DOCUMENT RESUME

ED 168 804 SE 024 415

AUTHOR	Carter, G. C., Ed.
TITLE	Applications of Phase Diagrams in Metallurgy and Ceramics: Proceedings of a Workshop Held at the National Bureau of Standards, Gaithersburg, Maryland, January 10-12, 1977. Volumes 1 [and] 2.
INSTITUTION	National Bureau of Standards (DOC), Washington, D.C.
REPORT NO	NBS-SP-496
PUB DATE	Mar 78
NOTE	1,633p.
AVAILABLE FROM	Superintendent of Documents, U.S. Government Printing Office, Washington, D.C. 20402 (Stock Number 003-003-01895-3; Sold in 2 volume sets only - $15.25 per set)
EDRS PRICE	MF14/PC66 Plus Postage.
DESCRIPTORS	*Ceramics; Computers; *Data Analysis; Industrial Arts; *Industry; *Metal Industry; *Metallurgy; Prediction; Theories; Thermodynamics; *Workshops
IDENTIFIERS	*Phase Diagrams

ABSTRACT

This document is a special National Bureau of Standards publication on a Workshop on Applications of Phase Diagrams in Metallurgy and Ceramics. The purposes of the Workshop were: (1) to assess the current national and international status of phase diagram determinations and evaluations for alloys, ceramics and semiconductors; (2) to determine the needs and priorities, especially technological, for phase diagram determinations and evaluations; and (3) to estimate the resources being used and potentially available for phase diagram evaluation. These proceedings reflect the detailed contents of the Workshop for both the tutorial and review sessions as well as four poster sessions and four panel sessions covering the following subjects: (1) critical phase diagram availability; (2) user needs of phase diagrams; (3) experimental methods of determination; (4) theoretical methods of calculation and prediction; (5) methods of phase diagram representations of calculation and prediction; (6) methods of phase diagram representations (especially multicomponent); and (7) distribution to the user. Three of the panels addressed the subject of phase diagram needs in industrial applications. (Author/GA)

****
* Reproductions supplied by EDRS are the best that can be made *
* from the original document. *
****

003-003-01895-3
C 13.10:496
#15.25/set
256-469
ERIC

SE

NBS SPECIAL PUBLICATION 496

U.S. DEPARTMENT OF COMMERCE / National Bureau of Standards

ED168804

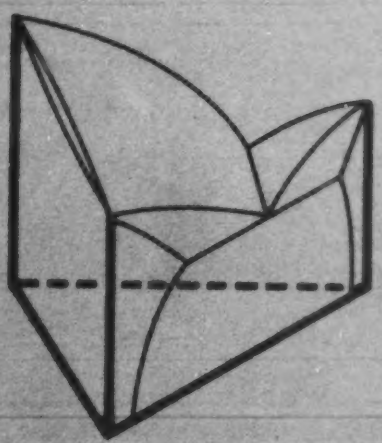

U.S. DEPARTMENT OF HEALTH, EDUCATION & WELFARE
NATIONAL INSTITUTE OF EDUCATION

THIS DOCUMENT HAS BEEN REPRODUCED EXACTLY AS RECEIVED FROM THE PERSON OR ORGANIZATION ORIGINATING IT. POINTS OF VIEW OR OPINIONS STATED DO NOT NECESSARILY REPRESENT OFFICIAL NATIONAL INSTITUTE OF EDUCATION POSITION OR POLICY

Applications of Phase Diagrams in Metallurgy and Ceramics

Volume 1

SE 024 415

NATIONAL BUREAU OF STANDARDS

The National Bureau of Standards[1] was established by an act of Congress March 3, 1901. The Bureau's overall goal is to strengthen and advance the Nation's science and technology and facilitate their effective application for public benefit. To this end, the Bureau conducts research and provides: (1) a basis for the Nation's physical measurement system, (2) scientific and technological services for industry and government, (3) a technical basis for equity in trade, and (4) technical services to promote public safety. The Bureau consists of the Institute for Basic Standards, the Institute for Materials Research, the Institute for Applied Technology, the Institute for Computer Sciences and Technology, the Office for Information Programs, and the Office of Experimental Technology Incentives Program.

THE INSTITUTE FOR BASIC STANDARDS provides the central basis within the United States of a complete and consistent system of physical measurement; coordinates that system with measurement systems of other nations; and furnishes essential services leading to accurate and uniform physical measurements throughout the Nation's scientific community, industry, and commerce. The Institute consists of the Office of Measurement Services, and the following center and divisions:

Applied Mathematics — Electricity — Mechanics — Heat — Optical Physics — Center for Radiation Research — Laboratory Astrophysics[2] — Cryogenics[2] — Electromagnetics[2] — Time and Frequency[2].

THE INSTITUTE FOR MATERIALS RESEARCH conducts materials research leading to improved methods of measurement, standards, and data on the properties of well-characterized materials needed by industry, commerce, educational institutions, and Government; provides advisory and research services to other Government agencies; and develops, produces, and distributes standard reference materials. The Institute consists of the Office of Standard Reference Materials, the Office of Air and Water Measurement, and the following divisions:

Analytical Chemistry — Polymers — Metallurgy — Inorganic Materials — Reactor Radiation — Physical Chemistry.

THE INSTITUTE FOR APPLIED TECHNOLOGY provides technical services developing and promoting the use of available technology; cooperates with public and private organizations in developing technological standards, codes, and test methods; and provides technical advice services, and information to Government agencies and the public. The Institute consists of the following divisions and centers:

Standards Application and Analysis — Electronic Technology — Center for Consumer Product Technology: Product Systems Analysis; Product Engineering — Center for Building Technology: Structures, Materials, and Safety; Building Environment; Technical Evaluation and Application — Center for Fire Research: Fire Science; Fire Safety Engineering.

THE INSTITUTE FOR COMPUTER SCIENCES AND TECHNOLOGY conducts research and provides technical services designed to aid Government agencies in improving cost effectiveness in the conduct of their programs through the selection, acquisition, and effective utilization of automatic data processing equipment; and serves as the principal focus within the executive branch for the development of Federal standards for automatic data processing equipment, techniques, and computer languages. The Institute consist of the following divisions:

Computer Services — Systems and Software — Computer Systems Engineering — Information Technology.

THE OFFICE OF EXPERIMENTAL TECHNOLOGY INCENTIVES PROGRAM seeks to affect public policy and process to facilitate technological change in the private sector by examining and experimenting with Government policies and practices in order to identify and remove Government-related barriers and to correct inherent market imperfections that impede the innovation process.

THE OFFICE FOR INFORMATION PROGRAMS promotes optimum dissemination and accessibility of scientific information generated within NBS; promotes the development of the National Standard Reference Data System and a system of information analysis centers dealing with the broader aspects of the National Measurement System; provides appropriate services to ensure that the NBS staff has optimum accessibility to the scientific information of the world. The Office consists of the following organizational units:

Office of Standard Reference Data — Office of Information Activities — Office of Technical Publications — Library — Office of International Standards — Office of International Relations.

---

[1] Headquarters and Laboratories at Gaithersburg, Maryland, unless otherwise noted; mailing address Washington, D.C. 20234.
[2] Located at Boulder, Colorado 80302.

Applications of Phase Diagrams in Metallurgy and Ceramics

Volume 1

Proceedings of a Workshop Held at the
National Bureau of Standards
Gaithersburg, Maryland, January 10-12, 1977

Edited by

G.C. Carter

Institute for Materials Research
National Bureau of Standards
Washington, D.C. 20234

Sponsored by:

Institute for Materials Research and
Office of Standard Reference Data, NBS
and by
National Science Foundation
Defense Advanced Research Projects Agency
Office of Naval Research
National Aeronautics and Space Administration
Energy Research and Development Administration
U.S. Army Research Office

U.S. DEPARTMENT OF COMMERCE, Juanita M. Kreps, Secretary

Dr. Sidney Harman, Under Secretary

Jordan J. Baruch, Assistant Secretary for Science and Technology

NATIONAL BUREAU OF STANDARDS, Ernest Ambler, Director

Issued March 1978

Library of Congress Catalog Card Number: 78-2201

National Bureau of Standards Special Publication 496/1
Nat. Bur. Stand. (U.S.) Spec. Publ. 496/1, 767 pages (March 1978)
CODEN: XNBSAV

U.S. GOVERNMENT PRINTING OFFICE
WASHINGTON: 1978

For sale by the Superintendent of Documents, U.S. Government Printing Office, Washington, D.C. 20402
Stock No. 008-003-01806-3 2-volume set; sold in sets only.
(Add 25 percent additional for other than U.S. mailing).

General Abstract

The proceedings of a Workshop on Applications of Phase Diagrams in Metallurgy and Ceramics, held at the National Bureau of Standards, Gaithersburg, Maryland, on January 10-12, 1977, is presented in this NBS Special Publication. The Workshop was co-sponsored by the Institute for Materials Research and the Office of Standard Reference Data, NBS, and the National Science Foundation, the Defense Advanced Research Projects Agency, the Office of Naval Research, the National Aeronautics and Space Administration, the Energy Research and Development Administration, and the U. S. Army Research Office.

The purpose of the Workshop was to assess the current national and international status of phase diagram determinations and evaluations for alloys, ceramics and semiconductors; to determine the needs and priorities, especially technological, for phase diagram determinations and evaluations; and to estimate the resources being used and potentially available for phase diagram evaluation. These proceedings reflect the detailed contents of the Workshop for both the tutorial and review sessions as well as four poster sessions and four panel sessions covering the subjects; critical phase diagram availability, user needs of phase diagrams, experimental methods of determination, theoretical methods of calculation and prediction, methods of phase diagram representations of calculation and prediction, methods of phase diagram representations (especially multicomponent) and distribution to the user. Three of the panels addressed the subject of phase diagram needs in industrial applications.

These proceedings represent documentation of this assessment, and constitute a valuable resource to workers in these areas, especially those planning to initiate phase diagram programs. Most subjects within the overall scope have been dealt with substantially in these proceedings; a few specialized topics such as surface and small particle phases, needed for the study of catalysis, have not been treated in detail. As the Alloy Data Center maintains a continuing phase diagram program, we would like to receive suggestions for similar topics of current and future interest, descriptions of new needs, or addenda and corrigenda to these proceedings. A tear-off sheet has been provided at the end of these proceedings for this purpose to be sent to the NBS Alloy Data Center.

KEY WORDS: Ceramics; computer predictions; critical evaluations; data compilations; electronic materials; industrial needs; metallurgy; phase diagrams; theory of phase diagrams; thermodynamics.

Foreword

Quantitative data on physical and chemical properties of materials form a key resource of modern technology. In the past a few dedicated scientists and engineers have performed an important service by compiling and evaluating such data for use by the technical community; an outstanding example is the work of Hansen on alloy phase diagrams. With the rapid growth of science and technology, this task has become too large and complex for a single individual. Organized programs with proper funding and continuity are essential if the technical community is to have the reliable data needed to solve the problems of modern society.

This Workshop represents an effort to coordinate and reinforce the current efforts on compilation of phase diagrams of alloys and ceramics. Many research groups and individual scientists throughout the world are concerned with phase equilibrium data.

Specialized expertise exists in small institutions as well as large laboratories. If this talent can be effectively utilized through a cooperative effort, the needs for such data can be met. The Office of Standard Reference Data, which serves as the program management office for the National Standard Reference Data System, is eager to work with all groups concerned with this problem. Through a cooperative international effort we can carry out a task which has become too large for an individual.

David R. Lide, Jr.
Chief
Office of Standard Reference Data
National Bureau of Standards

CONTENTS

	Page
General Abstract	iii
Foreword	v
Welcome - E. Ambler	xv
Overview of the Workshop - G.C. Carter	xvii
Workshop Organizing Committee	xviii

VOLUME 1

Present Status of Phase Diagram Compilation Activities

Phase Diagram Compilation Activities in Ceramics R.S. Roth, L.P. Cook, T. Negas, G.W. Cleek, and J.B. Wachtman, Jr.	1
Discussion	22
Present Status of Phase Diagram Compilation Activity for Semiconductors C.D. Thurmond	23
Phase Diagram Compilations for Metallic Systems - An Assessment of Ongoing Activities G.C. Carter	36
Organization of Phase Diagram Information in the Soviet Union N.V. Ageev, D.L. Ageeva, T.P. Kolesnikova, and L.A. Petrova	90
Discussion	95
A Survey of High Pressure Phases of Materials L. Merrill	100
Discussion (Jan. 10 - AM Session)	121
Phase Diagram Information from Computer Banks I. Ansara	123
An Overview of the Determination of Phase Diagrams F.N. Rhines	142
Discussion	163

Phase Diagram Compilation and Data Evaluation Activities

Proposal for a Comprehensive Handbook on "Ternary Phase Diagrams of Metals" F. Aldinger, E.-Th. Henig, H.L. Lukas, and G. Petzow	164
Phases and Phase Relations in the Binary Oxide Systems Containing WO_3 Luke L.Y. Chang	165

RIC in Phase with Rare-Earth Constitutional Diagrams
K.A. Gschneidner, Jr., M.E. Verkade and B.L. Evans..... 226

Evaluations of Phase Diagrams and Thermodynamic Properties of Ternary Copper Alloy Systems
Y.A. Chang, J.P. Neumann, U.V. Choudary..... 229

Phase Equilibria in Variable Valence Oxide Systems
W.B. White..... 251

Phase Diagrams for Ceramists
L.P. Cook, R.S. Roth, T. Negas and G.W. Cleek..... 257

NBS Crystal-Data Center
A. Mighell, H. Ondik, J. Stalick, R. Boreni..... 259

The NBS Alloy Data Center
G.C. Carter, D.J. Kahan, and L.H. Bennett..... 261

A Review of Phase Equilibria in the Na_3AlF_6-LiF-CaF_2-AlF_3-Al_2O_3 System
D.F. Craig, R.T. Cassidy, and J.J. Brown, Jr. 272

Methods of Compiling and Editing "Structure and Properties of Binary Metallic Systems"
A.E. Vol and I.K. Kagan..... 346
English Translation 351

Experimental Techniques in Phase Diagram Determinations

The Determination of Phase Diagrams for Liquid Oxides and Metallurgical Slags by Hot-Wire Microscopy
H.A. Fine..... 355

Experimental Techniques in Phase Diagram Determination of Superconducting Compounds Containing Volatile Components at Temperatures up to 2200°C
R. Flükiger and J.-L. Jorda 375

Application of Experimental Techniques and the Critical Determination of Phase Equilibria in Oxide Systems
F.P. Glasser..... 407

Protective Coatings for Superalloys and the Use of Phase Diagrams
M.R. Jackson and J.R. Rairden 423

Application of the Scanning Electron Microscope to the Study of High Temperature Oxide Phase Equilibria
L.P. Cook and D.B. Minor..... 440

Hyperfine Techniques and the Determination of Phase Diagrams
R.C. Reno, L.J. Swartzendruber, G.C. Carter, and L.H. Bennett..... 450

Experimental Determination of Phase Diagrams with the Electron Microprobe and Scanning Transmission Electron Microscope
A.D. Romig, Jr. and J.I. Goldstein..... 462

Interrelations Between Phase Diagrams and Hydriding Properties for Alloys Based on the Intermetallic Compound FeTi
G.D. Sandrock, J.J. Reilly, and J.R. Johnson..... 483

Phase Equilibria in the System MgO-RCl (R=Li, Na and K) Solution Under Hydrothermal Conditions by Means of a Capsule Bursting Method
Shigeyuki Sōmiya, Kazuo Nakamura, Shin-ichi Hirano and Shinroku Saito..... 508

High-Energy Ion Beams in Phase Diagram Determination
J.E. Smugeresky, and S.M. Myers..... 516

Phase Equilibrium Diagrams in Terms of Electronic Structure
F. E. Wang..... 545

Use of Segregation Phenomena in Solid Solutions as a Method for Determining Solidification Diagrams. Application to some Sc_2O_3 - Ho_2O_3 and Sc_2O_3 - Dy_2O_3 Systems
J.M. Badie..... 550

Studies of the Fe-C-B Phase Diagram by Autoradiography
T.B. Cameron and J.E. Morral..... 566

User Needs for Phase Diagrams
P. J. Fopiano..... 567

Phase Diagram of a Specimen at High Temperatures Under External Tensile or Shear Stress or Both
K.M. Khanna..... 575

Phase Diagram of a Metal-Gas System
V.K. Sinha..... 578

Methods of Phase Diagram Calculations

Theory of Alloy Phases
R.E. Watson, H.Ehrenreich and L.H.Bennett..... 592
Discussion..... 620

Computation and Prediction of Phase Diagrams (Panel I)

Estimation of Conjugate γ and γ' Compositions in Ni-Base Superalloys
R.L. Dreshfield..... 624
Discussion (Panel I - Jan. 11)..... 658

Review of Phase Diagram Representations, Format, and Distribution

The Representation of Phase Equilibria
A. Prince..... 660

Phase-Diagram Compilations - A User's View
J.D. Livingston..... 703

Some Thoughts on the Distribution of Reference Data
H. J. White, Jr..... 709

Remarks on Producing and Publishing Critically Evaluated Data
W.B. Pearson..... 720
Discussion (Jan. 11 - PM Session)..... 725

AUTHOR INDEX 725-A
SUBJECT INDEX 725-C
MATERIALS INDEX 725-J

VOLUME 2

Computational Techniques for Phase Diagram Construction

Computerized Characterization of the Au-Cu-Ni Ternary System
S.K. Tarby, C.J. Van Tyne, and M.L. Boyle..... 726

Correlations and Predictions of Metal-Boron Phase Equilibria
K.E. Spear..... 744

A Valence Bond Test for the Validity of Intermetallic and Semiconducting Structures
F.L.Carter..... 763

Computation of the Component Activities from Ternary Miscibility Gap Data: The Cu-Ag-S and Cu-Ag-Se Systems
U.V. Choudary and Y.A. Chang..... 774

The Mathematical Representation of Activity Data in Three Component Systems
I. Eliezer and R.A. Howald..... 803

A Program for Binary Phase Equilibria Using the Redlich-Kister Equations
I. Eliezer and R. A. Howald..... 846

Polynomial Representation of the Excess Free Energy of Multicomponent Systems and Their Use in Phase Diagram Calculations
H. Gaye and C.H. P. Lupis 907

Thermodynamic Data for the Fe-O System Evaluated Using a New Computer-Aided Strategy
J.L. Haas, Jr. and J.R. Fisher..... 909

Analysis and Synthesis of Phase Diagrams of the Fe-Cr-Ni, Fe-Cu-Mn and Fe-Cu-Ni Systems
M. Hasebe and T. Nishizawa..... 911

Optimization of Phase Diagrams by a Least Squares Method Using Simultaneously Different Types of Data
E.-Th. Henig, H.L. Lukas, B . Zimmermann and G. Petzow .. 955

Theoretical Calculation of Phase Diagrams Using the Cluster Variation Method
R. Kikuchi and D. de Fontaine 967

Fundamental Calculations of Coherent Phase Diagrams
D. de Fontaine and R. Kikuchi..... 999
Discussion..... 1017

Generation of Self-Consistent Gibbs Energy Functions for Binary Systems: The Fe-Cu System as an Example
J.P. Smith, D.M. Bailey and O. Kubaschewski..... 1027

Characteristics and Calculation of Stability Diagrams
S. McCormick and Y. Bilimoria..... 1047

The Effect of Irradiation on Phase Stability
L. Kaufman, J.S. Watkin, J.H. Gittus and A.P. Miodownik 1065

Facility for the Analysis of Chemical Thermodynamics (F*A*C*T) - A Computerized Canadian Thermodynamic Data Treatment Centre
A.D. Pelton, C.W. Bale, and W.T. Thompson..... 1077

The Calculation of Pourbaix Diagrams Using a Modified Linear Programming Technique
B.H. Rosof..... 1090

Theoretical Concepts Useful in the Calculation or Storage of Phase Diagrams of Ionic Systems
M.-L. Saboungi and M. Blander..... 1093

Estimation of Isothermal Sections of Ternary Phase Diagrams of Lithium Containing Systems: The Al-Li-Mg System
M.-L. Saboungi and C.C. Hsu..... 1109

Cybernetic Prediction of the Formation of Chemical Compounds in Uninvestigated Systems
E.M. Savitskii, V.P. Gribulya, and N.N. Kiselyeva 1139
English Translation..... 1151

The Determination and Representation of Metastable Phase Diagram Features and Other Thermal Characteristics of Metastable Alloys, Especially Amorphous Metals
B.C. Giessen..... 1161
Discussion..... 1183

The Calculation of Multicomponent Alloy Phase Diagrams at the National Physical Laboratory
T.G. Chart..... 1186

Synthesis of Binary Metallic Systems I. Ismorphous Systems II. Simple Eutectic Systems
S.S. Balakrishna, and A. K. Mallik..... 1200

Quantitative Fits to Phase Lines and High Temperature Thermodynamic Data for Systems Forming Semiconductor Compounds
R.F. Brebrick..... 1220

Format and Distribution of Phase Diagram Data

Table of Contents and Cumulative Subject Index for "Phase Diagrams of Metallic Systems," N.V. Ageev, editor, Volumes 1-19
C.M. Scheuermann..... 1237

Standards for Publication of Phase Equilibrium Studies
E.R. Kreidler..... 1307

Formatting and Distributing Evaluated Reference Data: The Office of Standard Reference Data at the National Bureau of Standards
S.P. Fivozinsky and G.B. Sherwood..... 1325

User Needs for Phase Diagram Information (Panel II)

Panel Discussion: Primary Metal Production
J.F. Elliott..... 1332

Needs for Phase Diagram Information in Non-Ferrous Industry
P.R. Ammann..... 1334
Discussion..... 1353

Primary Metals Production
H.R. Larson..... 1354
Discussion..... 1357

Use of Phase Diagrams in Iron and Steelmaking
R.D. Pehlke..... 1360
Discussion..... 1371

Materials Processing (Fabricating, Machining, Heat Treating, etc.) (Panel III)

User Needs for Phase Diagrams for Materials Processing: Glasses
R.C. Doman, and R.N. McNally 1378

Equilibrium Diagrams in Non-Ferrous Alloys
L.F. Mondolfo 1382

Phase Equilibria in the Development of High Temperature Structural Ceramics
S. Prochazka 1409

Phase Diagram Information for Processing of Superconductors
D. Dew-Hughes 1411

Product Applications (User Needs for Phase Diagram Information) (Panel IV)

Panel Discussion: Product Applications
F.L. VerSnyder 1418

Importance of Phase Diagrams in the Electric Power Industry
R.I. Jaffee 1420

Summary of Presentation on User Needs of Phase Diagrams: The Solar Energy Field
A.I. Mlavsky 1426

The Use of Phase Equilibria in the Manufacture of Spinel Ferrites
P. Slick 1427

The Application of the Phase Diagram to Thermal Energy Storage Technology
J.E. Beam and J.E. Davison 1428

The Needs for Phase Equilibria Data in the Development of Magnetohydrodynamics
R.A. Howald and I. Eliezer 1440
Discussion 1451

Summary Remarks
J. F. Elliott 1453

Evaluation of Conference
R.A. Howald 1470

Evaluation of Conference
J.E. Selle 1471

Comments on the Phase Diagram Workshop
D. de Fontaine..... 1472

Additional Contributed Papers to the Workshop

The Relation Between Bond Length and Crystal Structures in Metals
A.P. Miodownik..... 1479

On Computerized Construction of Multidimensional Phase Diagrams in a Factographic IRS
I.V. Tulupova and V.S. Stein..... 1506

REGISTRATION LIST..... 1520

AUTHOR INDEX..... 1529

SUBJECT INDEX..... 1531

MATERIALS INDEX..... 1538

Disclaimer

Certain commercial products and instruments are identified in this publication in order to specify adequately the experimental procedure. In no case does such identification imply recommendation or endorsement by the National Bureau of Standards, nor does it imply that the products or equipment identified are necessarily the best available for the purpose.

Welcome to the Workshop on Applications of Phase Diagrams in Metallurgy and Ceramics

E. Ambler

Good morning. It is my pleasure to welcome you this morning to the National Bureau of Standards and this Workshop on Applications of Phase Diagrams in Metallurgy and Ceramics. Evidence of the broad interest in and importance of this subject matter is seen when one notes that the National Science Foundation, Defense Advance Research Project Agency, Office of Naval Research, National Aeronautics and Space Administration, and U. S. Army Research Office have joined with the NBS Institute for Materials Research and NBS Office of Standard Reference Data in the sponsorship of this workshop.

As I looked over the material for this workshop, I found this group to be truly international and interdisciplinary in scope. There are participants here from Canada, France, Germany, India, Japan, the United Kingdom, Switzerland, the Union of Soviet Socialist Republics, and our own United States. You include representatives from data compilation groups, major industries and trade associations, and scientists from industry, government and university laboratories.

Of special interest to me is your banquet speaker, W. Dale Compton, who is the Vice President for Scientific Research at the Ford Motor Company. In addition, Dale is also a member of the NBS Visiting Committee - our Board of Directors so to speak - and the former chairman of the National Science Foundation Numerical Advisory Board. I look forward to joining you for the banquet and Dale's presentation.

For more than 100 years, phase diagrams have been a recognized and important tool in the development of science and technology. As one example, phase diagrams formed the basis for the development of new alloys and the respective heat treatments for these alloys. This resulted in new materials highly characterized and tailored to a host of specific uses. Today, phase diagrams are increasingly relevant to the development of new and substitute materials.

Now, as we stand at the threshold of this Workshop, it seems an appropriate time to spend a brief moment clarifying our perspective concerning the development of phase diagrams. Where do we stand in the study of phase diagrams and the compilation of phase diagram data? Clearly, the studies of and the techniques used today are vastly different than those of yesterday.

The optical microscope was used 100 years ago to study the character of alloys and minerals. By 1914, x-rays were used to confirm the crystalline structure of materials. The 1930's brought the advent of the electron microscope and a higher resolution of the materials being studied. From that evolved the electron microprobe which allowed us to determine the chemical composition of an individual phase on a spatial resolution of two to three μm in diameter. More recently, we have seen the development of the scanning electron microscope, the field ion microscope, and the Auger electron spectrometer.

Over the past 30 - 35 years, we have witnessed and participated in an evolution in experimental techniques. Today, we are able to determine phase diagrams to a high level and detail of accuracy. Certainly, our techniques are vastly improved. But the task we face is still enormous. Just consider the study of alloys. In the study of binarys, there are 1770 possible diagrams; with ternaries, there are 34,200 possible phase diagrams; and with quatranaries, there are many, many possible diagrams. To compound this task is the fact that it is the multicomponent materials which are of the greatest interest today.

To meet this problem, new techniques are now being developed which are based on a theoretical understanding of materials. We find that we can achieve "paper calculations" through theoretical prediction of phase diagrams. In addition, we can develop mathematical models that are predictive. However, the validity of these models is dependent on the availability of accurate data. Thus, while we strive to predict complicated phenomena, we do so with the clear understanding that we must first develop a simple, accurate data base.

An assessment of today's environment then shows that although we possess many new and improved tools, they are still not sufficient to perform the task that faces us. Therefore, we stand in a position where our first order of business should be an assessment of priorities. The goals of this workshop:

- To assess the current national and international status of phase diagram determination and evaluation for alloys, ceramics and semi-conductors;

- To determine the needs and priorities, especially technological, for phase diagram determinations and evaluations; and

- To estimate the resources being used and potentially available for phase diagram evaluation;

are quite timely. In fact, I think that the key statement for this workshop is found on page 1 of your program: "It is hoped that the workshop will provide the stimulus for the production of more relevant more useful, and more useable phase diagram data."

I concur with that statement and heartily endorse the goals of this workshop. Moreover, it is my personal belief that communication, such as this workshop is intended to foster, is a critical component to all scientific and technological ventures.

In closing, again let me welcome you to NBS. Our facilities are at your disposal and we would invite any inquiries about our specific programs that are of interest to you. I look forward to joining you Tuesday evening and I hope that your workshop is both stimulating and productive.

Overview of the Workshop

G. C. Carter

Knowledge of the structure of materials is important in understanding several industrially significant phenomena and applications such as aging, hardness, occurrence of brittle intermetallic compounds, magnetic transition temperatures, high-temperature solubility of impurities, corrosion resistance, solid electrolytes and non-crystalline solids. The study of a phase diagram appropriate to a particular material can often provide information important to its scientific and technical application.

Wide participation by industry, government, and university representatives was achieved at the Workshop. International participation was particularly successful among the data evaluation groups including important representations from the Soviet Union, Germany, France, the UK, Japan, and Canada. Other countries were represented; experimentalists and theorists determining phase diagrams were among the participants, as were a substantial fraction of phase diagram users from industry.

Specific subjects of investigation were:

... to assess the current national and international status of phase diagram determinations and evaluations for alloys, ceramics and semiconductors; to identify resources being expended that could be made more useful by appropriate coordination; to recognize unnecessarily overlapping efforts in determining phase diagrams; to suggest areas of international cooperation.

... to determine the needs and priorities, especially technological, for phase diagram determinations and evaluations; to gauge the relative importance of depth of coverage and range of materials including factors such as a) high precision, b) metastable phases, c) binary and higher order systems, d) magnetic, metal nonmetal and other phase transitions, e) high pressure data, f) integration of collateral information, and g) the role of impurities or trace additions.

... to review the strengths and limitations of various experimental techniques for determining phase diagrams,

... to briefly survey the status and merits of various predictive methods (CALPHAD, PHACOMP, psedupotential, etc.),

... to discuss diverse presentation methods, and

... to discuss effective and alternative means for dissemination of phase diagram data.

The workshop program was designed to stimulate interactions between (i) phase diagram data providers and users, (ii) metallurgists, geochemists, thermochemists, ceramics, solid state chemists, physicists, and scientists in other disciplines, (iii) representatives from industry, government, and the academia, (iv) phase diagram data centers throughout the world.

Plenary lectures introduced the subjects of present status of data availability from reference books, data centers and computerized files, the status of experimental data and theory of alloy phases. A panel on computation and prediction gave a more thorough introduction to that subject, and short reviews introduced the subjects of phase diagram representations and methods of distribution. Lively poster sessions followed these introductions. Three panel sessions were devoted to industrial needs in (i) Primary Metals Production, (ii) Materials Processing, and (iii) Product Applications. Discussion covered needs for multicomponent diagrams (up to 9 or 10 components) for industrial applications down to binary equilibrium diagrams, for various R & D programs, theoretical and prediction models, and other applications.

Four on-line demonstrations of computer-data handling systems related to phase diagrams were held and short instructional movies were shown during the poster session.

The workshop was organized by the Alloy Data Center and the group compiling "Phase Diagrams for Ceramists". The success of the Workshop program could not have been realized without invaluable assistance received from our very able organizing committee.

WORKSHOP ORGANIZING COMMITTEE

Members from NBS

L. H. Bennett, chairman
G. T. Armstrong, C. J. Bechtoldt, D. B. Butrymowicz, G. C. Carter, L. P. Cook, J. R. Cuthill, P. R. deBruyn, D. J. Kahan, M. B. McNeil, R. L. Parker, R. M. Waterstrat, H. J. White

Members from other Organizations

N. Ault, Norton Co., Worcester, MA
J. Elliott, M.I.T., Cambridge, MA
S. G. Epstein, Aluminum Association, New York, NY
L. Kaufman, ManLabs, Cambridge, MA
R. Laudise, Bell Telephone Laboratories, Murray Hill, NJ
J. D. Livingston, General Electric, Schenectady, NY
E. S. Osborne, Carnegie Geophysical Lab., Washington, DC
E. C. Van Reuth, Defense Advanced Res. Projects Agency, Arlington, VA
Schrade F. Radtke, Intl. Lead-Zinc Research Organization, New York, NY
R. Reynik, National Science Foundation, Washington, DC
E. Salkovitz, Office of Naval Research, Arlington, VA
L. M. Schetky, International Copper Research Assoc., New York, NY
C. Scheuermann, NASA Lewis Research Center, Cleveland, OH
M. Semchyschen, Climax Molybdenum Corp., Ann Arbor, MI
J. Swisher, Energy Research & Development Admin., Washington, DC

ARRANGEMENTS COMMITTEE

Ronald B. Johnson, Chairman
Sara R. Torrence

National Bureau of Standards SP-496, Applications of Phase Diagrams in Metallurgy and Ceramics
Proceedings of Workshop held at NBS, Gaithersburg, Md., January 10-12, 1977

PHASE DIAGRAM COMPILATION ACTIVITIES IN CERAMICS

R.S. Roth, L.P. Cook, T. Negas, G.W. Cleek, and J.B. Wachtman, Jr.

National Bureau of Standards
Institute for Materials Research
Washington, D.C. 20234

1.0 Introduction

Phase diagrams play an important role in the development of ceramic materials. Phase equilibria data are essential in meeting the expanding needs for refractories, electronic components, non-crystalline solids, and various other applications of interest to ceramic scientists and engineers. The chemical information generally summarized as a phase equilibrium diagram is extremely useful in many industrial processes. However, the necessary research involved in obtaining such information is often very costly. The average binary phase diagram can be estimated to take about one man year and a ternary diagram may take five times that effort. To avoid duplication, it is advantageous to have all existing diagrams compiled and distributed for easy access.

2.0 Compilation Activities in Ceramics

2.1 General Phase Diagrams

The major references in English for phase equilibria data are:

- E. M. Levin, et al., "Phase Diagrams for Ceramists" (3 volumes)

- G. J. Janz, et al., "Molten Salts" (4 volumes)

There is some duplication of compilation activity in the ceramic sciences but this is largely an international problem. The principal compilations in addition to "Phase Diagrams for Ceramists" are Russian. Such duplication is not necessarily wasteful, since any publication would have to be made available in both languages. Also, the two groups of publications, which are partly independent, can be cross-checked for inclusion of references otherwise missed.

The U.S.S.R. publications include:

- N. A. Toropov, et al., "Handbook of Phase Diagrams of Silicate Systems" (English translations available from NTIS)

- V. P. Barzanovskii, et al., "Phase Diagrams of the Silicate Systems", 2 volumes (in Russian)

- D. L. Ageeva, "Phase Diagrams of Non-Metallic Systems", 10 volumes (in Russian)

- F. V. Chukov, "Minerals: Phase Diagrams of Importance to Mineral Formation" (2 volumes - in Russian)

In Japan compilation activities have, so far, been confined mainly to refractories. These include:

- S. Somiya, "Zirconia Bearing Refractories" (in Japanese)

2.2 Compilation Activities - Metal Oxygen Systems

The link between metallurgy and ceramics is found in the equilibria data for the binary metal-oxygen systems. Special compilation activities in the United States for these systems began in 1961 with a group of reports by J. H. Westbrook, R. ". Carter and R. C. DeVries:

I. Rare Earth Metal - Oxygen Systems

II. Alkaline Earth - Oxygen Systems

III. Precious Metal - Oxygen Systems

Another compilation has been published in India by B. K. Rajput, A. M. George and M. D. Karkhanavala and pertinent portions will be extracted in the next supplement to "Phase Diagrams for Ceramists". The proceedings of this meeting contain a report of a more ambitious compilation attempt by W. B. White for the metal-oxygen systems (paper MPSI-5).

3.0 Phase Diagrams for Ceramists

The history of the compilation of Phase Diagrams for Ceramists dates back to 1933, when 157 diagrams collected by F. P. Hall and Herbert Insley were published in the October issue of the Journal of the American Ceramic Society. A supplement was published in the April 1938 issue of the same journal. A complete compilation of the diagrams appeared as Part II of the November 1947 Journal and contained 485 diagrams. In December 1949, H. F. McMurdie and F. P. Hall were authors of a supplement to the 1947 edition. In January 1956, the American Ceramic Society published a separate volume of phase diagrams edited by E. M. Levin, H. F. McMurdie and F. P. Hall. Part II of this volume appeared in 1959 authored by E. M. Levin and H. F. McMurdie. In 1964, a new complete compilation containing 2066 diagrams was published with E. M. Levin, H. F. McMurdie, and C. R. Robbins as authors. A supplement to the 1964 volume appeared in 1969 and contained another 2183 diagrams.

A third supplement, published in 1975 (850 diagrams), includes a discussion of the methods, data and interpretations made in the construction of each diagram. Since the death of E. M. Levin in 1974, this effort is being continued by a team of scientists actively engaged in phase equilibria studies in research centers in this country and abroad. This group is led by researchers at NBS who are assuming the responsibility for collecting data from the literature, distributing it among the group for evaluation, coordinating preparation of the publication, and preparing evaluations of systems in their own areas of expertise.

This latest supplement will include critical commentaries discussing preparation of starting materials, experimental methods, characterization of products, accuracy and precision of data and of diagram. The following experts in various fields are serving as Contributing Editors for the 1978 Supplement:

- J. J. Brown, Jr., Virginia Polytechnic Inst.
  Fluoride containing systems
- L. T. Y. Chang, Miami Univ.
  Tungstates, molybdates, carbonates
- R. C. DeVries, General Electric Co.
  High pressure studies
- F. P. Glasser, Univ. Aberdeen
  Alkali oxide containing systems
- F. A. Hummel, Pennsylvania State Univ.
  Sulfides, phosphates
- K. H. Jack, Univ. Newcastle Upon Tyne
  Nitrides, oxynitrides
- A. Muan, Pennsylvania State Univ.
  First row transition metal oxide containing systems
- C. Semler, Ohio State Univ.
  Anhydrous silicate - oxide systems
- C. A. Sorrell, Univ. Missouri-Rolla
  Aqueous salt systems
- K. H. Stern, Naval Research Laboratory
  Binary systems with halides only
- R. E. Thoma, Oak Ridge National Laboratory
  Fused salts
- D. R. Wilder and M. F. Berard, Iowa State Univ.
  R.E. oxide bearing systems
- H. S. Yoder, Jr., Carnegie Inst. Washington
  Hydrous silicate systems, high pressure silicate studies

Scientists at NBS (L. Cook, R. Roth and T. Negas) with the help of the American Ceramic Society (G. Cleek) are assuming much of the responsibility for gathering the data from the literature and coordinating the preparation of evaluations and final editing of diagrams.

Coverage according to chemical system for the various editions is as follows:

	1964	1969	1975	1978
Metal-oxygen systems	146	202	104	∿205
Metal oxide systems	855	408	401	∿655
Systems with oxygen containing radicals	172	228	68	∿120
Systems with halides only	483	718	145	∿365
Systems containing halides with other substances	214	273	72	∿160
Systems containing cyanides, sulfides, etc.	43	82	20	∿140
Systems containing water	151	131	40	∿250

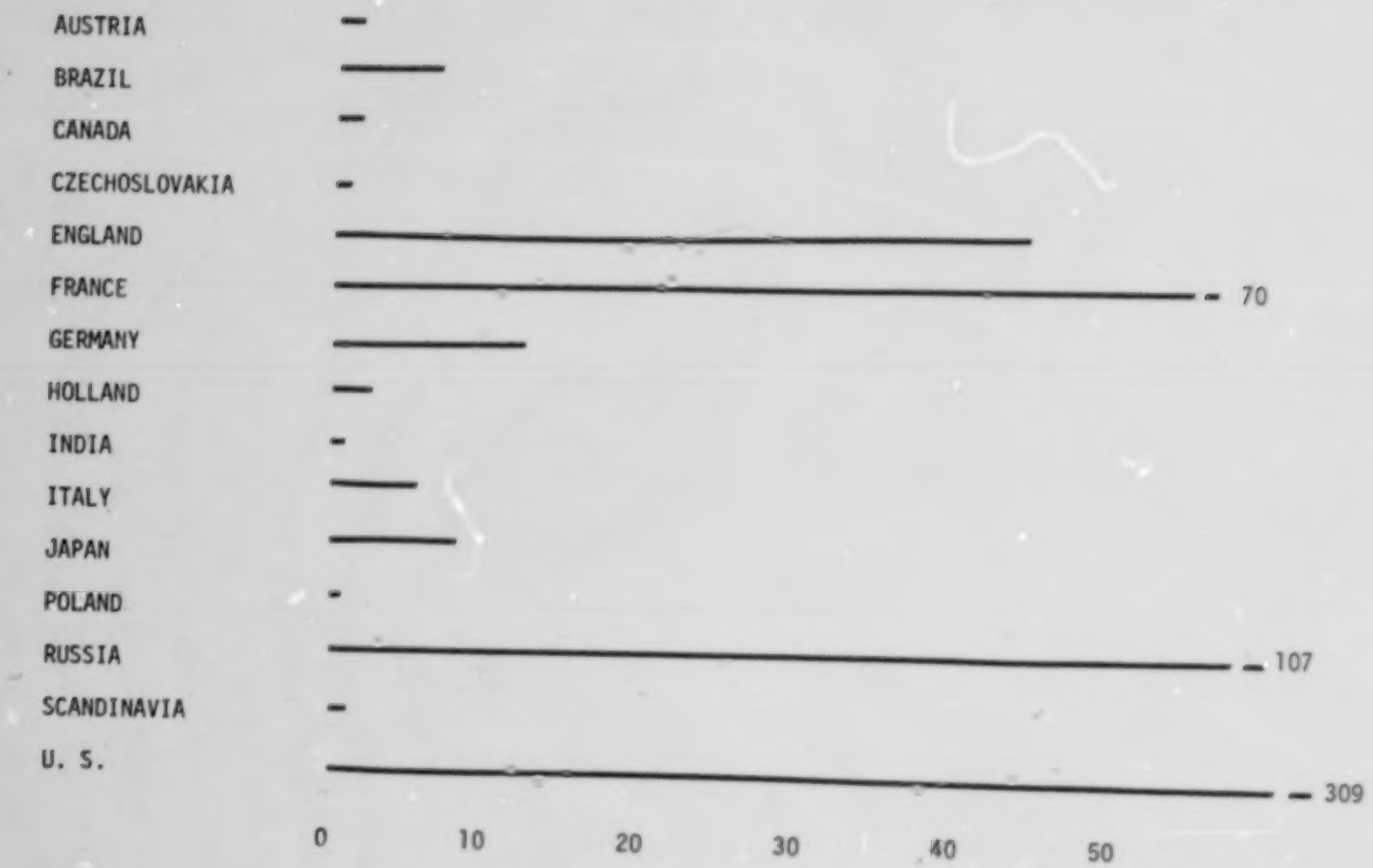

Figure 1. Publication of Oxide Systems by Country - 1975 Supplement.

A summary of the countries of publication of the phase diagrams reviewed in the 1975 Supplement is shown in Figures 1 and 2. The oxide systems by country are shown in a bar graph in Figure 1. It is evident that England, France, USSR and US are the major publishers of the diagrams. Figure 2 illustrates the distribution of the origin of other systems. The large number from the Soviet Union are mostly fused salt systems. It is highly probable that the distribution illustrated by these figures is biased by the techniques used to obtain the references and the reviewers' personal interests. It is hoped that any such bias will be eliminated in future supplements as greater attempts are made to make the compilation more complete and up-to-date.

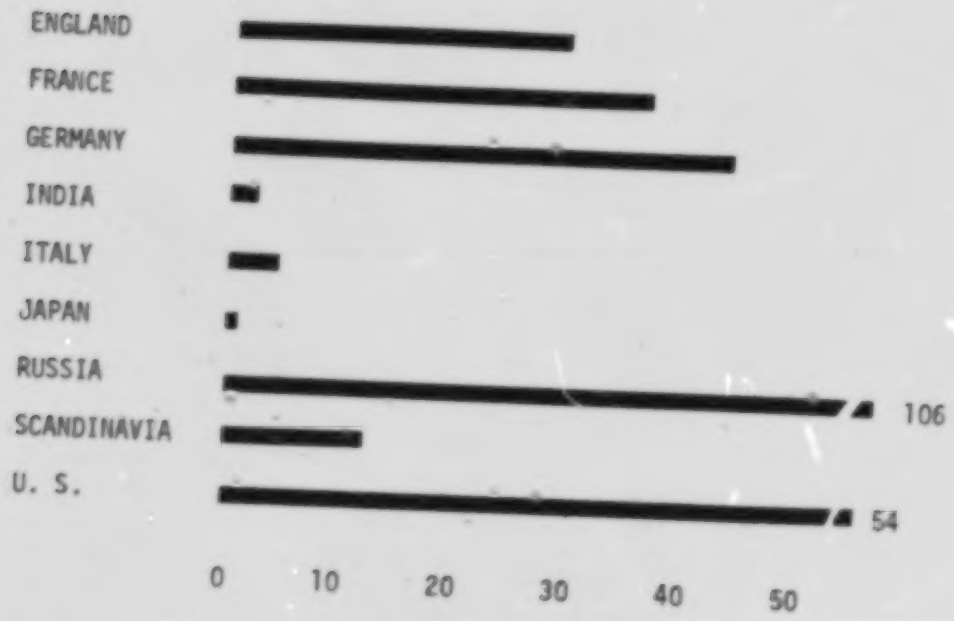

Figure 2. Publication of Other Systems by Country - 1975 Supplement.

4.0 Phase Diagrams for Ceramists - Survey of Users

A questionnaire was distributed by the American Ceramic Society in July 1976 to purchasers of the 1975 Supplement of "Phase Diagrams for Ceramists". The total number of questionnaires distributed was 460. The total number returned in the first three months was 186. This is a response of 40%, a remarkably large percent return, illustrating the great interest in the user community in this compilation. Table 1 gives the statistical breakdown of the origin of the returns. It should be noted that 81 or 44% of these are of domestic industrial users. The large response allows a determination of user needs in phase equilibria with a reasonably high statistical probability of success.

Table 1. PHASE DIAGRAMS FOR CERAMISTS PRELIMINARY RESULTS OF SURVEY OF USERS

Total Number Distributed - 460

Total Number Returned in First Three Months - 186

Response - 40%

- Unidentified - 25 (13%)
- Foreign - 37 (20%)
- Domestic
  1. Government and National Laboratories - 5 (3%)
  2. University and Non-Profit Laboratories - 38 (20%)
  3. Industrial - 81 (44%)

In this questionnaire, twenty-one questions were asked covering the four major categories:

I. Description of Respondent (1-7)

II. Uses of Phase Equilibria Data and Principles (8-10)

III. Evaluation of Phase Diagrams for Ceramists as a Publication of the American Ceramic Society (11-18)

IV. Important Needs for Experimental and/or Theoretical Work (not now being done) (19-21)

4.1 Description of Respondent (I)*

4.1.1 Personal Data

The first seven questions requested personal data and nature of employment. Under Type of Training 127 individuals (68%) identified themselves as scientists while 71 (38%) refer to themselves as engineers, with only four (or 2%) belonging to the "other" category. As scientists and engineers add up to more than 100% obviously some identify themselves with both groups. This breakdown along with the highest degree of the respondent is shown in Table 2. Note that 62% have a Ph.D. or equivalent. Their highest degree was generally in the fields of ceramics, chemistry, materials or geology (Table 3). In Table 4 the present type of work checked by the respondent is summarized by total number and percent. As the respondent was asked to check as many as appropriate, the totals again are greater than 100%. By far the largest group is in research and development although technical management and education activities are well represented. As shown in Table 5, 83% identify themselves as members of the American Ceramic Society and their division affiliations are mostly Basic Science, Refractories, Glass and Electronics.

* Roman numeral in parenthesis indicates Major Category.

Table 2. DESCRIPTION OF RESPONDENT (I)

Type of Training (1)

- Scientist - 127 (68%)
- Engineer - 71 (38%)
- Other - 4 (2%)

Highest Degree (2)

- BS or BA - 31 (17%)
- MS or MA - 30 (16%)
- PhD or ScD - 115 (62%)
- OTHER - 10 (5%)

Table 3. SPECIFIC FIELD OF HIGHEST DEGREE (2)

1. Ceramics (Technology, Engineering, Science) - 56 (30%)
2. Chemistry (Physical, Inorganic, Engineering, Industrial, Electrochemistry, etc.) - 40 (22%)
3. Materials Science (Engineering) - 17 (9%)
4. Geology - Mineralogy - 16 (9%)
5. Metallurgy - 12 (6%)
6. Physics - 5
7. Engineering - 4
8. Crystallography - 1
9. Natural Sciences - 1
10. No Identification - 33 (18%)

Table 4. PRESENT TYPE OF WORK (3)

- Research - 143 (77%)
- Development - 85 (46%)
- Production - 18 (10%)
- Technical Management - 40 (22%)
- Education - 46 (25%)
- Other - 9

Table 5. MEMBERSHIP IN THE AMERICAN CERAMIC SOCIETY (4a)

- Yes - 155 (83%)
- No - 28 (15%)

DIVISION AFFILIATION (4b)

1) Basic Science - 56
   Cement - 4
   Ceramic-Metal Systems - 5
4) Electronics - 21
3) Glass - 23
   Materials and Equipment - 4
   Nuclear - 5
2) Refractories - 29
   Structural Clay Products - 1
   White Wares - 1
   No Division - 12

4.1.2 Standard Industrial Categories of Employer (5)**

The respondents were requested to check one or more of a group of listed Standard Industrial Categories (SIC) which best describe their employer. Those categories receiving ten or more entries are listed in Table 6. The major industrial categories include stone, clay and glass products, electrical and electronic equipment, chemicals and non-metallic minerals. The name and address of the employer was given by 150 respondents and 174 listed their own name and address, indicating a (conditional) willingness to be contacted for further information.

Table 6. STANDARD INDUSTRIAL CATEGORIES OF EMPLOYER (5)

(10 or more checked)

SIC NO.	CATEGORY	NO. OF TIMES CHECKED
32	Stone, Clay and Glass Products	50
82	Educational Services	46
36	Electrical and Electronic Equipment	26
28	Chemicals and Allied Products	20
14	Nonmetallic Minerals, Except Fuels	19
33	Primary Metal Industries	15
34	Fabricated Metal Products	13
38	Instruments and Related Products	10
	Other	35

** Arabic numeral in parenthesis indicates Question Number.

4.2 Uses of Phase Equilibria Data and Principles (II)

4.2.1 Applications (8-9)

Question eight asked for areas of application of phase equilibria in the respondent's organization (check as many as possible). Fifteen categories were listed while the sixteenth, entitled "Other", requested specifics. Table 7 lists these categories rearranged according to decreasing number of responses.

Table 7. USES OF PHASE EQUILIBRIA DATA (8)

AREAS OF APPLICATION:

- Sintering of Ceramics - 117
- Search for New Compounds - 93
- Glass Processing - 63
- Education - 57
- Electronic Materials - 54
- Crystal Growing - 51
- Metal Coating or Processing - 41
- Smelting and Refining - 39
- Geology - 33
- Energy Conversion - 31
- Optical Materials - 29
- Magnetic Materials - 29
- Building Materials - 23
- Environment Effects - 17
- Nuclear Materials - 15
- Other - 19

Question nine, requesting specific application of phase equilibria data, elicited 127 responses. This may perhaps be the most important point in the questionnaire and will be treated in detail in a later publication. Table 8 summarizes these answers according to the type of material, the property of interest and the industry involved. One typical quote suffices to illustrate the simple yet very important uses which can be made by easy access to phase equilibria data:

> "Refractory attack occurred at bottom of furnace when metal temperature was lowered 50°C. Analysis of phase diagram showed that 50°C drop lowered bottom of furnace operating temperature below melting point of anorthite which built up during low end of temperature cycle. Upon heating to upper end of metal melting temperature, corrosive liquid was formed which ate the SiO_2 lining of the induction furnace. Bottom end of temperature range was raised 50°C and problem was eliminated."

Table 8. SPECIFIC APPLICATION OF PHASE EQUILIBRIA DATA (9)

Total Number of Answers - (127)

Industrial - (67)

MATERIAL

Oxide Ceramics (12)	Silicates (4)
Glass or Slag Plus Refractory (10)	Alumina (3)
Glass or Slag (9)	Metal + Slag (3)
Refractories (6)	Titanates, Etc. (2)
	Raw Materials (2)

PROPERTY

Identification of Phases (17)	Corrosion (4)
Glass Forming Regions (9)	Homogeneity (4)
Melting Points (6)	Chemical Reaction (4)
Liquidus (5)	Primary Phases (3)
Sintering (4)	Refractory Nature (3)

INDUSTRY

Glass (12)	Chemical (4)
Electronics (9)	Refining and Smelting (4)
Refractories (7)	Ceramics (2)
Electro-Optics (5)	Communications (2)
Iron and Steel (5)	Abrasives (2)

4.2.2 Classes of Systems of High Interest (10)

Question ten asked, "Which classes of systems are of high interest to you? Please indicate by 3 = High interest, 2 = Moderate interest, 1 = Some interest, 0 = No interest." Most respondents listed only 3 and 2. Table 9 lists the classes of systems divided into oxides, halides and general with the number of (3) answers given for each class, rearranged according to those of most interest in each category. Metal oxides and silicates are obviously of the highest interest with oxides in general being the most important. In the general category there is a significantly large vote for carbides and borides which are not covered in the present compilation, nor are there plans for inclusion of them. At the bottom of this list are arsenides, phosphides, selenides, and tellurides which are also not intended for coverage in the near future.

Table 9. CLASSES OF SYSTEMS OF HIGH INTEREST (10)

OXIDES	NO.	(%)
Metal Oxides	144	(77)
Silicates	107	(58)
Alkali Oxides	77	(41)
Alkaline Earths	53	(28)
Rare Earths	40	(22)
Phosphates	35	(19)
Borates	34	(18)

HALIDES	NO.	(%)
Fluorides	25	(13)
Chlorides	24	(13)
Bromides	1	
Iodides	1	

GENERAL	NO.	(%)
Carbides, Borides	43	(23)
Oxynitrides, Nitrides	32	(17)
Sulfates, Sulfides	32	(17)
Carbonates	31	(17)
Nitrates and Nitrites	18	(10)
Aqueous Systems at 1 atm	14	(8)
Hydrothermal Systems	12	(6)
Arsenides, Phosphides	10	(5)
Selenides, Tellurides	6	(3)

Other - 15 (8)

4.3 Evaluation of Phase Diagrams for Ceramists as a Publication of the American Ceramic Society (III)

In general the tone of evaluation in this section was very favorable, although it might be argued that the audience was biased in favor of the book as they had just ordered the latest supplement.

4.3.1 Value of Phase Diagrams for Ceramists as a Publication (11)

As shown in Table 10, an overwhelming majority (87%) considered "Phase Diagrams for Ceramists" very valuable; defined as "in the top priority category among special publications [Note: The Journal, Bulletin and Ceramic Abstracts are not special publications]". There were no votes for the category "No Value; should be discontinued".

Table 10. EVALUATION OF PHASE DIAGRAMS FOR CERAMISTS (11)

- Very Valuable - 162 (87%)
- Moderately Valuable - 20 (11%)
- Marginal Value - 1
- No Value - 0

4.3.2 Does Range of Systems Treated Span Range of Interest (12)

Question (12) asked: Considering the 1975 Supplement together with the 1969 Supplement and the 1964 volume, does the range of systems treated span your range of interests? This question elicited answers similar to those of question 10. Indeed, there was a large amount of redundancy deliberately built into the questionnaire specifically to obtain that opinion which most interested or bothered the respondent. In this category 126 or 68% of the respondents checked YES, indicating they were quite happy with the range of coverage. Only 38 or ∿20% answered NO and bothered to describe other systems which should be covered. These results are summarized in Table 11. Some of the suggested systems summarized under "not covered" are of course found in other non-ceramic compilations. Also note the similarity to the answers for question 19.

In Table 11 and succeeding tables the figures in brackets after the information refers to the number of times it was suggested. No number means it was only mentioned once. Unfortunately, the answers reflect the systems which the respondents want studied rather than compiled. There is very little published data in many of the categories listed. Many of the desired categories are outside the field of present coverage. Indeed some of them are outside the field of ceramics entirely. Other answers have nothing to do with the question; for instance, the comments "total coverage not adequate" and "time lag too great". These later points will be covered in the conclusion section.

Table 11. OTHER SYSTEMS WHICH SHOULD BE COVERED (12)

ALREADY COVERED	NOT COVERED
Glass Forming Systems (4)	Carbides, Borides, Nitrides (7)
Refractories (3)	Mixed Systems (5)
High Pressure (2)	Selenides, Tellurides (2)
Sulfides (2)	Silicides
Electronic Oxide Materials	Simple Metal Systems (2)
Oxyfluorides	Intermetallics
Hydrates	Metal-Gas Systems
Minerals	Refractories with Molten Metal
	Non-Oxide Containing Systems

IMPORTANT COMMENTS:

Systems with Variable P_{O_2} (8)

Total Coverage Not Adequate

Time Lag Too Great

4.3.3 Evaluation of Phase Diagrams for Ceramists (13-16)

In this section the respondent was asked to comment on (13) Gaps in Coverage, (14) More Attention During Experiment, (15) Is Information in Useful Format and (16) Are (1975) Commentaries Useful and of Right Length. The completely satisfied respondent would answer No, No, Yes, Yes, About Right to these questions. Table 12 shows the statistical summary of these answers and again it is evident that most people are fairly satisfied with the book as presently published.

4.3.3.1 Gaps in Coverage (13)

Table 13 shows that 67 answers considered that there were gaps in coverage. Again their written descriptions summarized in this table show that the gaps are mostly in the availability of experimental data rather than in the compilation of published data.

Table 12. EVALUATION OF PHASE DIAGRAMS FOR CERAMISTS (III)

(Completely Satisfied Checks No, No, Yes, Yes, About Right)

(13) Gaps in Coverage - No - 93
Yes - 67

(14) More Attention During Experiment - No - 89
Yes - 69
I Don't Know - 1

(15) Information in Useful Format - Yes - 165
No - 10

(16) (1975) Commentaries Useful - No - 7
Yes - 153

LENGTH: Too Long - 7
About Right - 129
Too Short - 9

Table 13. ARE THERE GAPS IN COVERAGE OR COMPILATION (13)

No - 93
Yes - 67

Summary of Answers

- Multicomponent Oxides - 34
- Systems with Variable P_{O_2} - 17
- Non Oxides - 14
- Hydrous, Hydrothermal and High Pressure - 5
- Metastable and Non-Equilibrium Phases - 3
- Commentaries for Important Systems from Vol I and II
- Compilation not Complete Because Some Published Diagrams not Included

Table 14. ARE THERE FEATURES WHICH NEED MORE ATTENTION DURING EXPERIMENTAL STUDIES? (14)

No - 89 (48%)

Yes - 69 (37%)

APPLICATIONS:

PRIMARY

Glass Forming Regions (3)

Viscosity (Even Qualitative)

SO_4^{-2} in Glass

Molten Metals vs Refractories and Slag

Slag and/or Other Wastes Plus Feldspar, Clay, etc.

More Property Measurements

EITHER

Ranges of Homogeneity (5)

Impurity Effects (5)

Kinetics (3)

Metastability (2)

Lattice Parameters vs Composition

Immiscibility Regions

Exsolution

SECONDARY

Effect of P_{O_2} on Equilibria (5)

P-T-X Equilibria and Vapor Pressure (2)

Phase Changes

Crystallographic Information

Magnelli-Type Phases

Nonstoichiometry

Methods of Detection of Solid Solution

"Opinions from Experts on Relative Accuracy of Conflicting Published Data"

4.3.3.2 Experimental Needs (14)

Question 14 asked "Are there features of the systems to which more attention should be given during experimental studies [such as solid solution below the one percent level]?" Only 18 people , or about 10%, specifically agreed with the suggestion concerning solid solution below the one percent level. They were about equally divided between industrial and university representatives. As pointed out by one individual in charge of the Materials Research Laboratory of a leading U.S. university, "This is very difficult data to get." The descriptions to the Yes answers of 69 individuals (37%) are summarized in Table 14, according to the type of applications of the features. Once again the answers are not necessarily those which have much relation to the question.

4.3.3.3 Useful Format (15)

A total of 165 respondents agreed that "the information given in the diagrams (was) presented in a useful format." Although only 10 persons indicated a No answer there were considerably more suggestions made for possible improvements. These are summarized in Table 15.

Table 15. IS INFORMATION IN PHASE DIAGRAMS IN USEFUL FORMAT (15)

1. The 1975 Format is Well Done (6)
2. State Whether Mole or Weight Percent (4)
3. Axes Should Always be Mole % not Wt %
   (Axes Should Always be Wt % not Mole %)
4. More Isothermal Sections (2)
5. Better Cross Referencing
   i.e. Ternary Liquidus to Binary Subsolidus
6. Exotic Formats Should Have Simplified Formats as Well
7. More Use of Descriptive Methods
8. P_{O_2} Assumed to be Air
9. All Diagrams Should be Reviewed for Theoretical Correctness

4.3.3.4 Information in Commentaries (17)

The respondents were asked to check four informational points (purity, accuracy, method and reference) as to their usefulness in the commentaries by using 3 = High value, 2 = Moderate, 1 = Marginal, 0 = No value. No one bothered to indicate zero value although certain portions were often without an entry. Table 16 indicates the number of times each of these points were given a 3 (High value). Purity of starting materials was considered to be the most important single factor to be included.

Table 16. IS IT USEFUL TO HAVE INFORMATION IN COMMENTARIES ON THE FOLLOWING: (17)

High Value:

Purity of Starting Materials - 103 (55%)

Information on Accuracy - 88 (47%)

Description of Method - 85 (46%)

References to Earlier Work - 61 (33%)

4.3.4 Additional Information for Commentaries (18)

Question 18 asked "What additional information, if any, would you suggest be included in the diagrams and/or the commentaries" and gave four blank lines for an answer. Only 43 people (23%) bothered to answer this question, and again, many answers had little bearing on the question. Tables 17 and 18 summarize the answers according to those possibly within the scope of the compilation, and those probably outside the scope of the compilation. In Table 19 four comments are given from answers to question 18 which are well worth considering, if not for inclusion in the commentaries, at least as a starting point for discussion.

Table 17. WHAT ADDITIONAL INFORMATION SHOULD BE INCLUDED? (18)

Return to '69 Format - (1)

Keep '75 Format - (9)

Answers Possibly Within Scope of Compilation

References (with titles) to Earlier Work (5)

Reaction Kinetics (4)

Purity (3)

References to X-Ray Diffraction Data (2)

Accuracy (2)

Stoichiometry

Metastable Phases (2)

Volatilization (2)

Comments on Possible Errors

More Complete Coverage

Table 18. WHAT ADDITIONAL INFORMATION SHOULD BE INCLUDED (18)

Answers Probably Outside Scope of Compilation

- Glass Forming Properties (3)
- Pptical Properties (2)
- Vapor Pressure
- Electrical Resistivity
- Dielectric Constant
- Mechanical Properties
- Free Energy Data
- Electronic Properties
- Viscosity of Liquidus

"Useful Data"

Table 19. WHAT ADDITIONAL INFORMATION SHOULD BE INCLUDED (18)

Noteworthy Comments:

1. Same Information in Same Order for Commentaries
2. A List of What Kind of Optical-Structural-Physical Data are Available in the Source Reference
3. Identify Which Part of Diagram is Theoretical and Which is Experimental
4. Comment on Rate of Volatilization and Attainment of Equilibrium to Indicate Probability of Real System Attaining Equilibrium Phase Composition

4.4 Important Needs for Experimental and/or Theoretical Work (IV)

In section IV of the questionnaire the respondent was asked to comment on "important needs for experimental and/or theoretical work not now being done". It was pointed out that "Compilers are usually also research workers and influence other workers. Your indication of the relative importance of certain research gaps might lead to filling some of these gaps". In general the response was very good. In fact, one respondent eloquently answered, "General increase in information on phase diagrams is needed. This is basic information of lasting value".

Table 20. NEEDS FOR EXPERIMENTAL OR THEORETICAL WORK NOT NOW BEING DONE (IV)

SPECIFIC SYSTEMS FOR WHICH DIAGRAMS ARE NEEDED (19)

TYPES:

- Silicates (9)
- Aluminates (5)
- Zincates (5)
- Rare Earths (4)
- Phosphates (3)
- Zirconates (3)
- Titanates (2)
- Stannates (2)
- Vanadates (2)
- Borates
- Carbides and Nitrides (9)
- Oxynitrides (6)
- Sulfides, Selenides, Tellurides (3)
- Fluorides, Oxyfluorides (3)
- Oxyhydroxides (2)
- Sulfates
- Metal-Oxygen Systems
- Ferrites
- Actinides

APPLICATIONS:

- Glass (7)
- Magnetics (3)
- Refractories (3)
- Steel Making (2)
- Cement
- Abrasives
- Semiconductors
- Ferroelectrics
- Electronics
- Optics

SPECIAL CATEGORIES:

- Ore Minerals
- Low P_{O_2}
- High Pressure Systems
- High Pressure Silicates
- Very Complex Systems (Five or More Components of Mixed Types)
- Oxy-Nitro-Carbides
- Oxide-Carbonate-Sulfates

4.4.1 Specific Systems for Which Diagrams are Needed (19)

Question 19 asked "Are there specific systems for which diagrams are needed and not available?" There were 44 No answers and 90 Yes answers. In describing their Yes answers the respondents were generally quite specific. However, for the purposes of this paper these answers can be summarized (Table 20) either by types of systems, by applications or in special categories. Note that the types of systems include most of those listed in question 10 and the applications cover most of those mentioned in question 8.

4.4.2 Existing Diagrams Which Need Updating or Correction (20)

Question 20 asked "Are there parts of existing diagrams for which more detailed data are needed or which you suspect of being in error?" There were 68 No answers and 42 Yes. The description of the Yes answers are summarized by categories in Table 21. Many of these were silicates, aluminates or zirconates.

Table 21. EXISTING DIAGRAMS WHICH NEED UPDATING OR CORRECTING (20)

No - (68)

Yes - (42)

CATEGORIES:

Silicates (14)	Sulfides
Aluminates (3)	Oxyfluoride
Zirconates (3)	Garnets
Titanates	Non-Stoichiometric Oxides
Chromates	Refractories
Phosphates	Ultra High Temperatures (>1800°C)
Uranates	

- Many Based on Assumed Equilibrium
- Many Determined Accurately Only if Need Arises

4.4.3 Aspects of Phase Equilibria Needed but Inadequately Explored (21)

Question 21 was worded, "Are there aspects of phase equilibria which are needed and generally inadequately explored in most studies? [for example, solid solution below one percent]" There were 61 No answers and 51 Yes. The Yes respondent was asked to "please describe the problem and, if possible, suggest experimental methods for obtaining such data". Fifteen people agreed with the example of solid solution below the one percent level as shown in Table 22, which also lists some other aspects given in the answers. In Table 23 a summary is given of some of the suggested experimental methods which might be used to obtain some of these hard to get data.

Table 22. ASPECTS OF PHASE EQUILIBRIA NEEDED BUT INADEQUATELY EXPLORED (21)

No - 63

Yes - 51

Example Given: Solid Solution Below One Percent (15)

Other Aspects:

- Explore Systems as a Function of P_{O_2} (6)
- Kinetics of Attainment of Equilibrium (5)
- Vapor Pressure (5)
- Immiscibility (Liquid and Solid) (3)
- Application of Phase Diagrams to Metastable or Non-Equilibrium Systems (2)

Table 23. ASPECTS OF PHASE EQUILIBRIA NEEDED BUT INADEQUATELY EXPLORED (21)

Experimental Methods for Obtaining Such Data

- Transmission Electron Microscopy
- Electron Diffraction (High Resolution Lattice Images)
- Vapor Pressure Measurements Across S.S. Region
- High Temperature X-Ray Diffraction in Mixed Gases
- Resistivity vs Temperature
- Scanning Electron Microscope
- Etch Techniques
- Neutron Diffraction
- IR Spectroscopy
- Neutron Activation Analyses

4.4.4 Some Conclusions from the Questionnaire

Several important points are worth summarizing as a result of the analyses of the answers received from this questionnaire. With regard to needed experimental data, there are two areas of experimental research which are apparently badly needed. The first involves the study of various elements and oxides capable of oxidation/reduction under conditions of variable P_{O_2}. There is very little such data available for compilation. Only the simplest systems have so far been studied. The second area needed involves mixed systems containing refractories with slag or melt plus metal. Such mixed ternary or more complex systems are not primarily the classical concern of either ceramists or metallurgists. Consequently very few "academic" studies of such nature have been

published. Probably a large amount of such data has been accumulated by individual industrial laboratories. Such data is generally considered proprietory and is very seldom published.

Regarding the compilation itself, there were several justified complaints which are worth reemphasizing. The first problem mentioned was that the time lag was too great between publication of the data and publication of the compilation. Attempting to supply a commentary for each diagram only increased the time lag. In answer to this criticism, the present technique utilizing guest editors for the commentaries has been established. It is obvious that 12 editors can produce more commentaries than one or two in the same amount of time. It remains to be proven that the system will work, but the coordinating editors presently hope to publish a new up-to-date supplement every three years with the next due in 1978.

The second comment is that the total coverage is not adequate. No matter how the editors try to find all published diagrams they are bound to miss some which were published in obscure journals or reports. Individuals have always been encouraged to submit references which they find have been missed, but this has never amounted to a large percentage. It is proposed that an advertisement for the publications be published several times a year in the trade journal(s) requesting readers to submit missed references from any date preceeding some fixed value. Hopefully this will increase the probability of obtaining responses from the large community of users.

Another problem which will eventually have to be faced by the editors involves commentaries for the diagrams published in the 1964 and 1969 editions. It seems most likely that only the more important systems would require commentaries. The decision as to which diagrams should be republished with commentaries will have to be faced in the near future.

DISCUSSION

F. P. Glasser - The audience should be aware that compilers frequently have difficulties determining in their evaluation, which information is estimated and which is determined. This question often prevents the possibility of a decision. Given the information as it exists in the literature, often the best a compiler can do is to point out the discrepancies to the reader, and let them make up their minds.

R. S. Roth - Dr. Glasser is speaking from experience. You most often cannot tell what was experimental and what was theoretical, and furthermore, that you usually do not question the experimenter's interpretation of his data according to the phase rule until you do experiments on the system yourself.

National Bureau of Standards SP-496, Applications of Phase Diagrams in Metallurgy and Ceramics
Proceedings of Workshop held at NBS, Gaithersburg, Md., January 10-12, 1977

PRESENT STATUS OF PHASE DIAGRAM COMPILATION ACTIVITY FOR SEMICONDUCTORS

by

C. D. Thurmond
Bell Laboratories
Murray Hill, New Jersey 07974

I. INTRODUCTION

There is no single compilation of semiconductor phase diagrams. There are, however, 3 principal compilations among which many of the important semiconductor phase diagrams are included. The phase diagrams compiled are for semiconductors belonging to the diamond-like class all having tetrahedral coordination with 4 valence electrons per atom. These semiconductors have proven to be important both because of their technologically important properties and because those properties have become understood at a fundamental level.

The class of elements and compounds that are tetrahedrally coordinated and average 4 valence electrons per atom is summarized in Table 1. Binary and ternary compounds are included.

In addition to 3 major compilations, certain other compilations will be mentioned. Brief mention will also be given to other semiconductors and some comments about other types of phase diagrams of interest to those in the semiconductor field.

II. PRINCIPAL COMPILATIONS

The most extensive compilation of semiconductor phase diagrams is contained in "Constitution of Binary Alloys," by Hansen, Elliott and Shunk.[1] These phase diagrams are only a small fraction of the total binary temperature-composition diagrams included in this work. Nevertheless, it contains more binary diagrams of semiconductors than any other compilation.

There are 76 diagrams for which 1 component is either Ge or Si. There are 8 diagrams containing a 3-5 compound and 7 containing a 2-6 compound (Table 2).

Panish and Ilegems[2] have critically reviewed a number of 3-5 compound binary and ternary phase diagrams. This includes a number of pseudobinary solid solutions of the types $A^3_xB^3_{1-x}C^5$ and $A^3B^5_xC^5_{1-x}$, i.e., with common "anion" and with common cation. There are 7 binary diagrams, 8 ternaries with common anion and 3 ternaries with common cation (Table 3).

Shay and Wernick[3] have included 26 phase diagrams in their book on "Ternary Chalcopyrites". Most are pseudo-binaries that include the chalcopyrite (Table 4). They include much information on the lattice parameters of the chalcopyrites and their composition dependence in solid solutions.

The level of evaluation of the phase diagrams in the 3 compilations is estimated in Table 5.

III. OTHER COMPILATIONS

Berezhnoi[4] has brought together silicon binary phase diagrams in a book published in Russia in 1958 and published in an English translation in 1960. The convenience of having silicon phase diagrams in 1 volume is offset by the volume now being somewhat out-of-date. The volumes of Hansen, et al.[1] contain. in general, the most up-to-date information on the binary silicon diagrams.

Goryunova[5] has expressly devoted her attention to the diamond-like, tetrahedrally coordinated semiconductors. Discussion of quaternary and higher systems is included. Few phase diagrams are given but there is useful related information and references.

IV. OTHER SEMICONDUCTORS

There are several classes of semiconductors not included among the tetrahedrally coordinated semiconductors described in Table 1 that should be mentioned. The most important of these is the class of 4-6 compounds, A^4B^6, for example, PbSe and the solid solutions formed between them, for example, $Pb_{1-x}Sn_xSe$. These semiconductors have the NaCl structure. A number of 4-6 phase diagrams are included in Hansen, et al.[1] Harman[6] has discussed the phase diagrams of 3 of the more important 4-6 ternary solid solutions.

There are two subclasses of semiconductors not previously mentioned that are usually thought to be members

of the diamond-like, tetrahedrally coordinated class of semiconductors. They are called defect semiconductors and excess semiconductors. The former can be thought of as tetrahedrally coordinated but with some fraction of one kind of site vacant. The semiconductor Ga_2S_3 is an example with 1/3 of its cation sites vacant. The excess semiconductors also have tetrahedral coordination but some fraction of normally vacant sites are occupied.

V. OTHER PHASE DIAGRAMS

The phase diagrams of Hansen, et al.,[1] Panish and Ilegems[2] and Shay and Wenick[3] by and large depict liquid-solid and solid-solid phase equilibria. There are other types of phase diagrams of special usefulness to those interested in semiconductor phase diagrams.

The technological importance of semiconductors arises primarily from the properties given to the semiconductor by donor and acceptor impurities. The maximum amount of impurity that can be added is of special interest. The solidus curves of impurities in Ge and Si have been compiled by Trumbore.[7] In order to display the characteristic low concentrations, a plot of T vs. log C is used. The solidus curve near the semiconductor melting point is of particular importance. It is described in terms of the ratio of the impurity concentration in the solid phase to its concentration in the liquid phase.

This ratio is the distribution coefficient $k = C_s/C_\ell$ and is constant for temperatures in a range near the melting point. Values of k have been included by Trumbore[7] for impurities in Ge and Si. Milnes[8] has compiled distribution coefficients for impurities in Ge and Si as well as for a number of 3-5 compounds.

Another type of phase diagram of particular significance for semiconductors is the Brouwer diagram. The dilute solution concentrations of impurities and defects as functions of temperature, concentration or partial pressure of particular components can be represented with considerable simplicity on log C-1/T or log C_1 vs. log C_2 or log P plots. Brouwer[9] has pointed out that such relationships for each component would be well approximated by a series of connected straight lines the slopes of which gave important information. A number of these diagrams may be found in "The Chemistry of Imperfect Crystals" by Kröger.[10]

An important class of semiconductor phase diagrams not included in Refs. 2 and 3 are the ternary diagrams giving the liquidus and solidus curves for an impurity in a compound semiconductor. As examples, Zn in GaAs and in GaP have received the most attention. Jordan[11] has considered these systems in some detail and gives critically evaluated liquidus and solidus information.

Other phase diagrams not included are the partial pressure-temperature diagrams giving the pressures of components of compound semiconductors for vapor-liquid-solid equilibria. Two examples are the GaAs and the GaP systems discussed by Thurmond.[12] In addition, the P-T diagrams for the pure semiconductor are of interest. Examples can be found in the paper by Jayaraman and Cohen.[13] A last example of phase diagrams not included in the principal compilations cited above is the solid-vapor equilibria of the multicomponent systems used to grow semiconductors from the vapor phase. Examples of such systems may be found in Shaw.[14]

SUMMARY

There is no compilation of phase diagram devoted exclusively to semiconductors. There are 3 compilations containing the most up-to-date information on binary and ternary tetrahedrally coordinated, 4 electrons per atom semiconductors. This is the largest and most important class of semiconductors. Phase diagrams of other semiconductors are mentioned. Some comments are included about other kinds of phase diagrams than the T-X diagram that are used for semiconductors.

REFERENCES

1. M. Hansen, Constitution of Binary Alloys, 2nd Ed., prepared in cooperation with K. Anderko (McGraw Hill), 1958; R. P. Elliott, First Supplement, 1965; F. A. Shunk, Second Supplement, 1969.
2. M. B. Panish and M. Ilegems, Phase Equilibria in Ternary III-V Systems, in Progress in Solid State Chemistry, eds., H. Reiss and J. O. McCaldin (Pergamon Press, New York) 1972, Vol. 7, p. 39-83.
3. J. L. Shay and J. H. Wernick, Ternary Chalcopyrite Semiconductors; Growth, Electronic Properties and Applications, (Pergamon Press, 1975).
4. A. S. Berezhnoi, Silicon and its Binary Systems, (Consultants Bureau, N. Y., 1960); Russian Edition, 1958.
5. N. A. Goryunova, The Chemistry of Diamond-Like Semiconductors, published in English (MIT Press, 1965); first published in Russian, 1963.
6. T. C. Harman, "Control of Imperfection in Crystals of $Pb_{1-x}Sn_xTe$, $Pb_{1-x}Sn_xSe$ and $PbS_{1-x}Se_x$," Physics of IV-VI Compounds and Alloys, (Gordon and Breach, N. Y.), S. Rabii Ed., p. 141, 1974.
7. F. A. Trumbore, "Solid Solubilities of Impurity Elements in Germanium and Silicon," Bell System Technical Journal 39, 205 (1960).

8. A. G. Milnes, Deep Impurities in Semiconductors, (John Wiley and Sons, 1973).

9. G. Brouwer, Philips Res. Rep. 9, 366 (1954).

10. F. A. Kröger, The Chemistry of Imperfect Crystals, Vol. 1, Preparation, Purification, Crystal Growth and Phase Theory, and Vol. 2, Imperfection Chemistry of Crystalline Solids, 2nd revised edition, 1974.

11. A. S. Jordan, "The Solid Solubility Isotherms of Zn in GaP and GaAs," J. Electrochem. Soc. 118, 781 (1971), and "The Liquidus Surfaces of Ternary Systems Involving Compound Semiconductors: Calculation of the Liquidus Isotherms and Component Partial Pressures in the Ga-As-Zn and Ga-P-Zn Systems. Met. Trans., 2, 1965 (1971).

12. C. D. Thurmond, "Phase Equilibria in the GaAs and the GaP Systems, J. Phys. Chem. Solids 26, 785 (1965).

13. A. Jayaraman and L. H. Cohen, "Phase Diagrams," Vol. 1 A. M. Alper Ed.(Academic Press, 1970).

14. D. W. Shaw, "Mechanisms of Vapor Epitaxy in Semiconductors," in Crystal Growth, Vol. 1, pp. 1-48 (1974). C. H. L. Goodman, Ed.,(Plenum Press).

TABLE 1

Tetrahedrally Coordinated Semiconductors
4 Electrons per Atom

Symbol	Example	Structure
A^4	Si	diamond
A^3B^5	GaAs	sphalerite (zincblende), wurtzite
A^2B^6	ZnS	sphalerite (zincblende), wurtzite
$A^2B^4C_2^5$	$ZnSiAs_2$	chalcopyrite, sphalerite, wurtzite
$A^1B^3C_2^6$	$AgGaSe_2$	chalcopyrite, sphalerite, wurtzite

TABLE 2

Number of Semiconductor Phase Diagrams in Hansen, Elliott and Shunk[1]

System	Number
A^4-B^n	76
A^3-B^5	8
A^2-B^6	7

TABLE 3

Number of Phase Diagrams in Panish and Ilegems[2]

Systems	Number
A^3-B^5	7
A^3-B^3-C^5	8
A^3-B^5-C^5	3

TABLE 4

Number of Phase Diagrams in

Shay and Wernick[3]

Systems	Number
A^1-B^3-C^6	14
A^2-B^4-C^5	7
A^2-B^3-C^4-D^5 $(A^2C^4D_2^5+B^3D^5)$	4
A^2-B^2-C^4-D^5 $(A^2C^4D_2^5-B^2C^4D_2^5)$	1

TABLE 5

	Depth of Treatment
Hansen, Elliott and Shunk[1]	2, 3, 4
Panish and Ilegems[2]	4
Shay and Wernick[3]	3, 4

1. Bibliography
2. Annotated Bibliography
3. Unevaluated Phase Diagrams and Bibliography
4. Critical Evaluation

National Bureau of Standards SP-496, Applications of Phase Diagrams in Metallurgy and Ceramics
Proceedings of Workshop held at NBS, Gaithersburg, Md., January 10-12, 1977

Phase Diagram Compilations for Metallic Systems - an Assessment of Ongoing Activities

G. C. Carter
Alloy Data Center
Metallurgy Division
Institute for Materials Research
National Bureau of Standards
Washington, D.C. 20234

Alloy phase diagrams provide a basis for solving many industrial problems. It is, therefore, not surprising to find critical phase diagram data compilation activities generally concentrated in the more industrialized countries. Large compilation projects are being carried out in Germany, France, the USSR, and the UK. Several notable projects are also carried out in other countries. Concise descriptions of all data centers we are aware of are given in Appendix A of this paper.

Historically, too, metallurgy was perfomed by the more culturally developed peoples, at first only creating ornamental objects, starting more than 10,000 years ago, with practical applications following at a much later date (1): Nearly all the industrially useful properties of matter, and shaping material, had their origins in decorative arts, writes Prof. C. S. Smith, the noted metallurgical historian. "The making of ornaments from copper and iron certainly precedes their use in weapons ..." Although metallurgical information was not quantified or documented accurately, a substantial amount must have been known in order to produce the fine artwork created in many cultures. Rather, metallurgical findings and fiction were relayed orally in a rather qualitative manner from master to apprentice.*

An early major quantitative physical property compilation for virtually every alloy known at the time was prepared by Achard in the 18th century in Germany, and is described in a review by C. S. Smith (3). It covered over 900 compositions, some with as many as seven components. Unfortunately, the compilation was written in the language of the Berlin Academy, which was French at that time (i.e. not the language of the German blacksmith), though the Academy's language was changed soon after. Another shortcoming described by Smith was that the compilation was devoid of theoretical speculation, and yet was not in a format attractive to engineers or artisans. It was noted that consequently, as far as could be determined, the compilation was never used. That is, user orientation of the compilation was important then, as much as it is today.

*as, for example, by the Samurai swordsmiths (2), giving the following data: "Heat the steel at final forging until it turns to the color of the moon about to set out on its journey across the heavens on a June or July evening (old calendar)", or, "After the final forging, place the sword in water which has a temperature of water in February or August (old calendar). They believed that water temperature in February or August was the same. Thus, when a swordsmith inscribed the month of manufacture on the sword, he generally used either February or August, regardless of the time of year the sword was actually made". This information, of course, states something semi-quantitatively about an Fe-C based alloy phase diagram, but was not interpreted in that perspective.

In the early 20th century, critical compilations were produced in Germany (this time in German) for binary (4) and "all" (5) phase diagrams, for which complete bibliographies of experimental determinations were collected and subsequently critical evaluations produced. This method of approach has been continued successfully in many smaller compilations up to today. The work by Hansen (6) (published in 1958 in English) was the last successfully produced complete critical compilation of all binary alloys. While two supplements to this volume were feasible (Elliott, 1965; Shunk, 1969) (7), a full re-working of these three volumes plus more recent literature, into a single reference book proved to be impracticable for a single group; the amount of literature to be evaluated has grown to prohibitive proportions.

This problem becomes amplified for ternaries and higher multicomponent alloys. However, methods of preparing critical phase diagram compilations have undergone substantial changes since large products such as the "Hansen" series (6,7) were produced. The reason is that in the past there existed an ample, though not excessive, amount of classical metallurgical data on the one hand, while, on the other hand, theoretical models and computerized methods to obtain phase diagrams from thermodynamic data were not yet adequate. In recent years tremendous progress has been made in this latter approach to phase diagram determination: improved computer facilities and increasingly sophisticated models either integrate existing experimental data with evaluated thermodynamic data, from which equilibrium diagrams can be calculated, or simply use the thermodynamic data to predict equilibrium diagrams. This latter method becomes invaluable for alloys for which classical phase diagram determination experiments are cumbersome, difficult, and lengthy (i.e. expensive), as is often the case for multicomponent alloys utilized in industrial applications. Especially for these alloys, specific groups of phase diagrams only in certain ranges of composition need to be evaluated, and comprehensive phase diagram compilations are not always a desired product for such specific needs. For example, Co-base and Ni-base superalloys tend to exhibit certain hard intermetallic phases precipitating after solidification (8), and data are only needed in those composition ranges in which the superalloys form (e.g. p. 624, Dreshfield).

An excellent review on the general topic of obtaining phase diagram information from thermodynamic data for various applications is given in reference (9). As a result of these computational developments, a large number of small projects are now underway in various countries. Several of these projects collaborate with each other, forming larger groups such as CALPHAD (see Appendix B for a listing of its members).

There are several other international collaborative programs. A prominent one is the Scientific Group of Thermodata Europe (SGTE), a thermochemical data bank, of which THERMODATA (10) represents very active french subgroup. THERMODATA is a bank of critically evaluated data including metallurgical thermodynamics for elements, stoichiometric compounds, alloys and non-stoichiometric phases. European scientific institutions from several countries, highly qualified in thermodynamics, select and critically evaluate the data, and review each other's evaluations before entering the data on an on-line accessible computer data bank.

Another international collaborative program is that organized by the International Atomic Energy Agency, Vienna. The IAEA has coordinated compilation and critical evaluation projects for thermodynamic and phase diagram data for the actinides on an international scale (Oetting et al. general editors), to be published in eleven parts (see under Oetting, Appendix A and C for further details), and a Special Issue series on elements and their alloys and compounds, for elements used heavily in the nuclear industry, with O. Kubaschewski as general editor (see under O. Knacke, and O. Kubaschewski, Appendix A and C for further details).

It is hoped that all compilation and critical evaluation projects for metallic phase diagrams will partake in yet increased international collaborative efforts in order to minimize costly and time consuming duplication of efforts, and to maximize availability of urgently needed reliable phase diagram data, not only for bulk equilibrium phases, but also for other phase diagram needs such as metastable phases, high pressure, small particle, surface phases, etc. Responses to this suggestion have been overwhelmingly favorable, although details of a large-scale collaborative effort must yet be developed.

As a preliminary start to the development of collaboration, a list has been prepared (see Appendix A) of all alloy phase diagram data compilation activities currently underway. This list represents an update to the one given in reference (11). The products of these compilation activities are included in a complete list of phase diagram compilations and handbooks as prepared by the Alloy Data Center (12), with the most recent edition given in Appendix C of this paper.

References

(1) P. Knauth, "The Metalsmith", in "The Emergence of Man" series, Time-Life Books, NY (1974).

(2) J. M. Yumoto, "The Samurai Sword - A Handbook", C. E. Tuttle Co., Rutland, VT., and Tokyo, Japan (1958).

(3) K. F. Achard, "Properties of Alloys" Berlin (1788), described by C. S. Smith, "Four Outstanding Researchers in Metallurgical History", American Society for Testing and Materials, Philadelphia (1963).

(4) M. Hansen, "Der Aufbau der Zweistofflegierungen" Springer-Verlag, Berlin (1936).

(5) E. Jänecke, "Kurzgefasstes Handbuch Aller Legierungen", Verlag von Robert Kiepert, Berlin-Charlottenburg (1940).

(6) M. Hansen and K. Anderko, "Constitution of Binary Alloys", McGraw-Hill, NY (1958).

(7) Supplements to ref (6): R. P. Elliott, Supplement I (1965), and F. A. Shunk, Supplement II (1969), McGraw-Hill, NY.

(8) L. R. Woodyatt, C. T. Sims, and H. J. Beatte, Trans AIME 218, 277 (1960), and W. J. Boesch and J. S. Slaney, Met. Prog. 86, 109 (1964).

(9) T. G. Chart, J. F. Counsell, G. P. Jones, W. Slough, and P. J. Spencer, Review 195 in "International Metallurgical Reviews" 20, 57 (1975).

(10) Y. Deniel, dir., Bibliotheque Universitaire des Sciences, Domaine Universitaire, B.P. 22, F-38402 Saint Martin d'Heres (Grenoble) France.

(11) L. H. Bennett, G. C. Carter, and D. J. Kahan, CODATA Conference, Boulder, Colo., June 1976.

(12) L. H. Bennett, D. J. Kahan, and G. C. Carter, Mat. Sci. and Eng. 24, 1 (1976).

Appendix A

Alloy Phase Diagram Compilation Activities

Prepared by G. C. Carter, D. J. Kahan, and L. H. Bennett

Persons or Centers conducting continuing phase diagram data programs as of January 1977 are listed below. Additional phase diagram calculation groups some of which also compile and critically evaluate phase diagram data are listed under CALPHAD Members, Appendix B. Generally, projects involved in computational techniques without specific compilation outputs are not included in this list. It is a natural activity for research scientists to collect their own data files on their own subjects of specialty. Unless specific efforts in compilation outputs are produced by such scientists, their activities are generally not included in this Appendix.

N. Ageev, President of the Scientific Council, and
O. S. Ivanov et al.
Physical & Chemical Bases of Metallurgal Processes
Academy of Sciences of the USSR
Leninski Prospekt 49
17334 Moscow, USSR

(unevaluated comprehensive data compilation for binary, ternary, and a few higher-order phase diagrams are published approximately annually; cumulative indices available, with the most recent one translated in English, and given in these proceedings by C. M. Scheuermann, TPSII-1; also see paper p. 90; to obtain, see under Mikhailov, VINITI).

I. Ansara and C. Bernard
Laboratoire de Thermodynamique et Physico-Chimie Metallurgiques
associe au CNRS
Institut National Polytechnique
B.P. 44-38401 St. Martin d'Heres
Grenoble, France

(computer prediction of phase equilibria from computer stored critical thermodynamic data; also see paper p. 123).

B. B. Argent
University of Sheffield
Sheffield S10 2TN S. Yorkshire
England

(experimental thermodynamic verification of Fe-based multicomponent systems, as a check on models used in phase diagram calculations).

T. I. Barry
National Physical Laboratory
Teddington, Middlesex, UK

(ceramic and glass pressure/temperature/composition diagrams are evaluated for specific customers).

L. Brewer
Inorganic Materials Research Div.
University of California
Berkeley, CA 94720

(prediction of high-temperature equilibria for binary and higher-order systems, presented in useful, two-dimensional, Brewer projection diagrams; review of all Mo binary alloy phase diagrams in preparation as part of the IAEA series; La alloys, Ac alloys, Fe alloys; surface phases in collaboration with G. A. Somorjai).

G. C. Carter
Alloy Data Center
Metallurgy Division
National Bureau of Standards
Washington, DC 20234

(coordination of phase diagram evaluation projects; evaluation of selected phase diagrams; automated, annotated bibliography of phase diagrams and physical properties; also see paper p. 909).

Y. A. Chang
Materials Department
College of Engineering and Applied Science
University of Wisconsin
Milwaukee, WI 53211

(ternary copper alloy phase diagrams are being critically evaluated see paper MPSI-4).

T. G. Chart
National Physical Lab.
Teddington, Middlesex, England

(bibliography being compiled on phase diagrams of binary and multicomponent systems of technologically important elements; critically evaluated thermochemical computer data file available through L. Kaufman's service (see below); evaluation of diagrams selected for use in prediction of multicomponent systems, currently mainly B-X, Si-X binaries upon which multicomponent superalloys are based; see paper p. 1186).

T. F. Connolly
Research Materials Information Center
Bldg 2,000, Oak Ridge Natl. Laboratory
P.O. Box X
Oak Ridge, TN 37830

(bibliography on all inorganic research materials (~4,000) for preparation of high quality research samples; unevaluated diagrams or abstracts thereof, stored in the systems, to prepare responses to specific queries).

R. Ferro
Instituto di Chimica Generale
University of Genoa
Genoa, Italy

(evaluated crystal structures for the IAEA series; see under O. Knacke, and under F. L. Oetting, below).

K. A. Gschneidner, Jr.
Rare Earth Information Center
Iowa State University
Ames, IA 50010

(the Center maintains a bibliographic file of papers dealing with many aspects of rare earths, including phase equilibria, crystallographic and thermodynamic data of rare earth alloys; reviews of rare earth alloy phase diagrams and other properties are published; see paper p. 226).

R. Hultgren, Prof. Emeritus
Dept. of Metallurgy
Lawrence Radiation Laboratory, Univ. of Calif.
Berkeley, CA 94720

(comprehensive data files of thermodynamic data and critical evaluations up to 1972; a small effort continues towards maintaining the bibliographic files of the center current).

International Atomic Energy Agency

(see under O. Knacke and under F. L. Oetting et al. of this appendix; for more details see Appendix C, under O. Kubaschewski, ed., of the phase diagram data section, and under F. L. Oetting, ed., of the thermodynamic data section).

L. Kaufman
ManLabs, Inc.
21 Erie St.
Cambridge, MA 02139

(computer prediction of phase equilibria from stored thermodynamic data; available to subscribers is an on-line file of critical thermodynamic data from the National Physical Laboratory (U.K.) and ManLabs, together with software for computation of binary and ternary phase diagrams, derived from the component metals Fe, Cr, Ni, Co, Al, Nb, Mo, Ti, C, and W).

K. M. Khanna
Materials Science Department
National Institute of Foundary and Forge Technology
P.O. Box Hatia
Ranchi 834003, India

(new program on phase diagrams of ferromagnetic materials).

Prof. Mats. Hillert
Dept. of Metallurgy, Divsion of Physical Metallurgy
10044 Stockholm 70, Sweden

(phase equilibria for iron-rich alloys)

O. Knacke and O. Kubaschewski
Institut für Theoretische Huttenkunde
Technische Hochschule
Aachen, Germany

(critically evaluated thermodynamic data, from which phase diagrams are deduced (see paper TPSI-13). Among the phase diagram evaluators are O. von Goldbeck; P. Spencer and others. Critical evaluation of Be, Hf, Nb, Pu, Ta, Th, and Zr-base alloy phase diagrams, begun in 1966, have been edited by O. Kubaschewski and published as Special Issues of the "Atomic Energy Review" (Vienna) (also see Appendix C, the phase diagram data section). Evaluations planned are Mo (see under Brewer, above), Hf, and Ta. In this series much of the phase diagram evaluations have been carried out by O. von Goldbeck. R. Ferro of the University of Genoa has contributed evaluations of crystal structures. P. T. Spencer: critical evaluations of mostly transition metal alloys, especially Fe).

D. J. Lam
Argonne National Laboratory
Argonne, IL 60439

(formation and crystal structures of binary and ternary actinide alloys; a publication in "The Actinides: Electronic Structure and Related Properties": II (1974), edited by A. J. Freeman and J. B. Darby, entitled "The Crystal Chemistry of Actinide Compounds").

V. C. Marcotte
IBM East Fishkill Facility
D/45k B/300-95
Hopewell Junction, NY 12533

(small scale compilation for the immediate area of liquid solder-solid metal interactions; file currently in the form of internal IBM reports, literature, and in-house research results).

L. Merrill
High Pressure Data Center
Brigham Young University
Provo, UT 84602

(the Center maintains a bibliographic file of papers dealing with properties of materials under high pressure, including phase transformations in metals; also see paper p. 100).

A. I. Mikhailov, Dir.
Institute for Scientific Information (VINITI)
Academy of Sciences of the USSR
Baltijskaya ul. 14
Moscow, USSR

(products include an Abstracts journal Metallurgy (Referativniy Zhurnal Metallurgiya) a Current Awareness Bulletin Metallurgia, magnetic data tapes starting 1977, "Phase Diagrams of Metallic Systems", editor N. V. Ageev et al., described in Appendix C under Ageev. Outputs are fomatted as bound volumes, microfiche, and, recently, magnetic tapes. Subscriptions to the Ageev series must be applied for, in the several months preceding the year for which the subscription is intended. This and the other VINITI material can be obtained through "Mezhdunarodnaya Kniga", Moscow, USSR, or through Prof. A. I. Mikhailov.

A. P. Miodownik
University of Surrey
Guildford, Surrey, England

(critical evaluation of Fe-Co and Fe-Ni phase diagrams, and reference to work on other Fe-base alloys exhibiting magnetic effects; bibliography on a wider range of alloys; effect of irradiation on phase diagrams; see paper p. 1065).

W. G. Moffatt
Metallurgy and Ceramics Laboratory
General Electric Research and Development Lab.
Schenectady, NY 12301

(compilation of mostly unevaluated binary phase diagrams, intended to complement the Hansen-Elliott-Shunk series, "Constitution of Binary Alloys" and supplements; also see Appendix C under his name).

F. L. Oetting
Div. of Research & Labs.
IAEA, Vienna, Austria

V. Medvedev
Inst. High Temp.
Moscow, USSR

M. H. Rand
Atomic Energy Res. Est.
Harwell, Oxfordshire OX11 ORA, UK

(the International Atomic Energy Agency has initiated an interational program of compilation for the Actinides. The above constitute the Advisory board. Eleven volumes are planned in this series. Further details are described in the thermodynamic data section of Appendix C).

A. D. Pelton and C. W. Bale
Dept de Genie Metallurgique
Ecole Polytechnique
Universite de Montreal
Montreal, Quebec H3C 3A7, Canada

and

W. T. Thompson
Dept. of Met. & Mining Eng.
McGill University
Montreal, Quebec, Canada

(a comprehensive critical computerized thermodynamic data treatment bank is being established; on-line capabilities are available with software packages; one for generalized predominance area diagrams, and one for the calculation of binary and ternary phase diagrams. This software can be applied to stored or user-supplied thermodynamic data; see paper p. 1077).

G. Petzow
Max-Planck-Institut fur Metallforschung
Institut fur Werkstoffwissenschaften
Stuttgart-80, Busnauerstr. 175
Germany

(a phase diagram data center is being established; a monumental compilation of ternary phase diagrams is being planned (see paper p. 164); currently experimental thermodynamic data are determined and CALPHAD-type computerized methods used to determine ternary phase diagrams; see paper p. 955).

A. Prince
Hirst Research Centre
General Electric Co. Ltd.
East Lane, Wembley, Middlesex, HA9 7PP
England

(critical evaluation of phase diagram data on Au-based alloys is in progress; compilation of a bibliography on multicomponent alloy constitution to update the 1956 bibliography by Haughton and Prince is being finalized (see Appendix C).

M. H. Rand
Atomic Energy Research Establishment
Harwell, Oxfordshire OX11 ORA, UK

(critical evaluation of phase diagrams of multicomponent alloys of some transuranic elements, including predictive methods from thermodynamic data. See Appendix C, under O. Kubaschewski, ed., in the phase diagram data section, and under F. L. Oetting, ed. in the thermodynamic data section, for listing of some of the compilations).

G. Raynor
Dept. of Physical Metallurgy and Science of Materials
University of Birmingham
Birmingham, B15 2TT
England

(critical evaluation of ternary and quaternary phase diagram data on Mg-based alloys is to be published shortly in Int. Metals Rev.; similar work for Be alloys may be planned).

R. S. Roth
Inorganic Materials Division
National Bureau of Standards
Washington, DC 20234

("Phase Diagrams for Ceramists" is prepared by this group; though dealing mainly with ceramic systems, some metal-metal-oxygen and metal-metal-sulfur diagrams are included).

E. Rudy
Materials Science Department
Oregon Graduate Center
Beaverton, OR 97705

(evaluated phase diagrams of refractory carbide and boride systems; see Appendix C).

E. M. Savitsky
A. A. Baikov Inst. of Metallurgy
Academy of Sciences of the USSR
Leninski Prospect 49
117334 Moscow USSR

(data compilations on metals and their applications are produced; see various entries of Appendix C).

C. M. Scheuermann
Alloys Branch
NASA Lewis Research Center
Cleveland, OH 44135

(compile binary and higher-order phase diagrams of Fe, Co, or Ni with Al, B, C, Ce, Hf, Mo, N, Nb, O, Re, Si, Ta, Ti, U, W, Y, or Zr; started in 1974; output in loose-leaf format).

S. P. Singhal
College of Engineering
State University of New York
Stonybrook, NY 11794

(critcally evaluated phase diagrams of Au-Pt, Ag-Pt, and some mixed oxide systems exhibiting metal-non metal transitions).

C. Smithells
Butterworths Publishers, Ltd.
London, England

(edits "Metals Reference Book" (5th ed., 1976) containing phase diagrams of many binary and some hydrogen-metal alloys, and a bibliography on ternary, quaternary, and higher-order alloy diagrams).

K. Spear
Materials Research Laboratory
Pennsylvania State University
University Park, PA 16802

(critical compilation of binary B-X diagrams, including predictions from electronic considerations, where experimental data are lacking; also see paper p. 744).

VINITI (see under A. I. Mikhailov)

A. E. Vol
Novocherkaskiy Prospekt Dom 20, Kvartia 31
Leningrad K-272
USSR

(has prepared three volumes of critically evaluated phase diagrams and other physical properties for binary systems. Volumes 4 and 5 are in preparation; see p. 346, and see entries in Appendix C).

R. W. Waterstrat (American Dental Association)
Polymers Division
National Bureau of Standards
Washington, DC 20234

(evaluates binary phase diagrams of Pt-group alloys with V, Cr, Nb and Ta metals, begun in 196?; a chart of certain transition metal combinations to be published).

M. Yukawa
Dept. of Metallurgy
Nagoya University
Nagoya, Japan

(have critically evaluated phase diagram of Cr-Ni to be applied to evaluation of up to quaternary Cr and Ni systems; results will appear in J. Inst. Met. Jap.).

Appendix B

CALPHAD Members: This group (CALculations of PHAse Diagrams) does computer predictions of phase diagrams using thermodynamic data bases. They meet about once a year and are currently producing a journal "CALPHAD", L. Kaufman general editor (see Appendix C for a complete citation).

B. S. Achar; P. O. Research Stn., London, England
I. Ansara; Inst. Nat. Polytechnique, Grenoble, France
C. Bernard; Inst. Nat. Polytechnique, Grenoble, France
T. G. Chart; Nat. Phys. Lab., Teddington, England
J. Counsell; Tech. Hochschule, Aachen, Germany
M. Hillert; Royal Inst. of Technology, Stockholm, Sweden
G. Inden; Max-Planck Inst. für Eisenforschung, Düsseldorf, Germany
L. Kaufman; ManLabs, Inc., Cambridge, MA, USA
G. Kirchner; Metallwerk Berndorf, Berndorf, Austria
O. Kubaschewski; Tech. Hochschule, Aachen, Germany
C. Lupis, Carnegie-Mellon University, Pittsburgh, PA, USA
A. P. Miodownik; University of Surrey, Guilford, England
H. Nesor; ManLabs, Inc., Cambridge, MA, USA
W. Pitsch; Max-Planck Inst. für Eisenforschung, Düsseldorf, Germany
M. Rand; Atomic Energy Agency, AERE Harwell, England
D. Spencer; Tech. Hochschule, Aachen, Germany

Appendix C

Compilations of Phase Diagram and Related Data

Prepared by D. J. Kahan, G. C. Carter, and L. H. Bennett

Alloy Data Center, NBS

(April 1977)

This compilation of existing phase diagram data compilations is prepared to be comprehensive for the subject of alloy phase diagrams only. Any suggested additions to this listing would be gratefully received. At the end of this compilation, a separate list of several thermodynamic t les is given, followed by a list of several crystallographic data compilations and a short list of some textbook treatments, theory and review. One of these latter lists are intended to be complete, nor do they repeat any of the pertinent entries that already appear in the phase diagram compilation list.

References are grouped into four sections: I (Phase Diagram Data Compilations), II (Thermodynamic Data Compilations), III (Crystallographic Data Compilations) and IV (Phase Diagrams - Theory and Review).

Assistance from our colleagues in bringing several compilations to our attention is gratefully acknowledged. Among these contributions are J. H. Westbrook, E. M. Savitskii, and I. Ansara.

I. Phase Diagram Data Compilations

Ageev, N. V., editor

Phase Diagrams of Metallic Systems
(A non-critical, comprehensive compilation of binary and ternary phase diagrams issued annually from Volume 1, for the 1955 literature (published in 1959) through Volume 20, for the 1974 literature (published in 1976); Volumes 21 and 22 in preparation; text in Russian; available from
Prof. A. I. Mikhailov, Director,
125219 Institute for Scientific Information (VINITI)
Academy of Sciences of the U.S.S.R.
Baltijskaya UL, No. 14
Moscow, USSR.
Subscriptions must be applied for in the several months preceding the year for which the subscription is intended.
A cumulative index translated in English is included into these workshop proceedings on p. 1237.

Phase Diagram Data Compilations

Ageev, N. V.
Ivanov, O. S., editors

Phase Diagrams of Metallic Systems, published by "Nauka", Moscow, 1971. Text in Russian.
(Several review papers cover data on a large number of binary and ternary diagrams.)

Ageeva, D. L.
Shvedov, L. V.

Phase Diagrams of Non-Metallic Systems (Oxides and Silicides of Metallic Elements), published by VINITI, Moscow, approximately annually since 1966 (most recent issue = 11, 1976). Text in Russian. Availability as in first entry.
(Phase diagrams for ternary metal-metal-oxygen systems, and for mixed oxide and oxide-silicide systems.)

Alisova, A. P.
Budberg, P. B.

Constitutional Diagrams of Metal Systems, English translation of Vol. 13 (1970) of Ageev's compilation (see above); available from NTIS as document AD 746,792.

American Society for Metals

Aluminum (A 3-volume set edited by K. R. van Horn and published by the American Society for Metals, Metals Park, Ohio, 1967.)
(28 binary, 19 ternary, and 4 quaternary diagrams are collected in an appendix; all are taken from other compendia.)

American Society for Metals

Metals Handbook (8th edition), Vol. 8: Metallography, Structures, and Phase Diagrams, edited by D. T. Hawkins and R. Hultgren (binaries) and by L. Brewer and S.-G. Chang (ternaries) and published by the American Society for Metals, Metals Park, Ohio, 1973.
(Approximately 400 binary and 50 ternary phase diagrams.)

Badaeva, T. A.

The Structure of Thorium Alloys, published by "Nauka", Moscow, 1968. Text in Russian.
(A compilation of phase diagrams, sometimes accompanied by crystallographic, metallographic, or hardness information, for 64 binary and 30 ternary Th alloy systems. A periodic chart on a large fold-out page summarizes the binary alloy diagrams.)

Phase Diagram Data Compilations

Baikov Institute

Diagrams of Ternary Metallic Systems (reference bibliography, 1972), published by the Institute of Metallurgy, Baikov Institute (Moscow), 1972. Text in Russian. (This bibliography covers papers published from 1910 to 1969; references are printed in their source language, mostly English and Russian, and listed by system; systems covered are listed in both Russian and English indexes; no diagrams.)

Battelle Memorial Institute

Cobalt Monograph, Battelle Memorial Institute, Columbus, Ohio, 1960. (Phase diagrams of 18 binary, 19 ternary, and a few higher order Co alloys; all of the binary diagrams are taken from Hansen.)

Berezhnoi, A. S.

Silicon and Its Binary Systems, published in Russian by Academy of Sciences of the Ukrainian SSR, Kiev (1958) and available in English translation from Consultants Bureau, New York, 1960. (Phase diagram and crystallographic structure data are systematically presented for most of the binary silicon alloys.)

Brewer, L.

Metals Handbook. (See under American Society for Metals.)

Brewer, L.

Molybdenum: Physico-Chemical Properties of Its Compounds and Alloys. (See under Kubaschewski.)

Butts, A.
Coxe, C. D.

Silver - Economics, Metallurgy, and Use, (Van Nostrand, New York, 1967) (21 binary and 14 ternary phase diagrams of Ag alloys; most of the binary diagrams have been taken from Hansen.)

Campbell, I. E.
Sherwood, E. M., editors

High-Temperature Materials and Technology (J. Wiley, New York, 1967) (A chapter on carbides includes a discussion of their crystallography and a small compilation of binary and ternary diagrams.)

Phase Diagram Data Compilations

Cannon, J. F.

Behavior of the Elements at High Pressures, an article in J. Phys. Chem. Ref. Data 3, 781, 1974.
(A critical compilation of P-T phase diagrams and crystal structure data for the elements; 431 references to the literature.)

Carlson, O. N.
Stevens, E. R.

A Compilation of Thorium Binary Phase Diagrams (published by Iowa State University as report No. IS-1752, 1968).
(phase relationships are discussed for 60 binary Th alloys; phase diagrams are given for most).

Carter, G. C.
Bennett, L. H.
Kahan, D. J.

Metallic Shifts In NMR, published in "Progress in Materials Science" 20, 1-2350 by Pergamon Press, Elmsford, N.Y. (1977).
(Phase diagrams are included for those binary systems for which critical NMR Knight shift evaluations have been prepared. The ∿ 800 binary diagrams have mostly been taken from the Hansen, Elliott and Shunk compilations (q.v.) and, occassionally, from other compilations, or original papers. Where diagram sections were available from different sources, these are condensed into a single diagram; all diagrams redrawn in a uniform format.)

Centre Nationale de la Recherche Scientifique

Index Thermochimique (Issued monthly since 1964 by the Centre d'Information de Thermodynamique Chimique Minerale, Grenoble.) Text in French.
(Bibliography of thermodynamic papers, including some on phase diagrams.)

Chang, S.-G.

Metals Handbook. (See under American Society for Metals.)

Diehl, J.
Schilling, W.
Schumacher, D., organizing comm.

International Conference on Vacancies and Interstitials in Metals, a 2-volume set of preprints of papers contributed to the conference (Sept. 1968), and available from the central library of the Kernforchgschgsanlage Jülich GmbH, Jülich, Germany. All papers are in English.
(A substantial amount of constitution-related data on vacancies and interstitials in metals is given; more than 900 pages.)

Phase Diagram Data Compilations

Donohue, J.

The Structures of the Elements, published by J. Wiley & Sons, New York (1974).
(Pressure-temperature phase diagrams and allotropic phase changes for elemental solids are compiled; structures and lattice parameters are treated thoroughly. Some 1500 references are cited; 435 pages.)

Efimov, Yu. V.
Baron, V. V.
Savitskii, E. M.

Vanadium and Its Alloys, published by "Nauka", Moscow, 1969. Text in Russian.
(Phase diagrams of binary and ternary V alloy systems are included in this review; the section on phase diagrams is divided into chapters on binary system compilation, ternary system compilation, and a review of crystallography and alloy theory.)

Elliott, R. P.

Constitution of Binary Alloys, First Supplement (McGraw-Hill, New York, 1965)
(Continuation of Hansen's compilation; see under Hansen.)

English, J. J.

Binary and Ternary Phase diagrams of Niobium, Molybdenum, Tantalum, and Tungsten (1961), available from NTIS as document AD 257,739.
(93 binary phase diagrams, and 68 ternary phase diagrams, each with a brief discussion, are included.)

Fromm, E.
Gebhardt, E., editors

Gase und Kohlenstoff in Metallen, published by Springer-Verlag, New York, 1976. Text in German.
(Thermodynamic principles and experimental techniques are reviewed in the first half of the book; the second half presents evaluated data on the thermodynamic properties and phase diagrams, including pressure dependences, of binary metal hydrides, carbides, nitrides and oxides, including extensive bibliographies; limited data are given for ternary compounds, also with bibliographies; 747 pages).

Phase Diagram Data Compilations

Supplement: "Gases and Carbon In Metals" (Fromm, E., Jehn, H. and Horz, G.) published by ZAED (Center for Atomic Energy Documentation Karlsruhe, Germany) as data compilation 5-1 (1976).

Giessen, B. C., editor

Developments in the Structural Chemistry of Alloy Phases, based on AIME Symposium held in 1967 (Published by Plenum Press, New York, 1969). (Several articles review the crystallography, packing, and other properties of metallic phases; one article reviews the occurrence of metastable phases in binary alloys, and presentation of this information.)

Gittus, J. H.

Uranium (A volume in the "Metallurgy of the Rarer Metals" series, Butterworths and Co., London, 1963.)
(More than 40 binary phase diagrams and 5 ternary phase diagrams of U alloys are compiled from various papers and evaluations.)

Gmelin, L., first editor

Gmelins Handbuch der Anorganischen Chemie (many volumes published, starting in 1817), available from Springer-Verlag, New York. Text in German.
(Single elements, or groups of similar elements, are treated in separate volumes; evaluated data include thermodynamic properties of the elements and their compounds and, in some volumes, phase diagrams.)

Gmelin, L., first editor

Gmelins Handbuch der Anorganischen Chemie - Zinn (Tiel D, Legierungen, 1974), available from Springer-Verlag, New York. Text in German.
(Data on a wide spectrum of physical properties, including crystallographic and thermodynamic, are compiled for binary, ternary, and some higher-order Sn alloys; phase diagrams are presented for many alloy systems; references cited throughout the text.)

Phase Diagram Data Compilations

Gmelin, L., first editor	Gmelins Handbuch der Anorganischen Chemie - Zirkonium (1958), available from Springer-Verlag, New York. Text in German. (The compilation of data on the physical, chemical, mechanical, and thermodynamic properties of Zr alloys and compounds occupies a major portion of the book. Phase diagrams and crystallographic information are presented for many binary Zr-metal and Zr-metalloid systems. References cited throughout the text.)
Gschneidner, K. A., Jr.	Rare Earth Alloys (Van Nostrand, New York, 1961). (Contains binary and ternary phase diagrams for some systems containing at least one lanthanide).
Gschneidner, K. A., Jr.	Selected Cerium Phase Diagrams (Published by Iowa State University as report no. IS-RIC-7, 1974.) (An up-to-date compilation of 19 binary phase diagrams, with bibliographies for each system.)
Gschneidner, K. A., Jr.	Inorganic Compounds and Alloys and Intermetallic Compounds, chapters 8 and 9, respectively, in "Scandium, its Occurence, Chemistry, Physics, Metallurgy, Biology and Technology (edited by C. T. Horovitz, et al.); published by Academic Press, New York, 1975. (Thermodynamic properties and phase diagrams are presented for several dozen binary and ternary hydrides, borides, carbides, nitrides, oxides, phosphides, arsenides, sulfides, halides, chalcogenides, and alloys; several hundred references cited).
Guertler, W. Guertler, M. Anastasidias, E.	A Compendium of Constitutional Ternary Diagrams of Metallic Systems; original German published in 1958; English translation (1969) available from NTIS as document TT 69-55069. (A major compilation of ternary systems, containing more than 100 phase diagrams.)
Hansen, M.	Constitution of Binary Alloys (McGraw-Hill, New York, 1958) (This volume, together with its supplements, constitutes one of the major critical data compilations on binary phase diagrams.)

Phase Diagram Data Compilations

Haughton, J. L.
Prince, A., editors

The Constitutional Diagrams of Alloys: A Bibliography (2nd edition), published by the Institute of Metals, London, 1956; a 3rd edition, by A. Prince, (for ternaries only) is nearing completion.
(The bibliography covers the literature (including Soviet work) through the end of 1954, with some 1955 citations included; while the greater portion of the bibliography refers to binary and ternary systems, references are given for alloys with up to 6 components.)

Hawkins, D. T.

Metals Handbook. (See under American Society for Metals.)

Hellwege, K. H. and A. M.

Landolt-Börnstein Tables (See under Landolt-Börnstein.)

Hoffman, W.

Lead and Lead Alloys - Properties and Technology, Springer-Verlag, New York, 1970.
(An extensive treatment of binary and ternary Pb alloys, including mechanical properties, crystallography, and more than 20 binary and more than 20 ternary phase diagrams.)

Hultgren, R.
Desai, P. D.
Hawkins, D. T.
Gleiser, M.
Kelley, K. K.
Wagman, D. D.

Selected Values of the Thermodynamic Properties of the Elements and Binary Alloys (in 2 volumes), (American Society for Metals, Park, Ohio, 1973).
(Evaluated thermodynamic data and phase diagrams, sometimes not found in other compilations, are included for the elements and for many binary alloys.)

Hultgren, R.
Desai, P. D.
Hawkins, D. T.
Gleiser, M.

The Metallurgy of Copper, published by INCRA and NSRDS, 1971; available from International Copper Research Assn., New York.
(Approximately 30 phase diagrams, and crystallographic and evaluated thermodynamic data, are given for Cu binary alloys.)

Hultgren, R.

Metals Handbook (See under American Society for Metals.)

Phase Diagram Data Compilations

Int'l. Atomic Energy Agency	Atomic Energy Review: Special Issues. The physico-chemical properties of metals and their compounds and alloys. (On metals important in nuclear reactor technology; see under the general editor, O. Kubaschewski, for complete listing.)
Int'l. Atomic Energy Agency	An 11-volume series presenting critically evaluated thermodynamic data and estimates where data are unavailable (see under the executive editor, F. L. Oetting, in the following section; Thermodynamic Data Compilations).
Ivanov, O. S.	Physical Chemistry of Alloys and Refractory Compounds of Thorium and Uranium, published in Russian by "Nauka", Moscow, 1968; English translation (1972) available from NTIS as document TT 71-50053 or AEC-TR-7212. (Phase diagrams for some binary Th and binary and ternary U alloys are scattered throughout the text; a bibliography is given for each system.)
Ivanov, O. S. Badaeva, T. A. Sofronova, R. M. Kishenevskii, V. B. Kushnir, N. P.	Phase Diagrams and Phase Transformations of Uranium Alloys, published by "Nauka", Moscow, 1972. Text in Russian. (Phase diagrams of more than 60 binary, more than 90 ternary, and about dozen higher-order uranium alloy systems are collected from the literature. Crystallographic information is frequently given, and a bibliography is included.)
Jänecke, E.	Kurzgefasstes Handbuch Aller Legierungen (Published by R. Kiepert, Berlin-Charlottenburg, 1940.) Text in German. (A systematized treatment of ternary and higher-order alloys is given, including over 800 phase diagrams and 80 tables.)
Jones, H. Suryanarayana, C.	Rapid Quenching from the Melt: An Annotated Bibliography 1958-72, an article in J. Matl. Sci. 8, 705-753, 1973. (This comprehensive bibliography lists several hundred papers on the subject, together with an index by alloy.)

Phase Diagram Data Compilations

Klement, W.

Phase Relations and Structures of Solids at High Pressures (A chapter in "Progress in Solid State Chemistry" 3, 289-376, 1967, edited by H. Reiss.)
(Review of high-pressure phases of the elements and phase diagrams for elements at high pressures.)

Kornilov, I. I.

Physico-Chemical Basis of Heat Resistant Alloys, published by Izdatel'stvo Akad. Nauk, Moscow, 1961. Text in Russian.
(Phase diagram information on systems with up to 7 components is scattered throughout the text.)

Kornilov, I. I.

The Chemistry of Metallides, published in Russian by "Nauka", Moscow, 1964; available in translation (1966) from Consultants Bureau, New York.
(Data on the chemical properties and phase equilibria of metal-metallide compounds are tabulated and reviewed; phase diagrams of many ternary and higher-order systems are shown; 267 references cited.)

Kornilov, I. I.
Matveeva, N. M.

Metallides, published by "Nauka", Moscow, 1971. Text in Russian.
(This collection of review papers includes a considerable amount of phase diagram and crystallographic data, especially for light metal systems.)

Kotel'nikov, R. B.
Bashl'kov, S. N.
Galiakborov, E. G.
Kashtanov, A. I.

Especially High-Melting Elements and Compounds, published by "Metallurgiya", Moscow, 1969. Text in Russian.
(Data on crystallographic, thermodynamic, electron transport, diffusion and other properties of transition elements, their alloys and metalloid intermetallic compounds are summarized; additional data, including phase diagrams for binary and ternary systems, comprises the greater portion of the book.)

Phase Diagram Data Compilations

Kubaschewski, O., editor

Atomic Energy Review: Special Issues, published by the International Atomic Energy Agency and available from UNIPUB, Inc., New York.

Plutonium: Physico-Chemical Properties of its Compounds and Alloys, by M. H. Rand, D. T. Livey, P. Feschotte, H. Nowotny, K. Seifert and R. Ferro; Special Issue No. 1 (1966).
(13 phase diagrams, plus crystallographic data and thermodynamic information, are compiled for binary Pu alloys.)

Niobium: Physico-Chemical Properties of its Compounds and Alloys, by V. I. Lavrentev, Ya. I. Gerassimov, P. Feschotte, D. T. Livey, O. Von Goldbeck, H. Nowotny, K. Seifert, R. Ferro and A. Dragoo; Special Issue No. 2 (1968).
(Phase diagrams, crystallographic data and thermodynamic information are compiled for approximately 20 binary and some ternary Nb alloys.)

Tantalum: Physico-Chemical Properties of its Compounds and Alloys, by Ya. I. Gerassimov, V. I. Lavrentev, O. Von Goldbeck, D. T. Livey, R. Ferro, and A. L. Dragoo; Special Issue No. 3 (1972).
(17 phase diagrams, plus crystallographic data and thermodynamic information, are compiled for binary Ta alloys.)

Beryllium: Physico-Chemical Properties of its Compounds and Alloys, by P. J. Spencer, O. Von Goldbeck, R. Ferro, K. Girgis, and A. L. Dragoo; Special Issue No. 4 (1973).
(16 phase diagrams, plus crystallographic data and thermodynamic information, are compiled for binary Be alloys.)

Kubaschewski, O., editor (continued)

Thorium: Physico-Chemical Properties of its Compounds and Alloys, by M. H. Rand, O. Von Goldbeck, R. Ferro, K. Girgis and A. L. Dragoo; Special Issue No. 5 (1975).
(Phase diagrams, crystallographic data and thermodynamic information are compiled for approximately 50 binary Th alloys.)

Zirconium: Physico-Chemical Properties of its Compounds and Alloys, by C. B. Alcock, K. T. Jacob, S. Zador, O. Von Goldbeck, H. Nowothy, K. Seifert, and O. Kubaschewski; Special Issue No. 6 (1976).
(Review of 65 binary systems, including 46 phase diagrams; chemical, thermodynamic, diffusion and crystallographic data for Zr binary alloys and compounds are compiled.)

Molybdenum: Physico-Chemical Properties of its Compounds and Alloys, by L. Brewer; Special Issue No. 7 (to be published).
Future compilations in this series are planned for Hafnium and Titanium.

Landolt-Börnstein

Landolt-Börnstein Tables - Zahlenwerte und Functionen aus Physik, Chemie, Astronomie, Geophysik und Technik; available from Springer-Verlag, New York.
Relevant data are contained in the following volumes:

I Band 4. Teil: Kristalle, 1955 (in German). (Includes data on crystal structures and lattice parameters of metals, alloys (mainly binary) and intermetallic compounds.)

II Band 2. Teil: Eigenschaften der Materie in Ihren Agregatzustanden.
a) Gleichgewichte Dampt - Kondensat und Osmotische Phänomene, 1960 (in German).
(Includes data on vapor pressures for the metals and some binary alloys, phase diagrams for binary alloys (also as a function of pressure) with information on some of the thermodynamic quantities related to phase transitions.)

b) Lösungsgleichgewichte I, 1962 (in German).
(Thermodynamic properties, such as solubilities of gases in metals and alloys, are given in this volume; also for the liquid phase.)

II Band 3. Teil: Schmelzgleighgewitchte und Grenzflachenerscheinungen, 1959 (in German).
(Includes a section on binary and ternary phase diagrams; lattice constants and discussions are not given.)

Levin, E. M.
Robbins, C. R.
McMurdie, H. F.

Phase Diagrams for Ceramists (1964), first supplement (1969), and second supplement (1975); third supplement envisioned, all published by the American Ceramic Society, Columbus, Ohio 43214.
(Evaluated phase diagrams are given for approximately 5,000 oxide, halide, salt and other ceramic systems, ranging from binaries to systems with six components; literature references cited for each diagram.)

Levinskii, Yu. V.

Phase Diagrams of Metals with Gases, published by "Metallurgiya", Moscow (1975). Text in Russian.
(Metal-gas equilibria as functions of temperature and pressure are reviewed; phase diagrams are given for 23 metal-hydrogen, 7 metal-nitrogen, and 6 metal-oxygen systems; more than 300 references cited.)

Ludwick, M. T.

Indium, published by Indium Corporation of America, Utica, New York, 1959.
(Contains phase diagrams for binary, ternary, and higher order In systems.)

Miller, G. L.

Zirconium (A volume in the "Metallurgy of the Rarer Metals" series, Butterworths & Co., London, 1975.)
(Approximately 30 phase diagrams of Zr alloys are compiled from various papers and evaluations.)

Miller, G. L.

Tantalum and Niobium (A volume in the "Metallurgy of the Rarer Metals" series, Butterworths & Co., London, 1959).
(Approximately 40 phase diagrams of Ta alloys and of Nb alloys are compiled from various papers and evaluations).

Phase Diagram Data Compilations

Moffatt, W. G., editor

Handbook of Binary Phase Diagrams, 1970 and 1972, published in 1976 and available from Business Growth Services, General Electric Co., 1 River Road, Schenectady, NY 12345. (This 2-volume loose-leaf compilation includes phase diagrams for more than 600 binary alloys not contained in or updated from the Hansen-Elliott-Shunk series; no crystallographic data are noted; references cited; includes a permuted alloy index indicating coverage of each system in Hansen, Elliott, Shunk and this compilation; semi-annual updating is projected.)

Molchanov, Y. K.

Atlas of Diagrams of State of Titanium Alloys, Translated from the Russian (1964) and available from NTIS as document AD 670,090 (1967); also available as Phase Diagram of Titanium Alloys, E. K. Molchanova, edited by G. S. Glazunov. (Translated by the Israel Program for Scientific Translations, Jerusalem, 1965.) (Extensive compilation of binary and ternary Ti phase diagrams.)

Mondolfo, L. F.

Metallography of Aluminum Alloys (J. Wiley and Sons, New York, 1943.) (Many binary, ternary and quaternary phase diagrams are given, with references to the original literature.)

Mondolfo, L. F.

Aluminum Alloys: Structure and Properties (Butterworths & Co., Boston and London, 1976.) (A major data compilation on Al metal and its binary and higher order alloys; evaluated phase diagrams, together with some chemical, physical and technological properties are reviewed; more details are presented for pure and commercial Al metal than the alloys. Evaluated phase diagram and crystallographic, mechanical, physical and corrosion behavior for approximately 70 binary Al alloys are given; crystallographic and (sometimes) phase diagram data for several hundred ternary and well-characterized higher order alloys are given; literature references are included throughout the text; a 971 page handbook.)

Phase Diagram Data Compilations

Mueller, W. M.
Blackledge, J. P.
Libowitz, G. G.

Metal Hydrides, published by Academic Press, New York, 1968. (Phase diagrams are presented for many binary and some ternary metal-hydrogen systems. Several pressure-composition isotherms, solubilities and other property data are tabulated throughout the text.)

Newkirk, H.

A Literature Survey of Metallic Ternary and Quaternary Hydrides, available from NTIS as document number UCRL-51244, Revision 1 (1975).
(Several figures of pressure-composition and pressure-temperature relations and some phase diagrams are given.)

Northcott, L.

Molybdenum (A volume in the "Metallurgy of the Rarer Metals" series, Butterworths & Co., London, 1956.)
(Phase diagrams of 13 binary and a few ternary Mo alloys are compiled from various papers and evaluations.)

Pascal, P., editor

Nouveau Traité de Chimie Minérale Vol. 20, in 3 parts; published by Maison & Cie, Paris, 1962-64. Text in French.
(Both binary and ternary phase diagrams are discussed; liberal reference listings; Part I: alloys of alkali, alkaline earth and light metals, and light metal - refractory metal alloys. Part II: alloys of Cu, Ag, Au and precious metal, refractory transition metal, and low melting alloys. Part III: alloys of Co, Fe, Mn, Ni, Th, U and transuranium metal, refractory transition metal and rare earth metal alloys.)

Prince, A.

Constitutional Diagrams of Alloys: Bibliography. (See under Haughton.)

Prokoshkin, D. A.
Vasil'eva, E. V.

Alloys of Niobium, edited by A. M. Samarian; published in Russian by "Nauka", Moscow (1964) and available in translation from the Israel Program for Scientific Translations, Jerusalem, 1965.
(Phase diagrams, crystallography and thermodynamic data are found throughout the book.)

Phase Diagrams Data Compilations

Rajput, B. K.
George, A. M.
Karkhanavala, M. D.

Binary Metal-Oxygen Phase Equilibrium Diagrams and Crystallographic Data, published by the Indian Atomic Energy Commision, Bombay, as document BARC-653 (1972) and available from the Bhabha Atomic Research Centre, Bombay.
(A compilation of phase equilibrium and crystallographic data.)

Raynor, G. V.

Compilation of Mg Alloy Phase Diagrams (not exact title); to be published in Int'l. Met. Rev. (1977).
(A phase diagram compilation of binary, ternary and quaternary Mg alloys.)

Reed, R. P.
Breedis, J. F.

Low-Temperature Phase Transformations, (published by ASTM as STP No. 387 (1966); available from the American Society for Testing Materials, Philadelphia.
(Low-temperature phase transformations are reviewed for alloys, including some ternary and higher-order systems.)

Rough, F. A.
Bauer, A. A.

Constitutional Diagrams of Uranium and Thorium Alloys, prepared at Battelle Memorial Institute and published by Addison-Wesley, Reading, MA (1958).
(Phase diagrams and descriptive text are given, together with crystallographic data for more than 100 binary and 18 ternary systems.)

Rudy, E.

Ternary Phase Equilibria in Transition Metal-Boron-Carbon-Silicon Systems - Part V. Compendium of Phase Diagram Data (originally published as Technical Report AD 689,843, 1969), available from NTIS as document no. AFML-TR-65-2, Part V.
(Phase diagrams and, in most cases, lattice parameters are compiled for over 50 binary, 36 ternary and four quaternary Ta_2C-X-Y alloys; a bibliography is included for each system; 689 pages.)

Samsonov, G. V.

Refractory Compounds, published by "Metallurgizdat", Moscow (1963).
Text in Russian.
(Data for crystallographic, physical, thermodynamic and mechanical properties are compiled; about 60 binary phase diagrams presented; 1100 references.)

Phase Diagram Data Compilations

Samsonov, G. V., editor	Aluminides, published by "Naukova Dumka", Kiev (1965). Text in Russian. (Phase equilibria data are presented for most binary, 69 ternary, 12 quaternary and 4 quintary alloy systems; copy not received by ADC - annotation by J. Westbrook.)
Samsonov, G. V.	Beryllides, published in Russian (1966), English translation available from NTIS as document no. JPRS 43,479 (1967). (Lattice constants are given for metal-beryllium compounds, and some phase diagrams are included.)
Samsonov, G. V.	The Oxide Handbook, published in Russian by "Metallurgiya", Moscow (1969); English translation (1973) available from Plenum Press, New York. (One chapter is devoted to presentation of metal-oxygen phase diagrams.)
Samsonov, G. V.	Nitrides, published by "Naukova Dumka", Kiev (1969). Text in Russian. (Crystallographic and thermodynamic data and many phase diagrams scattered throughout the text; more than 1,100 references.)
Samsonov, G. V., editor	Refractory Carbides, published in Russian by "Naukova Dumka", Kiev (1970); English translation (1974) available from Plenum Press, New York. (Preparation, properties and uses of refractory carbides are reviewed; crystallographic and thermodynamic properties for several (binary) carbides are compiled; phase diagrams of C-Mo-Ti, C-Ta-V, and C-Nb-Re are described.)
Samsonov, G. V.	Magnesides, published by "Naukova Dumka", Kiev (1971). Text in Russian. (A comprehensive review of both binary and ternary systems, including crystallographic data and phase diagrams; more than 1,400 references.)

Phase Diagram Data Compilations

Samsonov, G. V.
Bondarev, V. N.

Germanides, published in Russian by "Metallurgiya", Moscow (1968); English translation (1969) available from Plenum Publishing Corp., New York.
(A comprehensive review of binary and ternary Ge alloys includes data on phase diagrams, crystallographic and thermodynamic properties; nearly 500 references are cited.)

Samsonov, G. V.
Markovskii, L. Ya.
Zhigach. A. F.
Valyashko, M. G.

Boron, Its Compounds and Alloys, published by the Academy of Sciences of the Ukrainian SSR, Kiev (1960) and available, in English translation, in 2 volumes, from NTIS as document no. AEC-TR-5032, Books I and II.
(Constitutional and physical properties of binary, ternary and a few higher-order metal-boron alloys and compounds; phase diagrams and tables of various physical properties are scattered throughout the text; a bibliography cites over 500 references.)

Samsonov, G. V.
Portnoy, K. I.

Alloys Based On High-Melting Compounds, published in Russian by "Oborongiz", Moscow (1961); translation available from NTIS as document no. AD 283,859 (1962).
(Phase diagrams, crystallographic, physical and engineering properties are reviewed for binary alloys of metals with B, C, N or Si and for higher-order systems based on these alloys; binary systems formed between the non-metallic elements are also discussed; more than 316 references cited.)

Samsonov, G. V.
Serebryakova, T. I.
Neronov, V. A.

Borides, published by "Atomizdat", Moscow (1975). Text in Russian.
(Phase diagrams of many binary boron systems and tables summarizing physical and thermodynamic properties for selected boron compounds are scattered throughout the text; a bibliography cites over 1,000 references.)

Samsonov, G. V.
Upadkhaya, G. Sh.
Neronov, V. S.

Physical Metallurgy of Carbides, published by "Naukova Dumka", Kiev (1974). Text in Russian.
(Crystallographic data and many binary and ternary phase diagrams are scattered throughout the text.)

Phase Diagram Data Compilations

Savitskii, E. M., editor

Phase Diagrams of Metallic Systems, published by "Nauka", Moscow (1968). Text in Russian.
(Phase diagram and crystallographic data are reviewed for binary and ternary systems between IVA, VA and VIA group metals; systems based on these metals, but including an element from elsewhere in the periodic table, are presented, also.)

Savitskii, E. M.
Baron, V. V.
Efimov, Yu. V.
Bychkova, M. I.
Myzenkova, L. F.

Superconducting Materials, published in Russian by "Nauka", Moscow (1969); English translation (1973) available from Plenum Press, New York.
(Phase diagrams and cystallographic data for binary and ternary alloys showing superconducting behavior are reviewed in a chapter; 309 references.)

Savitskii, E. M.
Burkhanov, G. S.

Physical Metallurgy of Refractory Metals and Alloys, published by "Nauka", Moscow (1967); English translation (1970) available from Plenum Press, New York.
(Phase diagrams, crystallographic, some thermodynamic and other physical property data are given; most of the phase diagram data are found in Chapters II and III, largely for binary diagrams, some ternary diagrams and a quaternary Mo-Nb-W-Zr diagram; bibliographies follow each chapter. 287 pages.)

Savitskii, E. M.
Polyakova, V. P.
Tylkina, M. A.

Palladium Alloys (1967), translated from the Russian and published by Primary Sources, New York, 1969.
(Most of this book is devoted to a review of Pd metal and its binary and ternary alloys; assorted mechanical and physical property data are also given for many systems.)

Savitskii, E. M.
Polyakova, V. P.
Gorina, N. B.
Roshan, N. R.

Physical Metallurgy of the Platinum Metals, published by "Metallurgiya", Moscow (1975). Text in Russian; English translation to be published by "MIR", Moscow (1977).
(Several Pt metal phase diagrams are collected in one section of the book.)

Phase Diagram Data Compilations

Savitskii, E. M.
Terekhova, V. F.
Burov, I. V.
Markov, I. A.
Naumkin, O. P.

Rare Earth Alloys, published in Russian by the Academcy of Sciences of the USSR, Moscow (1962); English translation available from NTIS as document AEC-TR-6151.
(Binary and ternary phase diagrams of alloys containing a rare earth component are reviewed; tables of physical, chemical and mechanical property data are given; extensive bibliographies follow each chapter.)

Savitskii, E. M.
Tylkina, M. A.
Povarova, K. B.

Rhenium Alloys, published in Russian by "Nauka", Moscow (1965); English translation available from NTIS as document no. 69-55081.
(26 binary and 15 ternary Re phase diagrams are compiled, together with a general discussion of the Re diagrams.)

Schwartzkopf, P.

Refractory Hard Metals; Borides, Carbides, Nitrides, (and) Silicides, (Macmillan, New York, 1953).
(Phase diagram and crystallographic information is given for some of these materials.)

Selle, J.

Summary of Binary Phase Diagrams, prepared at the Mound Laboratory of Monsanto Research Corporation (1970).
(This large color wall chart shows the degree of solubility, number of intermetallic compounds, number of eutectics and other information for binary alloys.)

Shunk, F. A.

Constitution of Binary Alloys, Second Supplement (McGraw-Hill, New York, 1969)
(Continuation of Hansen's compilation; see under Hansen.)

Shunk, F. A.

Constitution of Alloys, a series of IIT reports (May 1972) updating sections of the Hansen series: Vols. 1A (systems Ac-H through Ag-Zr), 1B (Al-Am through Ar-U), 1C (As-Au through Au-Zr) and 2 (miscellaneous systems from B-Hg through Ge-Re); available from the Illinois Institute of Technology, Chicago.

Phase Diagram Data Compilations

Smithellas, C. J., editor
Brandes, E. A. asst. ed.

Metals Reference Book (5th edition, Butterworths & Co., Boston and London, 1976.)
(This summary of various data on alloys includes more than 300 binary phase diagrams (with literature references), bibliographies on more than 500 ternary and more than 50 quaternary alloy systems, and data on the solubility of gases in metals.)

Sōmiya, S.

Zirconia Bearing Refractories, published in "Kogyo Zairyo no Shinpo" (Progress of Engineering Materials): pages 201-234 (1964). Text in Japanese.
(23 phase diagrams, and 7 liquidus curves for binary and/or pseudo-binary systems and 29 phase diagrams and phase relation figures for ternary systems of zirconia or zircon are described.)

Sōmiya, S.
Hashimoto, K.-I.

Glossary for the Phase Diagrams, published in "Seramikkus" (Ceramics Japan) 2 (10), 817-827 (1967). Text in Japanese.

Smith, J. F.
Carlson, O. N.
Peterson, D. T.
Scott, T. E.

Thorium: Preparation and Properties (Iowa State University Press, Ames, Iowa, 1975.)
(Phase diagrams, crystallography and thermodynamics of several binary Th alloys are given in one of chapters.)

Sōmiya, S. editor

Application of Phase Diagrams in Refractories, published by the Ceramic Society of Japan (1968). Text in Japanese.
(A 119-page textbook.)

Spedding, F. H.
Daane, A. H.

The Rare Earths, published in 1961; reprinted in 1971 by R. E. Krieger Publishing Co., Huntington, N. Y.
(Phase diagrams of nearly 100 binary rare earth-metal alloys are presented; many are taken from Hansen.)

Phase Diagram Data Compilations

Spear, K. E.

Phase Behavior and Related Properties of Rare-Earth Borides, a chapter in "Phase Diagrams: Materials Science and Technology": IV, 91-159, 1976 (A. M. Alper, editor); published by Academic Press, New York.
(Evaluated binary phase diagrams, including predictions from electronic considerations, where experimental data are lacking, are presented for Sc, Y and all of the lanthanide-boron systems; crystal chemistry and electronic structure are reviewed; approximately 150 references cited.)

Staudhammer, K. P.
Murr, L. E.

Atlas of Binary Alloys (Marcel Dekker, New York, 1973)
(This book presents periodic tables of the elements, giving the characteristics of binary phase diagrams between each element in turn and all the other elements (e.g., Co with each of the other elements); information is given on degree of solubility, number of compounds, temperatures of lowest melting eutectic or peritectic and number of eutectics or peritectics; no diagrams are given.)

Storms, E. K.

The Refractory Carbides (Academic Press, New York, 1967)
(Phase diagrams, crystallography and thermodynamic properties, among others, are described for several refractory metal-carbon systems.)

Sully, A. H.

Manganese (A volume in the "Metallurgy of the Rarer Metals" series, Butterworths & Co., London, 1955.)
(Phase diagrams of approximately 30 binary and a few ternary Mn alloys are compiled from various papers and evaluations.)

Sully, A. H.
Brandes, E. A.

Chromium (A volume in the "Metallurgy of the Rarer Metals" series, 2nd edition, Plenum Press, New York, 1967.)
(Phase diagrams of 24 binary and 5 ternary Cr alloys are compiled from various papers and evaluations.)

Phase Diagram Data Compilations

Tananaev, I. V., editor	Physico-Chemistry of Rare Metals, published in Russian by "Nauka", Moscow (1972); English translation (1974) available from NTIS as document TT 73-58025 or AEC-TR-7409. (Review chapters on the theory and application of metals and alloys have been contributed by different authors; electrical, thermodynamic and other properties are treated; one chapter is devoted to computer prediction of phase diagrams. Phase data are scattered throughout the text of 324 pages. This collection is in dedication to E. M. Savitskii, and represents the subjects in physico-chemistry and physical metallurgy he has investigated throughout his career.)
Terekhova, V. F. Savitskii, E. M.	Yttrium - Properties, Phase Diagrams, Industrial Applications, published in Russian by "Nauka", Moscow (1967); English translation available from NTIS as document no. AEC-TR-6980 (1970). (Phase diagrams, crystallographic, physical and mechanical property data are compiled for many binary and a few ternary Y alloys. Elemental Y metal is treated in great detail; 280 literature references cited.)
Thoma, R. E., editor	Phase Diagrams of Nuclear Reactor Materials, available from NTIS as ORNL report 2548 (15th edition, 1959.) (Phase diagram compilation giving Zr-rich binary diagrams with Ag, In, Sb and Pb as minority component, five alkali-metal-halide systems, and many non-metallic binary and multicomponent diagrams.)
Toth, L. E.	Transitional Metal Carbides and Nitrides (Academic Press, New York, 1971.) (One chapter is devoted to phase diagrams; other chapters include crystallography, thermodynamic and other physical and engineering properties.)

Valignat, N.

Bibliographie Nb 2. Diagrammes de Phases et Structure des Systemes a base de Niobium, published by the Laboratorie de Thermodynamique et Physico-Chimie Metallurgiques de Grenoble, 1970. Text in French.
(This bibliography lists references to work on phase diagrams and crystallography in a large number of binary and ternary Nb alloys.)

van Horn, K. R.

Aluminum (See under American Society for Metals.)

Vines, R. F.

The Platinum Metals and Their Alloys (Edited by E. M. Wise; published by the Intl. Nickel Co., New York, 1941.)
(Phase diagrams for a few of these alloys are given.)

Vol, A. E.

Handbook of Binary Metallic Systems - Structures and Properties, Vol. 1 (1959) and Vol. 2 (1962), available in English translation from NTIS as documents TT-66 51149 and TT-66 51150 (1966), respectively; Vol. 3 (co-authored with I. E. Kagan) published by "Nauka", Moscow (1976), translation requested by the ADC; Volumes 4 and 5 in preparation.
(A major compilation of phase diagrams and data on physical, mechanical and chemical properties of binary alloys; Vol. 1: alloys of Ac, Al, Am, B, Ba, Be and N. Vol. 2: alloys of Bi, Dy, Eu, Fe, Ga, Gd, Ge, H, Hf, Ho, V and W. Vol. 3: alloys of Au, In, Ir, Y and Yb. Vol. 4: alloys of Ca, Cd and K. Vol. 5: alloys of Co, O and Si.)

Vol'skii, A. N.
Sterlin, Y. M.

The Metallurgy of Plutonium, published in Russian by "Nauka", Moscow (1967) and available in English translation from NTIS as document no. TT-70-500004.
(Pu binary and ternary alloy phase diagrams are compiled in this book.)

Wang, F. E.

Superconducting Critical Temperature, T_c, and Phase Equilibrium Diagram of A_3B (β-W) Type Compounds, an article in J. Phys. Chem. Sol. 35, 273-278, 1974.

Phase Diagram Data Compilations

(Phase diagrams (copied from the Hansen series) are presented for 23 systems in which a superconducting A_3B type compound is formed; superconducting transition temperatures are correlated with the solid solubility ranges of the A_3B compounds.)

Zhavoronkov, N. M., editor

Chemistry of Metallurgical Alloys, published by "Nauka", Moscow (1973). Text in Russian.
(Phase diagrams, crystallography and data on physical properties of binary and ternary systems are reviewed in several chapters.)

II. Thermodynamic Data Compilations

Bayanov, A. P.

Thermodynamics of the Interaction of the Lanthanides With Other Elements, an article in Russ. Chem. Rev.: 44, #2, 122, 1975.
(Thermodynamic characteristics (Gibbs free energies, enthalpies and entropies) for the interaction of the lanthanides with various elements to form hydrides, borides, carbides, silicides, pnictides, halides, chalcogenides and intermetallic compounds are reviewed.)

Blank, H.
Lindner, R., editors

Plutonium 1975 and other Actinides, Proceedings of the 5th International Conference on Plutonium and other Actinides 1975; published by North-Holland (1976) and available from American Elsevier, New York.
(Papers are presented on thermodynamic and other physical properties; many contributions relate to phase equilibria, though few phase diagrams are presented; nearly 1,000 pages.)

Brewer, L.

The Cohesive Energies of the Elements, published by Lawrence Berkeley Laboratory of the University of California at Berkeley as report LBL-3720 (1975).
(A tabulation of heats of atomization for the elements, extending the earlier work of Hultgren, et al., "Selected Values of the Thermodynamic Properties of the Elements", 1973.)

Eklund, S., editor

Thermodynamics of Nuclear Materials (Proceedings of a Symposium sponsored by the International Atomic Energy Agency in Vienna, 1962 and available from UNIPUB, Inc., New York.)
(Contributed papers on theory and experimental results on thermodynamic properties and phase diagrams of actinide metals and alloys; papers often include binary or multicomponent phase diagrams; especially to be noted is a paper by E. Rudy giving 19 ternary diagrams.)

Elliott, R. P.

Alloying Characteristics of the Rare Earth Elements with the Transition Elements (see in Crystallographic Data Compilations list).

Thermodynamic Data Compilations

Gluchko, V. P.	Thermodynamic Constants of Matter, Vol. VII (for Mn, Tc, Re, Cr, Mo, W, V, Nb, Ta, Ti, Zr and Hf metals and their compounds), published by the Academy of Science of the USSR, VINITI, Moscow (1974). (Data are tabulated for enthalpies and free energies of formation, room temperature entropies and specific heats and enthalpies and entropies of phase transformations and the temperatures and pressures at which the transformations occur; bibliography not included.)
Gschneidner, K. A., Jr. Kippenhan, N.	Thermochemistry of the Rare Earth Carbides, Nitrides and Sulfides for Steelmaking (published by Iowa State University as report no. IS-RIC-5, 1971.) (Heats of formation and free energies for selected rare earth compounds are compiled, in both tabular form (up to 2500 °K) and graphical form (up to 4000 °K); data sources are given in bibliography of 65 references.)
Gschneidner, K. A., Jr. Kippenhan, N. McMasters, O. D.	Thermochemistry of the Rare Earths: Part 1 (rare earth oxides), Part 2 (rare earth oxysulfides) and Part 3 (rare earth compounds with B, Sn, Pb, P, As, Sb, Bi, Cu and Ag), (published by Iowa State University as report no. IS-RIC-6, 1973.) (This report continues report no. IS-RIC-5 (1971) by Gschneidner and Kippenhan (see previous entry); heats of formation and free energies for many rare earth compounds are given in both tabular form (up to 2000-2700 °K) and graphical form (up to 4000 °K); a bibliography cites almost 100 references.)
Gschneidner, K. A., Jr.	Thermodynamic Stability and Physical Properties of Metallic Sulfides and Oxysulfides, a chapter in "Sulfide Inclusions in Steel" (edited by J. J. DeBarbadillo and E. Shape); published by the American Society for Metals, Metals Park, Ohio, 1975.

Thermodynamic Data Compilations

Kelly, K. K.

Contributions to the Data on Theoretical Metallurgy, bulletins compiled by the U. S. Bureau of Mines; available from the Government Printing Office, Washington, D. C.
Bulletin No. 542, Part XII: "Chemical Thermodynamics."

Bulletin No. 584, Part XIII: "High Temperature Heat Capacity, Heat Content, and Entropy. Data for the Elements and Inorganic Compounds", 1960 (232 pages). (Supersedes Bulletin No. 476.)

Bulletin No. 584, Part XIV: "Entropies of the Elements and Inorganic Compounds", by K. K. Kelly and E. G. King, 1961 (149 pages). (Supersedes Bulletin No. 477.)

Koslapova, T. Y.

Carbides, translated from the Russian and published by Plenum Press, New York, 1971.
(Phase relationships, crystallography, thermodynamic properties and other properties are compiled for many carbides.)

Kubaschewski, O.
Catterall, J. A.

Thermochemical Data of Alloys (Pergamon Press, New York, 1956.)
(Thermochemical data on 342 binary and 133 ternary alloy systems are given, including references to the original literature.)

Kubaschewski, O.
Alcock, C. B.

Metallurgical Thermochemistry (5th edition, published by Pergamon Press, New York, 1977.)
(Extensive tables of thermochemical data are included in this textbook.)

Landolt-Börnstein

Landolt-Börnstein Tables - Zahlenwerte und Functionen aus Physik, Chemie, Astronomie Geophysik und Technik, available from Springer-Verlag, New York.
II Band 4. Teil: Kalorische Zustandgrossen, 1961 (in German).
(Includes specific heats, entropies, enthalpies, free energies, and also some heats of mixing for alloys.)

Thermodynamic Data Compilations

Müller, W. Blank, H., editors	Heavy Element Properties, Proceedings of the Joint Sessions of the 4th International Transplutonium Element Symposium and the 5th International Conference on Plutonium and other Actinides 1975; published by North-Holland (1976) and available from American Elsevier, New York. (Nuclear, electronic, chemical and thermodynamic properties of the actinide and transplutonium metals and their alloys are reviewed; many data relating to alloy phase stability are presented, though phase diagrams, themselves, are not shown; 125 pages.)
Müller, W. Lindner, R., editors	Transplutonium 1975, Proceedings of the 4th International Transplutonium Element Symposium (1975); published by North-Holland (1976) and available from American Elsevier, New York. (Papers are presented on nuclear, chemical and physical properties of the transplutonium elements; many contributions relate to thermodynamics of the elements and their compounds; no phase diagrams are presented; nearly 500 pages.)
Oetting, F. L.	The Chemical Thermodynamic Properties of Plutonium Compounds, an article in Chem. Revs. 67, 261-297, 1967. (An evaluation of data for hydrides, carbides, nitrides, oxides, sulfides, sulfates, halides and oxyhalides.)
Oetting, F. L., executive editor Medvedev, V. Rand, M. H. Westrum, E. F., Jr., editors	The Chemical Thermodynamics of Actinide Elements and Compounds, published by the International Atomic Energy Agency and available from UNIPUB, Inc., New York. Volumes within the scope of this compilation are listed below: Part 1. The Actinide Elements (1976), by F. L. Oetting, M. H. Rand and R. J. Ackermann, Part 3. Miscellaneous Actinide Materials, by E. H. P. Cordfunke and P. A. G. O'Hare,

Part 4. The Actinide Carbides, by C. E. Holley, M. H. Rand and E. K. Storms,

Part 5. The Actinide Pnictides, by K. C. Mills, P. E. Potter and Y. Takahashi,

Part 6. The Actinide Chalcogenides, by J. Drowart, F. Grønvold and E. F. Westrum, Jr.,

Part 7. The Actinide Hydrides, by H. E. Flotow and S. Yamaguchi,

Part 8. The Actinide Alloys, by V. V. Akhachinskij, I. Ansara, P. Chiotti and M. H. Rand,

Part 9. Selected Ternary Systems, by H. Holleck, P. E. Potter and K. E. Spear,

Part 11. The Actinide Oxides, by R. J. Ackermann, F. Grønvold, F. L. Oetting, A. Pattoret and M. H. Rand.

Rand, M. H.
Kubaschewski, O.

The Thermochemical Properties of Uranium Compounds, published by Interscience, New York, 1963.
(Thermochemical data are compiled for alloys, hydrides, carbides, oxides, sulfides, halides and uranyl compounds; phase diagrams almost totally absent.)

Reed, T. B.

Free Energy of Formation of Binary Compounds: An Atlas of Charts for High - Temperature Chemical Calculations, published by the MIT Press, Cambridge, MA, 1974.
(Free energies of formation and enthalpy and entropy changes on formation of binary compounds are compiled for metallic hydrides, nitrides, oxides, sulfides, selenides, telurides and halides; data are compiled in both tabular and graphical form; plastic overlays are provided to enable the reader to determine the composition of reacting gases, equilibrium constants, EMF and other thermodynamic quantities directly from the data graphs; data are also

compiled for the free energies of ionization of some elements and changes in free energy, enthalpy and entropy of the elements upon condensation. Sources and accuracy of the data are noted in appendices; 35 references cited.)

Stull, D. R.
Prophet, H.

JANAF Thermochemical Tables, 2nd edition, 1971, published as NSRDS-NBS 37 and available from the Government Printing Office, Washington, D. C.; 1974 and 1975 Supplements, edited by M. W. Chase, et al., published in J. Phys. Chem. Ref. Data 3, 311-480, 1974 and 4, 1-175, 1975, respectively; reprints available from the American Chemical Society, Washington, D. C. (Thermodynamic data, including heat capacities, enthalpies and entropies, are tabulated mainly for compounds, but also for some metals.)

Teatum, E. T.
Gschneidner, K. A., Jr.

Compilation of Calculated Data Useful in Predicting Metallurgical Behavior of the Elements in Binary Alloy Systems, available from NTIS as document no. LA-4003 (1968); supersedes LA-2345.
(Radii for coordination number 12, atomic volumes, heats of sublimation, electronegativities, melting points and solubility parameters for the elements are tabulated; radius ratios, energy ratios, Mott numbers, Hildebrand factors and electronegativity differences are tabulated for elements as impurities in elemental hosts; 39 references to the literature.)

Voitovich, R. F.

Refractory Compounds (Thermodynamic Characteristics), published by "Naukova Dumka", Kiev (1971). Text in Russian.
(Graphical and tabular presentations of the temperature dependences of various thermodynamic quantities.)

Wagman, D. D.
Evans, W. H.
Parker, V. B.
Halow, I.
Bailey, S. M.
Schumm, R. H.

Selected Values of Chemical Thermodynamic Properties (NBS Tech Note 270, sections 3 (Jan. 1968) through 7 (Apr. 1973), sections 1 and 2 superseded; available from NTIS.
(Evaluated thermodynamic data for the elements.)

Thermodynamic Data Compilations

Wagner, C.

Thermodynamics of Alloys (Addison-Wesley, New York, 1952).
(Thermodynamic properties are given for some alloys in a chapter of this book.)

Weibke, F.
Kubaschewski, O.

Thermochemistry of Alloys (Thermochemie der Legierungen), published by Springer-Verlag, Berlin, 1943. Text in German.
(Review of experimental and theoretical treatment of the subject; critical compilation of thermochemical properties and often phase diagrams for some 250 binary alloy systems.)

Westrum, E. F.

Bulletin of Thermodynamics and Thermochemistry (Prepared under the auspices of IUPAC and published at the University of Michigan, Ann Arbor.)
(A monthly index to publications on metallic materials, among others.)

Wicks, C. E.
Block, F. E.

Thermodynamic Properties of 65 Elements - Their Oxides, Halides, Carbides, and Nitrides, available from the Government Printing Office, Washington, D.C. as Bureau of Mines Bulletin 605 (1963).
(A data book giving specific heats, enthalpies, entropies, free energies and other thermodynamic functions for about 50 metals and their compounds; 141 references cited.)

III. Crystallographic Data Compilations

Aronsson, B.
Lundstrom, T.
Rundqvist, S.

Borides, Silicides, and Phosphides, (J. Wiley, New York, 1965.)
(Crystallography discussed in general terms; no phase diagrams.)

Donnay, J. D. H.
Ondik, H. M., general editors

Crystal Data - Determinative Tables, 3rd edition, published in 2 volumes: Vol. 1 (Organic Compounds, 1972) and Vol. 2 (Inorganic Compounds, 1973); available from the Joint Committee on Powder Diffraction Standards, 1601 Park Lane, Swarthmore, PA 19081.

Donnay, J. D. H.
Ondik, H. M., general editors

Crystal Data - Determinative Tables, 3rd edition, published in 2 volumes: vol. 1 (Organic Compounds, 1972) and vol. 2 (Inorganic Compounds, 1973); available from the Joint Committee on Powder Diffraction Standards, 1601 Park Lane, Swarthmore, Pa. 19081.
(This major compilation includes crystallographic data for metals and intermetallic compounds; references are given to the original literature).

Elliott, R. P.

Alloying Characteristics of the Rare Earth Elements with the Transition Elements, published by the Illinois Institute of Technology Research Institute as report no. IITRI-578P19-13 (1964).
(The influence of electronic structure on the crystallography of intermetallic phases is reviewed, new data for several binary and ternary phases (including the variation of crystal structure and lattice parameters along pseudo-binary sections of ternary phase diagrams) are reported.)

Goldschmidt, H. J.

Interstitial Alloys (Plenum Press, New York, 1967).
(Includes extensive reviews of phase diagrams and crystallography of hydrides, borides, carbides, nitrides, oxides, and silicides, including some ternary systems).

Kornilov, I. I.
Matveeva, N. M.
Pryakhina, L. I.
Polyakova, R. S.

Metallochemical Properties of the Elements of the Periodic Table, published by "Nauka", Moscow (1966). Text in Russian.
(Atomic and physical properties of the metallic elements are summarized; limits of solid solubility and crystal prototypes of binary intermetallic phases are tabulated, though no phase diagrams are presented.)

III. Crystallographic Data Compilations

Lam, D. J.
Darby, J. B., Jr.
Nevitt, M. V.

The Crystal Chemistry of Actinide Compounds, a chapter in "the Actinides: Electronic Structure and Related Properties," edited by A. J. Freeman and J. B. Darby, Jr. II, 119-184, 1974.
(Crystal structure data, lattice parameters, symmetries and atomic positions are compiled for actinide intermetallic compounds; about 80 references cited.)

Landolt-Börnstein

Landolt-Börnstein Tables - Zahlenwerte und Functionen aus Physik, Chemie, Astronomie, Geophysik und Technik; available from Springer-Verlag, New York.
Selected Data of Elements and Intermetallic Phases, New Series, Group III, Vol. 6, 1971.
(Tabular compilation of evaluated data on space groups, lattice constants, and (sometimes) magnetic transition temperatures.)

McMasters, O. D.
Gschneidner, K. A., Jr.

Rare Earth Intermetallic Compounds, a chapter in the Proceedings of the International Symposium on Compounds of Interest in Nuclear Reactor Technology, 1964 (J. T. Waber, P. Chiotti and W. N. Miner, editors); published by the AIME as Nuclear Metallurgy 10, 93-158, 1964.
(Crystallographic data for rare earth intermetallic compounds are reviewed and tabulated; 164 references cited.)

Pearson, W. B.

Handbook of Lattice Spacings and Structures of Metals: Vol. I (1958) and Vol. II (1967); published by Pergamon Press, New York.
(Critical evaluation of space groups and lattice parameters for metals, alloys and intermetallic compounds.)

Pearson, W. B.

The Crystal Chemistry and Physics of Metals and Alloys (J. Wiley, New York, 1972)
(600 types of metallic structures are described and their crystal chemistry is discussed.)

Schubert, K.

Kristallstrukturen Zweikomoponentiger Phasen, published by Springer-Verlag, New York, 1964.
Text in German.
(Includes tables of lattice parameters for intermetallic compounds and binary compounds between a metal and a non-metal.)

IV. Phase Diagrams - Theory and Review

Alper, A. M., editor	Phase Diagrams: Materials Science and Technology, (Academic Press, New York) (This series is directed towards reviews of phase diagrams as applied to specific practical areas, such as solidification, joining and extractive metallurgy, as well as some more basic considerations. Some reviews of special interest in this list are entered separately; volumes published from 1970 to 1976.)
American Society for Metals	Theory of Alloy Phases, proceedings of a seminar (1955); published by the American Society for Metals, Metals Park, Ohio, 1956. (A collection of contributed papers on the electronic structure of metals and alloys and its relation to crystallography and phase stability.)
Bokii, G. B.	Introduction to Crystal Chemistry, published by Moscow University, 1954. Text in Russian. (Alloy crystallography and phase diagrams are reviewed.)
Brewer, L.	Prediction of High Temperature Metallic Phase Diagrams (proceedings of the Second Berkeley International Materials Conference, edited by V. F. Zackay, 1964), pgs. 12 - 103 (J. Wiley, New York, 1965).
Cahn, R. W., editor	Physical Metallurgy, North-Holland Publishing Co., Amsterdam, 1970. (A chapter on "Phase Diagrams and Their Determination," by G. V. Raynor, gives an overview of the subject.)
Chart, T. G. Counsell, J. F. Jones, G. P. Slough, W. Spencer, P. J.	Provision and Use of Thermodynamic Data for the Solution of High-Temperature Practical Problems, an article in Intl. Met. Revs. 20, 57, 1975. (Description and use of the NPL metallurgical data bank, including examples of phase diagram prediction and more than 200 references.)
Chernov, A. N. Evtyanova, E. N., editors	General Review of Phase Diagrams for Metallic Systems, published by "Nauka", Moscow (1973). Text in Russian. (Structural and crystallographic properties, among others, are reviewed for binary and ternary alloys.)
Darken, L. S. Gurry, R. W.	Physical Chemistry of Metals (McGraw-Hill, New York, 1953) (A textbook treatment of the subject.)

Phase Diagrams - Theory and Review

Findlay, A.	Phase Rule (Dover Publications, New York, 1951) (Development and use of the phase rule.)
Giessen, B. C. Willens, R. H.	Rapidly Quenched (Splat-Cooled) Metastable Alloy Phases; their Phase-Diagram Representation, Preparation Methods, Occurrence and Properties, a chapter in "Phase Diagrams: Materials Science and Technology" III, 103-141, 1970 (A. M. Alper, editor), published by Academic Press, New York. (Equilibrium and metastable phase diagrams for several binary alloys are compared and the representation of metastable compounds or phases together with the equilibrium diagram discussed; about 90 references cited.)
Gordon, P.	Principles of Phase Diagrams in Materials Systems (McGraw-Hill, New York, 1968) (Largely on the theory of phase diagrams.)
Gould, R. F., editor	Nonstoichiometric Compounds, published by the American Chemical Society in the "Advances in Chemistry" series, 39, 1963. (Contributed chapters treat the problem of nonstoichiometry in metal compounds; phase diagrams and related subjects are discussed; 253 pages.)
Hume-Rothery, W. Christian, J. W. Pearson, W. B.	Metallurgical Equilibrium Diagrams Institute of Physics, London, 1952) (Textbook-type treatment on the methodology of determining phase diagrams.)
Hume-Rothery, W.	The Engel-Brewer Theories of Metals and Alloys, a review in "Progress in Materials Science" 13 (#5), 1967, published by Pergamon Press, New York.
Ivanov, O. S. Alekseev, Z. M., editors	Structure of Phases, Phase Transformations, and Phase Diagrams of Metallurgical Systems, Proceedings of the 6th All-Union Conference on Research on the Structure of Phases, Phase Transformations and Phase Diagrams and Problems in the use of new Metallurgical Alloys (18-21 Sept. 1972, Baikov Inst., Moscow), published by "Nauka", Moscow (1974). Text in Russian. (Contributed papers deal with the subjects cited in the title; proceedings treat many ternary systems.)

Phase Diagrams - Theory and Review

Kaufman, L.	Computer Calculations of Phase Diagrams, With Special Reference to Refractory Metals (Academic Press, New York, 1970). (A how-to-do it book).
Kaufman, L.	The Stability of Metallic Phases, an article in Progress in Materials Science 14 (1971), edited by B. Chalmers and W. Hume-Rothery. (Discussion of phase diagram predictions based mainly on thermodynamic data.)
Kaufman, L., editor	CALPHAD: Computer Coupling of Phase Diagrams and Thermochemistry, a journal published quarterly beginning Jan. 1977, by Pergamon Press, New York. (A journal addressed to techniques and results of computer prediction of phase equilibria from thermodynamic data.)
Kubaschewski, O., editor	Metallurgical Chemistry, proceedings of a symposium held at Brunel University and NPL (July, 1971) and published by H.M.S.O. (London), 1972. (The proceedings include both review papers and reports of new experimental data. The prediction and determination of phase equilibria, lattice structures and thermodynamic data and the presentation of phase diagrams comprise the major portion of the proceedings. One session is devoted to the problem of data compilation and computer storage.)
Kubaschewski, O. Barin, I.	Phase Equilibria in Condensed Systems, an article in Pure and Appl. Chem. 38, 469-494, 1974. (Construction of phase diagrams from thermochemical data is reviewed and the results compared to experimentally determined diagrams.)
Lumsden, J.	Thermodynamics of Alloys (Academic Press, New York, 1966). (Textbook treatment on the thermodynamics of phase equilibria in metals and alloys.)
Masing, G.	Ternary Systems, Introduction to the theory of three component systems, published by Dover Publications, New York, 1960). (Easy-to-follow text; no data.)

Phase Diagrams - Theory and Review

Massalski, T. B., editor

Alloying Behavior and Effects in Concentrated Solid Solutions, published as the Proceedings of an AIME Metallurgical Society Conference, Vol. 29 (1965) by Gordon and Breach Science Publishers, New York.
(Invited conference papers dealing with the electronic structure and other aspects of alloy behavior are presented.)

Massalski, T. B.
Pops, H.

Intermediate Phases in Metallic Phase Diagrams, a chapter in "Phase Diagrams: Materials Science and Technology" II, 221-263, 1970 (A. M. Alper, editor); published by Academic Press, New York.
(Electronic and thermodynamic parameters which determine phase stability are reviewed, with a few binary phase diagrams and ternary sections given as illustrations; more than 50 references cited.)

Palatnik, L. S.
Landau, A. I.

Phase Equilibria in Multicomponent Systems (Holt, Rinehart and Winston, New York, 1964).
(Theory of phase diagrams, mostly for binary systems.)

Perel'man, F. M.

Phase Diagrams of Multicomponent Systems - Geometrical Methods, published in Russian by "Nauka", Moscow (1965); English translation (1966) available from Consultants Bureau, New York.
(The problems of representing multicomponent phase diagrams on a flat surface are discussed; representations for equilibria in two 6-component alloys are given; 59 references cited.)

Prince, A.

Alloy Phase Equilibria (Elsevier Publishing Corp., New York, 1966).
(Theory of binary, ternary and higher-order phase diagrams; descriptions of most phase diagram forms and topologies.)

Reisman, A.

Phase Equilibria (Academic Press, New York, 1970).
(Thermodynamics, applications, experimental determinations and graphical representations of alloy and non-metal phase equilibria are reviewed.)

Rhines, F. N.

Phase Diagrams in Metallurgy - their Development and Application (McGraw-Hill, New York, 1956).
(Textbook describing interpretation of both binary and ternary phase diagrams.)

Phase Diagrams - Theory and Review

Ricci, J. E.

The Phase Rule and Heterogenous Equilibrium (Peter Smith Publisher, Inc., Magnolia, Gloucester, MA, 1951).
(Application of the phase rule to binary, ternary and quaternary systems.)

Rudman, P. S.
Stringer, J.
Jaffee, R. I., editors

Phase Stability in Metals and Alloys, proceedings of a conference held in 1966; (McGraw-Hill, New York, 1967).

Salli, I. V.

Structure Formation in Alloys, published in Russian by "Metallurgizdat", Moscow (1963) and available in English translation (1964) from Consultants Bureau, New York.
(Theoretical survey of thermodynamics and kinetics of equilibrium and non-equilibrium phase transformations.)

Savitskii, E. M.
Gribulya, V. B.

A series of papers on the computer prediction of intermetallic phases in binary systems includes the following:

a. Dokl. Acad. Sci. USSR 178, #1, 79-81, 1968 (in Russian), on recognizing binary phase diagrams,

b. Dokl. Acad. Sci. USSR 183, #5, 1110-1112, 1968 (in Russian), on prediction of solubility ranges of A_3B type intermetallic compounds,

c. Dokl. Acad. Sci. USSR 185, #3, 561-563, 1969 (in Russian), on prediction of peritectic type reactions and solubility ranges,

d. Dokl. Acad. Sci. USSR 206, #4, 848-851, 1972 (in Russian), on prediction of phase stabilities,

e. Metallofizika: 46, 52-62, 1973 (in Russian), on prediction of laves phase occurrence,

f. Dokl. Acad. Sci. USSR 214, #5, 1059-1062, 1974 (in Russian), on prediction of occurrence of $CaCu_5$-type structures,

g. Metallofizika: 52, 84-86, 1974 (in Russian), on prediction of laves phase occurrence, and

h. Dokl. Acad. Sci. USSR 220, #6, 1066-1069, 1975 (in Russian), on prediction of solubility ranges and sigma phases.

Phase Diagrams - Theory and Review

Savitskii, E. M.
Devingtal', Yu. V.
Gribulya, V. B.

Superconducting Alloys and Compounds, published by "Nauka", Moscow (1972). Text in Russian.
(A 14-page paper in this volume; superconducting critical temperatures for binary compounds are predicted; annotation by J. H. Westbrook; copy not received by ADC.)

Savitskii, E. M.
Gribulya, V. B.

Structures and Properties of Heat-Resistant Metallurgical Materials, published by "Nauka", Moscow (1973). Text in Russian.
(An 8-page paper in this volume; melting points for binary compounds are predicted; annotation by J. H. Westbrook; copy not received by ADC.)

Swalin, R. A.

Thermodynamics of Solids, 2nd edition (J. Wiley, New York, 1972).
(This theoretical treatment includes, among other topics, discussions of defects and ordering in metals and alloys.)

Vozdvizhenskii, V. M.

Prediction of Binary Phase Diagrams, published by "Metallurgiya", Moscow (1975). Text in Russian.
(Thermodynamics of binary alloys, with emphasis on construction of phase diagrams, is reviewed.)

Zhavoronkov, N. M., editor

Chemistry of Metallurgical Alloys, published by "Nauka", Moscow (1973). Text in Russian.
(This volume, published as a tribute to N. V. Ageev, consists of many articles reviewing the field.)

(NTIS publications may be ordered from the National Technical Information Service at 5286 Port Royal Road, Springfield, VA 22161).

National Bureau of Standards SP-496, Applications of Phase Diagrams in Metallurgy and Ceramics
Proceedings of Workshop held at NBS, Gaithersburg, Md., January 10-12, 1977

Organization of Phase Diagram Information in the Soviet Union

N. V. Ageev, D. L. Ageeva, T. P. Kolesnikova, and L. A. Petrova

Baikov Institute of Metallurgy
USSR Academy of Sciences
Institute of Scientific Information
Moscow, USSR

Over two and a half centuries ago, in 1724, the Academy of Sciences was set up at St Petersburg by an edict of Peter the Great. From its early days, the Academy was paying unflagging attention to metallurgical problems [1]. In 1829, academician A. J. Kupfer published a study [2] on the congelation temperatures of a system of two metals - tin and lead. Towards the end of the 19th century, N. S. Kurnakov [3] began his famous research into phase diagrams and properties of metal alloys. His studies were markable for their systemic character, with the underlying principle being an analysis of relationships between the nature of alloy's phases, the phase diagram pattern, and the position of the respective components in the Periodic Table. All findings unequivocally pointed to Mendeleyev's Periodic Law as a sound basis for understanding the nature of metal alloys and their phase diagram patterns [4].

The study of phase diagrams of metal systems is important, not just for theory of metals, but also for many major practical issues of physical metallurgy and metals engineering. No less significant is the study of phase diagrams of nonmetal, both oxide and silicate systems. The present-day technological progress largely depends on development of new high-quality materials, their production and processing to endow them with properties needed for use in up-to-date technologies.

An efficient organisation of phase diagram studies and their theoretic and practical use requires that information supply on all publications in this field, be well in hand.

Studies by N. S. Kurnakov and his disciples (S. F. Zhemchuzhny, N. A. Pushin, N. S. Konstantinov, N. I. Stepanov, G. G. Urazov, V. A. Nemilov, and others) were carried in the Journal of the Russian Physico-Chemical Society, Transactions of the St Petersburg Polytechnical Institute, Transactions of the Institute for Platinum Studies, and also in foreign journals - Zeitschrift für anorganische Chemie and Journal of the Institute of Metals.

The first handbook on phase diagrams to appear in the Soviet Union was the translation of a comprehensive reference monograph by M. Hansen "Structure of Binary Metal Alloys" [5] published in 1941. In 1956, "Bibliography of Soviet Studies concerning Phase Diagrams of Metal Systems", edited by I. I. Kornilov, was published [6]. In 1959, the first volume of the reference book "Structure and Properties of Binary Metal Systems" by A. E. Vol appeared [7], followed by the second volume in 1962; subsequent volumes are ready for print and will appear within a few years' time. In 1962, a Russian translation of the two-volume handbook by M. Hansen and K. Anderko "Structure of Binary Alloys" [8] came off the press, and in 1970, another handbook by R. Elliott appeared under the same title and also in two volumes [9], and in 1973 - handbook by F. Schunk [10] under the same title.

In 1972, a bibliographic reference book "Phase Diagrams of Ternary Metal Systems, 1910-1969" (Ed. by N. V. Ageev) was published [11].

Along with emerging interest in particular metals used as alloy components, monographs and handbooks of phase diagrams of the respective systems were appearing. For example, in 1964 "Atlas of Phase Diagrams of Titanium Alloys", compiled by E. K. Molchanova and edited by S. G. Glazunov [12], was printed. In 1964, D. A. Prokoshin and E. V. Vasil'eva published a monograph on "Niobium Alloys". In 1968, T. A. Badaeva published a monograph on "Binary and Ternary Phase Diagrams of Thorium-Based Alloys. Structure of Thorium Alloys" [14]. The monograph by O. S. Ivanov, T. A. Badaeva, R. M. Safronova, V. B. Kishinevsky, and N. P. Kushnir "Phase Diagrams and Phase Transitions of Uranium Alloys: appeared in 1972 [15].

In 1973, O. S. Ivanov, A. S. Adamova, E. M. Tararyeva, and I. A. Tregubov published the monograph "Structure of Zirconium Alloys. Binary and Ternary Phase Diagrams" [16].

Since 1956, the All-Union Institute of Scientific Information of the USSR Academy of Sciences (VINITI) has been issuing an abstract journal "Chemistry" and since 1956 "Metallurgy". The formal journal includes a section for "Physico-Chemical Analysis" and the latter, sections for "Phase Equilibrium" and "Theory of Metallurgical Processes" covering studies on phase diagrams published in the USSR and elsewhere. Since 1959, VINITI has been publishing a yearbook titled "Phase Diagrams of Metal Systems", edited by N. V. Ageev. Thus far, twenty issues have appeared, which cover metal system diagrams described in 1955-1974 [17-35,52]. Issues XXI (1975) and XXII (1976) are being compiled. Each issue carries phase diagrams investigated and reported in the literature in a respective year. The yearbook covers papers describing or containing graphic images of complete phase diagrams or parts thereof (phase boundaries, solubility lines). Sources describing studies of crystal structures, physical and chemical properties and other features of individual phases are not included. Phase diagrams of metals with nonmetal elements are given only if the study has been conducted starting from 100 percent metal component. Diagrams are arranged according to increasing number of components, viz.: binary, ternary, quaternary, and so on; within each group, entries are ordered by Roman alphabet of component names. Roman alphabet has been adopted beginning with XVIII issue, for the benefit of users who are not familiar with the Russian language. All phase diagrams are described in accord with the following entry format: (1) materials used in the study; (2) methods of preparing and studying the alloy; (3) description of the diagram and its points and lines; (4) description of phases; (5) bibliographic details; and (6) note. Complete phase diagrams and sections of ternary or more complex systems are always reproduced from the original publication without any modification or a critical assessment of their reliability. Composition is mostly given in weight percentages, unless

otherwise indicated. Temperatures are centigrade, unless otherwise indicated. Each issue ends up with a table of contents indicating the pages containing phase diagrams. A cumulative index is compiled every ten years and inserted into the current issue. The first cumulation to issues I-X (1955-1964) of the "Phase Diagrams of Metal Systems" was printin 1964 [26]. The second cumulation for twenty years (issues I-XX) is inserted in issue XX.

Since 1966, VINITI has been issuing a series of handbooks under the general title - "Phase Diagrams of Nonmetal Systems", edited by D. L. Ageeva. So far, issues I to X have appeared, covering diagrams of oxide systems published from 1963 through 1974 [36-45,53]. The entry format is the same as described above for metal systems, but illustrations from originals are reproduced selectively.

On phase diagrams of silicate systems, three volumes of the reference book "Phase Diagrams of Silicate Systems" edited by V. P. Barzakovsky [46-48] were published in 1969, 1970 and 1972.

Primary publications dealing with study of phase diagrams in the Soviet Union are carried in the following main sources: Izvestia Akademii Nauk ("Metals" series); Doklady Akademii Nauk SSSR; Dopovidi Akademii Nauk URSR; Fizika metallov i metallovedenie; Izvestia Akademii Nauk SSSR (Non-Organic Materials series); Poroshkovaya metallurgia; Vestnik Moskovskogo Universiteta (Chemistry" series); Zhurnal neorganicheskoi khimii, as well as special subject compendia which are issued by various publishers.

A critical overview of the phase diagram information in the Soviet Union suggests that:

(1) information on phase diagrams covers not just binary, but also ternary and more complex systems;

(2) handbooks reproduce phase diagrams from original publications without any modification;

(3) regular published information on phase diagrams of metal and oxide systems is produced;

(4) primary publications dealing with studies of phase diagrams are not concentrated in any single source, but scattered over several journals and serials;

(5) times spent on bringing information to user's notice are: through VINITI's abstract journal - for Soviet publications, 3 to 5 months; for foreign publications, 4 to 8 months; through VINITI's handbooks, three years;

(6) no works on critical review of experimental data, such as the handbook of M. Hansen et al., are available;

(7) those handbooks that are being published are sold out too soon; and

(8) despite definite phase diagram description formats sanctioned by practice, there are no strict standard requirements, so that original publications often lack essential data for a judgement about reliability and quality of the phase diagrams.

From data covered by handbooks, one can conclude (see Figures 1, 2) that the Soviet Union holds a major place in studies of metal systems' phase diagrams. The work is under way in many research organisations across the country and coordinated by the USSR Academy of Sciences Scientific Council on Physico-Chemical Principles of Metallurgical Processes (117334, Moscow, Leninski prospekt, 49), which scrutinises the research programmes and the plans for conducting scientific conferences and meetings. Phase diagrams today are a product of experimental research. Phase diagrams calculated from thermodynamic data thus far only serve for reciprocal tests of computations and experiments, but as yet are no substitute for experiment. During experimental studies of phase diagrams, Soviet authors have been trying to improve the methods by studying samples of a variable composition which are produced by condensing films on a base [49] or by the diffusion layer method, which issued in studying phases formed by diffusion [50-51]. With these methods the sample is not in equilibrium state, so they are no adequate substitute for the study of particular samples of a definite composition brought into equilibrium state by thermal treatment.

It may be said in conclusion that cooperation between the researchers concerned with phase diagrams and the information officers is bound to improve and accelerate the work in the phase diagram field.

Research on computerized modelling of phase diagrams is also conducted in the Institute of Scientific Information (VINITI, USSR) [54-65].

DISCUSSION

W. B. Pearson - How many copies of each Ageev volume are printed?

T. Kolesinkova - 3,000 to 4,000 copies. These can be obtained through "International Books" [editor's note: see also description under Mikhailov (VINITI), p 44, in listing of international data compilation activities].

A. Navrotsky - Would you be able to tell us what publications on thermodynamic data are available in the Soviet Union?

T. Kolesnikova - There are many publications. We publish each year handbooks by a center of standard data. Eleven volumes have now been issued.

References

* Figures 1 and 2 may be obtained by contacting the authors.

1. Lomonosov, M. V., "The Basic Foundations of Metallurgy and Mining" (1763).

2. Kupfer, A. J., Ann. Chim., 40, 285, 1829.

3. Kurnakov, N. S., selected works, 611 pages, published by Izdatel'stvo Akademiia Nauk, Moscow (1961).

4. Ageev, N. V., Compt. Rend. (Chim. Phys.): 281, 287, 1952.

5. Hansen, M., "Structure of Binary Alloys", 2 volumes on the literature of ferrous and non-ferrous metallurgy, 1050 pages, published by the State Scientific-Technical Publishing House, Leningrad, 1941.

6. "Bibliography of Soviet Studies concerning Phase Diagrams of Metal Systems", edited by I. I. Kornilov, 38 pages, published by the Institute for Technical and Experimental Information, Academy of Sciences of the USSR, Moscow, 1956.

7. Vol, A. E., "Structure and Properties of Binary Metal Systems"; reference series, in 4 volumes, including physico-chemical properties of the elements; systems of Ac, Al, Am, B, Ba, Be, and N are treated in volume 1 (755 pages, 1959) systems of Bi, Dy, Eu, Fe, Ga, Gd, Ge, H, Hf, Ho, V, and W in volume 2 (982 pages, 1962) and systems of Au, In, Ir, Y, and Yb in volume 3 (814 pages, 1976); published by "Izdatel'stvo Fiziko-Matematicheskii Literatur" (Moscow).

8. Hansen, M. and Anderko, K., "Structure of Binary Alloys", translated from English and published by "Metallurgizdat," Moscow, 1962.

9. Elliott, R. P., "Structure of Binary Alloys, First Supplement", volumes 1 (455 pages) and 2(472 pages), translated from English and published by "Metallurgizdat", Moscow, 1970.

10. Shunk, F. A., "Structure of Binary Alloys, Second Supplement" 760 pages, translated from English and published by "Metallurgizdat," Moscow, 1973.

11. "Phase Diagrams of Ternary Metal Systems, 1910-1969" (bibliographic reference book), Ageev, N. V., editor, 189 pages, produced by the Institute of Metallurgy, Academy of Sciences of the U.S.S.R., and published by "Nauka", Moscow, 1972.

12. Molchanova, E. K., "Atlas of Phase Diagrams of Titanium Alloys",[2] 392 pages, published by "Izdatel'stvo Mashinostroenie," Moscow, 1964.

13. Prokoshkin, D. A. and Vasil'eva, E. V., "Niobium Alloys", 332 pages, published by "Nauka", Moscow, 1964.

14. Badaeva, T. A., "Structure of Thorium Alloys. Binary and Ternary Phase Diagrams of Thorium-Based Alloys," 177 pages, published by "Nauka," Moscow, 1968.

15. Ivanov, O. S., Badaeva, T. A., Sofronova, R. M., Kishinevsky, V. B., and Kushnir, N. P. (edited by Ivanov, O. S.), "Phase Diagrams and Phase Transitions of Uranium Alloys", 252 pages, published by "Nauka," Moscow, 1972.

16. Ivanov, O. S., Adamova, A. S., Tararyeva, E. M., and Tregubov, I. A., "Structure of Zirconium Alloys. Binary and Ternary Phase Diagrams", 199 pages, published by "Nauka," Moscow, 1973.

17. Alisova, S. P., Vul'f, L. B., Markovich, K. M., Novik, P. K., Petrova, L. A., and Rogachevskaya, Z. M. (edited by Ageev, N. V.), "Phase Diagrams of Metal Systems," vol. 1 (covering information published in 1955), 138 pages, published by VINITI, Moscow, 1960.

18. Ibid., vol. 2 (covering information published in 1956), 280 pages, published by VINITI, Moscow, 1960.

19. Ibid., vol. 3 (covering information published in 1957), 128 pages, published by VINITI, Moscow, 1960.

20. Ibid., vol. 4 (covering information published in 1958) 403 pages, published by VINITI, Moscow, 1961.

21. Rogachevskaya, Z. M. [edited by Ageev, N. V.], "Phase Diagrams of Metal Systems", vol. 5 (covering information published in 1959), 168 pages, published by VINITI, Moscow, 1962.

22. Ibid., vol. 6 (covering information published in 1960), 168 pages, published by VINITI, Moscow, 1962.

23. Ibid., vol. 7 (covering information published in 1961), 263 pages, published by VINITI, Moscow, 1963.

24. Ibid., vol. 8 (covering information published in 1962), 232 pages, published by VINITI, 1964.

25. Grankova, L. P., Mints, R. S., and Petrova, L. A. [edited by Ageev, N. V.] "Phase Diagrams of Metal Systems", vol. 9 (covering information published in 1963), 277 pages, published by VINITI, Moscow, 1966.

26. Alisova, S. P. and Budberg, P. B. [edited by Ageev, N. V.], "Phase Diagrams of Metal Systems", vol. 10 (covering information published in 1964), 240 pages, published by VINITI, Moscow, 1966.

27. ibid., vol. 11 (covering information published in 1965), 270 pages, published by VINITI, Moscow, 1968.

28. ibid., vol. 12 (covering information published in 1966), 272 pages, published by VINITI, Moscow, 1968.

29. ibid., vol. 13 (covering information published in 1967), 277 pages, published by VINITI, Moscow, 1970.

30. ibid., vol. 14 (covering information published in 1968), 272 pages, published by VINITI, Moscow, 1970.

31. ibid., vol. 15 (covering information published in 1969), 264 pages, published by VINITI, Moscow, 1971.

32. ibid., vol. 16 (covering information published in 1970), 308 pages, published by VINITI, Moscow, 1972.

33. ibid., vol. 17 (covering information published in 1971), 420 pages, published by VINITI, Moscow, 1973.

34. ibid., vol. 18 (covering information published in 1972), 268 pages, published by VINITI, Moscow, 1975.

35. ibid., vol. 19 (covering information published in 1973), 268 pages, published by VINITI, Moscow, 1976.

36. Ageeva, D. L., "Phase Diagrams of Non-Metallic Systems. Oxides and Silicides", vol. 1, 123 pages, published by VINITI, Moscow, 1966.

37. ibid., vol. 2, 224 pages, published by VINITI, Moscow, 1966.

38. ibid., vol. 3, 143 pages, published by VINITI, Moscow, 1968.

39. Dobroshvetov, B. L., ibid., vol. 4, 276 pages, published by VINITI, Moscow, 1969.

40. Ageeva, D. L. and Shvedov, L. V., ibid., vol. 5, 199 pages, published by VINITI, Moscow, 1970.

41. Ageeva, D. L., ibid., vol. 6, 232 pages, published by VINITI, Moscow, 1971.

42. Ageeva, D. L. and Shvedov, L. V., ibid., vol. 7, 161 pages, published by VINITI, Moscow, 1972.

43. Ageeva, D. L. and Shvedov, L. V., ibid., vol. 8, 155 pages, published by VINITI, Moscow, 1973.

44. Ageeva, D. L. and Shvedov, L. V., ibid., vol. 9, 155 pages, published by VINITI, Moscow, 1974.

45. Ageeva, D. L. and Shvedov, L. V., ibid., vol. 10, 115 pages, published by VINITI, Moscow, 1975.

46. Toropov, N. A., Barzakovskii, V. P., Lapin, V. V. and Kursheva, N. N., "Phase Diagrams of Silicide Systems" (part I, Binary Systems), 822 pages, published by "Nauka", Leningrad, 1969.

47. Toropov, N. A., Barzakovskii, V. P., Bondar, I. A., Udalov, Yu. P., ibid. (part II, Metal-Oxygen Phases in Silicide Systems), 372 pages, published by "Nauka", Leningrad, 1970.

48. Toropov, N. A., Barzakovskii, V. P., Lapin, V. V., Kurtseva, N. N., and Boikova, A. I., "Phase Diagrams of Silicide Systems" (reference book), vol. 3 (Ternary Systems), 448 pages, published by "Nauka", Leningrad, 1972.

49. Vekshchinskii, S. A., "Novel Method for Metallographic Study of Alloys," 252 pages, published by State Publishing House, Moscow, 1944.

50. Ivanov, O. S., et al., "Theoretical and Experimental Methods of studying Phase Diagrams of Metal Systems", pages 160-166, published by "Nauka", Moscow, 1969.

51. Tregubov, I. A., Kuzina, L. N., and Ivanov, O. S., Russian Metallurgy (English translation of Izvestiia Akademii Nauk SSSR - Metally): no. 4, 104-108, 1967.

52. Eroshchenkova, I. G., Olenicheva, V. G., and Petrova, L. A. [edited by Ageev, N. V.], "Phase Diagrams of Metallurgical Systems", vol. 20 (covering information published in 1974), 360 pages, published by VINITI, Moscow, 1976.

53. Ageeva, D. L., Shvedov, L. V., "Phase Diagrams of Non-Metal Systems. Oxide Systems", vol. 11, 110 pages, published by VINITI, Moscow, 1976.

54. Seifer, A. L., Stein, V. S., The topology of composition-property diagrams for binary systems. "Zhurnal Neorganicheskoi Khimii" (Journal of Inorganic Chemistry), 1961, 6, No. 12, p. 2719.

55. Seifer, A. L., Kleinermann, G. I., Stein, V. S., The principles of construction of a machine language for physico-chemical analysis. "Information Storage and Retrieval", 1963, No. 1, p. 13-18.

56. Stein, V. S., Principles of computer recording of phase regions in phase diagrams as exemplified by binary metallic systems. "Nauchno-Tekhnicheskaya Informatsiya" (Scientific and Technical Information), 1963, No. 3, p. 31-35.

57. Novik, P. K., Stein, V. S., Unification of names of regions of binary metallic systems. "Nauchno-Tekhnicheskaya Informatsiya" (Scientific and Technical Information), 1964, No. 5, p. 25-28.

58. Stein, V. S., Solution of some information problems of physico-chemical analysis by computers (in Russian). Dissertation, VINITI, USSR Academy of Sciences, 1966.

59. Stein, V. S., Design of an information retrieval system for physico-chemical analysis. In the book: "Prikladnaya dokumentatistika" (Applied documentation), Moscow, "Nauka" Publishers, 1968, (in Russian).

60. Adler, Iu. P., Stein, V. S., Composition-property diagrams: representation of information for computers. "Information Storage and Retrieval", 1969, 4, p. No. 4, p. 329-332.

61. Stein, V. S., Information language for representation of binary and ternary phase diagrams in computer memory for solving certain problems of physico-chemical analysis. In the book: "Diagrammy sostoyaniya metallicheskikh system" (Phase diagrams of metallic systems), "Nauka" Publishers, Moscow, 1968, (in Russian).

62. Stein, V. S., On certain methods of computer processing and retrieval of scientific information in diagrams of physico-chemical analysis. In the book: Teoreticheskiye i eksperimentalniye metody issledovaniya diagram sostoyaniya (Theoretical and experimental methods of research into phase diagrams), "Nauka" Publishers, Moscow, 1969, (in Russian).

63. Stein, V. S., Possibilities and problems of developing an information retrieval system for metallurgy. "Izvestiya Akademii Nauk SSSR", "Metally" (Metals), 1969, No. 2, (in Russian).

64. Tulupova, I. V., Stein, V. S., Topology of equilibrium diagrams of multicomponent systems and formal methods of their description. In the book: Struktura faz, fazoviye prevrashcheniya i diagrammy sostoyaniya metallicheskikh system. (Phase structure, phase conversion and phase diagrams of metallic systems). "Nauka" Publishers, Moscow, 1974, (in Russian).

65. Tulupova, I. V., Stein, V. S., Topology of equilibrium diagrams of multicomponent systems with a critical phase and formal methods of their description. Deposited at VINITI, N 2454-74, on 9 September, 1974, (in Russian).

Reference Notes

1. ref. 7 (Vol, A. E.): volumes 1, 2, and 3 have been published; volumes 4 and 5 are in press; see paper by Vol and Kagan (p.) for details, including the binary systems treated volumes 4 and 5.

2. ref. 12 (Molchanova, E. K.): English translation available from the National Technical Information Service, Springfield, VA 22161 as document AD 670,090 (1967).

National Bureau of Standards SP-496, Applications of Phase Diagrams in Metallurgy and Ceramics
Proceedings of Workshop held at NBS, Gaithersburg, Md., January 10-12, 1977

A SURVEY OF HIGH PRESSURE PHASES OF MATERIALS

Leo Merrill

High Pressure Data Center
5093 HBLL
Brigham Young University
Provo, Utah 84602 USA

A survey of polymorphic phase diagrams as a function of pressure and temperature is presented for the elements and simple inorganic compounds. Historically, the preparation and study of material phase were carried out as a function of temperature and composition. In 1955 with the successful synthesis of diamond[1], the importance of the use of high pressure in the synthesis of new materials became evident. In a few years a large number of new dense phases of the elements and compounds had been discovered and characterized. High pressure-high temperature phase studies of materials include the following formula types: elements (69)*, AB (87), AB_2 (78), AB_3 (8), ABO_2 (11), A_2B_3 (67), ABO_4 (54), and miscellaneous types (58) mainly of mineral systems or mineral analogs. All materials in this survey are those for which crystallographic data are available.

The preparation of high pressure phases falls into three principle categories: (1) pressure and temperature induced structural transformations of known elements or compounds, (2) synthesis of new compounds and (3) disproportionation reactions. In pressure induced structural phase transitions, materials proceed to structures with higher densities and generally to more efficient packing arrangements or higher cation coordination numbers. It would be impossible to discuss all the pressure induced phases, so reviews and compilations will be referenced and only the more interesting groups discussed. Since all successful theory of physical and transport properties are related to lattice symmetries, phase transformations will be discussed in terms of the crystal structures of the particular phases.

Why is high pressure useful in the preparation of new phases. Generally, the major effect of pressure is to force cations to adopt a higher coordination and to occupy sites in which they do not go naturally because of the unfavorable empirical radius ratio or their particular electronic configuration. Many compounds and/or phases of materials have no equilibrium configuration which can be prepared at atmospheric pressure. Compounds which cannot be formed due to high vapor pressure of one of its constituents are often synthesized at high pressure. In alloy systems pressure produces a change in solubility of one or both end members.

Elements. There are two excellent reviews of the high pressure-high temperature phases of the elements. Young[2] compiled phase diagrams of all the reported solid-solid and solid-liquid phase boundaries, which include approximately 80 phase diagrams. Cannon[3] published a similar report which is restricted to those materials for which the crystal structures of the high pressure phases have been identified by either x-ray or neutron diffraction techniques. This latter report, which contains 60 phase diagrams, is a critical evaluation of the phase boundaries and contains tables of the crystallographic data of the individual phases.

In an attempt to find some empirical relation which would predict which elements had pressure induced phase transformation Liu[4] plotted the room temperature densities of the elements with solid and liquid phases against atomic number. It was found that pressure induced polymorphic phase transformations of the solid elements appear to be closely correlated to the density periodicity. With the exception of Fe, all the solids with pressure induced phase transition lie below a straight line

$$\rho = 2.8 + 0.12Z$$

By using this correlation, Liu was able to predict new high pressure phases in Se, Tm, and Lu.

In general, the crystal structures of the metals are relatively simple as are their high pressure phases. In the phase diagrams of the metals it is very common for the bcc structure to be stable at high temperature adjacent to the melting curve. Starting in the first column of the period table Cs(fcc) undergoes a number of interesting transformations. Bridgmann[5] originally had observed two transitions at 23 and 43 kb which were detected by ΔV and electrical resistance anomalies. It was later shown that the resistance trace at 43 kb was not a cusp but two sharp discontinuities spaced about 0.5 kbar apart indicating the pressure of two closely spaced transitions at 42.2 and 42.7 kb. At 23 kb the transition is from bcc to fcc while at 42.2 kb the fcc phase transforms to a collapsed fcc' phase. The crystal structure above 42.7 kb could not be resolved.[6] An analogous transition occurs in Ce at 6 kb (fcc → fcc) and apparently involves an electronic transition. In cerium a critical point exists in the vicinity of 21.5 kb and 340°C. These transitions and others for the group B metals are summarized in Appendix A.

The rare earth metals form an interesting group and are structurally divided into two regions. The heavier elements from Gd have the hcp structure except Yb which is bcc. The lighter rare earth elements have more complicated structures as a result of different stacking sequences of close packed layers. The high temperature phases of the rare earth metals are mainly bcc. Jayaraman[7] has shown that the trend of the pressure induced structural phase transitions in the rare earth metals follow the sequence

$$\text{hcp} \rightarrow \text{Sm-type} \rightarrow \text{dhcp} \rightarrow \text{fcc}$$

which is in the direction of increasing cubic character. (Table I).

This is not true, however, for Eu and Yb which are divalent. Eu has no known high pressure phase while Yb undergoes a transition from fcc → bcc at 40 kb. The phase boundary of Eu has a negative slope and intersects the temperature axis near 800°C. The details of the phase diagrams and phases of Yb and Sr are almost identical.

The group IIIA through VIIA elements generally exhibit more complexity in both phase diagrams and the associated crystal structures. The phases of these elements are summarized in App. A. It should be noted that many of the polymorphic transitions of the elements do not undergo an increase in coordination as is particularly well illustrated in the transitions of the trivalent rare earth elements in which all the phases have coordination number 12.

AB Type Compounds. A recent review of the high pressure phases of the AB-type compounds[8] covers approximately 85 compounds with tables of crystallographic data and phase diagrams. The high pressure transitions in this group of compounds will in general be associated with an increase in cation coordination number. Experimentally, equilibrium values of the room temperature transitions are difficult to obtain due to poor kinetic effects in these compounds.

After the synthesis of diamond, the next significant discovery was the synthesis of the cubic form of boron nitride which is a high pressure analogue to diamond and also an abrasive. The principal groups of the AB type compounds which have been studied at high pressure are compounds of the halides, Group VA, and the chalcogenides. All the alkali halides with the exception of CsCl, CsBr and CsI crystallize in the 6 coordinated NaCl-type structure and have very simple phase diagrams. At high pressure the NaCl-type alkali halides transform to the 8 coordination CsCl-type structure.

Phase transitions in the ammonium halides, as well as their deuterium analogues, have been widely studied by a variety of methods. While a λ-transition at low temperatures is common to all these compounds, a pressure induced Fm3m (NaCl) to Pm3m (CsCl) transition is exhibited by ammonium chloride, bromide and iodide and their deuterated analogues at high temperature. Much of the theoretical work has been devoted to the λ transition in ammonium halides. In NH_4Br this transition is attributed to an order-disorder rotational orientation of the NH_4 groups.

AB-type compounds of the Group VA and VIA elements and Group 1B halides within the scope of this report have as the stable phases the αAgI, wurtzite, PbO, NaCl, ZnS or NiAs-type structure. The high pressure phases have the same or increased coordination (Appendix B) and consist mainly of HgS, CsCl, PbO, Wurtzite, NaCl, beta-Sn and HgS structure types.

Rare Earth Compounds. One of the particularly interesting areas where high pressure has been successful is with compounds of the rare earth elements. On the basis of high temperature synthesis it is usually found that there are regions where a particular structure cannot be formed (Table II). An empirical explanation is that in the higher rare earths the size of the ion is too small to form a stable compound. If as in the case of $LuTe_2$ the tellurium is more compressible than the rare earth member, high pressure can produce a favorable radius ratio for the formation of the particular series of compounds. Although this has been successful in synthesizing many new rare earth compounds, it is evident that other factors such as 4-f bonding play an important role.

The rare earth trialuminides[9] have layered type structures which have the Ni_3Sn, $BaPb_3$, $TiNi_3$, $HoAl_3$, and Cu_3Au type structures as shown in Table

III. These structure types are arranged according to increasing cubic character. The effect of high pressure on these layered compounds produces structures with greater cubic character.

Geological Studies. The use of high pressure has been extremely useful in studying the structure within the earth. The basis for dividing the earth's interior into various regions comes from seismic velocity data. From a knowledge of the ultrasonic properties of known minerals, the mineralogy can be predicted to approximately 200 km. In the region of the upper mantle known as the transition zone there are two major seismic discontinuities at about 400 km and 600 km. The discontinuity at 400 km is due to a transition of olivine to the spinel type structure and below 600 km silicon is in six fold coordination. Evidence for these phase changes comes principally from laboratory high pressure studies.

Of particular interest in this work was the discovery of new dense forms of quartz. Coesite containing Si in four fold coordination was prepared by Coes.[10] The synthesis of stishovite first prepared by Stishov and Popova[11] has the rutile structure with Si in octahedral coordination. A solution of the mineralogy of the lower mantle is not as straight forward as with the upper mantle. Present theory points to close packed oxide structures. One possible solution would be the existence of silicon in 8 fold coordination.

In order to test this possibility, the geologists began to look for analogue materials with rutile (octahedral coordination) type structures to see if pressure and temperature would favor the CaF_2-type structure. The use of analogue structure in the study of the structure of the earth's mantle has been a very productive technique.

Goldschmidt predicted that PbO_2 and MnF_2 would be the most likely rutile-type structures to undergo a transition to a CaF_2-type structure since their radius ratios are very close to critical value for the fluorite structure derived from simple geometrical considerations.

Experimental investigations confirmed PbO_2 and MnF_2, as well as CoF_2 and NiF_2, transform to the 8 coordinated fluorite structure. MnF_2 goes through a series of transformations; first to a 7-8 coordinated distorted fluorite, then to a 9 coordinated $PbCl_2$ phase and finally to the fluorite phase at high P and T. Fluorite phases of Ba, Sr, Cd, and Ca difluorides all transform to a 9 coordinated $\alpha PbCl_2$ structure.

In a recent experiment natural ilmenite (Fe,Mg) TiO_3 (pyroxene) was found to transform to the perovskite structure at high pressure and then to disproportionate into its component oxides (Fe,Mg)O and a cubic phase[12] of TiO_2 in which Ti is in 8 fold coordination. Other important transformations are those of olivine which transforms first to the spinel phase and finally to dense oxide phases. The pyroxenes at high pressure transform to spinel phases plus stishovite, etc. The success of this work has resulted from laboratory high pressure experiments.

(p-T-x) Phase Diagrams. While most of the high pressure studies have been devoted to the preparation of stoichiometric compounds, a number of researchers have investigated binary and ternary systems as a function of pressure, temperature and composition (p,T,x). Systems which have been reported in the literature include W-C, NiC, FeC, Fe-V, Fe-Cr, Fe-Si, Bi-Su, Bi-Tl, Bi-Pb, Bi-S, InS, Tl-In, Al-Si, Cu-Al, Ag-In and Au-Ga.

One of the best illustrations of the usefulness of phase diagrams at high pressure is the Ni-C system important in the production of synthetic

diamond (Fig. 1). At pressure less than 54 kbar there is no liquid - diamond region in the phase diagram which is necessary for the nucleation and growth of diamond crystals.[13] In connection with diamond production the Fe-C and Fe-Ni-C phase diagrams have been thoroughly investigated. The BN-Li_3BN_2 phase diagram is important for the production of the high pressure cubic BN. Relatively new products of commercial significance which are presently being developed are the sintered or polycrystalline forms of diamond and cubic boron nitride.

Considerable work is being done in the USSR on phase diagrams at high pressure. A review of this work has recently been published by Shinyaev (in Russian) of the Baikov Institute of Metallurgy.[14]

Displacive Transformations. Displacive phase transitions which are classified as second order or nearly second order are of particular interest in high pressure investigations. These are the soft mode type transitions in which the symmetry of the new phase can be related to either a temperature or volume dependent lattice instability in a mode of low energy. These transitions are important because they enable study of the basic physics of phase transitions.

In TeO_2 the elastic modulus (C_{11}-C_{12}) goes continuously to zero with pressure. $NaNo_3$ undergoes a paraelectric-ferroelectric ($R\bar{3}c$ - R3c) transition at 49 kbar. KH_2PO_4 (KDP) has a tricritical point at approximately 2 kbar. In $CaCo_3$, which has a displacive paraelectric-antiferroelectric ($R\bar{3}c$ - $P2_1/c$) transition, by the use of group theoretical calculations, a lattice mode has been identified which accounts for the observed displacements of the transition. Transitions of this type also occur in Sn at 90 kbar, KNO_3, $SrTiO_3$, the ammonium halides and others. Lattice dynamical

studies of the soft mode type phase transformation holds great promise in the development of basic theory of phase stability and structural phase transformations.

REFERENCES

* The number in parentheses is the number of materials which have been tabulated in each formula type.

1. H. T. Hall, Synthesis of Diamonds, J. Chem. Ed. 38, 484-489 (1961).

2. D. A. Young, Phase Diagrams of the Elements, UCRL 51902 Lawrence Livermore Laboratory (September 11, 1975).

3. J. F. Cannon, Behavior of the Elements at High Pressure, J. Phys. Chem. Ref. Data 3, 781-824 (1974).

4. L. G. Liu, Correlation of density periodicity to pressure induced polymorphic transformations in solid elements, J. Appl. Phys., 44, 2470-2474 (1973).

5. P. Bridgman, Proc. Am. Acad. Arts Sci., 76, 55-70 (1948).

6. H. T. Hall, L. Merrill, J. D. Barnett, High Pressure Polymorphism in Cesium, Science 146, 1297-1299 (1964).

7. A. Jayaraman, Solid-Liquid and solid-solid transformations in the Rare Earth Metals at High Pressure, Phys. Rev. 139A, 690-696 (1965).

8. L. Merrill, Behavior of the AB-Type compounds at High Pressure. (In press)

9. J. F. Cannon, H. T. Hall, Effect of High Pressure on the Crystal Structures of Lanthanide Trialuminides, J. Less Common Metals, 40, 313-328 (1975).

10. L. Coes, A new dense crystalline silica. Science 118, 131-133 (1953).

11. S. M. Stishov, S. V. Popova, New dense polymorphic modification of silica. Geokhimiya 8, 649-659 (1962).

12. L. G. Liu, High Pressure Phase Transformations and Compressions of Ilmenite and Rutile, I. Experimental Results, Phys. of the Earth and Planetary Interiors 10, 167-176 (1975).

13. H. M. Strong, R. E. Hanneman, Crystallization of Diamond and Graphite, J. Chem. Phys. 46, 3668-3676 (1967).

14. A. Ya. Shinyaev, Phase diagrams and properties of alloys at high pressure, Baikov Institute of Metallurgy of the Academy of Sciences USSR, 154p., 1973 Moscow.

Table I. Pressure Induced Phase Transformations for the Rare Earth Elements.

Metal	hcp	Sm-Type	dhcp	fcc
Gd,Tb,Dy,Ho,Tm,Lu	I ⟶ II			
Er	I ⟶ II			
Sm		I ⟶ II		
La,Pr,Nd			I ⟶ II	

Table II.

Rare Earth Series Compounds Showing Regions Where the Synthesis Range has been Extended by the use of Pressure.

R. E. Compound	La	Ce	Pr	Nd	Sm	Eu	Gd	Tb	Dy	Y	Ho	Er	Tm	Yb	Lu
RSb_2 ($LaSb_2$ Type)	*	*	P	*	*	-	P	P	-	-	-	-	-	-	-
RSb_2 ($HoSb_2$ Type)	-	-	-	-	-	-	P	P	P	P	P	P	P	-	-
RS_2 ($LaTe_2$ Type)	*	*	*	*	*	-	*	-	*	-	*	*	P	P	P
RTe_{2-x} ($0 \leq x \leq 0.3$)	*	*	*	*	*	-	*	*	*	P	P	P	P	*	P
RTe_3 (P4/nmm)	*	*	*	*	*	-	*	*	*	*	*	*	*	-	P
RCo_2 ($MgCu_2$ Type)	P														
RFe_2 ($MgCu_2$ Type)	-	-	P	P	*	-	*	*	-	*	P	-	-	P	*
RSn_3 ($AuCu_3$ Type)	*	*	*	*	*	*	*	P	P	P	P	P	-	*	-
RPb_3 ($AuCu_3$ Type)	*	*	*	*	*	-	*	*	*	*	*	*	*	*	P
RB_2	-	-	-	-	P	-	*	*	*	-	*	*	*	*	*
RB_{12}	-	-	-	-	-	-	P	*	*	-	*	*	*	*	*

Key: (-) Compound is unknown.
(*) Compound is prepared at atmospheric pressure and high temperature.
(P) Compound is prepared at high pressure and high temperature.

Table III. Pressure Induced Phase Transformations in the Rare Earth Trialuminides.

Compound	Ni_3Sn[1]	$BaPb_3$[2]	$TiNi_3$[3]	$HoAl_3$[4]	Cu_3Au[5]
$GdAl_3$	I ⟶ II				
$TbAl_3$		I ⟶ II			
$DyAl_3$			I ⟶ II		
$HoAl_3$				I ⟶ II	

Key:		Structure Type	Crystal Lattice	Space Group	Hexagonal Character (ABAB)	Cubic Character (ABCA)
	(1)	Ni_3Sn	hex	$P6_3/mmc$	100%	0%
	(2)	$BaPb_3$	rhomb	R3m	67%	33%
	(3)	$TiNi_3$	hex	$P6_3/mmc$	50%	50%
	(4)	$HoAl_3$	rhomb	R3m	40%	60%
	(5)	Cu_3Au	cubic	Pm3m	0%	100%

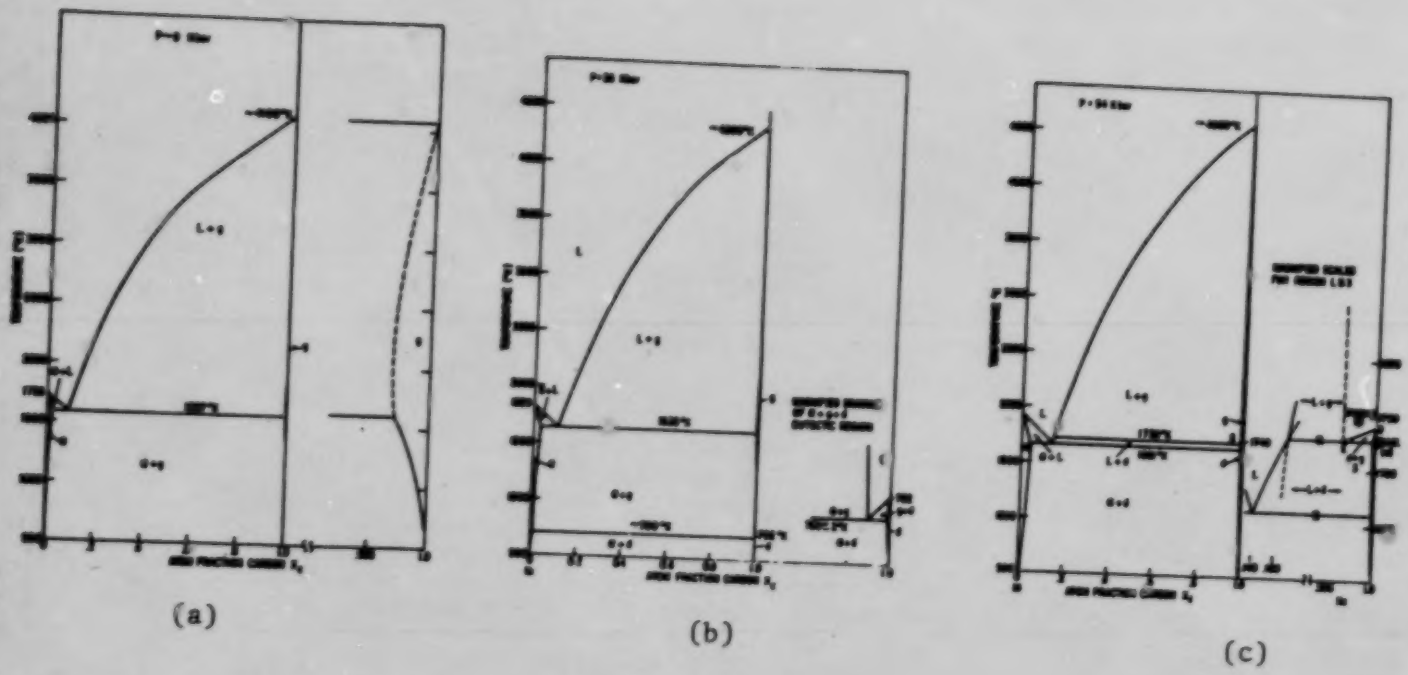

Figure 1. Isobaric sections of the Ni-C system equilibrium phase diagrams at (a) atmospheric pressure, (b) 26 kilobars, and (c) 54 kilobars.

Appendix A. Crystallographic data for the Elements.

Element	Pressure (kbar)	Temperature (°C)	Crystal System	Structure Type	a(Å)	b(Å)	c(Å)	Angle (°)	Z	Space Group
Cs(I)	R	25	cubic	bcc	6.141				2	Im3m
Cs(II)	25	R	cubic	fcc	6.465				4	Fm3m
Cs(III)	41.7	27	cubic	fcc	5.800				4	Fm3m
Sr(I)	R	25	cubic	fcc	6.0849				4	Fm3m
Ba(I)	R	25	cubic	bcc	5.013				2	Im3m
Ba(II)	58	R	hexagonal	hcp	3.901		6.154		2	$P6_3/mmc$
Ga(I)	R	24	orthorhombic		4.5197	4.5260	7.6633		8	Cmca
Ga(II)	>20	R	tetragonal	bct	2.808		4.458		2	I4/mmm
Tl(I)	R	18	hexagonal	hcp	3.4566		5.5248		2	$P6_3/mmc$
Tl(II)	R	262	cubic	bcc	3.882				2	Im3m
Tl(III)	60	R	cubic	fcc	4.778				4	Fm3m
C(I)	R	R	hexagonal	graphite	2.456		6.696		4	$P6_3mc$
C(II)	R	20	cubic	diamond	3.56679				8	Fd3m
Si(I)	R	25	cubic	diamond	5.4307				8	Fd3m
Si(II)	134	R	tetragonal	white-Sn	4.686		2.585		4	$I4_1/amd$
Si(III)	R	R	cubic		6.636				16	Ia3
Ge(I)	r	25	cubic	diamond	5.6575				8	Fd3m
Ge(II)	R	R	tetragonal		5.93		6.98		12	$P4_32_12$
Ge(III)	100	R	tetragonal	white-Sn	4.884		2.696		4	$I4_1/amd$
Sn(I)	R	25	tetragonal	white-Sn	4.8315		3.1814		4	$I4_1/amd$
Sn(III)	39	314	tetragonal	bct	3.81		3.48		2	I4/mmm
Pb(I)	R	25	cubic	fcc	4.9502				4	Fm3m
Pb(II)	139	R	hexagonal	hcp	3.265		5.387		2	$P6_3/mmc$
P(Black I)	R	22	orthorhombic		3.3136	10.478	4.3763		8	Cmca
P(Black II)	86	R	rhombohedral	As	3.524			57.25	2	R3m
P(Black III)	101	R	cubic	sc	2.377				1	
As(I)	R	23	rhombohedral	As	4.1318			54.13	2	R3m
As(II)	R	R	tetragonal		8.691		6.363			
Sb(I)	R	25	rhombohedral	As	4.5067			57.107	2	R3m
Sb(II)	64	R	cubic	sc	2.986				1	
Bi(I)	R	25	rhombohedral	As	4.746			57.23	2	R3m
Bi(II)	26	R	monoclinic		6.674	6.117	3.304	110.33	4	C2/m
Bi(V)	90	R	cubic	bcc	3.800				2	Im3m
Se(I)	R	25	hexagonal	Sc	4.3656		4.9590		3	$P3_121$
Se(II)										
Te(I)	R	25	hexagonal		4.4566		5.9268		3	$P3_121$
Te(III)	115	R	rhombohedral	β-Po	3.002			103.3	1	R3m
Tl(I)	R	25	hexagonal	hcp	2.9511		4.6843		2	$P6_3/mmc$

Appendix A. Crystallographic data for the Elements

Element	Pressure (kbar)	Temperature (°C)	Crystal System	Structure Type	a(Å)	b(Å)	c(Å)	Angle (°)	Z	Space Group
Ti(II)	R	900	cubic	bcc	3.3065				2	Im3m
Ti(III)	R	R	hexagonal		4.625		2.813		3	
Ti(IV)?	R	R	cubic	bcc	3.276				2	Im3m
Zr(I)	R	25	hexagonal	hcp	3.2312		5.1477		2	$P6_3/mmc$
Zr(II)	R	862	cubic	bcc	3.6090				2	Im3m
Zr(III)	R	R	hexagonal		5.036		3.109		3	
Zr(IV)?	R	R	cubic	bcc	3.568				2	Im3m
Fe(I)	R	20	cubic	bcc	2.8664				2	Im3m
Fe(II)	R	916	cubic	fcc	3.6468				4	Fm3m
Fe(III)	R	1394	cubic	bcc	2.9322				2	Im3m
Fe(IV)	151	R	hexagonal	hcp	2.461		3.952		2	$P6_3/mmc$
Rh	R	20	cubic	fcc	3.8044				4	Fm3m
Hg(I)	R	-46	rhombohedral	Hg	3.005			70.53	1	R3m
Hg(II)	R	-196	tetragonal	bct	3.995		2.825		2	I4/mmm
La(I)	R	R	hexagonal	dhcp	3.770		12.159		4	$P6_3/mmc$
La(II)	R	R	cubic	fcc	5.296				4	Fm3m
La(III)	R	887	cubic	bcc	4.26				2	Im3m
Ce(I)	R	23	cubic	fcc	5.1601				4	Fm3m
Ce(II)	R	25	hexagonal	dhcp	3.673		11.802		4	$P6_3/mmc$
Ce(III)	R	-196	cubic	fcc	4.85				4	Fm3m
Pr(I)	R	R	hexagonal	dhcp	3.6725		11.8354		4	$P6_3/mmc$
Pr(II)	R	821	cubic	bcc	4.13				2	Im3m
Pr(III)	40	R	cubic	fcc	4.88				4	Fm3m
Nd(I)	R	R	hexagonal	dhcp	3.6579		11.7992		4	$P6_3/mmc$
Nd(II)	R	883	cubic	bcc	4.13				2	Im3m
Nd(III)	50	R	cubic	fcc	4.80				4	Fm3m
Sm(I)	R		rhombohedral	Sm	8.996			23.22	3	R3m
Sm(III)	R	R	hexagonal	dhcp	3.618		11.66		4	$P6_3/mmc$
Gd(I)	R	20	hexagonal	hcp	3.6360		5.7826		2	$P6_3/mmc$
Gd(II)	R		cubic	bcc	4.06				2	Im3m
Gd(III)	R	R	rhombohedral	Sm	8.92			23.3	3	R3m
Tb(I)	R	R	hexagonal	hcp	3.6010		5.6936		2	$P6_3/mmc$
Tb(II)	R		cubic	bcc					2	Im3m
Tb(III)	R	R	rhombohedral	Sm	8.83			23.42	3	R3m
Dy(I)	R	R	hexagonal	hcp	3.5903		5.6475		2	$P6_3/mmc$.
Dy(II)	R		cubic	bcc					2	Im3m

Appendix A. Crystallographic data for the Elements.

Element	Pressure (kbar)	Temperature (°C)	Crystal System	Structure Type	a(Å)	b(Å)	c(Å)	Angle (°)	Z	Space Group
Dy(III)	75	R	rhombohedral	Sm	8.39			23.0	3	R3m
Ho(I)	R	R	hexagonal	hcp	3.5773		5.6158		2	$P6_3/mmc$
Ho(II)	R		cubic	bcc					2	Im3m
Ho(III)	85	R	rhombohedral	Sm	8.26			23.3	3	R3m
Er(I)	R	R	hexagonal	hcp	3.5588		5.5874		2	$P6_3/mmc$
Er(II)	R		cubic	bcc					2	Im3m
Tm(I)	R	R	hexagonal	hcp	3.5375		5.5546		2	$P6_3/mmc$
Tm(II)	116	R	rhombohedral	Sm	3.327		23.48		3	R3m
Yb(I)	R	R	cubic	fcc	5.4862				4	Fm3m
Yb(II)	R	23	hexagonal	hcp	3.8799		6.3859		2	$P6_3/mmc$
Yb(III)	39.5	R	cubic	bcc	4.02				2	Im3m
Lu(I)	R	R	hexagonal	hcp	3.5031		5.5509		2	$P6_3/mmc$
Lu(II)	230	R	rhombohedral	Sm	3.176		21.77		3	R3m
Th(I)	R	R	cubic	fcc	5.0845				4	Fm3m
Th(II)	R	1450	cubic	bcc	4.11				2	Im3m
U(I)	R	25	orthorhombic	U	2.8537	5.8695	4.9548		4	Cmcm
U(II)	R	720	tetragonal		10.759		5.656		30	$P4_2/mnm$
U(III)	R	805	cubic	bcc	3.524				2	Im3m
Np(I)	R	20	orthorhombic		6.633	4.723	4.887		8	Pnma
Np(II)	R	313	tetragonal		4.897		3.388		4	$P42_12$
Np(III)	R	600	cubic	bcc	3.52				2	Im3m
Pu(I)	R	21	monoclinic		6.183	4.822	10.963	101.79	16	$P2_1/m$
Pu(II)	R	190	monoclinic		9.284	10.463	7.859	92.13	34	I2/m
Pu(III)	R	235	orthorhombic		3.1587	5.7682	10.162		8	Fddd
Pu(IV)	R	320	cubic	fcc	4.6370				4	Fm3m
Pu(V)	R	500	cubic	bcc	3.638				2	Im3m
Am(I)		20	hexagonal	dhcp	3.4680		11.240		4	$P6_3/mmc$
Am(II)	R	22	cubic	fcc	4.894				4	Fm3m

Appendix B. Crystallographic data for the AB Type Compounds

Element	Pressure (kbar)	Temperature (°C)	Crystal System	Structure Type	a(Å)	b(Å)	c(Å)	Angle (°)	Z	Space Group
CsCl(I)	N	R	Cubic	CsCl	4.123				1	Pm3m
CsCl(II)	N	500	Cubic	NaCl	7.09				4	Fm3m
KBr(I)	N	R	Cubic	NaCl	6.599				4	Fm3m
KBr(II)	22		Cubic	CsCl	3.74				1	Pm3m
KCl(I)	N	R	Cubic	NaCl	6.2929				4	Fm3m
KCl(II)	22	R	Cubic	CsCl	3.58				1	Pm3m
KF(I)	N	R	Cubic	NaCl	5.344				4	Fm3m
KF(II)	35		Cubic	CsCl	3.06				1	Pm3m
KI(I)	N	R	Cubic	NaCl	6.0655				4	Fm3m
KI(II)	19	R	Cubic	CsCl	3.94				1	Pm3m
LiCl(I)	N	R	Cubic	NaCl	5.1399				4	Fm3m
NaCl(I)	N	R	Cubic	NaCl	5.6402				4	Fm3m
NaCl(II)	290	R	Cubic	CsCl	2.997				1	Pm3m
NaF(I)	N	R	Cubic	NaCl	4.628				4	Fm3m
NaI(I)	N	R	Cubic	NaCl	6.475				4	Fm3m
NH_4Br(I)	N	250	Cubic	NaCl	6.90				4	Fm3m
NH_4Br(II)	N	26	Cubic	CsCl	4.059				1	Pm3m
NH_4Br(III)	N	-73	Tetragonal		5.713		4.055		2	P4/nmm
NH_4Br(IV)	N	-170	*							
NH_4Cl(I)	N	250	Cubic	NaCl	6.52				4	Fm3m
NH_4Cl(II)	N	26	Cubic	CsCl	3.8758				1	Pm3m
NH_4Cl(III)	N	-185	Cubic		3.8200				1	P43m
NH_4F(I)	N	23	Hexagonal	Wurtzite	4.4385		7.1635		2	$P6_3mc$
NH_4F(II)	4	23	Tetragonal		10.2		3.37		8	
NH_4F(III)	11.5	23								
NH_4F(IV)	4	178	Cubic	NaCl	5.77				4	Fm3m
NH_4I(I)	N	R	Cubic	NaCl	7.259				4	Fm3m
NH_4I(II)	N	-17	Cubic	CsCl	4.38				1	Pm3m
NH_4I(III)	N	-100	Tetragonal		6.18		4.37		2	P4/nmm
NH_4I(IV)	10	-100	*							
ND_4Br(I)	N	-30	Cubic	CsCl	4.034				1	Pm3m
ND_4Br(II)	N	-71.5	Tetragonal		5.713		4.055		2	P4/nmm
ND_4Br(III)	N	-140	Cubic	4.010					1	P43m
ND_4F(I)	N	23	Hexagonal	Wurtzite	4.4378		7.1635		2	$P6_3mc$
ND_4F(II)	4	23	Tetragonal		10.2		3.37		8	
RbBr(I)	N	R	Cubic	NaCl	6.868				4	Fm3m

Appendix B. Crystallographic data for the AB Type Compounds

Element	Pressure (kbar)	Temperature (°C)	Crystal System	Structure Type	a(Å)	b(Å)	c(Å)	Angle (°)	Z	Space Group
RbBr(II)	5	R	Cubic	CsCl	4.09				1	Pm3m
RbCl(I)	N	R	Cubic	NaCl	6.590				4	Fm3m
RbCl(II)	5	R	Cubic	CsCl	3.91				1	Pm3m
RbF(I)	N	R	Cubic	NaCl	5.64				4	Fm3m
RbF(II)	5	R	Cubic	CsCl	3.29				1	Pm3m
RbI(I)	N	R	Cubic	NaCl	7.34				4	Fm3m
TlBr	N	R	Cubic	CsCl	3.838				1	Pm3m
TlCl	N	R	Cubic	CsCl	3.9846				1	Pm3m
TlF(I)	N	82	Tetragonal	Distorted NaCl	3.771	6.115			2	I4/mmm
TlF(II)	N	R	Orthorhombic		5.180	5.495	6.080		4	Fmmm
TlF(III)	12	R	*							
TlI(I)	N	R	Orthorhombic		5.24	4.57	12.92		4	Cmcm
TlI(II)	5	R	Cubic	CsCl	4.10				1	Pm3m
AgCN(I)	N	R	Rhombohedral		3.99		5.26		3	R3c
AgCN(II)	12	R	*							
AuCN(I)	N	25	Hexagonal		3.40		5.09		1	P6mm
AuCN(II)			*							
CsCN(I)	N	20	Cubic	CsCl	4.29				1	Pm3m
CsCN(II)	N	-80	Rhombohedral		5.79		7.78		3	R3m
KCN(I)	N	25	Cubic	NaCl	6.527				4	Fm3m
KCN(III)	30	100	Cubic	CsCl	3.808				1	Pm3m
KCN(IV)	25	23	Monoclinic		5.530	5.209	3.743	95	2	Cm
KCN(V)	N	-80	Monoclinic		8.04	4.53	7.47	109.4	4	Cc
KSCN(I)	N	160	Tetragonal		6.70		7.73		4	I4/mcm
KSCN(II)	N	20	Orthorhombic		6.66	7.58	6.635		4	Pcmb
KSCN(III)	20	450	*							
KSCN(IV)	28	500	*							
NaCN(I)	N	20	Cubic	NaCl	5.88				4	Fm3m
NaCN(II)	N	-10	Orthorhombic		4.71	5.61	3.74		2	Immm
NaSCN	N	R	Orthorhombic		13.45	4.10	5.66		8	Pnma or $Pn2_1a$
RbCN(I)	N	R	Cubic		6.834				4	$P2_13$
RbCN(II)	N	-182	Monoclinic		6.66	4.87	4.77	94.3	2	
PtB	N	R	Hexagonal		3.36		4.06		1	$P6_3/mmc$
MoC(I)	N	R	Hexagonal		2.898		2.809		1	

Appendix B, Crystallographic data for the AB Type Compounds

Element	Pressure (kbar)	Temperature (°C)	Crystal System	Structure Type	a(Å)	b(Å)	c(Å)	Angle (°)	Z	Space Group
MoC(I)	N	R	Hexagonal		3.00		14.58		6	
MoC(I)	N	R	Hexagonal		2.932		10.97		4	$P6_3/mmc$
MoC(II)	N	R	Cubic	NaCl	4.27				4	Fm3m
ReC	60	800	Hexagonal	γ-MoC	2.840		9.85		4	$P6_3/mmc$
BN(I)	N	35	Hexagonal	BN	2.502		6.661		6	$P6_3/mmc$
BN(II)	N	R	Cubic	ZnS	3.62				4	F43m
BN(III)	N	R	Hexagonal	Wurtzite	2.55		4.20		2	$P6_3mc$
BaO(I)	N	R	Cubic	NaCl	5.542				4	Fm3m
BaO(II)	100	R	Tetragonal		4.549		3.606		2	
BaO(III)	180	R	Tetragonal	PbO	4.397		3.196		2	P4/mmm
EuO(I)	N	R	Cubic	NaCl	5.143				4	Fm3m
EuO(II)	310	R	Cubic	NaCl	4.743				4	Fm3m
EuO(III)	400	R	Cubic	CsCl	2.92				1	Pm3m
FeO	N	R	Cubic	NaCl	4.312				4	Fm3m
SnO(I)	N	R	Tetragonal	PbO	3.796		4.816		2	P4/mmm
SnO(II)	60	R	Hexagonal	Wurtzite	3.42		5.62		2	$P6_3mc$
SrO(I)	N	R	Cubic	NaCl	5.142				4	Fm3m
SrO(II)	175	R	Tetragonal		4.912		4.949		4	
ZnO(I)	N	R	Hexagonal	Wurtzite	3.242		5.176		2	$P6_3mc$
ZnO(II)	N	R	Cubic	NaCl	4.28				4	Fm3m
NaOH(II)	N	R	Orthorhombic	TlI	3.397	11.32	3.397		4	Amam
NaOH(I)	N	300	Monoclinic		3.434	3.428	6.068	109.8	2	$P2_1/m$
NaOH(III)			*							
NaOH(IV)			*							
NaOH(V)			*							
BP	N	R	Cubic	ZnS	4.54				4	F43m
GaP(I)	N	1[illegible]	Cubic	ZnS	5.447				4	F43m
GaP(II)	220	R	*							
GeP(I)	N	R	Tetragonal		3.544		5.581		2	I4mm
InP(I)	N	[illegible]	Cubic	ZnS	5.868				4	F43m
InP(II)	N	[illegible]	Cubic	NaCl	5.71				4	Fm3m
SiP(I)	N	[illegible]	Orthorhombic		6.90	9.40	7.68		12	
SiP(II)	N	R	Cubic	ZnS	5.241				4	F43m
SnP(I)	N	R	Hexagonal		8.78		5.98		8	
SnP(II)	N	R	Tetragonal		3.831		5.963		2	
SnP(III)	N	R	Cubic	NaCl	5.536				4	Fm3m
CdS(I)	N	R	Hexagonal	Wurtzite	4.134		6.713		2	$P6_3mc$

Appendix B. Crystallographic data for the AB Type Compounds

Element	Pressure (kbar)	Temperature (°C)	Crystal System	Structure Type	a(Å)	b(Å)	c(Å)	Angle (°)	Z	Space Group
CdS(I)	N	R	Cubic	ZnS	5.835				4	F43m
CdS(II)	77	R	Cubic	NaCl	5.27				4	Fm3m
FeS(I)	N	R	Hexagonal	Triolite	5.946		11.72		12	P62c
FeS(II)	100	22	**							
FeS(III)	N	R	Hexagonal	NiAs	3.426		5.687		2	$P6_3/mmc$
HgS(I)	N	R	Cubic	ZnS	5.858				4	F43m
HgS(II)		R	Hexagonal	HgS	4.149		9.149		3	Pe_121
NiS(I)	N	R	Hexagonal	NiAs	3.428		5.340		2	$P6_3/mmc$
NiS(II)	20	R	Hexagonal	Wurtzite	**				2	$P6_3mc$
SmS(I)	N	R	Cubic	NaCl	5.863				4	Fm3m
SmS(II)	6.5	R	Cubic	NaCl'	5.70				4	Fm3m
ZnS(I)	N	R	Cubic	ZnS	5.406				4	F43,
ZnS(II)	N	R	Hexagonal	Wurtzite	3.811		6.234		2	$P6_3mc$
ZnS(III)	190	R	*							
ZnS(IV)	420	R	*							
BAs	N	R	Cubic	ZnS	4.777				4	F43m
GaAs(I)	N	R	Cubic	ZnS	5.654				4	F43m
GaAs(II)	190	R	*							
GaAs(III)	200	R	*							
GeAs(I)	N	R	Tetragonal		3.715		5.832		2	
InAs(I)	N	R	Cubic	ZnS	6.036				4	F43m
InAs(II)	100	R	Cubic	NaCl	5.514				4	Fm3m
MnAs(I)	N	R	Hexagonal	NiAs	3.710		5.691		2	$P6_3/mmc$
MnAs(II)	N	50	Orthorhombic	MnP	6.39	5.64	3.63		4	Pbnm
AlSb(I)	N	R	Cubic	ZnS	5.985				4	F43m
AlSb(II)	120	R	Tetragonal	β-Sn	5.375		5.911		2	$I4_1/amd$
GaSb(I)	N	R	Cubic	ZnS	6.135				4	F43m
GaSb(II)	90	R	Tetragonal	β-Sn	5.348		2.973		2	$I4_1/amd$
	1 atm.	90 K			5.47		3.06		2	
InSb(I)	N	R	Cubic	ZnS	6.474				4	F43m
InSb(II)	26	R	Tetragonal	β-Sn	5.862		3.105		2	$I4_1/amd$
InSb(III)	125	R	Hexagonal		6.099		5.708		2	
InSb(IV)	70	R	Orthorhombic		2.921	5.56	3.06		1	
CdSe(I)	N	R	Hexagonal	Wurtzite	4.30		6.02		2	$P6_3mc$
CdSe(II)	32	R	Cubic	NaCl	5.49				4	Fm3m
HgSe(I)	N	R	Cubic	ZnS	6.09				4	F43m
HgSe(II)	15	R	Hexagonal	HgS	4.32		9.62		3	$P3_121$

Appendix B. Crystallographic data for the AB Type Compounds

Element	Pressure (kbar)	Temperature (°C)	Crystal System	Structure Type	a(Å)	b(Å)	c(Å)	Angle (°)	Z	Space Group
InSe(I)	N	R	Hexagonal		4.05		16.93		4	$P6_3/mmc$
InSe(II)	40	520	*							
PbSe(I)	N	R	Cubic	NaCl	6.122				4	Fm3m
PbSe(II)	42	R	Orthorhombic		11.71	4.36	4.42		4	Pnma
CdTe(I)	N	R	Cubic	ZnS	6.478				4	F43m
CdTe(II)	30	R	Cubic	NaCl	5.92				4	Fm3m
CdTe(III)	100	R	Tetragonal		5.86		2.94		2	$I4_1/amd$
CdTe(III)	200	R	Tetragonal		5.62		2.96		2	$I4_1/amd$
EuTe(I)	N	R	Cubic	NaCl	6.591				4	Fm3m
EuTe(II)	100	R	Cubic	CsCl	3.755				1	Pm3m
GeTe(I)	N	R	Rhombohedral	As	4.171		10.661		3	
GeTe(II)	40	R	Cubic	NaCl	5.80				4	Fm3m
GeTe(II)	N	60	Cubic	NaCl	5.998				4	Fm3m
HgTe(I)	N	R	Cubic	ZnS	6.37				4	F43m
HgTe(II)	20	R	Hexagonal	HgS	4.51		10.13		3	$P3_121$
InTe(I)	N	R	Tetragonal	TlSe	8.437		7.139		8	I4/mcm
InTe(II)	30	R	Cubic	NaCl	6.160				4	Fm3m
InTe(II')	N	R	Tetragonal		6.06		6.55		4	
MnTe(I)	N	R	Hexagonal		4.148		6.710		2	$P6_3/mmc$
MnTe(II)		R	Cubic		6.003				4	Fm3m
PbTe(I)	N	R	Cubic	NaCl	6.36				4	Fm3m
PbTe(II)	43	R	Orthorhombic		11.61	4.00	4.39		4	Pnma
PrTe(I)	N	R	Cubic	NaCl	6.315				4	Fm3m
PrTe(II)	90	R	Cubic	CsCl	3.761				1	Pm3m
SmTe(I)	N	R	Cubic	NaCl	6.595				4	Fm3m
SmTe(II)	110	R	Cubic	CsCl	3.656				1	Pm3m
SnTe(I)	N	R	Cubic	NaCl	6.2956				4	Fm3m
SnTe(II)	20	R	Orthorhombic		11.59	4.37	4.48		4	Pnma
YbTe(I)	N	R	Cubic	NaCl	6.353				4	Fm3m
ZnTe(I)	N	R	Cubic	ZnS	6.101				4	F43m
ZnTe(II)			*							

Appendix B. Crystallographic data for the AB Type Compounds

Element	Pressure (kbar)	Temperature (°C)	Crystal System	Structure Type	a(Å)	b(Å)	c(Å)	Angle (°)	Z	Space Group
AgBr(I)	N	R	Cubic	NaCl	5.7745				4	Fm3m
AgBr(II)	70	R	Hexagonal	HgS	4.0		7.15		3	$P3_121$
AgCl(I)	N	R	Cubic	NaCl	5.547				4	Fm3m
AgCl(II)	74	R	Hexagonal	B9 (HgS)	4.06		7.02		3	$P3_121$
AgCl(II)	74	R	Orthrohombic		6.90	5.08	4.05		4	Pnma
AgF(I)	N	R	Cubic	NaCl	4.932				4	Fm3m
AgF(II)	25	R	Cubic	CsCl	2.945				1	Pm3m
AgF(III)		R	Hexagonal		3.246		6.226		2	
AgI(I)	N	145.8	Cubic	5.044					2	Im3m
AgI(II)	N	R	Hexagonal	Wurtzite	4.58		7.494		2	$P6_3mc$
AgI(II')	N	R	Cubic	ZnS	6.486				4	F43m
AgI(III)	4	R	Cubic	NaCl	6.07				4	Fm3m
AgI(IV)	3	R	Tetragonal		4.58		6.00		2	
AgI(V)	100	R	Tetragonal		4.615		5.020		4	
CsF(I)	N	R	Cubic	NaCl	6.008				4	Fm3m
CsF(II)	48	R	Cubic	CsCl	3.39				1	Pm3m
CuBr(I)	N	480	Cubic	αAgI	4.56				2	Im3m
CuBr(II)	N	430	Hexagonal	Wurtzite	4.06		6.66		2	$P6_3mc$
CuBr(III)	N	R	Cubic	ZnS	5.691				4	F43m
CuBr(IV)	50	R	*							
CuBr(V)	55	R	Tetragonal		5.40		4.75		4	
CuBr(VI)	75	R	Cubic	NaCl	5.14				4	Fm3m
CuCl(I)	N	410	Hexagonal	Wurtzite	3.91		6.42		2	$P6_3mc$
CuCl(II)	N	25	Cubic	ZnS	5.416				4	F43m
CuCl(III)	10	450	*							
CuCl(IV)	55	R	Tetragonal		5.21		4.61		4	
CuCl(V)	70	R	Cubic	NaCl	4.93				4	Fm3m
CuI(I)	N	440	Cubic	Disordered	6.14				4	F43m
CuI(II)	N	390	Hexagonal	Wurtzite	4.31		7.09		2	$P6_3mc$
CuI(III)	N	R	Cubic	ZnS	6.059				4	F43m
CuI(IV)	16	R	Rhombohedral		4.164		20.41		6	
CuI(V)	65	R	Tetragonal	Red PbO	4.02		5.70		2	P4/nmm
CuI(VI')	77	120	Cubic	S. C.	5.627				4	
CuI(VII)	20	800	*							
CuI(VIII)	120	R	Cubic	NaCl	5.15				4	Fm3m

DISCUSSION (Jan. 10 - AM Session)

T. B. Massalski, chairman - I would like to invite any further discussion on the subject of phase diagram compilations for which there exists a great need, and for which agencies should give financial assistance to projects carried out by qualified users.

Barry Rosof - I have one observation about the compilation, "Phase Diagrams for Ceramists". I have the feeling that metallurgists should look a little bit more carefully after their phase diagram needs in areas other than metallic systems. That is, perhaps we need more metallurgical input into the areas such as slags, oxides, oxichlorides, etc., that some of Dr. Roth's respondents alluded to. I'm sure that several of the diagrams in the areas that "Phase Diagrams for Ceramists" does not do a complete job on, are in areas of great interest to metallurgists.

P. Gallagher - I am a little concerned with Dr. Roth's removal of the vapor pressure on the phase diagram, treating it more as a physical property. I find it difficult to divorce vapor pressure from the study of phase diagrams. I would be interested to know whether other people felt the same way.

L. Kaufman - I believe that the integration of the vapor pressure and other thermochemistry, as it were, is an integral part of the phase diagram picture. I think only with the coupling of these two types of information that we begin to unscramble the different types of equilibria that can be observed experimentally and make some sense for example, out of the copper-lead system. Although, the job may be a lot more complicated, I think that's what will evolve over the next period of 5 to 10 years as an activity that will help bring some order to this field. I think it will be a costly activity, but I think the means to fund such efforts in this country and overseas will be found, because the needs for such information is really quite acute.

W. White - I think we have identified an interesting "gap problem" this morning, which is actually related to the band gap. If you have materials with band gaps 2 1/2 to 3 electron volts, there're called ceramics, and Dr. Roth described quite a wide range of such materials for which compilations exist. If the gap is zero or small, it is a metal or a semiconductor and several groups are working on that. In between, from about 0.5 to 2.5 electron volts, is a very large range of particular chalcogenide and pnictide systems, such as sulfides and selenides, for which, as near as I can tell, there are no systematic compilations at all. Most of these, incidentally, are P-T-X sytems and not simply T-X type systems.

L. Bennett - I'd like to respond to that. I do agree exactly with what you've said. I want to emphasize that one of the reasons for the organization of this meeting as a joint organization between Dr. Roth's group in ceramics and our own for metallic system, was to be sure that this in between part does not fall into the cracks. There will be some cases of overlap, but that is better than exclusion. The problem of gaps and overlap is something we with continue to pay attention to, and we plan to work together on that aspect.

R. Roth - I'll take this opportunity to answer some of these questions. First of all vapor pressure: I have worked for 25 years with the condensed phase rule and I tend to ignore not only vapor pressure but also partial pressures. However, I am just one voice in quite a large compilation effort. I think that any published phase equilibrium diagram in which vapor pressure is taken into account experimentally and properly will be included in "Phase Diagram for Ceramists". The other question is that which Bill White raised. The new editions of "Phase Diagrams for Ceramists" will make a chance to include all sulfides and all nitrides and oxinitrides in mixed materials of the Sialon type. We made a judgment based largely on consultation with Dr. Thurmond not to include semiconductors. So nobody is covering selenides and tellurides of the semiconducting type.

A. Navrotsky - In addition to interrelation between phase diagrams and thermodynamic data (and I agree with Larry Kaufman's comments), we also have to integrate phase diagrams, thermodynamic data and crystal structures. It's very important to characterize the phases that are being formed and realize what is going on in a structural scale and to let this tell us what is possible or impossible in terms of phase relations and what is sensible or nonsense in terms of thermodynamic parameters and thermodynamic equations we use.

National Bureau of Standards SP-496, Applications of Phase Diagrams in Metallurgy and Ceramics
Proceedings of Workshop held at NBS, Gaithersburg, Md., January 10-12, 1977

PHASE DIAGRAM INFORMATION FROM COMPUTER BANKS

BY

I. ANSARA

LABORATOIRE DE THERMODYNAMIQUE ET PHYSICO-CHIMIE METALLURGIQUES
ASSOCIE AU C.N.R.S., E.N.S.E.E.G., DOMAINE UNIVERSITAIRE, B.P. 44,
38401 - ST. MARTIN D'HERES, FRANCE.

Phase diagrams are usually determined by classical methods such as thermal analysis, N.M.R., and equilibrium techniques for relatively small composition and temperature ranges ; rather fewer are calculated from the thermodynamic properties because of the lack of experimental determinations. Although these two methods of establishing phase diagrams have been carried out independently, they can be reconcilied through thermodynamic principles to ensure a complete and consistent description of the system.

The experimental data are usually presented in the literature in the form of tables, equations or graphs, the analysis of which data is always tedious. When partial quantities of the thermodynamic properties relative to multicomponent solutions are determined, different methods are used to integrate the Gibbs-Duhem equation, all of them requiring limiting binary data which are not always critically analyzed.

A feature which is rarely achieved is the consistency between the thermodynamic properties of a solution and phase equilibria. This is due not only to the lack of complete information for both of these properties but also to the complexity of the problem.

And yet the need to develop computer techniques for phase diagram calculation and storage arises from a number of major practical considerations. Firstly, since the volume of in-

formation is very large both for phase diagrams and thermodynamic properties, computers provide a simple means of handling the data. Secondly, and certainly the most expensive of all, it is necessary to achieve consistency between the phase diagram and thermodynamic data, which requires extensive computation. Thirdly, modern technology requires that information be provided rapidly on the equilibrium phase stability of the materials that it uses. The computer enables such data to be calculated for the operating conditions of interest and to be presented in a comprehensive manner to the user.

Thus the establishment of a data bank for phase diagrams necessarily implies computer programs for the numerical treatment of raw data in order to perform a critical assessment. Kirchner(1) has used a computerized mathematical optimization procedure to analyze the experimental tie-lines for the Fe-Cr-Mn system in terms of a thermodynamic model. Zimmermann (2) has developped a method based on the least squares technique in order to facilitate critical assessment for binary and ternary systems, and an account of this work is described in these proceedings. Most of these programs should be designed so as to retrieve the thermodynamic properties of the system or to be used to predict them.

Bennett (3) has recently listed both existing phase diagram data compilations and the persons and centers (4) carrying out continuing phase data programs to which should be added the monographs co-ordinated by the International Atomic Energy Agency in Vienna, the Incra series and the individual contributions of the Calphad Members.

But to my knowledge, the only organized centers for the computation of phase diagrams from thermodynamic properties are those of the S.G.T.E. (Scientific Group of Thermodynamicists, Europe), and ManLabs (U.S.A.) Such calculations are carried out in the U.S.S.R. but emphasis is put on the mathematical representation of the phase "Surfaces" or Volumes" for multicomponent systems.

The organization of a data bank relative to the thermodynamic properties and the calculation of phase diagrams is summarized in Table I. The experimental information for the binary and multicomponent systems is critically analyzed. The equilibrium conditions for phase stability involved therein can be analyzed either by considering the equality of the partial Gibbs energies of the different components in the different phases or by minimizing the Gibbs energy of the system. In the latter case, the Gibbs energy of the multiphase system is equal to :

$$\Delta G = \sum_{j=1}^{j=\phi} P_j \left(\Delta G^{(j)} - \sum_{i=1}^{i=m} x_i \Delta G_i^{(j\rightarrow\phi)}\right)$$

$$\text{with } \Delta G^{(j)} = G^{(j)} - \sum_{k=1}^{k=m} x_k {}^{\circ}G_k^{(j)}$$

$$\text{and } \sum_{j=1}^{j=\phi} P_j = 1$$

where $\Delta G^{(j)}$ is the Gibbs energy of phase j referred to its pure elements in the same structural state and $\Delta G_i^{(j\rightarrow\phi)}$ the free energy difference due to the transformation of component i from the structural state j to that of ϕ. The number of variables, which are the composition at equilibrium for a given temperature, vary from 1 to (m-1), as is seen by considering the constraints imposed by the generalized lever rule. For a ternary system, that would correspond from the simplest case of a ternary phase in equilibrium between ternary phases.

From a practical point of view and especially for higher order systems, the use of integral quantities is preferable to that of the partial quantities because it reduces the number of mathematical operations. Numerical methods which do not require the calculation of derivatives such as the simplex method described by Nelder (6) are also preferable. This method can be established for nunknown compositions, where n is a variable parameter. After an iterative process, evaluated data are obtained, which can be stored and retrieved for various applications. In that framework, it is also possible to evaluate the thermodynamic properties from phase diagrams according to methods described by Wagner (7),

Hiskes (8,9,10), Rudman (11), Kaufman (12,13), Chiotti (14), Vieland (15) and Sundquist (16).

When the thermodynamic properties of a multicomponent system are not available, they can be calculated from equations which are derived from statistical thermodynamics (18 to 31) or are semi empirical (32 to 40) but always imply the knowledge of the limiting binary data. These equations have been reviewed elsewhere (17).

Apart from the quasi-chemical treatment which needs a resolution of a set of equations to derive the thermodynamic properties of mixing, all the other equations which are used to describe an excess property (for example the heat of mixing ΔH) can be written in the general form :

$$\Delta H = \sum_{i=1}^{i=n-1} \sum_{j=i+1}^{j=n} \alpha_{ij} \left(\Delta H_{ij}(x_i, x_j)\right) + \beta \prod_{k=1}^{k=n} x_k \sum_{i=1}^{i=n-1} \sum_{j=i+1}^{j=n} \left(\Delta \bar{H}^{\infty}_{i(j)} + \Delta \bar{H}^{\infty}_{j(i)}\right)$$

where ΔH_{ij} represents the heat of mixing of the binary system ij, $\Delta \bar{H}^{\infty}_{i(j)}$ the partial heat of mixing of component i in the concentrated solution of j, α_{ij} and β are parameters which vary according to the model or equation which is used. Table II presents the relationship between these quantities for seven equations. A computer subroutine can automatically establish the dependence between these quantities when the name of the model is given ; the analytical form of the equations describing the thermodynamic properties of the binary system can be of any type, generally related to the structure of the data file in the computer bank.

CALCULATION OF BINARY PHASE DIAGRAMS FROM THERMODYNAMIC PROPERTIES

Let us consider a system which exhibits different solution phases and intermetallic compounds like the Ni-Ti for example. Phase boundaries have been calculated by various numerical methods (Newton-Raphson or graphical methods) (9 to 12, 41, 42, 43) by considering all the possible two phase systems most of which are metastable with respect to the equilibrium phase diagram. When all the different possibilities have been assembled, the stable system can be

derived by inspection.

The other alternative is to design a computer program (44) which calculates the Gibbs energies of formation of all the different phases over the entire composition range and only those portions which have the lowest values are retained. If such curves intersect, there must be a common tangent to the two curves, whose point of contact lies on either side of the point of intersection. Thus the Gibbs energy is minimized at the point of intersection by any mathematical procedure which determines a common tangent. The phase diagram is then determined by a temperature scan. A metastable diagram can be obtained by deleting from the file the data corresponding to any given stable phase.

This procedure is similar to the method employed manually and has the advantage of considering all the phases simultaneously and of using integral quantities which may be represented either by polynomials or calculated by interpolation from tables using a spline function. In that case, a simplex method for minimization is preferable. Nevertheless, such a method can only be utilized if the thermodynamic properties of the different phases are given over the complete composition range ; thus the description of the hypothetical phases have to be included. For this, the lattice stabilities or the Gibbs energies of transformation of the pure elements have to be known. Kaufman (12) has derived these quantities for all the transition metals plus a certain number of others, and Michaels (45) has shown that Kaufman's approach could be extended to metals of group 1 to 3 and Lanthanides elements.

Similar procedures have been used by Hillert to calculate the Fe-S (46), Fe-N (47) and Mn-S (48) systems using a regular solution model. Kaestle (49) has also used simple models to calculate the binary phase diagram T=F(x) of the FeO-X (X=MgO, MnO, Al_2O_3, P_2O_5), CaO-Y (Y=MnO, MgO, Si_1O_2, Al_2O_3, P_2O_5), Si_1O_2-Z (Z=MnO,MgO, Al_2O_3), MnO-MgO,MnO-Al_2O_3 systems.

Mathematical procedures can be incorporated into the organization of a bank so as to represent the phase boundaries by analytical equations. The coefficients which are then obtained are stored in a reduced manner. Figures 1 and 2 represent the phase diagrams of the Al-Mn and Ni-Ti systems published by Hansen (50) and which have been retrieved from the data bank on a graph plotter.

When computer facilities are available, the results obtained for a particular system by these two methods can be compared on a graphical or visual display. Figure 2 illustrates an on-line calculation for which the $T=F(x)$ curve is static on the screen superimposed on the calculated phase diagram, for which the user can adjust the underlying thermodynamic data.

CALCULATION OF TERNARY PHASE DIAGRAM FROM THERMODYNAMIC PROPERTIES

Extensive work has been carried out on phase diagram calculation from thermodynamic properties for ternary systems (51 to 61). Information is required not only on phase boundaries but also on tie-lines, locus of univariant points (e.g. eutectic valleys) in a ternary system, crystallization paths, etc. All these problems are in essence the same and can be resolved by minor changes in computer programs.

Different strategies of computing phase boundaries can then be considered. For example, it seems easier to calculate a univariant line by considering the three-phase equilibrium rather than to determine it by intersection of two liquidus lines at a given temperature. The number of unknowns to be calculated does not lenghten the calculation. Figure 3 shows the the eutectic valley existing in the Ga-Sn-Zn calculated by this manner.

A similar strategy would be the most appropriate in quaternary and higher order systems. For example, once a three or four phase domain has been located at one temperature in such systems, it would be wise starting the calculation at other temperatures by determining the boundaries of this same region.

This strategy can be applied to the determination of the evolution of the composition of the liquid phase when a solid solution precipitates. For certain topologies of liquidus and solidus surfaces, the condition to precipitate a solid solution of fixed composition results from a straightforward calculation. Slightly different is the case where an imposed fraction of the liquid precipitates. In that case, a composition gradient in the solid may appear. Nevertheless optimum conditions can be defined. These two cases have been applied to the Ga-In-Sb system (63). Figures 4 and 5 show that below a certain temperature, a solid solution of fixed composition is obtained in both cases.

One has to be aware that if by using various models the phase boundaries differ only slightly, nevertheless the tie-line may differ appreciably. Figure 6 shows how the molar fraction of GaSb in the quasi-binary section $GaSb_x$-$InSb_{(1-x)}$ varies with respect to the molar fraction of gallium in the liquid solution when the regular solution (64,65) is used or when an "extended" Toop equation (54) is adjusted to agree with experimental ternary values.

The main problem in determining isothermal sections is the prediction of ternary intermetallic compounds or a limited intrusion of compound from the binary system into the ternary, for example the ternary sigma phase in the Fe-Cr-Ni system. Thus, the Gibbs energy of formation of the hypothetical sigma Ni-Cr phase must be estimated. Kaufman (60) and Rudy (66) have considered many of such cases.

Considerable work is being carried out on the use of the lattice simplex method (67 to 72). This technique was primarily used to establish a composition/property diagram in order to reduce lengthy experiments. The essence of such method, proposed by Scheffe (73) and analyzed by Gorman (74), consists in constructing mathematical models, usually polynomials, which correlate the property and composition of a test alloys. To calculate the coefficients of the equations, the properties are measured not at random, but according to a definite distribution within a simple lattice. A

possible selection of composition points for measuring responses is one that gives a uniform distribution of points over all possible mixtures of the components. Such a distribution is referred to a as a quadratic, cubic or quartic lattice, depending on the number of points. For example, a cubic model in a ternary system shown in figure 7 describing the property y would be :

$$y=\beta_1 x_1+\beta_2 x_2+\beta_3 x_3+\beta_{12} x_1 x_2+\beta_{13} x_1 x_3+\beta_{23} x_2 x_3+\gamma_{12} x_1 x_2 (x_1-x_2)$$
$$+\gamma_{13} x_1 x_3 (x_1-x_3)+\gamma_{23} x_2 x_3 (x_2-x_3)+\beta_{123} x_1 x_2 x_3$$

The coefficients β_i, β_{ij}, γ_{ij} and β_{123} are related to the value of the property for a lattice point which may be a single determination or the average of several determinations. The solidus volume of the Nb-W-Ti-Zr was calculated by this manner by Zakharov (72) in the niobium rich corner.

CONCLUSION

Since the first attempts at determining the miscibility gap and the spinodal surface in the Cd-Pb-Sn-Zn system (75,76), not much work has been performed on quaternary phase diagrams. If the systems involving carbon, oxygen and nitrogen (77 to 81) are excluded, the only ones studied are those of the III-V or II-VI elements (82 to 86) and a system involving low melting elements (87).

The development of an a priori calculation for reciprocal systems (88,89,90), metal gas equilibria (91 to 97), slags, systems of nuclear interest, chemical vapor deposition, geochemical applications is becoming increasingly important. Thus it is important that a data bank be as complete as possible and its application adapted to the user's needs. This is not the case at present. Existing data banks relative to the thermodynamic properties are limited to inorganic substances and alloy systems, and for many

of them, it is not yet possible to calculate the phase diagram over the complete composition and wide temperature ranges. The data are scattered in the literature and a considerable task still remains to be done.

The thermodynamic description of solution phases, stable or metastable in the complete composition range or enthalpies of formation for intermetallic compounds are essential when higher order systems are to be investigated, and more and more theoretical work of increasing precision on the phase stabilities of elements and alloys (98 to 103) in particular is being published.

If this contribution is limited mainly to metallic systems, it is satisfying to see the number of contributions which are presented in these proceedings and which may bring considerable progress in the prediction, assessment and compilation of phase diagrams of systems other than those involving metals.

BIBLIOGRAPHY

(1) G. Kirchner and B. Uhrenius, Acta Met., 1974, 22, 523
(2) B. Zimmermann, Dr. Rer. Nat. Thesis, Univ. Stuttgart, W.Germany, 1976.
(3) L.H. Bennett, D.J. Kahan and G.C. Carter, Mat. Sci. Eng., 1976, 24, 1.
(4) L.H. Bennett, G.C. Carter and D.J. Kahan, Proc. Vth Inter. Codata Conf., 1976, Boulder (U.S.A.).
(5) From N.P.L. (U.K.), A.E.R.E. (Harwell, U.K.), Vrije Univ. (Brussel Belgium), Rhein-Nest T.H. (Aachen, W. Gernamy), I.R.S.I.D. (Maiziere,France), Thermodata and L.T.P.C.M. - E.N.S.E.E.G. (St Martin d'Hères, France)
(6) J.A. Nelder and R. Mead, Comp. J., 1965, 7, 308.
(7) C. Wagner, Acta Met., 1958, 6, 309.
(8) R. Hiskes and W.A. Tiller, Mat. Sci. Eng., 1967/68, 2, 320.
(9) R. Hiskes and W.A. Tiller, Met. Sci. Eng., 1969, 4, 163.
(10) R. Hiskes and W.A. Tiller, Mat. Sci. Eng., 1969, 4, 173.
(11) P.S. Rudman, Adv. in Materials Research, Vol. IV, Inter-Science Publishers, N.Y. 1969.
(12) L. Kaufman and H. Bernstein, "Computer Calculations of Phase Diagrams", Academic Press, N.Y. (1970).
(13) L. Kaufman, "Metallurgical Chemistry", Proc. Symp. 1971, Ed. O. Kubaschewski (HMSO, London, 1972), P. 373.

(14) P. Chiotti, M.F. Simmons and Kateley J.A., "Nuclear Metallurgy", Vol. 15, Reprocessing of Nuclear Fuels, Met. Soc. Aime., Conf. 690801, CFSTI, NBS, Spring. Virginia, 1969.
(15) L.J. Vieland, Acta Met., 1963, 11, 137.
(16) B.E. Sundquist, Trans. Met. Soc. Aime., 1966, 236, 1111.
(17) I. Ansara, "Metallurgical Chemistry", Proc. Symp., 1971, Ed. O. Kubaschewski, (HMSO, London, 1972), p. 403.
(18) J.H. Hildebrand, Proc.Nat. Acad. Sci., Wash., 1927, 13, 167.
(19) J.H. Hildebrand, J. Amer. Chem. Soc. , 1929, 51, 66.
(20) E.A. Guggenheim, "Mixtures", Clarendon Press, Oxford, 1952.
(21) J.C. Mathieu, F. Durand and E. Bonnier, J. Chim. Phys., 1965, 11-12, 1289.
(22) J.C. Mathieu, F. Durand and E. Bonnier, J. Chim. Phys., 1965, 11-12, 1297.
(23) P. Hicter, J.C. Mathieu, Durand F. and E. Bonnier, J. Chim. Phys., 1967, 2, 261.
(24) C.H.P. Lupis, Ph.D. Thesis, M.I.T., Boston, 1965.
(25) C.H.P. Lupis and J.F. Elliott, Acta Met., 1967, 15, 265.
(26) B. Brion, J.C. Mathieu, P. Hicter and P. Desré, J. Chim. Phys., 1969, 66, 1238.
(27) B. Brion, J.C. Mathieu and P. Desré, J. Chim. Phys., 1970, 67, 1745.
(28) H.K. Hardy, Acta Met., 1953, 1, 202.
(29) N.A. Gokcen and E.T. Chang, "Metallurgical Chemistry", Proc. Symp. 1971, Ed. O. Kubaschewski (HMSO, London, 1972), p. 219.
(30) F. Durand, These Doctorat ès Sci. Phys., Grenoble, 1962.
(31) E. Bonnier, F. Durand and P.J. Laurent, C.R. Acad. Sci., 1962, 254, 107.
(32) K. Wohl, Trans. Amer. Inst. Chem. Eng., 1946, 42, 215.
(33) J.J. Van Larr, Z. Phys. Chem., 1913, 599.
(34) E. Bonnier and R. Caboz, C.R. Acad. Sci. 1960, 250, 527.
(35) G.W. Toop, Trans. Met. Soc. Aime., 1965, 233, 850.
(36) F. Kohler, Monatsch. Chemie, 1960, 91, 738.
(37) N.J. Olson and G.W. Toop, Trans. Met. Soc. Aime, 1966, 236, 590.
(38) H. Kehiaian, Bull. Soc. Pol. Sci. 1966, 14, 153.
(39) C. Chatillon-Colinet, I. Ansara, P. Desré and E. Bonnier, Rev. Int. Htes. Temp. et Réfract., 1969, 6, 227.
(40) C. Colinet, D.E.S. Fac. Sci., Univ. Grenoble, France, 1967.
(41) O. Kubaschewski and T.G. Chart, J. Inst. Metals, 1964, 93, 329.
(42) H. Gaye and C.H.P. Lupis, Scripta Met., 1970, 4, 685.
(43) H.Gaye and C.H.P. Lupis, Met. Trans., 1975, 6A, 1049.
(44) I. Ansara, J.N. Barbier and C. Bernard, Unpublished Results.
(45) K.F. Michaels, W.F. Lange III, R.Bradley and H.I.Aaronson, Met. Trans., 1975, 6A, 1843.
(46) M. Hillert and L. -I. Staffansson, Met. Trans., 1975, 6B, 3, 37.
(47) M. Hillert and M. Jarl, Met. Trans., 1975, 6A, 3, 553.
(48) L.-I. Staffansson, Met. Trans., 1976, 7B, 3, 131.
(49) C. Kaestle and K. Koch, Report "Zur Berechnung von Phasen-Diagrammen Oxidischer Mehrstoffsysteme Mit Hilfe von Mathematischen Thermodynamischen Modellen", Inst. Für Eisenhütt., Techn. Univ., Clausthal, 1976.

(50) M. Hansen and K. Anderko, "Constitution of Binary Alloys", McGraw-Hill Book Co. Inc., 1958, N.Y.
(51) S.M. Carmio and J.L. Meijering, Zeit. Für Metallkde., 1973, 64, 3, 170.
(52) M. Gaye and C.H.P. Lupis, Met. Trans. 1975, 6A, 1057.
(53) F. Ajersch, E. Hayer, J.N. Barbier and I. Ansara, Zeit. Für Metallkde., 1975, 66, 10, 624.
(54) I. Ansara, M. Gambino and J.P. Bros, J. Crystal Growth, 1976, 32, 101.
(55) P.E. Potter, J. Nucl. Mat., 1973, 47, 7.
(56) R.K. Iyengar and W.O. Philbrook, Met. Trans., 1973, 4, 2181.
(57) P.J. Spencer and J.F. Counsell, Zeit. Für Metallkde, 1973, 64, 9, 662.
(58) O. Kubaschewski and I. Barin, Pure and Appl. Chem., 1974, 38, 469.
(59) L. Kaufman and H. Nesor, Zeit. Für Metallkde, 1973, 64, 4, 249.
(60) L. Kaufman and H. Nesor, Can. Met. Quater., 1975, 14, 3, 221.
(61) L. Kaufman and H. Nesor, Met. Trans., 1974, 5, 7, Part 1 : 1617, Part 2 : 1623.
(62) L. Kaufman and H. Nesor, Met. Trans., 1975, 6A, Part 3 : 2115, Part 4 : 2123.
(63) I. Ansara, J.N. Barbier, J.C. Mathieu and B. Schaub, J. Crystal Growth, 1976, 36.
(64) G.M. Blom and T.S. Plaskett, J. Electrochem. Soc., 1971, 118, 1832.
(65) A. Joullié, R. Dedies, J. Chevrier and F. Bougnot, Rev. Phys. Appl., 1974, 9, 455.
(66) E. Rudy, Tech. Rep. Afml-TR-69-117, Part IX, 1970.
(67) G.I. Silman, Obshch. Zakonomern. Str. Diagramm Sost. Met. Sist., 1973, 94.
(68) V.N. Pervikova, F.S. Veselova, Y.U.K. Berendeev and L.I. Pryakhina, Obsch. Zakonomern. Str. Diagramm Sost. Met. Sist., 1973, 88.
(69) G.P. Vyatkin, V. YA. Mishchenko and D. YA. Povolotskii, Izvest. Vyssh. Ucheb. Zaved., Chern. Metall., 1974, 8, 9.
(70) V.I. Levanov, N.N. Sobolev, V.S. Mikheev and O.P. Elyutin, Fazovye Prevrashcheniya Diagrammy Sostoyaniya Metall. Sistem., Ed. O.S. Ivanov, Moscow, Izdatel'Stvo Nauka (1974).
(71) T.D. Dzhuraev, A.V. Vakhobov and K.K. Eshonov, Zavod. Lab., 1975, 41, 3, 335.
(72) A.M. Zhakharov, F.S. Novik and E.P. Daneliya, Izvest. Akad. Nauk SSSR, Met., 1970, 5, 212.
(73) H. Scheffé, J. Royal Statistical Soc., Series B, 1958, 20, 344.
(74) L.W. Gorman and J.E. Hinman, Technometrics, 1962, 4, 4, 463.
(75) J.F. Counsell, E.B. Lees and P.J. Spencer, DCS Rep. 9, N.P.L. Teddington, U.K., 1970.
(76) J.C. Chenavas, N. Valignat, I. Ansara and E. Bonnier, Chimie et Industrie, Génie Chimique, 1971, 104, 15, 1907.
(77) P.E. Potter, J. Nucl. Mat., 1972, 42, 1.
(78) H.Holleck and H. Kleykamp, J. Nucl. Mat., 1969, 32, 1.
(79) E. Rudy, J. Less Common Metals, 1973, 33, 43.
(80) G.G. Mikhailov and V.A. Kozheurov, SB. Nauchn. TR., Chelyab. Politekh. Inst., 1973, 118, 8.

(81) G.G. Mihkailov, V.A. Kohzeurov, A.M. Tupikin, M.A. Ryss and V.P. Zaiko, SB. Nauchn. TR., Politekh. Inst., 1973, 118, 14.
(82) N. Kazuo, O. Kozo and M. Yotaro, J. Electrochem. Soc., 1975, 122, 9, 1245.
(83) A.S. Jordan and M. Ilegems, J. Phys. Chem. Solids, 1975, 36, 329.
(84) A. Laugier, Sem. Chimie Etat Solide, (1974), Vol. 9, Masson 1975.
(85) G.B. Stringfellow, J. Cryst. Growth, 1974, 24, 21.
(86) A. Laugier, Rev. Phys. Appl., 1973, 8, 3, 259.
(87) A.D. Pelton, C.W. Bale and M. Rigaud, To be published in Zeit. Für Metallkde.
(88) M. Blander, Chem. Geol., 1968, 3, 33.
(89) M.L. Saboungi and M. Blander, J. Amer. Ceram. Soc., 1974. 58, 1-2, 1.
(90) H. Hillert and L.-I. Staffansson, Acta Met., 1976, 24, 1079.
(91) J.M. Pourbaix and C.M. Rorivé-Bouté, "The Physical Chemistry of Process Metallurgy", Discussion Far. Soc., N° 4, 1948.
(92) W. Hirschwald, O. Knacke and P. Reinitzer, Erzmetall, 1957, X, H-3, 123.
(93) C.B. Alcock, Can. Met. Quat., 1971, 10, 4, 287.
(94) A.S. Pashinkin, S.S. Bakeeva and M.I. Bakeev, TR. Khim.-Metall. Inst. , Akad. Nauk. Kaz. SSR, 1974, 25, 142.
(95) A.D. Pelton and H. Schmalzreid, Met. Trans., 1973, 4, 1395.
(96) J. Sticher and H. Schmalzreid, Report "Zur Geometrischen Darstellung Thermodynamischer Zustandsgrossen in Mehrstoff-Systemen Auf Eisenbasis", Techn. Univ. Clausthal, 1975.
(97) G. Eriksson, Chem. Src., 1975, 8, 3, 100.
(98) J. Van Der Rest, F. Gautier and F. Brouers, J. Phys. F: Metal Phys., 1975, 5, 2283.
(99) F. Gautier, J. Van Der Rest and F.Brouers, J. Phys F: Metal Phys., 1975B, 1884.
(100) A.R. Miedema, R. Boom and R. De Boer, J. Less Common Metals, 1975, 41, 283.
(101) A.R. Miedema, J. Less Common Metals, 1976, 46, 67.
(102) R. Boom, F.R. De Boer and A.R. Miedema, J. Less Common Metals, 1976, 45, 237.
(103) R. Boom, F.R. De Boer and A.R. Miedema, J. Less Common Metals, 1976, 46, 271.

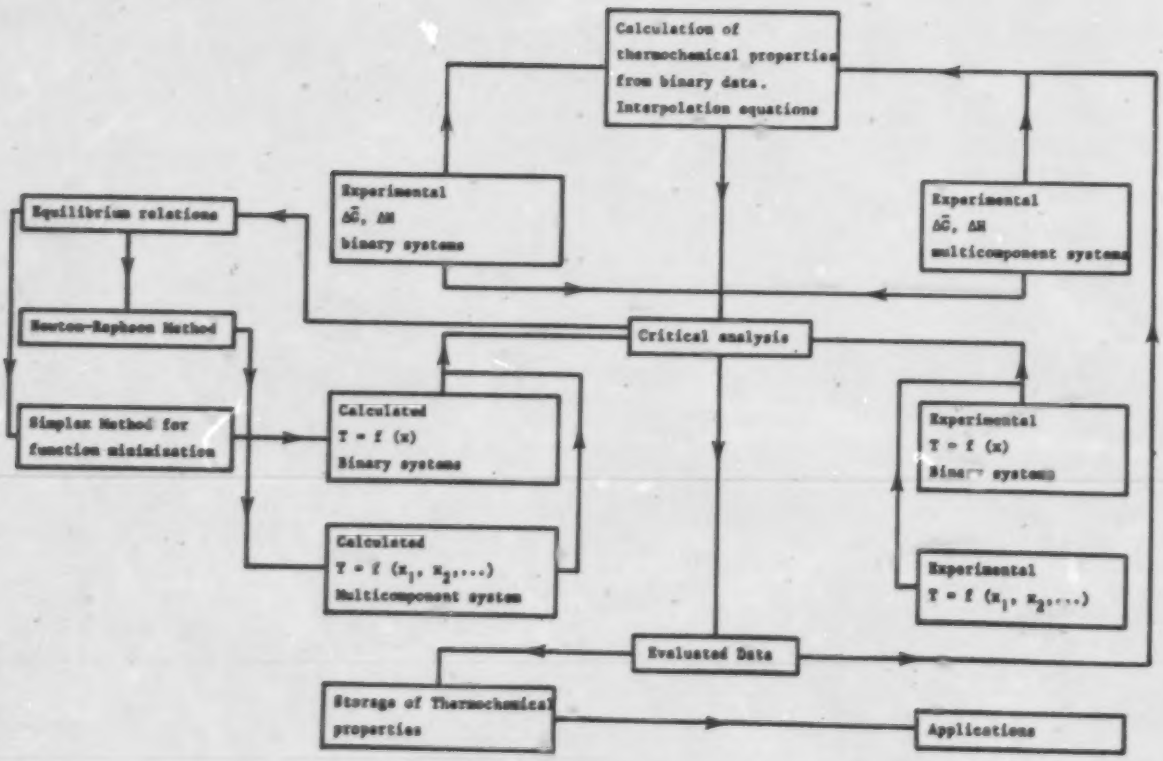
Calculation of thermochemical properties from binary data. Interpolation equations
Experimental $\Delta\bar{G}$, ΔH binary systems
Experimental $\Delta\bar{G}$, ΔH multicomponent systems
Equilibrium relations
Newton-Raphson Method
Simplex Method for function minimisation
Critical analysis
Calculated T = f (x) Binary systems
Calculated T = f (x_1, x_2,...) Multicomponent system
Experimental T = f (x) Binary systems
Experimental T = f (x_1, x_2,...)
Evaluated Data
Storage of Thermochemical properties
Applications

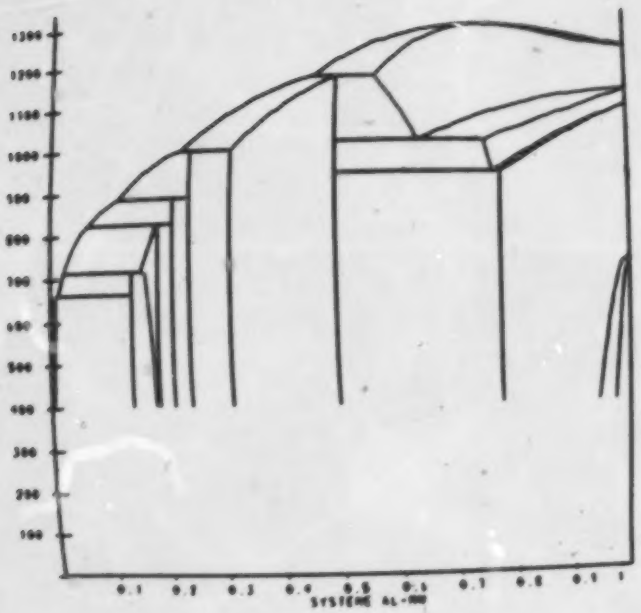

Fig. 1 : System Al-Mn from Ref, 50.

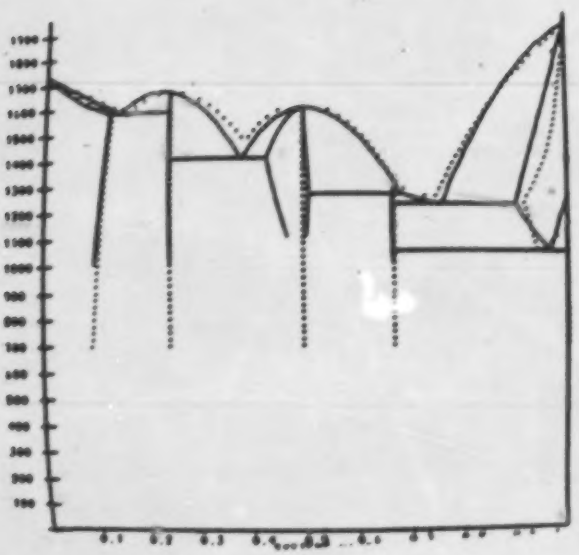

Fig. 2 : System Ni-Ti from Ref. 50 Calculated diagram in dotted lines.

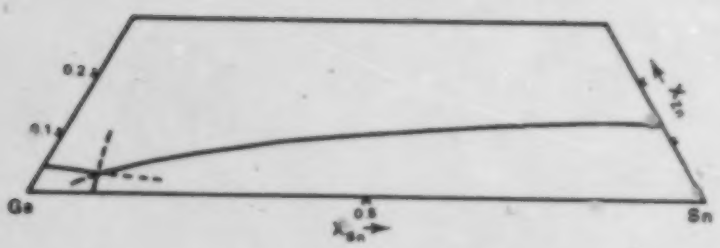

Fig. 3 : Eutectic valley in the Ga-Sn-Zn system.

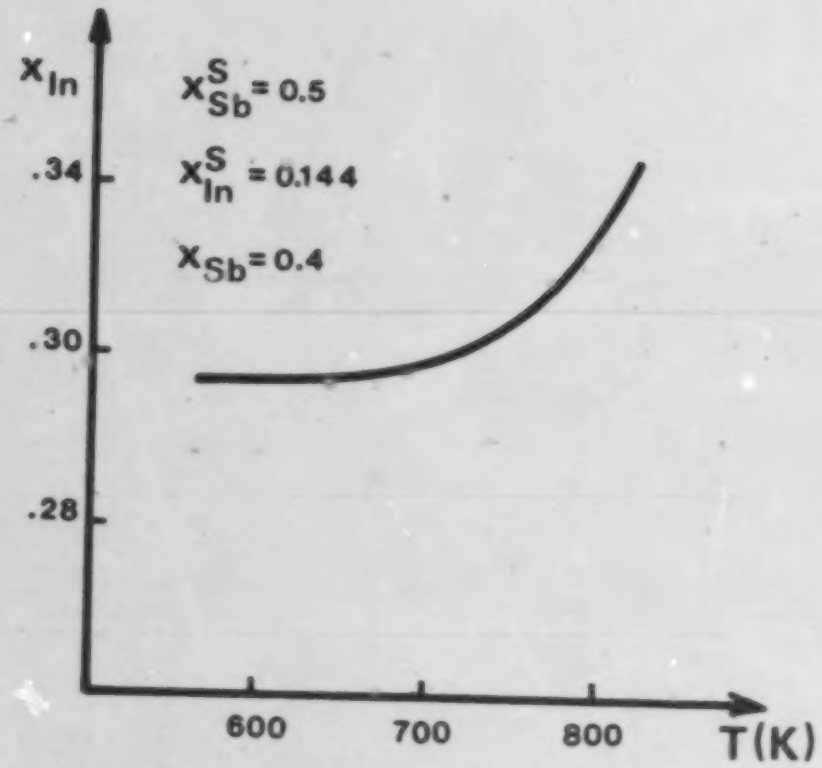

Fig. 4 : Variation of the molar fraction of In the two phase region with respect to temperature.

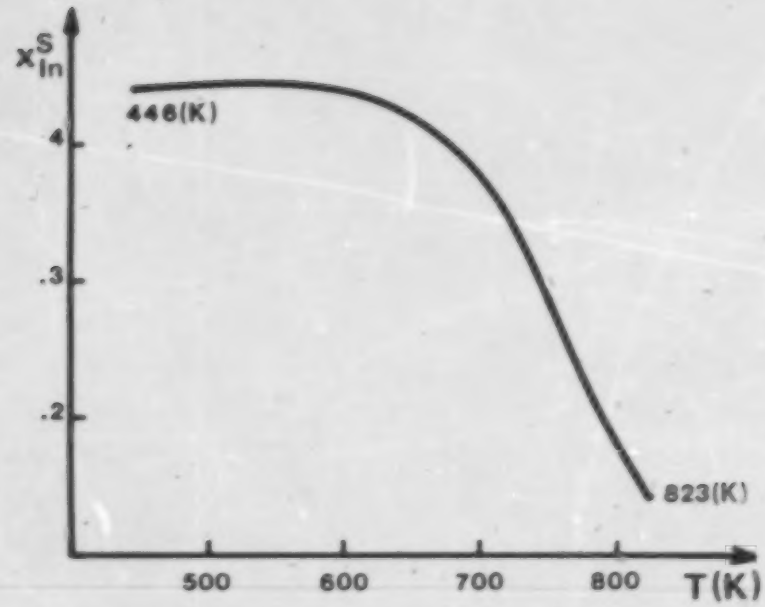

Fig. 5 : Variation of the molar fraction of In the quasi-binary solid solution with respect to temperature.

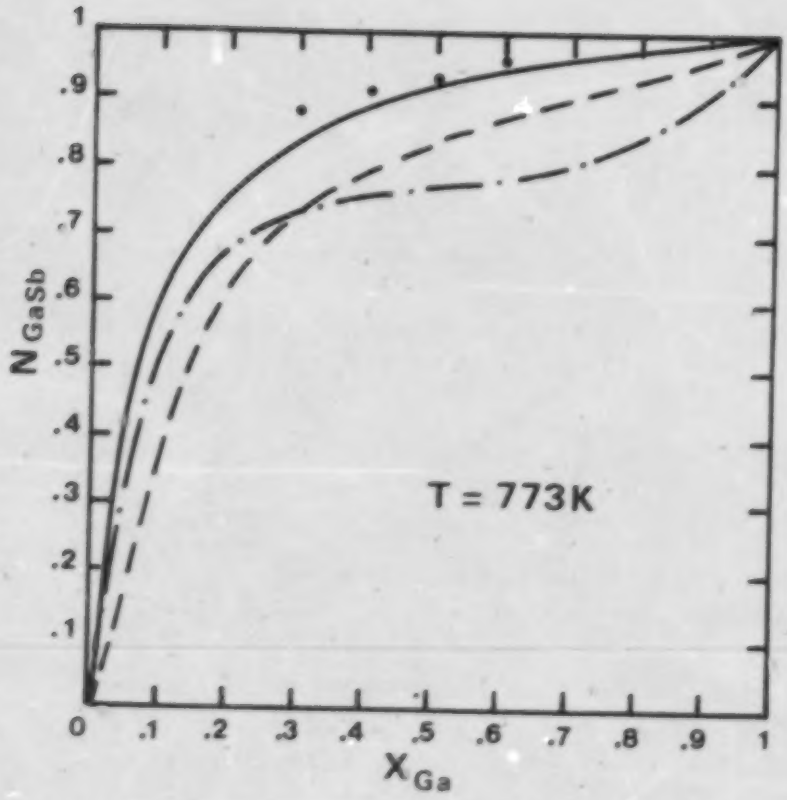

Fig. 6 : Variation of $N^{S}_{GaSb} = f(x^{l}_{Ga})$ at 773K. •Experimental values (G.A. Antypas, J. Electrochem. Soc., 1970, 8, 3, 259)

——— Calculated from experimental values in Réf. 54.

– – – – Recalculated from data in Réf. 64.

—·—·— Recalculated from data in Réf. 65.

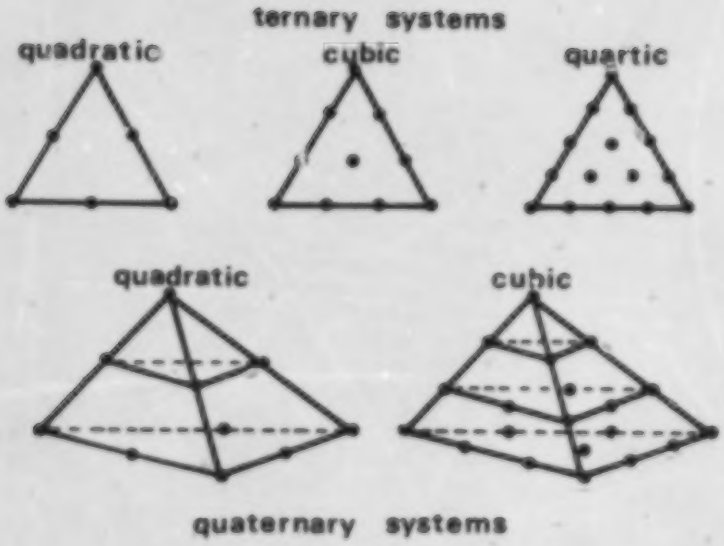

Fig. 7 : Simplex lattices.

	ΔH_{ij}	α_{ij}	RELATION BETWEEN BINARY AND TERNARY MOLAR FRACTION		β
Power series	$\sum_{n=1}^{n=m} x_i x_j v_n (x_i - x_j)^n$	1	$x_i = N_i$	$x_j = N_j$	1 **
Power serie Hardy type	$x_i x_j (\alpha + \beta (x_i - x_j))$	1	$x_i = N_i$	$x_j = N_j$	0
Power serie Hardy type	$x_i x_j (\alpha' x_i + \beta' x_j)$	1	$x_i = N_i$	$x_j = N_j$	$\frac{1}{2}$
Kohler	$\Delta H_{ij} = f(x_i, x_j)$	$(N_i + N_j)^2$	$x_i = \frac{N_i}{N_i + N_j}$	$x_j = \frac{N_j}{N_i + N_j}$	0
Toop	$\Delta H_{12} = f(x_1, x_2)$ $\Delta H_{13} = f(x_1, x_3)$ $\Delta H_{23} = f(x_2, x_3)$	$\alpha_{12} = \frac{N_2}{1 - N_3 i}$ $\alpha_{13} = \frac{1}{1 - N_j}$ $\alpha_{23} = (1 - N_1)^2$	$x_1 = N_1$ $x_1 = N_1$ $x_2 = N_2 / (N_2 + N_3)$	$x_2 = 1 - N_1$ $x_3 = 1 - N_1$ $x_3 = N_3 / (N_2 + N_3)$	0 0 0
Surrounded atom model	$x_i x_j (\alpha' x_i + \beta' x_j)$	1	$x_i = N_i$	$x_j = N_j$	1

* That equation is not symmetrical with respect to the component subscript ;

** Terms of higher order (used when experimental ternary data are available)

National Bureau of Standards SP-496, Applications of Phase Diagrams in Metallurgy and Ceramics
Proceedings of Workshop held at NBS, Gaithersburg, Md., January 10-12, 1977

AN OVERVIEW OF THE DETERMINATION OF PHASE DIAGRAMS

By: F. N. Rhines

Department of Materials Science and Engineering
University of Florida, Gainesville, Florida 32611

In view of the impressive progress that has been made toward complete coverage of at least the binary systems of the elements, one may well ask why we should continue to concern ourselves with methods of phase diagram investigation. The answer cannot be that we are generally dissatisfied with the phase diagrams that are being produced, because the improvement in the quality of constitutional determinations in the years since the second World War is every bit as impressive as is the outpouring of new diagrams. Rather, I see our present interest associated, first, with the fact that the systems that remain to be undertaken have special difficulties that have prevented their being attacked earlier and, second, with problems of refinement where there is importance in determining very small solubilities, in improving the accuracy of temperature measurement, in extending phase diagrams into regions of low and high temperatures and in exploiting the pressure variable.

A survey of current activity in the determination of phase diagrams makes it clear that the preponderance of investigations, even on exotic systems, is being conducted by the use of old time-tested methods, such as thermal analysis, dilatometry, diffusion couple analysis, metallographic

analysis, chemical analysis, x-ray crystallography and lattice parameter measurement, electrical conductivity and dip sampling. These methods are so well-known and their uses so commonly understood that it does not seem appropriate to review them upon this occasion. I shall direct my remarks, instead, to the newer, more sophisticated techniques, which seem destined to see increasing use in the years to come. Upon perusing the literature dealing with new methods, I find many of the authors understandably preoccupied with the details of the method to the near exclusion of consideration of the requirements of phase equilibrium. Since we are about to be instructed in some of the newer techniques, it may be worthwhile to begin by paying our respects to the Phase Rule and reflecting for a few minutes upon its meaning with respect to experimental methods.

A phase diagram is, of course, a graphical expression of the Phase Rule, where

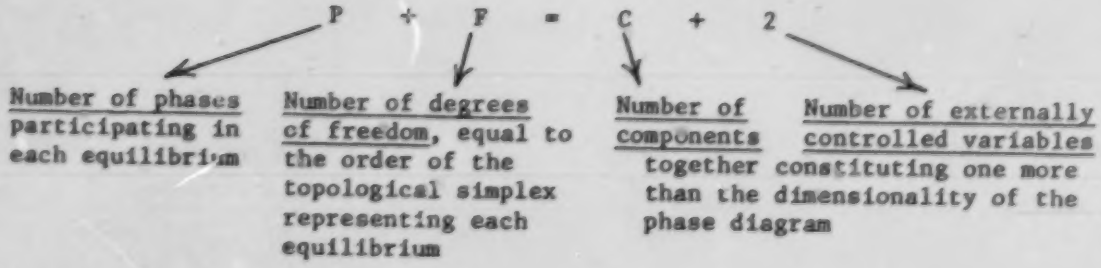
P + F = C + 2
Number of phases participating in each equilibrium
Number of degrees of freedom, equal to the order of the topological simplex representing each equilibrium
Number of components
Number of externally controlled variables
together constituting one more than the dimensionality of the phase diagram

This is a topological relationship, which means that it deals in whole numbers. It stands austerely aloof from concern with the texture of any of its numbers. Thus, the number of phases in an equilibrium is just number, nothing more. It is not necessary even to give the phases names, as long as

we can see that there are two, or three, or whatever number may be participating in the equilibrium. It is necessary and sufficient to identify phase difference at equilibrium. The same is true of each of the other factors of the Phase Rule, which is concerned with the number of components, not with what they are, and with the number of externally controlled variables, not with the specific temperature or pressure. In other words, the Phase Rule pertains to the form of the phase diagram, but not to its metric characteristics.

It is probably not widely appreciated that these distinctions intrude into the business of determining phase diagrams, where clarity of purpose and of procedure can be enhanced by recognition of the bifurcated nature of the problem. In the following, I shall preserve this distinction. I shall deal first with the topological aspects of phase diagram determination and separately with the metric aspects of the phase diagram.

Topological Aspects of Phase Diagram Determination

The concept of heterogeneous equilibrium presumes thermodynamically distinguishable states of matter in physical contact and so all at the same temperature, the same pressure and the same chemical potential. In determining the number of phases it is necessary, therefore, (1) to demonstrate physical contact, (2) to show thermodynamic difference of state and (3) to prove equilibrium. In the majority of cases these requirements are easily met. There are instances, however, in which conformity with these demands is not easily provable, or in which apparent adherence is false. Since we

are concerned here with the difficult and the special cases, some penetration into this field seems desirable.

Physical contact implies not only the existence of interface, but specifically of sharp interface, sharp in the sense that every atom in the system could be identified as belonging to one phase, or another, but never as being a shared atom. The latter provision is necessitated by the requirement of equilibrium that all of the system be at constant chemical potential, a state that could not exist if there were compositional gradients at the phase interfaces, instead of abrupt differences in composition. It is only since the development of the field-ion microscope that we have had direct evidence that such a sharply differentiated state can exist. The clear demonstration that sharpness of interface can prevail lends strength to the position that indefinite boundaries do not denote phase difference. An example exists in the case of the so-called "coherent precipitates," which must be regarded as inhomogeneities in the matrix state, rather than as members of a heterogeneous equilibrium. A related problem has long troubled the field of colloid chemistry, where there arose the question of how large a particle must be before it may be said to have a surface and, hence, be regarded as a separate phase. Perhaps the most positive resolution of the question of phase difference in cases of indefinite interface is to be had by demonstrating that the postulated equilibrium can be established by following a different experimental path. For example, if it could be shown that the coherent intermediate phase could be produced by isothermal diffusion between the terminal components, as well as by precipitation from a

supersaturated solid solution, then it would become evident that it is a phase member of an equilibrium system.

Evidently, those experimental methods which provide direct access to the physical nature of the interface can be of value in phase diagram determination. The battery of electronic microscope equipment that we now have at our disposal provides ever improving resolution of the detail of phase interface. The ultimate in this group is, of course, the field-ion microscope, especially with its adjunct, the atom probe. One of the most impressive accomplishments of this instrument, thus far, has been the demonstration that the ordered and disordered forms of Cu_3Au are separated by an atomically sharp interface and are, therefore, different phases of the Cu-Au system. No other instrument could have settled this question. Because of its experimental limitations and its newness, the field-ion microscope has not yet been broadly applied, but its future in phase diagram investigation seems to be assured.

Also highly useful, even though not capable of such great resolving power, are the transmission and reflecting electron microscopes and scanning electron microscopes. These bring within the range of observation particles of a degree of fineness that would altogether escape detection by the finest of optical instruments. In many cases, the resolution of such fine particles has been sufficient to reveal their shapes as being regularly idiomorphic. This I take as indirect evidence of sharpness of interface, because the formation of facets demands that the structure of the surface be controlled by the crystalline forces of the particle, rather than by some sort

of compromise with the matrix. Accordingly, I suggest that particle shape can give useful information in the ultra fine size range, where there is sometimes doubt concerning the reality of a second phase.

While sharpness of interface seems to be a necessary condition of phase difference, the presence of sharp interface is not alone sufficient evidence. A contrary example exists in the case of polycrystalline grain boundary, which can be seen to be atomically sharp, but which is clearly not a phase interface. Another classical case exists in the distinction between optically enantiomorphic forms of crystals, both forms (according to Ricci) constituting a single phase, although they are separated by sharp interface. The domain boundaries of long-range order fall in the same category. Evidently, something more than interface is necessary for the determination of the number of phases in an equilibrium.

Thermodynamic difference of state must also be demonstrated to prove difference of phase. In principle, this should be done with the phases in contact, at equilibrium. To accomplish this, it is necessary to make an energy sensing scan, which may be approached in any of four different ways. First, the system at equilibrium can be scanned by an energy sensing device that is responsive to localized differences and, thus, identifies phase difference *in situ*. Second, a composition sequence, or gradient, can be traversed with an energy sensing indicator. Third, the energy content of the system, as a whole, can be traced in the course of a temperature scan. Fourth, the same thing can be done by means of a pressure scan.

In multicomponent systems, the *in situ* scan is appropriate and its

simplest embodiment is to be found in optical, or electron, microscopy, where phase difference is visually apparent, although not necessarily reliably so. The element of relevance to difference in chemical state is introduced by the use of chemical etching which sometimes distinguishes between phases by their relative rates of chemical reaction. A more sophisticated application of the principle of chemical difference was once proposed by Mears and Brown who employed an electrochemical probe to associate a difference in solution potential with difference of phase. Probably the most generally reliable criterion of phase difference, however, lies in composition difference per se. Micro-chemical analysis has long been in use for this purpose, but its resolution, with respect to the subdivision of the microstructure, has been limited. This defect has been largely overcome by the development of the electron microprobe, which is useful down to a particle size of about 3 microns, and the STEM, which is said to be capable of analyzing a particle only one micron in diameter. In this connection, it should be noted that precision of analysis is not crucial where the objective is to ascertain the form of the phase diagram, as distinguished from its quantitative characteristics. All that is necessary is to show difference of phase.

Difference in crystal structure is a generally reliable means of distinguishing phases, although the absence of structural difference does not rule out phase difference. Here again, we have micro-tools such as micro x-ray diffraction and electron diffraction, which give access to a limited range of microstructures. Composition difference can sometimes be detected by the use of radioactive tracers coupled with auto-radiographic techniques.

Almost any physical property that can be measured directly upon the micro-constituent can be helpful in phase differentiation, but generally provides supplementary rather than primary phase differentiation. Included in this group are such properties as color, reflectivity, micro-indent hardness, and scratch hardness. Thermal conductivity has been used to distinguish phases by frost patterns. Osmond used micro-indentation patterns to distinguish alpha-iron from gamma-iron long before x-rays were known. Where particles are too fine to be resolved with the microscope, they have sometimes been separated from their matrix by selective chemical solution, have been concentrated by centrifuging and subsequently analyzed.

In applying such techniques, we must maintain vigilence to retain the condition of equilibrium in contact. Failure to do this has frequently been a source of error. There was a time when any compound that a chemist could make was given a place on the phase diagram. Similarly, the finding of crystal structures of transition states, as well as of compounds of subordinate stability, has intruded into the construction of phase diagrams to create confusion. Fortunately, we have been blessed with a generation of critical compilers of phase diagrams who have worked diligently to eliminate such extraneous matter.

Another very useful tool for the establishment of isothermal phase sequences is the diffusion couple. In its application to binary systems, the diffusion couple has the special advantage of displaying the phases in the order of their occurrence in the phase diagram. A suspicion that there may be a tendency for some of the proper phases to be omitted from the layers of

the diffusion couple has generally proved unfounded. This problem seems usually to have been associated with an insufficiently delicate observation of the layers. With the new high powered microscopes, this should cease to remain a problem. Lustman once provided an ingeneous solution when he dissolved the couple layer by layer, using an electrolytic cell and monitoring the emf of the reaction to distinguish each phase layer from the next.

There remains, however, a legitimate question concerning the validity of the phases that form in a diffusion couple, or, for that matter, in any chemical gradient. Some have contended that equilibrium can prevail locally upon the two sides of a phase interface, even though this is embedded in a chemical gradient. Others assert that equilibrium is impossible, because the system is continuing to undergo chemical change. Concerning the concept of localized equilibrium, they contend that under the kinetic state of continuing diffusion, the energy balance at the interface will be shifted, so that the compositions on the two sides of the boundary would not be those of the stable equilibrium. This could, but does not necessarily,mean that the couple would give qualitatively wrong information. For my own part, my experience with diffusion couples has been so consistently good that I am willing to use them, with a small reservation that I am conscious that I could be misled.

Thus far, the use of diffusion couples has been limited mainly to that range of temperature within which diffusion is sensible and melting does not interfere. They have been little used in the survey of ternary and higher order systems, because the composition path of diffusion cannot be foreseen.

With regard to temperature limits, we shall shortly be hearing about methods which are capable of analyzing such shallow diffusion zones that exploration is extended to relatively low temperatures. Very thin couples can be set up by ion implant methods, then analyzing the evolving couple by ion back-scattering. As for their application to ternary systems, it is possible to make a diffusion triple by drawing wires of the three components through a die to cold weld them into a single specimen, whereupon diffusion produces a two-dimensional model of the phases of the ternary system. It is also possible to so design a set of diffusion couples as to virtually guarantee coverage of the ternary span.

The temperature scan method, best known to metallurgists in the form of cooling curves and dilatometry, differs from the isothermal chemical scan in two fundamental respects; namely, that there is no pretense of establishing equilibrium in the course of the experiment and that the total energy content of the system is monitored in order to sense phase change. It offers the very considerable advantage, not only of identifying the temperatures at which the various equilibria occur, but, most particularly, of providing recognition of the variance of otherwise undocumented equilibria over an enormous temperature range. Its principal limitations arise (1) from the need for any new phase to be nucleated and to grow forthwith and (2) from the rather large proportion of any new phase that is normally required for detection. The requirement of nucleation and growth leads to undercooling and superheating effects, to the failure of some stable phases to be observed with the appearance of meta-stable, or transition states, instead, or in

addition. These are all familiar occurrences bearing upon the problem of achieving equilibrium and will be reserved for later discussion. The matter of the detection of small quantities of a new phase is, however, one which has been largely overcome in recent years and which will be considered upon this occasion. I have reference to the magnetic detection methods, i.e NMR and Mossbauer Effect measurements. Under favorable circumstances, these are very sensitive detectors of small quantities of a new phase. In their present form, they require expert interpretation, because there are some magnetic indications that are not connected with phase change. In proper use, however, they are capable of extending the knowledge of phase equilibria into systems that have not previously been open to study, because of their very narrow solubility limits.

The pressure scan also provides a very broad range of conditions and, like the temperature scan, depends upon the sensing of property changes in the bulk of the sample to reveal the occurrence of phase changes. The techniques that are available divide themselves naturally into two classes, the one relating to relatively high pressures at which the gas phase is absent, the other dealing with the medium to low pressure range within which the gas phase is usually present. For the high pressure range, piston type compression cells are usually employed. At a pressure where a phase change occurs, there is ordinarily a change in the specific volume of the test material, which can be sensed by an alteration in the volume/pressure ratio. For experimental reasons, this indication of phase change is often difficult to detect. It has been more common, therefore, to provide for

heating the cell and for reading the phase change by the use of a differential thermocouple implanted in the sample along with a reference material. Thus, the pressure variable and the temperature variable are scanned together. At each step in advance of the pressure, the cell is heated and cooled to explore for a phase change. Such experiments are usually conducted in a series of rising pressure steps, rather than the reverse, because the pressure seals become tighter with rising pressure, but tend to fail as the piston is retracted.

When the gas phase is present, the pressure of the system is determined by the equilibrium between the gas and the condensed phases. Thus, a temperature pressure scan is produced whenever a material is enclosed within an inert cell and is heated, or cooled. In order to define the equilibria traversed in this experiment, it is necessary to monitor both the temperature and pressure and to determine the compositions of the gas and of the condensed phases. In the field of chemistry where vapor pressures are readily measurable, such techniques are classical. The application of this method to metal systems, however, has seen less use, especially in alloy investigation. Boyle and I used it successfully for the determination of the gas-eutectic of the system Cd-Zn. We used a capsule composed of two glass bulbs joined by a capillary. The metallic sample was contained in one of the bulbs and the system was evacuated and sealed. The capsule was then held several days in a thermostat which kept the gas bulb about one degree hotter than the specimen bulb, in order to avoid condensation. At the end of the stabilization treatment, the capillary was sealed, by means of a hot wire,

the gas bulb was broken in a fixed volume of acid and the total composition of the gas thus analyzed. Knowing also the original volume of the bulb, the gas pressure was calculated. The solid phases were then analyzed separately to complete the description of the three-phase equilibrium at known temperature and pressure. This is a tedious procedure, but it does give us access to the PTX diagram of the alloy system.

Proof of thermodynamic equilibrium is probably the most uncertain factor in phase diagram determination, mainly because such proof can never be positive; it must always be based upon indirection of some kind. To prove that a system is in a state of minimum energy, one is burdened with the necessity of showing that all other states that can be attained with the same conditions of temperature, pressure and composition contain greater energy. Where the equilibrium is being approached isothermally and isobarically, it has been common simply to extend the time of stabilization until no further change can be observed. Equilibria that are intercepted in the course of temperature, or pressure, change, can be "boxed in" by traversing them in the opposite sense. Indeed, the true equilibrium temperature can be established to any desired degree of precision by taking cooling and heating scans at progressively lower rates of temperature change and extrapolating both cooling and heating indications to coincidence at long time. No matter how carefully the equilibrium is located, however, there can be a lingering doubt that the equilibrium is a true one and not some transition state, or a meta-stable state.

Probably the surest means for identifying meta-stable and unstable

states is to compare the results of two or more kinds of scan through the state. This is because most unstable states are arrived at through a specific sequence of temperature, pressure or composition change. If the equilibrium is approached so that the participating phases are formed by a different mechanism, the unstable form may not be generated. An interesting example exists in the case of carbon steels. When steel is cooled from its high temperature (gamma) state, the eutectoid product is invariably alpha-iron and cementite (Fe_3C) and not alpha-iron and graphite, as it should be in the stable state. The reason seems to be that graphite is not easily nucleated, so that the saturated gamma undercools, whereas Fe_3C nucleates with relative ease at only slightly lower temperature. Before any graphite has had an opportunity to form, all of the gamma has been transformed to the meta-stable state. If, on the other hand, one attempts to form cementite by isothermal diffusion of carbon into iron, none forms. Below 738°C, only alpha and graphite appear in the diffusion zone and this is stable down to low temperatures. Diffusion between iron and carbon above 738°C produces gamma iron, in addition to the alpha and graphite and the gamma must decompose upon cooling. Here, the phase change occurs, not isothermally, but with falling temperature and the gamma decomposes into alpha and cementite, as in any cooling cycle. Upon very long heating of the alpha-iron cementite alloy, the cementite gradually decomposes into alpha-iron and graphite. Thus, it is seen that the cementite is less stable than the graphite. This principle is capable of broad application.

Many of the kinds of experimentation that are used in phase diagram

determination are best conducted at room temperature (microscopy, for example). To accomplish this, we often resort to quenching the specimen from its equilibrium temperature, down to room temperature. The question then arises whether the quenched state is equivalent to the high temperature state. Again, it may be difficult to determine whether this is true. While increasing the rate of cooling usually secures the retention of the equilibrium state, this is not always the case. There are instances in which no diffusion is required to effect the transformation, so that the phase change may occur freely at room temperature. This is by no means confined to the martensitic transformation. It occurs also where the phases concerned are all of truly stable types. The case of the diffusionless transformation of beta to alpha brass is well-known, but widespread behavior of this type in the copper-based ternary alloys, as well as other alloys of the analogous type, is probably less widely recognized.

As with metastability, the incidence of quenching failure is not always obvious and may lead to confusion in the construction of the phase diagram. The most certain escape from this dilemma is, of course, to make all observations at the equilibrium temperature. This demands hot methods for microscopy, x-ray diffraction, microprobe analysis and so on. While methods for hot microscopy and x-ray diffraction have long been in use, they have been complicated by many difficulties and limitations, so that the development of better methods continues.

The number of components is perfectly straightforward as long as the elemental species are taken in total. This is usually done in the construc-

tion of phase diagrams of metal systems, so that the metallurgist is not commonly troubled by this factor. Where it is desired to designate compounds as components, as is commonly done in both inorganic and organic chemistry and in ceramics, it is necessary to exercise much care, because the equilibria that occur between two (or more) compounds may include compositions that cannot be described by mixtures of these compounds alone. The ceramic systems are particularly subject to this complication and the most troublesome problem facing the compiler of ceramic phase diagrams today is probably that of sorting out the true equilibrium diagrams from those that involve incompletely defined equilibria.

In principle, one is free to designate a quasi-binary system only when all tie-lines and all three-phase equilibrium lines lie in the plane of the diagram, or equivalently with the quasi-ternary or quasi-quaternary systems. Obviously, this condition cannot be guaranteed in advance of the experimental determination, so that it is prudent to examine this factor as a first order of business. All that is required is to equilibrate a composition somewhere in the middle of the system and to verify that the compositions of all of its phases lie upon the intended composition section. If this is true, then the likelihood of the system being other than the quasi-type intended is greatly diminished. If, however, one or more of the equilibrium phases proves to have a composition that lies off the intended sequence, then it is necessary to treat the system as being one of higher order. Too often, the fact of an assumed quasi-binary section not being such has come to light only when attempts were made to incorporate the section in a ternary, or higher order,

system. At such time, the failure of the section to connect properly with the rest of the diagram becomes painfully evident.

The question whether impurities should be included in the count of the components of a system is one that we tend to ignore as much as we can, because the answer is often embarrassing. We must, of necessity, handle our experimental materials in some kind of container, which is bound to enter into the equilibrium in some way and there are often other sources of contamination. Some of the more sophisticated experimental techniques, such as levitation melting and cold hearth melting, seek to minimize this problem, but to some degree it is always with us. The best that we can usually do is to select among potential contaminants those that will do the least damage. So long as we are concerned with the topological form of the phase diagram, as distinguished from its quantitative features, we can sometimes accept impurities that remain in solution and form no new phases. Where there is doubt on this score, the obvious remedy is to change the composition of the container system and compare the results for any evidence of a foreign phase. Unfortunately, it does not always follow that because an impurity remains in solution it has no influence upon the topology of the phase diagram. A memorable case is that of the effect of a small carbon impurity upon copper-iron alloys; in the presence of carbon, two-liquid immiscibility occurs, whereas the pure copper-iron system displays only liquid miscibility. Impurity effects remain one of the more difficult problems of phase diagram determination, especially because the problem is different from system to system.

The number of externally controlled variables is subject to reduction by fixing the pressure, the temperature, or both. So long as the fixed variable is maintained at constant value in a closed system, no problems arise and the phase diagram is reduced by one dimension for each variable that is held constant. For experimental reasons, and within reasonable limits of precision, the temperature variable may be fixed with no bad side effects. The same is true of relatively high pressure, because it is necessary to have the system confined. At ordinary and low pressure, however, it is common practice to handle the experimental materials in the open, upon the presumption that the pressure is being maintained at one atmosphere. This assumption is essentially correct for the mass of the specimen, but it may not apply at the surface. Unless the system is confined, so that the vapor phase is indeed in equilibrium with the rest of the sample, there is likely to be a non-equilibrium at the surface, resulting either in the loss of some of one of the components, or contamination by the ambient atmosphere. Continuously pumped vacuums are particularly damaging in this respect.

These matters have been inconsequential in much of the past experimentation, because the mass of the experiment was not affected and this was all that mattered. With the advent of some of the new techniques that involve very thin samples, either attached or not attached to a massive body, the state of the surface becomes a critical factor. We should pay heed to this matter in our deliberations at this gathering.

Quantitative Aspects of Phase Diagram Determination

From the point of view of the users of phase diagrams, the precision of the temperature and composition data, and sometimes of the pressure, are of first consideration. Justifiably, therefore, much of the effort that is devoted to phase diagram determination relates to accuracy of measurement. In approaching the sharpening of a datum point, it is generally presumed that the constitution of the system is already known qualitatively. Under such conditions, with the general characteristics of the system known and with the temperature and composition known approximately, it is possible to select a method of investigation and to tailor the experimental conditions to suit the specific case. This is a rather different situation from that which prevails in the exploratory type of experimentation.

Temperature of equilibrium measurements require first of all well-calibrated standards. This is taken for granted. The main problem then is the establishment of the equilibrium under conditions that permit an unobstructed measurement of temperature. For the majority of cases, the scheme of "boxing in" the true equilibrium temperature is usually the best solution. By this I mean approaching the equilibrium from both lower and higher temperature to identify a temperature of coincidence. The isothermal approach to equilibrium provides an excellent opportunity for exact temperature measurement, but the establishment of equilibrium may remain uncertain. The most sensitive measurement is usually obtained when the experiment is so arranged as to first encounter the appearance of a new phase, rather than its disappearance. Thus, cooling curves are best for locating liquidus points,

while heating curves are better for solidus determination; solubility limits are more readily detected through the beginning of precipitation than by the completion of solution.

The use of very thin specimens presents some problems that appear menacing. Ordinary temperature measuring techniques have to be miniaturized, or have to be replaced with less familiar methods. The small specimen is more responsive to temperature change and also is likely to support temperature gradients. Surface effects such as radiation and superficial reaction with the atmosphere must also be considered. The initiation of a phase change may also be sensitive to the mass of the specimen, where nucleation depends statistically upon the volume of the material. While the small specimen technology has much to recommend it, it behooves us to be wary of its pitfalls.

Finally, there is the problem of temperature determination at the extremes of temperature and pressure. This remains a field for the specialist. My personal experience in the use of optical and radiation methods for constitutional determination has often been less than satisfactory. The difficulties that I have met have not been so much connected with the measuring methods per se as with the maintenance of conditions under which they could be used. Fumes tend to obscure the path from the instrument to the specimen, sometimes fogging windows. Black body conditions are often awkward to arrange and radiation corrections unreliable. This seems to me to remain an area where innovation is needed.

The measurement of phase composition at equilibrium is especially sensi-

tive to the detailed characteristics of the system under consideration. Consequently, we have before us a broad array of methods, each having special advantages for certain situations. One of the most broadly applicable schemes is the physical separation of the phases to permit direct analysis by conventional means. Among chemists, this method has been exemplified by dip sampling. Eutectic liquids can sometimes be bled out of alloys during incipient melting and the beads of eutectic subsequently analyzed. Embedded particles of solid phases can sometimes be separated by selective dissolution and concentrated for analysis. Most of the general types of analytical techniques have already been discussed. Among the remainder are indirect methods, such as the measurement of the crystal lattice parameter for comparison with a composition standard. Such methods can be highly precise and reliable.

Closure

The objective of this overview has been to approach the field of phase diagram determination broadly, so as to bring out some general principles and to direct attention away from the experimental details, toward the basic requirements of the Phase Rule. If we are moved to receive the new methods, that will now be presented to us, in the light of their roles in the application of the Phase Rule, its mission will have been accomplished.

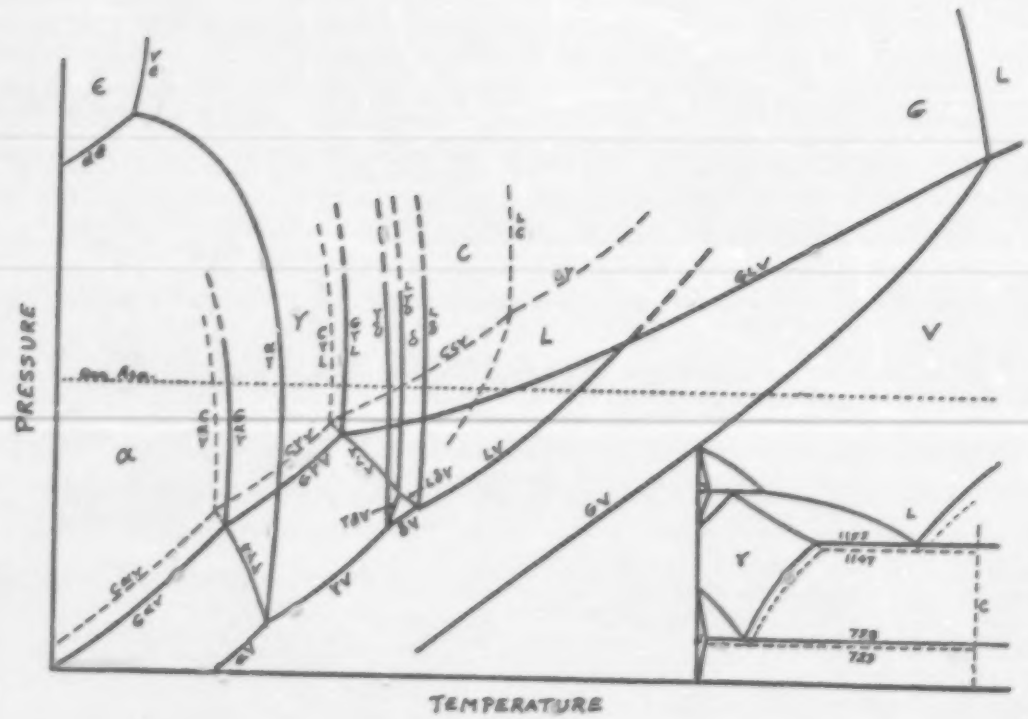

DISCUSSION

R. E. Watson - A future class of experiments for phase diagram research, that may be devolped in a half dozen years or so involves synchrotron light. Synchrotrons radiate intense white light in the soft and hard x-ray range, that can be focussed. This in turn will provide improvements for techniques such as x-ray photography, low angle- and diffuse x-ray scattering, and it promises to provide a bridge between x-ray microscopy and x-ray diffraction. Some studies are now being done on the dynamics of phase transitions. Depending on whether hard (or very soft) x-rays are being used, the x-rays can (or cannot) be sent through a window, thus allowing studies in isolated atmospheres, such as a vacuum, or varying temperatures.

O. J. Kleppa - A large number of phase diagrams have not really been tested for the reversibility of the equilibrium. Many of the experimental studies are by dynamic methods. In addition to the phase rule, other criteria such as the generalized Clausius-Clapeyron relation can be applied.

National Bureau of Standards SP-496, Applications of Phase Diagrams in Metallurgy and Ceramics
Proceedings of Workshop held at NBS, Gaithersburg, Md., January 10-12, 1977

Proposal for a Comprehensive Handbook on "Ternary Phase Diagrams of Metals"

F. Aldinger, E.-Th. Henig, H.L. Lukas, and G. Petzow
Max-Planck-Institut für Metallforschung,
Institut für Werkstoffwissenschaften,
Büsnauerstr.175, D-7000 Stuttgart-80

Today, constitutional data of ternary systems are available on a large scale, but they are scattered over a large number of different reports, journals, and books. In order to use this enormous amount of knowledge more extensively, it is most desirable to summerize all informations on ternary phase diagrams in a critically evaluated compilation in which the systems are presented in the alphabetical order of the chemical symbols. In order to make such a handbook useful not only for insiders but also for technical people and students, the form of the presentation of the systems should be comparable to that of the binary phase diagrams in the well-known book of Hansen and Anderko. And also, the content of such a handbook has to include a brief presentation of the fundamentals of the ternary phase equilibria together with a proper nomenclature, enabling to "read" ternary phase diagrams. The form of the presentation of the systems should cover the following content:

1. A brief critical review of the work which has been published in the literature
2. A discussion of special features of the binary systems related to the ternary phase diagram
3. Composition and structure of solid phases
4. Pseudobinaries
5. Invariant equilibria
6. Liquidus surface
7. Isothermal sections
8. Miscellaneous (e.g. solid solutions, tie-lines, vertical sections, ordering, lattice constants as a function of composition, etc.)
9. References.

The presentation has to have a minimum in extension and a maximum in distinctness.

A literature survey covering constitutional work carried out before 1974 comprises about 18000 references on about 6000 ternary systems of metals. A rough estimate shows that about one-forth of these systems are fully investigated and phase diagrams are available. About one-third of the systems are evaluated to some extent. Of the remaining systems constitutional data are available only on a rather limited scale.

According to the concept mentioned above this appreciable amount of results will comprise about 16000 pages in printed book form!

National Bureau of Standards SP-496, Applications of Phase Diagrams in Metallurgy and Ceramics
Proceedings of Workshop held at NBS, Gaithersburg, Md., January 10-12, 1977

Phases and Phase Relations in the Binary Oxide Systems Containing WO_3

Luke L. Y. Chang

Department of Geology, Miami University, Oxford, Ohio 45056

ABSTRACT

Phases and phase relations are reviewed in the systems of WO_3 with alkali oxides, alkaline earth oxides, scandium and yttrium oxides, rare earth oxides, titanium, zirconium and hafnium oxides, vanadium, niobium and tantalum oxides, molybdenum oxide, thorium and uranium oxides, manganese, iron, cobalt and nickel oxides, copper and silver oxides, zinc, cadmium and mercury oxides, boron, aluminum, gallium and indium oxides, tin and lead oxides, and phosphorus, arsenic, antimony and bismuth oxides.

165186

INTRODUCTION

The purpose of this review is to summarize phases and phase relations in WO_3-containing systems and to present a compilation of phase diagrams according to the types of chemical compounds. Fifteen tungstate groups have been selected for discussion and their phase diagrams are presented.

SYSTEMS ALKALI OXIDE - WO_3

Alkali tungstates have been studied extensively, but there are inconsistencies in the number, composition, and melting relations of reported phases. In the system $Li_2O \cdot WO_3$-WO_3 (Fig. 1), Hoermann (1928) reported the formation of both 1:2 and 1:4 (alkali oxide/WO_3 ratio) phases, However Spitsyn et al. (1938) and Kletsov et al. (1971) could not prepare the 1:4 phase. Recent work by Sakka (1968), Reau and Fouassier (1971), Hauck (1974), and Chang and Sachdev (1975) confirmed Hoermann's results. The marked difference among published phase relations in the system is in the nature of melting of the 1:2 phase. Hoermann (1928), Parmentier et al.(1972a), and Hauck (1974) all reported a congruent melting point at 745°C for the 1:2 phase, but Chang and Sachdev (1975), on the basis of x-ray diffraction and microscopic examination of polished sections, concluded that melting at 745°C is incongruent.

In the system $Na_2O \cdot WO_3$-WO_3 (Fig. 2), the existence of the 1:6 phase is the subject of controversy. It has been reported by Sakka (1968), and Chang and Sachdev (1975), but was not found by Hoermann (1928) or Caillet (1963). In addition, the melting point of the 1:4 phase determined by Chang and Sachdev is 50°C higher than that proposed by Hoermann and Caillet. Polymorphic relations in the 1:1 phase have been well established (Pistorius, 1966; Bottelberghs and van Buren, 1975). Three forms; α (orthorhombic), β (orthorhombic), and γ (cubic), have transition temperatures at 587.6°C (γ to β) and at 588.8°C (β to α).

In the system $K_2O \cdot WO_3$-WO_3 (Fig. 3), Hoermann (1928) and Mokhosoev et al. (1962) prepared two tungstates, 1:3 and 1:4, but Caillet (1963) reported 1:2 and 1:4 phases. Sakka (1968) and Guerin and Caillet (1970) reported the formation of 1:2, 1:3, 1:4 and 1:6 phases. Gelsing et al. (1965), who studied this system in some detail, identified 1:2, 1:3, 1:4 phases and two metastable phases (designated as X and Z). Chang and Sachdev (1975) confirmed all phases reported by Sakka and Guerin and Caillet, and also observed the formation of metastable phases. Chang and Sachdev stated that experimental evidence was not adequate to suggest the presence of two separate metastable phases, as proposed by Gelsing et al. The reported melting points of potassium tungstates show substantial variance. A comparison is shown

in Table 1.

Phase relations in the systems $Rb_2O \cdot WO_3$-WO_3 and $Cs_2O \cdot WO_3$-WO_3, as established by Chang and Sachdev, are very similar (Figs. 4 and 5). The 1:2 and 1:3 phases form a complete series of solid solution with melting points increasing and d-spacing decreasing from the 1:2 to the 1:3 phase. The 1:6 phases in both systems are the most refractory alkali tungstates. Chang and Sachdev confirmed the number and the composition of phases in the Rb-system as reported by Spitsyn and Kulesbov (1950). No other study on the Cs-system was found.

Several basic alkali tungstates have been reported. $3Li_2O \cdot 2WO_3$ is stable below 500°C (Parmentier et al., 1972b) $3Li_2O \cdot WO_3$ decomposes below 440°C, and $2Li_2O \cdot WO_3$ melts at 1350°C and is dimorphic with a transition point at 690°C (Hauck, 1974). In the Na-system, both $2Na_2O \cdot WO_3$ and $3Na_2O \cdot WO_3$ were prepared at 450°C in silver crucibles in sealed Vycol capsules (Reau et al., 1967). Reau et al. (1971) reported a 2:1 phase in the K-system, which decomposes at 650°C in dry oxygen to $K_2O \cdot WO_3$ and K_2O.

Among the alkali tungstates, crystal structures are known only for the 1:1 phases and the 1:2 phases of Li and Na. Chang and Sachdev suggested some structural relationships among them. $Li_2O \cdot WO_3$ and $Na_2O \cdot WO_3$ have phenakite (Zacharisen and Plettinger, 1961) and spinel (below 587.6°C)(Lindqvist, 1950)

structures, respectively. In both, structures are built up of isolated WO_4 tetrahedra linked together by alkali atoms. $K_2O \cdot WO_3$ and $Rb_2O \cdot WO_3$ are isostructural, a structure in which isolated WO_4 tetrahedra are linked by eight-coordinated alkali atoms to form layers (Koster et al., 1969; Kools et al., 1970). The $Cs_2O \cdot WO_3$ has β-K_2SO_4 structure (Kools et al., 1970), which also is characterized by the isolated WO_4 tetrahedra. The structures of the 1:2 phases, $Li_2O \cdot 2WO_3$ and $Na_2O \cdot 2WO_3$, are built up of continuous chains of WO_6 octahedra joined by bridging oxygen atoms and WO_4 tetrahedra (Lindqvist, 1950; Margarill, *et al.* 1973). Although the crystal structures of other alkali tungstates are not known, the WO_3 end member has a structure of solely WO_6 octahedra, linked by bridging oxygen atoms (Anderson, 1953), which suggests that in alkali tungstates the preference for the formation of the WO_6 octahedron increases in the direction from the 1:1 phase toward WO_3.

SYSTEMS ALKALINE EARTH OXIDE - WO_3

Alkaline earth tungstates of the 1:1 type have long been known and are well characterized. Structurally, they can be divided into two major classes: (1) Tungstates of large divalent cations which are tetragonal, usually described as the scheelite-type, and (2) Tungstates of small divalent cations which are monoclinic, usually described as the wolframite-type.

Steward and Rooksby (1951) prepared a series of tungstates of the 3:1 type and showed that their crystal structures are related to that of $(NH_4)_3FeF_6$. Calcium, strontium, and barium all form this compound.

Phase relations in the systems have been studied in detail by Chang et al. (1966a) and have showed a simple eutectic in the system $BeO-WO_3$ (Fig. 6), and compound formation in other systems. In the system $MgO-WO_3$ (Fig. 7), the wolframite-type, 1:1 phase is stable to 1165°C, where it transforms to a high-temperature phase with unkown structure. On the basis of x-ray powder diffraction data, this high-temperature phase does not not match with any of the known polymorphic forms of TiO_2, α-PbO_2, and $FeNbO_4$ (Laves et al., 1963). In addition, this phase does not have a form similar to $MgMoO_4$, which transforms to a wolframite-type structure under high pressure (Young and Schwartz, 1963).

In the system $CaO-WO_3$ (Fig. 8), the 1:1 phase is the mineral scheelite, and its structure is used to describe crystal structure of other 1:1 tungstates. The 3:1 phase has a distorted $(NH_4)_3FeF_6$-type structure. In high-temperature x-ray diffraction, the distortion in the 3:1 phase is gradually reduced as the temperature increases from 25° to 1200°C, but an ideal $(NH_4)_3FeF_6$ structure was not obtained. Nassau and Wills (1962) prepared a 6:1 phase, which apparently is metastable and is not present in equilibrium assemblages. Tokunov

and Kislyakov (1972) confirmed the phase relations determined by Chang et al. (1956a).

In the system $SrO-WO_3$ (Fig. 9), the 1:1 phase is isostructural with $CaO \cdot WO_3$, and the 3:1 phase, as compared with $3CaO \cdot WO_3$, is less distorted from the $(NH_4)_3FeF_6$-type structure. DTA shows an endothermal peak at 1100°C for the 3:1 phase and high-temperature x-ray diffraction indicates that it transforms to the ideal $(NH_4)_3FeF_6$ structure (cubic) above that temperature. Tokunov and Kislyakov (1972) confirmed the phase relations in the system reported by Chang et al. (1966a), except that they proposed a 2:1 phase which melts incongruently at 1500°C and forms a eutectic point with $SrO \cdot WO_3$ at 1470°C and 44.5 mole% WO_3.

In the system $BaO-WO_3$ (Fig. 10), published reports do not agree on the existence of a 2:1 phase. Scholder and Brixner (1955) first proposed such a phase and it was subsequently observed by Zhmud and Ostapchenko (1961), Kreidler (1972), and Tokunov and Kislyakov (1972). However, Purt (1962) and Chang et al. (1966a) found no evidence for the existence of a 2:1 phase. According to Kreidler, the 2:1 phase has three forms with transition temperatures at 1385° and 1490°C.

SYSTEMS $Sc_2O_3-WO_3$ and $Y_2O_3-WO_3$

Phase relations in the system $Sc_2O_3-WO_3$ have not been established as only a 1:3 phase is characterized. This phase melts at about 1650°C (Nassau et al., 1965) and is

orthorhombic. Its crystal structure is similar to the scheelite-type (Abraham and Bernstein, 1966), but scandium atoms are six-coordinated, rather than taking the eight-coordinated positions of calcium in scheelite.

In the system Y_2O_3-WO_3(Fig. 11), Borchardt (1963) reported five phases: 3:1, 9:4, 15:8, 1:1 and 1:3 and suggested some melting relations in the WO_3-rich portion. The 3:1 phase has a rhombohedrally distorted fluorite structure (Borchardt, 1963; Aitken et al., 1964) below 1700°C, above which it transforms to a f.c.c. phase. The 9:4 phase reported by Borchardt was later proved to have a 5:2 composition by McCarthy et al. (1972), and it has a pseudo-tetragonal, fluorite-related structure. McCarthy et al. also suggested a 7:4 composition for the 15:8 phase reported by Borchardt. The 1:1 phase is monoclinic (Trunov et al., 1968) and has a crystal structure related to that of scheelite. The 1:3 phase is isostructural with $Sc_2O_3 \cdot 3WO_3$ (Nassau and Shieve, 1972).

A 3:2 phase was found by Borchardt (1963) at temperatures between 750° and 1000°C. This phase disappears on heating at 1100°C and does not re-appear when any of the higher temperature phases are treated at 1000°C. As suggested by Borchardt, this phase is probably a metastable phase.

SYSTEMS RARE EARTH OXIDE - WO_3

Crystal chemistry of and compound formation in rare earth tungstates have been well documented by McCarthy et al. (1972) and Naussau and Shieve (1972). Also, phase relations have been established in several systems. Among the five phases present in the system La_2O_3-WO_3 (Fig. 12) (Ivanova et al., 1970), three (3:1, 1:1 and 1:3) are common to all RE_2O_3-WO_3 systems, and their crystal structures are in most cases type structures for tungstates of large-sized rare earths (for example, Pr, Ce). $3La_2O_3 \cdot WO_3$ has a distorted pyrochlore or ordered, defect fluorite structure (Chang and Phillips, 1964). Ivanova et al. (1970) suggested that this phase has three modifications, but these were not found by McCarthy et al. (1972). $La_2O_3 \cdot WO_3$ is probably monoclinic and its structure is scheelite-related (Polyanskaya et al., 1970a). $La_2O_3 \cdot 3WO_3$ is dimorphic, both forms have distorted scheelite structure with La atoms in the eight-coordinated positions (Nassau and Shieve, 1972). The structure of $3La_2O_3 \cdot 2WO_3$ is not known, and that of $La_2O_3 \cdot 2WO_3$ appears to be different from the rest of the $RE_2O_3 \cdot 2WO_3$ phases (McCarthy et al., 1972).

The system Sm_2O_3-WO_3 also has five phases (Fig. 13)(Chang et al., 1966b). $3Sm_2O_3 \cdot WO_3$ and $Sm_2O_3 \cdot 3WO_3$ are considered to be isostructural with their counterparts in

the La-system (Chang and Phillips, 1964), but Trunov et al. (1968) prepared $3Sm_2O_3 \cdot WO_3$ at 1250°C showing a pseudo-tetragonal symmetry. $7Sm_2O_3 \cdot 4WO_3$ may also be indexed on the basis of a cubic cell, but shows a few extra reflection lines (Chang et al., 1966b). McCarthy et al. (1972) suggested a pseudo-rhombohedral cell for this phase, which is the type structure for all rare earth tungstates of the same RE_2O_3/WO_3 ratio, except those of La, Pr and Tb. $Sm_2O_3 \cdot WO_3$ is monoclinic (Trunov et al., 1968) and has a scheelite-related structure (Polyanskaya et al.,1970a). $Sm_2O_3 \cdot 2WO_3$ is also monoclinic (McCarthy et al., 1972). In this structure, distorted WO_6 octahedra share edges to form W_2O_9 zig-zag chains, producing both eight and nine coordinated structural positions for the rare earth atoms (Klevtsov et al., 1967; Borisov and Klevtsova, 1970).

Phase relations in the system Nd_2O_3-WO_3 were studied by Rode and Karpor (1966) showing five phases: 3:1, 2:1, 1:1, 1:2 and 1:3 (Fig. 14). They are all isostructural with their counterparts in the Sm-system (Trunov et al., 1968; Polyanskaya et al., 1970a; McCarthy et al., 1972). In addition, a 3:2 phase was prepared hydrothermally which has a tetragonal unit cell (Polyanskaya et al., 1970b).

Five phases were also found in the system Dy_2O_3-WO_3 (Fig. 15)(Ivanova and Reznik, 1972). $3Dy_2O_3 \cdot WO_3$ has a

rhombohedrally distorted fluorite structure (Aitken et al., 1964), a type structure for $3RE_2O_3 \cdot WO_3$ of small rare earths (Tb - Yb). The $5Dy_2O_3 \cdot 2WO_3$ structure is also related to the fluorite structure but has a pseudo-tetragonal cell (McCarthy et al., 1972). $7Dy_2O_3 \cdot 4WO_3$, $Dy_2O_3 \cdot WO_3$ and $Dy_2O_3 \cdot 3WO_3$ are all isostructural with their corresponding Sm phases (Polyanskaya et al., 1970a; Nassau and Shieve, 1972). Ivanova and Reznik (1972) reported a monoclinic $Dy_2O_3 \cdot 3WO_3$ which transforms to an orthorhombic form at 970°C.

SYSTEMS TiO_2-, ZrO_2-, and HfO_2-WO_3

The system TiO_2-WO_3 contains no binary phase, and shows a simple eutectic relationship (Fig. 16)(Chang et al., 1967a), whereas a 1:2 phase characterizes both the ZrO_2-WO_3 and HfO_2-WO_3 systems (Figs. 17 and 18)(Graham et al., 1959; Chang et al., 1967b).

X-ray powder diffraction data of $ZrO_2 \cdot 2WO_3$ can be indexed on the basis of a cubic unit cell with no systematic absence of reflections (Chang et al., 1967b). The crystal structure of $ZrO_2 \cdot 2WO_3$ has not been determined, but Chang (1967a) suggested that it has a defect wolframite-type structure. $ZrO_2 \cdot 2WO_3$ has a lower stability limit at 1105°C, which was determined by treating the stoichiometric composition side by side with the phase previously prepared at 1200°C in a series of runs (Chang et al., 1967b).

Phase relations in the system HfO_2-WO_3 are much like those in the Zr-system, and $HfO_2 \cdot 2WO_3$ is isostructural with $ZrO_2 \cdot 2WO_3$.

SYSTEM V_2O_5-WO_3

Several vanadium tungstates have been reported (Mondet, 1968; Launay-Mondet, 1971), but they all are mixed-valence phases and have compositions deviant from that of the fully oxidized binary join. Preliminary results obtained from a study in progress in this laboratory indicate that this system has a simple eutectic relationship with an invariant point at about 660°C and 4 mole%WO_3.

SYSTEMS Nb_2O_5-WO_3 and Ta_2O_5-WO_3

A number of studies have been made on the system Nb_2O_5-WO_3. Kovba and Trunov (1962), Kovba et al. (1964), Felton (1965), and Gruehn (1965) reported the formation of several niobium tungstates. Goldschmidt (1960) and Fiegel et al. (1964) proposed extensive Nb_2O_5 solid solution, and Roth and Waring (1966) established phase relations in the system. The phase diagram shown in Fig. 19 is a modified version of Roth and Waring's (Levin et al., 1969). In it, the 9:16 and 9:17 phases replace the 6:11 phase and the 30:1 phase should be replaced by the phases 34:1, 20:1 and 13:1.

Roth and Wadsley (1965c) proposed a "Block Principle" and used it to describe crystal structures of niobium

tungstates and to predict possible compound formation in the system. The blocks are made of ReO_3-type octahedra of niobium extending by sharing corners in certain numbers in a- and c-directions and infinite in the third direction. These blocks are joined together by the four-coordinated tungsten atoms. Generally, niobium tungstates can be classed on the basis of unit cell symmetry into two groups: monoclinic and tetragonal. Crystal structures of monoclinic phases, $Nb_{12}WO_{33}$ and $Nb_{16}W_5O_{55}$, and of tetragonal phases, $Nb_{14}W_3O_{44}$ and $Nb_{18}W_8O_{69}$, were determined in detail (Roth and Wadsley, 1965a, 1965b).

In $Nb_{12}WO_{33}$, the blocks of Nb-octahedra are three wide, four long and infinite in the third direction, and are joined with tetrahedrally coordinated W atoms, ordered at the junctions of every four blocks. With W atoms in similar positions, the blocks in $Nb_{16}W_5O_{55}$ are four wide, five long and infinite along the third direction, and in $Nb_{14}W_3O_{44}$ are four wide, four long and infinite along the direction which is the four-fold axis. In $Nb_{18}W_8O_{69}$, the blocks are five wide, five long and infinite in the third direction. W atoms occupy the four coordinated positions, and also share the octahedral positions with Nb atoms in a random arrangement.

The formation of tantalum tungstates and their relative stabilities have been studied by Gruehn (1965), Roth

and Stephenson (1969), Roth et al. (1970), and Stephenson and Roth (1973a, 1973b, 1973c). The phase diagram proposed by Roth et al. is shown in Fig. 20.

Crystal structures of several tantalum tungstates have been described by Stephenson and Roth (1973a, 1973b, 1973c) in terms of UO_3-type subcell. The cations lie in sheets and have a h.c.p. arrangement within each sheet. Oxygen atoms form either distorted octahedra or pentagonal bipyramids around the cation to form the basic structural units. These units are linked together by edge-sharing to form chains within the (001) plane, and each chain is attached to other identical chains by corner-sharing along [001]. Each chain has a regular "herring-bone weave" and the folding causes distortions in crystal structures of tantalum tungstates as compared with the straight linkages in UO_3. The crystal structures of $Ta_{22}W_4O_{67}$ (Stephenson and Roth, 1973a), $Ta_{30}W_2O_{81}$ (Stephenson and Roth, 1973b), and $Ta_{38}WO_{98}$ (Stephenson and Roth, 1973c) are based on, respectively, 13, 8, and 19 subcells of UO_3-type.

SYSTEM MoO_3-WO_3

Phase relations in this system have not been well established, although numerous studies were made. Rieck (1943) proposed a simple eutectic relationship with an invariant point at 765°C and 2 mole%WO_3. Magneli (1949) reported a 1:1 phase

in the system, and Westman and Magneli (1958) found limited solid solutions between MoO_3 and WO_3. Semikina and Limonov (1968) examined x-ray powder diffraction data in the system, and suggested three types of $(Mo,W)O_3$ solid solution. Type I has compositions ranging between 84 and 66.5 mole%WO_3 (including both 1:2 and 1:3 phases), type II between 61.2 and 48 mole%WO_3 (including 1:1 phase), and type III between 44 and 27.5 mole%WO_3 (including both 2:1 and 3:1 phases).

The difficulty in attaining equilibrium in this system is to maintain molybdenum in its fully oxidized state at relatively high temperatures.

SYSTEMS ThO_2-WO_3 and UO_3-WO_3

In the system ThO_2-WO_3, there is a 2:1 phase (Trunov and Kovba, 1963; Spitsyn et al., 1968). This is in consistent with other systems including large tetravalent cations of Zr and Hf (Chang et al., 1967b). Unlike the 2:1 phases in Zr- and Hf-systems, this 2:1 phase of Th is polymorphic and has three forms: the α-form stable above 1360°C, the β-form between 1200° and 1360°C, and the γ-form below 1200°C. Spitsyn et al. also reported that phase assemblages of ThO_2+$ThO_2 \cdot 2WO_3$ and $ThO_2 \cdot 2WO_3$+WO_3 are stable at least to 1200°C.

Phase relations in the system UO_3-WO_3 have been studied in some detail. Trunov et al. (1961), Juenke and Bartram (1964), and Cordfunke (1969) found only one binary

phase $UO_3 \cdot WO_3$, whereas Ampe et al. (1968), and Hauck (1974) reported both $UO_3 \cdot WO_3$ and $UO_3 \cdot 3WO_3$. Phase relations shown in Fig. 21 (Hauck, 1974) were studied under one atmosphere of oxygen. In the system, UO_3 is not stable at relatively high temperatures and decomposes to U_3O_8, which has three forms with transition points at 630° and 850°C. The eutectic temperature given by Hauck is 25°C lower than that proposed by Cordfunke.

Crystal structures of both uranium tungstates are not known, although the unit cell symmetry of $UO_3 \cdot WO_3$ has been reported to be either cubic with a = 3.805Å (Trunov et al., 1961) or monoclinic with a = 7.205, b = 5.482, c = 13.57Å, and β = 104.35° (Juenke and Bartram, 1964).

A phase, $5UO_2 \cdot 19WO_3$, was reported in the system uranium dioxide and tungsten trioxide by Rozanova et al. (1971). It is orthorhombic with cell dimensions, a = 7.814, b = 7.271, and c = 38.67Å.

SYSTEMS Mn-, Fe-, Co-, Ni-Oxide - WO_3

Very few data have been reported on the phase relations in these systems; only that each system has a 1:1, wolframite-type phase (Keeling, 1957; Phillips et al., 1965; Ulka, 1967; Dach et al., 1967). The wolframite-type structure is made up of zig-zag strings of edge-sharing octahedra,

extending along the c-direction and these strings are linked together by sharing corners. Each string contains only one type of cation, either Mn (or Fe, Co, Ni) or W. Both octahedra are considerably distorted. Cell dimensions of $MnO \cdot WO_3$, $FeO \cdot WO_3$, $CoO \cdot WO_3$ and $NiO \cdot WO_3$ as well as other common wolframite-type 1:1 tungstates are listed in Table 2 (Sleight, 1972).

In the system Fe_2O_3-WO_3, a 1:1 phase was reported by Trunov and Kovba (1966). Waring (1965) proposed a 2:5 phase and suggested it to be isostructural with the 2:5 phase he found in the system Al_2O_3-WO_3. Determination of phase relations in this system is now in progress in this laboratory.

SYSTEMS Cu- and Ag-Oxide - WO_3

Gimelforb and Zelikman (1968) reported the formation of a phase with the composition of $Cu_2O \cdot WO_3$ in the process of oxidation of WC in the presence of copper, but its stability is unknown. In the system CuO-WO_3, two phases, 3:1 and 1:1, were prepared (Tkachenki et al., 1975) with melting points at, respectively, 930° and 920°C. The 1:1 phase has a triclinically distorted wolframite-type structure (Gebert and Kihlborg, 1967; Kihlborg and Gebert, 1970). The Cu atoms are surrounded by six oxygens, four of which are in approximately square planar arrangement with the remaining two at a

distance completing an elongated octahedron Van Uitert et al. (1963) reported that this 1:1 phase dissociates extensively at its melting point.

Phase relations in the system Ag_2O-WO_3 are not known.

SYSTEMS ZnO-, CdO-, and HgO - WO_3

All systems, ZnO-WO_3 (Fig. 22)(Kislyakov et al., 1973), CdO-WO_3 (Fig. 23)(Kislyakov and Lopatin, 1967), and HgO-WO_3 (Sleight and Licis, 1971), show the formation of a 1:1 phase. Both ZnO·WO_3 and CdO·WO_3 have the wolframite-type structure, but large distortion exists in CdO·WO_3 (Sharp 1960; Coing-Boyat, 1961; Chang 1967b; Sleight, 1972) Cell dimensions of both ZnO·WO_3 and CdO·WO_3 are listed in Table 2.

HgO·WO_3 is monoclinic (Sleight and Licis, 1971), and its structure has no obvious relationship with either the scheelite or wolframite structure.

SYSTEMS B_2O_3-, Al_2O_3-, Ga_2O_3-, and In_2O_3 - WO_3

Phase relations in the system B_2O_3-WO_3 as determined by Levin (1965)(Fig. 24) are of a simple eutectic type with an S-shaped liquidus and with a solidus near 450°C. No liquid immiscibility exists because, as suggested by Levin, the B - O bonds are not strong enough to maintain a separated B_2O_3-rich liquid phase.

A tentative phase diagram for the system Al_2O_3-WO_3 was given by Waring (1965)(Fig. 25) showing a congruently melting phase with a composition later refined to be 1:3 rather than 2:5 as shown in his phase diagram (Levin et al., 1969). Craig and Stephenson (1968) showed that in the structure, each WO_4 tetrahedron by corner-sharing of oxygen atoms is surrounded by four AlO_6 and each AlO_6 octahedron is surrounded by six WO_4. The 1:3 phase is orthorhombic with a = 12.588, b = 9.055, and c = 9.127Å.

The system Ga_2O_3-WO_3 has a simple eutectic relationship with no formation of a binary phase (Fig. 26), whereas a 1:3 phase exists in the system In_2O_3-WO_3 (Fig. 27)(Karpov and Korotkerich, 1973), and is isostructural with $Al_2O_3 \cdot 3WO_3$ (Abrahams and Berstein, 1966).

SYSTEMS Sn- and Pb-Oxide - WO_3

Tungstates of the Group IVA elements are known only in the tin and lead systems where the cations are in their di-

valent state. $SnO \cdot WO_3$ is dimorphic (Jeitschko and Sleight, 1972) with a transition temperature at 670°C. The low-temperature form is orthorhombic with a = 5.627, b = 11.649, and c = 4.997Å, and the high-temperature form is cubic with a = 7.299Å. Neither structure is related to either the scheelite or the wolframite structure (Sleight, 1972).

Phase relations in the system $PbO-WO_3$ are shown in Fig. 28 (Chang, 1971). The 1:1 phase has the scheelite-type structure and is stable to its melting point. The absence of a phase transition in $PbO \cdot WO_3$ confirms the results of an earlier study (Chang, 1967b). Jaeger and Germs (1921) proposed a phase change at 877°C, but they did not characterize the difference in the high and low temperature forms. It is known that in natural occurrences (Palache et al., 1944) two minerals have this composition; the scheelite-type stolzite and the wolframite-type raspite. Attempts to synthesize raspite under high-pressure failed (Chang, 1971), although a new phase of $PbO \cdot WO_3$ was synthesized in the pressure range between 10 and 35 kbars. Using natural raspite, Shaw and Claringbull (1955) determined an apparent upper stability limit at about 400°C.

SYSTEMS P-, As-, Sb-, and Bi-Oxide - WO_3

Two phases, 1:1 and 1:2, have been reported in the system $P_2O_5-WO_3$ (Schulz, 1955; Kierkegaard, 1958, 1960, 1962; Kierkegaard and Asbrink, 1964), but only the latter was con-

firmed by a recent study of Martinek and Hummel (1970). They reported that the 1:2 phase is stable at least to 1125°C in an open system at atmospheric pressure and has a range of solid solution extended to the 1:1 composition. The 1:2 phase has a framework-type structure (Kierkegaard 1960; Kierkegaard and Asbrink, 1964) made by joining WO_6 octahedra and PO_4 tetrahedra in such a way that each WO_6 is linked to four PO_4 and one other WO_6 and each PO_4 is linked to four WO_6. The 1:2 phase is monoclinic with a = 7.83, b = 12.48, c = 7.76Å, and β = 91.9°. The 1:1 phase, according to Kierkegaard (1958), has a layer structure made up of WO_6 octahedra and PO_4 tetrahedra. No arsenic tungstates have been reported.

Other members of Group VA elements, antimony and bismuth, show a trivalent state in their tungstate formation. In the system Sb_2O_3-WO_3, a 1:1 phase was prepared in sealed capsules under inert gas at 750°C and has a monoclinic symmetry with a = 9.27, b = 9.80, c = 11.05Å, and β = 100.4° (Parmentier et al., 1975).

Phase relations in the system Bi_2O_3-WO_3 have been studied in detail (Sillen and Lundborg, 1943; Smalyaninov and Belyaev, 1962; Gal'perin et al., 1966; Speranakaya, 1970; Hoda and Chang, 1975). Phase relations established by Hoda and Chang are shown in Fig. 29. The 7:1 phase has a tetragonal face-centered structure below 784°C with a = 5.52

and c = 17.39Å and transforms to a f.c.c. structure above 784°C. The 7:2 phase has a f.c.c. structure with a = 5.61Å and forms a complete solid solution series with the high-temperature form of Bi_2O_3 above 784°C. Both 1:1 and 1:2 phases are orthorhombic and have cell dimensions, respectively, of a = 5.45, b = 5.46, c = 16.42Å and a = 5.43, b = 5.41, c = 23.172Å.

Results obtained by Hoda and Chang (1974) confirm in general the limited information provided by Gal'perin et al. (1966), except for their extensive ranges of solid solution at 650°C. As Hoda and Chang stated, "it is suspected that the experimental procedure of those workers, which involved melting the samples at 900° to 1200°C, cooling them rapidly in water, annealing the quenched samples at 650°C for 2 hours, and furnace cooling before x-ray diffraction examination, could have resulted in misleading estimates of solid solution ranges". A better agreement between these two studies can be obtained when the solid solution ranges reported by Gal'perin et al. are considered to represent equilibrium at higher temperatures.

Phase relations proposed by Speranskaya (1970) resulted from annealing of nine compositions at 700°C and subsequent DTA. Neither x-ray diffraction data nor cell dimensions were reported.

207

REFERENCES

Abraham, S. C., and Berstein, J. L., J. Chem. Phys., 45, 2745-2752 (1966)

Aitken, E. A., Bartram, S. F., and Juenke, E. F., Inorg. Chem., 3, 949-954 (1964)

Ampe, B., Leroy, J. M., Thomas, D., and Tridot, G., Rev. Chim. Miner., 5, 789-800 (1968)

Andersson, G., Acta Chem. Scand., 7, 154-158 (1953)

Borchardt, H. J., Inorg. Chem., 2, 170-173 (1963)

Borisov, S. V., and Klevtsova, R. F., Kristallografiya, 15, 38-42 (1970)

Bottelberghs, P. H., and van Buren, R. R., J. Solid State Chem., 13, 182-191 (1975)

Caillet, P., C.R.H. Acad. Sci., 256, 1869-1889 (1963)

Chang, L. L. Y., Mineral. Mag., 36, 436-437 (1967a)

_____, Amer. Mineral., 52, 427-435 (1967b)

_____, J. Amer. Ceramic Soc., 54, 357-358 (1971)

_____, and Phillips, B., Inorg. Chem., 3, 1192-1194 (1964)

_____, and Sachdev, S., J. Amer. Ceramic Soc., 58, 267-270 (1975)

_____, Scroger, M. G., and Phillips, B., J. Amer. Ceramic Soc., 49, 385-390 (1966a)

_____, J. Inorg. Nucl. Chem., 28, 1179-1184 (1966b)

_____, J. Less-common Metals, 12, 51-56 (1967a)

_____, J. Amer. Ceramic Soc., 50, 211-215 (1967b)

Coing-Boyat, J., Acta Cryst., 14, 1100 (1961)

Cordfunke, E. H. P., J. Inorg. Nucl. Chem., 31, 1542-1545 (1969)

Craig, D. C., and Stephenson, N. C., Acta Cryst., B24, 1250-1255 (1968)

Dach, H., Stoll, E., and Weitzel, H., Zeit. Krist., 125, 120-129 (1967)

Felton, E. J., J. Less-common Metals, 9, 206-213 (1965)

Fiegel, L. J., Mohanty, G. P., and Healy, J. H., J. Chem. Eng. Data, 9, 365-369 (1964)

Gal'perin, E. L., Erman, L. Ya., Kolchin, I. K., Belov, M. A., and Chernyshev, K. S., Russ. J. Inorg. Chem., 11, 1137-1143 (1966)

Gebert, E., and Kihlborg, L., Acta Chem. Scand., 21, 2575-2576 (1967)

Gelsing, R. J. H., Stein, H. N., and Stevels, J. M., Rec. Trav. Chim., 84, 1452-1458 (1965)

Gimelfarb, P. A., and Zelikman, A. N., Izv. Vyssh. Ucheb. Zaved. Tsvet. Met., 10, 63-66 (1968). Chem. Abs., 68, 71809k (1968)

Goldschmidt, H. J., Metallurgia, 62, 211-218 and 241-250 (1960)

Graham, J., Wadsley, A. D., Weymouth, J. H., and Williams, L. S., J. Amer. Ceramic Soc., 42, 570 (1959)

Gruehn, R., Mont. Chim., 96, 1789-1792 (1965)

Guerin, R., and Caillet, P., C.R. Acad. Sci., Ser. C, 271, 814-817 (1970)

Hauck, J., J. Inorg. Nucl. Chem., 36, 291-298 (1974)

Hoda, S. N., and Chang, L. L. Y., J. Amer. Ceramic Soc., 57, 323-326 (1974)

Hoermann, F., Zeit. anorg. allgem. Chem., 177, 145-186 (1928)

Ivanova, M. M., Balagina, G. M., and Rode, E. Ya., Izv. Akad. Nauk SSSR, Neorg. Mater., 6, 914-919 (1970)

_____, and Reznik, E. M., Izv. Akad. Nauk SSSR, Neorg. Mater., 8, 981-983 (1972)

Jaeger, R. M., and Germs, H. C., Zeit. anorg. allgem. Chem., 119, 145-173 (1921)

Jeitschko, W., and Sleight, A. W., Acta Cryst., B29, 869-875 (1973)

Juenke, E. F., and Bartram, S. F., Acta Cryst., 17, 618 (1964)

Karpor, V. N., and Korotkerich, I. B., Zh. Neorg. Khim., 18, 520-521 (1973)

Keeling, R. O., Acta Cryst., 10, 209-213 (1957)

Kierkegaard, P., Acta Chem. Scand., 12, 1715-1729 (1958)

_____, Acta Chem. Scand., 14, 657-676 (1960)

_____, Ark. Kemi., 19, 51-74 (1962)

_____, and Asbrink, S., Acta Chem. Scand., 18, 2329-2336 (1964)

Kislyakov, I. P., and Lopatin, B. P., Zh. Neorg. Khim., 12, 3163-3165 (1967)

_____, Smirnova, I. N., and Boguslavskaya, G. I., Izv. Vyssh. Ucheb. Zaved., Khim. Khim. Tekhnol., 16, 1440 (1973)

Kihlborg, L., and Gebert, E., Acta Cryst., B26, 1020-1026 (1970)

Klevtsov, P. V., Kharchenko, L. Ya, and Klevtsova, R. F., Dokl. Akad. Nauk SSSR, 176, 575-577 (1967). Chem. Abs., 68, 24891w (1968)

_____, Kozeva, L. P., and Klevtsova, R. F., Izv. Akad. Nauk SSSR, Neorg. Mater., 7, 1461-1462 (1971)

Kools, F. X. N. M., Koster, A. S., and Rieck, G. D., Acta Cryst., B26, 1974-1977 (1970)

Koster, A. S., Kools, F. X. N. M., and Rieck, G. D., Acta Cryst., B25, 1704-1708 (1969)

Kovba, L. M., and Trunov, V. K., Dokl. Akad. Nauk SSSR, 147, 622-624 (1962)

_____, and Simanov, Ya. P., Zh. Neorg. Khim., 9, 1930-1933 (1964)

Kreidler, E. R., J. Amer. Ceramic Soc., 55, 514-519 (1972)

Launay-Mondet, S., Rev. Chim. Miner., 8, 391-422 (1971)

Laves, F., Bayer, G., and Panagas, A., Schweiz. Mineral. Petrog. Mitt., 43, 217-234 (1963)

Levin, E. M., J. Amer. Ceramic Soc., 48, 491-492 (1965)

_____, Robbins, C. R., and McMurdie, H. F., "Phase Diagrams for Ceramicsts", Amer. Ceramic Soc., 1969

Lindqvist, I., Acta Chem. Scand., 4, 1066-1074 (1950)

Magneli, A., Acta Chem. Scand., 3, 88-89 (1949)

Margarill, S. A., Klevtsova, R. F., and Bakakin, V. V., Kristallografiya, 18, 269-276 (1973)

Martinek, C. A., and Hummel, F. A., J. Amer. Ceramic Soc., 53, 159-161 (1970)

McCarthy, G. J., Fischer, R. D., Johnson, G. G., and Gooden, C. E., "Solid State Chemistry", NBS Spec. Publ., 364, 397-410 (1972)

Mokhosoev, M. V., Kuleshov, I. M., and Fedorov, P. I., Zh. Neorg. Khim., 7, 1628-1631 (1962)

Mondet, S., Acad. Soc. Paris., Sect. C, 267, 1689-1691 (1968). Chem. Abs., 70, 109803k (1969)

Nassau, K., and Mills, A. D., Acta Cryst., 15, 808-809 (1962)

_____, Levinstein, H. J., and Loiacona, C. M., J. Phys. Chem. Solids, 26, 1805-1816 (1965)

_____, and Shieve, J. W., "Solid State Chemistry", NBS Spec. Publ., 364, 445-456 (1972)

Palache, C., Berman, H., and Frondel, C., "Dana's System of Mineralogy", 7th ed., vol. II, John-Wiley & Sons, New York, 1944

Parmentier, M., Gleitzer, C., and Aubrey, J., C.R. Acad. Sci., Ser. c, 274, 1681-1683 (1972a)

_____, Reau, J. M., Fouassier, C., and Gleitzer, C., Bull. Soc. chim. Fr., 1743-1746 (1972b)

_____, Courtous, A., and Gleitzer, C., C.R.Hebd., Seances Acad. Sci., Ser. C, 280, 985-986 (1975)

Phillips, B., Chang, L. L. Y., and Scroger, M. G., Trans. AIME, Metal. Soc., 233, 1220-1226 (1965)

Pistorius, C. W. F. T., J. Chem. Phys., 44, 4532-4537 (1966)

Polyanskaya, T. M., Borisov, S. V., and Belov, N. V., Dokl. Akad. Nauk SSSR, 193, 83-86 (1970a)

_____, Kristallografiya, 15, 1135-1139 (1970b)

Purt, G., Zeit. Phys. Chem., 35, 133-138 (1962)

Reau, J. M., and Fouassier, C., Bull. Soc. chim. Fr., 398-402 (1971)

_____, and Hagenmuller, P., Bull. Soc. chim. Fr., 3873-3876 (1967)

Rieck, G. D., Rec. Trav. Chim., 62, 427-430 (1943)

Rode, E. Ya., and Karpor, V. N., Izv. Akad. Nauk SSSR, Neorg. Mater., 2, 683-687 (1966)

Roth, R. S., and Wadsley, A. D., Acta Cryst., 19, 32-38 (1965a)

_____, Acta Cryst., 19, 38-42 (1965b)

_____, Acta Cryst., 19, 42-47 (1965c)

Roth, R. S., and Waring, J. L., J. Res. NBS, 70A, 281-303 (1966)

_____, and Parker, H. S., J. Solid State Chem., 2, 445-461 (1970)

Roth, R. S., and Stephenson, N. C., "Chem. Extended Defects, Nonmetal Solids", Proc. Inst. Adv. Study, 167-182 (1969)

Rozanova, O. N., Kovba, L. M., and Trunov, V. K., Radiokhimiya, 13, 307-309 (1971). Chem. Abs., 75, 54496h (1971)

Sakka, S., Bull. Inst. Chem. Res., Kyoto Univ., 46, 300-308 (1968)

Scholder, R., and Brixner, L., Zeit. Natrforsch., B10, 178-179 (1955)

Schulz, I., Zeit. anorg. allgem. Chem., 281, 99-112 (1955)

Semikina, L. E., and Limonov, V. E., Zh. Neorg. Khim., 13, 1932-1935 (1968)

Sharp, W. E., Zeit. Krist., 114, 151-153 (1960)

Shaw, R., and Claringbull, G. E., Amer. Mineral., 40, 933 (1955)

Sillen, L. G., and Lundborg, K., Ark. Kemi., Mineral. Geol., 17A, 1-11 (1943)

Sleight, A. W., Acta Cryst., B28, 2889-2902 (1972)

_____, and Licis, M. S., Mater. Res. Bull., 6, 365-369 (1971)

Smolyaninov, N. P., and Belyaev, I. N., Zh. Neorg. Khim., 7, 2591-2595 (1962)

Speranskaya, E. I., Izv. Akad. Nauk SSSR, Neorg. Mater., 1, 149-151 (1970)

Spitsyn, V. I., and Kuleshov, I. M., Zh. Fiz. Khim., 24, 1197-1200 (1950)

_____, and Tikhomirov, I. I., J. Gen. Chem.,(USSR), 8, 1527-1533 (1938)

_____, Pokrovskii, A. N., Afonskii, N. S., and Trunov, V. K., Dokl. Akad. Nauk SSSR, 188, 1065-1068 (1968)

Stephenson, N. C., and Roth, R. S., Acta Cryst., 27, 1010-1017 (1973a)

_____, Acta Cryst., 27, 1018-1024 (1973b)

_____, Acta Cryst., 27, 1031-1036 (1973c)

Stewart, E. G., and Rooksby, H. P., Acta Cryst., 4, 503-507 (1951)

Tkachenki, E. V., Zhukovski, V. M., and Tel'nyk, T. F., Zh. Fiz. Khim., 49, 809 (1975). Chem. Abs., 83, 36904a (1975)

Tokunov, O. I., and Kislyakov, I. P., Izv. Vyssh. Ucheb. Zaved., Khim. Khim. Tekhnol., 15, 1609-1612 (1972)

Trunov, V. K., and Kovba, L. M., Vesta. Mosk. Univ., Ser. II, Khim., 18, 60-63 (1963). Chem. Abs., 59, 5878f (1963)

_____, Izv. Akad. Nauk SSSR, Neorg. Mater., 2, 151-154 (1966)

_____, and Spitsyn, V. I., Dokl. Akad. Nauk SSSR, 141, 114-116 (1961)

_____, Tynshevskaya, V., and Afronskii, N. S., Zh. Neorg. Khim., 13, 936-939 (1968)

Van Uitert, L. G., Rubin, J. J., and Boumer, W. A., J. Amer. Ceramic Soc., 46, 512 (1963)

Ulku, D., Zeit. Krist., 124, 192-219 (1967)

Waring, J. L., J. Amer. Ceramic Soc., 48, 493-494 (1965)

Westman, S., and Magneli, A., Acta Chem. Scand., 12, 363-364 (1958)

Young, A. P., and Schwartz, C. M., Science, 141, 348-349 (1963)

Zachariasen, W. H., and Plettinger, H. H., Acta Cryst., 14, 229-230 (1961)

Zhmud, E. S., and Ostapchenko, E. P., Zh. Strukt. Khim., 2, 33-45 (1961)

Table 1. Comparison of Reported Melting Points (°C) of Potassium Tungstates

Tungstate	Hoermann (1928)	Mokhosoev et al. (1962)	Gelsing et al. (1965)	Guerin and Caillet (1970)	Chang and Sachdev (1975)
$K_2O \cdot WO_3$	921°(c)	926°(c)	912°(c)	921°(c)	912°(c)
$K_2O \cdot 2WO_3$	-	-	654°(i)	619°(i)	684°(i)
$K_2O \cdot 3WO_3$	660°(i)	715°(i)	718°(i)	710°(i)	842°(i)
$K_2O \cdot 4WO_3$	930°(i)	930°(i)	898°(i)	812°(i)	912°(i)
$K_2O \cdot 6WO_3$	-	-	-	938°(i) (solid solution between 1:6 and 1:8 phases)	964°(i)

Table 2. Cell Dimensions of Common Wolframite-Type, 1:1 Tungstates (Sleight, 1972)

Tungstate	a, Å	b, Å	c, Å	β
$MgO \cdot WO_3$	4.687	5.675	4.928	90.71°
$MnO \cdot WO_3$	4.829	5.758	4.996	91.15°
$FeO \cdot WO_3$	4.724	5.705	4.961	90.00°
$CoO \cdot WO_3$	4.667	5.681	4.947	90.00°
$NiO \cdot WO_3$	4.599	5.665	4.910	90.00°
$ZnO \cdot WO_3$	4.690	5.718	4.926	90.64°
$CdO \cdot WO_3$	5.027	5.858	5.073	91.49°

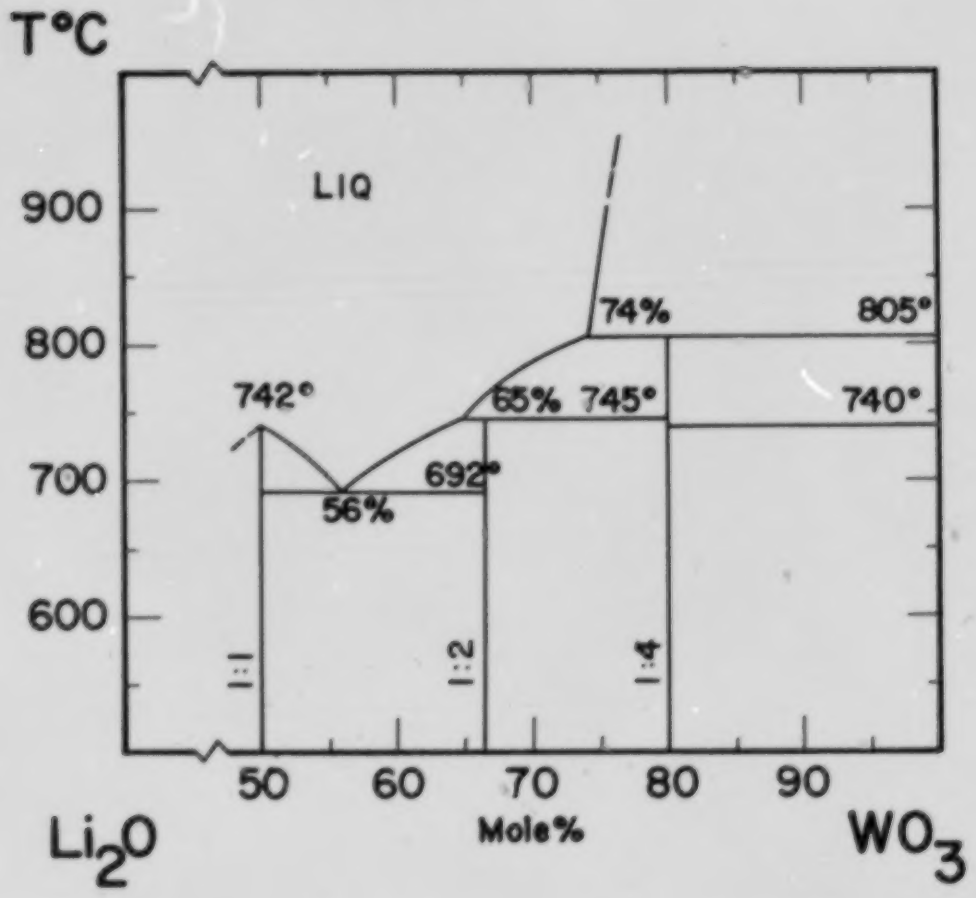

FIGURE 1. Phase relations in the system $Li_2O \cdot WO_3$-WO_3 (Chang and Sachdev, 1975)

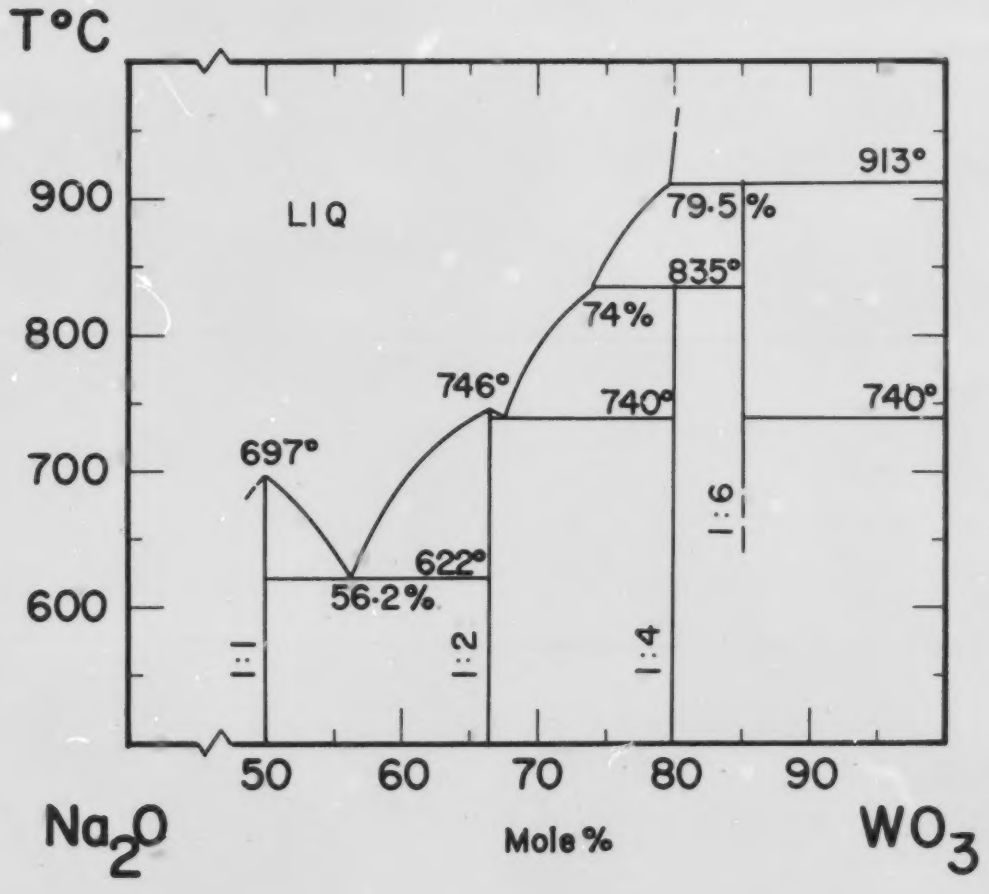

FIGURE 2. Phase relations in the system $Na_2O \cdot WO_3$-WO_3 (Chang and Sachdev, 1975)

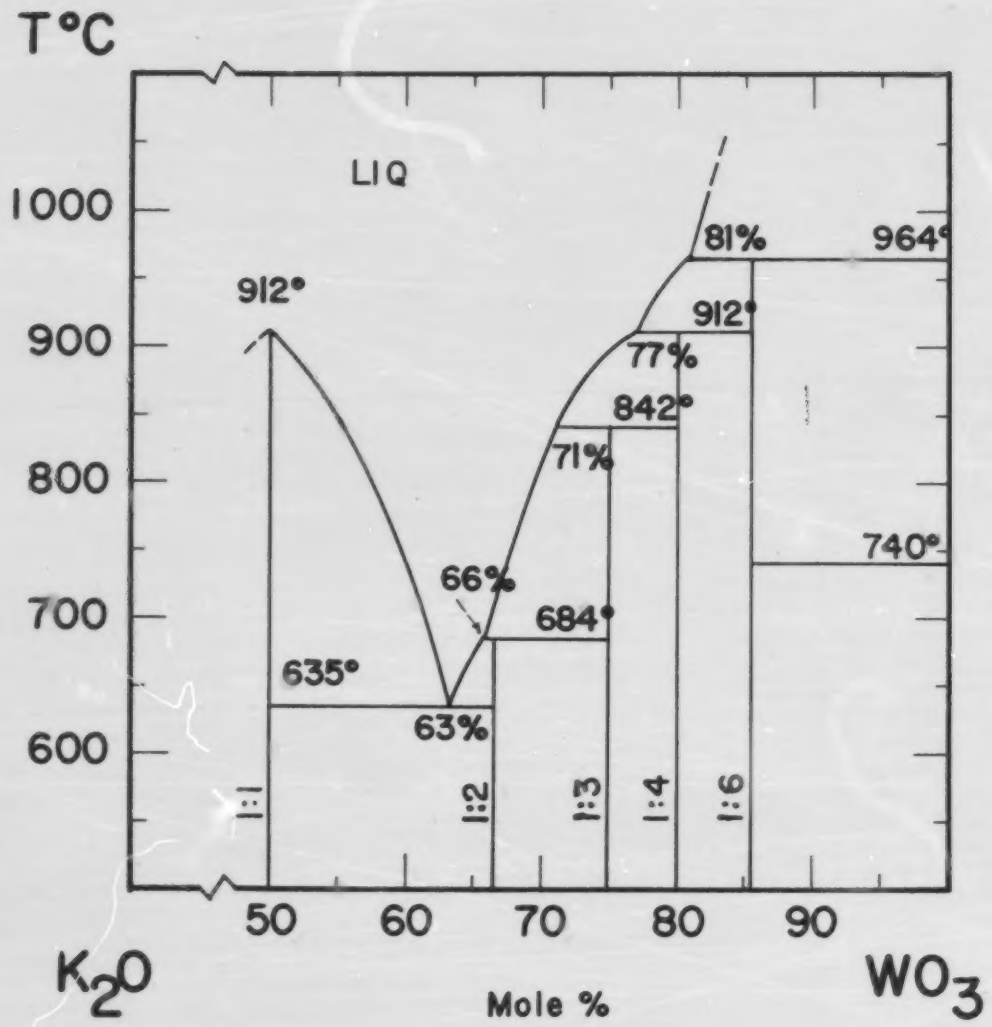

FIGURE 3. Phase relations in the system $K_2O \cdot WO_3$-WO_3 (Chang and Sachdev, 1975)

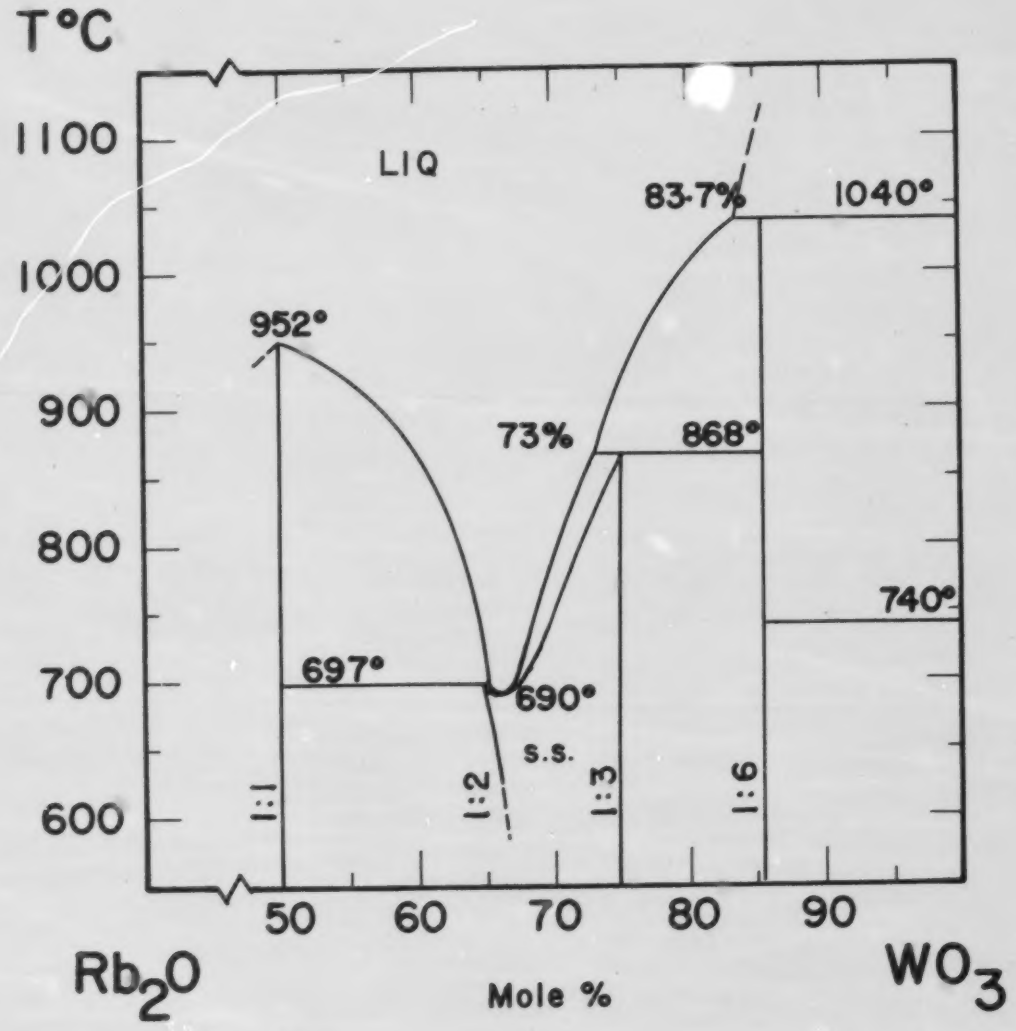

FIGURE 4. Phase relations in the system $Rb_2O \cdot WO_3$-WO_3 (Chang and Sachdev, 1975)

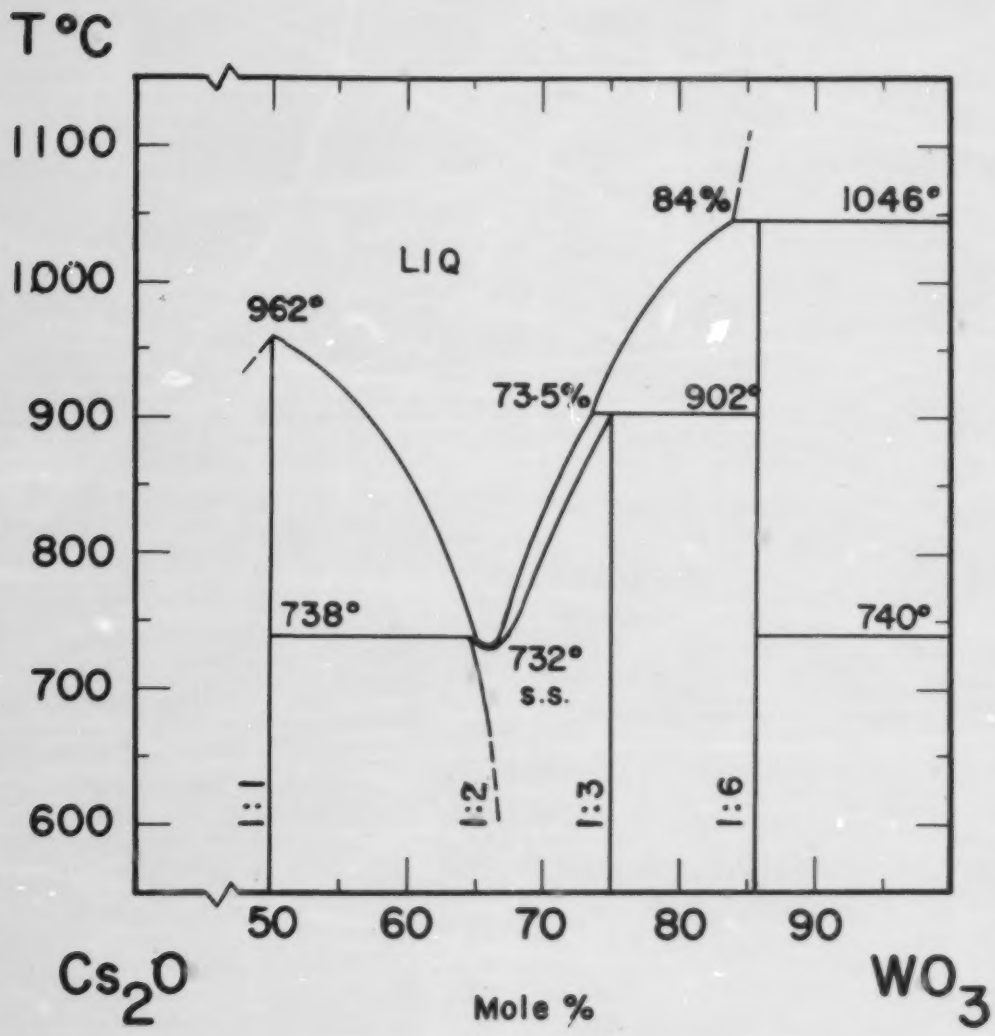

FIGURE 5. Phase relations in the system $Cs_2O \cdot WO_3$-WO_3 (Chang and Sachdev, 1975)

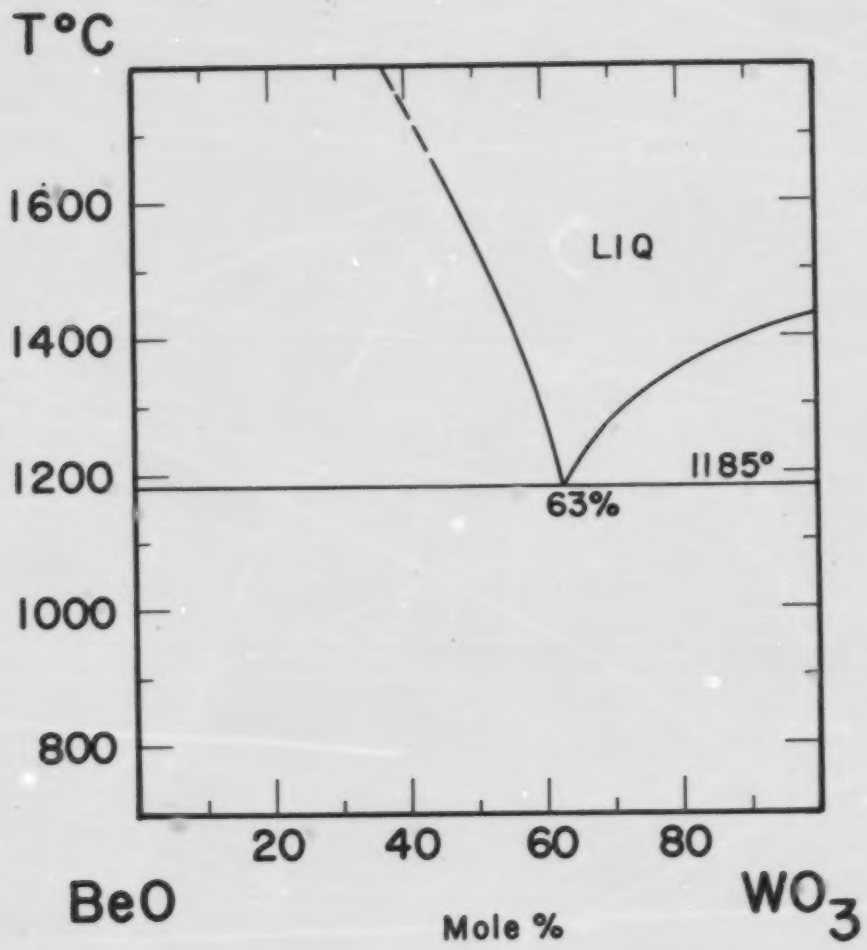

FIGURE 6. Phase relations in the system BeO-WO_3 (Chang et al., 1966a)

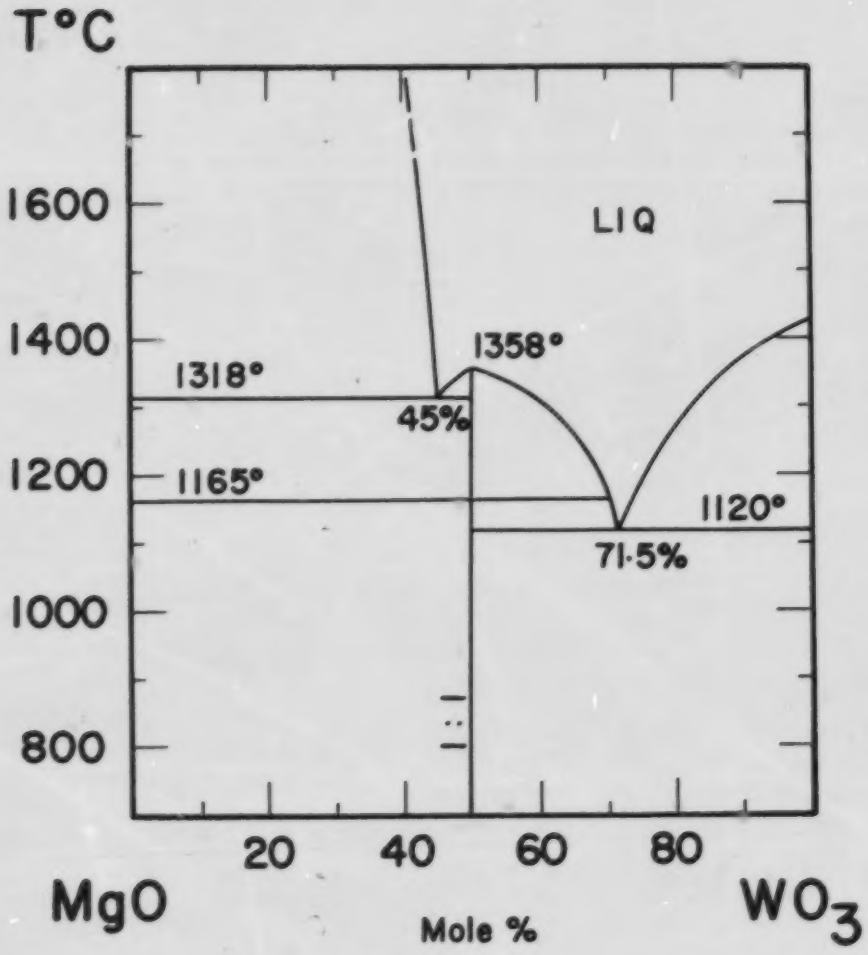

FIGURE 7. Phase relations in the system $MgO-WO_3$ (Chang et al., 1966a)

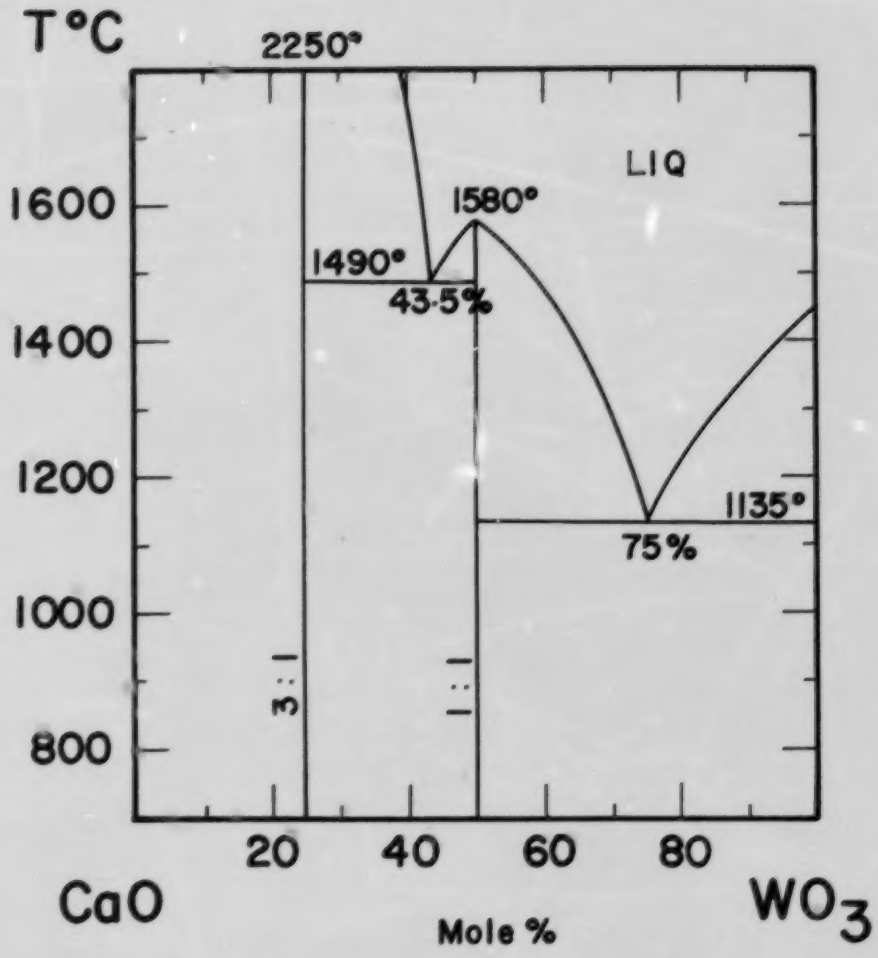

FIGURE 8. Phase relations in the system $CaO-WO_3$ (Chang et al., 1966a)

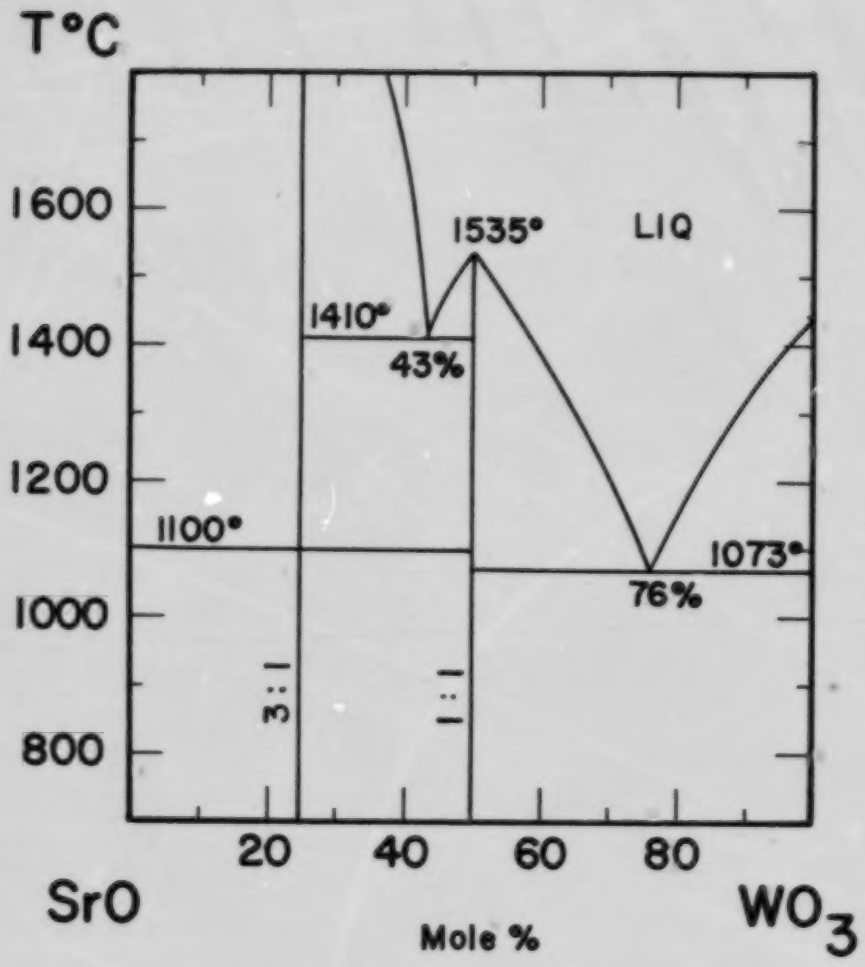

FIGURE 9. Phase relations in the system SrO-WO_3 (Chang et al., 1966a)

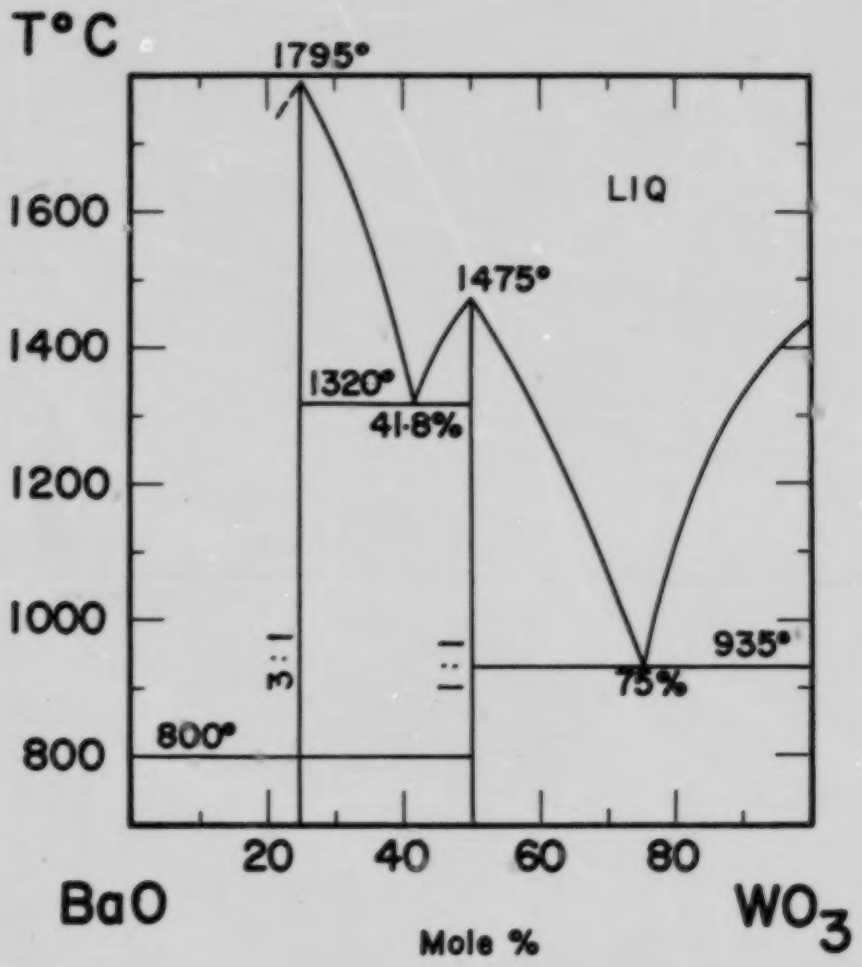

FIGURE 10. Phase relations in the system $BaO-WO_3$ (Chang et al., 1966a)

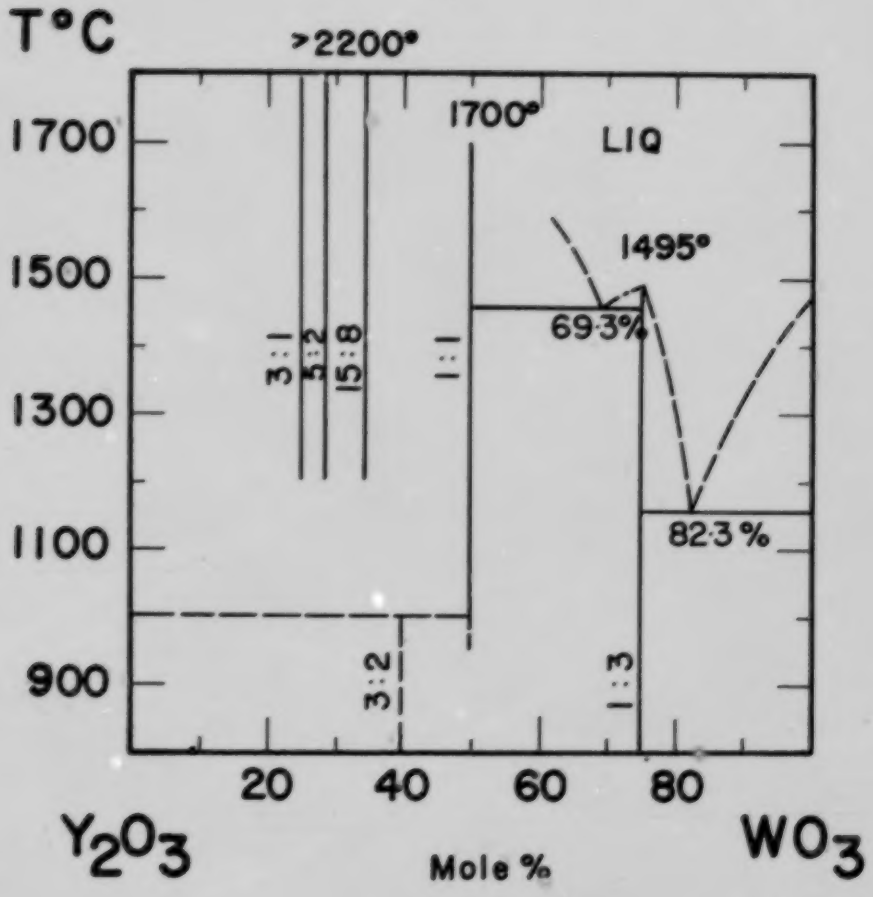

FIGURE 11. Phase relations in the system Y_2O_3-WO_3 (Borchardt, 1963)

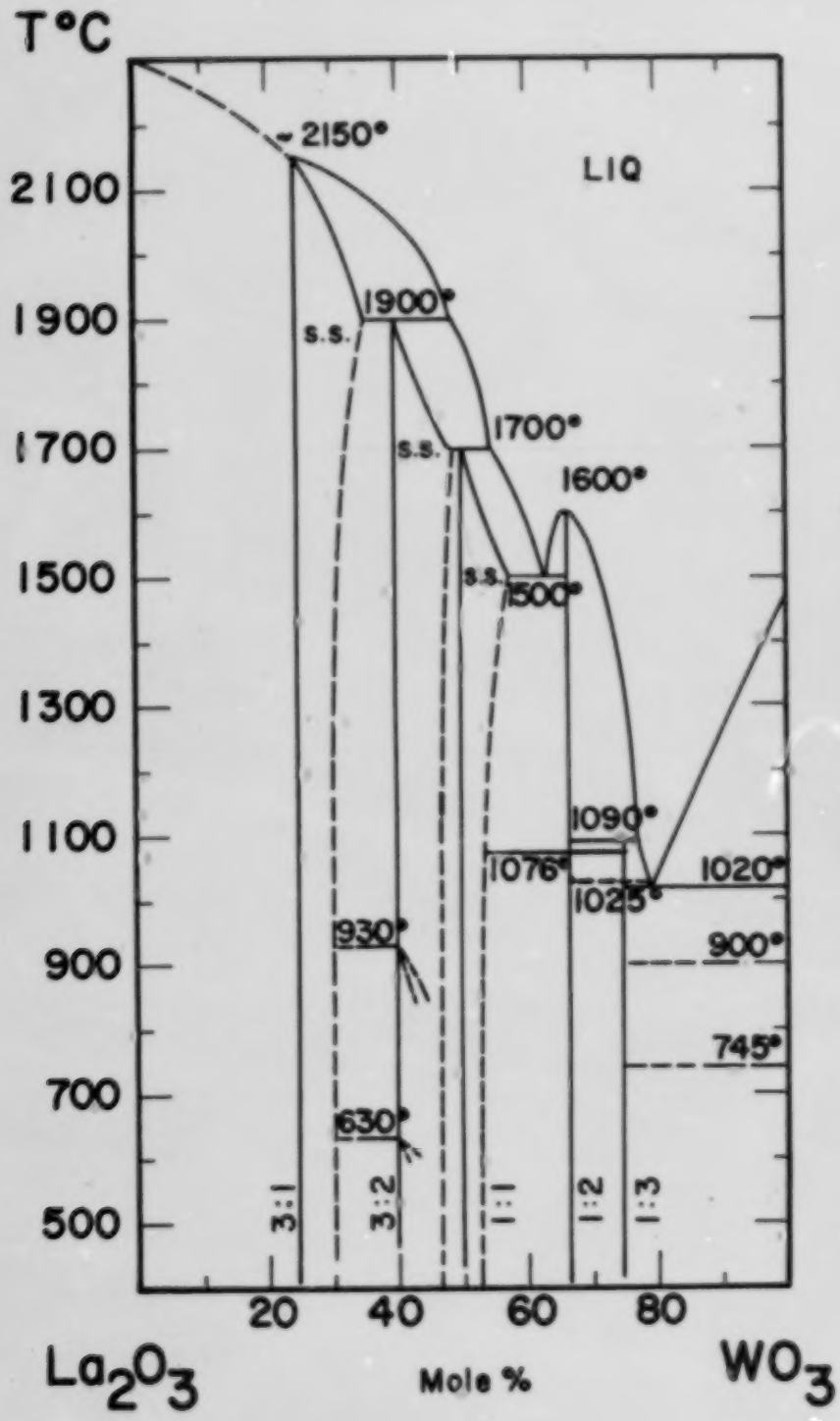

FIGURE 12. Phase relations in the system La_2O_3-WO_3 (Ivanona et al., 1970)

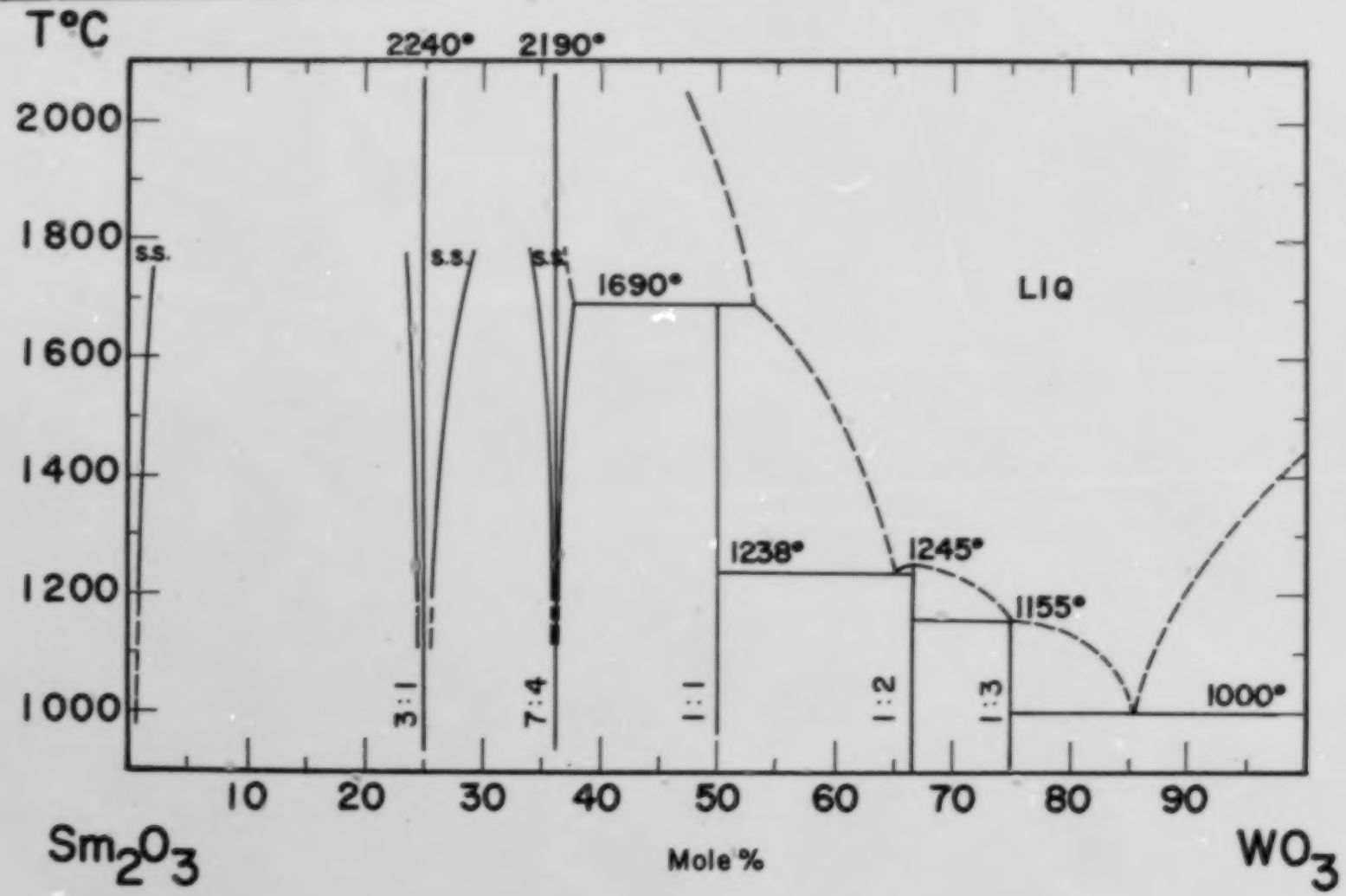

FIGURE 13. Phase relations in the system Sm_2O_3-WO_3

(Chang et al., 1966b)

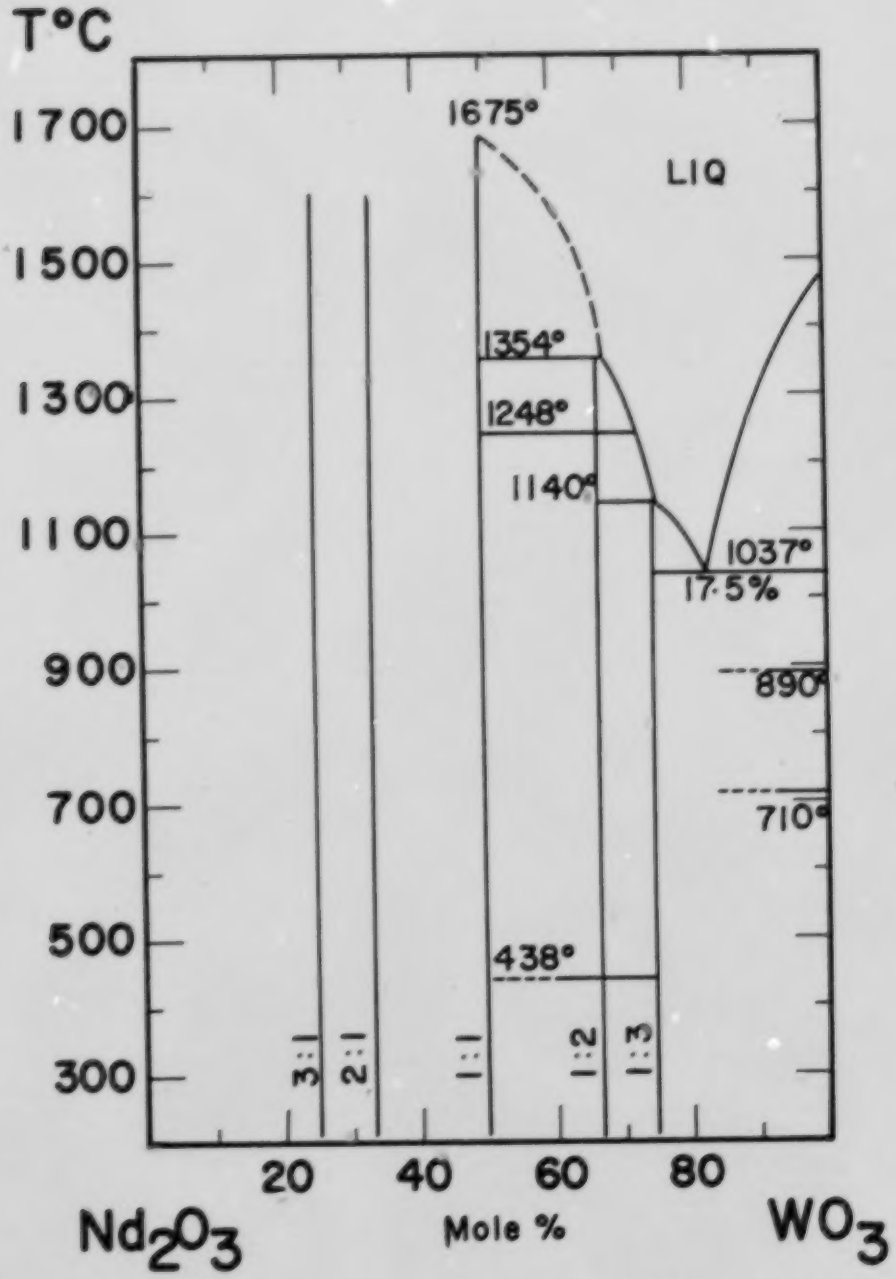

FIGURE 14. Phase relations in the system Nd_2O_3-WO_3 (Rode and Karpor, 1966)

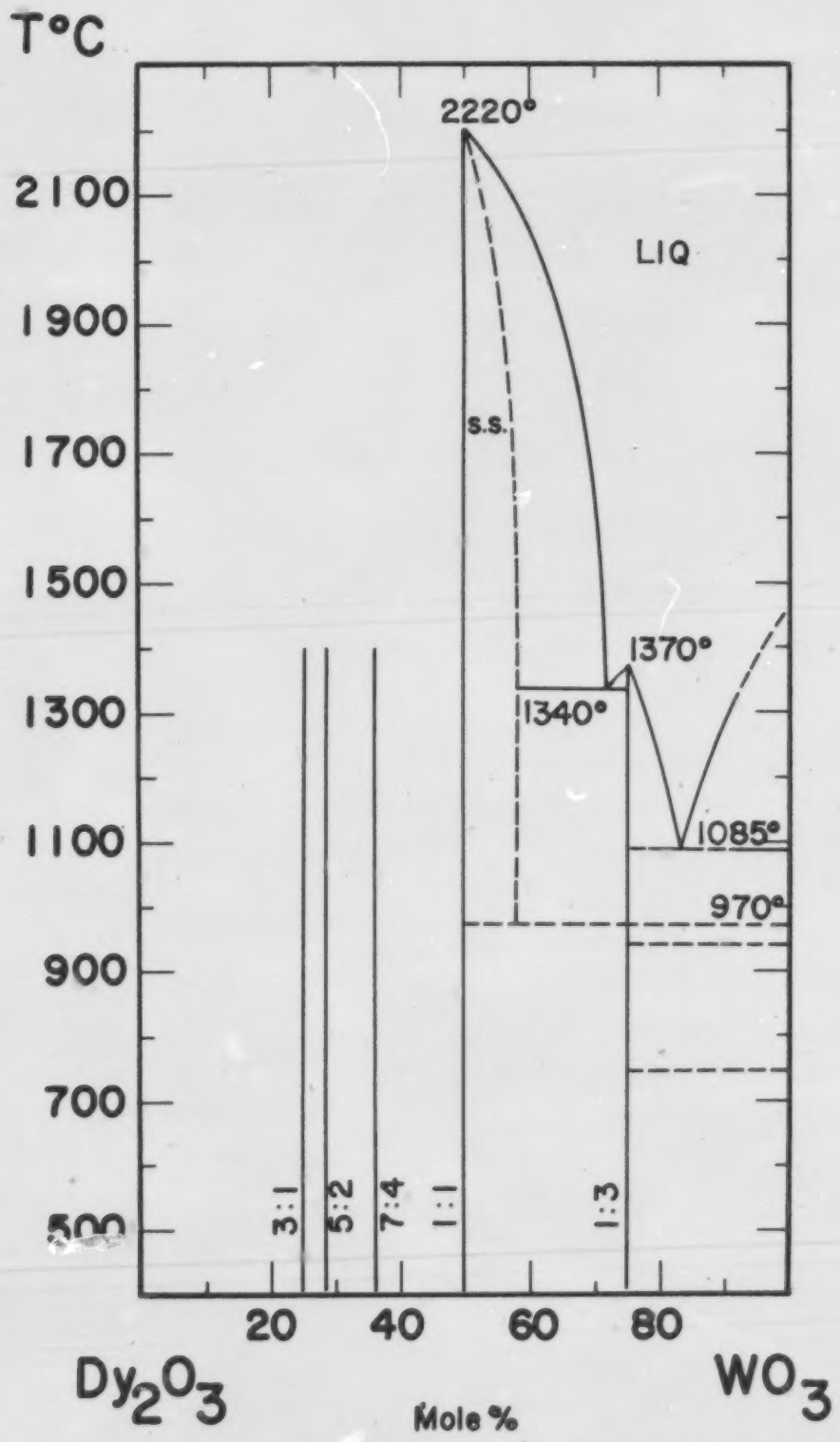

FIGURE 15. Phase relations in the system Dy_2O_3-WO_3 (Ivanova and Reznik, 1972)

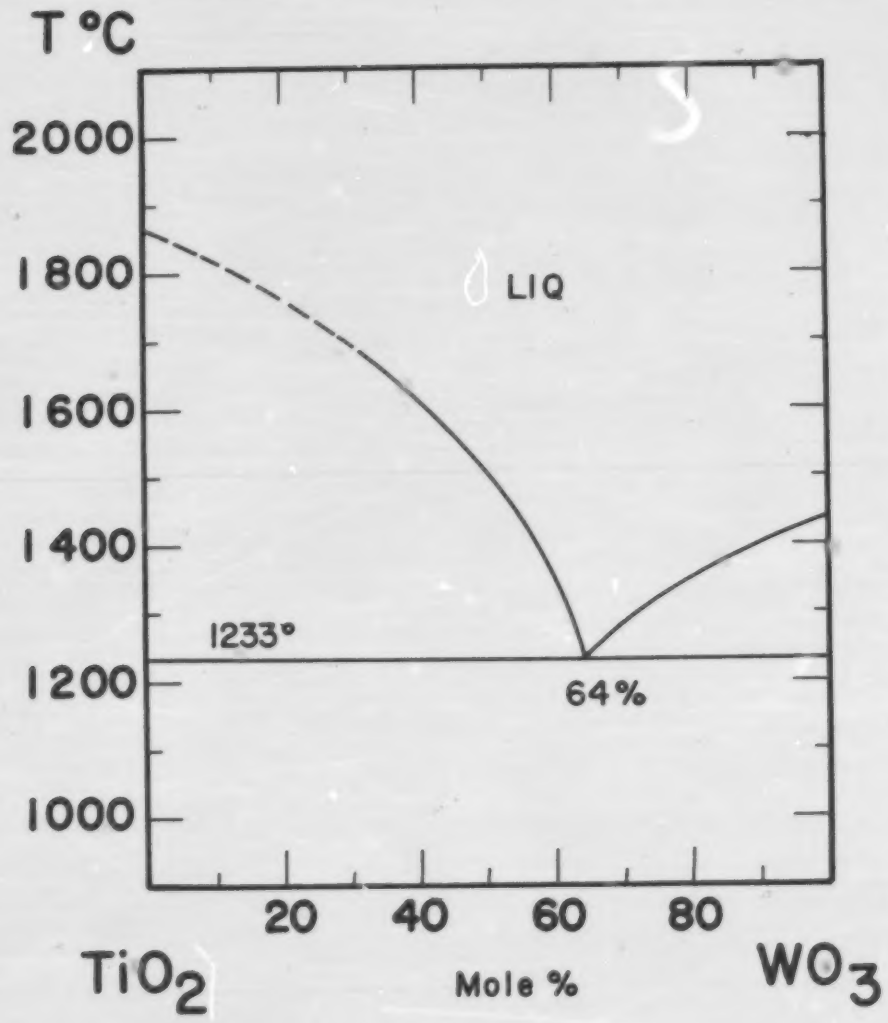

FIGURE 16. Phase relations in the system TiO_2-WO_3 (Chang et al., 1967a)

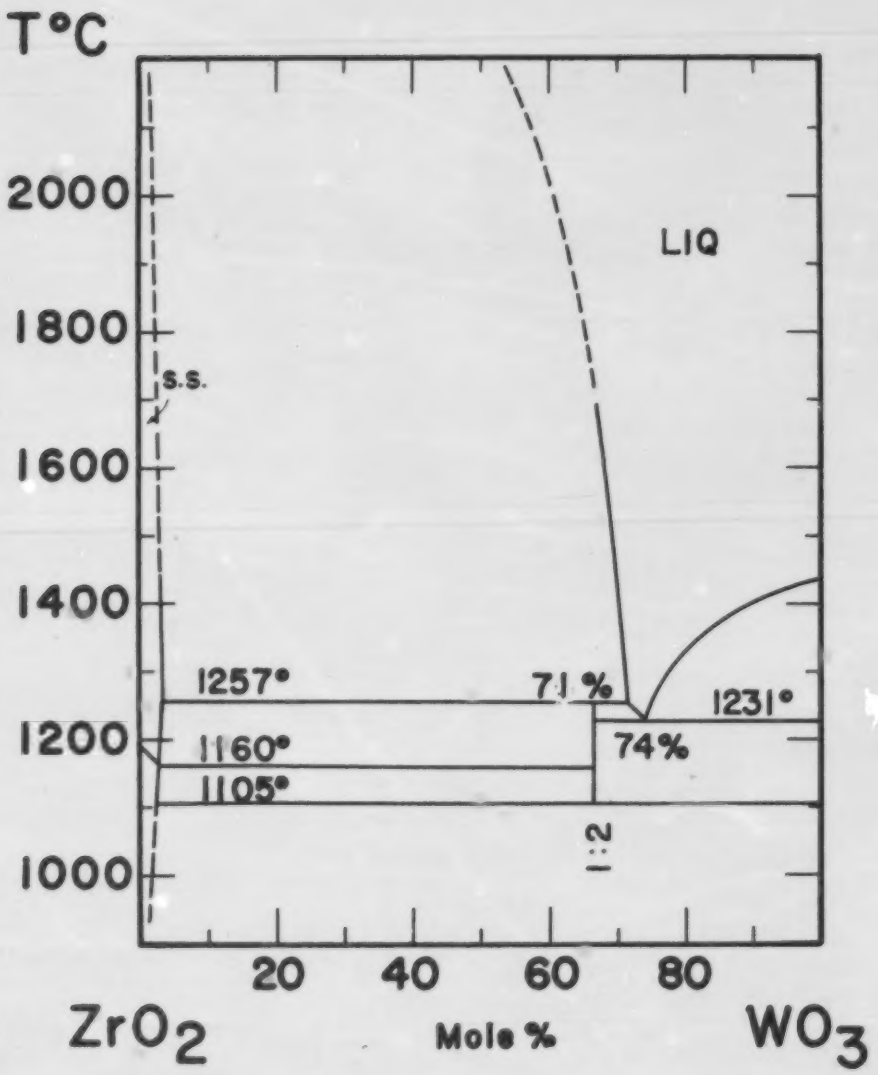

FIGURE 17. Phase relations in the system ZrO_2-WO_3 (Chang et al., 1967b)

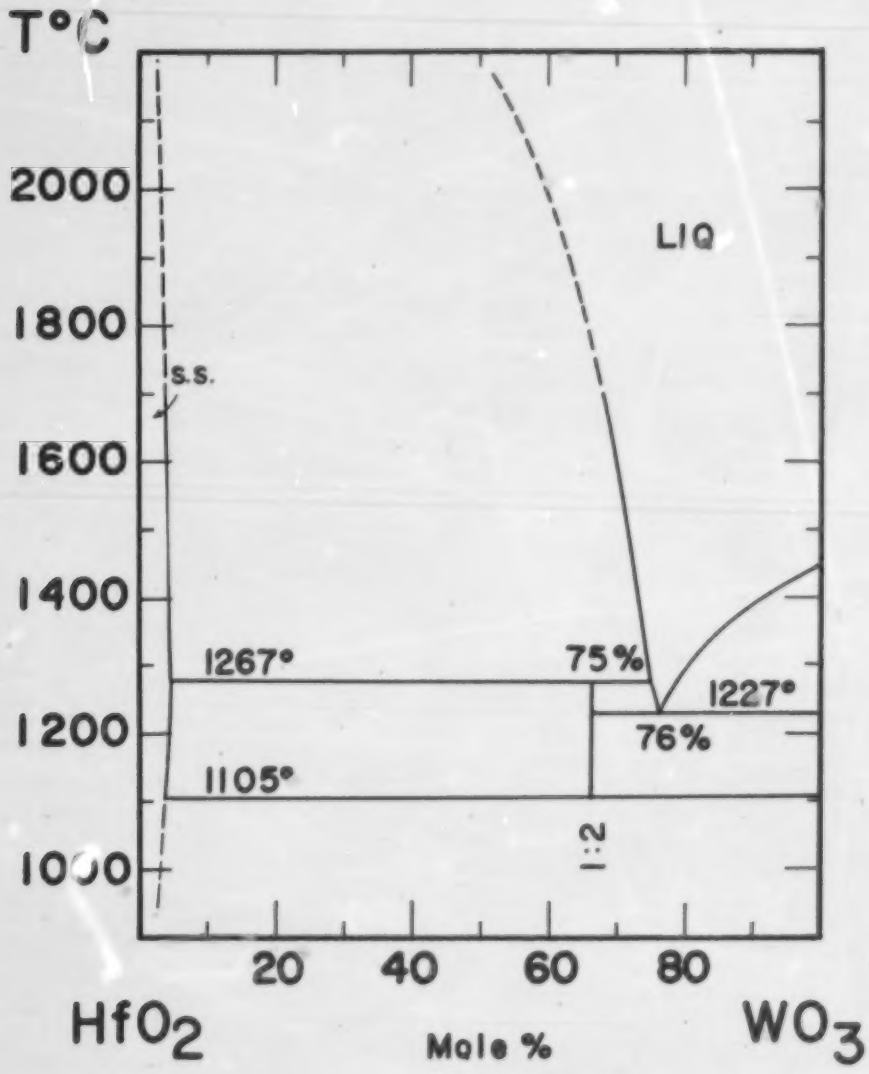

FIGURE 18. Phase relations in the system HfO_2-WO_3 (Chang et al., 1967b)

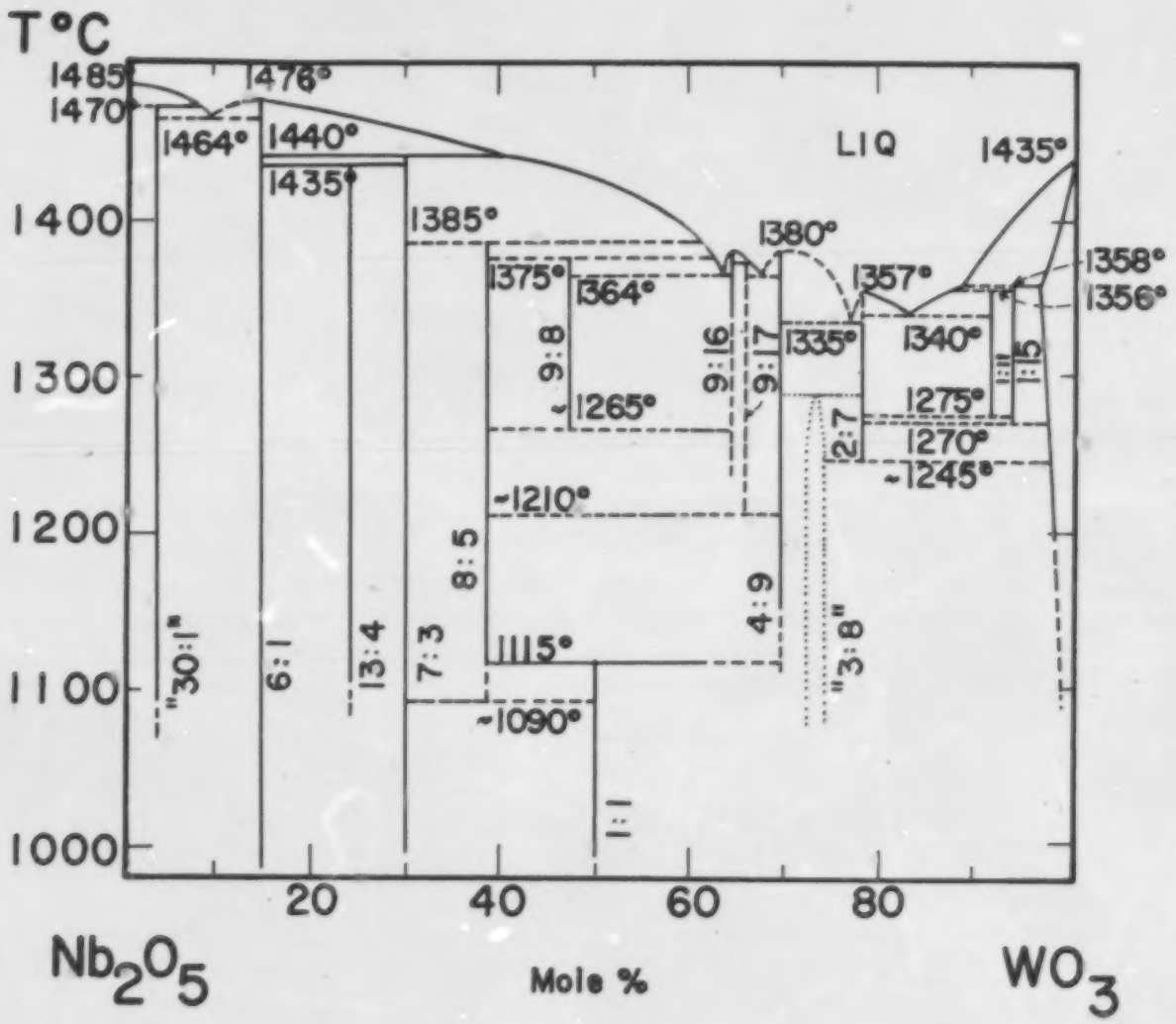

FIGURE 19. Phase relations in the system Nb_2O_5-WO_3 (Roth and Waring, 1966; Levin et al., 1969)

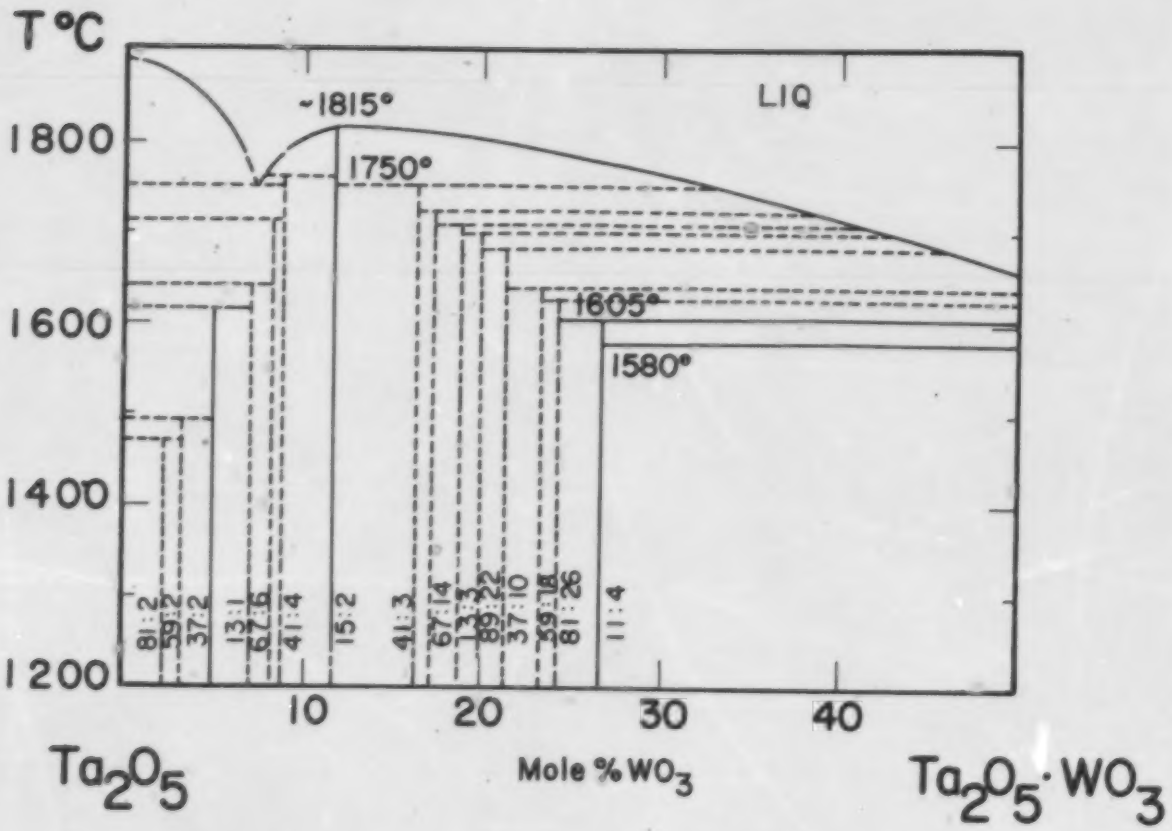

FIGURE 20. Phase relations in the system Ta_2O_5-WO_3 (Roth et al., 1970)

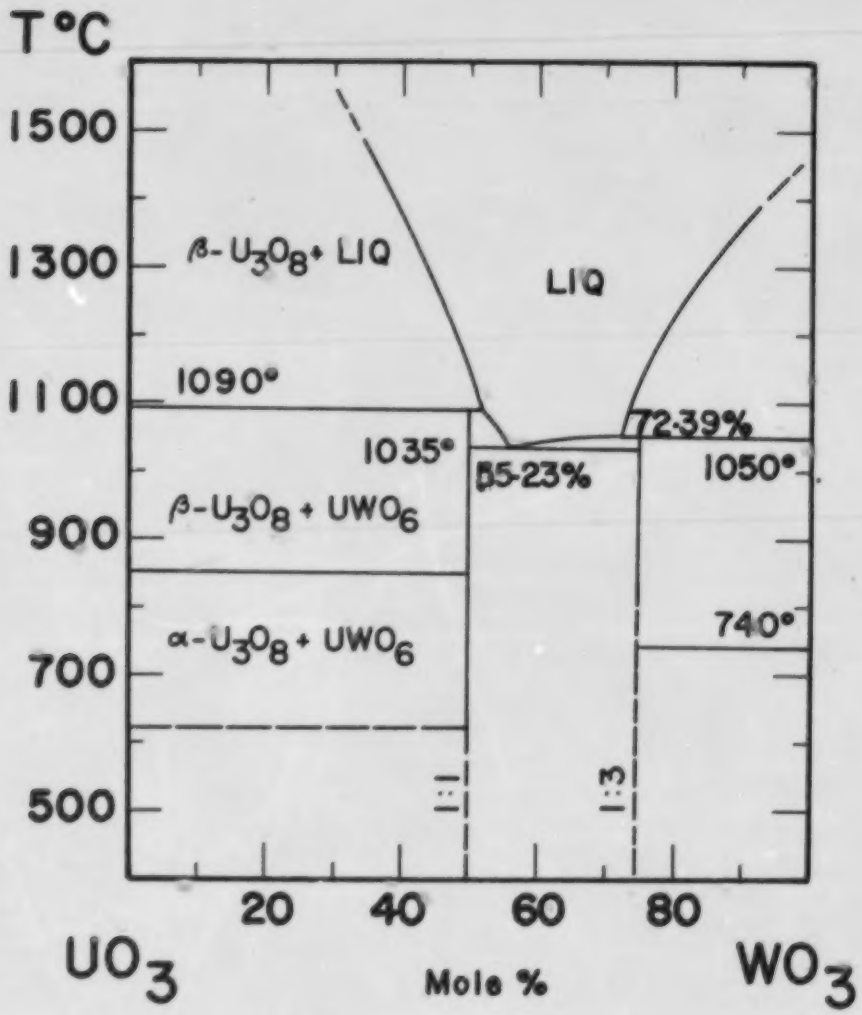

FIGURE 21. Phase relations in the system UO_3-WO_3 (Hauck, 1974)

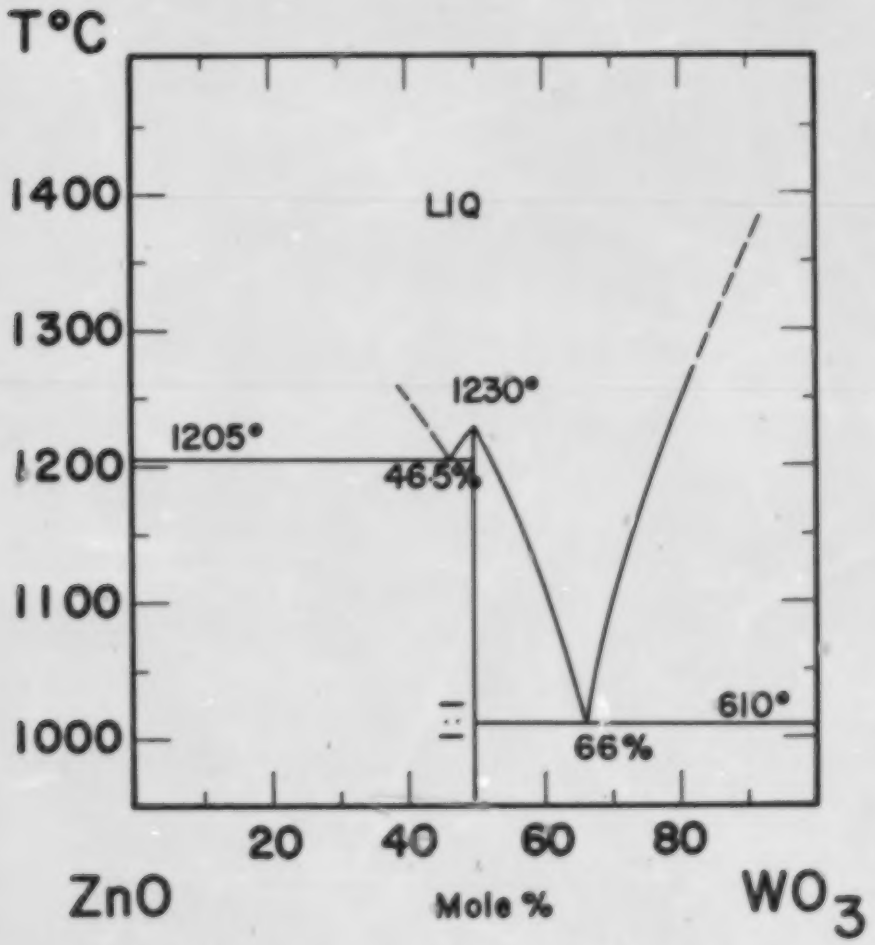

FIGURE 22. Phase relations in the system $ZnO-WO_3$ (Kislyakov et al., 1973)

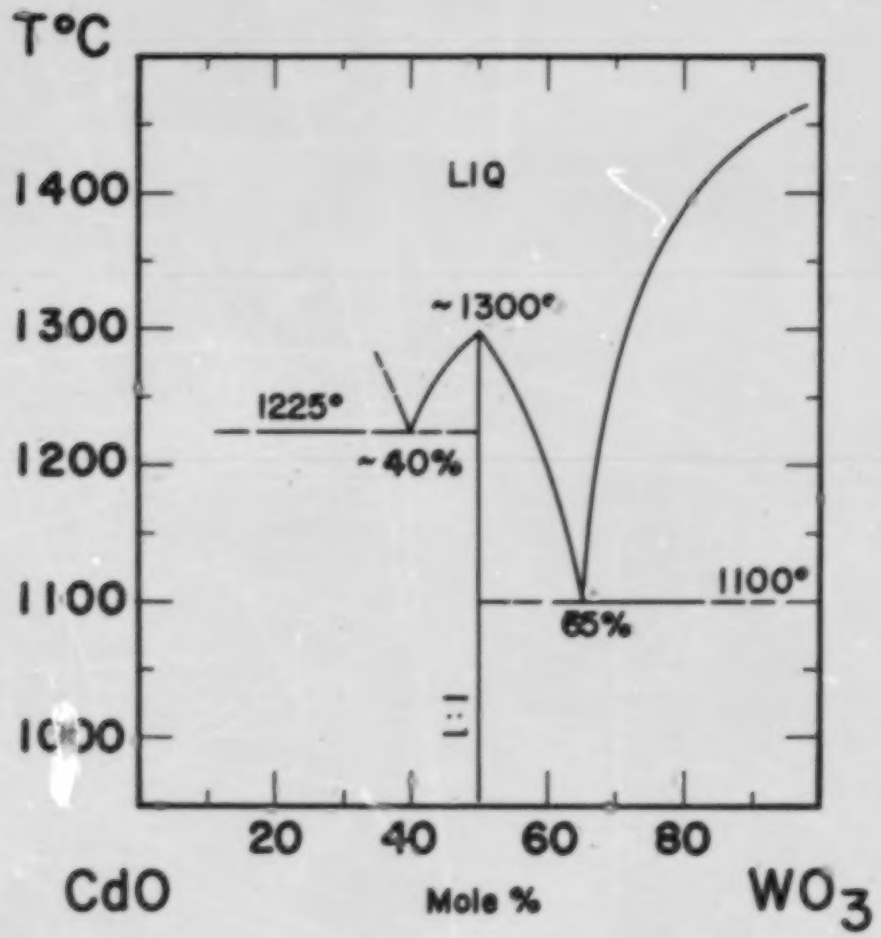

FIGURE 23. Phase relations in the system CdO-WO_3 (Kislyakov and Lopatin, 1967)

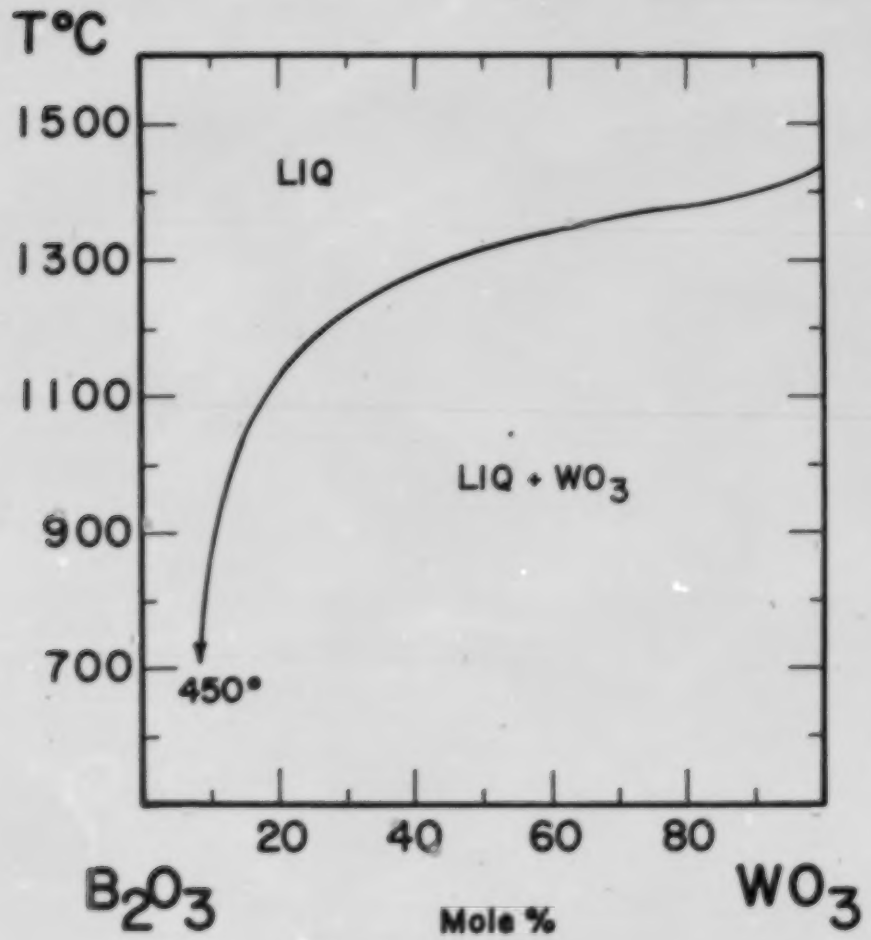

FIGURE 24. Phase relations in the system B_2O_3-WO_3 (Levin, 1965)

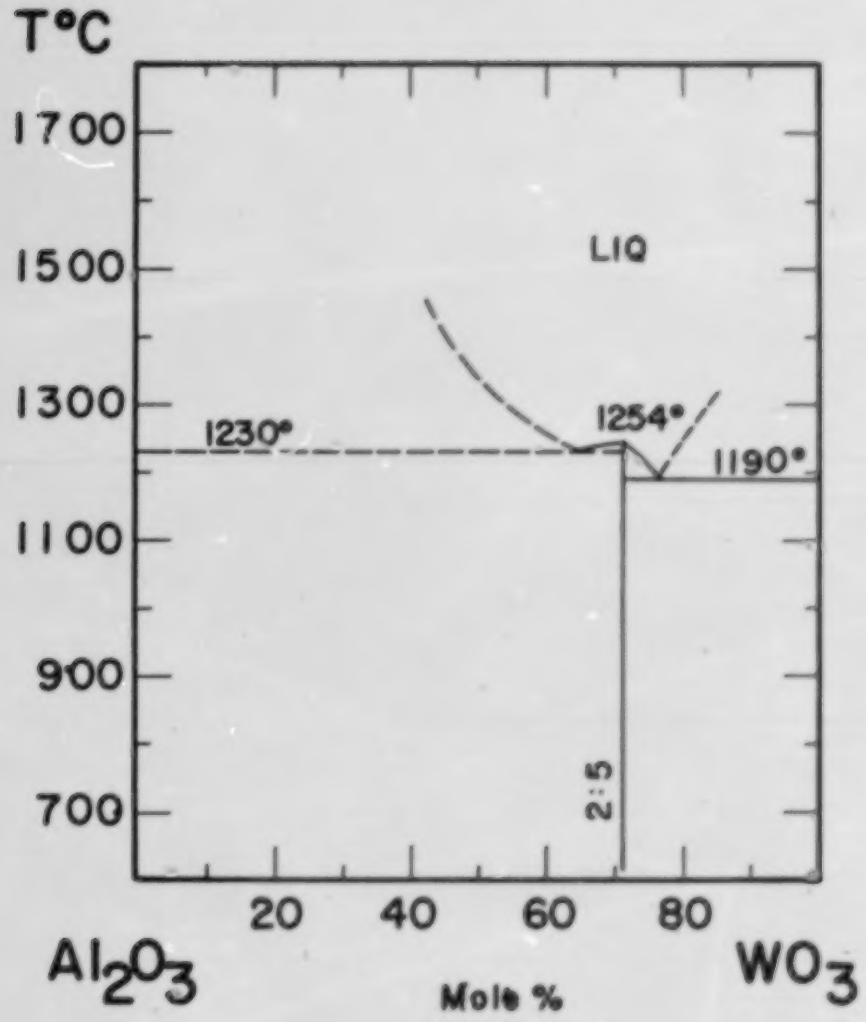

FIGURE 25. Phase relations in the system Al_2O_3-WO_3 (Waring, 1965; Levin et al., 1969)

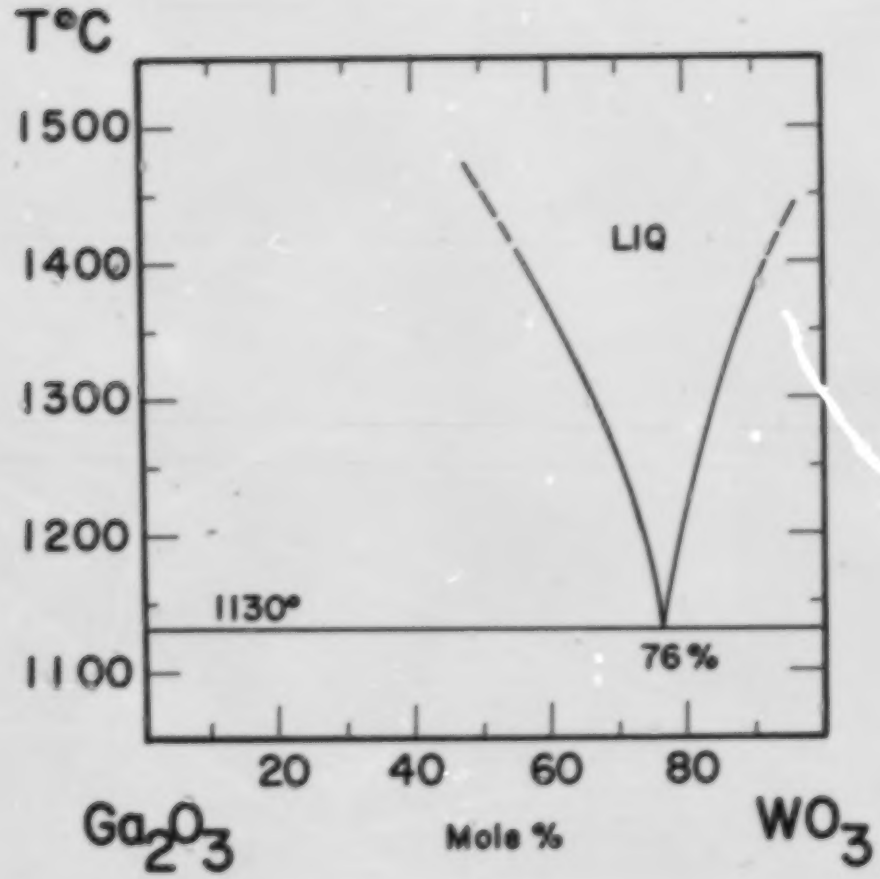

FIGURE 26. Phase relations in the system Ga_2O_3-WO_3 (Karpor and Korotkerich, 1973)

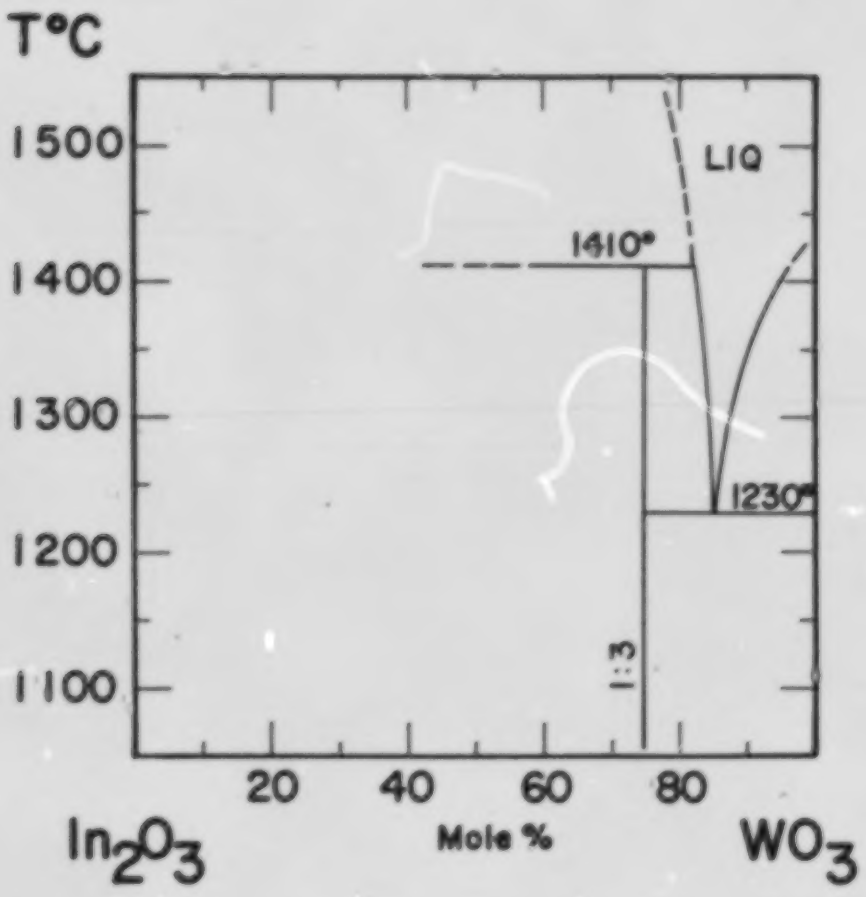

FIGURE 27. Phase relations in the system In_2O_3-WO_3 (Karpor and Korotkerich, 1973)

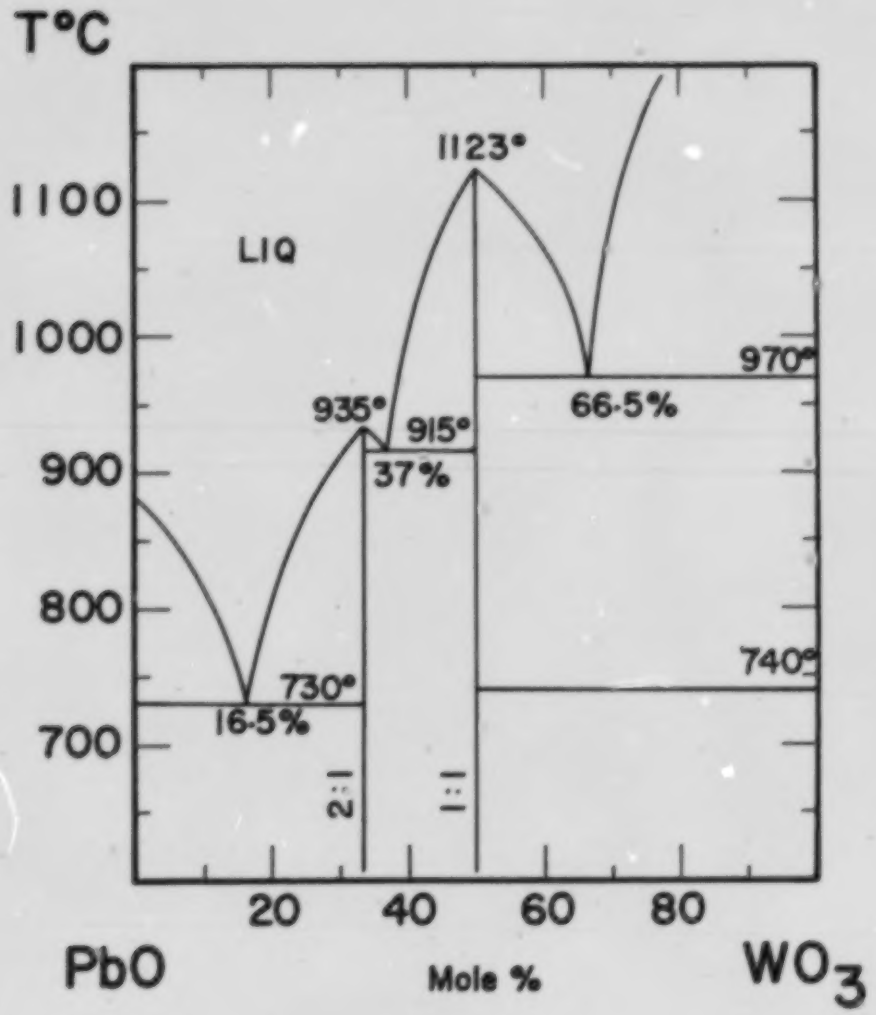

FIGURE 28. Phase relations in the system $PbO-WO_3$ (Chang, 1971)

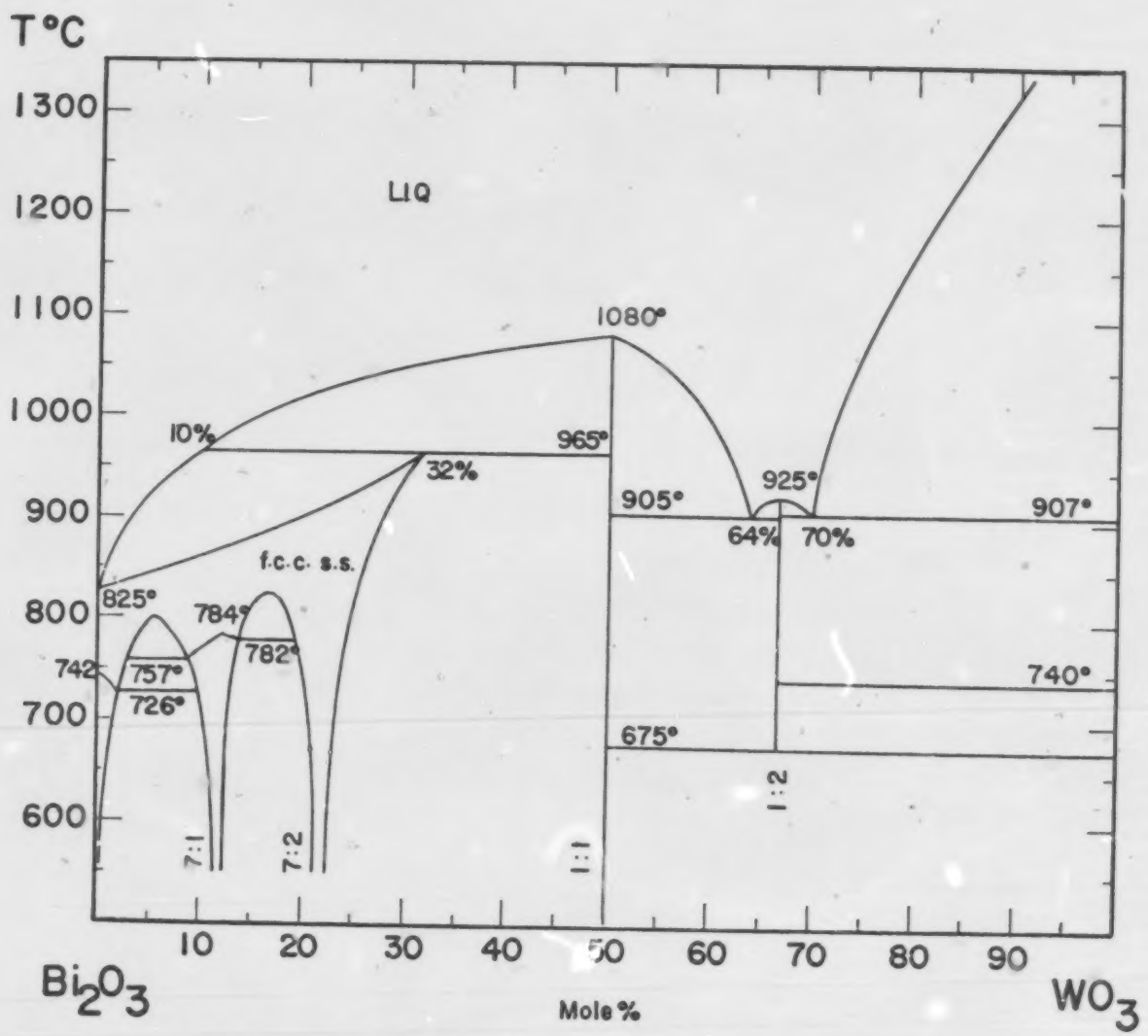

FIGURE 29. Phase relations in the system Bi_2O_3-WO_3 (Hoda and Chang, 1974)

National Bureau of Standards SP-496, Applications of Phase Diagrams in Metallurgy and Ceramics
Proceedings of Workshop held at NBS, Gaithersburg, Md., January 10-12, 1977

RIC IN PHASE WITH RARE-EARTH CONSTITUTIONAL DIAGRAMS

K. A. Gschneidner, Jr., M. E. Verkade and B. L. Evans

Rare-Earth Information Center (RIC)
Energy and Mineral Resources Research Institute
Iowa State University
Ames, Iowa 50011

Background

The Rare-Earth Information Center (RIC) was established at the Ames Laboratory by the U.S. Atomic Energy Commission's Division of Technical Information in 1966 and transferred to Iowa State University's Energy and Mineral Resources Research Institute (formerly Institute for Atomic Research) in 1968 with funding provided through grants from world-wide rare earth industries. The Center serves the scientific and technical community by collecting, storing, evaluating and disseminating rare earth information with particular emphasis on the physical metallurgy and solid state physics of the rare earth metals and their alloys.

Data Base

All available resources including books, journals, reports, conference proceedings, etc. are canvassed by the Center's technically trained staff of three (1 full time and 2 part time). Rapid and flexible retrieval of stored information is provided via a computerized system utilizing over 7400 key-word descriptors plus author indexing. Keyword descriptors are assigned following an examination of the original document rather than relying on only the title or abstract as do some indexing systems. Conversion of the information base from manually sorted punched cards to computer-read magnetic tape, begun in 1973, is about three-fourths completed and includes most of the approximately 14,000 journal articles held by the Center.

Publications

Utilizing this extensive information base, the Center engages in various publishing activities in addition to providing specialized literature searches on request. The RIC News, a quarterly newsletter containing items of current interest in science and technology of the rare earths, is distributed free

to over 3700 subscribers in the U.S. and abroad. State-of-the-art reviews, bibliographies and data compilations, prepared and published by RIC, have included a survey of rare earth metals in steel (IS-RIC-4), compilations of thermochemical data for rare earth compounds (IS-RIC-5 and IS-RIC-6), and a critical review of selected cerium binary phase diagrams (IS-RIC-7). These reports are currently available free from the Center or the sponsoring industry, Molycorp, Inc., which funded the study. Distribution of the reports is aided by publication announcements placed in appropriate scientific and trade journals, periodic notices in the RIC News and inclusion in abstracting journals.

Evaluation of Constitutional Diagrams

The staff of RIC has been involved over the past fifteen years with critical evaluation of phase equilibria, crystallographic and thermodynamic data on rare earth materials. The major effort has been primarily concerned with metallic systems. The evaluations on consitutional diagrams and crystal structures have been published as books, review articles or reports.

Rare Earth Alloys, K. A. Gschneidner, Jr., D. Van Nostrand Company, Inc., New York (1961) 449 + xiii pp.

"Rare Earth Intermetallic Compounds" by O. D. McMasters and K. A. Gschneidner, Jr., Nuclear Metallurgy 10, 93-158 (1964).

IS-RIC-7 "Selected Cerium Phase Diagrams" by K. A. Gschneidner, Jr. and M. E. Verkade (September 1974) 50 pp.

"Inorganic Compounds" by K. A. Gschneidner, Jr., and "Alloys and Intermetallic Compounds" by K. A. Gschneidner, Jr., Chapters 8 and 9 (pp. 152-251 and 252-323, respectively) of Scandium, Its Occurrence, Chemistry, Physics, Metallurgy, Biology and Technology, C. T. Horovitz, K. A. Gschneidner, Jr., G. A. Melson, D. H. Youngblood and H. H. Schock, Academic Press, New York (1975).

The RIC report on "Selected Cerium Phase Diagrams" (IS-RIC-7) contains several new innovations in addition to the standard features found in most phase diagram compilations. The new innovations are: 1. Text (discussion), phase diagram figures and crystallographic data are presented on two facing pages, and generally so are the references. Thus the reader does not need to turn pages back and forth to compare the figure while reading the text or examining the crystallographic data. If more than two pages are required the references are placed on the third page. 2. The phase

diagrams are presented twice, once in wt.% vs. temperature (°C) and once in at.% vs. temperature (°C). This way if the user is accustomed to phase diagrams in wt.% he (she) will find the left-hand figure more useful, but if one is more familiar with at.% the right-hand figure will be more useful.

The standard features include: 1. critical evaluation of published results, 2. composite diagram of several results (if there is more than one source of reliable information), and 3. a °F temperature scale in addition to the normal °C temperature scale.

Thermodynamic Evaluations

In addition to the above efforts the staff has also been involved in evaluating and estimating thermodynamic data for rare earth materials which are of special interest to the preparation and utilization of common metals, such as steel, ductile iron, superalloys, etc. These data compilations include:

IS-RIC-5 "Thermochemistry of the Rare Earth Carbides, Nitrides and Sulfides for Steelmaking" by Karl A. Gschneidner, Jr. and Nancy Kippenhan (August 1971) 27 pp.

IS-RIC-6 "Thermochemistry of the Rare Earths. Part 1. Rare Earth Oxides, Part 2. Rare Earth Oxysulfides, Part 3. Rare Earth Compounds with B, Sn, Pb, P, As, Sb, Bi, Cu, and Ag" by Karl A. Gschneidner, Jr., Nancy Kippenhan and O. Dale McMasters, (August 1973) 67 pp.

"Thermodynamic Stability and Physical Properties of Metallic Sulfides and Oxysulfides", by Karl A. Gschneidner, Jr., pp. 159-77 in SULFIDE INCLUSIONS IN STEEL, J. J. DeBarbadillo and E. Snape, eds., American Society for Metals, Metals Park, Ohio (1975).

National Bureau of Standards SP- , Application of Phase Diagrams in Metallurgy and Ceramics
Proceedings of Workshop held at NBS, Gaithersburg, Md., January 10-12, 1977.

Evaluations of Phase Diagrams and Thermodynamic Properties of Ternary Copper Alloy Systems

by

Y. Austin Chang
Joachim P. Neumann
U. V. Choudary

Materials Department
College of Engineering and Applied Science
University of Wisconsin-Milwaukee
Milwaukee, Wisconsin 53201

A status report on the compilation and evaluation of phase diagrams and thermodynamic properties of ternary copper alloy systems, sponsored by INCRA, is presented. As of November 1976, 90 ternary systems have been completed. These systems contain a total of 182 diagrams, 16 general references and 421 specific references. The format of presentation is briefly discussed and the actual evaluation is demonstrated by giving two systems as typical examples, Cu-Ag-Zn and Cu-Ca-Mg.

1. Introduction

Phase diagram and thermodynamic data for copper alloy systems are of considerable fundamental and practical interest in many aspects of extractive, chemical, and physical metallurgy. These data have been reported for binary copper alloy systems in a critical evaluation by Hultgren and Desai [Gen. Ref. 8], which forms one of the monographs in the series, "The Metallurgy of Copper," sponsored by the International Copper Research Association (INCRA). Since commercial alloys usually consist of more than two components, it is imperative to extend the work of Hultgren and Desai to higher order copper alloy systems. At the suggestion of Dr. L. McDonald Schetky of INCRA, a project to compile and evaluate phase diagrams and thermodynamic properties of ternary copper alloy systems was initiated in 1972 at the University of Wisconsin-Milwaukee. A total of 39 elements in addition to copper was considered for evaluation. These 39 elements are Ag, Al, Au, B, Be, Bi, C, Ca, Cd, Ce, Co, Cr, Fe, Ga, Ge, Hg, In, Mg, Mn, Mo, Nb, Ni, O, P, Pb, Pd, Pt, Re, S, Sb, Se, Si, Sn, Ta, Te, Ti, V, W, and Zn. The non-metallic elements C, O, P and S are included because of the technological importance of systems containing these elements. A simple calculation shows that the combinations of all 39 elements yield a total of 741 ternary copper alloy systems. A literature search, mainly based on Chemical Abstracts through June 1973, indicated that data were available for approximately 300 ternary copper alloy systems. In view of this rather large number of systems and because some of these systems are of less technological interest, the total number of systems for inclusion in this project was reduced to about 180. As of November, 1976, 90 systems have been completed. These 90 systems are given in Table I. They contain a total of 182 diagrams (liquidus projections, isothermal sections, isopleths and thermodynamic properties), 16 general references, and 421 specific references.

The results of the evaluations for the 20 ternary Cu-Ag systems will be published in the Journal of Physical and Chemical Reference Data. In the paper presented here, the format of presentation is briefly discussed and the actual evaluation is demonstrated by giving two systems, Cu-Ag-Zn and Cu-Ca-Mg, as typical examples.

2. Format of Presentation

The phase diagram and thermodynamic data have been evaluated for self-consistency, consistency with binary data, and consistency with known phase and thermodynamic relationships. Whenever conflicting data are reported by different groups of investigators, judgment has been made on the basis of the experimental methods used and the detailed experimental information reported by the investigators. The discussion of each system is divided into six sections: Phases and Structures, Phase Diagrams, Thermodynamic Properties, References, Tables, Figures.

2.1 Phases and Structures

Adopting the format of the Metals Handbook [Gen. Ref. 1], the following information is given for each of the binary and ternary intermediate phases: Designation, Composition, Symmetry, Symbol, and Prototype. The designations of Hansen and Anderko, Elliott, and Shunk [Gen. Refs. 3, 4, 5] are used whenever possible. If their designations cannot be used, they are given in parentheses next to the chemical formula in the composition column. For ternary intermediate phases, the designations T_1, T_2, T_3 ... are used. For the abbreviations of crystal symmetry, refer to pp. 243-250 of the Metals Handbook [Gen. Ref. 1]. For the structure symbols (Strukturbericht), refer to Pearson [Gen. Ref. 2]. A prototype phase is given whenever available.

2.2 Phase Diagrams

Following the notation of Rhines [Gen. Ref. 9], the three invariant four-phase equilibria are classified as types I, II, and III. If more than one four-phase equilibrium of the same type occurs, the equilibria are distinguished by

adding subscripts to the Roman numerals in order of descending temperature, I_1, I_2, I_3, etc. The chemical composition is given in wt.% and the temperatures are given in degrees Celsius. Solid lines are used for known phase boundaries, dashed lines for estimated phase boundaries, and dash-dotted lines for magnetic transformations.

In the liquidus projection, the binary eutectics, peritectics and monotectics are designated by e_1, e_2, e_3, ..., P_1, P_2, P_3, ..., and m_1, m_2, m_3, ..., respectively. The traces of the liquidus valleys, i.e., the univariant equilibria, are plotted, and the directions of their slopes toward lower temperature are indicated by arrows inscribed upon the lines. The primary phases of crystallization are given on either side of the traces of these valleys. The types of the four-phase equilibria at the intersections of the traces of the liquidus valleys are indicated by the Roman numerals I, II or III with the subscripts 1, 2, 3, etc. The melting points of congruently melting binary and ternary phases are marked with solid circles and the corresponding temperatures are given. For ternary saddle points (singular points), open circles are used.

In the isothermal sections, only the single- and two-phase regions are labelled, using the designations for the phases given in the section on Phases and Structures. For the terminal solid solutions, the chemical symbol of the base element in parentheses is used. Liquid phases are desginated by the letter L, with the subscripts 1, 2, etc., distinguishing different liquid phases.

In the case of isopleths, all single-, two- and three-phase regions are labelled.

2.3 Thermodynamic Properties

The Kelvin temperature scale is used to represent the temperature instead of the Celsius scale, and atom or mole fractions are used instead of weight percent. Thermodynamic activity data are generally presented in the form of iso-activity or iso-activity coefficient curves, using the Gibbs triangle.

Very often the thermodynamic properties of a particular component are known in infinitely dilute solutions. For such cases, the excess partial molar Gibbs energy is expressed in terms of the formalism suggested by Wagner [Gen. Ref. 12]:

$$\ln \gamma_i = \ln \gamma_i^o + \epsilon_i^i x_i + \epsilon_i^j x_j \qquad (1)$$

where γ_i is the activity coefficient of the solute i in a ternary dilute solution consisting of the solvent s and the solutes i and j; γ_i^o is the limiting activity coefficient of i in the binary system i-s; and the terms x_i and x_j are atom fractions of the solutes i and j. The terms ϵ_i^i and ϵ_i^j are the Gibbs energy self-interaction and the Gibbs energy interaction parameters.

2.4 References

The literature references which are pertinent to each particular system are given after the discussion. A number of frequently occurring references are cited as "General References"; they are listed in section 3.

2.5 Tables

Generally, the types and temperatures of the known invariant equilibria, as well as the compositions of the coexisting phases, are given in a table.

2.6 Figures

If the information is available, figures of the phase diagrams are generally presented in the following order: liquidus projection - isothermal sections - isopleths, including quasi-binaries. Graphical representations of the thermodynamic properties are given last.

3. General References

1. Metals Handbook, 8th Ed., Vol. 8, "Metallography, Structures and Phase Diagrams," American Society for Metals, Metals Park, Ohio, 1973.
2. Pearson, W. B., A Handbook of Lattice Spacings and Structures of Metals and Alloys, Vols. 1 and 2, Pergamon Press, London, 1958 and 1967.
3. Hansen, M., and Anderko, K., Constitution of Binary Alloys, 2nd Edition, McGraw-Hill, New York, 1958.
4. Elliott, R. P., Constitution of Binary Alloys, First Supplement, McGraw-Hill, New York, 1965.
5. Shunk, F. A., Constitution of Binary Alloys, Second Supplement, McGraw-Hill, New York, 1969.
6. Hultgren, R., Desai, P. D., Hawkins, D. T., Gleiser, M., and Kelley, K. K., Selected Values of the Thermodynamic Properties of Binary Alloys, American Society for Metals, Metals Park, Ohio, 1973.
7. Hultgren, R., Desai, P. D., Hawkins, D. T., Gleiser, M., Kelley, K. K., and Wagman, D. D., Selected Values of the Thermodynamic Properties of the Elements, American Society for Metals, Metals Park, Ohio, 1973.
8. Hultgren, R., and Desai, P. D., INCRA Monograph I, Selected Thermodynamic Values and Phase Diagrams for Copper and Some of Its Binary Alloys, The International Copper Research Association, Inc., New York, 1971.
9. Rhines, F., Phase Diagrams in Metallurgy, Their Development and Application, McGraw-Hill, New York, 1956.
10. Prince, A., Alloy Phase Equilibria, Elsevier, Amsterdam-London-New York, 1966.
11. Wagner, S., and Rigney, D. A., Metall. Trans., 1974, 5, 2155.
12. Wagner, C., Thermodynamics of Alloys (Translated by Mellgren, S., and Westbrook, J. H.), Addison-Wesley, Reading, Mass., 1952.

13. Lupis, C.H.P., and Elliott, J. F., Trans. Met. Soc. AIME, 1965, 233, 829; 1200.

14. JANAF Thermochemical Tables, 2nd Ed., NSRDS-NBS 37, U.S. Department of Commerce, National Bureau of Standards, Washington, D. C., 1971.

15. King, E. G., Mah, A. D., and Pankratz, L. B., INCRA Monograph II, Thermodynamic Properties of Copper and Its Inorganic Compounds, The International Copper Research Association, Inc., New York, 1973.

16. Diaz, C., INCRA Monograph III, The Thermodynamic Properties of Copper-Slag Systems, The International Copper Research Association, Inc., New York, 1974.

4. Personnel

Personnel who have contributed to this work are Y. A. Chang (YAC), U. V. Choudary (UVC), D. Goldberg (DG), D. K. Gupta (DKG), H. Ipser (HI), and J. P. Neumann (JPN). The evaluation of each system was the primary responsibility of one of the team members, whose initials are placed on the last page of the evaluation, following the list of references.

Dr. D. Goldberg is now with Westinghouse, Plant Apparatus Division, Pittsburgh, Pennsylvania; Dr. D. K. Gupta is now with Howmet Corporation, Whitehall, Michigan; and Dr. H. Ipser is now with the Institut für Anorganische Chemie, Universität Wien, Austria.

5. Acknowledgments

Financial support for this project is being provided by INCRA. The authors wish to thank Dr. L. McDonald Schetky of INCRA for his interest in this work and his initiation of support for this project.

6. Examples of Evaluations

Two typical examples of the evaluations that are being carried out are given below, the Cu-Ag-Zn and the Cu-Ca-Mg systems.

Table I. Ternary Cu-A-B Systems Completed As of November 1976

A \ B	Al	Au	B	Be	Bi	Cd	Ce	Co	Cr	Fe	Ge	In	Mg	Mn	Mo	Nb	Ni	P	Pb	Pd	Pt	Re	S	Sb	Se	Si	Sn	Ta	Te	Ti	V	Zn
Ag	x	x				x				x	x	x	x	x			x	x	x	x		x	x	x	x		x		x	x		x
Al				x	x	x	x	x	x	x	x	x			x	x	x		x	x			x			x		x			x	
Au								x		x							x		x	x							x					x
B																	x						x									
Be								x					x	x			x									x	x	x		x		
Ca											x		x													x						
Cd																							x									
Co									x	x				x			x			x						x	x					x
Cr										x				x		x	x			x			x					x		x		
Ga																							x									
Ge																							x									
Mn																							x									
Mo																							x									
Nb																							x									
Pb																							x									
Pd																					x											
Re																							x									
S																										x	x	x		x	x	x
Ta																															x	

259

Cu-Ag-Zn

Phases and Structures: The following intermediate phases appear in the Cu-Zn and Ag-Zn binary systems. No ternary phases have been found.

Designation	Composition	Symmetry	Symbol	Prototype
β_1	CuZn (HT)(β)	bcc	A2	W
β'	CuZn (LT)	ord bcc	B2	CsCℓ
γ_1	Cu_5Zn_8(γ)	ord bcc	$D8_2$	γ-brass
δ	$CuZn_3$	ord bcc	B2	CsCℓ
ϵ_1	~ 83% Zn (ε)	hcp	A3	Mg
β_2	AgZn (HT)(β)	bcc	A2	W
ζ	AgZn (LT)	ord hex	-	-
γ_2	Ag_5Zn_8 (γ)	ord bcc	$D8_2$	γ-brass
ϵ_2	~ 70% Zn (ε)	hcp	A3	Mg

The crystal structures are from the Metals Handbook (Gen. Ref. 1).

Phase Diagrams: After early investigations by Ueno [1], Keinert [2], and Weigert [3], Gebhardt, Petzow, and Krauss [4] later on thoroughly re-examined the phase relations in the ternary system. The liquidus, the isotherms at 600°, 500°, and 350°C, and the isopleths at 20% Ag and 20% Zn by [4] are shown here. Gebhardt, et al. also gave isopleths at 40% Ag, 60% Ag, 40% Cu, and 60% Cu.

The liquidus diagram shows the liquidus valleys extending from the binary eutectic or peritectic points into the ternary field. Two continuous

valleys (from p_8 to p_2 and from p_4 to p_5) are formed, the other valleys meet on planes of four-phase equilibria. The invariant reaction temperatures and compositions of the co-existing phases are shown in Table I.

In the solid state, the isotherms show that continuous solid solutions, designated β, γ, and ε, connect the isostructural β_1 and β_2, γ_1 and γ_2 and ε_1 and ε_2 binary phases, respectively. On the 350°C isotherm, the β and β' (ordered) regions were labelled incorrectly as β' and β, respectively, in the original paper [4]. No solid-state four-phase equilibria exist in this system.

The β' to β order-disorder transition temperature of $Cu_{.53-x}Ag_xZn_{.47}$ alloys was investigated by Murakami, Nakanishi, and Kachi [5]. The transition temperature decreases with increasing Ag content from about 465°C at $Cu_{.53}Zn_{.47}$ to about 223°C at $Ag_{.53}Zn_{.47}$. The latter temperature is estimated from an extrapolation to 0% Cu.

Thermodynamic Data: The partial pressure of zinc over the terminal (Cu) and (Ag) solid solutions at 1000 K were measured by Argent and Lee [6]. For the terminal copper solid solution, the data yield the following values:

$$\gamma^{o}_{Zn(\ell)} = 0.051$$

$$\varepsilon^{Zn}_{Zn} = +6.5$$

$$\varepsilon^{Ag}_{Zn} \simeq 0.$$

The few data available in the terminal silver solid solution do not permit a reliable evaluation of the activity coefficients; the values given must be considered as estimates:

$$\gamma^{o}_{Zn(\ell)} = 0.27$$

$$\varepsilon^{Zn}_{Zn} \simeq 0$$

$$\varepsilon^{Cu}_{Zn} \simeq -3.5.$$

For the solid solution of zinc in copper, Hultgren (Gen. Ref. 6) reports a value of 0.014 for $\gamma^{o}_{Zn(s)}$ at 773 K, which corresponds to $\gamma^{o}_{Zn(\ell)}$ = 0.048 at 1000 K. The data by [6] are in good agreement with this value. For the solid solution of zinc in silver, however, Hultgren (Gen. Ref. 6) reports a value of 0.199 for $\gamma^{o}_{Zn(s)}$ at 873 K, which corresponds to $\gamma^{o}_{Zn(\ell)}$ = 0.36 at 1000 K. This value is quite different from the one obtained from the data by Argent and Lee. Values for the partial enthalpies and partial entropies of zinc are also given by [6]. An insufficient number of data was taken to calculate integral properties.

References:

1. Ueno, S., Mem. Coll. Sci. Kyoto Imp. Univ., 1929, 12A, 347.
2. Keinert, M., Z. physik. Chem., 1932, A160, 15.
3. Weigert, K. M., Trans. AIME, 1954, 200, 233.
4. Gebhardt, E., Petzow, G., and Krauss, W., Z. Metallk., 1962, 53, 372.
5. Murakami, Y., Nakanishi, N., and Kachi, S., Acta Met., 1971, 19, 93.
6. Argent, B. B., and Lee, K. T., Trans. Faraday Soc., 1965, 61, 826.

Table I. Four-phase Equilibria in the Cu-Ag-Zn System

Reaction	Temp. °C	Co-existing Phases	Composition of Phases Wt.% Cu	Wt.% Ag	Wt.% Zn
I_1: $L = (Cu) + (Ag) + \beta$	665	L	20	56	24
		(Cu)	63	9	28
		(Ag)	5	75	20
		β	23	50	27
II_1: $L + \gamma = \varepsilon + \delta$	630	L	9.5	26	64.5
		γ	12	25	63
		ε	10.5	26	63.5
		δ	11	25	64

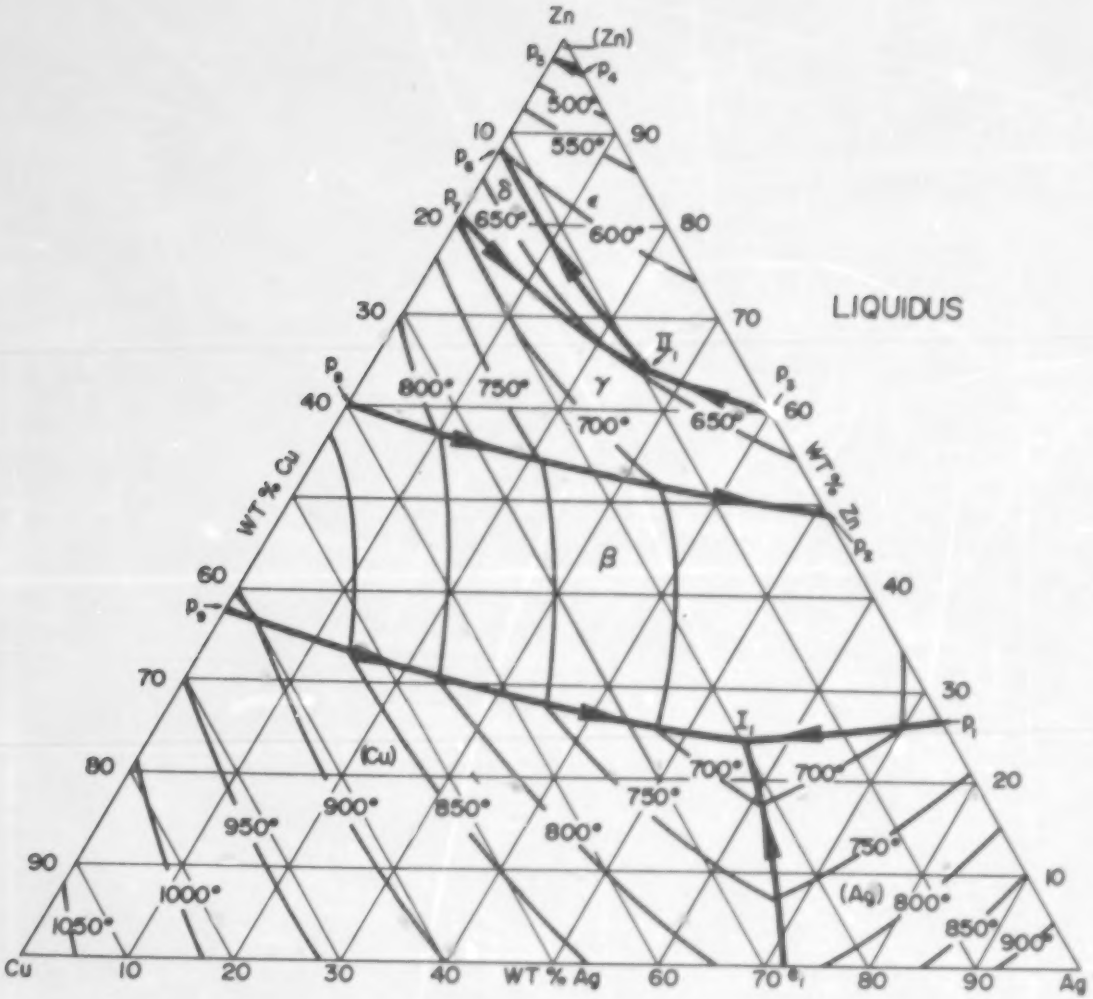
Zn
(Zn)
LIQUIDUS
WT % Cu
WT % Zn
WT % Ag
Cu
Ag
(Cu)
(Ag)
δ
ε
γ
β
P_3
P_4
P_5
P_6
P_7
P_8
P_1
E_1
U_1
U_2
500°
550°
600°
650°
700°
750°
800°
850°
900°
950°
1000°
1050°

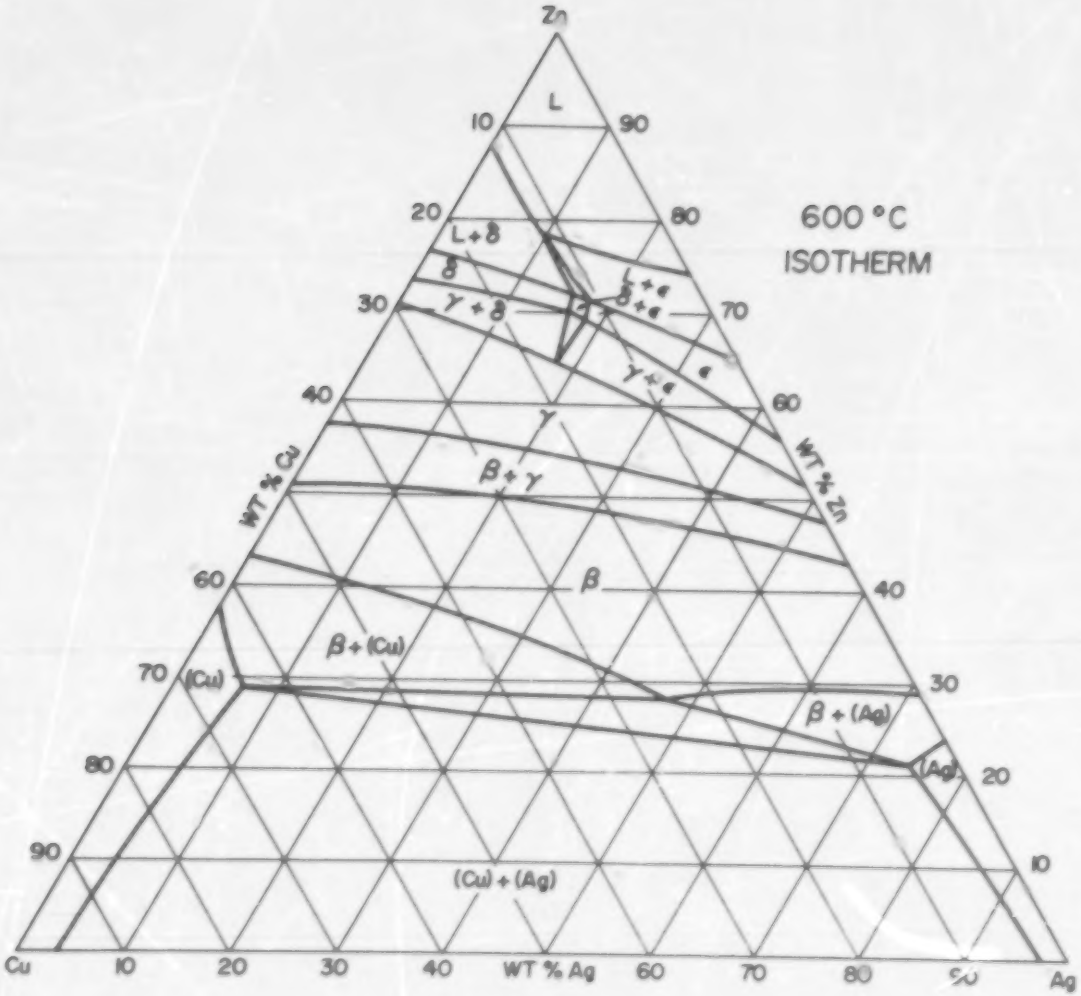
Zn
L
10
90
20
80
600 °C
ISOTHERM
L+δ
δ
L+ε
δ+ε
30
γ+δ
70
γ+ε
ε
40
γ
60
WT % Cu
WT % Zn
β+γ
β
60
40
β+(Cu)
70
(Cu)
30
β+(Ag)
80
(Ag)
20
90
10
(Cu)+(Ag)
Cu
10
20
30
40
WT % Ag
60
70
80
90
Ag

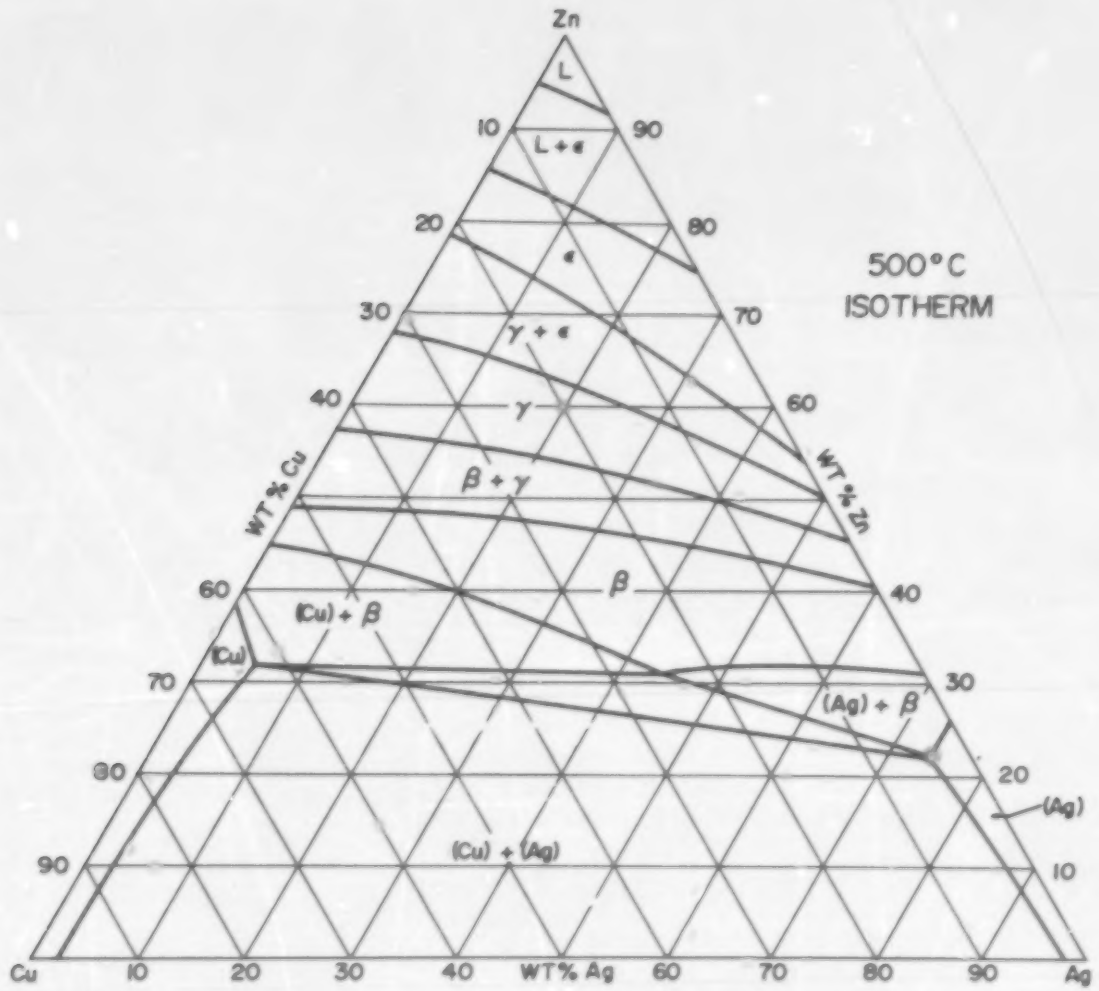
Zn
L
L + ε
ε
γ + ε
γ
β + γ
β
(Cu) + β
(Cu)
(Cu) + (Ag)
(Ag) + β
(Ag)
500°C
ISOTHERM
WT % Cu
WT % Zn
WT % Ag
Cu
Ag
10
20
30
40
60
70
80
90

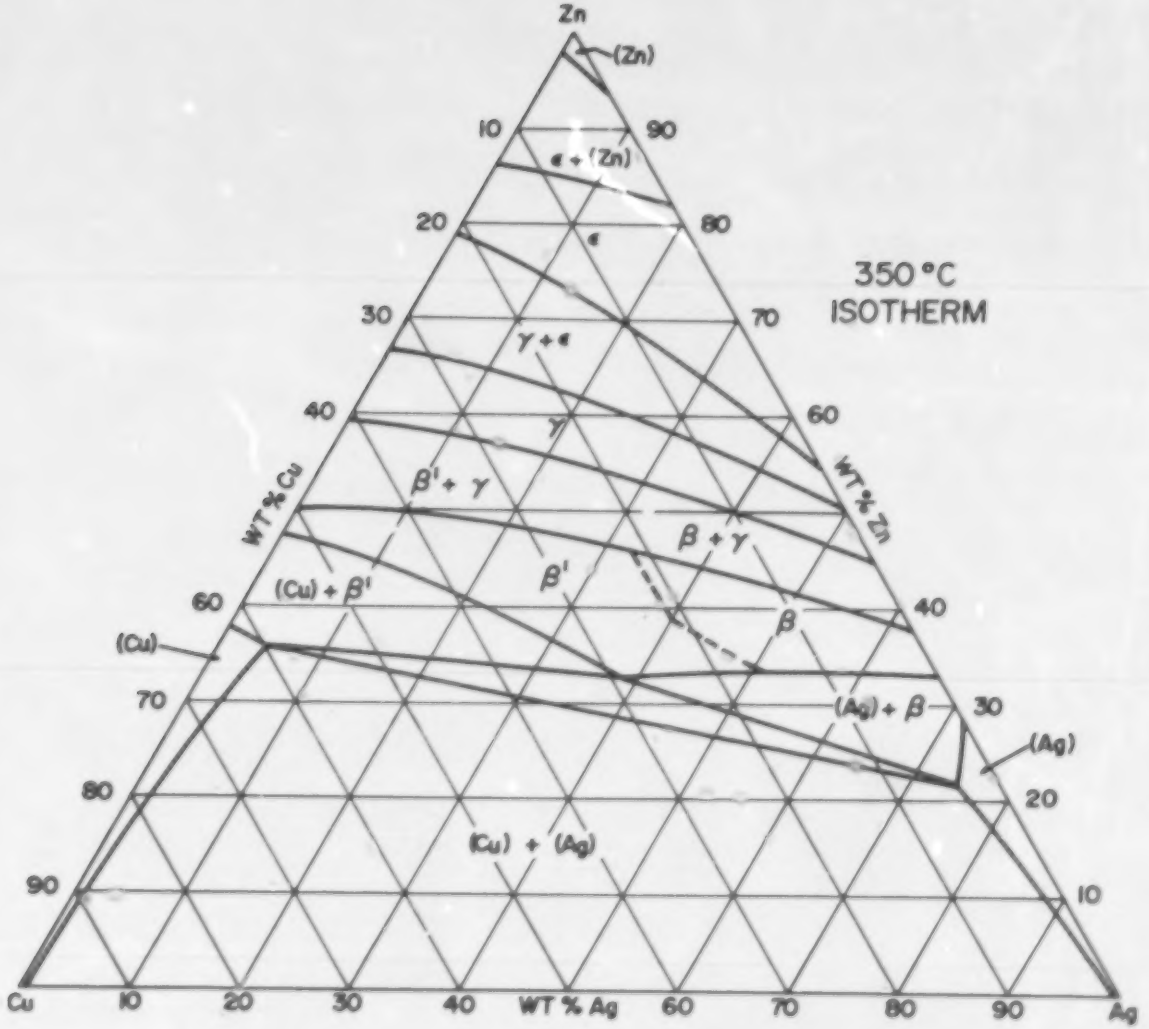
Zn
(Zn)
ε + (Zn)
ε
γ + ε
γ
β' + γ
β + γ
β'
β
(Cu) + β'
(Cu)
(Ag) + β
(Ag)
(Cu) + (Ag)
350 °C
ISOTHERM
WT % Cu
WT % Zn
WT % Ag
Cu
Ag
10
20
30
40
60
70
80
90

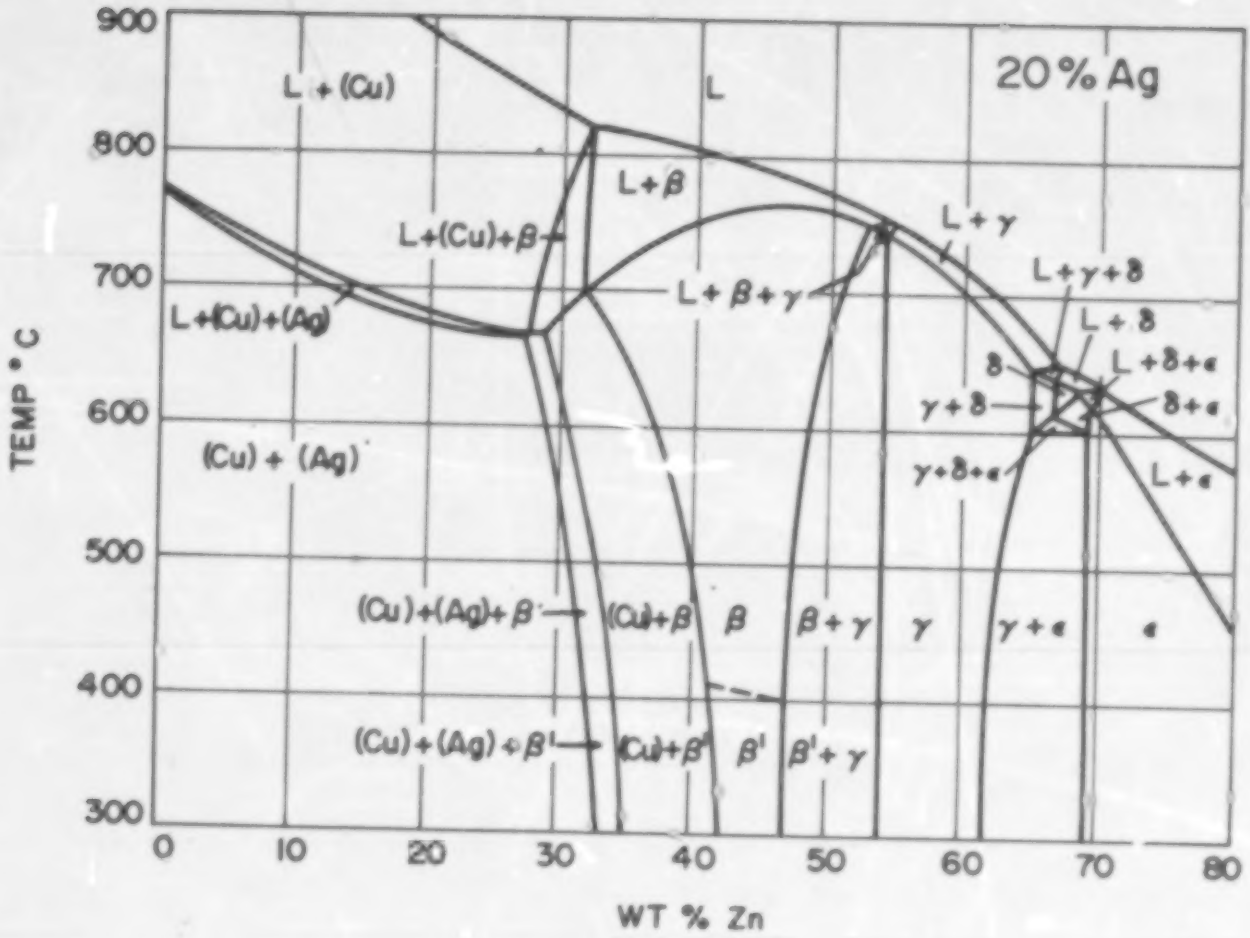
20% Ag
L + (Cu)
L
L+β
L+(Cu)+β
L+γ
L+γ+δ
L+β+γ
L+δ
L+(Cu)+(Ag)
δ
L+δ+ε
γ+δ
δ+ε
(Cu) + (Ag)
γ+δ+ε
L+ε
(Cu)+(Ag)+β
(Cu)+β
β
β+γ
γ
γ+ε
ε
(Cu)+(Ag)+β'
(Cu)+β'
β'
β'+γ
TEMP °C
900
800
700
600
500
400
300
0
10
20
30
40
50
60
70
80
WT % Zn

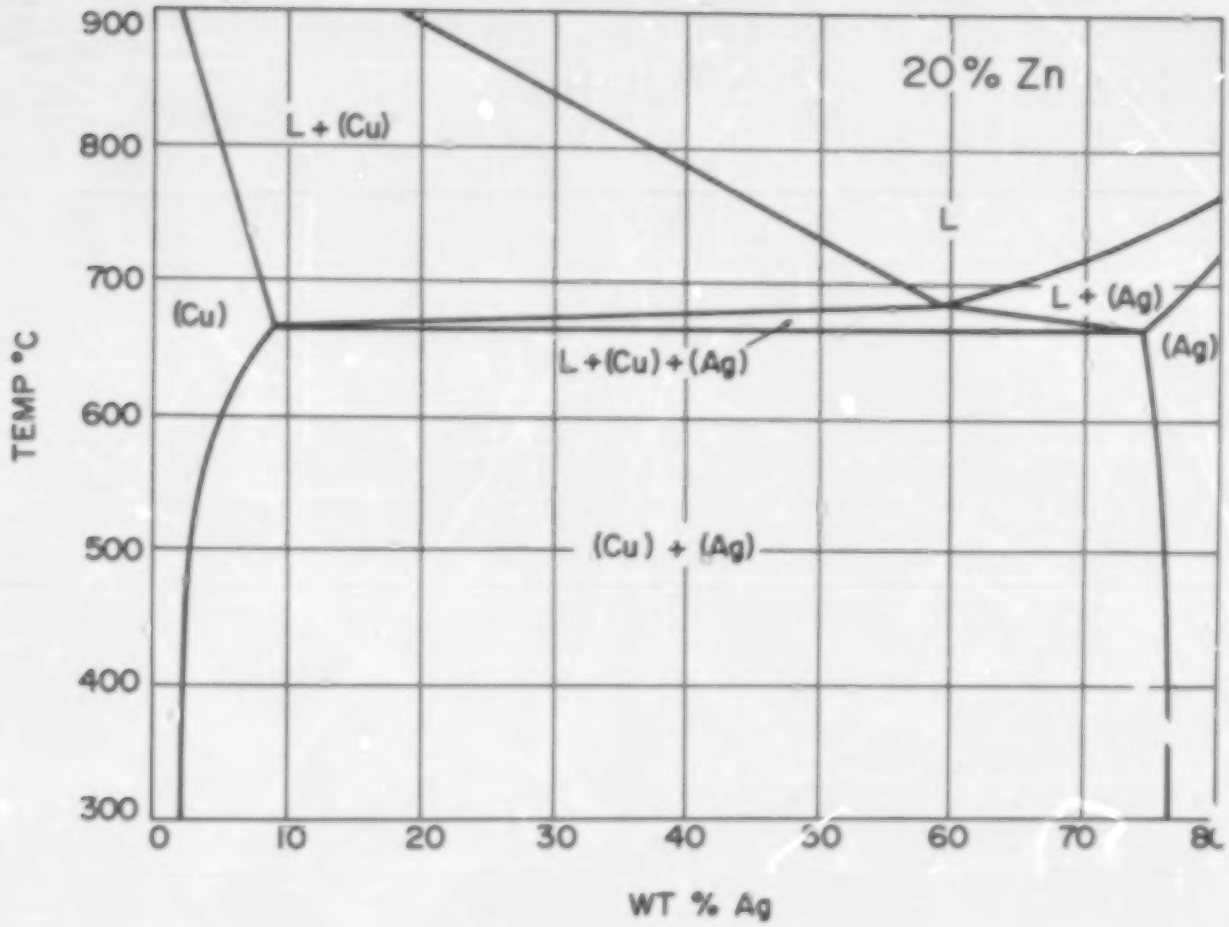
20% Zn
L + (Cu)
L
L + (Ag)
(Cu)
(Ag)
L + (Cu) + (Ag)
(Cu) + (Ag)
TEMP °C
900
800
700
600
500
400
300
0
10
20
30
40
50
60
70
80
WT % Ag

Cu-Ca-Mg

Phases and Structures: The following intermediate phases appear in the Cu-Ca, Cu-Mg, and Ca-Mg binary systems. No ternary phases have been found.

Designation	Composition	Symmetry	Symbol	Prototype
γ	Cu_5Ca	hex	$D2_d$	Cu_5Ca
η	CuCa	ortho	-	-
δ	$CuCa_2$	unknown	-	-
ε	Cu_2Mg	ord fcc	C15	Cu_2Mg
β	$CuMg_2$	ord ortho	-	-
ζ	$CaMg_2$	hex	C14	$MgZn_2$

The crystal structures of the Cu-Mg and Ca-Mg binary phases and the structure of the γ-Cu_5Ca phase are from the Metals Handbook (Gen. Ref. 1), whereas the structure of the η-CuCa phase is from Bruzzone [1].

Phase Diagrams: The liquidus and the 350° isotherm shown here are from the study of Myles [2]; however, the liquidus valleys have been slightly modified along the Cu-Ca binary system to bring them into agreement with the most recent data by Bruzzone [1]. This author confirmed the stoichiometry of the three Cu-Ca compounds found by Myles [2], but showed by means of a thermo-analytical investigation that η-CuCa and δ-$CuCa_2$ decompose peritectically instead of exhibiting congruent melting points as was assumed by Myles [2].

Three four-phase equilibria of type I and four of type II were found [2], they are given in Table I. The compositions of the coexisting phases are unknown as are the temperatures of the type II four-phase equilibria.

References:

1. Bruzzone, G., J. Less-Common Metals, 1971, 25, 361.
2. Myles, K. M., J. Less-Common Metals, 1970, 20, 149.

Table I. Four-phase Equilibria in the Cu-Ca-Mg System

Reaction	Temp.°C
I_1: $L = (Cu) + \varepsilon + \gamma$	700
I_2: $L = (Mg) + \beta + \zeta$	430
I_3: $L = (Ca) + \zeta + \delta$	350
II_1: $L + \beta = \varepsilon + \zeta$	
II_2: $L + \gamma = \varepsilon + \eta$	
II_3: $L + \varepsilon = \eta + \zeta$	
II_4: $L + \eta = \delta + \zeta$	

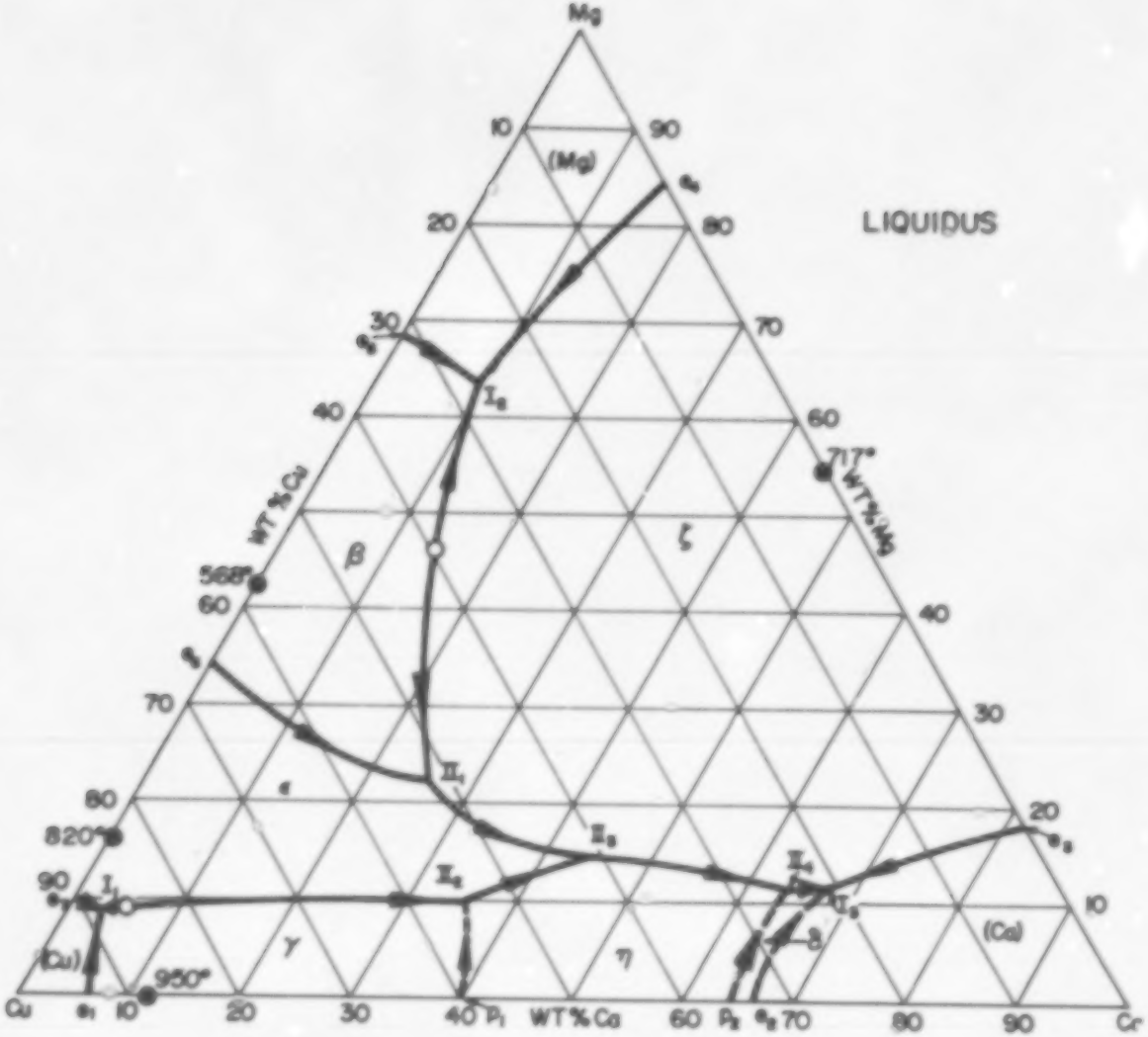
LIQUIDUS
Mg
Cu
Cr
(Mg)
(Cu)
(Cr)
WT % Cu
WT % Mg
WT % Cr
568°
820°
950°
1085°
β
ζ
ε
γ
η
δ
e1
e2
e3
e4
P1
P2
U1
U2
U3
U4
E1

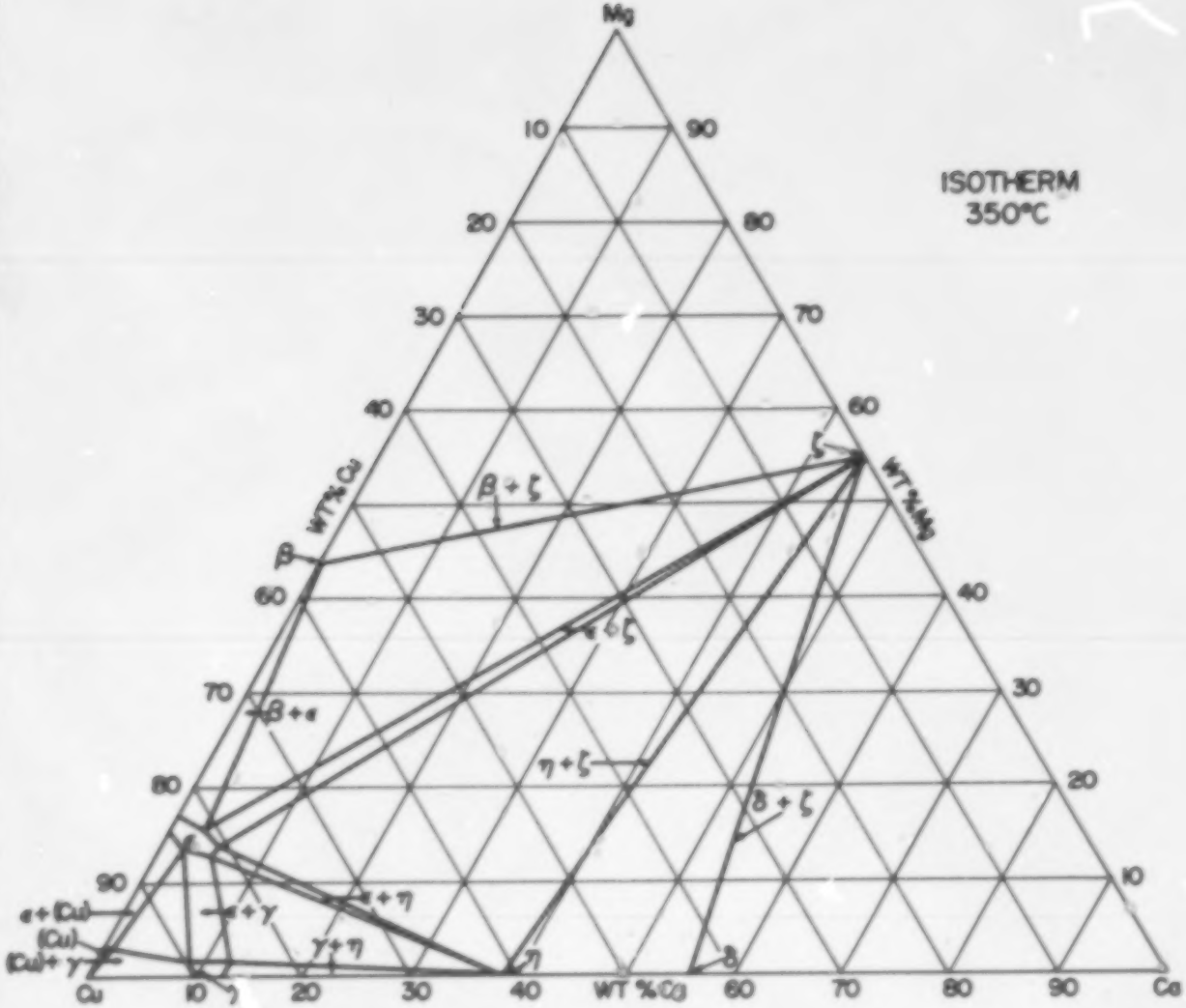
Mg
ISOTHERM
350°C
WT%Cu
WT%Mg
WT %Cd
Cu
Cd
β + ζ
β + α
α + ζ
η + ζ
δ + ζ
α + η
α + γ
γ + η
α + (Cu)
(Cu)
(Cu) + γ

National Bureau of Standards SP-496, Applications of Phase Diagrams in Metallurgy and Ceramics
Proceedings of Workshop held at NBS, Gaithersburg, Md., January 10-12, 1977

PHASE EQUILIBRIA IN VARIABLE VALENCE OXIDE SYSTEMS

William B. White

Materials Research Laboratory and

Dept. of Geosciences

The Pennsylvania State University

University Park, PA 16803

Abstract

A compilation of the phase diagrams for binary metal oxygen systems is being prepared. The objectives are to reduce the available literature data to sets of internally consistent diagrams. Crystal structure information on the phases, critical discussion and explanatory text, with the diagrams are intended to be eventually published in monograph form.

Introduction

Some 40 elements react with oxygen to form compounds in which the element appears in more than one valence state. These include most of the transition elements, in which variable valence is attained by varying the number of d-electrons in the partially filled d-orbitals. It includes a group referred to as the Rydberg elements in which there are two valence states, one with a d^{10} electron configuration and one two charges smaller with an outer non-bonding lone-pair ns^2 electron configuration. The remainder include a few of the lanthanide elements and most of the actinide elements in which variable valence is achieved by varying the number of f-electrons. Finally the elements Zn, Cd, and Hg are included. Although these elements exhibit only a single oxidation state, the defect structure and electronic properties of the oxide are so dependent on oxygen fugacity that the phase equilibria become important.

Objectives

The total literature on binary metal-oxygen systems is very large but also very fragmentary. The principal objective of this work is to compile various pieces of diagrams, decomposition reactions, and other bits of information into internally consistent phase diagrams. Where possible, thermochemical data are being used to calculate missing equilibrium data.

The number of oxide phases in some systems such as Ti-O, V-O, and W-O is very large. Crystal structure and other data on the individual oxide phases is also being collected so that lists of phases can be prepared to accompany the phase diagrams. Likewise the crystallographic relations between phases related by decomposition reactions can be examined.

The ultimate objective is the publication of a monograph which will contain the best estimate of the binary metal-oxygen phase diagrams, the lists of phases with key structural information (unit cell, space group and references to full structural analyses where such exist), and an explanatory text.

Representations

Presentation of phase equilibria in these systems must take account of temperature, total pressure, and oxygen activity. Careful distinction between open and closed systems must be made. Three types of systems can be distinguished as shown below.

Conditions	Vapor Phase	Type of Diagram
I. All oxides refractory to liquidus	Oxygen fugacity less than 100 bars Vapor phase essentially pure oxygen	T-X "condensed" diagrams with superimposed isofugacity lines. Also f_{O_2}-T projections
II. All oxides refractory to liquidus	Oxygen fugacity greater than 100 bars Vapor phase nearly pure oxygen	P_{O_2}-T diagrams for stoichiometric oxides. P-T-X sections for non-stoichiometric oxides
III. Volatile oxides	Vapor phase of variable composition	Closed system P-T-X diagrams

Systems with volatile oxides, of which Re-O and Os-O are examples, require the use of P-T-X type diagrams and closed systems. Oxygen isofugacity lines do not coincide with SSV equilibria as is the case for the diagrams of types I and II.

Status and Progress

A large body of literature has been compiled, some 500 mostly recent references. Sweeps through the older literature by means of citation indexing

must still be done. Compilation and calculation are nearly complete on a few systems and partial compilations are in hand for a few others. Things progress, although slowly.

A listing of the systems under study (Table 1) gives the type of representation necessary and the available data base from the literature. For those systems whose status is "+++" enough data are available to prepare nearly complete phase diagrams of the solid-vapor equilibria, the compositions of non-stoichiometric compounds as a function of oxygen fugacity, and sometimes including melting behavior. Systems listed as "++" are less complete and for systems listed as "+" there are only fragmentary data.

Difficulties and Obstructions

There is a great lack of liquidus data for many systems. This includes both the two-liquid region between liquid oxide and liquid metal that exists for most systems and also the eutectic and peritectic relations between different oxides. Many diagrams will appear with only the SSV portion of the P-T-X diagram.

There is great experimental difficulty in obtaining equilibrium or even a complete set of phases at low temperatures even at fairly high oxygen pressures. Many systems contain complex oxides of high valence state that remain poorly described.

Oxygen fugacities in the metal-rich side of many binaries are extremely low. Gas buffer techniques have a lower limit at about 10^{-22} bars so that oxygen isofugacity lines are not known in the region of many oxygen-stuffed metallic phases such as occur in the system Ti-O. In absence of good thermochemical data, data for many of the intermediate phases cannot be calculated either.

Several systems, of which Ti-O and V-O are spectacular examples, exhibit one or more homologous series of shear phases, some of which occur with very small stoichiometric and stability range differences. The evidence is that many of these phases are both homogeneous and stoichiometric. However, the difference in free energy and therefore the oxygen fugacity is so small that resolution of the oxygen fugacity "stair steps" between adjacent phases is extremely difficult. There is also a very real question of whether the higher shear structure phases actually order on a macroscopic scale or whether there are domains or regions of different composition. What do we mean by a "homogeneous" phase at this level of energy resolution?

Table 1

Status of Variable Valence Element-Oxygen

Binary Phase Diagrams

System	Type of Representation	Status	System	Type of Representation	Status
Transition Element Systems			Pt-O	P-T-X	++
Ti-O	f-T-X	+++	Au-O	P-T-X	+
V-O	f-T-X	++	Rydberg Systems		
Cr-O	P-T-X	+++	As-O	P-T-X	++
Mn-O	f-T-X P-T-X	++	Sn-O	f-T-X	++
Fe-O	f-T-X	+++	Sb-O	P-T-X	+
Co-O	f-T-X P-T-X	++	Tl-O	f-T-X	+
Ni-O	P-T-X	+	Pb-O	P-T-X	+++
Cu-O	f-T-X	++	Bi-O	P-T-X	++
Nb-O	f-T-X	+++	Lanthanide Systems		
Mo-O	f-T-X	+++	Ce-O	P-T-X	+++
Tc-O	P-T-X	+	Pr-O	P-T-X f-T-X	+++
Ru-O	P-T-X	+	Eu-O	f-T-X	+++
Rh-O	P-T-X	++	Tb-O	P-T-X f-T-X	+++
Pd-O	P-T-X	++	Actinide Systems		
Ag-O	P-T-X	++	U-O	f-T-X	+++
Ta-O	f-T-X	+++	Np-O	f-T-X	++
W-O	f-T-X	+++	Pu-O	f-T-X	++
Re-O	P-T-X	+	Am-O	f-T-X	+
Os-O	P-T-X	+	Cm-O	f-T-X	+
Ir-O	P-T-X	++	Bk-O	f-T-X	+

National Bureau of Standards SP-496, Applications of Phase Diagrams in Metallurgy and Ceramics
Proceedings of Workshop held at NBS, Gaithersburg, Md., January 10-12, 1977

PHASE DIAGRAMS FOR CERAMISTS

L.P. Cook, R.S. Roth, T. Negas and G.W. Cleek

Institute for Materials Research
National Bureau of Standards
Washington, D.C. 20234

Compilation of phase equilibria data of interest to ceramists is continuing, in accordance with the pattern established by the 1975 supplement to "Phase Diagrams for Ceramists". This latest supplement includes critical commentaries discussing preparation of starting materials, experimental methods, characterization of products, accuracy and precision of data and of diagram. The following experts in various fields are serving as Contributing Editors for the 1978 Supplement:

- J. J. Brown, Virginia Polytechnic Inst.
  Fluoride containing systems
- L. L. Y. Chang, Miami Univ.
  Tungstates, molybdates, carbonates
- R. C. DeVries, General Electric Co.
  High pressure studies
- F. P. Glasser, Univ. Aberdeen
  Alkali oxide containing systems
- F. A. Hummel, Pennsylvania State Univ.
  Sulfides, phosphates
- K. A. Jack, Univ, Newcastle Upon Tyne
  Nitrides, oxynitrides
- A. Muan, Pennsylvania State Univ.
  First row transition metal oxide containing systems
- C. Semlar, Ohio State Univ.
  Anhydrous silicate - oxide systems
- C. A. Sorrell, Univ. Missouri-Rolla
  Aqueous salt systems
- K. Stern, Naval Research Laboratory
  Binary systems with halides only
- R. Thoma, Oak Ridge National Laboratory
  Fused salts
- D. R. Wilder and M. Berard, Iowa State Univ.
  R.E. oxide bearing systems
- H. S. Yoder, Jr., Carnegie Inst. Washington
  Hydrous silicate systems, high pressure silicate studies

Scientists at NBS (Cook, Roth and Negas) with the help of the American Ceramic Society (Cleek, Smith and others) are assuming much of the responsibility for gathering the data from the literature and coordinating the preparation of evaluations and final editing of diagrams.

Coverage according to chemical system for the various editions is as follows:

	1964	1969	1975	1978
Metal-oxygen systems	146	202	104	∿205
Metal oxide systems	855	408	401	∿655
Systems with oxygen containing radicals	172	228	68	∿120
Systems with halides only	483	718	145	∿365
Systems containing halides with other substances	214	273	72	∿160
Systems containing cyanides, sulfides, etc.	43	82	20	∿140
Systems containing water	151	131	40	∿250

Results of a questionnaire are being analyzed to determine user interest as a function of chemical system and user opinion regarding the critical commentaries, in order to guide the preparation of future editions.

291

National Bureau of Standards SP-496, Applications of Phase Diagrams in Metallurgy and Ceramics
Proceedings of Workshop held at NBS, Gaithersburg, Md., January 10-12, 1977

NBS CRYSTAL-DATA CENTER

A. Mighell, H. Ondik, J. Stalick, R. Boreni

Institute for Materials Research
National Bureau of Standards
Washington, D.C. 20234

The NBS Crystal-Data Center abstracts and critically evaluates crystallographic data. For a substance to be included in the crystal-data file, cell parameters must be reported for the material. These parameters are determined primarily by powder and single-crystal x-ray diffraction. Crystallographic data results from a variety of disciplines and, consequently, is taken from over 300 scientific journals. The total number of crystalline compounds now in the file is over 40,000.

The output of the project includes:

1. *Crystal Data Determinative Tables*: Used to identify crystalline materials via the ratios of the cell parameters. The most recent volume published is the third edition.[1] A supplement to the third edition will be issued in 1977.

2. *Crystal Data Space-Group Tables*: Materials are arranged by space group. These tables can be used to identify materials of any given space group or symmetry, and to identify isostructural materials. These tables will be consonant with the third edition of *Crystal Data*. They will be published in the Journal of Physical and Chemical Reference Data in the Spring of 1977.

3. NBS Magnetic Tape #9:[2] This tape is an abbreviated version of the third edition of *Crystal Data* and contains cell, space group, density, formula, and determinative ratios. As supplements to the third edition are published the tape will be updated.

4. Component of CIS (Chemical Information System) which is being set up by NIH/EPA: The crystal-data file will be in the CIS system along with the powder-data file, the Cambridge structural file, the mass spectroscopy file and other scientific data bases. These files are to be used primarily in the identification of unknown crystalline materials.

A principal use of the cell and chemical data is the identification of unknown crystalline materials. Several recent developments give great promise for the identification of unknown materials via single-crystal work. They include the growth of the data base, advances in lattice theory, and automation of the single-crystal x-ray diffractometer. To identify an unknown, one can start with a single crystal, mount it on a diffractometer, determine a refined primitive cell, reduce the cell, and check against a file of known reduced cells. The entire procedure can be automated. As a result, the single-crystal x-ray diffraction method can now complement the powder method for the routine analysis of crystalline materials.

A major objective of the NBS Crystal-Data Center is to establish close ties with other data efforts with common interests and to coordinate our data evaluation with these centers (e.g. Joint Committee on Powder Diffraction Standards, Cambridge Crystallographic Data Centre, The Chemical Information System).

---

[1] J.D.H. Donnay and Helen M. Ondik, "Crystal Data Determinative Tables," Third Edition, Vol. 1 and 2, U.S. Department of Commerce, National Bureau of Standards, and the Joint Committee on Powder Diffraction Standards (1972, 1973).

[2] For information about the tape and its lease, contact the National Technical Information Service (NTIS), Department of Commerce, 5285 Port Royal Road, Springfield, VA 22151.

DEMONSTRATION: The NBS magnetic tape #9 described under item 3 of this abstract will be accessed in an accompanying demonstration of "On-Line Data Retrieval and Analysis Systems Such as OMNIDATA", by B. B. Molino and J. Hilsenrath, NBS.

National Bureau of Standards SP-496, Applications of Phase Diagrams in Metallurgy and Ceramics
Proceedings of Workshop held at NBS, Gaithersburg, Md., January 10-12, 1977

The NBS Alloy Data Center

G. C. Carter, D. J. Kahan, and L. H. Bennett
Metallurgy Division
Institute for Materials Research
National Bureau of Standards
Washington, D.C. 20234

Introduction

Knowledge of the structure of materials is important in understanding several industrially significant phenomena and applications such as aging, hardness, occurrence of brittle intermetallic compounds, magnetic transition temperatures, high-temperature solubility of impurities, corrosion resistance, solid electrolytes and non-crystalline solids, as well as many other physical properties. The study of a phase diagram appropriate to a particular material can often provide information important to its scientific and technical applications. In recent years it has become increasingly clear that the need for reliable phase diagrams far exceeds the availability, and the Alloy Data Center (ADC) is now addressing this problem in some detail.

Preliminary surveys concerning data availability have already been done by the ADC in the form of short reviews and compilations of existing phase diagram compilations (1) and of existing phase diagram data centers (2). Both of these are being kept current and a more extensive review together with these updated editions are given on page 36 of these proceedings. Earlier investigations on phase diagram and thermodynamic data needs had already been done via an NBS Impact study, and more recently with more specific questions by method of a questionnaire, distributed by the ADC to those showing an interest in our present phase diagram workshop.

This paper reports on the findings of the questionnaire, on general ADC activities, and on the present status and future plans of the ADC with regards to the subject of phase diagram data. Although thermodynamic data are an integral part of this subject, the present paper intends to concentrate primarily on phase diagrams.

User Needs and Data Availability - Questionnaire Results

About 150 questionnaires were sent to those persons who indicated (written or orally), an interest in the Phase Diagram Workshop. At the time of writing, 48 responses have been received. The questionnaire addressed both the topics of 1) User Needs, and 2) Data Availability. Since the papers of these workshop proceedings go into great detail in both of these areas, all results from these questionnaires will not have to be duplicated here, but rather, the results not expressed elsewhere will be described, with relation primarily to metallic alloys.

1. User Needs. The most often cited user needs were in the areas of superalloys, high temperature steels, and eutectics. Such materials are utilized in high temperature applications (e.g. turbine components), reactors, energy storage materials, etc. Other areas of needs were for coatings and their interactions with the alloys they coat, corrosion resistant alloys (e.g. Hastelloy, alloy C-267, corrosion properties versus phase diagrams), wear resistant alloys (certain carbides), impurity effects on phase diagrams in many of the instances given here, data on the effect of hot-working, heat treatments, segregation during soldification, data on materials used in ferromagnetic, mechanical, and superconducting applications (A-15 compounds and other), catalysis (metals), catalyst supports (ceramics), battery components and their corrosion properties (e.g. electrodes, high energy density batteries, lead acid batteries, etc.), memory alloys, effect of irradiation on phase transformations, dental alloys, data for specification of thermal practices, data on liquid solder-solid alloy interactions, hard steels, special steels, data on the σ-phase formation in transition metal alloys, and composite materials (e.g. refractory boride or carbide compounds with metal matrix). The occurrence of sulfur in alloys was mentioned occasionally in the questionnaires as a problem area where more data are needed, and the urgency of this subject was repeatedly mentioned during the third day of the workshop, devoted to user needs (Panels II, III, and IV). Applications of phase diagram data ranged from very specific problems such as turbines and batteries, to more general areas as materials development for materials substitution, or, in general, R & D. These needs for data on the above general categories of alloys can be rewritten in more chemical terms as needs for phase diagram data on: binary and multicomponent alloys based on Fe, Cu, Ni, Al, W, Pb, Mo, Nb, Cr, and other transition metal as well as some non-transition metal alloys, and on the carbides, sulfides, silicides, selenides, tellurides, as well as effects of impurities (O, N, C, S, and non-interstitial impurities) on all these materials.

Three tabular questions were also asked with regards to user needs (summary reproduced in Fig. 1). They query the subjects of relative needs for i) coverage in phase diagram compilations, ii) depth of evaluation (ranging from unannotated bibliographies to full critical evaluations), and iii) preferred formats of such compilations.

The urgent need for data on ternary and higher component phase diagram data is clearly demonstrated in Fig 1-i. High precision, metastable phase, impurities or trace additions, and crystallography were also of importance to many respondents. While the ADC will concern itself with all former topics, the topic of crystallography falls outside our scope. NBS' Crystal Data Center (see preceding paper, p. 259) concerns itself with this topic, and many critical compilation on crystallographic data are available (e.g. see refs 3-6, and the listing on pp. 82-83 of these proceedings).

Fig 1-ii demonstrates the preference for a full critical evaluation of binary alloys (i.e. an update of the Hansen (7) series), whereas for ternary or higher order multicomponent system, a lesser degree of evaluation will be helpful with the most weighting on unevaluated diagrams with a complete bibliography. Intermingled with this response is probably the fact that many users are accustomed to having a full evaluation for binaries and, therefore, prefer an update, whereas multicomponent data users are not so spoiled. It should be noted here that a major data project in the USSR does produce just that, giving an "unevaluated" (though some judgement has been made) phase diagram compilation with complete bibliography, issued annually (8). An English translation of a cumulative index to this Russian work has recently been completed and is enclosed in these workshop proceedings as paper TPSII-1. Other ternary phase diagram projects include the updating of the 1956 bibliography by Haughton and Prince (See p. 57, Appendix C) which is nearing completion and a new project in Germany under Petzow et al. (see p. 45, Appendix A), which plans to produce a complete, evaluated compendium of ternary diagrams.

Packaging of the output was addressed as well in tabular form in the questionnaire (Fig 1-iii). It appears that loose-leaf sheets are more popular than was anticipated. Several respondents qualified this preference noting that quick distribution was of high urgency. A bound volume could then follow at a later time. Also, insofar as many scientists have their own personal files of diagrams, loose-leaf distribution was said to be a desirable method for inclusion in private collections. Of course, bound volumes were also noted as being desirable.

Generally, the results of ii, and iii were weighted towards minimal evaluation minimal packaging in the interest of speed of distribution. To some extent the results suggest that people want new, improved versions of what they have used in the past. Very few marked magnetic tapes, microform, or on-line access as desirable forms of packaging. Although for microform there may not be much change in technology, and, therefore, popularity, the distribution of magnetic tapes, and especially the on-line access method could gain an increased popularity in the near future, since improved software is becoming available, and more and more groups are acquiring on-line terminals. Especially with the availability of software for the calculation of phase diagrams (e.g. see paper by A. D. Pelton, on p. 1077), such an alternative is becoming attractive.

2. Data Availability. The subject of data availability was also addressed in the questionnaire. As a result, a substantial amount of information was gathered, which has been added in Appendices A and C, pp. 40-80, representing a listing of on-going data activities and a listing of existing phase diagram compilations. Generally, between available books and current data projects, a fair amount of data is available. However, much of it is badly out of date, coverage is incomplete or lacking in several areas, and future products will not be out soon. For example, no comprehensive update of the critical compilation of binary phase diagrams (the old Hansen series) is being done yet; the compendium of critical ternary

phase diagrams, estimated at some 18,000 pages, is just in the initial stages (bibliography has been collected), and is not expected to be completed in the near future. Any higher order multicomponent systems are covered only very occasionally for very select systems (e.g. Raynor's Mg-alloy phase diagram compilation; see listing on p. 65). The questionnaire briefly went into the subject of experimental and calculational approaches to phase diagram determinations. Full conference papers by the respondents give a detailed account of the answers, and the present paper will not dwell on this subject.

The results of the questionnaire indicate

1. An excessively long time lag between supply and demand in those areas where data exist (this covers mostly binaries and ternaries).
2. A tremendous lack of data for multicomponent phase diagrams for alloys of immediate need, as described under User Needs, above.
3. An absence of data for multicomponent alloys in general, thereby providing no basis for materials substitution.
4. Certain gaps in coverage (as was pointed out during the workshop as well) in specific areas that lie outside the well-defined scopes of metals, ceramics, and electronic materials (e.g. semiconductors). For example, sulfur-containing materials fall in this category and tellurides were also mentioned in this context.

General ADC Activities

The Alloy Data Center is a part of the NBS' National Standard Reference Data System, under the Office of Standard Reference Data (OSRD). It maintains an awareness of about 150 physical properties in metals and alloys, evaluating only those properties for which a special need exists and for which qualified researchers are employed in the Alloy Physics Section (Metallurgy Division), in which the Alloy Data Center is located. In the past, critical compilations in soft x-ray emission spectroscopy (9) and nuclear magnetic resonance (10) were prepared (the latter including some 800 binary phase diagrams). Consequently, our current bibliographic files (11), which contain nearly all papers on the first two subjects published up to recent years are not being kept up-to-date for those subjects, while papers on phase diagrams are being annotated and entered at an increased rate for production of a comprehensive bibliographic file.

Another important function of the ADC is to maintain interactions with other existing data centers dealing with physical properties of metals and alloys, and to advise the OSRD in matters related to data activities in these areas. It is as a result of this function that the ADC has initiated its program on alloy phase diagrams, and plans to concentrate its efforts on this basic property which underlies most physical, metallurgical, or engineering properties of alloys.

ADC Phase Diagram Program

As is apparent from the compilation on pp. 40-48, several data centers throughout the world are engaged in collecting, critically evaluating, and disseminating phase diagram data. The Alloy Data Center plans to be a center of coordination and interaction for these groups and hopes to help avoid costly and time consuming duplicati .1 of efforts. It plans to continue interactions with the scientific, but more importantly the industrial, user to identify areas of greatest needs such as the four that have been identified above, and recommend programs in these areas. Other problems not yet identified by us as yet may exist today, and new ones will develop in the future. We take the task upon ourselves as a continuing data center, to continue to identify areas of needs, and to act as a liaison between the user and the data evaluation centers.

The ADC plans to assist other data centers and users in preparing bibliographies. Our currently existing computerized bibliographic files already contain many phase diagram citations and they are being entered at an increasing rate. In total, some 20,000 papers are in this system, and with the expected growth, an on-line system is being planned.

The Alloy Data Center plans to critically evaluate phase diagrams in specific areas, and has started with the metal-hydrogen systems applied to hydrogen storage, an area in which the Alloy Physics Section has expertise.

The ADC also will concern itself with the development of graphical methods in phase diagram data communication and presentation. Some preliminary considerations will be discussed below.

Interactive Graphic Demonstration

(given in conjunction with this poster presentation)

by

R. A. Kirsch and L. J. Swartzendruber
Institutes for Basic Standards and Materials Research, resp., of NBS

Introduction

Recently a considerable number of computer-based graphical display systems have become commercially available. The ease of use and sophistication of these systems have advanced to the point where it is worthwhile to consider their utility in the storage, manipulation, retrieval, and display of graphical phase diagram information.

The display of three dimensional surfaces in two dimensions is often used as an aid to visualizing the properties of ternary phase diagrams (and binary systems when pressure is also an important variable, e.g. in metal-hydrides). The use of a program which allows the surface to be plotted as it would appear to an observer when his eye is placed at any location with respect to the surface has been investigated (12). Using this program, the surface can be viewed from any number of positions, and the one position which best presents the salient features can be selected. The surface generated could then be used by a draftsman to prepare a figure for formal publication. Also, using this method, stereo pairs can be readily generated.

An example is shown in Fig. 2. To generate this figure, a mathematical formula was used to represent a surface *similar* to that found for the palladium-hydrogen system, with the vertical axis representing pressure and the other two axes representing composition and temperature. A 30 x 30 grid was used to generate the display. When using actual data such a grid would be generated using interpolation algorithms. Fig. 3 shows another view of the same surface using a 50 x 50 grid.

To illustrate the use of graphics in displaying binary phase diagrams, we have developed a system which stores the diagram information on mass storage in an abbreviated digital form. The program reads the digital information for the desired diagram from mass storage and uses it to generate a diagram using graphics software. Transformations on the temperature scale, changes between atomic and weight percent, and variations in diagrams size are readily made to obtain the diagram in desired format. Examples are shown in Fig. 4. Information for each line of the diagram is stored as follows: (1) vertical and horizontal lines are specified by their end points. (2) all other lines are specified by their end points and a fourth degree polynomial giving temperature as a function of composition. The polynomial was obtained as a least squares fit to a series of data point with a constraint requiring the curve to pass through the end points. Many other display formats, supplementary scales on each diagram, etc. are readily obtainable.

Using such a system a centralized bank of phase diagram information could be maintained, with each diagram maintained in up-to-date form. A user with access to a graphics terminal could quickly obtain any diagram in the format required. Outputs of any of all diagrams on, for example, microfilm could be supplied from such a centralized system to those without access to a graphics terminal. We have presented only a very brief glimpse at the possibilities inherent in interactive graphic display. As the problem of maintaining up to date compilations of phase diagram data becomes more extensive, such systems may offer a viable alternative.

References

(1) L. H. Bennett, D. J. Kahan, and G. C. Carter, Matls. Sci. Eng. 24, 1 (1976). The compilation of phase diagram books given in this paper is being kept current and the latest edition is given as Appendix C in paper M-3 of this conference.

(2) L. H. Bennett, "Alloy Phase Diagram Activities of the Alloy Data Center", 5th International CODATA Conference, Boulder, CO., June 28-July 1, 1976. The compilation of on-going activities given in this paper is being kept current and the latest edition is given as Appendix A in paper M-3 of this conference.

(3) J.D.H. Donnay and H. M. Ondik, "Crystal Data Determinative Tables", Third edition, Vol 1 and 2, U.S. Dept. of Commerce, NBS, and the Joint Committee on Powder Diffraction Standards (1972, 1973). A supplement to the third edition will be issued in 1977.

(4) W. B. Pearson, "A Handbook of Lattice Spacings and Structures of Metals and Alloys", Pergamon Press, N.Y., Vol 1 (1968), Vol. 2 (1967).

(5) R. W. G. Wyckoff, "Crystal Structures", Interscience, N.Y., Vol. I (RX_1, RX_2), (1963); Vol II (Inorganic Compounds, RX_n, RMX_2, $RnMX_3$, (1964).

(6) Landolt-Bornstein Tables, New Series, Group III, Vol 6, "Selected Data of Elements and Intermetallic Phases", Springer-Verlag, N.Y., (1971).

(7) M. Hansen "Constitution of Binary Alloys", McGraw-Hill, N.Y. (1958) Supplement I, R. P. Elliott (1965), Supplement II, F. A. Shunk (1969).

(8) N. V. Ageev, editor, "Phase Diagrams of Metallic Systems", issued annually in Russian (1955-1974). A cumulative index in english is available in paper TPSII-1 of this proceedings. Subscriptions to this series can be obtained by ordering only in the several months preceding the year for which the subscription is intended, from Prof. A. I. Mikhailov, Director, 125219 Inst tute for Scientific Information (VINITI), Academy of Sciences of the USSR, Baltijskaya UL 14, Moscow, USSR.

(9) J. R. Cuthill, A. J. McAlister, R. C. Dobbyn, and M. L. Williams, "Soft X-ray Emission Spectra of Metallic Solids: Critical Review of Selected Systems and Annotated Spectral Index", NBS Special Publication No. 369 (1974).

(10) G. C. Carter, L. H. Bennett, and D. J. Kahan, "Metallic Shifts in NMR", Progress in Materials Science 20, 1-2260, Pergamon Press (1977).

(11) File, described in NBS Technical Note 464, by G. C. Carter et al. (1968); the file holdings up to 1970 published in "The NBS Alloy Data Center: Permuted Materials Index", by G. C. Carter et al. (1971); the file holdings through 1972 made available in NBS Magnetic Tape 3, Alloy Data Center Tape and Documentation Parcel, Natl. Tech. Info. Ser., Springfield, VA 22151.

(12) This investigation was made by R. A. Kirsch and D. J. Orser, Applied Mathematics Division, NBS, using a program developed by T. K. Porter, LSU/CCB/DCRT/National Institutes of Health.

i) Importance of parameters (check appropriate items):

	very important	important	not important
high precision	|||||	|||||||||	||||
metastable phases	|||||	|||||||||	||||
ternary and higher order systems	|||||||||||	||||||||||	
magnetic and other transitions	|||||	||||||||	||||||||
high pressure	||	|||	||||||||||
impurities or trace additions	|||||||	||||||||	||||||||||
surface phases			||||||||	|||||||
related information: crystallography	||||||||	||||||||	||||
other (please specify): thermo data	|||		
" (intermediate or ordered phases)	||		
" (tie lines sol-liq. multicomp.)				
" (high T changes under tensile and shear stress)				
" (Vapor pressure, any thermal props for x-tal growth - inorg. res. matls.)				
" (decomposition pressures)				

ii) Minimum acceptable depth (check appropriate items):

depth	binary systems	multicomponent systems	other
bibliography	|||||||	|||||||||		
annotated bibliography	|||||	||||||||||	
unevaluated diagrams with bibliography	||	||||||||||||	||||||||||		
critical evaluation	||||||||||	||||||||||	|||||||||||||	
other (coordination with evaluation of thermochem. props. of phases					

iii) Most desirable form of "packaging" (check appropriate items):

	bibliographies	binary systems	multicomponent systems	other
loose-leaf sheets	||||||||||||||	||||||||	||||||||||||	
bound volumes	||||||||||	||||||||	||||||||||||||||		
microfilm or microfich.	|||	|||	||	||
magnetic tape	|||					
on-line computer access	|||||	|||	||||	||
other				

Figure 1. Summary of three of the questions asked in a phase diagram data need questionnaire.

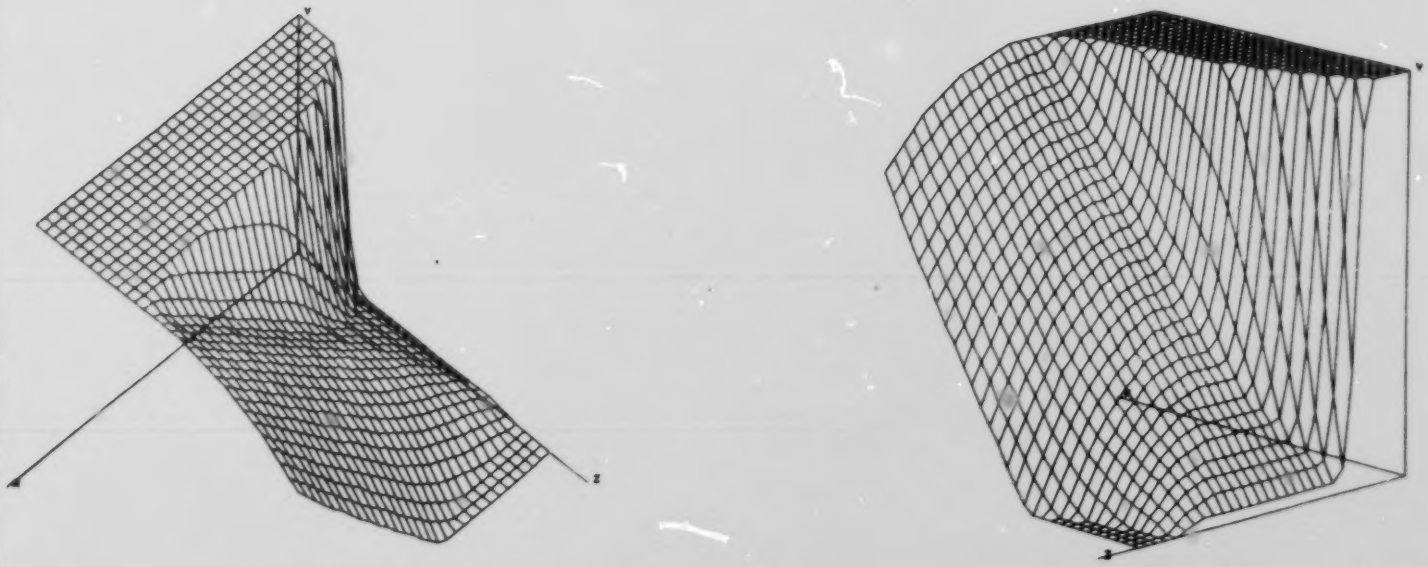

Fig. 2. Two views of a hypothetical pressure-composition-temperature plot of a metal-hydrogen system with properties similar to Pd-H. Vertical Y axis represents pressure, the Z axis composition, and the X axis temperature. The grid size is 30 points by 30 points.

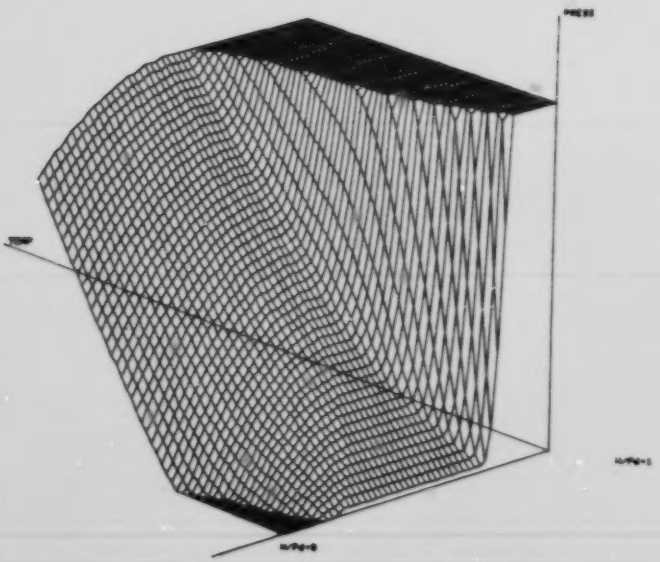

Fig. 3. Another view of the same surface shown in Fig. 2. A finer grid of 50 points by 50 points has been used.

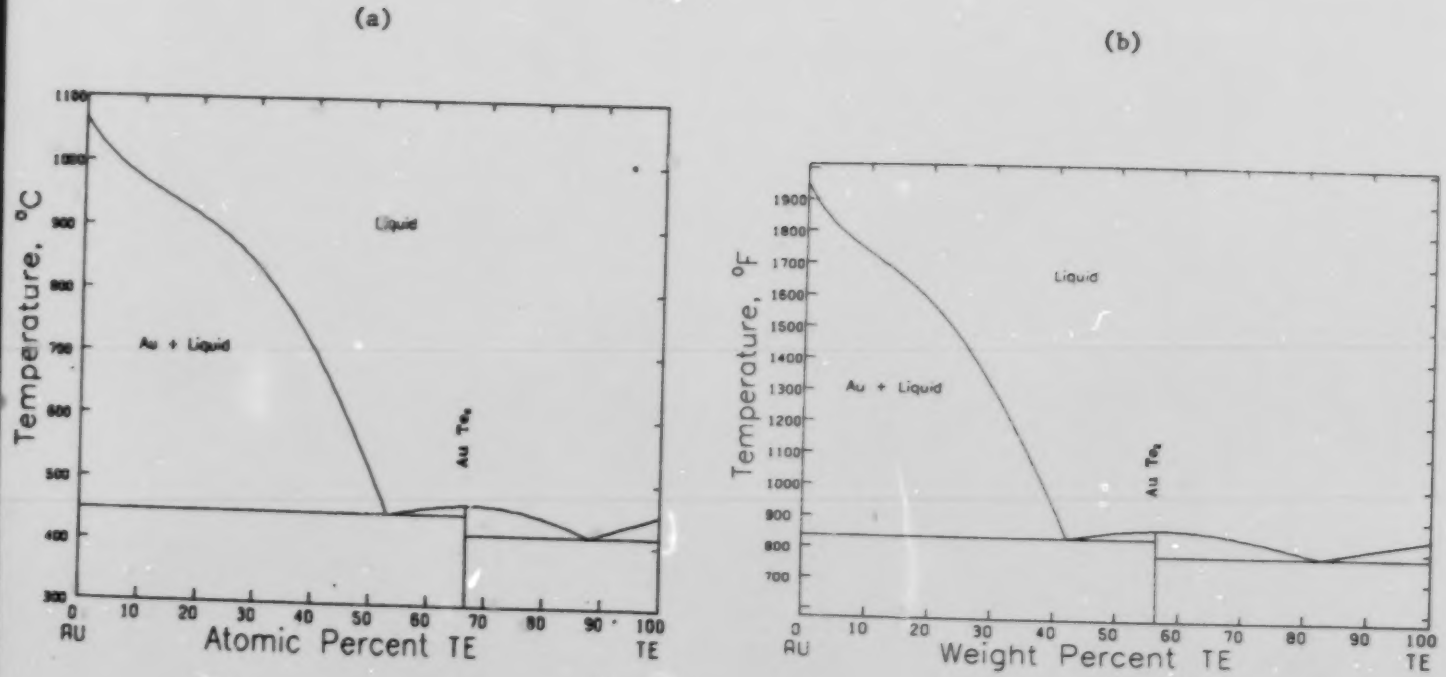

Fig. 4. (a) AuTe phase diagram as displayed on a graphics terminal. (b) AuTe diagram after software generated transformation to weight percent and degrees Fahrenheit. The scale lengths have also been altered slightly.

National Bureau of Standards SP-496, Applications of Phase Diagrams in Metallurgy and Ceramics
Proceedings of Workshop held at NBS, Gaithersburg, Md., January 10-12, 1977

A Review of Phase Equilibria in the Na_3AlF_6-LiF-CaF_2-AlF_3-Al_2O_3 System

Douglas F. Craig, Roger T. Cassidy, and Jesse J. Brown, Jr.
Department of Materials Engineering
College of Engineering
Virginia Polytechnic Institute and State University
Blacksburg, Virginia 24061

ABSTRACT

The electrolyte used in the Hall process for producing aluminum metal consists basically of a fused mixture of alumina (Al_2O_3) and cryolite (Na_3AlF_6). Other ingredients including AlF_3, LiF, and CaF_2 are added to modify properties such as bath density, electrical conductivity, and freezing temperature. The electrolyte composition now used was determined largely by trial and error because of the incompleteness of available phase equilibria data.

For the past five years, a research program jointly sponsored by the Alcoa Foundation and the VPI&SU Research Division has been underway in the Materials Engineering Department at VPI&SU. This program was designed to critically review the existing phase equilibria data on systems involving cryolite and to expand upon this body of knowledge by determining the liquidus-solidus phase relationships in a portion of the Na_3AlF_6-LiF-CaF_2-AlF_3-Al_2O_3 system.

Historically, a variety of experimental techniques have been employed to determine the phase diagrams of systems important to the Hall process. Many of the early experiments were conducted using open containers. This practice resulted in the publication of some inaccurate phase diagrams because of the decomposition of many of the fluoride

compounds at high temperatures. In more recent years, it has become standard procedure to encapsulate all samples in sealed platinum containers. Quenching and Differential Thermal Analysis (DTA) experiments using samples sealed in the platinum containers have been used to revise some of the early phase diagrams and to investigate new systems.

In this paper, the phase diagrams that are known in the Na_3AlF_6-LiF-CaF_2-AlF_3-Al_2O_3 system are reviewed in a systematic manner including the diagrams that have been determined at this University over the past five years. The result is a current review of the phase equilibria knowledge of cryolite containing oxy-fluoride systems of importance to the aluminum industry.

Table of Contents

		Page
A.	One Component Systems	277
	1. Cryolite	277
	2. Aluminum Fluoride	278
	3. Calcium Fluoride	279
	4. Aluminum Oxide	279
	5. Lithium Fluoride	280
B.	Two Component Systems	280
	1. System CaF_2-AlF_3	280
	2. System Na_3AlF_6-CaF_2	285
	3. System Na_3AlF_6-AlF_3	289
	4. System Na_3AlF_6-Al_2O_3	296
	5. System CaF_2-Al_2O_3	299
	6. System AlF_3-Al_2O_3	300
	7. System LiF-AlF_3	300
	8. System LiF-Na_3AlF_6	305
	9. System Na_3AlF_6-Li_3AlF_6	306
	10. System Li_3AlF_6-Al_2O_3	310
	11. System LiF-CaF_2	310
	12. System Li_3AlF_6-CaF_2	314
C.	Three Component Systems	314
	1. System CaF_2-AlF_3-Na_3AlF_6	314
	2. System Na_3AlF_6-AlF_3-Al_2O_3	322
	3. System Na_3AlF_6-CaF_2-Al_2O_3	325
	4. System CaF_2-AlF_3-Al_2O_3	328
	5. System Li_3AlF_6-Na_3AlF_6-Al_2O_3	328
	6. System LiF-AlF_3-Na_3AlF_6	329
	7. System Li_3AlF_6-LiF-CaF_2	329
D.	Four Component Systems	333
	1. System Na_3AlF_6-AlF_3-CaF_2-Al_2O_3	333
	2. System Na_3AlF_6-AlF_3-LiF-Al_2O_3	336
	3. System Na_3AlF_6-CaF_2-LiF-Al_2O_3	336

Aluminum is the most abundant metallic element in the earth's crust and ranks after oxygen and silicon as the third most abundant of all elements. Because of its strong affinity for oxygen, it is not found in nature in the elemental state but only in combined forms such as oxides, silicates, etc. In 1886 Charles Martin Hall and Paul L. T. Héroult discovered almost simultaneously the process in which alumina is dissolved in molten cryolite (Na_3AlF_6) and decomposed electrolytically. This reduction process is known as the Hall-Héroult process.

The electrolyte consists basically of a fused mixture of cryolite, aluminum fluoride, calcium fluoride, lithium fluoride, and alumina. Aluminum fluoride is added to the bath to alter the cryolite ratio ($3NaF/AlF_3$) from the stoichiometric value of 1.5 to some lower value. Calcium fluoride is added in amounts between 5 and 6 wt. % to permit lower operating temperatures with additions of approximately 0.1 wt. % LiF used to increase electrical conductivity.

While the basic process for the production of aluminum has not changed significantly since its discovery 90 years ago, the phase equilibrium diagrams involving the components of the electrolyte are in many cases contradictory and in some cases unknown. To some extent this is because of the experimental difficulties encountered in working in these systems. Cryolite decomposes on melting, AlF_3 is volatile, supercooling is often present and the primary crystallization of Al_2O_3 is difficult to detect by conventional techniques. The inter-relationships between the various fluorides in the bath and their influence on the melting temperature and alumina solubility of the electrolyte can best be understood when reliable phase diagrams for the electrolyte exist.

During the past few years an intensive study of the phase diagrams

involving the components of the electrolyte used in the smelting of aluminum has been underway in the Materials Engineering Department of the Virginia Polytechnic Institute and State University. The objectives of this study are to establish the phase equilibrium relationships in a portion of the Na_3AlF_6-LiF-CaF_2-AlF_3-Al_2O_3 system. This has required a critical review of the existing phase diagrams and, in some cases, experimental redeterminations of selected diagrams. Many pertinent binary and ternary systems were unknown and these were determined experimentally. The final goal of this study is to determine the invariant points in the systems Na_3AlF_6-AlF_3-CaF_2-Al_2O_3, Na_3AlF_6-AlF_3-LiF-Al_2O_3, and Na_3AlF_6-CaF_2-LiF-Al_2O_3. (These systems are of most interest because they contain Na_3AlF_6 and Al_2O_3, the two primary components in the Hall electrolyte.) In this paper, the phase relationships in these systems, as known at the present time, are reviewed.

A. One Component Systems

1. Cryolite

Cryolite, Na_3AlF_6, has been the subject of numerous investigations because of its importance in the industrial production of aluminum. The compound exists in both a low temperature (α) and high temperature (β) polymorphic form. The naturally occurring low temperature polymorph is monoclinic, space group $P2_1/n$, with cell parameters a_o = 5.40Å, b_o = 5.60Å, c_o = 7.78Å and β = 90°11'.[1] Between 560 and 572°C[2-6] cryolite undergoes a rapid reversible transition to the high temperature cubic form, a_o = 7.962Å, with a heat of transition of 2238 cal./mole.[2] Landon and Ubbelohde,[3] on the basis of electrical conductance and thermal arrest data, reported the existence of a third polymorphic variety which they designated γ-cryolite. The β-γ inversion reportedly took place at 881°C with an estimated heat of transition of 200 cal./mole. Attempts by Foster[7] to confirm this transition by electrical conductivity and high temperature X-ray diffraction methods were unsuccessful. More recent investigations have also failed to confirm the existence of a gamma form.

The melting point of natural cryolite has received a great deal of attention because of its importance in cryoscopic calculations. Melting points ranging from 977 to 1027°C have been reported[3-6,8-13] with the majority of the more recent investigations yielding values close to 1009°C. Foster[14], working with samples contained in sealed platinum tubes under carefully controlled conditions, used quenching methods to determine a melting temperature of 1009.2°C for natural Greenland cryolite. On the basis of a plot of the liquid fraction as a function of the temperature from which the samples were quenched the melting point of pure cryolite was determined as 1012 ± 2°C.

The determination of the melting point of cryolite is complicated by the fact that the compound partially dissociates into several ionic subspecies on melting. Frank and Foster [15] employed calculations based on experimental densities to compare several possible reaction mechanisms. It was concluded that cryolite dissociated into $NaAlF_4$ and NaF on melting according to the reaction:

$$Na_3AlF_6 = 2NaF + NaAlF_4$$

Foster and Frank [16] recognized that the calorimetric determination of the heat of fusion of cryolite (27.8 kcal./mole) included a heat effect due to partial dissociation. The true cryoscopic heat of fusion was determined to be 19.9 kcal./mole.

The refractive indices of the room temperature alpha form of cryolite are $\alpha = 1.3376$, $\beta = 1.3377$, and $\gamma = 1.3387$ [17].

2. Aluminum Fluoride

Aluminum fluoride is rhombohedral, space group $R\bar{3}$, with cell parameters $a_{rh} = 5.016\text{Å}$ and $\alpha = 58^{\circ}32'$ [18]. The compound is uniaxial positive with indices of refraction of 1.3765 and 1.3767 [19].

O'Brien and Kelley [4], during an investigation of the heat contents of Na_3AlF_6, AlF_3 and NaF, noted the existence of a new polymorph of AlF_3. The transition to the high temperature form took place at 454°C and was accompanied by a weak heat effect of approximately 150 cal./mole. Holm and Holm [20] used differential thermal analysis to confirm the existence of the polymorph, which they designated β-AlF_3, and set the transition temperature at 453°C. The new polymorph, also noted by Schultz et al. [21], could not be quenched to room temperature and no optical or X-ray diffraction data were reported. Shinn, Crocket and Haendley [22] reported the existence of a third (gamma) polymorph of

AlF_3, which could be obtained either by heating ammonium hexafluoroaluminate to 400°C or decomposing ammonium tetrafluoroaluminate. The transition to the new tetragonal form (a_o = 3.54Å and c_o = 6.00) took place at 300°C. No confirmation of the existence of this polymorph is found in the literature.

Mesrobian, Rolin and Pham [23] studied mixtures of NaF and AlF_3 under pressure using thermal arrest methods. A peak at 1300°C for samples containing more than 50 wt. % AlF_3 was interpreted as resulting from a previously unknown inversion of AlF_3. In addition, the triple point of pure AlF_3 was placed above 200 bars pressure and 1700°C. Aluminum fluoride is normally reported to sublime at 1291°C at 1 atmosphere pressure.

3. Calcium Fluoride

Calcium fluoride (fluorite) exists in only one form which has a face centered cubic structure, space group Fm3m, and a cell parameter a_o = 5.4626[24]. Kojima et al.[25] suggested that the variations in the melting point found in the literature[26] are caused by slight hydrolysis during heating ($CaF_2 + H_2O \rightarrow CaO + 2HF$). Using anhydrous HF as a deoxidyzing and purifying agent, the melting point of high purity CaF_2 was determined as 1423°C. The refractive index of the compound is 1.434[27].

4. Aluminum Oxide

Aluminum oxide, Al_2O_3, exists in at least seven crystalline modifications which are arbitrarily designated as alpha, gamma, delta, eta, theta, kappa, and chi. The most common form, α-Al_2O_3 or corundum, belongs structurally to space group $R\bar{3}c$ with cell parameters a_{hex} = 4.758Å and c_{hex} = 12.991Å[28]. Corundum is a uniaxial positive mineral with indices of refraction 1.768 and 1.760[27].

Eta aluminum oxide, like corundum, has been reported as the crystalline modification of Al_2O_3 present in certain areas of phase diagrams dealing with the electrolyte used in the smelting of aluminum[29]. The eta form is cubic with a spinel type structure and cell parameter $a_o = 7.94\text{Å}$[30]. The index of refraction is 1.670.

A metastable alumina phase designated as m-alumina by Foster[31] and later as tau-alumina by Wefers and Bell[32] has also been reported. Tau-alumina converts first to eta- and finally to alpha-alumina on heating. The X-ray diffraction pattern is similar to mullite.

5. Lithium Fluoride

Lithium fluoride exists in one crystalline modification. It has the cubic NaCl type structure with a cell parameter of $a_o = 4.0262$. The melting point of LiF has been reported to be between 845 and 848°C[33-42].

B. Two Component Systems

1. System CaF_2-AlF_3

The earliest investigation of the system was conducted by Fedotieff and Iljinsky[8]. On the basis of DTA data collected from samples heated in air, a eutectic system was identified. The invariant point was placed at 37.5 mole % AlF_3 and 820°C. Ravez and Hagenmuller[43] and Ravez et al.[44] reinvestigated the system using powder X-ray diffraction. Samples were encapsulated in copper and reacted at 600, 700, 800, and 840°C. One compound, $CaAlF_5$, was identified and found to exist in both a low (alpha) and high (beta) temperature polymorph. Debye Sherrer patterns of α-$CaAlF_5$ were used to index the compound in the orthorhombic system with cell parameters $a_o = 11.81 \pm 0.03\text{Å}$, $b_o = 9.16 \pm 0.02\text{Å}$ and $c_o = 6.35 \pm 0.01\text{Å}$. The high temperature polymorph was found to be isotypic with $CaFeF_5$ and was also indexed in the orthorhombic system ($a_o = 20.04 \pm$

0.03Å, b_o = 9.81 ± 0.01Å, and c_o = 7.31 ± 0.01Å). A structural analogy was noted between orthorhombic β-$CaAlF_5$ and tetragonal $SrAlF_5$ corresponding to the relationships:

$$\sqrt{2}\, a_{SrAlF_5} \approx a_{\beta\text{-}CaAlF_5}$$

$$b_{SrAlF_5} \approx \frac{\sqrt{2}}{2}\, b_{\beta\text{-}CaAlF_5}$$

$$c_{SrAlF_5} \approx c_{\beta\text{-}CaAlF_5}$$

DTA results established the transition and melting temperature of the compound at 820 and 850°C respectively. Pycnometric methods were used to determine the density of α- and β-$CaAlF_5$ as 3.09 and 2.96 g/cm^3.

Holm[45] provided the first phase diagram of the system (Figure 1). He confirmed the existence of the 1:1 compound and on the basis of DTA data showed the α-β transition to take place at 740°C. The compound formed highly twinned crystals with a mean refractive index of 1.375 and a density of 2.947 g/cm^3. Incongruent melting to AlF_3 and a liquid containing 44 mole % took place at 881°C. The eutectic for the system was located at 37 mole % AlF_3 and 828°C. Pronounced supercooling was noted in the area of the diagram containing 60% or more CaF_2 and DTA heating curves were therefore used to gather data in this region. No liquidus data were presented for the portion of the system richer in AlF_3 than the peritectic composition. Malinovsky, Vrbenska and Cakajdova[46] and Millet, Pham and Rolin[47] reinvestigated the system using thermal arrest methods and presented diagrams very similar to Holm's. Both studies confirmed the existence of $CaAlF_5$ in both a low

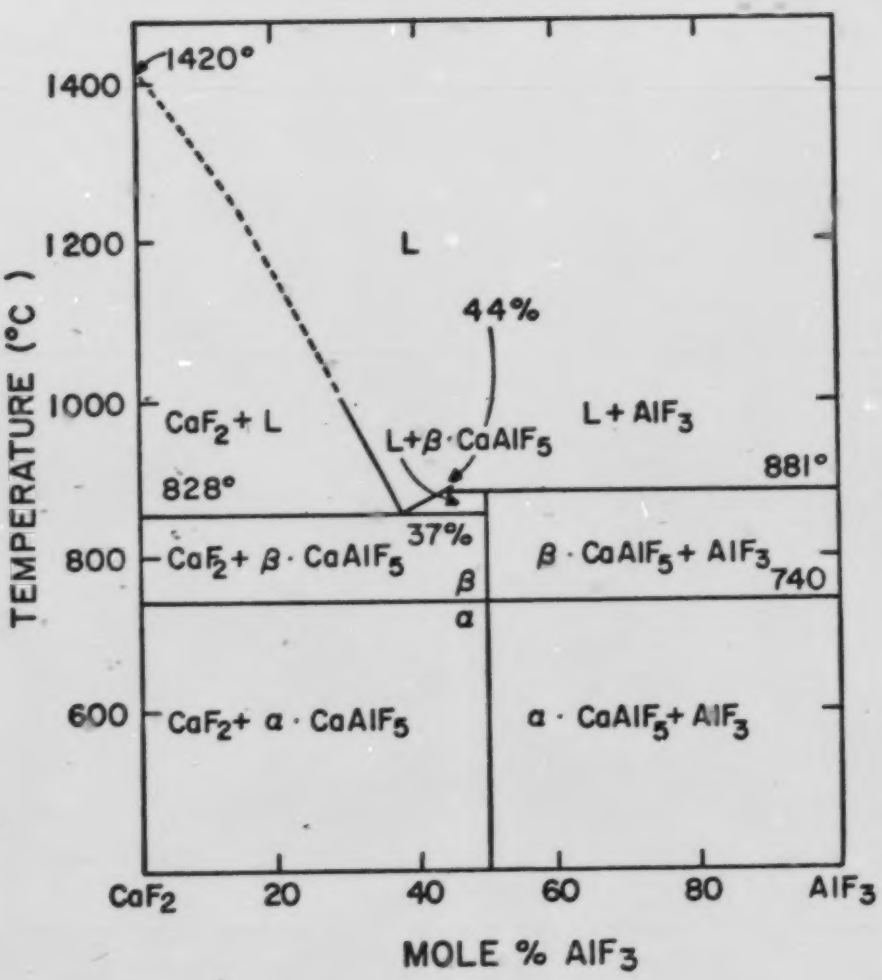

Figure 1. System CaF_2-AlF_3 (45).

and high temperature polymorphic form. Malinovsky et al. located the invariant points at 37.5 mole % AlF_3 and 829°C and 47.5 mole % AlF_3 and 893°C. Millet et al. reported slightly different compositions and temperatures (36 mole % AlF_3 and 820°C and 44 mole % AlF_3 and 880°C). The latter authors also noted that the extrapolation of the liquidus curve in the high AlF_3 end of the diagram indicated that the triple point of AlF_3 is in the neighborhood of 2250°C.

Craig and Brown[48], using a combination of optical microscopy, powder X-ray diffraction, quench techniques and differential thermal analysis, presented the phase diagram of the system shown in Figure 2. To prevent volatilization of AlF_3, all heat treatments and DTA experiments were performed on samples encapsulated in sealed platinum tubes. Since pronounced supercooling existed in the system, DTA heating curves at 3°C/min (as opposed to cooling curves) were used to obtain reaction temperatures. These temperatures were then verified by quenching experiments to insure they represented equilibrium data.

Two compounds were found to exist in the system. The 1:1 compound, noted by previous authors, melted incongruently at 873 ± 3°C to AlF_3 and a liquid containing 44 mole % AlF_3. The α-β inversion remained constant at 743 ± 3°C. A previously unreported 2:1 compound, Ca_2AlF_7, was found to melt incongruently at 845 ± 3°C to CaF_2 and a liquid containing 35 mole % AlF_3. The eutectic for the system was placed at 37.5 mole % AlF_3 and 836 ± 3°C.

The authors noted that while Ca_2AlF_7 had not been previously reported a hydrated form $Ca_2AlF_7 \cdot 2H_2O$ and a hydrated hydroxide $Ca_4Al_2(OH)_{14} \cdot 5H_2O$[49] are known to exist. The anhydrous compound was successfully formed using AlF_3, $AlF_3 \cdot 3H_2O$ or $CaAlF_5$ as a starting material. The absence of

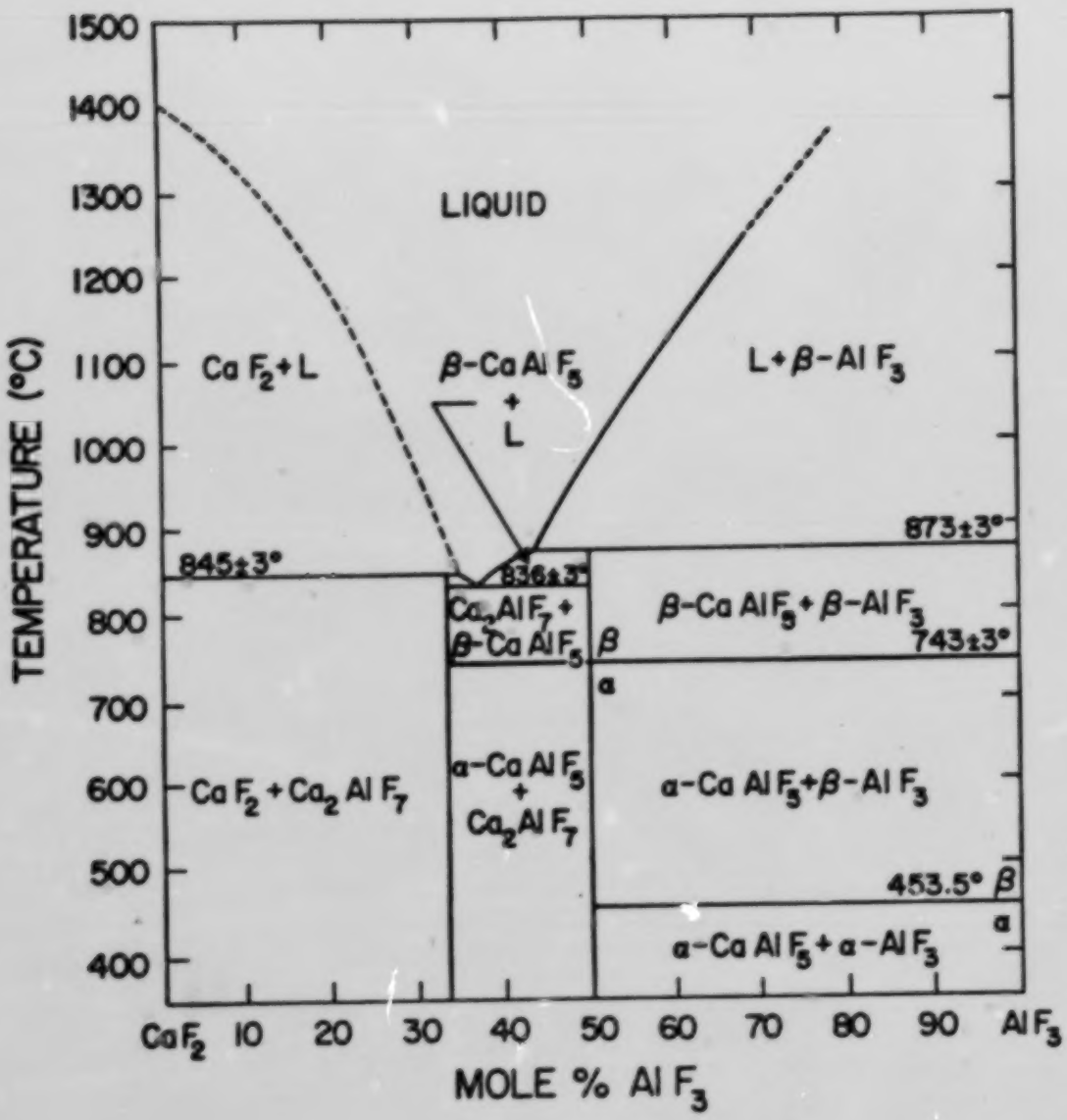

Figure 2. System CaF_2-AlF_3 (48).

308

any previous reports on the existence of the compound was attributed to its sluggish formation and to non-equilibrium cooling. Only the peritectic reaction was consistently observed during DTA heating experiments, but on cooling three peaks were observed. The lowest corresponded to the α-β $CaAlF_5$ inversion. Powder X-ray diffraction data of samples after DTA experiments showed a mixture of α-$CaAlF_5$ and AlF_3 which converted back to Ca_2AlF_7 on reheating.

The 2:1 compound was tentatively indexed on the basis of powder X-ray diffraction data (¼°2θ/min-CuK_α) as orthorhombic with lattice parameters a_o = 18.22Å, b_o = 9.06Å and c_o = 7.11Å (Table I). A least squares cell refinement program developed by Evans, Appleman and Handwerker[50] was used to obtain the final cell parameters.

The structural relationships between β-$CaAlF_5$ and $SrAlF_5$ noted by Ravez et al.[44] were also found to exist between Ca_2AlF_7 and Sr_2AlF_7. These suggest that the a and b parameters of the orthorhombic cell of Ca_2AlF_7 roughly coincide with the face diagonal and ½ the face diagonal of the (001) plane of the tetragonal cell of Sr_2AlF_7 with c being common to both cells.

2. System Na_3AlF_6-CaF_2

The first study of the Na_3AlF_6-CaF_2 binary system was conducted by Pascal[13] in 1913. He was primarily concerned with the liquidus curves reporting a eutectic at 47.8 mole % CaF_2 and 905°C. Minor modifications of the temperature and composition of the eutectic were made by Fedotieff and Iljinsky[8] (48.1 mole % CaF_2 and 930°C), Matiasovský and Malinovský[51] (50.5 mole % CaF_2 and 940°C), and Fenerty and Hollingshead[52] (48.6 mole % CaF_2 and 946°C).

TABLE I. Powder X-Ray Diffraction Data for the Compound Ca_2AlF_7*

d_{obs}	d_{calc}	I/I_o	(hkl)
5.34	5.35	5	111
4.06	4.06	10	220
3.82	3.82	30	021
3.55	3.55	75	602
3.49	3.49	100	102
2.983	2.980	10	130
2.885	2.880	65	610
2.744	2.749	35	131
2.702	2.705	15	330
2.637	2.637	5	521
2.444	2.444	10	701
2.274	2.275	20	113
2.248	2.248	55	140
2.169	2.169	40	801
2.099	2.100	15	023
2.029	2.029	10	440
1.946	1.946	40	532
1.910	1.911	5	042
1.877	1.876	65	812
1.848	1.849	35	920
1.835	1.835	30	632
1.778	1.777	35	004
1.745	1.744	20	204
1.685	1.684	25	450
1.598	1.598	10	504

other reflections

a = 18.22Å

b = 9.06Å

c = 7.11Å

*Evans, H. T., Appleman, D. E. and Handwerker, D. J., (1963) Least Squares Refinement.

In 1961, Rolin[53] reported solidus data for the system. Using thermal arrest cooling curves of closely spaced compositions containing up to 53.5 mole % CaF_2 the eutectic was placed at 47.3 mole % CaF_2 and 946°C. Samples higher in Na_3AlF_6 than the eutectic composition showed a marked decrease in the eutectic temperature with increasing cryolite content. Rolin concluded that a large solid solution of CaF_2 in cryolite must exist, extending almost to the eutectic composition at 946°C. Following Rolin's suggestion that before the phase relations could be definitely established the system should be re-examined by other methods, Holm[54] studied the system using a combination of thermal analysis, DTA, X-ray diffraction, quenching techniques, optical microscopy and density determinations. The lack of a real eutectic halt on the high cryolite side of the diagram was again observed during DTA; however, a small exothermic peak at 785°C was also noted. Since this temperature is close to the reported eutectic temperature for the system NaF-Na_3AlF_6-CaF_2[8] Holm postulated that the depression of the eutectic temperature seen by Rolin might be caused by volatilization of small amounts of AlF_3 or $NaAlF_4$ and not by solid solution. As further proof that solid solution of CaF_2 in Na_3AlF_6 does not exist, Holm noted that samples containing 5-90 mole % CaF_2 quenched from 950°C showed Na_3AlF_6 or CaF_2 in equilibrium with liquid. In addition, the densities of samples containing up to 60 mole % CaF_2 quenched from 970°C compared closely with calculated densities of mechanical mixtures of CaF_2 and Na_3AlF_6. Holm's simple eutectic system showing no solid solution and a eutectic at 50 mole % CaF_2 and 945.5°C is shown in Figure 3.

Verdan and Monnier[55], using DTA experiments of samples contained in sealed crucibles, studied the system to resolve the controversy between

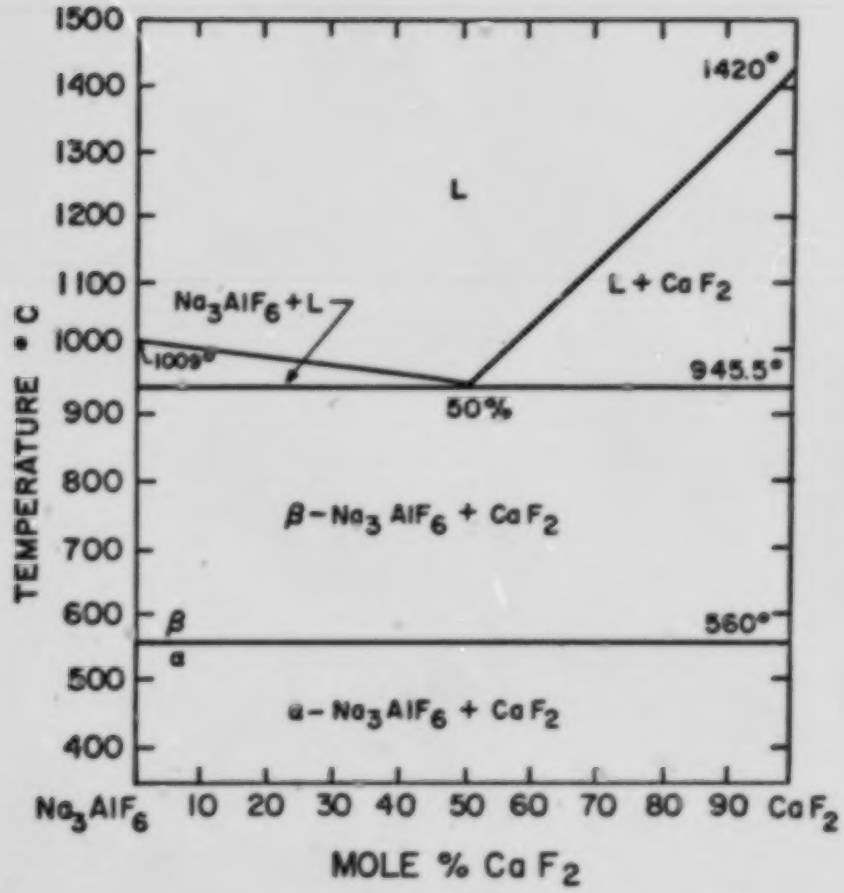

Figure 3. System Na_3AlF_6-CaF_2 (54)

Holm and Rolin over the existence of solid solution. They noted that the presence of a Na_3AlF_6 solid solution would explain the difficulty in purifying cryolite when CaF_2 is present. Liquidus and solidus data were obtained which indicated a solid solution of CaF_2 in Na_3AlF_6 approaching a maximum of 20 mole % CaF_2 at the eutectic temperature. A decrease in the α-β Na_3AlF_6 transition from 563°C for pure cryolite to 530°C for a sample containing between 5 and 6 mole % CaF_2 was also noted. A eutectoid reaction was, therefore, located at 5.5 mole % CaF_2 and 530°C (Figure 4).

Craig and Brown[56] studied samples containing 0-30 mole % CaF_2 using DTA of samples encapsulated in sealed platinum tubes. The α-β Na_3AlF_6 inversion remained constant at 567°C. No peaks corresponding to a solidus line were observed and all data agreed well with the simple eutectic diagram of the system presented by Holm.

3. System Na_3AlF_6-AlF_3

The system Na_3AlF_6-AlF_3 has been investigated periodically since the first published version by Fedotieff and Iljinsky[8] in 1923. Foster[57] gives an excellent review of the more recent publications. A slightly altered version of his table of reported invariant points, compositions and temperatures is reproduced in Table II. The majority of the diagrams agree well with respect to the liquidus curve up to 30 wt. % AlF_3; however, there is disagreement above this value as to the location and composition of the invariant point(s), shape of the chiolite ($Na_5Al_3F_{14}$) liquidus curve and identity of the primary phase in equilibrium with liquid in the high AlF_3 end of the diagram.

A major point of contention is whether $NaAlF_4$ exists as a stable phase. Grjotheim[5] reported $NaAlF_4$ to melt congruently at 731°C.

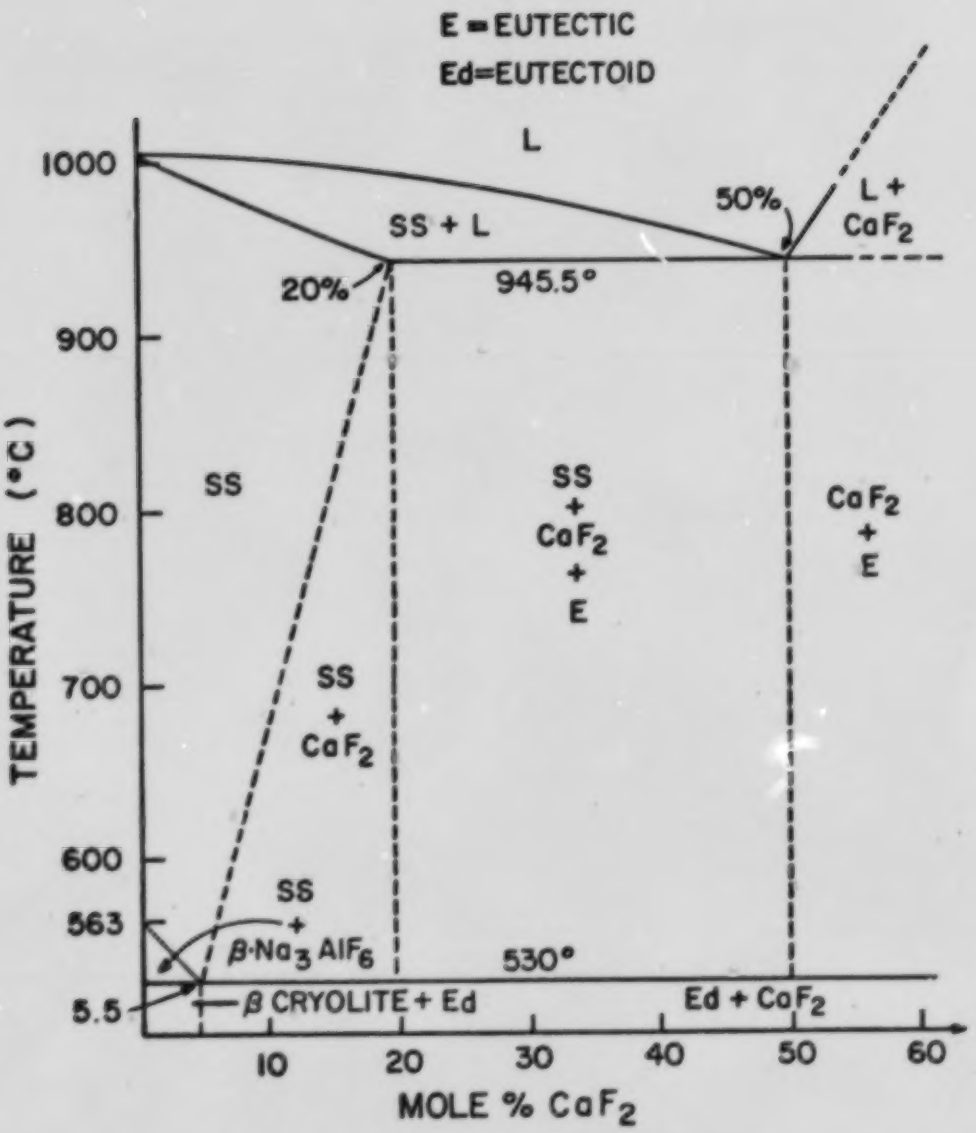

Figure 4. System Na_3AlF_6-CaF_2 (55).

TABLE II

Invariant Point Compositions and Temperatures in the System Na_3AlF_6-AlF_3

Ref.	Invariancy	Equilibrium Solid Phases	Liquid Composition (wt.%) AlF_3	Liquid Composition (wt.%) Na_3AlF_6	Temp. (°C)
5	Peritectic	Na_3AlF_6 $Na_5Al_3F_{14}$	28.6	71.4	734
	Eutectic (1)	$Na_5Al_3F_{14}$ $NaAlF_4$	35.3	64.7	690
	Eutectic (2)	$NaAlF_4$ AlF_3	49.8	50.2	704
10	Peritectic	Na_3AlF_6 $Na_5Al_3F_{14}$	30	70	734
	Eutectic	$Na_5Al_3F_{14}$ AlF_3	40	60	693
42	Peritectic	Na_3AlF_6 $Na_5Al_3F_{14}$	30	70	730
	Eutectic	$Na_5Al_3F_{14}$ AlF_3	38.5	61.5	684
37	Peritectic	Na_3AlF_6 $Na_5Al_3F_{14}$	30	70	739
	Eutectic	$Na_5Al_3F_{14}$ AlF_3	40	60	694
43	Peritectic	Na_3AlF_6 $Na_5Al_3F_{14}$	28.1	71.9	739
	Eutectic	$Na_5Al_3F_{14}$ AlF_3	36.6	63.4	700
44	Peritectic (1)	Na_3AlF_6 $Na_5Al_3F_{14}$	32.2	67.8	737
	Eutectic	$Na_5Al_3F_{14}$ $NaAlF_6$	37.5	62.5	690
	Peritectic (2)	$NaAlF_4$ AlF_3	38.7	61.3	710
	Eutectoid	$Na_5Al_3F_{14}$ $NaAlF_4$ AlF_3			680

TABLE II (Cont.)

Ref.	Invariancy	Equilibrium Solid Phases	Liquid Composition (wt.%) AlF_3	Liquid Composition (wt.%) Na_3AlF_6	Temp. (°C)
41	Peritectic	Na_3AlF_6 $Na_5Al_3F_{14}$	30	70	741
	Eutectic	$Na_5Al_3F_{14}$ AlF_3	39	61	694

Ginsberg and Wefers[58] agreed with Grjotheim that $NaAlF_4$ is a stable phase in the system but found it to melt incongruently 710°C. In addition, a eutectiod reaction was found at 680°C with $Na_5Al_3F_{14}$ and AlF_3 forming at the expense of $NaAlF_4$ (Figure 5).

Several other authors[10,52,59,60] have disagreed with the equilibrium existence of $NaAlF_4$ and presented diagrams showing AlF_3 as opposed to $NaAlF_4$ as an equilibrium solid at the eutectic. Holm[60] suggested that $NaAlF_4$ was not a stable phase since solid $NaAlF_4$ collected from the vapor above a melt of the same composition decomposed during differential thermal analysis at 500°C to $Na_5Al_3F_{14}$ and AlF_3.

Foster[57], working with samples in sealed platinum tubes, used a combination of optical microscopy, DTA, X-ray diffraction and quench techniques to establish the diagram shown in Figure 6. It was concluded that $NaAlF_4$ is not a stable phase since (1) it was only found when liquid was present before quenching; (2) samples quenched from the region reported to contain $NaAlF_4$ and chiolite in equilibrium showed only chiolite and AlF_3; (3) samples quenched from the region of the diagram reported to have $NaAlF_4$ and liquid in equilibrium showed AlF_3 to be the primary crystalline phase; and (4) DTA (in sealed tubes) of melts that precipitated $Na_5Al_3F_{14}$ as the primary phase did not show any peaks that would indicate a phase field containing solid $NaAlF_4$.

Mesrobian et al.[23] studied mixtures of AlF_3 and NaF and in addition to locating the triple point of AlF_3 above 200 bars pressure and 1700°C reported two new invariant lines in the system. The first was located by constant temperature peaks of thermal arrest cooling curves for compositions ranging from 45-95 wt. % AlF_3 at approximately 1300°C. It was postulated that the peaks were caused by an allotropic

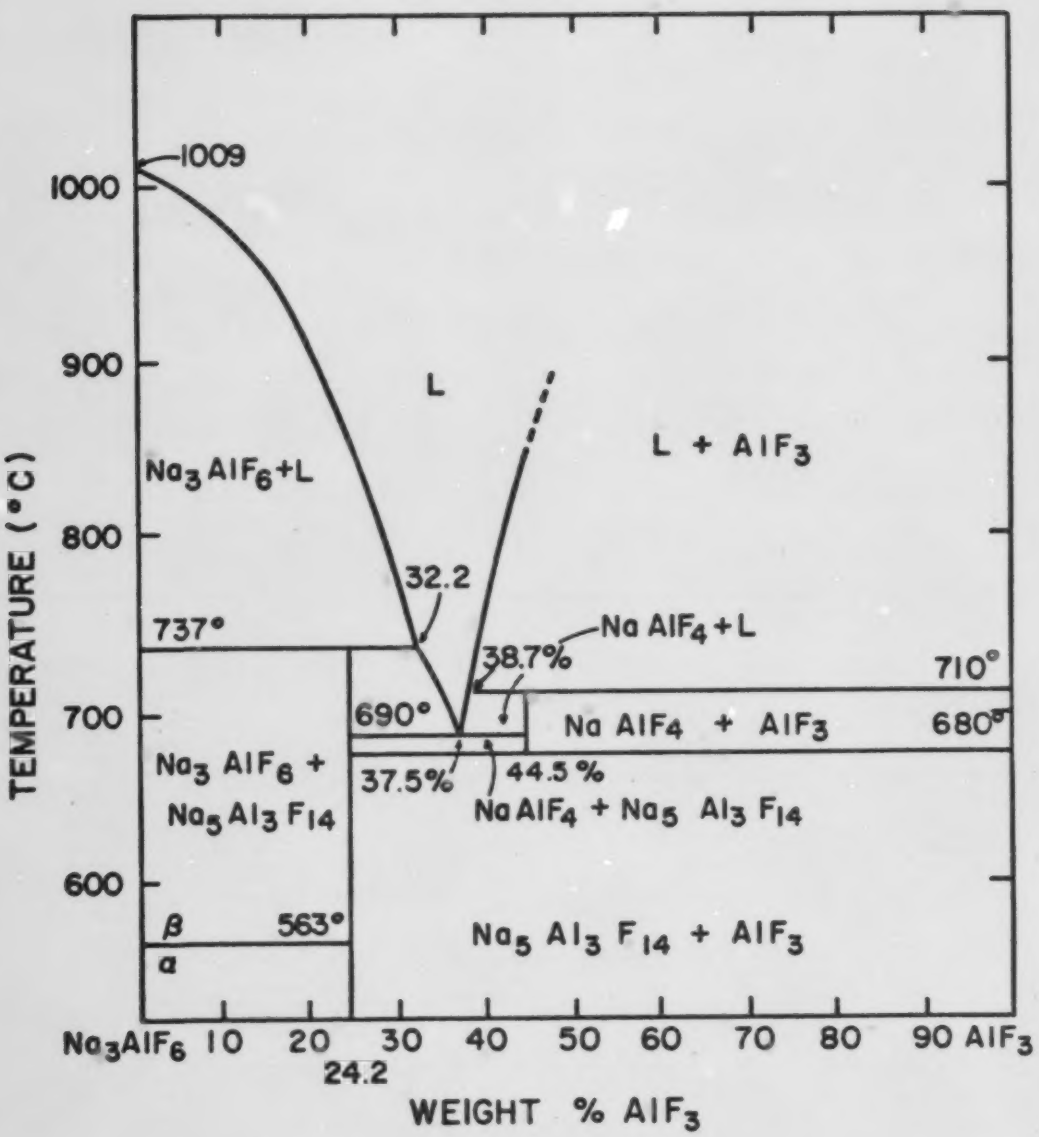

Figure 5. System $NaAlF_6$-AlF_3 (58).

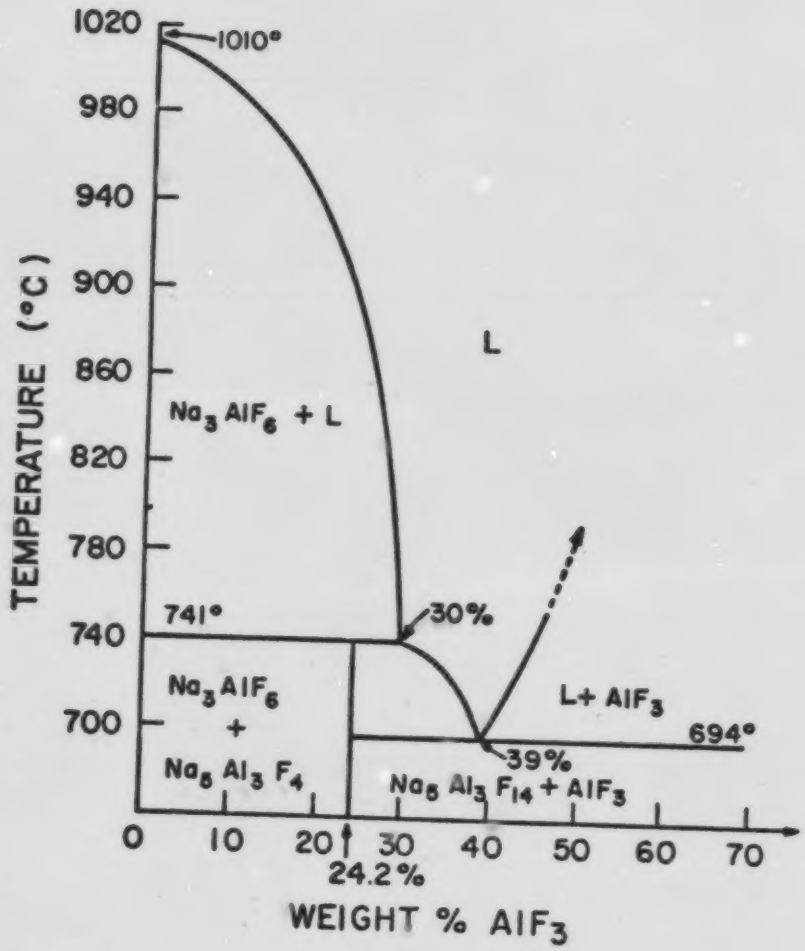

Figure 6. System Na_3AlF_6-AlF_3 (57).

transformation of AlF_3. A second set of peaks, measurable from 45-68 wt. % AlF_3 at 1250°C was considered to represent a peritectic line extending from an incongruently melting compound of possible composition $NaAl_2F_7$. It was felt that, like $NaAlF_4$, this new compound was unstable and decomposed on cooling and, therefore, is not seen in the subsolidus region.

4. System Na_3AlF_6-Al_2O_3

A number of phase diagrams exist in the literature for the system Na_3AlF_6-Al_2O_3. Roush and Miyake[61] reviewed the diagrams published up to 1925 and Phillips, Singleton and Hollingshead[10] summarized the more recent works. There were significant differences between the various diagrams with the eutectic for the system ranging from 10 to 18.5 wt. % Al_2O_3 and 930 to 962°C. Several diagrams showed appreciable solid solubility. The possibility of solid solubility of Al_2O_3 in cryolite creates particular interest in the system because of its significance in the interpretation of the solution mechanism of Al_2O_3 in the Hall electrolyte and in the determination by cryoscopic methods of the number and structure of entities present in the molten binary mixtures.

Foster[7,31] studied the cryolite-alumina binary using a combination of quench methods, optical microscopy and X-ray diffraction. The simple eutectic system with no solid solution and an invariant point at 10.5 wt. % Al_2O_3 and 961°C is shown in Figure 7. The primary phase on the low alumina side of the eutectic was identified by X-ray diffraction and refractive index measurements as cryolite. On the high alumina side of the eutectic the primary phase was found to be corundum. While the cryolite examined in the low-alumina end of the diagram was α-Na_3AlF_6,

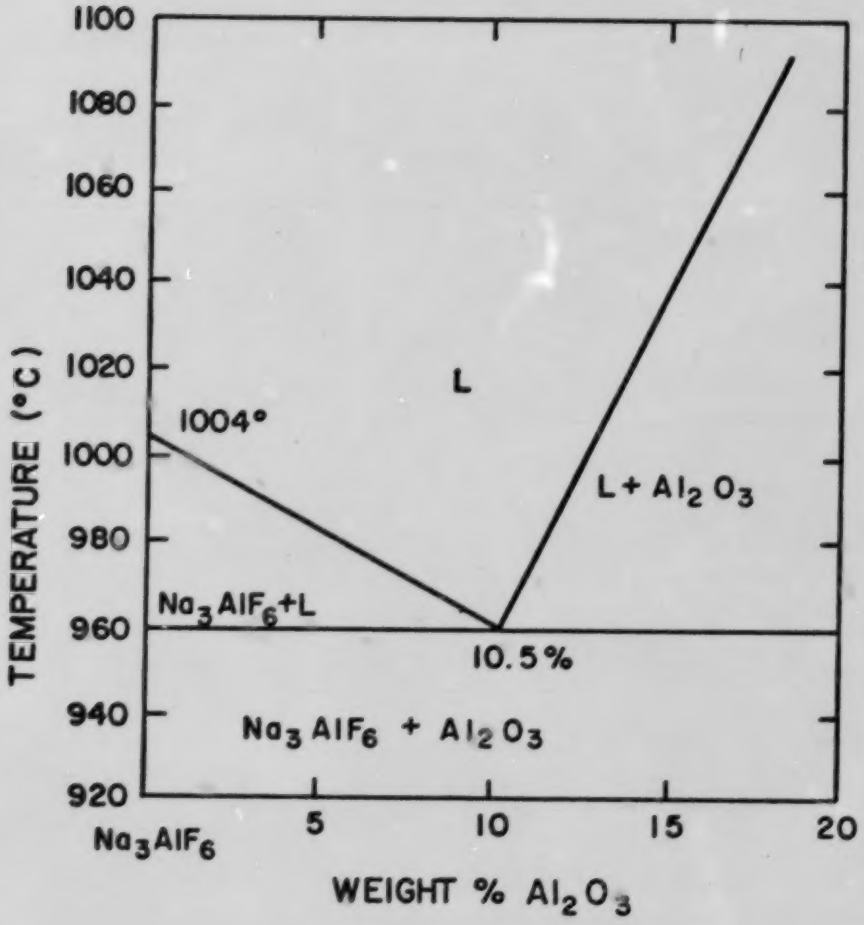

Figure 7. System Na_3AlF_6-Al_2O_3 [7,31].

the existence of a solid solution in the high temperature form was ruled out since the alpha form did not contain polycrystalline fractures with alumina segregating at the boundaries. It was also noted that extremely rapid quenching from the liquid resulted in a new alumina phase (m - or tau - alumina) with a diffraction pattern similar to mullite. On heating this phase transformed first to eta-alumina and then to corundum.

Rolin[62] reinvestigated the system using thermal arrest methods and arrived at the conclusion that if solid solution could not be totally disproved it was less than 1 wt. % Al_2O_3. He presented a simple eutectic diagram with the invariant point at 11.5 wt. % Al_2O_3 and 960°C. However, the reported eutectic arrest for a sample containing 1 wt. % Al_2O_3 occurred 18°C below the established eutectic temperature. The decrease was attributed to the inability to obtain thermal equilibrium because of the large mass of solid pre-existing at the moment of eutectic crystallization. Duruz and Monnier[63] attempted to prove this assumption by investigating the system using DTA techniques. In order to avoid the problem of volatility, samples were sealed in a nickel container. Compositions containing as little as 0.5 wt. % Al_2O_3 showed a eutectic peak at the same temperature as samples containing 10 wt. % or more Al_2O_3. Below 0.5 wt. % Al_2O_3 the sensitivity of the equipment was not sufficient to pick up the small thermal effect. A plot of the surface area of the eutectic peak versus the concentration of Al_2O_3 extrapolated through the origin indicated that no solid solution existed between 0 and 0.5 wt. % Al_2O_3.

A substantial amount of literature is also available on the reaction mechanism for the solution of alumina in cryolite-alumina melts. Foster and Frank[16] reviewed the proposed reaction mechanisms and used Temkin's ionic model to calculate activities. A graph of $-\log a_c$ versus

1/T was then constructed to demonstrate that the scheme $3F^- + Al_2O_3 = 3/2AlO_2^- + 1/2AlF_6^{3-}$ was the most probable. However, considerable controversy still exists over the true reaction mechanism[64].

5. System CaF_2-Al_2O_3

The binary system CaF_2-Al_2O_3 was first studied in 1913 by Pascal[13]. Extensive solid solution at both ends of the system was noted. At the eutectic temperature 20 wt. % Al_2O_3 was soluble in CaF_2 and 71.5 wt. % CaF_2 was soluble in Al_2O_3. The eutectic was placed at 26.5 wt. % Al_2O_3 and 1270°C.

Gunther et al.[65], during a study of the luminescence of phosphors of the aluminum oxide - calcium fluoride type, reported the existence of a 1:5 compound $CaAl_{10}O_{15}F_2$. The compound was obtained by heat treating CaF_2 and $NH_4(SO_4)_2 \cdot 12H_2O$ with small amounts of $MnSO_4 \cdot 4H_2O$ (added as an activator) in air at 1200-1450°C.

Using quench methods, Kuo and Yen[66] reported a simple eutectic diagram for the system with the invariant point at 7 mole % Al_2O_3 and 1290°C. Neither the extensive solid solution nor the compound formation reported earlier could be verified. The authors noted that, while in a closed system CaF_2 and Al_2O_3 were the stable coexisting phases, in open air under ordinary atmospheric conditions $CaAl_4O_7$ formed as the unique product according to one of the two reaction schemes shown below.

1. $CaF_2 + 2Al_2O_3 + H_2O \rightarrow CaAl_4O_7 + 2HF$
2. (a) $3CaF_2 + 7Al_2O_3 \rightarrow 3CaAl_4O_7 + 2AlF_3$

   (b) $2AlF_3 + 3H_2O \rightarrow Al_2O_4 + 6HF$

Chatterjee and Zhmoidin[67] reinvestigated the system by sintering samples in hermetically sealed capsules. Quenching, DTA, and optical microscopy were used to obtain data which suggested a eutectic system.

The invariant point was placed at approximately 2 wt. % Al_2O_3 and 1395°C. The liquidus curve had a pronounced "S" shape suggestive of metastable liquid phase separation.

6. System AlF_3-Al_2O_3

While numerous authors[29,68-71] have reported results in ternary and quaternary systems involving the binary system AlF_3-Al_2O_3, their investigations have been confined to portions of the diagrams far removed from the binary system. At the present time no phase equilibrium data are available on the system.

7. System LiF-AlF_3

The numerous investigations[69,72-78] of the LiF-AlF_3 system are summarized in Table III. Good agreement exists between the reported diagrams. One compound, lithium cryolite (Li_3AlF_6), melts congruently between 782°and 800°C and divides the system into two simple binaries (LiF-Li_3AlF_6 and Li_3AlF_6-AlF_3). The eutectic for the LiF-Li_3AlF_6 system has been reported between 14.5 and 16.5 mole % AlF_3 and between 705° and 715°C. The Li_3AlF_6-AlF_3 system has been reported to contain a eutectic between 35 and 37 mole % AlF_3 and between 690° and 711°C.

The representative diagram of the system shown in Figure 8 is that presented by Holm[42] based on TA and DTA.

The polymorphism and structure of the compound lithium cryolite have been the subject of four studies[79-82]. Garton and Wanklyn[79] used high temperature X-ray diffraction and standard DTA methods to identify five polymorphs, α-, β-, γ-, δ-, and ε-Li_3AlF_6.

The α-β transition took place at 210°C. Both forms were reported as hexagonal with cell parameters a = 9.70Å and c = 12.32Å and a = 13.71Å and c = 12.32Å respectively. The third polymorph, γ-Li_3AlF_6 was stable

TABLE III

Reported Eutectic Compositions and Temperatures in the System $LiF-AlF_3$ and the Melting Point of Li_3AlF_6

Author(s)	Equilibrium Solid Phases	Liquid Composition of Eutectic (Mole%)	Eutectic Temperature (C°)	M.P. Li_3AlF_6
Puschin and Baskow (72)	LiF, Li_3AlF_6	14.5 AlF_3 85.5 LiF	705	800
	Li_3AlF_6, AlF_3	37 AlF_3 63 LiF	690	
Fedotieff and Timofeeff (73)	LiF, Li_3AlF_6	15 AlF_3 85 LiF	715	790
	Li_3AlF_6, AlF_3	36 AlF_3 64 LiF	710	
Dergunov (74)	LiF, Li_3AlF_6	16.5 AlF_3 83.5 LiF	706	792
	Li_3AlF_6, AlF_3	--- ---	---	
Thoma et al. (75)	LiF, Li_3AlF_6	14.5 AlF_3 85.5 LiF	711	785
	Li_3AlF_6, AlF_3	36 AlF_3 64 LiF	710	
Rolin et al. (69)	LiF, Li_3AlF_6	--- ---	---	782
	Li_3AlF_6, AlF_3	35.5 AlF_3 64.5 LiF	---	
Malinovsky et al. (76)	LiF, Li_3AlF_6	15 AlF_3 85 LiF	711	782
	Li_3AlF_6, AlF_3	35 AlF_3 65 LiF	708	
Rolin et al. (77)	LiF, Li_3AlF_6	15.5 AlF_3 84.5 LiF	711	782
	Li_3AlF_6, AlF_3	--- ---	---	
Matiasovsky and Malinovsky (78)	LiF, Li_3AlF_6	15 AlF_3 85 LiF	711	782
	Li_3AlF_6, AlF_3	35 AlF_3 65 LiF	708	
Holm (42)	LiF, Li_3AlF_6	14.5 AlF_3 85.5 LiF	710	785
	Li_3AlF_6, AlF_3	35.5 AlF_3 64.5 LiF	709	
Garton and Wanklyn (79)	LiF, Li_3AlF_6	--- ---	---	783
	---	--- ---	---	

TABLE III (Cont.)

Author(s)	Equilibrium Solid Phases	Liquid Composition of Eutectic(Mole%)		Eutectic Temperature (C°)	M.P. Li_3AlF_6
Holm[80]	---	---	---	---	780
	---	---	---	---	

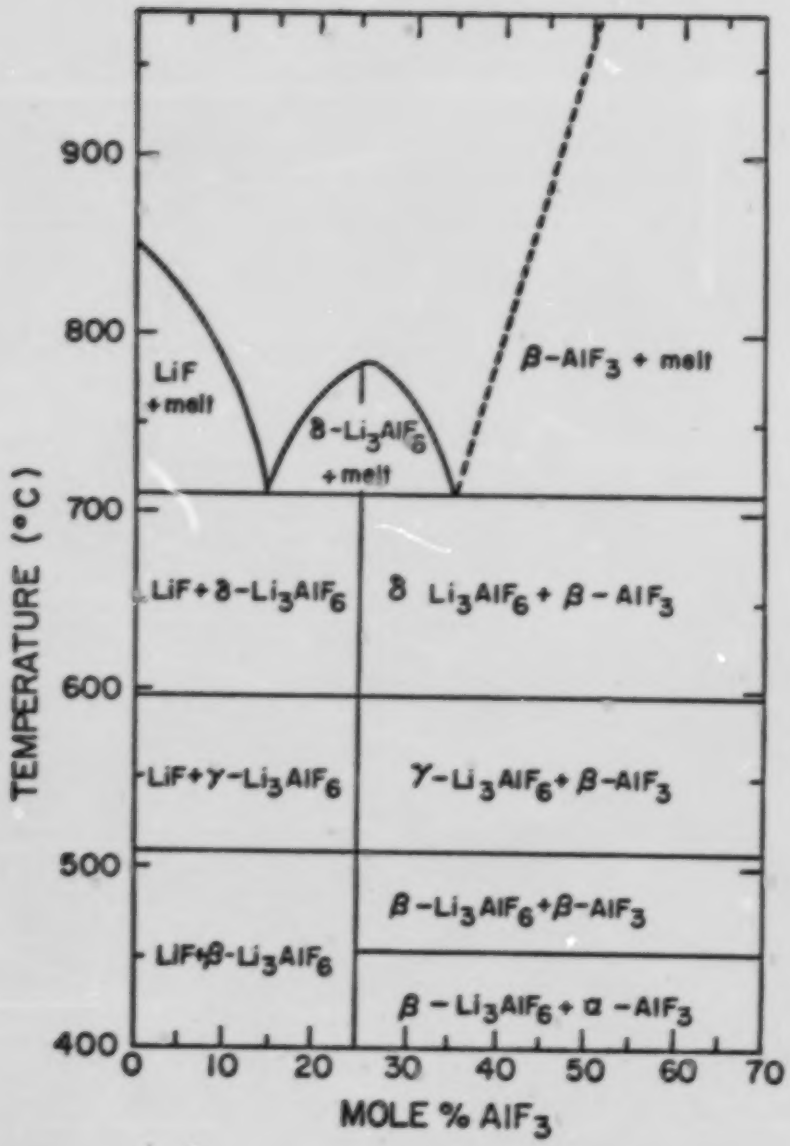

Figure 8. System LiF-AlF_3 [43].

between 515°C and 604°C where it converted to δ-Li_3AlF_6. Crystallographic data on the γ polymorph conformed with a cubic unit cell, a = 14.2Å (at 596°C). The high temperature polymorph, ε-Li_3AlF_6, was found to be stable from 705°C to its melting point at 703°C. No crystallographic data was reported for the δ and ε forms.

Holm[80] studied lithium cryolite using DTA methods and powder X-ray diffraction. He found 3 polymorphs of Li_3AlF_6 and inversion temperatures at 505°C and 597°C. The compound was reported to melt at 780°C. The high temperature form was reported to have the garnet structure with a cubic unit cell (a = 12.03 ± 0.05Å at 625 ± 10°C). The low temperature form was orthorhombic with cell dimensions a = 8.39Å, b = 11.92Å and c = 7.82Å. No data were reported on the intermediate temperature polymorph.

Burns, Tennissen and Brunton[81] used single crystal X-ray diffraction to study α-Li_3AlF_6. They reported an orthorhombic unit cell with parameters a = 9.510, b = 8.2295 and c = 4.8762Å. Their X-ray powder pattern agreed with the pattern reported for α-Li_3AlF_6 by Garton and Wanklyn[80].

The discrepancies in all reported parameters lead Holm and Jenssen[82] to reinvestigate the polymorphy and structure of Li_3AlF_6. DTA heating curves resulted in transformation peaks at 510°C and 597°C. These values were reported as the β⇌γ-Li_3AlF_6 and γ→δ-Li_3AlF_6 inversions. The α-Li_3AlF_6 polymorph was not seen after normal cooling, but was observed along with β-Li_3AlF_6 in samples quenched from 647°C and 790°C. The beta polymorph was reported to be orthorhombic with cell parameters a = 11.78Å, b = 8.43Å and c = 7.77Å. It was stable up to 510°C where it converted to the tetragonal gamma form with cell parameters of

a = 11.81Å and c = 8.74Å. The final transformation of Li_3AlF_6 took place at 592°C when γ-Li_3AlF_6 converted to a cubic polymorph designated δ. The cell edge of δ-Li_3AlF_6 is a= 11.98Å.

The authors believe that the 705°C peak reported by Garton and Wanklyn[80] corresponded to the eutectic in the LiF-AlF_3 system reported in the literature.

8. System LiF-Na_3AlF_6

The system LiF-Na_3AlF_6 has been investigated numerous times[33-42] with widely divergent results being reported. Diagrams of a simple eutectic, limited solid solubility of LiF and mutual solubility of both end members have all been reported. The reported extents of the solid solutions, in particular that of LiF in Na_3AlF_6, differ by as much as 60 mole %.

After studying the liquidus curve, Chu and Belyaev[33] reported the eutectic composition as 83.5 mole % LiF with a eutectic temperature of 700°C. Holm[34] reported a eutectic temperature of 693°C as did Jenssen[35]. Jenssen[35] located the eutectic composition at 15.4 mole % Na_3AlF_6.

Lewis[40] differed with earlier investigators and reported mutual solid solubility of the end members. Approximately 69 mole % LiF was soluble in Na_3AlF_6 and 3 mole % Na_3AlF_6 in LiF. The eutectic was located at 87 mole % LiF and 703°C.

The first investigation reporting the system to exhibit only partial solid solubility of LiF in Na_3AlF_6 was conducted by Matiasovsky and Malinovsky[37]. Using TA and X-ray phase analysis the extent of solution was set at 70 mole % LiF and the eutectic was located at 14.4 mole % Na_3AlF_6 and 700°C. Holm[38] reinvestigated the system and sharply decreased the amount of LiF soluble in Na_3AlF_6. The extent of solid solution was

12 mole % LiF and the eutectic was placed at 15 mole % Na_3AlF_6 and 694°C. Kostenska[39] further reduced the solubility of LiF to 6 mole % Na_3AlF_6 and 696°C.

Holm[42] used TA, DTA, quenching techniques and X-ray diffraction to study the system (Figure 9). He found the subsolidus region below 550°C to be a pseudobinary due to the presence of only two phases, α-Na_3AlF_6 and LiF. He reported the solid-liquid region to be part of the ternary reciprocal system

$$3LiF + Na_3AlF_6 \rightleftarrows Li_3AlF_6 + 3NaF$$

as a result of a formation of solid solutions between Li_3AlF_6 and Na_3AlF_6.

Foster[41], realizing the problem of volitization, encapsulated his samples in sealed platinum tubes. Working under carefully controlled conditions and employing both quench methods and refractive index measurements, he determined mutual solubility of both end members. By assuming Raoult behavior, the amount of LiF soluble in Na_3AlF_6 was calculated to be 14.4 mole %. Cryolite was found to be soluble in LiF up to 6.8 mole %. The eutectic was located at 85.3 mole % LiF. The diagram is shown in Figure 10.

9. System Na_3AlF_6-Li_3AlF_6

The Na_3AlF_6-Li_3AlF_6 system has been studied many times with little agreement between investigators[83-89]. The first study was made in 1936 by Drossbach[83]. Using thermal methods he reported a continuous solid solution between the end members. Solidus temperatures ranged from 10 to 15°C below the liquidus and a thermal minimum was located at 70 mole % Li_3AlF_6.

Mashovets and Petrov[84] found the system to be a simple eutectic with no solid solution. Thermal and optical studies were employed and the eutectic was found at 710°C and 62 mole % Li_3AlF_6.

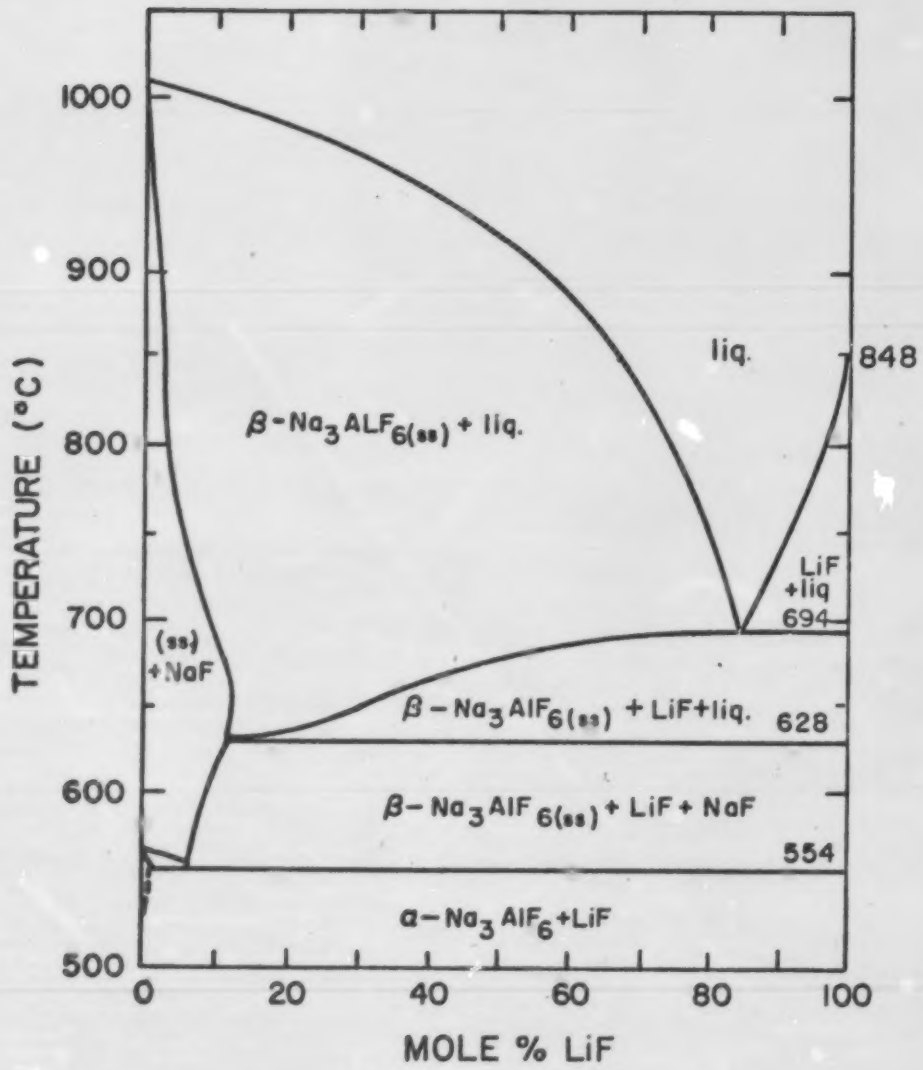

Figure 9. System Na_3AlF_6-LiF[42].

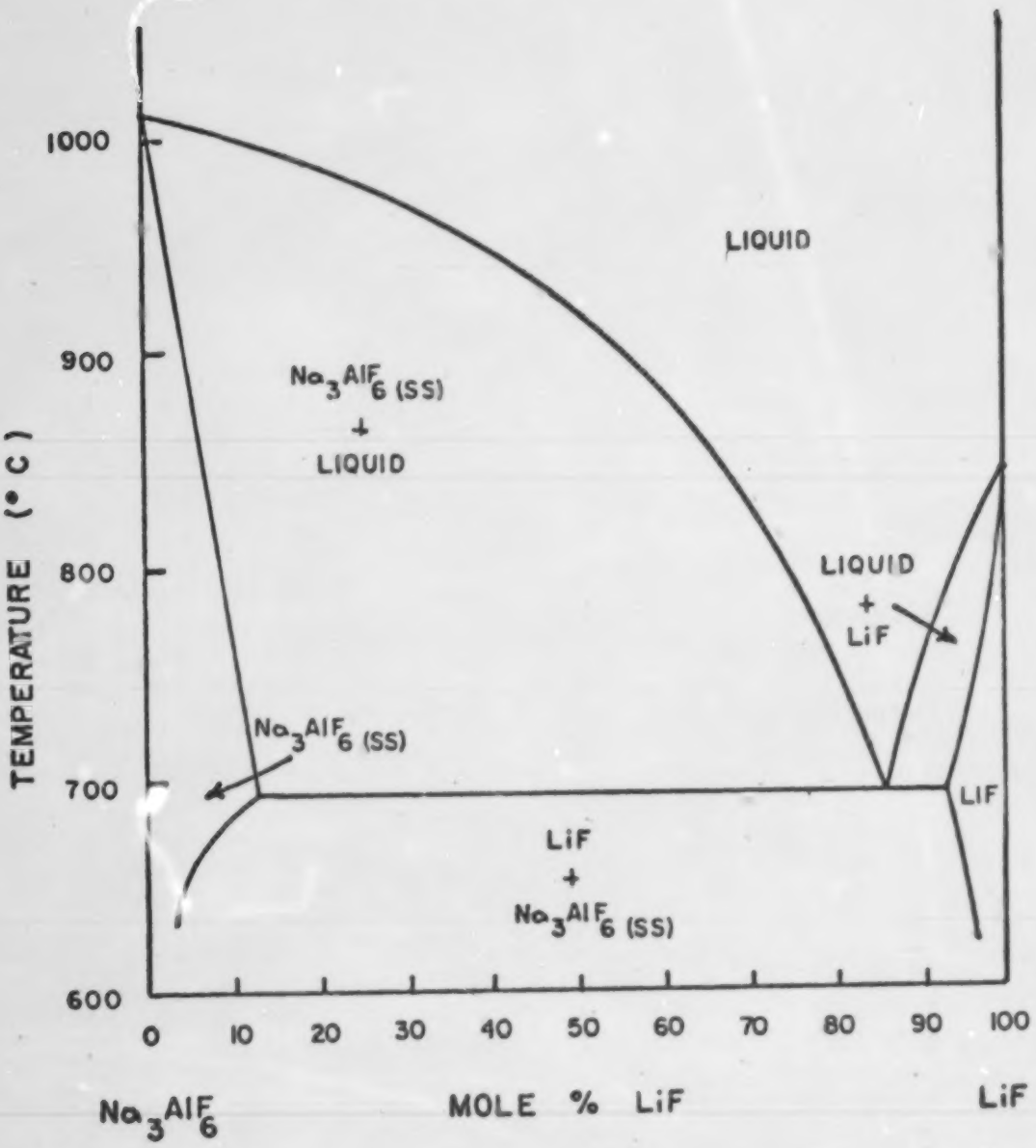

Figure 10. System Na_3AlF_6-LiF[41].

Another study[85] reported three compounds to exist. Beletskii and Saksonov reported compounds corresponding to the formulas $Li_3Na_6Al_3F_{18}$, $Li_6Na_3Al_3F_{18}$ and $Li_{15}Na_3Al_6F_{36}$. No compound having the formula of the naturally occurring mineral cryolithionite, $Na_3Li_3Al_2F_{12}$, was reported.

Rolin and Muhlethaler[69] used cooling curves to examine the system. They found a continuous series of solid solutions on the Li_3AlF_6 side up to the eutectic point of 62.3 mole % Li_3AlF_6 and 713°C. Solid solution extended to 36 mole % Li_3AlF_6 on the Na_3AlF_6 side.

Garton and Wanklyn[86] used X-ray analysis, quenching techniques, and DTA results in studying the system. Two compounds were found, one corresponding to the natural mineral cryolithionite, $Na_3Li_3Al_2F_{12}$ and another compound of the formula Na_2LiAlF_6. Cryolithionite was found to exist as a nonstoichiometric solid solution which decomposed to Li_3AlF_6 and a phase of Na_3AlF_6 at 680°C. The second compound, Na_2LiAlF_6 was found to decompose at 500°C.

Holm and Holm[87] used DTA and high temperature X-ray analysis to confirm the existence of the two compounds. Each existed up to approximately 500°C. Na_2LiAlF_6 was found to exist in two polymorphic forms. The α polymorph was indexed on the basis of a monoclinic unit cell with parameters a = 7.538Å, b = 7.516Å and c = 7.525Å. On heating, α-Na_2LiAlF_6 converted to cubic β-Na_2LiAlF_6 (a = 7.639Å at 445°C). The transformation could not be detected by DTA but high temperature X-ray diffraction showed the inversion to be complete at 420°C. $Na_3Li_3Al_2F_{12}$ was identical to naturally occurring cryolithionite (a = 12.127Å at 20°C). The study also revealed one new phase present between 560°C and 630°C from 90 to 99 mole % Li_3AlF_6. The new phase was indexed based on a tetragonal unit cell with parameters

a = 11.97Å and c = 8.73Å (625°C). Although no solid solution was found at room temperature, an extensive amount was reported at high temperatures. The liquidus curve reached a minimum at 64 mole % Li_3AlF_6 and 710°C.

Baylor et al.[88] found Li_3AlF_6 to be soluble in Na_3AlF_6 up to a maximum of 18 mole %. Cryolithionite and Na_2LiAlF_6 were reported to decompose between 500 and 600°C. Stinton and Brown[89] used DTA and X-ray diffraction to study the system. Samples were sealed in platinum tubes to prevent volatilization during firing and DTA experiments. Their liquidus curve agreed well with that of Holm and Holm[87]. The eutectic was placed at 64 mole % Li_3AlF_6 and 713°C and no solid solution was reported below 500°C. An intermediate solid solution denoted α'-Na_3AlF_6 was found to be stable between 530°C and 758°C and 10 and 38 mole % Li_3AlF_6. Their diagram is pictured in Figure 11.

10. System Li_3AlF_6-Al_2O_3

The first study of the system was made in 1936 by Drossbach[83] Using thermal methods he reported a simple eutectic system with the invariant point at 782°C and 1 wt. % Al_2O_3. Mashovets and Petrov[84] used samples containing up to 6 wt. % Al_2O_3 to revise the eutectic location to 775 ± 3°C and 1.1 mole % Al_2O_3. Cassidy and Brown[90] reexamined the system using samples encapsulated in sealed platinum tubes. Optical microscopy, X-ray diffraction, quench methods and DTA (on samples in platinum tubes) were used to place the eutectic at 773°C and 0.5 mole % Al_2O_3. The diagram is shown in Figure 12.

11. System LiF-CaF_2

The studies of the LiF-CaF_2 system are summarized in Table IV. All investigators[91-100] used thermal arrest methods and reported data consistent with a simple binary eutectic system. The invariant point was

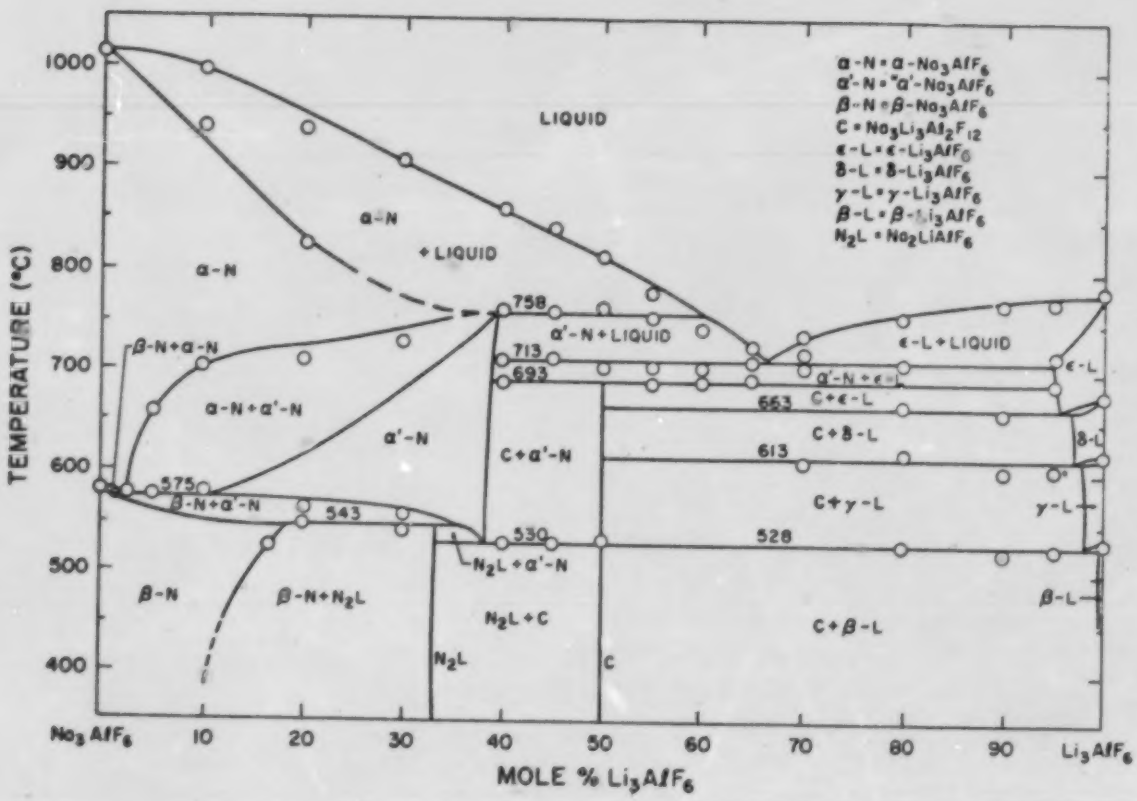

Figure 11. System Na_3AlF_6-Li_3AlF_6 (89).

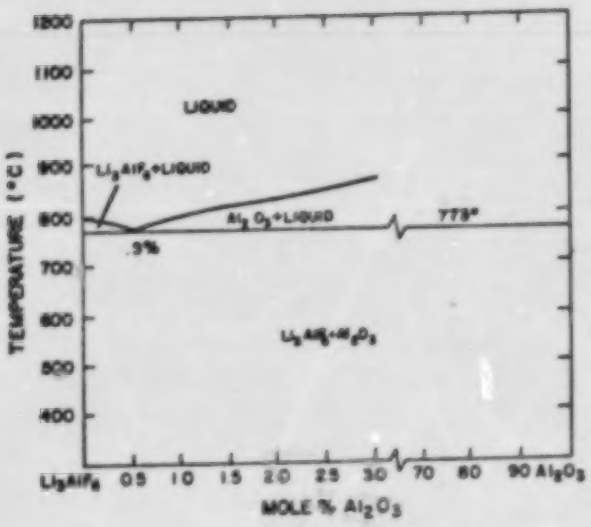

Figure 12. System Li_3AlF_6-Al_2O_3 (90).

TABLE IV

Composition and Temperature of the Eutectic in the System LiF-CaF_2

Author(s)	Composition of Liquid (Mole %) LiF	CaF_2	Temperature (°C)
Ruff and Busch[91]	79	21	765
Roake[93]	80.5	19.5	769
Barton, Bratcher and Grimes[95]	81	19	773
Bukhalova, Sulaymankulov and Bostandzhiyon[96]	85.5	14.5	766
Deadmore and Machin[97]	77	23	760
Vrbenska and Malinovsky[99]	79	21	755
Kostenska, Vrbenska and Malinovsky[100]	80.5	19.5	769

consistently reported to be between 77 and 85.5 mole % LiF and 755 to 773°C. The representative diagram for the system shown in Figure 13 is the most recent version reported by Kostenska et al.[100]

12. System Li_3AlF_6-CaF_2

The only study of the Li_3AlF_6-CaF_2 system reported in the literature is by Vrbenska and Malinovsky[99]. Based on data obtained by thermal analysis methods a simple eutectic system was presented (Figure 14). The eutectic was located at 703°C and 43 mole % CaF_2.

C. Three Component Systems

1. System CaF_2-AlF_3-Na_3AlF_6

Fedotieff and Illjinsky[8] presented a liquidus surface diagram of the CaF_2-AlF_3-NaF ternary system based on the results of differential thermal analysis experiments, performed in air, on over 100 compositions. At the time of the work no ternary compounds were known to exist and only chiolite and cryolite were identified in any of the binary systems. Two ternary eutectics were reported. The first was located at 50.2 mole % NaF, 5.0 % CaF_2 and 44.8% AlF_3 and 675°C with AlF_3 in equilibrium with Na_3AlF_6 and CaF_2. The second eutectic was placed at approximately 73 mole % NaF, 20% CaF_2 and 7% AlF_3 and 780°C with NaF in equilibrium with Na_3AlF_6 and CaF_2. A ternary peritectic was found at approximately 49 mole % NaF, 10% CaF_2 and 41% AlF_3 and 705°C with chiolite, cryolite and CaF_2 in equilibrium.

Rolin[101], using thermal arrest methods, investigated the portion of the CaF_2-AlF_3-Na_3AlF_6 system containing 24 and 62.5 mole % or less CaF_2 and AlF_3 respectively. Phases precipitating from the melt were identified by the shape and sharpness of the thermal arrest peaks. A ternary eutectic was located at 35.9 mole % cryolite, 56.7% AlF_3 and 7.4% CaF_2

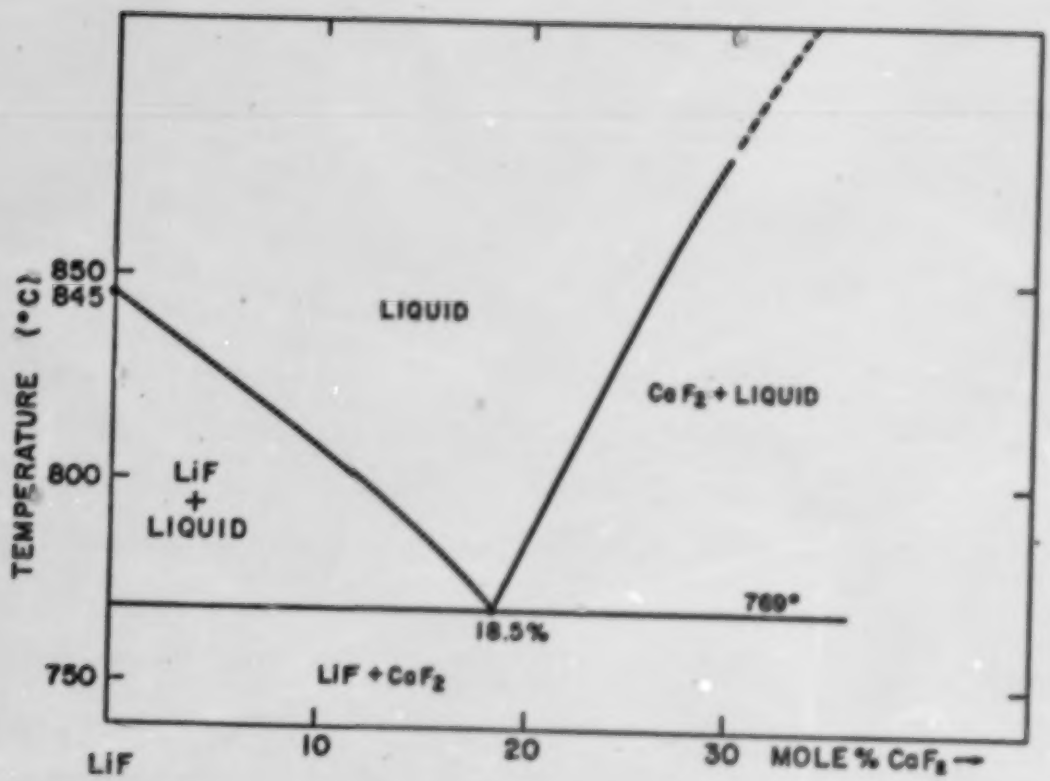

Figure 13. System LiF-CaF_2 (100).

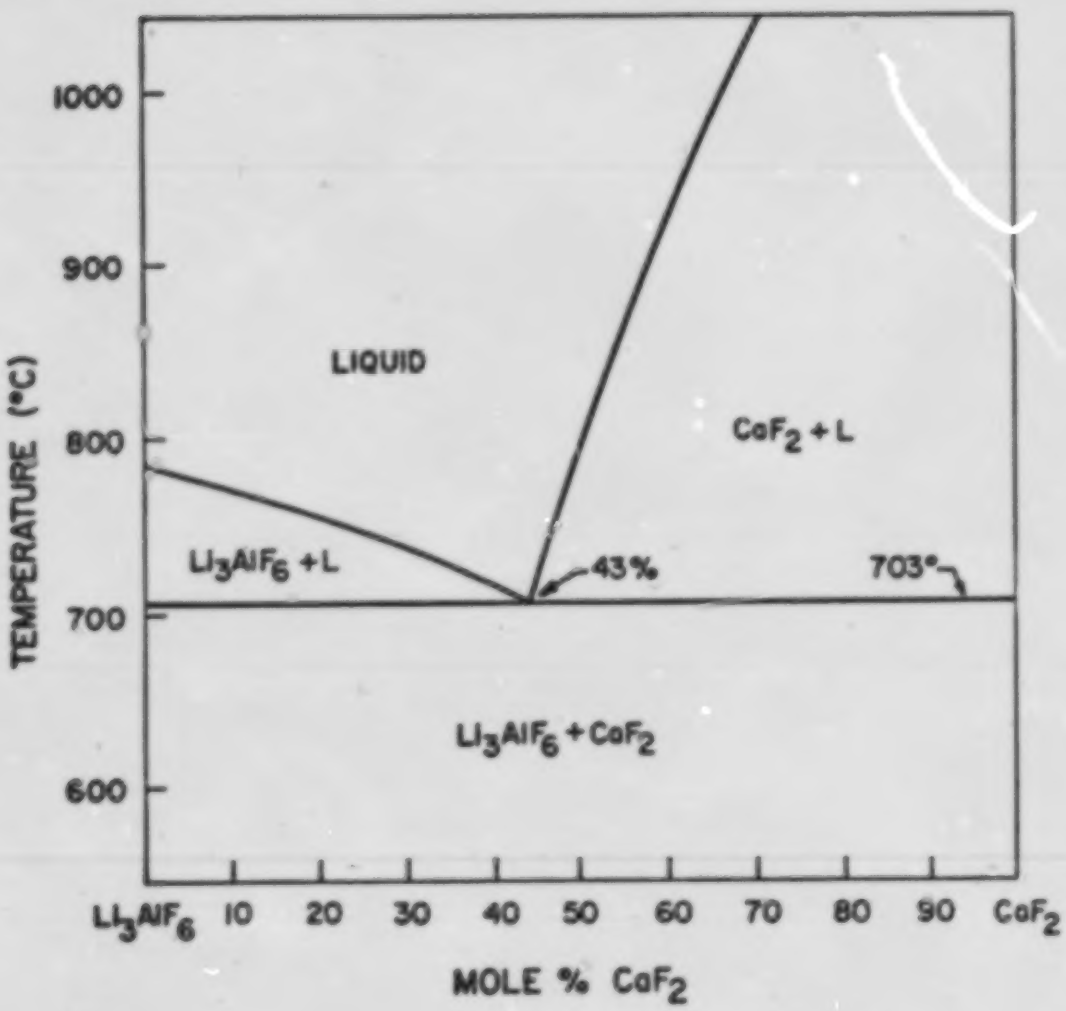

Figure 14. System Li_3AlF_6-CaF_2 [99].

and 682°C with chiolite in equilibrium with CaF_2 and AlF_3. Two points on the chiolite-CaF_2 boundary curve were also located, the first at 32.7 mole % cryolite, 50.5% AlF_3 and 16.8% CaF_2 and 689°C and the second at 34.3 mole % Na_3AlF_6, 52.7% AlF_3 and 13.0% CaF_2 and 688°C. A point on the CaF_2-AlF_3 boundary was located at 28.7 mole % Na_3AlF_6, 55.3% AlF_3 and 16.0% CaF_2 and 708°C. On the basis of these points a partial ternary diagram was present. Supercooling in the region of the diagram containing CaF_2 as the primary phase was noted. At the time of the work no compounds were known to exist either in the CaF_2-AlF_3 binary or the ternary system.

Pfundt and Zimmermann[102] investigated both the ternary system and the quasi-binary system NaF-$CaAlF_5$ using DTA of samples contained in pressure tight nickel crucibles. They agreed with the earlier investigations that the ternary system could be divided into two subsystems, NaF-Na_3AlF_6-CaF_2 and CaF_2-AlF_3-Na_3AlF_6. The invariant temperature for the NaF containing system was placed at 780°C.

The diagram of the quasi-binary system is presented in Figure 15. One compound, $NaCaAlF_6$, belonging to the system CaF_2-AlF_3-Na_3AlF_6 was found to melt incongruently at 740°C. The compound existed in both a low temperature (beta) and high temperature (alpha) form with the transition taking place at 653°C on heating. The beta form exhibited tetragonal symmetry with lattice parameters a_o = 7.32Å and c_o = 10.18Å. The existence of the high temperature polymorph at room temperature was noted in both air cooled and water quenched samples but no diffraction data was reported.

Working with samples encapsulated in sealed platinum tubes and using DTA heating curves taken at 3°C/min supplemented by optical microscopy, powder X-ray diffraction and quench experiments Craig and

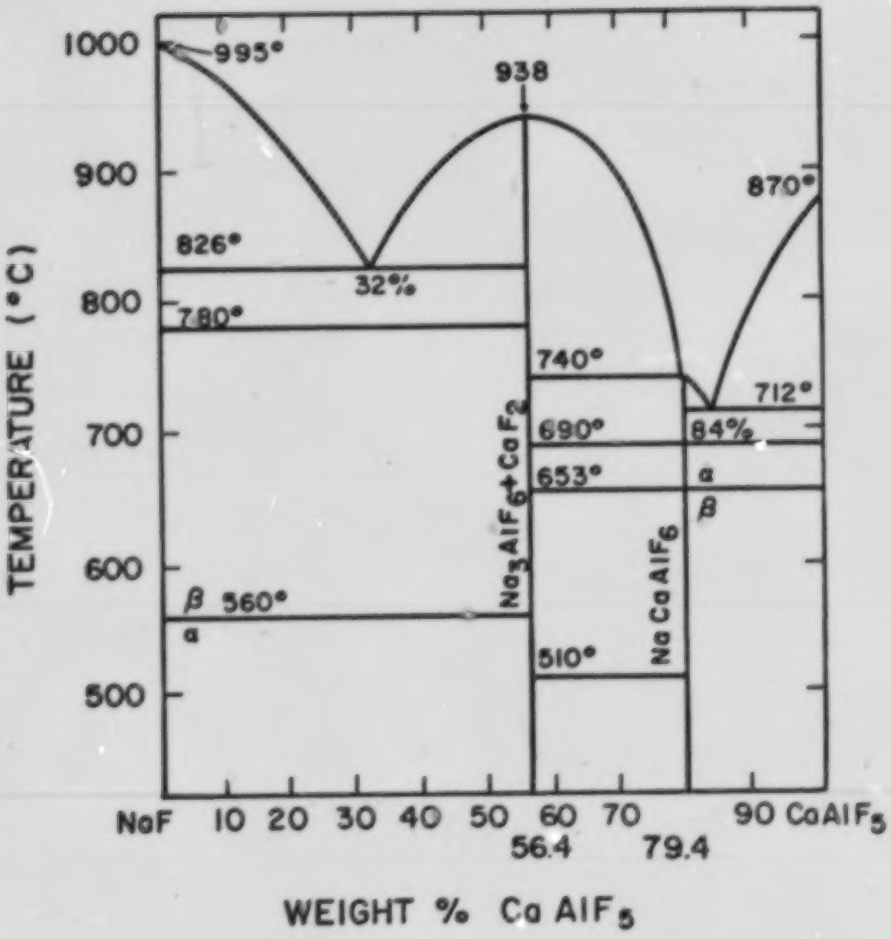

Figure 15. System NaF-$CaAlF_5$ (102).

Brown[56] investigated the CaF_2-AlF_3-Na_3AlF_6 ternary system. The compound $NaCaAlF_6$ first noted by Pfundt and Zimmermann[102] was found to exist in a previously unreported γ form in addition to the α and β polymorphs. DTA showed the inversion to the new form, characterized by a sharp but small exothermic peak, to take place at 720°C. Gamma-$NaCaAlF_6$ was not quenchable and no diffraction data was reported. The compound melted incongruently at 737°C to CaF_2 and a liquid. In addition to $NaCaAlF_6$, a previously unreported compound $NaCaAl_2F_9$ was identified. Based on powder X-ray diffraction data taken at scanning speeds of ¼°2θ/min. using CuK_α radiation the compound was indexed as body centered cubic (h + k + l = 2n) with a_o = 10.76Å (Table V). The compound melted incongruently to AlF_3 and a liquid at 715°C; however, metastable congruent melting at 723°C was often observed.

On the basis of samples reacted for 394 hrs. in the solid state, the subsolidus compatibility relationships shown in Figure 16 were established. In the compatibility triangles containing cryolite a decrease in the α-β inversion temperature was noted. Investigation of the $NaCaAlF_6$-Na_3AlF_6 ternary join revealed that this decrease from 567 to 525°C was caused by a solubility of approximately 7 mole % $NaCaAlF_6$ in α-Na_3AlF_6.

The authors noted, in support of Holm's[54] simple eutectic diagram for the CaF_2-Na_3AlF_6 system, that slight compositional errors introducing excess AlF_3 to the binary system would result in the solid solution diagrams for the system reported by Rolin[53] and Verdan and Monnier[55]. Craig and Brown[56] cited as additional evidence the work of Dewing[103] who postulated that a 50 fold increase in the conductivity of a sample in the CaF_2-AlF_3-Na_3AlF_6 system (as compared to pure Na_3AlF_6) could be explained by a solid solution of CaF_2 in Na_3AlF_6 and that such a

TABLE V. X-Ray Powder Diffraction Data for the Compound $NaCaAl_2F_9$

d_{obs}	d^*_{calc}	I/I_o	(hkl)
7.59	7.61	10	110
5.37	5.38	5	200
4.40	4.39	30	211
3.80	3.81	70	220
3.40	3.40	75	310
3.11	3.11	80	222
2.873	2.877	10	321
2.691	2.691	5	400
2.538	2.537	5	511,330
2.198	2.197	15	422
2.112	2.111	50	510,431
1.966	1.965	5	521
1.904	1.903	100	440
1.845	1.846	10	530,433
1.795	1.794	30	600,442
1.747	1.746	20	611,532
1.703	1.702	55	620
1.661	1.661	5	541
1.623	1.623	15	622
1,587	1.587	10	631

Other reflections

a = 10.765Å

*Evans, H. T., Appleman, D. E. and Handwerker, D. S., (1963) Least Squares Refinement.

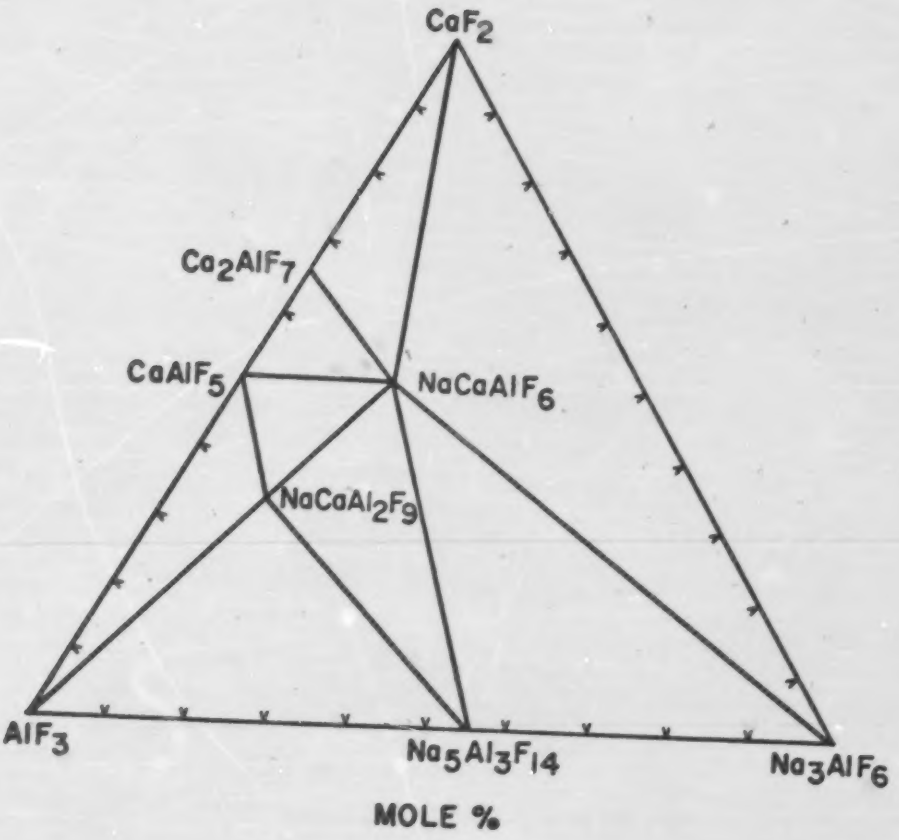

Figure 16. Subsolidus Compatibility Relationships in the System CaF_2-AlF_3-Na_3AlF_6 (56).

solid solution was only reasonable when AlF_3 was present. It was noted that while Dewing was unaware of the existence of $NaCaAlF_6$, the sample studied actually lay on the $NaCaAlF_6$-Na_3AlF_6 ternary join. The conductivity increase, therefore, should be attributed to a solid solution of $NaCaAlF_6$ in Na_3AlF_6 and not to CaF_2 in cryolite. While firm evidence of the solubility of $NaCaAlF_6$ in the low temperature form of cryolite exists, the use of DTA to investigate solubility in the high form of cryolite was complicated by the dissociation of Na_3AlF_6 near its melting point. While a peak corresponding to a solidus line was often observed on cooling, the dissociation of cryolite masked its existence (if indeed it was present) on heating. The solubility of $NaCaAlF_6$ is, therefore, difficult to conclusively confirm.

The full phase diagram for the CaF_2-AlF_3-Na_3AlF_6 presented by Craig and Brown is shown in Figure 17 and the compositions, temperatures, and phase assemblages of the invariant points are given in Table VI.

2. System Na_3AlF_6-AlF_3-Al_2O_3.

Fenerty and Hollingshead[52] investigated the liquidus curves in the cryolite rich portion of the system using cooling curve methods supplemented by visual observation of crystallization. The Na_3AlF_6-Al_2O_3 phase boundary showed a gradual decrease in Al_2O_3 up to 25 wt. % AlF_3. Above this value the boundary curved sharply with a rapid decrease in Al_2O_3 content. The ternary peritectic and eutectic were both located at alumina contents less than 1 wt. %. Rolin's[68] investigation of the system agreed well with the previous authors up to 25 wt. % AlF_3. Above this value, however, the boundary curve continued a smooth approach to the ternary peritectic located at 5 wt. % Al_2O_3, 28.5% AlF_3 and 66.5% Na_3AlF_6 and 710°C. A ternary eutectic was located at 60 wt. % Na_3AlF_6,

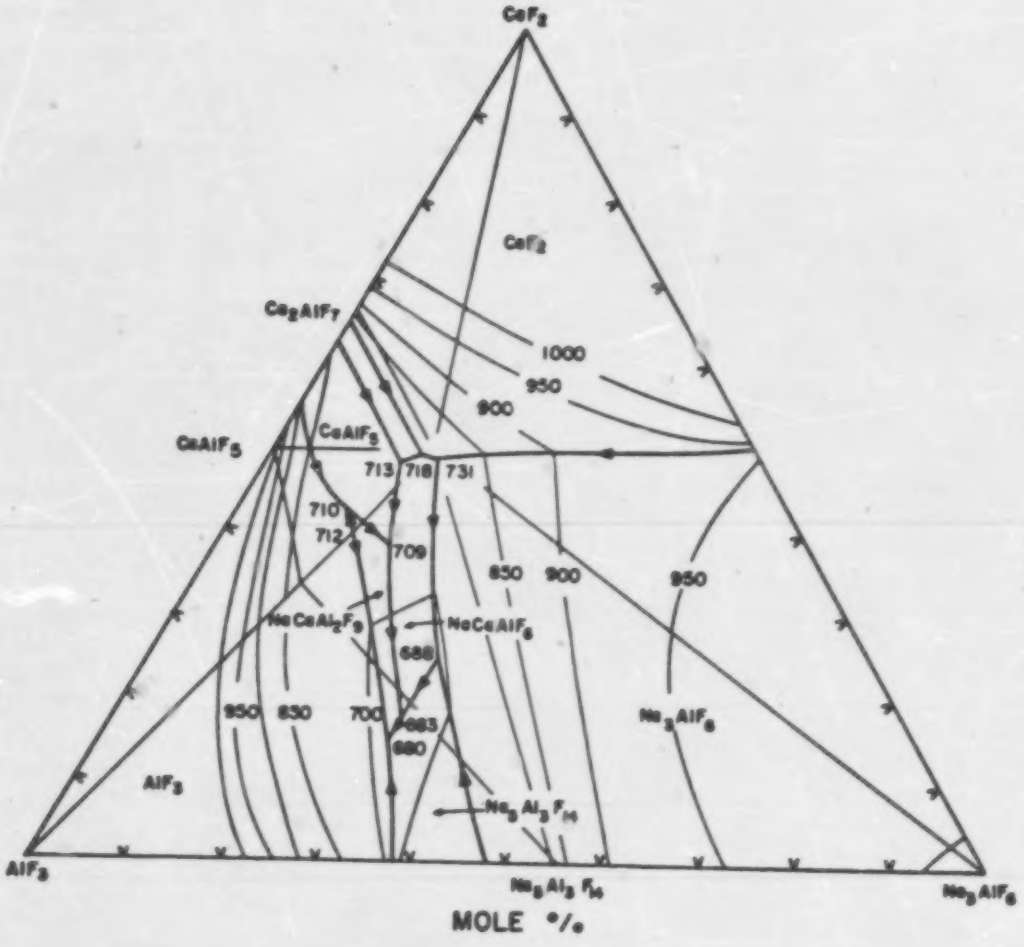

Figure 17. System CaF_2-AlF_3-Na_3AlF_6 (56).

347

TABLE VI. Invariant Points in the System CaF_2-AlF_3-Na_3AlF_6

Point No.	Mole % CaF_2	Mole % AlF_3	Mole % Na_3AlF_6	Type	T (°C)	Equilibrium Phase Assemblage
1	49.0	33.5	17.5	Peritectic	731	CaF_2 $NaCaAlF_6$ Na_3AlF_6
2	49.5	35.0	15.5	Peritectic	718	CaF_2 Ca_2AlF_7 $NaCaAlF_6$
3	48.5	37.5	14.0	Peritectic	713	Ca_2AlF_7 $CaAlF_5$ $NaCaAlF_6$
4	43.0	46.0	11.0	Peritectic	710	$CaAlF_5$ $NaCaAl_2F_9$ AlF_3
5	38.0	44.0	18.0	Peritectic	709	$CaAlF_5$ $NaCaAl_2F_9$ $NaCaAlF_6$
6	25.0	45.0	30.0	Peritectic	688	Na_3AlF_6 $Na_5Al_3F_{14}$ $NaCaAlF_6$
7	18.0	52.0	30.0	Peritectic	683	$NaCaAl_2F_9$ $Na_5Al_3F_{14}$ $NaCaAlF_6$
8	15.0	55.0	30.0	Eutectic	680	AlF_3 $Na_5Al_3F_{14}$ $NaCaAl_2F_9$
9	49.0	34.0	17.0	Saddle Point	735	CaF_2 $NaCaAlF_6$
10	39.5	47.5	13.0	Saddle Point	712	$NaCaAl_2F_9$ AlF_3

37% AlF_3 and 3% Al_2O_3 and 670°. Possible sources of error which could account for the previous results such as the slow dissolution of Al_2O_3, the lack of a thermal arrest corresponding to the primary crystallization of Al_2O_3 and the purity of starting materials were noted.

Using samples contained in sealed platinum tubes, Foster[104] employed quench methods, optical microscopy and X-ray diffraction to reinvestigate the cryolite rich portion of the diagram. In support of Rolin's diagram, the Na_3AlF_6-Al_2O_3 boundary fell regularly to the peritectic composition at 28.3 wt. % AlF_3, 4.4% Al_2O_3 and 67.3% Na_3AlF_6 and 723°C. The ternary eutectic was located at 37.3 wt. % AlF_3, 3.2% Al_2O_3 and 59.5% Na_3AlF_6 and 684°C (Figure 18). Compositions containing 20 wt. % or less AlF_3 precipitated α-Al_2O_3 in the primary phase field of Al_2O_3 while those containing 25 wt. % or more precipitated η-Al_2O_3. The line defining the limits of the α-η formation (broken line, Figure 18) is not isothermal and since no solid solution exists it must define a metastable region.

3. System Na_3AlF_6-CaF_2-Al_2O_3

Fenerty and Hollingshead[52] investigated the Na_3AlF_6-CaF_2-Al_2O_3 ternary diagram using the same procedure as in their investigation of the Na_3AlF_6-CaF_2 and Na_3AlF_6-AlF_3-Al_2O_3 systems. On the basis of results obtained for cuts taken at 5, 10, 15, 20, 22, 24, 25, and 26 wt. % CaF_2 a simple eutectic diagram with the ternary invariant point at 76.1 wt. % cryolite, 21% CaF_2 and 2.9% Al_2O_3 and 933°C was presented. A later investigation by Rolin[53], using the method of thermal arrest, placed the eutectic at 78 wt. % Na_3AlF_6, 17% CaF_2 and 5% Al_2O_3 and 927°C. The major difference between the works was in the Al_2O_3 content of the cryolite-alumina phase boundary. Rolin's diagram (Figure 19) showed the boundary

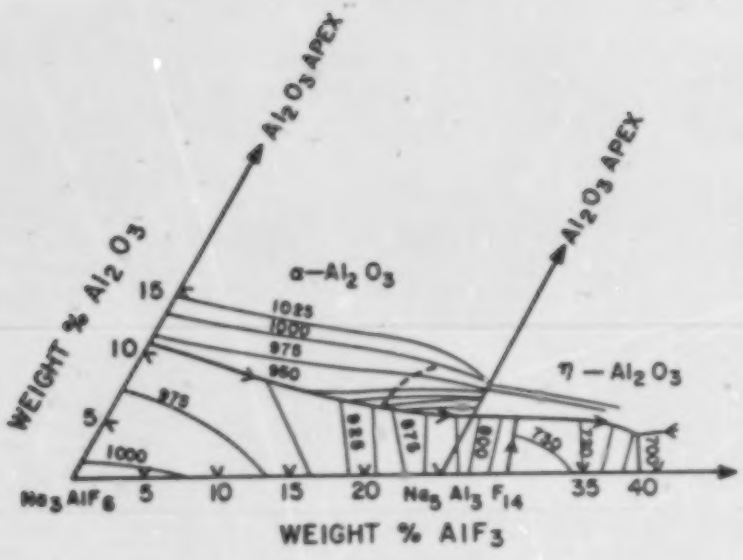

Figure 18. System Na_3AlF_6-AlF_3-Al_2O_3 (104).

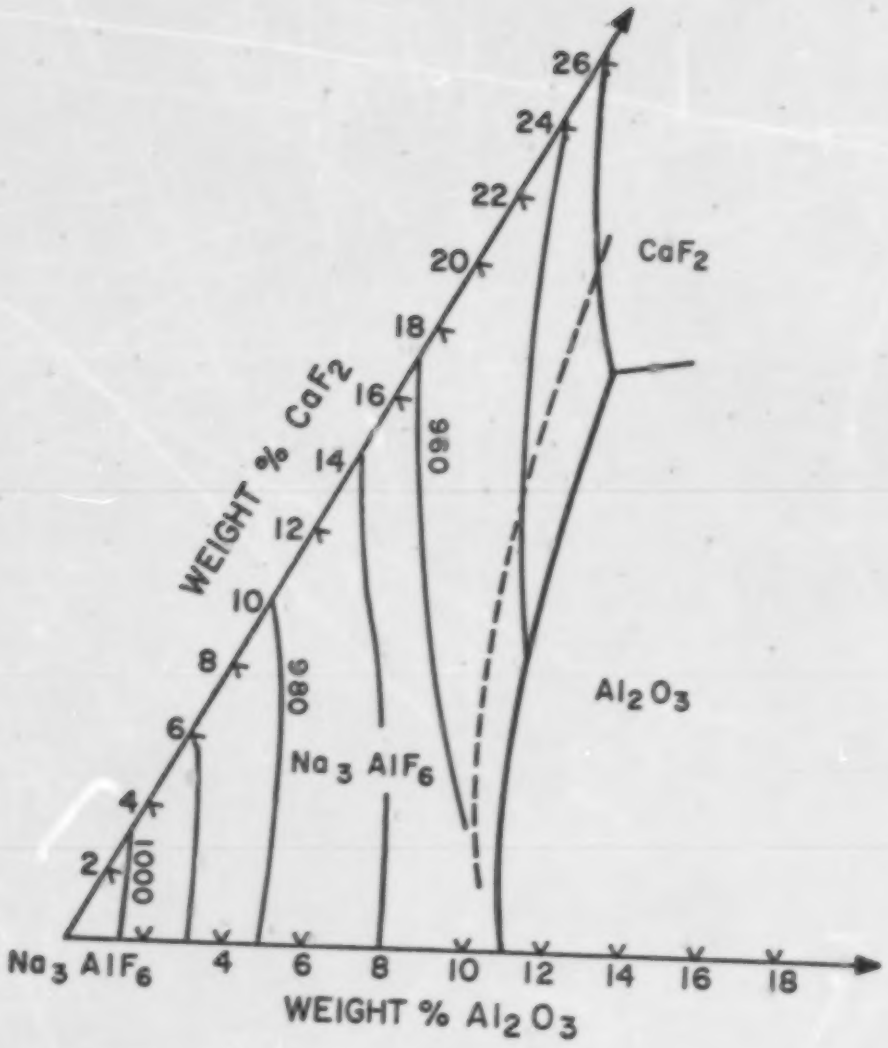

Figure 19. System Na_3AlF_6-Al_2O_3-CaF_2 (52).

curve to be higher in Al_2O_3 than that of Fenerty and Hollingshead (Figure 19, dashed line).

4. System CaF_2-AlF_3-Al_2O_3

In the CaF_2-AlF_3-Al_2O_3 ternary system only the CaF_2-AlF_3 and CaF_2-Al_2O_3 binary systems are known. Several authors[52,70,71,105] have investigated quaternary systems involving the ternary; however, their work has been confined to areas far removed from the ternary. At the present time no phase equilibrium data are available on the system.

5. System Li_3AlF_6-Na_3AlF_6-Al_2O_3

Drossbach[83] first investigated this system in 1936. Working near the Na_3AlF_6-Li_3AlF_6 side of the ternary, he determined a boundary curve extending from 10 weight % Al_2O_3 on the Na_3AlF_6-Al_2O_3 binary at 937°C to 38 weight % Li_3AlF_6 on the Na_3AlF_6-Li_3AlF_6 join at 810°C. No Li_3AlF_6 primary phase field was indicated.

Mashovets and Petrov[84] also worked in the Na_3AlF_6-Li_3AlF_6 side of the ternary and found a boundary curve extending from 15 weight % Al_2O_3 on the Na_3AlF_6-Al_2O_3 join to 7 weight % Al_2O_3 on the Li_3AlF_6-Al_2O_3 join.

Rolin and Muhlethaler[69] obtained similar results in their study of the diagram. Using data obtained from thermal arrest cooling curves they found a single boundary curve separating Al_2O_3 from the cryolite-lithium cryolite solid solution. The boundary curve paralleled the Na_3AlF_6-Li_3AlF_6 binary within 1 weight % from 45 to 100 weight % Li_3AlF_6. No ternary compounds were reported.

Cassidy and Brown[90] found the ternary to contain one reaction point, one peritectic point and one ternary eutectic point. Working in sealed platinum tubes and employing X-ray diffraction, DTA and

quench methods a primary phase field of the incongruently melting compound cryolithionite, $Na_3Li_3Al_2F_{12}$ was located. Three compatibility triangles were found in addition to one two phase region ($Na_3AlF_{6(ss)}$ + Al_2O_3). The second compound on the Na_3AlF_6-Li_3AlF_6 binary, Na_2LiAlF_6 which decomposes at 543°C[30] is never in equilibrium with liquid. The diagram is seen in Figure 20.

6. System LiF-AlF_3-Na_3AlF_6

Holm and Holm[20] worked in the Li_3AlF_6-Na_3AlF_6-LiF portion of the ternary diagram in 1973. They found a ternary eutectic at 684°C and 83 mole % LiF, 7% AlF_3 and 10% Na_3AlF_6. Thoma et al.[75] studied the NaF-LiF-AlF_3 ternary system and found the LiF-AlF_3-Na_3AlF_6 portion of the diagram to contain a eutectic in each of the two compatibility triangles Na_3AlF_6-AlF_3-Li_3AlF_6 and Na_3AlF_6-LiF-Li_3AlF_6. No evidence of either Na_2LiAlF_6 or $Na_3Li_3Al_2F_{12}$ was reported.

Rolin and Muhlethaler[69] presented a diagram of the Na_3AlF_6-Li_3AlF_6-AlF_3 ternary system (Figure 21) showing a peritectic at 647°C and 47 weight % Na_3AlF_6, 34.5% Li_3AlF_6 and 18.5% AlF_3 and a eutectic at 36 weight % Na_3AlF_6, 41% Li_3AlF_6 and 23% AlF_3 and 607°C.

To avoid the problem of volatilization, Stinton and Brown[106] encapsulated all samples in platinum tubes. DTA, quench methods, and X-ray analysis were employed to determine the system shown in Figure 22. Seven compatibility triangles, three eutectics, one peritectic, a reaction point and two regions of cryolite - $Li_3AlF_{6(ss)}$ were identified.

7. System Li_3AlF_6-LiF-CaF_2

Only one study of the Li_3AlF_6-LiF-CaF_2 system exists in the literature. Using thermal arrest methods Vrbanska and Malinovsky[99]

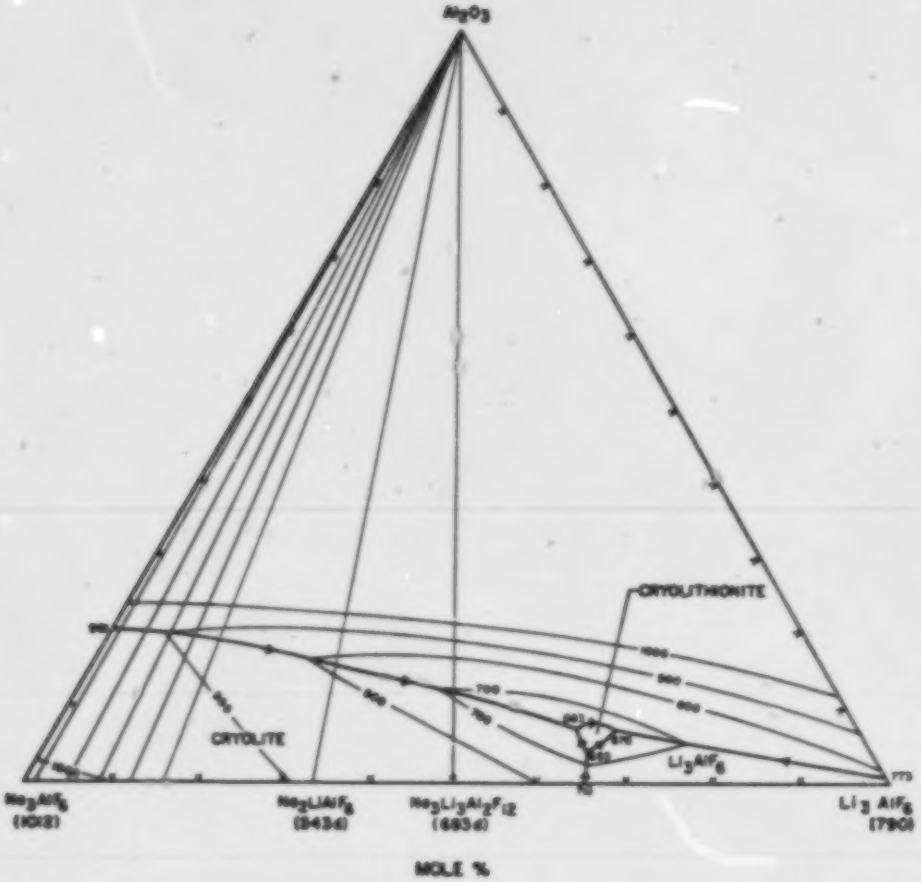

Figure 20. System Li_3AlF_6-Na_3AlF_6-Al_2O_3 (90).

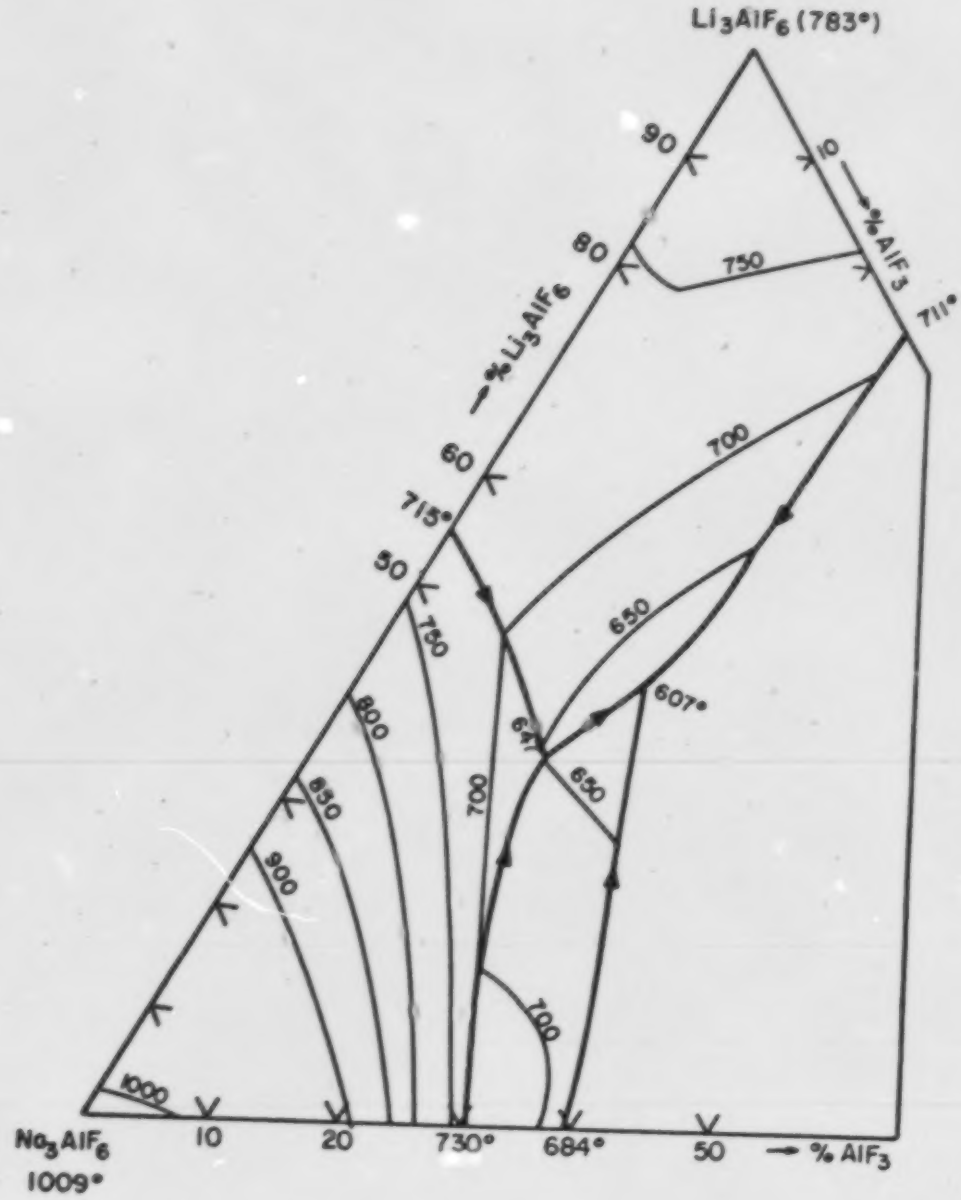

Figure 21. System Na_3AlF_6-Li_3AlF_6-AlF_3 (69).

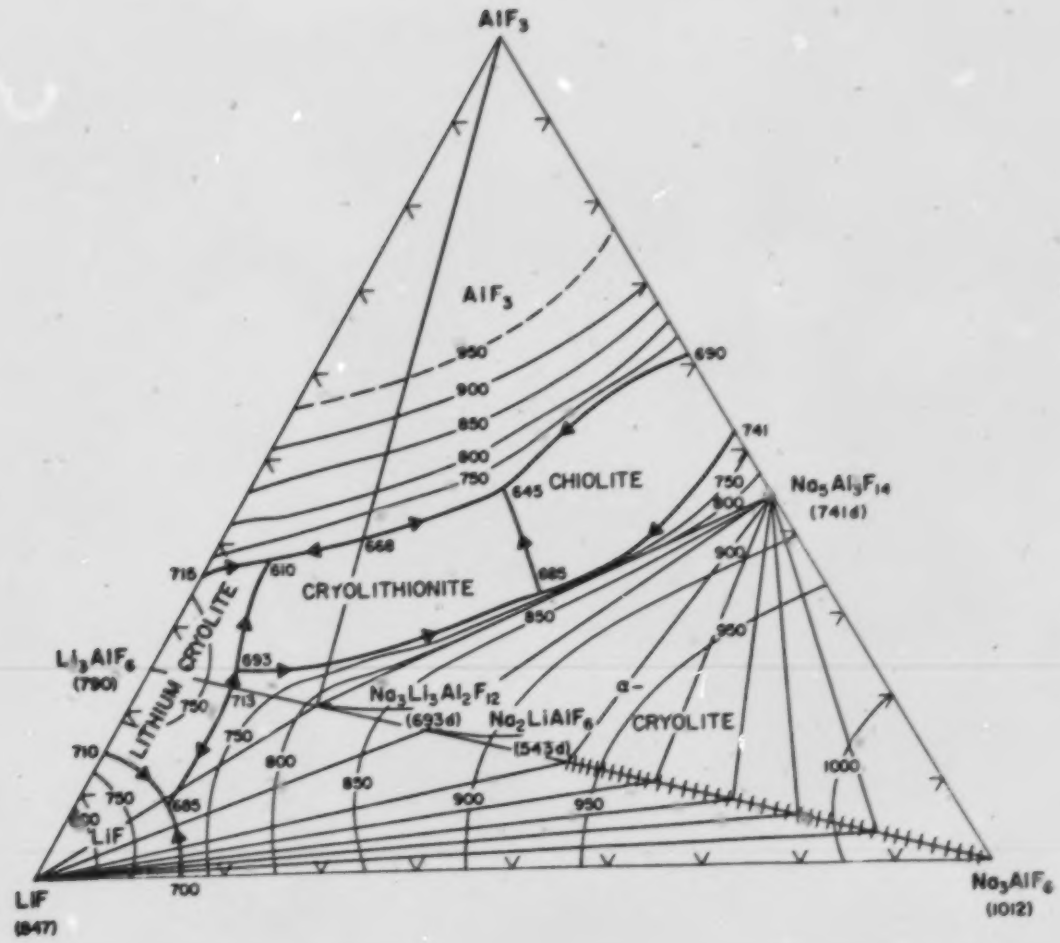

Figure 22. System $LiF-AlF_3-Na_3AlF_6$ (106).

located the invariant point for the ternary eutectic system (Figure 23) at 665°C and 25 mole % Li_3AlF_6, 52% LiF and 25% CaF_2.

D. Four Component Systems

1. System Na_3AlF_6-AlF_3-CaF_2-Al_2O_3

The quaternary system Na_3AlF_6-AlF_3-CaF_2-Al_2O_3 has been investigated several times. The studies were performed prior to the reported existence of any ternary compounds and were concerned only with very limited portions of the liquidus surface of the system.

Abramov[70] et al. studied the $Na_5Al_3F_{14}$-CaF_2-Al_2O_3 cross section of the quaternary system. The liquidus surface of the section contained phase fields for cryolite, Al_2O_3 and CaF_2. A quaternary peritectic at 34.5 mole % Na_3AlF_6, 45.9% AlF_3, 13.9% CaF_2 and 5.7% Al_2O_3 and 685°C in addition to a quaternary eutectic temperature of 665°C were reported.

Fenerty and Hollingshead[52] studied the system by noting the change in the Na_3AlF_6-Al_2O_3 and Na_3AlF_6-CaF_2 boundary curves as mixed additions of up to 15 wt. % AlF_3 and 20 wt. % CaF_2 were added to the system Na_3AlF_6-Al_2O_3. An addition of 10 wt. % AlF_3 moved the ternary eutectic for the system Na_3AlF_6-CaF_2-Al_2O_3 from 21 wt. % CaF_2 and 933°C to 13 wt. % CaF_2 and 927°C.

Rolin[71] investigated the portion of the system bounded by 10 wt. % CaF_2 and 20% AlF_3. On the basis of thermal arrest data, a partial diagram of the cryolite rich end of the quaternary system showing the boundary surface between cryolite and Al_2O_3 was presented (Figure 24). Foster[105] also presented a few selected liquidus curves in the NaF-AlF_3-CaF_2-Al_2O_3 system for compositions with constant NaF/AlF_3 ratios.

Craig and Brown[56] working with samples encapsulated in sealed platinum tubes (reacted in the solid state and in the presence of liquid) established the eight compatibility tetrahedra for the system CaF_2-AlF_3-

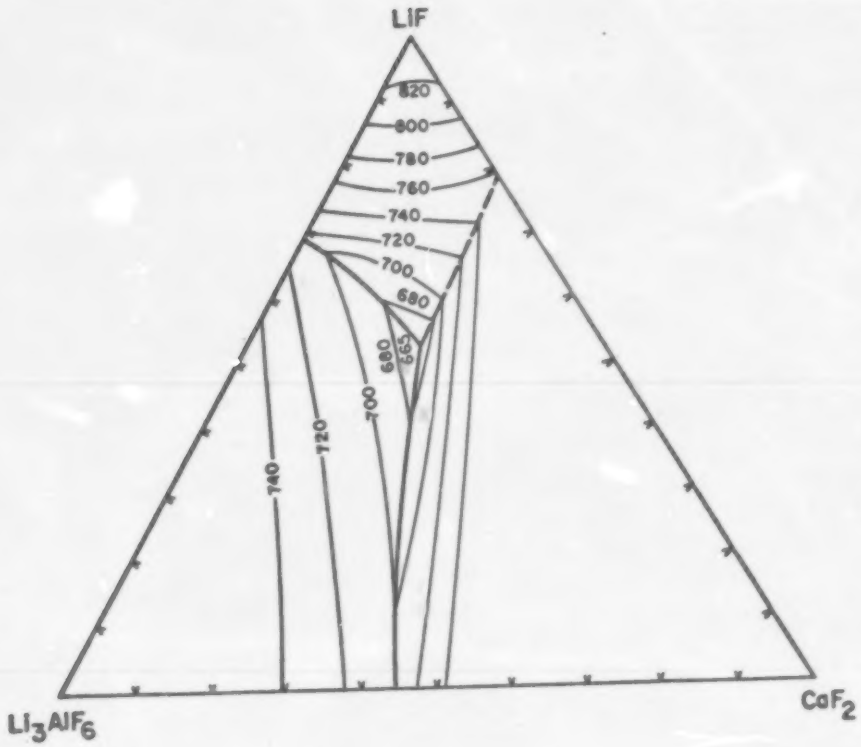

Figure 23. System Li_3AlF_6-LiF-CaF_2 [99].

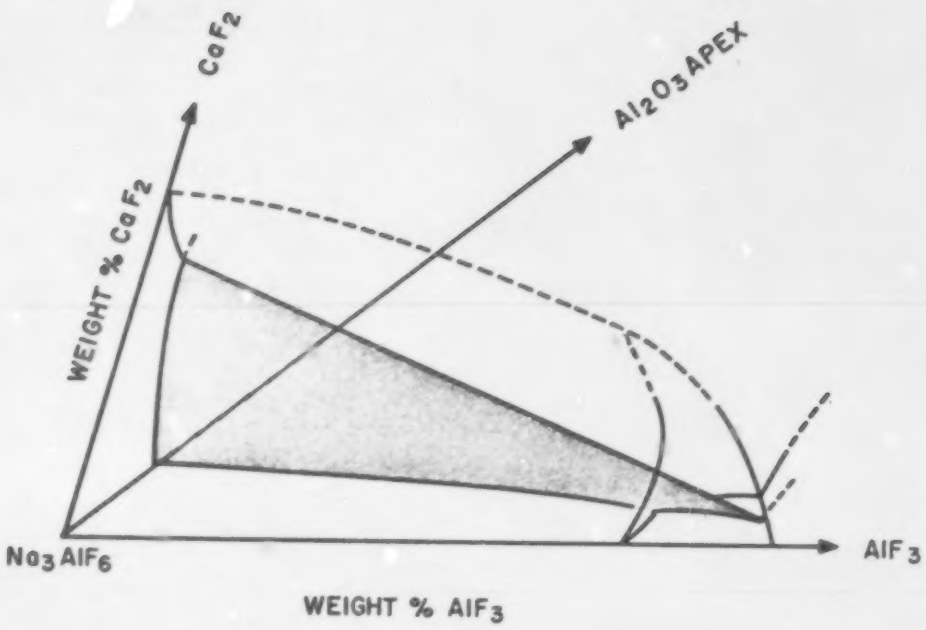

Figure 24. System Na_3AlF_6-AlF_3-CaF_2-Al_2O_3 (71).

Na_3AlF_6-Al_2O_3 shown in Figure 25. No quaternary compounds were found to exist and in all cases where Al_2O_3 was present it was identified by X-ray diffraction as α-Al_2O_3.

2. System Na_3AlF_6-AlF_3-LiF-Al_2O_3

Based on the data thus far presented, it is possible to draw a "not impossible" quaternary diagram for the system. This is shown in Figure 26. As depicted, the system contains seven compatibility tetrahedra, thus giving rise to as many as seven invariant points involving liquid. These invariant points are possibly very important to the Hall electrolyte and should be determined.

3. System Na_3AlF_6-CaF_2-LiF-Al_2O_3

There are no reported compounds in the Na_3AlF_6-CaF_2-LiF-Al_2O_3 system; however, there is little information available on the LiF-Al_2O_3 binary subsystem. If there are no compounds in either this binary or any of the ternary subsystems, it is likely that there is only one compatibility tetrahedron in this system. This would suggest that there exists only one quaternary invariant point involving liquid. The location and temperature of this point should be determined.

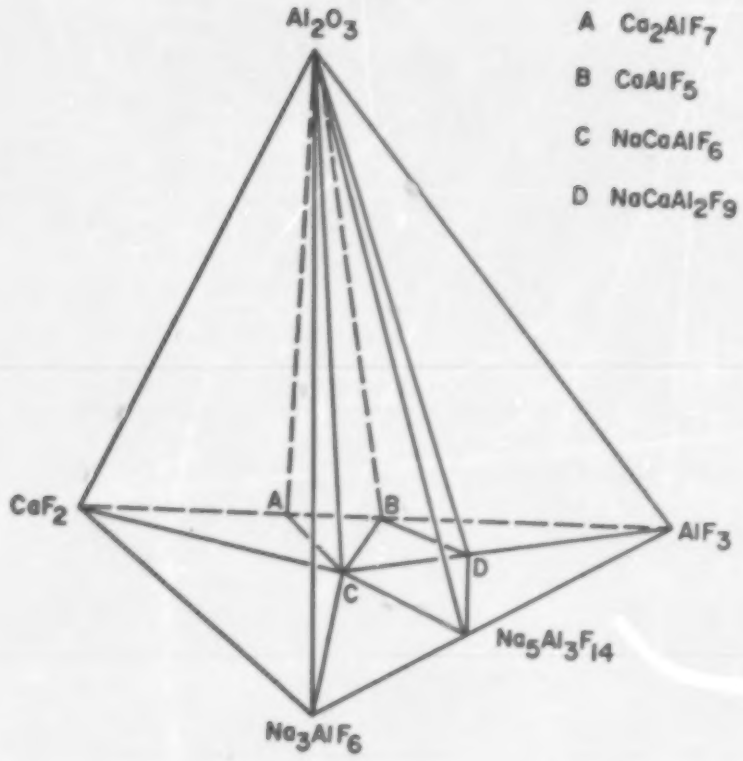

Figure 25. Subsolidus Compatibility Relationships in the system Na_3AlF_6-AlF_3-CaF_2-Al_2O_3 (56).

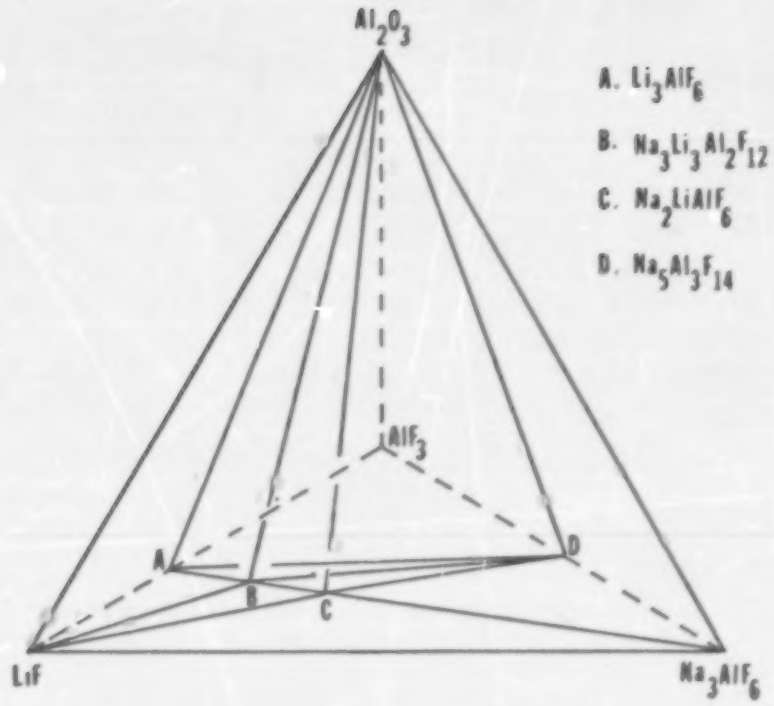

Figure 26. Possible phase diagram for the system Na_3AlF_6-AlF_3-LiF-Al_2O_3.

REFERENCES

1. Powder Diffraction File, 12-257, Joint Committee on Powder Diffraction Standards, Philadelphia, PA.

2. A. J. Majumdar and R. Roy, "Test of the Applicability of the Clapeyron Relationship to a Few Cases of Solid-Solid Transitions", J. Inorg. Nucl. Chem. 27 1961-73 (1965).

3. G. J. Landon and A. R. Ubbelohde, "Melting and Crystal Structure of Cryolite ($3NaF, AlF_3$)", Proc. Roy. Soc. (London) A240 160-72 (1957).

4. C. J. O'Brien and K. K. Kelley, "High Temperature Heat Contents of Cryolite, Anhydrous Aluminum Fluoride and Sodium Fluoride," J. Am. Chem. Soc. 79 5616-18 (1957).

5. K. Grjotheim, "Theory of Aluminum Electrolysis", Kgl. Nor. Vidensk. Selsk. Skr. 2 (5) 1-90 (1957).

6. W. B. Frank, "Thermodynamic Considerations in the Aluminum-Producing Electrolyte," J. Phys. Chem. 65 (11) 2081-87 (1961).

7. P. A. Foster, Jr., "Determination of the Cryolite-Alumina Phase Diagram by Quenching Methods," J. Am. Cer. Soc. 43 (2) 66-68 (1960).

8. P. P. Fedotieff and W. P. Iljinsky, "Uber die Schmelzbarkeit des Ternaren Systems: Natriumfluorid, Calciumfluorid, Aluminumfluorid", Z. Anorg. Chem. 129 93-107 (1923).

9. M. G. Petit, "Etude Cryoscopique de Solutions de Certains Oxydes Metalliques dans l'Eutectique Cryolithe-Fluorure de Sodium," Compt. Rend. 234 1281-83 (1952).

10. N. W. F. Phillips, R. H. Singleton and E. A. Hollingshead, "Liquidus Curves for Aluminum Cell Electrolyte," J. Electrochem. Soc. 102 (11) 648-49 (1955).

11. J. L. Holm, "Structural Interpretation of the System Cryolite + Sodium Aluminate," Trans. Faraday Soc. 58 (11) 1104-7 (1962).

12. P. A. Foster, Jr., "A Cryolite Melting Point Through Quenching Methods," J. Phys. Chem. 61 (7) 1005-6 (1957).

13. P. Pascal, "Die Elektrometallurgie des Aluminums. I. Das Ternare System Tonerde-Fluorit-Kryolith.," Z. Electrochem. 19 610-13 (1913).

14. P. A. Foster, Jr., "Melting Point of Cryolite," J. Am. Cer. Soc. 51 (2) 107-9 (1968).

15. W. B. Frank and L. M. Foster, "The Constitution of Cryolite and NaF-AlF_3 Melts," J. Phys. Chem. 64 (1) 95-8 (1960).

16. P. A. Foster and W. B. Frank, "The Structure of Cryolite-Alumina Melts," J. Electrochem. Soc. 107 (12) 997-1001 (1960).

17. C. Palache, H. Berman and C. Frondel eds., Dana's System of Mineralogy, John Wiley and Sons, Inc., New York, 1951.

18. F. Hanic, K. Matiasovsky, D. Stempelova and M. Malinovsky, "Uber die Kristallstruktur Von AlF_3," Acta Chim. Hung. Tomus 32 309-13 (1962).

19. E. Staritzky and L. B. Asprey, "Aluminum Trifluoride, AlF_3," Anal. Chem. 29 984 (1957).

20. J. L. Holm and J. B. Holm, "Phase Relations and Thermodynamic Properties in the Ternary Reciprocal System LiF-NaF-Na_3AlF_6-Li_3AlF_6," Thermochimica Acta. 6 (4) 375-98 (1973).

21. A. H. Shultz, B. Bieker and J. Krogh-Moe, "Phase Equilibrium in the System BaF_2-AlF_3," Acta Chem. Scand. 26 (7) 2623-30 (1972).

22. D. B. Shinn, D. S. Crocket and H. M. Haendler, "The Thermal Decomposition of Ammonium Hexafluoroferrate (III) and Ammonium Hexafluoroaluminate. A New Crystalline Form of Aluminum Fluoride," Inorg. Chem. 5 (11) 1927-33 (1966).

23. G. Mesrobian, M. Rolin and H. Pham, "Etude Sous Pression des Melanges Fluorure de Sodium-Fluorure d'Aluminum Riches en Fluorure d'Aluminum," Rev. Int. Hautes Temp. Refract. 9 (1) 139-46 (1972).

24. Swanson and Tatge, "Calcium Fluoride, CaF_2", Nat'l. Bur. Std. Circ. 539 Vol. 1, 69-70 (1953).

25. H. Kojima, S. G. Whiteway and C. R. Masson, "Melting Points of Inorganic Fluorides," Can. J. Chem. 46 (18) 2968-71 (1968).

26. E. M. Levin, C. R. Robbins and H. F. McMurdie, eds., Phase Diagrams for Ceramists, American Ceramic Society, Inc., Columbus, Ohio (1964).

27. F. D. Bloss, An Introduction to the Methods of Optical Crystallography, Holt, Rinehart and Winston, New York (1961).

28. Nat. Bur. Stand. U.S. Circ. 539 (9) 3 (1959).

29. P. A. Foster, Jr., "The System Sodium Fluoride-Alumina Investigated by Quenching Methods," J. Am. Cer. Soc. 45 (4) 145-48 (1962).

30. H. C. Stumpf, A. S. Russell, J. W. Newsome and C. M. Tucker, "Thermal Transformations of Aluminas and Alumina Hydrates," Ind. Eng. Chem. 42 (7) 1398-1403 (1950).

31. P. A. Foster, Jr., "The Nature of Alumina in Quenched Cryolite-Alumina Melts," J. Electrochem. Soc. 106 (11) 971-75 (1959).

32. K. Wefers and G. M. Bell, "Oxides and Hydroxides of Aluminum," Tech. Paper No. 19 Aluminum Co. of America, Pittsburgh, PA, p. 37 , 1972.

33. Y. I. Chu and A. I. Belyaev, Izv. Vyssh Ucheb. Zaved., Tsvet. Metal. p. 59 (1959).

34. J. L. Holm, Lic. Thesis. NTH, Trondheim, 1963; cited from 39.

35. B. Jenssen, Lic. Thesis, NTH, Trondheim, 1969; cited from 39.

36. M. A. Kuvakin, Zh. Neorg. Khim. 14 282 (1969).

37. K. Matiasovsky and M. Malinovsky, Hutn. Listy. 24, 515 (1969).

38. J. L. Holm, Thesis for a Doctorate Degree. NTH, Trondheim, 1971; cited from 39.

39. I. Kostenska, J. Corba, and M. Malinovsky, "On Solid Solutions in the System LiF-Na_3AlF_6," Chem. Zvesti, 28, 546-552 (1974).

40. R. A. Lewis, Process Metallurgy Division Monthly Report, May, 1948, cited from 41.

41. P. A. Foster, Jr., "The Phase Diagram of the Na_3AlF_6-LiF System," Unpublished Data, Aluminum Company of America, ALCOA Center, Pa. (1968).

42. J. L. Holm, Thermodynamic Properties of Molten Cryolite and Other Fluoride Mixtures, Inst. of Inorganic Chem., The University of Trondheim, NTH Norway, 1971.

43. J. Ravez and P. Hagenmuller, "Les Systemes CaF_2-AlF_3 et SrF_2-AlF_3," Bull. Soc. Chim. 7 2545-48 (1967).

44. J. Ravez, J. Viollet, R. DePape and P. Hagenmuller, "Les Systems MF_2-FeF_3(M=Ba,Sr,Ca). Les Fluoferrites Alcalino-Terreux," Bull. Soc. Chim. 4 1325-31 (1967).

45. J. L. Holm, "Phase Equilibria in the System CaF_2-AlF_3," Acta Chem. Scand. 19 (6) 1512-14 (1965).

46. M. Malinovsky, J. Vrbenska and I. Cakajdova, "Phasediagramm dis Systems CaF_2-AlF_3," Chem. Zvesti. 21 (1967).

47. J. Millet, H. Pham and M. Rolin, "Les Diagrammes de Phase des Systemes Binaires NaCl-AlF_3 et CaF_2-AlF_3: Extrapolation du Point Triple du Fluorure d'Aluminum," Rev. Int. Hautes Temp. Refract. (11) 4, 277-83 (1974).

48. D. Craig and J. Brown, Jr., "Phase Equilibria in the System CaF_2-AlF_3" accepted for publication, J. Am. Cer. Soc. 1977.

365

49. H. Grunhager and J. Mergoil, "Decouverte d'Hydrocalamite et Afwillite Associees a l'Ettringite dans les Porcelonites de Boissejour pres Ceyrat (puy-de-Dome), Bull. Soc. Franc. 86 149-57 (1963).

50. H. Evans, D. Appleman, and D. Handwerken, Amer. Crystallographic Assoc. Annual Program Meeting 42-43 (1963).

51. K. Matiasovsky and M. Malinovsky, "Physicochemical Study of Some Species Important in the Production of Aluminum, II. The Phase Diagram of the System Na_3AlF_6-CaF_2-NaCl," Chem. Zvesti. 14 353-64 (1960) Chem. Abst. 54 (20-21) 22100g (1960).

52. A. Fenerty and E. A. Hollingshead, "Liquidus Curves for Aluminum Cell Electrolyte III. Systems Cryolite and Cryolite-Alumina with Aluminum Fluoride and Calcium Fluoride," J. Electrochem. Soc. 107 (12) 993-97 (1960).

53. M. Rolin, "Le Diagramme Binaire Cryolithe-Fluorure de Calcium. La Diagramme Ternaire Cryolithe-Fluorure de Calcium-Alumine," Bull. Soc. Chim. 1120-25 (1961).

54. J. L. Holm, "The Phase Diagram of the System Na_3AlF_6-CaF_2, and the Constitution of the Melt in the System," Acta Chem. Scand. 22 (3) 1004-12 (1968).

55. M. Verdan and R. Monnier, "Etude du Systeme Na_3AlF_6-CaF_2 au Moyen de l'Analyse Thermique Differentielle en Creuset Scelle," Rev. Int. Hautes Temp. Refract. 9 (2) 205-8 (1972).

56. D. Craig and J. Brown, Jr., unpublished results.

57. P. A. Foster, Jr., "Phase Equilibria in the System Na_3AlF_6-AlF_3," J. Am. Cer. Soc. 53 (11) 598-600 (1970).

58. H. Ginsberg and K. Wefers, "Thermochemische Unter Suchungen am System NaF-AlF_3," Erzmetall 20 (4) 156-61 (1967).

59. M. Rolin, "Sur la Structure Ionique de la Cryolithe pure Fondue II - Determination Experimentale du Diagramme Binaire Cryolithe. AlF_3," Bull. Soc. Chim. (4) 671-77 (1960).

60. J. L. Holm, Investigation of Structure and Phase Ratio of Some Systems in Connection with Alumminum Electrolytes, Norweigan Technical Institute, Trondheim, Norway 7-13 (1963).

61. G. A. Roush and M. Miyake, "Equilibrium of the Series Cryolite-Alumina," Trans. Am. Electrochem. Soc. 48 153-57 (1925). Chem. Abst. 19 (8-16) 2455 (1925).

62. M. Rolin, "Le Diagramme Binaire Cryolithe-Alumine. I. Partie Experimentale," Bull. Soc. Chim. (6) 1201-3 (1960).

63. J. J. Duruz and R. Monnier, "Une Methode d'Analyse Thermique Differentielle pour les Substances Volatiles a Point de Fusion Eleve: Application au Systeme Cryolithe-Alumine," Chimia 21 (12) 572-5 (1967).

64. E. W. Dewing, "The Structure of Cryolite-Alumina Melts," J. Electrochem. Soc. 108 (6) 611-12 (1961).

65. G. Gunther, G. Anderson and H. Perlitz, "On the Luminescence of Phosphors of the Aluminum Oxide-Calcium Fluoride Type Activated with Manganese," Arkiv Kemi 1 565-72 (1950).

66. C. Kuo and T. Yen, "Phase Equilibria and Chemical Reactions in the System CaF_2-Al_2O_3," Hua Hsueh Hsueh Pao 30 (4) 381-7 (1964). Chem. Abst. 61 (12-13) 15401h (1964).

67. A. K. Cahtterjee and G. I. Zhmoidin, "The Phase Equilibrium Diagram of the System CaO-Al_2O_3-CaF_2," J. Mater. Sci. 7 (1) 93-7 (1972).

68. M. Rolin, "Le Diagramme Ternaire Cryolithe-Fluorure d'Aluminium-Alumine." Bull. Soc. Chim. 1112-1120 (1961).

69. M. Rolin and R. Muhlethaler, "Etude du Systeme Cryolithe de Sodium-Cryolithe de Lithium en tant que Solvant de l'Alumine," Bull. Soc. Chim. 2593-99 (1964).

70. G. A. Abramov, A. A. Kestyukov and L. B. Kulakov, "The Structural Diagram of the Quaternary System Cryolite-Aluminum Fluoride-Calcium Fluoride-Alumina," Electromet. Tsvetnykh Metal. No. 188 45-57 (1957). Chem Abst. 53 (13-16) 11975g (1959).

71. M. Rolin, "Le Diagramme Quaternaire Cryolithe-Fluorure d'Aluminium-Fluorure de Calcium-Alumine," Bull. Soc. Chim. 1404-7 (1961).

72. N. Puschin and A. Baskow, "Das Gleichgewicht in binaren Systemen einigen Fluorverbindungen; Z. Anorg. Chem. 81 354 (1913).

73. P. P. Fedotieff and K. Timofeeff, "Schmelzdiagramme der Systeme KF-AlF_3 und LiF-AlF_3," Z. Anorg. Chem. 206 266 (1932).

74. E. P. Dergunov, Doklady Akad. Nauk. SSSR 60 (1948) 1185, cited from 42.

75. R. E. Thoma, B. J. Sturm, and E. H. Guinn, U. S. Atom. Energy Comm. ORNL-3594 (1964).

76. M. Malinovsky, I Cakajdova, and K. Matiasovsky, Chem. Zvesti, 21 794 (1967).

77. M. Rolin, H. Latreille, and H. Pham., "Etude de la Dissociation de la Cryolite de Lithium a la Fustion, Comparaison avec celle de la Cryolite de Sodium," Bull. Soc. Chim. 2271 (1969).

78. K. Matiasovsky and M. Malinovsky, "Physico-Chemical Properties of Molten LiF-AlF_3 Mixtures," Coll. Czech. Chem. Comm., 36 3746-3751 (1971).

79. G. Garton and B. M. Wanklyn, "Polymorphism in Li_3AlF_6," J. Inorg. Nucl. Chem., 27, 2466-2469 (1965).

80. J. L. Holm, "Phase Transitions and Structure of Lithium Cryolite," Acta Chem. Scand. 20, 1167-1169 (1966).

81. J. H. Burns, A. C. Tennissen, and G. D. Trunton, "The Crystal Structure of α-Li_3AlF_6," Acta. Cryst., B24, 225-230 (1968).

82. J. L. Holm and B. Jenssen, "A Note on the Polymorphy and Structure of Li_3AlF_6," Acta Chem. Scand. 23, 1065-1068 (1969)

83. P. Drossbach, "Zur Elektrometallurgie des Aluminiums," Z. Elektrochem., 42 (2) 65-70 (1936).

84. V. P. Mashovets and V. I. Petrov, "Phase Diagram of the System Na_3AlF_6-Li_3AlF_6-Al_2O_3," Zh. Prikl. Khim., 30 (11), 1695-1698 (1957).

85. M. S. Beletskii and Y. G. Saksonov, "Phases in the System Na_3AlF_6-Li_3AlF_6," Zh. Neorg. Khim. Vol. II, No. 2, 414-416 (1957).

86. G. Garton and B. M. Wanklyn, "Reinvestigation of the System Na_3AlF_6-Li_3AlF_6," J. Amer. Cer. Soc., 50 (8) 395-399 (1967).

87. J. L. Holm and B. J. Holm, "Phase Investigations in the System Na_3AlF_6-Li_3AlF_6," Acta Chemica. Scand., 24, 2535-2545 (1970).

88. R. Baylor, Jr., D. P. Stinton, and J. J. Brown, "Subsolidus Equilibria in the System LiF-AlF_3-Na_3AlF_6," J. Amer. Ceram. Soc., 57, (11) 470-471 (1974).

89. D. P. Stinton and J. J. Brown, "Phase Equilibria in the System Na_3AlF_6-Li_3AlF_6," J. Amer. Ceram. Soc., 58 (5-6) 257 (1975).

90. R. T. Cassidy and J. J. Brown, Jr., Unpublished data, Virginia Polytechnic Institute and State University (1977).

91. O. Ruff and W. Z. Busch, "Elektrolytische Gewinnung von Magnesium usw," Z. Anorg. Chem., 144, 96 (1925).

92. G. A. Bukhalova and A. G. Bergman, Dokl. Akad. Nauk. SSSR, 66, 67 (1949), cited from 101.

93. W. E. Roake, "The Systems CaF_2-LiF and CaF_2-LiF-MgF_2," J. Electrochem. Soc., 104, 661 (1957).

94. G. A. Bukhalova and V. T. Berezhnaya, Zh. Neorg. Khim. 2, 1409 (1957), cited from (100).

95. C. J. Barton, L. M. Bratchev, and W. R. Grimes, Phase Diagrams of Nuclear Reactor Materials. (R. E. Thoma, Ed.) Oak Ridge Natl. Lab., ORNL 2548, 29 (1959).

96. G. Bukhalova, K. Sulaymankulov, and A. K. Bostandzhiyan, "The Melting Diagram of the System Consisting of Fluorides of Lithium, Sodium and Calcium," Zh. Neorg. Khim., 5, 1138-1140 (1959).

97. D. L. Deadmore and J. S. Machin, "Phase Relations in the Systems CsF-LiF, CsF-NaF, and CaF_2-LiF," J. Phys. Chem., 64, 825 (1960).

98. V. A. Gladushchenko and M. A. Zakharchenko, Zh. Neorg. Khim., 11 916 (1966), cited from 101.

99. J. Vrbenska and M. Malinovsky, "Phasendiagramm des Dreistoffsystems Li_3AlF_6-LiF-CaF_2," Chem. Zvesti. 21 819 (1967).

100. I. Kostenska, J. Vrbenska, and M. Malinovsky, "The equilibrium 'solidus-liquidus' in the system lithium fluoride-calcium fluoride," Chem. Zvesti, 28 531-538 (1974).

101. M. Rolin, "Le Diagram Ternaire Cryolithe-Fluorure d'Aluminium-Fluorure de Calcium," Bull. Soc. Chim. 1351-54 (1961).

102. H. Pfundt and H. Zimmermann, "The Quasi Binary System NaF-$CaAlF_5$, An Investigation from the Ternary System NaF-$AlF_3$$CaF_5$," Ertzmetall 25 (11) 564-72 (1972).

103. E. W. Dewing, "Solid Solubility of CaF_2 in Cryolite," Tran. of The Metal. Soc. of AIME 245 (8) (1969).

104. P. A. Foster, Jr., "Phase Diagram of a Portion of the System Na_3AlF_6-AlF_3-Al_2O_3," J. Am. Cer. Soc. 58 (7-8) 288-91 (1975).

105. P. A. Foster, Jr., "Liquidus Curves in the Quaternary System NaF-AlF_3-CaF_2-Al_2O_3," J. Am. Cer. Soc. 43 (8) 437-38 (1960).

106. D. P. Stinton and J. J. Brown, Jr., "Phase Equilibria in the System LiF-AlF_3-Na_3AlF_6," J. Am. Ceram. Soc., 58, 264 (1976).

National Bureau of Standards SP-496, Applications of Phase Diagrams in Metallurgy and Ceramics
Proceedings of Workshop held at NBS, Gaithersburg, Md., January 10-12, 1977

Краткие сведения
о содержании третьего, четвертого и пятого томов труда А.Е.Вол и И.К.Каган "Строение и свойства двойных металлических систем" и методах работы по их составлению.

Во всех томах принят единый принцип расположения материала, а именно, как металлы, так и образуемые ими двойные системы располагаются в алфавитном порядке по их наименованиям на русском языке. При этом для каждой системы, в зависимости от степени ее изученности, приводятся следующие данные:

I. Диаграмма состояния и кристаллическая структура;

2. Физические и механические свойства (термодинамические, механические, электрические, термоэлектрические и магнитные свойства, поверхностное натяжение и вязкость, упругость паров, плотность, теплоемкость, теплопроводность, термическое расширение);

3. Химические свойства (коррозионная стойкость в атмосферных условиях, а также в различных агрессивных средах и в газах, стойкость против окисления при высоких температурах);

4. Список использованной литературы.

Авторы уделяют очень большое внимание вопросу более полного использования, имеющихся в литературе данных по каждой рассматриваемой системе. При написании третьего тома, в который вошли системы золота, индия, иридия, иттербия и иттрия, были использованы данные, опубликованные по 1970-71 гг включительно. При подготовке материалов для 4-го тома, в который войдут системы кадмия, калия и кальция, используются данные, опубликованные по 1973-74 гг. включительно. Для составления 5-го тома, в который войдут системы кислорода, кобальта и кремния, будут использованы литературные данные, опубликованные по 1975-76 гг. включительно.

В третьем томе (объем ~ 70 печатных листов), выход которого из печати ожидается в ноябре-декабре 1976 г., приводятся данные

по 288 двойным системам, в том числе для 116 систем приведены диаграммы состояния во всей области концентраций и сделан подробный обзор свойств сплавов; для 23 систем приведены диаграммы состояния не во всей области концентраций и менее подробное описание свойств; сведения о растворимости в жидком и твердом состояниях, составе промежуточных фаз с описанием в ряде случаев отдельных свойств, приведены для 149 двойных систем.

При построении диаграмм состояния предпочтение отдавалось данным, полученным при исследовании наиболее чистых сплавов с одновременным применением нескольких современных методов физико-химического анализа. В тех случаях, когда имеющихся в распоряжении авторов данных было недостаточно для однозначного решения, в книгу помещали два варианта одной и той же диаграммы состояния с указанием литературных данных, использованных для построения каждой из них (см. например системы Au-In, Au-Pu, In-Mg, In-Na, In-Tℓ, Ir-Ti).

Объем использованной в 3-м томе литературы можно иллюстрировать такими примерами: при рассмотрении системы Au-Cu использовано 345, системы In-Sb - 214, системы Au-Ag - 162 литературных источника. Таким образом, только для этих трех систем использовано более 700 литературных источников.

В 4-м томе (объем около 50 печатных листов) рассмотрено 163 системы. В этом томе для 54 систем приведены диаграммы состояния во всей области составов и сделан подробный обзор свойств сплавов. Для остальных 109 систем приведены сведения о взаимной растворимости компонентов системы и (или) составе образуемых ими промежуточных фаз с описанием в ряде случаев свойств сплавов.

Объем 5-го тома предполагается ~ 50 печатных листов с рассмотрением около 140 систем.

В качестве основных материалов для написания перечисленных

выше трудов авторы используют свою обширную картотеку, начало которой было положено одним из них (А.Г.Вол) еще в 1931 г., когда подготавливались к изданию книги "Цинк и его сплавы" (Стандартгиз, 1933 г.), "Никель и его сплавы" (Цветметиздат, 1932г.) и "Кремнистые бронзы и их промышленное применение" (Объедин. научно-технич. изд-во, 1935г.). Эта картотека продолжала непрерывно пополняться по новым литературным источникам и в настоящее время включает в себя карточки по литературным данным по 1973–1974 г.г. включительно. Каждая карточка является подробным рефератом с приложением графиков и таблиц оригинального источника по двойным системам и содержит данные, используемые авторами в своих трудах при описании той или иной системы. Карточки составляются только по первоисточникам. Даже в тех случаях, когда имеется заслуживающая доверия компиляция (например книги Хансена, Эллиотта и Шенка по двойным системам), имеющиеся в них ссылки на оригинальные работы, используются как библиографические данные для составления подробной карточки по первоисточникам. Это обусловлено тем, что в упомянутых работах приводятся только диаграммы состояния и нет никаких данных по свойствам сплавов, исследования которых послужили основанием для построения этих диаграмм. В случае невозможности ознакомления с первоисточниками – используются данные компилятивных работ с ссылками как на первоисточник, так и на компилятивную работу.

Выбор статей для составления подробных карточек производится:

1. путем систематического просмотра целого ряда журналов, издаваемых в СССР и в других странах (перечень журналов см. ниже);

2. путем систематического просмотра Metallurgical Abstracts in Journal Institute of Metals (London);

3. путем систематического просмотра реферативных журналов "Металлургия" и "Химия", издаваемых в СССР.

Классификация карточек в картотеке полностью отвечает принятой для издания трудов. Каждому элементу периодической системы Д.И.Менделеева присвоен порядковый номер, соответствующий его расположению по наименованию в русском алфавите, а бинарная система обозначается дробным числом, состоящим из порядковых номеров обоих входящих в нее элементов. По этой классификации, например, азот обозначен цифрой I, алюминий - цифрой 3, ванадий - цифрой 7, а сплавы систем: азот-алюминий - дробным числом I/3, алюминий - ванадий - 3/7, азот - ванадий - I/7 и т.д. Такая нумерация карточек дает возможность быстро рассортировать их и расположить в картотеке в той последовательности, в какой описываются системы.

Перечень систематически просматриваемых журналов:

I. Атомная энергия,
2. Доклады Академии Наук СССР,
3. Журнал неорганической химии,
4. Журнал прикладной химии,
5. Журнал структурной химии,
6. Журнал физической химии,
7. Известия Академии Наук СССР. Неорганические материалы,
8. Известия Академии Наук СССР. Металлы,
9. Известия Высших учебных заведений. Цветная металлургия,
I0. Кристаллография,
II. Металловедение и термическая обработка металлов,
I2. Украинский химический журнал,
I3. Физика металлов и металловедение,
I4. Acta Crystallographica,
I5. Acta Metallurgica,
I6. Comptes rendus Acad. Sci., Paris,
I7. Journ. Less-Common Metals,
I8. Journ. Institute of Metals,

19. Transactions ASM,
20. Transactions AIME (Trans. Metallurg. Soc. AIME), } за 1970 г.
21. Metallurgical Transactions за 1970 г.
22. Zeitschrift für anorganische Chemie,
23. Zeitschrift für Kristallographie,
24. Zeitschrift für Metallkunde.

Brief Summary

The 3rd, 4th, and 5th volumes of the "Handbook of Binary Metallic Systems" and the Methods of compilation & editing.

by A. E. Vol & E. K. Kagan
Leningrad, USSR

National Bureau of Standards SP-496, Applications of Phase Diagrams in Metallurgy and Ceramics
Proceedings of Workshop held at NBS, Gaithersburg, Md., January 10-12, 1977

An English translation prepared by G. Marinenko, Analytical Chem. Div., NBS

Brief Information on the Content of the Third, Fourth, and Fifth Volumes of the Collection "Structure and Properties of Binary Metallic Systems" by A. E. Vol and I. K. Kagan, As Well As Presentation Of The Methods Of The Work In Compilation Of These Volumes

A. E. Vol and I. K. Kagan
Leningrad, USSR

In all of the volumes a single principle of organizing the material was adhered to; namely, both metals, as well as the binary systems which these metals form, were arranged in alphbetical order in accordance with their chemical symbols in the Russian language. At the same time for each system, depending on the degree to which the system was studied, the following data were cited:

(1) Phase Diagram and Crystal Structures;
(2) Physical and Mechanical Properties (Thermodynamic, Mechanical, Electrical, Thermoelectric and Magnetic Properties, Surface Tension and Viscosity, Vapor Pressure, Density, Heat Capacity, Thermoconductivity, and Thermal expansion);
(3) Mechanical Properties (Corrosion Stability under atmospheric conditions, as well as in various other corrosive media and gasses, Oxidation Stability at elevated temperatures);
(4) Enumeration of bibliography which was used.

The authors devote extremely great attention to the question of fuller utilization of data which are available in the literature on each of the considered systems. In writing the third volume, which contained systems of Au, In, Ir, Yb, and Y, data were utilized which were published until 1970-1971 inclusively. In preparation of the materials for the fourth volume which included Cd, K, and Ca systems, data were utilized which were published until 1973-1974 inclusively. In compilation of the fifth volume, which contains O, Co, and Si systems, literature data published until 1975-1976 inclusively were utilized.

The third volume (amounting to approximately 70 printed pages), publication of which is expected to be in Nov.-Dec. 1976* the data are cited on 288 binary systems, including phase diagrams over the entire composition range and detailed studies of the properties for 116 systems; for 23 systems phase diagrams are provided, but not over the entire composition range and the descriptions of the properties are less detailed; information on the solubility in liquid and solid states, composition of the intermediate phases with the description in a number of cases of individual properties are given for 149 binary systems.

In constructing the phase diagrams the preference was given for data which were obtained with the study of the purest alloys with simultaneous use of several modern methods of physico-chemical analysis. In those cases where the data available to the authors were insufficient for a single-valued decision, two variations were included in the book for the same phase diagram indicating the literature data which were utilized for the construction of each of these (see for example the following systems: Au-In, Au-Pu, In-Mg, In-Na, In-Tl, Ir-Ti).

The scope of literature utilized in the third volume can be illustrated with the following example: in considering the Au-Cu system, 345 literature sources were used, for In-Sb system 216 sources were used, while for Au-Ag system, 162 sources were utilized. Thus, for these three sytems only, more than 700 lfterature sources were utilized.

In the fourth volume (approximated 50 printed pages) 163 systems are considered. Phase diagrams are provided over the whole composition range and a detailed review of the properties of 54 alloy systems is made. For the remaining 109 systems, information is given on the mutual solubility of the components of the [illegible] or composition of the intermediate phases which are formed by the component metals along with a description of the properties of the alloys in a number of cases.

The fifth volume is expected to be approximately 50 printed pages and to contain approximately 140 systems.

---

*Translator's note: has been published by "Nauka", Moscow, 1976.

The basic materials which were used for compilation of the above cited work were the extensive card file of the authors, which was initiated by one of the authors (A. E. Vol) back in 1931, when the books "Zinc and Its Alloys" ("Standartgiz" Publishing House, 1933), "Nickel and Its Alloys" ("Tsvetmetizdat" Publishing House, 1932) and "Silicon Bronzes and Their Industrial Aplications" ("Ob'Yedin. Nauchno-Tkhnich." Publishing House, 1935) were being prepared for publication. This card file was continuously updated from new literature sources and at present includes literature data up to 1973-1974 inclusively. Each card is a detailed reference with the attached graph and tables of the original source on the binary systems and contains data which are utilized by authors in their work in describing these various systems. The cards are compiled only from the original sources. Only in those cases, when reliable compilations are available (for example, the books by Hansen, Elliott, and Shunk on binary systems), the references contained in those books to the original works were utilized as bibliographic data for the compilation of a detailed card file on primary sources. This results from the fact that in the above works only phase diagrams are given and there are no data on the properties of alloys, the studies of which served as the basis for the construction of these phase diagrams. In a case when it is not possible to become familiar with the primary source, the data of compiled works are utilized with references both to the primary source as well as to the compilation utilized.

Choice of articles for compilation of the detailed card file is performed as follows:

1. By systematic review of the whole series of journals which are published in the USSR and other countries (for a list of journals, see below);
2. By systematic review of the Metallurgical Abstracts in the Journal of Institute of Metals (London);
3. By systematic search of the reference journals ("Referativni Zhurnal") "Metallurgiya" and "Khimiya", published in the USSR.

The classification of cards in the card file corresponds completely to the format used in publishing the work. An ordinal number is given to each of the elements of the peroidic system of elements of D. I. Mendeleev, which corresponds to its alphabetical position in a list of chemical symbols in the Russian language, and binary systems are denoted by fractional numbers, which consist of both ordinal numbers of the elements which comprise the system. In accordance with this classification, for example, nitrogen

is designated by 1, Aluminum by 3, Vanadium by 7, and the alloys of the systems: nitrogen-aluminum by 1/3, aluminum-vanadium by 3/7, nitrogen-vanadium by 1/7, etc. Such numbering of cards enables one to quickly sort them and place them into the card file in the sequence which corresponds to the description of the system.

The list of journals which are systematically searched:

1. Atomnaya Energiya (Atomic Energy),
2. Doklady Akademii Nauk SSSR (reports of the Acadeny of Sciences of the USSR),
3. Zhurnal Neorganicheskoy Khimii (Journal of Inorganic Chemistry),
4. Zhurnal Prikladnoy Khimii (Journal of Applied Chemistry),
5. Zhurnal Strukturnoy Khimii (Journal of Structural Chemistry),
6. Zhurnal Fizicheskoy Khimii (Journal of Physical Chemistry),
7. Izvestiya Akademii Nauk SSR. Neorganicheskiye Materialy (News of the Academy of Sciences of the USSR, Inorganic Materials),
8. Izvestiya Akademii Nauk SSSR. Metally (News of the Academy of Sciences of the USSR, Metals),
9. Izvestiya Vysshikh Uchebnykh Zavedeniy. Tsvetnaya Metallurgiya (News of the Institutions of Higher Learning. Nonferrous Metallurgy),
10. Kristallografiya (Crystallography),
11. Metallovedeniya i Termicheskaya Obrabotka Metallov (Metal Science and the Thermal Treatment of Metals),
12. Ukrainskiy Khimicheskiy Zhurnal (Ukrainian Chemical Journal),
13. Fizika Metallov i Metallovedeniya (Physics of Metals and Metal Science),
14. Acta Crystallographica,
15. Acta Metallurgica,
16. Comptes rendus Acad. Sci., Paris,
17. Journ. Less-Common Metals,
18. Journ. Institute of Metals,
19. Transactions ASM,
20. Transactions AIMME (Trans. Metallurg. Soc. AIME),
21. Metallurgical Transactions c1970,
22. Zeitschrift fur anorganische Chemie,
23. Zeitschrift fur Kristallographie,
24. Zeitschrift fur Metallkunde.

National Bureau of Standards SP-496, Applications of Phase Diagrams in Metallurgy and Ceramics
Proceedings of Workshop held at NBS, Gaithersburg, Md., January 10-12, 1977

The Determination of Phase Diagrams for Liquid Oxides and Metallurgical Slags by Hot-Wire Microscopy

by

H. Alan Fine
Department of Metallurgical Engineering
University of Arizona
Tucson, Arizona 85721

Hot-wire microscopy has been used successfully to determine the liquidus surfaces for many oxide systems. The technique, which lends itself to measurements in all temperature ranges, can be used to determine liquidus temperatures for transparent or semi-transparent melts under reducing, neutral or oxidizing conditions.

A review of the development of hot-wire microscopy is presented. The limitations and the experimental idiosyncrasies of the technique are discussed and special equipment necessary for atmosphere control within the hot-wire microscope are described.

INTRODUCTION

The phase diagrams for liquid oxides and slags that occur in metallurgical operations are important tools for developing a better understanding of the phase relations and physical chemistry of the processes. The classical quenching technique used for determination of these phase diagrams was, however, a very long and tedious procedure. Consequently, many important phase diagrams were not known. Within the last twenty-five years, a new technique known as hot-wire or hot-filament microscopy has been developed for direct observation of oxide melts. Using this device, the liquidus surfaces of many phase diagrams have been easily and quickly determined. This article reviews the development of the hot-wire microscope, with special emphasis being placed on its use for determination of the liquidus surfaces of oxide mixtures and metallurgical slags. Modifications to the standard hot-wire microscope which are being used to study blast-furnace slags in atmospheres containing an oxygen partial pressure of 10^{-15} atm. are also described.

HOT-WIRE APPARATUS

The development of micro-furnaces for the direct microscopic observation of melts dates back to 1891[1]. However, it was the development of a micro-furnace by Ordway[2] in 1952, which could be used to contain, heat and monitor the temperature of a sample, that lead to the hot-wire technique for the determination of the liquidus surfaces of oxides. In Ordway's original apparatus, a small sample was held by capillarity on a Pt/Pt-10% Rh thermocouple. The thermocouple, made from 0.25 mm wires, served as the heating element, i.e. furnace, and the container for the sample. A high frequency current produced by an audio amplifier, which was driven by an audio oscillator, was used to heat the thermocouple and sample. The simultaneous measurement of the thermocouple emf was made by placing a low-pass filter between a second pair of leads connected to the thermocouple and a voltage measuring device, such as a potentiometer.

A modification suggested by Welch[3] to the electrical circuit substantially simplified and reduced the cost of Ordway's unit. In Welch's circuit, a high-speed polarized relay which vibrated at the power main frequency (50 or 60 hz.) was used to replace the low-pass filter and to eliminate the need for a high-frequency heating current. The relay simply switched connections within the circuit so that heating of the thermocouple by the main current was done during one half of the power cycle, while temperature measurement was made during the other. To attain higher operating temperatures and to eliminate the need for a cold junction, Welch also suggested that the Pt/Pt-10% Rh thermocouple used by Ordway be replaced by a Pt-5% Rh/Pt-20% Rh thermocouple.

A microscope with a working distance of approximately 25 mm was also commonly used with the unit to facilitate observation of the sample and thermocouple assembly. Modifications to protect the microscope from damage by the hot-wire unit were not necessary because of the small thermal capacity and low power dissipation (usually much less than 50 W) from the sample.

Even though the aim of Ordway's initial work was to develop a furnace for growing single crystals of refractory materials, the usefulness of this apparatus for liquidus determinations was evident. Within a few years of the report of his work, the hot-wire microscope had been successfully used by Welch[4] and Baldwin[5] to determine blast furnace slag liquidus temperatures. The work of Welch[4] proved that the hot-wire method was a viable technique for liquidus measurement, by showing that excellent agreement could be obtained from experiments performed using hot-wire microscopy, the classical quenching technique and thermal analysis. A comparison of results of experiments performed by Welch and Baldwin[5] showed that excellent agreement on tests performed in different laboratories was also possible.

Further modifications to the hot-wire unit reduced contact wear and stray voltages that were produced in the relay. A simultaneous reduction in the variations in sample temperature resulting from main power drift was also achieved.[6,7] Slightly different circuit designs allowed the hot-wire unit to be used for thermal analysis[8] and differential thermal analysis[9]. The use of an Ir-40% Rh/Ir-60% Rh thermocouple increased the working temperature of the unit to 2150°C [10].

EXPERIMENTAL PROCEDURE AND SOURCES OF ERROR

The procedure for liquidus temperature determination consists of a sample preparation step and a temperature measurement step. A discussion of the complete procedure and sources of error follows.

Sample Preparation - The hot-wire technique requires that a small sample, usually around one milligram, of known composition, be held by capillarity on a thermocouple junction. Samples of this size are, however, quite difficult to prepare. Hence, representative samples of a larger master sample of known composition are studied. To insure that representative samples are obtained, most investigators have thoroughly mixed a several-gram sample of the oxide mixture. The sample is then fused, equilibrated for approximately an hour and quenched to prevent segregation during solidification. The master sample is then finely ground and if necessary, fused, etc. again. Hot-wire samples are taken by moistening the thermocouple junction and inserting the junction into the finely powdered master sample. The moisture in the small sample is then driven off by heating the sample above 100°C and holding it at that temperature for several minutes.

Perhaps the most serious error when using the hot-wire technique is associated with obtaining a representative sample of the oxide mixture. Sample homogeneity, however, is easily checked using the hot-wire technique, as a sample that is not well mixed will produce a wide band of experimental results for the same master slag sample.

Temperature Measurement - After drying a sample on the thermocouple, the sample is usually heated until molten and held for several minutes. The sample is then slowly cooled until the first crystal

solidifies within the melt and the temperature is noted. The temperature at which this crystal is in equilibrium with the melt is the liquidus temperature of the sample. It is usually best to determine a rough estimate of this temperature and then refine the value by slowly heating and cooling the sample in the temperature range around the initial estimate.

Another experimental error can arise if formation of the first crystal of solid does not occur at the thermocouple junction. As shown by Cavalier[11], temperature differences as large as 30°C can exist within the oxide sample. It is, therefore, necessary that the first crystal which solidifies from the melt be in equilibrium with the melt and at the thermocouple junction.

Several different methods have been used to correct this problem. A second small thermocouple which has been inserted into the melt has been used to measure the liquidus temperature[11,12]. In this procedure, the second thermocouple acts like a heat sink, causing solidification to occur on this thermocouple. However, an error may still be present with this procedure, as the thermocouple wires will tend to carry heat away from its junction, and produce a temperature gradient in the melt. Consequently, care must be taken to measure the liquidus when the first crystal on the secondary thermocouple is stable, i.e. not growing or melting. Perhaps a more satisfactory method for making the first crystal form on the thermocouple junction is to adjust the shape of the thermocouple, i.e. the furnace. In principle, by making the coldest portion of the thermocouple the junction, the first crystalization should be forced to occur at the

junction. In Ordway's[2] and Welch's[3,4] work a V-shaped thermocouple with the junction at the base of the V was used to produce solidification at the junction. Baldwin[5] used a U-shaped element with a smaller diameter junction at the base of the U to obtain the same results. A thermocouple with three leads, the extra lead to facilitate emf measurement, may also result in first solidification at the junction, because of less power generation due to a larger cross-section at this point[13]. There is probably not a single solution to this problem. The type of junction that should be used is probably dependent on the particular experiments. However, regardless of the type of junction used, extreme care must be taken to assure that the first crystal forms on the junction and is stable, to obtain a correct liquidus measurement.

Even when precautions are taken to obtain a stable crystal, it is still possible to make an incorrect measurement. Some oxide mixtures, and especially those high in SiO_2, do not crystallize easily upon solidification[14]. It is thus possible to "miss" the liquidus temperature. Under these circumstances, it is necessary to solidify and crystallize the oxide mixture. Then, slowly heating the solid and observing the temperature at which the last crystal is in equilibrium with the melt will allow measurement of the liquidus[15,16]. Again, care must be taken to have the last crystal at the thermocouple junction. In order for this to occur, it may be necessary to use a differently shaped thermocouple.

When elements such as FeO and/or MnO are present in the oxide, the liquidus may be missed because the sample becomes opaque. To aid

in the observation of solidification within the melt, polarized light or ultra-violet light can be used. However, in general the technique works best for transparent melts and the accuracy decreases as the melt becomes opaque. For transparent melts, overall experimental errors of $\pm$1°C have been obtained in calibration experiments[5]. Errors of $\pm$3°C have been estimated for liquidus temperature measurements[4,5]. Larger errors would be anticipated for melts that were not transparent.

MODIFICATIONS FOR THE CURRENT INVESTIGATION

The vast majority of the previous studies which employed hot-wire microscopy were done on oxide mixtures made of very stable oxides, such as CaO, MgO, SiO_2 and Al_2O_3. For these oxides, almost any atmosphere would be "inert", i.e. would not change the melt composition. Consequently, the studies were done within a small container to minimize temperature variations produced by convection and the container was filled or continuously flushed with air.

In the present work, the effect of the minor constituents of blast furnace slag, such as FeO, MnO, Na_2O and TiO_2, on the liquidus surface of the CaO - SiO_2 - MgO - Al_2O_3 system was to be determined. In this study, the oxygen partial pressure would affect the state of oxidation of the minor constituents. Hence, careful control of the atmosphere at an oxygen partial pressure of 10^{-15} atm. was necessary. A description of the system used to produce a controlled atmosphere for these experiments follows. Several other modifications to the basic hot-wire microscope are also described and the results of several preliminary experiments are given.

Gas System - The standard procedure for fixing the oxygen potential of a gas phase is based upon the reaction

$$CO(g) + \frac{1}{2} O_2(g) = CO_2(g) \qquad (1)$$

$$\text{or} \quad H_2(g) + \frac{1}{2} O_2(g) = H_2O(g) \qquad (2)$$

At equilibrium

$$P_{O_2} = \frac{1}{K_c} \frac{P_{CO_2}}{P_{CO}}^2 \qquad (3)$$

$$\text{or} \quad P_{O_2} = \frac{1}{K_H} \frac{P_{H_2O}}{P_{H_2}}^2 \qquad (4)$$

where P_{O_2}, P_{CO_2}, ... are the partial pressures of O_2, CO_2, ..., respectively. K_c and K_h are the equilibrium constants for reaction 1 and 2, respectively and are both functions of temperature.

In hot-wire microscopy, a very small sample is contained within an otherwise cold enclosure. It was anticipated that a large temperature gradient would exist in the general region next to the surface of the sample, making it impossible to accurately determine the temperature of the gas in this region. Without an accurate temperature, K_c and K_h cannot be determined. Hence, proper gas mixture cannot be made. Therefore, this standard technique would not work for hot-wire microscopy.

The solution to this problem was to build a gas system that produced an inert gas that contained the specified partial pressure of oxygen. This was accomplished by passing dried nitrogen through a

fluidized-bed reactor that contained a mixture of -200 mesh Fe_3O_4 and Fe_2O_3, see Fig. 1.

Equilibrium is attained very rapidly in Fluidized beds[17]. Consequently, the partial pressure of oxygen in the nitrogen was fixed by the Fe_3O_4/Fe_2O_3 equilibrium and was dependent on bed temperature only. A solid electrolytic cell[18] contained in an auxilliary furnace, see Fig. 2, that could be inserted into the gas system was occasionally used to check oxygen partial pressures. Excellent agreement was obtained between calculated values based upon Fe_3O_4/Fe_2O_3 equilibrium and the electrolytic cell. Further verification of the technique was made by replacing the Pt/Pt-10% Rh thermocouple with a Cu/Constantan thermocouple. Measuring the temperature at which the copper oxidized in the atmosphere, again gave good agreement between the calculated and experimental temperatures.

Thermocouples - The manufacture of a large number of small thermocouples for use in the hot-wire unit can be a very costly and time-consuming process. An inexpensive and easily done technique for making small butt-weld thermocouples which had been developed earlier was therefore used[14].

A large number of thermocouples were made by electron-beam welding the edge of a 0.05 mm sheet of platinum to the edge of a 0.05 mm sheet of platinum-10% rhodium. The sheets were then sheered perpendicular to the welded seam to produce thermocouples that had a uniform cross-section and were 0.05 mm thick, 0.2 mm wide and approximately 25 mm long.

For many slag compositions, it was often necessary to perform heating experiments. A thermocouple bent into a U-shape with a

slightly larger bottom than top works well in both heating and cooling experiments, see Fig. 3. The support stantions for the hot-wire unit were made from 0.8 mm platinum and platinum-10% rhodium wires. All other connections to the unit were made from compensating wire. The complete probe is shown in Fig. 4.

Electrical Circuit - An electrical circuit modified from one used by Haupin[19] for measuring thermal conductivities, was used in this study, see Fig. 5. Temperature control to 1°C was attained by using three variacs; one as a coarse adjustment, one as a fine adjustment and one to set the span of the fine adjustment. A Doric DS-100 integrating millivoltmeter was used for emf measurement. This unit together with the low-pass filter in the circuit reduced the ac heating voltage and noise to less than 1 μV and permitted temperature measurement to 0.1°C.

Calibration of the thermocouples and electronics was done by measuring the melting point of $Na_2 SO_4$. The results of many experiments performed on several different thermocouples were always within $\pm$1°C of the published value[20].

Initial Experiments - The effect of small additions of Na_2O on the liquidus surface of the $CaO - SiO_2 - MgO - Al_2O_3$ system were studied first. The result of one set of experiments are tabulated below and shown in Fig. 6. A measurement of the liquidus temperature of the slag without an addition of Na_2O was not made. However, the value of 1513°C obtained by extrapolation of the line fit by least-square regressional analysis. To 0% Na_2O is in excellent agreement with the value of 1510°C determined from the expanded section of the phase diagram determined by Snow[21].

THE EFFECT OF Na_2O ON THE LIQUIDUS TEMPERATURE OF BLAST-FURNACE SLAGS

Sample Number	Weight percentage					Measured liquidus temp °C
	CaO	MgO	SiO_2	Al_2O_3	Na_2O	
2_1	48.66	3.97	36.75	10.16	(0.43)	1502 ± 1
2_2	48.71	3.98	36.78	10.17	(0.35)	1503 ± 2
2_3	48.54	3.96	36.66	10.13	(0.69)	1488 ± 2
2_4	48.77	3.98	36.82	10.18	(0.23)	1504 ± 2
2_5	48.79	3.98	36.84	10.19	(0.17)	1506 ± 2

Compositions listed in parentheses have been determined by chemical analysis.

CONCLUDING REMARKS

The hot-wire microscope with its maximum operating temperature of 2150°C under reducing, neutral or oxidizing conditions, has been shown to be a useful tool for determination of the liquidus temperatures of oxide mixtures. Because of its simplicity and low cost, the technique should be considered by phase diagram researchers, when dealing with transparent or semi-transparent melts.

ACKNOWLEDGMENTS

The author wishes to thank Janna McIntosh and Sabri Arac for their help in preparing this paper. The American Iron and Steel Institute is also gratefully acknowledged for financial support of the blast furnace slag work.

REFERENCES

1. Joly, J., Proc. Rev. Irish Acad. 2 (1891), 38.
2. Ordway, F., J. Res. Nat. Bur. Stand. 48 (1952), 152.
3. Welch, J. H., J. Sci. Instrum. 31 (1954), 458.
4. Welch, J. H., J. I. S. I. 183 (1956), 275.
5. Baldwin, B. G., J. I. S. I. 186 (1957), 388.
6. Welch, J. H., British Patent Application No. 24573/59, 1959.
7. Welch, J. H., J. Sci. Instrum. 38 (1961), 402.
8. Mercer, R. A. and Miller, R. P., J. Sci. Instrum. 40 (1963), 352.
9. Miller, R. P. and Sommer, G., J. Sci. Instrum. 43 (1966), 293.
10. Gutt, W., J. Sci. Instrum. 41 (1964), 393.
11. Cavalier, G., Cer. Bul. 39 (1960), 142.
12. Derge, G., Trans. AIME 239 (1967), 1480.
13. Causer, R. L., J. Sci. Instrum. 43 (1966), 650.
14. Fine, H. A., Sc. D. Thesis, M.I.T., Cambridge, Mass., 1973.
15. Ohno, A. and Ross, H. U., Can. Met. Quat. 2 (1963), 243.
16. Rennie, M. S. et al., J. S. African Inst. Min. Met. 73 (1972), 1.
17. Frantz, J. F., Chem. Eng. 69 (1962), 89.
18. Kiukkola, K. and Wagner, C., J. Electrochem. Soc. 104 (1957), 379.
19. Haupin, W. E., Cer. Bul. 39 (1960), 139.
20. Handbook of Chemistry and Physics, 48th ed., Chemical Rubber Co., Cleveland, Ohio, 1967, p. 13-226.
21. Snow, R. B., Proc. Blast Furnace, Coke Oven and Raw Mat. Conf., AIME, 1962, p. 21.
22. Arac, S., M. S. Thesis, U. of AZ., Tucson, Arizona, 1976.

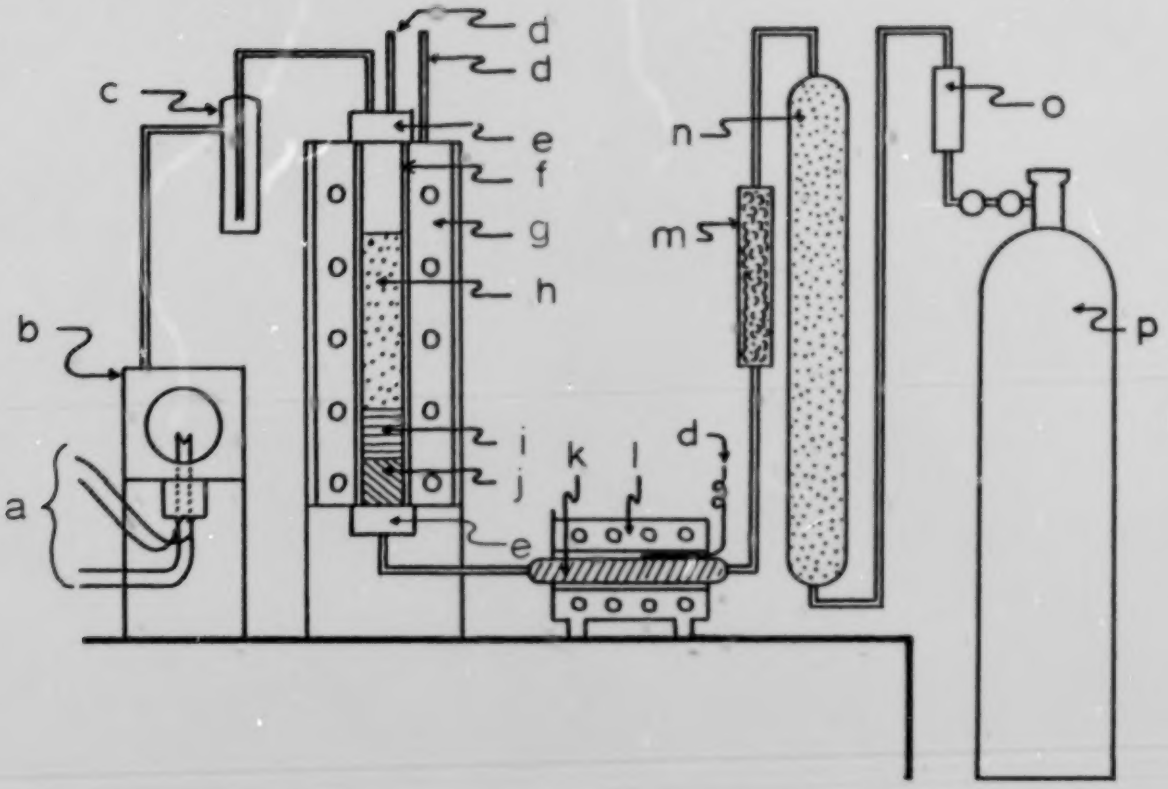

Fig. 1 Gas system; (a) hot-wire thermocouple leads, (b) hot-wire unit and container, (c) dust filter, (d) chromel/alumel thermocouple , (e) brass fitting, (f) quartz tube, (g) tube furnace, (h) Fe_3O_4/Fe_2O_3 fluidized bed, (i) quartz wool, (j) mullite chips, (k) pyrex wool, (l) tube furnace, (m) P_2O_5, (n) drierite, (o) flow meter, and (p) N_2 supply. All other gas connections were made with pyrex glass. (Modified from Ref. 22).

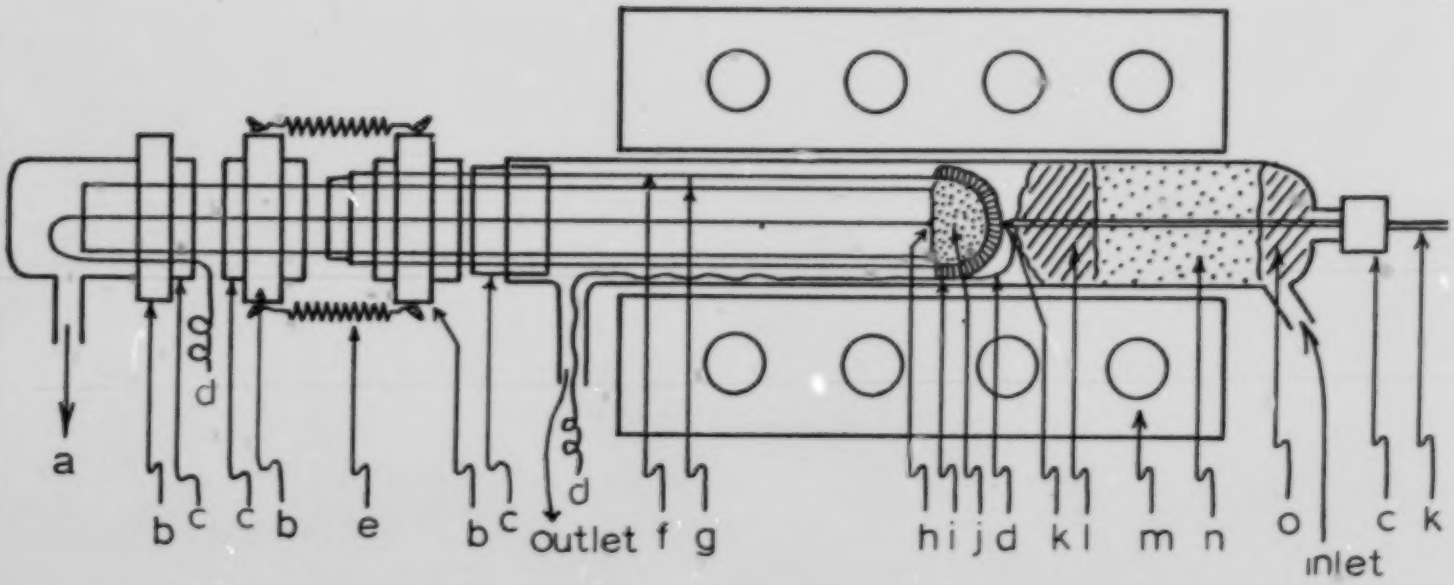

Fig. 2 Oxygen probe; (a) to vacuum pump, (b) metal clamp, (c) rubber seal, (d) Pt wire, (e) springs (f) lime-stabilized Zirconia tube, (g) mullite tube, (h) Pt foil, (i) Pt-gauze, (j) Ni/NiO reference electrode, (k) chromel/alumel thermocouple, (l) quartz wool, (m) tube furnace, (n) silica sand, (o) pyrex wool. (Modified from Ref. 22).

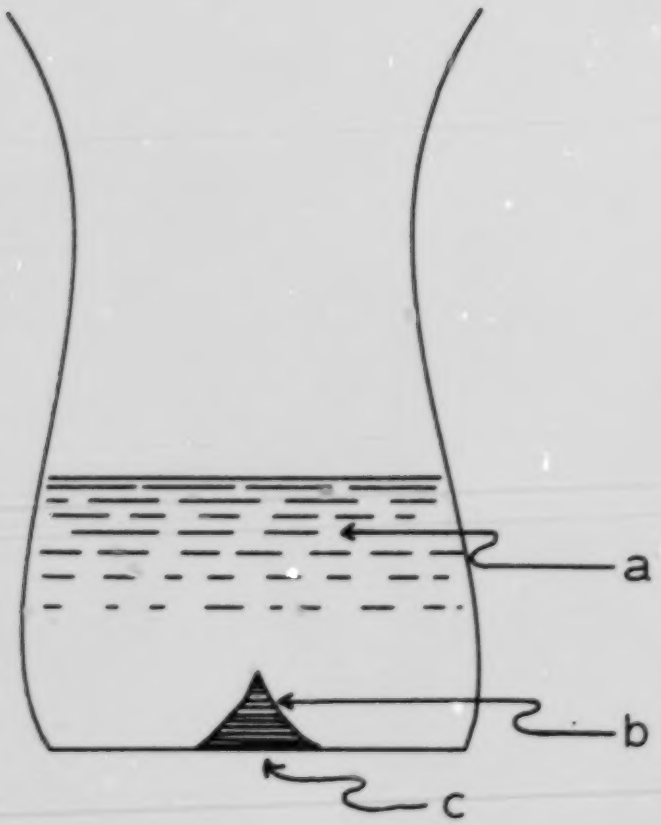

Fig. 3 Schematic representation of hot-wire thermocouple; (a) melt, (b) first crystal, and (c) thermocouple junction (Modified from Ref. 22).

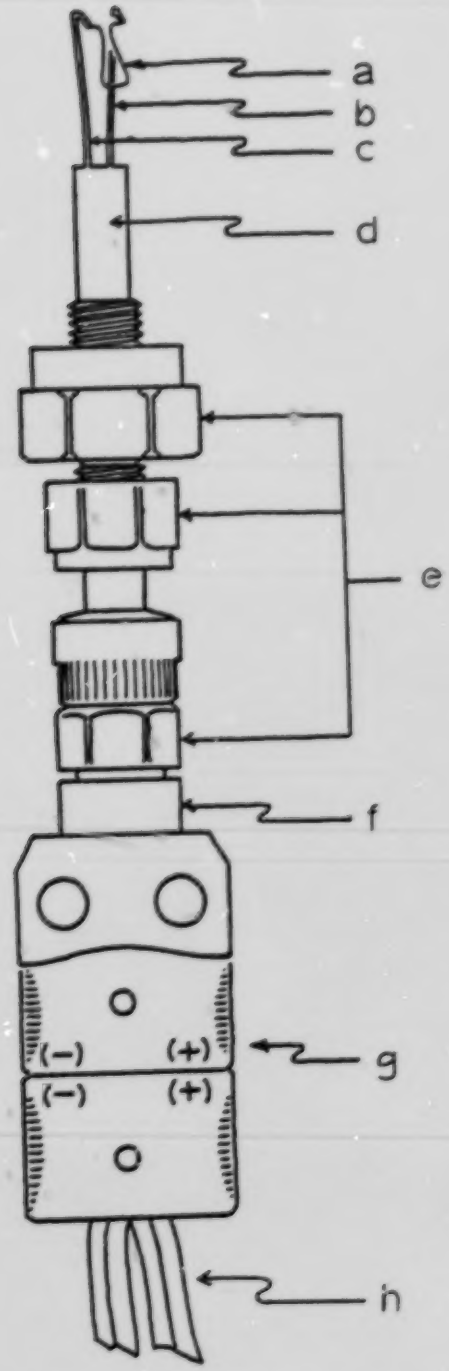

Fig. 4 Complete hot-wire assembly; (a) thermocouple, (b) Pt support and lead, (c) Pt-10% Rh support and lead, (d) Al_2O_3 insulator, (e) Swage lok fittings, (f) tube clamp, (g) Omega Eng. thermocouple connector, and (h) compensating wire for Pt/Pt-10% Rh thermocouples (Modified from Ref. 22).

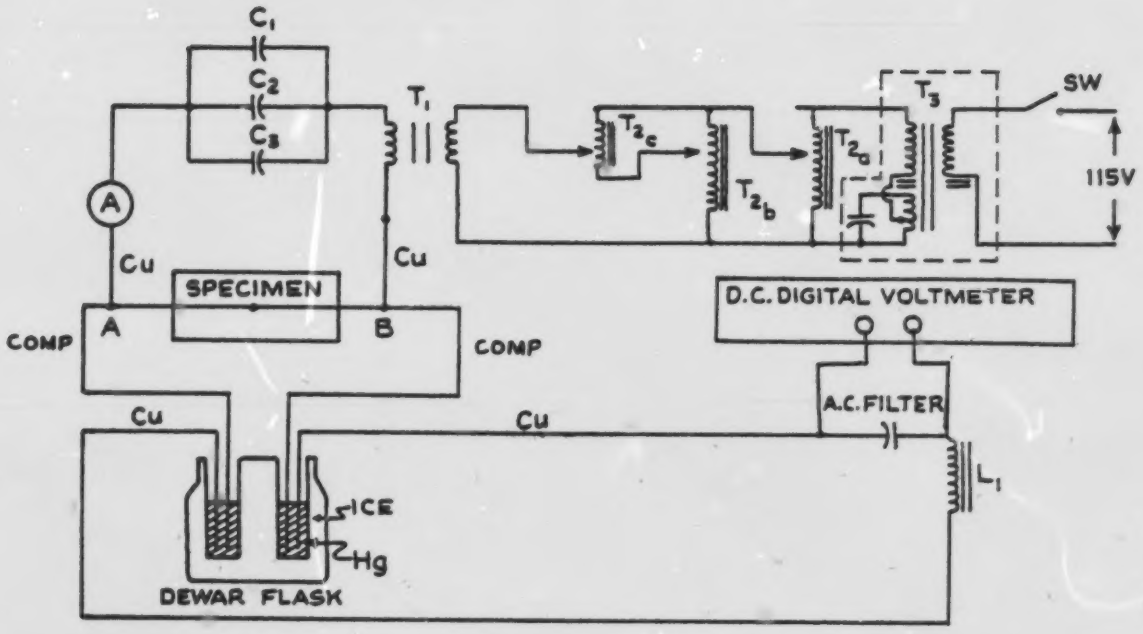

Fig. 5 Schematic diagram for electronic circuit; (C_1, C_2, C_3) 250 μF, 2.5 V ac electronic capacitor, (C_4) 500 μF, 1.5 V dc electronic capacitor, (L_1) 10H, 200 mA, 140 Ω choke, (T_1) 115 to 25 V, 250 VA transformer, (T_2) 115 V, 420 VA variable transformer, (T_{2_A}) coarse adjustment, (T_{2_B}) span adjustment, (T_{2_C}) fine adjustment, (T_3) 115 V, 250 VA voltage regulating transformer, (A) 0-5 A ammeter, (S W) on-off switch, (Cu) copper wire, and (Comp) compensating wire. (Modified from Ref. 19 and 22)

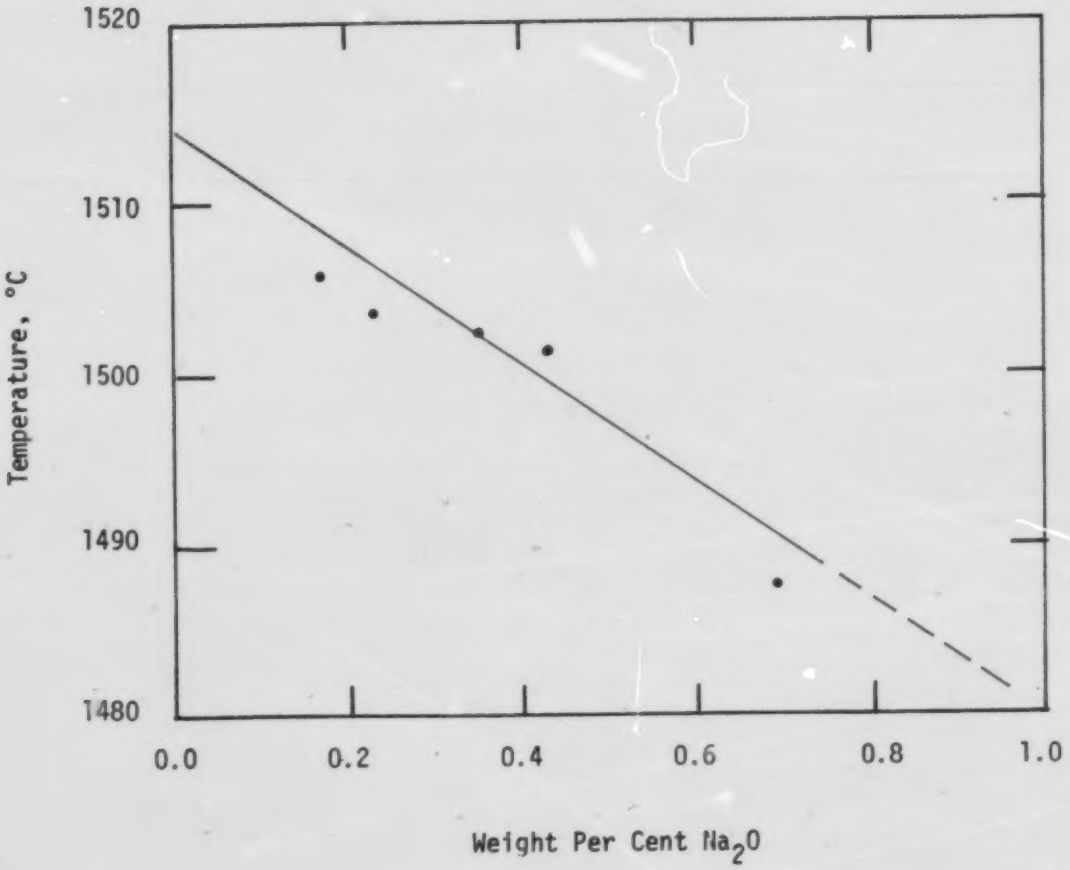

Fig. 6 The effect of Na_2O on the liquidus temperature of an oxide melt having a % CaO + % MgO/% SiO_2 + % Al_2O_3 ratio of 1.12.

National Bureau of Standards SP-496, Applications of Phase Diagrams in Metallurgy and Ceramics
Proceedings of Workshop held at NBS, Gaithersburg, Md., January 10-12, 1977

EXPERIMENTAL TECHNIQUES IN PHASE DIAGRAM DETERMINATION OF SUPERCONDUCTING COMPOUNDS CONTAINING VOLATILE COMPONENTS AT TEMPERATURES UP TO 2200 °C

by

R. FLÜKIGER and J.-L. JORDA

Département de Physique de la Matière Condensee
24, quai Ernest-Ansermet
1211 - Geneve - 4
Switzerland

I - INTRODUCTION

In addition to their individual metallurgical properties, a great number of binary and ternary intermetallic compounds possess a further important property : they are superconducting. The superconducting transition temperature, T_c, of a compound is strongly related to its electronic structure and phonon spectrum. It is now widely accepted that to a well-defined superconducting bulk compound there corresponds a well-defined value of T_c. Within the homogeneity range of a given crystallographic structure, T_c has been found to vary more or less with the atomic composition. Thus superconductivity can be used as an additional technique in establishing phase diagrams. This means in turn that a precise knowledge of the phase field gives some indication about the maximum value of T_c which can be reached in a given phase.

The technically most promising superconductors known to date, such as the A15 type compounds or the $R\bar{3}$ type compounds (Chevrel phases), generally form at temperatures well above 1700°C. Almost all of them contain at least one volatile component, e.g. Ga, Al, Sn,... for the A15 type compounds or S, Se, Te, Pb, Sn... for the $R\bar{3}$ type compounds. At the formation temperature of these superconducting phases, i.e. in the range of $1700 < T < 2200$°C, the contamination of the alloys by the crucible material or by impurities in the heating chamber becomes increasingly important. Furthermore, the evaporation of such a compound at these temperatures increases the fluctuations on the DTA base line, which

in addition shows a more or less important curvature, thus rendering the detection of thermal arrests very difficult. The analysis under these conditions presents another inconvenience, namely the short lifetime of the measuring cell which may be affected by the reactivity of the metal vapors either with the thermocouples or with the ceramics. It is thus not surprising that the high temperature phase fields of the majority of these systems are far from being really known.

In this article we will show from some selected cases that the high temperature details of the phase field of a superconducting phase are of importance in attempting to reach the maximum superconducting transition temperature for a given compound. It should be noted that the precise determination of these high temperature details has to be carried out very carefully in order to prevent contamination. The high temperatures involved require specially designed measuring devices, which will be described in detail.

II - EXPERIMENTAL TECHNIQUES

From the above mentioned difficulties encountered in the study of the high temperature part of compounds containing volatile components, it follows that the results obtained using a given experimental device have to be treated with scepticism,unless their accuracy has been confirmed by other experiments under different conditions. Even still, when changing the experimental conditions one has to be careful to eliminate the causes which really influence the measured values.

On the other hand, the extreme concentrations in a phase field, which are often stable at high temperatures only, have to be quenched at sufficiently high rates in order to be retained for a subsequent analysis. Quenching experiments are, however,

dependent on kinetics and thus give only an indirect image of the high temperature behavior. This image does not necessarily correspond to the real situation: it can even represent a non-equilibrium. Thus quenching experiments alone cannot give a definite answer to the question of the equilibrium phase limits at high temperatures. The only way of solving the problem with accuracy is to combine the quenching experiments with the direct high temperature observations.

A. DIRECT METHODS OF OBSERVATION

By direct observation methods we define all techniques which are independent of kinetics, i.e. which reflect the real behavior at high temperatures. The methods used in the present investigation are described in the next section.

A.1. Differential Thermal Analysis (DTA)

The commonly used method for the detection of phase transformations at high temperatures is DTA {1}. A DTA apparatus working up to 2200°C under an inert gas pressure up to 10 atm. is not commercially available : it was thus necessary to develop such a device. Carbon was found to be the heating resistance material having the longest lifetime under the required working conditions. In order to ascertain that the carbon impurities did not affect the phase relations of interest, we have compared the DTA results of all investigated systems with those obtained using a carbon-free device, which will be discussed in Section A.2. Theoretically, the best material for the heating resistance is tungsten. It was excluded because of its brittle nature, which is mainly caused by recrystallization and reaction of the tungsten with small amounts of oxygen present in the furnace atmosphere. The latter is contained in the argon (99.995%) or arises from the water adsorbed at the surface of the ceramics or of the furnace walls.

Our cylindrical carbon resistance, supplied by Sétaram (France), has a total length of 400 mm and an inner diameter of 34 mm. By applying a power of 8 kw, it develops a temperature of 2400°C at the hot zone. The resistance has a complex shape, designed for a homogeneous temperature zone of approximately 40 mm length at 1900°C. The temperature gradient in this zone, parallel to the axis of the cylinder is of the order of 0.5°C/cm. Due to the considerable length of the heating resistance, the sample-holder has a total length of 450 mm. In order to avoid the mechanical problems due to the softening of the central 4-hole BeO tube at high temperatures, it was mounted so that it hung from the top of the furnace. The details of this holder are shown in Fig. 1. The materials used for its construction are BeO and molybdenum, which form a cylindrical box of the approximate size of the homogeneous zone. The samples, contained by small BeO crucibles, are located at the centre of the box in a plane normal to the axis. The junction measuring the temperature was placed at the centre of this plane. The melting points of platinum (1772°C) and rhodium (1966°C) were used as temperature standards. The size of these crucibles was kept as small as possible in order to minimize the temperature variation in the samples, which is estimated to be at less than 0.1°C. The mass of the crucibles is comparable to that of the samples (0.2 - 0.25g). The BeO crucibles were supported by the thermocouple junctions and the samples separated from the latter by a thin BeO wall of 0.4 mm thickness, thus providing a good thermal contact.

For linear variation of the temperature, a proportional feedback temperature programmer was used. It was driven by a supplementary W-3% Re vs. W-25% Re thermocouple placed just below the sample-holder. The DTA signal was measured with a nanovoltmeter and registered with a multi-channel recorder. All parts of the sample-holder can serve for numerous runs, except the thermocouples, which have to be changed after 10 to 20 runs, depending on the substance under investigation and on their thickness (which, in our experiments, varied between 0.25 and 0.5 mm). Apart from the above mentioned non-linear deviations of the base-line, the described DTA apparatus enables very sensitive measurements up to 2200°C or more to be made. As an illustration, we have presented the results of a DTA run on the alloy $Nb_{.74}Ga_{.26}$ in Fig. 2. Although this apparatus works satisfactorily under these conditions, the measured thermal arrests may be affected by several parameters such as the carbon and the oxygen content of the furnace atmosphere and the choice of the crucible material. In order to determine if these parameters had some influence on our DTA results, two methods, described in the next sections, appeared to be particularly useful in this respect.

A.2. Simultaneous Stepwise Heating

The obvious advantage of a long-life carbon heating element is counter-balanced by the presence of carbon impurities in the furnace atmosphere. Therefore the DTA results obtained have to be confirmed by measurements effectuated under the same conditions as in the DTA apparatus, but in a carbon free atmosphere. The horizontal lines in the phase diagram, such as eutectic or peritectic temperatures appear to be particularly convenient for the proposed comparison. We have checked these temperatures by using a very simple technique, "simultaneous stepwise heating", which is based

on the fact that the number of liquid phases changes by crossing the eutectic or a portion of the peritectic line. This technique consists of heating pieces of the same master sample at different temperatures above and below the desired eutectic or peritectic temperature. After cooling, they are analyzed visually or microscopically in order to decide if the solidus had been reached during the high temperature exposure. The step between the annealing temperatures being of the order of 5°C, the value of the eutectic or the peritectic temperature can be found with good precision, and can be compared with that obtained by DTA.

When studying the phase diagrams of the binary systems Nb-Ge and Nb-Ga, we found in addition that this technique furnishes precise information on the extreme Ga or Ge solubility in the A15 phase if several samples of different, but neighbouring compositions are heated simultaneously. It is thus possible to study at the same time the influence of carbon impurities on the eutectic or peritectic temperature and the extreme composition of a given phase which renders the method as being quite powerful.

Fig. 3 illustrates the high temperature cell which was used for the "simultaneous stepwise heating" experiments. These were carried out in a 30 kW high frequency furnace under the same pressure conditions with the same inert gas as in the DTA apparatus. The samples were contained in BeO crucibles located inside a double walled molybdenum cylinder, which, in turn, was placed in a tantalum susceptor. Because of the cylindrical symmetry, the difference in temperature between the samples is less than 5°C at 1800°C. As for DTA, the temperature was measured with a W-3% Re vs. W-25% Re thermocouple, which was in good thermal contact with one of the BeO crucibles.

A.3. Thermal Analysis on Levitating Samples

At first sight, the possible influence of the crucible material on the DTA results seems to be easily avoidable by using different materials. However, the number of commercially available ceramics which can be used at 1800°C and more is small. In addition, the costs of DTA crucibles of the same shape as in Fig. 1 made from ThO_2 or HfO_2 are prohibitively high. The generalized use of BN at T>1800°C is problematic because of the hygroscopic behavior of this material. A technique which completely eliminates the problem of contamination by crucibles is electromagnetic levitation, introduced by Fogel et al.(2). We performed the thermal analysis on levitating samples weighing 1-2 g using a 30 kW h.f. generator at a frequency of 300 kc and a watercooled Cu induction coil as shown in Fig. 4.

As in usual thermal analysis, the temperature of the sample is varied by a gradual change of the generator power. The sample temperature was measured with a Leybold two-color pyrometer.

The main problem arising from such temperature measurements lies in the unknown behaviour of the emissivity of our alloys as a function of the observing wavelength of the pyrometer (4500 and 6500 Å). The observed alloys, however, do not necessarily behave like grey bodies, as required for an accurate temperature determination with a two-color pyrometer. In addition, the window absorption has to be corrected, even using a two-color pyrometer, which disagrees with the currently used selling arguments for these instruments. Thus, a reliable determination of the temperature requires a calibration of the pyrometer. This calibration has been carried out by measuring simultaneously the temperature of a sample with a thermocouple and the pyrometer, up to 1900°C. The sample was placed in a BeO crucible which was contained by the "simultaneous stepwise heating" device discribed above (Fig. 3).

With the variation of the composition on a given binary system, as Nb-Ge or Nb-Ga, the emissivity is expected to undergo a variation. Nevertheless, we have found that a horizontal line (the eutectic), as it occurs in the systems Nb-Ga and Nb-Ge can be reproduced as a horizontal line by the pyrometer method. This indicates that for these systems the variation of the emissivity as a function of the Ga or the Ge concentration, at least for the mentioned composition range, can be neglected. This is a very encouraging argument for the proposed technique, which, in addition to the elimination of the crucible problem, presents another advantage: rapidity. In fact, since the sample is the only part heated, the furnace is ready to be opened a few minutes after the measurements. We are currently trying to improve this thermal analysis method, the precision in the absolute temperature beeing better than 15°C at 1800°C. A more detailed work is in press (13).

B. INDIRECT METHODS OF OBSERVATION

In order to retain a high temperature phase or a composition of this phase which is stable at high temperatures only, more or less severe quenching is necessary. The quenching rete is considered to be sufficient if it is higher than the rates of phase transformations or segregation occurring during the cooling process. However, from the analysis of a quenched sample alone it cannot be affirmed with certainty if it really reflects the equilibrium high temperature relationships: it may represent a non-equilibrium situation due to an insufficient cooling rate. The latter possibility has to be taken into account, particularly if solid samples have to be quenched. Liquid samples of the same material can be quenched at much higher rates.

B.1. Splat Cooling on Liquid Samples

This method was first used by Duwez et al.(4) and has since been modified by many authors. We used a combination of magnetic levitation and two watercooled Cu pistons, an illustration of which is shown in Fig. 4. By suddenly switching off the h.f. power, the levitating, molten sample falls through the levitation coil and is squeezed by the polished front of the Cu pistons, which are accelerated against each other by two strong electromagnets. The magnets are activated by the h.f. power switch with an appropriate time delay which takes into account the falling time of the sample. The thickness of the splat-cooled sample varies between 50 and 100 μ, the initial quenching speed being estimated at $\sim 10^6$ °C.

B.2. Argon Jet Quenching on Solid Samples

A solid sample can be quenched by falling into a liquid metal

(Ga or Ga-Sn) or an oil bath. However, this method has a disadvantage: as the hot sample enters into the bath, the liquid in contact with its surface evaporates, forming an insulating layer which reduces the heat exchange and thus the cooling speed. We have used another method, the argon jet quenching, which allows higher cooling rates to be reached, provided the sample is small enough. On samples having a mass of 0.3 g, we have measured initial quenching rates of the order of 10^4 °C, i.e. 100 times less than for the splat cooled samples.

Our argon jet apparatus (Fig. 5) was mounted in an h.f. furnace, which has the advantage that the total mass of the heated assembly is small, which is a stringent condition for a rapid quench. The argon gas is introduced through a thin-walled tantalum tube into the high temperature cell. This cell consists of a double-walled molybdenum cylinder made from rolled Mo sheets of 0.1 mm thickness. It is designed in such a manner that the top and the bottom of the cylinder can be blown away by the argon jet, leaving the thermocouple in place. The sample hangs on a tantalum wire fixed inside the tantalum tube and is located at the centre of the cell, just above the W-3% Re vs. W-25% Re thermocouple.

C. SUPERCONDUCTIVITY AS A SUPPLEMENTARY ANALYSIS METHOD.

The analysis of the samples studied has been carried out by classical methods, such as metallography, microhardness, X-ray diffraction combined with chemical and electron microprobe analyses. For a more detailed description of these current analytical methods, we refer to the articles which deal with the Nb.Ga(5) and Nb-Ge phase diagrams. In this section we discuss the role of the superconductivity and, more precisely, the superconducting transition temperature, T_c, as an additional analytical method in the determination of the phase limits of a given phase.

The value of T_c characterizes a bulk superconducting compound as well as for example the lattice constant: there is a reproducible relation between the variation in composition within the homogeneity range of a superconducting phase and the variation of T_c. For hexagonal phases this may be illustrated by Fig. 6. This figure shows only a small part of the known data, the other systems having been omitted for clarity. Since the crystal structures of the compounds represented in Fig. 6 are disordered (A3 type structures), the attainment of T_{cmax} (shown by arrows in the lower figure) depends only on the quenching speed, which has to be fast enough to retain the extreme concentration limit of the superconducting phase after high temperature treatments at the appropriate temperature. This compositional effect also works for ordered phases such as the A15 type compounds. However, for the latter compounds, the situation is somewhat complicated by the fact that rapid quenching introduces a partial disordering, thus lowering T_c (see Section III).

C.1. Analysis of the Superconducting Data

The superconducting transition temperature can be determined either by induction methods or by measuring the resistivity of a sample by the four points method. As several measuring devices have been reported in the literature (6), we limit our discussion to the practical problems related to the analysis of the measured T_c values.

Screening Effects

The vast majority of erroneous results on measurements of the superconducting transition temperature of a given bulk sample belonging to a given structure are due to screening effects. These effects are connected with the presence of additional phases having a higher value of T_c than that of the phase

under study. The presence of these additional phases may be due to several causes:

a) the microstructure of the sample shows that the phase of interest is enclosed in a matrix of another phase,

b) an additional phase is formed at the surface due to contamination during the heat treatment in quartz tubes,

c) one of the components of the alloy evaporates during the heat treatment, creating at the surface a layer of the same phase, but at different concentration,

d) the layer formed in c) is of another phase type.

The screening effects are caused by different mechanisms, depending on the measuring technique applied. When measuring the electrical resistance, the superconducting layer at the surface short-circuits the current passing through the sample, thus masking all transitions at lower T_c. On the other hand, the screening effects encountered on inductive measurements are due to the expulsion of the magnetic field at the surface of the superconducting sample(Meissner effect). The surface layer will thus act as a shield which prevents the weak applied magnetic field penetrating the sample.

A layer thickness of several μ is sufficient for a total screening of the lower superconducting transitions. After grinding, the screening effects are thus eliminated for the cases b),c) and d), while they persist for the case a), as to be expected from the microstructure. For this case, the lower superconducting transitions appear only after the crushing of the samples down to particles of the order of the grain size. From these remarks it can be said that in order to determine the value of T_c which really corresponds to the measured bulk sample, it is generally useful to grind the sample at the surface and then to crush it down to 10μ particle size.

III - RESULTS

The binary compounds having the highest known value of T_c are Nb_3Ge (23.2°K {7}) and Nb_3Ga (20.7°K {8}). Both systems contain a component which can be said to be volatile at the formation temperature of the A15 phase in these systems, i.e. higher than 1800°C. This is illustrated in Fig. 2 which shows for the alloy $Nb_{.74}Ga_{.26}$ an increased evaporation at the liquidus temperature. In addition, we found in our investigations that these compounds react with most crucible materials and thus particular attention has been paid to this problem. The techniques described in this article appear to be the most convenient for studying the high temperature behavior of these systems.

A. The system Nb-Ga

The phase diagram of the binary system Nb-Ga has been studied by several authors, who have centered their attention on the superconducting A15 phase. Some recent works have been published by Webb et al. {7}, Oden et al. {9}, Feschotte et al. {10} and Ashby et al. {11}. A very careful investigation of the high temperature part which was recently undertaken in our laboratories using the techniques described above is currently in press {5}. A comparison of the A15 phase fields reported by the different authors, shows that there is general agreement concerning the peritectic formation of this phase which was found to occur between 1850°C {11} and 1900°C {9}, {10}. The A15 phase limits, however, vary considerably from one author to another : they have been reproduced in Fig. 7 for comparison. It is seen that the Ga-rich limit and particularly its variation with temperature, is controversial. All the phase limits in Fig. 7 having been obtained by means of the electron microprobe, this illustrates the drastic variation between

different investigations which can be attributed to the use of different standard materials and different correction programmes. In one case {11}, the oxygen content of the samples may cause a shift in composition. We have checked our microprobe results {5} by comparing them with the maximum weight loss observed after arc-melting under an argon pressure of several atmospheres. From this comparison it follows that the maximum error of our microprobe results is around ± 1 at.%. Another important point is the shift of the Ga-rich A15 phase limit with temperature : its maximum value was determined to 2 at.% by Feschotte et al. {10} and Ashby et al. {11}, while Jorda et al. {5} reported 4.2 at.%. This discrepancy is essentially due to the different cooling rates after high temperatures annealings : it was found that initial quenching rates of more than 10^3 °C/sec, obtained by spraying with an argon jet, are necessary to prevent the segregation which occurs on cooling. Webb et al. {8} obtained similar cooling rates by dropping the samples in a Ga-Sn bath, while the same method, used by Ashby et al. {11} who replaced the Ga-Sn bath by water, was apparently not successful. This is shown by an analysis of the lattice constants (Fig. 8) : the values obtained for the water-quenched samples {11}are considerably higher than those obtained by dropping in a metal bath {7} or by argon jet quenching {5}, thus suggesting Ga contents markedly lower than 25 at.%. It therefore appears that the segregation into the A15 + Nb_5Ga_3 phases, which could not be avoided, is responsible for the apparently temperature independent Ga-rich phase limit.

If such a curved phase limit really corresponds to the equilibrium, it must be reversible. Jorda et al. {5} confirmed this reversibility on the basis of micrographic observations, lattice constant measurements and microprobe analysis. However the best method for demonstrating this reversible behaviour is seen from superconductivity measurements, as was recently found {12}. From the results shown in Fig. 9 it is seen that the superconducting temperature T_c increases strongly

with the temperature at which the samples were treated before argon jet quenching. This increase of T_c is correlated with the variation of the Ga solubility in the A15 phase, which occurs after quenching from different temperatures. The highe[illegible] value of T_c (18°K) corresponding to the stoichiometric composition could be obtained after quenching from 1740°C, the eutectic temperature.

Subsequent annealings at temperatures low enough so that segregation does not occur (<700°C) cause an increase of the long-range order (LRO) parameter {13}, {14} and thus a further increase of T_c to its maximum value, 20.7°K {8}, {12}.

This example shows a concrete application of the superconductivity as a supplementary argument in determining the precise limits of a given phase, which is of course connected with the problem of determining the maximum possible value of T_c in a compound. For Nb_3Ga, the "simultaneous stepwise heating", together with the electron microprobe and DTA measurements suggest that the stoichiometric composition has been reached within less than 1 at.%. A spectacular further increase of T_c above 20.7°K is thus not to be expected.

B. THE NIOBIUM-GERMANIUM SYSTEM

By means of splat cooling experiments, Matthias et al. {15} suggested that the Ge-rich limit of the A15 phase in the system Nb-Ge had a curved shape, as in the system Nb-Ga : the Ge solubility of the A15 phase increases with temperature, tending towards the stoichiometric composition. This fact was partly confirmed by Pan et al. {16}, who have investigated the complete phase diagram of the system Nb-Ge. In Fig. 10 where we have reproduced the Nb-rich part of their diagram {16}, it is seen that the Ge-rich limit of the A15 phase varies from 18 at.% Ge at 1000°C to approximately 20 at. % Ge at the eutectic temperature. On the same figure we have superposed the shape of the A15

phase field as reported by Müller {17} who found nearly temperature independent phase limits.

The question which arises is whether the quench-induced extension of the A15 phase found by Matthias et al.(15) really corresponds to a high temperature equilibrium situation. The T_c value for Nb_3Ge as found from the quenching experiment was 17^oK, while a value of 23^oK has been reported by Gavaler et al. (18), which they obtained from sputtered samples. It is therefore seen from the lower values of T_c, which are parallel to an increase of the lattice constant, that even splat-cooling experiments do not allow the retention of the stoichiometric composition Nb_3Ge for which T_c is maximum.

It is of fundamental interest to know if the values of T_c above 20^oK really correspond to the binary Nb-Ge compound or if some impurities, introduced during the sputtering process have an effect on its superconducting transition temperature. We thus decided to reinvestigate the high temperature part of the Nb-Ge system. However, the experimental difficulties encountered studying this system are even greater than those for Nb-Ga. The main reason is the extreme reactivity of this material with most refractory ceramics such as Al_2O_3, ZrO_2, BeO and ThO_2, particularly at temperatures above 1870^oC. The only exception is BN which allowed at least one DTA run up to 1950^oC before it also reacted {19}. In all these cases, reaction means that the peritectic temperature was in some cases considerably lowered by the presence of the ceramics, particularly by ZrO_2. It is interesting to note that this lowering effect was observed only on concentrations less than 20 at.% Ge. Thus the only valid measurements for the peritectic temperature have been obtained by using the "simultaneous stepwise heating", using tungsten as crucibles. However, even the tungsten vapor has been found to react at the surface of the samples, thus

lowering their melting points. By reducing the high temperature exposure time, it was possible to limit this effect to the surface. On the other hand, the eutectic temperature, which is only 35°C lower, was measured on samples containing 23 to 30 at.% Ge without difficulty.

Because of the contamination problems already mentioned, the only possible way of obtaining meaningful results seems to be thermal analysis on levitating samples. As described in the preceding section, the actual precision of this technique is not better than ±15°C at 1800°C, but we estimate that our results shown in Fig. 11 are representative.

The thermal analysis on levitating samples is particularly useful in determining the solidus lines of a phase diagram. It is thought that it can be used for the liquidus lines, too. In the case of Nb-Ge however, the evaporation makes the precise determination of the temperature very difficult and additional corrections have to be used. The extent of these corrections is, as yet, unknown, and has to be found by other measurements. This is currently being done in our laboratories.

From Fig. 11 it can be seen that the peritectic and the eutectic temperatures are very close to each other: 1900 ± 15°C and 1865 ± 10°C, respectively. The formation temperature of the Nb_5Ge_3 phase was found to be 2100 ± 20°C at 36 ± 1 at.% Ge, which is just between the values 2150°C and 2065°C, reported by Pan et al.(16) and Müller(17) respectively. The eutectic composition as determined micrographically was found at 26 ± 1 at.% Ge which is comparable to the values given in Ref. 16 and 17, which are 27 and 22 at.% Ge respectively.

The most important value, the maximum Ge solubility of the A15 phase, could not be determined with the desired precision but we estimated it at 22 ± 1 at.% Ge. Further measurements are

in progress to improve the accuracy of this value. Nevertheless, it can be stated without any doubt that the stoichiometric composition is not included in the equilibrium phase field of the A15 phase.

It is thus not surprising that quenching experiments did not produce transition temperatures above 17 or 18°K: this value corresponds to the high temperature phase limit of approximately 22 at.% Ge. This means that the further increase of T_c up to 23°K (18) can be attributed to compositional effects. If we take in account that
a) the superconducting transition temperature of ordered alloys depends only on the composition and the LRO parameter (12), and
b) the variation of 1 at.% in composition causes the same change of 2.5°K for the systems Nb_3Al, Nb_3Ga and Nb_3Sn(12), it appears that a further spectacular increase of T_c for Nb_3Ge is not to be expected.

IV. CONCLUSION

It is a fact that a great majority of high T_c superconductors contain elements which are volatile at their formation temperatures. At these temperatures they are characterized by a strong reactivity with the crucible material which makes the correct determination of the high temperature relationships quite difficult. We have discussed in this paper several methods which seem particularly useful to overcome this problem. We emphasize that a high temperature result on the investigated compounds cannot be accepted as accurate without further confirmation by at least another, independent measurement. This is a consequence of the considerable amount of perturbing factors, such as the contamination by the crucible material,

the oxygen content of the furnace atmosphere, the reaction of the metal vapors with the thermocouples and other materials.

The present work was originally undertaken to study the possibilities of increasing the superconducting transition temperature by extending the phase fields of selected compounds. From our investigations it emerged that superconductivity represents a useful supplementary analytical method for a precise determination of the phase fields. At the first sight, it may seem surprising that low temperature properties can be used for understanding high temperature relationships.The reason becomes apparent, however, if one takes into account the fact that this property (present in a large number of materials) is a function of the atomic composition for a given compound, as for example the lattice constant. This illustrates the role of physical properties as a supplementary means for precise phase diagram determinations.

REFERENCES

{1} W.Wm. Wendtlandt, "Thermal Analysis Methods", Ed. P.J. Elving and I.M. Kolthoff, John Wiley & Sons, 1964

{2} A.A. Fogel, T.A. Sidorova, V.V. Smirnov, Z.A. Guts and I.V. Korkin, Russ. Met., 2, 89 (1968)

{3} J.L. Jorda and R. Flükiger, to be published in J. Appl. Phys.

{4} P. Duwez, "Progress in Solid State Chemistry", Pergamon Press, New York, Vol. 3, p. 377 (1966)

{5} J.L. Jorda, R. Flükiger and J. Muller, to be published in J. Less-Common Metals

{6} A.L. Schavlov and G.E. Devlin, Phys. Rev. 113, 120 (1959)

{7} L.R. Testardi, J.H. Wernick and W.A. Royer, Sol. State Comm. 15, 1 (1974)

{8} G.W. Webb, L.J. Vieland, R.E. Miller and A. Wicklund Sol. State Comm., 9, 1769 (1971)

{9} L.L. Oden and R.E. Siemens, J. Less-Common Met., 14, 33 (1968)

{10} P. Feschotte and F.L. Spitz, J. Less-Common Met., 37, 233 (1974)

{11} D.A. Ashby and R.D. Rawlings, J. Less-Common Met., 50, 111 (1976)

{12} R. Flükiger and J.L. Jorda, accepted by Sol. State Comm.

{13} E.C. van Reuth, R.M. Waterstrat, R.D. Blaugher, R.A. Hein and J.E. Cox, Proc. LT10, Moscow, Vol. 1b, Viniti, p. 137 (1967)

{14} R. Flükiger, J.L. Staudenmann and P. Fischer, J. Less-Common Met., 50, 253 (1976)

{15} B.T. Matthias, T.H. Geballe, R.H. Willens, E. Corenzwit and G.W. Hull, Phys. Rev., 139, A1501 (1965)

{16} V.M. Pan, V.I. Latyscheva and E.A. Shishkin, Phys. Chem. and Metal Phys. of Superconductors, Izd. Nauka, Moscow, p. 157 (1967)

{17} A. Müller, Z. Naturforschung, 25a, 1659 (1970)

{18} J.R. Gavaler, Appl. Phys. Lett., 23, 480 (1973)

{19} BN has to be treated at 1900°C under 1 atm. argon pressure before it can be used as crucible at T > 1800°C.

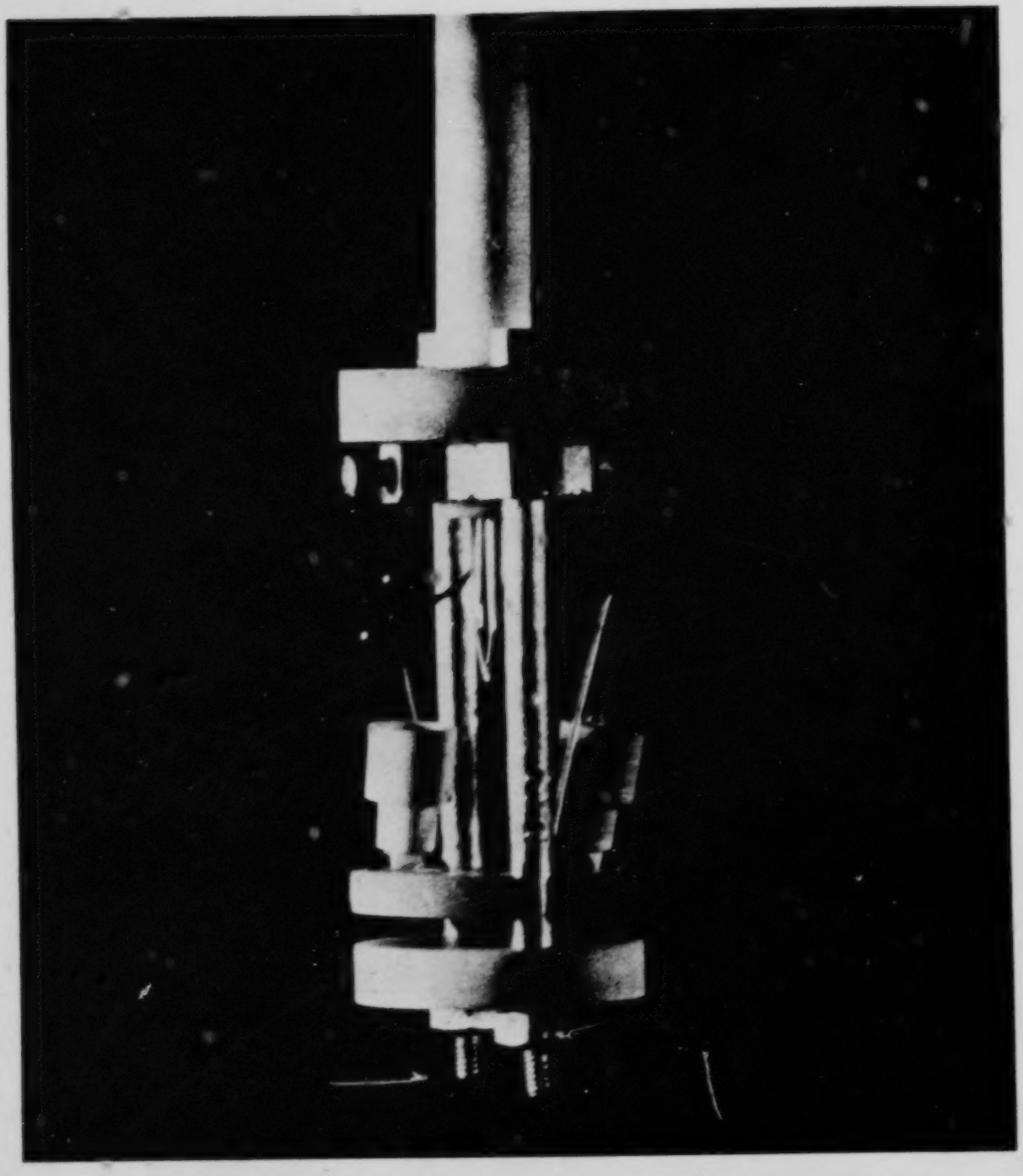

FIGURE 1. The DTA sample-holder used up to 2200°C. It is entirely constructed on BeO and Mo. As thermocouple material, W-3% Re vs. W-25% Re wires of 0.25 or 0.5 mm diameter were used. The BeO crucibles are directly supported by the thermocouple junctions.

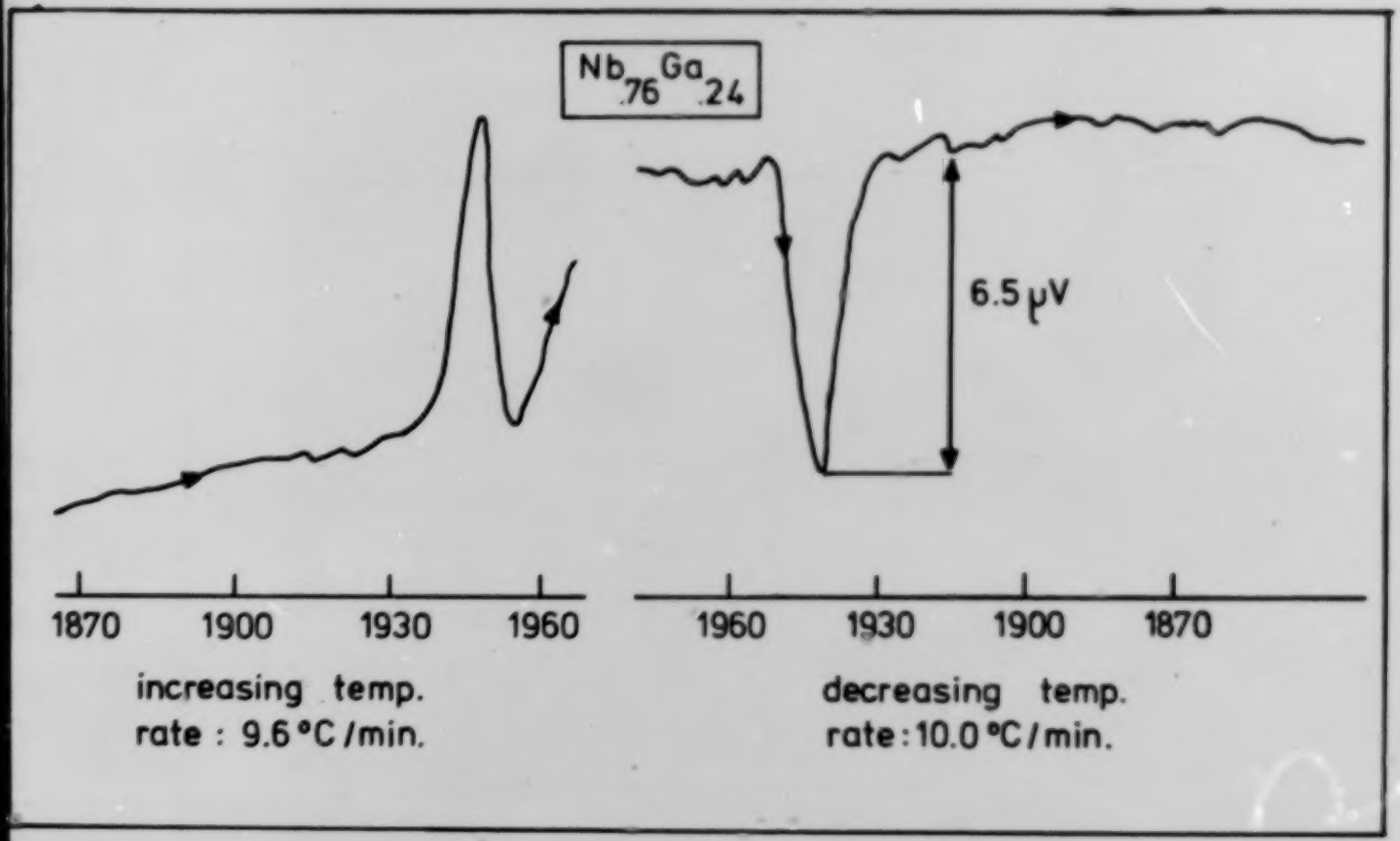

FIGURE 2. A high temperature DTA run of the alloy $Nb_{.76}Ga_{.24}$. The observed thermal arrest corresponds to the liquidus temperature. Note the strong curvature of the base line on increasing temperature, showing beginning evaporation.

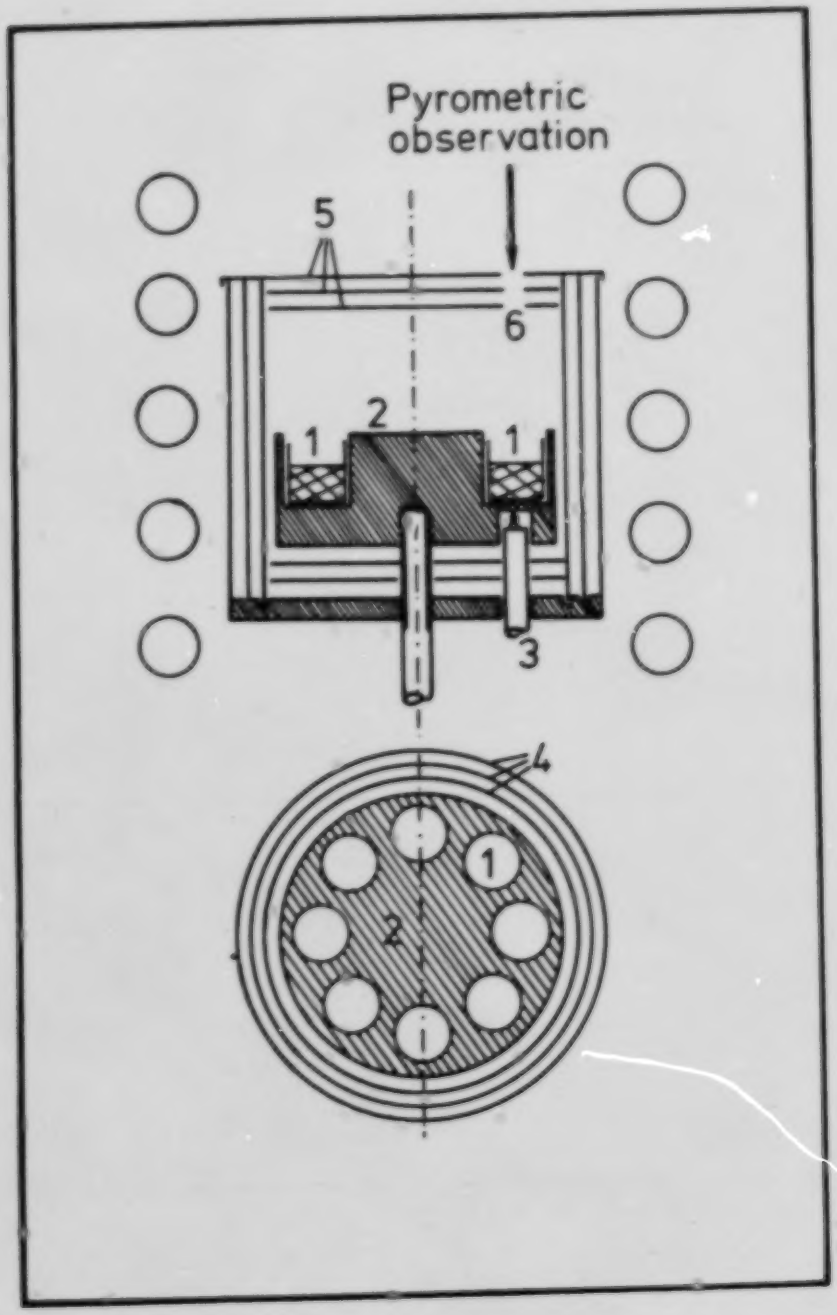

FIGURE 3. The high temperature cell for the "simultaneous stepwise heating", mounted in a HF coil. The sample temperature is measured both by thermocouples and a two-color pyrometer, allowing a "calibration" of the latter for measurements at higher temperatures. 1 : samples, 2 : Molybdenum block, 3 : Thermocouple, 4,5 : Molybdenum shields, 6 : hole for pyrometric observation.

FIGURE 4. Splat cooling device, consisting in a levitation coil and two copper pistons which are accelerated against each other.

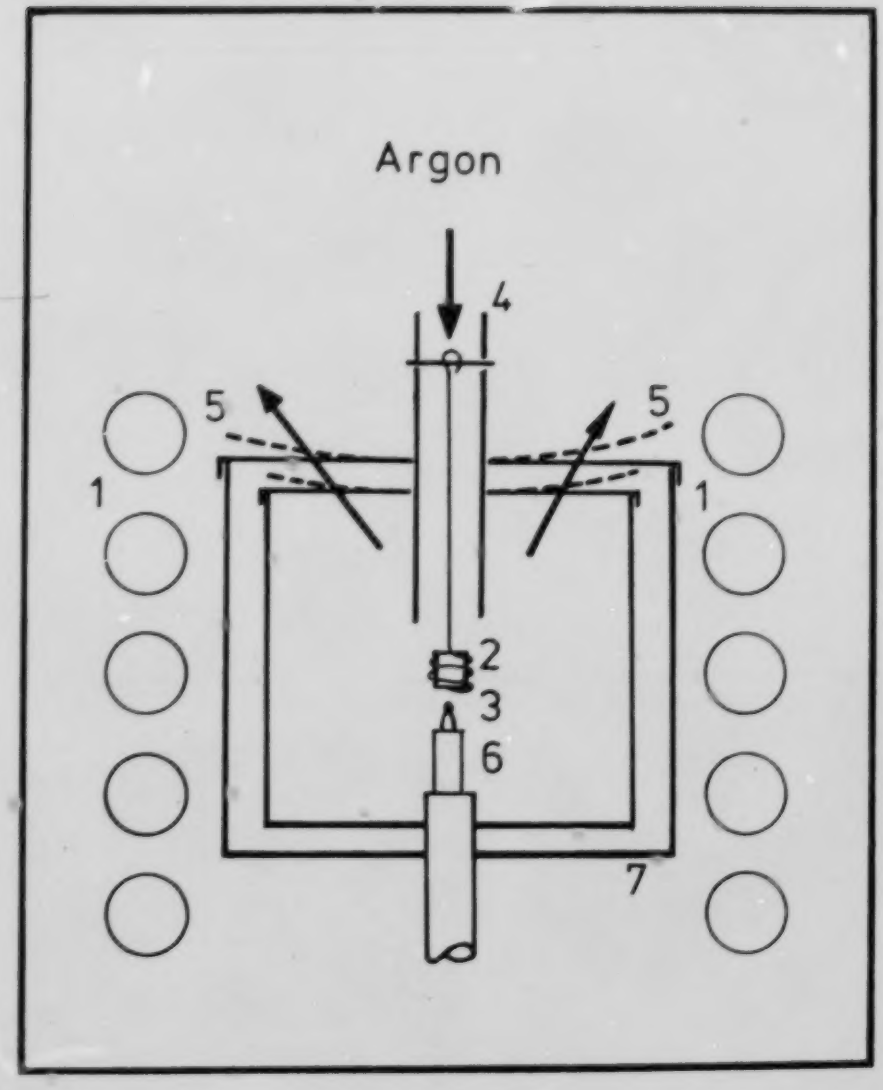

FIGURE 5. The argon jet quenching device. 1 : HF coil, 2 : sample, hanging on a tantalum wire, 3 : Thermocouple, 4 : Tantalum tube, 5 : Molybdenum lid, is blown away by the argon jet, 6 : 2 hole BeO tube for the thermocouple wires.

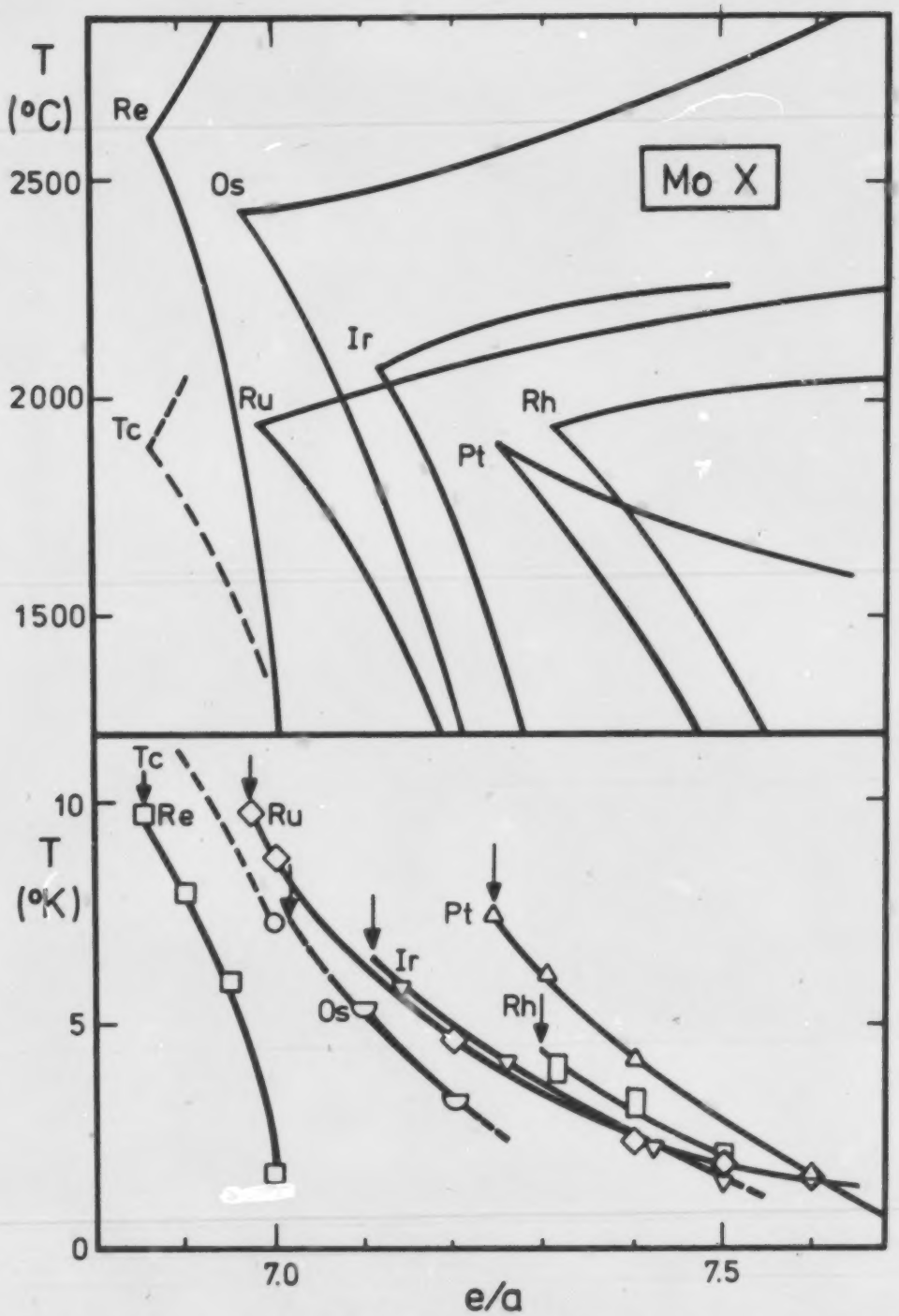

FIGURE 6. The dependence of T_c on the number of electrons per atom for several hexagonal Mo-X compounds. The arrows denote the highest value of T_c in a given system, corresponding to the extreme solubility limit of the hexagonal phase at high temperature, as it follows from the upper picture.

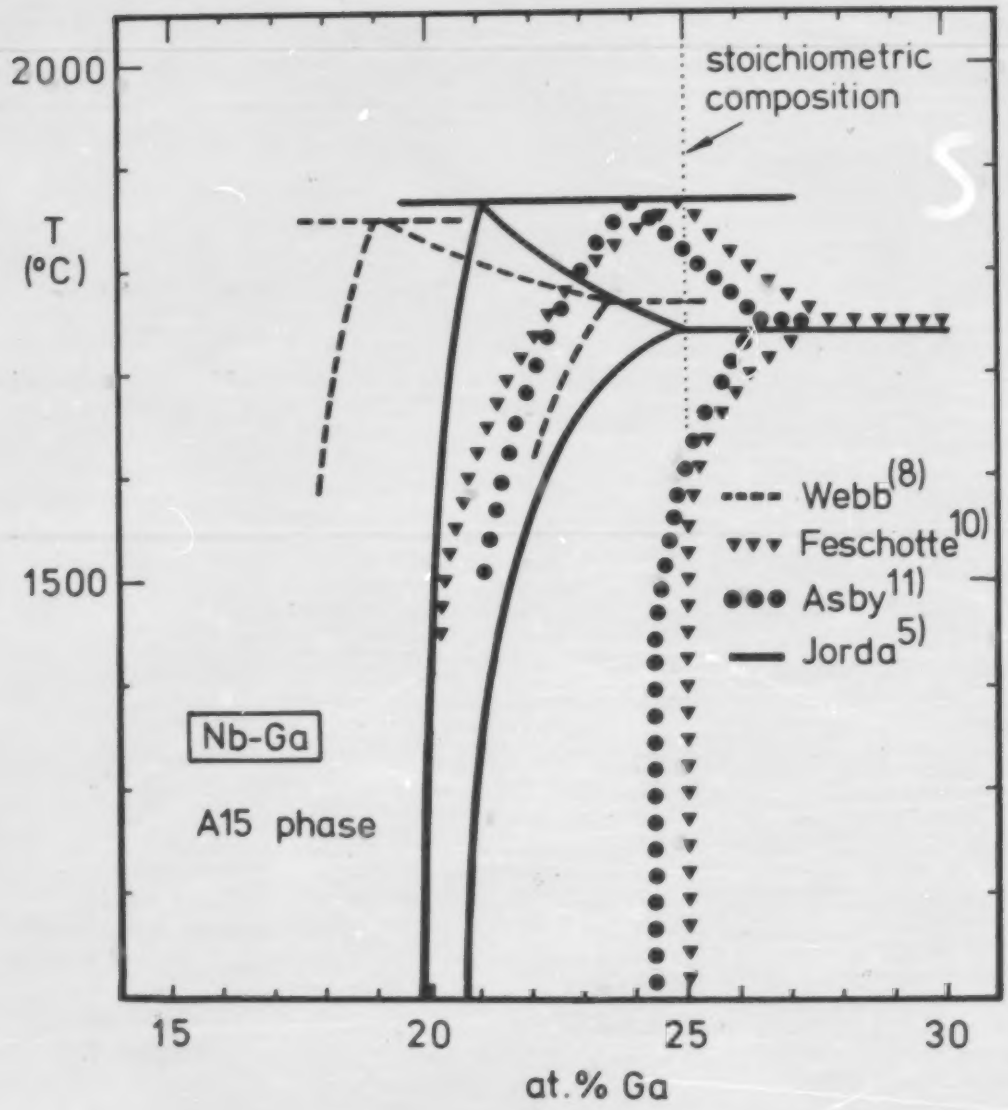

FIGURE 7. The A15 phase field in the Nb-Ga system as reported by different authors. The strong dependence of the Ga-rich limit on the temperature observed by Jorda et al. [5] was obtained using argon jet quenching at different temperatures between 1100 and 1740°C.

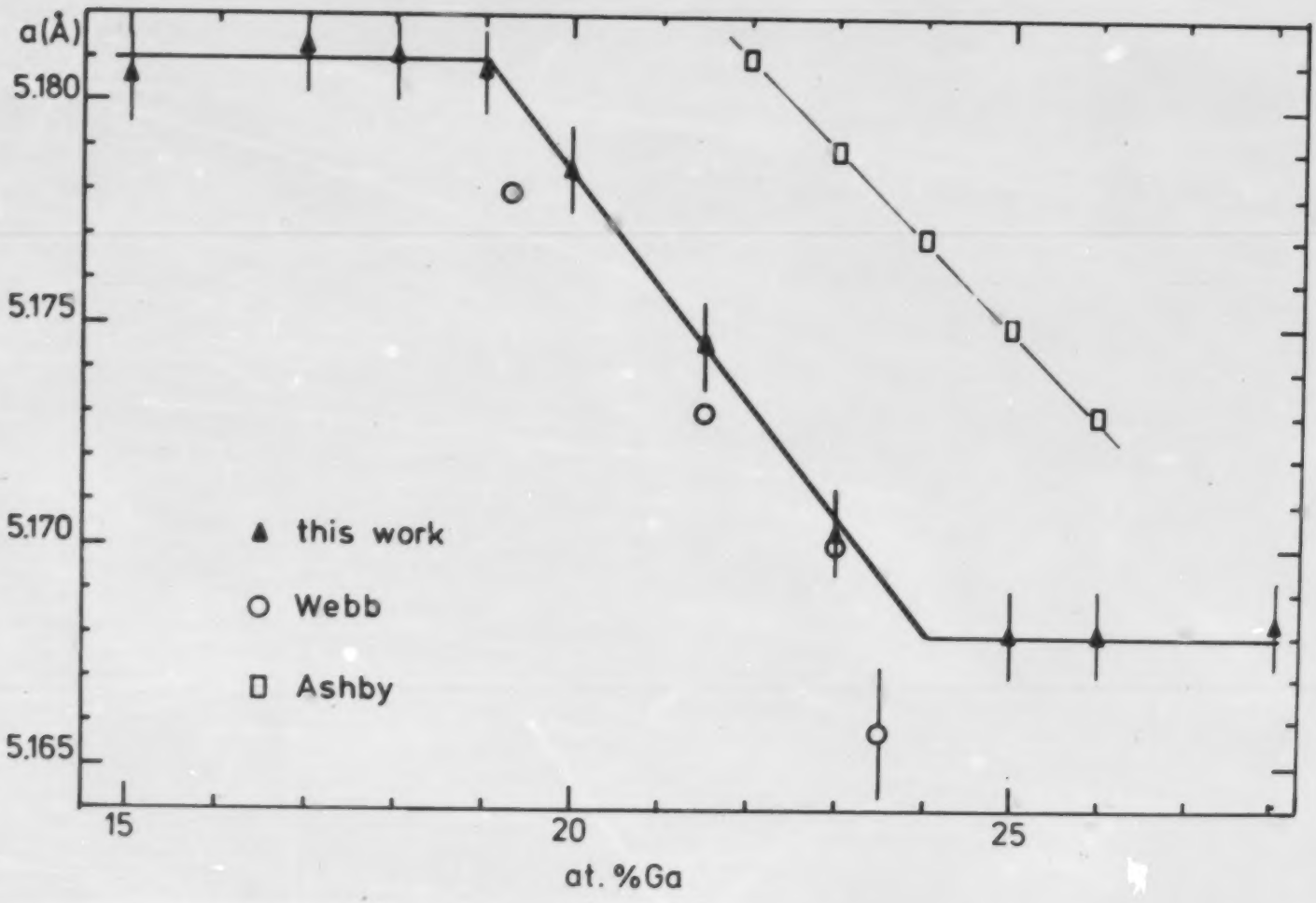

FIGURE 8. The variation of the lattice constant for the A15 phase of the Nb-Ga system. The values of Ashby et al. {11} can be brought to cover with those of Webb et al. {8} and Jorda et al. {5} by a shift of 3 at.% Ga.

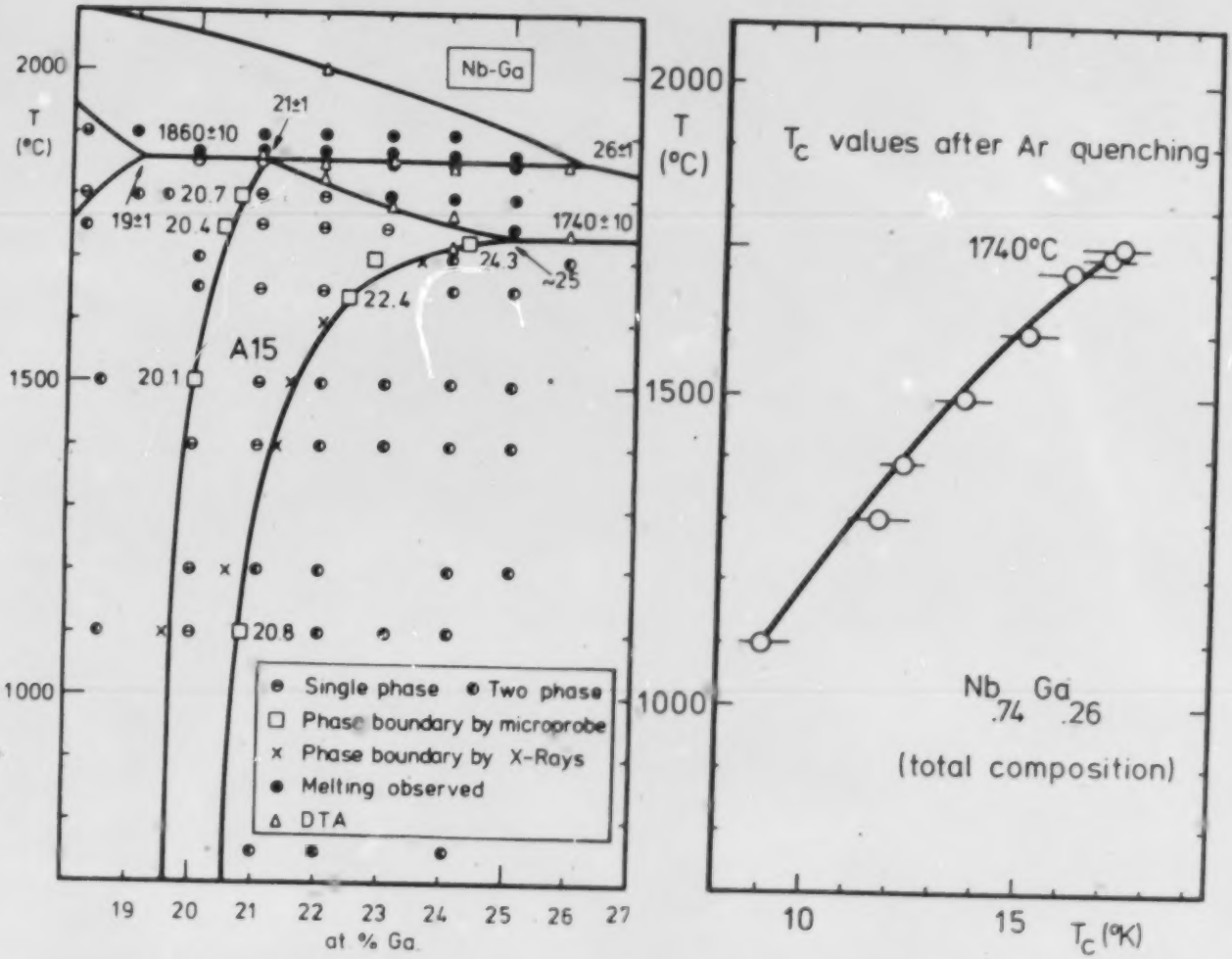

FIGURE 9. The variation of T_c for the compound $Nb_{.74}Ga_{.26}$ after quenching from different temperatures by a jet of cold argon. In the range $1100 < T < 1740^{\circ}C$, it corresponds to the curvature of the Ga-rich limit of the A15 phase Nb_3Ga (12).

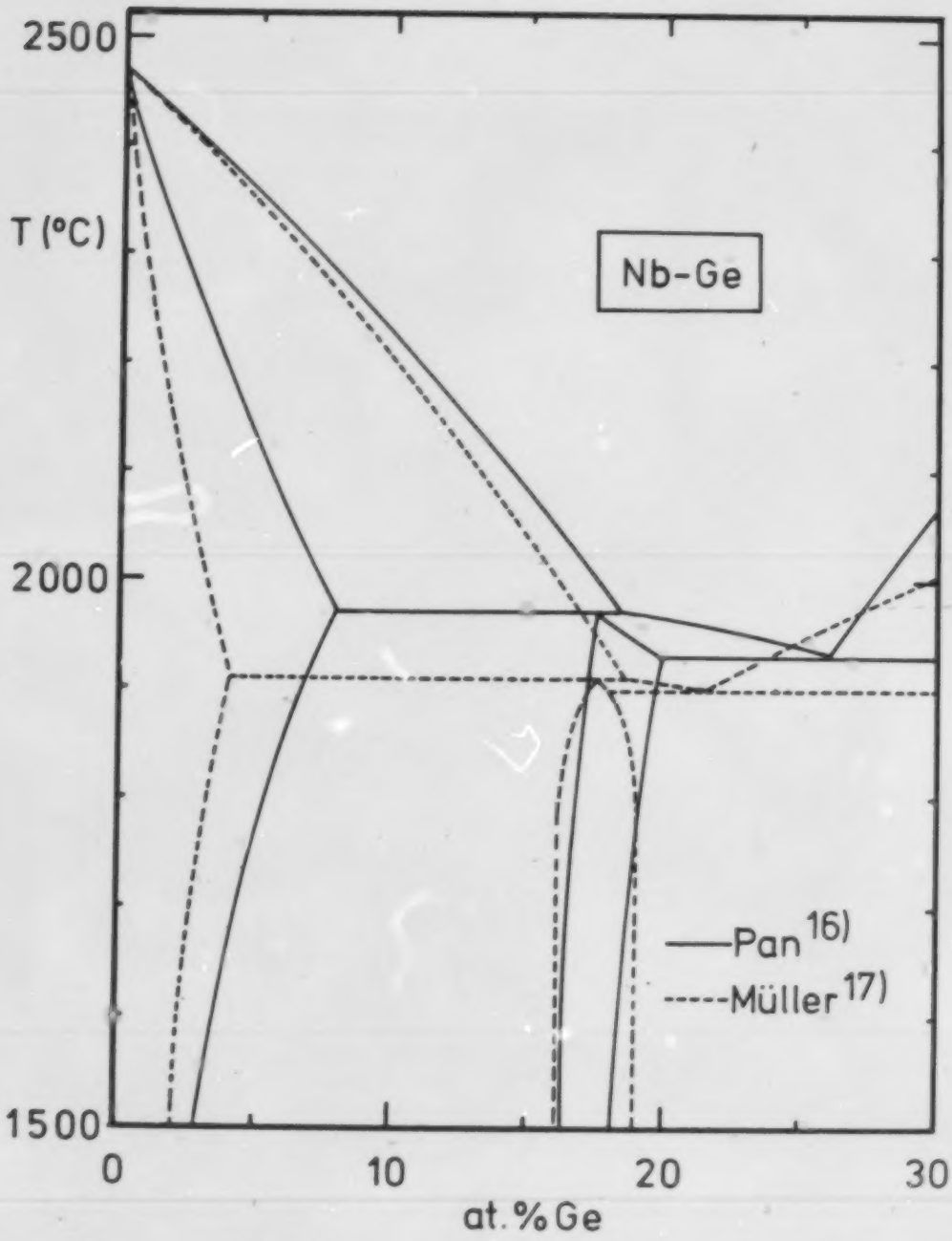

FIGURE 10. The high temperature part of the Nb-Ge system as reported by Pan et al. {16}and Müller {17}.

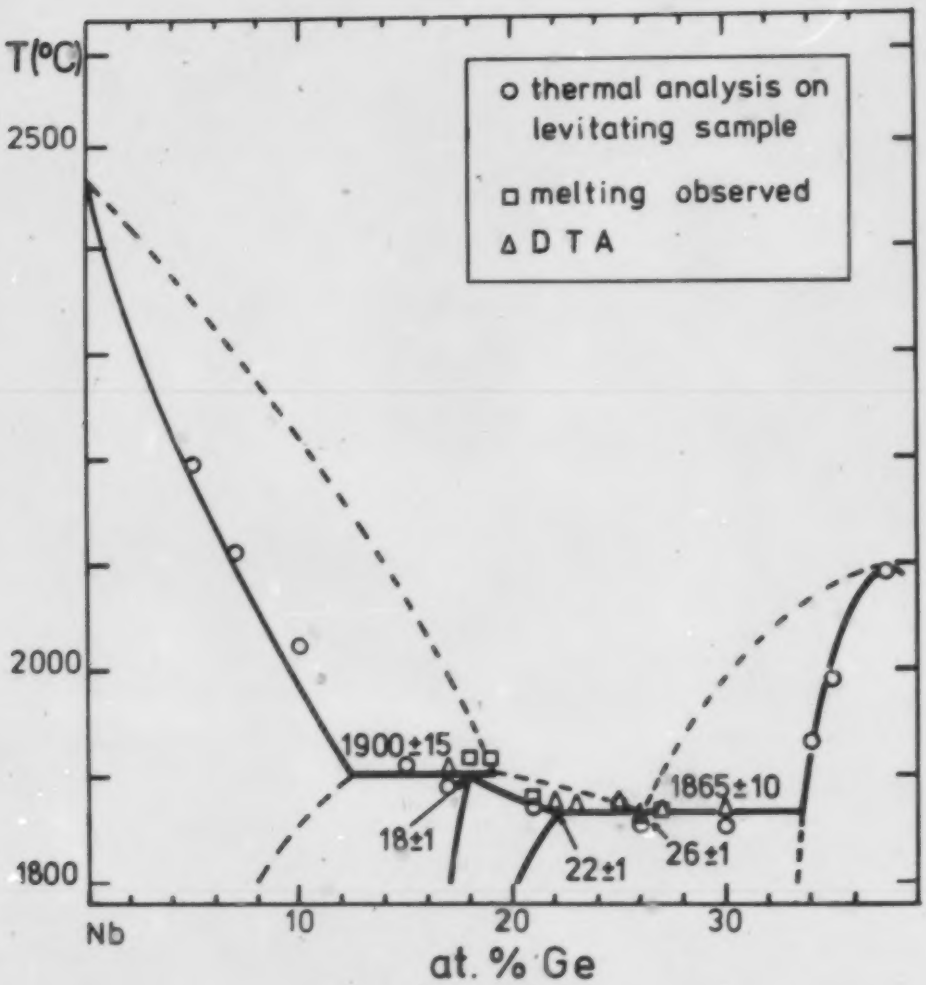

FIGURE 11. The high temperature part of the Nb-Ge phase diagram as obtained by thermal analysis on levitating samples, combined with DTA and "simultaneous stepwise heating".

National Bureau of Standards SP-496, Applications of Phase Diagrams in Metallurgy and Ceramics
Proceedings of Workshop held at NBS, Gaithersburg, Md., January 10-12, 1977

APPLICATION OF EXPERIMENTAL TECHNIQUES AND THE CRITICAL DETERMINATION OF PHASE EQUILIBRIA IN OXIDE SYSTEMS

F.P. GLASSER

Department of Chemistry, University of Aberdeen,
Old Aberdeen, AB9 2UE, Scotland.

ABSTRACT

Experimental determination of phase equilibria in oxide systems has been greatly assisted by improvements in technique. For example, the focussing X-ray camera is superior to the diffractometer in its ability routinely to detect small quantities of a second phase and its more general use is advocated. It is almost always necessary to use another method of phase identification in conjunction with X-rays: optical microscopy, if possible. Selected applications of single-crystal data to the determination of phase composition is illustrated and the use of continuous high-temperature X-ray diffraction as a complimentary technique to DTA is described. It is concluded that despite the existence of critical compilations of data on oxide systems, the need exists for more experimental work to be done before our existing store of data can be considered reliable.

1. INTRODUCTION

During the past decade, the writer has increasingly been concerned at the general lack of critically-determined phase equilibrium data on oxide systems. Two principal areas of concern exist: firstly, the low reliability of data on systems which have supposedly been critically studied in the past, and secondly, the general attitude that it will be extremely difficult to extend studies on 'simple' systems to yet more complex systems by experiment. For example, the attitude is prevalent that quaternary oxide systems are, in general, too complex to study within the time scale usually available to the experimenter. Of course, if reliable data are not available on the limiting unary, binary or ternary portions of a complex system, it is not surprising that experimenters are unable to produce data on hitherto-unexplored systems quickly.

Critical compilations, such as the 1975 edition of "Phase Diagrams for Ceramists", are of only limited value in producing correct phase diagrams. While the compiler

can point out or correct obvious errors or inconsistencies - for example, violations of the phase rule - thereby at least producing consistent diagrams, these will not necessarily be correct. Errors such as the omission of compounds, undetected polymorphic transitions, etc., will almost inevitably not be detected by the compiler, without recourse to experiment. Errors in the literature thereby tend to become perpetuated in compilations and data banks.

Our experimental activities have largely been confined to systems containing oxides which are abundant in the crust of the earth. Most of these contain Al_2O_3 or SiO_2 or both : a list of systems studied in the writers' laboratory is given in the Appendix. This choice of systems is deliberate, for we believe that critically-determined data on these are most needed by technology, yet because they lack glamour are unlikely to be the subject of special funding. It follows that trained personnel have not always been available to work on our program and it has usually been necessary to work through students, giving each the necessary formal training both in theory and method. However, a judicious blend of modern equipment and procedures, combined with an enthusiastic and able team, enable complex oxide systems to be determined experimentally with an accuracy and rapidity which was not until recently possible. We remain optimistic about prospects for experimental studies of phase equilibria in oxide systems.

This paper does not seek to give a comprehensive account of the techniques of phase diagram determination : several Chapters in the series edited by Alper* fill this need. I concentrate on describing several useful techniques which have not been adequately described elsewhere.

---

*"Phase Diagrams - Materials Science and Technology" Ed., A.M. Alper, 3 Vol. Academic Press, New York.

2. X-RAY POWDER DIFFRACTION METHODS

X-ray powder diffraction was first applied to phase equilibrium studies within a few years of the discovery of X-ray diffraction. Since that time, many improvements have been made in the ease of recording the pattern; for example, the combination of electronic measurement and automatic recording of the diffraction pattern which makes the diffractometer possible. Although the latter is certainly more convenient and more rapid than the powder camera, its response is basically no more sensitive than that of the conventional Debye-Scherrer camera. Most experimental studies of phase equilibrium have tended routinely to rely on the diffractometer for phase identifications but few investigators would regard it as a sufficiently sensitive method for the location of a second phase to rely on it accurately to locate phase boundaries. Significant advances in the technique have, however, occurred. An example is the development of the focussing X-ray powder camera. In focussing cameras, an intense beam of X-radiation is produced which is not only strictly monochromatized but which is also focussed. This is achieved by using a strong Bragg reflection, for example $10\bar{1}1$ of quartz, and simultaneously bending the crystal by applying mechanical pressure to achieve a focussing effect. Photographs may be obtained in the transmission mode using the Guinier geometry. Typically, a modern focussing camera gives exposures in 15 - 30 min. and requires 1.0 - 20 mg of sample. The time taken is comparable with that required to record a diffractometer trace, although it is of course necessary to process a strip of film. Nevertheless, the combination of the human eye and photographic film gives a better signal-to-noise ratio than can be obtained by diffractometry. Admittedly, the 'smear' method of preparation — often used in diffractometry — is not the best method of sample preparation, but it is quicker and often the quantity of sample available is only sufficient for a 'smear'. Moreover, while the X-ray system itself

may be at or near optimum performance, other variables - especially specimen preparation - may detract from obtaining the optimum results. In the course of studying a moderately complex system, it might be necessary to X-ray several hundred specimens: it is rarely possible to optimize all the variables affecting the quality of the diffraction pattern for each individual specimen. Therefore X-ray records obtained either from films or diffractometer traces, and which provide evidence of the phase distribution, are likely to be obtained under average rather than optimum conditions of system performance. These factors combine to give the focussing camera a marked advantage over the diffractometer.

A practical illustration of the relative ability to resolve mixtures of phases using optical and X-ray powder diffraction techniques will now be given. It is based upon data obtained in the course of a critical re-examination of the MgO-Al_2O_3-SiO_2 system. In the Al_2O_3-rich corner of this system, two binary phases are encountered - mullite, $Al_6Si_2O_{13}$ and spinel, $MgAl_2O_4$ - as well as two ternary phases: cordierite, $Mg_2Al_4Si_5O_{18}$, and sapphirine, $Mg_4Al_{10}Si_2O_{23}$. These formulae are approximate but suffice for present purposes. Let us examine the problems involved. All the phases have distinctive powder patterns except for those of sapphirine and spinel, which are similar. Good structural reasons exist for the similarity between the powder X-ray patterns of the two phases. Sapphirine contains cubic close packed oxygens in an arrangement which is almost identical to that of spinel : moreover, many of the cations in sapphirine occupy positions spatially similar to those which they would have in a spinel. One consequence of this similarity is that the sapphirine powder pattern resembles that of spinel in the positions and intensity of its more intense reflections, although the greater structural complexity of sapphirine creates another, and characteristically weaker, set of powder lines which are absent in spinel. The main powder reflections of both

phases overlap, and in mixtures of the two phases they tend to be superimposed except at low d-spacings. Therefore, positive confirmation of the presence of sapphirine in mixtures with spinel depends crucially upon the ability to locate the weaker set of reflections which are characteristic of the latter phase, whereas the identification of spinel in the presence of sapphirine depends upon resolving closely-spaced reflections : in particular the (440) reflection of spinel from the adjacent reflections due to sapphirine. The resolution of mixtures of the two phases is therefore handicapped to some extent by similarities in the powder X-ray patterns of spinel and sapphirine. Such similarities are not isolated occurrences. Several phases in a system may frequently share the same basic substructure; failure to recognize that this may occur frequently leads to mistaken judgments concerning the number of phases which exist, as is shown in this instance by the length of time which it took for sapphirine to be recognized as a phase which was chemically and structurally distinct from spinel.

3. X-RAY AND OPTICAL METHODS COMPARED

An exact comparison between optical and X-ray methods is rendered difficult because much depends upon the skill of the microscopist. Table 1 contrasts both of these methods. The comparison is based on samples which have been heated to within $\sim 20^{\circ}C$ of the solidus. This results in comparatively large crystals (2 - 5μ) developing in heat treatments of 24 - 48 h duration, so that the optical character of the crystals may readily be determined. In these, sapphirine may readily be distinguished from spinel on account of the weak birefringence of the former and from cordierite by the lower mean refractive index of the latter. Mullite is readily recognized even in traces on account of its needle-like or elongated lath-shaped crystals.

TABLE 1

Sensitivity of X-ray and Optical Methods Used to Determine the Presence of a Second Phase Occurring with Sapphirine Compared.

Nature of Second Phase		Minimum Quantity Required For Reliable Identification	
NAME	FORMULA	X-RAY	OPTICAL
SPINEL	$MgAl_2O_3$	1%	1%
CORDIERITE	$Mg_2Al_4Si_5O_{18}$	0.5%	Difficult
MULLITE	$Al_6Si_2O_{13}$	2.0%	1.0%
CORUNDUM	Al_2O_3	2.0%	Difficult

The X-ray data shown in this table were obtained from trials made using weighed mixtures of phases and the detection limits cited were obtained using focussing cameras and 'routine' exposure conditions, as described previously. Similar trials using 'smear' mounts and a modern diffractometer, show that a gain in sensitivity of 4 to 5 times is achieved with the focussing camera. The comparison appears very favourable to optical methods: however, as the sintering temperature is decreased, the mean size of the crystals also decreases and the sensitivity of phase detection by optical methods decreases rapidly. X-ray methods are much less susceptible to variations in sensitivity arising from changes in particle size until line-broadening eventually occurs. Therefore, X-ray methods are especially useful in determining the phases present in experiments made below the solidus. On the other hand, as temperatures approach and eventually exceed the solidus, the appearance of liquid - even in traces - is readily revealed by optical examination. Even if the liquid cannot at first directly be perceived, the microstructure usually undergoes an abrupt change when the solidus temperature is exceeded. Therefore, optical and X-ray examination are complementary rather than competitive techniques. It is to be regretted that it is becoming increasingly difficult for those entering the field to obtain

the good training in microscopy which scientists of previous generations took for granted.

4. X-RAY DIFFRACTION COMBINED WITH OTHER TECHNIQUES

a. Determination of phase composition. Many systems which supposedly have been thoroughly studied are found when re-examined to show hitherto undetected phases. For example, the Na_2O-SiO_2 system was studied by Kracek (Phase Diagrams for Ceramists: Fig. 192) who found a simple eutectic between α-$Na_2Si_2O_5$ and SiO_2 (quartz). However, a re-examination of this system disclosed that compositions between 70 - 75 mol % SiO_2 gave a powder X-ray pattern which was not that of mixtures of any known polymorphs of SiO_2 and $Na_2Si_2O_5$. Investigation showed that a hiterto unidentified phase occurred. Persistent but incompletely - confirmed reports in the literature of a "sodium trisilicate" led us first to suspect that this phase was the elusive $Na_2Si_3O_7$. The composition of the newly-discovered phase was determined unequivocally as follows. Although it melted incongruently, one temperature-composition region of the phase diagram was found in which small laths 20 - 30 μ in length could be grown in contact with liquid. Single laths were isolated on the stage of a petrographic microscope. These were not completely free from adhering glass, but the latter does not interfere with a determination of the symmetry of the crystal. Single crystal X-ray photographs were obtained : these were consistent with monoclinic symmetry, although the crystals were geometrically orthorhombic. Systematic absences indicated the space group $P2_1/c$: $\underline{a}$ = 4.90 Å, $\underline{b}$ = 23.4 $\underline{c}$ = 15.4 Å, β = 90.0°. The unit cell volume was 1768 $Å^3$. Meantime, sintering of compositions close to the trisilicate ratio at subsolidus temperatures disclosed that at both 74 and 75% SiO_2 quartz remained in excess, while at 72 and 73% SiO_2, an apparently single phase preparation resulted. However, at 71% SiO_2, $Na_2Si_2O_5$ was definitely present. Therefore, the phase appeared not to be the trisilicate. The density of the apparently homogeneous sinters obtained at the 72 and 73% compositions were both 2.495 ± 0.002 g/cc. We note

also that the unit cell contents must obey the restriction that they must fill the unit cell volume to give the observed density. Moreover, this space-group symmetry places an additional restriction on the possible unit cell contents; namely, that barring a statistical distribution of atoms, the content must have an even number of each species – Na, Si and O. With this in mind, we can construct a plot, shown in Fig. 1, of the unit cell contents of some hypothetical sodium silicates having V = 1768 $\AA^3$ and a density of 2.50 g/cc : two other parallel lines are shown to allow for errors in the density determination of ± 0.05 g/cc. Bearing in mind the symmetry-imposed restriction, possible fits within this regions occur at the ratios of $Na_2O:SiO_2$ equal to 14:30, 12:32 and 10:34. These ratios correspond respectively to ≃ 68, 72.7 and ≃ 77 mol % SiO_2. However, from observing the phase purity of the sintered preparations we can readily exclude the 14:30 ratio as this composition was observed to yield much $Na_2Si_2O_5$, while the 10:34 ratio yielded much unreacted SiO_2. This leaves only the 12:32 ratio, which must therefore be the only empirical formula which is consistent with all the data. Hence the phase is unequivocally shown to be $3Na_2O.8SiO_2$, or $Na_6Si_8O_{19}$. It is important to note that other ratios close to 3:8 could not be excluded except by using the additional constraints imposed by crystallographic symmetry.

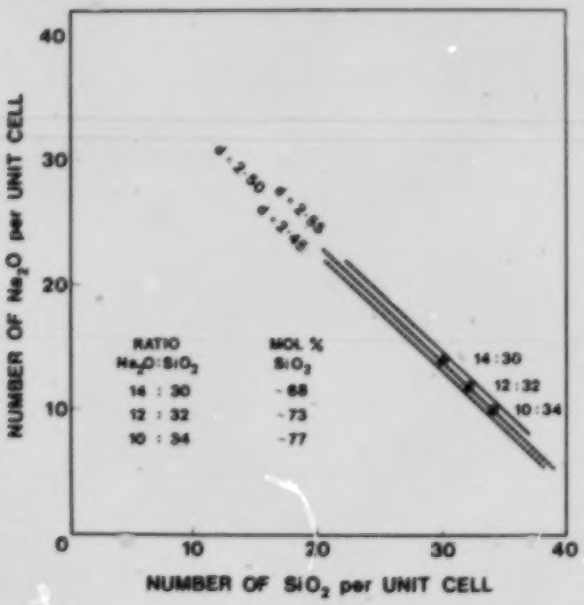

FIG. 1. Applications of Crystal Data to Sodium Silicates.

It is noteworthy that, although $Na_2Si_3O_7$ is not a thermodynamically stable phase at any temperature, it is readily prepared by devitrifying glasses (ref. 11, appendix) the same procedures were again applied to prove that the formula of this metastable phase was $Na_2Si_3O_7$.

A useful additional check on the validity of this type of calculation is to apply the Lorentz-Lorenz relation, which states

$$R = \frac{n^2 - 1}{n^2 + 2} \times \frac{M}{d}$$

where R is the atomic refractivity, n the mean refractive index, M the formula weight and d the density. We take the value of R for Si from the low-density phases of SiO_2, in which $R_{Si} \simeq 0.0$ and those of Na and O from sodium silicates, in which $R_{Na} \simeq 1.6$ and $R_O \simeq 3.7$. For example, knowing that the mean refractive index of $Na_3Si_8O_{19}$ is 1.503 (its birefringence is low) we can calculate its density. The value thus obtained, 2.47 ± 0.03 g/cc, agrees well with the observed density.

The principle has been explained with reference to an example from a two-component system but it is even more useful when applied in systems of greater chemical complexity: thus when a ternary compound stable to its incongruent melting point was encountered in the Na_2O-CaO-SiO_2 system, classical phase equilibrium methods were again combined with crystallographic data (symmetry, unit cell size and density) to show that the phase was $Na_2CaSi_5O_{12}$ (ref. 12, appendix). In the Na_2O-BaO-SiO_2 system (ref. 18 - 20 appendix) this combination of techniques was again sufficient to determine that the composition of a ternary phase was $Na_2Ba_4Si_{10}O_{25}$, despite the rather large unit cell size arising from the long $\underline{c}$ axis ($\underline{a} = 39.3_5$ Å) and the low symmetry of this phase (ref. 18, appendix).

It is almost always practicable to obtain single crystals sufficient for crystallographic measurements. With care and practise, crystals which are only 10 - 20 μ in maximum dimension will usually suffice. During the course of phase

equilibrium studies, one would expect to encounter a particular phase in the course of making many experiments in which time, temperature and bulk composition were important variables. Observing the relative size of the crystals would generally suffice to indicate conditions most favourable for crystal growth, should it be required specially to grow crystals. If, however, it proves impossible to obtain crystals of sufficient size for X-ray diffraction, electron diffraction may instead be used to obtain the necessary crystallographic data.

The crystallographic information required to implement the procedures described above do not require that a full structure determination be made. There are, however, some instances in which full structure determination is required. Thus, a structure determination has been helpful, for example, in understanding the cation distribution in sapphirine.* But it is by no means certain that all sapphirine must have the composition - close to the molar ratio $7MgO.9Al_2O_3.3SiO_2$ - of the crystal which was studied. Therefore, even the best crystal structure determinations will not necessarily suffice to determine the limits of homogeneous single-phase formation, although refinements based on site occupancy factors may correctly show the composition of an individual crystal. Moreover, an accurate crystal structure determination may not be possible if the crystals suffer from twinning and polytypism or both. Examples of the latter occur in the system Na_2O-BaO-SiO_2 (refs. 19, 20, Appendix) in which two phases, designated X and Y were encountered. Not only did the crystals prove to be difficult subjects for growth at liquidus temperatures, but crystals of both phases had extremely large and complex unit cells. We therefore had to be content with the best estimate of the compound compositions, taking into account the results of subsolidus equilibration. Tentatively, X was ascribed the formula $Na_2Ba_{18}Si_{28}O_{75}$ and Y, $Na_2Ba_{45}Si_{73}O_{192}$.

---

* Moore, P.B. Amer. Miner., 54, 31 (1969).

If it is possible to obtain chemical data on the composition of a phase by some direct technique, e.g., from microprobe analyses, this information should of course be utilized to the fullest. During our studies of silicate systems containing alkali ions, we have frequently made microprobe analyses in order to determine the alkali and SiO_2 contents of crystalline phases. In general, the quantitative worth of the results has been disappointing. When the phases being analyzed contained a preponderance of low atomic-weight elements, the volume which is sampled by the electron beams for analytical purposes may be approximately equivalent to a sphere of 100 - 200 μ diameter, even though the focal spot of the beam may be much smaller, typically 1 - 2 μ. In my experience, it is impracticable routinely to grow crystals of sufficient size to obtain reliable probe analyses for Na, Mg, etc. The advent of new types of electron-optic instruments with analytical capabilities, e.g., STEM, CORA, etc., give real hope that it will be possible to obtain 'spot' analyses which are able to more accurately determine the phase composition especially of micron-size crystals that are apt to occur in sintered mixtures.

b. Continuous High-Temperature X-ray Diffraction: a complementary tool to DTA. On a focussing camera all X-ray reflections within the range of the instrument are recorded simultaneously. This is unlike the diffractometer which 'scans' the pattern, thereby making it almost essential that in a high temperature diffractometer, all other variables (temperature, pressure) should remain at least approximately constant during each individual scan. The different mode of operation of the focussing camera has lead to an ingeneous commercially-available design for a high-temperature instrument in which a sheet of photographic film is translated past a set of narrow (2 - 4 mm wide) slits, thereby exposing only a small strip at any instant. Starting from the origin, distance along the strip is proportional to θ (or (2θ), as in a normal photograph. However, the film translation motion is linked to a temperature programmer, so that the direction

on the film normal to the θ axis becomes an axis of changing temperature. The X-ray reflections in this direction are recorded continuously as a function of temperature. Typical heating and cooling rates using in the camera are 1° - $2^{\circ}C\ min^{-1}$, or about an order of magnitude lower than those usually employed in DTA. The two techniques are, in general, complimentary and it is frequently helpful to have both. Usually, the same interpretation can be reconciled with both sets of data. There are, however, instances in which apparently different interpretations of the same events are required. In this connection, it is relevant to recount an actual example concerning the polymorphism of $Na_2Si_2O_5$. Fig. 2 shows schematically the most probable free-energy- temperature relations at 1 atm. The α phase and its variants are stable between 710° and the melting point (874°) but readily persist to lower temperatures. Samples of α $Na_2Si_2O_5$ can readily be heated and cooled on the DTA without converting to the more stable β phase. The α phase is thermally active: it undergoes two rapidly-reversible inversions one at 680° the other at $707^{\circ}C$.

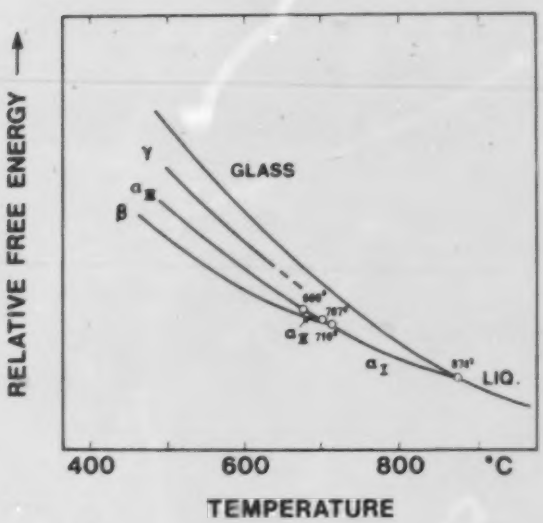

FIG. 2 Schematic free energy vs temperature diagram for Na_2SiO_5 at 1 atm. pressure.

However, when examined by continuous X-ray diffraction, only one change in the powder X-ray pattern - at 707° - is recorded. This apparently contradictory state of affairs is explained as follows: the low, or α_{III}, phase is orthorhomic. At 680°, it converts to the monoclinic, geometrically orthorhombic α_{II} phase having an orthorhombic pseudocell with cell dimensions identical to those of the α_{III} phase and, presumably because the atomic coordinates also change little, a powder pattern which is essentially identical to that of the α_{III} phase. At the 707° phase change the monoclinicity increases, resulting in a splitting of reflections which were previously coincident in the α_{II} and α_{III} phases.

However, α_I also has a much smaller b axis periodicity relative to the α_I and α_{II} phases. Therefore, above 707° some reflections which were present both in α_I and α_{II} phases also disappear. Without this interplay of techniques, it would not be possible to explain in such detail the nature of the phase transitions and to realize that each technique senses only a part of the picture. It would, however, be unwise to conclude that DTA is generally more sensitive than powder X-ray as a way of detecting phase transitions. By DTA, the γ family appears to have three rapid inversions, suggesting its subdivision into γ_I, γ_{II}, γ_{III} and γ_{IV} phases. However, the high-temperature X-ray suggests that the true picture is more complex, and the presumption is that the DTA fails to record those phase transformations for which ΔH is fortuitously equal to or very close to zero.

5. ROLE OF EXPERIMENTAL TECHNIQUES IN THE CRITICAL DETERMINATION AND EVALUATION OF PHASE RELATIONS.

Within the next decade, much effort will certainly be devoted to predicting phase relations in oxide systems. This is a welcome development especially to the technologist who almost always needs to 'stretch' the available data to predict the behaviour of chemically complex systems. At first sight, the development of predictive methods might appear to end or at least greatly to reduce the need to have recourse to experiment in order to determine phase relations. This is unlikely to be the case for a number of reasons. Firstly, there are many systems on which the necessary data either do not exist or are too fragmentary to be adequate. These system must, in the first instance, be studied experimentally. Secondly, there exists a less obvious region in which we appear to have much data for a particular system. Yet, upon intensive critical study, these data are shown to be incorrect. We have given several examples, but offer one more. The system $CaO\text{-}MgO\text{-}Al_2O_3\text{-}SiO_2$ is one of the great importance to petrologists and one which has apparently been thoroughly studied and a critical compilation made*. Together, these show that the

*Osborn, E.F., Gee, K.H., Muan, A, Roeder, P.L. and Ulmer, G.C. Bull. Earth, Min. Sci. Expt. Station, Penn. State Univ., 85 pp 80 (1969).

system does not have any quaternary compounds: i.e., it has no phases which require essential quantities of all four oxides in order to have a range of thermodynamic stability. However, Parker* has reported the existence of a quaternary compound (Q) to which he assigned the formula $6CaO.4MgO.Al_2O_3.SiO_2$. Compilations made subsequently have omitted this compound : the compilers were probably influenced by the fact that sintered oxide preparations made at that composition do not yield Q. However, a re-examination of this system (ref. 25, Appendix) has shown that the Q can readily be prepared by sintering, and that judged by all criteria usually used to decide if a phase is stable, it should be admitted to the phase equilibrium diagram. The difficulty in preparaing Q arose because the composition given by Parker was wrong. It was therefore necessary to resort to experiment and ultimately to show that a single-phase sinter could be obtained at the composition (in wt %) 42.2 CaO, 45.4 Al_2O_3, 4.1 MgO and 8.2 SiO_2. The existence of Q and R phases (the system in fact contains two quaternary phases, the second having been designated R) considerably alter phase relations in the MgO-rich portions of the quaternary system. The important point to be made here is that no amount of compilation acitivity divorced from experiment is likely to provide validated data on complex oxide systems. It is important, therefore, that the application of predictive methods should not be handicapped by the lack of these data.

Finally, phase equilibrium determinations frequently encounter persistent non-equilibrium states. While the existence of some of these states might be predicted, others may not. In any event, our knowledge of the kinetics of solid-state reactions is generally insufficient to enable us to predict how persistent a given metastable state would be or what specific conditions would favour development of a particular metastable state. This is another advantage of having experimental data, which readily reveals the existence of persistent metastable phases.

---

*Parker, T.W. Proc. Intl. Symp. Chem. Cement (London, 1952) 485.

S U M M A R Y

During the past decade, no revolutions have occurred in the experimental methods used to study phase relations in oxide systems. Nevertheless, steady progress has been made and it is now possible to study complex oxide systems more rapidly yet with greater precision than in the past. The writer's experience has been that even susposedly well-known systems require major modifications to 'accepted' phase diagrams. It is considered especially important if predictive studies are to be given a fair start that a store of validated data on oxide systems must be available upon which to base calculations : at present, it is felt that this store is not adequate. Hence the need for continuing experimental studies on oxide systems with an emphasis on those of fundamental importance to technology.

A P P E N D I X

SUMMARY OF PHASE EQUILIBRIA STUDIES IN SILICATE AND ALUMINATE SYSTEMS UNDERTAKEN AT THE UNIVERSITY OF ABERDEEN

System	Ref.	System	Ref.
Li_2O-SiO_2	1,2,3	MgO-Al_2O_3-TiO	22
Li_2O-BaO-SiO_2	4	MgO-Al_2O_3-SiO_2	23
Li_2O-ZnO-SiO_2	5,6		
Li_2O-MgO-ZnO-SiO_2	7,8	CaO-SrO-BaO-SiO_2	24
Li_2O-Pd-O	9	CaO-MgO-Al_2O_3-SiO_2	25
Na_2O-SiO_2	10,11	CaO-Al_2O_3-Fe_2O_3	26,27
Na_2O-CaO-SiO_2	12,13,14	CaO-Al_2O_3-FeO-Fe_2O_3	28,29
Na_2O-CaO-MgO-SiO_2	15	CaO-Al_2O_3-Fe_2O_3-SiO_2	30,31
Na_2O-CaO-Al_2O_3-SiO_2	16		
Na_2O-CaO-SrO-SiO_2	17	PbO-SiO_2	32
Na_2O-BaO-SiO_2	18,19,20		
K_2O-BaO-SiO_2			

References

1. Phys. Chem. Glasses 8, [6] 224 - 32 (1967).
2. Mater. Res. Bull. 5, 837 - 43 (1970)
3. Advances in Nucleation and Crystallization in Glasses Amer. Ceram. Soc. Spec. Pub. 5 (1972) (pp. 151 - 65).
4. Trans. and Jour. Brit. Ceram. Soc. 73, 207 - 11 (1974).
5. Jour. Mater. Sci. 5, 557 - 65 (1970).
6. " " " 5, 676 - 88 (1970).
7. " " " 6, 1100 - 10 (1971).
8. " " " 7, 895 - 908 (1972).
9. Jour. Solid State Chem. 6, 329 - 34 (1973).
10. Science 148, No. 3677, 1589 - 91 (1965).
11. Phys. Chem. Glasses, 7 [4], 127 - 38 (1966).
12. Jour. Amer. Ceram. Soc. 53 [7], 423 (1970).
13. Phys. Chem. Glasses, 12, 50 - 7 (1971).
14. " " " 15, 6 - 11 (1974).
15. " " " 13, 27 - 42 (1972).
16. " " " 17, 45 - 53 (1976).
17. Trans. & Jour. Brit. Ceram. Soc. 73, 199 - 206 (1974).
18. Phys. Chem. Glasses, 13, 125 - 30 (1972).
19. Trans. & Jour. Brit. Ceram. Soc., 72 [7], 299 - 305 (1973).
20. J. Amer. Ceram. Soc. 57, 201 - 4 (1974).
21. " " " 58, 233 - 6 (1976).
22. Trans. & Jour. Brit. Ceram. Soc. 72 [5], 215 - 20 (1973).
23. Jour. Mater. Sci. 11 [8] 1459 - (1976).
24. Zeit. Krist. 141, 437 - 50 (1975).
25. Trans. & Jour. Brit. Ceram. Soc. 4 [4], 113 - 9 (1975).
26. "Science of Ceramics" Vol. 3, Academic Press London (1967) pp. 191 - 214.
27. Trans. & Jour. Brit. Ceram. Soc. 66 [7], 293 - 306 (1967).
28. " " " " " 70 [6], 227 - 34 (1971).
29. " " " " " 72 [5], 221 - 28 (1973).
30. " " " " " 74 [7], 253 - 6 (1975).
31. " " " " " 75 [5], 95 - 103 (1976).
32. Jour. Amer. Ceram. Soc. 57 [9], 378 - 82 (1974).

National Bureau of Standards SP-496, Applications of Phase Diagrams in Metallurgy and Ceramics
Proceedings of Workshop held at NBS, Gaithersburg, Md., January 10-12, 1977

PROTECTIVE COATINGS FOR SUPERALLOYS AND THE USE OF PHASE DIAGRAMS

M. R. Jackson and J. R. Rairden
General Electric Company
Corporate Research & Development
Schenectady, New York

Abstract

Compositional modifications to increase the strength of superalloys have produced parallel decreases in environmental resistance, both for oxidation limited jet engine applications and hot corrosion limited gas turbine applications. Simple aluminide coatings have been formed by pack aluminization, but with greater demands on oxidation resistance, MCrAl(Y) coatings have come into use (M is Ni, Co and/or Fe), and duplex coatings have been formed by aluminizing the MCrAl(Y) coatings. Other elements are also of interest as additions to coatings, either homogeneously distributed throughout the coating or localized as an inner or outer layer of the coating.

Phase equilibria in ternary and higher order systems can be extremely useful in correlating coating/substrate compositions, microstructures and behavior. For example, the time-temperature changes in formation and degradation of coatings on superalloy surfaces can be understood in terms of multi-element diffusion between the elements added and the elements in the substrate by mapping the diffusion paths through the appropriate phase diagrams. This understanding can be useful in developing improved coating compositions.

Specific examples of the application of phase diagrams to the understanding of coating formation and degradation are presented: aluminization of superalloys, duplex aluminized coatings, and aluminization of platinide coatings on superalloys. Systems where only limited diagrams exist are also discussed.

INTRODUCTION

Coatings are used in many metallurgical applications to create composite systems whose properties are optimized with (a) a surface layer for stabilized interfacing with the environment, and (b) a substrate for economically meeting the mechanical requirements. Common examples are galvanized steel to resist rusting, and carburized steel to resist wear. In both these systems, coating formation is at high temperature, but service is at relatively low temperature. Coating formation involves diffusive interactions with the substrate, but coating degradation in service involves predominantly the interaction with the environment.

In contrast, coatings for hot gas components must resist high temperature oxidation and corrosion in the severe environment of gas turbines and jet engines.[1] The Ni-base superalloy substrates are protected with coatings that form dense, adherent oxide scales. For these coatings, degradation in high temperature service (as well as coating formation) involves interdiffusion between the coating and substrate.[2] For many applications, compositions for resistance to oxidation and/or hot corrosion have been identified. Successful coatings form and retain a desired surface structure for times approaching several years at 1000°C.

An understanding of the phase distribution established between coating and substrate, and how that distribution changes in service as the system tries to move toward equilibrium, can be achieved in terms of the relevant phase diagrams. When the diagrams are available, the diffusion path taken by the coating/substrate system can be considered directly. When the diagrams are unavailable, a study of the diffusion path taken can be used to gain phase diagram information. To advance current coating technology, a detailed definition of relevant phase diagrams over a range of temperatures is needed. This information can be used to devise coatings which maintain the desired surface structure by following diffusion paths through the phase diagram chosen to minimize the rate of approach to equilibrium.

The Ni-base superalloys contain on the order of 10-25% Cr, 0-10% Co and 2-10% Al, by atom percentages, as well as lesser amounts of other elements for further strengthening.[3] The major phases present are the fcc Ni solid solution (γ) and an ordered precipitate phase based on Ni_3Al (γ'). Some elements, such as Ti or Ta, are added to strengthen the γ'

phase, while others, such as Mo or W, are added to strengthen the γ matrix. Further additions are made to form carbides or borides, generally in amounts of less than 2 v/o of either phase.

A typical superalloy composition specification may include 9-14 different elements. These complex alloys might appear to prohibit any use of phase diagrams to understand their behavior. However, some simplifying assumptions can be made, similar to these made in "phacomp" stability calculations.[3] Since the borides and carbides represent a small volume fraction of the system, they generally have a small influence on phase equilibrium of the superalloy, although they are not inert. The elements involved in these phases can be subtracted from the bulk chemistry proportionately to their presence in these phases. Furthermore, elements which influence the phase equilibrium in a manner similar to Cr can be treated as additional Cr atoms.[4] This includes Mo, W and V. The elements Ta, Ti and Nb influence the phase equilibrium in a manner similar to Al, and can be treated as additional Al atoms.[4] These simplifications reduce the complex chemistry of most superalloys to Ni, Co, Cr and Al. For most alloys, Co can be equated to Ni, and the alloys can be treated as ternary systems of Ni, Cr and Al.

Rules governing the description of diffusion paths in multicomponent systems have been discussed in the literature.[5-7] It should be noted that for diffusion paths plotted on phase diagrams, dashed lines do not represent distance in the actual diffusion couple, but represent an interface. In a true ternary system, a three-phase field will have no width in a diffusion couple because of the constant chemical potentials within that field.[6] In the ternary approximations of 10-12 element systems, we have not observed three-phase fields in diffusion couples.[4] However, for practical systems such as silicided superalloys, we have observed three-phase structures developing in the diffusion couples.[8]

We will illustrate the use of existing diagrams for protective coatings on superalloys by examples of aluminization, and then go on to generation of phase diagram information by the use of diffusion path studies where details are unavailable. Finally, further systems of interest for which incomplete information exists will be discussed.

ALUMINIZATION

Compositional modifications to increase the strength of the superalloys have usually involved reductions in Cr content. The greater strengths permit the use of the superalloys at higher temperatures. For both oxidation limited jet engine applications and hot corrosion limited gas turbine applications, lower Cr and higher temperatures have necessitated the use of coatings.[1] Initially, simple diffusion aluminide coatings were formed by pack aluminization.[9] The part to be coated is placed in a pack consisting of Al_2O_3 powder mixed with a small percentage of aluminum or aluminum-bearing powder. Generally, the pack is "activated" by inclusion in the pack of a halide such as NH_4F. The pack is heated to a high temperature (850-1150°C) for a period of several hours, during which time Al is transported to and deposited on the substrate surface. The generally accepted view is that the deposition is an approximately steady-state process,[10] although we have recent experimental evidence which indicates that Al transfer is largely completed by the time the pack reaches the aluminizing temperature, and that the time at temperature is predominantly a diffusion heat treatment.[4] In any event, the coating/substrate microstructure can be observed and the structures formed can be plotted in the ternary phase diagram. The binary Ni-Al diagram[11] has been used successfully to describe aluminization of Ni,[12,13] but aluminization of more complex alloys requires higher order diagrams.

The observed microstructure formed in aluminizing a complex Ni-base superalloy, IN-738, is illustrated in Figure 1. Phase identification for this type of microstructure involves metallographic examination, electron microprobe analysis of the phase chemistries, and x-ray diffraction to verify chemistries on the basis of crystal structures known from each of the binary systems involved.[4] The diffusion path through the ternary diagram is shown in the schematic diagram of Figure 1. The diagram is based on information in the literature, but is hypothetical for Al-rich compositions beyond the $\beta+\alpha$ field.[11,14-16] The $\delta+\alpha$ (Ni_2Al_3 + Cr solid solution) field is observed experimentally in aluminized structures, while the higher Al fields are assumed. In the Ni-Cr-Al diagram, the $\gamma'+\alpha$ field is prevented by a $\gamma+\beta$ field at temperatures greater than ~1000°C. However, for the superalloys, the additions of Ta, Ti and Nb raise the temperature of the $\gamma'+\alpha \rightleftarrows \gamma+\beta$ transition.[17] For the alloys IN-738, IN-100,

and René 80, for example, the $\gamma'+\alpha$ field is observed at 1060°C, but not at 1160°C.[4] One further point to be made about the diagram involves the presence of α. For alloys high in Mo and/or W, a topologically close-packed phase (σ) intervenes between γ and α.[18] Therefore, depending on the substrate composition and the coating/substrate interaction, $\gamma'+\sigma$ may be observed rather than $\gamma'+\alpha$.

The path shown in Figure 1 is for the coating formed by aluminizing IN-738.[4] The initial couple can be considered as between IN-738 and Al. Typically, aluminization of a turbine blade involves the deposition of $\sim$6 mg/cm^2 of Al which is equivalent to the deposition of an $\sim$25μm thick layer on the substrate. Therefore, the IN-738 acts as an infinite sink for a finite amount of Al. For IN-738 (11.8 a/o Al, 19.5 a/o Cr in the ternary approximation), the final equilibrium for a coated .25cm thick substrate would be 12.7 a/o Al, 19.3 a/o Cr, still well within the $\gamma+\gamma'$ field for the substrate. Since this composition would be only marginally more resistant to the environment than the base composition of IN-738, it is desirable to minimize the rate of equilibration of the coating with the substrate and to retain the high-Al β and δ phases for long service life. During coating formation, the outermost part of the coating corresponds in the phase diagram to the first completely solid phase field intersected by a line joining the terminals of the couple, IN-738 and Al. The remainder of the path is governed by the relative diffusivities of Ni, Cr and Al. Presumably, Cr is the slowest in diffusion in the phases formed in the coating,[19] so the path swings away from the Cr corner of the diagram initially, and then swings back toward the Cr corner, crossing the line joining the terminals of the couple in order to maintain the Cr mass balance.

In service, the coating degrades by two mechanisms.[9] (1) The interaction with the environment causes the preferential oxidation of Al and Cr. These elements are lost when the oxide scale spalls and additional Al and Cr from the coating are required to form a new oxide layer. (2) The interaction with the substrate causes a loss of Al from the coating to the substrate by inward diffusion and a gain of Ni in the coating by outward diffusion. In the microstructure, the β phase is seen to grow at the expense of δ as Al is lost at the surface. The disappearance of the

δ phase in service generally occurs rapidly. The IN-738 terminal of the couple does not change location, but the Al-rich terminal migrates toward the IN-738 terminal, as shown in Figure 1c. In a closed system, the diffusion path would have to cross the line joining Al and IN-738 so that mass balance would be maintained. Although spallation of oxidized material eases that restriction, the general observation is that the path does cross that line throughout the useful service life of the coating.

OVERLAYER AND DUPLEX COATINGS

The most advanced higher temperature capability Ni-base superalloys have quite low Cr contents. For many of these materials, operation at the extreme of their capability requires more environmental resistance than can be provided by a simple diffusion aluminide coating. Coatings known as MCrAlY's (the M being the major element, Ni, Co and/or Fe) have been devised which contain enough Cr and Al to be extremely resistant to high temperature agressive environments.[1] The amount of Y present in the actual coating is generally small, on the order of 0.05 a/o, and is localized primarily at grain boundaries in the coating. For phase equilibrium purposes, we can ignore Y, although its presence is very important. As a protective Al, Cr oxide scale forms at the surface of the coating, Y_2O_3 forms at the boundaries and is interconnected with the surface oxide.[20] The interconnection serves to promote adherence of the surface scale to the coating. Because of differences in expansion coefficient between coating and oxide, temperature cycling can cause stresses which act to spall the protective oxide and degrade the coating by allowing new scale formation. The presence of Y tends to prolong the adherence of the protective surface scale.

The MCrAlY overlay coatings can be deposited by several methods. Physical vapor deposition is accomplished by heating a source of the desired composition with an intense electron beam to produce melting and vaporization.[21] Another commonly used technique involves thermal spraying where the coating is deposited by passing powder of the desired composition through a plasma torch impinging on the substrate or by passing the coating as a wire source through a high temperature flame.[22]

As noted earlier, the Ni-Cr-Al ternary diagram exhibits the transition $\gamma+\beta \rightleftarrows \gamma'+\alpha$, with $\gamma+\beta$ present above 1000°C, and $\gamma'+\alpha$ present below 1000°C (Figure 2). In the superalloys, γ' is stabilized by additions of elements such as Ta, Ti and Nb, so that the transition occurs at somewhat higher temperatures. This leads to some complications for understanding microstructures for NiCrAlY coatings on Ni-base superalloys after service in the range of 1000-1100°C. For example, consider a coating whose composition is located in the $\gamma'+\alpha$ field at low temperatures and the $\gamma+\beta$ field at high temperatures. Above 1000°C, the bulk of the coating will be in the $\gamma+\beta$ field. However, at the coating/substrate interface, sufficient interdiffusion may occur in service so that γ' stabilizing elements reach levels in the coating sufficient to raise the transition temperature above the service temperature and form $\gamma'+\alpha$. This can occur for compositions outside the narrow range already described. For example, compositions in the $\gamma+\gamma'+\alpha$ field at low temperature may fall in $\gamma+\gamma'+\beta$, $\gamma+\beta$ or $\gamma+\beta+\alpha$ at high temperatures, and interdiffusion can lead to differences in the ternary section which describes the structure in the different parts of the coating. for example, a coating of Ni-20a/o Cr-20a/o Al with 0.05 a/o Y on IN-738 at 1060°C is $\gamma+\beta$ for the bulk of the coating, but produces $\gamma'+\alpha$ at the coating/substrate interface.[4] As Al and Cr diffuse from the coating into the substrate, σ precipitates within the substrate.

Coatings of the CoCrAlY type are very similar to the NiCrAlY coatings, but there are differences. The γ phase of the coating transforms to the hexagonal close-packed ε phase at temperatures below about 800°C.[11] However, for use temperatures where interdiffusion is rapid, the CoCrAlY coatings consist principally of the γ fcc phase. There is a pronounced influence of Co on the NiAlCr phase equilibrium.[17] The γ' phase is destabilized, and with sufficient amounts of Co, the $\gamma+\beta$ field is stable to room temperature and $\gamma'+\alpha$ does not form.

Interdiffusion between Ni-base substrates and CoCrAlY overlayers can be plotted in the quaternary diagrams, (Figure 2). The paths can change considerably with coating composition, and frequently traverse the interior of the quaternary section. At present, there is no convenient way to represent the paths visually, and we will not attempt to do so here. For

the bulk of the interaction, however, the paths will be quite close to the ternary faces of the quaternary sections. For example, a thick CoCrAlY coating will not have high Ni concentrations until very far into its useful life. The interdiffusion path for the outer region of the coating will lie very close to the CoCrAl surface of the quaternary, and for the major portion of the coating life, Ni that diffuses to the outer region of the coating can be treated as additional Co atoms and the path can be plotted in ternary space. Similarly for the substrate/coating interaction in the substrate, insufficient Co will be present to move the diffusion path significantly far from the NiCrAl ternary surface. The remainder of the coating will have a diffusion path which traverses the quaternary section too far from a ternary surface to be represented visually in two dimensions. It should also be noted in Figure 2 that Co tends to stabilize the σ phase in the simple quaternary alloys.[23] For the Ni-base superalloys, where σ is nearly stable, diffusion of Co into the substrate may alter the appropriate diagram to include the σ phase.

Coatings of the FeCrAlY type present equally difficult problems of visualization. The major phase of the coating is bcc and for many FeCrAlY compositions that is the only phase.[24] For these coatings the diffusion couple is α versus $\gamma+\gamma'$. Since Fe tends to stabilize a $\gamma+\beta$ field in favor of a $\gamma'+\alpha$ field when added to the Ni-Cr-Al systems,[17,25] diffusion paths again can be quite complex and are strongly dependent on the coating composition. Stabilization of σ by additions of Fe occurs at lower temperatures, although not for the temperature of the section shown in Figure 2.

The overlayer coatings can be described in terms of diffusion paths just as was the case for aluminization of superalloys. However, little detailed information is available regarding the interior of the Ni-Cr-Al-Fe and Ni-Cr-Al-Co quaternary sections at any temperature. The diagrams of Figure 2 contain many field boundary locations that are completely hypothetical. In fact, the Co-Cr-Al system is not well characterized, even though the CoCrAlY coatings are in use for their exceptional resistance to hot corrosion. Much work could be done to improve our understanding of the quaternary systems which could lead to optimum environmental coatings.

Duplex aluminizing of MCrAlY coatings on Ni-base substrates is a simpler case for coating formation. The situation for aluminization of NiCrAlY, CoCrAlY and FeCrAlY coatings can be treated as ternary diffusion problems, without difficulties that arise in the more complex superalloys. Since γ' stabilizing elements are not present, the ternary diagram for Ni-Cr-Al is accurate and the temperature for the $\gamma+\beta \rightleftarrows \gamma'+\alpha$ transition is better defined. However, consideration of coating degradation by reaction with the environment and interdiffusion with the Ni-base substrate still requires more detailed evaluation of the appropriate quaternary systems.

PLATINUM ALUMINIDE COATINGS

Another coating system is extremely resistant to hot corrosion environments.[26-28] A 10-20μm layer of Pt is deposited on the Ni-base substrate and the structure is pack aluminized. Many different coating microstructures can be formed, depending on the relative amounts of Pt and Al present in the coating.[29] Coating degradation involves interdiffusion of the coating and substrate at temperatures of 875-1000°C.

The phases present in the Al-Pt diagram have not been completely characterized.[30,31] However, a recent study appears to give the best definition of the system.[32] Our studies of the aluminization of pure Pt[29] are consistent with the diagrams of Chatterji, et al.[32] In aluminizing for very short times, the phases that develop are $PtAl_3$, $PtAl_2$, Pt_2Al_3 and PtAl. After 1/2 hour of treatment, the $PtAl_3$ and $PtAl_2$ phases are eliminated by rapid interdiffusion. The major phase is Pt_2Al_3, but small amounts of Pt_2Al and Pt_3Al also are observed.

Since the Pt-Al diagram has not been characterized fully, it is difficult to consider platinum aluminide coatings on Ni-base superalloys in terms of the Ni-Cr-Al-Pt phase diagram. We have performed microstructural and microchemical analyses of coated IN-738, and as a result we now have a limited picture of the phase diagram.[29] The IN-738 substrate was coated with Pt so that a non-uniform thickness was deposited on the circular cross-section. The Pt layer varied in thickness from zero to 25μm. After aluminization, a single microsection contained a large spectrum of Pt/Al ratios. Several paths are plotted in Figure 3 to show some of the possible coating/substrate systems. The Al-Cr-Pt diagram is not critical to the explanation, and too little data are available

to permit speculation on the appearance of the ternary isothermal section. Paths through the interior of the quaternary cannot be mapped on the unfolded diagram. However, most paths observed traversed the pyramid along ternary faces or just below the faces.

The path marked 1 is for the case of a Pt coating that is thick relative to diffusion distances. The initial part of the path is that seen for aluminization of bulk Pt, and the remainder is for diffusion that occurs between bulk Pt and IN-738. Path 2 is for 1060°C aluminization of the ~25μm thick-Pt coated IN-738 just as the pack reaches temperature. The path departs from that of bulk Pt below the PtAl layer and enters the two-phase PtAl + βNiAl phase field, but it quickly crosses to Pt-rich γ and finally to γ+γ' substrate. The diagram is drawn so that a PtAl + γ field exists. It is possible, however, that this field does not exist but is blocked by Pt_2Al + β and Pt_3Al + β fields. These fields may not be observed because of kinetics of formation of Pt_2Al and Pt_3Al.

Path 3 is based on observations of the 3-hour aluminization of the thick-Pt coated IN-738. Diffusion of Al inward has eliminated the outer $PtAl_2$ region, and γ has been replaced with β(Ni, Pt)Al. Microanalysis indicates the β phase contains about 12.5 a/o Pt, with Pt apparently substituting for up to one-fourth of the Ni. For path 3, a three-dimensional depiction of its position is really more accurate. The path is shown as far as β in the Ni-Al-Pt ternary, and beginning again at β in the Ni-Al-Cr ternary. The path leaves β to form the β+α Cr finger zone, and then goes to the γ+γ' substrate. The dashed lines indicate that β+α and γ+γ' have a planar interface. The γ'+α phase field, as would be expected for the Ni-Al-Cr ternary isotherm, is not observed. The β+α phase field has between 5 and 8 a/o Pt which may put the actual path far enough into the quaternary isotherm that a ternary description is no longer valid. As Pt is added to a composition initially in the γ'+α field, the composition may move into a γ+γ'+α field, and then to a γ+β+α field. Path 3 may pass from β+α to γ+γ' at the interface describing passage through the γ+β+α field.

Path 4 describes the aluminization of thin-Pt coated IN-738 just as the pack reaches temperature. The path begins along the Pt-Al binary but quickly moves into the Ni-Pt-Al ternary isotherm. The Pt content reaches zero in the β phase, so path 4 is expected to be entirely in the Ni-Cr-Al ternary isotherm from that point on. As is seen for the aluminization of bare IN-738, the path exhibits two finger zones: $\beta+\alpha$ and $\gamma'+\alpha$. Path 5 for the 3-hour condition, thin-Pt coated IN-738, begins well into the ternary Ni-Pt-Al. Again, Pt drops to zero in β, and the remainder of the path duplicates path 4. Path 6 is the path for 0 Pt; i.e., for aluminization of bare IN-738. For very thin Pt coatings on IN-738, the microstructure would be expected to follow path 6.

A pattern emerges from the observed microstructures: for Pt coatings that are thick relative to diffusion distances for a given time-temperature treatment, the system behaves as two unconnected couples, IN-738/Pt and Pt/Al. As the Pt layer becomes thinner relative to diffusion distances, the two couples begin to interact through the common Pt terminus. With increasing time at temperature, the diffusion paths tend to move in the direction of less Al and less Pt at the surface, as expected. Commercial Pt-Al coatings are frequently heat treated at lower temperatures and longer times, but they probably go into service with a coating described by path 3 or 5. If Al is consumed in service by oxidation or by more rapid inward diffusion than that for Pt diffusion into the substrate, the outer surface composition may again move toward the Pt corner of the quaternary isotherm.

The platinum aluminide coating system for Ni-base superalloys is an example of the generation of phase diagram information from coating formation studies. However, a detailed characterization would be helpful in developing optimum coatings. As noted, path 3 may be that followed by coatings going into service, yet much of this path traverses the interior of the pyramidal section where we have little information.

OTHER COATING SYSTEMS

The Ni-base superalloys can also be protected using coatings which contain other elements. Additions of Si to NiCrAlY coatings have resulted in improved oxidation resistance.[8,33] Depending on the amount of Si present, phases in addition to those in the Ni-Cr-Al ternary system may or may not be present. Additions of Hf have been shown to have a dramatic influence on the oxidation resistance of other NiCrAl coatings.[34] Phase diagram analyses for the coating formation and service temperatures are not well characterized for either of these additions. It seems likely that as coating development proceeds, other elements will become important ingredients in high temperature coatings. These other additions, such as Ta , Ti or W, may be present in amounts sufficient to alter the phase equilibrium as described in the simple Ni-Cr-Al diagram.

SUMMARY

We have attempted to show how the appropriate phase diagrams can be used to characterize the coating formation and degradation processes in simple aluminide coatings and in overlayer MCrAlY and duplex coatings for high temperature Ni-base superalloys. Even for these systems, the available phase diagram information is inadequate in many cases to be useful in coating design to retain the desired phases for extended service life. In more complex systems, such as platinum aluminide coatings, the study of coating microstructure and microchemistry has allowed the development of a qualitative description of the Ni-Cr-Al-Pt phase diagram. However, much more detailed information would be needed to be more useful in coating design. The area of environmentally resistant high temperature coatings would be benefited by a better definition of the appropriate ternary, quaternary and possibly quinary systems.

REFERENCES

1. S. J. Grisaffe, in The Superalloys, ed. C. T. Sims and W. C. Hagel, John Wiley, New York, p. 341, 1972.
2. G. W. Goward, D. H. Boone and C. S. Giggins, ASM Trans., Quart., 60, 228 (1967).
3. R. F. Decker and C. T. Sims, in The Superalloys, ed. C. T. Sims and W. C. Hagel, John Wiley, New York, p. 33, 1972.
4. J. R. Rairden and M. R. Jackson, "The Aluminization of Nickel-Base Superalloys," submitted to Met. Trans.
5. J. B. Clark and F. N. Rhines, Trans., ASM, 51, p. 199 (1959).
6. J. S. Kirkaldy and L. C. Brown, Canadian Met. Quart., 2, p. 89 (1963).
7. J. Kirkaldy, Can. J. Phys., 36, p. 907, 1958.
8. J. R. Rairden and M. R. Jackson, General Electric Co., Schenectady, N.Y., unpublished research, 1976.
9. G. W. Goward and D. H. Boone, Oxidation of Metals, 3, 475 (1971).
10. R. L. Wachtell, Science and Technology of Surface Coating, Edited by B. N. Chapman and J. C. Anderson, Academic Press (1974).
11. M. Hansen and K. Anderko, Constitution of Binary Alloys, McGraw-Hill Book Co., Inc., New York (1958).
12. M. M. P. Janssen and G. D. Rieck, Trans., TMS-AIME, 239, 1372 (1967).
13. A. J. Hickl and R. W. Heckel, Met. Trans., 6A, 431, 1975.
14. A. Taylor and R. W. Floyd, J. Inst. of Metals 81, p. 451 (1952-53).
15. A. Taylor, Trans. AIME, 206, p. 1356 (1956).
16. I. I. Kornilov and R. S. Mints, Russ. J. Inorg. Chem., 3 p. 214, 1958.
17. M. R. Jackson and J. L. Walter, in Superalloys: Metallurgy and Manufacture, ed. B. H. Kear, D. R. Muzyka, J. K. Tien and S. T. Wlodek, Claitor's Publishing, Baton Rouge, p. 341, 1976.
18. Appendix A, Phase Diagrams, The Superalloys, ed., C. T. Sims and W. C. Hagel, John Wiley, New York, p. 577, 1972.

19. R. T. DeHoff, K. J. Anusavice and C. C. Wan, Met. Trans., 5, p. 113, 1974.

20. E. J. Felton, J. Electrochem. Soc., 108, p. 490, 1961.

21. Vapor Deposition, ed. C. F. Powell, J. H. Oxley and J. M. Blocher, Jr., John Wiley, New York, 1966.

22. H. S. Ingham and A. P. Shepard, Metco Flame Spray Handbook, Vol. III., Plasma Flame Process, Metco, Inc. Westbury, New York, 1965.

23. K. R. Gupta, N. S. Rajan and P. A. Beck, Trans., AIME., 218, p. 617, 1960.

24. Metals Handbook, 8th ed., 8, American Society for Metals, Metals Park, Ohio, 1973.

25. M. R. Jackson, in Conference on In Situ Composites-II, ed. M. R. Jackson, J. L. Walter, F. D. Lemkey and R. W. Hertzberg, Xerox-Individualized Publishing, Lexington, Mass., p. 67, 1976.

26. G. Lehnert and H. W. Meinhardt, D.E.W., Tech. Ber., 11, p. 236, 1971.

27. G. Lehnert and H. W. Meinhardt, Electrodep. Surface Treat., 1, p. 189, 1972-1973.

28. G. Lehnert and H. W. Meinhardt, Electrodep. Surface Treat., 1, p. 71, 1972-1973.

29. M. R. Jackson and J. R. Rairden, "The Aluminization of Platinum and Platinum-Coated IN-738," accepted for publication, Met. Trans.

30. F. A. Shunk, Constitution of Binary Alloys, 2nd Supplement, McGraw Hill, 1969.

31. R. Huch and W. Klemm, Z. Anorg. Chemie, Band 329, p. 123, 1964.

32. D. Chatterji, R. C. DeVries and J. F. Fleischer, J. Less-Common Metals 42, p. 187, 1975.

33. G. J. Santoro, D. L. Deadmore and C. E. Lowell, NASA TN D-6414, NASA, Lewis Research Center, Cleveland, Ohio, 44135, 1971.

34. D. R. Chang, "The Oxidation Behavior of Aluminide Coatings on René 120 and René 125", Abstract #108, Abstract Book for 1975 Materials Science Symposium, American Society for Metals, Metals Park, Ohio, p. 30, 1975.

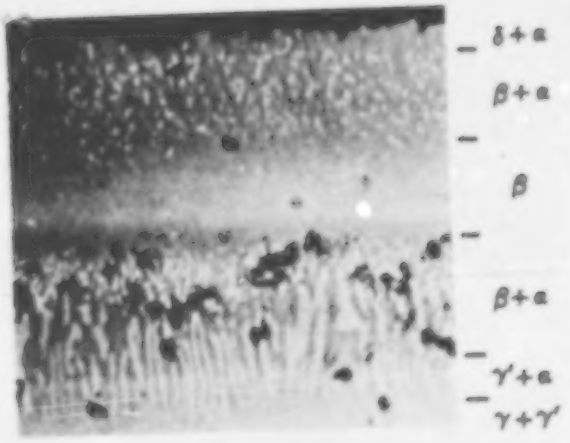

a

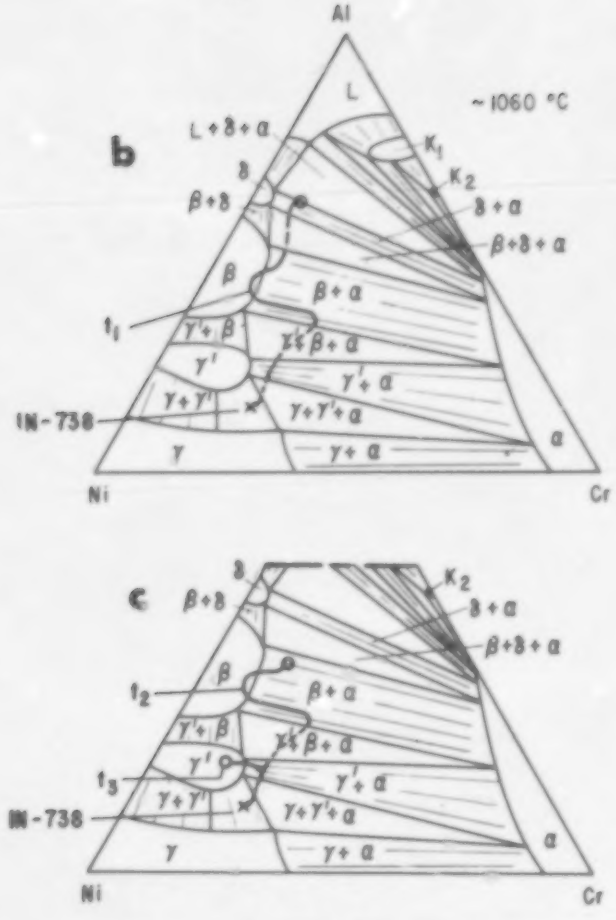

Fig. 1: (a) The microstructure formed on aluminizing IN-738 and the phase diagram Ni-Cr-Al with diffusion paths describing (b) coating formation and (c) degradation.

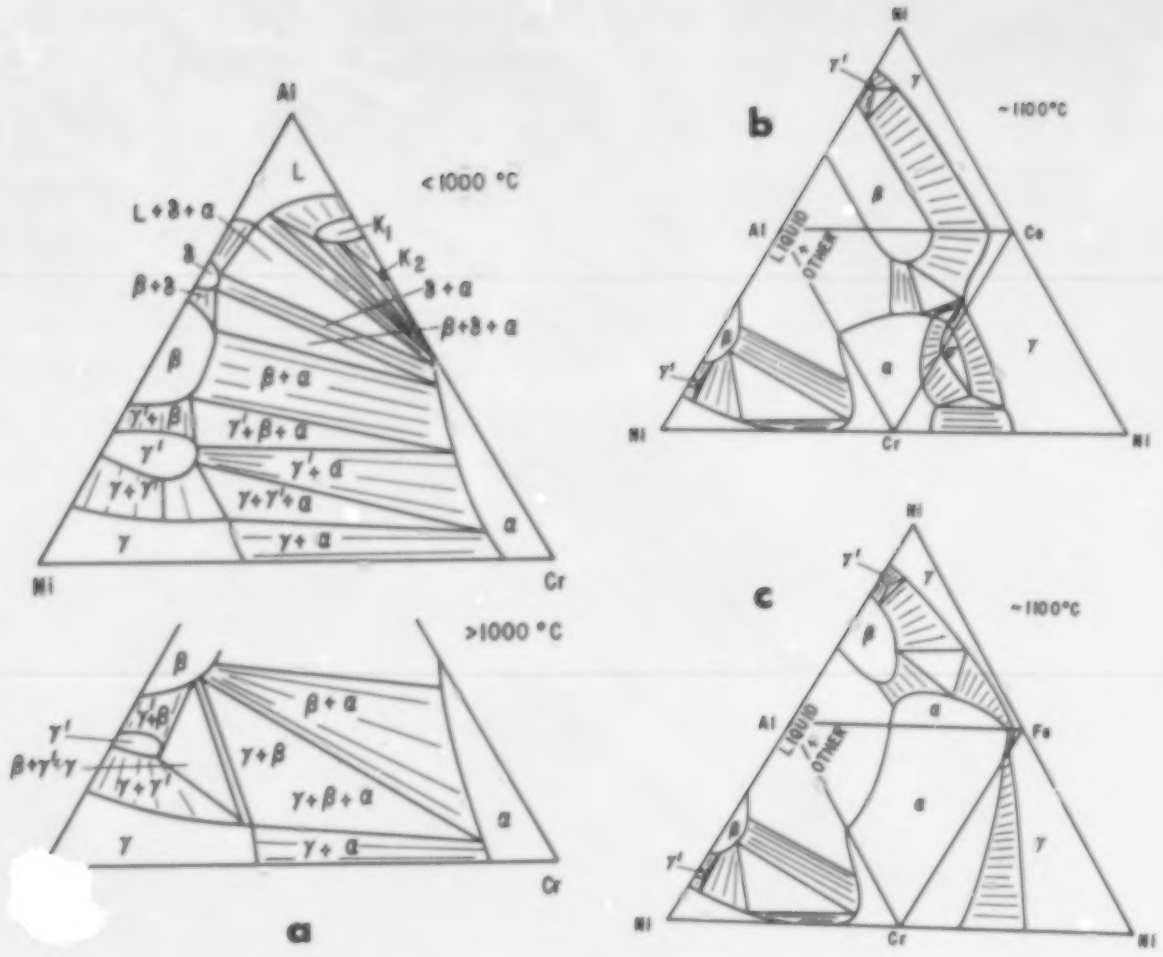

Fig. 2: Phase diagrams for coatings on superalloys; (a) Ni-Cr-Al, (b) Ni-Cr-Al-Co, (c) Ni-Cr-Al-Fe.

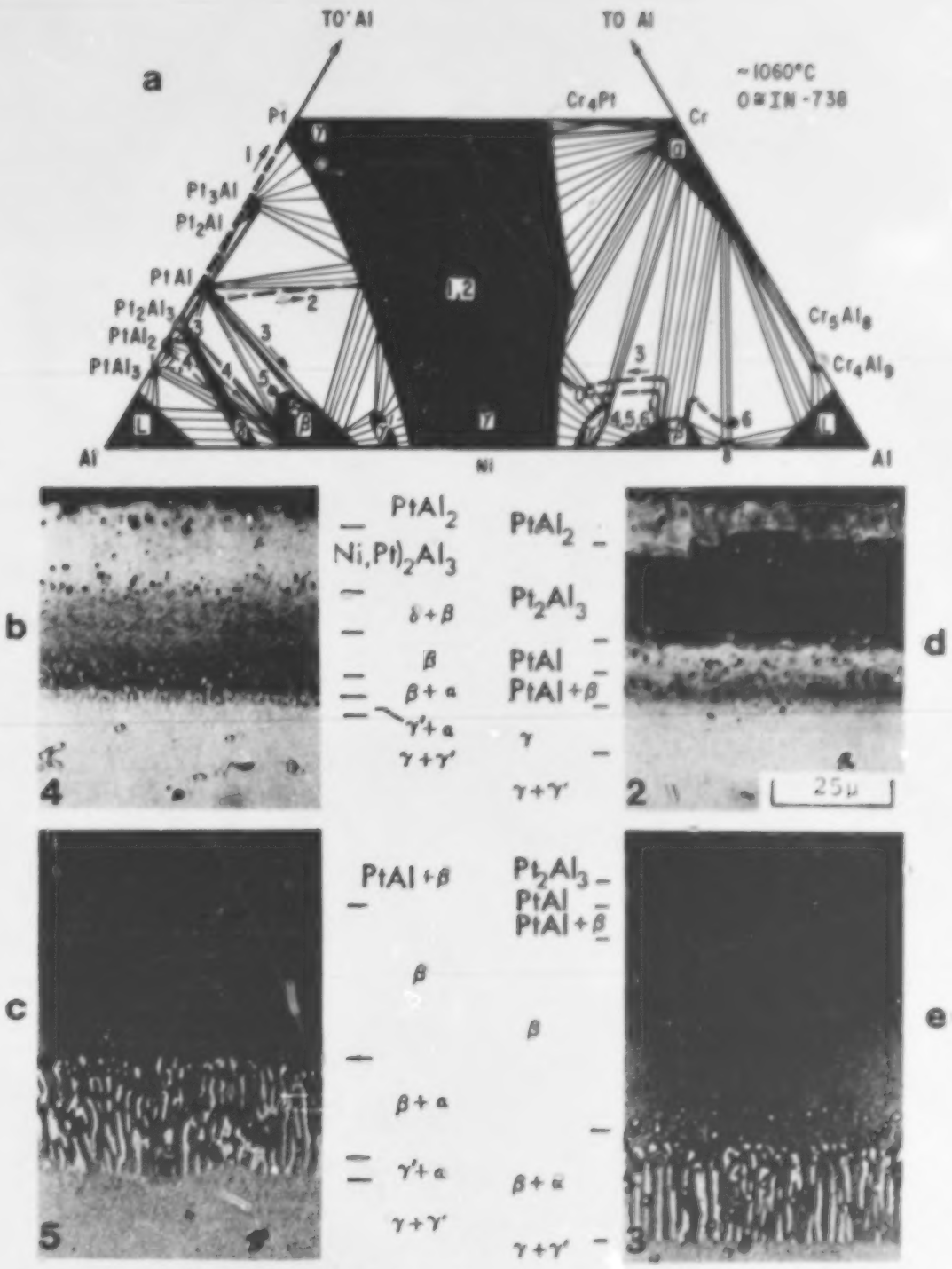

Fig. 3: (a) Schematic phase diagram for Ni-Cr-Al-Pt with diffusion paths describing platinum aluminide coating formation on IN-738 in a 1060°C pack for (b) 5μm Pt as the pack reaches temperature, and (c) after 3 hours at 1060°C, and for (d) 25μm Pt as the pack reaches temperature and (e) after 3 hours at 1060°C.

National Bureau of Standards SP-496, Applications of Phase Diagrams in Metallurgy and Ceramics
Proceedings of Workshop held at NBS, Gaithersburg, Md., January 10-12, 1977

APPLICATION OF THE SCANNING ELECTRON MICROSCOPE TO THE STUDY OF HIGH TEMPERATURE OXIDE PHASE EQUILIBRIA

L. P. Cook and D. B. Minor

National Bureau of Standards
Institute for Materials Research
Washington, D. C. 20234

INTRODUCTION

Instrumentation

An early scanning electron microscope (1) was built several years before invention of the electron microprobe x-ray analyzer by Castaing (2), yet the latter was the first type of analytical electron beam instrument available commercially in a fully developed form. In the last ten years, electron microbeam instrumentation has evolved rapidly and the distinction between microprobes and SEM's has in many respects vanished. It is convenient to differentiate modern electron microprobes by the presence of wavelength dispersive spectrometers and high precision stages. High resolution SEM's usually employ energy dispersive x-ray analysis (EDX) systems, more convenient for the rapid accumulation of spectral information. Since the work of Fitzgerald et al. (3), EDX resolution and associated software have developed to the point where quantitative analyses are possible if proper operating conditions and data reduction methods are employed (4).

Reviews of basic microprobe and SEM instrumentation are given by Fitzgerald (5), Wells (6) and others. EDX instrumentation and operation are discussed by Lifshin et al. (7) and Gedcke (8).

Application

Microchemical characterization aids significantly in the determination of phase diagrams (9). Examples of electron microprobe application to the study of oxide phase equilibria are numerous (see for example, 10). However as Keil (11) notes, use of classical microprobe methods in the study of fine grained experimental products has been limited by the relatively poor spatial resolution of x-ray information (1.0 to 0.1 μm).

One of the first SEM uses in the study of ceramic systems is the work of Thornley and Cartz (12); subsequent SEM studies of ceramic materials have been published at an increasing rate (13). Although reviews have been written on SEM application to ceramic studies (see for example, 14), SEM potential in phase equilibrium investigations has not been emphasized. We will demonstrate in this paper how the SEM/EDX combination is a particularly powerful tool in the study of oxide phase equilibria, where otherwise unobtainable information can be gathered for reactants. Examples given below are primarily from experiments made using the quenching technique, but SEM/EDX has application to the results of other methods used in the determination of oxide phase diagrams such as DTA, TGA, and the various hydrothermal, effusion, diffusion and electrochemical techniques.

EXAMINATION OF EXPERIMENTAL PRODUCTS

Subsolidus Studies

While much of the characterization of reactions in the solid state must be done by x-ray diffractometry, SEM studies of polished surfaces can sometimes detect small amounts of a second phase not present in large enough quantities to give an easily detectable x-ray powder diffraction pattern. Moreover SEM examination in such cases can give an indication of textural relationships. Figure 1 shows an iron Kα x-ray map of Fe_2O_3 exsolution laths in a (Mg, Al, Fe)-spinel matrix. These laths are at the limit of x-ray spatial resolution and x-ray maps must be supplemented with the SEM image (Figure 2) for proper interpretation. It should be noted that surface preparation was of utmost importance in this example. The difference in atomic number is the main contrast mechanism when examining smooth polished surfaces such as this and because backscattered electrons are involved, resolution is correspondingly less, of the order of 30 nm (15) as opposed to 7 nm or better for high resolution secondary electron images.

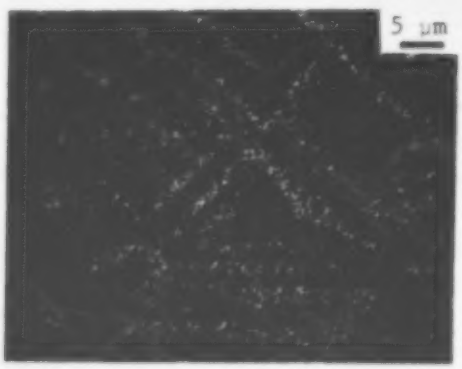

Figure 1. Fe Kα x-ray map of polished surface showing exsolution of Fe_2O_3 in (Mg,Al,Fe)-spinel (see Figure 2).

Figure 2. Secondary electron image of area corresponding to Figure 1. 20 kV, 45° tilt.

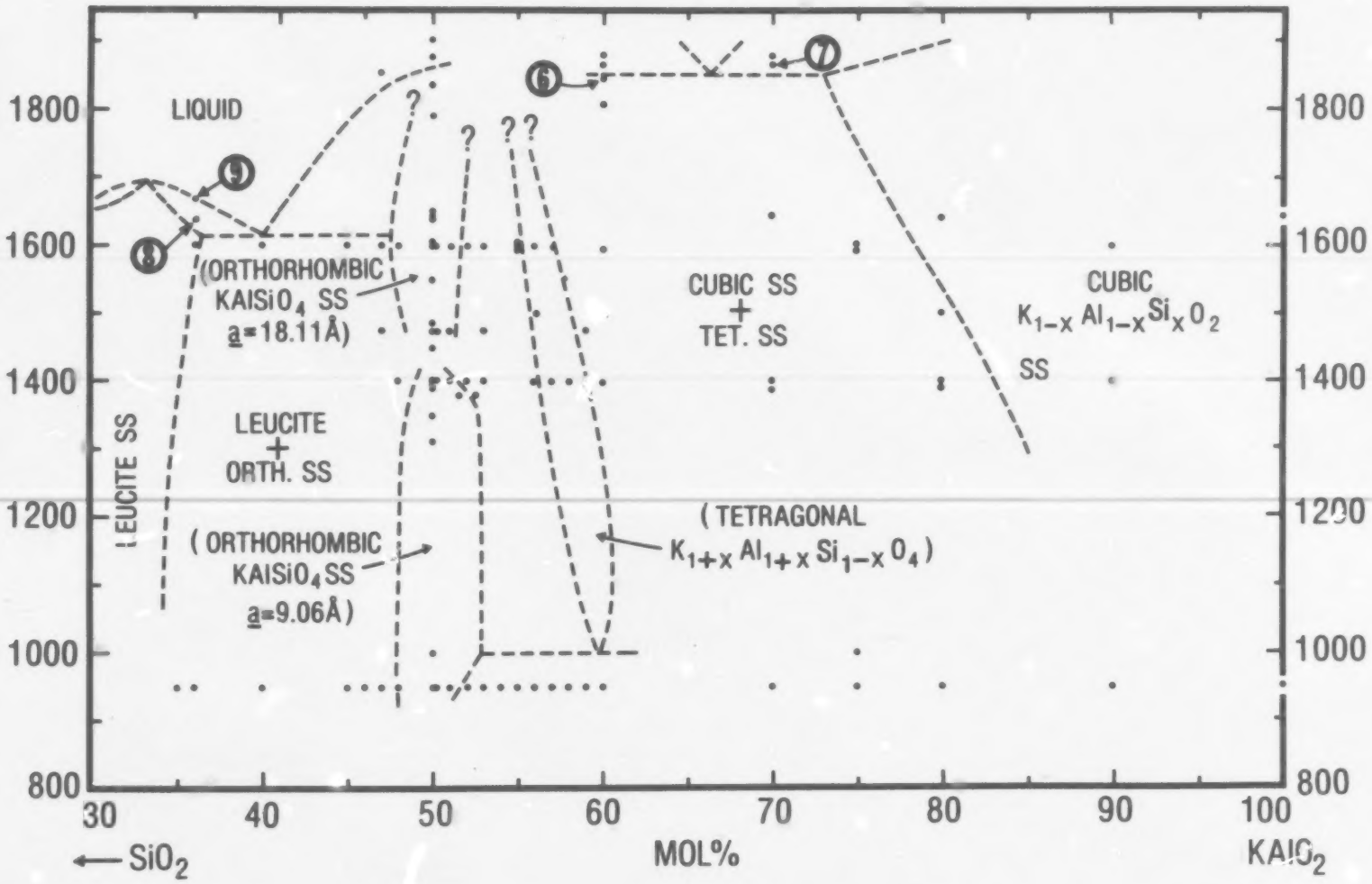

Figure 3. Hypothetical phase diagram of the $KAlO_2$-SiO_2 system, showing some of the experiments examined with the SEM. Numbers refer to Figures in which micrographs of experimental products are shown.

In some cases, especially where solid-liquid and solid-gas equilibria are involved high resolution secondary electron images allow one to determine the type of solid phase present, and the reaction which is occurring, on the basis of crystal morphology (16, 17). If morphologies are distinctive this can be done in situ for sparse crystals which could not be investigated by other means.

We have made particular use of SEM/EDX methods to correlate the results of flux syntheses with quench experiments in the system $KAlO_2$-SiO_2 (Figure 3). Flux-grown single crystals were used for x-ray diffraction precession analyses to establish the unit cell and space group of the solids appearing on the phase diagram, then mounted on a carbon planchet using the technique described by Brown and Teetsov (18). Semi-quantitative analyses were performed for single crystals of orthorhombic and tetragonal (Figure 4) phases, by normalizing and comparing intensities with those from standard glasses (a typical EDX spectrum is shown in Figure 5). During analysis the electron beam was rapidly rastered over an area 100 μm x 100 μm to prevent specimen charging and compositional changes. The SEM goniometer stage was of particular use in selecting an uncontaminated flat face on the crystal and orienting it as precisely as possible for analysis. For both tetragonal and orthorhombic phases, semi-quantitative analyses of single crystals (excluding fluorine) allowed us to state that: 1) single crystals plot on or near the join $KAlO_2$-SiO_2; 2) they plot close to or within the phase regions outlined by quench experiments.

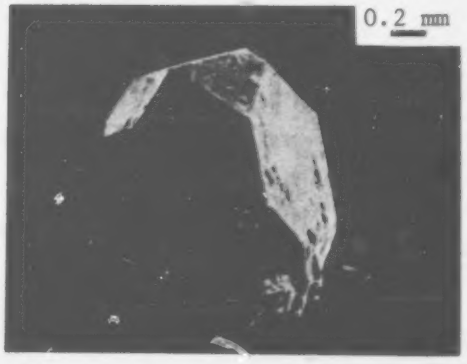

Figure 4. Single crystal of flux-grown tetragonal $K_{1+x}Al_{1+x}Si_{1-x}O_4$. Note flat faces suitable for semi-quantitative analysis. 20 kV, 0° tilt.

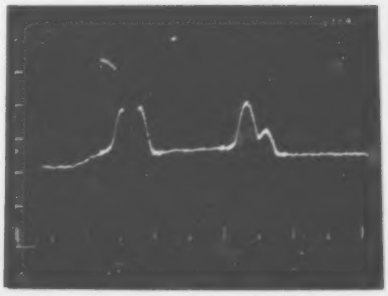

Figure 5. A typical EDX spectrum of material in Figure 4.

Solidus Studies

For many high temperature applications equilibria may be very complicated and yet a detailed phase diagram is needed. Such systems may have steeply dipping liquidii and closely spaced compounds. A major problem then comes in interpreting the character of quench experiments: does sintering result from grain boundary growth and annealing, or does it result from small amounts of quenched equilibrium melt, recrystallized equilibrium melt, or some combination thereof? This problem has been approached with the SEM in our preliminary work on the system $KAlO_2$-SiO_2. The overall appearance of both specimens shown in Figures 6 and 7 suggested melting when results were examined with the binocular microscope. Light optical examination of immersion mounts also proved inconclusive, and so both were subjected to SEM examination at high magnification. In the $(KAlO_2)_{60}(SiO_2)_{40}$ specimen (Figure 6) the melting was apparently a transitory phenomenon, perhaps spurred by the presence of a non-equilibrium solid assemblage or by the requirement to minimize surface free energy. Grain boundaries appear sharp and equant throughout the sample (Figure 6-c), and no areas suggestive of melt segregation can be found. The recrystallization was more intense in some areas of the sample (Figure 6-b) than others (Figure 6-a), suggesting limited migration of a metastable melt during recrystallization.

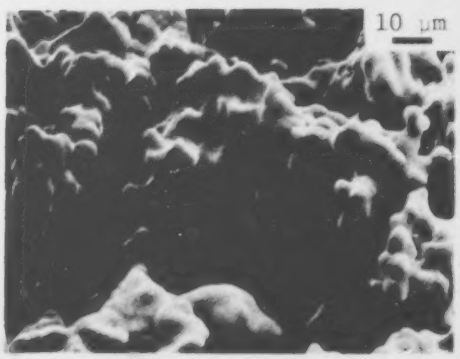

6a) Weakly sintered area.

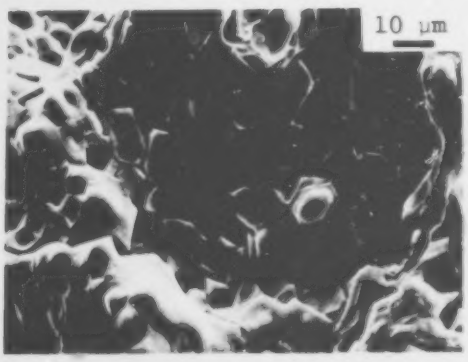

6b) Highly sintered area.

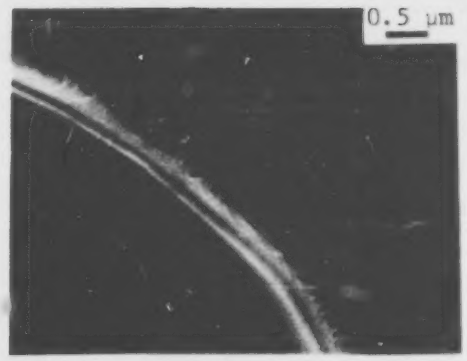

6c) High magnification micrograph of grain boundary in (a). Note sharpness compared to Figure 7-c.

Figure 6. Solidus studies - experiment below solidus. $K_{60}S_{40}$, 1850°C. Micrographs taken at 20 kV, 45° tilt.

469

By contrast, the $(KAlO_2)_{70}(SiO_2)_{30}$ sample (Figure 7) contains fine grained low-lying areas between larger grains (Figure 7-a) suggestive of recrystallized equilibrium melt (Figure 7-b). The grain boundary in Figure 7-c shows what appears to be an intergranular phase. Owing to the difficulty of temperature control with the induction furnace used, this run was of short duration at maximum temperature attained and any melt formed may not have had time to segregate completely into larger volumes. Alternatively, since the grain boundaries in Figure 7-c were close to the area of melt in Figure 7-b, we may be looking at the effect of capillary action.

The $K_{60}S_{40}$ example above is similar in some respects to the recrystallization of $MgAl_2O_4$ observed by Daw and Nicholson (19). Froschauer and Fulrath (20) have observed formation of a liquid phase at grain boundaries during sintering of particles on a high temperature stage in the SEM.

Liquidus Studies

In many instances there are advantages in looking at the undisturbed quench specimens, as removed from the capsule. Figures 8-a, b are micrographs of the surface of a sample of $(KAlO_2)_{36}(SiO_2)_{64}$ heated at 1641°C. Dendritic outlines protruding into areas of low relief suggest non-equilibrium crystallization from the melt during quench. Also present on the surface of the specimen are coarser crystals having well developed sharp boundaries and roughly equant shapes, interpreted as formed under equilibrium conditions. In contrast, the surface of a sample of $(KAlO_2)_{36}(SiO_2)_{64}$ heated at 1658°C, that was completely melted, is largely featureless (not shown).

As shown in Figures 8-c, d the manner in which glass fractures allows the detection of crystalline phases on fracture surfaces with the SEM. For the $KAlO_2$-SiO_2 experiments mentioned above, conclusions drawn from outer surfaces and fracture surfaces are similar. Coarser grains, presumably formed at equilibrium are conspicuous because of the regular, structurally controlled features visible on fracture surfaces (Figure 8-c). The fine-grained quench structures are less apparent, but nonetheless distinguishable (Figure 8-d). The completely melted sample (Figure 9) shows only a smooth conchoidal fracture surface.

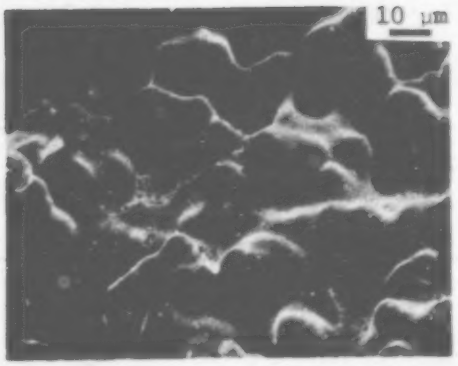

7a) Micrograph showing rounded grains separated by voids and areas with fine structure.

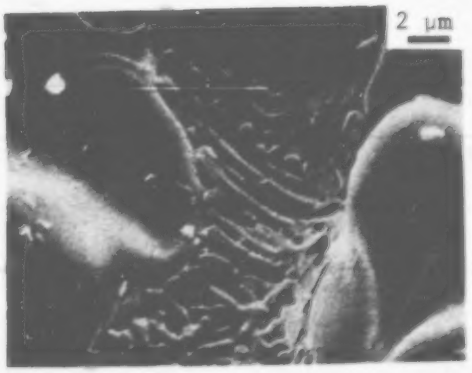

7b) Detail of (a). Dendritic texture is interpreted as recrystallized melt.

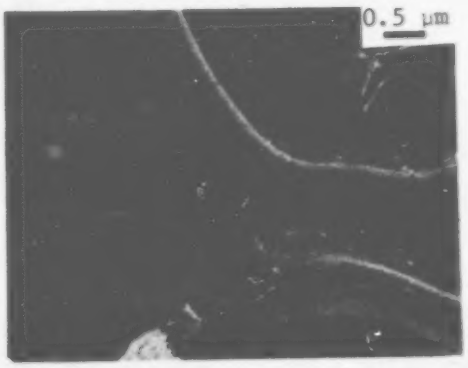

7c) High magnification micrograph of area in upper left of (b). Note what is interpreted as film of quenched melt along grain boundaries.

Figure 7. Solidus studies - experiment above solidus. $K_{70}S_{30}$, 1880°C. Micrographs taken at 20 kV, 45° tilt.

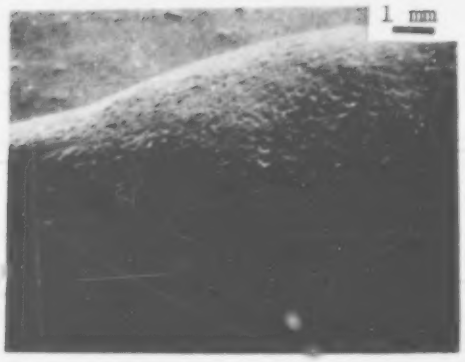

8a) Low magnification micrograph of outer surface of experiment.

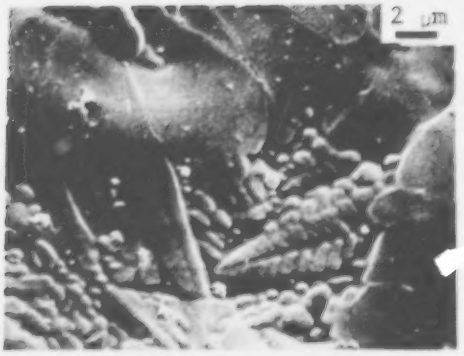

8b) High magnification detail of (a). Dendritic texture suggests growth from melt upon quench. Grains at top and right may represent solids in equilibrium with melt.

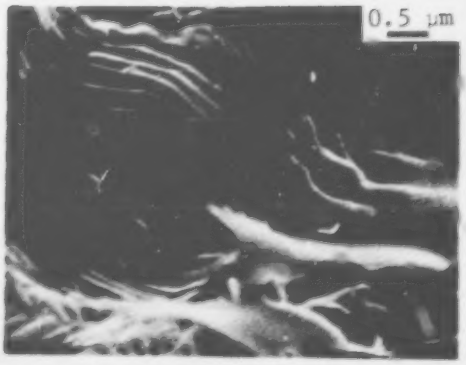

8c) Fracture surface. Relatively large crystal (corrugated surface) in glass, interpreted as formed at equilibrium.

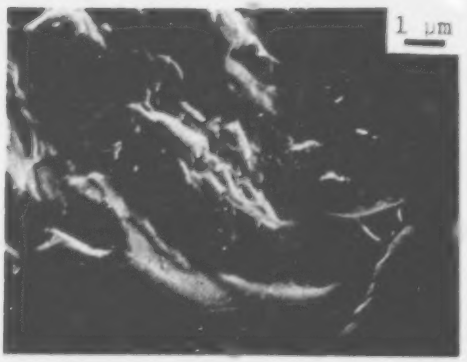

8d) Fracture surface. Fine grained aggregate of crystallites in glass, interpreted as forming on the quench.

Figure 8: Liquidus studies - experiment below the liquidus. $K_{36}S_{64}$, 1641°C. Micrographs taken at 20 kV, 45° tilt.

Figure 9. Liquidus studies - experiment above liquidus. $K_{36}S_{64}$, 1658°C. Fracture surface, no evidence of crystalline phases in glass. 20 kV, 45° tilt.

CONCLUSIONS

The scanning electron microscope can be applied to the study of high temperature oxide phase equilibria for examination of experimental results. Many of the functions of conventional light microscopy in the analysis of phase equilibria products can be performed, at higher magnification, and without disrupting the specimen. Correlation between single crystal syntheses and quench experiments is facilitated. Precise determination of solidus boundaries in complex systems using the quenching technique is made more feasible. Perhaps the most important advantage of the SEM/EDX technique is the presentation of textural relations between phases which are not as conveniently studied at high magnification with the immersion method of light microscopy. This advantage arises not only because of the superior resolution of the SEM, but also because of its much greater depth of focus.

ACKNOWLEDGEMENTS

The authors wish to thank Dr. R. S. Roth for stimulating discussion which has led to preparation of this paper. Dr. T. Negas kindly supplied the micrographs in Figures 1 and 2. J. Waring and C. Harding performed the high temperature experiments. E. Farabaugh and Dr. D. Newbury improved the manuscript through their critical reviews.

REFERENCES

1. V. K. Zworykin, J. Hillier, and R. L. Snyder, ASTM Bull. 117, 15 (1942)

2. R. Castaing, Ph.D. Thesis, Univ. of Paris, 1951.

3. R. Fitzgerald, K. Keil and K.F.J. Heinrich, Science 159, 528 (1968).

4. C. E. Fiori, R. L. Myklebust and K.F.J. Heinrich, Microbeam Anal. Soc., Proc. 11th Ann. Conf. Miami Beach, 1976, Paper 12.

5. R. Fitzgerald, in "Microprobe Analysis", C. A. Andersen, Ed., Wiley-Interscience, New York, 1973, pp 1-51.

6. O. C. Wells, "Scanning Electron Microscopy," McGraw-Hill, New York, 1974, 421 p.

7. E. Lifshin, M. F. Ciccarelli, and R. B. Bolon, in "Practical Scanning Electron Microscopy", J. I. Goldstein and H. Yakowitz, Eds., Plenum Press, New York, 1975, pp. 263-297.

8. D. A. Gedcke, in "Quantitative Scanning Electron Microscopy," D. B. Holt, M. D. Muir, P. R. Grant and I. M. Boswara, Eds., Academic Press, New York, 1974, pp. 403-450.

9. A. D. Romig, Jr., and J. I. Goldstein, Workshop on Applications of Phase Diagrams in Metallurgy and Ceramics. National Bur. Standards, Gaithersburg, MD, January 1977, Paper MPSII-7.

10. K. L. Keester and W. B. White, J. Amer. Ceram. Soc. 53, 39 (1970).

11. K. Keil, in "Microprobe Analysis", C. A. Andersen, Ed., Wiley-Interscience, New York, 1973, pp. 189-239.

12. R. R. M. Thornley and L. Cartz, J. Amer. Ceram. Soc. 45, 425 (1962).

13. V. E. Johnson, in "Scanning Electron Microscopy/1974", O. Johari and I. Corvin, Eds., IIT Research Inst., Chicago, 1974, pp. 763-812.

14. E. W. White and R. Roy, in "Scanning Electron Microscopy/1968", O. Johari, Ed., IIT Research Inst., Chicago, 1968, pp. 89-94.

15. O. C. Wells, in "Scanning Electron Microscopy/1974", O. Johari and I. Corvin, Eds., IIT Research Inst., Chicago, 1974, pp. 361-368.

16. S. T. Liu, G. H. Nancollas and E. A. Gasiecki, J. Crystal Growth 33, 11 (1976).

17. S. Chatterji and J. W. Jeffrey, Nature 209, 1233 (1966).

18. J. A. Brown and A. Teetsov, in "Scanning Electron Microscopy/1976", O. Johari, Ed., IIT Research Inst., Chicago, pp. 385-392.

19. J. D. Daw and P. S. Nicholson, J. Amer. Ceram. Soc. 58, 109 (1975).

20. L. Froschauer and K. M. Fulrath, J. Mater. Sci. 10, 2146 (1975).

National Bureau of Standards SP-496, Applications of Phase Diagrams in Metallurgy and Ceramics
Proceedings of Workshop held at NBS, Gaithersburg, Md., January 10-12, 1977

Hyperfine Techniques and the Determination of Phase Diagrams

R. C. Reno*

Department of Physics

University of Maryland, Baltimore County

Baltimore, MD 21228

and

L. J. Swartzendruber, G. C. Carter and L. H. Bennett

Institute for Materials Research

National Bureau of Standards

Washington, DC 20234

I. Introduction

Within any material there exist internal electric and magnetic fields which are produced by the positively charged atomic nuclei and the negatively charged core and valence electrons. The fields depend upon the arrangement of these constituents (e.g., spatial ordering of the ion cores) as well as interactions between the constituents (e.g., chemical bonding and electron exchange effects). Of particular interest are the internal fields present at the positions of the atomic nuclei. These "hyperfine" fields interact with the nuclei and shift the discrete energy levels, allowing nuclear transitions which can be observed by a number of techniques[1].

This review will discuss three well-established techniques for measuring the nuclear hyperfine interaction - nuclear magnetic resonance (NMR)[2,3], the Mössbauer effect (ME)[2] and the perturbed angular correlation of gamma rays (PAC)[4]. It will discuss how the hyperfine interaction is influenced by the chemical, magnetic, and structural properties of the material involved and will illustrate how each of the above techniques can be used to provide information useful in constructing phase diagrams.

II. Description of the Techniques

All three of the above hyperfine techniques detect a change in the nuclear energy levels of the atom in the material studied by observing transitions between levels.

The ^{57}Fe nucleus can best illustrate the similarities and differences in the three techniques. In addition to the ground state, ^{57}Fe has two excited nuclear energy levels as shown in Fig. 1. The ground state

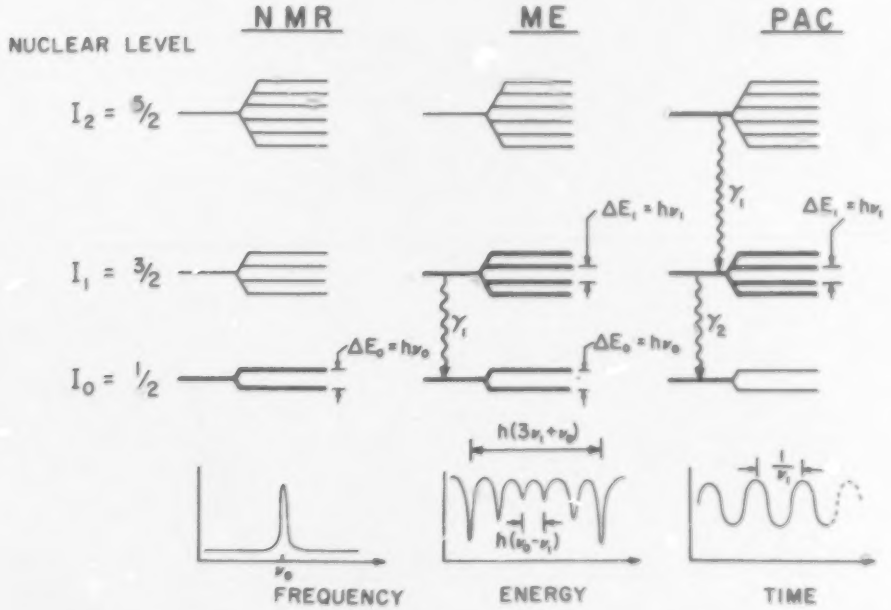

Fig. 1. An example of the energy levels and transitions used in nuclear magnetic resonance (NMR), Mossbauer effect (ME), and perturbed angular correlation experiments. The nuclear spins and energy levels shown are those appropriate for an ^{57}Fe nucleus in the presence of a magnetic field. The types of resonances observed for each method are also illustrated.

nucleus has a spin of 1/2 while the first and second excited states have spins 3/2 and 5/2, respectively. When ^{57}Fe nuclei interact with a hyperfine field, these levels will be split into discrete sublevels, the number and spacing of which depend on the type and strength of the field. If, for example, a static magnetic field, H, acts on the nucleus, the levels will be split in accordance with the well known Zeeman effect, as shown in the figure. The degree of splitting of the ground state will differ from that of the excited states since each state has a different magnetic moment, μ. It will be sufficient to consider only the ground state splitting ($\Delta E_o = \mu_o H$) and the first excited state splitting ($\Delta E_1 = \mu_1 H$).

In a nuclear magnetic resonance experiment, the nuclei of interest are those in the ground state (the lowest energy configuration), where $\Delta E_o = \mu_o H$ is small compared to the energy difference between ground and first excited state. The presence of electromagnetic radiation will promote transitions between the two sublevels of the ground state. A resonant absorption of energy is observed when the frequency, ν_o, satisfies the condition $h\nu_o = \mu_o H$ where h is Planck's constant, and ν_o is on the order of radio frequencies.

In the Mössbauer effect, one observes transitions between the first excited state and the ground state. The magnetic hyperfine field will cause Zeeman splittings in both of these states and therefore eight (4x2) transitions could occur between the excited state and the ground state. Of these eight, only six are allowed by quantum mechanical selection rules and they are observed by measuring the six energies necessary to

excite nuclei from their ground state to the first excited state. The excitation energies are measured by doppler shifting the exciting radiation (14 keV gamma rays) until a recoilless absorption occurs and a resonant dip appears in gamma ray transmission through the sample. The positions of the six resonant energies depend upon ΔE_o and ΔE_1, both of which depend upon the magnetic field strength.

In perturbed angular correlation experiments, the nucleus is prepared in the second excited state and is then allowed to decay spontaneously to the ground state by the two step process, $I_2 \xrightarrow{\gamma_1} I_1 \xrightarrow{\gamma_2} I_o$. This involves the emission of two gamma rays γ_1, and γ_2 in time coincidence, the delay between emissions being on the order of 10^{-7} sec. The presence of a hyperfine field H at the nucleus during this time interval will cause the coincidence rate to vary sinusoidally in time with a period T equal to $1/\nu_1$. This is the Larmor period - the time necessary for the nuclear spin to precess once about the field direction - and depends upon the field strength since $1/\nu_1 = h/\mu_1 H$.

Thus, all three techniques sense the splitting in one or more nuclear levels produced by interaction with the hyperfine field. While the above discussion used a *magnetic* field for illustrative purposes, the same type of effects will be observed for the interactions between the nuclear quadrupole moment and *electric field gradients*. Magnetic fields may be either externally applied, or internally generated by the presence of permanent or induced magnetic moments. Electric field gradients of sufficient magnitude to give observable effects cannot be externally applied, and are present only when the nucleus is in a non-cubic environment.

Although the information obtained by all three techniques is similar, the mode of detection varies considerably and each technique has limitations

as well as advantages. Table I summarizes the salient differences between NMR, ME, and PAC.

III. Applications

The hyperfine field at an atom in a material depends on the crystal structure in the region of the atom and on the electronic structure of the atom and its neighbors. Common types of hyperfine interactions include electric field gradients due to non-cubic crystal symmetry, isomer and Knight shifts due to electron density changes and magnetic fields due to co-operative electron spin effects (magnetism). The hyperfine field often changes measurably when the material changes phase. This property can provide a signature by which to identify each phase. Furthermore, two-phase mixtures can be analyzed with the three presently described hyperfine techniques, using a lever rule which becomes enhanced due to the preferential concentration of the field-sensing atoms in one phase. This "enhanced" lever rule[5] can be expressed for an A-B alloy with an α and β phase, as

$$R = \frac{C_\alpha f_\alpha}{C_\beta f_\beta}$$

where R is the ratio of the intensity of the NMR, ME, or PAC signal from the B atoms in the α phase to the intensity from those in the β phase, C_α and C_β are the concentration of B atoms in the α and β phase, respectively, and f_α and f_β are the fractions of α phase and β phases present, as given by the ordinary lever rule. When close to the α-phase boundary, the "enhancement" of the signal from the minority β phase arises from the high concentration of B atoms in the β phase. An example of the signals obtained from the psuedo-binary system $AuAl_2$-$AuIn_2$ is shown in Fig. 2.

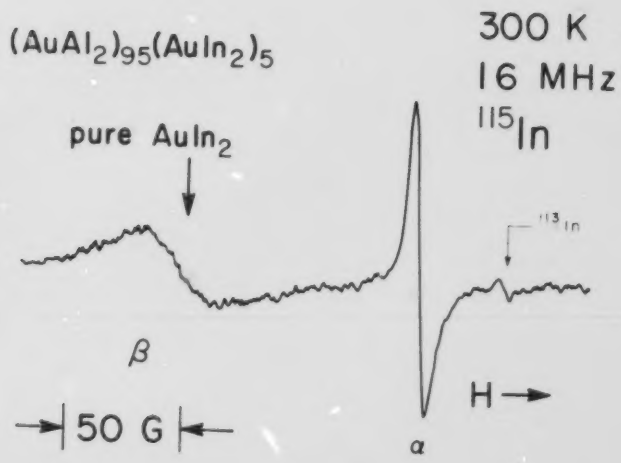

Fig. 2. ^{115}In NMR spectrum for the alloy $(AuAl_2)_{95}$ showing a separate resonance for the indium nuclei in each of the two phases. The separation of the two resonances is due to the NMR metallic shift (known as the Knight Shift) caused by different hyperfine fields at the In sites in the two different phases. From this resonance, the solubility of $AuIn_2$ in $AuAl_2$ (at the homogenization temperature of 500°C) can be obtained very accurately (from ref. 5).

NMR contributions to phase determinations include measurements of: the solubility of $AuAl_2$ in $AuIn_2$[6]; liquid-solid phase equilibria in Cu-Te alloys[7]; phase changes in La, Nb and Ta hydrides[8]; phase identification in Na-Tl alloys[9]; and Hg concentration in Cd-Hg alloys[10]. The NMR measurements on Cu-Te alloys[7] are extremely useful since one phase is liquid and some alternative techniques, such as x-ray diffraction, cannot be utilized. The measurements on Na-Tl[9] provided evidence that an ordered compound $NaTl_2$ exists with the same crystal structure as NaTl - a fact hard to obtain from x-ray analysis alone since Na has a much smaller scattering factor than Tl and both lattices have the same arrangements of Tl atoms.

Mössbauer measurements of multi-phase systems include: detection of microprecipitates in Fe-Cu-Ni alloys[11], the observation of a metastable (θ) phase in Fe-Ti[12], a study of phase boundaries in TiFe-H[13], an examination of phase changes during the sintering of β-Fe_5Ge_3[14]; and studies of surface-induced changes in supported Pt and Pd particles as small as 3nm[15]. Some spectra of TiFe-H are shown in Fig. 3. The Mössbauer

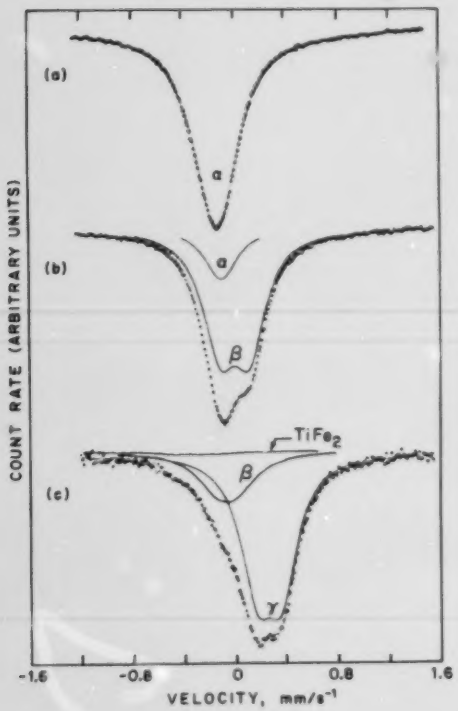

Fig. 3. Room temperature Mössbauer absorption spectra for $TiFeH_x$. The line through the data points is a least-squares fit which is the sum of the the contributions from the individual phases. (a) x = 0.1, 100% α phase. (b) x = 0.9, 19% α phase and 81% β phase. (c) x = 1.7, which consists of 23% β phase, 75% γ phase, and 2% of spurious $TiFe_2$. (After Ref. 13).

measurements on Fe-Cu-Ni alloys[11] indicated the maximum solubility of Fe in a Cu-Ni alloy and showed that excess Fe formed precipitates too small to be observed by conventional techniques. The presence of these precipitates could be correlated with increased corrosion of the alloy in saline environments. The measurements on Fe-Ge[14] illustrate the kinetics involved in the transformation of Fe and Ge to β-Fe_5Ge_3. During the sintering

process the following phases were observed: Fe, γ-FeGe, ε-Fe_3Ge, η-$Fe_{1.4}Ge$ and β-Fe_5Ge_3. The η phase has not been observed unambiguously by x-ray diffraction but clearly shows up in Mössbauer spectroscopy.

Perturbed angular correlation measurements of multi-phase systems are less numerous than those done by NMR and Mossbauer effect, primarily because the sample under study must be made radioactive. Studies do exist, however, on Ni-Hf alloys[16], Zr-Hf hydrides[17], and In-Bi liquid alloys[18]. The data on In-Bi liquid alloys seem to indicate that some ordering takes place in the liquid phase since liquids around the composition In_2Bi show hyperfine interactions characteristics of an ordered array of atoms. NMR studies have also given qualitative evidence for the existence of In_2Bi groupings in liquid In-Bi alloys[19].

In addition to hyperfine studies which detect two or more phases simultaneously, there exist a wide range of NMR, Mössbauer and PAC measurements that are concerned with single phase materials that undergo first or second order phase transitions. Numerous hyperfine measurements have been done, for example, on the transition from ferromagnetic (or antiferromagnetic) to paramagnetic behavior in pure, single phase materials[20-22]. Hyperfine techniques have also been used to study structural phase transitions[23,24] and ferroelectric transitions[25-27].

References

*Also a consultant, Alloy Physics Section, Institute for Materials Research, National Bureau of Standards.

1. e.g. Hyperfine Interactions, ed. by A. J. Freeman and R. B. Frankel, (Academic Press, New York, 1967).
2. I. D. Weisman, L. J. Swartzendruber, and L. H. Bennett, Nuclear Resonances in Metals: Nuclear Magnetic Resonance and Mossbauer Effect, chapter VI-2, in Techniques of Metals Research, ed. by. R. F. Bunshah (John Wiley & Sons, 1973).
3. G. C. Carter, D. J. Kahan and L. H. Bennett, Metallic Shifts in NMR, Progress in Materials Science 20, 1 (1976).
4. M. Frauenfelder and R. M. Steffen, in Alpha-, Beta- and Gamma-Ray Spectroscopy, Vol. 2, ed. by K. Seigbahn (North Holland Pub. Co., Amsterdam, 1966). p. 997.
5. L. H. Bennett and G. C. Carter, Metallurgical Transactions 2, 3079 (1971).
6. G. C. Carter, I. D. Weisman, L. H. Bennett and R. E. Watson, Phys. Rev. B 5, 3621 (1972).
7. W. W. Warren, Charge Transfer/Electronic Structure of Alloys, ed. by L. H. Bennett and R. H. Willens (Metallurgical Society of America, New York, 1974) p. 223.
8. D. Zamir and R. M. Cotts, Phys. Rev. 134, A666 (1964); D. S. Schreiber and R. M. Cotts, Phys. Rev. 131, 1118 (1963); B. Pedersen, T. Krogdahl and O. E. Stokkeland, J. Chem. Phys. 42, 72 (1965).
9. L. H. Bennett, Acta. Met. 14, 997 (1966).

10. V. V. Zhukov, I. D. Weisman and L. H. Bennett, J. of Research 77A, 713 (1973).

11. L. H. Bennett and L. J. Swartzendruber, Acta. Met. 18, 485 (1970).

12. M. M. Stupel, M. Ron and B. Z. Weiss, Journal de Physique, Colloque C6, 35, 483 (1974).

13. L. J. Swartzendruber, L. H. Bennett and R. E. Watson, J. Phys. F: Metal Phys. 6, L331 (1976).

14. D. Eliezer, S. Nadiv and M. Ron, Journal de Physique, Colloque C6, 35, 477 (1974).

15. C. H. Bartholomew and M. Boudart, J. Catalysis 29, 278 (1973); R. L. Garten and D. E. Ollis, J. Catalysis 35, 232 (1974).

16. E. Gerdau, H. Winkler, W. Gebert, B. Giese and J. Braunsfurth, Hyperfine Int. 1, 459 (1976).

17. R. L. Rasera, University of Maryland, Baltimore County, private communication.

18. S. Tamaki, Y. Tsuchiya, A. Furusawa and H. Okazaki, J. Phys. F: Metal Phys. 6, 2009 (1976).

19. G. A. Styles, Adv. Phys. 16, 275 (1967).

20. NMR studies of magnetic phase transitions include: P. Heller, Phys. Rev. 146, 403 (1966); E. Sawatsky and M. Bloom, Canad. J. Phys. 42, 647 (1964); S. D. Senturia and G. B. Benedek, Phys. Rev. Letters 17, 475 (1966); A. M. Gottlieb and P. Heller, Phys. Rev. B3, 3615 (1971); P. J. Segranean, W. G. Clark, Y. Chabre, and G. C. Carter, J. Phys. F: Metal Phys. 6, 453 (1976).

21. Mossbauer studies of magnetic phase transitions include:
G. K. Wertheim, H. J. Guggenheim and D. N. E. Buchanan, Phys. Rev. 169, 465 (1968); H. C. Benski, R. C. Reno, C. Hohenemser, R. Lyons and C. Abeledo, Phys. Rev. B6, 4266 (1972); R. S. Preston, J. Appl. Phys. 39, 1231 (1968); D. G. Howard, B. D. Dunlap and J. G. Dash, Phys. Rev. Letters 15, 628 (1965); M. A. Kobeissi and C. Hohenemser, AIP Conf. Proc. 29, 497 (1976).

22. PAC Studies of magnetic phase transitions include:
R. C. Reno and C. Hohenemser, Phys. Rev. Letters 25, 1007 (1970); R. M. Suter and C. Hohenemser, AIP Conf. Proc. 29, 493 (1976); J. L. Oddou, J. Berthier and P. Peretto, Phys. Letters 45A, 445 (1973).

23. D. N. Pipkorn, C. K. Edge, P. Debrunner, G. dePasquali, H. G. Drickamer and H. Frauenfelder, Phys. Rev. 135, A 1604, (1964).

24. T. A. Kovats and J. C. Walker, Phys. Rev. 181, 610 (1969).

25. PAC papers include:
H. V. Einsiedel and S. S. Rosenblum, Phys. Stat. Sol. (b) 65, K5 (1974); S. P. Solv'ev, V. V. Zakurkin, Z. I. Shapiro, V. A. Klyucharev, V. I. Bozhko and A. P. Gaidamaka, Ferroelectrics (GB) 8, 543 (1974).

26. Mossbauer papers include:
G. D. Sultanov, F. A. Miriskli and I. H. Ismailzade, Ferroelectrics (GB) 8, 539 (1974); E. A. Samuel and V. S. Sundaram, Phys. Letters 47A, 421 (1974).

27. NMR papers include:
J. Y. Nicholson and J. F. Soest, J. Chem. Phys. 60, 715 (1974); D. Slotfeldt-Ellingsen and B. Pedersen, Phys. Stat. Sol. (a) 24 191 (1974).

Table I: Comparison of Hyperfine Techniques

Property:	NMR	ME	PAC
Sensitive Chemical species	Most elements in the periodic table are suitable for NMR	Fe, Sn, Sb are routine; Ge, Zn, Dy, Au and several others can be done under specialized conditions	Hf, Cd, Sc, In Re, Rh, Ru, Fe, Pd, Tc and Cs are routine; Dy, Yb, Lu, F, Hg, Pb Te and others can be done under specialized conditions
Source and Detecting apparatus	RF generation & detection, signal averaging, recorder, static magnetic field	Gamma ray source, non-radioactive absorber, gamma ray counting	Radioactive sample, $\gamma\gamma$ coincidence spectroscopy
Sample	Stable elements	Stable elements (absorber expt.) or radioactive tracers (source expt.)	Radioactive tracers
Number of sensitive nuclei needed	$\sim 10^{21}$	$\sim 10^{15}$ (source expt.) $\sim 10^{20}$ (absorber expt.)	$\sim 10^{12}$
Physical form of sample	solids, liquids	solids only	solids, liquids

National Bureau of Standards SP-496, Applications of Phase Diagrams in Metallurgy and Ceramics
Proceedings of Workshop held at NBS, Gaithersburg, Md., January 10-12, 1977

Experimental Determination of Phase Diagrams with the Electron Microprobe and Scanning Transmission Electron Microscope

A. D. Romig, Jr. and J. I. Goldstein
Department of Metallurgy and Materials Science
Lehigh University, Bethlehem, PA 18015

ABSTRACT

Within the past dozen years the electron microprobe (EMP) has proven itself a valuable tool in the determination of phase diagrams (solid phase regions). A literature survey indicates that over thirty (30) metallic systems have been determined with this instrument.

An important advantage of this technique is that one can determine equilibrium tie lines even when the bulk phases themselves are not in equilibrium. This advantage is best realized when one is considering a system where diffusion rates are so slow that the bulk equilibrium condition cannot be reached in a reasonable time period, or where the phase diagram contains a metastable phase that will decompose if heat treatments long enough to produce homogeneous phases are used.

Several factors affect the accuracy of the EMP measurements: (1) spatial resolution; (2) X-ray absorption; and (3) X-ray fluorescence. Even under optimum conditions it is not possible to generate X-rays from a volume with a diameter less tha 1 μm and interface compositons must be determined by extrapolation to the interface position. This is a reasonable procedure, unless the concentration gradient is too steep. The use of the EMP technique is illustrated by its application to the Fe-Ni-Co and Fe-Ni-C systems.

The newly developed scanning transmission electron microscope (STEM) will allow X-ray excitation from regions less than 0.10 μm in diameter. The technique requires thin foils which are transparent to the incident electron beam (typically 80/100 kV). The use of thin foils and high excitation voltages usually eliminates the fluorescence and absorption problems preser in microprobe analysis, thus permitting the application of a relatively simple matrix correction technique. The STEM methods have now been developed to the point where phase diagram determination is possible. Measurements of the Fe-Ni-Co system using this technique are presented and agreement with the accepted diagram is demonstrated.

Introduction

The experimental determination of solubility limits and tie lines in the solid regions of multicomponent phase diagrams is difficult. The phases which are present are often small, and sometimes the bulk specimen is not even equilibrated. In addition the necessary heat treatment cycles are usually lengthy and a large number of specimens are usually required. Many experimental techniques have been employed including X-ray diffraction, metallography and differential thermal analysis. All of these techniques require well equilibrated samples for analysis. The electron microprobe (EMP) has been used since the mid-1960's to determine the composition of the equilibrated phases directly. One specific advantage of the EMP technique is the spatial resolution which approaches 1 μm. This technique enables one to obtain tie line compositions directly, even in alloys with three or more components. Composition-distance profiles can be used in special cases even when bulk equilibration has not been attained.

The purpose of this paper is to describe the use of the EMP in the determination of multicomponent phase diagrams. Heat treatment cycles, EMP spatial resolution, and the accuracy of tie line measurements will be discussed. Examples of the use of the EMP in determining isothermal sections of ternary phase diagrams will also be discussed. In addition a description of the newly developed scanning transmission electron microscopy (STEM) technique for phase diagram analysis will be given.

Sample Analysis Techniques

Two techniques have been developed to obtain suitable samples for EMP analysis: 1) diffusion couple and 2) heat treatment.[1] The diffusion

couple technique requires the bonding of two pieces of single phase material (a pure metal or alloy) and the subsequent annealing at a desired temperature.[2] The resulting concentration gradient is then measured. The composition gradient will vary continuously through solid solutions and exhibit a sharp discontinuity at the boundary of a two phase region. As long as the two phases at the interface are in local equilibrium,[2] the compositions at the interface correspond to an equilibrium tie line. The diffusion couple technique is applicable to binary, ternary, and higher order systems. The basic requirement is that the interface compositions be resolved with the EMP. The concentration gradients which result must not be too steep or accurate extrapolation to the two phase interface cannot be accomplished.

The second technique involves the heat treatment of an alloy within a 2 or 3 phase field at a desired temperature. The sample is usually one phase and compositionally homogeneous before heat treatment. A second or third phase is obtained by a specified heat treatment cycle.

After heat treatment, the composition of the resulting phases is measured with the EMP. In some cases the bulk alloy may not be equilibrated. Even so appropriate tie line measurements can be obtained if local equilibrium is maintained at phase interfaces[2] and if composition gradients in the various phases measured with the EMP are small. The heat treatment technique has been applied to a large number of alloy systems and is used more often than the diffusion couple technique.

For ternary two phase alloys the measured tie line need not go through the bulk alloy composition unless the sample is completely equilibrated after heat treatment. This effect is illustrated in Figure 1 where the 650°C isothermal section of the iron rich portion of the FeNiCo phase diagram[3] is given. The measured $\alpha + \gamma$ tie lines do

not pass through the bulk composition of the alloys but are displaced to higher Co contents. The requirements of interface mass conservation and local equilibrium in ternary systems permit phase growth to occur by continuous adjustment in the tie line selected and in the rate of growth of the precipitate.[4] Note that in the low Co alloy #9, equilibrium has been achieved in the heat treatment time allotted.

Specimen Preparation

Usually sample preparation involves melting an alloy of appropriate composition from either pure elements or master alloys of known composition. Induction melting, arc melting, resistance furnace melting, and other methods may be used depending on the specific alloy or oxide system. After melting, the sample should be homogenized to insure uniform composition throughout the sample. The time and temperature required for homogenization will again depend on the alloy or oxide system. Homogenization can be established by mounting-polishing selected samples and by using standard EMP analysis techniques.[5] In some cases the as-cast alloy is used directly for the heat treatment cycle without prior homogenization. This procedure is not recommended in that the EMP data obtained from the sample will vary from place to place across the alloy.

Diffusion couples can be produced by standard techniques. Usually the interfaces between the two single phase samples are polished and are clamped together by an appropriate device until bonding is achieved. The clamp is often removed before the final diffusion treatment.

The number of heat treatment samples necessary for a phase diagram study can be minimized by use of the EMP technique. The same samples may be used to determine several isotherms. In addition for ternary systems

only one sample is necessary to determine the outline of an entire 3 phase field. A few strategically located alloys may in fact serve to determine an entire isothermal section.

Several heat treatment cycles are available for a given sample. These heat treatment cycles are:

(A) Annealing cycle. The sample (usually one phase) is rapidly cooled from a high temperature directly to the temperature of interest (usually in a two or three phase field) and held at that temperature until sufficient phase growth occurs. This type of cycle is used to avoid unwanted phases from forming during heat treatment and to promote nucleation.

(B) Quench and anneal cycle. The sample (usually one phase) is quenched from a high temperature to a low temperature and is reheated to the temperature of interest (usually in a two or three phase field). The sample is held at that temperature until sufficient phase growth occurs. This type of cycle is often used to promote nucleation of the phases of interest. In some alloy systems a martensitic structure is formed during the quench.

(C) Controlled cooling cycle. In this scheme the sample (usually one phase) is cooled from a high temperature to the temperature of interest (usually in a two or three phase field) by some continuous and/or step cooling sequence. The sample is maintained at this temperature for a specified time period. This type of cycle controls the amount of nucleation of a second phase during cooling and increases the amount of growth of the phases which form.

491

In all of these heat treatment cycles the sample is quenched immediately after removal from the final isothermal treatment.

Cycles (B) and (C) were used in the determination of the $\alpha + \gamma$ tie lines of the FeNiCo system.[3] The quench and anneal technique (B) (heated up cycle--Fig. 1) yields fine platelets of γ which have precipitated from a martensitic α_2 structure and whose compositions can be measured directly with the EMP. The controlled cooling cycle (C) (cooled down cycle--Fig. 1) yields α grain boundary allotriomorphs in a γ matrix. The α phase composition can be measured directly. However a steep Ni concentration spike was measured in γ making a measurement of the γ tie line composition impossible using cycle C.

The controlled cooling cycle (C) may be required when one is attempting to determine phase equilibria with a metastable phase. For example, when attempting to determine the composition and temperature range over which $(Fe,Ni)_3C$, cohenite, can exist in the Fe-Ni-C system it was discovered that the carbide cannot be grown by either cycles (A) or (B). The cohenite is metastable with respect to metal plus graphite and the conventional heat treatment cycles, (A) and (B), produced the stable assemblage. However, cohenite precipitates, up to 5 microns in size, which are sufficiently large for EMP analysis, have been grown with the controlled cooling cycle technique.

Electron Microprobe Analysis

After the heat treatment cycle the sample is mounted and polished with standard metallographic techniques. Etching, surface marking, and repolishing may be necessary if the microstructure cannot be seen in the as-polished condition. The sample is then coated with a thin conducting layer to prevent charging during EMP analysis.

To obtain the most meaningful results from the probe analysis the operating conditions must be optimized. Operating potential, sample current, and counting time are perhaps the most critical parameters. The optimization of these parameters have been discussed in detail[5] and will only be described briefly in this paper.

A ratio of operating voltage to excitation potential for the measured characteristic X-ray lines of approximately 2 to 3 is desirable in order to maximize peak to background ratios and minimize the X-ray source size-resolution. Hence, if the characteristic X-rays being detected vary greatly in excitation potential, a multiple analysis at more than one operating potential may be necessary. The sample current is chosen so that X-ray counts are maximized for a statistically meaningful analysis without greatly increasing the electron beam size. Count times must be sufficiently long to allow the collection of enough X-ray counts for statistically meaningful results. The total number of counts accumulated is the critical variable in determining the detectability limit and sensitivity for each element in the analysis. The X-rays generated may be detected by either wavelength dispersive or energy dispersive spectrometers. Both systems have specific advantages and the choice will depend on the alloy system. For example, in systems containing light elements and/or overlapping spectra the wavelength dispersive spectrometer would most likely be selected. In many modern EMP systems both types of spectrometers can be used simultaneously.

Accuracy of Phase Diagram Determination

The accuracy of phase boundary measurement with the EMP is limited by three main factors: X-ray spatial resolution, X-ray absorption and

X-ray fluorescence. These factors are discussed in turn in the following paragraphs.

The X-ray source size or X-ray spatial resolution in which primary X-rays are produced is much larger than the size of the electron beam. The X-ray source size is defined by the amount of elastic scattering which occurs in a solid sample and is almost always 1 μm or larger in diameter even under optimum conditions.[5] Therefore the direct measurement of the phase boundary composition is impossible within a distance equivalent to the X-ray source size of the analyzed phase. Typically then, the interface composition is determined by extrapolation to the interface position. The extrapolation procedure can only be used if the concentration gradient is small. Deconvolution techniques have been developed to account for "smeared" interface gradients. These techniques are not very useful when compositional accuracy of the type necessary for phase diagram measurements is desired. In most cases, the necessity for extrapolation is the most serious limitation of the EMP technique.

The X-ray absorption effect occurs when X-rays produced at one point within the specimen travel through material of different composition, and perhaps different mass absorption coefficients on their way to the spectrometer. To avoid such an absorption effect, it is necessary to orient the interface perpendicular to the surface of the specimen and the interface parallel to the X-ray path to the spectrometers.

The X-ray fluorescence effect occurs when characteristic lines of a given element are excited by the continuum and the characteristic spectrum of other lines at a distance away from the electron beam ($\geq 5\,\mu m$). In this case additional X-ray excitation may occur on one side of the two phase interface even though the electron beam and the analysis point is on the

other side of the interface. In such a situation, it is best to determine how large the effect is by using undiffused couples and to correct the data accordingly.

In addition the measured X-ray counts from the EMP must be converted to composition (weight percent). The most common method used in solid materials applications is the (ZAF) matrix correction technique. The X-ray counts from the point of beam impingement are ratioed against the counts obtained from a homogeneous standard of known composition. Weight percents are obtained from these ratios after correcting for effects of atomic number, absorption, and fluorescence.

Application of the EMP to the Determination of the Fe-Ni-C Phase Diagram

In the Fe-Ni-C system equilibrium occurs between the f.c.c. (γ) phase, b.c.c. (α) phase, and the metastable line compound $(Fe,Ni)_3C$. Figure 2 shows the metallography of an Fe-3.75 wt% Ni-1.0 wt% C alloy obtained by continuous cooling from 1000°C at 25°C/hour to 730°C with an isothermal 24 hour hold at that temperature. The matrix of the alloy is now martensite, produced at the end of the heat treatment when γ was quenched from 730°C to room temperature. The grain boundary precipitate is $(Fe,Ni)_3C$. Microprobe traverses were made across the carbides. One such traverse is shown in Figure 3. The interface compositions are indicated on the figure and the corresponding tie line is plotted on the 730°C isotherm, Figure 4. Several other measured tie lines are shown in this Figure. It should be noted that the tie lines in the $\gamma + Fe_3C$ phase field do not go through the bulk alloy compositions.

Summary - EMP Technique

The method of phase diagram determination with the EMP is well developed and has been used to determine phase diagrams in over 30 systems. Table 1 lists several systems where the EMP has been used to determine at least part of the phase diagram.

The utility of the technique has been fully described in this work, yet it is not without its shortcomings. One area where improvement is possible is in spatial resolution. Errors attributable to extrapolated interface compositions could be minimized and steeper gradients could be measured if a small excitation volume could be obtained.

Application of STEM Techniques to Phase Diagram Determination

In the last few years the scanning transmission electron microscope has been developed. It is now possible to focus the primary electron beam of this instrument to $\leq 100\text{Å}$ spot size on the specimen. Similar to the EMP, the excited characteristic X-rays can be measured in a suitable detector and used for localized chemical analysis. The major advantage of this technique is that, by using electron microscope thin films and operating voltages of 80 to 200 kV, little electron scattering occurs in the sample. The X-ray source size obtained is < 0.1 μm, a factor of 10 better than the EMP. With sufficiently thin samples, the X-ray source size may be < 0.01 μm. In addition, the use of thin films at high electron beam excitation voltages eliminates, in most cases, the need to correct for absorption and fluorescence effects in the conversion of X-ray data to composition.

As an example of the use of the STFM technique for phase diagram determination the Fe-Ni-Co system will be considered. The phase diagram has recently been redetermined by microprobe analysis at several temperatures.[3] The 650°C isotherm is given in Figure 1. The alloy samples used for this isotherm were heat treated for times of up to 6 months and analyzed with the EMP techniques previously described. The 6 month treatment time was necessary to produce γ plates ≥ 5 μm in width for EMP analysis. To evaluate the applicability of the STEM to phase diagram determination an Fe-8.96 wt% Ni-7.92 wt% Co alloy was prepared using a quench and anneal cycle (B). The alloy sample was heat treated at 650°C for only 2 weeks and the γ plates produced were 0.3-0.5 μm in width. A thin foil transmission microscope sample was prepared from the specimen by ion etching.

Figure 5 shows a scanning transmission image of the γ plates and α matrix prior to data acquisition. A Philips 300 STEM instrument was used with an operating potential of 80 kV and with the specimen tilted at 36°. Data was taken across the γ platelets and the α matrix with an electron beam ~ 320Å in diameter. The position of the beam during analysis are visible due to sample contamination as shown in Figure 6.

X-ray data was collected on a solid state X-ray detector with a counting time of 60 sec. per point. The $Fe_{K\alpha}$ and $Ni_{K\alpha}$ integrated peak intensities were measured and the continuum background was subtracted. A plot of I_{Ni}/I_{Fe} vs. distance was constructed and is shown in Figure 7. The circles represent data points as measured on the STEM. The 2 σ error bars were calculated from the accumulated X-ray counts on the specimen. The bulk alloy I_{Ni}/I_{Fe} value was determined by scanning the electron beam over the entire area of Figure 5.

The diameter of the X-ray generation region is indicated on Figure 7 by R(x). For the EMP R(x) is a nominal 1 μm and represents the diameter of the X-ray excitation volume. For the STEM, R(x) represents the 320Å beam diameter plus an estimate of the amount of beam spreading in the specimen, about 200Å for a 1000Å iron thin foil.[6]

Cliff and Lorimer[7] have outlined a simple technique to carry out the quantitative analysis of thin foils with the STEM analytical electron microscope. For very thin foils where X-ray absorption and fluorescence can be neglected, the following expression may be used:

$$\frac{I_A}{I_B} = (k_{AB})^{-1} \frac{C_A}{C_B} \qquad (1)$$

where I_A and I_B are the measured characteristic X-ray intensities, and C_A, C_B are the weight fractions of two elements A and B in the thin film. The constant k_{AB} varies with operating voltage but is independent of sample thickness and composition if the two intensities are measured simultaneously. This method has been often referred to as the standardless method in that pure bulk standards are not needed for the analysis.

These k_{AB} values can either be measured or calculated. The value of k_{NiFe} used in this experiment was calculated using the expressions developed by Goldstein et al.[6] A value of $k_{NiFe} = 1.081$ for 80 kV operating potential was calculated using the method of Goldstein et al.[6] which corrects for the absorption of the Be window in the detector and the relativistic nature of the electron beam.

STEM - Discussion

Using Equation 1 and the calculated k_{NiFe} value one can calculate the expected I_{Ni}/I_{Fe} ratios for the α and γ phase compositions using measured C_{Ni}, C_{Fe} values obtained from a tie line drawn through the bulk

composition of the Fe-8.96 wt% Ni-7.92 wt% Co alloy at a temperature of 650°C (Figure 1). The solid lines of I_{Ni}/I_{Fe} plotted on Figure 7 for the α and γ phases were determined by this procedure. The bulk alloy intensity ratio was calculated similarly. It is apparent that excellent agreement has been obtained between measurements of tie line compositions by EMP and STEM techniques.

It is clear from this example that phase diagram determination by STEM techniques has a promising future. The increased spatial resolution will allow analyses of phases 0.5 μm in size and possibly smaller. Growth times for precipitates will also be greatly reduced by this technique. A major advantage will be the extension of phase diagram analysis to lower temperatures than have been possible to date. Problems of contamination, X-ray absorption, and thin film preparation in STEM analysis have yet to be completely solved, however.

Acknowledgements

The authors wish to thank D. Richards for the preparation of the STEM sample and R. Korastinsky for assistance with the STEM analysis work. We thank D. Williams and S. Widge for helpful discussions and suggestions. This work was supported by NASA Grant NGR 39-007-056.

REFERENCES

1. Goldstein, J. I. and Ogilvie, R. E. in X-ray Optics and Microanalysis, ed. by R. Castaing, P. Deschamps and J. Philibert, Hermann, Paris (1966), pp. 594.

2. Ogilvie, R. E., Sc.D. Thesis, MIT, (1953).

3. Widge, S. and Goldstein, J. I., Met. Trans. A, to be published (1977).

4. Randich, E. and Goldstein, J. I., Met. Trans. 6A, 1553 (1975).

5. Goldstein, J. I. and Yakowitz, H., eds. Practical Scanning Electron Microscopy, Plenum, New York (1975).

6. Goldstein, J. I., Costley, J. L., Lorimer, G. W. and Reed, S. J. B. in SEM/1977, ed. by O. Johari, to be published (1977).

7. Cliff, G. and Lorimer, G. W., Proc. Fifth Euro. Conf. on EM, Institute of Physics, London, 1972, pp. 140-141.

8. Rexer, J., Z. Metallkde, v. 62, (1971), pp. 844-848.

9. Kirchner, G., Nishizawa, T. and Uhrenius, B., Met. Trans., v. 4, (1973), pp. 167-174.

10. Waterstrat, R. M., Met. Trans., v. 4, (1973), pp. 1585-1592.

11. Kirchner, G., Harvig, H. and Uhrenius, B., Met. Trans., v. 4, (1973), pp. 1059-1067.

12. Goldstein, J. I. and Ogilvie, R. E., Trans. TMS-AIME, v. 233, (1965), pp. 2083-2087.

13. Hofmann, H., Löhberg, K. and Rerf, W., Arch. Eisenhüttenwes, v. 41, (1970), pp. 975-982.

14. Wald, F. and Sturmont, R. W., Trans. TMS-AIME, v. 242, (1968), pp. 72-74.

15. Heijwegen, C. and Rieck, G., Z. Metallkde, v. 64, (1973), pp. 450-453.

16. Meussner, R. and Goode, R., Trans. TMS-AIME, v. 233, (1965), pp. 661-671.

17. Waterstrat, R., Met. Trans., v. 4, (1973), pp. 455-466.

18. Maxwell, I. and Hellawell, A., Met. Trans., v. 3, (1972), pp. 1487-1493.

19. Urednicek, M. and Kirkaldy, J., Z. Metallkde, v. 64, (1973), pp. 419-427.

20. Cisse, J. and Davies, R., Met. Trans., v. 1, (1970), pp. 2003-2006.

21. Rosenbach, K. and Schmitz, J., Arch. Eisenhüttenwes, v. 45, (1974), pp. 843-847.

22. Karnowsky, M. and Yost, F., Met. Trans. A, v. 7A, (1976), pp. 1149-1156.

23. Carmio, S. and Meijering, J., Z. Metallkde, v. 3, (1973), pp. 170-175.

24. Benz, R., Elliott, J. and Chipman, J., Met. Trans., v. 4, (1973), pp. 1975-1986.

25. Sharma, R. and Kirkaldy, J., Can. Met. Quat., v. 12, (1973), pp. 391-401.

26. Reinbach, R. and Baer, H., Z. Metallkde, v. 5, (1969), pp. 453-456.

27. Schultz, J. and Merrick, H., Met. Trans., v. 3, (1972), pp. 2479-2483.

28. Massalski, T. and Perepezko, J., Z. Metallkde, v. 3, (1973), pp. 176-181.

29. Budurov, S., Krassimir, R., Kovatchev, P., Toncheva, S. and Komenova, Z., Z. Metallkde, v. 65, (1974), pp. 683-685.

30. Doan, A. and Goldstein, J. I., Met. Trans., v. 1, (1970), pp. 1759-1767.

31. Chiang, P.-W. and Gluck, J. V., Trans. TMS-AIME, v. 242, (1968), pp. 2229-2236.

32. Brunch, A. and Steeb, S., Z. Metallkde, (1974), pp. 714-720.

33. Wald, F., Bates, H. and Weinstein, M., Trans. TMS-AIME, v. 242, (1968), pp. 760-761.

501

Table I

Summary of Phase Diagrams

Tabulation of systems where the EMP has been used in the determination of solid solubility limits, tie-lines, tie-triangles, and phase identification.

System	Temperature Range (°K)	Technique*	Measured Parameter (Phase Relationship)
Al-Mo [8]	1673-1873	D.C.	solubility limits: Al_3Mo_3 - $Al_{63}Mo_{37}$ AlMo - $AlMo_3$ - Mo
Cr-Fe [9]	1123-1373	HTB	tie-lines: $\alpha + \gamma$
Cr-Pt [10]	970-2133	HTB	tie-lines: $\gamma+\beta$, $\beta+\alpha$, $\gamma'+\beta$
Fe-Mo [11]	1073-1773	HTB	tie-lines: $\alpha+\gamma$
Fe-Ni [12]	773-1073	HTB,D.C.	tie-lines: $\alpha+\gamma$
Fe-P [13]	1133-1273	D.C.	solubility limits: α - Fe_3P
Fe-PbTe [14]	1073-1195	HTB	solubility limits: Fe-PbTe
Fe-W [11]	1173-1813	HTB,D.C.	tie-lines: $\alpha+\lambda$, $\lambda+\mu$, $\alpha+\mu$, $\mu+$'W'
Mo-Ni [15]	1073-1568	D.C.	tie-lines: (Mo) $+\zeta$, (Ni) $+\zeta$, $\zeta+\gamma$ (ζ - MoNi, γ - $MoNi_3$, β - $MoNi_4$)
Nb-Zn [16]	1293-1393	HTB	compound identification: $NbZn_3$, $NbZn_2$, $NbZn_{1.5}$, NbZn
Pt-V [17]	1173-1973	HTB	tie-lines: $\zeta+\beta$, $\alpha+\beta$, $\gamma+\beta$ (β - V_3Pt, ζ - VPt)
Al-B-Ti [18]	923	HTB	compound identification: Al_3Ti, AlB_2, TiB_2
Al-Fe-Zn [19]	723	solid-liquid equilibration	phase and compound identification: FeAl, $FeAl_2$, Fe_2Al_5, δ_1, ζ, two ternary phases solubility limits: compounds-terminal phase
Al-Nb-Ni [20] (Ni_3Al-Ni_3Nb-Ni)	1073-1473	HTA,D.C.	solubility limits: γ'-Nb tie-lines: $\gamma+\gamma'$
Al_2O_3-Cr_2O_3-FeO [21]	1923-2073	HTB	solubility limits: FeO · Cr_2O_3 - FeO · Al_2O_3 quasi-binary
Au-In-Pb [22]	432-706	HTB	phase identification: AuIn, $AuIn_2$

Table I (continued)

System	Temperature Range (°K)	Technique*	Measured Parameter (Phase Relationship)
Au-Ni-Pt[23]	1085-1533	HTB	tie-lines: solid 1 - solid 2 miscibility gap
C-Fe-Mn[24]	1163-1373	HTB	tie-lines: $\gamma + M_3C$ phase identification: M_3C, $M_{15}C_4$, $M_{23}C_6$, ϵ
C-Fe-Ni[25]	773-1003	HTB,HTC	tie-lines: $\alpha+\gamma$, $\gamma + (Fe,Ni)_3C$, $\alpha + (Fe,Ni)_3C$
C-Fe-P[13]	873-1173	D.C.	solubility limits: α - $(Fe,Ni)_3P$
Co-Be-Cu[26]	673-1373	HTB	solubility limits: α - β, α - γ_2, α - γ_1
Co-Fe-Ni[3]	926-1073	HTB,HTC	tie-lines: $\alpha+\gamma$
Cr-Fe-Ni(Al,Nb,Si,Ti)[27]	1089-1533	HTB	solubility limits: α' - γ tie-lines: $\alpha'+\gamma$
Cu-Al-Ag[28]	848-898	HTB	solubility limits: terminal regions (α_1 - (Ag), α_2 (Cu))
Fe-Mn-Zn[29]	893-1273	HTB	tie-lines: $\alpha+\gamma$
Fe-Mo-W[11]	1373-1578	HTB	tie-lines: $\alpha+\gamma$, $\alpha+\mu$, $\alpha+R$
Fe-Ni-P[30]	823-1373	HTB,HTC	tie-lines: $\alpha + (Fe,Ni)_3P$, $\gamma + (Fe,Ni)_3P$, $\alpha+\gamma$, α + liquid, γ + liquid
Sb-Te-Tl[31]	483-518	HTB	phase identification: α (Tl_2,Te_3), δ (Sb_2Te_3), ϵ ($SbTlTe_2$), β(Te)
Ti-V-Zr[32]	1073	HTA	tie-lines: $\alpha+\gamma$, $\beta+\gamma$, $\delta+\beta$, $\gamma+\delta$
C-Cr-Ni-Si[33]	1173	HTB	phase identification: Cr_3C_2 solubility limit: γ - Cr_3C_2

* Codes: D.C. - diffusion couple

HTA - heat treatment A - quench from high temperature to temperature of interest (annealing cycle)

HTB - heat treatment B - quench from high temperature to low temperature, then reheat at temperature of interest (quench and anneal cycle)

HTC - heat treatment C - controlled cooling from high temperature to temperature of interest (controlled cooling cycle)

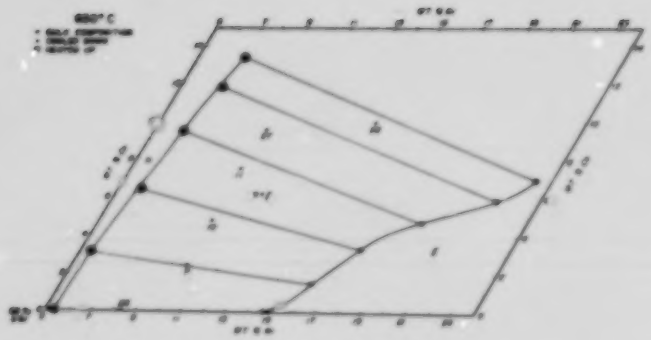

Figure 1

Isothermal section of Fe-Ni-Co ternary diagram at 650°C.[3] Origin is at 95Fe-5Ni, and heat treatments are as indicated in the text.

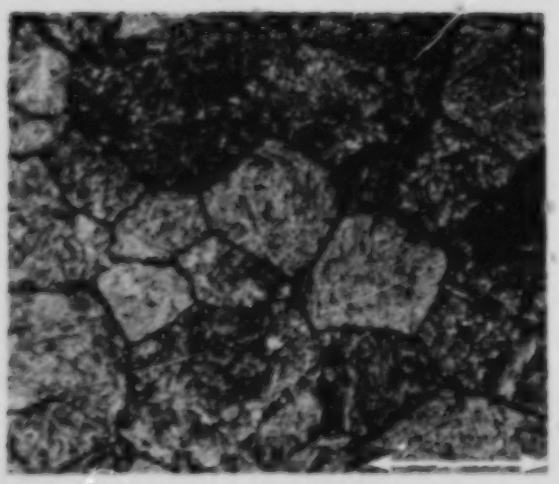

Figure 2

Microstructure of an Fe-3.75 wt% Ni-1.0 wt% C alloy. Austenitized at 1000°C and then cooled to 730°C at 25°C/hour and isothermally treated for 24 hours. Matrix is martensite and grain boundary precipitate is $(Fe,Ni)_3C$. 2% Nital Etch. Scale Bar = 200 μm.

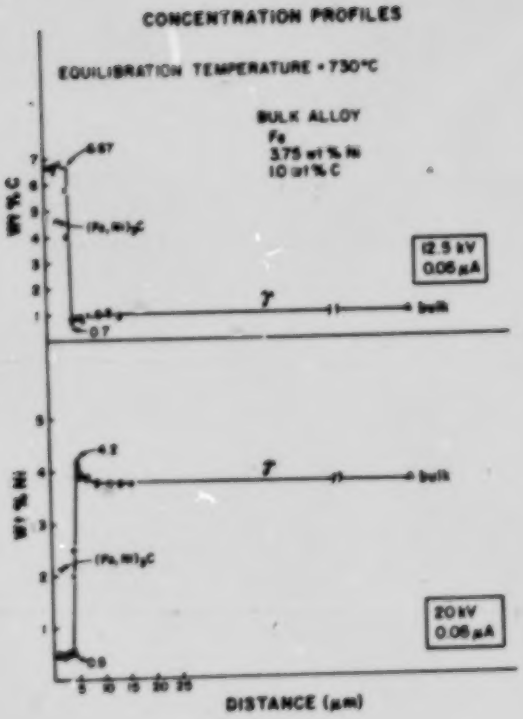

Figure 3

Microprobe traces taken in an Fe-3.75 Ni-1.0 C alloy. x and o represent data points from two separate traces.

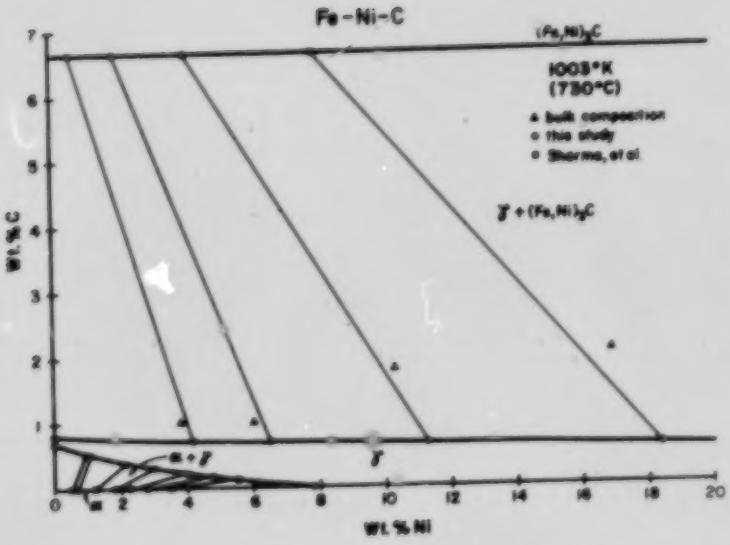

Figure 4

Fe-Ni-C 730°C isotherm.

505

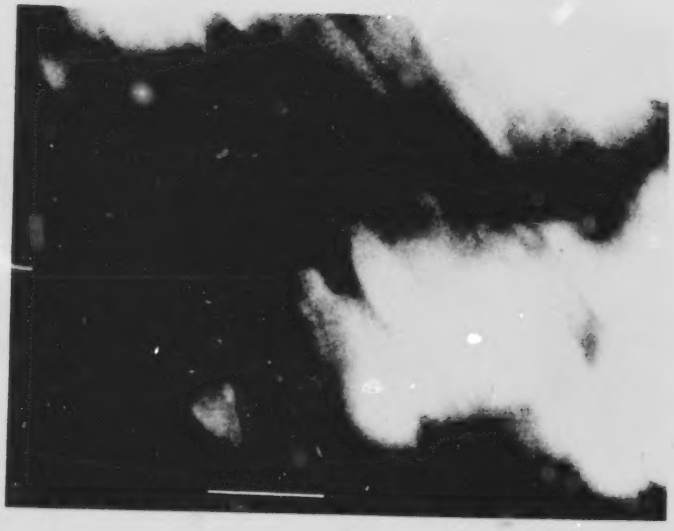

Figure 5

Fe-8.96 wt% Ni-7.92 wt% Co alloy treated at 650°C using the quench and anneal cycle. STEM image of the thin foil prior to composition analysis. Scale Bar = 1 μm.

Figure 6

Fe-8.96 wt% Ni-7.92 wt% Co alloy treated at 650°C using the quench and anneal cycle. STEM image of the thin foil after composition analysis. Scale Bar = 1 μm. The analysis points can be observed by the contamination spots left on the foil. The white dots are placed on the photograph to more clearly indicate the analysis points.

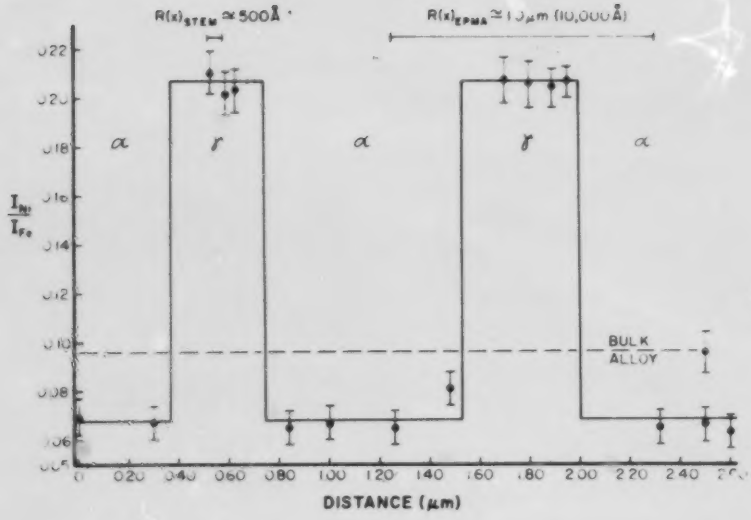

Figure 7

STEM trace across the α and γ phases formed in a Co alloy annealed at 650°C for 2 weeks. Solid circles are data points and 2 σ error bars are shown. The solid lines are calculated from the known Fe-Ni-Co phase diagram and the dashed line is calculated from the bulk alloy composition. The spatial resolution of the STEM and typical resolution of the EMP are also shown.

507

National Bureau of Standards SP-496, Applications of Phase Diagrams in Metallurgy and Ceramics
Proceedings of Workshop held at NBS, Gaithersburg, Md., January 10-12, 1977

THE INTERNATIONAL NICKEL COMPANY, INC.
PAUL D. MERICA RESEARCH LABORATORY
STERLING FOREST
SUFFERN, NY 10901

INTERRELATIONS BETWEEN PHASE DIAGRAMS AND HYDRIDING PROPERTIES FOR ALLOYS BASED ON THE INTERMETALLIC COMPOUND FeTi

by

G.D. Sandrock*, J.J. Reilly** and J.R. Johnson**

ABSTRACT

Hydriding alloys based on the intermetallic compound FeTi have potential for the safe and convenient storage of hydrogen, both for mobile and stationary applications. In spite of its simple formula, the hydriding behavior of FeTi is quite complex and a strong function of alloy microstructure. The alloy microstructure, in turn, depends on composition, not only deviations from stoichiometry but also various impurities. In this paper we discuss some of the interrelations among composition, microstructure, and hydriding behavior that can be related to phase diagram information. In particular, we discuss the Fe-Ti, Fe-Ti-O, and Fe-Ti-Mn phase diagrams and their relationships to hydriding properties. The use of hydriding data to infer metal-hydrogen phase diagrams is also briefly discussed.

*The author is with The International Nickel Company, Inc., Paul D. Merica Research Laboratory, Sterling Forest, Suffern, NY
**The authors are with Brookhaven National Laboratory, Department of Applied Science, Upton, NY

INTRODUCTION - FeTi FOR HYDROGEN STORAGE

In the past few years considerable interest has developed in using rechargeable metal hydrides for hydrogen storage, both for stationary and vehicular applications(1-4). Of particular interest has been the hydrogen storage properties of the intermetallic compound FeTi(5). In spite of its simple formula, however, the hydriding behavior of FeTi is complex and a strong function of alloy microstructure(6,7). Alloy microstructure, in turn, is influenced by deviations from stoichiometry and various impurities. As with other engineering alloys, phase diagram information can be very useful in interpreting the microstructures of FeTi and relating these microstructures to hydriding data. In this paper we present a few specific examples of these interrelations.

Before discussing specific examples of the use of phase diagrams to interpret hydriding data, however, a brief introduction to ideal (high purity) FeTi hydriding behavior should be given. At ambient temperatures and a few atmospheres pressure, FeTi reacts with hydrogen to form a monohydride and a dihydride according to the approximate reactions:

$$FeTi + 1/2\ H_2 \rightleftarrows FeTiH \qquad (1)$$

$$FeTiH + 1/2\ H_2 \rightleftarrows FeTiH_2 \qquad (2)$$

The hydriding reaction is similar to corrosion reactions such as oxidation as shown metallographically in Figure 1.

There is a positive volume change during the hydriding reaction so that the brittle FeTi cracks as a result of stresses generated during first hydriding (activation). After activation each particle is highly cracked on a fine scale (Figure 2) and thus provides a relatively large surface area for the occurrence of subsequent hydriding and dehydriding reactions. Because the reactions are easily reversible, FeTi can be effectively charged and discharged, thus serving as a solid "sponge" for the storage of hydrogen. Examples of charging and discharging curves are shown in Figure 3. Once the alloy is fully activated (finely cracked) kinetics are very rapid and are for practical purposes determined by the rate the heat of reaction can be removed from the bed during hydriding or added to the bed during dehydriding.

PHASE DIAGRAM - HYDRIDING INTERRELATIONS

The curves shown in Figure 3 were obtained with carefully prepared, high purity, nearly stoichiometric FeTi. Practical production of engineering quantities of FeTi for hydrogen storage will result in alloys that are less than perfect from stoichiometry and purity points of view. Phase diagrams can be very useful in understanding these deviations from ideality and can provide useful production targets. In this section we present a few examples of the use of phase diagrams in the interpretation of FeTi hydrogen storage behavior. In particular we will consider the Fe-Ti,

Fe-Ti-O and Fe-Ti-Mn phase diagrams, although others have been consulted in our studies of FeTi(7). The hydriding properties we will concentrate on most will be hydrogen storage capacity, although others such as activation and decrepitation (particle size breakdown with cycling) have been considered(6,7).

Fe-Ti BINARY SYSTEM

An understanding of the metallurgy of FeTi should begin with the Fe-Ti binary phase diagram, reproduced in Figure 4. Hydrogen desorption curves for selected binary alloys are shown in Figure 5. The phase of interest for hydrogen storage purposes is the FeTi phase which exists over a narrow (∿2.5%) composition range near the center of the phase diagram. For maximum hydrogen storage capacity it is important that the alloy composition be within the single phase FeTi field. If the prepared composition is only slightly deficient in Ti (<∿49.5 at. % Ti) the two-phase FeTi + Fe_2Ti field is entered. The presence of Fe_2Ti in the microstructure is undesirable because it apparently does not hydride. Thus the overall storage capacity is reduced by the presence of the inert Fe_2Ti phase. From the phase diagram, it is evident from the lever rule that only moderate decreases in Ti content below 49.5 at. % can result in substantial amounts of Fe_2Ti. For example, an alloy of ∿41 at. % Ti would contain ∿50% Fe_2Ti. The drastic reduction in hydrogen storage capacity accompanying such a decrease in Ti content is shown in Figure 5.

On the other hand, if the Ti content of the prepared alloy is in excess of ∿52 at. %, the two-phase FeTi + Ti solid solution (α-or β-Ti) field is entered. The Ti solid solution phase hydrides readily, tending to form essentially TiH_2. Unfortunately, however, this hydride is not readily reversible (i.e., it is much too stable) and is thus not useful for reversible hydrogen storage purposes at near ambient temperatures. Thus, as graphically confirmed by the right curve in Figure 5, alloys with substantial excess free Ti should also be avoided for maximum reversible storage capacity. From the geometry of the phase diagram (Figure 4) a given error is somewhat less deleterious if it is on the Ti-rich side rather than the Ti-lean side of 50-50 at. % Fe-Ti. This, coupled with the fact the equiatomic alloy solidifies through a peretectic reaction (i.e., as shown in Figure 4, the first few crystals to form in the cooling melt are Fe_2Ti), makes it desirable in practice to aim for slightly Ti-rich alloys (say 50.5-51 at. % Ti).

Depending on the hydriding properties desired, there may be advantages to use alloys slightly richer than 51 at. % Ti. As shown in Figure 5, excess Ti (say ∿53 at. %) lowers the overall dissociation pressure and makes the plateau much more inclined. The reason for this is not completely clear, but appears to involve non-equilibrium segregation effects during solidification (i.e., effects not directly relatable to the equilibrium phase diagram).

In addition we have qualitatively found that the presence of some free Ti solid solution in the microstructure aids activation by providing preferred paths for initial hydride penetration. Fe_2Ti probably also aids activation. In fact, most second phases seem to assist the activation process.

Fe-Ti-O TERNARY SYSTEM

Of the common trace element impurities in FeTi, oxygen is the most influential on the hydriding properties. Like most other high-Ti alloys, liquid FeTi has a very high affinity and solubility for oxygen. Of importance to the hydriding behavior is the microstructural role oxygen plays in the solidified alloy.

After studying this problem in some detail, we conclude the role of oxygen can be explained well by the Fe-Ti-O ternary phase diagram of Rostoker(9), shown in Figure 6. Rostoker's diagram indicates that the introduction of oxygen results in the formation of a ternary "T-phase" (Ti_4Fe_2O-Ti_3Fe_3O). In fact, we metallographically find that the amount of a second phase increases directly with increasing oxygen content. This is shown in Figure 7. Microprobe analysis of the second phase particles conform reasonably well with the homogeneity range of the T-phase. Our data points cluster around the approximate stoichiometry $Fe_7Ti_{10}O_3$ (Figure 6). This phase is crystallographically equivalent to that reported originally by Rostoker(9) and again recently by Pick and Wenzl(10) in O-contaminated FeTi. The only

difference we note between our observations and Rostoker's phase diagram (Figure 6) is that we see eutectic $Fe_7Ti_{10}O_3$ particles in as-cast microstructures with O-contents as low as 0.01 wt. % (Figure 7a), whereas Rostoker suggests a solubility (at 1000°C) of 1-2 at. % (0.3-0.6 wt. %) oxygen in the FeTi phase.

The problem with $Fe_7Ti_{10}O_3$ is that it does not hydride, at least at the temperatures and pressures routinely used for FeTi. This, coupled with the fact that each O-atom ties up about 17/3 = 5.67 metal atoms, results in a substantial loss in hydrogen storage capacity. This is shown graphically in Figure 8, which presents a series of desorption isotherms for FeTi samples with different O-contents. The measured loss in capacity corresponds closely with that which would be predicted by the Fe-Ti-O phase diagram; i.e., calculated assuming all the oxygen goes to form an inert $Fe_7Ti_{10}O_3$ phase.

The presence of $Fe_7Ti_{10}O_3$ affects other hydriding properties such as activation and decrepitation(6,7). As with other second phases, the $Fe_7Ti_{10}O_3$ particles accelerate activation by serving as sites for preferred hydride penetration and nucleation. In a related way, decrepitation (particle size breakdown) is also accelerated by the presence of the ternary O-rich phase. In summary, it is desirable to heed the overall lesson of the Fe-Ti-O phase diagram in the production of FeTi and set as a target the minimum O-contamination practical so as to minimize the amount of $Fe_7Ti_{10}O_3$ in the microstructure.

Fe-Mn-Ti TERNARY SYSTEM

A number of transition metal elements (e.g., Mn, Cr, V, Co or Ni) can be at least partially substituted into the FeTi lattice(11). Which element (Fe or Ti) the ternary addition substitutes for, as well as the rough limits of substitution can often be qualitatively inferred from existing binary or ternary phase diagram information(7). However, an equilibrium phase diagram can be slightly misleading in attempting to interpret the hydriding behavior of non-equilibrium microstructures that often result from solidification at conventional rates.

An example of this can be seen with the Fe-Mn-Ti ternary system. A portion of the ternary phase diagram is shown in Figure 9. The dotted lines indicate the limits of 1000°C homogeneity reported for the Ti(Fe,Mn) phase by Murakami and Enjyo(12). They indicate that the FeTi phase has a substantial solubility for Mn and in fact the homogeneity range for the phase is actually widened by the substitution of Mn. We find that this diagram, determined by annealing samples at 1000°C, is not representative of as-cast structures. Shown on Figure 9 are a number of ternary alloys prepared and metallographically examined during our study. In no case was a strictly single phase Ti(Fe,Mn) microstructure found, but invariably some $(Fe,Mn)_2Ti$ and Ti solid solution was found within the single phase region of the reported phase diagram. This, of course, does not contradict the work of Murakami and Enjyo, but merely

repeats the well established fact that "equilibrium" phase diagrams can be misleading under non-equilibrium solidification conditions.

The implications of this particular example on the hydriding behavior of Fe-Mn-Ti alloys are as follows. By substituting Mn directly for Fe (i.e., along the $TiFe_{1-x}Mn_x$ line in Figure 9) the two-phase Ti(Fe,Mn) + $(Fe,Mn)_2Ti$ is quickly entered in as-cast alloys. Assuming one does not wish to go to the expense of extensively annealing to establish the equilibrium single phase, the result is some loss in H-storage capacity because the $(Fe,Mn)_2Ti$ phase does not hydride. An example of this is shown by the $TiFe_{0.7}Mn_{0.3}$ desorption curve in Figure 10. For maximum storage capacity it is desirable to maximize the amount of the Ti(Fe,Mn) phase. As shown by the as-cast results of Figure 9, this can be done by melting slightly Ti-rich [i.e., at an atomic ratio (Fe+Mn)/Ti slightly less than 1]. The improved storage capacity of such an alloy, $TiFe_{0.7}Mn_{0.2}$, is shown in Figure 10.

There are other aspects of the curves in Figure 10 that are not explained by phase diagrams. The general lowering of the hydride pressures by substitution of Mn into the FeTi structure is a consequence of subtle bonding effects not directly reflected in the phase diagram(6). Similarly the sloping plateaus that result in the Mn-containing alloys are a result of non-equilibrium segregations of Mn that occur within the Ti(Fe,Mn) phase itself during solidification.

Although phase diagrams do not answer all the questions regarding the complex hydriding behavior of FeTi and its related alloys, they are very important to establishing the basic metallurgical understanding of this system which must accompany engineering use for hydrogen storage.

USE OF HYDRIDING DATA TO INFER METAL-HYDROGEN PHASE DIAGRAMS

Thus far we have discussed the use of metal-metal phase diagrams to rationalize observed hydriding data. The situation may be somewhat reversed, whereby hydriding data as a function of temperature may be used to infer the M-H phase diagram. As an example we will briefly show the application of this to the FeTi-H phase diagram(5).

A series of hydrogen desorption isotherms for high purity FeTi (49.6 at% Fe) is shown in Figure 11. Each curve has essentially five regions. Starting from the left of the plot they are: (a) an almost vertical portion, which represents the solubility limit of H in FeTi; (b) a horizontal plateau, which represents a two-phase mixture of hydrogen saturated FeTi and the monohydride (~FeTiH); (c) a rising portion which represents some increased solubility of H in the monohydride; (d) another plateau, representing the two-phase monohydride + dihydride field; and (e) another steeply rising portion, representing a slight further increase in the solubility of H in the dihydride phase. By plotting the approximate points separating these five regions in Figure 11, the FeTi-H phase diagram of Figure 12 was created. Such

a construction only helps to infer a phase diagram and must, of course, be supported by independent x-ray diffraction data. A limited amount of room temperature XRD confirming data is shown in Figure 12.

The gradual elimination of the upper plateau at higher temperatures has been tentatively interpreted as a closing off of the two-phase $\beta + \gamma$ field at a consolute temperature of about 60°C, although the exact temperature is rather difficult to determine from the hydriding data (Figure 11). Above this temperature it is assumed the monohydride can continuously change to the dihydride by hydrogen absorption in a manner similar to the formation of the V, Nb, Ta and Pd hydrides at high temperatures(13). It should be noted, however, that this has not yet been confirmed for the FeTi case by x-ray diffraction.

CONCLUSION

The optimum use of hydriding alloys for hydrogen storage requires an intimate knowledge of the metallurgy of the alloys involved. We have shown for FeTi, and related hydrogen storage alloys, the application of metallurgical phase diagram information can greatly aid the interpretation of hydriding data. In a related manner, hydriding data can be used in the construction of metal-hydrogen phase diagrams

and, as an example, the FeTi-H phase diagram was derived. The generalities derived from work such as this on FeTi should be applicable to other rechargeable hydride systems.

REFERENCES

1. K.C. Hoffman, J.J. Reilly, F.J. Salzano, C.H. Waide, R.H. Wiswall and W.E. Winsche, "Metal Hydride Storage for Mobile and Stationary Applications", Hydrogen Energy, 1, 133 (1976).

2. D.L. Henriksen, D.B. Mackay and V.R. Anderson, "Prototype Hydrogen Automobile Using a Metal Hydride", Proc. 1st World Hydrogen Energy Conf., III, 7C-1, Miami Beach, 1976.

3. R.E. Billings, "A Hydrogen-Powered Mass Transit System", Proc. 1st World Hydrogen Energy Conf., III, 7C-27, Miami Beach, 1976.

4. A. Buchner and H. Saüfferer, "The Short and Medium Term Development and Practical Application of Hydrogen-Powered Vehicles", 2nd Symposium on Low Pollution Power Systems Development, Duesseldorf, 1975.

5. J.J. Reilly and R.H. Wiswall, Jr., "Formation and Properties of Iron Titanium Hydride", Inorganic Chem., 13, 218 (1974).

6. G.D. Sandrock, J.J. Reilly and J.R. Johnson, "Metallurgical Considerations in the Production and Use of FeTi Alloys for Hydrogen Storage", Proc. 11th Intersociety Energy Conversion Engineering Conference, I, 965 (1976).

7. G.D. Sandrock, "The Interrelations Among Composition, Microstructure and Hydriding Behavior for Alloys Based on the Intermetallic Compound FeTi", Final Report, Contract BNL-352410S, June 30, 1976.

8. T. Lyman, Editor, Metals Handbook, Vol. 8, American Society for Metals, Metals Park, OH, 1973, p. 307.

9. W. Rostoker, "Selected Isothermal Sections in the Titanium-Rich Corners of the Systems Ti-Fe-O, Ti-Cr-O, and Ti-Ni-O", Trans. AIME, 203, 113 (1955).

10. M.A. Pick and H. Wenzl, "Physical Metallurgy of FeTi-Hydride and Its Behavior in a Hydrogen Storage Container", Proc. 1st World Hydrogen Energy Conf., II, 8B-27, Miami Beach, 1976.

11. J.J. Reilly and J.R. Johnson, "Titanium Alloy Hydrides; Their Properties and Applications", Proc. 1st World Hydrogen Energy Conf., II, 8B-3, Miami Beach, 1976.

12. Y. Murakami and T. Enjyo, "Investigation of Ti-Rich Ti-Fe-Mn Alloy System on the Solid Equilibrium Relation in the Ti-Fe-Mn System", Nippon Kinzoku Gakkaishi, 22, 328 (1958).

13. G.G. Libowitz, The Solid State Chemistry of Binary Metal Hydrides, Benjamin Press, New York (1965), pp. 34-37.

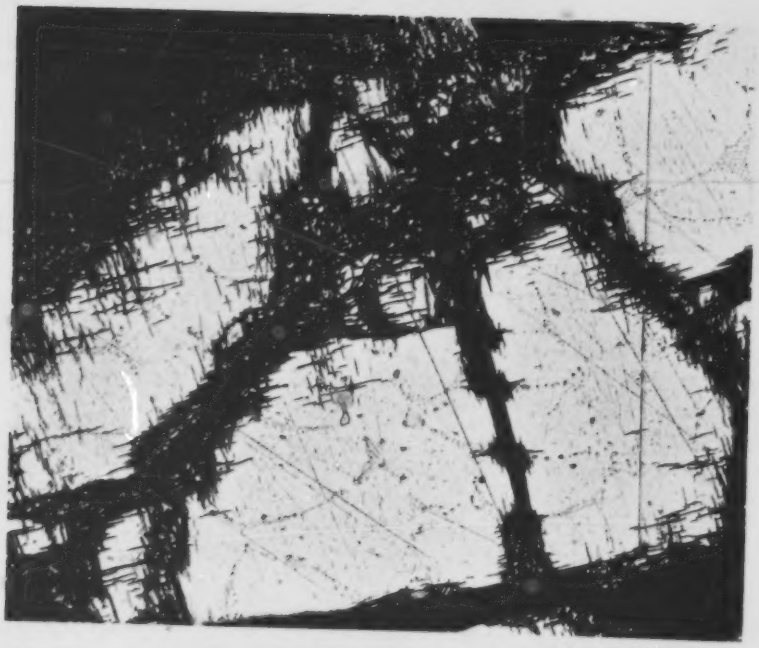

FIGURE 1

PARTIALLY HYDRIDED PARTICLE OF FeTi
200X

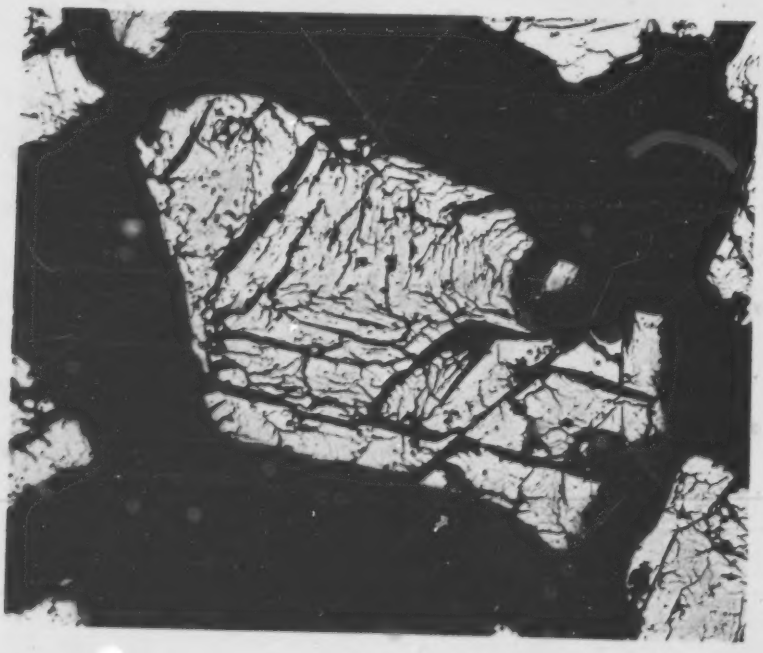

FIGURE 2

FULLY ACTIVATED PARTICLE OF FeTi (IN
DEHYDRIDED CONDITION)
200X

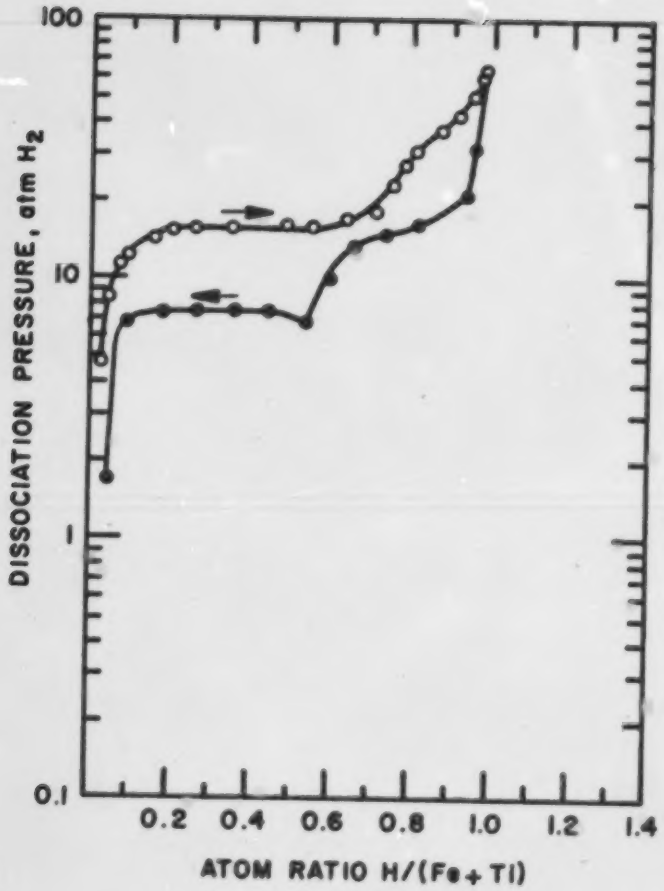

FIGURE 3 - FeTi-H CHARGING AND DISCHARGING CURVES AT 40°C.

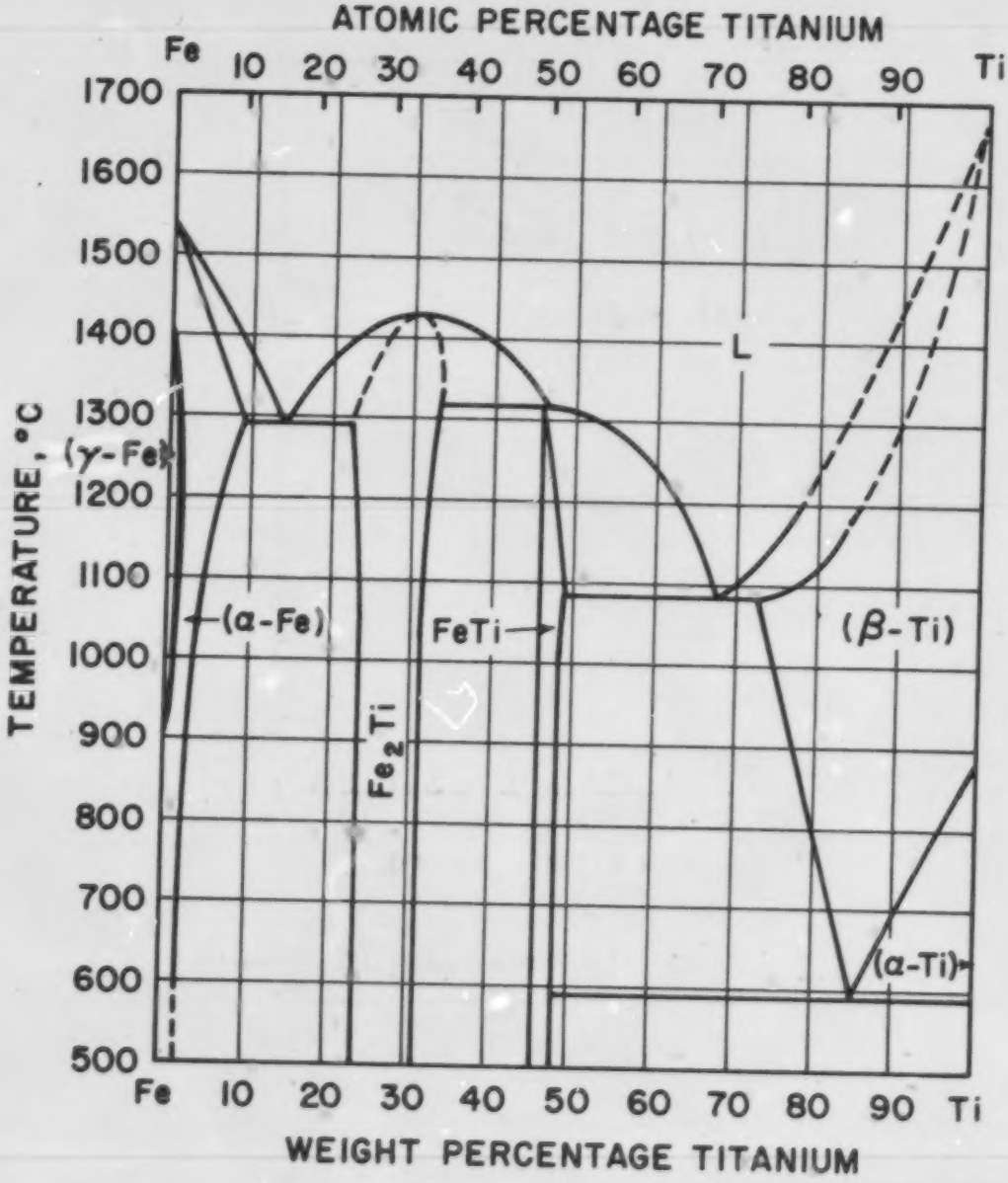

FIGURE 4 - Fe-Ti PHASE DIAGRAM. (AFTER REF. 8)

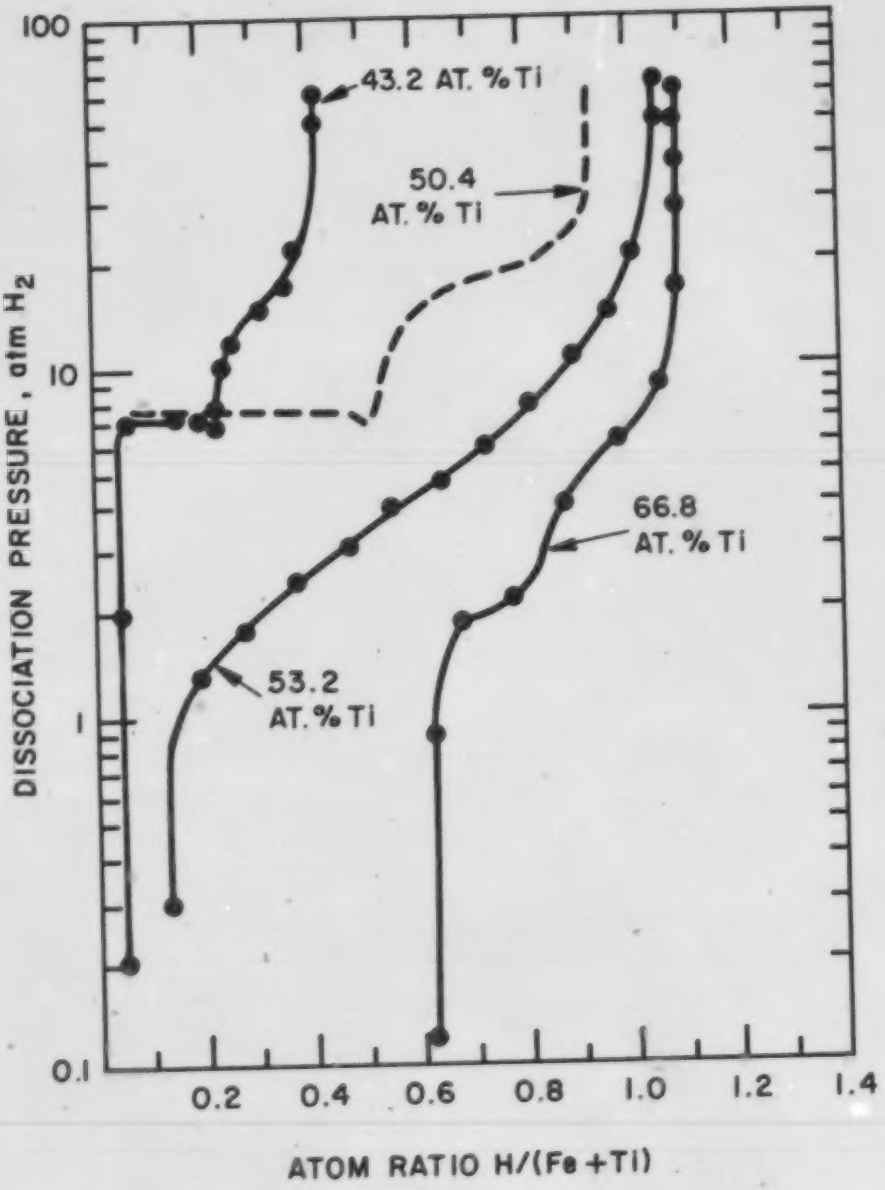

FIGURE 5 - EFFECT OF Ti CONTENT ON 40°C DESORPTION ISOTHERM OF Fe-Ti ALLOYS.

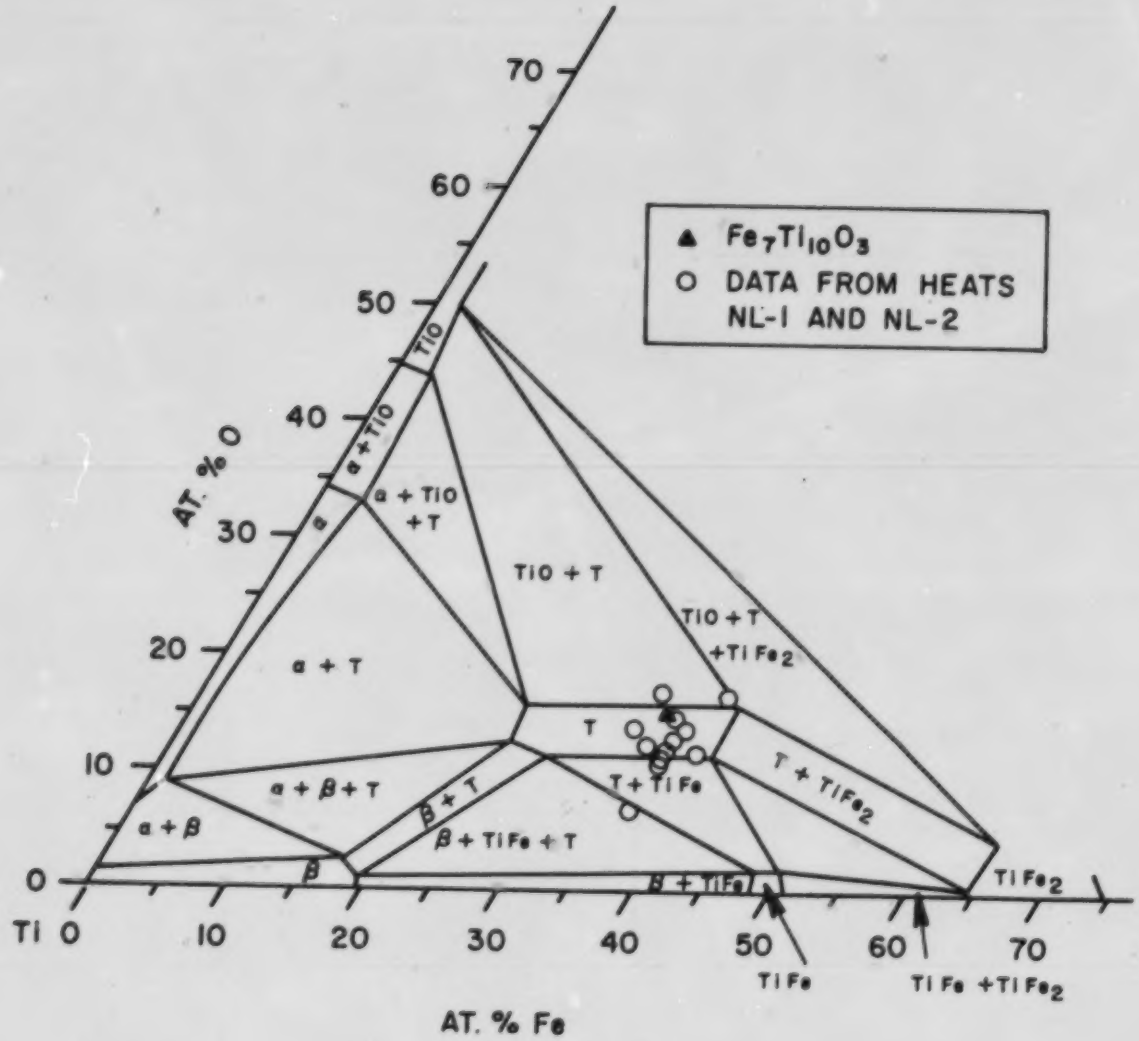

FIGURE 6 - MICROPROBE DATA FOR O-RICH SECOND PHASE PARTICLES FOUND IN MICROSTRUCTURE OF O-CONTAINING FeTi HEATS COMPARED TO THE Ti-Fe-O TERNARY PHASE DIAGRAM OF ROSTOKER (REF. 9). HEATS STUDIED CORRESPOND TO FIG. 7b AND c.

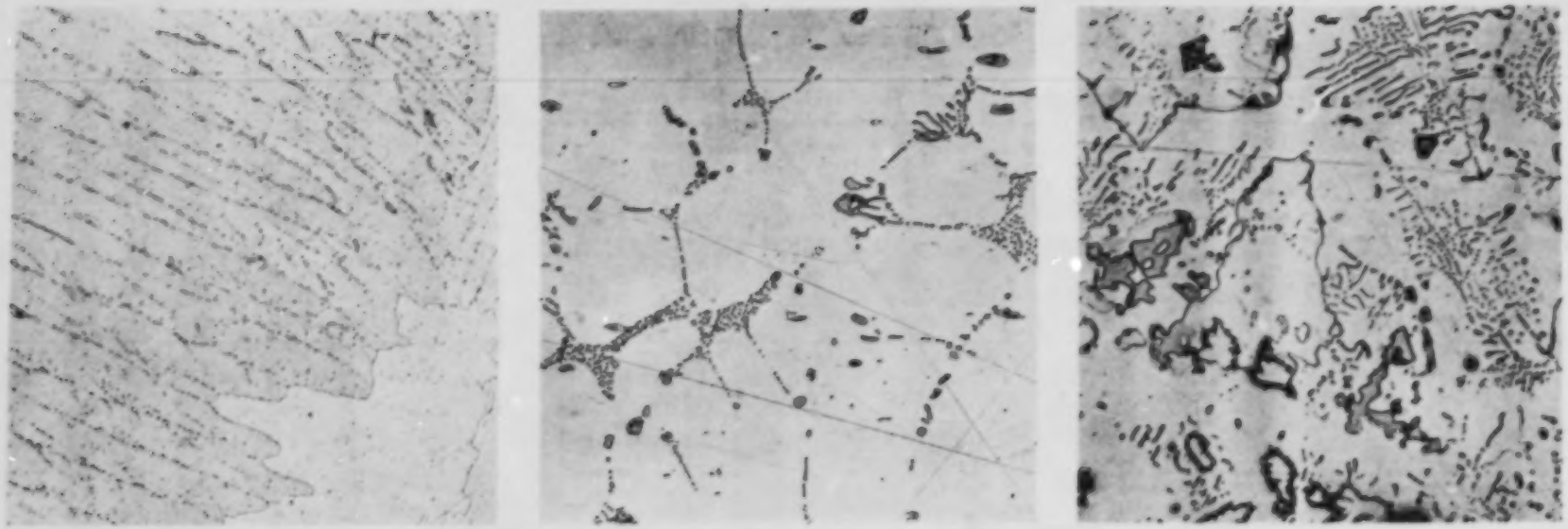

(a) 0.010% O (b) 0.062% O (c) 0.30% O

FIGURE 7

EFFECT OF OXYGEN CONTENT (IN WT. %) ON THE MICROSTRUCTURE OF FeTi
250X

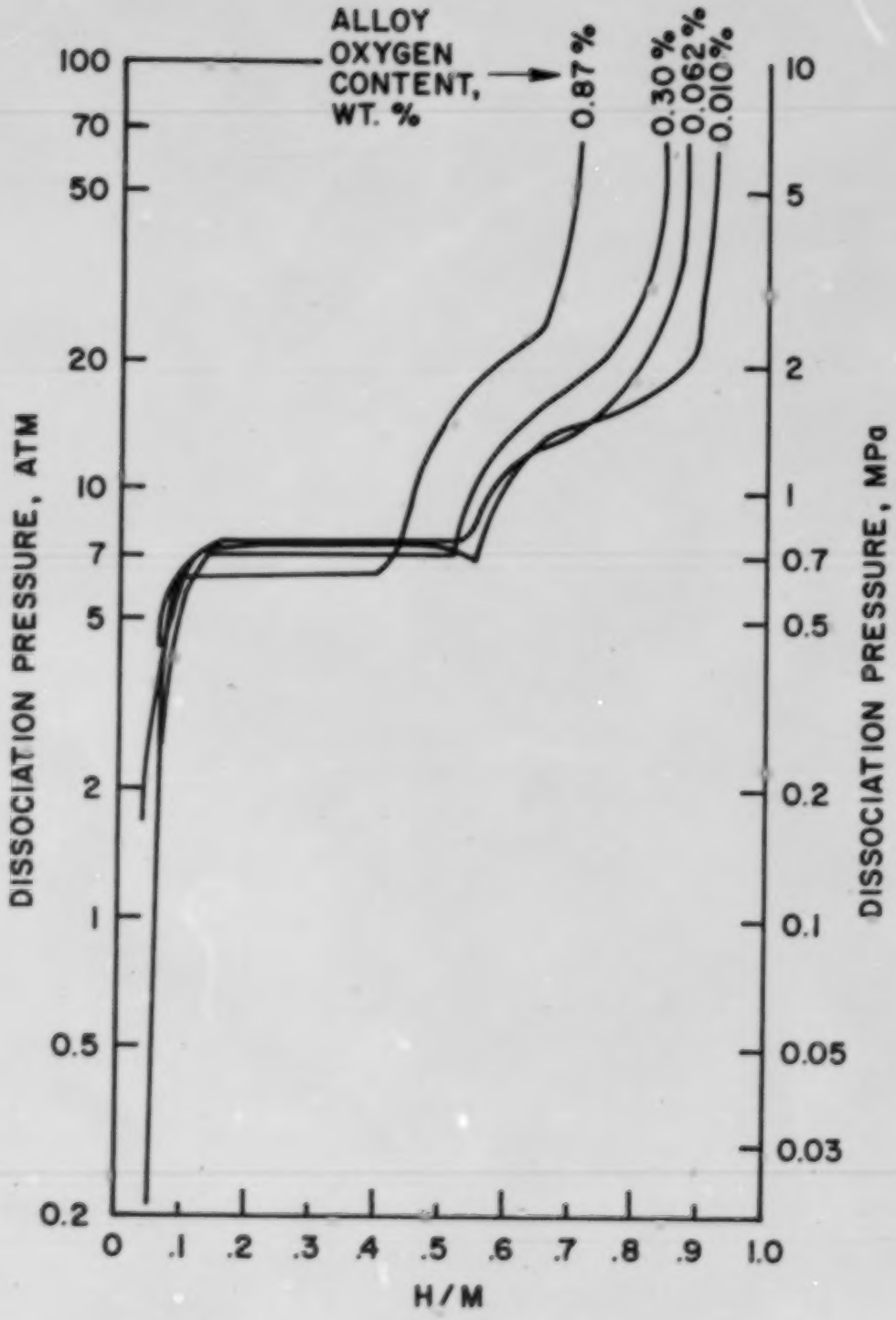

FIGURE 8 - EFFECT OF ALLOY OXYGEN CONTENT ON THE 40°C HYDROGEN DESORPTION ISOTHERM OF FeTi.

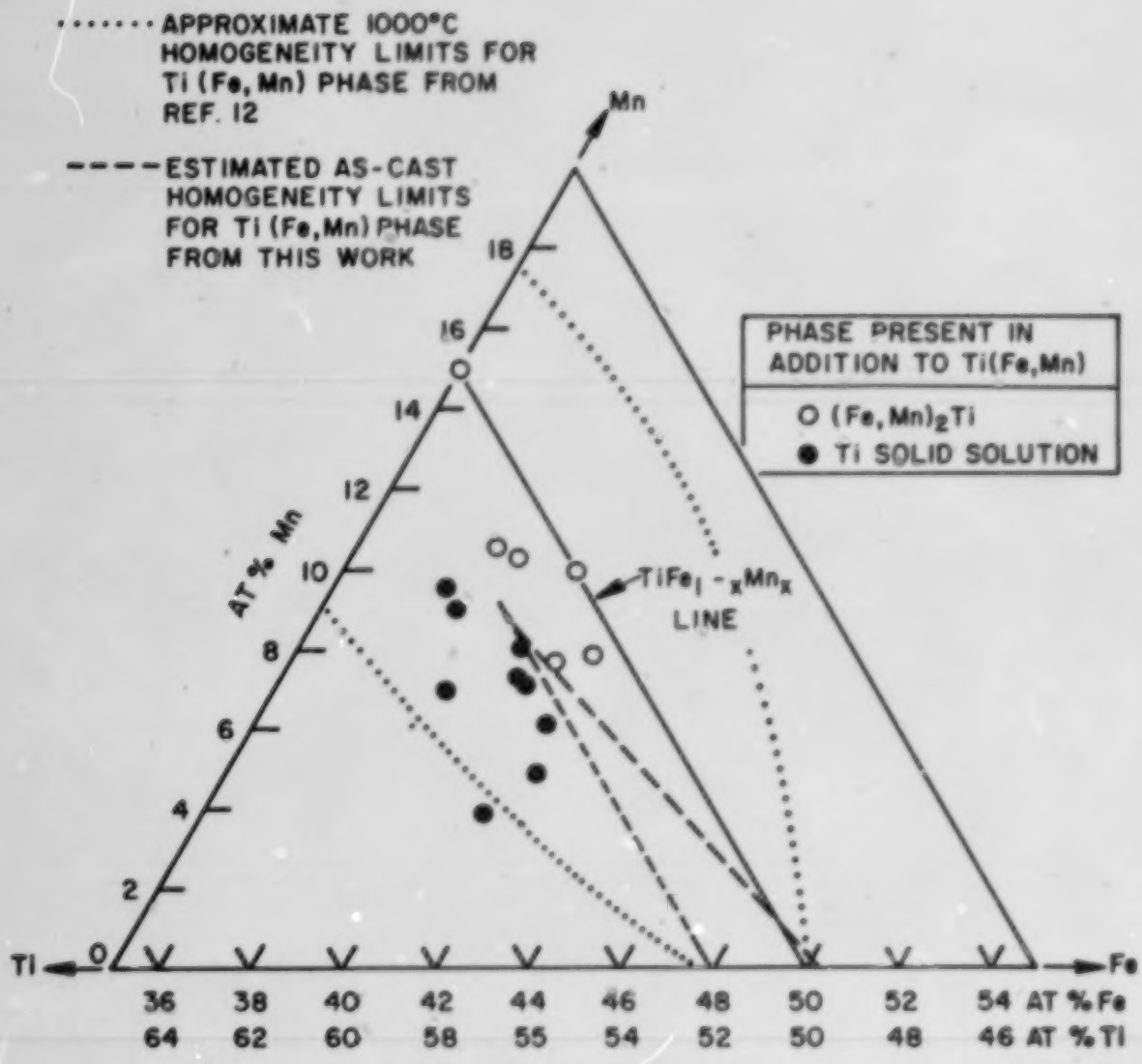

FIGURE 9 - Ti-Fe-Mn ALLOYS STUDIED IN AS-CAST CONDITION COMPARED TO THE 1000°C TERNARY PHASE DIAGRAM OF REF. 12.

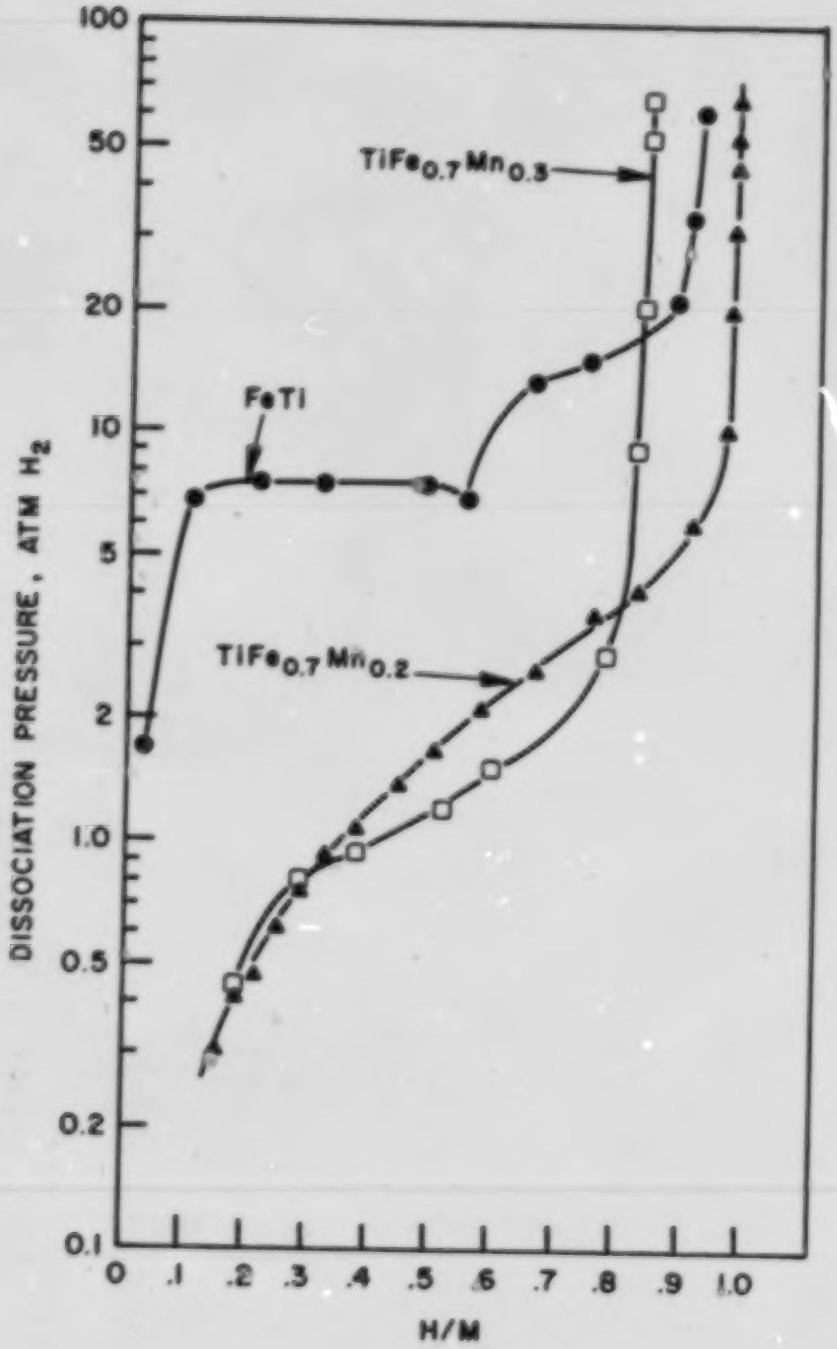

FIGURE 10 - EFFECT OF Mn SUBSTITUTION ON THE 40°C DESORPTION ISOTHERM OF FeTi.

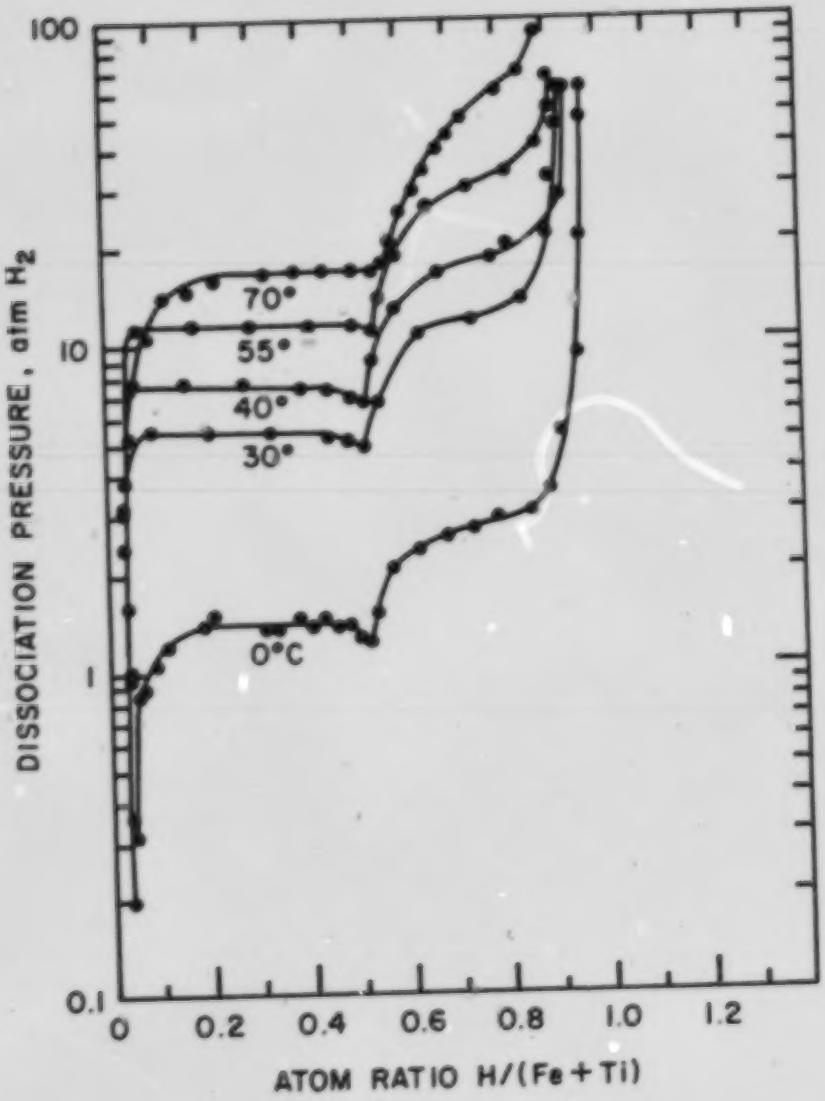

FIGURE II - PRESSURE-COMPOSITION ISOTHERMS FOR THE FeTi-H SYSTEM.

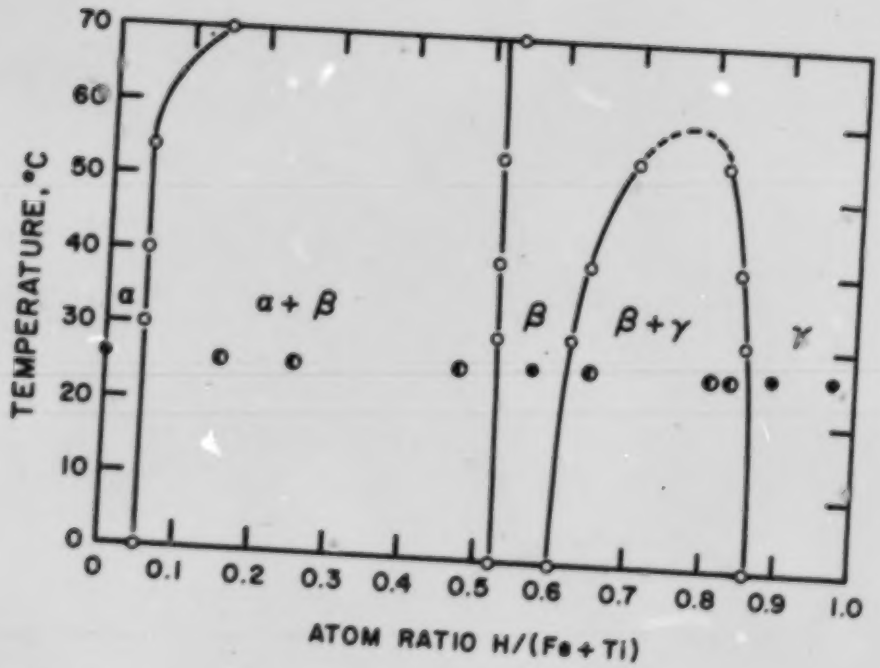

FIGURE 12 - PHASE DIAGRAM OF THE FeTi-H SYSTEM AS DERIVED FROM PRESSURE-COMPOSITION DATA. X-RAY DIFFRACTION PATTERNS TAKEN AT COMPOSITIONS INDICATED: ●, ONE SOLID PHASE, ◐, TWO SOLID PHASES. α = FeTi, $\beta \approx$ FeTiH, $\gamma \approx$ $FeTiH_2$.

National Bureau of Standards SP-496, Applications of Phase Diagrams in Metallurgy and Ceramics
Proceedings of Workshop held at NBS, Gaithersburg, Md., January 10-12, 1977

Phase Equilibria in the System MgO-RCℓ (R=Li, Na and K) Solution under Hydrothermal Conditions by Means of a Capsule Bursting Method

Shigeyuki Somiya, Kazuo Nakamura, Shin-ichi Hirano and Shinroku Saito

Research Laboratory of Engineering Materials
Tokyo Institute of Technology
Ookayama, Meguroku, Tokyo, 152, Japan

Introduction

Brucite $Mg(OH)_2$, is one of the raw materials to produce basic bricks. Brucite is obtained from sea water by precipitation or as natural rock which occurs in hydrothermal veins. The researches on the phase equilibrium in the system MgO-$Mg(OH)_2$ in pure water have been carried out by many researchers by means of various methods including the thermodynamic calculation. The phase equilibrium curves obtained, however, dispersed in wide temperature range because of the difficulty of quench of periclase, MgO.

It is well known that the hydrothermal solutions often contain alkali chlorides. But the literature that can be found on the phase equilibria in the system MgO-$Mg(OH)_2$ in alkali chloride solution, was scarce.

The purpose of the present work is to clear up the effect of the kind of the alkali chloride such as LiCℓ, NaCℓ and KCℓ on the phase equilibrium curve of the system MgO-$Mg(OH)_2$ up to 1,500 kg/cm^2 by means of a capsule bursting method.

Experimental

In this investigation test-tube-type hydrothermal vessels were employed and water was used as a pressure medium. Pressure was measured with a 12 inch Heise Bourdon tube pressure gauge. Temperature was measured with a platinel thermocouple calibrated against the melting points of gold (1,064.4°C) and zinc (419.5°C). Temperature

was controlled with an automatic electronic controller combined with a SCR system (Ohkura Electric Co. Ltd., Tokyo, Japan) within ±3°C. The accuracy of pressure during a run was ±30 kg/cm^2.

The starting material of MgO was prepared by calcination at 600°C in Pt crucible for 24 hrs from magnesium nitrate, which had been obtained by the reaction of reagend grade nitric acid (Wako Pure Chemical Industry, Osaka, Japan) and magnesium metal (99.94% Furukawa Magnesium, Tokyo Japan). Five molar percent solutions were prepared from reagend grade alkali chloride (Wako Pure Chemical Industry) and redistilled water.

A gold capsule, 3.0 mm in OD, 2.7 mm in ID and 35 mm in length, including the desired quantity of MgO powder and 5 mol% RCℓ solution was sealed by an electric arc. The quantity of H_2O in the capsule was from 0.6 to 0.8 in molar ratio necessary to convert MgO into $Mg(OH)_2$.

The process of hydrothermal treatment are the same as in the study of the system MgO-$Mg(OH)_2$ in pure water[1]; that is, pressure was initially applied to the desired value and then the temperature was increased to the desired value at the constant pressure. Samples were subjected to the constant temperature and pressure for a given duration. After the run pressure was released quickly to the atomospheric pressure and subsequently the vessel was quenched in cold water. This process is called "Capsule Bursting Method".

If the set point of temperature and pressure was on the higher temperature side of the equilibrium curve, the capsule would be burst by unreacted solution. In contrast, if it was on the lower temperature side, water inside the capsule was completely consumed up to form $Mg(OH)_2$. Therefore the capsule would not be burst but squeezed. After the run, the sample taken out of the capsule was examined by the Xray powder diffraction method using copper K_α radiation. The result was accepted when the results of Xray powder diffraction coincided with those of the capsule bursting method of two set of the capsules in one vessel.

Results and Discussion

The outside feature of the capsule showed the stable phase which existed in the capsule at each temperature and pressure in the system containing alkali chloride solution as in the system with pure water.

The phase equilibrium curves in LiCℓ solution, NaCℓ solution and KCℓ solution obtained are shown in Figs. 1, 2 and 3, respectively. Fig. 4 shows these curves including one in the system of MgO- pure H_2O which was studied by authors with the same method.[1] The equilibrium temperatures of each system at 500, 1,000 and 1,500 kg/cm^2 are shown in table 1. For example, equilibrium temperatures at 1,000 kg/cm^2 are 517°C in 5 mol% LiCℓ solution, 559°C in 5 mol% NaCℓ solution and 537°C in 5 mol% KCℓ solution. On the other hand it is 595°C in pure water.

All the equilibrium curves in RCℓ solution are in lower temperature side than that in pure water except for the region below about 200 kg/cm^2 in NaCℓ solution. The three equilibrium curves in RCℓ solution are nearly parallel and steeper than that in pure water. The effect of LiCℓ on lowering the equilibrium temperature is the greatest among the three kinds of solutions. The order of the effect, however, does not obey the order in the periodic table. It is known that such the effect is raised by the decrease of the fugacity of water due to the interaction of solute with water.[2]

From these results, the capsule bursting method is recognized as one of the acceptable methods for the study of phase equilibria under hydrothermal conditions whenever the reaction rate of hydration is rapid.

Reference

1) S. Hirano, K. Nakamura and S. Sōmiya
Am. J. Sci, submitted

2) H. L. Barnes and W. G. Ernst, Am. J. Sci, 261 129 (1963)

Table 1. Phase equilibrium temperatures of the system $Mg(OH)_2$-MgO in pure water, 5 mol% LiCℓ solution, 5 mol% NaCℓ solution at 500, 1,000 and 1,500 kg/cm^2.

	Pressure (kg/cm^2)		
	500	1,000	1,500
System of $Mg(OH)_2$-MgO			
pure water[1)]	567	595	614
5 mol% LiCℓ solution	505	517	524
5 mol% NaCℓ solution	553	559	562
5 mol% KCℓ solution	530	537	544

537

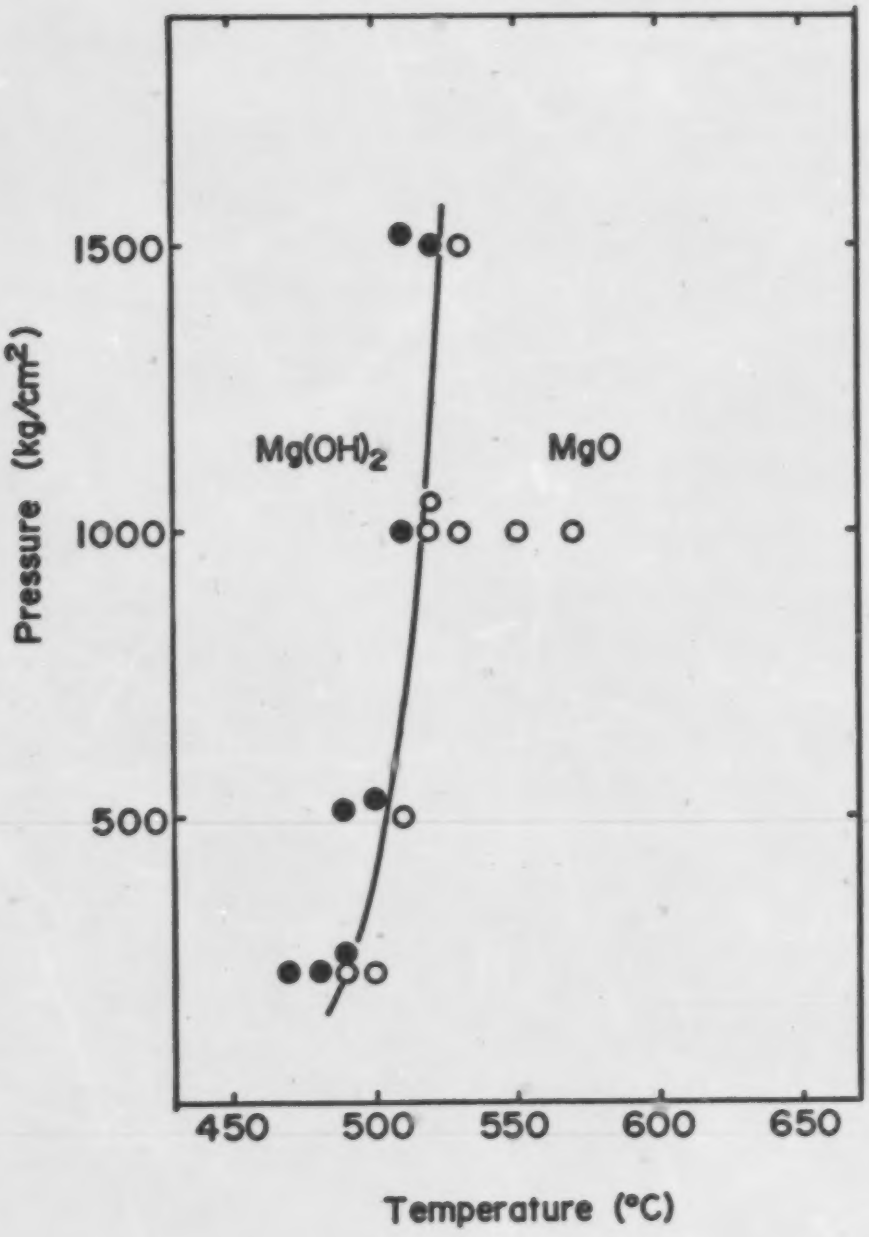

Fig.1 P-T diagram of the system $MgO-Mg(OH)_2$ in 5 mol% LiCl solution.

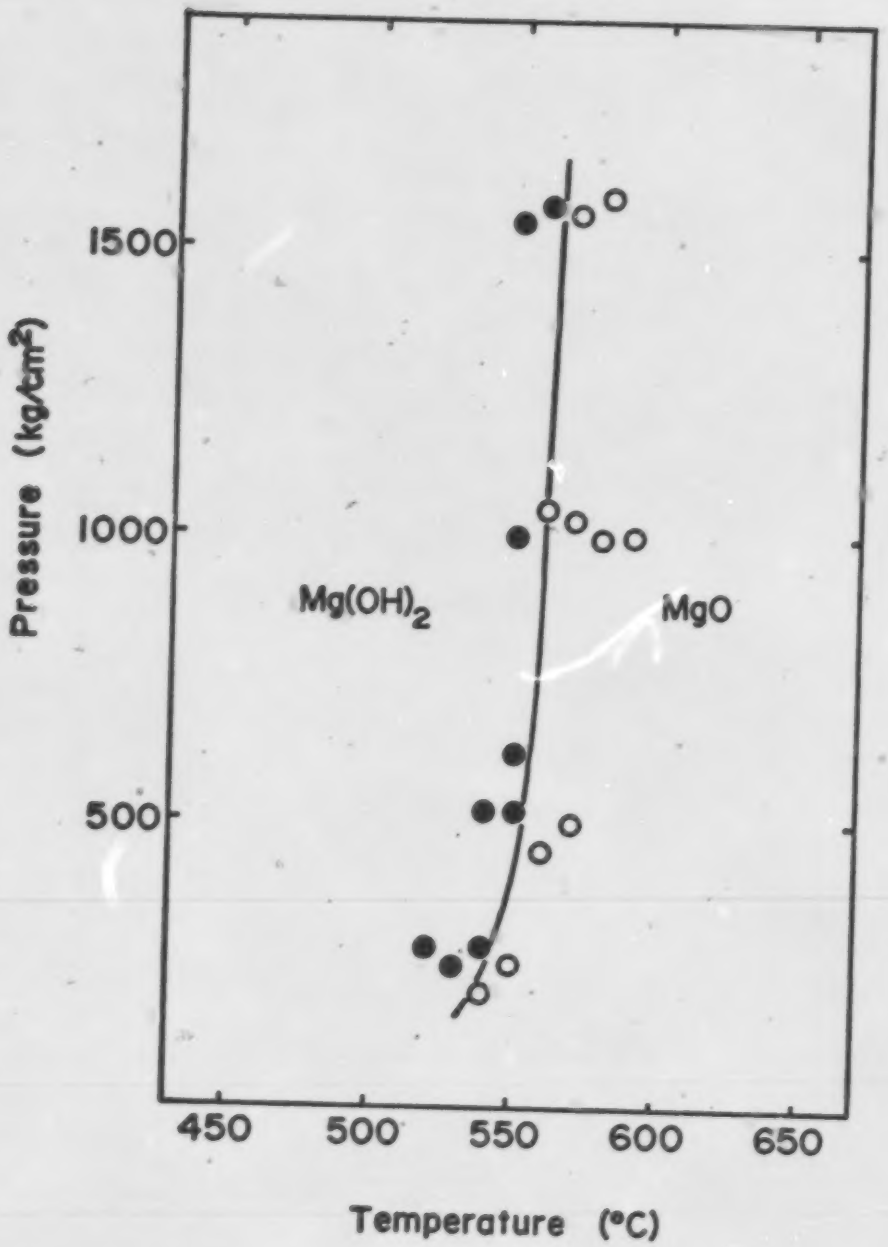

Fig.2 P-T diagram of the system MgO-Mg(OH)$_2$ in 5 mol% NaCl solution.

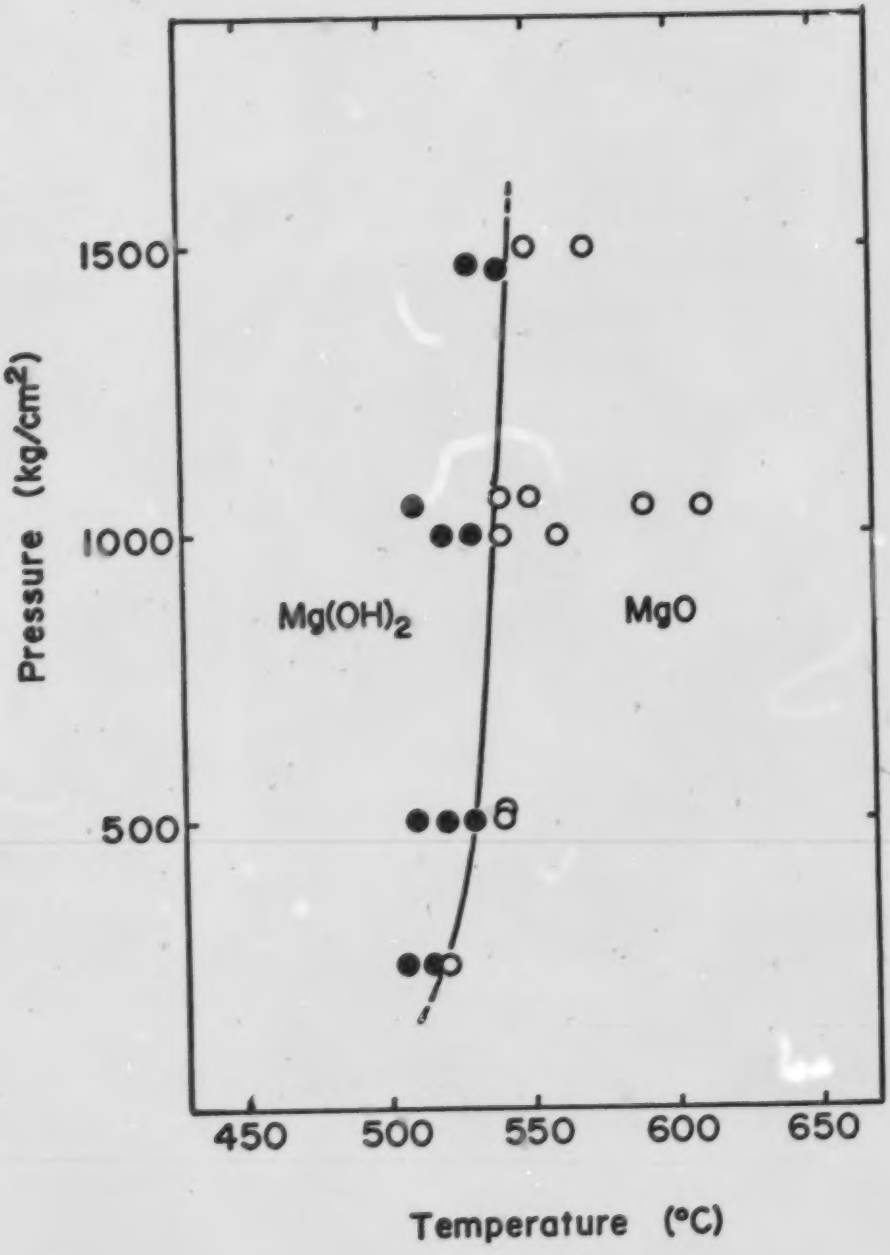

Fig.3 P-T diagram of the system $MgO-Mg(OH)_2$ in 5 mol% KCl solution.

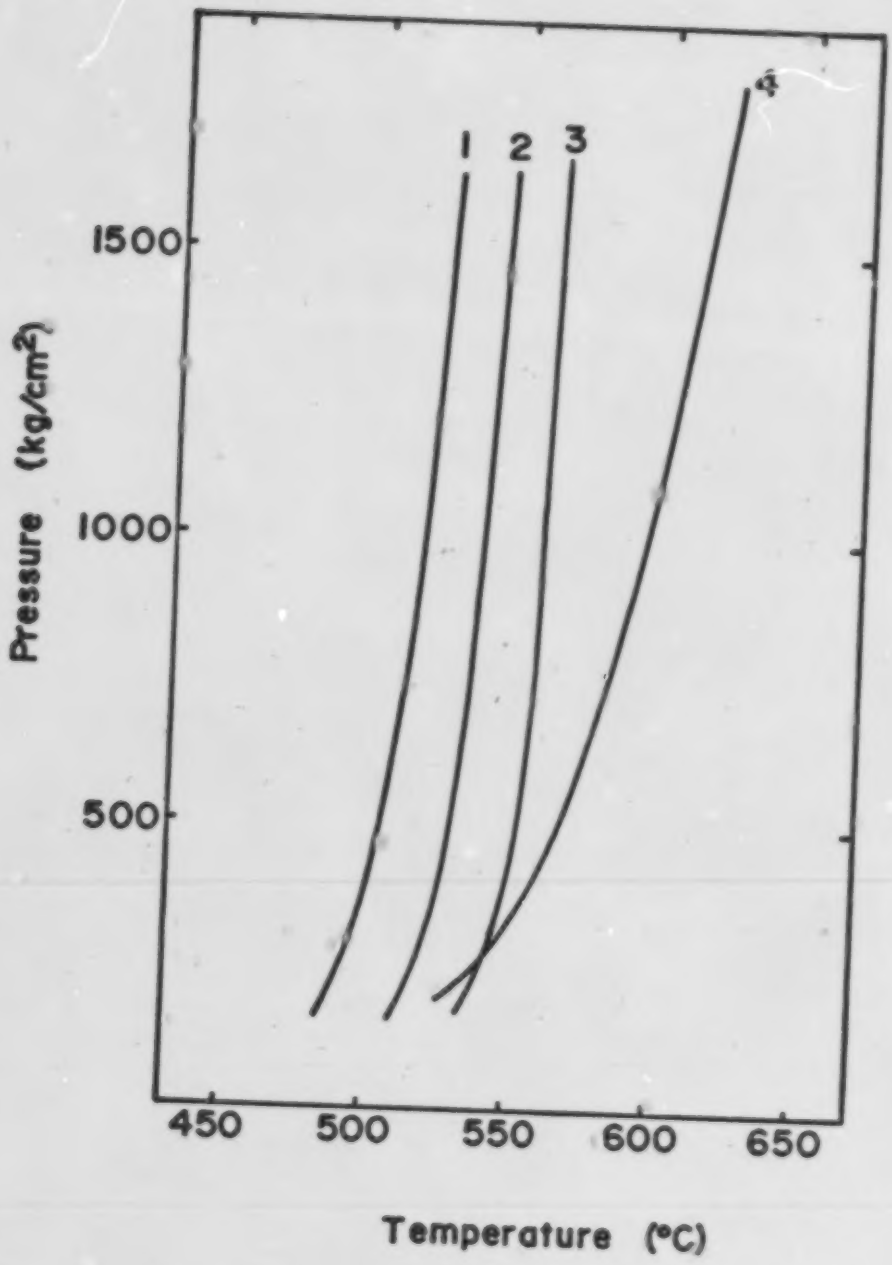

Fig. 4 P-T diagram of the system $MgO-Mg(OH)_2$ in 5 mol% LiCl soln.(1), 5 mol% KCl soln. (2), 5 mol% NaCl soln.(3) and pure water (4).

National Bureau of Standards SP-496, Applications of Phase Diagrams in Metallurgy and Ceramics
Proceedings of Workshop held at NBS, Gaithersburg, Md., January 10-12, 1977

HIGH-ENERGY ION BEAMS IN PHASE DIAGRAM DETERMINATION*

J. E. Smugeresky
Metallurgy & Electroplating Division 8312

S. M. Myers
Ion-Solid Interactions Division 5111
Sandia Laboratories

ABSTRACT

Phase boundaries can now be investigated by a new approach which uses high-energy ion beams. The technique makes use of ion implantation and ion backscattering analysis combined with diffusion annealing treatments. Ion implantation of solute elements into the matrix is used to create a supersaturated solid solution in the first ≈0.1 μm of the sample. During isothermal annealing the composition-versus-depth profile is monitored nondestructively via 2 MeV He backscattering. These profiles and the appropriate boundary conditions for the diffusion equation can be used to obtain the phase boundaries. The advantages of this technique are threefold: (1) solubility measurements can be made at lower temperatures than by other techniques; (2) the composition can be accurately tailored in complex systems; and (3) very low solubilities can be monitored. This technique has been applied to both binary and ternary systems, and solubilities as low as 70 appm and at temperatures lower by almost 300K have been measured.

*This work was supported by the United States Energy Research and Development Administration. Contract Number AT-(29-1)-789.

HIGH-ENERGY ION BEAMS IN PHASE DIAGRAM DETERMINATION

Introduction

The various methods used in phase diagram determination include classical quenching techniques, thermal analysis, electrical conductivity measurements, metallographic methods, thermal gravimetric analysis, dilatometric analysis, X-ray diffraction techniques, and electromotive force measurements in galvanic cells.[1,2] The most widely used method involves thermal analysis or differential thermal analysis. However, in cases where temperatures are low, phase transformations tend to be sluggish and the temperature of transformation becomes difficult to assess. In addition, there are cases in which the solid solubility is quite low and thus the accurate determination of phase boundaries becomes quite difficult. It is these situations that led the authors to develop a new technique which uses high-energy ion beams to determine these boundaries more easily and accurately.

In this paper, we will first describe in general terms the technique used to measure solid solubilities, then give the analytical details of the technique, and finally discuss specific examples of its application thus far in both binary and ternary systems.

General Description of Method

It is helpful to first consider the sample schematically (Figure 1) by dividing it into three regions: A, the near-surface region; B, the underlying bulk region; and C, the unaffected bulk region equivalent to the starting condition of the sample. Initially, all regions are identical. Then solute ions are accelerated toward the surface with sufficient energy to penetrate the sample and occupy region A. Although the width of this implanted region and the amount of solute contained within it can vary, this region is typically 0.1 μm (100 nm) wide and the distribution of solute generally approximates a Gaussian peak. The peak concentrations in region A are typically greater than the solubility, the amount being dependent on the particular systems studied. However, no precipitation of second phases occurs, because the implantation is done at room temperature where the atom mobilities are essentially nil. In effect, the implanted region consists of a supersaturated solid solution.

The implanted concentration can easily be tailored to concentrations much less than 100 percent solutes as is the case in most simple diffusion couples. This is an important benefit most useful when more complex situations are under study, as in the ternary systems described below.

After implantation, an ion backscattering profile is taken to establish the starting conditions. This is done by analyzing the helium backscattering spectrum. From this spectrum, both the identity and the depth distribution of solute or impurity elements can be determined. At this point regions B and C are identical and represent the original condition of the sample.

Next, a diffusion anneal at a temperature of interest is given to the sample. During the anneal, the atoms become mobile enough for precipitation of a second phase, or phases, to occur in region A, the implanted region. At the same time, the excess solute atoms diffuse from the implanted layer into the underlying bulk of the sample (region B). However, precipitation in the implanted region occurs much faster than the diffusion of excess solute into the underlying bulk, so that almost all of an anneal sequence consists of a flow of solute between two well-defined phases at the interface of regions A and B. The situation is not much different from that of a diffusion couple in which a condition of thermodynamic equilibrium exists between these regions, i.e.,

Consequently, the composition of the various phases remains constant during annealing, provided there is an excess of solute atoms in the implanted region. The change that takes place during annealing is in the relative amounts of each phase.

Following the anneal, a second backscattering spectrum is obtained to provide a composition-versus-depth profile. A mathematical analysis of the annealing kinetics allows both the solid solubility and the diffusivity of the solute to be determined. This analysis consists of the application of Fick's law with the appropriate boundary condition.

The measurement of solid solubilities at lower temperatures than by other techniques is possible because of the microscopic scale of the experiment. The implanted layer is typically 0.1 μm thick, so that diffusion

distances need not be very large. Consequently, shorter annealing times are sufficient to get the data at low temperatures. Ion backscattering analyses are ideally suited for microscale situations because of the capability of probing to small depths at high resolution. For helium ions, the maximum depth that can be probed is 2 μm while the resolution is of the order of 0.01 μm. This is a nondestructive technique that can follow the changes in concentration with time. The high resolution and the straightforward quantitative calibration in both depth and concentration are its best assets. Even in cases which require more time, the time necessary for the anneal can be shortened by a factor of typically one to two orders of magnitude by using a modified implant sequence to enhance the diffusion of the solute of interest. By implanting either a lighter element or the solvent element somewhat deeper than the solute implant, a region in which the diffusion rate is greatly enhanced is created between regions A and B as seen in Figure 1. While this modification may not work in all cases, it does allow measurements of solubility to be made at temperatures even lower than those of the unmodified procedure. Now that a general description of the method has been given, some details of the analysis will be described.

Ion Backscattering Analysis

The backbone of this technique is the ion backscattering spectrum. This spectrum is a plot of yield Y, in counts per keV, versus the energy E, in MeV of the backscattered ions. The energy of the backscattered helium ions is dependent upon the atomic mass m of the elements present in the target and the incident ion energy before backscattering. Hence, the fraction of incident ion

energy that is retained by the backscattered ions increases with the atomic mass, as shown in Figure 2. The yield is related to the amount of that element present, as well as to its atomic number Z. The depth at which the element is located also affects the energy of the backscattered ions. Continuous energy losses occur as a result of electronic excitations as the ion traverses the lattice before and after backscattering. Consequently, if all of a particular element were present at the surface, a spike in the yield would occur at the energy corresponding to the fraction of retained energy for that element. For example, a 2 MeV helium ion would retain 0.753 of its incident energy if iron were present and a spike in yield would appear at an energy equal to 1.506 MeV. Several elements and the corresponding fractions of retained energy are indicated on the right margin of Figure 2. If one or more of these impurities is distributed within the sample, the corresponding spike becomes a concentration profile indicating just how the impurity is distributed with depth into the sample. This can best be seen by considering Figure 3, a schematic ion backscattering spectrum for a sample having three impurities present where $m_A > m_B > m_C$. In this example, element A is confined to an infinitely thin layer on the surface; element B is present in the first y μm of surface at a constant concentration, while element C has a Gaussian concentration distribution with a peak located a distance p from the surface.

The concentration at a given depth x is obtained by analytically transforming the yield-versus-energy (Y vs E) spectrum into a concentration-versus-distance (C vs x) profile for each element k present. Thus

$$Y_k = Y(E) \quad \text{for} \quad E \leq E_k \tag{1}$$

is transformed into

$$C_k = C_k(x) \qquad (2)$$

where E_k corresponds to the energy retained by element k. Such a transformation is schematically shown in Figure 4 for a profile of an as-implanted element k. Consequently, one can study the change in profile during annealing by comparing the transformed spectra. The exact analytical expression for the concentration profile is found in the work of Chu, et al.;[3] its evaluation in the general case is complex and requires numerical methods described by Brice.[4] Calculations include electronic stopping rates for pure elements; these are taken from experimental results in the literature.[5]

Solubility Determination

Following a diffusion anneal, the concentration profiles are analyzed and both the solid solubility and the diffusion coefficient D can be determined. During the anneal, a discontinuity in the concentration profile exists at the interface of the implanted layer and the underlying bulk, i.e., the boundary between regions A and B as shown in Figure 5. When this discontinuity remains constant with annealing time at a given concentration C_0, it indicates that a condition of local thermodynamic equilibrium exists at the interface between regions A and B. This concentration value C_0 is the solubility of the implanted element, and the profile in region B is described by solving the diffusion equation

$$\frac{\partial C(x,t)}{\partial t} = D\frac{\partial^2 C(x,t)}{\partial x^2} \qquad (3)$$

where D, the diffusion coefficient, is assumed constant. The initial condition is

$$C(x>0,\ t=0) = 0 \tag{4}$$

and the boundary condition is

$$C(x=0, t) = C_0 \tag{5}$$

where x is measured from the intersection of the peak and a diffused tail (i.e., boundary of regions A and B in Figure 5). The solution is readily obtained[6] as

$$C(x, t) = C_0 \operatorname{erfc}\left(\frac{x}{2\sqrt{Dt}}\right) \tag{6}$$

When the actual data are compared with a family of plots for different values of D, the curve with the best fit gives the diffusion coefficient. Since the emphasis here is on phase boundaries, details for diffusivity studies are not described, but they can be found in References 7, 8, and 9.

Enhanced Diffusion

As the temperature of the diffusion anneal becomes lower, the time required for sufficient diffusion to occur becomes longer. Even though the ion beam technique is on a microscopic scale and thus requires only small diffusion distances, the lower temperature diffusion anneals can still become prohibitively long. In these cases, diffusion can be enhanced by implanting a second element in addition to the solute and deeper than the solute. In effect, this introduces an intermediate region between regions A and B in Figure 1, which we will call region A'. The as-implanted profile of the solute of interest

is essentially unaffected by this procedure. However, after the anneal, the shape of the diffused tail is qualitatively different, in that it exhibits a plateau in region A'. The concentration profile in region A is essentially the same as for the normal implant procedure, while in region B much less solute diffuses because of the low temperature and short anneal time. The implantation of the second element, which can be an inert element such as neon or the solvent itself, produces lattice damage in the sample just beyond the implanted solute. This allows the solute to diffuse more rapidly than before so that the concentration builds up to the solubility limit more rapidly in the damaged lattice. Consequently, the plateau concentration corresponds to the solubility. However, the equilibrium diffusion coefficient cannot be determined by this procedure. In addition, the applicability of enhanced diffusion may not be as general as the normal implantation procedure described above. It has been applied to several systems but has not been successful in all cases. Now that the techniques have been discussed generally, a deeper insight can be gained from the specific examples described below.

Applications

(a) Binary Cases The first systems investigated by the authors used beryllium as the solvent. This metal perhaps represents the most ideal case, since it has so low a Z that any impurity or solute element of interest has a higher Z. Consequently, the backscattered energy of the host material

is lowest and this allows easy resolution on the backscattered spectrum of any solute of interest. The implanted solute species were copper, iron, and aluminum.[7,8] The as-implanted backscattered spectrum for the beryllium-copper binary system is shown in Figure 6. In these experiments, the usual configuration for ion backscattering measurements with 2 MeV helium was used.[3]

A magnetically analyzed helium beam from a Van de Graff accelerator was collimated to a 1 mm square and allowed to strike the sample normal to its surface. A silicon surface-barrier detector of 25 mm^2 surface area and 13 keV FWHM (full width at half maximum) resolution faced the sample at a distance of 180 mm at an angle of 170 degrees from the incident beam. The backscattered ions produced a current pulse with an amplitude proportional to energy and a spectrum of these energies was accumulated by a multichannel analyzer. The beam current was ≈40 nA and an accumulated charge of the order of 20 μC (i.e., $\sim 10^{16}$ He/cm^2) per spectrum was used. Effects of the helium analysis beam on the experimental results were checked by sampling a virgin spot periodically, but no significant differences were ever found. An additional measure when the solubilities were low involved use of a second set of collimation slits to reduce halo effects[7] about the incident beam.

The transformed data are shown in Figure 7 for both the as-implanted and after-annealing conditions. Actual values of solubility of copper in beryllium were measured at 593K, 673K, 773K and 1023K.[8,9] A plot of the solubility versus T^{-1} (Figure 8) resulted in the following relation for the solubility:

$$C_0(\text{Cu}) = (12.6 \text{ atomic percent}) \exp\left(\frac{-842\text{K}}{T}\right) \quad (7)$$

Included in the plot are values from other workers,[10,11] showing the excellent agreement between data obtained using high-energy ion beams and data obtained by other techniques.

In the Be-Fe system, the solubility of iron is very low and is complicated by the role played by aluminum in commercial purity beryllium.[12] Previous workers[10,13,14] had measured the solid solubility, but only at temperatures above 973K. By using this high-energy ion beams technique, the present authors[7] made measurements at temperatures as low as 773K. A plot of the solubilities, which are less than 0.2 at.%, versus T^{-1} (Figure 9) resulted in the relation:

$$C_0(\text{Fe}) = (14.0 \text{ at.}\%) \exp\left(\frac{-5246\text{K}}{T}\right) \quad (8)$$

A comparison with data gathered at higher temperatures[10,13] showed excellent agreement.

The validity of the application of the diffusion equation and assumed boundary condition was subjected to two additional checks: (1) the amplitude of the diffused tail at the discontinuity should be independent of both anneal time and the amount of implanted iron at a given temperature and (2) the amount of iron per unit area L which has diffused from the implanted region should vary with the isothermal anneal time t as[7]

$$L(t) = C_0 \left(\frac{4Dt}{\pi}\right)^{1/2} \quad (9)$$

Both of these criteria were satisfied with the relationship between L and t shown in Figure 10.

In the case of aluminum, the solubility was below the limits of detectability of the apparatus. The upper bound was established as 70 appm at both 873 and 1073K.

The enhanced diffusion technique has been used in the Be-Cu system to determine the solubility at 593K. The second implanted species was neon, which was immobile during the anneal. The concentration profiles for Cu and Ne after the anneal are shown in Figure 11. Here it is seen that the plateau in the copper profile overlaps the neon-implanted region. This technique resulted in an anneal time of only 175 hours instead of the six months required for normal diffusion rates. Thus the time required to do the experiment was dramatically reduced.

As a consistency check, the enhanced diffusion technique was also used for 673K. The solubilities measured were 3.62 at. % for the normal diffusion case and 3.50 at. % for the enhanced diffusion case, both well within the experimental error.

(b) Ternary Cases The ternary systems investigated were Be-Fe-Al, Be-Cu-Al, Be-Cu-Si.[7,8] The primary concern here was the effect of the third element on the solubility of the primary solute: in essence, the effects of aluminum and/or silicon on the solubility of iron and copper in beryllium.

The ternary solute effect was strongest for the Be-Fe-Al system, in which the presence of aluminum reduced the solubility of iron below the limits of detectability by this technique, i.e., less than 100 appm for temperatures less than 1123K. This represents an order of magnitude decrease.

In the case of Be-Cu-Al,[8] the effect was well within the experimental error. At 773K the solubility of Cu is 4.25 atomic percent, while in the presence of aluminum, a value of 4.15 atomic percent was measured.

Silicon, however, made a measurable difference. At 673K the measured solubility of copper was 3.6 atomic percent in the binary case but dropped to 2.82 atomic percent in the presence of silicon.

In each of the ternary cases noted here, the implantation concentration was sufficient to ensure the establishment of equilibrium at the interface between regions A and B of the sample. The situation is entirely analogous to the binary if the implant concentration is high enough and the overall composition of regions A and B in Figure 1 is in a three-phase region of the phase diagram. Thus the implanted concentration must not only exceed the solubility on the binary leg of a ternary diagram, but also ensure establishment of a three-phase equilibrium locally. With reference to Figure 12, this amounts to being at points Y or Z instead of X. In these situations, the diffusion equation solutions used for the binary case are still valid. However, if the sample is at composition X in Figure 12, more complex analytical solutions are required. As yet, these have not been developed.

As a check on the establishment of equilibrium consistent with points Y and Z in three-phase equilibrium, samples were examined by transmission electron microscopy.[15] The presence of these phases was established by diffraction analysis. Similar confirmation has also been obtained for binary systems.[15]

In the ternary cases, the requirement of obtaining specific concentrations to ensure the attainment of equilibrium for three phases at various regions of the phase diagram is easily satisfied by ion implantation. The local concentration corresponding to the peak of the Gaussian distribution can easily be modified and does not have to be 100 percent as is the case in vapor-deposited layers in diffusion couple studies. In the examples described above, peak concentrations were of the order of 20 atomic percent at a depth of approximately 0.04 μm with a full width at half amplitude of 0.04 μm; this is in excellent agreement with values calculated from the ion range theory of Brice.[16] This ability to tailor the composition locally greatly facilitates studies in complex situations.

Summary

We have described here a new technique for determining phase equilibria in condensed systems. It consists of ion implantation of solute species in the first $\approx$0.1 μm of the sample at concentrations less than 100 percent, combined with ion backscattering analysis of samples subjected to diffusion anneals.

By an analytical transformation of the ion backscattering spectrum, the concentration profile of the solute species is obtained. An analysis of this profile, along with the application of the diffusion equation, allows determination of the solid solubility, but can also be used to obtain the diffusion coefficient of the solute. This technique can be applied to both binary and ternary systems for solid solubility measurements. The main

advantages are (1) solubility measurements at lower temperatures than by other techniques (examples were given for almost 300K lower); (2) the ability to tailor the implanted composition accurately at values considerably less than 100 percent to suit the needs of complex situations; and (3) the ability to measure very low solubilities. The technique is best applied to situations in which the solute elements have a higher atomic number than the solvent. So far, this technique has been applied to both binary and ternary systems where beryllium was the solvent, with the solubilities of iron and copper being measured at temperatures almost 300K lower than had been previously reported.

REFERENCES

1. A. Reisman, Phase Equilibria, Academic Press, 1970.
2. J. B. Macchesney and P. E. Rosenberg, Phase Diagrams, Vol. 1, ed. by A. M. Alper, Academic Press, 1970, p. 114.
3. See W. K. Chu, J. W. Mayer, M. A. Nicolet, T. M. Bach, G. Ansel, and F. Eisen, Thin Solid Films, 17 (1973) 1, for a review of ion beam analysis.
4. D. K. Brice, Thin Solid Films, 19 (1973), p. 121.
5. See, for example, J. F. Ziegler and W. K. Chu, Atomic Data and Nuclear Data Tables, 13 (1974), p. 463.
6. P. G. Shewmon, Diffusion in Solids, McGraw Hill, 1963.
7. S. M. Myers and J. E. Smugeresky, Met. Trans. 7A (1976), p. 795.
8. S. M. Myers and J. E. Smugeresky, to be published in Met. Trans. A.
9. S. M. Myers, S. T. Picraux, and T. S. Prevender, Phys. Rev. B 9 (1974), p. 3953.
10. M. L. Hammond, A. T. Davinroy and M. I. Jacobson, Beryllium-Rich End of Five Binary Systems, Air Force Materials Laboratory Report, AFML-TR-65-233, 1965.
11. A. R. Kaufmann, P. Gordon, and D. W. Lillie, Trans. ASM, 42 (1950), p. 785.

12. S. H. Gelles, Impurity Effects in Beryllium, Metals and Ceramics Information Center, Report MCIC 72-06, 1972, Columbus, OH.

13. G. Donze, R. LeHazif, F. Maurice, D. Dutilloy, and Y. Adda, Compt. Rendu., 254 (1962), p. 2328.

14. S. H. Gelles, J. J. Pickett, E. D. Levine, and W. B. Nowak, in "The Metallurgy of Beryllium," Inst. of Metals Monograph, London (1963), p. 588.

15. J. E. Smugeresky, G. J. Thomas, and S. M. Myers, unpublished research 1976.

16. D. K. Brice, Radiation Effects, 11 (1971), p. 227.

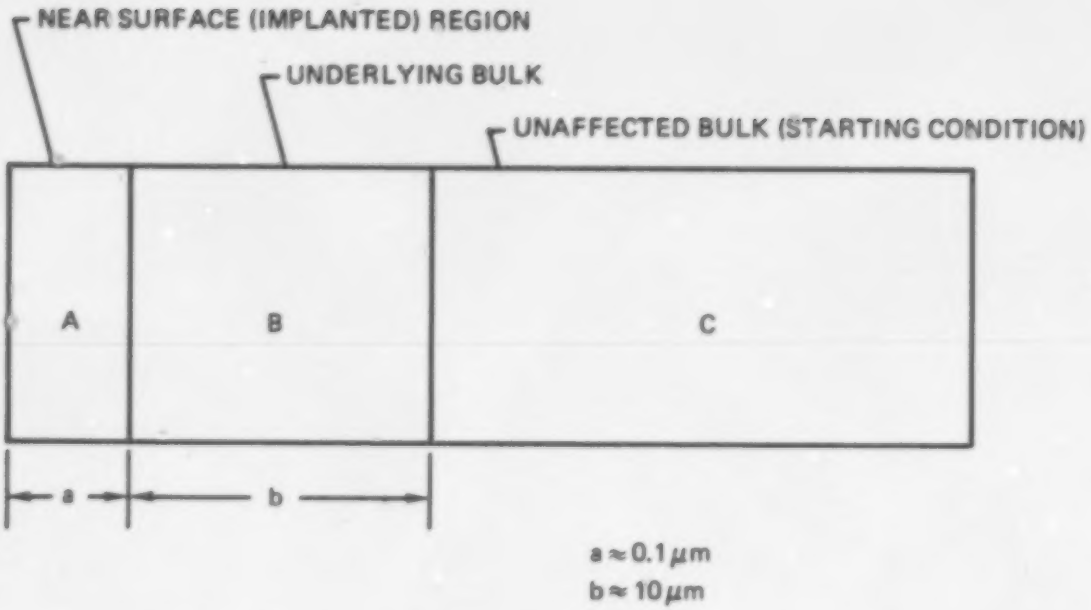

Figure 1. Schematic of sample showing implanted region (A), underlying bulk (B), and unaffected bulk (C). Diffusion of solute from region A occurs in region B during annealing.

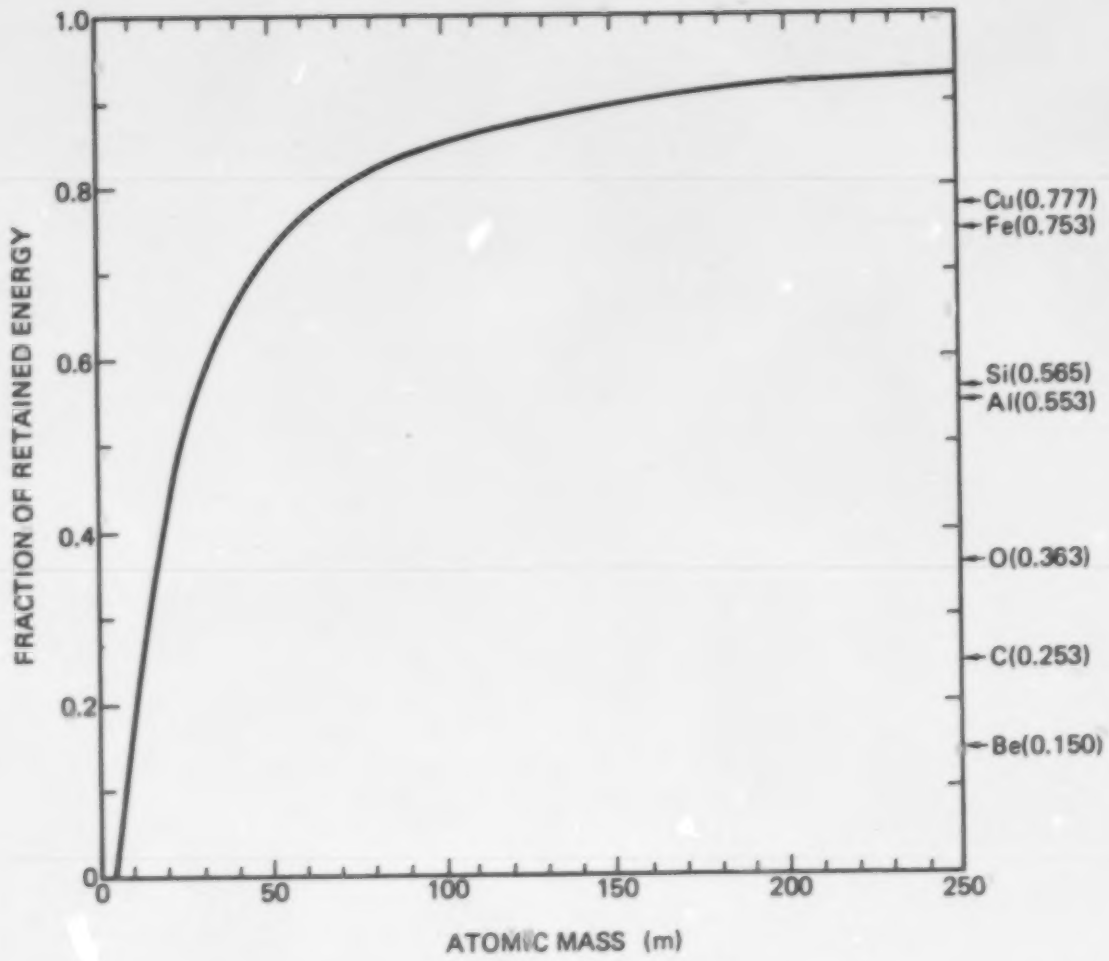

Figure 2. Relation between energy of backscattered ions and atomic mass of scattering species for backscattered angle of 170°. Values for several elements are listed at right.

530

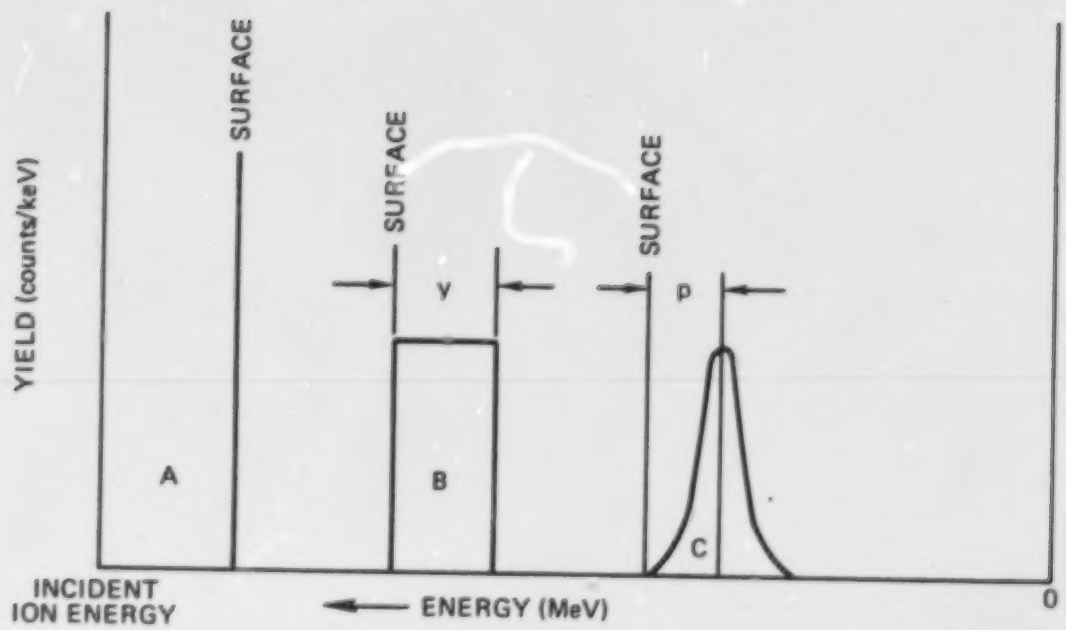

Figure 3. Schematic ion backscattering spectrum of sample containing three impurities: A, B, and C where $m_A > m_B > m_C$. In each case the impurity distribution is located near the surface.

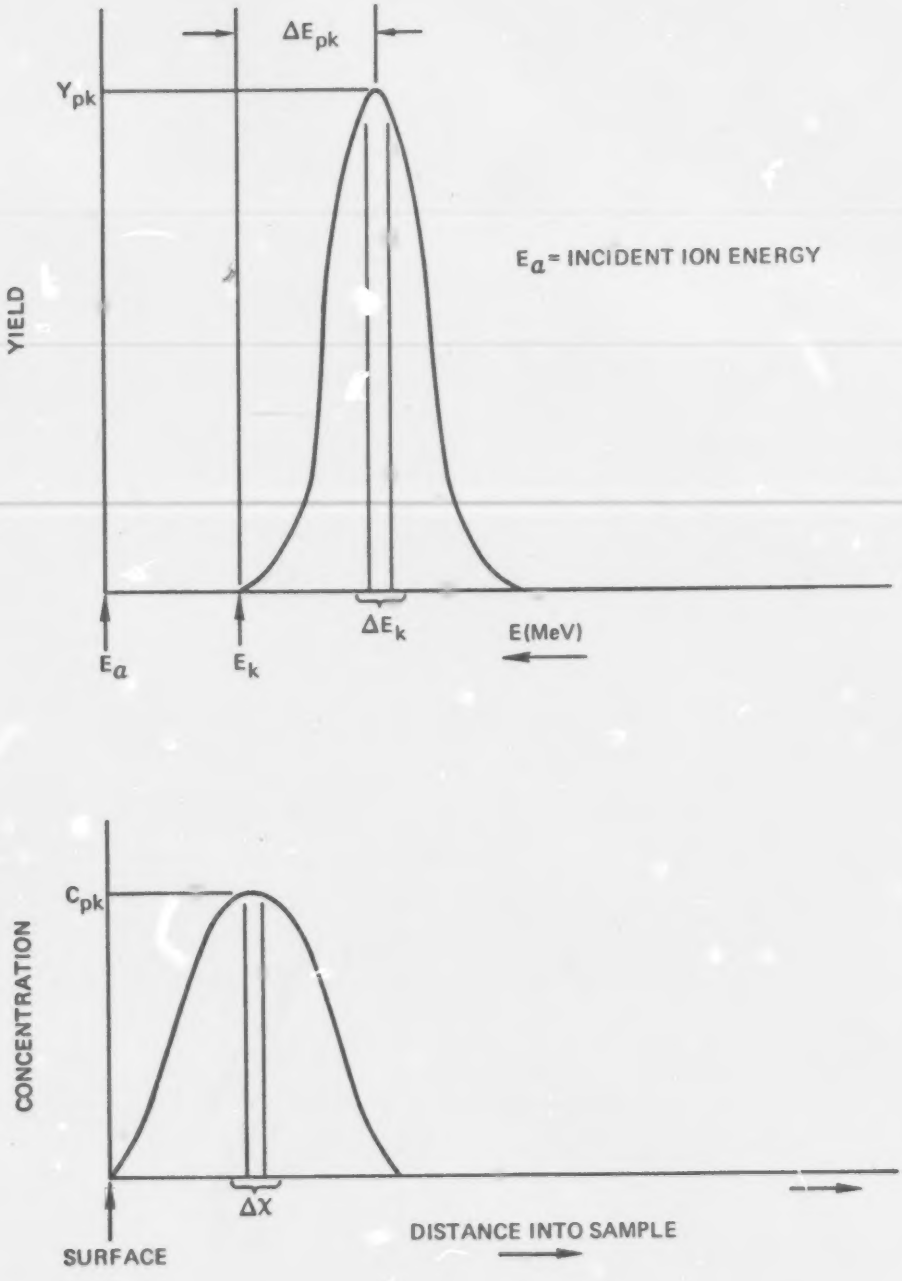

Figure 4. Schematic of ion backscattering spectrum of implanted region showing its transformation to a concentration profile. Note that E_k corresponds to element k present at the surface of the sample.

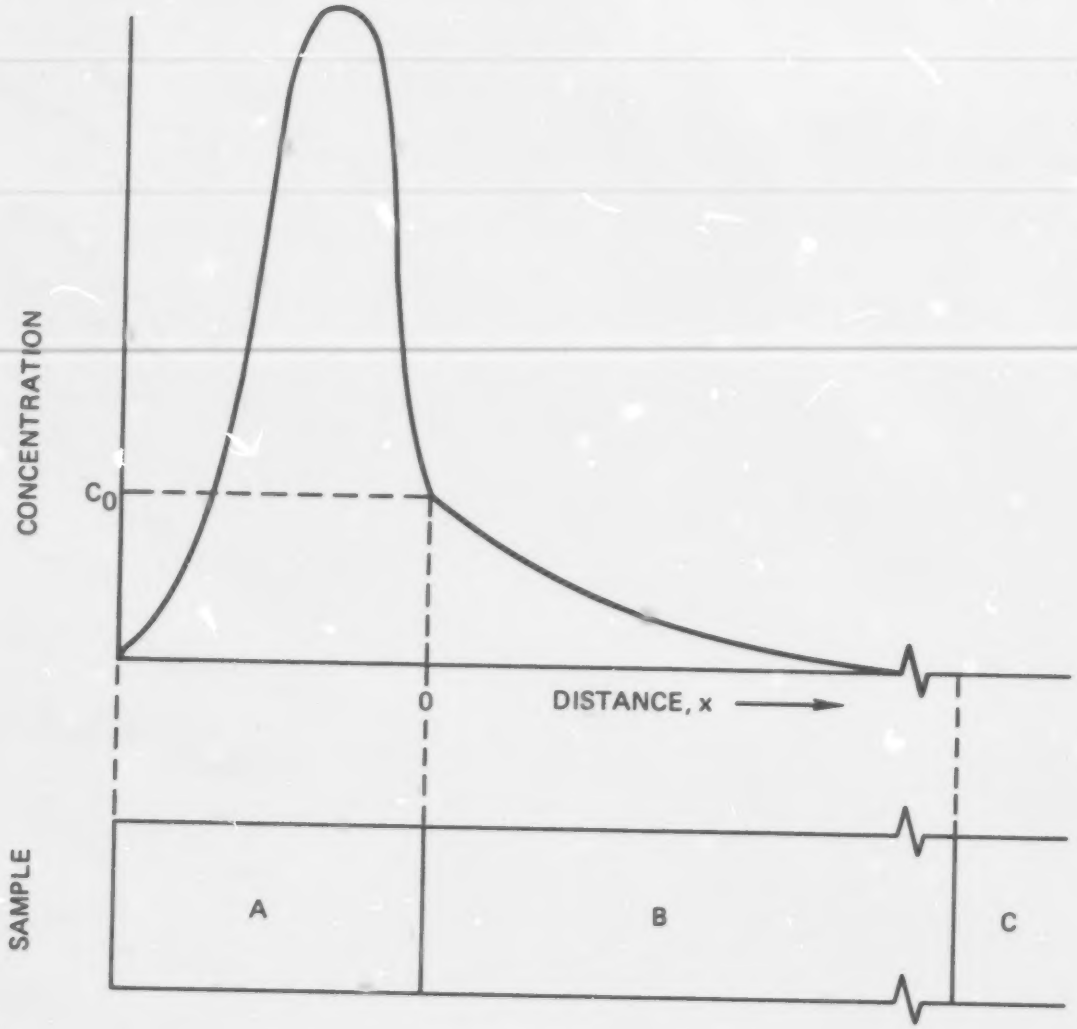

Figure 5. Schematic of diffused tail region showing discontinuity at C_0 and the concentration profile for the regions of interest in the sample.

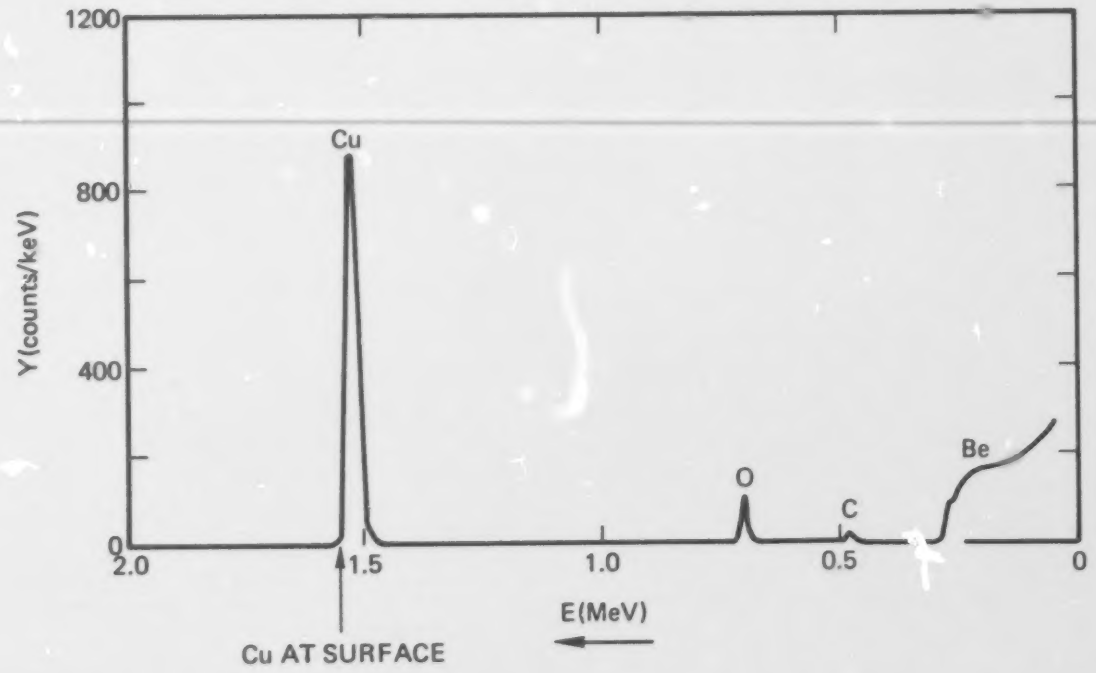

Figure 6. Actual ion backscattering spectrum of yield versus energy of backscattered ions for 2 MeV incident ions. Note that energy increases to the left.

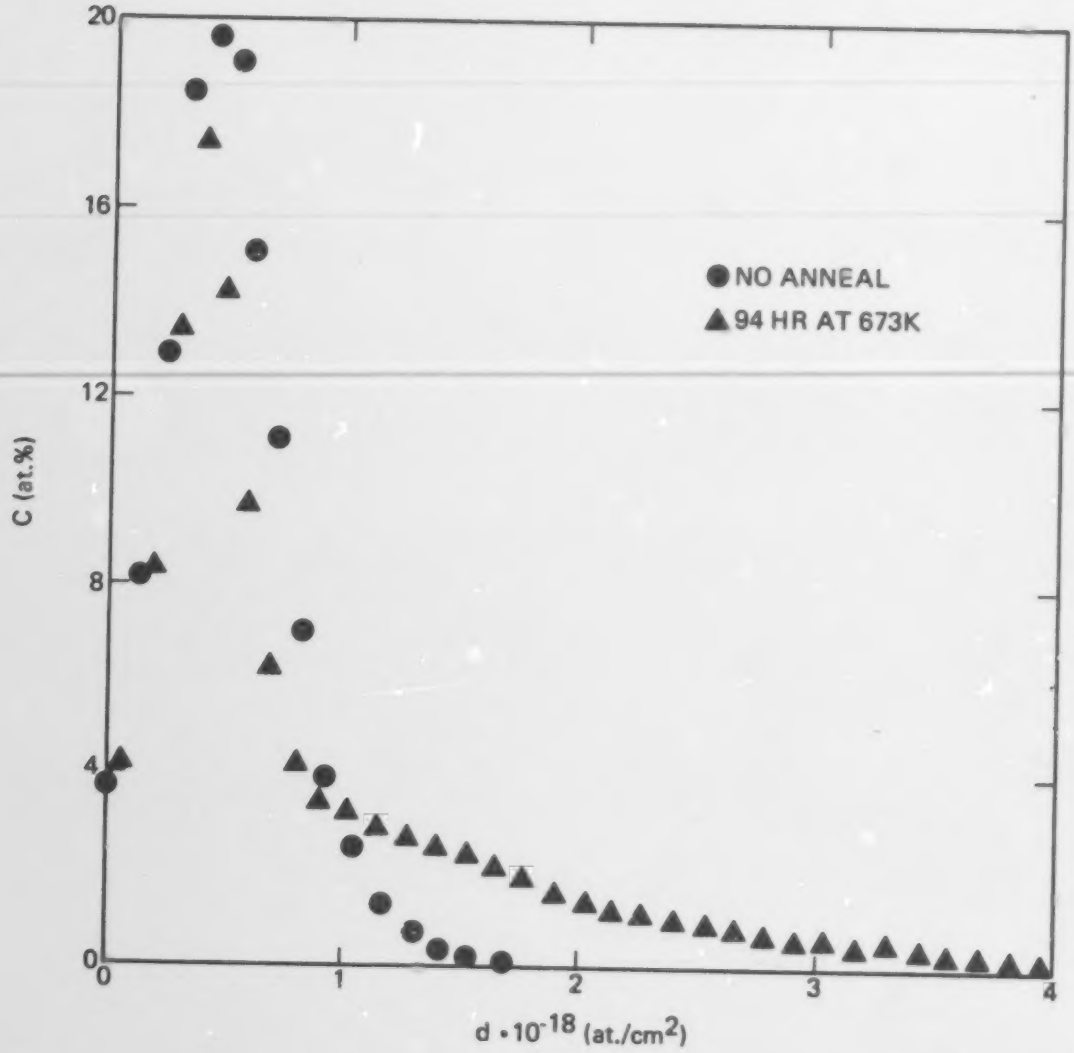

Figure 7. Concentration profile of copper implanted into beryllium before and after anneal, showing discontinuity in actual data.

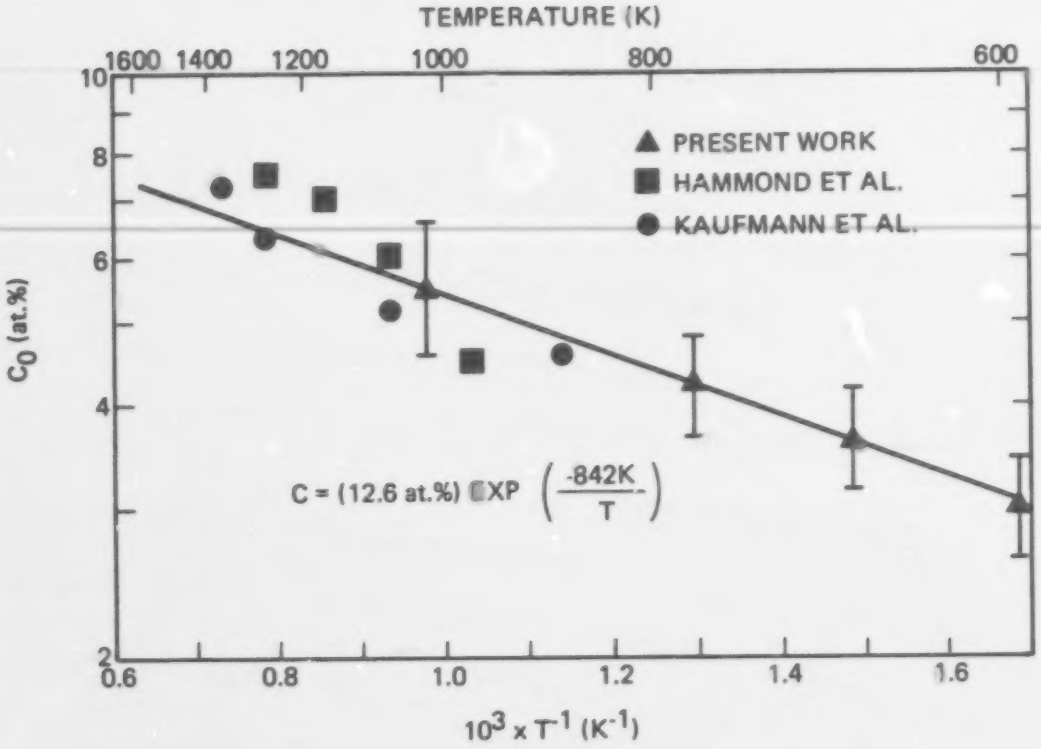

Figure 8. Solubility of copper in beryllium as a function of temperature on a log solubility versus T^{-1} plot. Plot shows data, while analytical expansion represents best fit.

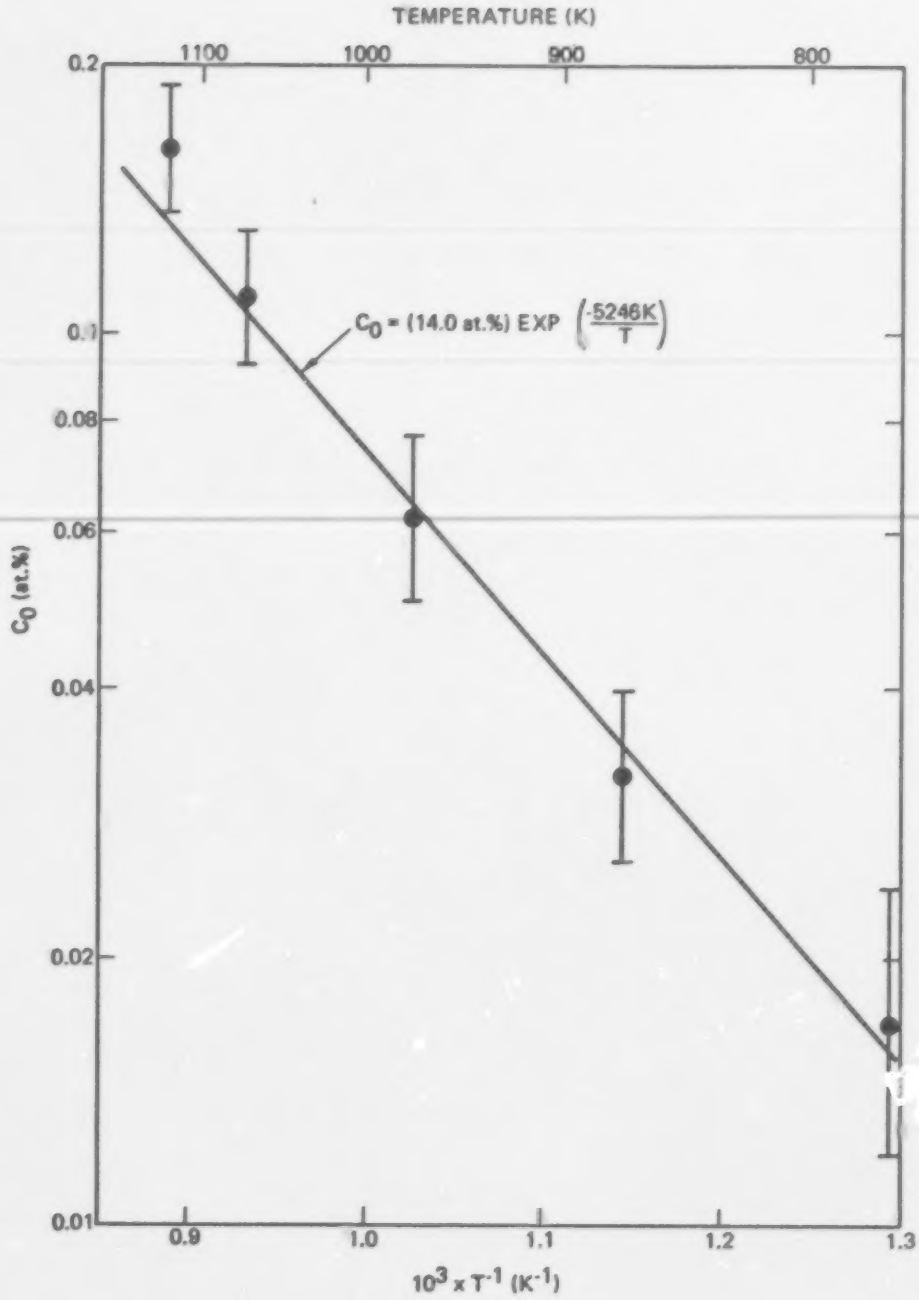

Figure 9. Solubility of iron in beryllium as function of temperature. Plot shows data, while analytical expression was obtained from best fit.

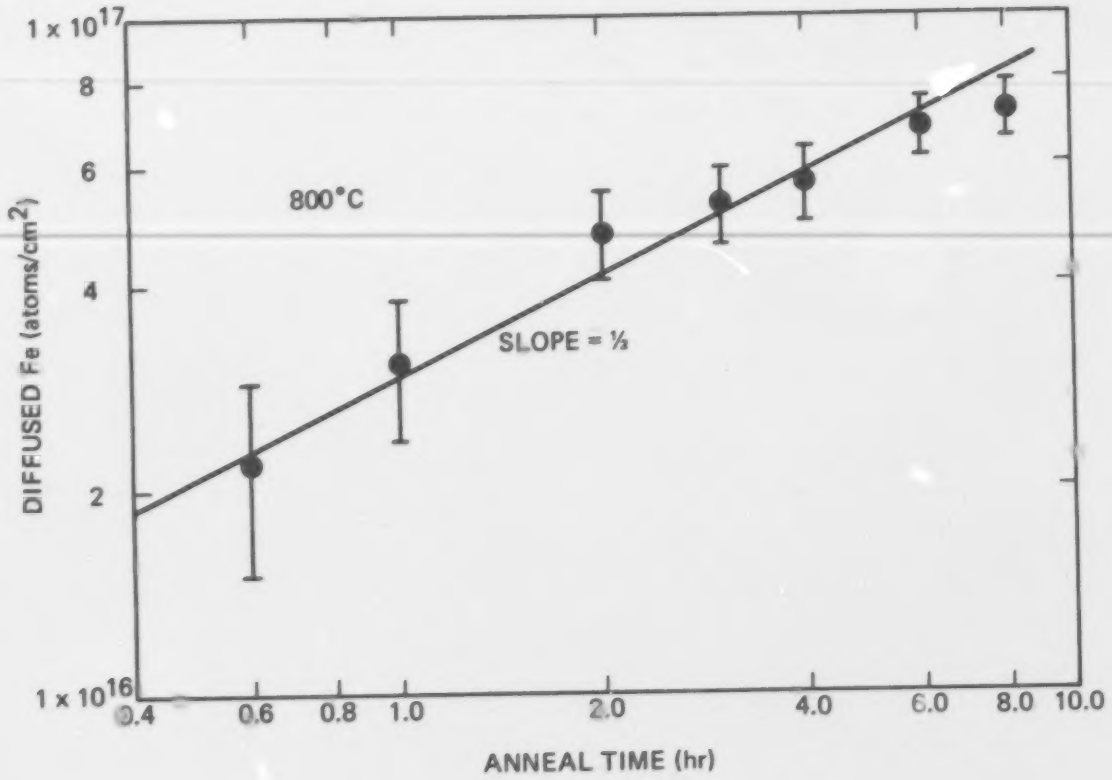

Figure 10. Time dependence of the amount of iron diffused into sample from implanted region during anneal at 800°C. Slope of 1/2, predicted from analysis, supports validity of assumptions.

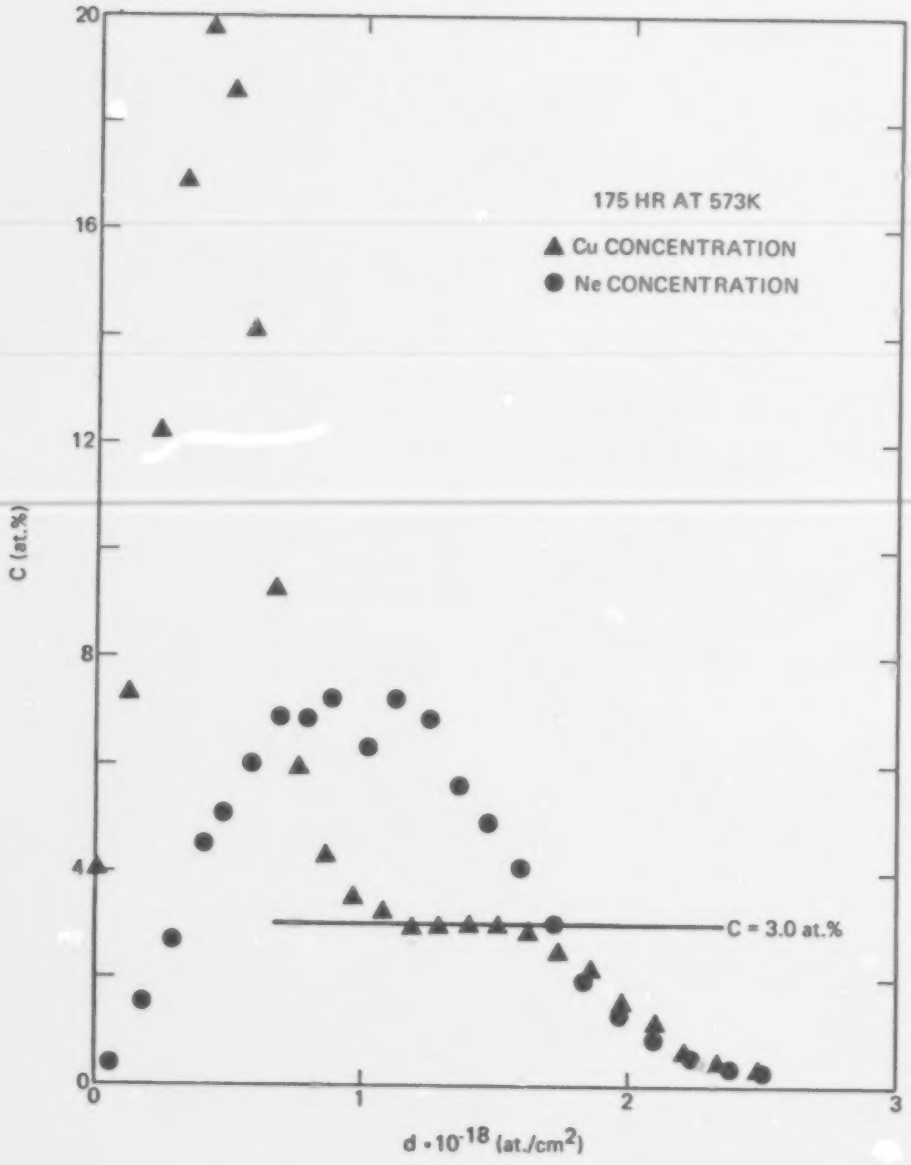

Figure 11. Concentration profile after annealing for enhanced diffusion experiment. Note overlays of plateau region of copper concentration and neon profile as implanted.

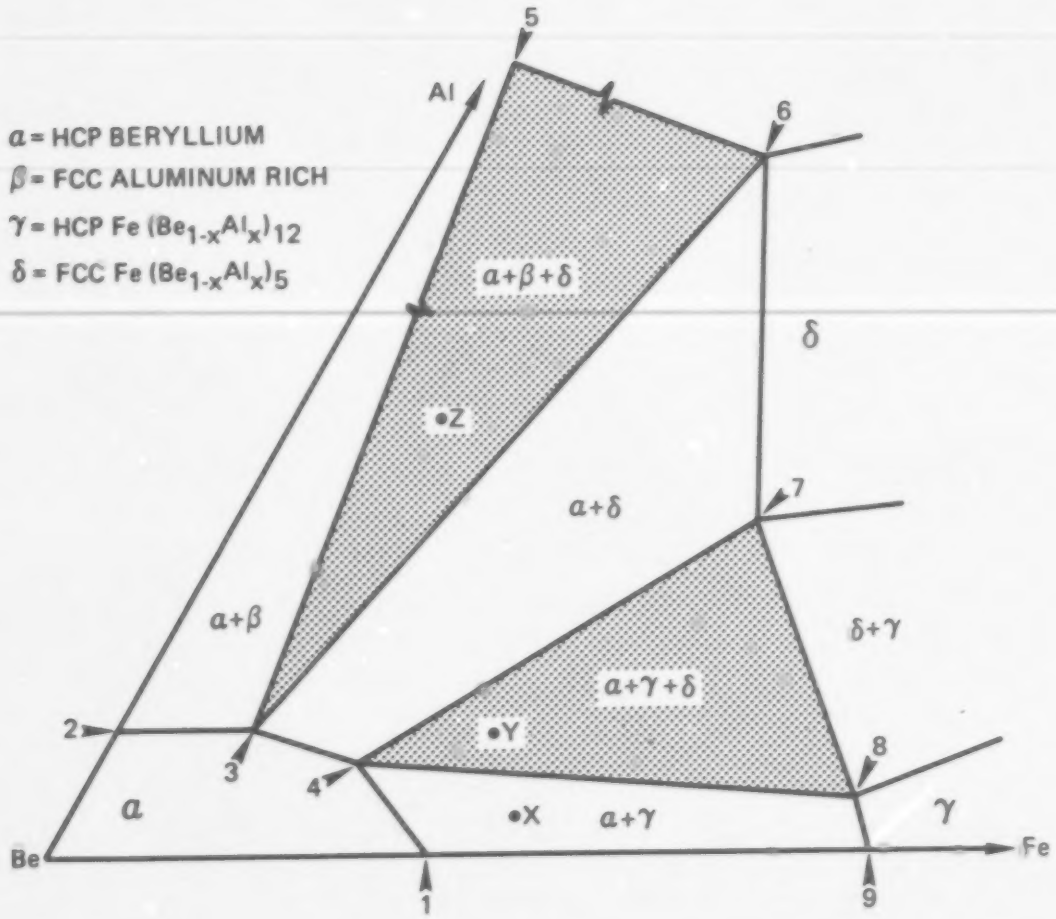

Figure 12. Schematic ternary phase diagram for Be-Fe-Al system showing relationship between two-phase and three-phase regions. Sample concentration during anneals must be in three-phase region, e.g., at points Y and Z, but not at X.

National Bureau of Standards SP-496, Applications of Phase Diagrams in Metallurgy and Ceramics
Proceedings of Workshop held at NBS, Gaithersburg, Md., January 10-12, 1977

PHASE EQUILIBRIUM DIAGRAMS IN TERMS OF ELECTRONIC STRUCTURE

Frederick E. Wang

Materials Division
Naval Surface Weapons Center
White Oak, Silver Spring, Md. 20910

In a continuing effort[1,2] to understand the nature of superconductivity in the A_3B(A15-type) compounds, I have observed[3] not too long ago some interesting correlations between the superconducting characteristics and the phase equilibrium diagrams of these compounds. These correlations were interpreted in terms of a proposed "A-chain integrity"[4] in the superconductivity of the A15 compounds and subsequently related to the electronic structure of the compounds.

The correlations thus observed are aesthetically satisfying on two accounts:

1) The importance of "A-chain integrity" in the superconducting characteristics of these compounds is supported by a number of experiments and observations, e.g., the isotopic substitution of A or B elements,[5] Matthias' rule is followed only when the e/a ratio is reached by B element substitution(A element substitution invariably degrades T_c),[6] and more recently direct evidence of T_c degradation due to "A-chain" disruption through thermal neutron bombardment.[7]

2) Since a phase equilibrium diagram is a manifestation of all the thermodynamic properties, it must contain information concerning electronic arrangements as well as atomic arrangements. The manifestation of electronic arrangements, while subtle in phase diagrams, can therefore be related with a phenomenon that is supersensitive to their electronic property, i.e., superconductivity.

However, experimentally the correlations are not obeyed rigorously(as was indicated in the original paper,[3] e.g., V_3Si, Mo_3Os

systems). It was pointed out that these deviations from the correlations may be attributable to the following possibilities: a) the phase diagrams reported may be in error, b) the T_c's reported may be inaccurate(or the T_c's may be measured correctly but the material under investigation may contain fractional impurities leading to an erroneous T_c). Therefore, the final acceptance or abandonment(or modification) of the correlation requires more(in number) and better(accurate) phase diagrams and T_c data for the A15 compounds.

A significant number of new or revised phase diagrams have appeared in the literature since the original paper[3]: the Cr-Ir,[8] V-Au,[9] V-Ga,[10] V-Rh[11], V-Si[12], V-Pt[13], Nb-Au[14], Nb-Ga[15], Nb-Os[16], and Nb-Pt[14] systems. While the majority of these systems conform to the correlations, there are a few systems that appear to directly contradict the correlation. For example, V_3Rh and Nb_3Os are both peritectically formed and have SSR(solid solubility range) of 12 and 4 at/o respectively, and yet, V_3Rh is not superconducting(even at 0.015°K)[17] while Nb_3Os has a T_c of only 0.94°K[17]. A close inspection of these phase diagrams, however, indicates that the SSR for both systems are lopsided on the B-rich side(no solubility range at all on the A-rich side). This implies that the "A-chain integrity" in these two systems are practically non-existent (or extremely weak) and consequently are not superconducting(or have very poor superconducting characteristics). These two systems, therefore, not only do not contradict the correlation(based on the "A-chain integrity" concept) but in fact lend further support to it. To be sure, some modification in the stated correlation is required. More detailed explanation including all other newly characterized systems and modification of the correlation will be published elsewhere[18]. However, it is reasonable to conclude at this point that the correlation appears sound and should not be abandoned.

In view of these facts, further investigations into new and/or reinvestigations of the phase diagrams that contain A15 compounds are urgently needed. These phase diagram investigations should include(or pay special attention to) a) an accurate determination

of the SSR of each A15 compound and b) an unequivocal characterization of the nature of its formation(congruent vs. incongruent).

Acknowledgement

I wish to thank Dr. R.M.Waterstrat of the National Bureau of Standards for pointing out a number of new systems in the literature to me.

References

1. F.E.Wang, J.Sol.Stat.Chem. 6, 365(1973).
2. F.E.Wang, and J.R.Holden, Sol.Stat.Comm. 17, 225(1975).
3. F.E.Wang, J.Phys.Chem.Sol. 35, 273(1974).
4. M.Weger, Rev.Mod.Phys. 36, 175(1965).
5. G.E.Devlin, and E.Corenzwit, Phys.Rev. 120, 1964(1960); B.T.Matthias, T.H.Geballe, E.Corenzwit, and G.W.Hull, Phys.Rev. 129, 1025(1963).
6. B.T.Matthias, T.H.Geballe, and V.B.Compton, Rev.Mod.Phys. 35, 1(1963); B.T.Matthias, T.H.Geballe, L.D.Longinotti, E.Corenzwit, G.W.Hull, R.H.Willens, and R.H.Maita, Science 156, 645(1967).
7. A.R.Sweedler and D.G.Schweitzer, Phys.Rev.Lett. 33, 168(1974).
8. R.M.Waterstrat, and R.C.Manuszewski, J.Less Comm.Met. 32, 79(1973).
9. R.Flukiger, C.Susz, F.Heiniger, and J.Muller, J.Less Comm.Met. 40, 103(1975).
10. J.H.N.vanVucht, H.A.C.M.Bruning, H.C.Donkersloot, and A.H.Gomes de Mesquita, Phil.Res.Rept. 20, 407(1965).
11. R.M.Waterstrat, and R.C.Manuszewski, J.Less Comm.Met.(in press).
12. H.A.C.M.Bruning, Phil.Res.Rept. 22, 349(1967).
13. R.M.Waterstrat, Trans.AIME 4, 455(1973).
14. J.Muller, R.Flukiger, A.Junod, F.Heiniger, and C.Susz, Proc. 13th International Conference in Low Temperature Physics.
15. D.A.Ashby and R.D.Rawlings, J.Less Comm.Met. 50, 111(1976).
16. R.M.Waterstrat, and R.C.Manuszewski, J.Less Comm.Met. 51, 55 (1977).
17. B.W.Roberts,"Survey of Superconductive Materials and Critical Evaluation of Selected Properties," J.Phys.Chem. Ref.Data, 5, No.3(1976).
18. F.E.Wang. To be published.

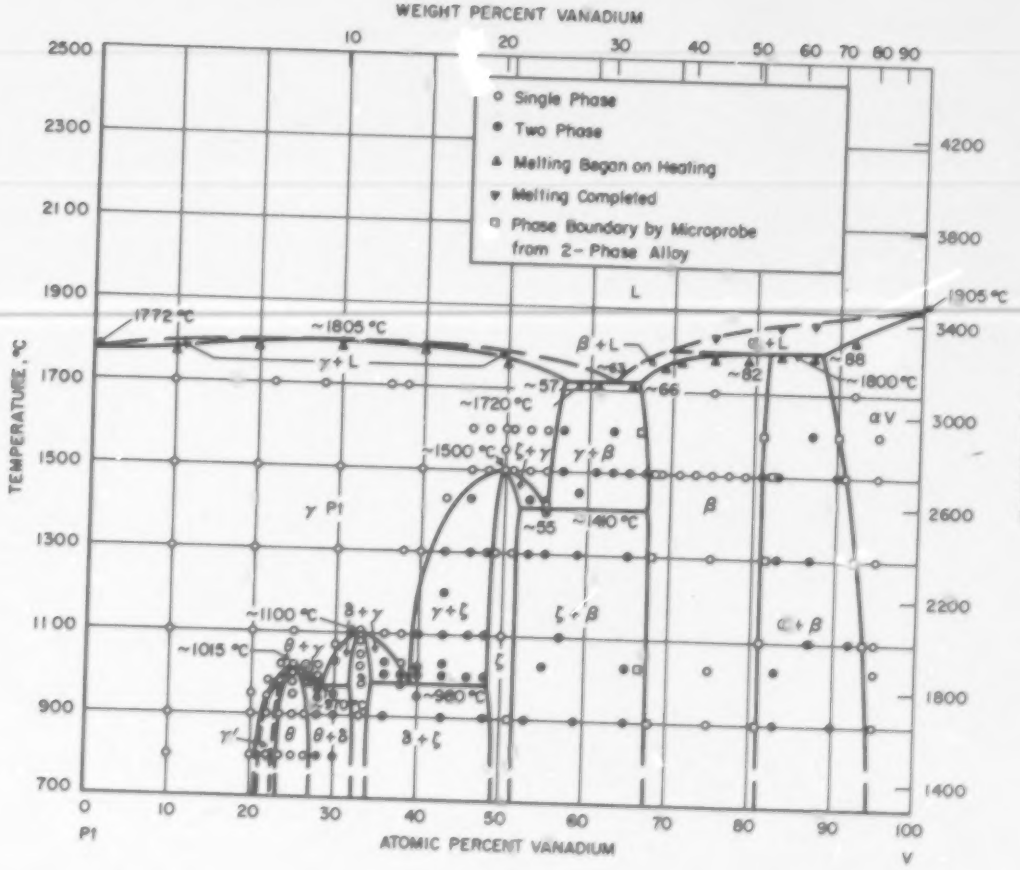

Fig. 1. The Vanadium-Platinum Constitution Diagram.

National Bureau of Standards SP-496, Applications of Phase Diagrams in Metallurgy and Ceramics
Proceedings of Workshop held at NBS, Gaithersburg, Md., January 10-12, 1977

An English translation may be obtained by contacting the author.

APPORT DE L'ÉTUDE DES SÉGRÉGATIONS DANS LES SOLUTIONS SOLIDES À LA DÉTERMINATION DE DIAGRAMMES DE SOLIDIFICATION. APPLICATION À L'ÉTUDE DES SYSTÈMES Sc_2O_3 - Ho_2O_3 ET Sc_2O_3 - Dy_2O_3

J. M. Badie
Lab. Ultra-Refractaires, Odeillo
66120 Font-Romeu, France

I. INTRODUCTION.

La solidification contrôlée (1) offre des possibilités très intéressantes pour la détermination de courbes ou de surfaces liquidus et solidus de systèmes à deux ou plusieurs constituants. Ces possibilités ne sont que très rarement exploitées.

Nous nous sommes plus particulièrement attachés à l'étude des ségrégation, dans les solutions solides. L'apparition de tels phénomènes implique nécessairement une diffusion faible dans le solide au cours de la solidification. La nature des observations que l'on peut faire par analyse à température ambiante de ces phénomènes est donc étroitement liée à celle du diagramme de solidification et de phases à haute température.

Les résultats de cette étude sont comparés à ceux dus notamment à l'utilisation de méthodes expérimentales permettant un examen "in situ" à haute température telles que la diffraction des rayons X à haute température (2) et l'analyse thermique directe à l'aide d'un four solaire (3).

2. PREPARATION DES ECHANTILLONS.

Les mélanges intimes d'oxydes (pureté 3 N), de 500 mg à 1 gramme, sont fondus au four solaire sur un support réfrigéré. Le globule (Ø ≈ 5mm), entièrement liquide, est déplacé, dans le gradient de température vertical du four solaire, en s'éloignant du miroir concentrateur. La solidification progresse depuis la base de l'échantillon au contact du support réfrigéré jusqu'à sa partie supérieure où elle se termine. Ces solidifications progressives dirigées ont été effectuées avec deux vitesses de déplacement de l'interface liquide-solide. Ces deux vitesses sont respectivement de 5.10^{-3} mm/s et 10 mm/s. Dès la fin de solidification, le globule est retiré du foyer ; il se refroidit alors rapidement (5.10^{+2}°C/s) au contact du support et de l'atmosphère ambiante.

3. METHODES EXPERIMENTALES D'ANALYSE.

a) Diffraction des rayons X à température ambiante.

Chaque globule est broyé en totalité. La poudre obtenue, d'une granulométrie de l'ordre de quelques microns, est analysée (Cu K_α et Fe K_α) à l'aide d'un dispositif classique : goniomètre vertical Philips et système d'enregistrement des intensités diffractées par compteur proportionnel. Les enregistrements sont effectués à la vitesse de 1° en 2θ à la minute.

La diffraction par un solide homogène dont la taille des grains est supérieure à quelques milliers d'angstrons conduit à des raies enregistrées dont la largeur à mi-hauteur ne dépend en première approximation que des conditions expérimentales d'analyse (4). Elle est en moyenne de l'ordre de 0,25° en 2θ pour nos conditions d'analyse.

L'existence de ségrégations dans les solutions solides peut être mise en évidence par l'élargissement, dissymétrique, des raies caractéristiques de la structure de la solution. Chaque raie est l'enveloppe d'une série de pics élémentaires diffractés par les divers domaines, homogènes en composition, constituant le mélange solide. Les pentes de cette enveloppe définissent deux pics élémentaires dont les positions peuvent être déterminées en tenant compte de leur largeur moyenne à mi-hauteur, ainsi que le montre la figure 1. Ce traitement des raies permet de calculer une valeur approchée des paramètres des solutions extrêmes présentes dans le mélange.

Les courbes représentatives du paramètre de maille, des solutions cubiques à base de Sc_2O_3, en fonction de la concentration ne présente pas d'écarts notables à la loi de Végard. Cette relation nous a permis d'atteindre la composition des solutions solides par mesure du paramètre de maille. Nous avons ainsi pu suivre dans de très bonnes conditions l'évolution de la composition des solutions extrêmes en fonction de la composition globale du solide et des conditions variables de la solidification. La sensibilité de la méthode est, en effet, très grande du fait de l'important écart paramétrique qui existe entre Sc_2O_3, a = 9,848 Å et Ho_2O_3, a = 10,606 Å ou Dy_2O_3, a = 10,665 Å. La détermination des paramètres qui est faite à 5.10^{-3} Å près permet de déceler des variations de composition de l'ordre de 1 mol %.

b) Analyse chimique ponctuelle.

Les globules sont sectionnés par leur milieu, parallèlement à la direction de progression du front de solidification. Les analyses des deux éléments métalliques sont effectuées, à l'aide d'une microsonde de Castaing, sur cette section suivant des axes parallèles à la direction de déplacement du globule au cours du refroidissement. La vitesse de déplacement de l'échantillon pendant les analyses est de 17,4 microns par minute. Les compositions sont déterminées avec une précision de l'ordre de 0,5 à 1 mol %. Les références utilisées sont les oxydes de base fondus.

Un résultat d'analyse présenté sur la figure 2 permet de juger de la résolution spatiale de l'appareillage utilisé.

4. RESULTATS DES ANALYSES ET INTERPRETATION.

a) Système Sc_2O_3 - Ho_2O_3.

Les figures 2 et 3 mettent bien en évidence la présence de ségrégations et les variations du profils des raies de diffraction enregistrées en fonction des conditions de préparation des échantillons.

Seules les interférences caractéristiques de la forme cubique de Sc_2O_3 sont observables dans tous les diffractogrammes, ce qui indique que ce système présente une miscibilité complète dans le solide, tout au moins à haute température.

L'évolution des paramètres extrêmes a_1 et a_2 (fig. 4), en fonction de la composition globale du solide, montre que l'amplitude des ségrégations et maximum vers 75 mol % Sc_2O_3 nulle à 45 mol % Sc_2O_3. Des élargissements trop faibles des raies, pour les échantillons plus riches en Ho_2O_3, ne permettent pas un calcul des deux paramètres extrêmes. En fonction, des conditions de solidification, on peut observer une variation notable du paramètre a_2 qui est celui de la solution la moins riche en Sc_2O_3 dans le mélange ($a_2 > a_1$) alors que a_1 reste sensiblement constant.

On peut déduire de ces observations :

- que le diagramme de solidification (à deux fuseaux) présente un point invariant à 45 mol % Sc_2O_3 - 55 mol % Ho_2O_3,
- que ce point invariant est un minimum de solidification ; dans l'hypothèse d'un maximum, nous aurions du observer une variation du paramètre a_1 jusqu'à une valeur égale à celle de Sc_2O_3 à la limite,

- que la diffusion dans le solide est effectivement négligeable dans nos conditions expérimentales ; la détermination de la composition N_1 de la solution extrême de paramètre a_1 permet une première approche satisfaisante de la largeur du fuseau de solidification dans cette partie du diagramme, ainsi que le montrent les résultats rassemblés au tableau 1.

Les résultats que nous avons obtenus, par diffraction des rayons X à haute température, analyse thermique et calcul des courbes d'équilibre C - L (modèle des solutions régulières) et, qui sont rassemblés à la figure 5 permettent de juger de l'intérêt de ce type d'étude. Le diagramme de phases complet, compatible avec le polymorphisme de Ho_2O_3, qui est proposé est représenté figure 6.

b) Système Sc_2O_3 - Dy_2O_3.

Seules les solutions cubiques à base de Sc_2O_3 nous ont permis, compte tenu de nos conditions de préparation des échantillons, d'observer des phénomènes de ségrégation nets.

La diffraction par des échantillons contenant moins de 15 mol % Dy_2O_3 ne donne que les interférences caractéristiques de la forme cubique C. A ces dernières s'ajoutent celles du composés $DyScO_3$, de structure pérovskite P, à déformation orthorhombique, pour des teneurs plus fortes en Dy_2O_3 (fig. 7).

La présence de deux variétés cristallines dans la plupart des mélanges et l'évolution des paramètres a_1 et a_2 (fig. 8) des solutions extrêmes montrent :

- que la miscibilité est limitée par la formation d'un mélange eutectique. La composition de l'eutectique est de 40 mol % Dy_2O_3 - 60 mol % Sc_2O_3. C'est la composition de l'échantillon pour lequel l'amplitude des ségrégations s'annule ($a_1 = a_2$). Une analyse par microsonde conduit à une teneur de 41 ± 1 mol % Dy_2O_3 dans l'eutectique,
- que la dissolution limite de Dy_2O_3 dans Sc_2O_3 à la température eutectique est voisine de 22 mol % Dy_2O_3 ($a_0 = a_2$). a_0 est le paramètre de la solution homogène obtenu par trempe à partir d'un équilibre réalisé à haute température. La courbe représentative de a_0 en fonction de la composition obéit à la loi de Végard,
- que nous sommes en présence d'un "faux eutectique" (5) entre 15 et 22 mol % Dy_2O_3. Ces mélanges ont en effet, une composition globale extérieure à la lacune de miscibilité ($a_2 < a_0 < a_1$) (fig. 8 et 9) ; leur température de fin de solidification a été abaissée, du fait des ségréga-

tions, jusqu'à la température eutectique. Une certaine quantité d'eutectique, mis en évidence par les interférences de la phase P, a pu ainsi être formée en fin de solidification contrairement à ce que pouvait laisser prévoir un tel diagramme.

La mesure du paramètre a_1 permet là aussi, de remonter à une valeur approchée de la composition du premier solide déposé à l'équilibre à partir d'un mélange liquide de composition globale connue (fig. 9).

Les figures 9 et 10 montrent respectivement les résultats expérimentaux obtenus au cours de l'étude complète du diagramme et la proposition qui en est faite, compatible avec le polymorphisme de Dy_2O_3.

5. CONCLUSION.

Nous avons obtenu, par interprétation de l'évolution des ségrégations dans les solutions solides en fonction de la composition et des conditions de la solidification des informations en bon accord avec les résultats expérimentaux des analyses "in situ" à haute température. L'étude à température ambiante des échantillons préparés par solidification contrôlée solidification "normale" dans notre cas ou fusion de zone, présente donc un grand intérêt pour la détermination de diagrammes de solidification. Nous pensons en particulier aux systèmes pour lesquels des études directes "in situ" à haute température sont rendues très difficiles sinon impossible en raison de problèmes liés, à la réactivité de leurs constituants avec les supports ou contenants ou plus simplement aux quantités de produits réclamées par ces analyses.

BIBLIOGRAPHIE

1. W.G. PFANN. Zone Melting (1966) (Wiley)
2. J.M. BADIE, M. FAURE, J.P. TRAVERSE, 3è colloque International sur les méthodes analytiques par rayonnement X, Nice 16 Septembre 1974
3. M. FOEX, Rev.Int.Htes Temp. et Réfract. 3.309 (1966)
4. A. GUINIER, Théorie et Technique de la radiocristallographie (1964) (Dunod)
5. P. GORDON, Principles of Phases Diagrams in Materials Systems (1968) (Mc Graw Hill).

N_o	N_1 cal	N_1 obs		N_2 obs	
	$x_{«A»}$	$x_{«A»}^{RX}$	$x_{«A»}^{M}$	$x_{«A»}^{RX}$	$x_{«A»}^{M}$
$0,9\ Sc_2O_3 - 0,1\ Ho_2O_3$	0,98	0,95	0,96	0,65	0,50
$0,8\ Sc_2O_3 - 0,2\ Ho_2O_3$	0,96	0,90	0,93	0,52	0,44
$0,7\ Sc_2O_3 - 0,3\ Ho_2O_3$	0,91	0,83	0,87	0,52	0,44
$0,6\ Sc_2O_3 - 0,4\ Ho_2O_3$	0,83	0,70	—	0,52	—

Tableau I: Concentration $x_{<<A>>}$ en Sc_2O_3 dans les solides de composition extrême N_1 et N_2 determinée experimentalement par RX et microsonde (M) sur des produits fondus de composition globale No. Les valeurs les plus riches en Sc_2O_3 sont comparées a celles, calculées, du premier solide déposé a partir du liquide No.

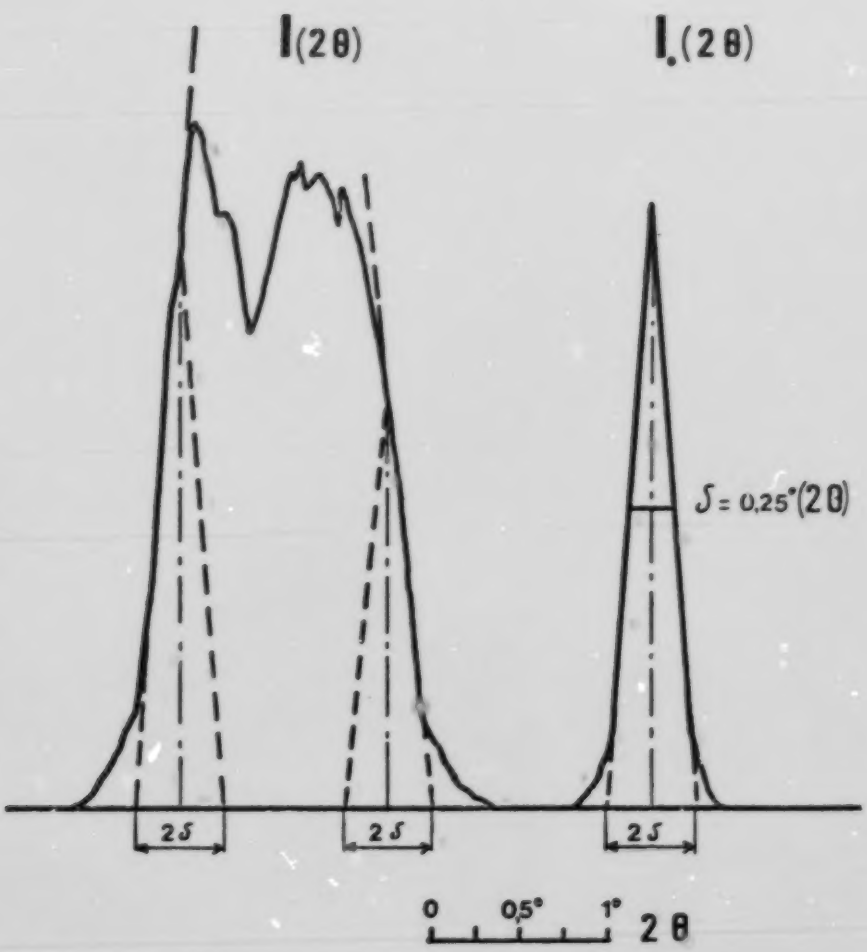

Fig. 1 - Schema de la determination des composantes extrèmes d'une "raie" de diffraction enregistrèe. La raie I (2θ) est l'enveloppe d'une serie de raies elementaires de profil I_o (2θ).

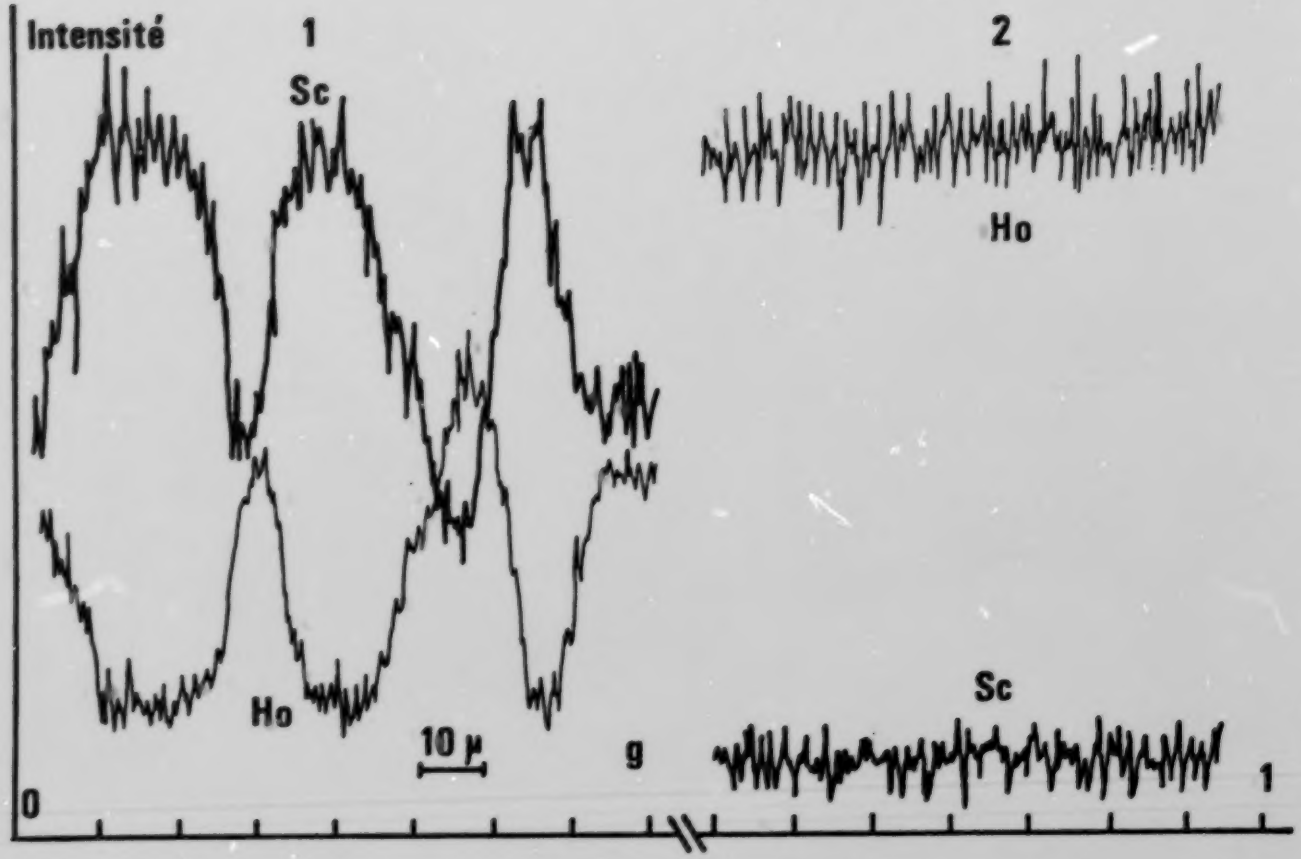

Fig. 2 - Profils des concentrations en Ho et Sc enregistrés par analyse à la microsonde pour un échantillon contenant 80 mole % Sc_2O_3 et préparé par solidification progressive unidirectionnelle.

1. Dans les premières fractions "g" de solide déposé, $0 < g < 0{,}05$ ($\sim$ 100 µ)
2. Dans les dernières fractions "g" de solide déposé, $0{,}95 < g < 1$ ($\sim$ 100 µ)

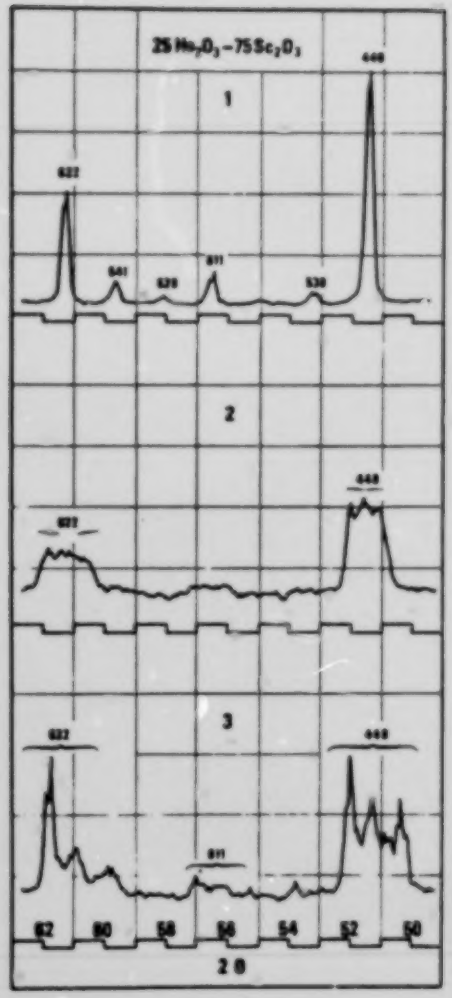

Fig. 3 - Evolution de la largeur des raies de diffraction enregistrées pour un échantillon de composition 25 mole % Ho_2O_3 - 75 mole % Sc_2O_3 en fonction des conditions de traitement thermique.

1. Trempe de la solution solide à l'équilibre aux environs de 2100°C
2 et 3. Trempe après solidification unidirectionnelle progressive, vitesse de déplacement de l'interface solide liquide 10 mm/s et 0,005 mm/s respectivement.

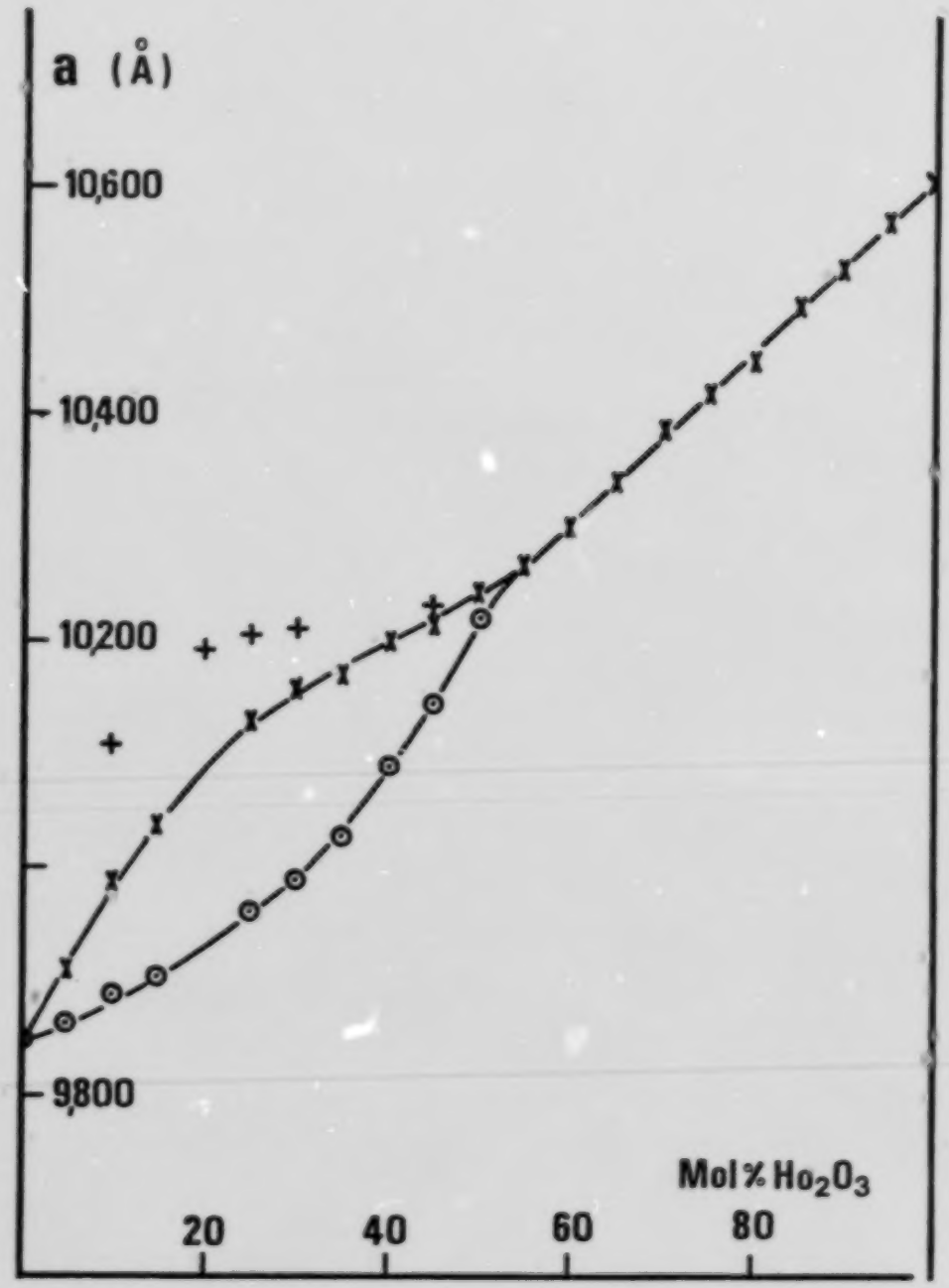

Fig. 4 - Evolution des paramètres a_1 et a_2 des solutions solides cubiques extrêmes dans les produits fondus en fonction de la composition globale des mélanges pour le système Sc_2O_3-Ho_2O_3. Vitesses de déplacement de l'interface solide liquide :
v = 10 mm/s (X, ⊙) et v = 0,005 mm/s (+, ⊙).

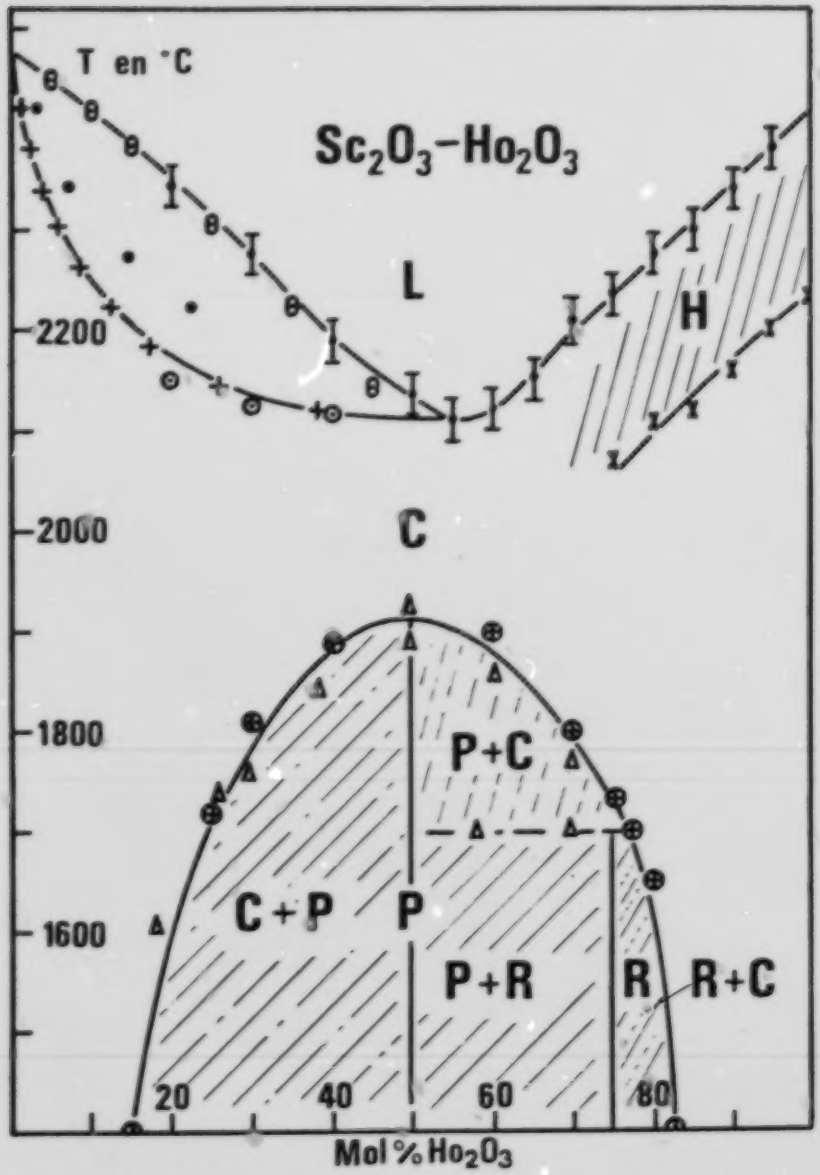

Fig. 5 - Domaines d'existence des différentes phases observées. Résultats expérimentaux et calculés :

I, ⊕, analyse thermique - Δ diffraction X à haute température

X, analyse thermique et diffraction X à haute température

●, diffraction X sur produits trempés

θ,+, liquidus et solidus calculés

●, solidus déduit de l'étude des ségrégations.

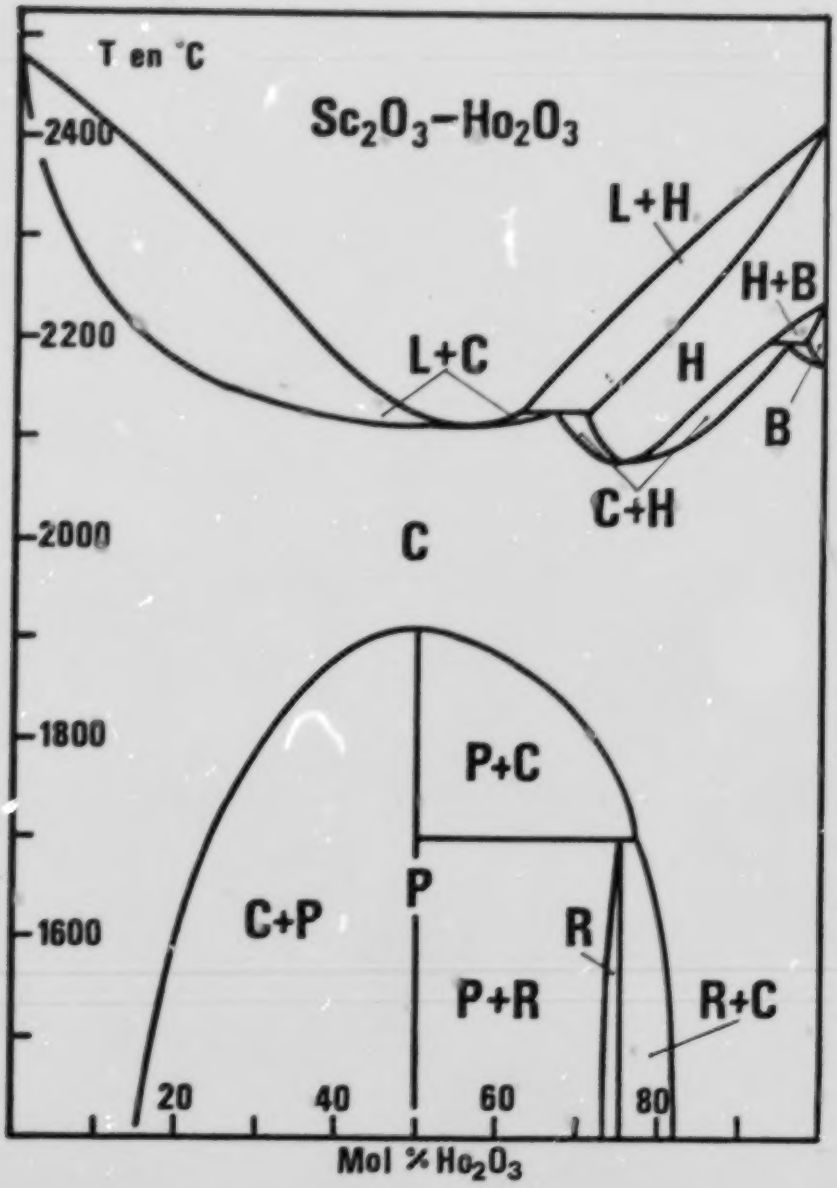

Fig. 6 - Diagramme de phases proposé compatible avec le polymorphisme de Ho_2O_3.

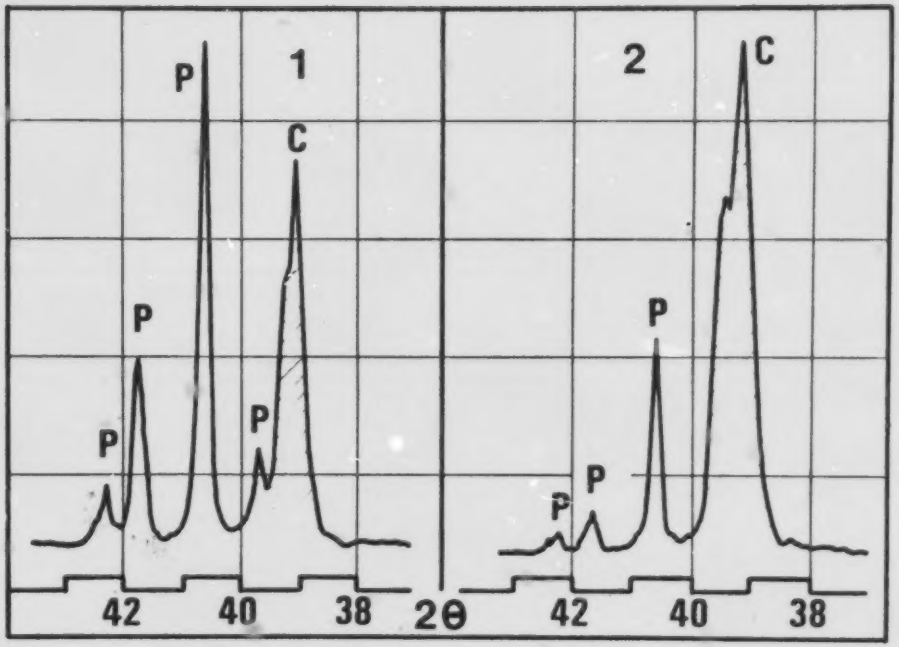

Fig. 7 - Manifestation des phénomènes de ségrégations dans le cas d'un système à miscibilité partielle dans le solide. Produits fondus analysés à T ambiante.

1. Diagramme de poudre d'un échantillon de produit fondu contenant 30 mole % Dy_2O_3.
2. Diagramme de poudre d'un échantillon de produit fondu contenant 20 mole % Dy_2O_3.

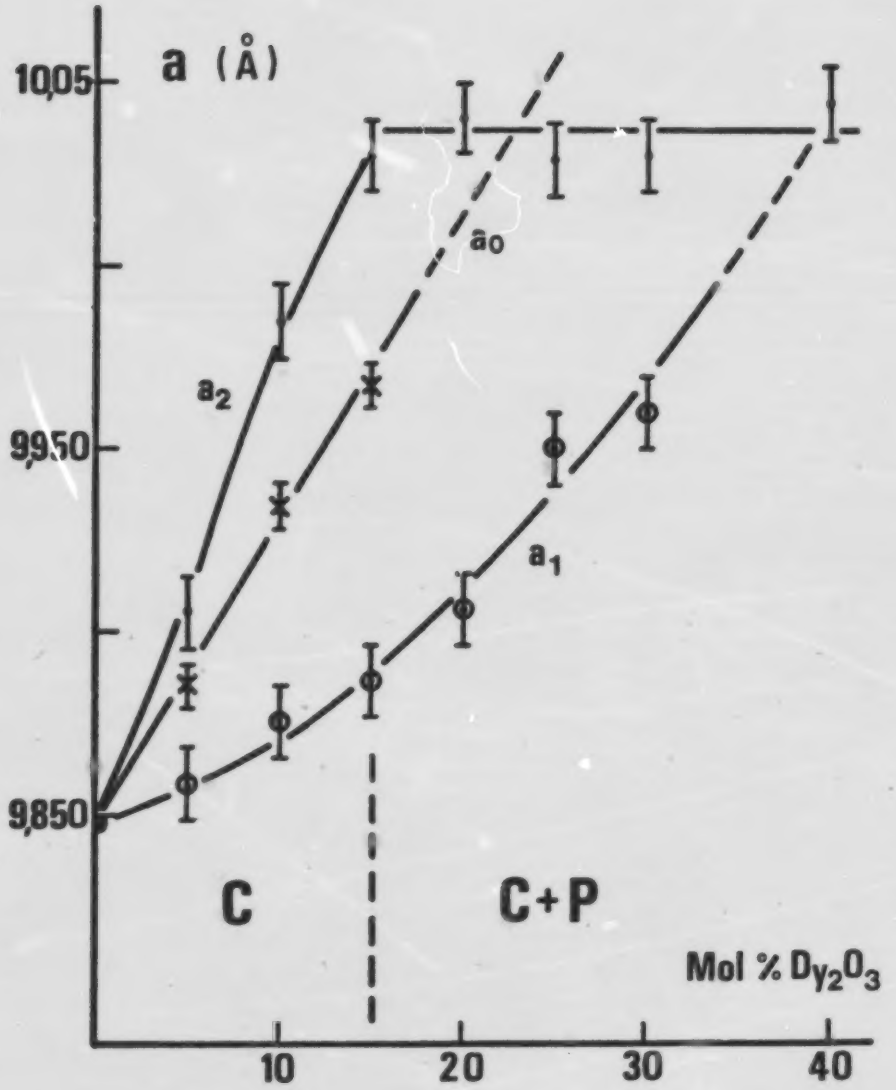

Fig. 8 - Evolution des paramètres a_1 et a_2 des solutions solides cubiques extrêmes présentes dans les produits fondus trempés en fonction de leur composition globale. Ces valeurs sont comparées à celles du paramètre a_0 de la solution homogène obtenue par trempe du solide à l'équilibre à haute température.

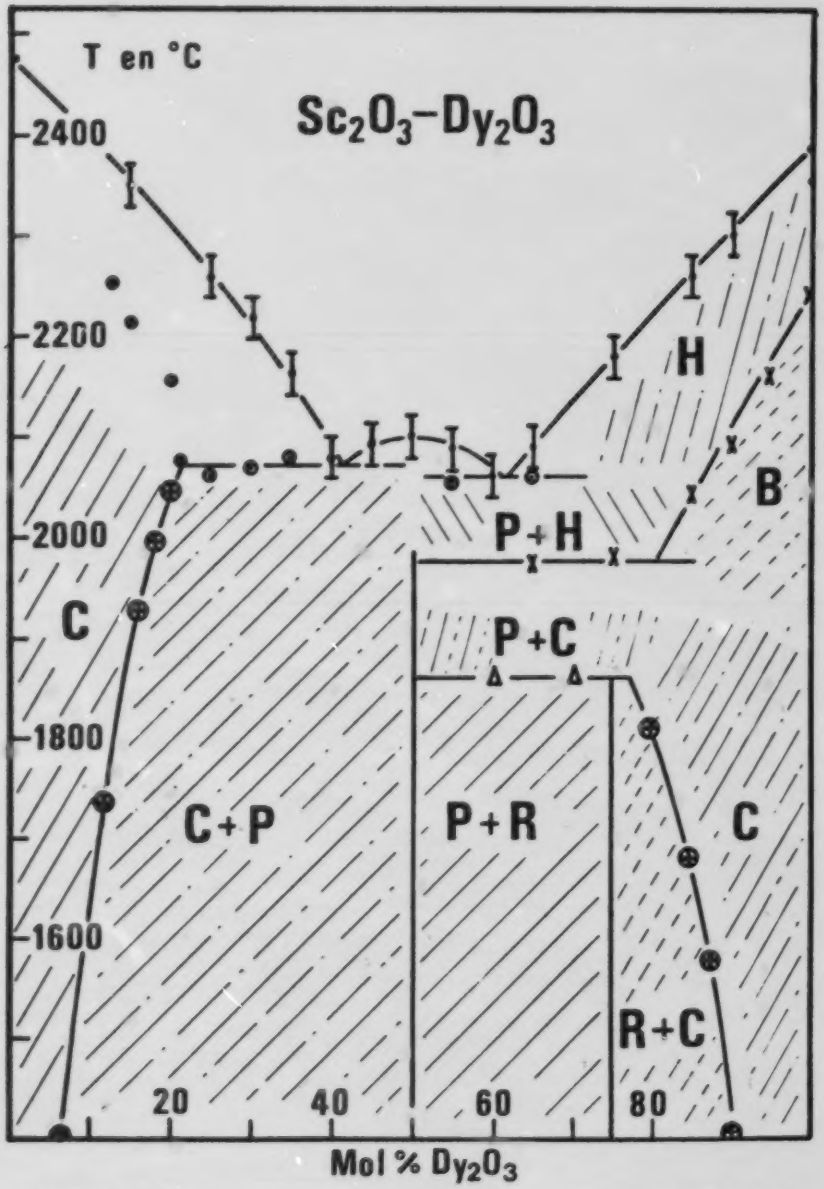

Fig. 9 Domaines d'existence des différentes phases observées (hachures).
Résultats expérimentaux :
I, ●, analyse thermique - Δ diffraction X à haute température,
X, analyse thermique et diffraction X à haute température
●, diffraction X sur produits trempés
●, solidus déduit de l'étude des ségrégations.

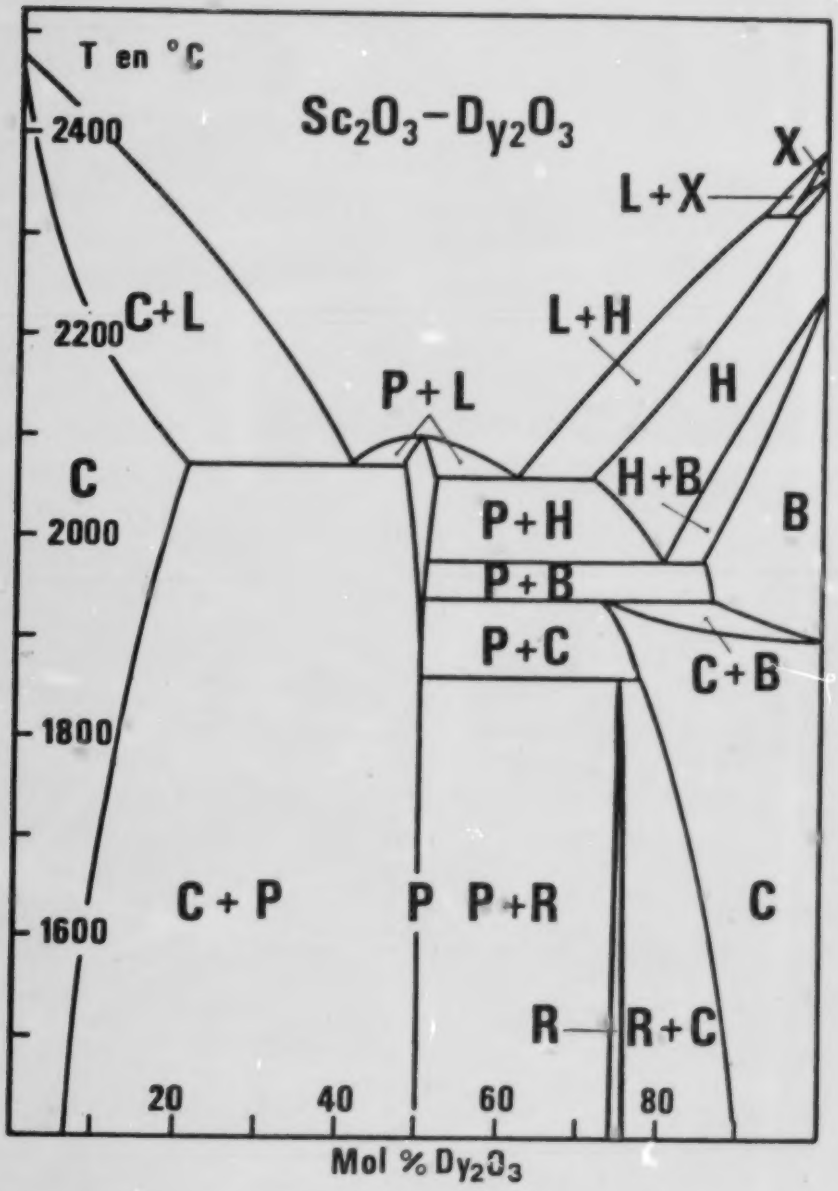

Fig. 10 - Diagramme de phases proposé compatible avec le polymorphisme de Dy_2O_3.

National Bureau of Standards SP-496, Applications of Phase Diagrams in Metallurgy and Ceramics
Proceedings of Workshop held at NBS, Gaithersburg, Md., January 10-12, 1977

STUDIES OF THE Fe-C-B PHASE DIAGRAM BY AUTORADIOGRAPHY

Thomas B. Cameron and John E. Morral
Department of Metallurgy and
Institute of Materials Science, U-136
University of Connecticut
Storrs, CT 06268

The iron rich corner of the Fe-C-B phase diagram is being investigated in the first step of a study probing the mechanism behind boron hardenability in steel. The major problems encountered in this type of study are first, obtaining accurate measurements of soluble boron concentrations, on the order of 30 ppm or less; and second, maintaining high purity samples since boron will react with other elements, notably nitrogen, in the ppm range. For these reasons a novel approach is being used in the phase diagram study. Boron concentrations are being measured by neutron autoradiography along the carbon gradient of a carburized Fe-B alloy. The autoradiography technique allows measuring boron concentrations of 5 ± 1 ppm and the use of somewhat massive samples prevents contamination during processing. Isothermal sections of the austenite - borocarbide solvus are obtainable by this technique.

National Bureau of Standards SP-496, Applications of Phase Diagrams in Metallurgy and Ceramics
Proceedings of Workshop held at NBS, Gaithersburg, Md., January 10-12, 1977

USER NEEDS FOR PHASE DIAGRAMS

by

Dr. Paul J. Fopiano
Army Materials & Mechanics Research Center
Watertown, Massachusetts 02172

In multicomponent systems where two ore more phases have important effects on the properties of the alloy, it is rare that the phase compositions are known. Sometimes these compositions can be ignored with impurity but other times this is not the case. In the latter category, the determination of a single tie line only may be required or, because of the prevalence of several alloys using the same alloying elements, a more thorough investigation of phase compositions is justified. In few of these cases, however, is the construction of a phase diagram carried out and widely disseminated. As a result, much otherwise useful data is lost before it can become a useful part of a databank. Examples of one of each type of application are included to indicate the normal limits to which we go to satisfy a specific need. It might be added that without the advent of the probe microanalyzer, little of this work would have been carried out.

TYPICAL EXAMPLES OF PHASE COMPOSITION

Determinations in Commercial Alloys

Titanium-Aluminum-Vanadium Alloys

In the investigation of the phase transformations which occur during the heat treatment of commercial titanium alloys, the presence of two or more phases complicates the interpretation of the mechanical and physical property data. The major strengthening mechanisms can often be related to the compositions of the alpha and beta phases in equilibrium at the solution temperature. Many titanium alloys of commercial interest employ aluminum and vanadium as major alloying elements.

Several standards were made up with various amounts of aluminum and vanadium. The nominal compositions are given in Table 1. Chemical analyses of these alloys were also determined. A probe analysis of these standards yield for our experimental conditions the calibration curve in Figure 1. The least square slope of these lines is given analytically as:

$$\text{w/o V} = \frac{I_V - 629}{486}$$

$$\text{w/o Al} = \frac{I_{Al} + 27}{1048}$$

where w/oV, w/oAl = weight percent vanadium and aluminum.

Table 1. NOMINAL COMPOSITIONS OF STANDARD ALLOYS IN WEIGHT PERCENT

Specimen	Al	V
76	2	2
77	2	4
78	2	8
81	4	2
82	4	4
83	4	8
84	8	2
85	8	4
86	8	8
43	12	0
44	0	12

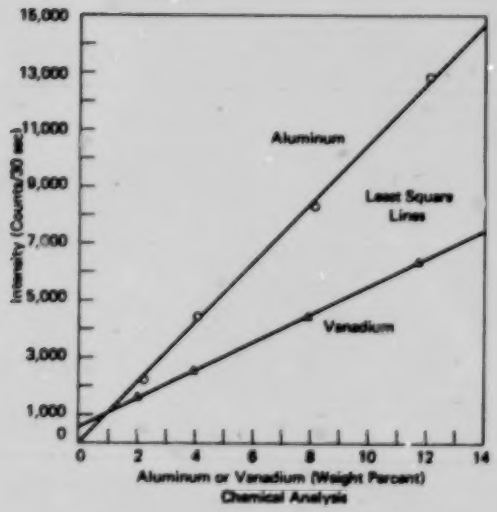

FIGURE 1. Mean Number of Counts (per 30 sec.) Versus Chemical Analysis of Aluminum and Vanadium Standards

I_V = counts (vanadium)/30 seconds

I_{Al} = counts (aluminum)/30 seconds

Utilization of this data for the most popular commercial alloy of titanium, Ti-6Al-4V is illustrated in the following discussion. Five solution-treated conditions (all in the alpha beta field) were investigated (Figure 2); i.e.,

Table 2. NUMBER OF COUNTS (per 30 sec) AND CORRESPONDING COEFFICIENT OF VARIATION FOR THE ALPHA AND BETA PHASES FOR SEVERAL SOLUTION TREATMENT CONDITIONS

Sample Designation (and Solution Temp)	Phase (α or β)	Counts/30 Seconds (Coeff. of Variation)	
		Al	V
P-1 (1750 F)	α	7301 (2.5)	1307 (2.9)
	β	6052 (2.6)	2519 (4.3)
P-2 (1700 F)	α	7849 (1.5)	1475 (2.0)
	β	6150 (1.1)	3040 (2.3)
P-3 (1650 F)	α	7078 (4.2)	1593 (2.2)
	β	5779 (1.6)	3686 (3.7)
P-4 (1600 F)	α	7664 (1.4)	1709 (2.5)
	β	5570 (2.2)	4062 (2.3)
P-5 (1550 F)	α	7398 (1.3)	1747 (4.7)
	β	4723 (2.8)	4551 (3.7)

1750, 1700, 1650, 1600, 1550 F with designations P-1 through P-5 respectively. In order to get large enough fields to examine with the probe microanalyzer, it was necessary to heat all specimens to 1850 F for one hour furnace cool to the solution temperature (Figure 3 - 1550 F) and hold for the times indicated in Figure 2.

Probe analysis data of both the alpha and beta phases are presented in Table 2. The measured compositions of the alpha and beta phases are shown in Table 3 (P-1 through P-5). Estimated compositions from published literature is also shown in Table 3 for specimens solution treated at 1562, 1652, and 1742 F. An approximate retrofit of our data to published work on the Ti-6Al-4V alloy is shown in Figure 4. The published work was done before the probe was generally available and was typical of a type of publication then popular. In no sense, however, could it be considered a complete phase diagram even for the titanium-rich corner.

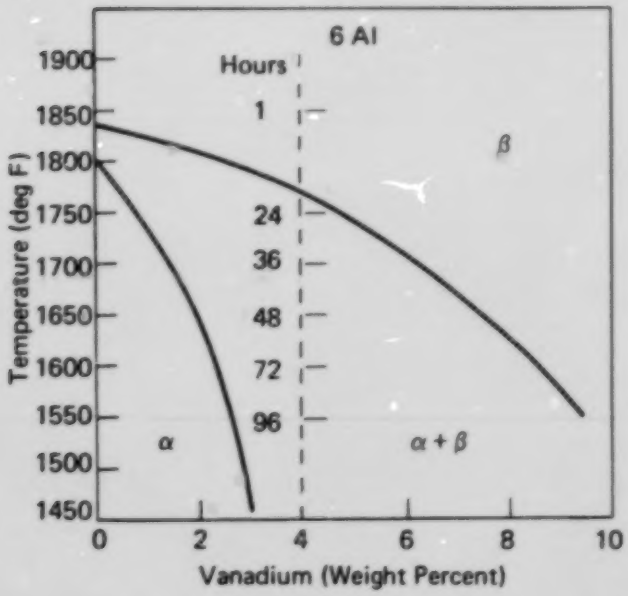

FIGURE 2. Schematic Representation of the 6Al Section of Titanium Corner of Ti-Al-V Ternary

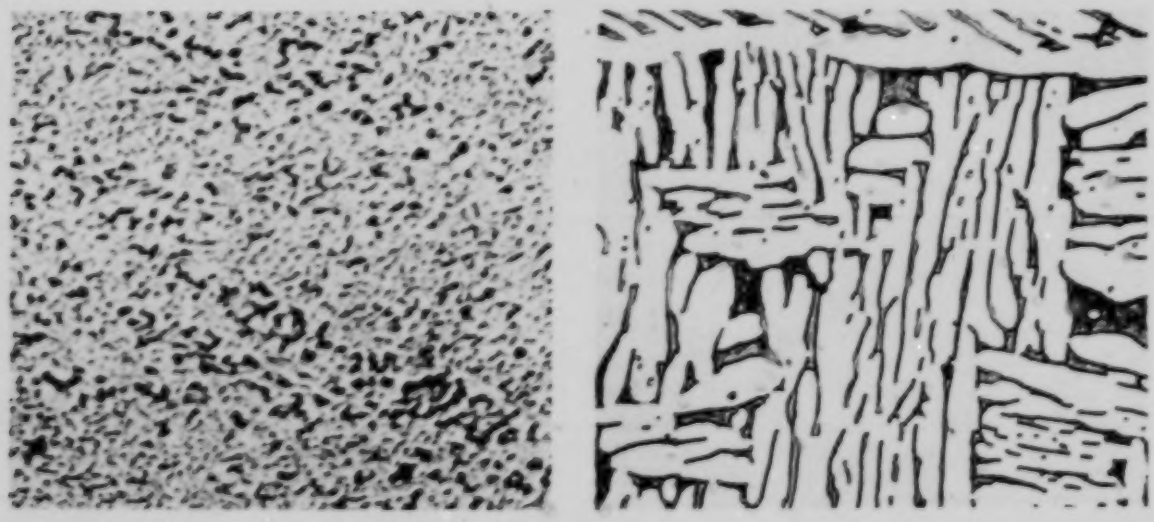

FIGURE 3. Solution-treated Ti-6Al-4V Alloy. Mag. 500X

Table 3. EFFECT OF SOLUTION TEMPERATURE ON THE COMPOSITIONS OF THE ALPHA AND BETA PHASES IN Ti-6Al-4V

Solution Treatment Temperature (deg F)	Weight Percent				Vol % β
	Alpha		Beta		
	Al	V	Al	V	
1550 (P-5)	7.08	2.30	4.53	8.07	
1562	8	2-1/2	2	8	25
1600 (P-4)	7.34	2.22	5.34	7.06	
1650 (P-3)	6.78	1.98	5.54	6.26	
1652	9	2-1/2	2	6-1/2	38
1700 (P-2)	7.52	1.74	5.89	4.96	
1750 (P-1)	6.99	1.40	5.80	3.89	
1742	10	2	4	5	64

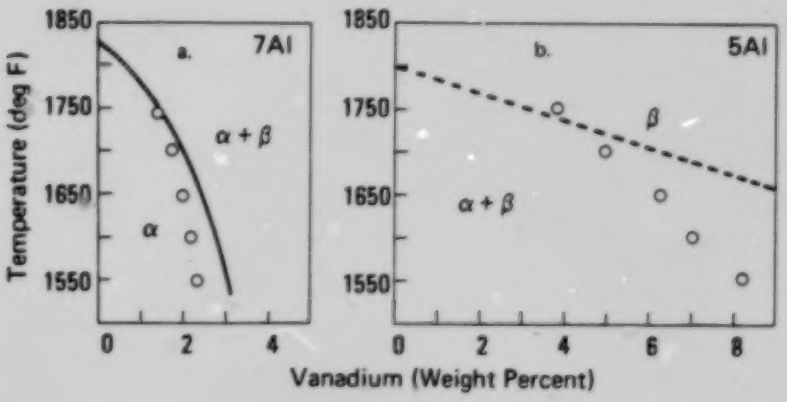

FIGURE 4. Correlation of Probe Data with Published Isothermal Sections (Ref. 5)

43XX Steel

Even though the 43XX steels have been utilized for many years, no phase diagram was available in the literature when the investigation on "Partially Austenitized 43XX Steel" was initiated. A "pseudo" iron-carbon phase diagram was then determined by microstructural analysis. A copy of this "pseudo"

iron-carbon phase diagram for 4300 steels is shown in Figure 5. This is an example where even a very rudimentary phase diagram data was helpful and necessary to develop an optimum compositional and temperature requirements for a new application of a very old alloy.

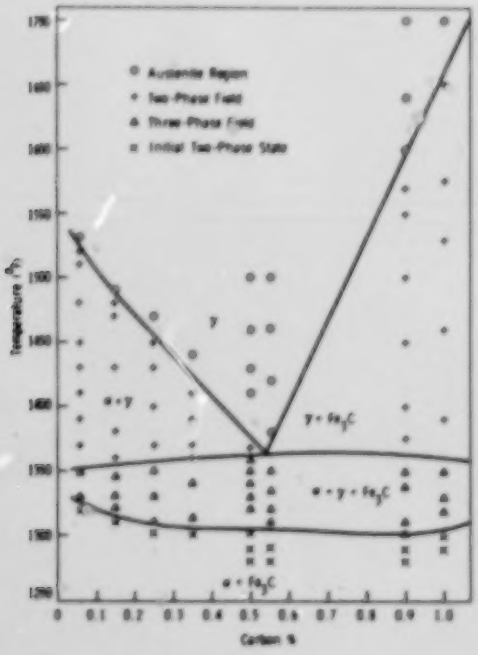

FIGURE 5. Constitution Diagram for 43XX Steels

Partitioning of Impurity Elements in Iron-Carbon Alloys

The addition of even small amounts of certain impurity elements to iron-carbon alloys can result in a severe loss in ductility when tempered at 500 C. The partitioning of these elements between the ferrite and the carbide phases was felt critical to better understanding of the problem. Electron probe microanalysis, carbide extraction, and x-ray diffraction techniques were employed to this end. Figure 6 shows some of the data and Figure 7 shows the iron-rich end of the binary phase diagram for one of the impurity elements, antimony. Again, the phase diagram was gemain to the better understanding of the problem.

Heat Treatment of a Modified Tool Steel

In the heat treatment of a modified tool steel where the carbon level is lowered considerably, a much higher hardening temperature than normal was required to eliminate the low temperature ferrite phase which was considered

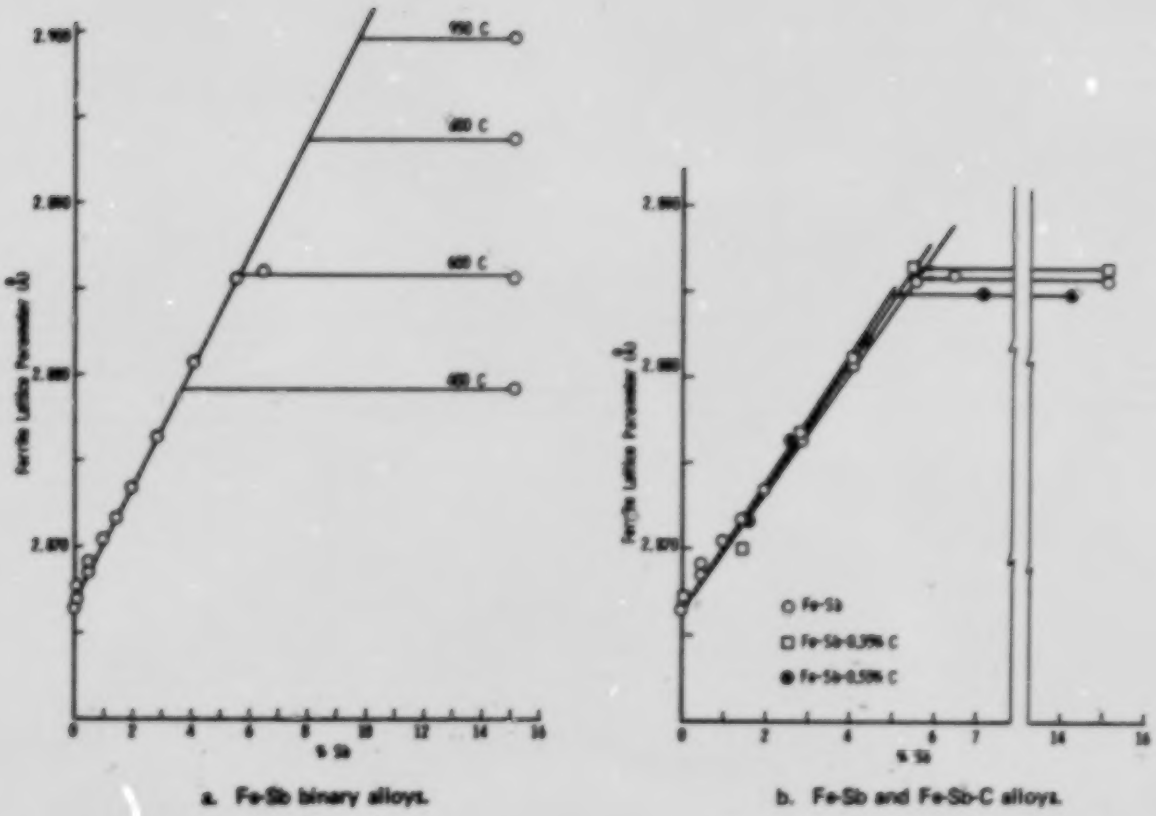

FIGURE 6. Ferrite Lattice Parameter as a Function of Antimony Concentration Alloys were Annealed at 600 C Unless Otherwise Indicated

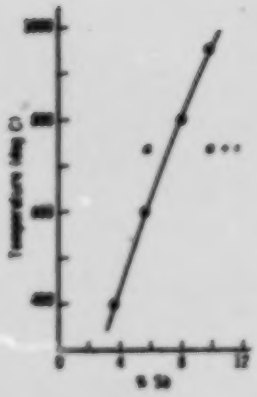

FIGURE 7. The Iron-Rich End of the Iron-Antimony Binary Phase Diagram Based Upon Present Results, Showing the α-Solvus

undesirable for the application. It turned out, however, that the ferrite could be reduced only to an irreduceable limit before the hardening temperature became so high as to create a distortion problem. A qualitative probe analysis indicated no significant alloy transfer to the ferrite for normal hardening times and the relatively low amount of delta ferrite could be ignored. This is a very simple example but, in general, phase amounts and compositions would be invaluable in the investigation of the general class of tool steels.

The above examples are typical of the needs of the metallurgist in his investigations of alloys for the important information contained in phase diagrams. Any help that the metallurgist can get in this area whether it be a data bank of available (readily retrievable) information or approximate computational diagrams (generally for multicomponent systems) would be welcome.

600

National Bureau of Standards SP-496, Applications of Phase Diagrams in Metallurgy and Ceramics
Proceedings of Workshop held at NBS, Gaithersburg, Md., January 10-12, 1977

Phase Diagram of a Specimen at High Temperatures under external tensile or Shear Stress or both.

By

K.M. Khanna
Head, Materials Science Deptt.,
National Institute of Foundry
and Forge Technology,
Hatia, Ranchi-834003, India.

Abstract:

Phase Diagrams are graphs that give relationships between various phases in a system as a function of temperature, pressure and composition. To my mind, phase changes at high temperatures under tensile or shear stress or both have not been studied so far. Similarly the corresponding phase diagrams have also not been studied. It will be interesting to plot the phase diagram of a specimen under external tensile or shear stress or both, keeping pressure constant and varying the temperature. Having done so we can have a better insight into the control of micro-structure. We can have an idea of the life time of a specimen that works at high temperatures under external tensile and shear stress. Experimental studies can be made by providing a tensometer type attachment to the dilatometer.

Basic Theory and Discussion:

Let a specimen be under external stress and the temperature gradient. As a consequence of the thermal agitation, the charge density of the electrons at any point and at any instant of time is reduced by an amount which depends only on the temperature under constant external stress. Let the decrease in the charge density be represented by a (T). Thus the charge density at any point x can be written as,

$$\rho(x) = \frac{2e}{L} \sum_{n=1}^{N} \sin^2 \frac{n\pi x}{L} - a(T) \qquad (1)$$

where L is the side of the box in which the electrons are enclosed and e is the charge on the elctron. Eq.(1) can be written as,

$$\rho(x) = e\left[\frac{N}{L} - \frac{\sin 2\pi N x/L}{2\pi x}\right] - a(T)$$

$$= \rho_0 - \rho_0 \frac{\sin 2\pi N x/L}{2\pi N x/L} - a(T) \qquad (2)$$

where

$$\rho_0 = \frac{eN}{L} \qquad (3)$$

or

$$\frac{\rho(x)-\rho_0}{\rho_0} = \rho = -\frac{\sin 2\pi N x/L}{2\pi N x/L} - \frac{a(T)}{\rho_0} \qquad (4)$$

The quantity L will be a function of the external stress F and the temperature T, such that,

$$L = L(F,T) = L_0 + \alpha_F F + \alpha_T T \qquad (5)$$

We can write,

$$d\rho = \frac{\partial \rho}{\partial F} dF + \frac{\partial \rho}{\partial T} dT \qquad (6)$$

where,

$$\frac{\partial \rho}{\partial F} = \frac{\alpha_F}{L} \cos \frac{2\pi N x}{L} - \frac{\alpha_F}{2\pi N x} \sin \frac{2\pi N x}{L}$$

$$\frac{\partial \rho}{\partial T} = \frac{\alpha_T}{L} \cos \frac{2\pi N x}{L} - \frac{\alpha_T}{2\pi N x} \sin \frac{2\pi N x}{L}$$

Eq. (6), therefore, shows that in plotting phase diagrams of specimens under external stress and temperature, the density variations of electrons in the specimen must be taken into account. This concept will add new element of information to the existing knowledge on phase diagrams.

National Bureau of Standards SP-496, Applications of Phase Diagrams in Metallurgy and Ceramics
Proceedings of Workshop held at NBS, Gaithersburg, Md., January 10-12, 1977

PHASE DIAGRAM OF A METAL - GAS SYSTEM

By

V.K. SINHA*, B.Sc. Engg.(Met.), Ph.D.

ABSTRACT

A simple technique for determining various phase relations in metal - gas systems is discussed. The difficulties associated with interpretation of conventional phase diagrams of metal - gas systems are highlighted and a modified format in this context is suggested. The method of computing various thermodynamic quantities from the modified phase diagram is demonstrated. Some of the results obtained for the Zr - H_2 and Zr - Nb - H_2 systems are also included for illustration.

---

* The author is with Department of Materials Science, National Institute of Foundry and Forge Technology, Hatia, Ranchi-834003, Bihar State, India.

Introduction:

The phase diagram is an indispensable means for representing physico - chemical state of a system in terms of the state variables, pressure (P), composition (C), and temperature (T). For metallic or other systems the phase diagram is conventionally represented [1-3] in the form of T - C diagrams at fixed pressure of 1 atm. which suits most of the practical purposes unless otherwise pressure variations are too large. A similar representation for the phase diagram of a metal - gas system is, however , inadequate because of the pronounced effect of gas partial pressure in fixing the physico - chemical state. In the past, [1-3] the phase diagrams of metal - gas systems have also been compiled as T - C diagrams which lack information and are difficult to interpret. The author, therefore, recommends that in the latter cases the T - C diagrams must be supplemented either with the isothermal P - C diagrams or the constant composition P - T isochores or both. The P - C - T data contained therein will then provide not only a better understanding of the existence of equilibrium phases in terms of the state variables but also an easy means for computing the various thermodynamic functions.

The purpose of the present paper is to demonstrate a better format of representing the phase diagram of a metal - gas system, with particular reference to the binary Zr - H_2 system. The method of determining various thermodynamic quantities from the modified phase diagram is also discussed.

Discussion:

When a metal (M) at a given temperature is placed in contact with a gas (G), the latter is taken up until its concentration in the metal reaches a particular value. This concentration depends only on the pressure of the gas at that temperature. The phase relations in a metal - gas system can therefore be most conveniently determined with the help of standard thermodynamic relations using the measured pressure of the gas in equilibrium with the metal as a function of temperature and composition. In a binary metal - gas system schematically shown in Fig. 1(a) the dissolution reaction of gas in the α- phase, for example, may be represented as,[4,5]

$$\tfrac{1}{2}\, G_2 = G \text{ (dissolved in } \alpha \text{)}$$

At equilibrium, $\tfrac{1}{2} F_{G_2} = \bar{F}_G(\alpha)$, where F_{G_2} is molar free energy of the gas and $\bar{F}_G(\alpha)$ is the partial gram - atomic free energy of gas in the α- phase. Assuming the gas to behave ideally, $F_{G_2} = F^{o}_{G_2} + R\,T \ln P_{G_2}$ and hence its partial gram - atomic free energy of mixing in the α - phase is,

$$(\bar{F}_G - \tfrac{1}{2} F^{o}_{G_2}) = \tfrac{1}{2} RT \ln P_{G_2} \qquad (1)$$

The partial gram - atomic enthalpy of mixing of gas, $(\bar{H}_G - \tfrac{1}{2} H^{o}_{G_2})$ in the α- phase of composition $M_x G_y$ is obtained from the van't Hoff equation,

$$\left[\partial \ln P_{G_2} / \partial (1/T)\right]_{M_x G_y} = \frac{2(\bar{H}_G - \tfrac{1}{2} H^{o}_{G_2})}{R} \qquad (2)$$

In equations (1) and (2) P_{G_2} is the gas partial pressure, $P^{\circ}_{G_2}$ is the free energy in the standard state, y/x is the atomic ratio of gas to metal, T is the temperature in degrees Kelvin and R is the gas constant. The mean partial molar entropy of mixing of gas, $(\bar{S}_G - \frac{1}{2} S^{\circ}_{G_2})$ may be computed from the free energy and enthalpy values. The partial molar quantities of mixing of the metal component and the integral thermodynamic quantities may be obtained from the numerical integration of the Gibb's - Duhem equation. If variables other than P, C, and T are excluded the hetrogeneous equilibria can be described by the Gibb's Phase Rule, $\Psi + \Phi = n+2$, where n is the number of components, Φ is the number of phases, and Ψ is the degrees of freedom or independently adjustable variables. Since the metal - gas alloys cannot exist except in equilibrium with the gas phase the equation reduces to $\Psi + \Phi = n+1$. In binary systems, the phase Rule predicts two degrees of freedom in single phase regions and therefore pressure depends both on temperature and composition. In the two - phase regions, there is only one degree of freedom and total composition can vary without affecting the pressure - temperature curve. The thermodynamic properties and Phase Rule lead to determination of various phase fields with the help of the following two methods;

Method I : P - C isotherms ;

Pressure - composition measurements may be carried out experimentally at different temperatures. The points of intersection of steeply sloping isotherms with the plateaus determine the composition

limits of one - phase and two - phase fields. This is illustrated in Fig. 1 (b) at typical temperatures T_1, T_2, T_3 and T_4. The composition limits derived from Fig. 1 (b) are marked in the T - C diagram [Fig. 1 (a)].

Method II: P - T isochores;

In the van't Hoff plot of $\ln P_{G_2}$ against 1/T at constant gas concentrations, the one - phase and two - phase regions would be represented by areas and lines respectively. The shape of the line in the two - phase region is determined by the distribution of gas between the two co-existing phases, which is a function of gas solubility and relative amounts of the two phases. If these factors vary with temperature, the line would in general be non-linear[6]. Also, the partial gram - atomic enthalpy of mixing of gas obtained from the slope of the plot would be different for different phases. The P - T isochores for a large number of alloys of varying gas content is schematically shown in Fig. 1 (c) and the various phase fields are also labeled therein. The two - phase regions are ascertained by a non-linear $(\alpha+\beta)$ curve and two straight lines denoting the $(\beta+\delta)$ and $(\alpha+\delta)$ fields. It is observed that the P - T curves representing the $(\alpha+\beta)$, $(\beta+\delta)$ and $(\alpha+\delta)$ fields intersect at a triple point, T_e, which defines the $\beta \rightleftharpoons \alpha+\delta$ eutectoid horizontal of the T - C diagram [Fig. 1 (a)]. For an alloy M_xG_y, the line AB in Fig. 1 (c)

represents the $(\alpha+\delta)$ two - phase region. The intersection of the lines CB and AB at B represents the temperature T_1 at which the equilibrium $\alpha - (\alpha+\delta)$ exists. Similarly the intersection point C represents the temperature T_2 for the $\alpha - (\alpha+\beta)$ equilibrium and that of point D represents the temperature T_3 for the $(\alpha+\beta) - \beta$ equilibrium in the T - C diagram [Fig. 1 (a)]. Some of the experimental results of the present author[7-10] on the Zr - H_2 and Zr - Nb - H_2 systems are shown in Figs. 2 - 5.

The above mentioned techniques along with other conventional methods like dilatometric, X-ray diffraction, electrical resistivity, metallographic, tensimetric, thermal gradient, heat capacity measurement etc. have been used by numerous investigators to determine phase relations in various metal - gas systems. For the Zr - H_2 system, the widely accepted T - C diagram [11] with modifications[12, 13] is shown in Fig. 6. The diagram gives instantaneous information about state of the system as a function of temperature and composition, however, without any idea of the hydrogen partial pressure which maintains the equilibrium. Consequently, for full details, the original published work of different investigators are to be referred which is cumbersome and as such the objectives of having separate compilation of phase diagrams are considerably diluted. The author, therefore, recommends that the phase diagram of the Zr - H_2 system or other metal - gas systems must be compiled in a uniform format as schematically shown in Figs. 1 (a), 1 (b) and 1 (c), where the T - C diagram has been

supplemented with the P - C isotherms and the P - T isochores. This provides not only a better understanding of the various phase relations but also an easy means to readily compute the various thermodynamic quantities from the P - C - T data through equations (1), (2) and the Gibb's - Duhem equation. Some of the author's computed results published elsewhere [5] are shown in Fig. 7. The modified phase diagram therefore eliminates the necessity of even a separate compilation of the thermodynamic data.

Conclusions:

1. The phase diagram of a metal - gas system should be represented in the form of T - C diagram supplemented either by the P - C isotherms or the P - T isochores or both.
2. The modified phase diagram may be readily used to compute the various thermodynamic quantities and hence a separate compilation of the latter may not be essential.

Acknowledgement:

The author is grateful to the Director, National Institute of Foundry and Forge Technology for according permission to present the paper.

....

610

References:

1. M. Hansen and K. Anderko, Constitution of Binary Alloys, Mc Graw - Hill, New York, 1958.

2. R. P. Elliott, Constitution of Binary Alloys, First Supplement, Mc Graw - Hill, New York, 1965.

3. F. A. Shunk, Constitution of Binary Alloys, Second Supplement, Mc Graw - Hill, New York, 1969.

4. V.K. Sinha and K.P. Singh, Trans. Ind. Inst. Metals, 1974, Vol. 27, p. 289.

5. V.K. Sinha, Met. Trans., 1976, Vol.7A, p. 472.

6. R. Speiser, Metal Hydrides, W. M. Mueller, J.P. Blackledge and G.G. Libowitz, eds., p. 51, Academic Press, New York, 1968.

7. V.K. Sinha and K.P. Singh, J. Nucl. Mater., 1970, Vol. 36, p. 211.

8. V.K. Sinha and K.P. Singh, Met. Trans., 1972, Vol.3, p. 1581.

9. V.K. Sinha, J. Chem. Soc. Faraday Trans. 1976, Vol. 72, p. 134.

10. V.K. Sinha, J. Nucl. Mater, 1976, Vol. 59, p. 201

11. Ref. 2, p. 513.

12. K.E. Moore and W.A. Young, J. Nucl. Mater., 1968, Vol.27, p.316.

13. S. Mishra, K.S. Shivaramakrishnan and M.K. Asundi, J. Nucl. Mater., 1972/73, Vol. 45, p. 235.

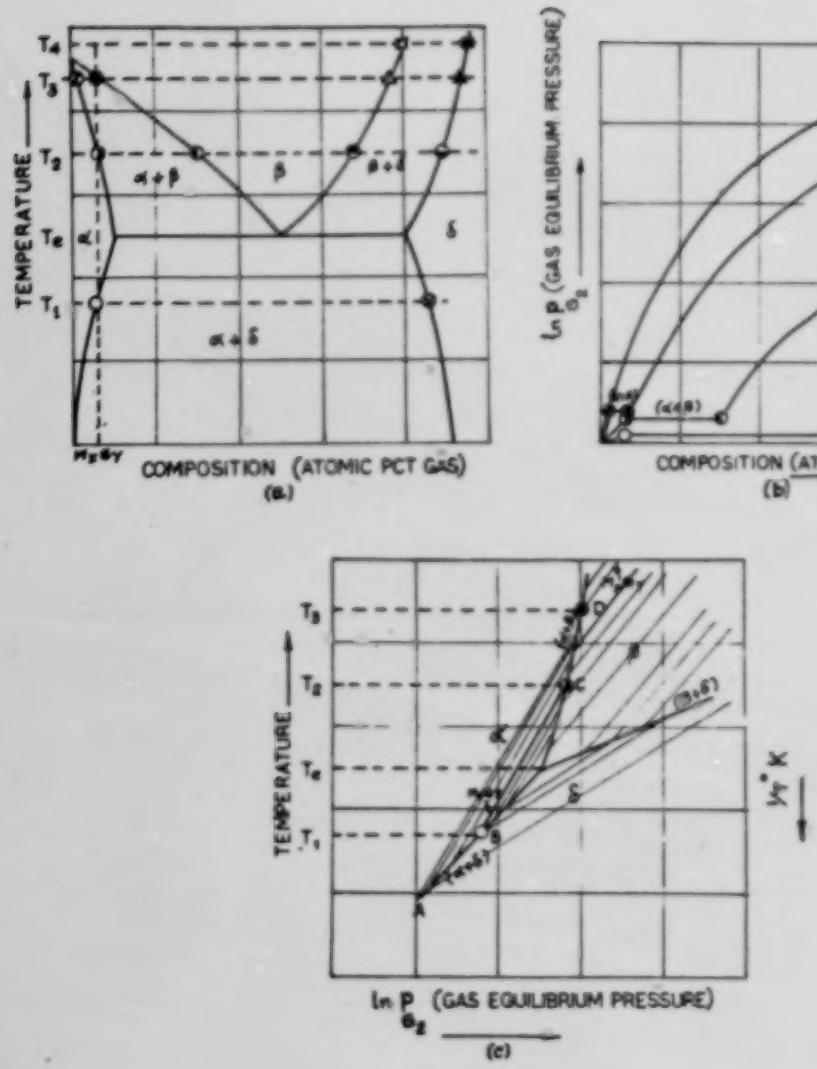

Figure 1. Phase-Diagram of Metal-Gas System (Schematic) (a) Temperature-composition Diagram (b) Pressure-Composition Isotherms (c) Pressure-Temperature Isochores

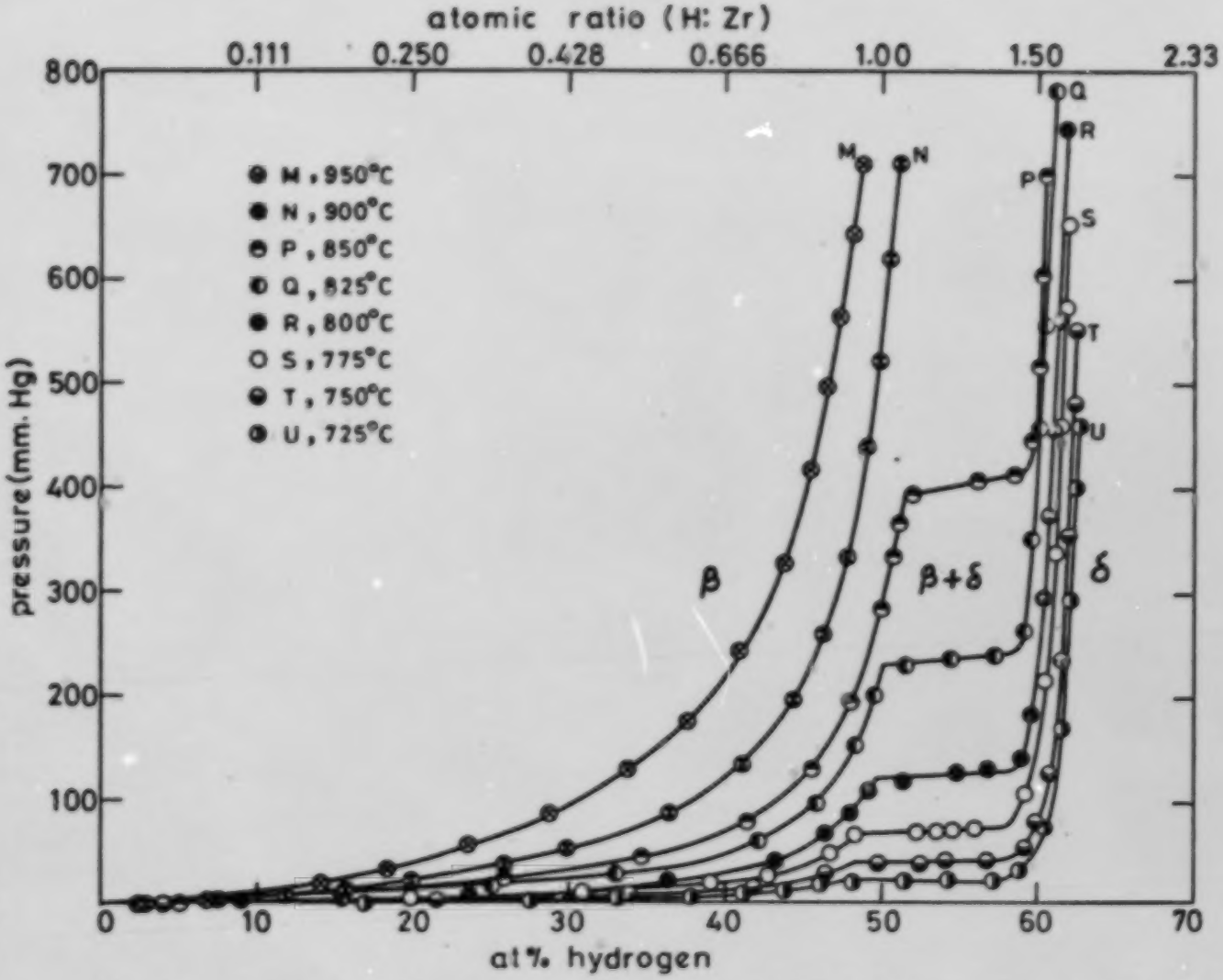

Fig. 2 Isothermal pressure against at% hydrogen for unalloyed Zr in the temperature range 725 to 950°C.

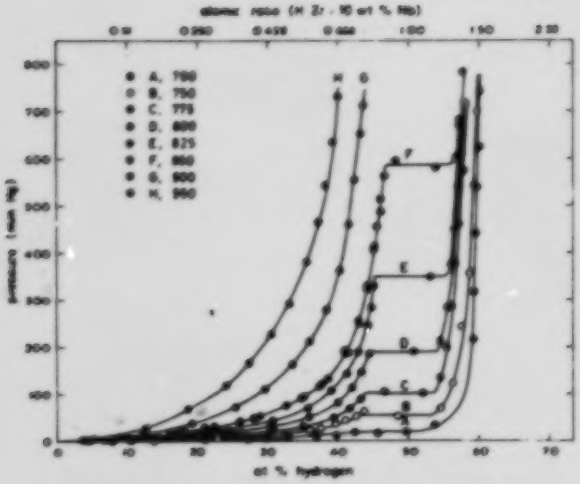

Fig. 3—Isothermal pressure against at. pct H for Zr-10 wt pct Nb alloy in the temperature range 700° to 950°C.

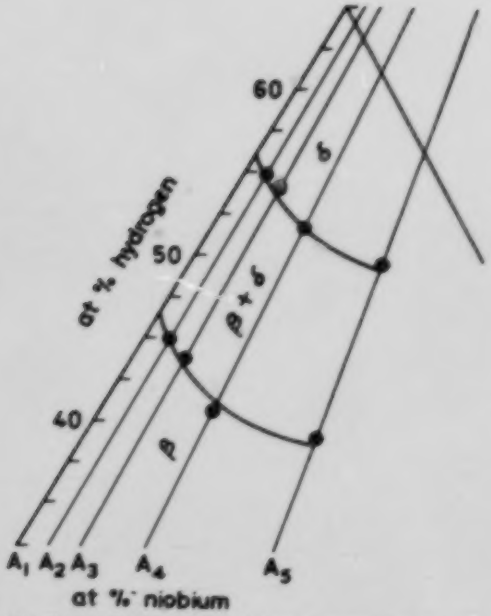

Fig. 4—Isothermal section for the ternary system Zr-Nb-H at 700°C. A_1, 0.0 at. pct Nb; A_2, 2.46 at. pct Nb; A_3, 4.91 at. pct Nb; A_4, 9.84 at. pct Nb; A_5, 19.71 at. pct Nb.

614

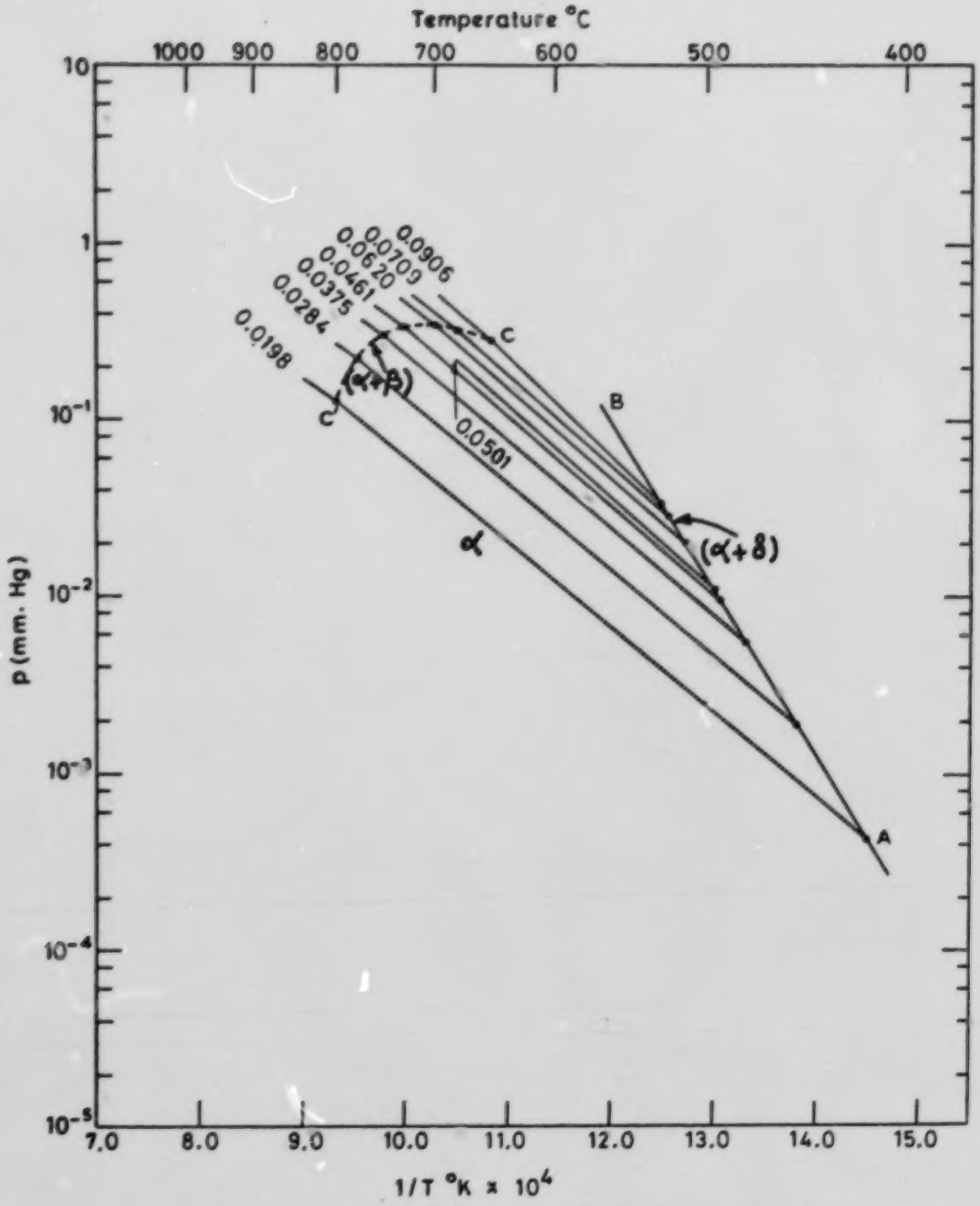

Fig. 5 Summary plot of decomposition pressure vs. reciprocal of temperature for different zirconium-2.5 wt% niobium-hydrogen alloys. The number on a plot represents the H/(Zr-2.5 wt% Nb) atomic ratio

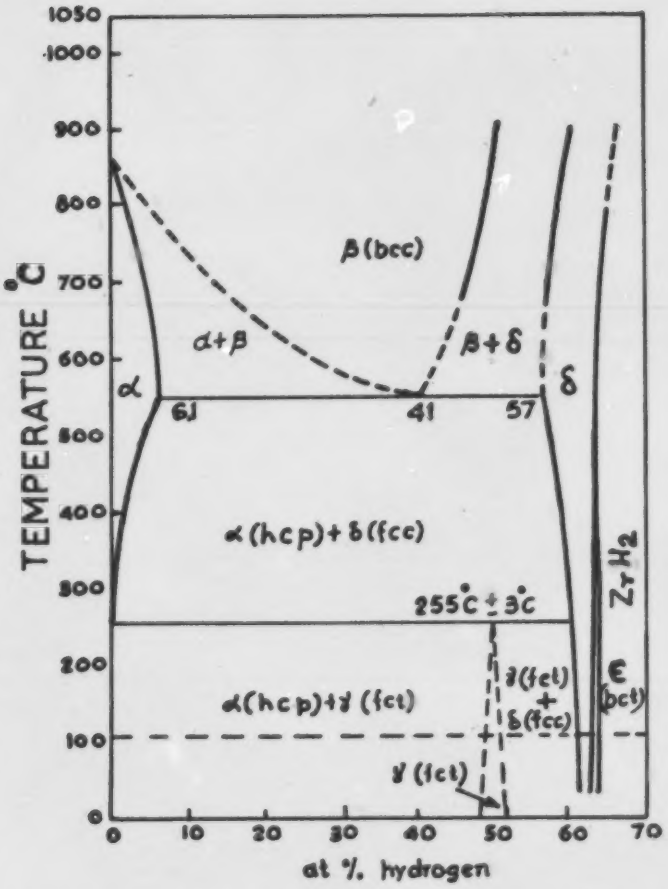

FIG.6. THE EQUILIBRIUM PHASE RELATIONS IN ZIRCONIUM-HYDROGEN SYSTEM

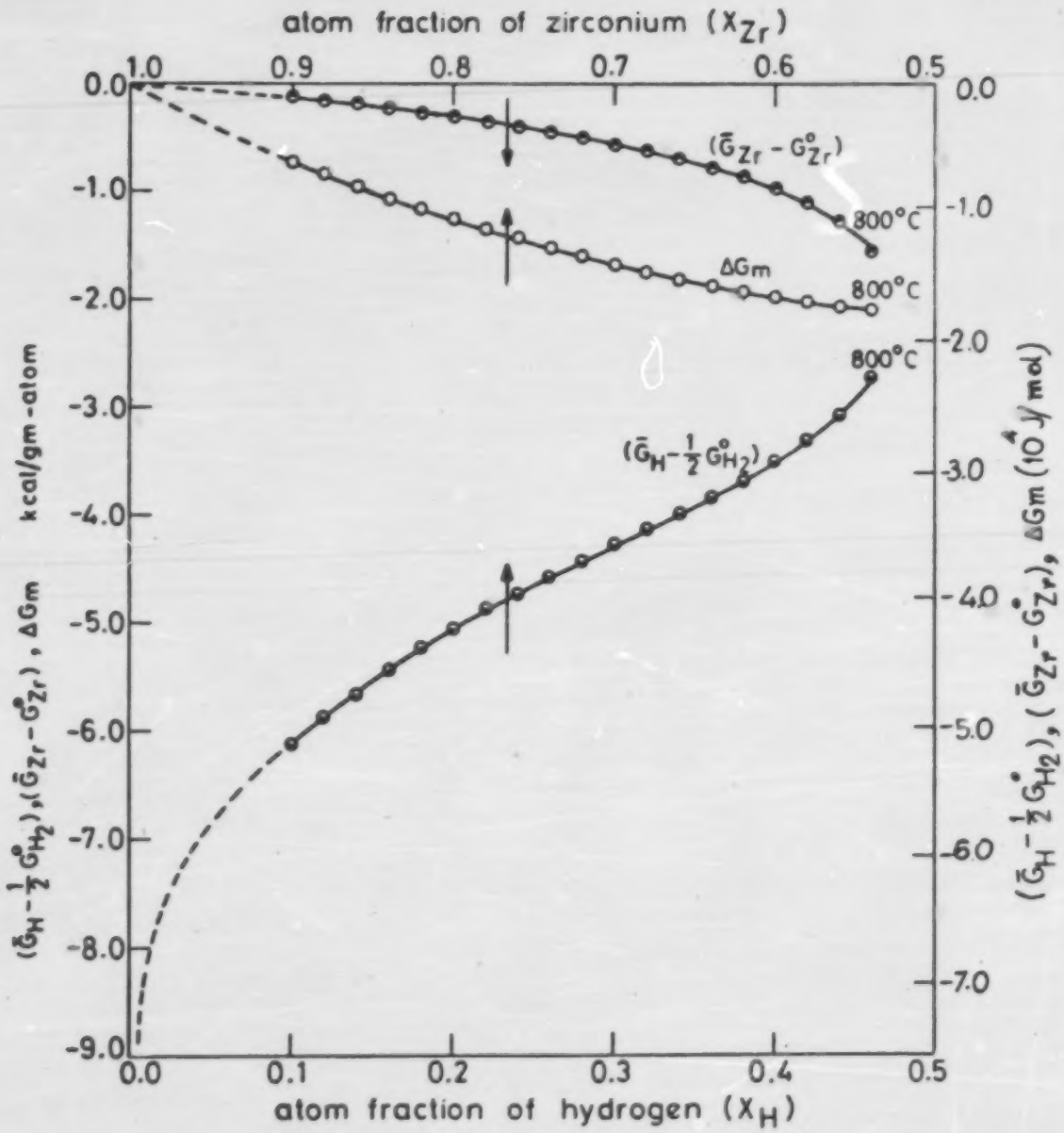

Fig. 7 Free energy against atom fraction of hydrogen plot in the ß-phase of Zr-H_2 system at 800°C. •, $(\bar{G}_H - \frac{1}{2}G^{\circ}_{H_2})$; •, $(\bar{G}_{Zr} - G^{\circ}_{Zr})$; o, ΔGm. The arrow indicates the direction in which an isothermal curve shifts with increase in temperature.

National Bureau of Standards SP-496, Applications of Phase Diagrams in Metallurgy and Ceramics
Proceedings of Workshop held at NBS, Gaithersburg, Md., January 10-12, 1977

THEORY OF ALLOY PHASES

R. E. Watson
Brookhaven National Laboratory*
Upton, NY 11973

H. Ehrenreich†
Harvard University
Cambridge, MA 02138

and

L. H. Bennett
Institute of Materials Research
National Bureau of Standards
Washington, DC 20234

I. Introduction

The problem of understanding and predicting phase diagrams may be attacked in a variety of ways ranging from the successful thermodynamic approaches of Kaufman and others to the a priori band theory estimates of the solid-state physicist. In one of his last papers, Samsonov produced[1] a "global map" (Fig. 1) that indicates the dilemma of talking about the subject of this tutorial. The work-horses of this meeting are in the lower part of the diagram, sitting on the ground so-to-speak. In the heavens is Schrödinger's equation, surrounded by a variety of practical and impractical schemes, including faulty transliterations (e.g. Prof. Brewer, who is on the program of the Workshop, is called Bluer). The orderliness of Fig. 1 is only apparent - the real life situation is much more complicated. The purpose of the present article is to explore various non-thermodynamic approaches from the viewpoint of solid-state physics. We will not attempt complete coverage of the subject but will, instead, try to indicate the scope of activity and to indicate some of the progress which has been made.

It appears to be within the means of present day a priori energy

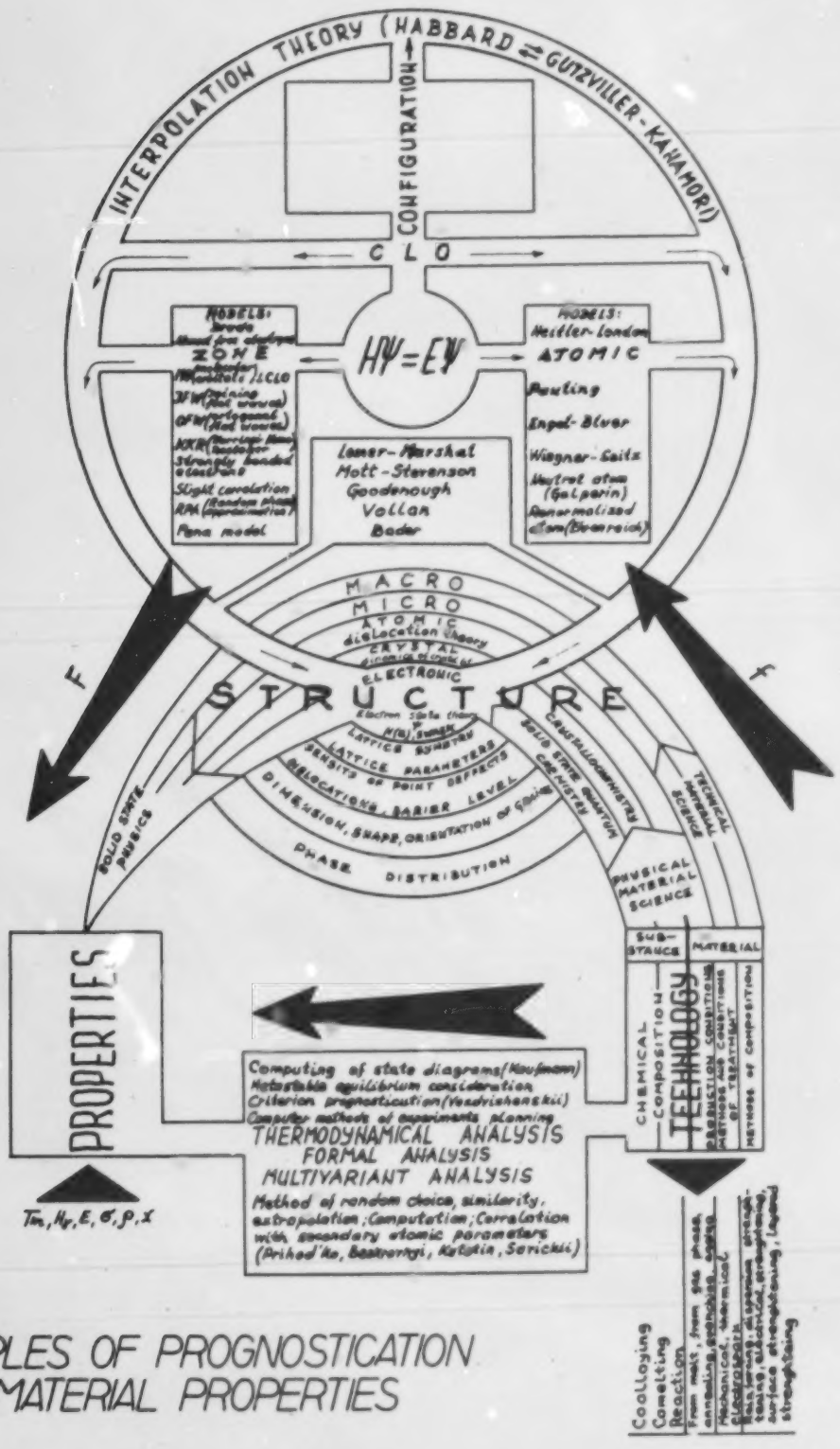

PRINCIPLES OF PROGNOSTICATION OF MATERIAL PROPERTIES

Fig. 1. Samsonov's organization[1] of a variety of schemes for predicting phase diagrams and other properties of solids.

band theory to estimate the phase diagram of a binary system, provided sufficient care is taken in the choice of the system. The computer costs would be high and the results would probably indicate little that wasn't already understood. This type of approach will be of minor concern here. Instead we will ask what solid-state theory, as practiced in either a chemistry or physics department, has to say concerning various model approaches to phase diagram predictions and what physical basis there is for choosing the relevant parameters entering these approaches. We will also consider several classes of questions concerning solubility or tendencies for martensitic transformations, which are appropriate to ask of a band theory calculation. Finally, we will remind the reader of a few of the approximations, which are often used but not always justified, in solid state theory.

Section II will be concerned with transition metal cohesion, magnetic effects and alloying. This will be followed by consideration of potentials and pseudo-potential applications. Section IV will discuss electronegativities and pair-potential approaches. This will be followed by consideration of Madelung effects and the problem of defining atomic size and charge. The final sections will cover some aspects of what can be learned from band theory calculations concerning such matters as alloy solubility, as well as some activities by the solid-state community of which the metallurgist and ceramist should be aware.

As has already been admitted, this will be a broad-brush review. We apologize to those workers whose results are either neglected or, worse, dealt with inadequately.

II. Transition Metals: Cohesion, Magnetic Effects and Alloying

It is useful to begin by considering the cohesion of the pure transition metals. The various factors[2] contributing to a band theory estimate of cohesion in Ti are indicated in Fig. 2. The atomic ground configuration is $3d^2 4s^2$, (a), whereas the $3d^3 4s$ configuration is more appropriate to the metal. The resulting atomic excitation, (a) → (b), is the familiar Brewer promotion energy. The atomic charge

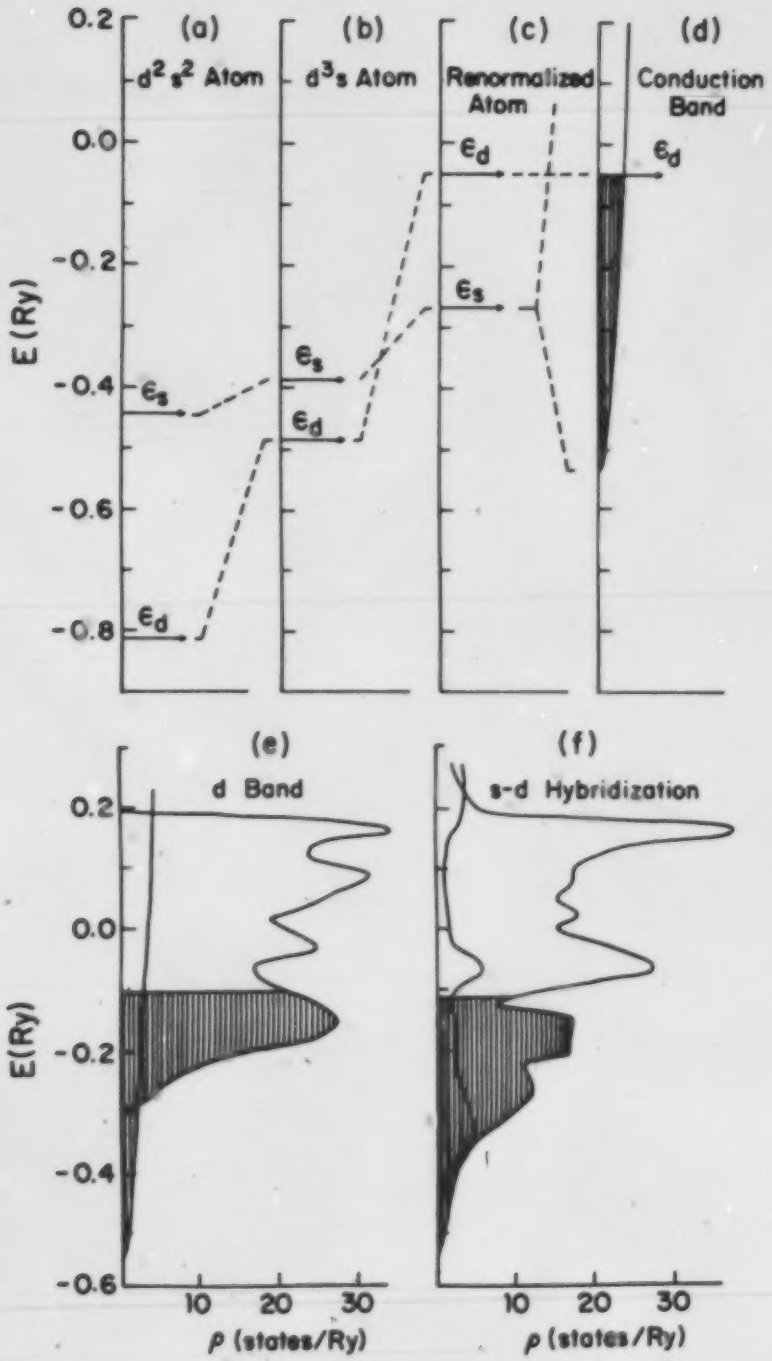

Fig. 2. The various factors contributing to the electron energy structure of a transition metal. As an example of these, Ti is taken from its free atom ground state to the metal. See Ref. 2 for details.

within the metal is constrained to be within the atomic Wigner-Seitz cell whereas some of the charge is considerably outside this volume in the free atom. The resulting compression of charge increases the valence electron contributions to the coulomb potential and raises the one-electron energy levels, ε_s and ε_d, as is seen in (c). The s level broadens into a non-d conduction band, as in (d). The bottom-most level of this band is determined by the boundary condition that the wavefunction be flat at the Wigner-Seitz radius. This condition lets the electron have a compressed charge density without a severe cost in kinetic energy and, as a result, substantially lower energy than the ε_s of the renormalized atom. As was pointed out[3] by Wigner and Seitz, this is the essential feature of cohesion in the alkali metals: the center of gravity of the occupied levels in the resulting conduction band lies lower than the free atoms one-electron level, ε_s. This does not have to be the case in the transition metals due to more important d-electron contributions. As is indicated in (e), the d level broadens into a band whose center of gravity remains at ε_d finally, the conduction and d bands hybridize (the two curves in (f) indicate the relative weights of d and non-d characters in the final density of states). As Friedel and his associates[4] have emphasized, it is the broadening of the d levels into a band structure which is essential to the variation in cohesion across a transition metal row. Putting one electron per atom in the d bands gains the difference in energy between ε_d and the center of gravity of the occupied levels. Putting in a second electron per atom yields less energy than the first, since one must fill states lying closer to ε_d. Once the band is half filled, some of the benefits of band broadening are lost since states above ε_d are being occupied. Once the band is completely filled, band broadening makes no further contribution to cohesion since the center of gravity of the occupied levels is the equal to ε_d. Estimates of the various contributions to cohesion of the 3d and 4d transition metal rows are indicated in Fig. 3 (see ref. 2 for details of these calculations). Agreement with experiments is quite

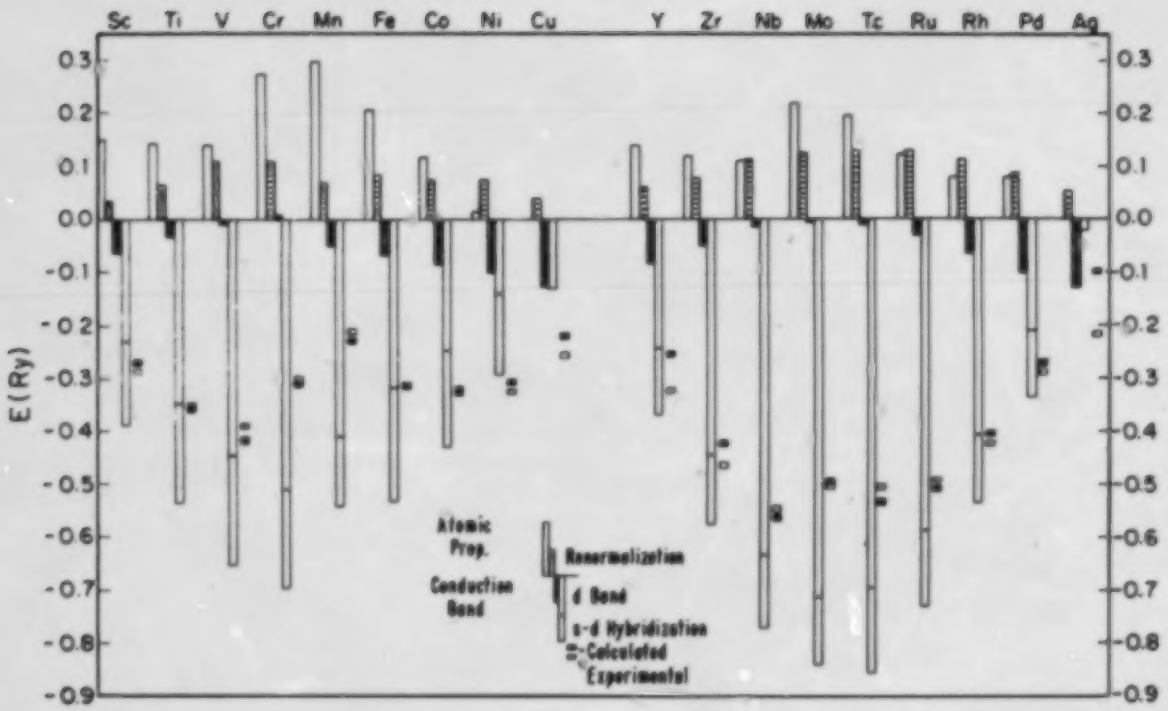

Fig. 3. Theoretical estimates of the various contributions to the cohesion of the 3d and 4d row transition metals. The breakdown of the contributions follows from Fig. 2: These are the preparation of the atom into the proper atomic configuration, renormalization to the metallic volume, conductor and d-band broadenings, and the effects of s-d hybridization. See Ref. 2 for details of the calculation.

good in this set of estimates. The effects of d-band broadening and of promotion of the free atom into the configuration most appropriate to the solid are most important in determining the variation of cohesion across the rows. Cu and Ag with their filled d bands have no d-band broadening contributions. There are significant contributions arising from hybridization between d and conduction bands. For the other metals, the band-broadening contribution depends on the extent to which the d-band is filled and is proportional to the band width of the metal in question. Friedel and Ducastelle[5] have pointed out that the band width, and hence its contributions to cohesion, does not arise from a sum of atom-atom pair interaction terms.

Band calculations such as these typically yield non-d electron counts of 1 ± 1/4 electrons across a transition metal row. This is consistent with Engel-Brewer theory, as it is commonly defined, for the body-centered and hexagonal metals, but not for the face centered cubic metals encountered in the Ni and Cu columns of the periodic table. The Brewer or Pauling view emphasizes the role of non-d electrons in transition metal structures while the band theory view, as exemplified in Fig. 3, suggests that d electrons play the essential role.

The difference in energy on going from one structure to another is, of course, much smaller than the total cohesive energy. Nevertheless band theory has had modest success in predicting the experimental trends. Pettifor, for example, has taken[7] electron densities of states, $\rho_i(\varepsilon)$, such as that plotted for the fcc structure in Fig. 2, and has evaluated the energy differences

$$\Delta E = \Delta \int_{\text{band bottom}}^{\text{Fermi level}} \varepsilon \rho_i(\varepsilon) d\varepsilon \ , \qquad (1)$$

between fcc, bcc and hcp structures. After modest adjustment of parameters (e.g. band width and position), his results reproduce the experimental trends.

It has been recognized for some time that the presence of local magnetic moments sensibly alters a transition metal's lattice constant[8]. These magnetic contributions have been the object of calculations by

Poulsen et al.[9] and by Janak and Williams[10]. The latter's results for the Wigner-Seitz radii and for bulk moduli, calculated for paramagnetic metals, are shown in Fig. 4. Calculation agrees with experiment for the 4d metals which are paramagnetic, but breaks are seen in the middle of the 3d row where magnetic moments occur. Janak and Williams, using exchange polarized band calculations, went on to estimate the derivatives of the plotted quantities with moment and, using the experimentally accepted moment values, obtained the results of Fig. 5. The agreement with experiment is quite good, but perhaps deceptively so in the case of Mn which occurs in four allotropes whose Wigner-Seitz radii do not correlate with the moments which occur. Two of the four allotropes, the γ and δ phases, are close packed and, of the two, the phase with the larger moment has the smaller Wigner-Seitz radius contrary to the model employed in Fig. 5. Poulsen et al.'s calculations were limited to the Fe and Ni columns of the periodic table. They obtained similarly good results and were able to discuss the relative stability of the fcc and bcc phase of iron.

For the case of the properties of disordered transition metal alloys, the coherent potential approximation (CPA) has been developed[11]. In this scheme, the d-electrons maintain their atomic character, e.g. in Cu-Ni alloys, the d-electrons are Cu-like at Cu sites and Ni-like at Ni sites, in first approximation. Efforts, largely in France, have been made[12,13] applying CPA and various perturbation schemes to the prediction of phase stability in such alloys. In general these employ model densities of states of the constituent metals. A sample[12] of the results is shown in Fig. 6 where comparison is made with Kaufman's thermodynamic approach[14]. This is not the only, or necessarily the best example we could have chosen, but is particularly interesting because of the contact it makes with the thermodynamic predictions methods discussed elsewhere in this workshop. The technology of such calculations is being actively studied and improved. Questions concerning how to improve quantum mechanical models for real alloys, which remain computationally tractable are the object of study. The calculations have reached the stage where the question

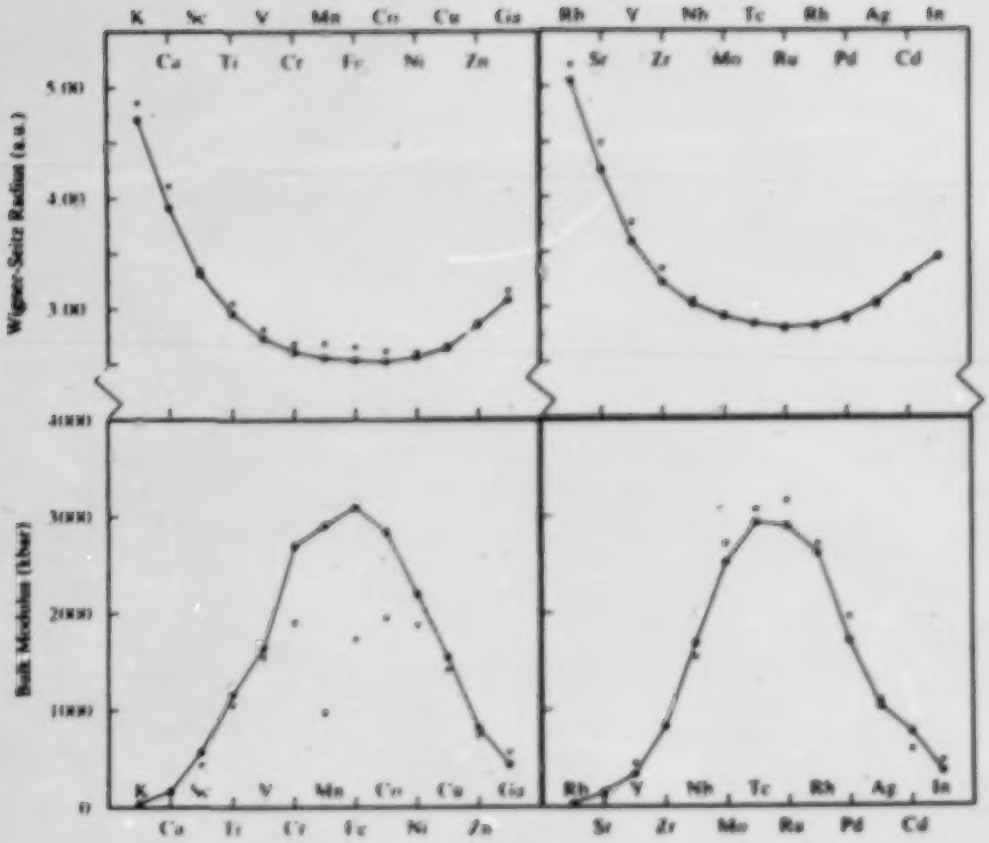

Fig. 4. Janak and Williams' band theory estimates[10] of the Wigner-Seitz radii and bulk moduli of 3d and 4d transition metals in the paramagnetic states. The crosses are experimental values. Note that there are significant deviations for Cr through Ni, which have magnetic moments.

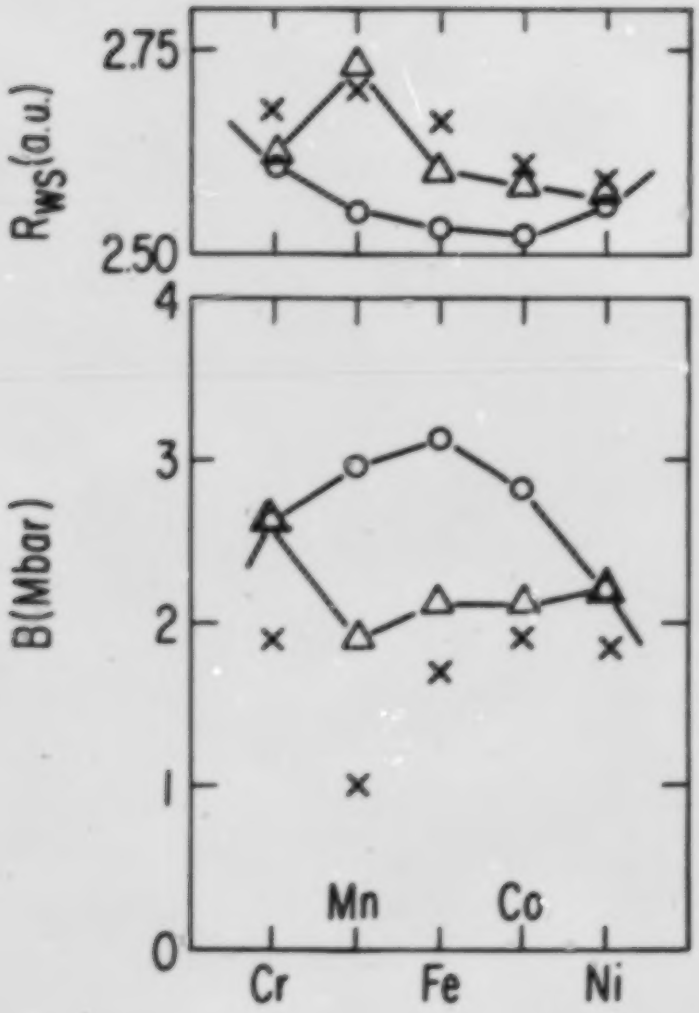

Fig. 5. Janak and Williams' estimates[10] of Wigner-Seitz radii and bulk moduli for the paramagnetic (circles) and magnetized (triangles) transition metals Cr through Ni. The crosses are the experimental values.

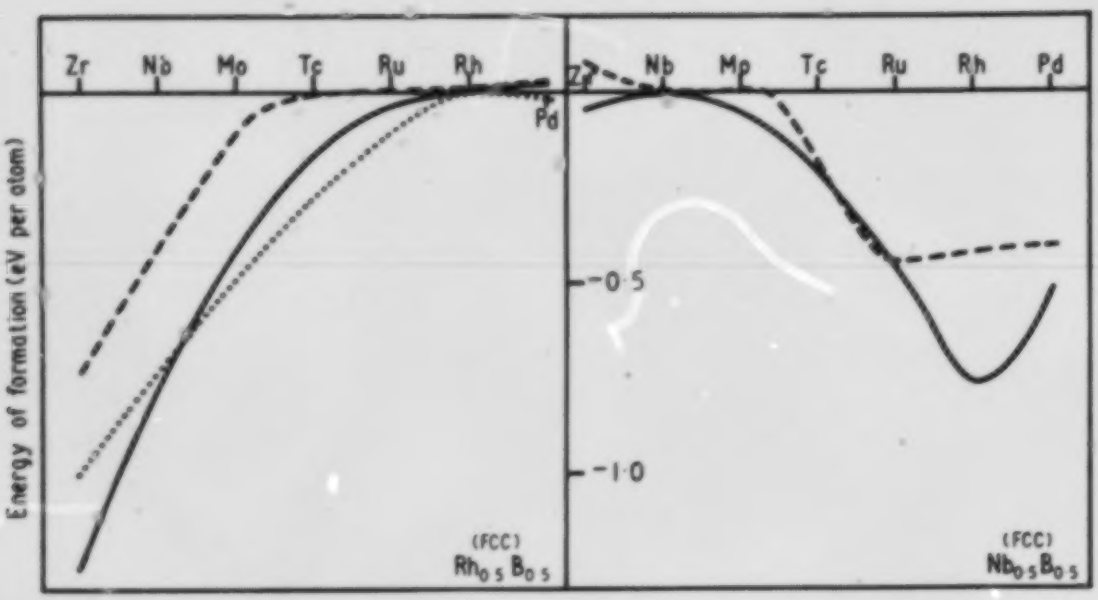

Fig. 6. van der Rest et al.'s estimates[12] of the energy of formation of equiconcentrational rhodium and niobium based alloys with elements of the second transition metal row having the fcc structure. The dashed lines are their standard solutions, the dotted obtained with an improved model density of states. Comparison is made with thermodynamic estimates of Kaufman (solid lines).

of how well theory agrees with experiment is also being addressed. Few, if any, real qualitative contradictions have been found thus far for the relatively small number of alloy systems that have been carefully studied. This indicates that the models used are at least qualitatively adequate and may be used to obtain insight into the physical mechanisms important to alloy formation.

III. Approximations, Potentials and Pseudopotentials

Of the several approximations made in some of the calculations cited here, two deserve special mention. One is associated with estimating total energy differences and the other with potentials. Approximations are often computationally necessary and less frequently quantitatively justifiable. Accordingly one must be alert to their possible implications.

The total energy of a many-electron system having one-electron energies ϵ_i that are characteristic of the interacting system is

$$E = \sum_{i}^{\substack{\text{all}\\ \text{electrons}}} \epsilon_i - \sum_{i}^{\substack{\text{all}\\ \text{electrons}}} \sum_{j<i} \left[\left\langle ii \left| \frac{e^2}{r_{ij}} \right| jj \right\rangle - \left\langle ij \left| \frac{e^2}{r_{ij}} \right| ji \right\rangle \right] \qquad (2)$$

Since each ϵ_i has contributions from interaction with <u>all</u> other electrons, j, a simple sum of one-electron energies double counts electron-electron interaction terms which thus are subtracted to obtain a correct expression for the total energy E. Now it is normally the difference in total energy which is of concern and usually there is an atomic core common to the states being compared: if so, we may rewrite Eq. (2)

$$E = E_c + \sum_{i}^{\substack{\text{valence}\\ \text{electrons}}} \epsilon_i - \sum_{i}^{\substack{\text{valence}\\ \text{electrons}}} \sum_{j<i} \left[\left\langle ii \left| \frac{e^2}{r_{ij}} \right| jj \right\rangle - \left\langle ij \left| \frac{2}{r_{ij}} \right| ji \right\rangle \right] \qquad (3)$$

where the sums are limited to the valence electrons and E_c is the core energy involving the kinetic and nuclear potential energies of the

core electrons plus core-core interelectronic terms. There still remains a subtraction of valence electron - valence electron interaction terms which is often computationally inconvenient when calculating an energy difference characteristic of two phases. When taking such energy differences it is often assumed that the differences in the double sum may be neglected, yielding

$$\Delta E = \Delta \sum_{\substack{\text{valence} \\ \text{electrons}}} \varepsilon_i \tag{4}$$

which, in its integral form, is Eq. (1). This approximation is frequently valid, though rarely is the justification presented in a published paper. Indeed, there are cases where the approximation is inapplicable. Consider the case of a transition metal where alloying or compound formation has led to an increase (decrease) in d electron count with a compensating decrease (increase) in the number of non-d electrons. Being more compact, the interaction energy between a pair of d electrons is roughly twice that among non-d or between d and non-d electrons. Eqs. (1) and (4) are not applicable if interchange between d and non-d electrons is significant.

Approximations are also involved in the potentials used in calculating energies and wavefunctions of many-electron systems. "Non-local" effects occur because one electron acts to avoid another due to the repulsive e^2/r_{ij} interaction. The potential sampled by electron i depends on that electron's spatial distribution. While exchange (and correlation) terms can be manipulated so that the potential multiplying the wave funciton ϕ_i is a function only of coordinates i, the resulting potential $V(\vec{r},i)$ is only appropriate to electron i. In other words, there is a term

$$V(\vec{r},i)\ \phi_i(\vec{r})$$

in the one-electron, Schrödinger equation rather than

$$V(\vec{r})\ \phi_i(\vec{r})$$

where $V(\vec{r})$ is a "local" potential common to all electrons.

Hartree-Fock theory, for example, includes non-local effects associated with exchange. Calculations employing different potentials for different electrons are computationally inconvenient and normally avoided for solids. Sometimes ℓ-dependent potentials are used where electrons, or more precisely, wavefunction components of differing angular quantum number ℓ, "sample" different potentials. The results of Figs. 2 and 3 are an example in which d and non-d electrons were allowed differing, hence non-local, potentials as is desirable on physical grounds. More specifically, these calculations employed Hartree-Fock-Wigner-Seitz potentials. These potentials differ from Hartree-Fock theory in that they include a self-Coulomb exchange-correlation hole which is centered, and contained within, the atomic site at which the potential is defined. Put another way, the potential is such that each electron in the neutral unit cell samples the potential due to all the others in that cell, excluding the full charge associated with itself. Such potentials are expected to provide a good approximation to correlation effects for d electrons; they are less appropriate for the less localized non-d electrons for which the hole should be centered about the electron in question.

Starting with the work of Slater[15] and of Kohn, Hohenberg and Sham[16], among others, there has been considerable work directed toward defining a single potential to serve all electrons. Hedin and Lundqvist[17] have derived a local potential which incorporates correlation as well as exchange effects. The dielectric response of metallic electrons to an external perturbation was evaluated. This permitted an estimate of their contribution to the potential sampled by an electron. The result is an exchange - correlation potential which is a function of the electron density at the point at which the potential is evaluated. Hedin and Lundqvist's potential is widely used in energy band calculations. This has been extended by von Barth and Hedin[18] to the magnetic case where separate exchange-correlation potentials are constructed for electrons of majority and minority spin. It is likely that someone will

generate an ℓ-dependent variant of this class of potential to differentiate between d and non-d electrons in transition metals. Whatever the gains, the beauty and simplicity of a unified local exchange-correlation potential will have been sacrificed.

Pseudopotentials are often used, particularly for semiconductors and simple metals. In this constant, a repulsive term is added to the potential which accounts for orthogonalization to the atomic core. This allows one to deal with a wavefunction- which does not have the wiggles, associated with core orthogonalization, in the interior of an atom. Both local and ℓ-dependent pseudopotentials are in common usage. Calculations for silicon suggest what can happen. Using a local pseudopotential, Walter and Cohen computed[19] the charge density of the silicon valence electrons, as portrayed by the "contour map" in the middle of Fig. 7. Note the ellipsoids of charge built up between Si atoms. The experimental results appearing at the top of the figure were obtained[20] by Yang and Coppens from "forbidden" x-ray reflections - - reflections, which, by symmetry, would be absent if the density were simply a sum of spherical contributions. There are ellipsoids of charge of about the same magnitude as those computed, but with their long axis parallel, rather than normal to the Si-Si line. Using a two term ℓ dependent pseudopotential, Chelikowsky and Cohen obtained[21] the results at the bottom of the figure. Better agreement is obtained in both the magnitude and the shape of the ellipsoid. In order to get the shape of the bonding charge correct, use of a nonlocal potential was thus required. The importance of this to total energies and, in turn, to the prediction of phase stability has not yet been assessed. Local pseudopotentials are very useful for many problems but one must be alert to their potential shortcomings. The applicability of this method has been extended to transition metals[22], but due to technical reasons, its utility appears to be limited.

Stroud and Ashcroft used local pseudopotentials in their estimate[23] of the relative stability of the hcp, bcc and fcc struc-

Experimental
(Yang and Coppens)

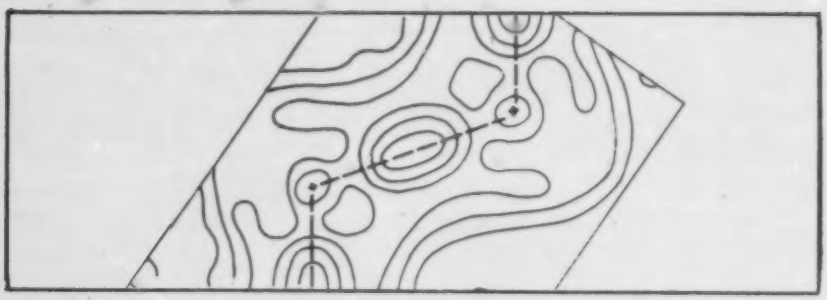

Local Pseudopotential
(Walter and Cohen)

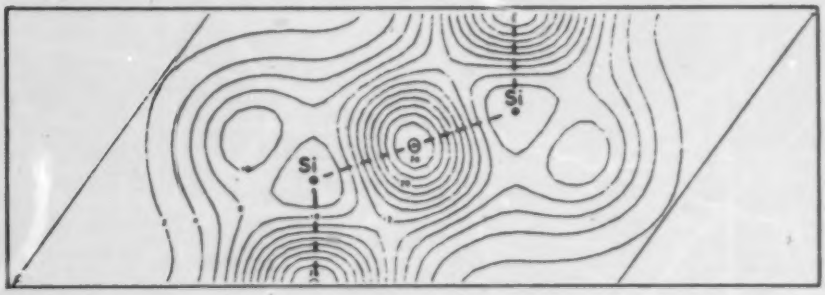

Nonlocal Pseudopotential
(Chelikowsky and Cohen)

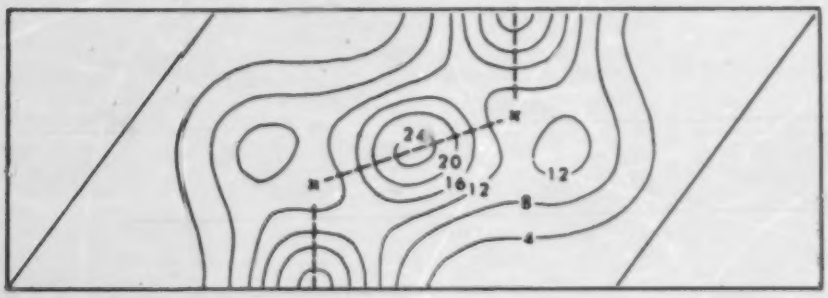

Fig. 7. The valence electron distribution in silicon as inferred experimentally from forbidden x-ray reflection data (top figure); from local pseudopotential theory (middle figure) and from non-local pseudopotential theory (bottom figure). (Refs. 20, 19 and 21 respectively.)

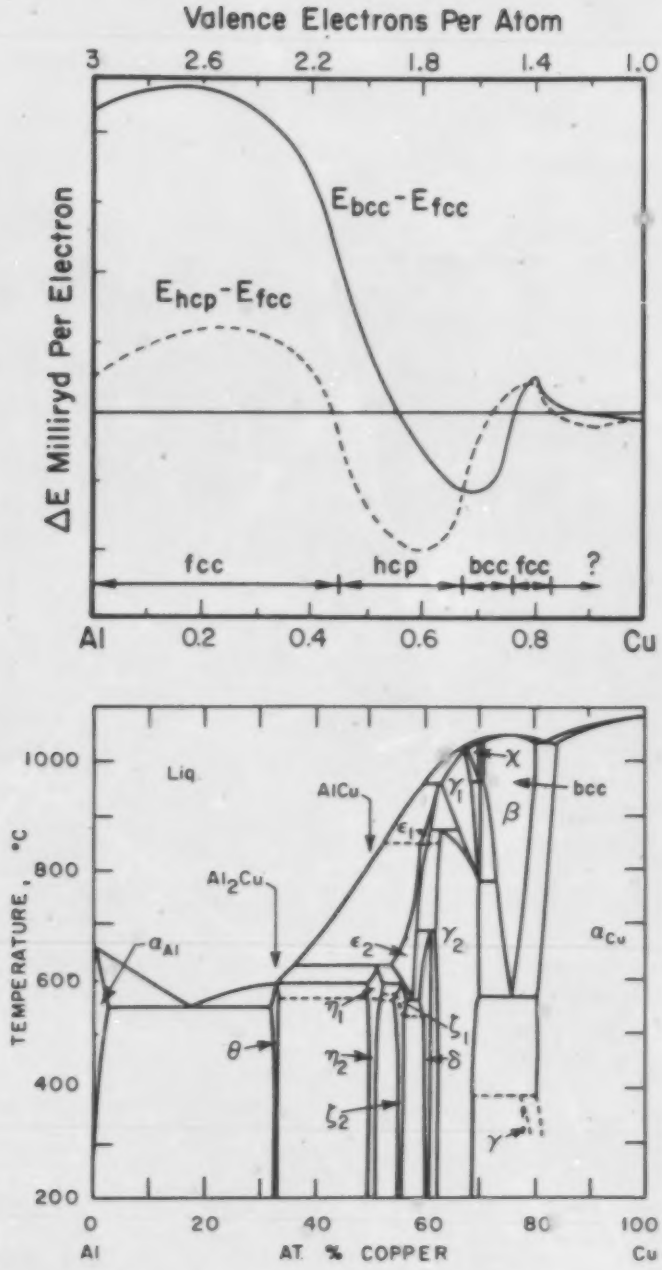

Fig. 8. The relative stability of the fcc, hcp and bcc structures in the CuAl alloy system as estimated by Stroud and Ashcroft[23]. The actual phase diagram of the system is shown for comparison. Note that the bcc region (β phase) is correctly predicted for $0.7 < x < 0.8$ and that complex phases, not considered in the calculations occur for $0.45 < x \leq 0.7$ where the hcp structure is predicted. While the hcp is predicted for $x > 0.85$, the results are too close to call in this region.

tures for the Cu-Al system. Their results are shown in Fig. 8. The prediction of stable phases is indicated at the bottom of the plot. At the Cu rich end the computed phase energies are too close to one another to call. It is gratifying that the predicted bcc phase stability falls in just the region where the bcc β phase occurs. The region of predicted hcp stability is one where a variety of complicated structures occur to which the calculations are not relevant (though the η and ε phases are hexagonal, approximately close-packed structures). The predictions seen here are rather more successful than is typical for such calculations.

Girifalco has recently noted[24] that he can correlate alloy solubility by considering ion core radii, which are basically the radii of the repulsive cores of pseudopotentials instead of atomic sizes. If the core radii of homovalent constituents differ by more than 20%, there will not be mutual solubility. Whether this is more properly viewed as a size effect, or, instead, as a measure of the potential and in turn the electronegativity is difficult to say. We are inclined to the latter view.

Before leaving pseudopotentials, we should note that the machinery has been developed[25] to deal with ternary systems. Its much more complicated than the binary case and to our knowledge has not yet been used in actual calculations.

As has been indicated above, there are many classes of potential available to the band theorist. They often yield predictions of Fermi surfaces, optical spectra, and other properties that are consistent with experiment. While the evidence is somewhat limited, it would appear that potentials which yield consistent predictions for other properties do <u>not</u> yield consistent results for the alloy phase stability problem where small differences between large quantities are involved. Attention to this issue by solid-state theorists may yield insight into the problem of understanding alloy formation.

IV. Electronegativities and Pair Potential Approaches

The idea of electronegativity - the tendency for some atomic species to attract or donate electronic charge - is useful and intuitively satisfying. There are some problems associated with its use. First, there is no universal scale. Pauling and others consider Au the most electronegative among the metallic elements. This means that it attracts electrons from sites occupied by other metal constituents more strongly than any other metal. On the other hand most electronegativity scales employed by metallurgists, in connection with solubility or phase structure considerations, have a number of the transition metals such as Pt and Ir more electronegative than Au. On this point we believe the Pauling scale to be the "truer" measure of charge flow. What is more in addition to electronegativity, it appears to be necessary to have at least a second parameter to describe the metallurgical effects of concern to us here. There is, however, considerable difficulty in finding a parameter that is truly independent. Consider, for example, Miedema's scheme[26].

Miedema and his associates introduced a metallurgical electronegativity scale which used experimental workfunctions as a starting point. For this scale, Pt is more electronegative than Au. Instead of defining the second parameter, say, in terms of the atomic size, they used the electronic density at the outer part of the atomic cell appropriate to the atom in its elemental solid form. When constructing a compound or alloy of several atomic species there would be density mismatches which must be removed. This would cost energy unlike the electronegativity mismatches which cause charge flow and compound stabilization. The result is a plot for the elements as in Fig. 9: this is not Miedima's most recent set of parameters but serves present purposes well. Miedema's point was that, for alloys, one could draw two lines, in this case through H, thereby producing predictions for the heat of formation of H-metal alloys. The electronegativity dominates in the top and

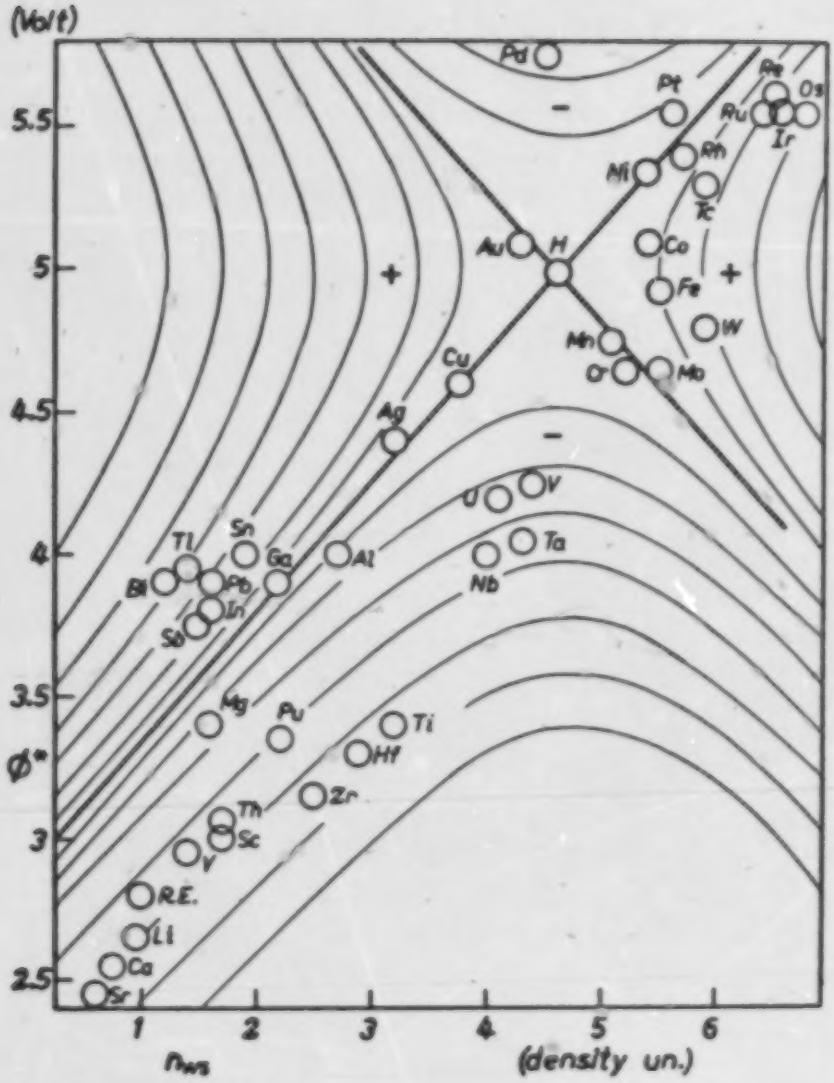

Fig. 9. A plot of Miedema's chemical potential and electron density parameters[26] for the purpose of predicting alloy heats of formation. Taking hydrogen alloys as an example, the straight lines divide regions of positive and negative heats of formation. The top and bottom quadrants, where the chemical potential dominates, produce alloys stabilized in energy whereas the left and right quadrants cost energy to form. One can draw contours of constant heat of formation as is done schematically with the light curves.

637

bottom quadrants leading to gains in energy on alloy formation. The density mismatch dominates in the side quadrants causing energy loss. Only one other factor had to be introduced for the scheme to predict the sign of heats of formation rather satisfactorily: in a case involving the alloying of a polyvalent p band metal such as Sn with a transition metal, a p-d hybridization term, whose value is independent of the particular pair involved, would have to be added. Miedema has drawn energy contour lines going away from the crossed lines, such as seen for the H-metal alloys in Fig. 9, and these types of contours, he reports, quite satisfactorily give the magnitudes of the hears of formation for a variety of alloy systems. Whatever its numerical success, there is one factor bothersome to a solid-state theorist, namely, to the extent that the electronegativity is a function of a single physical parameter, that parameter must be an electron density. No solid-state theorist has really calculated an electronegativity scale from first principles, but Lang and Kohn have calculated[27] its near equivalent - namely the work function which is a measure of the Fermi level and hence the chemical potential. Their electron gas results, with the average electron density the only independent variable, are in rather good agreement with experiment. This is suggested by Miedema's parameters plotted in Fig. 9 for the points lie close to a universal curve. One might say that the number of independent parameters involved lies somewhere between one and two, a situation not uncommon to most schemes. Atomic size, core "size", electronegativity, valence and electron density are intimately connected with one another column by column in the periodic table, making it almost impossible to deal with independent or almost independent variables.

Simons, St. John and Bloch[28] have dealt with another aspect of electronegativities namely that different valence shells make separate "orbital" electronegativity contributions to the total. This idea is found in Mulliken's concept of electronegativity.

They[28] introduced a term which is given approximately by

$$X_\ell \sim E_\ell/Z \tag{5}$$

where E_ℓ is the binding energy of an $n\ell$ valence electron outside the ion stripped to its core and Z is the charge of the stripped ion. This reflects the notion that electronegativity is some measure of the attractive interaction between a valence electron and the atomic core. The total electronegativity becomes

$$X_{tot} = a\sum_{\ell=0}^{2} X_\ell + b\ . \tag{6}$$

The constants a and b are chosen so that X_{tot} reproduces Paulings' values[29] for first row elements. Having done this, the resulting electronegativities obtained for all but the transitions metals lie between the Pauling and Phillips[30] scales - agreeing when these two scales agree and providing a compromise when they do not. St. John and Bloch took as a second parameter a measure of the relative role of s and p bonding with the fraction

$$S \equiv (X_o - X_1)/X_o \tag{7}$$

Using this and X_{tot}, they obtained the map of the structures of the non-transition elements displayed in Fig. 10. It has been recognized for some time that the more electronegative elements tend to form covalent structures while the most electropositive such as the alkali metals tend to be bcc. Introduction of S allows one to differentiate between hcp, fcc and covalent structures for the elements of intermediate electronegativity. A similar mapping is seen in Fig. 11 for the so called octet compounds - fifty-fifty compounds with eight valence electrons per molecular unit. Here the independent parameters are the electronegativity <u>difference</u> and the <u>average</u> of the S values. Again boundaries can be drawn between regions apparently favoring different structures. By introducing ℓ dependent orbital electronegativities which are measures of an

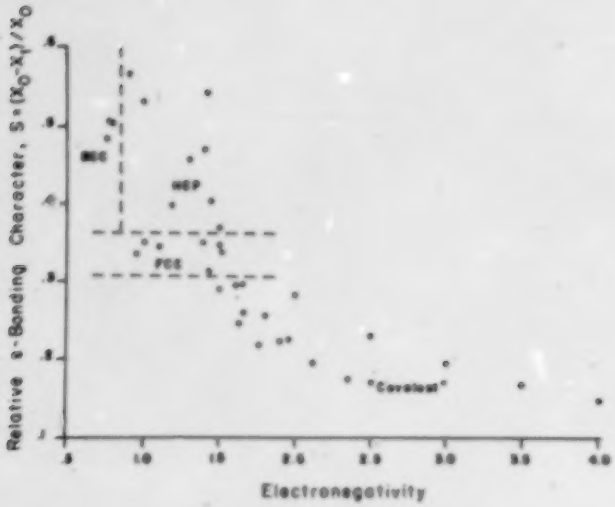

Fig. 10. Correlation of the structures of the non-transition metal elements with electronegativity and fraction of s characters in the bonding as obtained by St. John and Bloch[28].

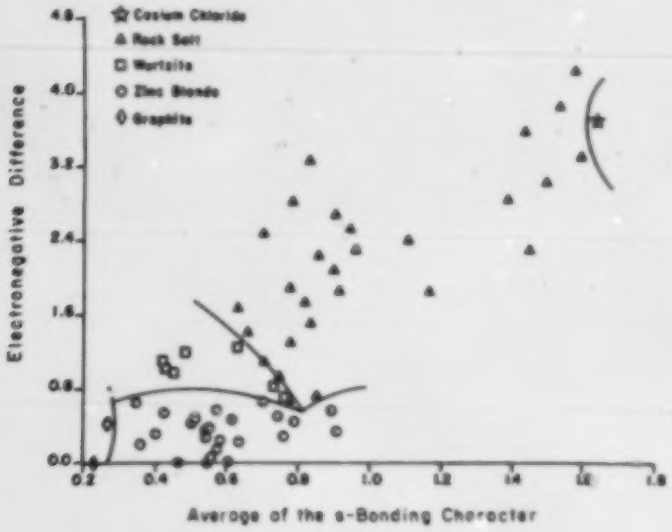

Fig. 11. Mapping of the structures of the $A^N B^{8-N}$ "octet" compounds as a function of electronegativity difference and average s fraction of bonding as obtained by St. John and Bloch[28].

ℓ dependent pseudopotential, Simons, St. John and Bloch have provided a non-local potential description of bonding in those materials. Still needed is theoretical justification for the parameters used.

In the transition and noble metals changes in d, and non-d electron counts, denoted respectively by Δn_d and Δn_{cond}, tend to oppose one another upon alloying. The Mössbauer isomer shift[31], which measures the charge density at the nucleus, indicates that as much as one non-d conduction electron's worth of charge flows on or off the site of a given atom upon alloying. The flow is always onto the site in the case of Au. However, adding dilute amounts of Ag to Au causes the Au 5d bands to drop relative to the Fermi level as is evident from the more silvery color of the alloy. A lowering of the d bands implies a more attractive potential and hence charge flow off the site, opposite to the isomer shift result. The picture which has emerged[32] is that the occupied d bands of Au, which lie beneath the Fermi level, are hybridized with electron states belonging to the other constituent of the alloy causing a reduction (a negative Δn_d) of the 5d count in the bands. This is more than compensation by a flow of non-d charge onto the Au site (a positive Δn_{cond}) producing a small net negative charge on that site. The d electrons, being more, make a larger repulsive coulomb contributions to the potential. Therefore, a decrease in the d count causes a drop in core level and d band energies. While Au has filled d bands and is electronegative, a transition metal such as Ti has almost empty d bands and is electropositive. Hybridization fills empty d levels causing Δn_d to be positive. The counterflow of conduction electron charge leads to a depletion of charge at the site.

A recent analysis[33] of the available isomer shift data for various transition metals suggests that not only is the ratio $\Delta n_d / \Delta n_{cond}$ negative but that to a remarkable degree it is a constant independent of the transition metal impurity in question or of the other constitutents in the alloy host.

Machlin has recently incorporated[34] electronegativity effects

into the traditional pair potential approach to alloying. He took an interaction potential of the form

$$V(r_{ij}) = \frac{-A}{r_{ij}^{4}} + \frac{B}{r_{ij}^{8}} \qquad (8)$$

where r_{ij} is the distance between an atom pair. The powers of r_{ij} were chosen somewhat arbitarily: fractional powers would have done a bit better. Such an interaction potential can be related to pseudopotentials, at least for simple metals, and in turn to such parameters as atomic size. Machlin obtained the parameters A and B by fitting to lattice constants and cohesive energies of the pure elements. By assuming that the atomic radius scales with the valence electron screening distance of the ion core and, in turn, employing Gordy and Thomas's view of electronegativity which was related to such screening, Machlin was able to introduce the effect of charge transfer on A and B. In doing this he used enlightened empiricism: if the scheme introduced a systematic error in the prediction of lattice constants for some class of compounds, the electronegativity contribution would be scaled to bring the lattice constants into line. Phase stability problems were considered after this. In regard, for example[34], to the competition of the A15 and Ll_2 structures for compounds such as Nb_3Sn, the scheme predicted the stable phase correctly in 66 out of 73 cases considered. In subsequent consideration of competition between the A15 and A2 structures it correctly predicted the A2 structure for V_3Al and the A15 for the 21 other compounds considered. The scheme is more precise in its predictions than say, Miedema's. It should be, since the input information is more detailed. Whatever its success or failure there are arguments against its applicability to transition metals. As pointed out in Section II, Friedel and Ducastelle have noted[4,5] that the d-band broadening contribution to transition metal cohesion, after the manner of Figs. 2 and 3, does not arise from a sum of atom-atom pair interaction terms (it is something more like the square root of a sum of squares). Moreover Krause has recently argued[35] that a two-body interaction potential description of the phonons of the noble metals implies that the fcc structure is unstable with respect to a sliding of [111] planes and the hcp structure is favored. Higher order interaction terms appear

in schemes such as that of de Fontaine discussed elsewhere in these proceedings. Such terms are quite small numerically but crucial to his predictions.

V. Charge and Volume

One question which has not been dealt with is the preference for a alloy to form an ordered versus a disordered structure. Perturbation theories exist which should be useful for such a question. The stumbling block is the Madelung term associated with the ordered phase. It requires an assignment of charge to the constituent atoms. One way to assign charge is to integrate the charge density over the volume of an atomic site but this, then, requires the definition of the atomic volumes. Unfortunately there is[36] no universally accepted and useful way to define atomic charge and volume. Lacking this, the order-disorder problem becomes difficult.

Consider the case of V_3Si for which Staudemmann, Coppens and Muller[37] obtained the electron distribution from x-ray diffraction data. Given data throughout the unit cell one can infer the charge associated with V or Si sites as a function of their relative size as is done in Fig. 12. A physically plausible definition of the boundary region, between sites is where the valence charge is a minimum. This would correspond to a flat in the integrated density plot. Staudenmann et al. concluded that the structure in the region $R_V/R_{Si} \sim 1.6$ corresponds to such a flattening and therefore to a compound consisting of roughly $Si^{+2.1}$ and $V^{-0.7}$ sites. Although these charges involve flow opposite to conventional electronegativity assignments, the difference in electronegativity between Si and V is not large and changes in the Si electronegativity associated with a metallic environment might well lead to the deduced direction of charge flow. On the other hand, the metallic radii[38] of Teatum, Waber and Geschneidner place R_V/R_{Si} at 1.02 and at this ratio V and Si have their atomic valence charge density, i.e. they are neutral. Two reasonable choices of atomic size yield two very different conclusions concerning charging in this system.

It should be noted that ionic charges of $\pm$ 0.1e correspond to Madelung terms of 5-10 kcal/mole. Charging of at least $\pm$ 0.1e is typically inferred from many experimental results. In 1936 Mott showed that a Madelung energy with an effective charge of 0.06e accounts for the order-disorder transition of brass. The situation is particularly difficult for refractory hard metals such as WC. It is generally agreed that these materials have covalent

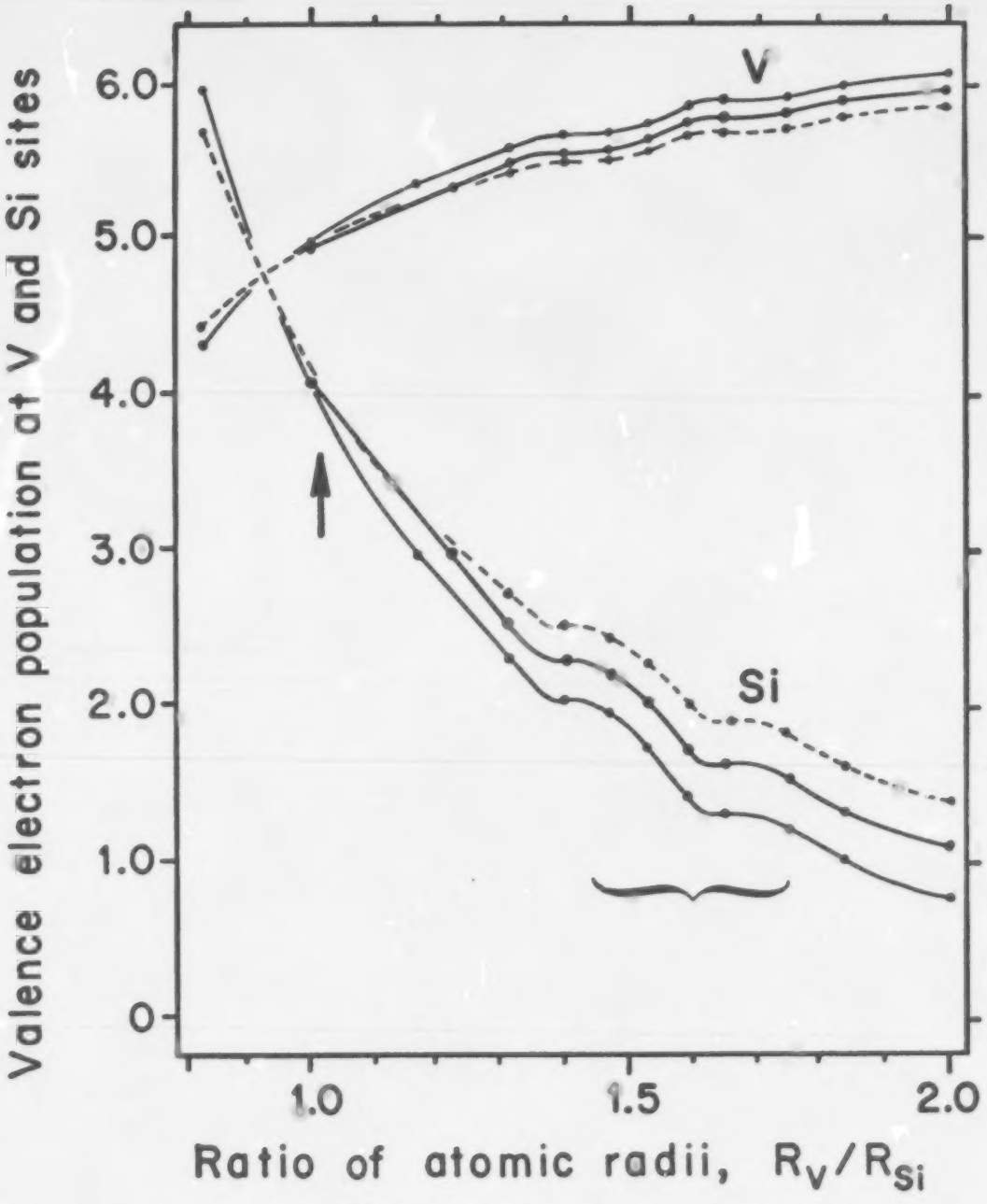

Fig. 12. V and Si site charge in V_3Si as a function of the ratio of V to Si atomic radii[37]. The spread is associated with various estimates of x-ray extinction coefficients. The bracket marks the region of flattening cited in text, where the boundary between atoms corresponds to some minimum in the average valence electron density. This leads one to infer substantial charging of atomic sites. The arrow at ~1.0 marks the ratio appropriate to a standard choice of atomic radii[38]: there is little or no charging of the V and Si sites with this definition of site volumes.

and metallic bonding character and it is often argued that there is significant ionic charging as well but there is no general agreement as to the direction in which that charge flows.

VI. Band Theory

The technology of doing energy band calculations has advanced substantially in recent years. Self-consistent results for pure elements and compounds are becoming commonplace as are results for disordered systems where the energy levels have widths associated with finite lifetimes. Wave functions as well as eigenvalues are being obtained and aspherical terms are sometimes incorporated into the potentials. Total energies, however, are not easy to obtain to the accuracy relevent for the purposes of the present meeting. Bank theory results are nevertheless very useful in understanding why certain effects occur.

Switendick, for example, has considered[39] hydrogen solubility in Ni, Pd and Pt. Pd readily accepts H whereas Pt does not. Switendick has shown that hydrogen solubility in these metals correlates with the presence of d states, above the Fermi level in the pure metal, which have s-like symmetry at the interstitial hydrogen site. Not only are these states available for filling upon addition of a proton into the lattice but the presence of the proton lowers their energy causing them to lie deep in the d-bands.

Gelatt, Weiss and Ehrenreich[40] have employed band theory in estimates of the heats of formation of 3d and 4d transition metal hydrides. The principal ingredients are (1) the formation of a metal-hydrogen bonding band; (2) the lowering of the d bands due to the presence of the proton and (3) the binding of the extra electron associates with the H atom.

Band structure information can also provide insights into distorted structures or into martensite transitions leading to distorted structures. Often an undistorted structure has degenerate, partially filled levels at the Fermi level. A distortion which splits the degeneracy can often be stabilized by the energy lowering of the one set of sublevels. Switendick has discussed[41] the Ti-V-H phase diagram in such terms.

VII. Other Matters

There are a variety of activities which, as a matter of record, deserve mention in this talk. We will close by citing two.

There has been a beautiful series of work by Wagner and Horner at Jülich concerned with dilute hydrogen in metals[42]. At dilute concentrations the hydrogens interact via strain fields which are long ranged. Classical theory works in such a case and results depend on the shape of the host on a macroscopic scale.

Finally, an area of major activity[43] in statistical mechanics has been second order phase transitions and critical points. Whether it be a structural, a superfluid or a magnetic transition, the order parameters involved display universal temperature dependences in the vicinity of the transition temperature. While much work has been done on the tricritical point in the helium system, it is relevant to tricritical points in other phase diagrams including the metal hydrides. Some of the most vigorous intellectual activity in solid-state physics and chemistry is in this area. In contrast, the theory of first-order phase transitions is in poor shape.

In this superficial survey we have tried to give a physicist's view of some of the things that work in metallurgy, of some of the pertinent activities in solid-state theory, and of some of the secrets that we hide.

DISCUSSION

Question - One must introduce temperature dependence. This is a profound problem.

R. Watson - Sorry! I should at the onset have admitted that I was going to legislate entropy out of existence for the purpose of my talk among a variety of other subjects. (Something else I would have liked to discuss are the, what we call, glassy systems. I'm thinking of the transition metal glasses). There are included some efforts but they are an order of two magnitudes more rudimentary in nature. Some solid state theorists do admit temperature exists, in a variety of ways. But for instance a mariage of say some pseudopotentials predictions with a temperture dependence, this type of technology has not yet arrived in a comfortable way.

F. Carter - Many years ago Pauling freely mixed s-p-d orbitals, and physicsts at the time said that was wrong. Now they agree that s and d ought to be mixed. What has happened to the p-orbitals? How well do they fit into the renormalization scheme?

R. Watson - In transition metals the p's where always there. They where higher up. In a continuum band picture, you went from pure s-character at the bottom of the band to something which went smoothly into p- character. In fact, when you are interested in the noble metals, it is worth putting a p level on that plot as well, because there are symmetry points in the zone of high p character. For instance, this becomes important in the question of why silver is different from copper or gold. It's the s-d-p separation, that counts if you're dealing with a noble metal. So, when I said s, it was s-p.

Footnotes

*Supported by U. S. Energy Research and Development Administration.
†Supported in part by the National Science Foundation.

(1) G. V. Samsonov, Science of Sintering 8, 5 (1976).

(2) G. D. Gelatt Jr., H. Ehrenreich, R. E. Watson, Phys. Rev. B15, 1613 (1977).

(3) E. P. Wigner and F. Seitz, Solid St. Phys. 1, 97 (1955).

(4) J. Friedel, Physics of Metals I, J. M. Ziman, Ed., (Cambridge Univ. Press, 1969) and F. Ducastelle and F. Cyrot - Lackmann J. Phys. Chem. Sol. 32, 285 (1971).

(5) F. Ducastelle, J. Physique 31, 1055 (1970).

(6) W. Hume-Rothery, Progress in Materials Science, 13, 5, "The Engel-Brewer Theories of Metals and Alloys", 1967. L. Brewer, in "High-Strength Materials", edited by V. F. Zackay, (Wiley, New York, 1965), pp. 12-103. L. Brewer, in Phase Stability in Metals and Alloys, edited by P. Rudman, J. Stringer, and R. I. Jaffee, (McGraw-Hill), New York, 1967), pp. 39-61, 241-9, 344-6, and 560-8. L. Brewer, Science, 161, 115 (1968). N. N. Engel, "Alloy Phase Stability Criteria", Developments in the Structural Chemistry of Alloy Phases, edited by B. C. Giessen, (Plenum Press, New York, 1969) pp. 25-40.

(7) D. G. Pettifor, J. Phys. C 3, 367 (1970).

(8) e.g., See M. Shiga, AIP Conf. Proc. 18, 463 (1974).

(9) U. K. Poulsen, J. Kollar and O. K. Andersen, J. Phys. F. 6, L241 (1976).

(10) J. F. Janak and A. R. Williams, Phys. Rev. B14, 4199 (1976).

(11) P. Soven, Phys. Rev. 156, 809 (1967); B. Velicky; S. Kirkpatrick and H. Ehrenreich, Phys. Rev. 175, 747, (1968), and H. Fukuyama, H. Krakauer and L. Schwartz, Phys. Rev., B10, 1173 (1974).

(12) J. van der Rest, F. Gautier and F. Brouers, J. Phys. F. 5, 2283 (1975).

(13) F. Gautier, J. van der Rest and F. Brouers, J. Phys. F. 5, 1884 (1975), and M. Cyrot and F. Cyrot-Lackmann, J. Phys. F. 6, 2257 (1967.

(14) L. Kaufman and H. Bernstein, Computer Calculation of Phase Diagrams, (Academic Press, New York, 1970) p. 89-90.

(15) J. C. Slater, Phys. Rev. 81, 385 (1951).

(16) P. Hohenberg and W. Kohn, Phys. Rev. 136, B864 (1964); W. Kohn and L. Sham, Phys. Rev. 140, A1333 (1965) and L. Sham and W. Kohn, Phys. Rev. 145, 561 (1966).

(17) L. Hedin and B. I. Lundqvist, J. Phys. C. 4, 2064 (1971).

(18) U. von Barth and L. Hedin, J. Phys. C. 5, 1629 (1972).

(19) J. P. Walter and M. L. Cohen, Phys. Rev. B4, 1877 (1971).

(20) Y. W. Yang and P. Coppens, Sol. St. Comm. 15, 1555 (1974).

(21) J. R. Chelikowsky and M. L. Cohen, Phys. Rev. Letters 33, 1339 (1974).

(22) W. A. Harrison, "Pseudopotentials in the Theory of Metals", W. A. Benjamin, New York, 1966.

(23) D. Stroud and N. W. Ashcroft, J. Phys. F. 1, 113 (1971).

(24) L. A. Girifalco, Acta Met. 24, 759 (1976).

(25) G. M. Rooney, A. L. Kipling, B. A. Lambos, J. Phys. Chem. Sol. 36, 677 (1975).

(26) A. R. Miedema, F. R. de Boer and P. de Chatel, J. Phys. F 3, 1558 (1973); A. R. Miedema, J. Less Common Met. 32, 117 (1973); A. R. Miedema, R. Boom and F. R. de Boer, J. Less Common Met. 41, 283 (1975) and 46, 54 (1976) and A. R. Miedema, J. Less Common Met. 46, 67 (1976).

(27) N. D. Lang and W. Kohn, Phys. Res. B3, 1215 (1971).

(28) J. St. John and A. N. Bloch, Phys. Rev. Let. 33, 1095 (1974) and references therein.

(29) L. Pauling, The Nature of the Chemical Bond (Cornell Univ. Press, Ithaca, NY (1960) 3rd ed.

(30) J. C. Phillips, Phys. Rev. Let. 20, 550 (1968).

(31) e.g. See N. N. Greenwood and T. C. Gibb, Mössbauer Spectroscopy (Chapman and Hall, London 1971).

618

(32) R. E. Watson, J. Hudis and M. L. Perlman, Phys. Rev. B4, 4139 (1971); R. M. Friedman, J. Hudis, M. L. Perlman and R. E. Watson, Phys. Rev. B 2433 (1973); C. D. Gelatt, Jr., and H. Ehrenreich, Phys. Rev. B10, 398 (1974), and T. S. Chou, M. L. Perlman and R. E. Watson, Phys. Rev. B14, 3248 (1976).

(33) R. E. Watson and L. H. Bennett, Phys. Rev. B15, 502 (1977).

(34) E. S. Machlin, Acta Met. 22, 95 (1974); Machlin, Acta Met. 22, 109 (1974), and E. S. Machlin and S. H. Whang, J. Phys. Chem. Sol. 37, 555 (1976).

(35) C. W. Krause, Phys. Let. 57A, 390 (1976).

(36) R. E. Watson and L. H. Bennett, Charge Transfer in Alloys: The Blind Men and the Elephant, Charge Transfer/Electronic Structure of Alloys, L. H. Bennett and R. H. Willens, ed. (Metallurgical Society of the American Institute of Mining, Metallurgical, and Petroleum Engineers, 1973).

(37) J. L. Staudenmann, P. Coppens and J. Muller, Sol. St. Comm. 19, 29 (1976).

(38) E. T. Teatum, K. A. Gschneidner, Jr. and J. T. Waber, Los Alamos Report LA-4003 (1968) unpublished.

(39) A. C. Switendick, Proc. Hydrogen Economy Miami Energy Conf., Coral Gables, Florida, paper S6-1 (1974).

(40) C. D. Gelatt, Jr., J. A. Weiss and H. Ehrenreich, Solid State Comm. 17, 663 (1975).

(41) A. C. Switendick, J. Less Common Metals 49, 283 (1976).

(42) H. Wagner and H. Horner, Advances in Phys. 23, 587 (1974).

(43) e.g. D. P. Landau, Mag. and Mag. Mat'ls-76, AIP Conf. Proc. 34, 373 (1976) and the series Phase Transitions and Critical Phenomena, ed. C. Domb and M. S. Green (Academic Press, NY) vols. 1-6.

PANEL I

COMPUTATION AND PREDICTION OF PHASE DIAGRAMS

(Methods of Phase Diagram Calculations)

Moderator: O. J. Kleppa, The James Franck Institute, University of Chicago, Chicago, IL

Panel Members:

L. Brewer, Inorganic Materials Research Div., Lawrence Berkeley Laboratories, University of CA, Berkeley, CA

D. de Fontaine, Materials Dept., University of CA, Los Angeles, CA

R. L. Dreshfield, Materials Processing and Joining Section, NASA Lewis Research Center, Cleveland, OH

B. C. Giessen, Dept. of Chemistry and Mechanical Engineering, Northeastern University Boston, MA

L. Kaufman, ManLabs, Inc., Cambridge, MA

A. Navrotsky, Chemistry Dept., Arizona State University, Tempe, AZ

Several of these panel members' texts appear in the poster session "Computational Techniques in Phase Diagram Construction", where there were further presentations by these authors. General remarks follow Dr. Dreshfield's paper, on p. 659.

National Bureau of Standards SP-496, Applications of Phase Diagrams in Metallurgy and Ceramics
Proceedings of Workshop held at NBS, Gaithersburg, Md., January 10-12, 1977

ESTIMATION OF CONJUGATE γ AND γ' COMPOSITIONS IN Ni-BASE SUPERALLOYS

by Robert L. Dreshfield

Lewis Research Center

ABSTRACT

To control the formation of unwanted phases, superalloy metallurgists have developed methods of estimating the composition of the matrix phase of alloys. That composition is then used to estimate the alloy's propensity toward sigma and other unwanted phase formations upon prolonged exposure to elevated temperatures in service. This paper reviews two approaches for estimating phase composition from the melt composition. One method is based on assigning essentially fixed stoichiometry to precipitating phases and is typified by "PHACOMP." The second method uses analytical geometry to interpret phase diagrams and is shown to be applicable to a two-phase region of a six-component Ni-base system. The geometric method is also shown to be applicable to commercial Ni-base superalloys.

INTRODUCTION

The nickel-base superalloys used in the hot section of gas turbines have been developed to the point where they have useful strength at approximately 80 percent of their melting point (ref. 1). Over 50 such alloys are commercially available.

Typical nickel-base superalloy contain nickel, aluminum, chromium, titanium, zirconium, carbon, and boron. In addition molybdenum, tungsten, niobium, tantalum, hafnium and other reactive or refractory metals may be added to the melt. The two major phases in the alloys are a face centered cubic matrix, γ, and a dispersed, usually coherent, ordered face centered cubic phase, γ'. Small amounts of carbides and borides (usually <3 percent) and other intermetallic compounds are frequently

651

present and are responsible for profound changes in mechanical properties. These alloys are clearly described as multicomponent-multiphase alloys typically containing 6 to 13 intentionally added alloy elements and three to five phases.

Since the sigma phase instability was identified in Ni-base superalloys (ref. 2) and the presence of sigma was correlated with a loss of stress rupture life (refs. 3 to 6), the superalloy industry has sought methods to prevent or minimize its occurrence in the alloys. This paper deals with two approaches which have been offered to control the melt compositions to minimize the occurrence of sigma and other undesirable phases in superalloys. The first approach, as exemplified by "PHACOMP" (ref. 7) and the method of reference 8 uses a chemical stoichiometric calculation to estimate the composition of the γ phase. The propensity of the alloy toward phase instability is then determined by calculating the average electron vacancy concentration ($\overline{N}_v$) of the γ. The second approach is to estimate the composition of the conjugate phases (γ and γ') by applying analytical geometry to existing phase diagrams (refs. 9 to 11). The analysis is continued to determine if the melt composition is likely to fall in a phase field containing unwanted phases. In both methods, an attempt is made to estimate the composition of at least one of the conjugate phases (usually γ) from the melt composition.

This paper will review the stoichiometric and geometric approaches for estimating the compositions of conjugate phases in superalloys. It will also show that the geometric approach can be used to develop a description of a two-phase region of a six-component system and show that the description of the six-component system can be applied to commercial Ni-base superalloys.

STOICHIOMETRIC APPROACH

Methodology. - The first efforts to control sigma phase in superalloys were those of Boesch and Slaney (ref. 8) and Woodyatt and coworkers (ref. 7). These methods made use of a two step computation. In the first

step the melt composition was used to calculate a "residual matrix" or γ-phase composition. In the second, the $\bar{N}_v$ of the γ was compared to an empirically determined value to estimate the propensity of the alloy to form unwanted phases. The procedure is exemplified by the method described in reference 12 which follows:

A. Calculate γ matrix composition in atomic percent:

1. Calculate composition of carbides and borides as follows:

a. Half the carbon forms mono-carbides in the sequence TaC, NbC, ZrC, TiC, and VC.

b. Half the carbon forms either $Cr_{23}C_6$ or $Cr_{21}(Mo, W_2)C_6$ if Mo or W are present. If Mo + W is greater than 6 weight percent, $[NiCo_2(Mo, W)_3]C$ forms instead of $M_{23}C_6$.

c. A boride, $(Mo_{0.5}Ti_{0.15}Cr_{0.25}Ni_{0.10})_3 B_2$ forms.

d. All of the Al, Ti, and Nb remaining following formation of carbides and borides plus 3 percent of the melt's Cr form γ' of the stoichiometry $Ni_3(Al, Ti, Nb, Cr)$. If there is insufficient Ni, β will also form having a stoichiometry Ni(Al, Ti, Nb, Cr).

e. The residual γ matrix resulting from subtracting the amount of compounds in (a) to (d) is scaled to 100 percent.

B. The $\bar{N}_v$ of the residual γ matrix is calculated by

$$\bar{N}_v = \sum_{i=1}^{n} f_i (N_v)_i \qquad (1)$$

where

f_i atomic fraction of the nth element

$(N_v)_i$ 4.66 for Cv, Mo, W; 3.66 for Mn; 2.22 for Fe; 1.61 for Co 0.61 for Ni

($(N_v)_i$ may be taken as 10.66 - group number if no value is known.) If $\bar{N}_v$ is approximately 2.45 or greater the alloy is prone to form σ or other undesirable phases.

Discussion. - This method has been successfully used to control the melt composition of several commercial superalloys (ref. 12). While it would be interesting to review all the additional work in this area, it is considered beyond the scope of this paper and interested readers are referred to references 12 to 17. To summarize the additional work, it should be noted that much of it has been directed at finding a universal critical $\overline{N}_v$, that is, a value of $\overline{N}_v$ appropriate to all alloys or toward finding a systematic method of defining the critical $\overline{N}_v$ for a particular melt. It has been proposed that for some elements N_v be altered and that the γ' composition be altered from those first proposed. No method has been successful in finding a γ' composition and a series of elements' N_vs which can properly estimate σ and other instabilities at a single value of $\overline{N}_v$ for all alloys.

It should be noted that the methods which rely on a nearly fixed γ' stoichiometry necessarily assume that no Al, Ti, Nb (and perhaps other γ' formers), C and B are soluble in the γ. Mihalisin and Pasquine (ref. 17) suggested that this treatment of γ' was in error and could account for problems observed in predicting the stabilities of alloy 713C and alloy 713LC. They suggested that actual chemical analysis of the γ' phase be made and that a mass balance, also using the measured volume fraction of γ', be used to calculate the residual γ matrix composition. The propensity toward forming σ phase of that γ was estimated in a manner similar to that described earlier for PHACOMP in that the $\overline{N}_v$ was calculated and compared to an empirically selected value. The presence of significant Al in the γ was also noted in reference 18 for Udimet 700. While the method of reference 17 is likely to better estimate the γ composition than PHACOMP, it suffers from the need for preparing a melt from which the γ' can be analyzed. Therefore the method of reference 17 is of reduced value in alloy development programs.

654

GEOMETRIC APPROACH

The Ni-Al-Ti-Cr System at 750° C

Background. - The work of Kriege and Baris (ref. 19) confirmed the presence of significant Al and Ti in the γ phase of 15 commercial Ni-base superalloys. Further, their work showed, while γ' was nearly stoichiometric, that variations in its compositions occur which could affect a PHACOMP calculation.

In an effort to avoid reliance on a fixed or predictable γ' composition to predict γ composition, references 9 to 11 used analytic geometry to interpret the Ni-Al-Ti-Cr phase diagrams of Taylor and co-workers (refs. 20 to 23). The problem addressed that of finding the composition of the γ phase, given the melt composition and assuming the melt lies in the two-phase ($\gamma + \gamma'$) field. The approach was to find the intersection of the tie line on which the two-phase alloy lies and the $\gamma - \gamma'$ solvus surface (the locus of γ compositions saturated with respect to γ').

Methodology. - As a first step the $\gamma - \gamma'$ solvus surface of the Ni-Al-Ti at 750° C was curve fit using the method of least squares. This equation was then altered to fit the Ni-Al-Ti-Cr $\gamma - \gamma'$ solvus resulting in the equation

$$Al + 1.5Ti = 1.33Cr^2 - 0.566Cr + 0.12 \qquad (2)$$

That equation (2) is a good simulation of the $\gamma - \gamma'$ solvus at low Ti concentrations can be seen in figure 1 by comparing the solid lines surface (eq. (2)) and the double-dashed line from reference 23.

The next step was to deduce the tie line behavior in the alloy systems. Fortunately, Taylor and Floyd showed some tie lines in their ternary diagrams in references 20 to 22. The tie line system in the four component systems has to include the tie lines of the three component systems as a limit and further, the tie lines in the four component systems must not intersect each other in the two-phase field. The details of the system proposed are described in references 10 and 11. The procedure will now be briefly reviewed for the Ni-Al-Ti-Cr system at 750° C. Three assumptions are made to allow a closed form solution:

1. Assume that for the system Ni-Cr-Al tie lines (for $\gamma + \gamma'$) intersect at (Ni, 0.25Al) (fig. 2).

2. Assume that for the system Ni-Cr-Ti that η and γ' are mutually soluble and tie lines intersect at (Ni, 0.25Ti) (fig. 3).

3. Assume that for the system Ni-Al-Ti that $\gamma + \gamma'$ tie lines intersect at (Ni, -0.05Al) (fig. 4). (Also shown as point S in fig. 1.)

In the specific construction to be used, a tie line is formed by the intersection of two planes. One plane has a zone axis (for this paper defined as a line common to all planes in the set) from the Cr corner to point S in figure 1. The other plane has line U-V as a zone axis (fig. 1). The Al to Ti to Ni ratio of the alloy governs the selection of the plane from the Cr-S set and the Cr concentration selects the plane from the U-V set.

Because U-V and Cr-S are zone axes for the two planes determining the tie line, the only places where the tie line families can intersect are on U-V or Cr-S. Both of these lines are outside of the two-phase field; therefore, Gibbs' phase rule is followed.

The details of the construction by which the composition of the γ phase in a two-phase quaternary alloy is determined from the above analysis follows. In figure 1 the composition of the two-phase quaternary alloy is projected on the Ni-Al-Ti diagram by passing a line from the Cr corner of the quaternary, through the two-phase alloy A to the Ni-Al-Ti ternary. This construction locates a point T in the ternary diagram that has the same relative Ni, Al, and Ti concentration as in the quaternary alloy. This is shown as line Cr-A-T. The intersection of U-V (the line connecting 0.25Al, 0.75Ni, and 0.25Ti, 0.75Ni) and T-S (the tie line in the Ni-Al-Ti ternary) established point X on the tie line (containing the two-phase quaternary alloy A). The tie line on which alloy A lies is X-A-G. The composition of G (γ phase) is determined by finding the intersection of X-A with the solvus surface.

The mathematics of this treatment can be followed in reference 10 or 11. The approach was adapted to commercial superalloys by using a stoichiometric approach to account for carbides, borides, and γ' formed by Nb, Ta, Zr, and V. The Mo and W in γ were treated by analogy to Cr. Comparison of γ predicted by the geometric method for the

alloys in Table I and that determined by references 18 and 19 are shown in Table II. Note that both Co and Ti were in error by a constant amount and factor, respectively.

Discussion. - While the application of the procedure to commercial alloys was encouraging, it required some extra assumptions. It was felt that the general techniques of using analytic geometry to interpret two-phase regions of multicomponent phase diagrams had been demonstrated.

The Ni-Al-Cr-Ti-W-Mo System at 850° C

Background. - Analysis of the work of references 10 and 11 suggested that a better superalloy phase diagram could be developed by including W and Mo directly in the system's phase diagram. Further, it was clear from references 10 and 11 that to predict conjugate phase compositions it was not necessary to graph a phase diagram, only to describe its significant features by mathematical expressions. These ideas from references 10 and 11 coupled with a quantitative analytical procedure for γ' (ref. 19) encouraged the author to initiate a study to determine the compositional limits of γ and γ' in the Ni-Al-Cr-Ti-W-Mo system at 850° C (refs. 24 and 25). The temperature of 850° C was selected as it was thought to be near the temperature at which σ and related phases precipitate rapidly (refs. 4 to 6).

Experimental approach. - The experimental details of the study are available in reference 25. They will only be summarized here. After checking two preliminary alloys, a series of melts were made, the compositions of which were based on a fraction of a three-level factorial design (ref. 26). The experimental design is shown in Table III. The compositions of the two-phase alloys melted are shown in Table IV. The alloys were homogenized for 4 hours at 1190° C and air cooled to room temperature. They were heated at 850° C for 1008 hours before being air cooled to room temperature. The γ' was quantitatively extracted from the heat treated two-phase alloys using the method of reference 19. After the γ' residues and the alloys were chemically analyzed, the composition of γ was calculated by a mass balance.

This experimental approach allowed the determination of the conjugate γ and γ' compositions with a single melt. The solvus hypersur-

faces were then described by fitting a third degree equation to the γ and γ' compositions using linear regression analysis (ref. 27).

The average composition and amount of γ' are shown in Table V. The range of composition is consistent with that of other investigations (refs. 17 to 19, and 28 to 30). Also shown in Table V is the sample standard deviation (S) for each element except Ni. The value of S is less than one-third the range of each element observed which suggests the spread in observed compositions is significant when compared to analytical errors.

The average composition of γ is shown in Table VI. The sample standard deviation (S), also shown in Table VI for each element can be seen to be less than one-third the range of each element, again suggesting that the observed spread is greater than would be expected from experimental errors. The range of γ compositions is consistent with the ranges observed in other work (refs. 17 to 19, and 28 to 30).

Gamma-gamma prime relationship. - The compositions of the γ in Table VI and γ' shown in Table V are compositions of the phases from two-phase alloys. These compositions, therefore, represent points on the solvus hypersurfaces, and when considered in pairs (one γ and one γ') from a heat, these are, in fact, the compositions of conjugate phases.

To obtain a more useful description of these solvus hypersurfaces, the data points from each extraction were fitted with curves using a multiple linear regression computer program (ref. 27). The model equation used to fit both sets of data was:

$$\begin{aligned} Al = {} & B_0 + B_1 \times Cr + B_2 \times Mo + B_3 \times Ti + B_4 \times W \\ & + B_5 \times Cr^2 + B_6 \times Mo^2 + B_7 \times Ti^2 + B_8 \times W^2 \times W \\ & + B_9 \times Cr \times Mo + B_{10} \times Cr \times Ti + B_{11} \times Cr \\ & + B_{12} \times Mo \times Ti + B_{13} \times Mo \times W + B_{14} \times Ti \times W \\ & + B_{15} \times Cr \times Mo \times Ti + B_{16} \times Cr \times Mo \times W \\ & + B_{17} \times Cr \times Ti \times W + B_{18} \times Mo \times Ti \times W + error \end{aligned} \qquad (3)$$

where Al, Cr, Mo, Ti, and W are in atomic percent, B_0 is a constant, and $B_1, B_2, \ldots, B_{18}$ are coefficients.

For both solvus hypersurfaces, the regression program rejected coefficients with less than a 25-percent significance level. The low significance level was chosen because it is recognized that the independent variables have errors associated with them. Although it is desirable to simplify the equations, the regression analysis assumption that the independent variables are known without error is violated. The low significance level is believed to avoid rejecting significant terms.

The constant and coefficients for both solvus equations are shown in Table VII. The multiple regression coefficient (R^2) for the γ is 0.89 and for the γ', R^2 is 0.87.

These two equations may be used to plot sections of the hypersurfaces or simply to estimate the amount of a particular element in a phase if four others are known. The usefulness of these equations could be increased if they could be used to estimate the compositions of conjugate phases, given the composition of a two-phase alloy.

The compositions obtained in this investigation for γ and γ' are the compositions of conjugate phases. Therefore a tie line is known to pass through the γ composition, the alloy composition and the γ' composition. Direction numbers for the tie lines were calculated by:

$$DN_i = \frac{I_\gamma - I_{\gamma'}}{Cr_\gamma - Cr_{\gamma'}} \qquad (4)$$

where

DN_i direction number for the ith element

I_γ composition of I in γ

$I_{\gamma'}$ composition of I in γ'

Cr_γ composition of Cr in γ

$Cr_{\gamma'}$ composition of Cr in γ'

These direction numbers for each element (Cr being 1) indicate the change in amount of the element along a tie line per unit change in Cr. These, in effect, describe the slope of the tie lines.

To determine the phase compositions from the alloy composition by using the tie lines, the direction number of the tie line needs to be known as a function of the composition of the alloy. The direction numbers were estimated from the alloy compositions by using a multiple linear regression program (ref. 27) to fit the direction numbers for Al, Mo, Ti, and W to equations of the form:

$$DN_i = B_0 + B_1 \times Al + B_2 \times Cr + B_3 \times Mo + B_4 \times Ti + B_5 \times W + error \qquad (5)$$

The full model was used since the uncertainties involved in rejecting terms of low significance seemed large when compared to the small gain obtained in simplifying these equations. The values of the constants and coefficients for these equations are summarized in Table VIII.

The two-phase region of this alloy system can now be described by using the equations for the solvus hypersurfaces and those which relate the direction numbers of the tie lines to the alloy chemistry. In principle, these equations could be solved simultaneously to find the composition of the γ and γ' for an alloy of known composition. This approach was not used because errors resulting from the least squares curve fitting were expected (and did) result in conditions where the tie lines fail to intersect the solvus hypersurfaces. Furthermore, because the solvuses are parabolic in shape, it is possible that two real and positive solutions exist.

The procedure used to find the compositions of the conjugate phases from the composition of a two-phase alloy is described below. It was programmed in FORTRAN IV for a time-sharing IBM 360 computer (ref. 25). First, the composition of the alloy is used to establish direction numbers for Al, Mo, Ti, and W by using the equations from Table VIII. Next, the alloy composition is changed by an increment of Cr and the new values for the other elements are calculated from the direction numbers. The composition is therefore still on the tie line. The new values of Cr, Mo, Ti, and W are used in the solvus equation to calculate the Al for the solvus, if the other four elements were as just estimated. This procedure is repeated until the Al compositions on the tie line and on the solvus agree to within 0.005 percent or until it is obvious

that no intersection will be found. If it appears that a second solution is likely, the procedure is repeated. If no intersection is located, the closest approach of the tie line to the solvus (as defined by the least difference in Al) is displayed as a solution.

To solve for γ composition, the Cr is increased from the alloy composition. To solve for the γ' composition, the Cr is decreased from the alloy composition. The closest approach is taken as a solution if no intersection is found for γ when Al is 0 percent or Cr is 40 percent. The closest approach is used for γ' if Al is 30 percent or Cr is 0 percent. Where two intersections were found, the higher Cr solution for γ and the lower Cr solution for γ' appeared to be closer to the experimental values.

The results of this calculation for the two-phase experimental alloys are compared to the experimental results in Table IX. The experimental compositions and those calculated by the phase analysis procedure are in good agreement. Except for γ composition in two alloys (ref. 25) the agreement was excellent. It is assumed that the two exceptions were the result of accumulated error.

Occurrence of additional phases. - The primary purpose of the investigation reported in references 24 and 25 was to define the $\gamma + \gamma'$ region of the Ni-Al-Cr-Ti-W-Mo system. During the conduct of the investigation, 51 alloys were melted. Two alloys were determined to contain only γ, 27 alloys contained only γ and γ', and the remaining 22 alloys were multiphase alloys containing phases other than γ and γ'. This section will relate primarily to the latter group of multiphase alloys which contained from three to six identifiable phases.

The composition of the multiphase alloys and phases (other than γ and γ') present are listed in Table X. The phases observed were σ, μ, and two body centered cubic phases, one having a lattice constant (A_0) similar to Cr, the other having an A_0 similar to W and Mo. No alloy in Table X contains more than 74.5 percent Ni and only alloys 3 and 44 contain in excess of 70 percent Ni. When one converts the two-phase alloys of Table IV to atomic percent, it is seen that these alloys had greater than 65.5 percent Ni and all but two alloys had greater than 67 percent Ni. This compares well with the $\gamma - \sigma$ boundary of 62 to

64 percent Ni + Co reported in reference 31 and the γ - α boundary of 60 percent in reference 20, see figure 5.

While the alloy composition offers a quick check for stability it should be more revealing to examine the γ composition as in PHACOMP. Instead of using an N_v approach, however, a more direct treatment of the phase diagram is proposed here. Reference 31 shows that Mo and W are 1.75 times more potent than Cr in promoting σ formation. By using an analogy to the 67 percent Ni limit for two-phase alloys, it is suggested that the [Cr + 1.75(Mo + W)] for the γ should be less than 33 percent (100 - 67 percent). For the stable alloys in Table VI, only two (alloy 15 and alloy 37) have values of the function Cr + 1.75(Mo + W) which were greater than 33 percent. The maximum value was 36.1 for alloy 15. For the multiphase alloys, the γ composition could only be estimated by use of the computer program previously mentioned from reference 25. The lowest value of the function was 20.2 percent but only three alloys of 14 for which a computation could be made, had values less than 30 percent.

A third parameter which appears capable of assisting in the prediction of additional phases is the rate of change of Al with respect to Cr (Al direction number) along the $\gamma + \gamma'$ tie line. For the two-phase alloys, only two alloys had Al direction numbers which measured greater than -0.30, the maximum value being -0.22. For the multiphase alloys, the minimum value estimated from the computer program of reference 25 was -0.20. Eight of 22 alloys had values greater than 0.0.

The relationship of the direction number of a tie line to a phase boundary is shown in figure 5. The line Q-R is the boundary between a two-phase ($\gamma + \gamma'$) field and a three-phase (γ ' γ' + α) field. It can be seen in the $\gamma + \gamma'$ field as Cr increases from the Ni-Al binary to line Q-R, the Al direction number increases from negative ∞ to -0.74. While the difference between the experimental limit of about -0.30 does not compare too well with that predicted by the Ni-Al-Cr phase diagram, one can see that there is a basis for the concept.

The three parameters for estimating occurrence of multiphase alloys are shown in figure 6. They are shown schematically as a Venn diagram to imply that as more than one of the conditions is satisfied, the probability of occurrence of additional phases increases.

APPLICATION TO COMMERCIAL ALLOYS

Phase diagram. - The alloys studied in reference 19 are typical of current commercial Ni-base superalloys. The heat treatments for these alloys, except for Udimet 700, are typical of the condition in which the alloys may be placed in service. In addition to the six elements studied in the last investigation, the commercial alloys in reference 19 contain C and may have intentional additions of Co, Nb, Fe, Ta, and V. The compositions from reference 19 were used to determine whether the "phase diagram" could be applied to commercial alloys.

The compositions from reference 19 were first converted to atomic percent to test the "phase diagram." The composition was then adjusted for carbide formation by using the procedures suggested in reference 32. The adjusted composition was then treated as an alloy composition using the computer program described earlier. The procedure in effect treated all elements other than Al, Cr, Mo, Ti, and W as if they were Ni. This appears to be a reasonable assumption for Co and Fe, but Ta and Nb are shown in reference 19 to be γ' formers.

The results of these calculations of γ and γ' compositions are compared to the compositions reported in reference 19 in Table XI. The compositions of γ calculated compared well with those reported except for alloys IN 100, Mar M200, Nimonic 115 and Nicrotung. For the γ' compositions, only alloys Inconel X-750 and Unitemp AF 1753 failed to show good agreement between the calculated and observed values. For alloy Unitemp AF 1753, the estimating procedure reported the alloy composition for the γ composition. This can be considered to indicate the alloy to be single phase.

The "phase diagram" of this investigation is capable of describing one phase in all of the commercial alloys examined. Of the six phase analyses which were not in reasonable agreement, four were for the γ phase. This is probably because the γ' composition was directly determined in both this investigation and reference 19 and a greater undertainty should exist for the composition of the γ phase. The two alloys for which the γ' estimate was poor had the lowest weight fraction γ' of the alloys examined. Errors in estimating the tie line direction numbers would be expected to be magnified in the composition of the phase more

distant from the alloy composition because of a leverage effect.

The results of the above comparisons indicate that the techniques developed in this investigation should be capable of being adapted for use in commercial alloys. It appears that the discrepancies between the estimates based on the current work and reference 19 are partly the result of the fact that the alloys in reference 19 were heat treated for shorter times and at different temperatures than the current work. The other obvious source differences is that the current work made no attempt to account for additional elements, except as they enter into carbide reactions.

Additional phases. - The alloys of reference 19 were also used to test the applicability of the parameters related to formation of additional phases. The three parameters (Ni in alloy; Cr + 1.75(Mo + W) in γ; and Al direction number on the $\gamma + \gamma'$ tie line) were calculated using the data from reference 19. These parameters are shown in Table XII. Also shown in Table XII are the phases that Collins and Kortovich (ref. 15) observed in these alloys. (It should be noted that the composition of the alloys varied slightly between refs. 15 and 19.) Reference 19 did not report on the stability of the compositions.

While the phase boundary between the two-phase and multiphase alloys is not identical to that of reference 25, it can be seen that the three parameters show similar critical regions. Alloys with less than 67 percent Ni + Co + Fe were multiphase alloys. γ phase with Cr + 1.75(Mo + W) greater than 31.5 formed additional phases. While it is difficult to find a critical value for the Al direction number, the average value for alloys having a high propensity toward forming σ and μ is -0.44 while it is -0.55 for the stable alloys. The difference between the averages is significant at the 95 percent level.

The three parameters identified in reference 25 do appear to be appropriate in determining if commercial alloys are likely to form undesirable phases. The specific composition of IN 100, which is shown from reference 15 as a σ former in Table XII, may have been stable in reference 19. IN 100 is one of the alloys which may be stable or σ forming within its normal composition limits (refs. 3 to 6).

CONCLUDING REMARKS

A review of two methods of estimating conjugate phase compositions in Ni-base superalloys has been presented. Both methods had as an ultimate objective the estimation of a melt's propensity for forming unwanted phases such as σ.

One method as exemplified by PHACOMP uses the chemical stoichiometric approach. This method reduces from the melt composition the elements that are believed to precipitate and arrives at the residual matrix by difference. The stability of the alloy is determined by calculating the average electron vacancy concentration ($\overline{N}_v$) of the residual matrix and comparing that with an empirically determined critical $\overline{N}_v$.

The method has been successfully used as a quality control tool for several commercially produced alloys where the range of compositions is limited and the critical $\overline{N}_v$ was empirically determined. However, when used as a research tool, no single γ' composition or elemental $\overline{N}_v$ s could be found to allow one critical $\overline{N}_v$ for sigma formation. One reason for this problem is that γ' has been experimentally shown to have a variable stoichiometry and perhaps of greater significance is that γ' formers are soluble in γ in varying amounts.

It is believed that the stoichiometric approach also can be successfully used in systems where the precipitate is in essence a line compound (solvus independent of composition), has little solubility in the second phase, or is present in small amounts. This may be the case for the carbides and borides in the Ni-base superalloys.

The analytical geometric approach to estimating the composition of conjugate phases has been demonstrated for Ni-base alloys containing up to six components. The work reviewed here has shown that the two-phase region ($\gamma + \gamma'$) of the Ni-Al-Cr-Ti-W-Mo systems at 850° C can be satisfactorily modeled. If one is given a melt composition the composition of the conjugate γ and γ' can be determined from the model. Furthermore, I believe that the approach that was applied to a six-component Ni-base system can be used in either higher order Ni-base systems and in other alloy bases.

In developing the geometric approach for estimation of conjugate phase compositions, it was observed that the propensity toward formation

of additional phases could be estimated from parameters available from the geometric analysis. Specifically it was observed that the Ni in the alloy, the parameter Cr + 1.75(Mo + W) and the Al direction number along the $\gamma + \gamma'$ tie line, can be used to estimate the propensity of an alloy toward additional phase formation. All three parameters can be related to solvus curves on conventional phase diagrams. It is suggested that additional study in relating phase diagram parameters to solvus surfaces can further refine this approach and make it applicable to different alloy bases, higher order systems and perhaps three or four phase regions. For years the phase diagram literature has touched on mathematical modeling of systems; however, in practice the industry has settled for what it can draw on a plane sheet or model in three-dimensional space.

In closing, I would like to offer that the work reviewed here should encourage more work on multicomponent systems where the computer can allow interpretation of the modeled diagrams. This approach has been demonstrated here and its extension to commercial alloys has been indicated.

REFERENCES

1. Quigg, R. J. and Collins, H. E., Superalloy Development for Aircraft Gas Turbines, ASME Paper 69GT-7, Cleveland, Ohio (March 1968).
2. Wlodek, S. T., Trans. ASM 57 (1), 110 (1964).
3. Ross, E. W., J. Met. 19 (12), 12 (1967).
4. Dreshfield, R. L. and Ashbrook, R. L., NASA TN D-5185 (1969).
5. Dreshfield, R. L. and Ashbrook, R. L., NASA TN D-6015 (1970).
6. Dreshfield, R. L. and Ashbrook, R. L., NASA TN D-7654 (1974).
7. Woodyatt, L. R., Sims, C. T., and Beattie, H. J., Jr., Trans. AIME 236 (4), 519 (1966).
8. Boesch, W. J. and Slaney, J. S., Met. Prog. 86 (1), 109 (1964).
9. Dreshfield, R. L., NASA TM X-52530 (1969).

10. Dreshfield, R. L., NASA TN D-5783 (1970).

11. Dreshfield, R. L., Metall. Trans. 2 (5), 1341 (1971).

12. Sims, C. T., in The Superalloys, Sims, C. T. and Hagel, W. C., eds. (John Wiley & Sons, Inc., New York, N. Y., 1972), Chapter 9.

13. Barrows, R. G. and Newkirk, J. B., Metall. Trans. 3 (11), 2889 (1972).

14. Wallace, W., Nat. Res. Coun. Can. Q. Bull. No. 3, 1 (1974).

15. Collins, H. E. and Kortovich, C. S., J. Mater. 4 (1), 62 (1969).

16. Barrett, C. S., J. Inst. Met. 100, 65 (1972).

17. Mihalisin, J. R. and Pasquine, D. L., in International Symposium on Structural Stability in Superalloys (Metall. Soc. AIME, New York, N. Y., 1968), p. 134.

18. Kriege, O. H. and Sullivan, C. P., Trans. ASM 61 (2), 278 (1968).

19. Kriege, O. H. and Baris, J. M., Trans. ASM 62 (1), 195 (1969).

20. Taylor, A. and Floyd, R. W., J. Inst. Met. 81, 451 (1952-1953).

21. Taylor, A. and Floyd, R. W., J. Inst. Met. 80, 577 (1951-1952).

22. Taylor, A. and Floyd, R. W., J. Inst. Met. 81, 25 (1952-1953).

23. Taylor, A., Trans. AIME 206 (10), 1356 (1956).

24. Dreshfield, R. L. and Wallace, J. F., Metall. Trans. 5 (1), 71 (1974).

25. Dreshfield, R. L. and Wallace, J. F., The Effect of Alloying on Gamma and Gamma Prime in Nickel-Base Superalloys, Case Western Reserve Univ., 135 pages (May 1972); also NASA CR-120940.

26. Connor, W. S. and Zelen, M., Fractional Factorial Experiment Designs for Factors at Three Levels. National Bureau of Standards Applied Mathematics Series No. 54, 12 (May 1959).

27. Sidik, S. M., NASA TN D-6770 (1972).

28. Loomis, W. T., Freeman, J. W., and Sponseller, D. L., Metall. Trans. 3 (4), 989 (1972).

29. Mihalison, J. R., Rev. High-Temp. Mater. 2 (3), 243 (1974).

30. Kishkin, S. T., Kozlova, M. N., and Lashko, N. F., Izv. Akad. Nauk SSSR, 170 Met. (Jan.-Feb. 1972).

31. Kirby, G. N., Sponseller, D. L., and Van Vlack, L. H., Metall. Trans. 5 (6), 1477 (1974).

32. Decker, R. F., Strengthening Mechanisms in Nickel-Base Superalloys, presented at Steel Strengthening Mechanisms Symposium, Zurich, Switzerland (May 5-6, 1969).

668

TABLE I. - COMPOSITION OF ALLOYS

Alloy	Reference	Heat treatment	Weight percent (balance is nickel)											
			Cr	Co	Al	Ti	W	Mo	Nb	Ta	V	Fe	C	B
B-1900	19	1	7.9	9.8	5.9	1.0	----	5.7	-----	4.5	----	----	0.09	----
GMR 235		1	15.9	-----	3.5	2.0	----	5.0	-----	---	----	9.8	.15	----
Inconel 700		2	14.3	28.5	3.0	2.5	----	3.9	-----	---	----	.7	.12	----
Alloy 713C		1	12.6	-----	6.8[a]	.8	----	4.7	2.1	---	----	----	.16	----
Inconel X-750		3	14.6	-----	.8	2.4	---	----	.8	---	----	6.5	.04	----
IN 100		1	9.8	15.0	5.6	5.7[a]	----	3.1	-----	---	0.9	----	.19	----
Mar-M 200		1	8.9	9.5	4.5	1.9	12.3	----	1.1	---	----	----	.16	----
Nicrotung		1	11.0	9.9	4.4	4.2	8.0	----	-----	---	----	----	.07	----
Nimonic 115		4	14.8	14.8	4.8	3.9	----	3.5	-----	---	----	----	.14	----
René 41		5	19.0	10.7	1.5	3.1	----	9.7	-----	---	----	----	.09	----
TRW 1900		1	10.1	10.3	6.7	1.0	9.2	----	1.6	---	----	----	.14	----
Udimet 500		6	18.7	19.3	2.9	3.0	----	4.3	-----	---	----	----	.07	----
Udimet 700		7	15.4	18.8	4.4	3.4	----	5.0	-----	---	----	----	.06	----
Unitemp AF 1753		8	16.4	7.7	2.0	3.4	8.3	1.5	-----	---	----	9.0	.23	----
Waspaloy		9	18.6	13.0	1.4	2.9	----	4.2	-----	---	----	----	.05	----
Alloy 713C	17	1	13.23	-----	5.86	.79	----	4.46	[b]2.09	---	----	.10	.11	0.01
Alloy 713LC (heat 07)		1	12.32	-----	5.90	.72	----	4.46	[a]2.13	---	----	.20	.06	.01
Alloy 713LC (heat 17)		1	12.52	-----	5.90	.60	----	4.41	[a]2.10	---	----	.15	.03	.01
IN 731 X		1	9.80	9.72	5.60	4.66	----	2.46	-----	---	.85	.23	.16	.01

Heat treatment	Description
1	As cast
2	2160° F/ 2 hr/air cool + 1600° F/ 4 hr/air cool
3	2100° F/ 2 hr/air cool + 1550° F/ 24 hr/air cool + 1300° F/20 hr/air cool
4	2175° F/1½ hr/air cool + 2010° F/ 6 hr/air cool
5	1950° F/ 4 hr/air cool + 1400° F/ 16 hr/air cool
6	1975° F/ 4 hr/air cool + 1550° F/ 24 hr/air cool + 1400° F/16 hr/air cool
7	2140° F/ 4 hr/air cool + 1800° F/136 hr/air cool
8	2150° F/ 4 hr/air cool + 1650° F/ 6 hr/air cool
9	1975° F/ 4 hr/air cool + 1550° F/ 24 hr/air cool + 1400° F/16 hr/air cool

[a]Value higher than AMS specification for alloy.

[b]Reported in ref. 17 as Nb + Ta.

669

TABLE II. - COMPARISON OF PROPOSED METHOD AND ANALYZED DATA

Element	Average difference, $\bar{d}$,[a] wt %	Sample standard deviation of difference, s_d
Cr	1.1	2.05
Al	.007	.57
Ti[b]	.007	.28
Co[b]	.017	2.74
Mo	.136	1.36
Fe	1.38	1.10
W	-3.73	3.52

[a] $\bar{d} = \sum_{i=1}^{n} \frac{\text{literature - calculated}}{n}$.

[b] $\bar{d}$ was forced to be essentially zero.

TABLE III. - EXPERIMENTAL DESIGN

Element	Level	Alloying addition, at.%, Ni is balance, heat number	
		1-36	37-49
Al	Low	4.0	4.0
	Medium	9.0	8.0
	High	13.0	12.0
Ti	Low	0.25	0.25
	Medium	1.75	1.75
	High	4.75	3.75
Cr	Low	6.5	6.5
	Medium	13.5	12.5
	High	20.5	18.5
W	Low	0	0
	Medium	2.0	1.5
	High	4.0	3.0
Mo	Low	0	0
	Medium	3.0	2.0
	High	6.0	4.0

TABLE IV. - COMPOSITION OF

TWO-PHASE ALLOYS

Heat	Composition, wt %					
	Al	Cr	Mo	Ni	Ti	W
98	2.9	9.4	0	76.9	1.5	9.3
99	3.9	11.2	9.3	73.9	1.7	0
2	4.1	12.5	4.8	78.4	.2	0
5	1.5	5.9	4.2	75.7	1.3	11.2
7	3.9	6.8	0	80.0	3.3	6.0
12	3.7	5.5	4.6	72.4	.1	13.7
14	6.4	5.7	0	81.0	1.4	5.5
15	2.2	20.0	5.1	65.1	1.5	6.1
16	1.9	6.5	10.2	77.4	3.9	0
[a]21	1.7	6.2	0	85.9	.2	5.9
22	1.8	12.1	5.2	79.4	1.5	0
23	4.8	6.3	10.8	76.6	1.5	0
28	7.4	6.3	0	74.3	.2	11.9
31	4.7	17.7	0	70.6	1.2	5.8
33	1.9	5.9	9.6	75.7	1.2	5.7
34	2.1	13.3	0	80.7	3.9	0
35	4.7	5.4	4.8	81.4	3.6	0
37	3.9	13.2	6.8	70.2	1.3	4.6
38	6.5	12.8	4.0	73.5	3.2	0
39	5.4	6.6	6.8	81.1	.1	0
40	5.9	11.2	0	72.6	1.6	9.0
41	1.8	12.3	6.7	72.2	3.0	4.0
42	4.1	18.9	3.7	68.9	.1	4.3
46	4.1	10.9	7.9	68.6	.3	8.2
47	5.6	11.5	3.5	73.2	1.3	4.8
48	3.6	17.5	0	75.2	3.8	0
49	5.5	17.2	0	75.6	1.7	0

[a]Alloy contain less than 1 percent γ' - no analysis of γ' could be made.

TABLE V. - COMPOSITION AND AMOUNT OF GAMMA PRIME

Heat	Element, at.%						Amount of γ', wt%
	Ni	Al	Cr	Mo	Ti	W	
98	78.0	12.5	2.7	---	3.7	3.1	40.1
99	76.1	13.8	2.6	2.9	3.9	---	39.4
2	74.5	17.3	5.1	2.4	.7	---	29.3
5	75.7	13.3	2.1	1.1	5.1	2.7	[a]5.6
7	76.9	11.7	2.4	---	7.1	1.9	39.2
12	77.8	14.6	1.9	1.5	.3	3.9	31.9
14	73.3	15.9	4.2	---	2.8	3.8	18.4
15	74.3	11.3	4.9	1.1	6.3	2.1	16.8
16	75.6	10.3	1.5	2.3	10.3	---	20.3
22	76.2	7.8	8.9	2.2	4.9	---	8.5
23	74.2	15.9	2.7	3.9	3.3	---	44.5
28	72.1	16.9	3.5	---	.3	7.2	32.1
31	74.3	16.0	4.0	---	3.3	2.4	41.3
33	77.1	10.8	2.4	2.4	5.9	1.4	[a]1.4
34	73.1	10.1	2.9	---	13.9	---	21.5
35	77.3	12.1	2.3	1.7	6.6	---	54.5
37	74.7	15.7	2.7	1.7	3.5	1.7	35.3
38	74.7	15.1	3.5	1.6	5.1	---	34.2
39	77.5	15.5	3.2	3.5	.3	---	44.7
40	76.0	15.1	3.3	---	2.3	3.3	55.7
41	72.4	10.6	2.1	2.9	9.5	2.5	23.9
42	73.6	17.5	4.6	1.3	.3	2.7	27.1
46	76.6	14.9	2.9	1.7	.4	3.5	29.3
47	75.8	15.3	3.2	1.3	2.4	2.0	55.6
48	76.1	13.1	3.9	---	6.9	---	38.7
49	75.9	15.3	6.1	---	2.7	---	51.9
S		0.851	0.336	0.573	0.502	0.852	

[a]Electrolyte was H_3PO_4 - extraction not quantitative in amount of γ'.

673

TABLE VI. - COMPOSITION OF GAMMA

Heat	Element, at.%, balance is Ni				
	Al	Cr	Mo	Ti	W
98	2.1	16.4	---	0.5	2.9
99	4.3	19.1	7.5	.8	---
2	4.7	17.2	3.0	0	---
7	6.1	10.9	---	1.7	1.9
12	5.5	8.9	3.7	.1	5.0
14	12.7	6.6	---	1.5	1.2
15	3.5	26.5	3.6	.9	1.9
16	2.1	9.2	7.5	3.1	---
22	3.4	13.9	3.2	1.5	---
23	5.1	10.7	8.7	.5	---
28	15.4	8.5	---	.1	2.2
31	5.5	29.9	---	.1	1.3
34	2.5	17.7	---	1.9	---
35	6.9	10.3	4.2	1.2	---
37	4.3	21.8	5.5	.5	1.3
38	11.9	18.5	2.7	2.9	---
39	7.6	10.5	4.3	0	---
40	9.5	23.3	---	1.5	2.1
41	1.9	17.8	4.5	1.9	.9
42	5.5	25.7	2.5	.1	.8
46	6.7	16.7	6.3	.4	2.3
47	7.5	24.4	3.1	.5	.8
48	3.5	27.7	---	2.5	---
49	6.2	30.7	---	1.1	---
S	0.640	0.391	0.224	0.256	0.374

674

TABLE VII. - REGRESSION ANALYSIS OF GAMMA AND GAMMA PRIME

$$\left[\text{Equation: } Al = \sum_{n=0}^{n=18} B_n \times F_n\right]$$

n	Phase		Factor, F_n
	γ Coefficient, B_n	γ' Coefficient, B_n	
0	13.3992	7.42647	Constant
1	-1.07392	3.59713	Cr
2	1.80069	0	Mo
3	0	.849058	Ti
4	15.3168	-.589230	W
5	.0318507	-.292157	Cr^2
6	.0455815	.149930	Mo^2
7	1.53473	-.0256415	Ti^2
8	-2.59870	-.0398181	W^2
9	-.100793	-.127831	Cr × Mo
10	-.204796	-.310730	Cr × Ti
11	-.504191	.290021	Cr × W
12	-2.12721	-.245979	Mo × Ti
13	.598921	.876515	Mo × W
14	-7.75600	-.155343	Ti × W
15	.153165	.0675603	Cr × Mo × Ti
16	0	-.275617	Cr × Mo × W
17	.486625	0	Cr × Ti × W
18	-1.43936	.0226054	Mo × Ti × W
R^2	.89	.87	

TABLE VIII. - LEAST SQUARES ANALYSIS OF DIRECTION NUMBERS

$$\left[\text{Equation: Direction number} = \sum_{n=0}^{n=5} B_n \times F_n\right]$$

n	Element				Factor, F_n
	Al coefficient, B_n	Mo coefficient, B_n	Ti coefficient, B_n	W coefficient, B_n	
0	-2.4316	-0.0032572	-1.04691	-0.52841	Constant
1	.066096	-.0010339	.046595	-.054240	Al
2	.059819	-.013136	.030941	.030041	Cr
3	.0088685	.087981	.026712	.020858	Mo
4	.14622	.021598	-.070565	.054511	Ti
5	.090661	.024404	.040548	.14031	W
R^2	.64	.72	.76	.37	
a_T	.35	.09	.96	.29	

a_T is the significance level of the least significant coefficient.

676

TABLE IX. - COMPARISON OF ANALYZED DATA AND CALCULATION FOR EXPERIMENTAL ALLOYS

Element	Phase	Average difference, $\bar{d}$,[a] at. %	Sample standard deviation of difference, S_d
Al	γ	-0.50	1.6
	γ'	.59	1.5
Cr	γ	.93	4.8
	γ'	.90	1.8
Mo	γ	.18	.54
	γ'	-.09	.72
Ti	γ	.12	.82
	γ'	.12	1.28
W	γ	.23	.95
	γ'	-.66	1.6

[a] $\bar{d} = \sum_{i=1}^{i=n} \left(\frac{\text{observed - calculated}}{n} \right)$.

TABLE X. - OCCURRENCE OF PHASES

Alloy	Element, at. %						Phase			
	Al	Cr	Mo	Ti	W	Ni	Cr	[a]Mo, W	σ	μ
3	14.6	8.4	5.5	0.2	---	71.2				×
4	12.9	11.9	---	1.3	4.1	69.8		×		
6	7.3	21.6	5.6	1.4	3.6	60.5		×	×	
8	13.1	21.9	2.8	4.3	1.8	56.1	×	×	×	
9	4.0	14.8	5.4	5.1	2.1	68.6		×		×
10	9.7	23.5	6.4	.4	4.6	55.4		×	×	
13	8.8	15.2	5.5	1.8	1.8	67.1				×
17	8.6	23.4	---	4.3	---	63.7	×			
18	15.3	14.0	3.0	4.9	---	62.9	×		×	
19	9.9	17.8	3.1	.1	2.1	67.0		×		×
20	15.7	13.1	5.4	.2	2.0	63.5		×	×	
24	14.2	20.7	---	1.4	---	63.6	×			
25	13.3	7.1	2.9	4.6	3.4	68.6		×	×	
26	3.9	21.8	5.6	4.5	3.6	60.6		×	×	×
27	7.1	17.0	---	4.6	4.0	67.2	×	×		
29	4.1	22.7	3.2	.1	3.8	66.1		×		
30	9.8	14.8	5.8	.1	3.8	65.7		×		×
32	14.7	13.7	3.1	1.7	1.9	65.3	×	×	×	
36	14.8	21.0	6.4	4.5	---	55.3	×	×	×	
43	12.9	12.5	4.1	4.9	1.3	64.2				×
44	10.9	6.4	2.0	3.3	2.9	74.5	Unidentified			
45	3.6	19.6	4.1	3.9	2.6	66.2		×		

[a]Mo and W cannot be differentiated by X-ray diffraction.

BCC phase with A_0 at approximately 3.15 Å.

678

TABLE XI. - COMPARISON OF OBSERVED AND ESTIMATED PHASE COMPOSITIONS IN COMMERCIAL ALLOYS

Alloy	Phase	Element, at.%									
		Al		Cr		Mo		Ti		W	
		Obs[a]	Est[b]	Obs	Est	Obs	Est	Obs	Est	Obs	Est
B-1900	γ	5.1	1.8	18.3	20.5	5.4	5.7	0	0	---	---
	γ'	17.2	16.4	3.0	4.4	2.3	2.6	1.9	1.7	---	---
GMR 235	γ	3.8	3.5	20.6	22.5	3.2	3.3	.6	.4	---	---
	γ'	17.6	14.3	2.3	6.0	1.4	2.2	5.1	4.4	---	---
Inconel 700	γ	4.0	4.8	19.4	16.9	2.4	2.3	1.0	1.7	---	---
	γ'	13.6	13.0	4.3	5.7	1.2	1.8	6.7	6.4	---	---
Inconel 713C	γ	8.1	5.4	24.3	27.2	3.9	3.6	.1	.6	---	---
	γ'	19.2	18.0	3.5	6.5	1.5	2.3	1.3	.6	---	---
Inconel X-750	γ	.6	.5	17.9	16.9	---	---	1.2	2.0	---	---
	γ'	6.9	15.5	2.3	1.5	---	---	12.8	12.5	---	---
IN 100	γ	4.8	10.4	24.0	14.8	3.1	2.4	.5	3.0	---	---
	γ'	14.0	13.4	3.4	1.2	.7	.6	8.6	10.7	---	---
Mar M 200	γ	3.2	.5	20.4	29.4	---	---	0	0	4.2	2.1
	γ'	14.8	13.5	3.1	3.4	---	---	3.7	3.6	4.0	4.9
Nicrotung	γ	.9	8.4	26.1	18.3	---	---	1.0	1.8	2.9	2.1
	γ'	14.9	10.6	3.3	4.9	---	---	7.6	8.2	2.3	3.0
Nimonic 115	γ	4.6	8.6	26.5	19.1	2.9	2.1	.6	2.6	---	---
	γ'	15.7	12.8	4.1	3.6	.6	1.4	7.2	8.4	---	---
Rene 41	γ	1.3	.5	26.8	27.6	7.0	8.2	.7	1.1	---	---
	γ'	9.2	9.3	3.5	5.3	1.3	1.0	10.9	9.2	---	---
TRW 1900	γ	7.6	7.4	24.1	27.3	---	---	.4	.9	3.0	1.8
	γ'	17.4	17.5	3.9	3.9	---	---	1.4	.9	2.6	6.6
Udimet 500	γ	2.3	3.7	28.6	26.7	3.0	2.6	.6	1.0	---	---
	γ'	13.5	10.7	2.9	5.6	1.0	2.1	7.9	8.3	---	---
Udimet 700	γ	5.3	6.8	24.3	24.0	3.9	3.8	1.5	1.3	---	---
	γ'	13.9	12.5	2.7	4.0	.9	1.5	8.1	7.6	---	---
Unitemp AF 1753	γ	2.4	4.4	22.5	18.1	1.1	.9	1.1	2.7	2.7	3.4
	γ'	11.6	7.9	1.3	8.0	.3	.9	11.6	5.9	1.8	0
Waspaloy	γ	1.1	.5	25.0	24.6	3.2	2.6	.7	1.2	---	---
	γ'	9.5	11.2	2.4	4.3	.7	2.1	12.5	10.6	---	---
$\bar{d}$[c]	γ	-0.82		0.99		0.15		-0.69		0.85	
	γ'	.83		-1.5		-.60		.55		-.95	
S_d	γ	3.1		4.8		.56		.75		1.2	
	γ'	3.1		2.1		.49		1.7		2.4	

[a]Obs is the experimentally observed value (ref. 19).

[b]Est is the value estimated by the calculation.

[c] $\bar{d} = \sum_{i=1}^{n} \left(\frac{\text{observed - calculated}}{n} \right)$.

670

TABLE XII - PHASE OCCURRENCE IN COMMERCIAL ALLOYS

Alloy	Parameters			Phase[b]
	Alloy Ni + Co + Fe,[a] at.%	Gamma Cr + 1.75 × (Mo + W),[a] at.%	Al DN[a]	
Inconel X-750	78.9	17.9	-0.40	n
Mar M 200	73.1	27.4	-.67	n
Inconel 700	72.6	23.6	-.64	n
B-1900	72.5	27.0	-.79	n
Nicrotung	70.7	31.2	-.61	n
Waspaloy	70.5	30.6	-.37	n
GMR 235	69.9	26.2	-.75	--
TRW 1900	69.1	29.4	-.49	n
IN 100	68.7	29.4	-.45	σ
Unitemp AF 1753	68.4	29.2	-.43	n
Nimonic 115	67.7	31.6	-.50	σ
Udimet 500	67.6	33.9	-.44	σ
Udimet 700	67.5	31.1	-.40	σ
Inconel 713C	67.5	31.1	-.53	σ
Rene 41	65.6	39.1	-.34	μ

[a]From Kriege and Baris (ref. 19).
[b]From Collins (ref. 15).

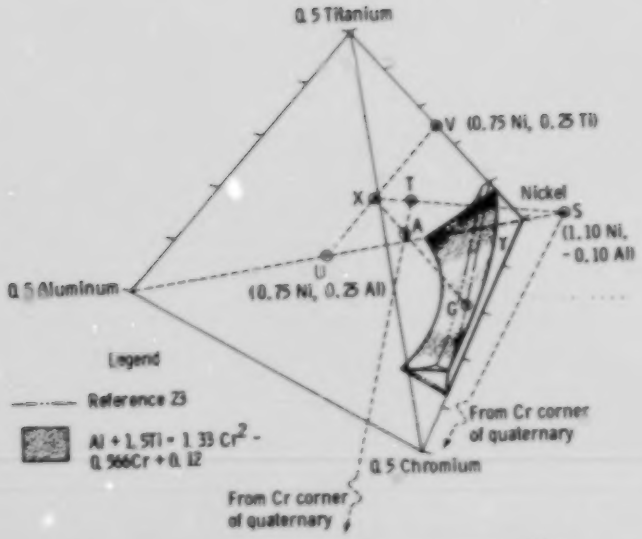

Figure 1. - Nickel-rich region of Ni-Al-Cr-Ti system at 750° C.

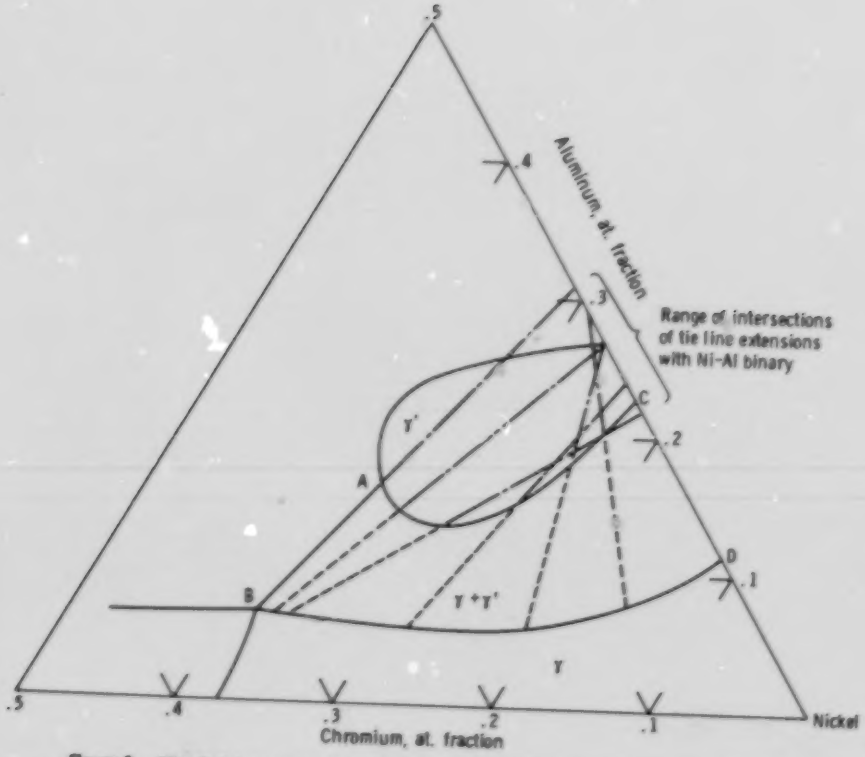

Figure 2. - Nickel-rich region of Ni-Cr-Al system at 750° C (after Taylor and Floyd (ref. 20)).

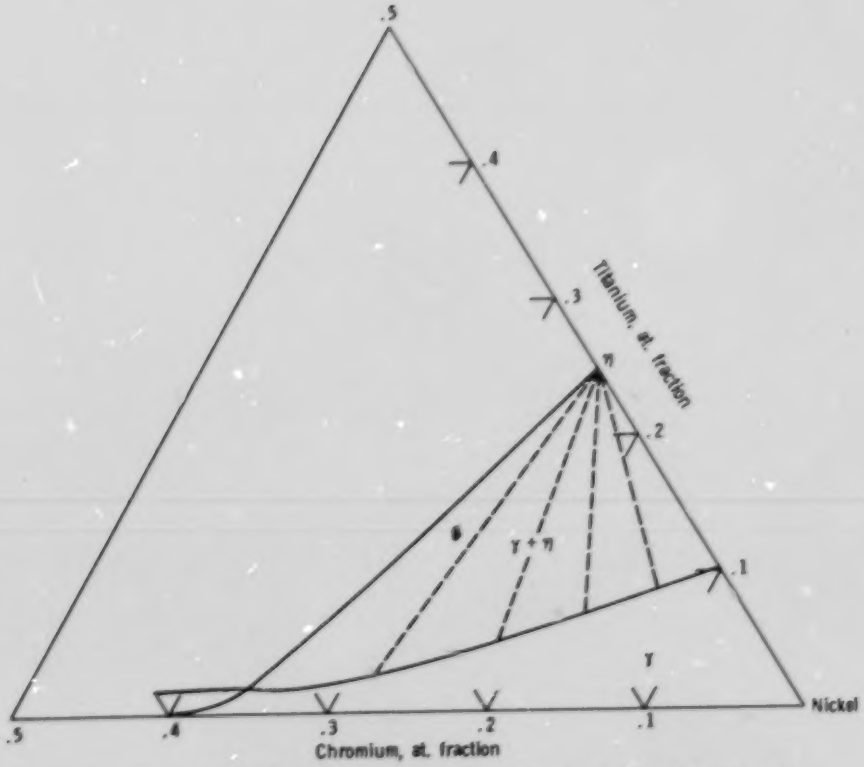

Figure 3. - Nickel-rich region of Ni-Cr-Ti system at 750° C (after Taylor and Floyd (ref. 21)).

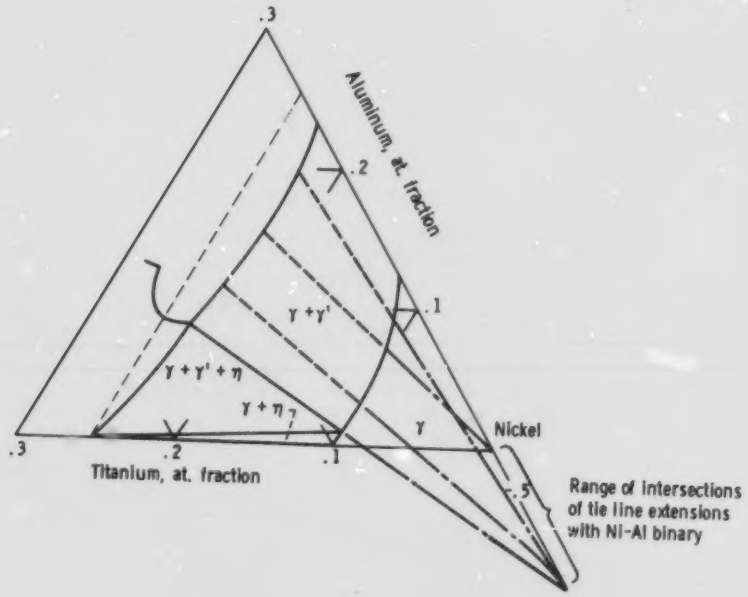

Figure 4. - Nickel-rich region of Ni-Ti-Al system at 750° C (after Taylor and Floyd (ref. 22)).

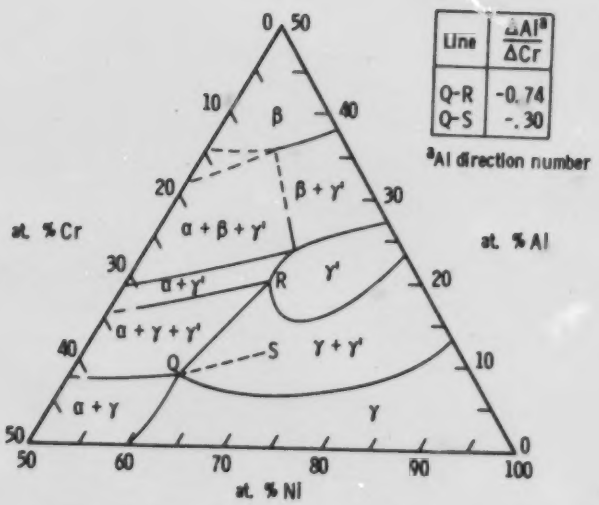

Line	$\frac{\Delta Al^a}{\Delta Cr}$
Q-R	-0.74
Q-S	-.30

[a]Al direction number

Figure 5. - The Ni-Cr-Al phase diagram at 850° C from reference 20.

694

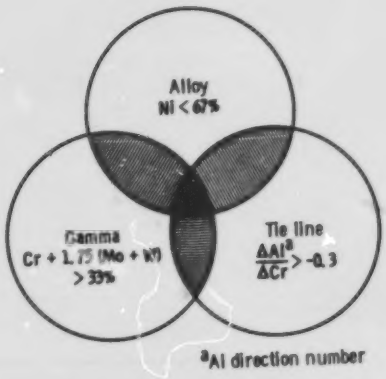

Figure 6. - Occurrence of BCC and TCP phases in experimental alloys.

Discussion following the Panel I presentations on Tues Jan 11.

George Armstrong - I am pleased to see Prof. Brewer is going to publish his solvus curves in a numerical form, because as I will attempt to show later, one of my beliefs is that one does not have to be able physically to look at a phase diagram to extract useful information, but only be able to massage it numerically.

J. Elliott - I have a comment I would like to make: we're going to have to do some experiments. We are interested in what constitute the phases in equilibrium in a number of systems of technological importance; the Fe-Cr-Ni-C for example. What we would like, is to do a few measurements and do a lot of calculations. The trouble is that we have a complicated set of interactions. We have written down a complicated program similar to that which Larry Kaufman has, and have compared experimental liquidus results in the Fe-Cr-Ni-C system with these calculations and there is quite a difference. Adjusting the data and going through another calculation improves certain features, but it depends on your taste as to whether this gives a better fit. We have not used ternary and higher order coefficients in our calculations. These would then give a better fit. The trouble then arises: when do we use such a "better" set of data for other calculations such as for the Fe-Cr-Mn-C system or Fe-Ni-Mn-C system. And the result of this is that we are not quite as optimistic as we were at the outset that we would be able to do a limited set of experimental points to be able to rapidly predict what the liquidus surfaces are.

L. Kaufman - It depends on your viewpoint. Your calculation seems to indicate that we could be out by as much as 2 to 3 percent. For most practical kinds of applications you are really not interested in this close detail, as, for example, in an application like Bob Dreshfield's where you want to know roughly where the liquidus surfaces are. It depends on what you want. We are not trying to imply that you shouldn't do the experiment.

F. L. Carter - My question is to Dr. Kaufman as well as the others: Are the x-ray parameters and distances used in the calculations and do the calculations predict lattice parameters or compositions of phases?

L. Kaufman - Not on the ones that we are currently doing. In the kind of considerations that Leo Brewer does, volumes can be important.

L. Brewer - Yes. They are very important because, particularly in solid solubility, the strain energies are very important term.

A. Navrotsky - Volume considerations certainly are important in the high pressure oxide work and the crystallography is important in chosing appropriate forms of equations in complicated silicate systems. For example, questions of how many sites are involved in mixing, and things of this sort, are to be considered.

National Bureau of Standards SP-496, Applications of Phase Diagrams in Metallurgy and Ceramics
Proceedings of Workshop held at NBS, Gaithersburg, Md., January 10-12, 1977

The Representation of Phase Equilibria

Alan Prince
(The General Electric Co. Ltd.,
Hirst Research Centre, Wembley, England)

In two years we will see the 150th anniversary of the first investigations of alloy phase equilibria. F. Rudberg[1] of Sweden produced a tabular representation of what we would call nowadays the inverse-rate cooling curves of the Pb-Sn alloy series. The importance of this early work is not so much the fact that Rudberg tabulated his data on the familiar temperature-concentration axes, but the detailed conclusions he drew from his work[2]. The Russian A. Ya. Kupfer in examining the specific gravity of Pb-Sn alloys also determined the liquidus temperatures of these alloys[3]. Over the past century and a half there has been a great increase in our knowledge of alloy phase equilibria, especially of binary systems. Multicomponent systems have been less well studied. To the end of 1973 some 6223 ternary systems had been examined, 1237 quaternary systems, 149 quinary systems, and 27 senary systems. This represents a minute percentage of possible systems and it must be remembered that very few of the systems studied have been investigated in any detail.

In terms of phase equilibria it is important to consider the representation of binary, ternary, and quaternary systems. Methods need to be available for the representation of more complex systems but little experimental data exists on which to apply these methods.

Phase diagrams are graphical representations of the phase relationships in heterogeneous systems. The phase diagram can be considered to consist of a coordinate framework enclosing geometrical elements (the phase complex) representative of the phase relationships. The coordinate framework is based on a concentration simplex, which is equated to the concentration diagram of the system, combined with other geometrical elements representing such additional externally variable parameters as temperature and pressure, figure 1. This terminology appears unduly academic at first glance. However its introduction by the Russian metallurgist Kurnakov[4] paved the way for a consideration of multicomponent systems by topological techniques.

Representation of Concentration - The Concentration Simplex

A ternary system with components A, B, and C is represented by two concentration axes. This follows from the relation

$$X_A + X_B + X_C = 100$$

where X_A, X_B, X_C are the molar, weight, or atomic percentages of components A, B, and C respectively. The concentration diagram is a two-dimensional simplex, figure 2a, containing three vertices, three edges, and one surface. It contains no internal diagonals and all lines and surfaces connecting the vertices of a simplex coincide with its edges and surfaces. The number of vertices of a simplex exceeds by one the dimension of the space in which it exists.

Simplexes can have edges of equal or unequal length. A two-dimensional regular simplex with equal edges is normally used to represent concentrations in ternary systems. It is the well-known Gibbs triangle or concentration triangle, figure 2b. Any alloy with a composition defined by a point within this triangle has the concentrations of its components defined by dropping perpendiculars from the point to the three sides of the triangle. Alternatively concentrations of any component can be equated to the area of the triangle including the alloy and the edge containing the other two components.

This elementary preamble leads to a consideration of the Kurnakov method for representing concentrations in multicomponent systems. For n-component systems

$$\sum_{i=A}^{n} X_i = 100$$

Concentrations are represented in n-component systems by (n-1)-dimensional simplexes with n vertices. The concentrations X_i (i = A, B, ..., n) for any alloy in the n-component system are defined by the lengths of the perpendiculars dropped from the point representing the alloy on to the (n-2)-dimensional hyperfaces of the concentration simplex. Alternatively the concentrations X_i are given by the ratio of the hypervolume of the simplex containing the point representing the alloy and all the vertices of the concentration simplex except vertex i to the hypervolume of the concentration simplex :-

$$X_i = \frac{V_i}{V}$$

In ternary systems the hypervolumes of the simplexes are the areas of appropriate triangles. In quaternary systems four vertices, A, B, C, D, in three-dimensional space define the concentration simplex. The normal representation is by means of an equilateral tetrahedron, as first suggested by Roozeboom[5], figure 3. The concentration of any component in alloy M is the ratio of the volume of the tetrahedron opposite the vertex of the component to the volume of the concentration tetrahedron, e.g.

$$X_A = \frac{V_A}{V} = \frac{\text{Volume MBCD}}{\text{Volume ABCD}}$$

It is not possible to visualise or graphically represent a quinary concentration diagram since this would require four-dimensional space. Since the number of geometrical elements in any simplex is determined by the relation

$$\sum_{1}^{n} S(n) = 2^n - 1 = {}^nC_1 + {}^nC_2 + \ldots\ldots + {}^nC_n$$

we can deduce that for a quinary system with n = 5 there will be

$^{n}C_{1}$ = 5 vertices, $^{n}C_{2}$ = 10 edges, $^{n}C_{3}$ = 10 surfaces, $^{n}C_{4}$ = 5 volumes, and $^{n}C_{5}$ = 1 hypervolume. The vertices correspond to the components, edges to the constituent binary systems, surfaces to the ternary systems, volumes to the quaternary systems and the hypervolume to the quinary system itself. All we can now do is to project such a quinary simplex, a pentahedroid, as a three-dimensional figure, figure 4 or, as will be noted later to consider two-dimensional projections of the simplex.

Representation of Concentration - Secondary Methods

In most compilations of constitutional data concentrations have been expressed in weight percentages or atomic percentages of the components. The industrial metallurgist normally works in weight percentages. He recognises the eutectoid point in the Fe-C system as containing 0.80 weight percentage carbon not as containing 3.61 atomic percentage carbon.

Notwithstanding this practice there are cogent scientific reasons for considering alternative methods for representing concentrations. The historic paper by W. Hume-Rothery and co-workers[6] introduced the concept of electron concentrations - the ratio of valency electrons to atoms - as a powerful tool in understanding phase relationships in binary alloys. For Cu and Ag alloys with favourable size-factors it was shown that the maximum solid solubilities of B - subgroup elements corresponds to an electron concentration of about 1.4. The electron compounds were shown to occur at specific electron concentrations, corresponding to electron: atom ratios of 3:2, 21:13, and 7:4. Later workers[7] have used electron concentrations in studying ternary alloy systems to show how the interplay of size-factors and electronic structure influence the formation of ternary solid solutions based on binary electron compounds at constant e:a ratios.

Electron concentration effects also apply to some solid solutions in binary transition metals. Difficulties in assigning a valency to the transition metals led Hume-Rothery to describe concentrations in terms of average group numbers (AGN) of the alloys. Group numbers from 1 to 10 are allotted to the elements of Groups 1A to VIIIC respectively. If all the electrons outside the rare-gas shell are counted the AGN is identical with the electron concentration.

Another method of representation, used extensively in researches on superalloys, uses the electron-vacancy number, N_v, which is related to the electron concentration by the relation $N_v = 10.66 - e/a$, where N_v represents the electron vacancies in the 3d subshell. In the series V, Cr, Mn, Fe, Co, Ni the electron vacancy numbers assigned are 5.66, 4.66, 3.66, 2.66, 1.71, 0.66 respectively. Elements in the same group have identical values of N_v, e.g. Mo = 4.66. One of the major aims in the superalloy field is the constitutional avoidance of topologically close-packed phases, particularly the sigma phase. The basic problem addressed by the PHACOMP method is to calculate the solubility limits in terms of an average N_v for the fcc residual matrix phase in multicomponent alloys. This requirement has led to novel methods for representing constitutional data[8] in terms of polar diagrams. One of the refractory metals Cr, Mo, W

is placed at the centre of the plot and the elements of the first long period are sequentially displayed on the perimeter, figure 5. The binary systems of Mo with the transition elements are represented by the radial segments Mo-Ni, Mo-Co, etc. Ternary systems are represented by the sectors Fe-Mo-Mn, Mn-Mo-Cr, etc. They can also be represented by more than two radial segments. For example the system Fe-Mo-Cr can be regarded as the summation of Fe-Mo-Mn and Mn-Mo-Cr since the radial segment Mo-Mn can be regarded as the line joining Mo to an Fe-Cr alloy with an electron vacancy equal to 3.66 (the 50 atomic percent Fe-Cr alloy). Iso-electron vacancy lines can be drawn which spiral outwards in a counter-clockwise direction. The solid solubility limits for the fcc phase follow this pattern of behaviour.

In their later form[9] polar diagrams have been stacked on each other to give a three-dimensional representation.

The Coordinate Framework

The coordinate framework normally considered in alloy systems is the concentration-temperature diagram. Pressure is not one of the external parameters often used. For binary systems a two-dimensional diagram suffices. Ternary systems are represented by a three-dimensional diagram, a right triangular prism. Quaternary systems require four-dimensional space for representation of the concentration-temperature diagram. Assuming constant pressure conditions quaternary systems can be represented by a series of isothermal sections which are individual tetrahedra. To represent such systems in three or two dimensions it is necessary to use projections of the four-dimensional diagram. For higher component systems projections are obligatory. Emphasis will be placed on quaternary systems with some reference to quinary systems.

Projection Methods

Ternary diagrams are frequently represented by two-dimensional projections of the space model (i.e. the coordinate framework and the phase complex) on to the Gibbs triangle. Nothing further need be said about such systems.

There is no difficulty in projecting any point in a ternary space model on to the concentration triangle since the concentration coordinates of the point do not change on projection. The position is more difficult in quaternary systems. We will consider the projection of any point within the tetrahedron so as to establish a relationship between the coordinates of the point, representing a quaternary alloy, and the coordinates of its projection on one of the concentration triangles of the tetrahedron. Two general methods have been used, the perspective projection and the parallel projection.

Perspective Projections

Projections are made from one of the vertices of the tetrahedron to the opposite triangular face. In figure 6 an alloy of composition X is projected from vertex B on to the triangle ACD. The coordinates of the

quaternary alloy are a, b, c, d where a is the content of component A etc. The coordinates of the projected point x_1 are a_1, c_1, d_1 i.e. alloy x_1 is a ternary alloy with a content a_1 of component A etc.

Since any point on a line from a vertex to the opposite face of a tetrahedron contains the same ratio of the components associated with that face, then

$$a : c : d = a_1 : c_1 : d_1$$

But $$a + b + c + d = 100$$

and $$a_1 + c_1 + d_1 = 100$$

Knowing the composition of the quaternary alloy X the composition of the projected point x_1 can be obtained. In alloy x_1 the relative concentrations of A, C, and D ($a_1 : c_1 : d_1$) are known. The absolute values are given by the relations

$$a_1 = \frac{100\ a}{a + c + d}$$

$$c_1 = \frac{100\ c}{a + c + d}$$

$$d_1 = \frac{100\ d}{a + c + d}$$

The reverse problem, that of finding the quaternary alloy composition from the projected point, requires the use of two projections. If the two projections are x_1 ($a_1 = 60$, $c_1 = 30$, $d_1 = 10$) and x_2 ($b_2 = 71\,^3/_7$, $c_2 = 21\,^3/_7$, $d_2 = 7\,^1/_7$) then

$$a_1 : c_1 : d_1 = 60 : 30 : 10 = a : c : d$$

$$b_2 : c_2 : d_2 = 500 : 150 : 50 = b : c : d$$

or $$b_2 : c_2 : d_2 = 100 : 30 : 10$$

whence $$a : b : c : d = 60 : 100 : 30 : 10$$

As $a + b + c + d = 100$ it follows that $a = 30$, $b = 50$, $c = 15$, $d = 5$.

The perspective method of projection has been used extensively for the examination of quaternary phase equilibria. G. Phragmen's extensive publication on Al-base alloys uses perspective projections throughout[10] and the recent textbook by L.F. Mondolfo also uses this type of projection[11]. In each case the projection is made from the Al vertex of the tetrahedron.

Parallel Projections

In perspective projections all alloys within the tetrahedron are projected from lines radiating from a vertex of the tetrahedron. If the vertex were removed to infinity the lines would be parallel. We can differentiate two basic types of parallel projections. The first uses projections parallel to one of the edges of the tetrahedron; the second uses orthogonal projections (perpendicular to specific faces).

In figure 7 x_3 is the parallel projection of quaternary alloy X (a, b, c, d) on to the concentration triangle ACD. The direction of the projection is parallel to edge BD of the tetrahedron. The advantage of this type of projection is that two of the coordinates of alloy X remain the same in the projected point x_3. In this case the coordinates a and c are identical in alloy X and its projection x_3.

$$Da_3 = a_3 = Ba = a$$

$$Dc_3 = c_3 = Bc = c$$

$$d_3 = Ae = Ad_3 + d_3e = d + d_3e$$

$$AD = a + b + c + d = Da_3 + b + a_3e + Ad_3$$

$$\text{i.e. } b = d_3e$$

$$\text{Hence } d_3 = b + d$$

A second projection parallel to the edge AB on to the concentration triangle BCD gives a projected point x_4. The c and d coordinates of quaternary alloy X and projected point x_4 are identical. The third coordinate for x_4 (b_4) = a + b. The two projections give the a, c, and d values for alloy X. They define the composition of X.

Orthogonal projections involve projecting any point within the tetrahedron at right angles to the plane of the projection. This plane is usually one of the concentration triangles or it can be a plane parallel to two mutually perpendicular, but not intersecting, edges of the tetrahedron. In the former case a quaternary alloy X (a, b, c, d) is projected on to triangle ACD as x_1 (a_1, c_1, d_1), figure 8a. From X draw planes XX_1X_2, XX_1X_3, and XX_2X_3 parallel to the faces ABC, ABD, and BCD respectively. Triangle $X_1X_2X_3$ has at its centre of gravity point x_1.

From figure 8b

$$EX_1 = JL = d;\ Jx_1 = d_1.\ Lx_1 = d_1 - d$$

$$GD = MK = a;\ Kx_1 = a_1.\ Mx_1 = a_1 - a$$

$$FX_1 = ON = c;\ Ox_1 = c_1.\ Nx_1 = c_1 - c$$

In any equilateral triangle $Lx_1 = Mx_1 = Nx_1$

$$\text{i.e. } d_1 - d = a_1 - a = c_1 - c.$$

But $a + b + c + d = 100$ and $a_1 + c_1 + d_1 = 100$.

Hence $a_1 - a + c_1 - c + d_1 - d = b$.

It follows that $a_1 - a = c_1 - c = d_1 - d = \frac{b}{3}$

In other words the coordinates a_1, c_1, d_1 of the projected point x_1 are related to the coordinates a, b, c, d of the quaternary alloy X by the relations

$$a_1 = a + \frac{b}{3} \quad c_1 = c + \frac{b}{3} \quad d_1 = d + \frac{b}{3}$$

If the coordinates of two projected points, x_1 and x_2, are known one can determine the coordinates of alloy X. This follows from the previous relations and a similar set of relations for projection x_2 on, say triangle BCD.

$$b_2 = b + \frac{a}{3} \quad c_2 = c + \frac{a}{3} \quad d_2 = d + \frac{a}{3}$$

Alternatively it is possible to take a second projection parallel to the basal concentration triangle on to one of the side triangles. G. Petzow and A.O. Sampaio[12] used the parallel orthogonal projection method in work on the U - UMn_2 - UAl_2 - UFe_2 system. Projecting the T phase at the 760°C invariant reaction on to the U - UAl_2 - UMn_2, figure 9a, produces a composition of 6.87% U, 50.84% UAl_2, 42.29% UMn_2 or 37.92% U, 33.89% Al, 28.19% Mn. Projecting parallel to the U - UMn_2 - UAl_2 face on to the U - UMn_2 - UFe_2 face allows the % UFe_2 in phase T to be read directly as 7.63%. The % Fe = 5.09. The T phase therefore has a composition

$$37.92 = U + \frac{5.09}{3}, \quad 33.89 = Al + \frac{5.09}{3}, \quad 28.19 = Mn + \frac{5.09}{3}$$

leading to T (36.2 U, 32.2 Al, 26.5 Mn, 5.1 Fe).

A second type of orthogonal projection is the square orthogonal projection[13]. This is formed by rotating the tetrahedron about an edge, say AC, until the edge BD is horizontal and orthogonally projecting the rotated tetrahedron on to a plane parallel to both non-intersecting edges of the tetrahedron. The projection plane is a square with the two edges, AC and BD, of the tetrahedron as its diagonals, figure 10b. A quaternary alloy X (a, b, c, d) lies on plane $A_1 B_1 C_1 D_1$, figure 10a, parallel to edges AC and BD. Let point O represent the intersection of AC and BD in the projection, figure 10b. The x axis is taken from O along OC, the y axis from O along OB. The coordinates of X in the projection are

$$Ox_1 = \frac{a_1 X + Xc_1}{2} - Xc_1 = \frac{a_1 X - Xc_1}{2}$$

$$Oy_1 = \frac{d_1 X + Xb_1}{2} - Xb_1 = \frac{d_1 X - Xb_1}{2}$$

The lengths Xa_1, Xb_1, Xc_1, and Xd_1 are equal to the concentrations of components A, B, C, and D (a, b, c, d) in alloy X. Therefore

$$Ox_1 = \frac{c - a}{2} \quad \text{and} \quad Oy_1 = \frac{b - d}{2}$$

A second square orthogonal projection is produced by rotation about edge AD until edge BC is horizontal, figure 8c. On this projection

$$Ox_2 = \frac{b - c}{2} \quad \text{and} \quad Oy_2 = \frac{a - d}{2}$$

The coordinates of quaternary alloy X can be derived from the coordinates of the two projections. Since $100 - (b + c + d) = a$

$$100 - (2x_1\,0 + 2y_1\,0 - 4y_2\,0) = 4a$$

$$a = \frac{50 - x_1 0 - y_1 0 + 2y_2\,0}{2}$$

The remaining coordinates follow from the previous relations.

In an extensive study of quaternary systems Cayron[14] makes use of an orthogonal projection of the tetrahedron on to one of the faces, say ACD figure 11b, linked with a second projection along a plane perpendicular to one edge of face ACD, say edge AD, figure 11c.

F.M. Perel'man has developed what she calls "optimal projections", these being the most convenient projections of multidimensional figures for the quantitative determination of phase equilibrium relationships. As applied to quaternary systems the optimal projection of a regular tetrahedron is obtained by turning say triangle BCD about the edge CD on to the adjoining triangle ACD. Triangle BCD is thereby projected on to triangle ACD without any distortion of scale. Triangles ABC and ABD, figure 12, project as line segments on edges AC and AD respectively, and vertex B coincides with vertex A. An optimal projection of this type can be used to consider the phase relationships in alloys rich in components C or D. A second optimal projection derived by projecting triangle ABC on to triangle ACD can be used to consider phase relationships in alloys rich in components A or C. From two such parallel projections the compositions of such invariant points as M or points on the monovariant curves WM, XM, YM, and ZM can be determined quantitatively. The standard text by Perel'man[15] discusses the method of optimal projections and applies it to a variety of problems, such as the estimation of the liquidus temperatures of multicomponent alloys. According to Palatnik and Landau[16] the optimal projection method has not found extensive application in the analysis of multicomponent systems since "this is a consequence of the complexity of the geometrical constructions, and of the fact that substantial distortions of shape, and even complete omission of whole regions of coexistence of phases and the interfaces between them, as well as of certain important details of the phase diagrams of multicomponent heterogeneous systems often occurs".

The projection methods outlined above do not exhaust the subject. Ricci[17] considers other methods and the inter-relation of various projections. Which method is used will depend to a large extent on the region of the system that is being investigated and the preference of the authors in choosing a projection method that presents the data in the clearest possible manner.

Quaternary systems have been dealt with at some length. This is justifiable on the grounds that the conceptually simple ternary systems, together with quaternary systems, are those on which experimental data exists. Little experimental data is available on quinary and higher-component systems.

Projection techniques for the graphical representation of quinary systems have been published by Perel'man[15, 18] and in Chapter 4 of Cayron's book[14]. Phragman has also dealt with the perspective projection of quinary Al alloys on to a concentration tetrahedron[10]. The complexity of these projections methods makes one doubt whether sectioning techniques do not provide a better method of representation of the equilibria. The next section considers this topic.

Sectioning Methods

As previously noted no difficulty is experienced in representing the temperature - concentration diagrams of binary and ternary systems. For quaternary and higher-component systems some form of sectioning is required to allow a graphical representation of the system in two- or three-dimensions. Assuming isobaric conditions sections of phase diagrams are $(n - \lambda)$-dimensional, where λ is the number of external factors assumed constant in the given section of the n-component phase diagram.

In quaternary systems the application of one constraint to the system gives three-dimensional sections. If the temperature is assumed constant the isothermal section appears as a three-dimensional tetrahedron. A series of such tetrahedra relating to various temperatures provides a useful, if laborious, means for tracing the variation of the equilibria as a function of temperature[19]. F.N. Rhines has made extensive use of isothermal sections combined with an exploded representation of each phase region[20]. Figure 13 is an example of an isothermal section at a temperature equal to the binary BD eutectic temperature. Liquid whose composition is represented on the surfaces 4-5-6 or 5-7-8 is in equilibrium with solid β or solid α whose compositions are represented by corresponding points on surfaces 1-2-3 and 9-10-11 respectively.

If a series of isothermal sections are projected on to the concentration tetrahedron a three-dimensional polythermal projection of the quaternary system is produced. Each triangular face represents a polythermal projection of the appropriate ternary system whilst the interior of the tetrahedron represents the polythermal projection of the quaternary system. Such projections are useful in tracing the course of freezing of quaternary alloys. However not many systems have been studied in sufficient experimental detail to allow this type of representation.

Another type of three-dimensional section is produced if, instead of assuming constant temperature, the content of one component is maintained constant. A section at a constant %B is a triangular plane acd parallel to the basal triangle ACD, figure 14. Temperature-concentration diagrams are drawn for each of the three ternary systems at the constant %B - sections ac for the system ABC, cd for BCD, and ad for ABD. From these the quaternary section at constant %B is produced. The method has been advocated by A. Schrader and M. Hanemann[21]. It provides information on the sequence of phase fields through which any quaternary alloy on the section acd passes through on cooling or heating. It does not indicate the compositions of coexisting phases since these lie outside the plane of the section.

If two constraints are applied to a quaternary system (P = constant) the resulting sections will be two-dimensional. Referring to figure 9, a section at a constant %UFe_2 through an isothermal tetrahedron will be a triangle[12]. A similar result would obtain if an isothermal section were taken through the temperature-concentration diagram of figure 14. Alternatively one may take a section at a constant percentage of one component through a polythermal section of the quaternary system, to produce a polythermal representation of the equilibria. Examples are given in the paper by G. Petzow and F. Aldinger[22].

Finally two-dimensional sections are produced if two of the component concentrations are assumed constant. This is equivalent to sectioning the three-dimensional temperature-concentration diagram, figure 14, at a constant percentage of component A, B, or C. In experimental work it would be normal to determine two-dimensional sections at constant concentrations of two components. It is not necessary to assume this restriction since temperature-concentration sections can be produced for any line segment through a quaternary system. L.S. Palatnik and A.I. Landau[16] have described a variety of methods for producing two-dimensional temperature-concentration sections of multicomponent systems. These have been summarised in a review by the author[23].

The combinatorial method of number chains relies on the description of the indices of the individual hypervolumes intersected by a one-dimensional concentration axis passing through a polythermal projection of the n-component system. As a simple example consider the polythermal projection of a ternary eutectic system. It is required to construct the temperature-concentration section ab, figure 15. The components are denoted 1,2,3; binary eutectics as 12, 13, 23; the ternary eutectic as 123 or E; the liquid phase as O. The section ab intersects the projected areas (1)(12)(123), (1)(13)(123), (3)(13)(123) and (3)(23)(123). The sequence of indices produced is called a numerical chain. It provides a representation of the phase composition and the sequence of phase regions in the required section. To construct the section a table of phase compositions must be produced from the numerical chain. The first area cut by the section ab is tabulated in full. Each succeeding area is tabulated only insofar as the one number which distinguishes it from the preceding area. The last area cut by the section ab is tabulated in full. This gives a table of phase compositions of the form:

1		3	3
12	13		23
123			123

The numeral O, representing the liquid phase, is added to all indices and those indices underlined by which an area differs from its preceding area:

01		<u>03</u>	03
012	<u>013</u>		<u>023</u>
0123			0123

A lattice is constructed to represent the number of columns and rows in the table. All underlined indices are denoted by a point on the lattice:

01		03	03
012	013		023
0123			0123

The points are now joined together so that they conform to the rule of adjoining phase regions and the cross rule. The rule of adjoining phase regions states that the dimension of the phase diagram or regular section, R, is related to the dimension of the boundary between neighbouring phase regions, R_1, by the relation:

$$R_1 = R - D^- - D^+$$

where D^- and D^+ represent, respectively, the number of phases that disappear and the number of phases that appear in a transition from one phase region to the other. The cross rule concerns the phase distribution in the four phase regions meeting at a point in a two-dimensional phase diagram or regular section. Of the four phase regions one will have the minimum number of phases; neighbouring phase regions will each have an additional phase; the fourth phase region is joined to the phase region with the minimum number of phases through the central point and it contains the maximum number of phases, figure 16. Inspection will show that the rule of adjoining phase regions is obeyed for all transitions from one phase region to another in figure 16.

We can now complete the construction of the temperature-concentration section ab of figure 15. This leads to the

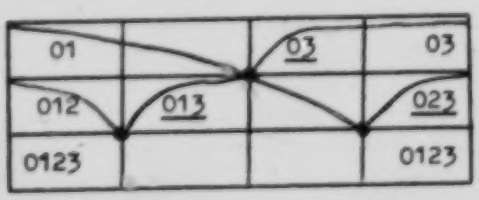

well-known section illustrated in figure 17. The area 0123 represents the coexistence of the liquid phase with the three components. It is the invariant ternary eutectic. When all liquid is consumed all alloys would be represented by the index 123.

The utility of the combinatorial method of numerical chains for constructing two-dimensional sections is only evident when quaternary and higher-component systems are considered. An alternative method proposed by A.I. Landau, the shadow method, involves casting a shadow of the concentration axis of the required two-dimensional section on to the coordinate simplex of the system. In quaternary eutectic systems it is assumed that a light is placed at the quaternary eutectic point in the concentration tetrahedron and that the light casts a shadow of the concentration axis on to the side faces of the tetrahedron. The concentration axis passes through individual volumes in the three-dimensional polythermal projection of the quaternary system and its shadow passes through the corresponding areas on the side faces of the projection in the same sequence. For simplicity the concentration tetrahedron is unfolded about its base triangle into four planar

triangles, figure 18. The shadow of the concentration axis ab lays in areas that produce the numerical chain (1)(12)(124), (1)(12)(123), (1)(13)(123), (3)(13)(123), (3)(23)(123), (3)(23)(234). The corresponding table of compositions is therefore:

01		03		03
012		013		023
0124	0123		023	0234

The corresponding phase diagrams of section ab is illustrated in figure 19.

Reciprocal Systems

Reciprocal systems involve double decomposition reactions of the type $AB + CD \rightleftharpoons AD + CB$. Such systems are met when dealing with salt systems such as $KF + NaCl \rightleftharpoons KCl + NaF$. The system is ternary since all compositions can be expressed in terms of any three of the compounds (components), i.e. in terms of NaCl, KCl, and NaF since KF = KCl + NaF - NaCl. By appropriate choice of components it is possible to express any composition in terms of positive percentages of three-components. Figure 20 illustrates the graphical representation of a reciprocal system. Two triangles are placed together to form a square. The composition X is a ternary eutectic mixture of KCl + KF + NaF. If it is assumed that the side of the square is equal to 100% of the three components, aX = % KCl, bX = % NaF and cX = % KF. The composition Y is similarly derived as fY = % KCl, ey = % NaF and hY = % NaCl. Alternatively Y can be referred to the three components outside the triangle in which it is placed. In figure 20 Y would then have a composition dY = % KCl, gY = % NaF and hY = - % KF. The negative sign for the % KF indicates that this component does not enter the phase composition of Y in reality. It also ensures that the total % of the three components adds to 100% since dY + gY - hY = dY + gh = de. Ricci[17] gives an extensive treatment of reciprocal systems to which those interested in pursuing the topic are recommended.

Systems with Variable Valency of a Component

Probably the most important system to consider is the Fe-O system. Figure 21a gives the phase stability diagram in relation to the temperature and partial pressure of the oxygen. As its name implies this diagram indicates the ranges of temperature and P_{O_2} under which condensed phases are stable. Within the magnetite field the Phase Rule indicates that the temperature and P_{O_2} are independent variables. ($P + F = C + 2$. $F = 2 + 2 - 2 = 2$). There are two degrees of freedom since two phases are involved - the magnetite and the gas phase. The boundary curves, such as that between magnetite and wustite represent conditions for the coexistance of these phases - magnetite, wustite and the gas phase - implying a monovariant equilibrium. A particular temperature is associated with a fixed P_{O_2}.

If we choose to maintain a large gas reservoir at $P_{O_2} = 10^{-8}$ atmospheres and slowly heat a sample of hematite in this reservoir the phase stability diagram indicates the temperature ranges over which the condensed phases are stable. Hematite is stable to point 1; at this

temperature it is in equilibrium with magnetite; from 1 to 3 magnetite is stable etc. The drawback to this method of representation is that the compositions of the condensed phases are not shown. To overcome this objection one may represent the Fe-O phase diagram as a normal-temperature concentration diagram but with a series of curves showing identical values of partial pressures of oxygen in the gas phase in equilibrium with the condensed phases. In figure 21b one such curve is drawn at $P_{O_2} = 10^{-8}$ atmospheres. If the sample of hematite is slowly heated in an atmosphere with $P_{O_2} = 10^{-8}$ atmospheres, the hematite will remain unchanged until 875°C is reached. At this temperature hematite of composition 1 is in equilibrium with magnetite of composition 2 in accordance with the reaction $3Fe_2O_3 = 2Fe_3O_4 + \frac{1}{2}O_2$. Increase of temperature involves the completion of the reaction with disappearance of the hematite phase. With increasing temperature the oxide composition changes slightly across the magnetite field, 2-3, until at 1275°C magnetite of composition 3 is in equilibrium with wustite of composition 4 in accordance with the reaction $Fe_3O_4 = 3FeO + \frac{1}{2}O_2$. Subsequently the oxide is converted wholly to wustite whose composition than changes along the curve 4-5. At 1400°C solid wustite, 5, is equilibrated with liquid oxide, 6. Further increase in temperature moves the liquid composition to saturation with Fe at 1635°C at point 7. At 1635°C liquid oxide is in equilibrium with O_2-saturated liquid Fe according to the reaction $FeO_{(liquid)} = Fe_{(liquid)} + \frac{1}{2}O_2$. Beyond 1635°C the liquid oxide phase disappears and the liquid Fe is reduced in dissolved oxygen content.

The relation between the two representations are indicated in figure 21 by dotted lines at the invariant reaction temperatures.

A.D. Pelton and H. Schmalzried[24] have considered the generalised geometrical representation of phase diagrams, particularly with the aim of optimising thermodynamic information for multicomponent systems in two-dimensional diagrams. Three types of phase diagrams were studied:

1. diagrams whose coordinate framework consisted of two thermodynamic functions. Temperature, pressure, and chemical potential are the defined thermodynamic functions.
   Such diagrams would include T-log P_{O_2} diagram, figure 21a, T-P diagrams, and the log P_{Cl_2}-log P_{O_2} diagram for the U-O-Cl system[25]

2. diagrams whose coordinate framework consists of one thermodynamic function and a ratio of conjugate extensive variables. Typical of such diagrams are plots of $T\text{-}X_O/X_{Fe} + X_O$, figure 21b, and plots of log P_{O_2}-$X_{Cr}/X_{Fe} + X_{Cr}$ for an isotherm of the Fe-Cr-O system

3. diagrams whose coordinate framework consists of two ratios of conjugate extensive variables.
   In the Fe-Cr-O system an isotherm could be plotted with coordinates $X_O/X_{Fe} + X_{Cr} - X_{Cr}/X_{Fe} + X_{Cr}$[24].

Analytical Representation of Phase Equilibria

The complexity of most quaternary and higher-component systems makes their graphical representation a difficult task for all concerned. For this reason increasing interest is being taken in analytical methods for representing phase equilibria. O.S. Ivanov[26] has considered this technique using the polythermal projection of the Al-Mg-Zn system to illustrate the applicability of the approach. It was found that quadratic

equations of the form

$$T = k_o + k_1 a + k_2 b + k_3 a^2 + k_4 ab + k_5 b_2^2$$

(T = liquidus temperature; a = Al content in weight %; b = Mg content in weight %)

were adequate to describe the liquidus surface in this ternary. Expressions for the monovariant curves could be derived by appropriate computer programming and indeed the computer could be used, with peripheral devices, to construct projections and sections and to generate the space model of the ternary system.

N.N. Sobolev and colleagues have considered the analytical representation of the solidus surface of the Mo-Nb-Ti-V quaternary system[27]. They used the method of simplex lattice designs, devised by H. Scheffé[28] to investigate the properties of multicomponent systems as a function of composition and extended by J.W. Gorman and J.E. Hinman[29]. The basis of this method is the selection of compositions on a lattice arrangement and determination of some corresponding property at each composition. In the present case solidus temperatures were determined for each alloy composition on the lattice. The solidus surface, or hypersurface for the Mo-Nb-Ti-V system, is then represented by a polynomial equation relating the solidus temperature to composition. Coefficients in the polynomial are functions of the measured temperature at the lattice points.

To obtain a uniform distribution of alloy compositions in the quaternary system a quadratic, cubic, or quartic lattice is selected, figure 22. The proportion of any component in the quadratic lattice is either 0, $\frac{1}{2}$, or 1 since each edge of the concentration simplex has one lattice point at its centre. Similarly the proportion of any component in the cubic and quartic lattices are 0, $\frac{1}{3}$, $\frac{2}{3}$, 1 and 0, $\frac{1}{4}$, $\frac{1}{2}$, $\frac{3}{4}$, 1 respectively.

The polynomials relating the solidus temperature, t, to the alloy composition ($x_1 + x_2 + x_3 + x_4 = 1$) are:-

quadratic model

$$t = \sum_{1 \leq i \leq 4} \beta_i x_i + \sum_{1 \leq i < j \leq 4} \beta_{ij} x_i x_j$$

cubic model

$$t = \sum_{1 \leq i \leq 4} \beta_i x_i + \sum_{1 \leq i < j \leq 4} \beta_{ij} x_i x_j + \sum_{1 \leq i < j \leq 4} \gamma_{ij} x_i x_j (x_i - x_j)$$

$$+ \sum_{1 \leq i < j \leq 4} \beta_{ijk} x_i x_j x_k$$

quartic model

$$t = \sum_{1 \le i \le 4} \beta_i x_i + \sum_{1 \le i < j \le 4} \beta_{ij} x_i x_j + \sum_{1 \le i < j \le 4} \gamma_{ij} x_i x_j (x_i - x_j)$$

$$+ \sum_{1 \le i < j \le 4} \delta_{ij} x_i x_j (x_i - x_j)^2 + \sum_{1 \le i < j < k \le 4} \beta_{iijk} x_i^2 x_j x_k$$

$$+ \sum_{1 \le i < j < k \le 4} \beta_{ijjk} x_i x_j^2 x_k + \sum_{1 \le i < j < k \le 4} \beta_{ijkk} x_i x_j x_k^2$$

$$+ \sum_{1 \le i < j < k < l \le 4} \beta_{ijkl} x_i x_j x_k x_l$$

The coefficients in the polynomials are functions of the experimentally determined solidus temperatures at the lattice compositions selected in the model used. In Scheffé's nomenclature the solidus temperature of a pure component, i, is denoted by t_i; the solidus temperature of a binary alloy containing $\frac{1}{2}$ i and $\frac{1}{2}$ j is denoted by t_{ij} where i and j are integers and $i < j$. Designating the components as 1, 2, 3 and 4 a 50:50 alloy of components 1 and 2 would have a solidus temperature t_{12}. The number of distinct numbers in the subscript indicates how many components are involved in the alloy, and the number of times a specific number appears indicates the relative proportions of the components. A binary alloy with $\frac{3}{4}$ x_1 and $\frac{1}{4}$ x_4 would have a solidus temperature designated as t_{1114}; a ternary alloy with $\frac{1}{4}$ x_2, $\frac{1}{2}$ x_3, $\frac{1}{4}$ x_4 would have a solidus temperature designated as t_{2334}. Figure 23 illustrates the nomenclature for the solidus temperatures of the 35 alloys in the quartic model of a quaternary system. If the solidus temperatures of these 35 alloys are determined experimentally the coefficients in the fourth-order polynomial can be calculated (see Appendix). It will be noted that all the coefficients are functions of the experimentally determined solidus temperatures.

Having determined the coefficients it remains to test the particular model used for the system under study. The fourth-order polynomial for a quaternary system has 35 coefficients, the same as the number of alloy lattice points. The polynomial will exactly match the value of temperature for each alloy. To test the model additional alloy compositions are necessary. A number of arbitary alloys, whose compositions do not coincide with the regular lattice of compositions, are checked for solidus temperature and these experimental results are compared with those calculated from the polynomial. If the t-test as used in statistics indicates no significance in the difference between experimental and calculated results the model is acceptable. Sobolev and co-workers fitted their data for 35 alloys in the Mo-Nb-Ti-V system, only one alloy of which was a quaternary, to a fourth-order polynomial. Ten arbitary alloys were used as a check on the applicability of the model with the calculated coefficients. Of these, three were quaternary alloys. The differences in solidus temperatures were negligible for two;

the third alloy was quoted as having an experimentally determined solidus of 1930°C as against the calculated value of 1980°C. This latter alloy was included in a section of the quaternary system studied by R.S. Polyakova[30] whose value of 2000°C for the solidus is close to the calculated value.

The difficulty with this method of representation is the need to decide which model is appropriate to the system under consideration. The simplest model, involving a quadratic model, requires only 10 experimental alloys to be examined in order to derive the coefficients of the polynomials for a quaternary system. As the complexity of the model increases or as the number of components in the system increases so does the number of experimental observations increase. This point is illustrated in the table below.

	MODEL		
	Quadratic	Cubic	Quartic
Quaternary	10	20	35
Quinary	15	35	70
Senary	21	56	126

The Mo-Nb-Ti-V system is a simple system in that the constituent binaries and ternaries all show complete solid solution series. Complicated hypersurfaces for the solidus are not anticipated. As Sobolev and his co-workers have shown it is feasible to produce an analytical expression for the solidus surface in this quaternary system which accords well with limited experimental data. The equation of the solidus surface can then be used to compute sections of the quaternary system. Sections at constant % Ti are given in the original paper.

Experimental data on phase equilibria could well be stored in the memory of a computer. With sufficient data and suitable programmes the computer could be used to produce analytical representations of phase boundaries. Three-dimensional diagrams and two-dimensional sections or projections could be computed and presented in graphical or tabular form. This extension of the traditional techniques for graphical representation of phase equilibrium data will mainly apply to multicomponent systems, in particular to the more complex quaternary systems and to all higher-order systems when experimental data begins to accumulate.

References

1. F. Rydberg, K. Svenska Vet. Akad. Handl., 1829, 157; Pogg. Ann., 1830, 18, 240

2. A. Prince, Annals Sci., 1955, 11, (1), 58

3. A. Ya. Kupfer, Ann. chim. phys., 1829, 40, 285

4. N.S. Kurnakov, "Collected Works", Vol. 1, 1961, Moscow (Acad. Sci. U.S.S.R.)

5. H.W.B. Roozeboom, Z. physikal. Chem., 1894, 15, 145

6. W. Hume-Rothery, G.W. Mabbott, and K.M. Channel-Evans, Phil. Trans. Roy. Soc., 1934, (A), 233, 1

7. T.B. Massalski and J.H. Perepezko, Z. Metallkunde, 1973, 64, 176

8. C.T. Sims, J.Metals, 1966, 18, (10), 1119

9. C.S. Barrett, J. Inst. Metals, 1972, 100, 65

10. G. Phragmen, J. Inst. Metals, 1950, 77, 489

11. L.F. Mondolfo, "Aluminium Alloys : Structure and Properties", Butterworths, London, 1976

12. G. Petzow and A.O. Sampaio, Z. Metallkunde, 1966, 57, 625

13. F.A.H. Schreinemakers, Z. physikal. Chem., 1909, 65, 553

14. R. Cayron, "Etude Theorique des Diagrammes D'Equilibre dans les Systemes Quaternaires", Institut de Métallurgie, Louvain, 1960

15. F.M. Perel'man, "Phase Diagrams of Multicomponent Systems. Geometric Methods", Consultants Bureau, New York, 1966

16. L.S. Palatnik and A.I. Landau, "Phase Equilibria in Multicomponent Systems", Holt, Rinehart and Winston Inc., New York, 1964

17. J.E. Ricci, "The Phase Rule and Heterogeneous Equilibrium", Chapter 16, D. Van Nostrand Co., New York, 1951 ; Dover Publications Inc., New York, 1966

18. F.M. Perel'man, "Methods for the Representation of Multicomponent Systems. Five-Component Systems", Moscow, Acad. Sci. U.S.S.R., 1959

19. A. Prince, "Alloy Phase Equilibria", Chapter 15, Elsevier, 1966

20. F.N. Rhines, "Phase Diagrams in Metallurgy", NcGraw-Hill, New York, 1956

21. A. Schrader and M. Hanemann, Z. Metallkunde, 1943, 35, 185

22. G. Petzow and F. Aldinger, Z. Metallkunde, 1968, 59, 145

23. A. Prince, Metallurgical Rev., 1963, 8, (30), 213

24. A.D. Pelton and H. Schmalzried, Metall. Trans., 1973, 4, 1395

25. O. Knacke, "Metallurgic l Chemistry", Proc. Symposium N.P.L./Brunel Univ., July 1971, H.M.S.O. (London), 1972, p. 549

26. O.S. Ivanov, Izvest. Akad. Nank SSSR., Metally, 1969, (1), 204

27. N.N. Sobolev, V.I. Levanov, O.P. Eliutin and V.S. Mikheev, Izvest. Akad. Nauk SSSR., Metally, 1974, (2), 217

28. H. Scheffé, J. Roy. Statistical Soc., 1958, 20B, 344

29. J.W. Gorman and J.E. Hinman, Technometrics, 1962, 4, 463

30. R.S. Polyakova, Izvest. Akad. Nank SSSR., Metally, 1970, 3, 199

APPENDIX

Solutions for the coefficients in the fourth-order polynomial

$$\beta_i = t_i$$

$$\beta_{ij} = 4t_{ij} - 2t_i - 2t_j$$

$$\gamma_{ij} = \frac{8}{3}(-t_i + t_j + 2t_{iiij} - 2t_{ijjj})$$

$$\delta_{ij} = \frac{8}{3}(-t_i - t_j + 4t_{iiij} + 4t_{ijjj} - 6t_{ij})$$

$$\beta_{iijk} = 32(3t_{iijk} - t_{ijjk} - t_{ijkk}) + \frac{8}{3}(6t_i - t_j - t_k) - 16(t_{ij} + t_{ik}) - \frac{16}{3}(5t_{iiij} + 5t_{iiik} - 3t_{ijjj} - 3t_{ikkk} - t_{jjjk} - t_{jkkk})$$

$$\beta_{ijjk} = 32(3t_{ijjk} - t_{iijk} - t_{ijkk}) + \frac{8}{3}(6t_j - t_i - t_k) - 16(t_{ij} + t_{jk}) - \frac{16}{3}(5t_{ijjj} + 5t_{jjjk} - 3t_{iiij} - 3t_{jkkk} - t_{iiik} - t_{ikkk})$$

$$\beta_{ijkk} = 32(3t_{ijkk} - t_{iijk} - t_{ijjk}) + \frac{8}{3}(6t_k - t_i - t_j) - 16(t_{ik} + t_{jk}) - \frac{16}{3}(5t_{ikkk} + 5t_{jkkk} - 3t_{iiik} - 3t_{jjjk} - t_{iiij} - t_{ijjj})$$

$$\beta_{ijkl} = 256_{ijkl} - 32(t_{iijk} + t_{iijl} + t_{iikl} + t_{ijjk} + t_{ijjl} + t_{jjkl} + t_{ijkk} + t_{ikkl} + t_{jkkl} + t_{ijll} + t_{jkll} + t_{ikll}) + \frac{32}{3}(t_{iiij} + t_{iiik} + t_{iiil} + t_{ijjj} + t_{jjjk} + t_{jjjl} + t_{ikkk} + t_{jkkk} + t_{kkkl} + t_{illl} + t_{jlll} + t_{klll}).$$

706

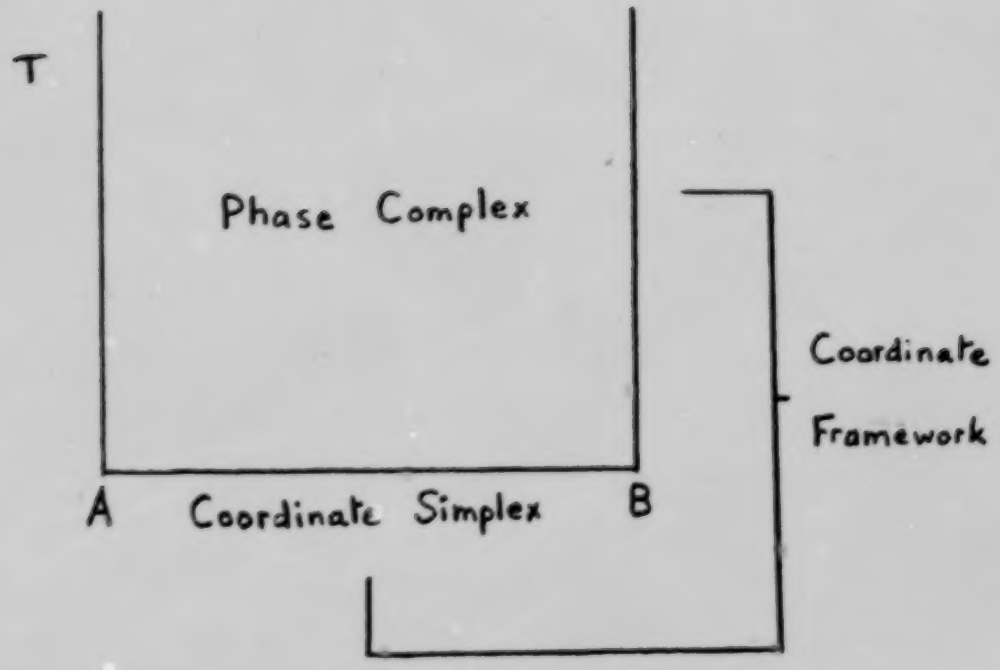

FIGURE 1. BINARY PHASE DIAGRAM WITH T-X COORDINATE FRAMEWORK

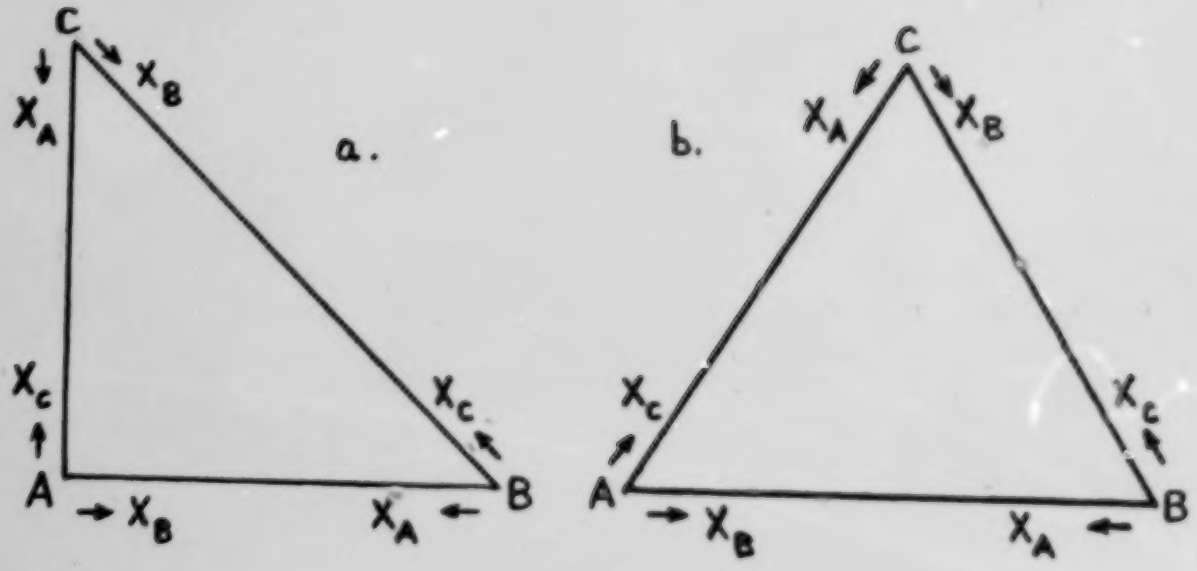

FIGURE 2. a) Ternary System Concentration Diagram
b) The Gibbs triangle

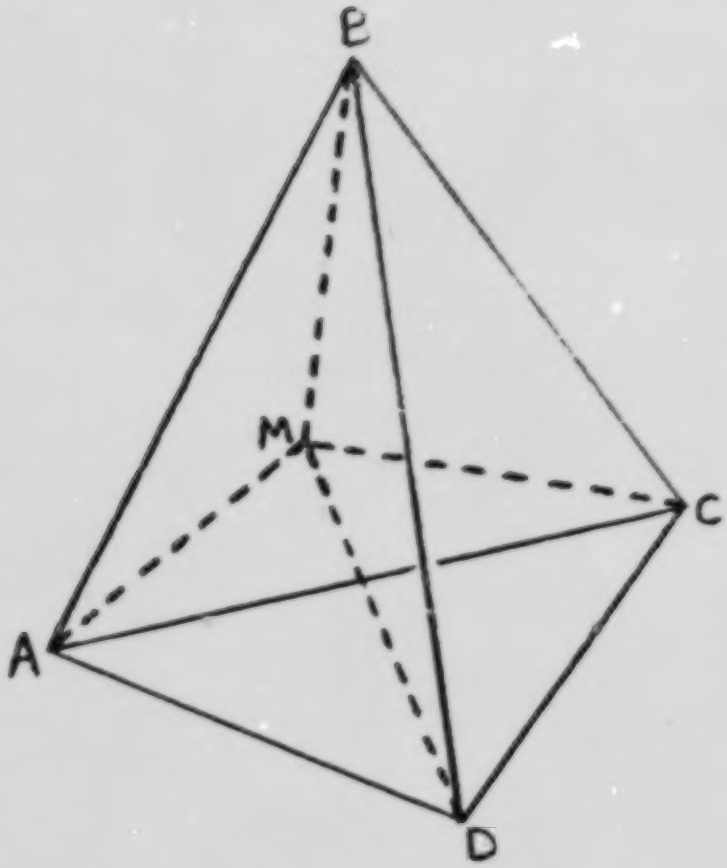

FIGURE 3. Quaternary System Concentration Diagram

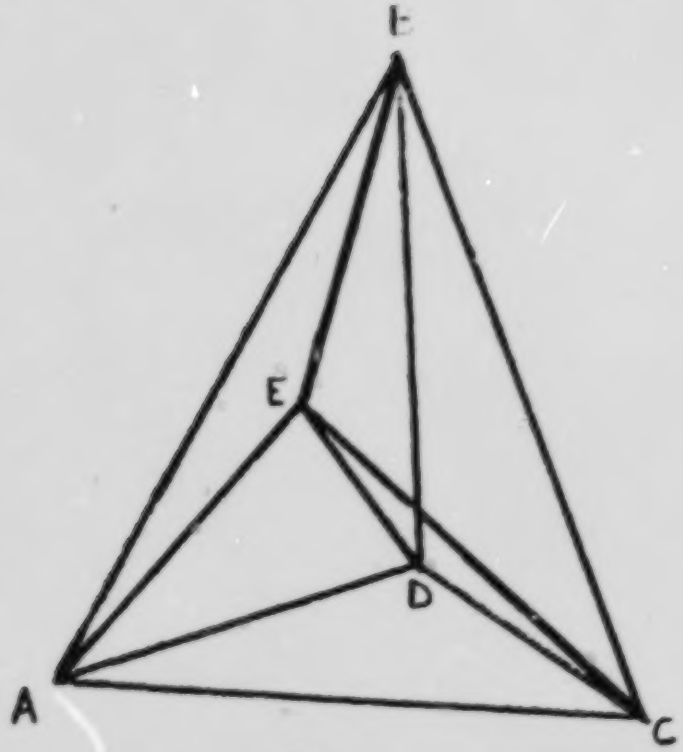

FIGURE 4. Three-dimensional projection of a Quinary System Concentration Diagram

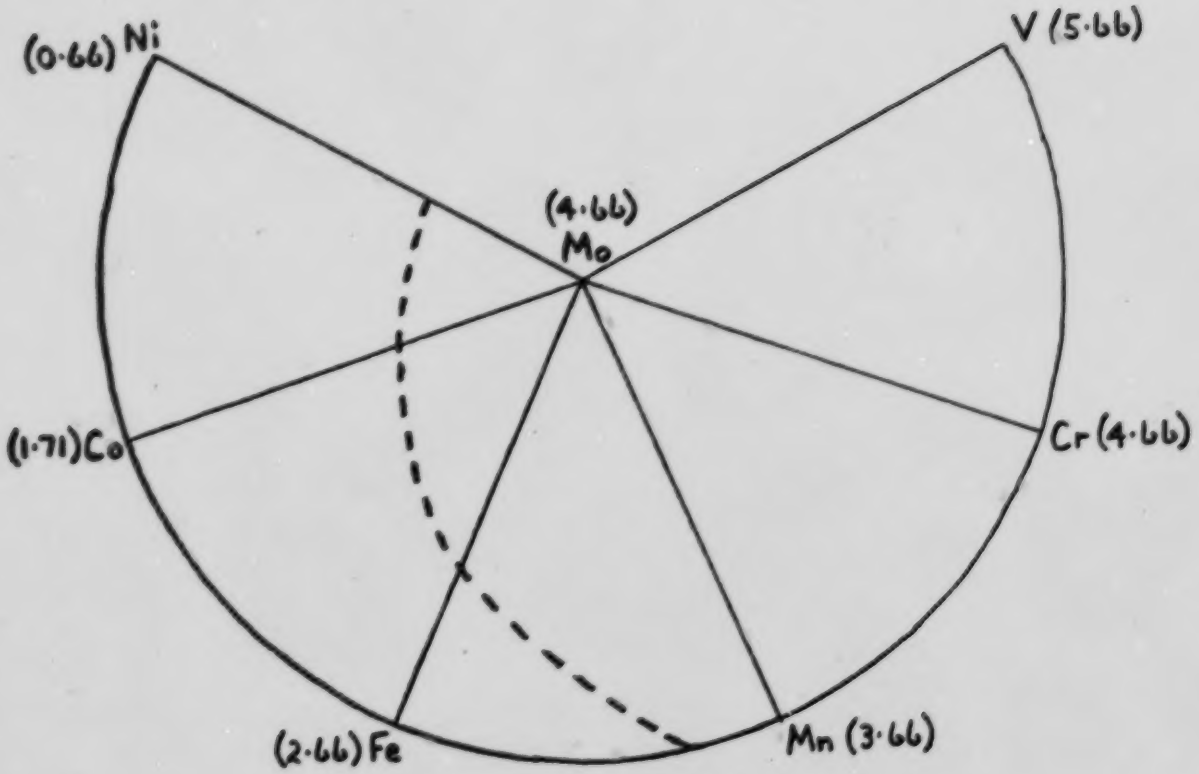

FIGURE 5. Polar Diagram for Mo Alloys
(--- $N_v = 3 \cdot 5$)

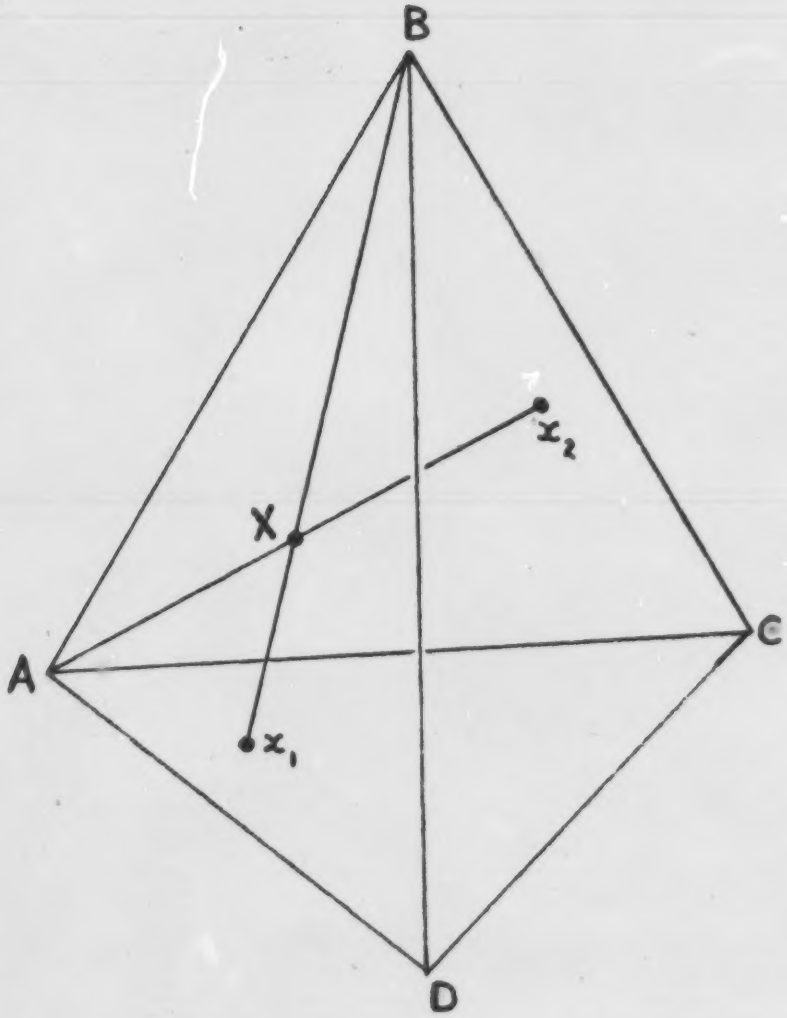

FIGURE 1. Perspective Projection of Quaternary Alloy X

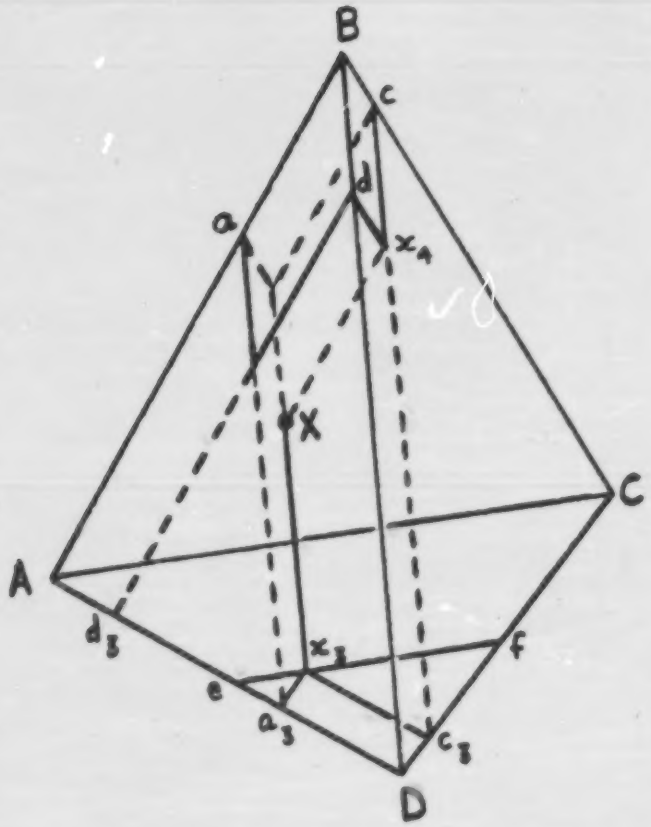

FIGURE 7. Parallel Projection of Quaternary Alloy X

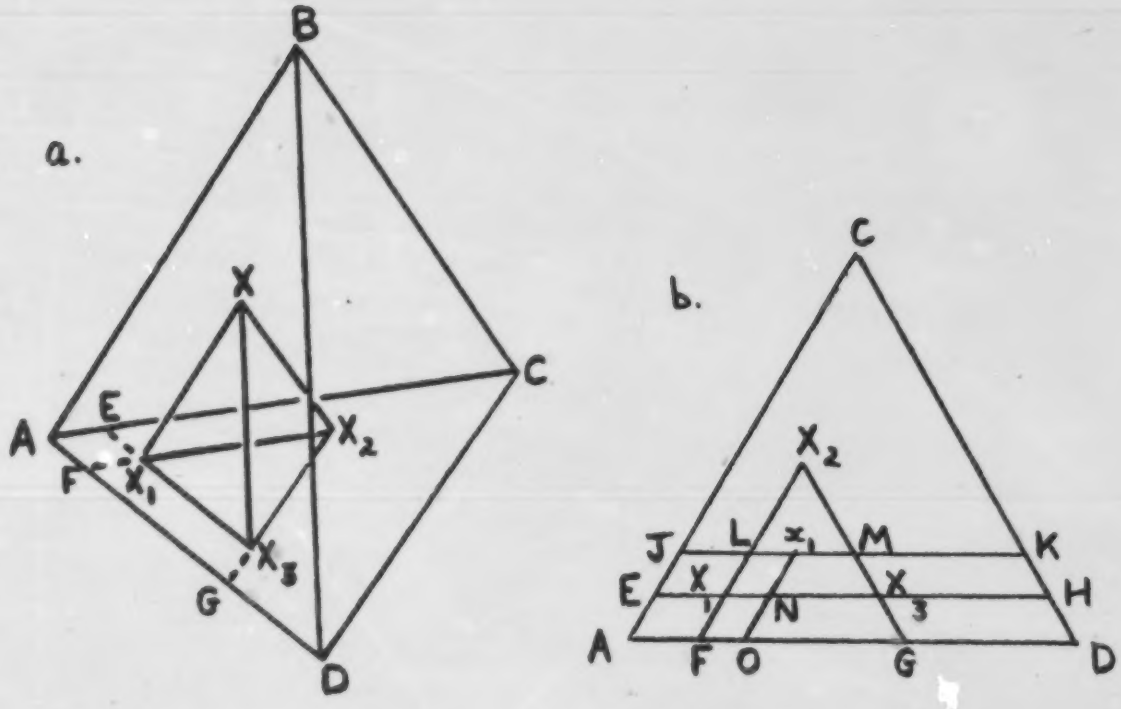

FIGURE 8. Orthogonal Parallel Projection of Quaternary Alloy X

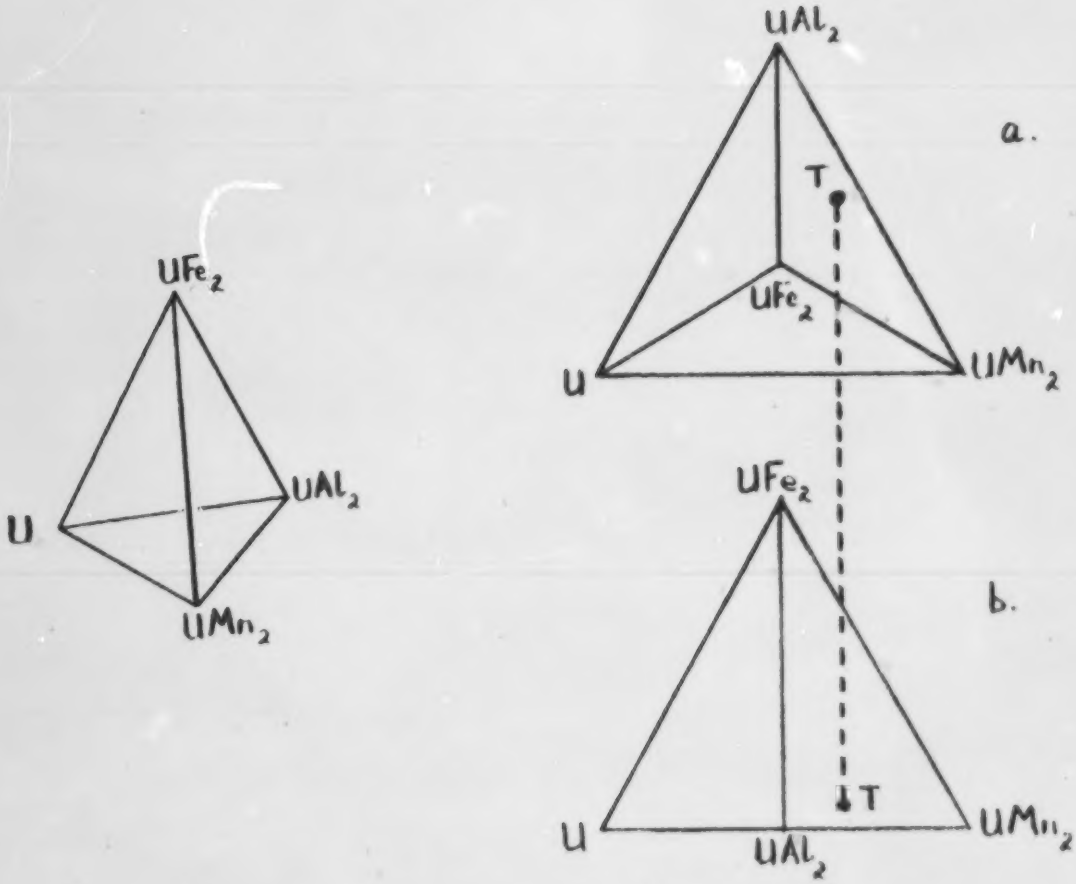

FIGURE 9. Projection of the U-UMn_2-UAl_2-UFe_2 System

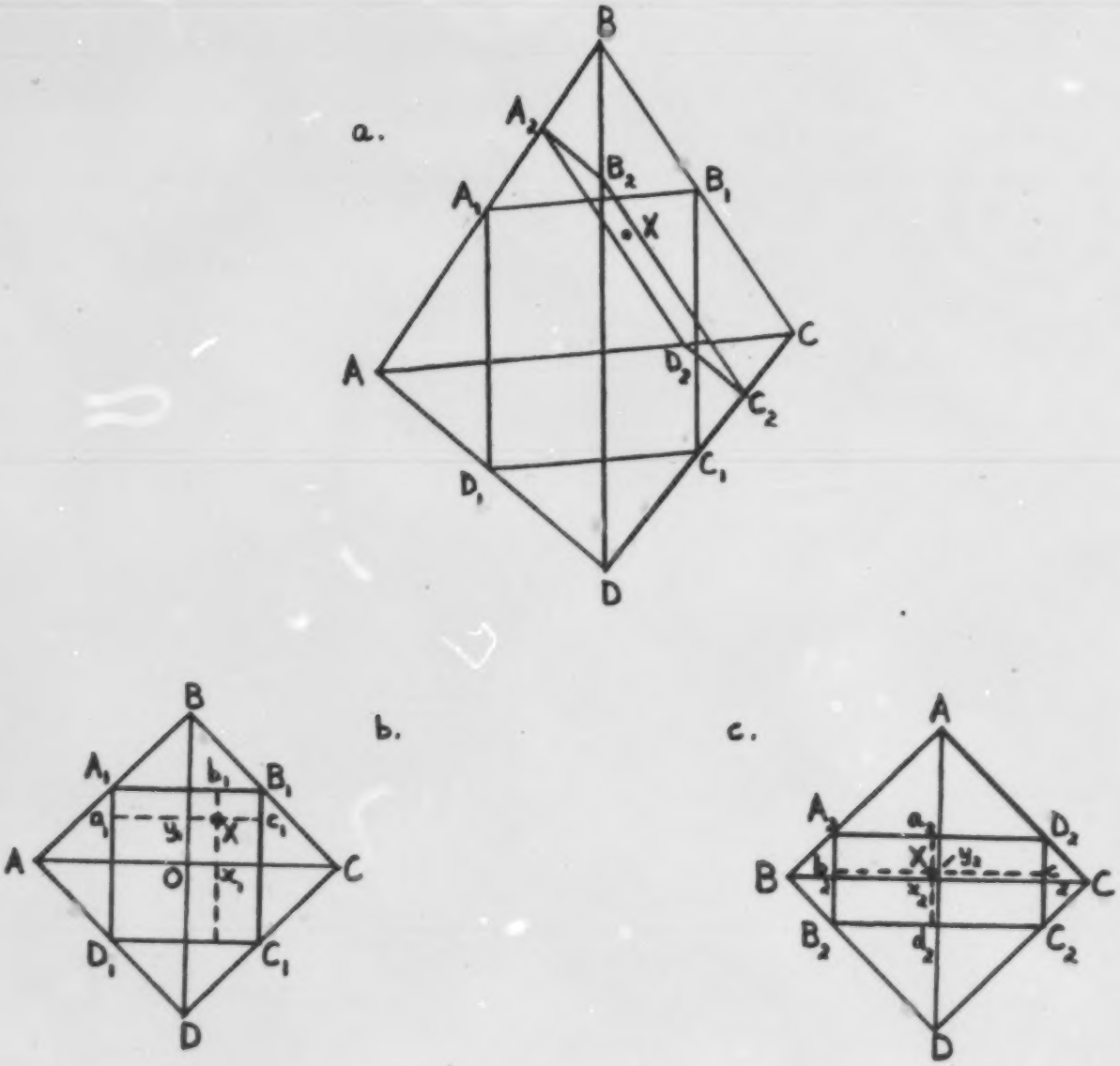

FIGURE 10. Square Orthogonal Projection of Quaternary Alloy X

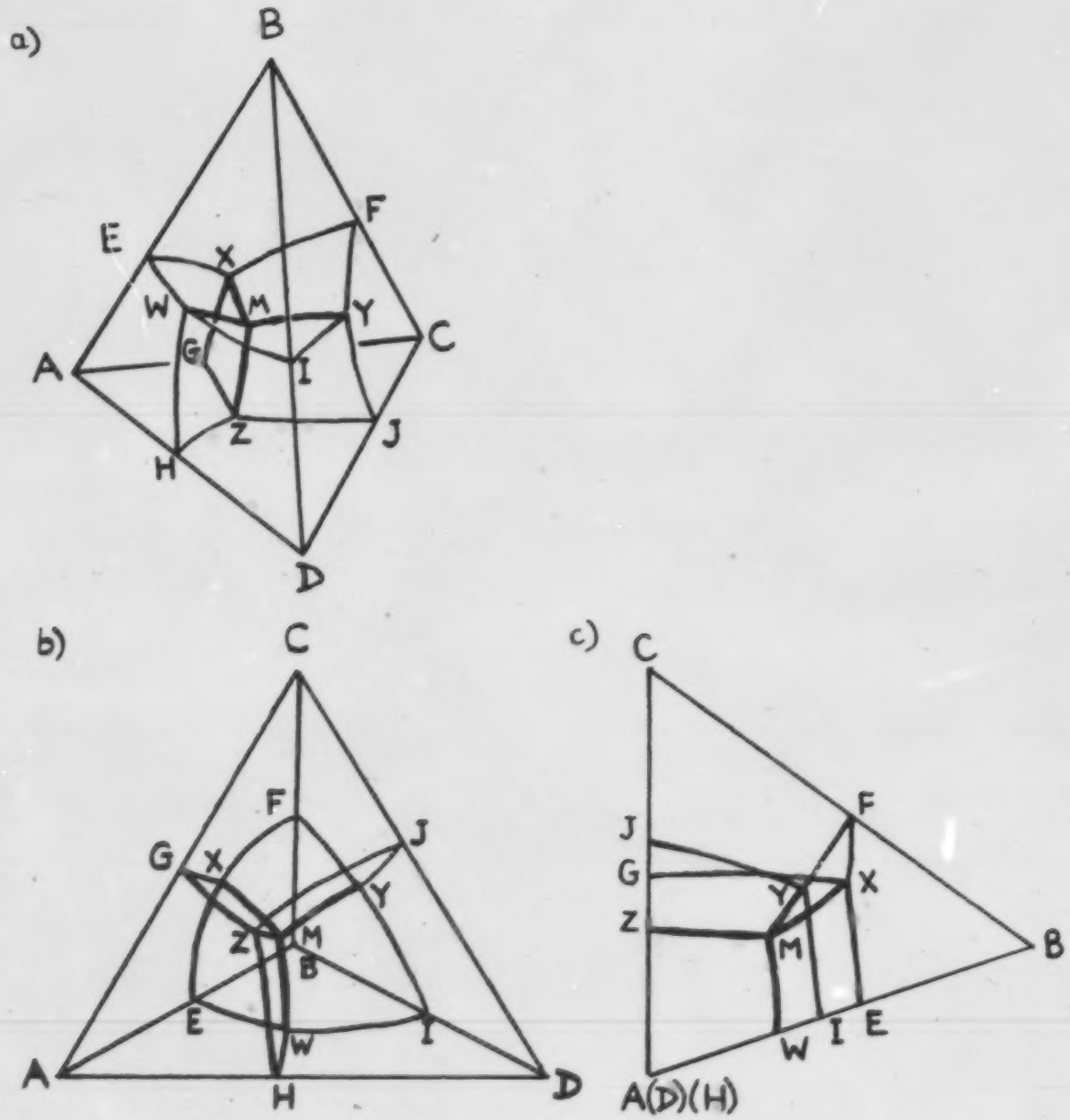

FIGURE 11 CAYRON ORTHOGONAL PROJECTION OF A SIMPLE QUATERNARY EUTECTIC SYSTEM

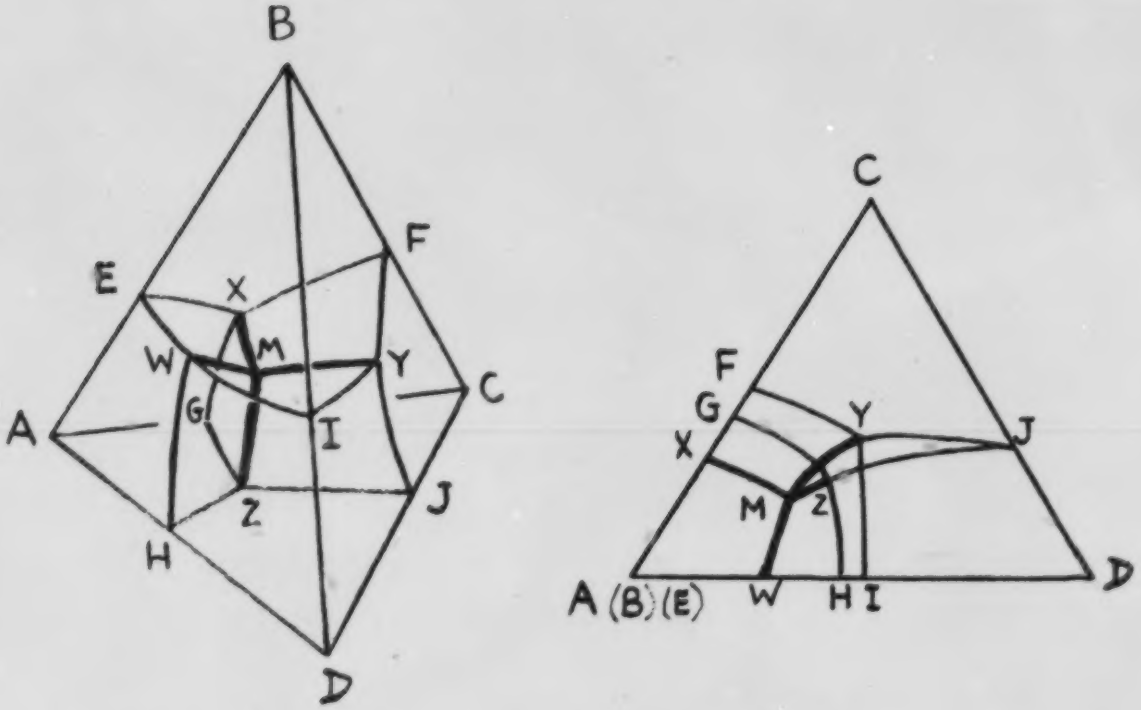

FIGURE 12. PEREL'MAN OPTIMAL PROJECTION OF A SIMPLE QUATERNARY SYSTEM.

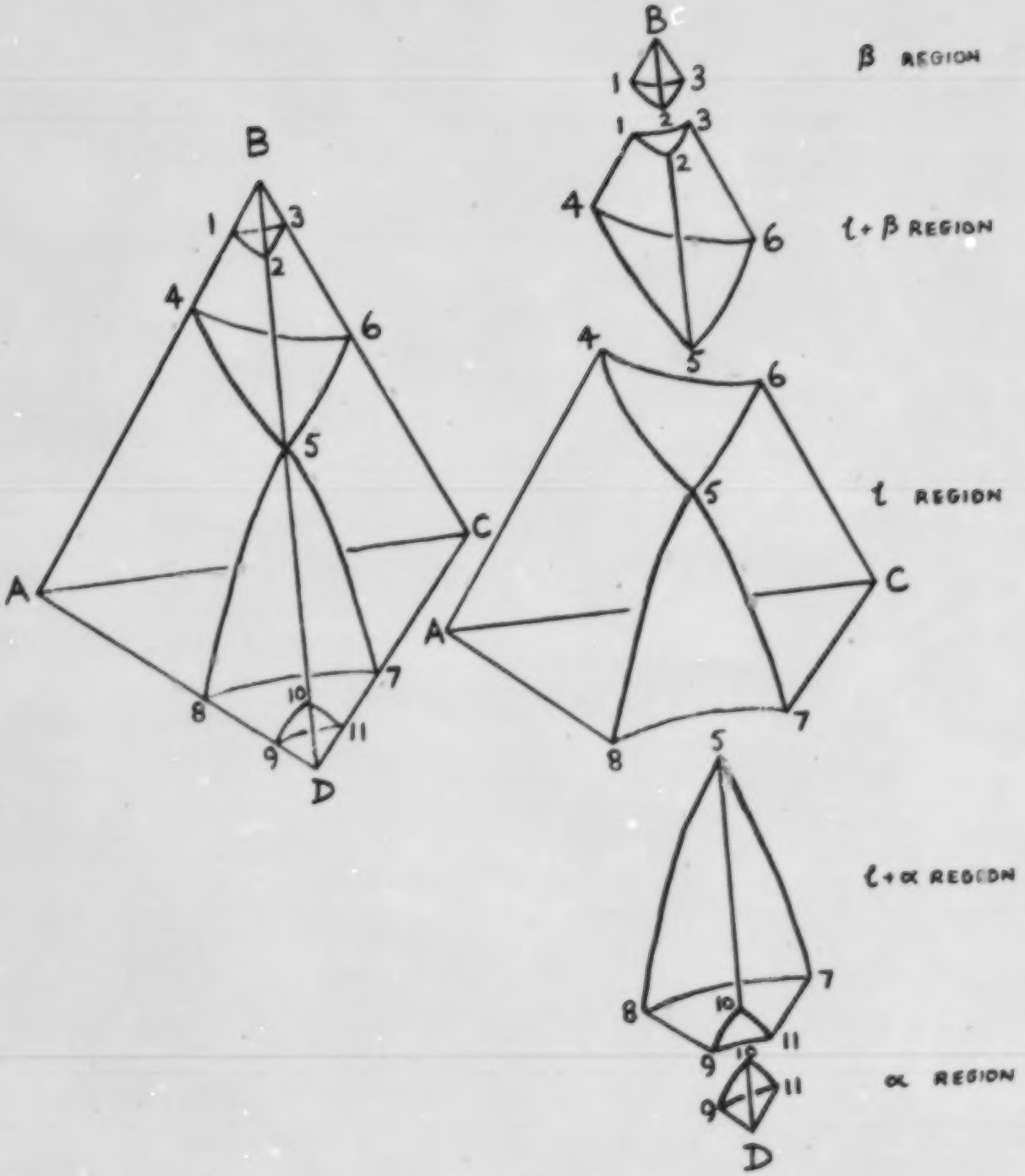

FIGURE 13. ISOTHERMAL SECTION WITH EXPLODED MODEL OF PHASE REGIONS.

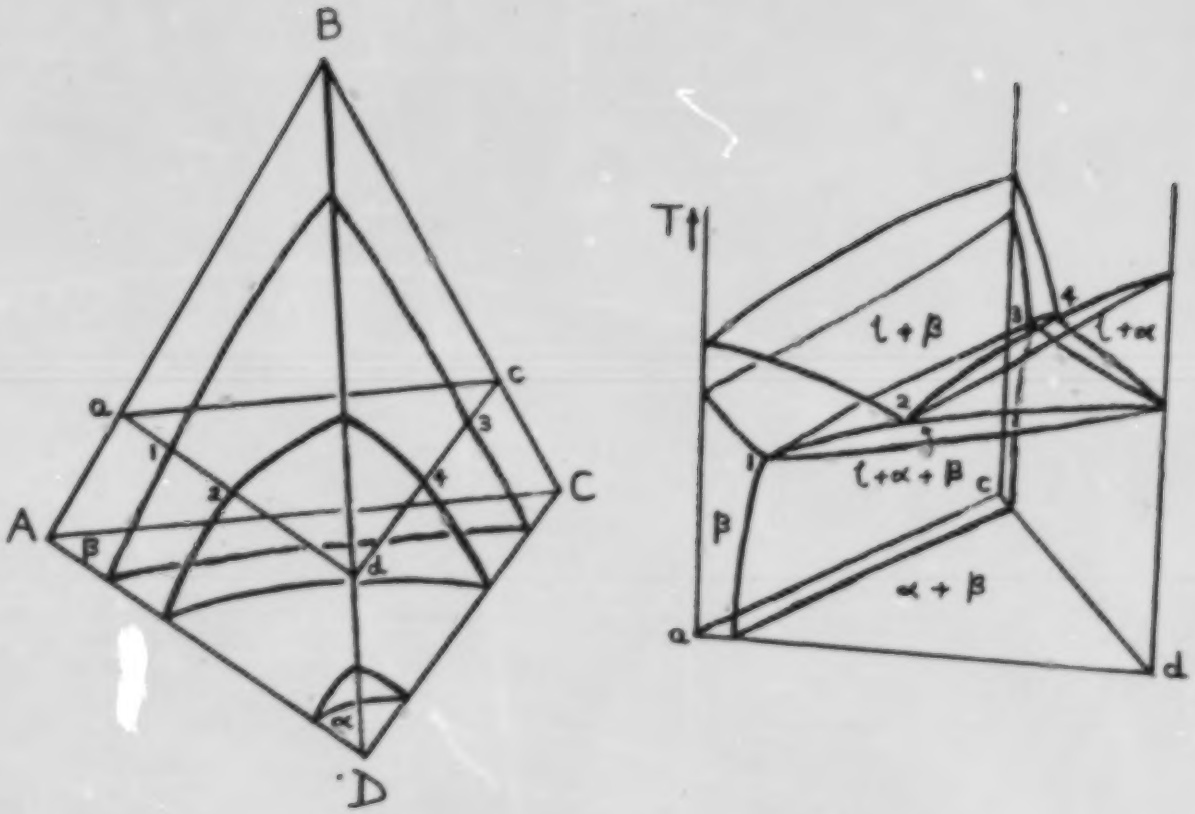

FIGURE 14. THREE - DIMENSIONAL TEMPERATURE - CONCENTRATION SECTION OF A QUATERNARY SYSTEM AT CONSTANT % B.

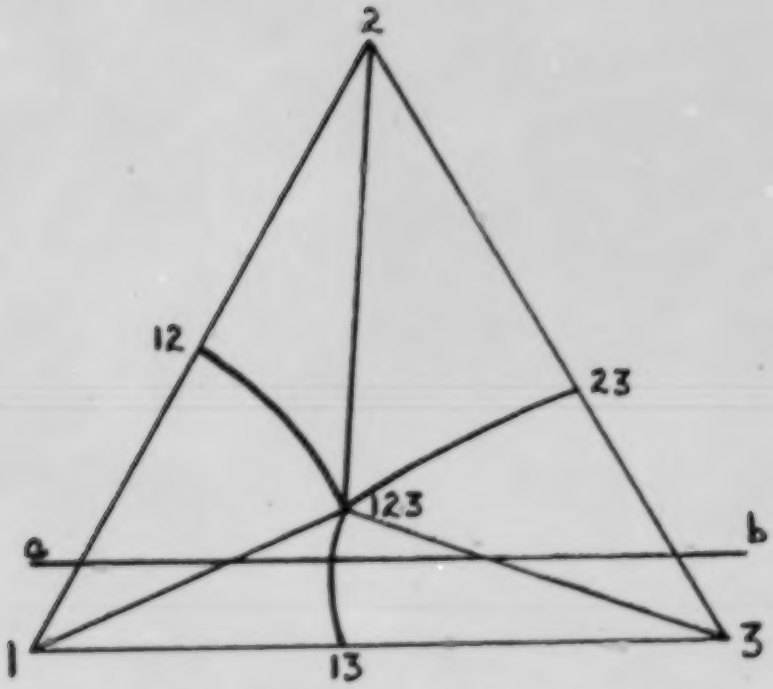

FIGURE 15. Section ab of the Ternary Polythermal Projection 234

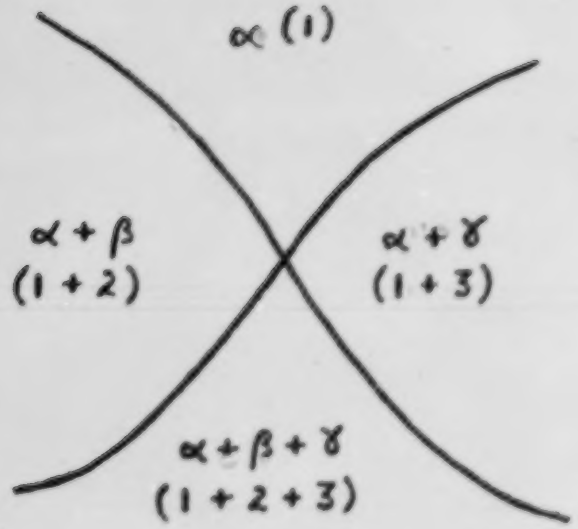

FIGURE 16. Illustration of the Cross Rule

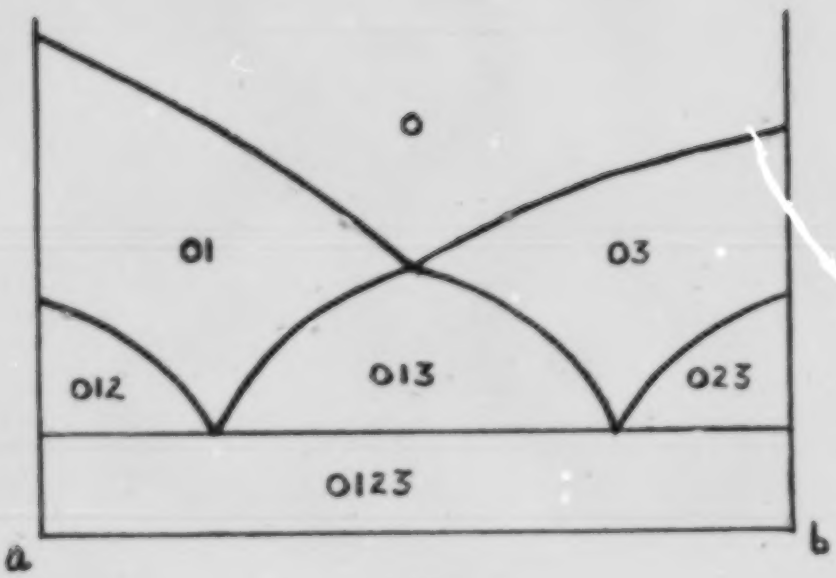

FIGURE 17. Two-dimensional Section along ab

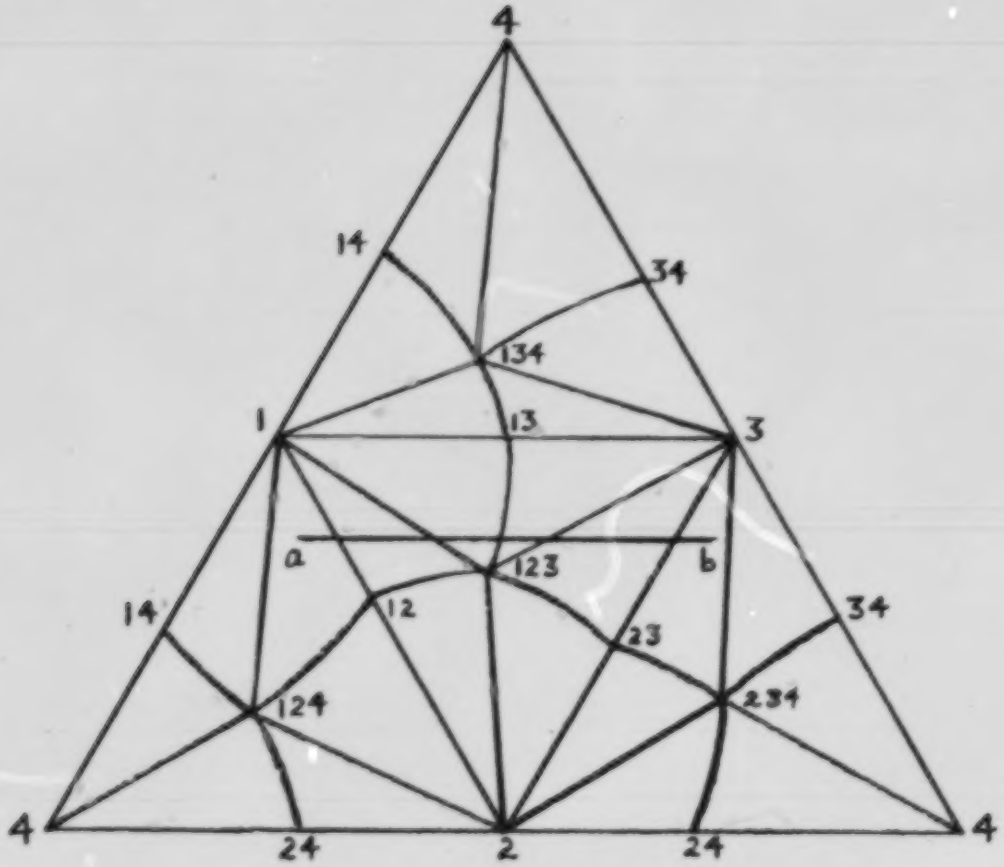

FIGURE 18. The Concentration Tetrahedron Unfolded About the Basal Triangle

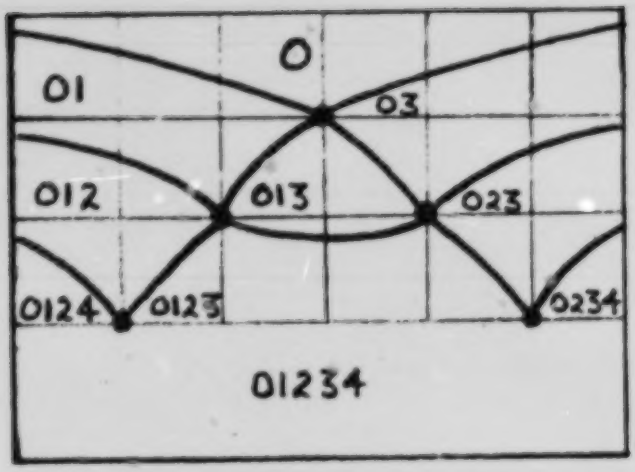

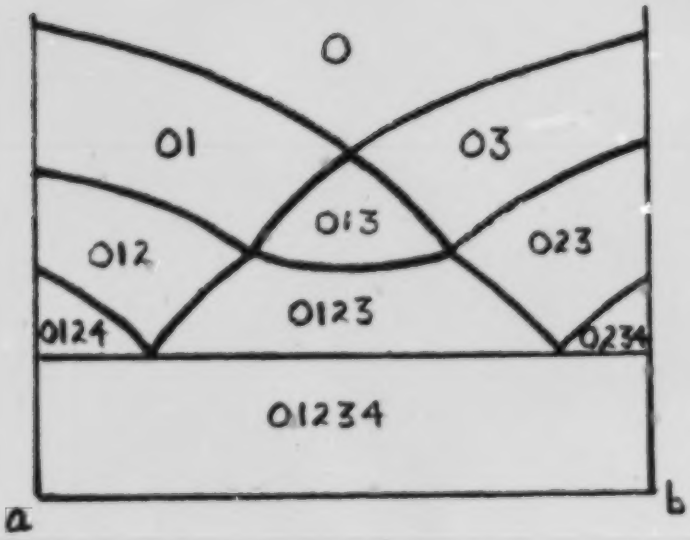

FIGURE 19. Two-dimensional Section Along ab

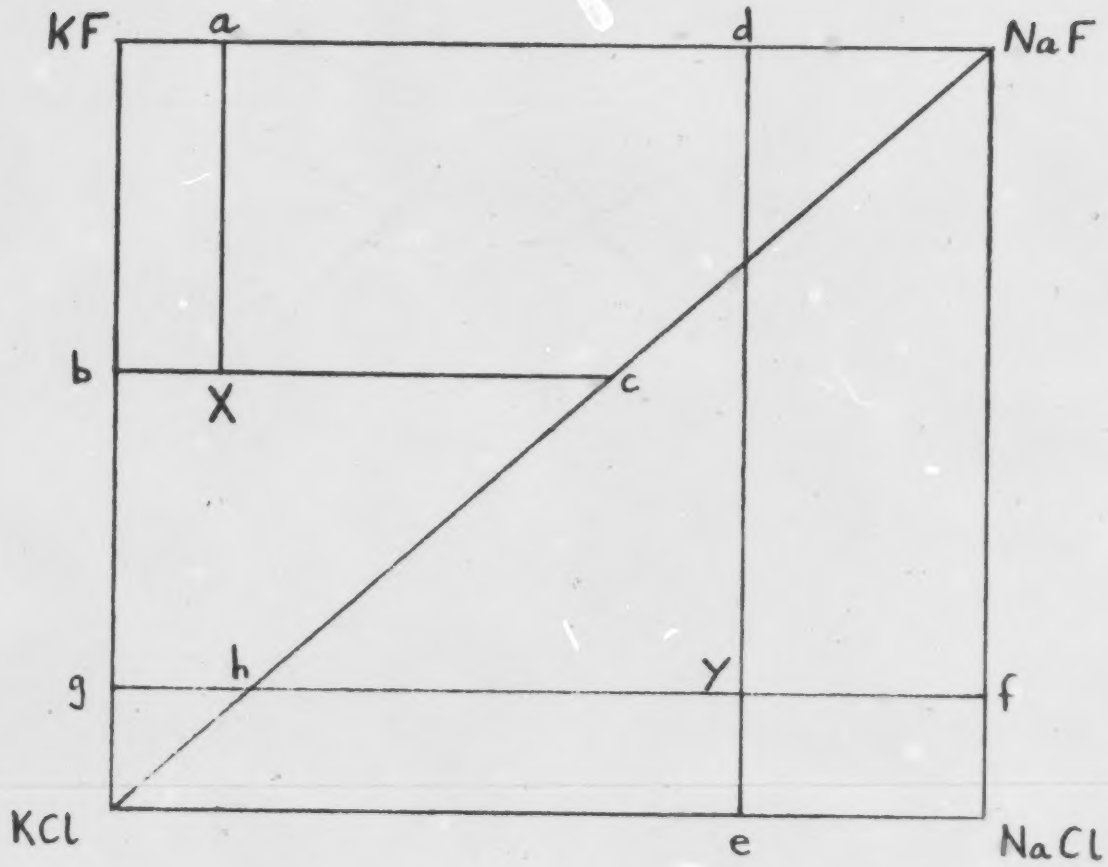

FIGURE 20. Representation of a Reciprocal System

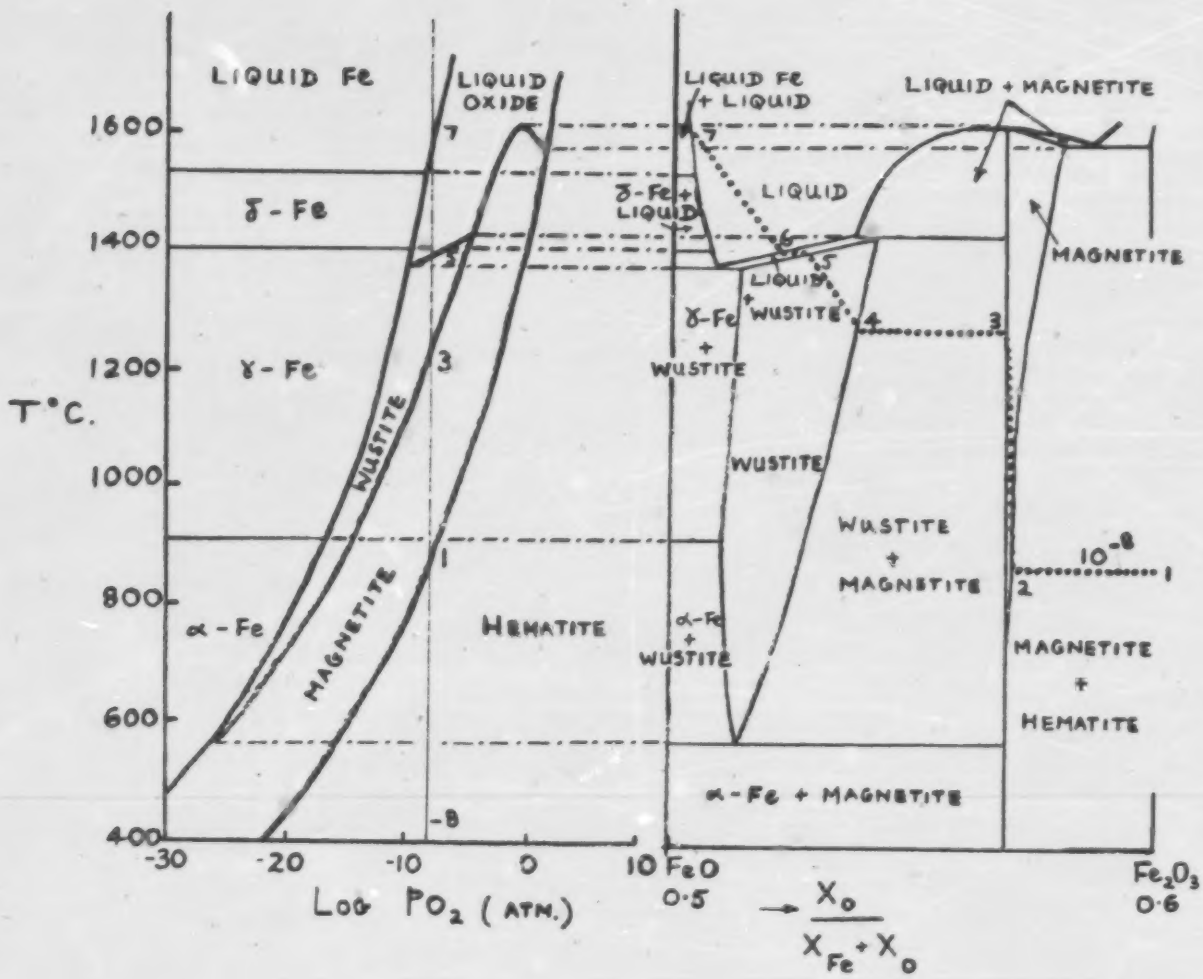

FIGURE 21a) PHASE STABILITY DIAGRAM FOR THE Fe-O SYSTEM. b) PHASE DIAGRAM OF THE Fe-O SYSTEM.

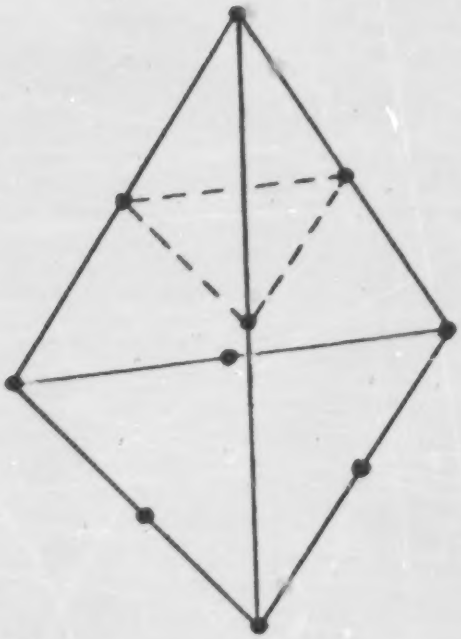

a) Quadratic Lattice

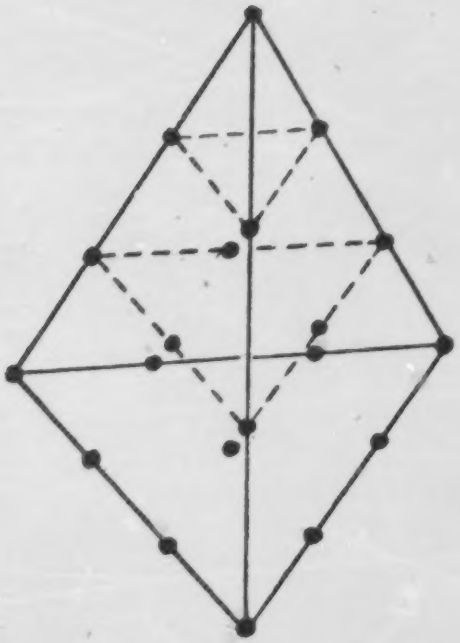

b) Cubic Lattic-

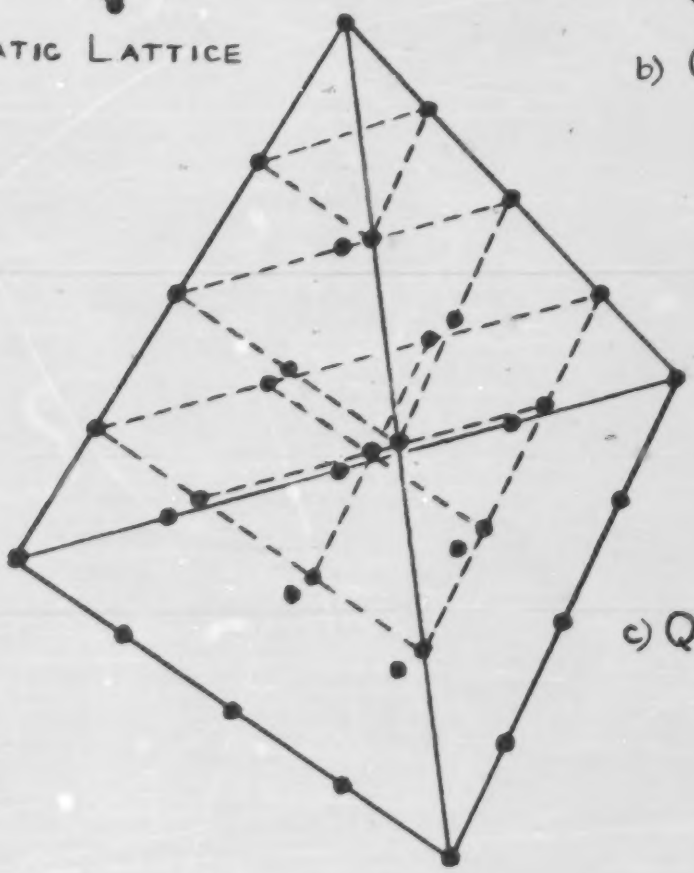

c) Quartic Lattice

Figure 22. Lattice types for a quaternary system

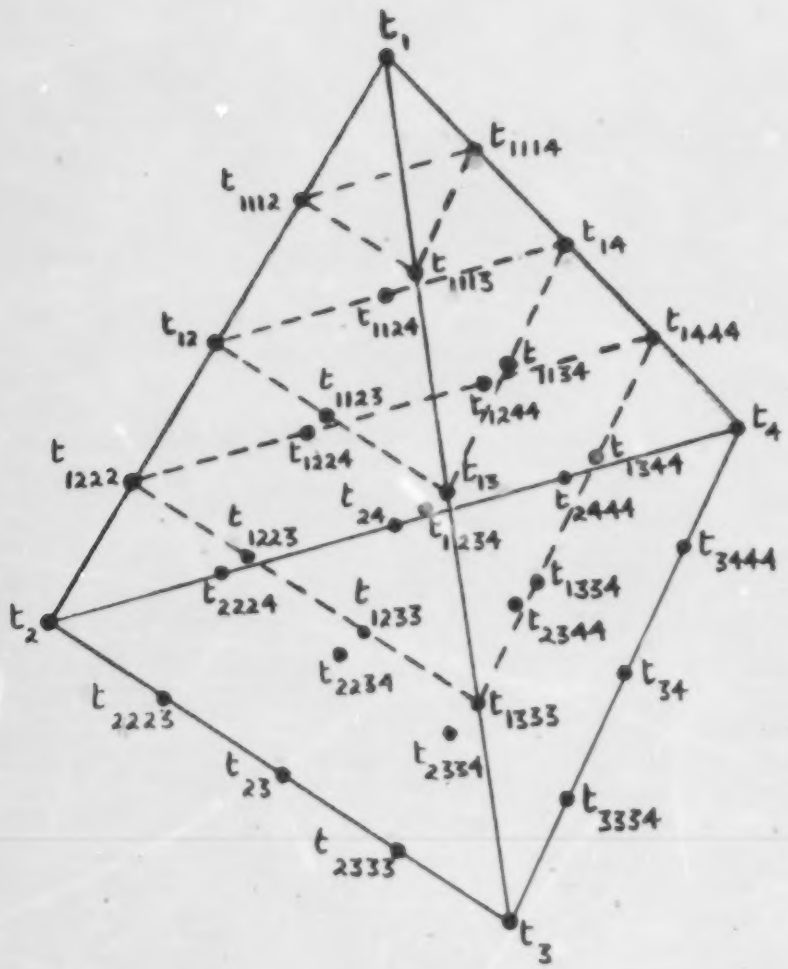

FIGURE 23. Nomenclature for Solidus Temperatures in a Quaternary System According to the Quartic Model

National Bureau of Standards SP-496, Applications of Phase Diagrams in Metallurgy and Ceramics
Proceedings of Workshop held at NBS, Gaithersburg, Md., January 10-12, 1977

Phase-Diagram Compilations - A User's View

J. D. Livingston
General Electric Company
Corporate Research and Development
Schenectady, New York

INTRODUCTION

A major goal of this Workshop is to assess the current status of phase-diagram compilations in metallurgy and ceramics, and users' needs for such information, in order to assist the NBS Alloy Data Center in setting priorities for their newly-initiated efforts in this area. I was asked to present for discussion a user's view of the type of format and means of distribution most desirable for phase-diagram information. The views presented will represent my own bias, that of a research metallurgist in an industrial laboratory. However, they also have been influenced by discussions with many others, and by the results of two recent questionnaires, one sent to registrants of this Workshop, and one sent to a group of prominent metallurgists in the United Kingdom by Dr. A. Prince.

TYPES OF USE

User needs for phase-diagram information vary considerably in their breadth and depth. On the one extreme, a worker initiating a research program on a particular alloy system is usually willing to devote considerable time to a study of past results. In such a case of in-depth need, a phase-diagram compilation serves only as a starting point for entry into the literature, and the worker will go to the original references for most of his information. Papers more recent than the compilation will be located through abstract journals and Citations Index.

On the other extreme, many metallurgists must often find quick answers to such questions as, "What's the minimum melting point in the Pb-Sb system?", "How much Ni dissolves in Cr at 1000°C?", "What intermetallics form between Au and Sn?". Here the need is for quick access to a compilation as broad and as up-to-date as possible, preferably available on his own bookshelf. Between these two extremes ranges an entire spectrum of phase-diagram needs of varying depth.

In my own research, I have often found phase-diagram compilations useful in surveying alloy systems to select a suitable alloy for an experimental program. For example, when starting a research program on eutectoid reactions several years ago, I used phase-diagram compilations to tabulate known eutectoid reactions, their temperatures, phases, etc., prior to selecting a few systems for specific experiments. For such a use, breadth and currency of coverage, and compactness of format, were of prime importance.

In industrial research, the alloys of interest usually contain many components. Binary phase-diagram information, although helpful, goes only part of the way towards providing the necessary answers. Ternary phase-diagram information can be extremely useful in unraveling such complex problems. For quaternary, quinary, and higher-order systems, however, the difficulty of representation and interpretation of phase-diagram information becomes so great that a compilation of published information becomes of doubtful value.

TYPES OF DISTRIBUTION

There are many ways in which data compiled at an information center can be distributed to potential users. On a limited scale, information can be directly supplied in response to individual telephone requests. If the data are appropriately computerized, a user with access to an appropriate terminal can conduct an on-line search for the information he needs. However, it seems very clear that for the immediate future most materials scientists and engineers will prefer phase-diagram compilations in book form.

For alloys, the best-known source of phase-diagram information is the Hansen-Elliott-Shunk series.[1] These books present critically-evaluated phase diagrams for binary alloys and considerable crystallographic and other information, and are extremely useful. However, the explosive growth in metallurgical literature made this task increasingly difficult, time-consuming, and expensive. The latest supplement, prepared by Shunk, required over 700 pages to cover only the three-year period 1962 to 1964. A later attempt to continue this series and consolidate the earlier volumes eventually was discontinued because of the magnitude of the necessary effort and the lack of sufficient funding. Thus this series, which has been of great value to the metallurgical profession, is now 12 years out of date.

In addition to the problems of time and expense, the preparation of critical evaluations a la Hansen has another problem - a critical evaluation may be wrong. For example, Shunk's supplement devotes over four pages to the Nb-Sn system*, and one of the most clearcut conclusions reached was the following: "That Nb_3Sn is stable only at high temperatures is well established." This "well established" conclusion is now known to be completely wrong.

A less expensive, less time-consuming, and less subjective approach to compiling the literature on metallurgical phase diagrams is that which has been taken by the Institute of Scientific Information of the USSR Academy of Sciences. On an annual basis, they compile phase diagrams direct from the literature, with no attempt at evaluation or correlation with earlier results. In addition, in a prescribed format, they present considerable additional information describing the work. This series now includes 20 volumes, covering the literature from 1955 through 1974.(2) An important feature of this series is that it includes ternary and higher-order systems, making this the most extensive compilation of ternary phase-diagram information available. Use of this series was cumbersome in the past, because they lacked a cumulative index and the annual indices were alphabetized in Russian. However, volume 20, which recently appeared, contains a cumulative index for all 20 volumes and is alphabetized by the standard chemical symbol. A similar index for volumes 1-19 was recently published by NASA.(3)

An approach involving even less time and expense is that of simply compiling phase diagrams in compact form, with little or no evaluation or further information beyond a bibliographic reference. Such an approach was used for the 1964 and 1969 editions of Phase Diagrams for Ceramists.(4) Each of these editions compiled over 2000 diagrams in about 600 pages, sometimes including as many as six diagrams on a single page. Despite the limited information presented, these handbooks have been found to be extremely useful by workers in the field. The 1975 supplement to this series now accompanies the diagram with a brief descriptive text, but as a result this volume contains only about 800 diagrams. For metals, similar but much less comprehensive compilations can be found in such handbooks as Smithells' Metals Reference Book (5) and ASM's Metals Handbook. (6) Since these handbooks are aimed more at metallurgical engineers than research scientists, diagrams are presented in weight percent rather than atomic percent.

---

*Actually, this diagram appears in Shunk as Cb-Sn. Elliott's supplement also spelled niobium with a C, a mistake that Hansen did not make.

A very recent compilation is Moffatt's Handbook of Binary Phase Diagrams[7], which covers the literature since 1954, and hence supplements the Hansen-Elliott-Shunk series. Diagrams, which are presented with no explicit evaluation, are presented in loosleaf format. This allows annual updating to be interpolated into alphabetical order when supplements arrive. Another interesting feature is a double-entry index, with each diagram indexed for both elements. This can be much more convenient than the usual single-entry system when surveying, for example, the binary alloys of Zn or Zr. The index also integrates the indices of Hansen, Elliott, and Shunk.

For workers with easy access to a good technical library, a simple bibliography on phase-diagram information can be very useful. Haughton and Prince[8] compiled a bibliography of phase-diagram literature through 1954, and Spengler[9] reviewed the literature from 1949 to 1960. Prince[10] has prepared a bibliography on ternary and higher-order systems covering the literature from 1955 through 1973. Containing 18,000 references, this will be published this year.

The Alloy Data Center of NBS has prepared a comprehensive list of all existing phase-diagram compilations and of current data centers active in this area. They are also preparing a comprehensive index by alloy system incorporating 12 major phase-diagram compilations. Such lists and indices can guide the individual researcher to the appropriate compilations or data centers.

As we move from indices and bibliographies to simple diagram compilations (like Moffatt and the early volumes for ceramists) to diagram compilations including additional information (like the Russian series) to compilations of critical evaluations (*a la* Hansen), the product becomes increasingly useful but the time and expense required for preparation increases substantially. Because user needs vary so greatly in breadth and depth, no single format will be best for all needs. However, any decisions on future projects must clearly balance the information desired by the users - which is often "as much as possible" - against the time and expense involved in preparing the compilation.

CURRENT STATUS AND NEEDS

The current status of phase-diagram compilation in English is poor,

but it is improving. For binary alloys, the Hansen-Elliott-Shunk series is now 12 years out of date, but the recent appearance of Moffatt's Handbook partly fills this gap. Although a critically-evaluated compilation of all binary systems has now become an impractical task, evaluations limited to particular metals of industrial importance are feasible and desirable. A recent example is that of Mondolfo[11] dealing with aluminum-base systems.

A more serious gap exists in the compilation of ternary phase-diagram information, which is of particular importance to industrial researchers dealing with complex alloys. The bibliography by Prince[10], which will appear this year, will be a very welcome tool for locating such information. A comprehensive compilation of evaluated ternary diagrams has been proposed to Gmelin by a group at Stuttgart under Petzow.[12] However, this proposed work is estimated to require about 18,000 pages, and, when it finally appears, will probably be priced beyond the reach of individuals and small libraries.

There would be considerable utility to a book on ternary phase diagrams falling between Prince's bibliography and Petzow's proposed compendium. A format similar to the early volumes of Phase Diagrams for Ceramists would allow the presentation of one to two thousand of the most important diagrams in a single handy volume. Alternatively, a looseleaf format such as Moffatt's might be the most practical approach, since it easily incorporates updating. The 20 volumes of Russian compilations would provide many of the necessary diagrams without the need for consulting all of the original literature. Thus the task could be accomplished with modest requirements of time and money. In my view, such a compilation would be of considerable value to industrial metallurgists.

ACKNOWLEDGMENTS

I am grateful to A. Prince for the results of his questionnaire, and for a preprint of his paper on multicomponent alloy constitution data compilations. I am grateful to G. C. Carter for the results of the questionnaire sent to workshop registrants. Also of great help were conversations with many colleagues, especially W. G. Moffatt and J. H. Westbrook.

References

1. M. Hansen and K. Anderko, Constitution of Binary Alloys, 2nd Edition, McGraw-Hill, New York, 1958; R. P. Elliott, 1st Supplement, 1965; F. A. Shunk, 2nd Supplement, 1969.
2. Phase Diagrams of Metallic Systems, N. V. Ageev, ed., Russian Institute for Scientific and Technical Information, Moscow, 20 annual volumes.
3. NASA Technical Translation NASA TT F-17296, C. M. Scheuermann, Lewis Research Center, 1976; reproduced in these proceedings as paper TPSII-1.
4. E. M. Levin, C. R. Robbins, and H. F. McMurdie, Phase Diagrams for Ceramists, American Ceramic Society, 1964; Supplement, 1969; 2nd Supplement, 1975.
5. Metals Reference Book, C. J. Smithells, ed., Butterworths, U.K., 5th ed., 1976.
6. Metals Handbook, Vol. 8, Metallography, Structures, and Phase Diagrams, American Society for Metals, Metals Park, Ohio, 1973.
7. W. G. Moffatt, Handbook of Binary Phase Diagrams, General Electric Co., Schenectady, N.Y., 1976.
8. J. L. Haughton and A. Prince, The Constitution of Alloys: A Bibliography, The Institute of Metals, London, 2nd ed., 1956.
9. H. Spengler, Metall. 15, 883, 1004 (1961).
10. A. Prince, A Bibliography of the Constitution of Multicomponent Alloy Systems (1955-1973), to be published.
11. L. F. Mondolfo, Aluminum Alloys: Structure and Properties, Butterworths, U.K., 1976.
12. F. Aldinger, E.-Th. Henig, H. L. Lukas, and G. Petzow, paper MPSI-1, this workshop.

National Bureau of Standards SP-496, Applications of Phase Diagrams in Metallurgy and Ceramics
Proceedings of Workshop held at NBS, Gaithersburg, Md., January 10-12, 1977

Some Thoughts on the Distribution of Reference Data

Dr. Howard J. White, Jr.
Office of Standard Reference Data
National Bureau of Standards
Washington, D.C.

ABSTRACT

Some of the characteristics of the existing methods of distributing reference data are discussed. Strengths and weaknesses of the various methods are pointed out. There does not appear to be one superior method, but rather various methods or combinations of methods are indicated for individual cases. The problem of distributing reference data on phase diagrams is considered specifically.

KEY WORDS

Distribution of phase diagrams; distribution of reference data; formats for reference data.

736

I. INTRODUCTION

The generation of phase diagrams and their utilization to solve technological and scientific problems are covered in other sessions of this Workshop. This paper is focussed on the format and distribution of phase diagrams; that is, on the advantages and disadvantages of the various methods that might be considered for transferring phase diagrams from their generators to their users. After a general consideration of the possible methods of transferring data, the problem of phase diagrams is taken up specifically and some recommendations for the future are made.

II. METHODS OF TRANSFERRING DATA

The following listing would appear to cover the principal methods that are currently used for transferring data.

a) Personal conversations and letters

b) Lectures

c) Loose-leaf data sheets

d) Technical papers in journals

e) Monographs

f) Computer tapes and card decks

g) Responsive computer programs available

  i) for query by batch method

  ii) for interactive query via terminal

h) Handbooks

The methods listed above will be considered in some detail. However, two conclusions can be cited immediately. First, none of the above is the universal solution to the data distribution

problem. Each has its strengths and weaknesses. Secondly, the suitability of each of the above depends on the nature of the data and the nature of the interest group involved.

III. INTEREST GROUPS

An interest group can be defined as those individuals with a direct, immediate, or continuing interest in the data in question because they generate them or need to use them. An interest group may be small, medium-sized, or large; and its properties will vary accordingly.

1. The Small Interest Group

There appear to be several reasons why an interest group may be small. However, the basic properties of the group seem to be the same whatever the reason.

First of all, the data may represent a field that is blossoming. As yet, only a few appreciate the value of the data. It is probable that each member of the interest group knows the work of the other members and may know a number of them personally. The users and generators of the data tend to be the same people. There is no one else involved. A small interest group may also result from a field that is so narrow that only a few can profit from the availability of the data. The users and generators of the data are often linked by a public or private mission-oriented agency which supports the effort for its own purposes. Alternately, a narrow portion of a large field might be developed rapidly for a specific purpose. Again, users and generators may be linked by a mission-oriented agency which provides support. An example might be the JANAF Project which

originally provided thermodynamic data for purposes of rocket design. Finally, generators and users of the data may be closely coordinated because of unusual constraints in the field. Again, there is often a common support agency. High-energy accelerator physics with its extremely expensive equipment can be cited as an example.

In all of the cases mentioned, the members of the interest group can be expected to know of one another and know how to obtain the pertinent literature in the field.

2. Medium-Sized Interest Group

The data of interest to such a group have proved their worth over a range of problems. The members of the group are no longer closely connected. Few know or know of all members of the group. The members have several reasons to want the data. However, the members in general have the same technical background, know about the same journals and books, and hear of and attend the same lectures.

3. Large Interest Groups

If the interest group is large, the data have proved their worth in many fields. The members of the group do not know one another and may not have similar backgrounds. Potential users do not necessarily know all sources of data, and generators are not aware of all possible uses for their data.

The above brief characterizations of the interest groups can serve to establish some of their properties and the differences between them. It is clear that the problem of reaching

the members of an interest group will change with the size of the group. The large interest group is different from the small one not only in size but also in nature.

IV. PROPERTIES OF METHODS FOR TRANSFERRING DATA

The various methods for transferring data have been listed in a previous paragraph. Some properties of these methods will now be considered. These properties have been stated from the standpoint of a user's needs and refer to a vantages or disadvantages a given method may have with respect to fulfilling the user's needs. The properties to be considered may be listed as follows:

a) Rapidity of response to perceived need

b) Degree of responsiveness to need

c) Permanence, suitability for reference, and transferability

d) Restrictions on the audience

e) Restrictions on data

f) Restrictions on use

Cost is an obvious property which has not been mentioned. It will be considered along with the properties which are listed. Each of the methods for transferring data cited in the first section of this paper will now be considered in terms of these properties.

A. Personal Communication

The response is generally very rapid. Since personal communication, whether verbal or by letter, is interactive, it is fully responsive. In other words, the prospective user can

obtain the data he needs and any collateral information about it which is necessary to substantiate its suitability. However, the results of personal communication are essentially unsuitable for reference or transfer. There is no information other than the name of the source that can be used by a third person to substantiate the data for his own purposes. Personal communication is essentially limited to a small audience. It is inexpensive when provided as a professional service, but may become expensive when provided as a consulting service. It is limited to small amounts of data and the user and producer of the data must make direct contact.

B. Lectures

Although a lecture requires more formal preparation, it is still quite a rapid method for transferring information. It is reasonably responsive and some interaction in the form of questions and answers is often possible during or after the lecture. Unless converted into a technical paper, it is ephemeral and unsuited to reference. It is limited to quite small amounts of data, and the user and producer must make direct contact.

C. Loose-Leaf Data Sheets

These represent a reasonably rapid method of transferring data. Changes can be made in a short period of time by substitution of individual data sheets. The format is fixed and non-interactive. As a result, responsiveness depends on the design of the data sheet. Loose-leaf data sheets are permanent as a collection although individual sheets may be replaced from time to time.

In principle, they are suitable for reference although the organization, indexing, replacement, etc. of the individual sheets open the way to multiple errors in filing and the inadvertent use of obsolete sheets. Collections of loose-leaf data sheets are heartily disliked by librarians. In theory there is no limit to the audience that can be served; in practice the method is limited to a moderate audience by the cost and complexity of the dissemination procedures. Again, there is no limit in principle on data content although cost and complexity increase with size. The user must contact the distributor and remain in contact with him.

D. Technical Papers

These are slower. The more formal method of presentation and the details of the publication process limit the rapidity of response. It is also necessary to find a journal willing to publish the data in question. The format is fixed and non-interactive, and the responsiveness depends on the nature of the paper. They are subject to unrecognized obsolescence. Technical papers are permanent, easily referenced, and transferrable. Technical journals have a larger audience and, in fact, are too expensive for a smaller one unless they are subsidized. The feasibility of presenting data through papers in a journal again depends on the availability of a journal willing to accept the papers. There are essentially no restrictions on the data and no direct connection between the user and author is required.

E. Monographs

The characteristics of monographs are essentially the same

as those of technical papers. They tend to be more massive and slower in coming out. The problem of finding a publisher may be a serious one.

F. Computer Tapes and Card Decks

The initial response may be slow because the development of software may be needed to produce the tapes. Updating can be quite rapid. These, too, are of fixed format and non-interactive, and the responsiveness depends on the design of the product. They are permanemt and can be transferred, but no systematic reference system is currently available. There is no inherent restriction on the size of the audience, but the use may require a substantial investment in equipment and probably software. These costs tend to limit applicability to sophisticated, high-volume users. There are no restrictions in principle on the data. In fact, tapes are excellent for very large files. Use requires the availability of suitable hardware and software.

G. Responsive Computer Programs

These are rapid, once established. Batch systems are fixed in format; limited flexibility is often provided with interactive systems. Again, no systematic reference system is available. There are a few restrictions on the use of batch systems. The user of an interactive system must have access to a terminal. They are good in principle for all sizes of fields. Large files are expensive to maintain on the computer and may be expensive to search unless very carefully designed. Someone must pay for software-development costs and for up-time on the computer.

H. Handbooks

These are slow in being generated, and in general are preceded by one or several of the other methods. They are fixed in format, non-interactive, and responsiveness depends on design of the handbook. A handbook is permanent, transferrable, and easily referenced in itself. However, unless it is carefully put together, it may present difficulties to those who wish references to a definitive source of the data. Handbooks tend to be widely available and are often designed to assist in data transfer between different groups. They are strongly advertised and marketed. There is no restriction on the amount of data contained. The limitations on the quality of the data are often difficult to determine.

V. APPLICATIONS TO DATA ON PHASE DIAGRAMS

The phase-diagram field is a mature field with a large interest group. There are many sources for data which must be incorporated into phase diagrams, and there are many practical engineering applications of phase diagrams. In fact, phase diagrams are among the most pervasive data there are with uses ranging from metallurgy and the formation of ceramic materials through an entire spectrum of applications in the materials field. As a result, formal mechanisms for finding, transferring, and providing references are needed. Although the more ephemeral methods of transferring data may have uses in specific instances, the more permanent mechanisms must clearly play the major role.

The monograph has been the historic method of choice with such classical examples as Hansen's "Constitution of Binary Alloys"

and "Phase Diagrams for Ceramists." It seems probable that the monograph will continue to be extensively used for distributing phase diagrams.

An article in a journal is also an attractive possibility. Such an article could cover a smaller area than the comprehensive monographs and would be published more rapidly. At the same time, the needed permanence and ease of reference would be obtained. The problem, of course, is in finding a journal to publish such compilations. Standard research journals are usually unwilling to publish compilations of phase diagrams. In this regard, the Journal of Physical and Chemical Reference Data should be considered. This relatively new Journal is devoted to the publication of reference data. Thus, a compilation of phase diagrams, if prepared to the editorial specifications of the Journal, would be a suitable article for publication. In fact, one compilation of phase diagrams has already been accepted for publication. I would recommend that serious thought be given to publication of suitable compilations of phase diagrams in this Journal on a systematic basis.

Finally, some consideration should be given to the data center. A data center as a formal entity is a relatively new concept. It consists of a group or "groups" who have accepted responsibility for compiling and evaluating data in a given field. Examples are the Alloy Data Center in the field of metals and the group producing phase diagrams for ceramists in the non-metallic field. The data center has the potential to provide any of the techniques for transferring data which

have been discussed above along with a degree of institutional permanence. Thus, it can be personal and interactive and still provide a stable, recognizable reference point.

National Bureau of Standards SP-496, Applications of Phase Diagrams in Metallurgy and Ceramics
Proceedings of Workshop held at NBS, Gaithersburg, MD., January 10-12, 1977

Remarks on Producing and Publishing Critically Evaluated Data

W. B. Pearson
Faculty of Science, University of Waterloo
Waterloo, Ontario, Canada

As somebody who has been concerned for nearly thirty years with critical compilations of phase equilibria and structural data on metals and alloys in particular[1 - 5], I offer some thoughts on "how to get the job done". This may be valuable since my experience runs through the days of "bits of paper" to "quick-sort" filing cards with the 102 perimetrically punched holes, to the advent of Xerox copying, and finally into the computer age. Secondly it encompasses various organization systems from the "do it yourself" to the international "moonlighting" system of Structure Reports and, by observation, to fully (though perhaps inadequately) funded systems, based either on government grant financing, or on commercial sales. In all I have directly written or edited over 19,000 pages of critically evaluated data.

My general conclusions are as follows: a fully computer-based operation, is by far the most elegant, since with appropriate programming it can lead to books printed directly from magnetic tapes, but such a system requires very considerable financial backing, even if it goes no further than data handling and storage and does not proceed to the ultimate step of book production direct from the data files. Although computer programmes can be readily used to calculate and check data, the use of computers in no way obviates the need for experts to find the data in the literature and to critically evaluate it. In contrast to computer-based operations, a system of data handling by hand, using part-time typists as required, although far less elegant, is still workable and gives the final product at less cost.

Secondly, in order to get a critical data compilation prepared (unless there is sufficient money available to employ as many full-time assessors as is necessary), it is much better to support a single person (or possibly two) full-time for the two or three years that may be required for the project, than to

organize a team of many people on a "moonlighting" basis for nominal honoraria, each of whom is expected to complete a portion of the compilation. In the latter case the work is likely to become indefinitely delayed due to some members of the "team", for various reasons, not completing their assignments.

Perhaps some recollections of the works that I have undertaken will give substance to these conclusions, and the experience apparent therein will be useful to those contemplating undertaking and publishing critical assessments of data.

In preparing the first volume of "The Lattice Spacings and Crystal Structures of Metals and Alloys"[2] (1044 pp.), I read all of the relevant literature and transcribed the pertinent data onto "quick-sort" cards with the 102 perimeteral holes assigned to the elements by atomic number. This handled cross-referencing satisfactorily and although shaking out the required cards from a wire was clumsy, it was just adequate for the job that existed at that time. However, rewriting all of the data and typing and checking the ms. in preparation for the publisher proved to be very time consuming and inefficient.

My choice of the method of producing Volume 2 of this work[3] (1446 pp.) was more fortunate than I realized at the time, and indeed in retrospect, had I not adopted that method, it is very doubtful whether I would ever have been able to complete the work. As I read each paper that contained pertinent data, I wrote it up immediately in a form suitable for publication, and also constructed a running tabulation of data. These portions of ms. were then immediately typed, checked and set aside for final processing. When the total literature survey was completed and treated in this way, Xerox copying machines were just becoming generally available. Therefore, all that I did in constructing the final ms. for the publishers, was to assemble all of the written reports on any particular alloy system. I then cut out the parts that I selected from any of these reports, pasted them in the required order on a sheet of paper, together with the required references at the bottom of the page, and finally copied the synthesized page by

Xerox to give a flat page for the publisher. In this way construction of the final ms. was exceedingly rapid requiring only scissors, glue and a Xerox copying machine. The amount of connecting material that had to be written and typed at this stage turned out to be negligibly small, as also did the number of reports that had to be completely rewritten. Generally they could be assembled by a sentence cut from this, and a sentence from that report. The assembly of the extensive tables of structural data (490 pp.) in appropriate alphabetical order was handled in a similar manner.

Whether such a method could be now used to assemble a third volume of the same work is a good question, but I think it could if the person had his full time to devote to it and the help of one other person. However, I doubt that as an alternative, a committee of say ten people on a part-time basis would be too successful; data would probably accumulate more rapidly than it could be processed.

As a general editor of Structure Reports for some 15 years[4], I have further experience of organizing numerous co-editors. Structure Reports is a series of annual volumes, which report in critical fashion all crystal structure determinations published in the year to which the volume is attributed. It is divided into three sections: Metals, Inorganic and Organic, each having its own co-editor assigned for the year in question. The work of a section co-editor thus comprises reading the appropriate literature, checking data and producing critical reports thereon which, when appropriately combined and edited, constitute the ms. The general editor is responsible for producing lists of structural papers to be read and for general coordination and checking of the different ms., reading proofs, etc. The trouble with this organization, where each editor takes on the work out of a sense of goodwill to the crystallographic community and in exchange for a relatively small honorarium, was that due to accidents or personal problems, one section of a volume frequently delayed the publication of the whole for several years. At one point the situation was so bad that Structure Reports volumes were

only being published some 10 years after the year whose work was critically reported. Recently this back-log has been eliminated and Structure Reports now are appearing in the shortest possible time; only 2-3 years after the work that they report is published. Thus all volumes and up to and including 1973 were published by the end of 1975.

This changed state of affairs resulted from three factors - the first two are mentioned for completeness although they are trivial in the present context; the third is more interesting. First, only those section co-editors were assigned volumes whose record indicated that they could produce ms. rapidly. Secondly, the general editor no longer covered the world literature and produced lists of papers to be reported: the main subject journals were reported by the co-editors as they were received and Bulletin Signalétique abstracts #161, "Cristallographie" were used simultaneously as a source of references of papers containing structural data.

The third reason for the rapid publication transpired to be a switch to direct photo-offset printing of typed ms. instead of having printers set the ms. in monotype, as was the earlier practice. This change was adopted primarily because the cost of typesetting the volumes was making them too expensive for individuals to purchase. At the time of the change, using any typing service to produce pages with justified lines was as expensive as setting the ms. in monotype, so "moonlighting" typists were engaged to type the pages of ms. in a standard format. The general editor then read the pages in proof and had corrections done before the ms. was assembled and sent to the publisher for photo-offset printing. It so happened that this process turned out to be very much more rapid than the original one where the ms. was sent to the publisher who then went through it marking it for the printer, who set it in print. Thereafter the general and section editors went through up to four proofs to ensure correctness of the data. From this, one may conclude that unless a continuous data-bank operation is to be established at the same time as the production of ms., hand-typing operations may still be cheaper and as rapid as computer-based operations, unless these are fully funded to provide

day workers necessary for the operation. These observations are very cogent to the production of volumes of critically assessed data on phase equilibria, since computer handling of such operations is likely to require the development and successful operation of special programmes.

Finally a remark or two on comparative costs may be interesting. When I first became general editor of Structure Reports producing volumes in the early 1960s, a consumer buying the volumes obtained an average of 7 pages per Dutch florin (D fl) spent, whereas critically evaluated data on a similar subject produced by a commercial company ran at one page only per D fl., if my recollection is correct. Nevertheless, the production of Structure Reports was unsubsidized, and over the years they were self-financing and made a modest profit. In more recent years the costs of typesetting volumes of Structure Reports began to increase alarmingly so that the price per page doubled. However, the changeover from typesetting to photo-offset printing of hand-typed ms. pages again halved the cost of a printed page. A certain lost of elegance results from the change from type-set pages to typed pages with unjustified lines, but as far as I am aware this has not produced adverse comments, the users finding that any moves to reduce costs are welcome.

References

1. Vanadium and its Alloys. J. Iron and Steel Inst., 1950, Vol. 164, pp. 149-159.

2. Lattice spacings and structures of metals and alloys. Pergamon Press, London, 1958, pp. 1044.

3. Lattice spacings and structures of metals and alloys. Vol. 2, Pergamon Press, Oxford, 1967, pp. 1446.

4. Structure Reports. International Union of Crystallography, Oosthoek, Utrecht. Volumes 17, 18, 19, 20, 21, 22, 23, 24, 25, 26, 27, 28, 29, 30A, 30B, 31A, 31B, 32A, 32B, 33A, 33B, 34A, 34B, 35A, 35B.

5. The Crystal Chemistry and Physics of Metals and Alloys, Wiley & Sons, New York, 1972, pp. 806.

Discussion Following the Tuesday Afternoon Session on Representations, Format, and Distribution

K. Gschneidner - In our compilation of binary cerium diagrams, we have given the diagram in atomic percent for the researcher, and on the opposite page in weight percent for the industrial user.

T. Livingston - You can do that if you have the luxury of the space available. Usually there is a financial limitation. The question is, "What is the minimum acceptable depth?" The way I view it, if you plot increasing information, starting from bibliographies increasing to evaluated compendia, the value probably goes up monotonically, but I feel it has a decreasing slope and the cost may go up, but it may have an increasing slope.

L. Brewer - But what do you do if there are six or more contradictory diagrams, do you give them all in your compendium?

T. Livingston - There is always *some* evaluation involved. Moffat does some evaluation too. For example, if a melting point is obviously off, this gets taken care of. But, how many man-hours can you spend? Another question is, how good is the person doing it? There is some optimum there in man-hours you can spend. It may come to the point where you may want to put - maybe not all 6... (you can throw out some of them because maybe they violate the phase rule or something!) - but several in your compilation.

J. Cahn - There is a danger with evaluated data. The melting point of maganese sulfide just went up over 100 degrees and it was recorded as early as the 1930's that it was higher. All the weight of the evaluated phase diagrams came down on the wrong figure. You can't always rely on the evaluators.

D. Kahan - A full evaluation is going to be costly not only in money, but also in time and delay in getting it to the users.

J. Livingston - In loose leafing you can update periodically, but you may still be a few years behind. Dr. Pearson and a few other people suggested that maybe there would be a market for some sort of a current awareness journal, something like the Diffusion and Defect Data Journal, or Structure Reports.

B. Rosof - The participants here know a lot about phase diagrams, but many metallurgists (not only PhD's, but also bachelor's degrees), can't evaluate phase diagrams for themselves. For them, I think, evaluated compendia are far more important than for people here who are researchers in the field.

J. Livingston - There is obviously a whole range of user needs and we are trying to get a feeling for what the priorities are. Maybe we should go after the best evaluated product, but I think that many people I speak to in industry, at least, would rather have a compendium of a thousand diagrams, some of which may not be right, or many of which may be wrong. They're not all interested in the third decimal.

Author Index

Ageev, N. V., 90
Ageeva, D. L., 90
Aldinger, F., 164
Ammann, P., 1334
Ansara, I., 121

Badie, T. M., 550
Bailey, D. M., 1027
Balakrishna, S. S., 1200
Bale, C. W., 1077
Beam, J. E., 1428
Bennett, L. H., 261, 450, 592
Bilimoria, Y., 1047
Blander, M., 1093
Boreni, R., 259
Boyle, M. L., 726
Brebrick, R. F., 1220
Brown, J. J., Jr., 272

Cameron, T. B., 566
Carter, F. L. 763
Carter, G. C., 36, 261, 450
Cassidy, R. T., 272
Chang, L. L. Y., 165
Chang, Y. A., 229, 774
Chart, T. G., 1186
Choudary, U. V., 229, 774
Cleek, G. W., 1, 257
Cook, L. P., 1, 257, 440
Craig, D. F., 272

Davison, J. E., 1428
de Fontaine, D., 967, 999
Dew-Hughes, D., 1411
Doman, R. C., 1378
Dreshfield, R. L., 624

Ehrenreich, H., 592
Eliezer, I., 803 846, 1440
Elliott, J. F., 1332, 1453
Evans, B. L., 226

Fine, H. A., 355
Fisher, J. R., 909
Fivozinsky, S. P., 1325
Flukiger, R., 375
Fopiano, P. J., 567

Gaye, H., 907
Giessen, B. C., 1161
Gittus, J. H., 1065
Glasser, F. P., 407
Goldstein, J. I., 462
Gribulya, V. B., 1139, 1151
Gschneidner, K. A., Jr., 226

Haas, J. L., Jr., 909
Hasebe, M., 911
Henig, E.-Th., 164, 955
Hirano, S., 508
Howald, R. A., 803, 846, 1440, 1470
Hsu, C. C., 1109

Jackson, M. R., 423
Jaffee, R. I., 1420
Johnson, J. R., 483
Jorda, J.-L., 375

Kagan, E. K., 346, 351
Kahan, D. J., 261
Kaufman, L., 1065
Khanna, K. M., 575
Kikuchi, R., 967, 999
Kiseleva, N. N., 1139, 1151
Kolesnikova, T. P., 90
Kreidler, E. R., 1307
Kubaschewski, O., 1027

Larson, H., 1354
Livingston, J. D., 703
Lukas, H. L., 164, 955
Lupis, C. H. P., 907

Mallik, A. K., 1200
McCormick, S., 1047
McNally, R., 1378
Merrill, L., 100
Mighell, A., 259
Minor, D. B., 440
Miodownik, P. A., 1065, 1479
Mlavsky, A. I., 1426
Mondolfo, L., 1382
Morral, J. E., 566
Myers, S. M., 516

Nakamura, K., 508
Negas, T., 1, 257
Neumann, J. P., 229
Nishizawa, T., 911

Ondik, H. 259

Pehlke, R. D., 1360
Pelton, A. D., 1077
Pettrova, L. A., 90
Petzow, G., 164, 955
Prince, A., 660
Prochazka, S., 1409

Rairden, J. R., 423
Reilly, J. J., 483
Reno, R. C., 450
Rhines, F. N., 142
Romig, A. D., Jr., 462
Rosof, B. H., 1090
Roth, R. S., 1, 257

Saboungi, M.-L., 1093, 1109
Saito, S., 508
Sandrock, G. D., 483
Savitskii, E. M., 1139, 1151
Scheuermann, C. M., 1237
Selle, J. E., 1471
Sherwood, G. B., 1325
Sinha, V. K., 578
Slick, P., 1427
Smith, J. F., 1027
Smugeresky, J. E., 516
Sōmiya, S., 508
Spear, K. E., 744
Stalick, J., 259
Stein, V.S., 1506
Swartzendruber, L. J., 450

Tarby, S. K., 726
Thompson, W. T., 1077
Thurmond, C. D., 23
Tulupova, I. V., 1506

Van Tyne, C. J., 726
Verkade, M. E., 226
VerSnyder, F. L., 1418
Vol, A. E., 346, 351

Wachtman, J. W., 1
Wang, F. E., 545
Watkin, J. S., 1065
Watson, R. E., 592
White, H. J., Jr., 709
White, W. B., 251

Zimmermann, B., 955

SUBJECT INDEX

Each paper has been indexed under one or more of these entries for ease of retieval. This index is cursory rather than exhaustive. Those papers giving numerical phase diagram data or phase diagrams on specific systems are listed in the Materials Index.

Acceptor solubilities 26-27
Activity coefficients 726-727, 774, 777-786, 803-845, 1047-1048, 1052-1055
Additive systems (salts) 1093, 1098-1108
Ageev, translated cumulative index 1237-1306
Aircraft industry 262, 1396, 1418-1419
Allen and Cahn 1012, 1017
Alloy physics 84-89, 592-623
  (Also see under spcific terms)
Alloys (see under Metallic systems)
Amorphous materials 261-268, 1161-1185
Analytical representations 672-675
Angular correlation 450-461
Applications (see under Needs and Applications, under main headings of
  Ceramics systems, Semiconductor systems, High pressure diagrams,
  or specific terms)
Atomic deposition methods 151, 516-544
  - summary 1172
Autoradiography 566

Bale-Pelton polynomials and coefficients 846-847, 874-875, 902-903, 1445
Band theory 619
Batteries 262, 1109-1138
Bonding, chemical (see also Crystal chemistry) 612-614, 763-773
  -, transient liquid phase (TLP) 1418-1419
Bonnier and Caboz 956
Bragg-Williams 978, 1000, 1008
Brouwer diagrams 27

Calculations of phase diagrams (see under Theories of phase diagrams,
  specific topics, and see Tuesday's poster session on this subject,
  pp 726-1236)
Calphad 37, 49, 1188
Calorimetry (including differential scanning calorimetry, DSC)
  1171, 1173
Capsule bursting method 508-515
Ceramic systems (see also under specific systems, Materials Index)
  - compilation activities, review 2-5, 12-22, 121-122, 165, 252-256, 257-258,
    1327-1331, 1460-1471
  - compilations, review 1-2, 14-22, 256, 407, 1326, 1374
  - needs and applications (see also under Panels II, III, and
    IV on User Needs, pp 1332-1452) 9-22, 121, 703-708, 1352, 1356-1357,
    1361-1366, 1371, 1375-1377, 1378-1381, 1409-1410, 1427, 1442-1450,
    1451-1452, 1455-1457, 1471, 1475
  - questionnaire review 5-22

Charge distribution, transfer 607, 615-619, 766
Chatillon-Colinet 141
Chemical analysis 143, 552, 1379
Chemical scan (isothermal) 151
Cluster variation (theory) 967-998, 999-1026, 1474
Coatings of materials 262, 423-439
Coherent phase diagrams 999-1026
Cohesion, cohesion energy 594-603, 616
Compilations (see under Ceramic systems, Semiconductor systems, Metallic systems, High pressure diagrams)
Compilation methods 22, 163, 658, 720-725, 1475-1478
Composites 1378-1381
Compounds (see also the Materials Index) 100-200, 763-773, 1378-1381
Compound prediction 763-773, 1112, 1139-1150, 1151-1160, 1220-1236, 1473
Computerized data banks (see under Crystallography and under Thermodynamics)
Concentration simplex 660-662
Concorde, alloys in use 1396
Coordination numbers, 1479-1491
- generalized 767
Crystal chemistry 84-89, 101, 545-547, 620-621, 745-746, 763-772, 1139-1150, 1479-1491
Crystallography
- compilations 82-83, 259-260, 720-725, 1326
- computerized data bank 259-260
- theory and prediction of phases 100-109, 659, 763-773, 1139-1150, 1151-1160

Data banks, computerized
- crystallography 259-260
- thermodynamics and thermochemistry 37, 40, 41, 43, 45, 49, 121-124, 1077-1089, 1186-1199
Data compilations (see under Cermic systems, Semiconductor systems, Metallic systems, High pressure diagrams, under the subtopic "compilations")
Density of states (esp Ti) 595
Differential thermal analysis, DTA (see under Thermal analysis)
Diffusion couple analysis 142, 149-151, 465, 522-524, 913
Dilatometry 142, 151, 517
Dip sampling 143
Distribution and publication of phase diagrams 262-264, 703-708, 709-719, 720-725, 1325-1326
Donor solubilities 26-27

Electrical conductivity (experimental phase change det.) 143, 517
Electrochemical probe 148
Electron densities 611
Electron diffraction 148
Electron distribution 607, 615-619, 766
Electron energies 594-609

Electron microprobe 148, 156, 462-471
- microscope, reflecting, transmission, scanning (SEM, STEM) 146, 148, 440-449, 462, 471-474
Electronegativity 610-613, 766
Electronic density of states (esp Ti) 595
Electronic materials (see under narrower term, Semiconductor systems, or specific topics)
Ellingham diagrams (see also Metal-gas phase diagrams Solid-vapor diagrams and Pourbaix diagrams) 1077-1088, 1428
Emf measurements in galvanic cells 517
Energy storage/conversion 262, 1109-1138, 1426, 1428-1439, 1440-1450, 1458
Experimental techniques of phase diagram determination (see under specific techniques)

F*A*C*T (Facility for the Analysis of Chemical Thermodynamics) 1077-1089
Field ion microscope 146
Format of phase diagrams
- representation 16-18, 262-264, 265-271, 578-591, 658, 660-702, 1093-1108, 1315-1324, 1458-1460. 1506-1519
- distribution and publication 262-264, 703-708, 709-719, 720-725, 1325-1326
- publication standards 1307-1324

Geometric description of superalloys 628-658
Gibbs energy function, generation of 1027-1046
Glasses (see also specific glasses in the Materials Index)
- ceramic 1378-1381
- metallic 261-268, 1161-1185
- needs 1378-1381
Graphical methods 45, 265-271, 628-658, 1077-1089, 1506-1519

Hardy-type power series 141
High pressure phase diagrams
- compilation activities, review 100-120
- compilations, review 101-108
- needs and applications 261-268, 703-708
- P-T, P-T-X diagrams 121-122, 153, 578-591
Hillert 956
History of data compilations 2, 36, 90, 100
Hot stage microscopy 1310
Hot wire microscopy 355-374
Hume-Rothery 662
Hyperfine techniques (see also under nuclear magnetic resonance, Mossbauer effect, perturbed angular correlation) 450-461

Industrial needs and applications
- ceramics 1378-1381, 1409-1410, 1427, 1440-1450, 1455
- composites 1378-1381
- glasses 1378-1381
- intermetallics 1378-1381
- ionic systems (see salt systems)
- iron and steelmaking 567-574, 1360-1377, 1378-1381, 1421-1423
- non-ferrous 567-574, 1334-1353, 1354-1359, 1378-1381, 1382-1408, 1418-1419, 1423-1425, 1427
- salt systems 1426, 1428-1439
- superconductors 1411-1417
Interaction parameters 1210-1214
Intermetallics (see also under Compounds, or see under specific systems in the Materials Index)
- needs 1378-1381
Internal pressue 1210-1214
International Atomic Energy Agency (IAEA) 38, 45, 60-61, 78-79
Ion backscattering methods 151, 516-544
- implantation methods 151, 516-544
Ionic systems (see also Salt systems, and also specific systems in the Materials Index) 115-120, 165-225, 251-256, 272-345, 1093-1108
Iron and steelmaking (needs) 1360-1377, 1378-1381, 1421-1423
Irradiation effects 1065-1076

Kaburagi and Kanamori 1012, 1017
Kohler 141, 956

Least squares method of optimizing phase diagrams 955-966
Lever rule, enhanced 454

Magnetic effects 594-603
Margules 848, 872, 874, 876, 903
Matte 1356-1357, 1456
Metal-gas phase diagrams (see also Solid-vapor, Pourbaix-, Ellingham diagrams, etc) 1047-1064, 1077-1088, 1090-1092, 1332-1333
Metallic-nonmetallic component diagrams 1047-1064, 1077-1088, 1090-1092
Metallic radii 763
Metallic systems (see also under specific systems, Materials Index)
- compilation activities, review 37-38, 40-48, 49, 92-94, 122, 164, 226-228, 229-250, 751, 1186-1199, 1327-1331, 1460-1471
- compilations, review 36-38, 50-74, 90-94, 122, 227, 234, 346-350, 351-354, 744-762, 1237-1306, 1326, 1374, 1406
- needs and applications (see also under Panels II, III, and IV on user needs, pp 1332-1452) 121, 261-262, 567, 703-708, 725, 1109, 1180-1182, 1352, 1355-1357, 1361-1366, 1371, 1375-1377, 1378-1381, 1382-1408, 1411-1417, 1427, 1447-1448, 1451-1452, 1455-1457, 1471, 1475
- questionnaire review 261-266
Metallographic analysis 142-143, 156, 517

Metastable phases 261-266, 1161-1185, 1421, 1457
Mossbauer effect 152, 450-461, 615
Microanalysis 913, 1379
Microchemical analysis 148, 440
Micro-furnace 357
Micro-indent hardness 148
Micro x-ray diffraction 148
Microscopy (see under specific type, e.g. optical, electron, etc.)

Natural iteration (theory) 967, 974-978
Needs and Applications (see under Ceramics systems, Semiconductor system, Metallic systems, High pressure, etc., and see under Industrial needs).
Newton-Raphson iteration method 967, 976-977, 1017
Non-ferrous phase diagram industrial needs 1334-1353, 1354-1359, 1378-1381, 1382-1408, 1418-1419, 1423-1425, 1427
Non-stoichiometry prediction 770
Nuclear Magnetic Resonance (NMR) 121, 152, 450-461

Olson 730-731
Optical microscopy (color, reflectivity, other) 148, 411-413
Order-disorder 984-998, 999-1026

P-T, P-T-X, diagrams 28, 121-122, 153, 253, 578-591, 1421, 1456
Pair approximation (theory) 968-973, 1009-1010, 1017
Pair potentials 610, 616, 1424
Pauling 620, 763-773, 1479-1491
Perturbed angular coorelation (PAC) 450-461
Phacomp 37, 624-627, 1423
Phase rule 143-144, 162
Physical chemistry and metallurgy, general 84-89
Potential-composition diagrams 1077-1088
Potential-potential diagrams 1077-1088
Potentials (see also under specific potentials) 603-609, 1011-1015
Polar diagrams 662-663, 684
Pourbaix diagrams (see also Metal-gas diagrams, Solid-vapor diagrams, Ellingham diagrams, Stability diagrams, etc.) 1090-1092, 1[illegible]
Predictive methods (see under Theories of phase diagrams, Thermodynamic theories, or under specific topics)
Predominance area phase diagrams 1077-1088
Pressure scan 152
Projection methods
- parallel 664-668
- perspective 663-664
Pseudopotentials 603-609, 1014
Publication and distribution 262-264, 703-708, 709-719, 720-725, 1325-1326
Publication standards 1307-1324

Quenching (see also spat-cooling) 1310
- argon jet 383
- rapid quenching methods, summary 1172
Quenched phase plots 1166
Questionnaire, reviews
- ceramic system 5-22
- metallic systems 261-268

Radioactive techniques 148
Raoultian activity coefficient 726-727
Reciprocal systems, representations of 671
- salt systems 1093-1108
Redlich-Kister 803-845, 846-906, 1445
Representations of phase diagrams 16-18, 262-264, 265-271, 578-591, 660-702, 1093-1108, 1315-1324, 1507-1520
Russian literature 44, 46, 50, 51, 92-99, 346-350, 351-354, 1237-1306

Salt systems (see also Ionic systems and see specific systems in the Materials Index) 1093-1108
- needs 1426, 1428-1439
Scratch hardness 148
Second order phase transitions 620
Sectioning methods for phase diagram representations 668-671
Selective chemical solution 148
Semiconductor systems
- compilations, review 23, 346-350, 351-354
- needs and applications (see also under Panels II, III, and IV on User Needs, pp 1332-1452) 27-28, 121, 703-708, 1426, 1471, 1475
Semiconductor compounds, predictive methods 1220-1236
Sigma phase 625-658, 916, 1065
Slags (see also under Materials Index for specific systems) 362-366, 908, 1334-1353, 1356, 1361, 1368-1369, 1374, 1440, 1456
Smelting
- copper 1336-1339, 1342-1349, 1354
- lead 1354
- nickel 1339-1340, 1350-1352
- zinc 1354
Solid state physics (see under Alloy physics or under specific topics)
Solid-vapor diagrams (see also Metal-gas phase diagrams Pourbaix-Ellingham diagrams, etc.) 28, 121-122, 362-374, 1047-1064, 1077-1088, 1090-1092, 1332-1333
Solubilities, donor, acceptor 26-27
Speiss 1357
Splat cooling 383, 1171
Stability diagrams (see also under Pourbaix, Ellingham) 1047-1064, 1077-1088, 1428, 1456
Standards of publication 1307-1324
Stoichiometric description of superalloys 625-627

Strain energy 1210-1214
Strain fields 620
Stress, phase diagrams under external tensile -, or shear stress 575-577
Structural instabilities 769
Sulfur: desulfurization 1372, 1456
Superalloys 37, 262, 423-439, 624-658, 1186
- stoichiometric description 625-627
- geometric description 628-658
- phacomp 37, 624-627, 1423
Superconductivity as technique in phase diagram determination 384-386
Superconductors 262, 375, 387-392, 401, 545-549, 616-618, 770 1148, 1158, 1326, 1411-1417
- needs 1411-1417
Surface phases 262, 268, 1459-1460
Surrounded atom model 141

Temperature scan method 151
Tetrahedron approximation 968, 978-983, 1008
Theories of phase diagrams (see review article pp 592-623, Tuesday's poster session on the topic pp 726-1236, and see under specific topics)
- listing of treatments of the subject 84-89
Thermal analysis, including differential thermal analysis, DTA) 121, 142 377-382, 407, 417-419, 517, 1171, 1310
Thermal gravimetric analysis 517
Thermochemistry (see Thermodynamics)
Thermodata 37, 122
Thermodynamics
- compilations 37, 53, 75-81, 196, 228, 229-250
- computerized data banks 37, 49, 121-124, 1077-1089, 1186-1199, 1451
- theory, including computerized methods (see also Tuesday's poster session on the topic pp 726-1236; and see under specific topics) 37, 121-128, 143-144, 163, 803-845, 846-906, 1077-1089, 1100, 1457-1458, 1472-1475
- listing of treatment of theory 84-89
Toop 141, 730-731, 956
Transient Liquid Phase (TLP) bonding 1418-1419

Variable valency in representation of phase diagrams 671-672
VINITI (see under Russian literature)

Wiederkehr 960

X-ray analysis 143, 156, 407-422, 440-449, 517, 551
- synchrotron light 163

MATERIALS INDEX

This index represents a listing of pages on which quantitative information is given for specific systems: 1) all pages are noted on which phase diagram figures appear; 2) generally, those pages are noted on which data evaluation is discussed; 3) generally, those pages are noted on which related thermodynamic data, or sometimes related crystallographic data appear. A few summarizing data tables occur in these proceedings. No attempt has been made to list these under each individual material. Rather, these are noted under the general material category (e.g. "rare earths", etc.). Alloys have been listed with their components in alphabetical order under the component of lowest alphabetical occurrence. For compounds, the formulas have been alphabetized, but compounds forming components of salt systems are not broken up to further alphabetize, in order to preserve chemical meanings (e.g. CaF_2-AlF_3-Al_2O_3 is listed under AlF_3-Al_2O_3-CaF_2, rather than Al-Ca-F-O).

A-15 compound formation prediction 1148, 1158

$A_2^{III}B^{IV}O_7$ compound formation prediction 1149-1150, 1159-1160

Ac-B 762

Ag laves phase prediction 1147, 1157

Ag-B 770

Ag-Cu 780

Ag-Cu-S 774-797

Ag-Cu-Se 774-802

Ag-Cu-Zn (several temps) 237-246

Ag-Pd 1218

Ag-S 779-780

Ag-Si 219

Al 1407

Al-Au-In 455

Al-B 749, 753-757

Al-Be-Fe 544

Al-Ca-O-Si 1370

Al-Co-Cr-Ni 438

Al-Co-Fe-Si 1392, 1405

Al-Cr-Fe-Ni 438

Al-Cr-Fe-Si 1392, 1405

Al-Cr-Mo-Ni-Ti-W 630-635

Al-Cr-Nb	1189-1190, 1199
Al-Cr-Ni	628-630, 655, 658
Al-Cr-Ni-Pt	439
Al-Cr-Ni-Ti	628-630, 654
Al-Cr-Zr	1189-1190, 1194-1189
Al-Cu	608
Al-Cu-Mg-Si	1389-1390, 1402
Al-Fe-Mn	1391, 1403
Al-Fe-Mn-Si	1392, 1405
Al-Fe-Ni-Si	1392, 1405
Al-Fe-Si	1392, 1394, 1404, 1407
Al-Ge-Nb	1415
Al-Li	1115-1118, 1128-1131
Al-Li-Mg	1109-1138, 1134-1138
Al-Mg	1118-1119, 1128-1129, 1132
Al-Mg-Zn	1385-1386, 1399
Al-Mn	134
Al-Ni-Ti	628-630, 657
Al-Sn	1219
Al-Ti-V (Ti-6Al-4V)	567-574
Al-Zn	1393, 1406
$AlCa_2F_7$, and related cpds.	283-285
$AlCaF_5$-FNa	318
Al_2CaF_9Na	320
AlF-CaF_2	280-285
AlF_3	278
AlF_3-AlF_6Li_3-AlF_6Na	329, 331
AlF_3-AlF_6Na_3-CaF_2	314, 317-324
AlF_3-AlF_6Na_3-Al_2O_3	322-326
AlF_3-AlF_6Na_3-Al_2O_3-CaF_2	333, 335-337

AlF_3-AlF_6Na_3-Al_2O_3-CaF_2-FLi	272-354
AlF_3-AlF_6Na_3-Al_2O_3-CaF_2-FLi	336, 338
AlF_3-AlF_6Na_3-FLi	229, 332
AlF_3-Al_2O_3-CaF_2	328
AlF_3-FLi	300-305
AlF_6Li_3-AlF_6Na_3	306-311
Al_6Li_3-AlF_6Na_3-Al_2O_3	228-330
AlF_6Li_3-Al_2O_3	310, 312
AlF_6Li_3-CaF_2	314, 316
AlF_6Li_3-CaF_2-FLi	329, 333-334
AlF_6Na_3	277
AlF_6Na_3-AlF_3	289-296
AlF_6Na_3-Al_2O_3	296-299
AlF_6Na_3-Al_2O_3-CaF_2	325-328
AlF_6Na_3-CaF_2	285-290
AlF_6Na_3-FLi	305-308
$AlKO_2$-O_2Si	442
Al_2O_3	279
Al_2O_3-AlF_3	300
Al_2O_3-CaF_2	299-300
Al_2O_3-CaO-MgO-Na_2O-O_2Si	362-366, 374
$AlO_{1.5}$-$KO_{0.5}$	884
Al_2O_3-WO_3	221
Alloy 713 and 713LC	642
Am-B	752-756, 762
As-Ga	1233-1234
As-In	1233-1234
Au laves phase prediction	1147, 1157
Au-B	771
Au-Cu	726-743, 984-985, 988, 997-998, 1007-1011, 1020-1024

Au-Cu-Ni	726-743
Au-Mn	1013, 1025
Au-Ni	726-743
Au-Sb (including metastable diagram)	1173
Au-Si	1219
Au-Si (including metastable data)	1178
Au-Te	271
B-Ba	748, 753-757
B-Be	748, 752-757
B-C-Fe	566
B-Ca	748, 753-757
B-Co	749, 752-756, 761
B-Cr	749, 753-756, 759, 768
B-Fe	749, 753-756, 760
B-Fe (including metastable data)	1177, 1178
B-Hf	749, 753-756, 758
B-Ir	749, 753-756, 761
B-La	749, 753-756, 758
B-Mg	748, 753-757
B-Mn	749, 753-756, 760, 768
B-Mo	749, 753-756, 759
B-Nb	749, 753-756, 759, 768
B-Ni	750, 753-756, 761
B-Np	752-756, 762
B-Os	749, 753-756, 760, 770
B-Pa	762
B-Pd	750, 753-756, 761
B-Pt	750, 752-756, 761
B-Pu	752-756, 762
B-Re	749, 753-756, 760

B-Rh 749, 753-756, 761
B-rich systems 752
B-Ru 749, 753-756, 760, 770-771
B-Sc 749, 753-756, 758
B-Sr 748, 753-757
B-Ta 749, 753-756, 759, 768
B-Tc 749, 753-756, 760
B-Th 752-756, 762
B-Ti 749, 753-756, 758
B-transition metal 751
B-U 752-756, 762
B-V 749, 752-756, 759
B-W 749, 753-756, 759, 771
B-Y 749, 753-756, 758
B-Zr 749, 753-756, 758
B-1900 642, 652-653
B_2O_3-WO_3 220
BaO-WO_3 206
BeCu 539, 543
Be-Cu-Ne 543
Be-Fe 541
Be-Si 1219
Be-Ti (including metastable data) 1177
Be-Ti-Zr 1174
BeO-WO_3 202
Bi-Nb 1219
Bi_2O_3-WO_3 225
Brasses 1383-1385, 1398

C	857
C-Cr-Fe	1058
C-Cr-Fe-O	1048, 1060
C-Fe	155, 572, 885, 1368
C-Fe (metastable data)	1367
C-Fe-H-O-S	1081
C-Fe-Ni	470, 480, 880
C-Fe-Sb	573
C-H-Ni-O-S	1081
C-Ni (at three pressures)	111
C-Ni	891-901, 904
C-W	770
CO_3-HO-Li-Na	1098, 1108
Ca-Cu-Mg (several temps)	247-250
Ca-Fe-O-Si	1368
CaF_2	279
CaF_2-FLi	310, 313-315
Ca-O-Si	1369
$CaO-WO_3$	204
$CdO-WO_3$	219
Cl-F-K-Li	1095, 1107
Cl-F-Li-Na	1095, 1105-1106
$ClK-(HO)_2Mg-MgO$	511, 514-515
$ClLi-(HO)_2Mg-MgO$	511-512, 515
$ClNa-(HO)_2Mg-MgO$	511, 513, 515
Co-Fe-Ni	479
Co-Gd (including metastable data)	1177
Co-Sm	769
Cr-Fe	916, 935

Cr-Fe-Mg-O	1062
Cr-Fe-Ni	911-954
Cr-Fe-Ni (including irradiation effects)	1066-1069, 1071, 1074-1075
Cr-Fe-O	1059, 1061
Cr-Ni	916, 939
Cr-Ni-Ti	628-630, 656
Cr-O-S	1424
Cr-U (including metastable data)	1177
$Cs_2O \cdot WO_3$-WO_3	201
Cu-Fe	916, 924, 938, 1027-1046
Cu-Fe-Mn	911-954
Cy-Fe-Ni	911-954
Cu-Fe-O-SiO_2	1333
Cu-Fe-O-S-Si	1343
Cu-Fe-S	1333, 1343
Cu-Ge-Nb	1417
Cu-Mn	916, 940
Cu-Nb-Sn	1416
Cu-Ni	726-743, 916, 941
Cu-Ni-S	1350
Cu-O-S	1090-1092
Cu-S	779
Cu smelting	1336-1339, 1342-1349, 1354
Cu ternary alloys	229-250
Cu-Zn	1383-1385, 1398
Cu-Zr (including metastable data)	1177, 1178
Dy_2O_3-O_3Sc_2	553-565
Dy_2O_3-WO_3	211

F-Li	280
Fe-H-O-Ti	503
Fe-H-Ti	456, 498, 500, 506-507
Fe-Mn	916, 936
Fe-Mn-Ti	490-492, 504-505
Fe-Ni	916, 937, 1082, 1084
Fe-Ni (including irridation effects)	1065, 1068-1069
Fe-Ni-Mn (including irridation effects)	1065, 1068, 1072-1073
Fe-Ni-O	1078, 1082-1086
Fe-Ni-O-S	1077-1089
Fe-O	700, 909-910, 1080, 1084
Fe-O-S	1080, 1424
Fe-O-Si	1343
Fe-O-Ti	488-489, 501
Fe-Sb	573
Fe-Ti	486-488, 499
Ga-In-Sb	137, 138, 139
Ga-Nb	387-389, 397, 402-404
Ga-Sb	1233-1234
Ga-Sn-Zn	136
GaO_3-WO_3	222
Ge-Nb	389-392, 405-406
GMR 235	642, 652-653
graphite	857
H-Zr	587, 590-591
HfO_2-WO_3	214
H-Nb-Zr	588-589
H_2O-$(HO)_2Mg$-MgO	511, 515
Ho_2O_3-O_3Sc_2	552-565

In-Sb	1233-1234, 1236
In_2O_3-WO_3	223
IN 100	642, 652-653
IN 731 X	642
Inconel 700	642, 652-653
Inconel 713 C	642, 652-653
Inconel X-750	642, 652-653
Ir laves phase prediction	1147, 1157
$KO_{0.5}$-O_2S	902, 906
$K_2O \cdot WO_3$-WO_3	199
La_2O_3-WO_3	208
Li-Mg	1119-1120, 1128, 1133
$Li_2O \cdot WO_3$-WO_3	197
M 316 stainless (including irradiation effects)	1065
Mar - M 200	642, 652-653
Metal hydrides	610-612
Mg-Pb	1388, 1401
Mg-Si	1386, 1400
Mg-Zn (including metastable data)	1177, 1178
MgO-WO_3	203
Mn-O-S	1424
Mo-P	770
Mo-V	1218
Mo-W	1218

$Na_2O \cdot WO_3 - WO_3$	198
Nb-Ni (including metastable data)	1177
Nb-Ti	1218
Nb-W	1218
$Nb_2O_5 - WO_3$	215
$Nd_2O_3 - WO_3$	210
Ni-based (superalloys)	624-658
Ni-O-S	1078-1080, 1424
Ni smelting	1340-1341, 1350-1352
Ni-Ti	135, 769
Nicrotung	642, 652-653
Nimonic 115	642, 652-653
O-Si	882
Os laves phase prediction	1147, 1157
Oxide systems	165-225, 251-256, 257-258, 272-345, 355-374, 410-422, 440-449, 508-514, 550-562, 909
$PbO-WO_3$	224
Pb-Sn (including metastable data)	1175
Pb-Te	1235
Pd laves phase prediction	1147, 1157
Pd-Si (including metastable data)	1177, 1178
Pt laves phase prediction	1147, 1157
Pt-V	549

Rare earths	
- tabulation of structure vs pressure	110, 226-228, 751-752, 763
	110, 112-120
$Rb_2O \cdot WO_3 - WO_3$	200
René 41	642, 652-653
Re-W (including irradiation effects)	1066, 1068-1069, 1076
Rh Laves phase prediction	1147, 1157
Ru Laves phase prediction	1147, 1157
$Sm_2O_3 - WO_3$	209
Sn-V	770
$SrO - WO_3$	205
Steels: 43XX steel	571-572
$Ta_2O_5 - WO_3$	216
$TiO_2 - WO_3$	212
Ti-rich, commercial (Ti-6Al-4V)	567-574
Tool steels	572-573
TRW 1900	642, 652-653
Udimet 500	642, 652-653
Udimet 700	642, 652-653
Unitemp AF	642, 652-653
$UO_3 - WO_3$	217
V-W	1218

Waspaloy	642, 652-653
$Y_2O_3 - WO_3$	207
$ZnO - WO_3$	218
$ZrO_2 - WO_3$	213

NBS-114A (REV. 11-77)

U.S. DEPT. OF COMM. BIBLIOGRAPHIC DATA SHEET	1. PUBLICATION OR REPORT NO. NBS SP-496	2. Gov't Accession No.	3. Recipient's Accession No.

4. TITLE AND SUBTITLE

Applications of Phase Diagrams in Metallurgy and Ceramics—Volume 1
Proceedings of a Workshop Held at the National Bureau of Standards, Gaithersburg, Maryland, January 10-12, 1977

5. Publication Date: March 1978

6. Performing Organization Code

7. AUTHOR(S): G. C. Carter, Editor

8. Performing Organ. Report No.

9. PERFORMING ORGANIZATION NAME AND ADDRESS

NATIONAL BUREAU OF STANDARDS
DEPARTMENT OF COMMERCE
WASHINGTON, D.C. 20234

10. Project/Task/Work Unit No.

11. Contract/Grant No.

12. Sponsoring Organization Name and Complete Address (Street, City, State, ZIP)
National Bureau of Standards; National Science Foundation; Defense Advanced Research Projects Agency; Office of Naval Research; National Aeronautics & Space Administration; Energy Research & Development Administration; U.S. Army Research Office

13. Type of Report & Period Covered

14. Sponsoring Agency Code

15. SUPPLEMENTARY NOTES

Library of Congress Catalog Card Number: 78-2201

16. ABSTRACT (A 200-word or less factual summary of most significant information. If document includes a significant bibliography or literature survey, mention it here.)

The proceedings of a Workshop on Applications of Phase Diagrams in Metallurgy and Ceramics, held at the National Bureau of Standards, Gaithersburg, Maryland, on January 10-12, 1977, is presented in this NBS Special Publication. The Workshop was co-sponsored by the Institute for Materials Research and the Office of Standard Reference Data, NBS, and the National Science Foundation, the Defense Advanced Research Projects Agency, the Office of Naval Research, the National Aeronautics and Space Administration, the Energy Research and Development Administration, and the U. S. Army Research Office.

The purpose of the Workshop was to assess the current national and international status of phase diagram determinations and evaluations for alloys, ceramics and semiconductors; to determine the needs and priorities, especially technological, for phase diagram determinations and evaluations; and to estimate the resources being used and potentially available for phase diagram evaluation. These proceedings reflect the detailed contents of the Workshop for both the tutorial and review sessions as well as four poster sessions and four panel sessions covering the subjects; critical phase diagram availability, user needs of phase diagrams, experimental methods of determination, theoretical methods of calculation and prediction, methods of phase diagram representations of calculation and prediction, methods of phase diagram representations (especially multicomponent) and distribution to the user. Three of the panels addressed the subject of phase diagram needs in industrial applications. Cont.

17. KEY WORDS (six to twelve entries; alphabetical order; capitalize only the first letter of the first key word unless a proper name; separated by semicolons)
Ceramics; computer predictions; critical evaluations; data compilations; electronic materials; industrial needs; metallurgy; phase diagrams; theory of phase diagrams; thermodynamics.

18. AVAILABILITY

[x] Unlimited

[ ] For Official Distribution. Do Not Release to NTIS

[x] Order From Sup. of Doc., U.S. Government Printing Office Washington, D.C. 20402, SD Stock No. 003-003-01956-3

[ ] Order From National Technical Information Service (NTIS) Springfield, Virginia 22151

19. SECURITY CLASS (THIS REPORT)	21. NO. OF PAGES
UNCLASSIFIED	767
20. SECURITY CLASS (THIS PAGE)	22.
UNCLASSIFIED	

USCOMM-DC 60329-P78

16. ABSTRACT (*A 200-word or less factual summary of most significant information. If document includes a significant bibliography or literature survey, mention it here.*)

These proceedings represent documentation of this assessment, and constitute a valuable resource to workers in these areas, especially those planning to initiate phase diagram programs. Most subjects within the overall scope have been dealt with substantially in these proceedings; a few specialized topics such as surface and small particle phases, needed for the study of catalysis, have not been treated in detail. As the Alloy Data Center maintains a continuing phase diagram program, we would like to receive suggestions for similar topics of current and future interest, descriptions of new needs, or addenda and corrigenda to these proceedings. A tear-off sheet has been provided at the end of these proceedings for this purpose to be sent to the NBS Alloy Data Center.

☆ U.S. GOVERNMENT PRINTING OFFICE : 1979 O—256-480

(cut here)

If you wish to send us your suggestions for additional topics of current and future data compilation needs, or if you have any other addenda or corrigenda to these proceedings, please note them on this page and return to the

Alloy Data Center
National Bureau of Standards
Bldg. 223, Room B-150
Washington, DC 20234

Name _____

Affiliation _____

Address _____

City _____ State _____ Zip Code _____

Suggestions:

NBS TECHNICAL PUBLICATIONS

PERIODICALS

JOURNAL OF RESEARCH—The Journal of Research of the National Bureau of Standards reports NBS research and development in those disciplines of the physical and engineering sciences in which the Bureau is active. These include physics, chemistry, engineering, mathematics, and computer sciences. Papers cover a broad range of subjects, with major emphasis on measurement methodology, and the basic technology underlying standardization. Also included from time to time are survey articles on topics closely related to the Bureau's technical and scientific programs. As a special service to subscribers each issue contains complete citations to all recent NBS publications in NBS and non-NBS media. Issued six times a year. Annual subscription: domestic $17.00; foreign $21.25. Single copy, $3.00 domestic; $3.75 foreign.

Note: The Journal was formerly published in two sections: Section A "Physics and Chemistry" and Section B "Mathematical Sciences."

DIMENSIONS/NBS

This monthly magazine is published to inform scientists, engineers, businessmen, industry, teachers, students, and consumers of the latest advances in science and technology, with primary emphasis on the work at NBS. The magazine highlights and reviews such issues as energy research, fire protection, building technology, metric conversion, pollution abatement, health and safety, and consumer product performance. In addition, it reports the results of Bureau programs in measurement standards and techniques, properties of matter and materials, engineering standards and services, instrumentation, and automatic data processing.

Annual subscription: Domestic, $12.50; Foreign $15.65.

NONPERIODICALS

Monographs—Major contributions to the technical literature on various subjects related to the Bureau's scientific and technical activities.

Handbooks—Recommended codes of engineering and industrial practice (including safety codes) developed in cooperation with interested industries, professional organizations, and regulatory bodies.

Special Publications—Include proceedings of conferences sponsored by NBS, NBS annual reports, and other special publications appropriate to this grouping such as wall charts, pocket cards, and bibliographies.

Applied Mathematics Series—Mathematical tables, manuals, and studies of special interest to physicists, engineers, chemists, biologists, mathematicians, computer programmers, and others engaged in scientific and technical work.

National Standard Reference Data Series—Provides quantitative data on the physical and chemical properties of materials, compiled from the world's literature and critically evaluated. Developed under a world-wide program coordinated by NBS. Program under authority of National Standard Data Act (Public Law 90-396).

NOTE: At present the principal publication outlet for these data is the Journal of Physical and Chemical Reference Data (JPCRD) published quarterly for NBS by the American Chemical Society (ACS) and the American Institute of Physics (AIP). Subscriptions, reprints, and supplements available from ACS, 1155 Sixteenth St. N.W., Wash., D.C. 20056.

Building Science Series—Disseminates technical information developed at the Bureau on building materials, components, systems, and whole structures. The series presents research results, test methods, and performance criteria related to the structural and environmental functions and the durability and safety characteristics of building elements and systems.

Technical Notes—Studies or reports which are complete in themselves but restrictive in their treatment of a subject. Analogous to monographs but not so comprehensive in scope or definitive in treatment of the subject area. Often serve as a vehicle for final reports of work performed at NBS under the sponsorship of other government agencies.

Voluntary Product Standards—Developed under procedures published by the Department of Commerce in Part 10, Title 15, of the Code of Federal Regulations. The purpose of the standards is to establish nationally recognized requirements for products, and to provide all concerned interests with a basis for common understanding of the characteristics of the products. NBS administers this program as a supplement to the activities of the private sector standardizing organizations.

Consumer Information Series—Practical information, based on NBS research and experience, covering areas of interest to the consumer. Easily understandable language and illustrations provide useful background knowledge for shopping in today's technological marketplace.

Order **above** *NBS publications from: Superintendent of Documents, Government Printing Office, Washington, D.C. 20402.*

Order **following** *NBS publications—NBSIR's and FIPS from the National Technical Information Services, Springfield, Va. 22161.*

Federal Information Processing Standards Publications (FIPS PUB)—Publications in this series collectively constitute the Federal Information Processing Standards Register. Register serves as the official source of information in the Federal Government regarding standards issued by NBS pursuant to the Federal Property and Administrative Services Act of 1949 as amended, Public Law 89-306 (79 Stat. 1127), and as implemented by Executive Order 11717 (38 FR 12315, dated May 11, 1973) and Part 6 of Title 15 CFR (Code of Federal Regulations).

NBS Interagency Reports (NBSIR)—A special series of interim or final reports on work performed by NBS for outside sponsors (both government and non-government). In general, initial distribution is handled by the sponsor; public distribution is by the National Technical Information Services (Springfield, Va. 22161) in paper copy or microfiche form.

BIBLIOGRAPHIC SUBSCRIPTION SERVICES

The following current-awareness and literature-survey bibliographies are issued periodically by the Bureau:

Cryogenic Data Center Current Awareness Service. A literature survey issued biweekly. Annual subscription: Domestic, $25.00; Foreign, $30.00.

Liquified Natural Gas. A literature survey issued quarterly. Annual subscription: $20.00.

Superconducting Devices and Materials. A literature survey issued quarterly. Annual subscription: $30.00. Send subscription orders and remittances for the preceding bibliographic services to National Bureau of Standards, Cryogenic Data Center (275.02) Boulder, Colorado 80302.

NBS SPECIAL PUBLICATION 496

U.S. DEPARTMENT OF COMMERCE / National Bureau of Standards

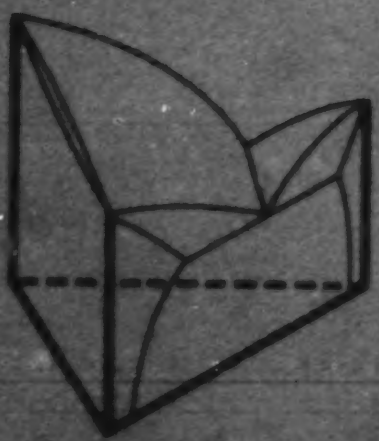

Applications of Phase Diagrams in Metallurgy and Ceramics

Volume 2

778

NATIONAL BUREAU OF STANDARDS

The National Bureau of Standards[1] was established by an act of Congress March 3, 1901. The Bureau's overall goal is to strengthen and advance the Nation's science and technology and facilitate their effective application for public benefit. To this end, the Bureau conducts research and provides: (1) a basis for the Nation's physical measurement system, (2) scientific and technological services for industry and government, (3) a technical basis for equity in trade, and (4) technical services to promote public safety. The Bureau consists of the Institute for Basic Standards, the Institute for Materials Research, the Institute for Applied Technology, the Institute for Computer Sciences and Technology, the Office for Information Programs, and the Office of Experimental Technology Incentives Program.

THE INSTITUTE FOR BASIC STANDARDS provides the central basis within the United States of a complete and consistent system of physical measurement; coordinates that system with measurement systems of other nations; and furnishes essential services leading to accurate and uniform physical measurements throughout the Nation's scientific community, industry, and commerce. The Institute consists of the Office of Measurement Services, and the following center and divisions:

Applied Mathematics — Electricity — Mechanics — Heat — Optical Physics — Center for Radiation Research — Laboratory Astrophysics[2] — Cryogenics[2] — Electromagnetics[2] — Time and Frequency[2].

THE INSTITUTE FOR MATERIALS RESEARCH conducts materials research leading to improved methods of measurement, standards, and data on the properties of well-characterized materials needed by industry, commerce, educational institutions, and Government; provides advisory and research services to other Government agencies; and develops, produces, and distributes standard reference materials. The Institute consists of the Office of Standard Reference Materials, the Office of Air and Water Measurement, and the following divisions:

Analytical Chemistry — Polymers — Metallurgy — Inorganic Materials — Reactor Radiation — Physical Chemistry.

THE INSTITUTE FOR APPLIED TECHNOLOGY provides technical services developing and promoting the use of available technology; cooperates with public and private organizations in developing technological standards, codes, and test methods; and provides technical advice services, and information to Government agencies and the public. The Institute consists of the following divisions and centers:

Standards Application and Analysis — Electronic Technology — Center for Consumer Product Technology: Product Systems Analysis; Product Engineering — Center for Building Technology: Structures, Materials, and Safety; Building Environment; Technical Evaluation and Application — Center for Fire Research: Fire Science; Fire Safety Engineering.

THE INSTITUTE FOR COMPUTER SCIENCES AND TECHNOLOGY conducts research and provides technical services designed to aid Government agencies in improving cost effectiveness in the conduct of their programs through the selection, acquisition, and effective utilization of automatic data processing equipment; and serves as the principal focus within the executive branch for the development of Federal standards for automatic data processing equipment, techniques, and computer languages. The Institute consist of the following divisions:

Computer Services — Systems and Software — Computer Systems Engineering — Information Technology.

THE OFFICE OF EXPERIMENTAL TECHNOLOGY INCENTIVES PROGRAM seeks to affect public policy and process to facilitate technological change in the private sector by examining and experimenting with Government policies and practices in order to identify and remove Government-related barriers and to correct inherent market imperfections that impede the innovation process.

THE OFFICE FOR INFORMATION PROGRAMS promotes optimum dissemination and accessibility of scientific information generated within NBS; promotes the development of the National Standard Reference Data System and a system of information analysis centers dealing with the broader aspects of the National Measurement System; provides appropriate services to ensure that the NBS staff has optimum accessibility to the scientific information of the world. The Office consists of the following organizational units:

Office of Standard Reference Data — Office of Information Activities — Office of Technical Publications — Library — Office of International Standards — Office of International Relations.

---

[1] Headquarters and Laboratories at Gaithersburg, Maryland, unless otherwise noted; mailing address Washington, D.C. 20234.
[2] Located at Boulder, Colorado 80302.

Applications of Phase Diagrams in Metallurgy and Ceramics

Volume 2

Proceedings of a Workshop Held at the
National Bureau of Standards
Gaithersburg, Maryland, January 10-12, 1977

Edited by

G.C. Carter

Institute for Materials Research
National Bureau of Standards
Washington, D.C. 20234

Sponsored by:

Institute for Materials Research and
Office of Standard Reference Data, NBS
and by
National Science Foundation
Defense Advanced Research Projects Agency
Office of Naval Research
National Aeronautics and Space Administration
Energy Research and Development Administration
U.S. Army Research Office

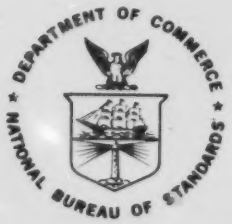

U.S. DEPARTMENT OF COMMERCE, Juanita M. Kreps, Secretary

Dr. Sidney Harman, Under Secretary

Jordan J. Baruch, Assistant Secretary for Science and Technology

NATIONAL BUREAU OF STANDARDS, Ernest Ambler, Director

Issued March 1978

780

Library of Congress Catalog Card Number: 78-2201

National Bureau of Standards Special Publication 496/2
Nat. Bur. Stand. (U.S.) Spec. Publ. 496/2, 847 pages (March 1978)
CODEN: XNBSAV

781

U.S. GOVERNMENT PRINTING OFFICE
WASHINGTON: 1978

For sale by the Superintendent of Documents, U.S. Government Printing Office, Washington, D.C. 20402
Stock No. 003-003-01895-3 2-volume set; sold in sets only.
(Add 25 percent additional for other than U.S. mailing).

General Abstract

The proceedings of a Workshop on Applications of Phase Diagrams in Metallurgy and Ceramics, held at the National Bureau of Standards, Gaithersburg, Maryland, on January 10-12, 1977, is presented in this NBS Special Publication. The Workshop was co-sponsored by the Institute for Materials Research and the Office of Standard Reference Data, NBS, and the National Science Foundation, the Defense Advanced Research Projects Agency, the Office of Naval Research, the National Aeronautics and Space Administration, the Energy Research and Development Administration, and the U. S. Army Research Office.

The purpose of the Workshop was to assess the current national and international status of phase diagram determinations and evaluations for alloys, ceramics and semiconductors; to determine the needs and priorities, especially technological, for phase diagram determinations and evaluations; and to estimate the resources being used and potentially available for phase diagram evaluation. These proceedings reflect the detailed contents of the Workshop for both the tutorial and review sessions as well as four poster sessions and four panel sessions covering the subjects; critical phase diagram availability, user needs of phase diagrams, experimental methods of determination, theoretical methods of calculation and prediction, methods of phase diagram representations of calculation and prediction, methods of phase diagram representations (especially multicomponent) and distribution to the user. Three of the panels addressed the subject of phase diagram needs in industrial applications.

These proceedings represent documentation of this assessment, and constitute a valuable resource to workers in these areas, especially those planning to initiate phase diagram programs. Most subjects within the overall scope have been dealt with substantially in these proceedings; a few specialized topics such as surface and small particle phases, needed for the study of catalysis, have not been treated in detail. As the Alloy Data Center maintains a continuing phase diagram program, we would like to receive suggestions for similar topics of current and future interest, descriptions of new needs, or addenda and corrigenda to these proceedings. A tear-off sheet has been provided at the end of these proceedings for this purpose to be sent to the NBS Alloy Data Center.

KEY WORDS: Ceramics; computer predictions; critical evaluations; data compilations; electronic materials; industrial needs; metallurgy; phase diagrams; theory of phase diagrams; thermodynamics.

782

Foreword

Quantitative data on physical and chemical properties of materials form a key resource of modern technology. In the past a few dedicated scientists and engineers have performed an important service by compiling and evaluating such data for use by the technical community; an outstanding example is the work of Hansen on alloy phase diagrams. With the rapid growth of science and technology, this task has become too large and complex for a single individual. Organized programs with proper funding and continuity are essential if the technical community is to have the reliable data needed to solve the problems of modern society.

This Workshop represents an effort to coordinate and reinforce the current efforts on compilation of phase diagrams of alloys and ceramics. Many research groups and individual scientists throughout the world are concerned with phase equilibrium data.

Specialized expertise exists in small institutions as well as large laboratories. If this talent can be effectively utilized through a cooperative effort, the needs for such data can be met. The Office of Standard Reference Data, which serves as the program management office for the National Standard Reference Data System, is eager to work with all groups concerned with this problem. Through a cooperative international effort we can carry out a task which has become too large for an individual.

David R. Lide, Jr.
Chief
Office of Standard Reference Data
National Bureau of Standards

CONTENTS

	Page
General Abstract	iii
Foreword	v
Welcome - E. Ambler	xv
Overview of the Workshop - G.C. Carter	xvii
Workshop Organizing Committee	xviii

VOLUME 1

Present Status of Phase Diagram Compilation Activities

Phase Diagram Compilation Activities in Ceramics R.S. Roth, L.P. Cook, T. Negas, G.W. Cleek, and J.B. Wachtman, Jr.	1
Discussion	22
Present Status of Phase Diagram Compilation Activity for Semiconductors C.D. Thurmond	23
Phase Diagram Compilations for Metallic Systems - An Assessment of Ongoing Activities G.C. Carter	36
Organization of Phase Diagram Information in the Soviet Union N.V. Ageev, D.L. Ageeva, T.P. Kolesnikova, and L.A. Petrova	90
Discussion	95
A Survey of High Pressure Phases of Materials L. Merrill	100
Discussion (Jan. 10 - AM Session)	121
Phase Diagram Information from Computer Banks I. Ansara	123
An Overview of the Determination of Phase Diagrams F.N. Rhines	142
Discussion	163

Phase Diagram Compilation and Data Evaluation Activities

Proposal for a Comprehensive Handbook on "Ternary Phase Diagrams of Metals" F. Aldinger, E.-Th. Henig, H.L. Lukas, and G. Petzow	164
Phases and Phase Relations in the Binary Oxide Systems Containing WO_3 Luke L.Y. Chang	165

RIC in Phase with Rare-Earth Constitutional Diagrams
K.A. Gschneidner, Jr., M.E. Verkade and B.L. Evans..... 226

Evaluations of Phase Diagrams and Thermodynamic Properties of Ternary Copper Alloy Systems
Y.A. Chang, J.P. Neumann, U.V. Choudary..... 229

Phase Equilibria in Variable Valence Oxide Systems
W.B. White..... 251

Phase Diagrams for Ceramists
L.P. Cook, R.S. Roth, T. Negas and G.W. Cleek..... 257

NBS Crystal-Data Center
A. Mighell, H. Ondik, J. Stalick, R. Boreni..... 259

The NBS Alloy Data Center
G.C. Carter, D.J. Kahan, and L.H. Bennett..... 261

A Review of Phase Equilibria in the Na_3AlF_6-LiF-CaF_2-AlF_3-Al_2O_3 System
D.F. Craig, R.T. Cassidy, and J.J. Brown, Jr. 272

Methods of Compiling and Editing "Structure and Properties of Binary Metallic Systems"
A.E. Vol and I.K. Kagan..... 346
English Translation 351

Experimental Techniques in Phase Diagram Determinations

The Determination of Phase Diagrams for Liquid Oxides and Metallurgical Slags by Hot-Wire Microscopy
H.A. Fine..... 355

Experimental Techniques in Phase Diagram Determination of Superconducting Compounds Containing Volatile Components at Temperatures up to 2200°C
R. Flukiger and J.-L. Jorda 375

Application of Experimental Techniques and the Critical Determination of Phase Equilibria in Oxide Systems
F.P. Glasser..... 407

Protective Coatings for Superalloys and the Use of Phase Diagrams
M.R. Jackson and J.R. Rairden 423

Application of the Scanning Electron Microscope to the Study of High Temperature Oxide Phase Equilibria
L.P. Cook and D.B. Minor..... 440

Hyperfine Techniques and the Determination of Phase Diagrams
R.C. Reno, L.J. Swartzendruber, G.C. Carter, and L.H. Bennett 450

Experimental Determination of Phase Diagrams with the Electron Microprobe and Scanning Transmission Electron Microscope
A.D. Romig, Jr. and J.I. Goldstein 462

Interrelations Between Phase Diagrams and Hydriding Properties for Alloys Based on the Intermetallic Compound FeTi
G.D. Sandrock, J.J. Reilly, and J.R. Johnson 483

Phase Equilibria in the System MgO-RCl (R=Li, Na and K) Solution Under Hydrothermal Conditions by Means of a Capsule Bursting Method
Shigeyuki Sōmiya, Kazuo Nakamura, Shin-ichi Hirano and Shinroku Saito 508

High-Energy Ion Beams in Phase Diagram Determination
J.E. Smugeresky, and S.M. Myers 516

Phase Equilibrium Diagrams in Terms of Electronic Structure
F. E. Wang 545

Use of Segregation Phenomena in Solid Solutions as a Method for Determining Solidification Diagrams. Application to some Sc_2O_3 - Ho_2O_3 and Sc_2O_3 - Dy_2O_3 Systems
J.M. Badie 550

Studies of the Fe-C-B Phase Diagram by Autoradiography
T.B. Cameron and J.E. Morral 566

User Needs for Phase Diagrams
P. J. Fopiano 567

Phase Diagram of a Specimen at High Temperatures Under External Tensile or Shear Stress or Both
K.M. Khanna 575

Phase Diagram of a Metal-Gas System
V.K. Sinha 578

Methods of Phase Diagram Calculations

Theory of Alloy Phases
R.E. Watson, H.Ehrenreich and L.H.Bennett 592
Discussion 620

Computation and Prediction of Phase Diagrams (Panel I)

Estimation of Conjugate γ and γ' Compositions in Ni-Base Superalloys
R.L. Dreshfield..... 624
Discussion (Panel I - Jan. 11)..... 658

Review of Phase Diagram Representations, Format, and Distribution

The Representation of Phase Equilibria
A. Prince..... 660

Phase-Diagram Compilations - A User's View
J.D. Livingston..... 703

Some Thoughts on the Distribution of Reference Data
H. J. White, Jr..... 709

Remarks on Producing and Publishing Critically Evaluated Data
W.B. Pearson..... 720
Discussion (Jan. 11 - PM Session)..... 725

AUTHOR INDEX 725-A
SUBJECT INDEX 725-C
MATERIALS INDEX 725-J

VOLUME 2

Computational Techniques for Phase Diagram Construction

Computerized Characterization of the Au-Cu-Ni Ternary System
S.K. Tarby, C.J. Van Tyne, and M.L. Boyle..... 726

Correlations and Predictions of Metal-Boron Phase Equilibria
K.E. Spear..... 744

A Valence Bond Test for the Validity of Intermetallic and Semiconducting Structures
F.L.Carter..... 763

Computation of the Component Activities from Ternary Miscibility Gap Data: The Cu-Ag-S and Cu-Ag-Se Systems
U.V. Choudary and Y.A. Chang..... 774

The Mathematical Representation of Activity Data in Three Component Systems
I. Eliezer and R.A. Howald..... 803

A Program for Binary Phase Equilibria Using the Redlich-Kister Equations
I. Eliezer and R. A. Howald..... 816

Polynomial Representation of the Excess Free Energy of Multicomponent Systems and Their Use in Phase Diagram Calculations
H. Gaye and C.H. P. Lupis 907

Thermodynamic Data for the Fe–O System Evaluated Using a New Computer-Aided Strategy
J.L. Haas, Jr. and J.R. Fisher..... 909

Analysis and Synthesis of Phase Diagrams of the Fe–Cr–Ni, Fe–Cu–Mn and Fe–Cu–Ni Systems
M. Hasebe and T. Nishizawa..... 911

Optimization of Phase Diagrams by a Least Squares Method Using Simultaneously Different Types of Data
E.-Th. Henig, H.L. Lukas, B . Zimmermann and G. Petzow .. 955

Theoretical Calculation of Phase Diagrams Using the Cluster Variation Method
R. Kikuchi and D. de Fontaine 967

Fundamental Calculations of Coherent Phase Diagrams
D. de Fontaine and R. Kikuchi..... 999
Discussion..... 1017

Generation of Self-Consistent Gibbs Energy Functions for Binary Systems: The Fe–Cu System as an Example
J.F. Smith, D.M. Bailey and O. Kubaschewski..... 1027

Characteristics and Calculation of Stability Diagrams
S. McCormick and Y. Bilimoria..... 1047

The Effect of Irradiation on Phase Stability
L. Kaufman, J.S. Watkin, J.H. Gittus and A.P. Miodownik 1065

Facility for the Analysis of Chemical Thermodynamics (F*A*C*T) – A Computerized Canadian Thermodynamic Data Treatment Centre
A.D. Pelton, C.W. Bale, and W.T. Thompson..... 1077

The Calculation of Pourbaix Diagrams Using a Modified Linear Programming Technique
B.H. Rosof..... 1090

Theoretical Concepts Useful in the Calculation or Storage of Phase Diagrams of Ionic Systems
M.-L. Saboungi and M. Blander..... 1093

Estimation of Isothermal Sections of Ternary Phase Diagrams of Lithium Containing Systems: The Al–Li–Mg System
M.-L. Saboungi and C.C. Hsu..... 1109

Cybernetic Prediction of the Formation of Chemical Compounds in Uninvestigated Systems
E.M. Savitskii, V.P. Gribulya, and N.N. Kiselyeva 1139
English Translation..... 1151

The Determination and Representation of Metastable Phase Diagram Features and Other Thermal Characteristics of Metastable Alloys, Especially Amorphous Metals
B.C. Giessen..... 1161
Discussion..... 1183

The Calculation of Multicomponent Alloy Phase Diagrams at the National Physical Laboratory
T.G. Chart..... 1186

Synthesis of Binary Metallic Systems I. Ismorphous Systems II. Simple Eutectic Systems
S.S. Balakrishna, and A. K. Mallik..... 1200

Quantitative Fits to Phase Lines and High Temperature Thermodynamic Data for Systems Forming Semiconductor Compounds
R.F. Brebrick..... 1220

Format and Distribution of Phase Diagram Data

Table of Contents and Cumulative Subject Index for "Phase Diagrams of Metallic Systems," N.V. Ageev, editor, Volumes 1-19
C.M. Scheuermann 1237

Standards for Publication of Phase Equilibrium Studies
E.R. Kreidler..... 1307

Formatting and Distributing Evaluated Reference Data: The Office of Standard Reference Data at the National Bureau of Standards
S.P. Fivozinsky and G.B. Sherwood..... 1325

User Needs for Phase Diagram Information (Panel II)

Panel Discussion: Primary Metal Production
J.F. Elliott..... 1332

Needs for Phase Diagram Information in Non-Ferrous Industry
P.R. Ammann..... 1334
Discussion..... 1353

Primary Metals Production
H.R. Larson..... 1354
Discussion..... 1357

Use of Phase Diagrams in Iron and Steelmaking
R.D. Pehlke..... 1360
Discussion..... 1371

Materials Processing (Fabricating, Machining, Heat Treating, etc.) (Panel III)

User Needs for Phase Diagrams for Materials Processing: Glasses
R.C. Doman, and R.N. McNally 1378

Equilibrium Diagrams in Non-Ferrous Alloys
L.F. Mondolfo 1382

Phase Equilibria in the Development of High Temperature Structural Ceramics
S. Prochazka 1409

Phase Diagram Information for Processing of Superconductors
D. Dew-Hughes 1411

Product Applications (User Needs for Phase Diagram Information) (Panel IV)

Panel Discussion: Product Applications
F.L. VerSnyder 1418

Importance of Phase Diagrams in the Electric Power Industry
R.I. Jaffee 1420

Summary of Presentation on User Needs of Phase Diagrams: The Solar Energy Field
A.I. Mlavsky 1426

The Use of Phase Equilibria in the Manufacture of Spinel Ferrites
P. Slick 1427

The Application of the Phase Diagram to Thermal Energy Storage Technology
J.E. Beam and J.E. Davison 1428

The Needs for Phase Equilibria Data in the Development of Magnetohydrodynamics
R.A. Howald and I. Eliezer 1440
Discussion 1451

Summary Remarks
J. F. Elliott 1453

Evaluation of Conference
R.A. Howald 1470

Evaluation of Conference
J.E. Selle 1471

Comments on the Phase Diagram Workshop
D. de Fontaine..... 1472

Additional Contributed Papers to the Workshop

The Relation Between Bond Length and Crystal Structures in Metals
A.P. Miodownik..... 1479

On Computerized Construction of Multidimensional Phase Diagrams in a Factographic IRS
I.V. Tulupova and V.S. Stein..... 1506

REGISTRATION LIST..... 1520

AUTHOR INDEX..... 1529

SUBJECT INDEX..... 1531

MATERIALS INDEX..... 1538

Disclaimer

Certain commercial products and instruments are identified in this publication in order to specify adequately the experimental procedure. In no case does such identification imply recommendation or endorsement by the National Bureau of Standards, nor does it imply that the products or equipment identified are necessarily the best available for the purpose.

Welcome to the Workshop on Applications of Phase Diagrams in Metallurgy and Ceramics

E. Ambler

Good morning. It is my pleasure to welcome you this morning to the National Bureau of Standards and this Workshop on Applications of Phase Diagrams in Metallurgy and Ceramics. Evidence of the broad interest in and importance of this subject matter is seen when one notes that the National Science Foundation, Defense Advance Research Project Agency, Office of Naval Research, National Aeronautics and Space Administration, and U. S. Army Research Office have joined with the NBS Institute for Materials Research and NBS Office of Standard Reference Data in the sponsorship of this workshop.

As I looked over the material for this workshop, I found this group to be truly international and interdisciplinary in scope. There are participants here from Canada, France, Germany, India, Japan, the United Kingdom, Switzerland, the Union of Soviet Socialist Republics, and our own United States. You include representatives from data compilation groups, major industries and trade associations, and scientists from industry, government and university laboratories.

Of special interest to me is your banquet speaker, W. Dale Compton, who is the Vice President for Scientific Research at the Ford Motor Company. In addition, Dale is also a member of the NBS Visiting Committee - our Board of Directors so to speak - and the former chairman of the National Science Foundation Numerical Advisory Board. I look forward to joining you for the banquet and Dale's presentation.

For more than 100 years, phase diagrams have been a recognized and important tool in the development of science and technology. As one example, phase diagrams formed the basis for the development of new alloys and the respective heat treatments for these alloys. This resulted in new materials highly characterized and tailored to a host of specific uses. Today, phase diagrams are increasingly relevant to the development of new and substitute materials.

Now, as we stand at the threshold of this Workshop, it seems an appropriate time to spend a brief moment clarifying our perspective concerning the development of phase diagrams. Where do we stand in the study of phase diagrams and the compilation of phase diagram data? Clearly, the studies of and the techniques used today are vastly different than those of yesterday.

The optical microscope was used 100 years ago to study the character of alloys and minerals. By 1914, x-rays were used to confirm the crystalline structure of materials. The 1930's brought the advent of the electron microscope and a higher resolution of the materials being studies. From that evolved the electron microprobe which allowed us to determine the chemical composition of an individual phase on a spatial resolution of two to three μm in diameter. More recently, we have seen the development of the scanning electron microscope, the field ion microscope, and the Auger electron spectrometer.

Over the past 30 - 35 years, we have witnessed and participated in an evolution in experimental techniques. Today, we are able to determine phase diagrams to a high level and detail of accuracy. Certainly, our techniques are vastly improved. But the task we face is still enormous. Just consider the study of alloys. In the study of binarys, there are 1770 possible diagrams; with ternaries, there are 34,200 possible phase diagrams; and with quatranaries, there are many, many possible diagrams. To compound this task is the fact that it is the multicomponent materials which are of the greatest interest today.

To meet this problem, new techniques are now being developed which are based on a theoretical understanding of materials. We find that we can achieve "paper calculations" through theoretical prediction of phase diagrams. In addition, we can develop mathematical models that are predictive. However, the validity of these models is dependent on the availability of accurate data. Thus, while we strive to predict complicated phenomena, we do so with the clear understanding that we must first develop a simple, accurate data base.

An assessment of today's environment then shows that although we possess many new and improved tools, they are still not sufficient to perform the task that faces us. Therefore, we stand in a position where our first order of business should be an assessment of priorities. The goals of this workshop:

- To assess the current national and international status of phase diagram determination and evaluation for alloys, ceramics and semi-conductors;

- To determine the needs and priorities, especially technological, for phase diagram determinations and evaluations; and

- To estimate the resources being used and potentially available for phase diagram evaluation;

are quite timely. In fact, I think that the key statement for this workshop is found on page 1 of your program: "It is hoped that the workshop will provide the stimulus for the production of more relevant more useful, and more useable phase diagram data."

I concur with that statement and heartily endorse the goals of this workshop. Moreover, it is my personal belief that communication, such as this workshop is intended to foster, is a critical component to all scientific and technological ventures.

In closing, again let me welcome you to NBS. Our facilities are at your disposal and we would invite any inquiries about our specific programs that are of interest to you. I look forward to joining you Tuesday evening and I hope that your workshop is both stimulating and productive.

Overview of the Workshop

G. C. Carter

Knowledge of the structure of materials is important in understanding several industrially significant phenomena and applications such as aging, hardness, occurrence of brittle intermetallic compounds, magnetic transition temperatures, high-temperature solubility of impurities, corrosion resistance, solid electrolytes and non-crystalline solids. The study of a phase diagram appropriate to a particular material can often provide information important to its scientific and technical application.

Wide participation by industry, government, and university representatives was achieved at the Workshop. International participation was particularly successful among the data evaluation groups including important representations from the Soviet Union, Germany, France, the UK, Japan, and Canada. Other countries were represented; experimentalists and theorists determining phase diagrams were among the participants, as were a substantial fraction of phase diagram users from industry.

Specific subjects of investigation were:

... to assess the current national and international status of phase diagram determinations and evaluations for alloys, ceramics and semiconductors; to identify resources being expended that could be made more useful by appropriate coordination; to recognize unnecessarily overlapping efforts in determining phase diagrams; to suggest areas of international cooperation.

... to determine the needs and priorities, especially technological, for phase diagram determinations and evaluations; to gauge the relative importance of depth of coverage and range of materials including factors such as a) high precision, b) metastable phases, c) binary and higher order systems, d) magnetic, metal nonmetal and other phase transitions, e) high pressure data, f) integration of collateral information, and g) the role of impurities or trace additions.

... to review the strengths and limitations of various experimental techniques for determining phase diagrams,

... to briefly survey the status and merits of various predictive methods (CALPHAD, PHACOMP, psedupotential, etc.),

... to discuss diverse presentation methods, and

... to discuss effective and alternative means for dissemination of phase diagram data.

The workshop program was designed to stimulate interactions between (i) phase diagram data providers and users, (ii) metallurgists, geochemists, thermochemists, ceramics, solid state chemists, physicists, and scientists in other disciplines, (iii) representatives from industry, government, and the academia, (iv) phase diagram data centers throughout the world.

Plenary lectures introduced the subjects of present status of data availability from reference books, data centers and computerized files, the status of experimental data and theory of alloy phases. A panel on computation and prediction gave a more thorough introduction to that subject, and short reviews introduced the subjects of phase diagram representations and methods of distribution. Lively poster sessions followed these introductions. Three panel sessions were devoted to industrial needs in (i) Primary Metals Production, (ii) Materials Processing, and (iii) Product Applications. Discussion covered needs for multicomponent diagrams (up to 9 or 10 components) for industrial applications down to binary equilibrium diagrams, for various R & D programs, theoretical and prediction models, and other applications.

Four on-line demonstrations of computer-data handling systems related to phase diagrams were held and short instructional movies were shown during the poster session.

The workshop was organized by the Alloy Data Center and the group compiling "Phase Diagrams for Ceramists". The success of the Workshop program could not have been realized without invaluable assistance received from our very able organizing committee.

WORKSHOP ORGANIZING COMMITTEE

Members from NBS

L. H. Bennett, chairman
G. T. Armstrong, C. J. Bechtoldt, D. B. Butrymowicz, G. C. Carter, L. P. Cook, J. R. Cuthill, P. R. deBruyn, D. J. Kahan, M. B. McNeil, R. L. Parker, R. M. Waterstrat, H. J. White

Members from other Organizations

N. Ault, Norton Co., Worcester, MA
J. Elliott, M.I.T., Cambridge, MA
S. G. Epstein, Aluminum Association, New York, NY
L. Kaufman, ManLabs, Cambridge, MA
R. Laudise, Bell Telephone Laboratories, Murray Hill, NJ
J. D. Livingston, General Electric, Schenectady, NY
E. S. Osborne, Carnegie Geophysical Lab., Washington, DC
E. C. Van Reuth, Defense Advanced Res. Projects Agency, Arlington, VA
Schrade F. Radtke, Intl. Lead-Zinc Research Organization, New York, NY
R. Reynik, National Science Foundation, Washington, DC
E. Salkovitz, Office of Naval Research, Arlington, VA
L. M. Schetky, International Copper Research Assoc., New York, NY
C. Scheuermann, NASA Lewis Research Center, Cleveland, OH
M. Semchyschen, Climax Molybdenum Corp., Ann Arbor, MI
J. Swisher, Energy Research & Development Admin., Washington, DC

ARRANGEMENTS COMMITTEE

Ronald B. Johnson, Chairman
Sara R. Torrence

National Bureau of Standards SP-496, Applications of Phase Diagrams in Metallurgy and Ceramics
Proceedings of Workshop held at NBS, Gaithersburg, Md., January 10-12, 1977

COMPUTERIZED CHARACTERIZATION OF THE Au-Cu-Ni TERNARY SYSTEM

by

S. K. Tarby, C. J. Van Tyne, and M. L. Boyle
Department of Metallurgy and Materials Science
Lehigh University, Bethlehem, Pa. 18015

Abstract

Information synthesized from binary systems by a computer method was used to characterize the Au-Cu, Au-Ni, and Cu-Ni binary systems. This characterization allows for the calculation of binary thermodynamic properties and binary phase equilibria. An extension of this characterization to the ternary Au-Cu-Ni system was made through the use of Kohler's equation of mixing. Not only did this yield thermodynamic information about the ternary, but it also permitted the calculation of a miscibility gap in the system. The predicted miscibility gap agrees extremely well with one determined experimentally. Currently, work with a computer optimization technique is being performed for the prediction of solid-liquid, two-phase equilibria in a ternary system.

Introduction

A computer program[1] employing a least squares technique has been developed to analyze concurrently activity data, integral heat of mixing data, and phase diagram data in order to generate a set of α-parameters for binary systems. The α-parameter is defined as

$$\alpha_{12} = \ell n\ \gamma_1/(1-X_1)^2 \qquad (1)$$

where γ_1 is the Raoultian activity coefficient and X_1 is the atom fraction of component 1. These α-parameters were given a composition and inverse temperature dependence of the form

$$\alpha_{12} = \sum_{i=o}^{n} (A_{2i} + A_{2i+1}/T) \cdot X_2^i \qquad (2)$$

where n is the order of the α-parameter representation, the A_j's are constants determined by the least squares analysis, and T is absolute temperature. Each α-parameter characterizes a single phase region in a binary system. The integral and partial molar solution thermodynamic quantities as well as the activities of each component can be calculated from the α-parameter for any given temperature and composition in a one phase region. A pair of α-parameters for two different phases can be used to predict two phase equilibria in a binary system.

The Cu-Ni, Au-Ni, and Au-Cu binary systems have been analyzed by such a technique[1] and the constants for the α-parameter representation are given in Table I.

TABLE I - Calculated Liquid and Solid α-Parameter Constants for the Cu-Ni, Au-Ni, and Au-Cu Binary Systems

	α^L_{Cu-Ni}	α^S_{Cu-Ni}	α^L_{Au-Ni}	α^S_{Au-Ni}	α^L_{Au-Cu}	α^S_{Au-Cu}
A_1	1.590	.8909	-18.34	-1.994	5.483	-3.654
A_2	-1538.	-816.4	27000.	2757.	-10750.	1252.
A_3	-3.076	-.6033	46.22	10.31	-7.777	5.391
A_4	5702.	2229.	-80160.	-4737.	11260.	-4859.
A_5	-	-	-55.90	-18.73	-	-
A_6	-	-	116500.	7813.	-	-
A_7	-	-	32.33	9.100	-	-
A_8	-	-	-69830.	-1267.	-	-

This study shows how the α-parameter representation can be utilized in the prediction of solution thermodynamic and phase equilibria properties of ternary systems.

α-Parameter Representation of Ternary Systems

A simple approach to the prediction of thermodynamic properties and phase diagrams in multicomponent systems is to employ a formalism based entirely on binary and pure component data. Ansara[2] has presented the highlights of several models that have been proposed for an approach of this sort. The equations developed by Kohler[3] have been selected from this group. According to Kohler, the excess molar free energy of a ternary solution can be given as

$$\frac{G^{XS}_{123}}{RT} = (1 - X_3)^2 \left.\frac{G^{XS}_{12}}{RT}\right|_{X_1/X_2} + (1 - X_2)^2 \left.\frac{G^{XS}_{13}}{RT}\right|_{X_1/X_3} + (1 - X_1)^2 \left.\frac{G^{XS}_{23}}{RT}\right|_{X_2/X_3} \qquad (3)$$

where along the constant composition path X_1/X_2

$$\left.\frac{G^{XS}_{12}}{RT}\right|_{X_1/X_2} = \frac{X_1}{1 - X_3} \; \frac{X_2}{1 - X_3} \; \alpha_{12} \qquad (4)$$

Similar relations hold for $\left.\frac{G^{XS}_{13}}{RT}\right|_{X_1/X_3}$ and $\left.\frac{G^{XS}_{23}}{RT}\right|_{X_2/X_3}$.

If the α functions are constant, then Eq. (3) reduces to the so-called regular solution form, i.e.,

$$\frac{G^{XS}_{123}}{RT} = \alpha_{12} X_1 X_2 + \alpha_{13} X_1 X_3 + \alpha_{23} X_2 X_3 \qquad (5)$$

This symmetrical form has been used by many investigators including Meijering,[4,5] Benedict et al.,[6] Oriani and Alcock,[7] Toop,[8] Olson and Toop,[9,10] and Wohl.[11]

In this study the α-parameters were not constant but were given the variability described by Eq. (2).

The activity coefficient of component 1 in a ternary solution may be expressed in terms of the binary data by differentiating Eq. (3) with

respect to X_1 at constant X_2/X_3. The result[10] is

$$\ell n\ \gamma_1^{123} = ((1-X_3)\ \ell n\ \gamma_1^{12} + X_3(1-X_3)\ [\ell n\ \gamma_1^{12} + \ell n\ \gamma_2^{12}])\Big|_{X_1/X_2}$$

$$+ ((1-X_2)\ \ell n\ \gamma_1^{13} + X_2(1-X_2)\ [\ell n\ \gamma_1^{13} + \ell n\ \gamma_3^{13}])\Big|_{X_1/X_3}$$

$$- (1-X_1)^2\ [\ell n\ \gamma_2^{23} + \ell n\ \gamma_3^{23}]\Big|_{X_2/X_3} \qquad (6)$$

Similar relations for $\ell n\ \gamma_2^{123}$ and $\ell n\ \gamma_3^{123}$ can also be formulated. Olson and Toop[9] have shown that both Eqs. (3) and (6) can be applied to systems that are non-regular. Thus, these equations can be quite useful for making predictions of ternary thermodynamic properties of non-regular systems where measured data are often lacking.

The addition of the ideal terms to Eq. (3) gives the molar free energy of mixing, i.e.,

$$\frac{\Delta G^M_{123}}{RT} = (1-X_3)^2\ \frac{G^{XS}_{12}}{RT}\Big|_{X_1/X_2} + (1-X_2)^2\ \frac{G^{XS}_{13}}{RT}\Big|_{X_1/X_3}$$

$$+ (1-X_1)^2\ \frac{G^{XS}_{23}}{RT}\Big|_{X_2/X_3} + X_1\ \ell n\ X_1 + X_2\ \ell n\ X_2 + X_3\ \ell n\ X_3 \qquad (7)$$

Results of Calculation

Figures 1, 2, and 3 show the iso-free energy of mixing curves, determined from Eq. (7), for solid Au-Cu-Ni alloys at 500°, 800°, and 1100°K, respectively. Figure 4 is a three dimensional representation of the free energy of mixing values at 800°K. Table II lists the 1100°K values of the free energy of mixing across the ternary system. Because of the temperature dependency assigned to the α-parameters, enthalpy of mixing and entropy of mixing values can also be determined for the ternary.

TABLE II - Free Energy of Mixing for the Au-Cu-Ni Ternary at 1100°K (J/mole).

	X_{Cu}/X_{Ni}										
X_{Au}	10/0	9/1	8/2	7/3	6/4	5/5	4/6	3/7	2/8	1/9	0/10
0.0	0	-2206	-3109	-3525	-3642	-3559	-3330	-2978	-2485	-1738	0
0.1	-4282	-6050	-6614	-6714	-6522	-6126	-5575	-4886	-4040	-2929	- 878
0.2	-6975	-8366	-8678	-8562	-8168	-7567	-6801	-5882	-4789	-3423	-1176
0.3	-8829	-9887	-9990	-9713	-9180	-8451	-7555	-6500	-5263	-3753	-1438
0.4	-9967	-10736	-10677	-10282	-9660	-8858	-7898	-6783	-5491	-3940	-1673
0.5	-10422	-10943	-10768	-10305	-9643	-8822	-7858	-6752	-5482	-3980	-1864
0.6	-10181	-10499	-10256	-9776	-9129	-8346	-7440	-6410	-5238	-3869	-1996
0.7	-9203	-9362	-9100	-8657	-8083	-7401	-6620	-5738	-4741	-3588	-2048
0.8	-7403	-7453	-7223	-6872	-6431	-5914	-5326	-4667	-3927	-3076	-1961
0.9	-4603	-4598	-4455	-4250	-4001	-3713	-3388	-3026	-2620	-2156	-1558

Olson and Toop[9] have proposed a method for determining ternary phase boundaries. The technique gives a fair approximation of ternary phase diagrams exhibiting miscibility gaps and was used to investigate the miscibility gap in the Au-Cu-Ni system. The underlying principle of this method is that the ends of the tie lines connecting two phases are located where each of the three components has the same activity in both phases. These tie lines may be determined by plotting the ternary activities of two components along an isoactivity line for the third component and then graphically locating the unique points where the activities of these two components are the same in both phases.

With the use of Eq. (6) in a computer program, the ternary compositional grid of the Au-Cu-Ni system was scanned to find points of equal activity for any component in this ternary system. Figure 5 shows the results of one of these scans. For this figure and in the activity search, nickel was chosen as component 1 and points of nickel activity equal to 0.92 in solid Au-Cu-Ni

alloys at 1100°K were determined by the grid search program. With the grid points of the isoactivity of nickel known, the activities of gold and copper were calculated directly from Eq. (6). The activities of gold and copper were plotted versus a composition ratio to find the unique set of points a_{Au}(PHASE 1) = a_{Au}(PHASE 2) and a_{Cu}(PHASE 1) = a_{Cu}(PHASE 2). An example of this determination may be seen in Figure 6. Here, the unique pair of points were found to be

$$\frac{X_{Ni}}{1-X_{Cu}} = 0.4575 \text{ and } \frac{X_{Ni}}{1-X_{Cu}} = 0.9517$$

Figure 7 shows the two points where the above composition ratios occur along the nickel isoactivity curve; hence, the ends of the tie line are now defined. A range of nickel isoactivity curves and associated tie lines are presented in Fig. 8. This technique was applied at several temperatures and the resulting calculated miscibility gap is shown in Fig. 9. It was estimated by this graphical method that the ternary critical point is between 1225° and 1250°K.

Discussion

Raub and Engel[12,13] have conducted the only extensive phase boundary determinations of the Au-Cu-Ni miscibility gap. The results of their experiments are found in Figs. 10a and 10b. The difference between the calculated and experimentally determined phase boundaries for this system is extraordinarily small. The only major difference is the predicted intersection of the miscibility gap with the Cu-Ni binary.

Although the approach of Olson and Toop is suitable for predicting the phase equilibria of a miscibility gap, a different approach is required for the more general case of two phase equilibria in a ternary system. A method currently under investigation is described below.

The ends of a two phase tie line are determined by the compositions which cause the partial molar Gibbs free energy of a component to be equal in the two phases. In essence, the problem becomes one of determining four unknowns--the atom fractions of two components in each of two phases. To obtain a unique solution for the location of the phase boundaries, it is necessary to have four equations for these unknown compositions. Three equations can be generated by equating the partial molar Gibbs free energy for each component in the two phases

$$\bar{G}_1 \text{ (PHASE 1)} = \bar{G}_1 \text{ (PHASE 2)} \qquad (8a)$$

$$\bar{G}_2 \text{ (PHASE 1)} = \bar{G}_2 \text{ (PHASE 2)} \qquad (8b)$$

$$\bar{G}_3 \text{ (PHASE 1)} = \bar{G}_3 \text{ (PHASE 2)} \qquad (8c)$$

The fact that tie lines are straight lines allows for the development of a fourth equation from geometrical considerations.

With the use of α-parameters synthesized from the three binaries, the problem of phase boundary determination in the ternary system ultimately reduces to one of solving four non-linear equations for four unknowns. In our present study of this problem, the approach being used sets all the equations equal to zero, e.g.,

$$\bar{G}_1 \text{ (PHASE 1)} - \bar{G}_1 \text{ (PHASE 2)} = 0 \qquad (9)$$

and then an optimization procedure is used to determine the four composition values which minimize on the error between the actual value of these equations and zero. Preliminary results from the determination of liquidus and solidus lines on isotherms of the Ag-Au-Cu system are very encouraging.

Conclusion

It appears that α-parameters which have been synthesized from data on binary systems can be used to predict solution thermodynamic and phase equilibria properties in ternary systems. Indeed, calculations made in this study gave a predicted miscibility gap in solid Au-Cu-Ni alloys that

was in excellent agreement with an experimentally determined one. Although the method described here is purely predictive since it relies only on binary and pure component data, it could prove useful in estimating properties of ternary systems for which experimental data are lacking.

References

1. M. L. Boyle: M.S. Thesis, Lehigh University, Bethlehem, Pa., 1976.
2. I. Ansara: Metallurgical Chemistry Symposium 1971, O. Kubaschewski, Ed., pp. 403-430, Her Majesty's Stationary Office, London, 1972.
3. F. Kohler: Monatshefte für Chemie, 1960, vol. 91, pp. 738-740.
4. J. L. Meijering: Philips Research Reports, 1950, vol. 5, pp. 333-356.
5. J. L. Meijering: Philips Research Reports, 1951, vol. 6, pp. 183-210.
6. M. Benedict, C. A. Johnson, E. Solomon and L. C. Rubin: Transactions A.I.Ch.E., 1945, vol. 41, pp. 371-392.
7. R. A. Oriani and C. B. Alcock: Transactions TMS-AIME, 1962, vol. 224, pp. 1104-1115.
8. G. W. Toop: Transactions TMS-AIME, 1965, vol. 233, pp. 850-855.
9. N. J. Olson and G. W. Toop: Transactions TMS-AIME, 1969, vol. 245, pp. 905-910.
10. N. J. Olson and G. W. Toop: Transactions TMS-AIME, 1966, vol. 236, pp. 590-592.
11. K. Wohl: Transactions A.I.Ch.E., 1946, vol. 42, pp. 215-249.
12. E. Raub and A. Engel: Zeitschrift für Metalkunde, 1947, vol. 2, pp. 11-16.
13. E. Raub and A. Engel: Zeitschrift für Metalkunde, 1947, vol. 2, pp. 147-158.

Acknowledgement

We wish to thank the United States Steel Foundation for their support of the Chemical Metallurgy Program at Lehigh University.

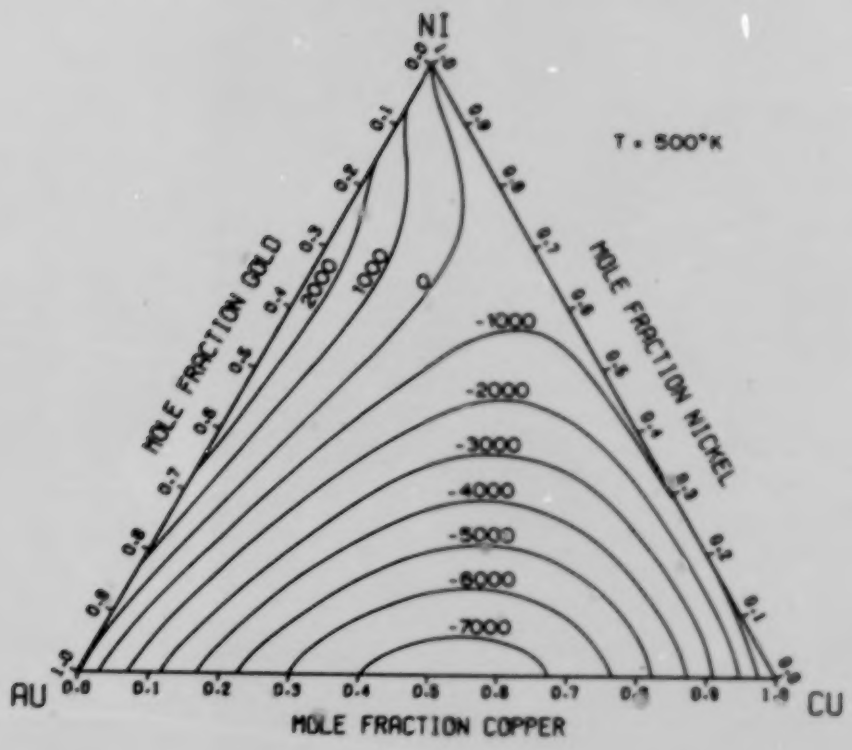

Figure 1. Iso-Free Energy of Mixing Curves for Solid Au-Cu-Ni Alloys at 500°K. Energy in units of J mol^{-1}.

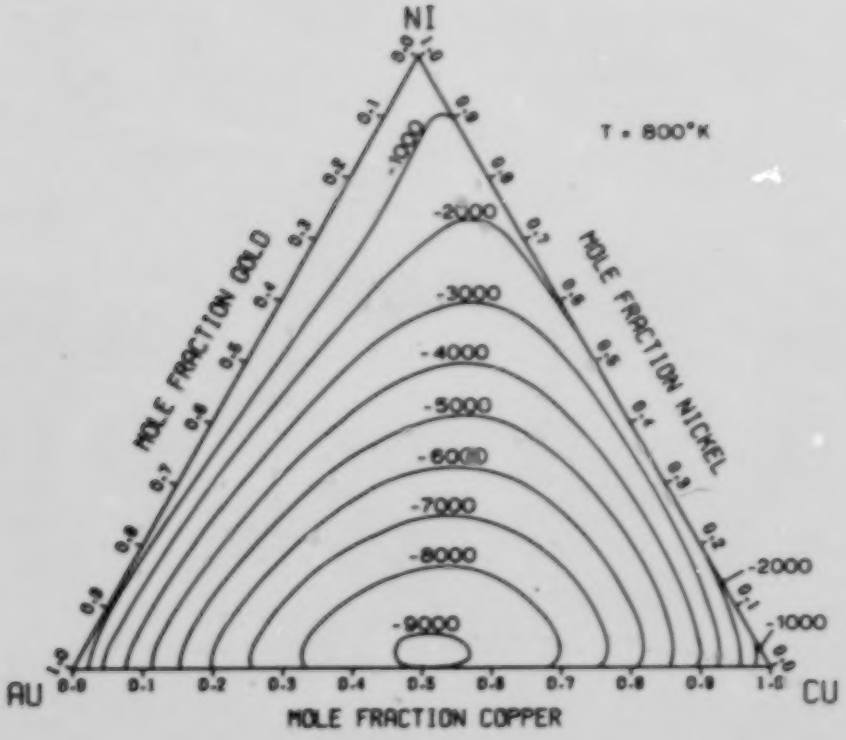

Figure 2. Iso-Free Energy of Mixing Curves for Solid Au-Cu-Ni Alloys at 800°K. Energy in units of J mol^{-1}.

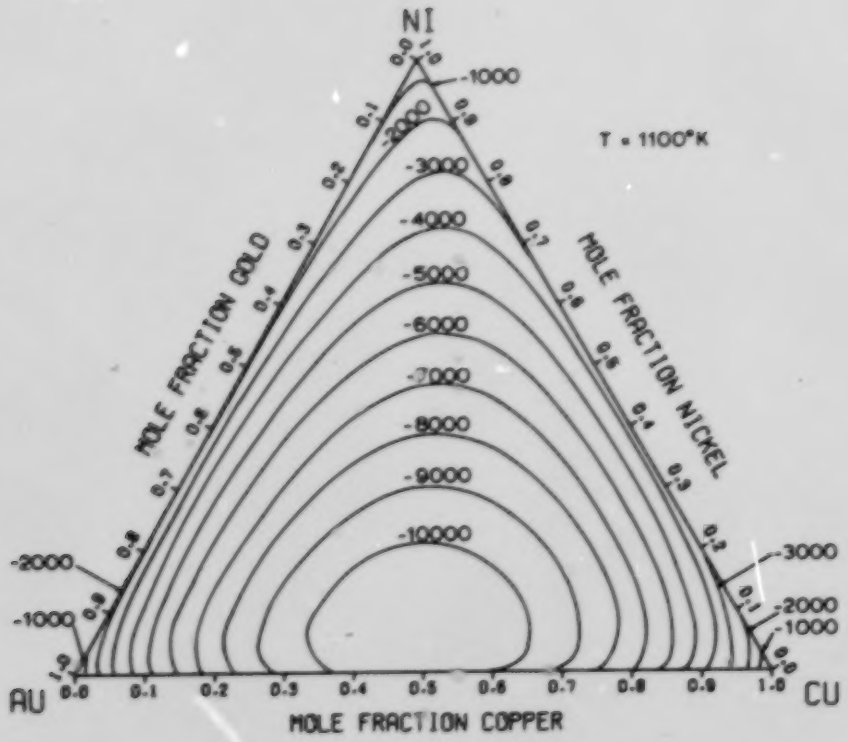

Figure 3. Iso-Free Energy of Mixing Curves for Solid Au-Cu-Ni Alloys at 1100°K. Energy in units of J mol^{-1}.

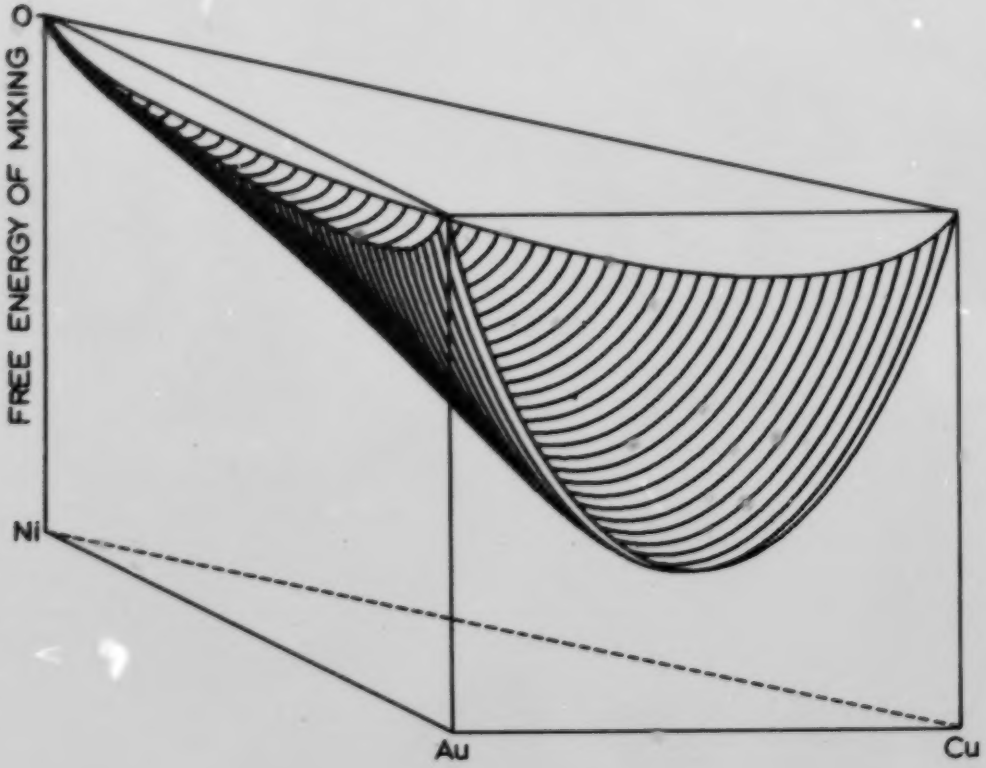

Figure 4. Three Dimensional Representation of the Free Energy of Mixing for Solid Au-Cu-Ni Alloys at 800°K.

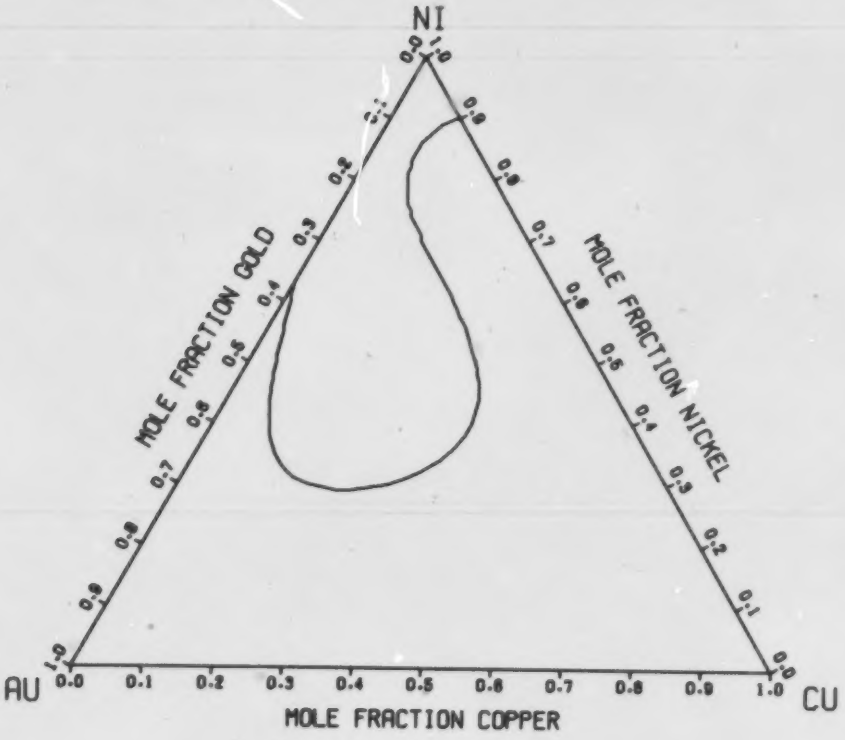

Figure 5. Iso-Activity of Nickel Curve Equal to 0.92 in Solid Au-Cu-Ni Alloys at 1100°K.

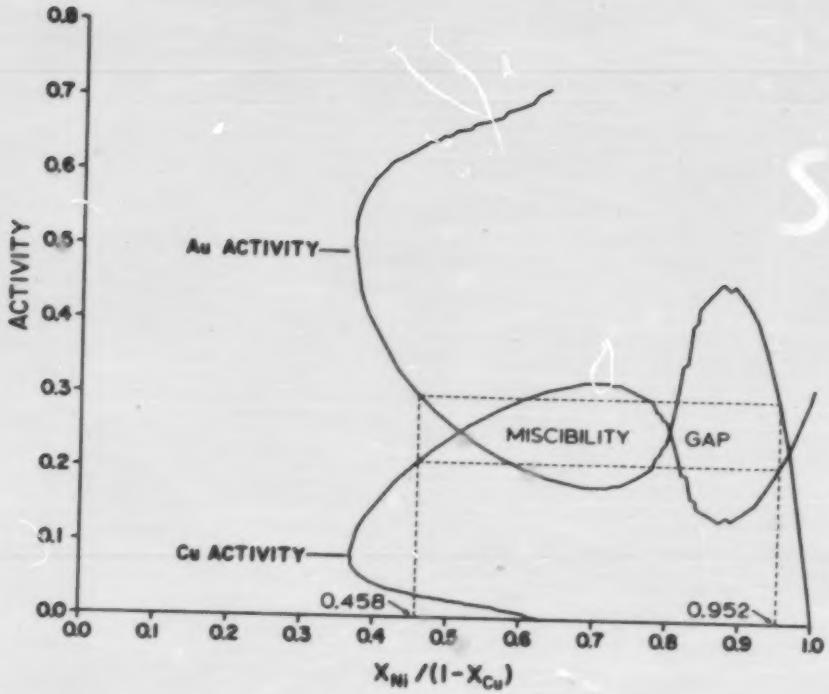

Figure 6. Graphical Determination of Miscibility Gap Boundaries as Proposed by Olson and Toop[9] in Solid Au-Cu-Ni Alloys at 1100°K.

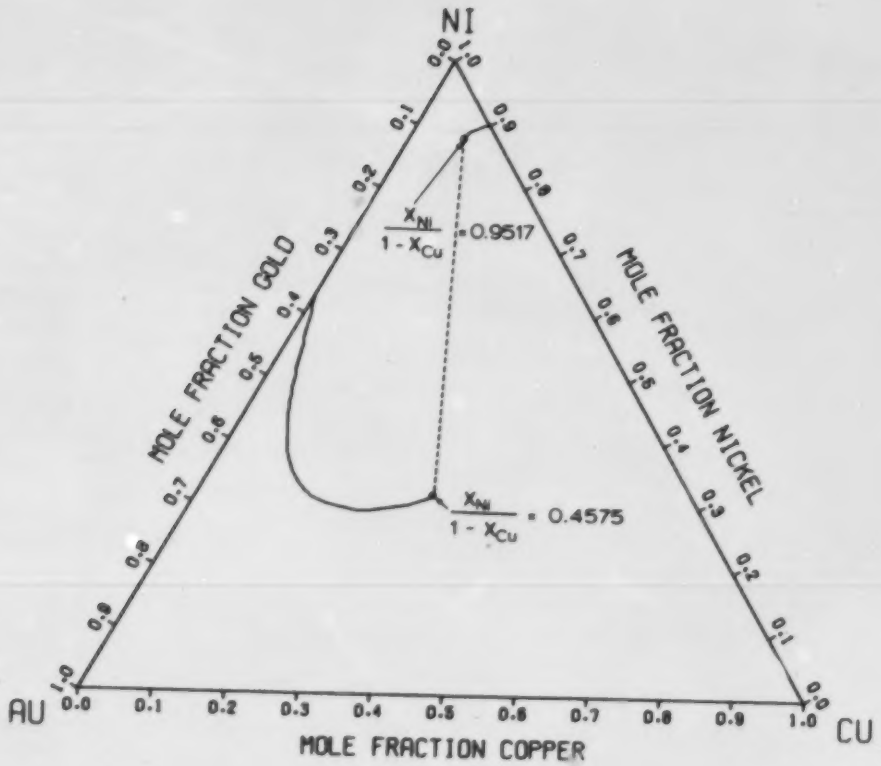

Figure 7. Placement of the Ends of the Graphically Determined Miscibility Gap Boundary in Solid Au-Cu-Ni Alloys at 1100°K.

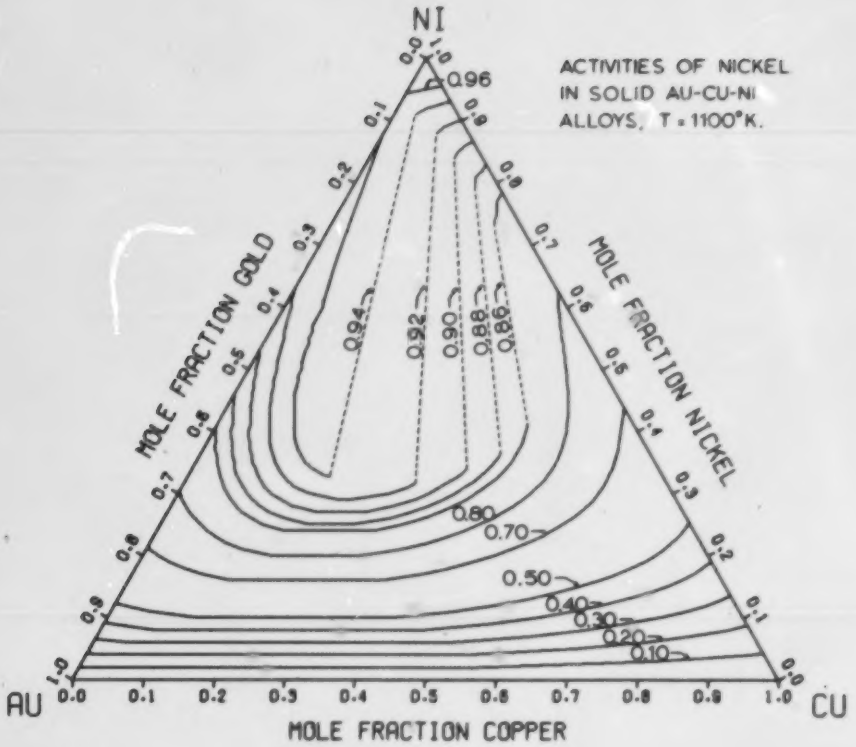

Figure 8. Miscibility Gap Tie Lines and Associated Nickel Iso-Activity Curves in Solid Au-Cu-Ni Alloys at 1100°K.

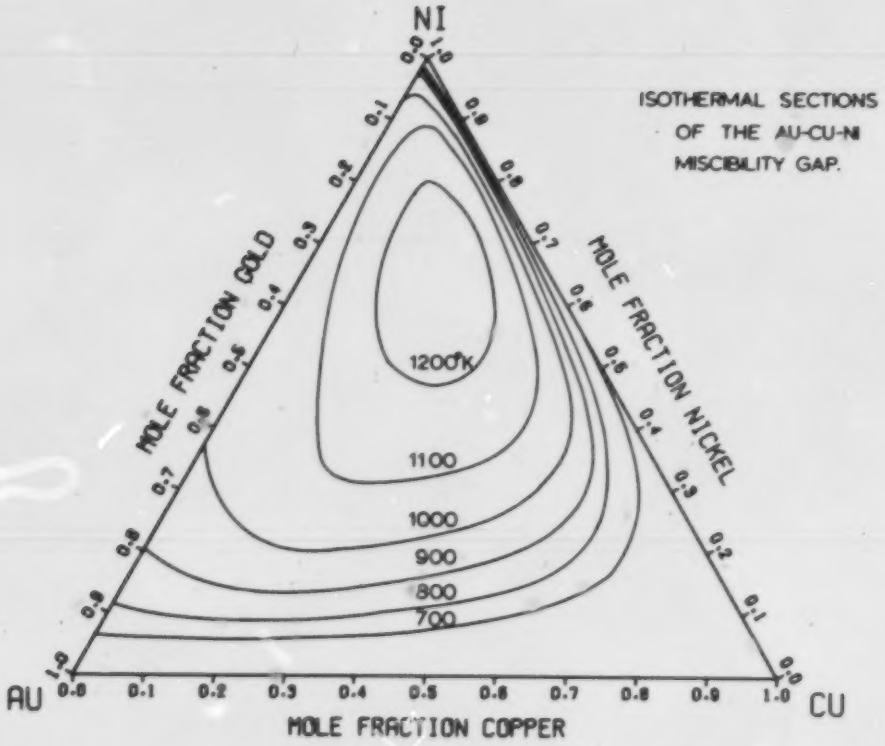

Figure 9. Graphically Determined Isothermal Sections of the Au-Cu-Ni Miscibility Gap.

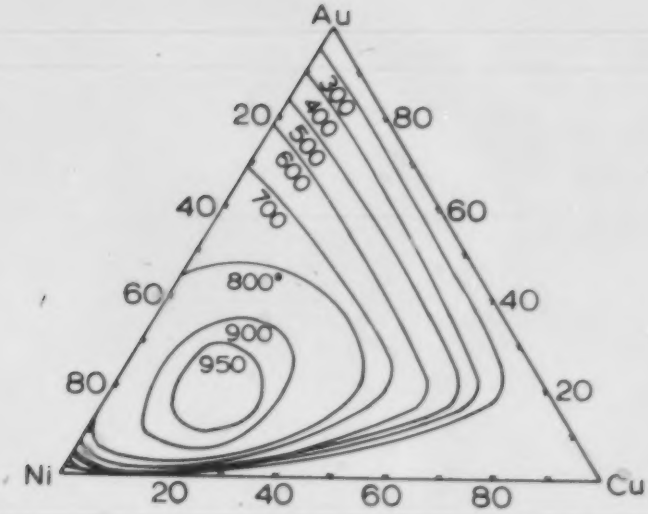

Figure 10a. Experimentally Determined Isothermal Sections of the Au-Cu-Ni Miscibility Gap from Raub and Engel.[12,13] (Temperature in °C, Composition in Atomic Percent.)

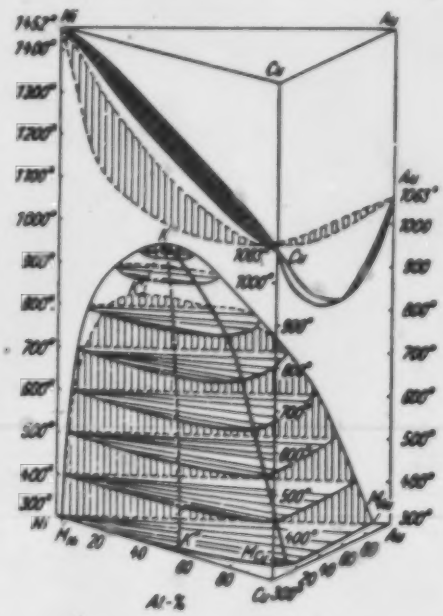

Figure 10b. Three Dimensional View of the Au-Cu-Ni Miscibility Gap from Raub and Engel.[12,13] (Temperature in °C.)

National Bureau of Standards SP-496, Applications of Phase Diagrams in Metallurgy and Ceramics
Proceedings of Workshop held at NBS, Gaithersburg, Md., January 10-12, 1977

CORRELATIONS AND PREDICTIONS OF METAL-BORON PHASE EQUILIBRIA*

Karl E. Spear
Materials Research Laboratory
Materials Science Department
The Pennsylvania State University
University Park, Pennsylvania 16802

ABSTRACT

Attempts have been made to find correlations relating the binary metal boride phase equilibria, the boride crystal chemistry, and the positions of the metals in the periodic chart. These correlations are used along with available experimental data and phase equilibria logic to predict unmeasured properties and to construct phase diagrams for binary metal-boron systems. Earlier research of this type on rare-earth boride systems was recently completed in the form of a critical analysis and compilation; the research published here is not yet that complete and should be considered as an interim report for the Workshop.

I. INTRODUCTION

This paper briefly summarizes our attempts to correlate and predict phase equilibria information for binary metal-boron systems. Our early research in this area (see Spear, 1976) emphasized RE-B systems, where RE is one of the metals Sc, Y, La, or a rare-earth Ce through Lu. We compiled and critically analyzed reported data for these systems and predicted unmeasured properties with the help of correlations, published limits, and phase equilibria logic so that we could construct phase diagrams for all 17 RE-B systems. These diagrams serve as graphical summaries of reported information, indicate reasonable estimates of unmeasured properties, and point out needed experimental research.

Our current efforts are aimed at extending the RE-B research to include transition metal and actinide metal boride systems as well as what little information has been published about the borides of metals from groups IA, IIA, and IIIA. This extended research is not yet a "critical analysis and compilation" as is the rare-earth boride publication, but is a current study being documented in the spirit of the Workshop at which this research was first presented.

* Research supported by the National Science Foundation, grant No. DMR76-14448.

The heart of this paper is presented in four sections. Section II outlines crystal chemical correlations for metal-boron phases and systems. An understanding of these correlations is particularly helpful in understanding and predicting the relationships among the boride phase equilibria properties since boron-boron bonding is so prominent in the majority of borides. Correlations and predictions of phase behavior are given in Section III, and are based on methods similar to those used in the RE-B studies.

Phase diagrams are given in Section IV for 37 metal-boron systems which form intermediate binary compounds. Not given are the RE-B diagrams for Ce through Lu since they have been published elsewhere (Spear, 1976), nor are the alkali metal-boron diagrams which have not yet been reviewed in enough detail to make predications.

We have not given specific references for information tabulated in the subsequent tables and figures, but instead have listed our main sources of information in Section V, the reference section at the end of the text. The references are listed under five topical headings to aid in finding information. A critical assessment and compilation which includes more specific references will be published later.

II. BORIDE CRYSTAL CHEMISTRY

The crystal chemistry of metal boride phases is dominated by the boron configurations in the structures. Boron-boron bonding occurs in most borides containing greater than 35 at.% boron. The B-B bond distances are practically identical in these boride structures and in pure boron.

The common types of boron configurations found in metal boride structures are shown in Figure 1. These configurations include (i) the "no connections" exhibited by metal-rich structures which exhibit no boron-boron bonding, (ii) the various types of boron chains, (iii) two-dimensional graphite-like nets, and (iv) a number of three-dimensional frameworks which are found in the boron-rich phases. The structure types which exhibit these configurations are listed in Table 1.

Figure 2 shows that the larger metals and those with unfilled d-shells favor the formation of the boron-rich phases, the phases which exhibit 2- and 3-dimensional boron frameworks. The smaller metals, and particularly those with a significant number of d-electrons, tend to form metal-rich phases which have few boron-boron bonds. The more noble metals such as Ru, Rh, and Pd have a greater tendency than the other metals to form defect structures. For ..me

crystal chemical details, one should refer to Aronsson et al. (1965), Lundstrom (1969, 1977), and Spear (1976).

III. PHASE EQUILIBRIA CORRELATIONS AND PREDICTIONS

A few specific correlations used to help in predicting phase equilibria properties are discussed in this section. Other estimates based on drawing "reasonable" phase diagrams which do not violate the phase rule are not discussed, but are evident from the constructed diagrams shown in Section IV.

In the previous section, the crystal chemical compositional trends with the position of the metal in the periodic chart were mentioned. The highest melting metal boride in a given M-B system tends to follow similar compositional trends with the size and number of metal d-electrons. The MB_6 phase is the highest melting in systems containing the larger rare-earth metals. This shifts to the MB_4 phases for the smaller rare-earths, then to the MB_2 phases for Sc, the Ti group metals, V and Nb, and Cr. The more metal-rich borides or defect diborides are the highest melting intermediate phases in systems with metals further to the right in the periodic chart.

The diboride with the AlB_2-type structure is the most common metal boride phase found. This group includes the most stable and the highest melting metal borides known. The metals forming this phase possess a wide range of sizes and electronic configurations. The reason for the common occurrence of this phase appears to be related to the ability of the metals in this structure to deform their electron cloud from an approximately spherical shape. The bond strengths between the metals are enhanced without drastically reducing the boron-boron bond strengths (Spear, 1976).

Correlations of the diboride melting temperatures along with those for other boron-rich phases are shown in Table 2. The fact that 2- and 3-dimensional boron frameworks dominate the structures of boron-rich compounds causes one to expect similar melting temperatures for these phases, particularly for those within a group exhibiting the same structure. The general correlations shown in Table 2 confirm these expectations. Unmeasured melting temperatures for similar phases are expected to lie approximately within the given range for the particular structure type and subgroup listed in the table.

The metals forming only intermediate boride phases with B/M atomic ratios of two and greater can be grouped into families, as is shown in Table 3. The

metals involved include the alkaline-earths, all the group III metals, the rare-earths, and the actinides. Zirconium also fits into this scheme. These metals are all fairly large and do not possess a large number of d-electrons. The RE-B systems have already been thoroughly analyzed and correlated (Spear, 1976), so only the other metal-boron systems will be discussed to a significant extent. This correlation does not include the new Sm_2B_5-type phase formed by Sm and Gd, nor the recently discovered REB_x ($x<4$) phases in the Nd and Pr system.

The metals within a given family are expected to show similarities in their binary phase diagrams, as well as in their other properties. The alkaline earths Ca, Sr, and Ba have only one confirmed intermediate boride phase, the hexaboride. They are similar to Eu in this respect, and in the fact that Eu is divalent in its hexaboride phase (Spear, 1976). (The YbB_6 phase is similar to EuB_6, but Yb forms other borides and converts to a trivalent state like most of the other rare earths. These phenomena will not be discussed further here.) The respective melting and boiling temperatures for Eu and the alkaline earth metals are also very similar, as is shown below, so it would be very surprising if their respective binary M-B phase diagrams were not also similar.

Metal	T°C(fusion)	T°C(boiling)
Eu	826	1491
Ca	850	1483
Sr	770	1367
Ba	710	1622
Ra	700	1527

Data are from Hultgren et al. (1973)

If Ra is not too large to form a hexaboride, its phase diagram would also be expected to be similar.

The Ac-B system has not been studied because of the extreme radioactivity of Ac, but its diagram is expected to be similar to La-B; both metals belong to group III. The Am-B system is expected to be similar to the next family forming three phases. The AmB_6 phase is congruently vaporizing, just like the hexaborides in the RE-B systems of the same family. The next smaller rare-earth, Gd, has a congruently vaporizing tetraboride. The lattice constants for AmB_4 are slightly smaller than those for ThB_4, indicating that Am is not too large to form the AmB_{66} phase, even though only AmB_4 and AmB_6 have been reported.

The unstudied Pa-B system should be intermediate between Th-B and U-B in behavior. It is assumed that it is similar to the Gd-B system. The Pu-B and Np-B systems clearly fall in the next family containing Tb-B, Y-B, Dy-B, and Ho-B systems. The phase behavior of these four RE-B systems is very similar, and the diagrams of Pu-B and Np-B are expected to be similar as well. All six systems have a congruently vaporizing tetraboride phase. The NpB_{66} phase has not been reported, but no other metal is known to exhibit the UB_{12}, AlB_2, ThB_4, and CaB_6 type phases without also forming a stable YB_{66} type phase.

The next actinide metal boride system is U-B, and it appears to fall in an intermediate stage between the Lu-B and the Sc-B systems. The UB_{66} phase has been searched for, but not found. The last family represents the smallest metals to form the dodecaboride phase.

IV. BINARY METAL-BORON PHASE DIAGRAMS

Binary temperature-composition phase diagrams for 37 metal-boron systems have been constructed and are shown in Figures 3-8. The metals include the alkaline earths, aluminum, the transition metals in groups III through VIII, and the actinide metals Ac through Am. These diagrams do not yet represent a thorough critical assessment in many cases, and much of the information has been estimated. The estimates of the alkaline earth and actinide boride diagrams are probably more reliable than those of the later transition metals. In order that the reader may better judge the reliability of the diagrams, some specific comments and references are given below for each system. The comments for diagrams given in the same figure are grouped together. The figures contain groups of systems organized according to the positions of the metals in the periodic chart. The actinide boride systems are given last.

Figure 3:

Be-B : Based on information from Stecher and Aldinger (1973). The composition of the dashed boron-rich phase lies somewhere between BeB_6 and BeB_{12}.

Mg-B : The decomposition temperatures for 1 atm vapor are strictly guesses. The general type of diagram shown is the type that the Mg-B system will exhibit, but the given critical temperatures may be grossly in error.

Ca-B, Sr-B, Ba-B: A discussion of the similarities of these estimated diagrams and the Eu-B diagram is given in Section III of the text..

Al-B : Many of the boron-rich phases reported have been shown to be impurity stabilized phases (Shunk, 1968). Otherwise, the diagram is generally the same as is given by Elliott (1965).

Figure 4:

Sc-B, Y-B, La-B: Based on diagrams from Spear (1976).

Ti-B, Zr-B, Hf-B: Based on diagrams from Rudy (1969).

Figure 5:

V-B, Nb-B, Ta-B: Based on diagrams from Rudy (1969), except for the addition of the V_5B_6 and V_2B_3 phases to the V-B system based on data by Spear and Gilles (1969).

Cr-B : Based on diagram by Portnoi and Romashov (1972), plus possible formation of Cr_4B phase, and the CrB_4 phase discussed by Lundstrom (1977).

Mo-B, W-B: Based on diagrams by Rudy (1969).

Figure 6:

Mn-B : Diagram estimated to be similar to Cr-B system; both systems form similar intermediate phases.

Tc-B : Diagram estimated to be similar to Re-B system. Both systems form similar intermediate phases.

Re-B : Based on diagram by Portnoi and Romashov (1972).

Fe-B : Based on diagram by Portnoi and Romashov (1972), but leaving out B-rich FeB_n phase shown by Carlsson and Lundstrom (1970) to be a solution of Fe in B.

Ru-B, Os-B: Estimated to be similar to neighboring diagrams, with the trend toward lower boride melting temperatures with an increase in metal d-electrons being observed. The defect diborides are estimated to have relatively high melting temperatures since all diborides appear to be relatively stable.

Figure 7:

Co-B : Based on diagram by Schobel and Stadelmaier (1966).

Rh-B, Ir-B: Estimated to have lower melting temperatures for their intermediate boride phases, as appears to be the trend with increasing number of metal d-electrons.

Ni-B : Based on diagram by Portnoi and Romashov (1972), but with slight modifications in Ni_4B_3 and NiB region to show similarities with Fe-B and Co-B diagrams. The B-rich NiB_n phase was left out since Carlsson and Lundstrom (1970) have shown this to be a solution of Ni in boron.

Pd-B : Estimated to be similar to its neighboring M-B systems.

Pt-B : Based primarily on diagram by Wald and Rosenberg (1965).

Figure 8:

A more detailed discussion of these seven actinide-boron systems and the correlations involved in the predictions of their properties is given in Section III. The papers published on the actinide borides are listed in the reference section.

Each phase diagram in Figures 3-8 is for a constant total pressure of 1 atm. A vapor phase is shown only when the total metal plus boron vapor pressure reaches 1 atm. which for these systems occurs first at the boiling (or 1 atm. sublimation) temperature for the metal. Data for the elements, including boron, were taken from Hultgren et al. (1973).

On the constructed diagrams shown in the figures, a fine line was used to represent estimated parts of the diagrams and a heavier line was used when at least some experimental evidence was available.

The (B/M) atomic ratios for common metal boride phases are shown on each diagram, with the tic-marks representing these ratios being drawn outside the diagram. The ratios of phases existing in a particular binary system are indicated by extending the specific tic-marks downwards into the graphed region of the diagram. No attempt has been made to indicate specific compositions of defect structures, or the homogeneity ranges of phases (although most boride homogeneity ranges are relatively small).

Again, the reader is reminded that the given diagrams are intended to serve as graphical summaries of reported information and reasonable estimates of unmeasured properties. Researchers are encouraged to send new information to the author of this paper so that a continual updating of these diagrams can be accomplished.

V. REFERENCES

General For Elements and For Borides

R. Hultgren, P. D. Desai, D. T. Hawkins, M. Gleiser, K. K. Kelley, and D. D. Wagman (1973). Selected Values of The Thermodynamic Properties of the Elements, Am. Soc. Metals, Metals Park, Ohio.

M. Hansen and K. Anderko (1958). Constitution of Binary Alloys, McGraw-Hill, New York.

R. P. Elliott (1965). ibid., First Supplement.

F. A. Shunk (1968). ibid., Second Supplement.

B. Aronsson, T. Lundstrom, and S. Rundqvist (1965). Borides, Silicides, and Phosphides, Wiley (Methuen), New York.

Reviews of Transition Metal-Boron Systems

E. Rudy (1969). "Compendium of Phase Diagram Data," AFML-TR-65-2, Part V, Air Force Materials Laboratory, Wright-Patterson Air Force Base, Ohio.

K. I. Portnoi and V. M. Romashov (1972). "Binary Constitution Diagrams of Systems Composed of Various Elements and Boron - A Review," Russ. Powder Met. 5 (113), 378-384.

T. Lundstrom (1969). "Preparation and Crystal Chemistry of Some Refractory Borides and Phosphides," Arkiv fur Kemi 31 (19), 227-266.

T. Lundstrom (1977). "Transition Metal Borides," Chapter in Boron and Refractory Borides (V.I. Matkovich, ed.) Springer-Verlag, Berlin (in press).

Review of Rare-Earth Metal-Boron Systems

K. E. Spear (1976), "Phase Behavior and Related Properties of Rare-Earth Borides," Chapter II in Phase Diagrams: Materials Science and Technology, Vol. IV (A. M. Alper, ed.) Academic Press, New York, pp. 91-159.

Actinide Metal-Boron Systems

Th-B — P. Stecher, F. Benesovsky and H. Nowotny (1965), "Study of the Alloy Behavior of Borides in the Ternary Systems Cerium-Thorium (Uranium)-Boron," Planseeber. Pulvermet. 13, 37-46.

U-B — B. W. Howlett (1959), "A Note on the Uranium-Boron Alloy System," J. Inst. Metals 88, 91-92.

R. W. Mar (1975). "The U-B System," J. Am. Ceram. Soc. 58 (2), 145-146.

Pu-B — H. A. Eick (1965),"Plutonium Borides," Inorg. Chem. 4 (8), 1237-1239.

Am-B, Np-B — H. A. Eick and R. N. R. Mulford (1969), "Americium and Neptunium Borides," J. Inorg. Nucl. Chem. 31, 371-375.

Other Specific Systems and Phases Types

AlB_2-Type — K. E. Spear (1976), "Chemical Bonding in AlB_2-Type Borides," J. Less-Common Metals 47, 195-201

Be-B — J. Stecher and F. Aldinger (1973), "Uber den Aufbau des Systems Beryllium-Bor," Z. Metallke. 64 (10), 684-689.

Co-B — J. D. Schobel and H. H. Stadelmaier (1966). "Das Zweistoffsystem Kobalt-Bor," Z. Metallkde. 57 (4), 323-325.

Pt-B — F. Wald and A. J. Rosenberg (1965), "Constitutional Investigations in the Boron-Platinum System," Trans. AIME 233, 796-799.

V-B — K. E. Spear and P. W. Gilles (1969), "Phase and Structure Relationships in the Vanadium-Boron System", High Temp. Sci. 1 (1), 86-97.

B-Rich — J. O. Carlsson and T. Lundstrom (1970). "The Solution Hardening of β-Rhombohedral Boron," J. Less-Common Metals 22, 317-320.

Table 1: Metal Boride Structures Which Exhibit Specific Types of Boron Configurations.

BORON CONFIGURATION*	STRUCTURE TYPES EXHIBITING THESE CONFIGURATIONS
No Connections	Mn_4B, Re_3B, Ni_3B, Pd_5B_2, Ru_7B_3, Fe_2B, PtB, RuB, $IrB_{1.1}$
Partial Chains	Cr_5B_3, V_3B_2, $Ru_{11}B_8$, Ni_4B_3
Single Chains	FeB, CrB, MoB
Multiple Chains	V_5B_6, Ta_3B_4, V_2B_3
2-D Nets (Perfect)	AlB_2
2-D Nets (Defect AlB_2)	$Ir_2B_{3-x}(IrB_{1.35})$, $Ru_2B_{3-x}(Ru_2B_3)$, RuB_2, ReB_2, $Mo_2B_{5-x}(Mo_2B_5)$, $W_2B_{5-x}(W_2B_5)$, $Mo_{1-x}B_3(MoB_{4-6})$
3-D Frameworks	Sm_2B_5, CrB_4, ThB_4, NaB_6, CaB_6, AlB_{12}, UB_{12}, YB_{66}

*See Fig. 1 for illustrations of the Boron Configurations.

Table 2: Correlations of Melting Temperatures of Boron-Rich Metal Boride Phase Types.

Structure Type	Subgroups	Limiting Melting Temperatures Observed	
		Lowest T_{fus} °C	Highest T_{fus} °C
AlB_2	Groups IVA, VA	>2500	3400
	Other Metals	2000	<2500
ThB_4	Congruent Melting	2500	2800
	Peritectic Melting*	2350	2400
CaB_6	Congruent Melting	2550	2715
	Peritectic Melting	2200	2600
UB_{12}	All Phases	2000	2250
YB_{66}	All Phases	2050	2150

*LaB_4 melts at 1800°C. The limited stability of LaB_4 with respect to decomposition to LaB_6 and a metal-rich melt is explained by the fact that La is the largest metal to form this phase.

Table 3: Families of Metals Forming Higher Borides.

Metal in M-B System	Phase Types				
	UB_{12}	AlB_2	YB_{66}	ThB_4	CaB_6
Ba, Sr, Eu, Ca, Yb[a]					X
La, Ce, Pr, (Ac)[b]				X	X
Th, Nd, Sm, (Pm)[b], Am			X	X	X
Gd, (Pa)[b]		X	X	X	X
Tb, Y, Dy, Ho, Pu, Np	X	X	X	X	X
Er, Tm, Yb[a], Lu	X	X	X	X	
U	X	X		X	
Sc, Zr, Al	X	X			

(a) Yb is listed in both the first and sixth groups because it is divalent in YbB_6 while it is trivalent in its other borides.

(b) These M-B systems have not been studied, but are predicted to form the indicated compounds.

824

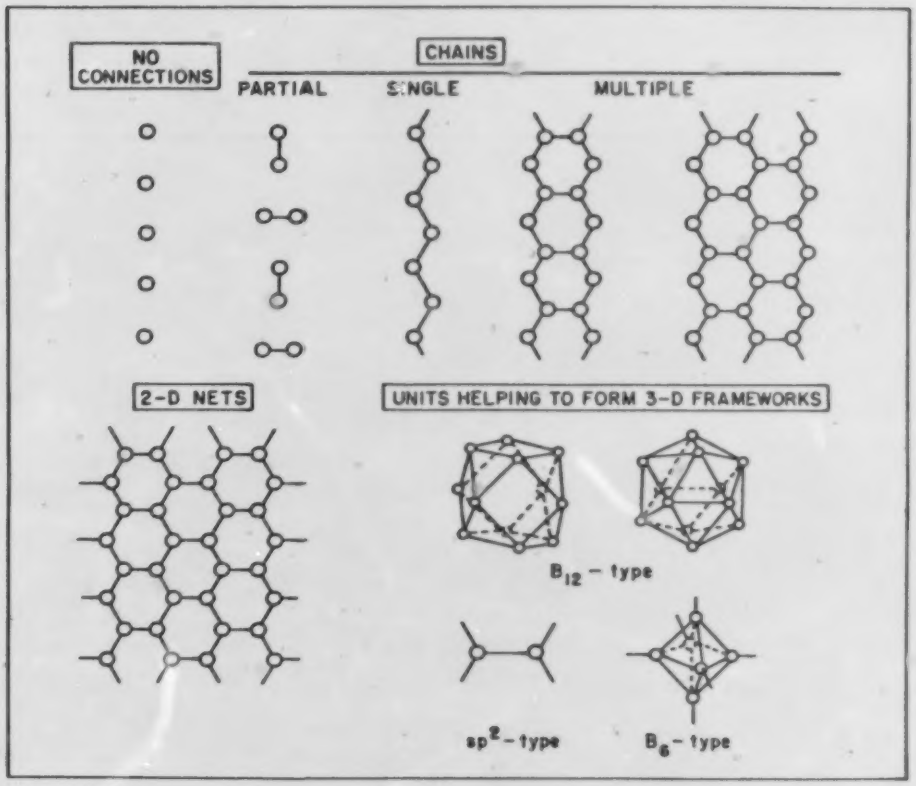

Figure 1: Common Types of Boron Configurations Found in Metal Boride Structures.

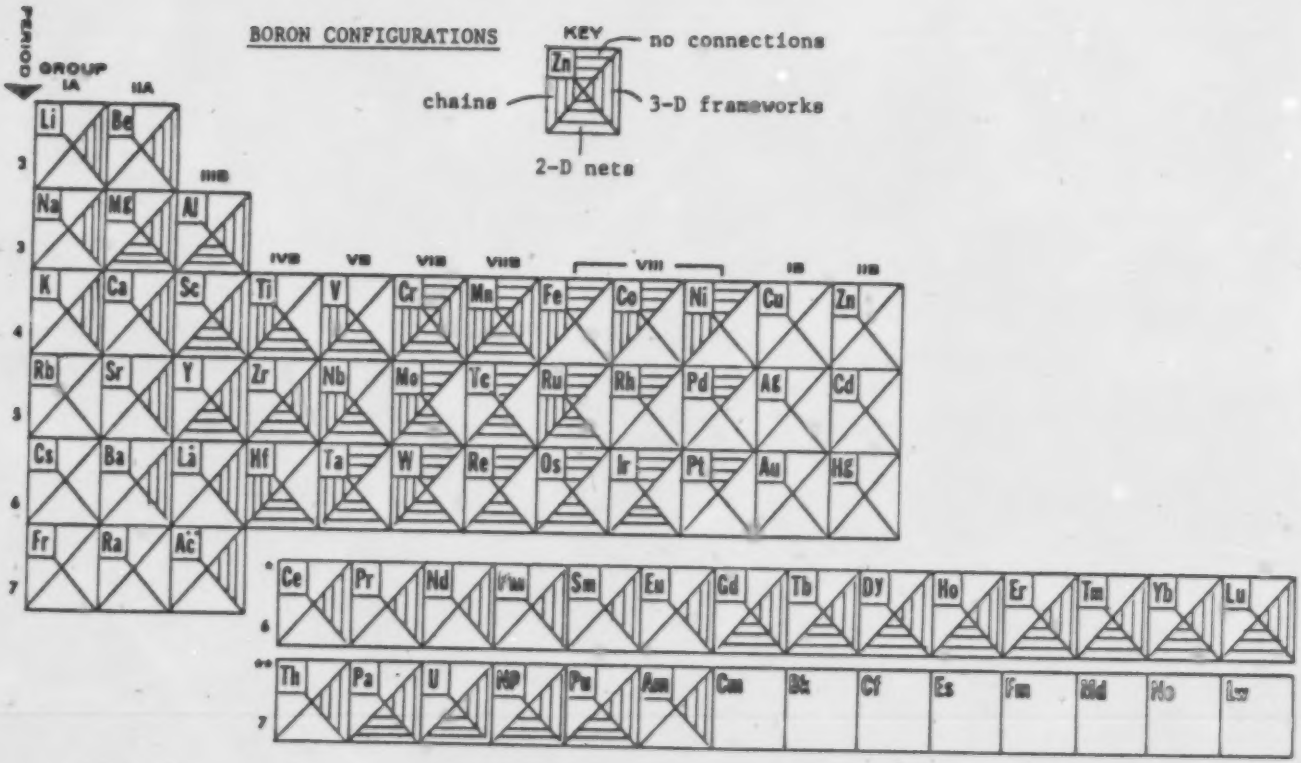

Figure 2: Partial Periodic Chart Showing the Types of Boron Configurations Exhibited by the Borides of the Various Metals.

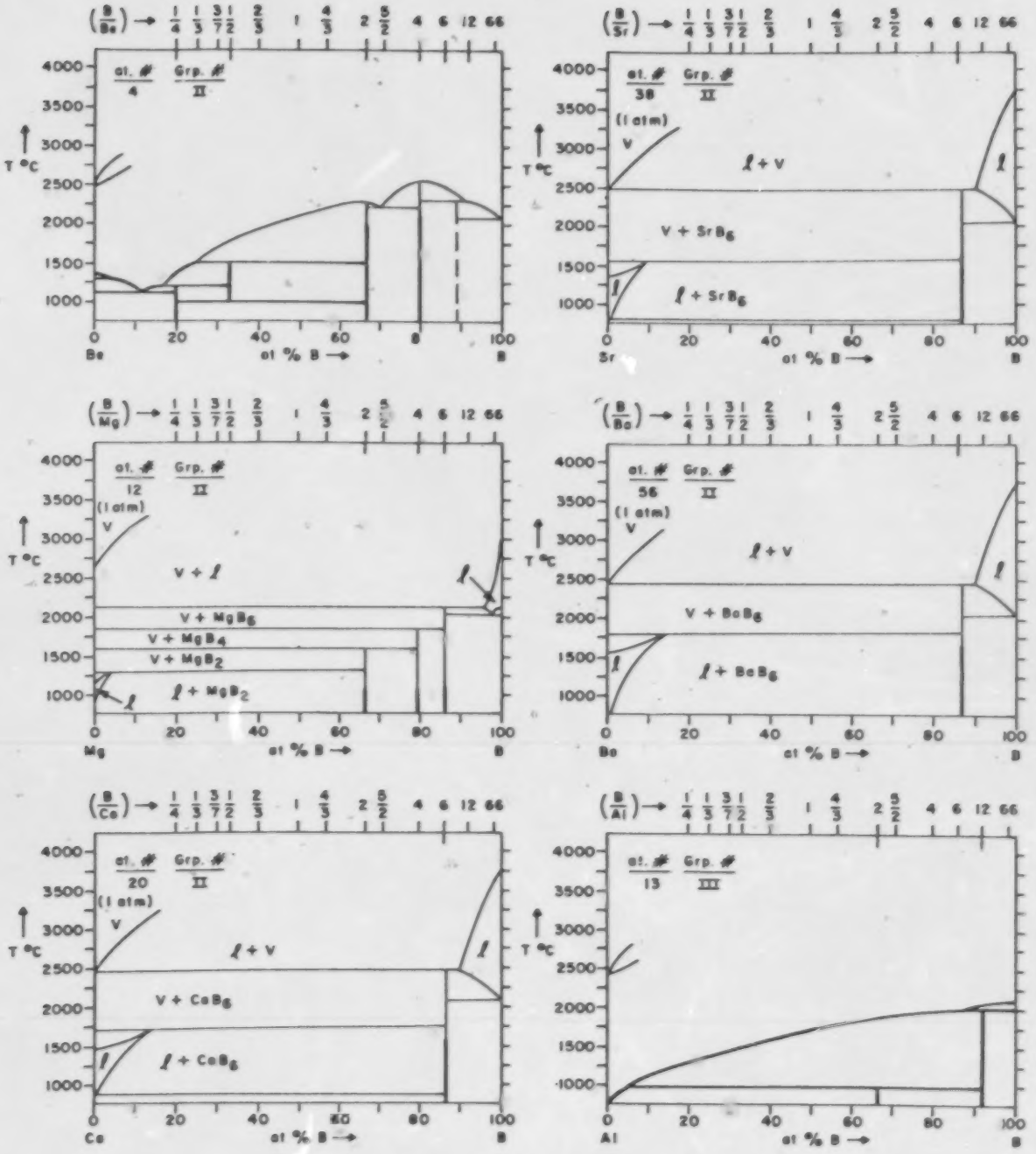

Figure 3: Phase Diagrams for the Metal-Boron Systems of the Alkaline-Earth Metals and Aluminum.

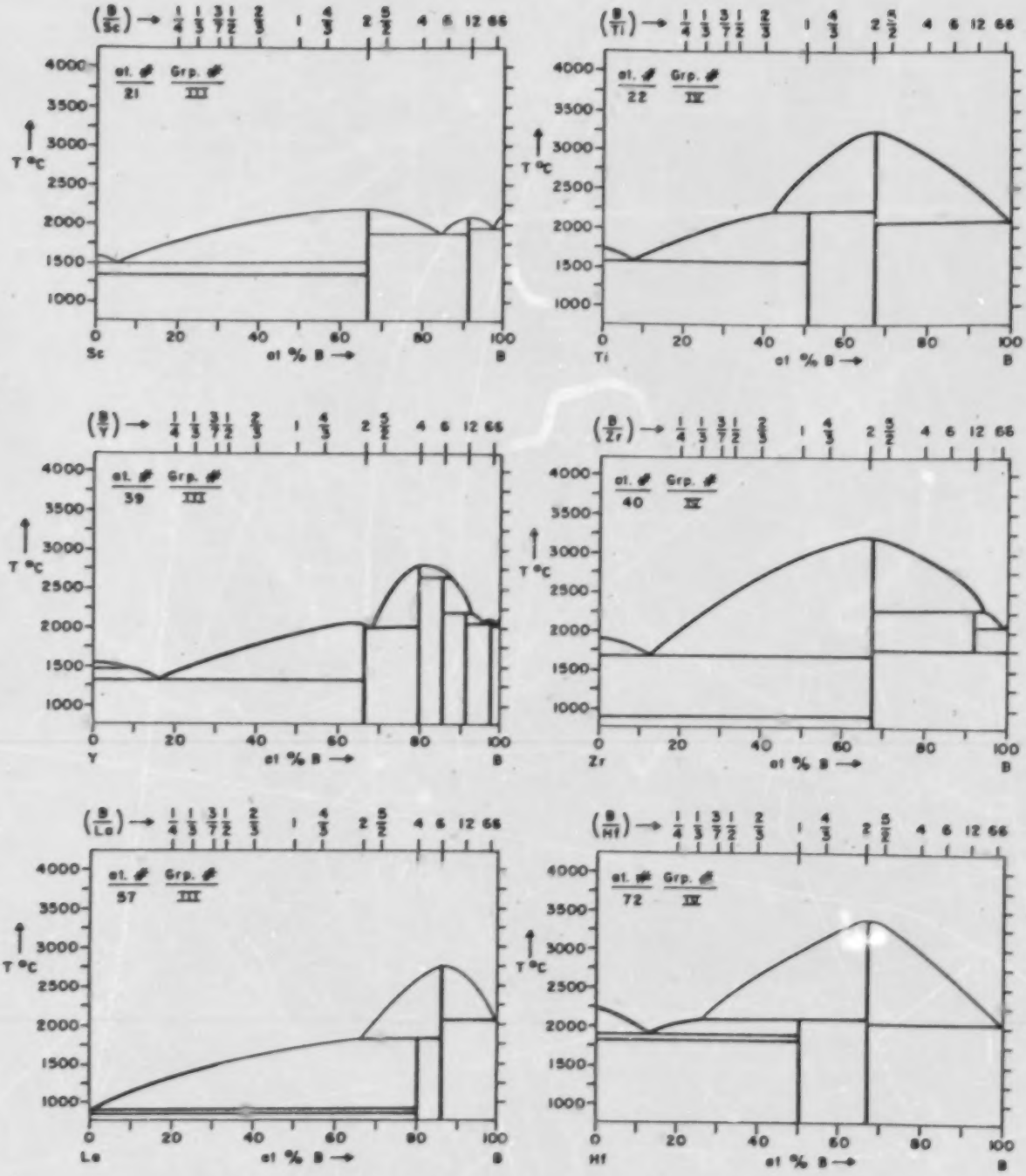

Figure 4: Phase Diagrams for the Metal-Boron Systems of the Transition Metals from Groups IiI and IV.

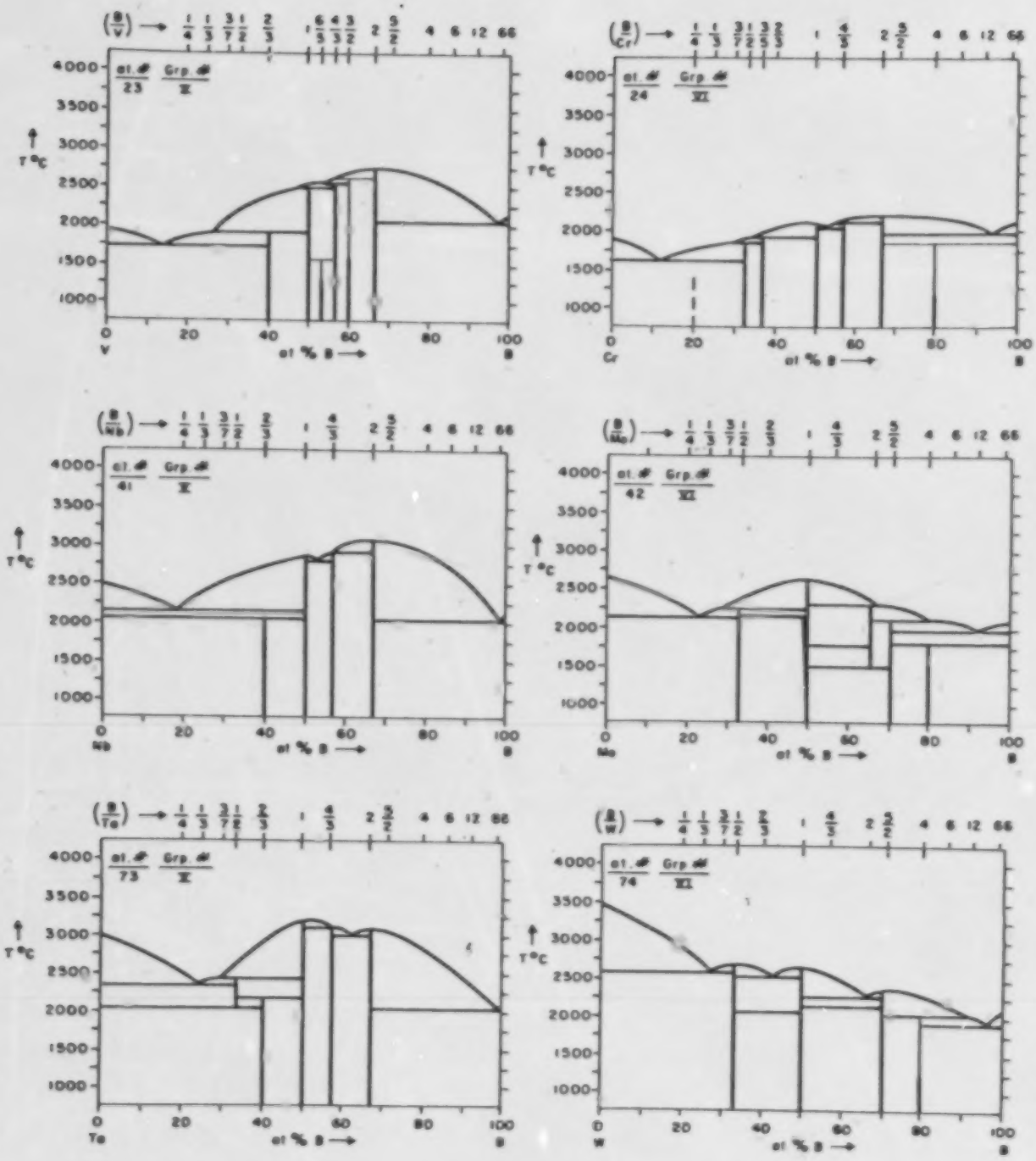

Figure 5: Phase Diagrams for the Metal-Boron Systems of the Transition Metals from Groups V and VI.

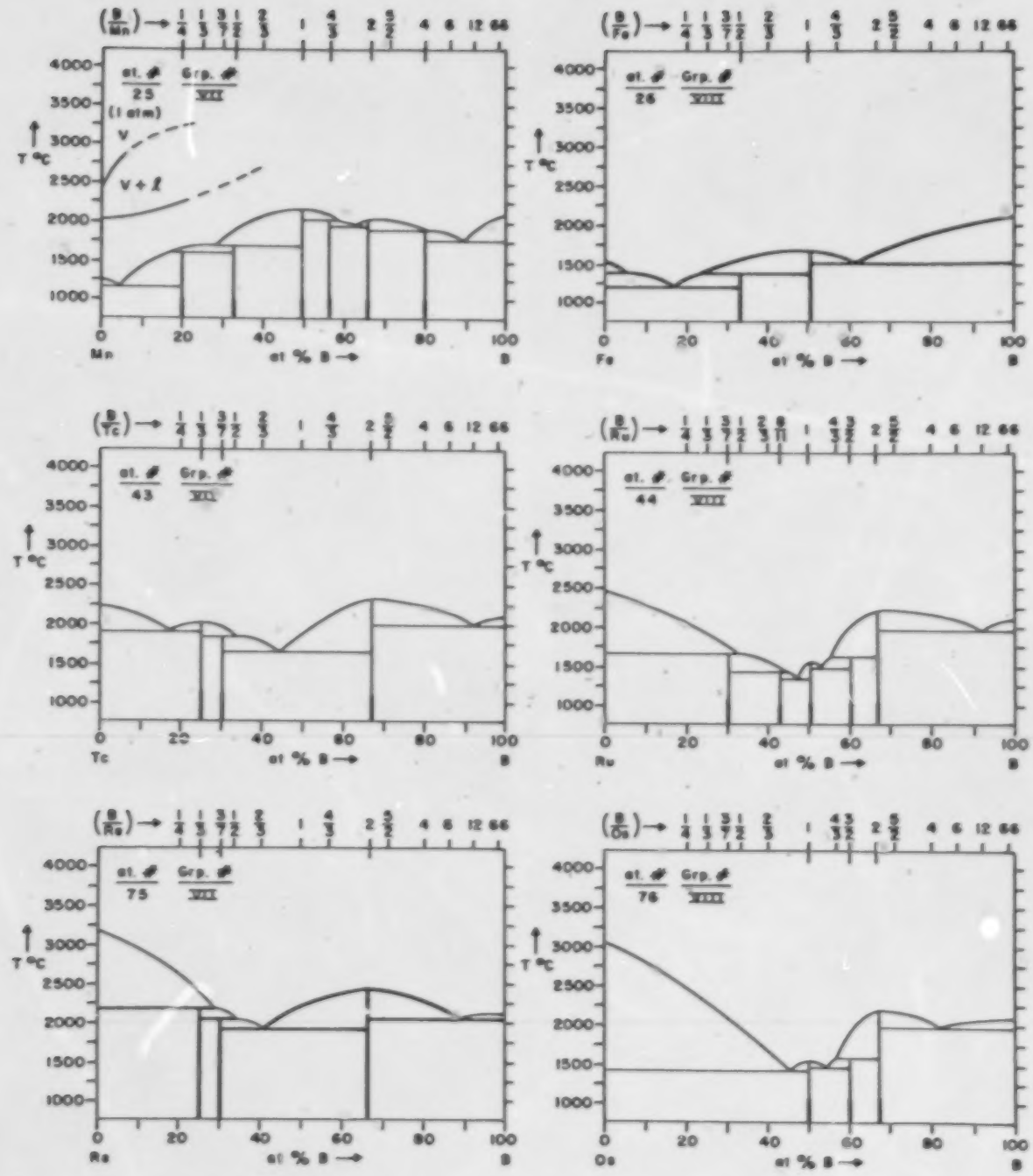

Figure 6: Phase Diagrams for the Metal-Boron Systems of the Transition Metlas from Groups VII and VIII.

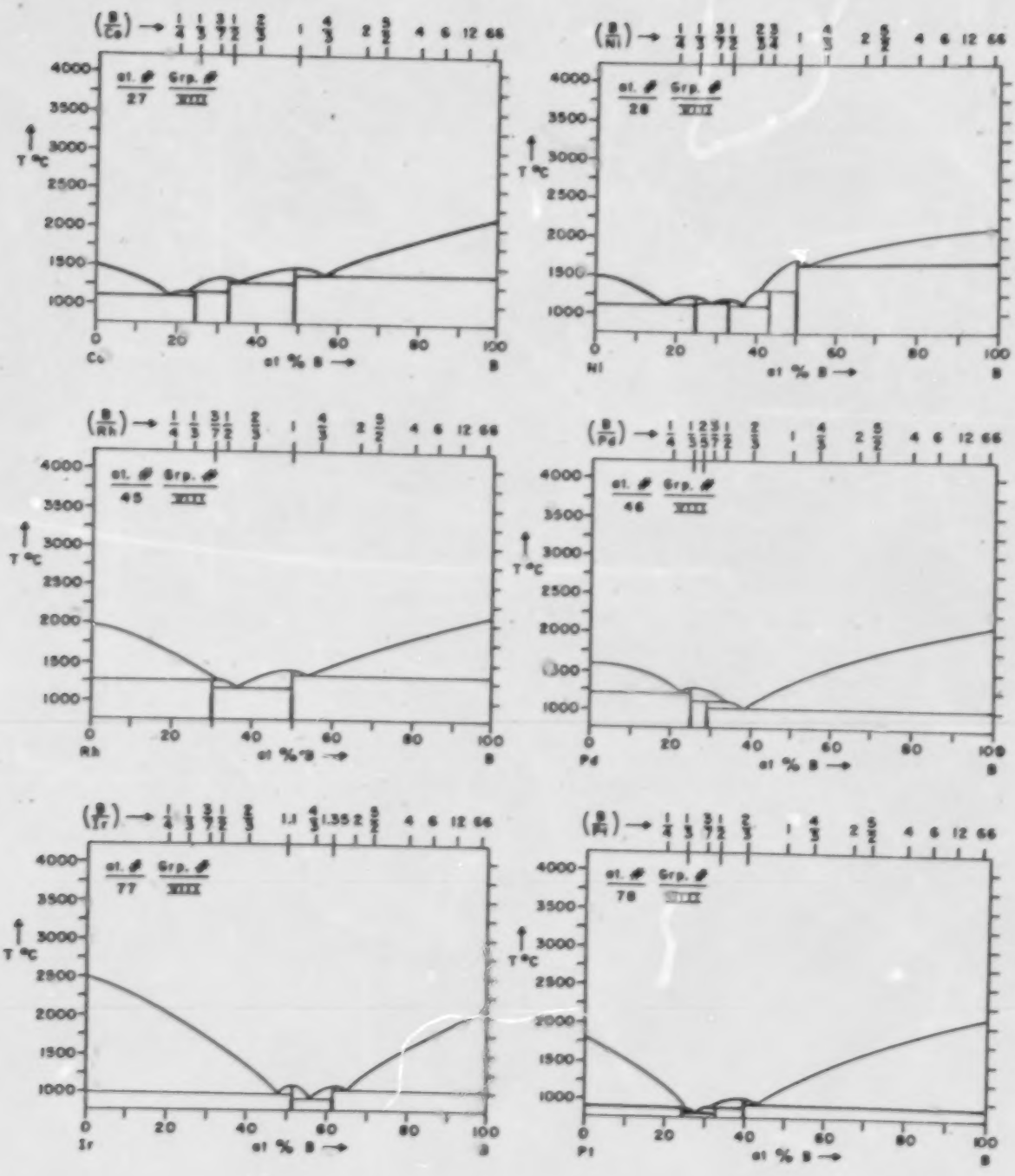

831

Figure 7: Phase Diagrams for the Metal-Boron Systems of the Transition Metals from Group VIII.

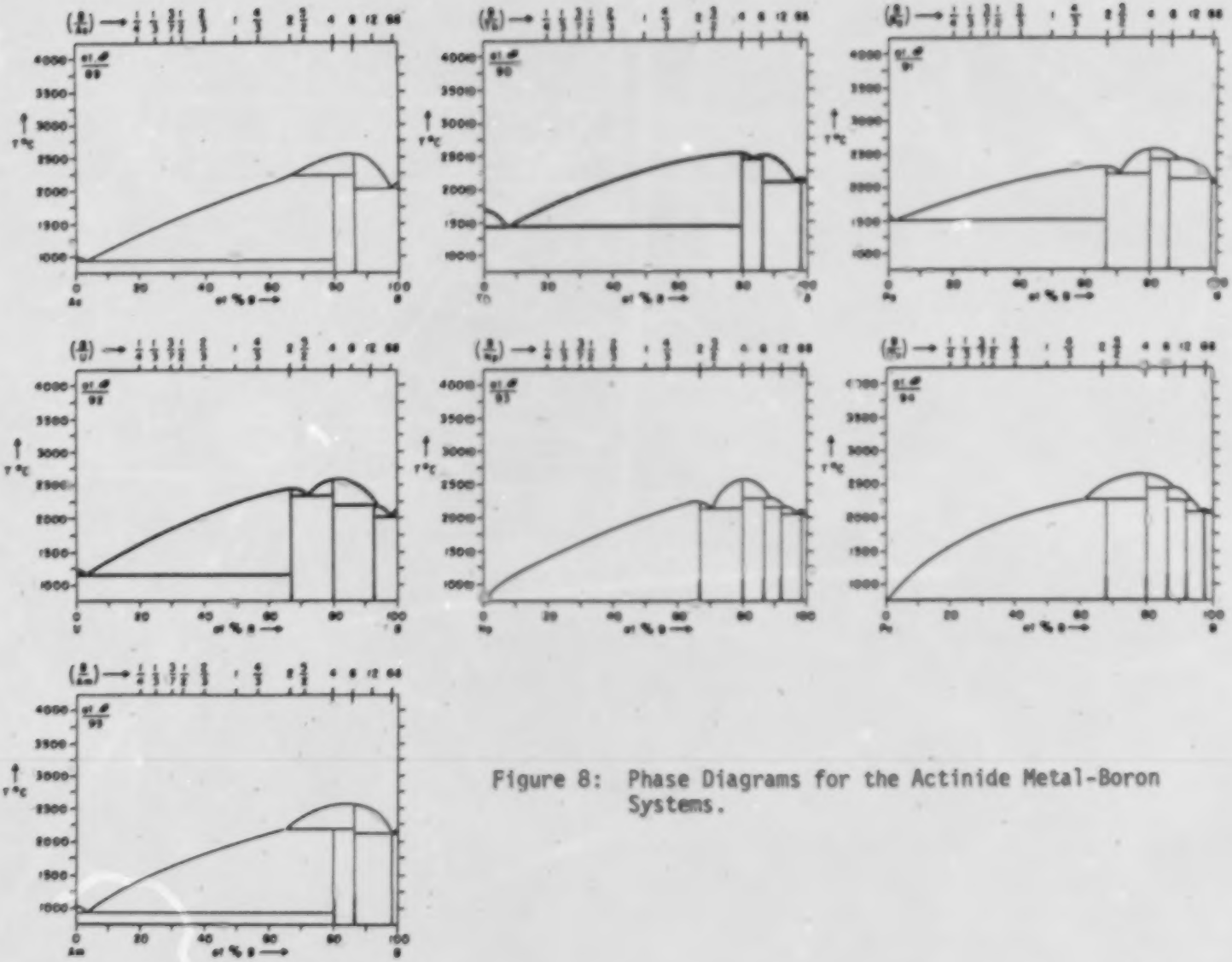

Figure 8: Phase Diagrams for the Actinide Metal-Boron Systems.

National Bureau of Standards SP-496, Applications of Phase Diagrams in Metallurgy and Ceramics
Proceedings of Workshop held at NBS, Gaithersburg, MD., January 10-12, 1977

A VALENCE BOND TEST FOR THE VALIDITY OF INTERMETALLIC AND SEMICONDUCTING STRUCTURES

Forrest L. Carter
Naval Research Laboratory
Washington, D.C. 20375

Abstract

The existence and stability of compounds is reflected primarily by the local coordination of and atomic distances between the constitute atoms. The most universally valid method to make use of this important primary information is the system of metallic radii developed by Pauling. We have found that if these metallic radii cannot be applied in a self-consistent manner to reputedly "known" compounds, then the crystal structure and/or composition of the "known" compound should be questioned. Examples are primarily drawn from the transition metal borides, pnictides, and intermetallic compounds, including those of the rare earths. The advantages and limitations of this approach are discussed, and the plan for its future development as a sharper diagnostic, as well as predictive, tool is indicated.

Introduction

The validity of intermetallic and semiconducting structures can be tested via the use of Pauling's single bond metallic radii [1]. The general correctness of this assertion has become increasingly clear during the course of our several studies of chemical bond formation in transition metal and rare earth compounds. With experience, we have learned that if the semiempirical approach of Pauling cannot be self-consistently applied within certain limits (to be discussed), then either the structure or composition is seriously in error. In short, for a very wide selection of compounds, one has a test for the correctness of a phase description, provided x-ray data are available.

After discussing the basis of Pauling's metallic radii in the next section, we will then describe its advantages as well as its limitations. The succeeding sections will then provide examples where this approach suggests (a) crystallographic refinement is desirable, (b) structural instability exists, (c) compositional data are incorrect, and (d) failure of the material to exist as reported. The final section will indicate our plans to strengthen the powers of this approach to include a predictive capability.

Pauling's Metallic Radii:

The semiempirical single bond metallic radii, R(1), of Pauling are much more than a set of hard sphere radii of a few elements useful only for a particular class of compounds. Rather, they are a set of radii for most of the periodic table, calculable from a few simple equations firmly based on the chemical concepts of covalency and hybridization.

From the observed crystallographic interatomic distances d_{ij}, the corresponding bond order n_{ij} between atoms i and j may be readily calculated from Eq. (1):

$$d_{ij} = R_i(1) + R_j(1) - 0.600 \log n_{ij} \qquad (1)$$

If atoms i and j form a single bond between them, then $n_{ij} = 1$, since each atom contributes one electron to the formation of that bond. From Eq. (1) we see that d_{ij} is then the sum of the single bond radii, $R_i(1) + R_j(1)$. Usually, however, d_{ij} is larger than the sum of the R(1), corresponding to a bond order less than 1.0; double bonds ($n_{ij} = 2$) are very rare in transition metal semiconductors and intermetallics. From the observed bond distances, one may calculate the valence of atom i by summing up the corresponding n_{ij}, Eq. 2:

$$V_i = \Sigma_j n_{ij} \qquad (2)$$

The single bond radii $R_i(1)$ are readily calculated for the Fe-transition elements as:

$$R_i(1) = 1.825 - 0.043z_i - (1.600-0.100z_i)\ \delta_i, \qquad (3)$$

where z_i is the number of electrons outside the rare gas core minus Q_i, the number of electrons transferred from atom i to its neighbors j. The d-character, δ_i, associated with the bond of atom i has a strong influence on the $R_i(1)$ of the transition elements, as we shall see shortly. As seen from Fig. 1, the equation for $R_i(1)$ of the Pd-transition elements is very similar to that of Eq. (3) and, excepting the interruption caused by the lanthanides, the equation for R(1) of the long row of Pt-transition elements is also closely related.

In Fig. 1 we note that the single bond radii $R_i(1)$ are marked by circles and linked by solid lines. The dotted lines correspond to tetrahedral radii of sp^3 type hybridization with the radii R(tet) having the form of Eq. (3) with zero d character, $\delta_i = 0$, thusly:

$$R_i(tet) = 1.825 - 0.043z_i \qquad (4)$$

834

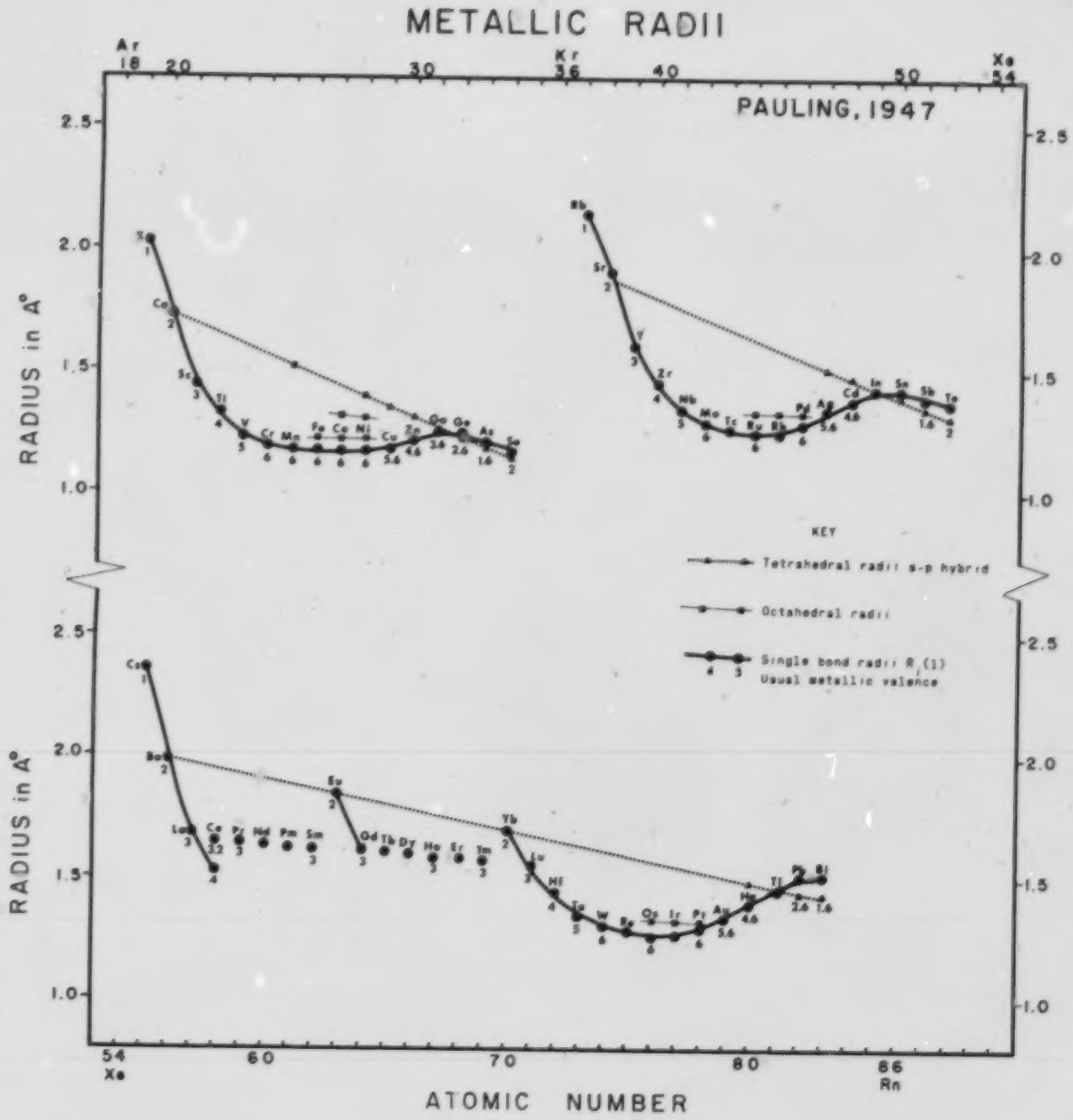

Fig. 1. The single bond radii of Pauling depend on valence and hybridization in a readily understandable fashion (see text).

We further note that the slope for the tetrahedral radii (-0.043) is the same for both the Fe- and the Pd-transition series elements and similar to that of the Pt-transition elements (-0.030). Further, Pauling provided for pure p-hybridization bonding by changing the constant of Eqs. 3 and 4, 1.825(sp^3) to 1.855(p). Accordingly, we can see (as a chemist would expect) a systematic dependence of $R_i(1)$ on the atomic number and hence on the hybridization.

The valence of the element also plays an important role in the single bond radius. This is suggested in several ways. For example: (1) in the beginning of each series, the sharp decline in $R_i(1)$ is due both to valence increases, as in the sequence K(1) → Ca(2) → Sc(3) → Ti(4), and to hybridization changes s → sp → spd. (2) For Fe, Co, and Ni, we find octahedral radii for different valent states midway between the solid R(1) curve and the dotted R(tet) line. For the rare earths, the divalent states of Eu and Yb are on the tetrahedral dotted line while the trivalent rare earths are significantly smaller. Thus it is quite clear from Fig. 1 that the atomic size is a significant function of both bond hybridization and valence. In contrast to the ionic picture, the single bond radii are only a weak function of formal charge Q_i (via the z_i parameter), usually with $|Q_i| < 1.5$.

In the application of Pauling's metallic radii to a given structure, it is usually desirable and often necessary to perform the calculation in an iterative manner to obtain self-consistent results. Starting with an atom's normal valence as an estimated valence, V(est), one calculates from the known interatomic distances d_{ij}, the associated bond orders n_{ij} (Eq. 1) and then a calculated valence V(calc) via Eq. 2. A new V(est) may be taken as an average of V(calc) and the prior V(est). During the iterative process, charge transfer and/or some hybridization change in δ_i may be necessary to achieve the self-consistency in which for each atom $V_i(est) = V_i(calc)$. Generally, charge transfer is allowed to take place only to maintain a filled octet (as for sulfur) or to increase the bonding power of one atom without impairing that of a neighbor. From the formal charges and adjusted electronegativity differences, one may estimate ionic bond character and hence the bond polarization. The resultant effective charge for an atom is then

$$Q_i(\text{eff}) = Q_i(\text{formal}) - \Sigma_j n_{ij} \left(1-\exp(-(x_i-x_j)^2/4)\right) * \text{sign}\ (x_i-x_j) \qquad (5)$$

where x_i is the electronegativity of the ith atom. Usually the bond polarization occurs in such a way as to reduce the formal charge.

Advantages and Limitations:

Compared to any hard sphere model, the use of Pauling's metallic radii has several advantages. First of all, it can handle compounds involving combinations of any of more than 75 elements. It also provides approximate atomic valences and, through bond order calculations, an estimate of the relative strength and importance of various bonds. In addition, the method permits an estimate of effective charges which are generally in reasonable agreement with ESCA results (but not with the naive ionic models). Further, the method calls attention to any unusual hybridization conditions. From the simple bookkeeping of electrons and their relative s-, p-, and d-character, one may estimate the maximum number of unpaired d-electrons for comparison with magnetic and neutron diffraction data.

Two additional advantages are associated with the use of a self-consistent set of single bond radii for a compound: (1) the metallic radii can serve as atom sizes for a computer program [2,3] that calculates polyhedral atomic volumes (PAV) using a Voronoi-like cell construction. This result is useful for unequivocally establishing which atom undergoes a volume change upon compound formation and how much change there is. (2) The second use permits one to calculate generalized coordination numbers, CN_i, for non-symmetric as well as symmetric coordinations via the formula of Eq. 6 [2.4].

$$\frac{1}{CN_i} = \Sigma\left(\frac{n_{ij}}{V_i}\right)^2 \qquad (6)$$

Hard sphere models offer none of these special chemical advantages.

The limitations of Pauling's metallic radii are of various sorts. First of all, the approach is not generally applicable to extremely ionic materials like halides or oxides, although the application to conducting halides and oxides might be both interesting and useful. Secondly, values of $R_i(1)$ and the variation of $R_i(1)$ with valence and d- or f-hybridization have not been developed for the actinide elements. Further, we note two kinds of difficulties with the rare earths: (1) the polyhedral atomic volumes of rare earths in most of their compounds are 10 to 15% smaller than calculated from the elements (see refs. 3 and 5), which indicates that the elemental $R_i(1)$ are generally too large (or the δ value is too small). The second problem is that in the rare earths, there is some evidence that bond hybridization is not isotropic, namely that f orbital participation may be strong for some bonds but not for others.

Finally, we note that the successful application of Pauling's metallic radii often requires some experience with the method. For example, for a particular compound it may be possible to achieve self-consistency *via* either a large charge transfer or through a vastly increased d-character. In such a case, it is difficult to know *a priori* which is more reasonable or what combination of these two approaches to use. In the future we hope to avoid this problem *via* the minimization of energy terms while iterating for self-consistency (details to be discussed later).

In summary of this section, we have found as a user (and not the originator) that the advantages of Pauling's metallic radii scheme render it far superior to any other proposed approach and that the method provides much useful information on innumerable phases, notwithstanding the limitations.

Applications:

Examples of the application of Pauling's metallic radii will be wholly drawn from our own experience, although the literature bulges with Pauling's contributions to elemental, compound, and alloy phases (for Si, see [6]). It is conceivable that the reader will be more convinced of the correctness of this method if it is argued by someone without Pauling's easy facility. In the examples we have chosen, we hope to demonstrate both the variation in criticality and the usefulness of this test for the validation of phases.

Refinement of Structure: Pauling's metallic radii can be used to indicate that a structure is probably correct but that refinement is necessary. In the case of ZnSb, the structure was solved in essence by Almin [7] using powder data. However, when it appeared that a Zn-Zn single bond was present as well as an Sb-Sb single bond, and that the metallic valence of Zn approached 4, it was decided that a structural redetermination was in order using a single crystal. In the results of Carter and Mazelsky [8], the Sb-Sb single bond was found correct, but the Zn-Zn bond order decreased to a more normal 0.31. The coordination of Sb is tetrahedral, while that of Zn is nearly trigonal planar. The use of Pauling's metallic radii suggests that antimony transfers approximately one electron to Zn, thereby permitting each to increase its valence by one (to 4 and 3, respectively, in agreement with their coordination). This increased bonding power presumably more than compensates for the energy cost of the electron transfer.

In the second example, we consider the isomorphous series Cr_3B_4, Mn_3B_4, Nb_3B_4, and Ta_3B_4, where accurate position parameters are available only for Cr_3B_4 (see Pearson [9]), and where the latter compounds probably were deemed too simple to be worthy of a full structure analysis. In using the metallic radii approach, the primary problem appears in terms of the valence of B2 (boron

No. 2, as catalogued by Pearson [9]), which increases from a reasonable value of 3.31 for Cr_3B_4 to 4.0 for Mn_3B_4, and in excess of 4.0 for the Nb and Ta analogues. A boron valence greater than 4 is not chemically reasonable, since there are only four atomic orbitals available ($2s2p^3$). An analysis of the bond orders for B2 shows that there is an unusually strong B2-B2 bond ($n \cong 0.95$), which is much too strong for this composition. The metallic radii approach, then, suggests that structural refinement is in order and the parameters of B2 should change in such a way that the B2-B2 bond should lengthen. As a third example, in [2], we consider the single crystal structure determination of $Ru_{11}B_8$ in which light atoms are sought in the presence of heavy ones. Again, the valences of boron are too high (B2, V = 4.04; B4, V = 4.61), indicating too many short contacts. Here it is unfortunate that neutron diffraction techniques cannot be of ready assistance.

Structural Instability: In our next two examples, we indicate how the application of Pauling's metallic radii suggests structural instability for two unusual materials which are important for special purposes in DoD devices. As our first example, we will discuss TiNi, a material known both for its "memory" and its sound attenuation properties. Its high temperature structure is CsCl-type, but upon cooling below 700°C, it undergoes a diffusion-controlled transition to a trigonal unit cell. Cooling further below 160°C, TiNi begins a long series of poorly understood, martensitic transitions that are involved in both its memory and its sound attenuation properties [10]. The room temperature powder pattern, however, still appears to be closely related to the CsCl structure. In an attempt to understand this material and how it might transform, we applied the metallic radii approach to TiNi as if it were CsCl type (since the real structure was unknown). The large size of elemental Ti prevented the attainment of self-consistency and suggested an excessive Ti valence of V(calc) = 5.6, and a corresponding excessive Ti charge of -1.6. However, Ni in the structure seemed to possess a near-normal valence of 5.40. In order to obtain self-consistency without charge transfer, it was necessary to increase the d-character of Ti from δ = 0.27 to 0.37. Not only was such a d-character objectionably high for Ti, but it also resulted in abnormally low valences for both Ti and Ni. In short, no reasonable adjustment of the parameters available in the metallic radii method resulted in a useful discussion of the bonding in TiNi as an ambient CsCl structure. This result was in agreement with the experimental facts; namely, TiNi was CsCl only above 700°C.

In a similar treatment of the super-permanent magnet material, $SmCo_5$, the two different kinds of cobalt (trigonal and icosohedral coordination) appeared as normal cobalts, but the Sm radius was obviously too large. In order to achieve a self-consistent treatment, Sm required not only an increased d-character and some charge transfer, but an anisotropic hybridization as well. Thus the final

model suggested f-orbital hybridization in the basal plane where Sm is encircled by a small ring of six cobalts. This structure prompted us to predict [3] that the structure was unstable at ambient conditions, which was found later to be the case experimentally by the co-workers of Buschow[11]. In short, if Pauling's metallic radii cannot be readily applied, then the stability and/or existence of the phase should be questioned.

Predicted Non-stoichiometry: In a consideration of the reported transition metal diborides of the AlB_2 structure, several reported diborides failed to iterate to self-consistent results at the ideal stoichiometry. Compounds for which this was the case and which might be non-stoichiometric members of the AlB_2 structure are RuB_2, OsB_2, and AgB_2 [12]. The results for RuB_2 are fairly typical of an extreme case. The boron calculated valence was an impossible 5.9, while V(est) = 3.64, even though $\delta = 0.53$ for Ru instead of a normal $\delta = 0.50$. Boron deficiency ameliorates this situation and if these compounds exist as an AlB_2 type, their stoichiometry deviates significantly from the ideal; thus for $RuB_{2(1-x)}$, $x > 0.4$. For RuB_2 and OsB_2, this composition had been previously questioned by Przybylska, Reddoch and Ritter for other reasons [13].

Structural Variation of Hybridization: Although Pauling's metallic radii method does not depend per se on coordination, we have found that the resultant hybridization changes away from his normal values are usually in agreement with what a chemist is led to by simple valence bond considerations. For example, in our treatment of compounds having the WC structure [12], we found that without reducing the R(1) value of P in MoP, self-consistency was not obtainable for P; thus V(calc) = 4.95 while V(est) = 3.11. However, by introducing a small amount of phosphorous d-character, 4-8%, the R(1) value is reduced, so that self-consistency is readily obtainable. Thus, at $\delta(p) = 0.04$, self-consistency occurs with V(calc) = V(est) = 4.16. In the WC structure, the non-metal is in trigonal prismatic coordination, for which d-character is required if a valence bond construction is employed. One valence bond method which discusses the trigonal prismatic coordination at low d-character is that employing the Bidirectional Orbital Approximation (BOA), wherein a single orbital forms half-bonds with two (not one) near neighbors [14]. Three such bidirectional orbitals of mostly p-character but 7-8% d-character can bond six atoms in a trigonal prismatic coordination like that of P in MoP. In short, this is approximately the same amount of d-character suggested by the metallic radii approach.

Another example where the metallic radii agree with valence bond arguments is represented by the V_3Sn-type superconducting intermetallic compounds having the A-15 structure. In this structure, the V site atom has an unusual bond situation in that it has two very strong V-V bonds ($n_{VV} = \approx 0.6$ to ≈ 1.5) to form a linear chain

while it bonds twelve other atoms in a much weaker manner (n_{vj} = 0.05 to ≈0.35). A valence bond estimate of the d-character required in such a situation is 48.6% (an average of five bonding models) [15].

In order to obtain self-consistency in the metallic radii calculations for some forty of these intermetallic compounds having the A15 structure, it was found necessary to increase the d-character (δ_i) of the V site atom by the following amounts: Ti, from 0.27 to 0.37; V, from 0.35 to 0.39; Cr, good at 0.39; Nb, from 0.39 to 0.43; and Mo, from 0.43 to 0.44. In each case, we note that the required d-character is high and that any change in d-character is to increase it toward the valence bond estimate of 48.6%. Thus, while the metallic radii approach is certainly empirical in nature, it contributes to and reinforces our chemical interpretation.

Non-existent Compounds: For some compounds reported in the literature, the results of the metallic radii approach are so unreasonable that the stated existence of the compound should be seriously questioned. Such an example is AuB_2, where the metallic d-character had to be decreased from δ = 0.36 to δ = 0.30 [12]. This is a very unusual and unlikely circumstance. In addition, the valence of boron was 2.64, significantly below a minimum boron valence of 3.0. There is, therefore, good evidence that this compound does not exist as reported.

Another example is W_2B_5, in which both a large charge transfer occurs to the boron atoms and the tungsten d-character must be increased to unlikely levels before self-consistency is obtainable. This result confirms the earlier suspicions of Lundstrom [16]. The situation for the analogous compound, Ru_2B_5, is even more suspect based on the metallic radii approach [17].

In summary of this section, then, we see that the Pauling metallic radii not only constitute a useful test for phase existence but also provide information on valence, effective charge, bond strengths, composition, and hybridization.

Future Directions:

In order to maximize the utility of Pauling's metallic radii approach beyond the mere testing for the validity of a phase and toward a capacity for prediction, it is desirable that energy terms be added. Thus one could seek a least squares fit to the observed distances (or between V(calc) and V(est)) and minimize an "energy of formation" at the same time. The energy terms to be included should depend on bond orders, n_{ij}, electronegativity differences, promotion energies for unusual hybridization, charge transfer energies, and a Madelung constant term. The Madelung term might be dependent upon coordination number in a manner

related perhaps to Templeton's suggestion [18] for a "reduced Madelung constant." Such terms should be initialized, of course, to give the known results for the elemental structures and other well-characterized compounds. Such an approach in the application of the metallic radii method would eliminate the current uncertainties (e.g., does one achieve self-consistency by charge transfer or by increased d-character hybridization?). More important, it would extend the approach toward the predictability required by the cost-effectiveness orientation of modern research managers.

Restatement

We have, it is to be hoped, argued the general soundness of the following two assumptions for this work and have demonstrated therein convincingly the forcefulness of the conclusion (3, below).

1. The existence and stability criteria for compounds are reflected primarily in their composition and crystal structure (i.e., bond distances).

2. This information can be most universally interpreted for semi-conducting and metallic materials via application of Pauling's metallic radii.

3. If Pauling's semi-empirical approach cannot be readily adjusted to a crystal's stated structure, the crystal structure and/or composition should be questioned.

References

1. L. Pauling, "Nature of the Chemical Bond," 3rd ed., Cornell University Press, Ithaca, N.Y., 1960, p. 400 ff.

2. F. L. Carter, J. Less-Common Metals, 47, 157 (1976).

3. F. L. Carter, "Valence Bond Formation in the Rare Earth Compounds Having the $CaCu_5$ Structure," Proceedings of the 9th Rare Earth Research Conference, Virginia Polytechnic Institute and State University, 10-14 Oct 1971, Vol. II, p. 617.

4. F. L. Carter, submitted for publication, Acta Cryst.

5. F. L. Carter and G. C. Carter, Proc. of 10th Rare Earth Research Conference, Carefree, Ariz., 30 April - 3 May, 1973, Vol. II, p. 1044.

6. Prof. L. Pauling has recently written a note indicating that a suggested high density form of Si "must be wrong, because of poor values of the bond lengths." Private communication.

7. Almin, K. E., Acta Chem. Scand. 2, 400 (1945).

8. F. L. Carter and R. Mazelsky, J. Phys. Chem. Solids, 25, 571 (1964).

9. W. B. Pearson, in G. V. Raynor (ed.), A Handbook of Lattice Spacings and Structures of Metals and Alloys-2, Vol. 8, Pergamon Press, Oxford, 1967.

10. F. L. Carter, "A Mechanism for the High Temperature Transformation and the Resultant Premartensitic TiNi(II)," Symposium on TiNi and Associated Compounds, F. E. Wang, ed., 20 Feb 1968, NOLTR 68-16.

11. F. J. A. Den Broeder and K. H. J. Buschow, J. Less-Common Metals, 29, 65 (1972).

12. F. L. Carter, in R. S. Roth and S. J. Schneider (eds.), Solid State Chemistry, Nat. Bureau Stand. Spec. Publ. No. 364, 1972, p. 515.

13. M. Przybylska, A. H. Reddoch, and G. J. Ritter, J.A.C.S., 85, 407 (1963).

14. F. L. Carter, in L. Bennett (ed.), Electron Density of States, Nat. Bureau Stand. Spec. Publ. No. 323, 1971, p. 385.

15. F. L. Carter, "Valence Bending in Alloys Having the β-Tungsten Structure," Westinghouse Paper 64-929-442-P3, 23 March 1964 (copy available from author).

16. T. Lundstrom, Ask. Kemi., 30, 115 (1968).

17. See discussion, ref. [2].

18. D. H. Templeton, J. Chem. Phys., 23, 1826 (1955).

National Bureau of Standards SP-496, Applications of Phase Diagrams in Metallurgy and Ceramics
Proceedings of Workshop held at NBS, Gaithersburg, Md., January 10-12, 1977

Computation of the Component Activities from Ternary Miscibility Gap Data: the Cu-Ag-S and Cu-Ag-Se Systems

U. V. CHOUDARY and Y. A. CHANG
Materials Department
College of Engineering and Applied Science
University of Wisconsin-Milwaukee
Milwaukee, Wisconsin 53201

ABSTRACT

The high temperature phase relations in the ternary Cu-Ag-S and Cu-Ag-Se systems at 1473 K have been analyzed in light of the recently developed thermodynamic method by the authors. From a knowledge of the experimental tie-line distribution data in the ternary miscibility gap, the boundary binary thermodynamics and the limiting activity coefficients of sulfur in the copper-silver melts, a consistent set of thermodynamic activities is derived in the Cu-Ag-S system. A similar analysis of the Cu-Ag-Se phase relations yields the metal activities and the relative selenium potentials; the absolute activities of selenium could not be determined due to lack of reliable Gibbs energies of mixing data in the Cu-Se and Ag-Se boundary binaries. An extension of the present method to obtain precise values of thermodynamic stabilities of binary and ternary carbides from the ternary metal-metal-carbon phase relations is pointed out.

INTRODUCTION

Phase equilibria and thermodynamic properties of alloy systems are closely interrelated. For instance, if the Gibbs energies of all the competing phases in any binary or ternary system are known as a function of composition and temperature, the phase diagram of the system can be computed. Conversely, from the experimentally determined phase diagrams, useful thermodynamic data of the alloy phases can often be extracted. This approach becomes extremely useful when it is experimentally difficult if not impossible to determine the appropriate thermodynamic properties.

Recently, Choudary and Chang[1] developed a thermodynamic method to calculate the thermodynamic activities (or the chemical potentials) of the component elements A, B, and C from a knowledge of the tie-line distribution data in the ternary miscibility gap (see Fig. 1), the thermodynamics of the boundary binary systems, and the limiting activity coefficients of C in solutions of A and B. This method is particularly applicable to ternary systems where the third component C is a non-metal such as O, S, Se, B, C. Many of these systems are of extractive metallurgical interest and are characterized by a ternary miscibility gap in the melt with one of the boundaries lying close to the A-B binary. Although experimental phase relations in the ternary miscibility gap are known for some of these systems, the chemical potentials of the components A, B, and C have not been determined and are usually difficult to derive experimentally. Yet, a basic knowledge of the thermodynamics of ternary systems such as A-B-O and A-B-S is essential for assessing the complex interactions in the multi-component solutions of metal-matte-slags encountered in extractive metallurgical operations.

In order to derive such basic data of importance in the smelting and refining processes of copper and lead, the present thermodynamic method has been used successfully to compute the chemical potentials of the component elements in the Cu-Pb-O[1] and Cu-Pb-S[2] systems at 1473 K. In the Cu-Pb-S[2]

system, the activity values of lead determined experimentally and those derived from this method are in good accord. For the Cu-Pb-O system, no experimental activity data are available. Since the method was developed from classical thermodynamics, the derived chemical potentials of the components should be exact if the phase equilibria data are correct.

To further our understanding of the metal-matte chemistry in copper extraction, the high temperature phase relations of the Cu-Ag-S system are analyzed to derive the activities of the components. Furthermore, a knowledge of the thermodynamic properties of the Cu-Ag-S system is of significant interest to mineralogists. In view of the importance of the quantitative knowledge of Cu, Ag and Se interactions in the recovery of Ag and Se from copper anode slimes, the phase relations in the Cu-Ag-Se ternary system are also analyzed.

THERMODYNAMIC TREATMENT

Since the thermodynamic method has been presented in detail elsewhere[1], only a brief description of the method is given here. From a knowledge of the tie-line distribution within the two liquid-phase field (see Fig. 1), the limiting activity coefficients of component C, γ_C^o, in the A-B solutions, and the thermodynamic properties of the boundary binaries, the chemical potentials of the component elements along the miscibility gap can be calculated from the relations developed in this section.

The Wagner's relation[1,3]

$$\left(\frac{\partial \ln (\gamma_B/\gamma_A)}{\partial y_C}\right)_{y_B} = \left(\frac{\partial \ln \gamma_C}{\partial y_B}\right)_{y_C} \equiv \theta \qquad [1]$$

can be integrated from $y_C = 0$ to $y_C = y_C^*$ at constant y_B to obtain the following equation for the ratio of activity coefficients of B and A along the metal-rich miscibility gap as:

$$\left(\ln \frac{\gamma_B}{\gamma_A}\right)_{\substack{y_B \\ y_C = y_C^*}} = \left(\ln \frac{\gamma_B}{\gamma_A}\right)_{\substack{y_B \\ y_C = 0}} + (\theta\, y_C^*)_{y_B} \qquad [2]$$

In the above equation, θ is assumed to be constant in the compositional range $0 < y_C < y_C^*$ which is a valid approximation for $y_C^* \simeq 0$. Thus the value of $\theta)_{y_B^*}$ can be evaluated from the experimentally determined limiting activity coefficient of C in the A-B solutions. Even if the values of γ_C^o are not available as a function of y_B, they may be estimated either from one of the several formulations of the quasichemical solutions models[4-10], the Wagner model[11] or the extended Wagner model by Chiang and Chang[12]. The parameters for the Wagner model as well as the extended Wagner model may be predicted from correlations proposed by Chiang and Chang[12] and Kuo and Chang[12]. Knowing the ratios of the activity coefficients of B and A as a function of y_B from Eq. [2], it is possible to

calculate the activities of all three components by integrating the following equations between the appropriate compositional limits along the miscibility gap boundary:

$$d\left(\ln a_i\right)_{y_B^* \text{ or } y_B'} = Z_i \, d\psi^* \qquad [3]$$

where ψ^* denotes $\ln \left(\frac{a_B}{a_A}\right)_{y_B^*}$ which is equal to $\ln \frac{\gamma_B}{\gamma_A}\Big)_{y_B^*} + \ln \frac{y_B}{y_A}\Big)_{y_B^*}$, and the subscript i stands for A, B, or C. The integration functions – Z_A, Z_B, and Z_C – defined as

$$Z_A = \frac{y_B' \, y_C^* - y_B^* \, y_C'}{y_C' - y_C^*} \qquad [4]$$

$$Z_B = 1 + Z_A \qquad [5]$$

$$Z_C = \frac{y_B^* - y_B'}{y_C' - y_C^*} \qquad [6]$$

are calculable from the tie-line distribution data in the ternary miscibility gap.

APPLICATION TO THE CU-AG-S SYSTEM

Since the calculation of the chemical potentials of the components along the miscibility gap depends on a knowledge of the phase relationships and the thermodynamic properties of the boundary binary and the ternary systems, they will be briefly reviewed. The thermodynamic values to be discussed hereafter refer to the temperature of 1473 K unless stated otherwise.

Cu-S

Kellogg[13] has critically evaluated the high temperature phase relations and the thermodynamic properties of the Cu-S system; the selected values employed in the present analysis are taken from his evaluation. The atom fraction of sulfur at saturation, x_S^*, is taken to be 0.0226 ± .001. The values of the limiting activity coefficient of sulfur in liquid copper, $\gamma^o_{S(Cu)}$, and the Gibbs energy self interaction parameter, $\epsilon^S_{S(Cu)} = (\partial \ln \gamma_S / \partial x_S)$, are derived as 3.97 (± 0.4) x 10^{-3} and -14 ± 2, respectively. Thus, the values of a_{Cu}, a_S, and p_{S_2} in the miscibility gap are found to be 0.981 ± .002, 6.53 x 10^{-5} and 9.37 (± 1.5) x 10^{-7} atm., respectively. The standard states are Cu(ℓ) and S(ℓ). The change of standard states for sulfur from $\frac{1}{2}$ S_2(g) to S(ℓ) is made using the data from JANAF[14].

The equilibrium constant, $K_{CuS_{1/2}}$, for the reaction

$$Cu(\ell) + \frac{1}{4} S_2(g) = Cu\ S_{1/2}\ (\ell) \qquad [7]$$

is found to be 32.3, while the values of a_{Cu}, a_S, and p_{S_2} at the stoichiometric composition Cu_2S are 0.437 ± 0.02, 3.36 x 10^{-4}, and 2.53 (± 2) x 10^{-5} atm., respectively.

Ag-S

Recent thermodynamic investigations of the Ag-Ag_2S system over the temperature interval 1273-1473 K by Yazawa and Schnalek[15] are in excellent accord with the earlier extensive phase equilibria and thermodynamic determinations of Rosenqvist[16] in the temperature range 773-1523 K. Mills[17] has reviewed and critically assessed the various thermodynamic studies of the Ag-S system; his suggested high temperature thermodynamic properties at 1373 and 1523 K are mainly based on the investigations of Rosenqvist, and Yazawa and Schnalek.

At 1473 K, the Ag-S system does not exhibit a miscibility gap; the critical point lies at approximately 24 at.% S and 1400 K. In conjunction with appropriate JANAF data, $\gamma^{o}_{S(Ag)}$ is derived as 0.045 ± .004 from the investigations of Rosenqvist[16] and Yazawa and Schnalek[15]. Since none of the above authors' investigations extend up to the composition corresponding to Ag_2S at 1473 K, the activities of silver and sulfur can be extrapolated from Rosenqvist's values of a_{Ag}, a_S, and $\Delta\bar{H}_S$ values at 1398 K. Also, the extrapolated values have to be consistent with the derived values of activities in the Ag-rich region of the miscibility gap. From these considerations, the values of a_{Ag}, a_S, and p_{S_2} at $x_S = 0.333$ and T = 1473 K are selected to be 0.691 ± 0.004, 8.2×10^{-3}, and $1.5(\pm 0.6) \times 10^{-2}$ atm, respectively. The standard states are pure liquid silver and sulfur. From the above selected values, the equilibrium constant, $K_{AgS_{1/2}}$, for the reaction

$$Ag(\ell) + \frac{1}{4} S_2(g) = AgS_{1/2}(\ell) \qquad [8]$$

is found to be 4.13 ± .4 from the above selected values.

Cu-Ag

The thermodynamic properties of Cu-Ag solutions pertinent to the present analysis are taken from Hultgren, et al.[18]

Cu-Ag-S

The high temperature phase relations in the ternary Cu-Ag-S system have been investigated by Gerlach, et al.[19], and Kristovnikov, et al.[20] The tie-line distributions at 1473 K, depicted in Fig. 2, are taken from Gerlach, et al. The silver-rich portion of the miscibility gap, shown as dashed line in Fig. 2, is drawn to be consistent with the fact that Ag and S are completely miscible at this temperature[16]. No thermodynamic properties have been reported along the miscibility gap. Kristovnikov, et al.[20], have studied the Cu_2S-Ag_2S system and found it to be pseudo-eutectic; Cu_2S and Ag_2S are completely miscible in the liquid state at 1473 K.

Solid solutions of Cu_2S-Ag_2S have been investigated in the temperature range 703-980 K by Perrot and Jeannot;[21] the activities of $CuS_{1/2}$ and $AgS_{1/2}$ exhibit small positive deviations from ideality at 980 K.

The limiting activity coefficient of S in Cu-Ag solutions has been determined by Cheng;[22] his experimental values for y_{Ag} = 0 to 1 at 1358 K are also available in a paper by Fruehan and Richardson.[23] Jacob and Jeffes[9] have reported that the experimental values of Cheng are in good accord with the predicted values from their quasichemical model. Hence, in the present analysis, the values of $\ln \gamma_S^o$ in Cu-Ag solutions at 1473 K are computed from the following quasi-chemical relation of Jacob and Jeffes:[9]

$$\ln \gamma^o_{S(Cu-Ag)} = y_{Cu} \ln \gamma^o_{S(Cu)} + y_{Ag} \ln \gamma^o_{S(Ag)} - 2 \frac{\Delta H}{RT} \qquad [9]$$

where ΔH is the enthalpy of mixing for the Cu-Ag solution and R is the universal gas constant.

Computation of the Activities of Cu, Ag and S in the Miscibility Gap

From Eqs. [2] and [9], and the standard thermodynamic relationship between the integral and partial quantities, an expression for calculating the ratio of activities of silver and copper along the metal-rich miscibility gap can be written as:

$$\psi^* = \left(\ln \frac{a_{Ag}}{a_{Cu}}\right)_{\substack{y_{Ag} \\ y_S = y_S^*}}$$

$$= \left(\ln \frac{\gamma_{Ag}}{\gamma_{Cu}}\right)_{\substack{y_{Ag} \\ y_S = 0}} + \left(\ln \frac{y_{Ag}}{y_{Cu}}\right) + y_S^* \left\{\ln \frac{\gamma^o_{S(Ag)}}{\gamma^o_{S(Cu)}} + \frac{2}{RT}\left(\frac{\Delta H - \Delta \bar{H}_{Ag}}{1 - y_{Ag}}\right)\right\} \qquad [10]$$

where $\Delta\bar{H}_{Ag}$ represents the relative partial molar enthalpy of silver in the Cu-Ag solutions.

Utilizing the calculated values of ψ^* from the above expression and integrating Eq. [3] with $y^*_{Ag} = 0$ as the lower limit, activities of the components can be derived as:

$$\left(\ell n\ a_i\right)_{y^*_{Ag}} = \left(\ell n\ a_i\right)_{y^*_{Ag}=0} + \int_0^{y^*_{Ag}} Z_i\ d\psi^* \qquad [11]$$

where the subscript i stands for Cu, Ag, or S, and Z_{cu}, Z_{Ag}, and Z_S represent the integration functions calculable from Eqs. [4] to [6].

The pertinent integration plots are presented in Figs. 3 and 4 while the derived activities of Cu, Ag and S are shown in Figs. 5, 6, and 7. The activities of Cu and Ag are also presented in Fig. 8 for sulfur-free (y_S=0) and sulfur-saturated ($y_S = y^*_S$) solutions as a function of the metal atom ratio. The positive deviations from ideality are less pronounced for the sulfur-saturated melts. The maximum uncertainty in the activities from all the sources is estimated to be ± 8%.

Computation of the Sulfur Potential in the Cu_2S-Ag_2S Psuedo-Binary

The sulfur potentials along the Cu_2S-Ag_2S join are not known experimentally, but may be computed using the method described below. However, the computed values must be consistent with (i) the known values of p_{S_2} at the stoichiometric compositions Cu_2S-Ag_2S; (ii) Wagner's relation represented by Eq. [2]; (iii) derived values of p_{S_2} in the miscibility gap. From Eqs. [7] and [8], the ratio of activity coefficients of the sulfides, $CuS_{1/2}$ and $AgS_{1/2}$, can be related to the ratio of activity coefficients of the metals, and that of the respective equilibrium constants as:

$$\ln \frac{\gamma_{AgS_{1/2}}}{\gamma_{CuS_{1/2}}} = \ln \frac{\gamma_{Ag}}{\gamma_{Cu}} - \ln \frac{K_{AgS_{1/2}}}{K_{CuS_{1/2}}} = \ln \frac{\gamma_{Ag}}{\gamma_{Cu}} - 2.06 \qquad [12]$$

For the mid-range composition, where the miscibility gap lies close to the $CuS_{1/2}$ - $AgS_{1/2}$ join, the value of $\ln \frac{\gamma_{Ag}}{\gamma_{Cu}}$ on the join may be calculated from the value at the S-rich side of the miscibility gap at constant y_{Ag} from Wagner's relation expressed in Eq. [2]. From these considerations, slight positive deviations from ideality are inferred in the $CuS_{1/2}$ - $AgS_{1/2}$ quasi-binary. The estimated sulfur potentials along the pseudo-binary join and the derived values along the miscibility gap are shown in Fig. 9. The maximum uncertainties in $\ln p_{S_2}$ values are ± 0.3 and ± 0.7 along the miscibility gap and $CuS_{1/2}$ - $AgS_{1/2}$ join, respectively.

APPLICATION TO THE CU-AG-SE SYSTEM

The phase relations in the Cu-Cu_2Se-Ag_2Se-Ag section have been well established by the determinations of Asano, et al.,[24] over the temperature interval 873-1473 K. At 1473 K, the miscibility gap in the Cu-Se system extends all the way to the Ag-Se system. Based on the chemical analysis of nearly twenty melts in the miscibility gap, Asano, et al.,[24] have determined the tie-line distribution at 1473 K; it is in essential agreement with that of Emicke[25] for the silver-rich portion at 1223 K. The Cu_2Se-Ag_2Se quasi-binary has been found to be of the pseudo-eutectic type by Asano, et al.; a single liquid exists throughout the compositional range at 1473 K.

Reliable high temperature thermodynamic data are not available for the boundary binaries Cu-Se, Ag-Se and the ternary system. However, a thermodynamic analysis of the phase relations at 1473 K may be carried out assuming the variation of the limiting activity coefficient of Se with atom ratio of Ag is approximately the same as that of S in the Cu-Ag melts. The pertinent integration plots based on the tie-line

distribution data of Asano, et al., are presented in Figs. 10 and 11. The derived metal activities with an estimated overall maximum uncertainty of ± 10% are shown in Figs. 12 and 13. Since the activity of Se is not known at either of the boundary binaries, only the relative activity is presented in Fig. 14. Once the high temperature thermodynamic properties of either Cu-Se or Ag-Se melts are known, absolute selenium activity can be readily obtained from the derived relative selenium activity.

ANALYTICAL APPROACH TO THE PRESENT THERMODYNAMIC METHOD

The thermodynamic properties of the boundary binary solutions (A-B) as well as the limiting activity coefficient of C in solutions of A and B can often be expressed as a simple function of the metal atom ratio. In such cases, thermodynamic activities along the miscibility gap can be represented analytically at least in a limited compositional range. Further, if the tie-line distribution data is extensive, the integration function Z and the ℓn (activity ratio) may be fitted to a suitable function of y_B and the pertinent integrations may be performed analytically to derive the activities.

To facilitate discussion in this section, the following nomenclature is adopted:

$$\xi = y_{Ag}; \qquad \eta = y_S; \qquad \psi = \ell n \frac{a_{Ag}}{a_{Cu}}$$

$$\phi = \ell n \frac{\gamma_{Ag}}{\gamma_{Cu}}; \quad Y = \ell n \frac{y_{Ag}}{y_{Cu}}; \qquad \theta = \frac{\partial \ \ell n \ \gamma_S}{\partial \xi} = \frac{\partial \phi}{\partial \eta}$$

The superscript 'o' is used to designate the values in C-free A-B binary.

The thermodynamic properties of Cu-Ag solutions at 1473 K can be adequately described by the regular solution model. Thus, the ratio of the activity coefficients of Ag and Cu may be expressed as a linear function of the metal atom ratio

$$\phi^o = \frac{\epsilon}{RT} (1 - 2\xi) \qquad [13]$$

where the regular solution parameter, ε, for Cu-Ag system is taken to be 3366 cal, based on the selected thermodynamic properties by Hultgren, et al.[18] Also, the variation of the limiting activity coefficient of sulfur in Cu-Ag melts is a simple linear function of ξ:

$$\theta^* \approx \theta^o = -0.5 + 5.8\ \xi \qquad [14]$$

Since $\eta^* = 0.02 \pm .004$, the activity ratio along the miscibility gap can be expressed from Eqs. [2], [13] and [14] as:

$$\psi^* = \psi^o + \theta^o\ \eta^* = (1.14 - 2.184\ \xi) + \ln \frac{\xi}{1-\xi} \qquad [15]$$

Also, the integration functions Z_{Cu}, Z_{Ag} and Z_S have been found to vary linearly for $0 < \xi^* < 0.7$, i.e., $Z_{Cu} = -1.11\ \xi^*$ and $Z_S = 1.68\ \xi^*$. Thus, analytical integration of Eqs. [3] to [5] yield the following expressions for the activities of components in the compositional range $0 < \xi < 0.7$ along the miscibility gap.

$$\ln a_{Cu} = -.02 + 1.212\ \xi^2 + 1.11 \ln (1-\xi) \qquad [16]$$

$$\ln a_{Ag} = 1.14 - 2.184\ \xi + 1.212\ \xi^2 + \ln \xi + 0.11 \ln (1-\xi) \qquad [17]$$

$$\ln a_S = -9.64 - 1.84\ \xi^2 - 1.68 \ln (1-\xi) \qquad [18]$$

$$\ln p_{S_2} = -13.88 - 3.68\ \xi^2 - 3.36 \ln (1-\xi) \qquad [19]$$

Noting that $Z_{Cu} = -1.033\ \xi^*$ and $Z_{Se} = 1.231\ \xi^*$ for $0 < \xi^* < 0.7$, metal [illegible] and the relative selenium activities can be similarly represented along the miscibility gap in the Cu-Ag-Se system.

$$\ln a_{Cu} = -.02 + 1.28\ \xi^2 + 1.033 \ln (1-\xi) \qquad [20]$$

$$\ln a_{Ag} = 1.12 - 2.184\ \xi + 1.128\ \xi^2 + \ln \xi + 0.033 \ln (1-\xi) \qquad [21]$$

$$\left(\ln a_{Se}\right)_{\xi^*} - \left(\ln a_{Se}\right)_{\xi^*=0} = -1.834\ \xi^2 - 1.68 \ln (1-\xi) \qquad [22]$$

EXTENSION OF THE PRESENT THERMODYNAMIC METHOD TO OTHER SYSTEMS

The present method can be extended to ternary systems where all the components A, B and C are metals, provided the miscibility gap lies close to one of the boundary binaries. Even in the absence of limiting experimental activity coefficients of C in A-B alloys, activities in the miscibility gap can be computed from the boundary binary thermodynamics by assuming a linear variation of $\ell n\ \gamma_C^o$ with metal atom ratio. Even if the ternary systems are not characterized by a miscibility gap, Wagner's relation given by Eq. [2] is highly valuable to check the internal consistency of experimental or derived thermodynamic properties from various solution models.

Recent analysis of ternary phase relations in metal-metal-carbon systems such as Fe-Mn-C,[26] Fe-Cr-C in solid[26] as well as liquid[27] state up to graphite saturation, shows that highly reliable Gibbs energies of formation for the binary and ternary carbides can be derived utilizing the present method. Since phase relations are well established for many of the ternary carbon systems, analysis of them in light of the present method will be useful for obtaining hitherto unavailable precise thermodynamic properties of transition metal carbides. Similar analysis of solid state phase relations in other ternary systems such as A-B-O, A-B-S will also be valuable for assessing the stabilities of oxides, sulfides, silicates and spinels.

ACKNOWLEDGMENTS

The authors wish to acknowledge partial support of this research from the International Copper Research Association.

REFERENCES

1. U. V. Choudary and Y. A. Chang: Met. Trans., 1976, vol. 7B, pp. 655-660.
2. U. V. Choudary, Y. E. Lee and Y. A. Chang: Met. Trans., in review.
3. C. Wagner: Met. Trans., 1975, vol. 6B, pp. 395-398.
4. C. B. Alcock and F. D. Richardson: Acta Met., 1958, vol. 6, pp. 385-95; 1960, vol. 8, pp. 882-87.
5. G. R. Belton and E. S. Tankins: Trans. TMS-AIME, 1965, vol. 233, pp. 1892-98.
6. U. Block and H. P. Stüwe: Z. Metallkunde, 1969, vol. 60, pp. 766-71.
7. N. A. Gokcen: Scripta Met., 1969, vol. 3, pp. 157-60.
8. R. J. Fruehan and F. D. Richardson: Trans. TMS-AIME, 1969, vol. 245, pp. 1721-26.
9. K. T. Jacob and J.H.E. Jeffes: Trans. Inst. Min. Met., 1971, vol. C80, pp. 32-41.
10. K. T. Jacob and C. B. Alcock: Acta Met., 1972, vol. 20, pp. 221-32.
11. C. Wagner: Acta Met., 1973, vol. 21, pp. 1297-1303.
12. T. Chiang and Y. A. Chang: Met. Trans., 1976, vol. 7B, pp. 453-67; S. Kuo and Y. A. Chang: Met. Trans. in review.
13. H. H. Kellogg: Can. Met. Quart., 1969, vol. 8, pp. 3-23.
14. JANAF Thermochemical Tables, 2nd edn., National Bureau of Standards, 1971.
15. A. Yazawa and F. Schnalek: Freiberger Forschrift, 1967, vol. 118B, pp. 7-24.
16. T. Rosenqvist: Trans. AIME, 1949, vol. 185, pp. 451-60.
17. K. C. Mills: Thermodynamic Data for the Inorganic Sulfides, Selenides, and Tellurides, Butterworths, London, 1974, pp. 102-8.
18. R. Hultgren, P. D. Desai, D. T. Hawkins, M. Gleiser, and K. K. Kelley: Selected Values of the Thermodynamic Properties of Binary Alloys, ASM, Metals Park, 1973.

19. J. Gerlach, U. Hennig, and K. Trettin: Erzmetall, 1966, vol. 19, pp. 458-63.

20. A. N. Kristovnikov, A. Yu. Mendelevich, and V. M. Glazov: R. J. Inorg. Chem., 1968, vol. 4, pp. 1047-8.

21. P. Perrot and C. Jeannot: Rev. Chim. Miner., 1971, vol. 8, pp. 87-97.

22. L. L. Cheng: Ph.D. Thesis, University of London, 1959.

23. R. J. Fruehan and F. D. Richardson: Trans. TMS-AIME, 1969, vol. 245, pp. 1721-60.

24. N. Asano, K. Wase, and T. Nomura: Nippon Kogyo Kaishi, 1971, vol. 87, pp. 485-90.

25. K. Emicke: Erzmetall, 1962, 15, pp. 15-20.

26. U. V. Choudary and Y. A. Chang: unpublished research, 1976, to be submitted to Met. Trans.

27. U. V. Choudary and G. R. Belton: unpublished research, 1976, to be submitted to Met. Trans.

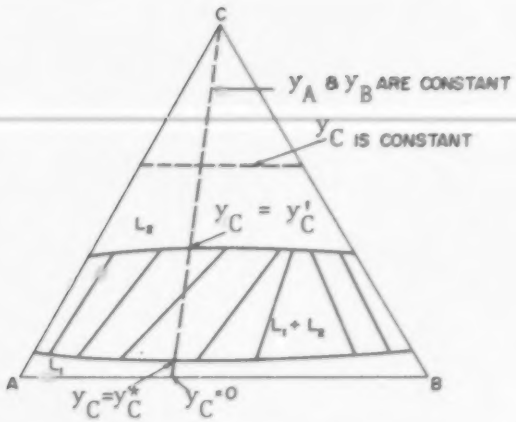

Fig. 1. A schematic of an isothermal section showing a miscibility gap in a ternary system A-B-C.

$$\text{Atom Ratio of i} = y_i \equiv \frac{n_i}{n_A + n_B} \equiv \frac{x_i}{1-x_C} \; ; \; y_B \equiv \xi; \; y_C = \eta$$

n_i - No. of atoms of the ith component; x - atom fraction.

'*' - Denotes the value at the metal-rich boundary

'′' - Denotes the value at the matal-deficient boundary

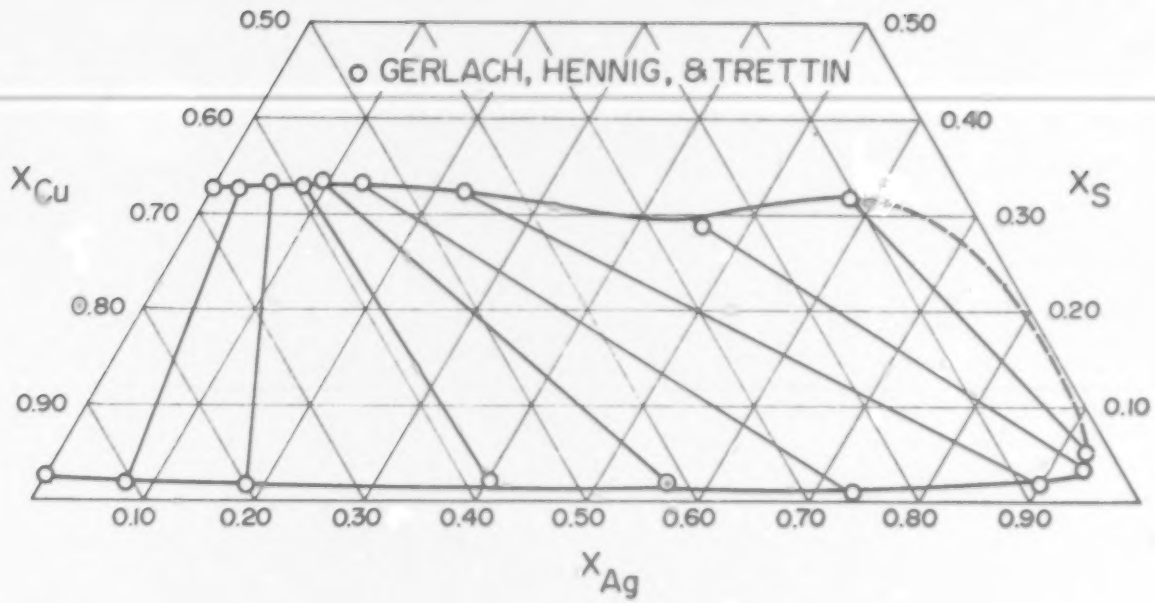

FIGURE 2. Experimental tie-line distributions along the ternary miscibility gap of the Cu-Ag-S system at 1473 K.

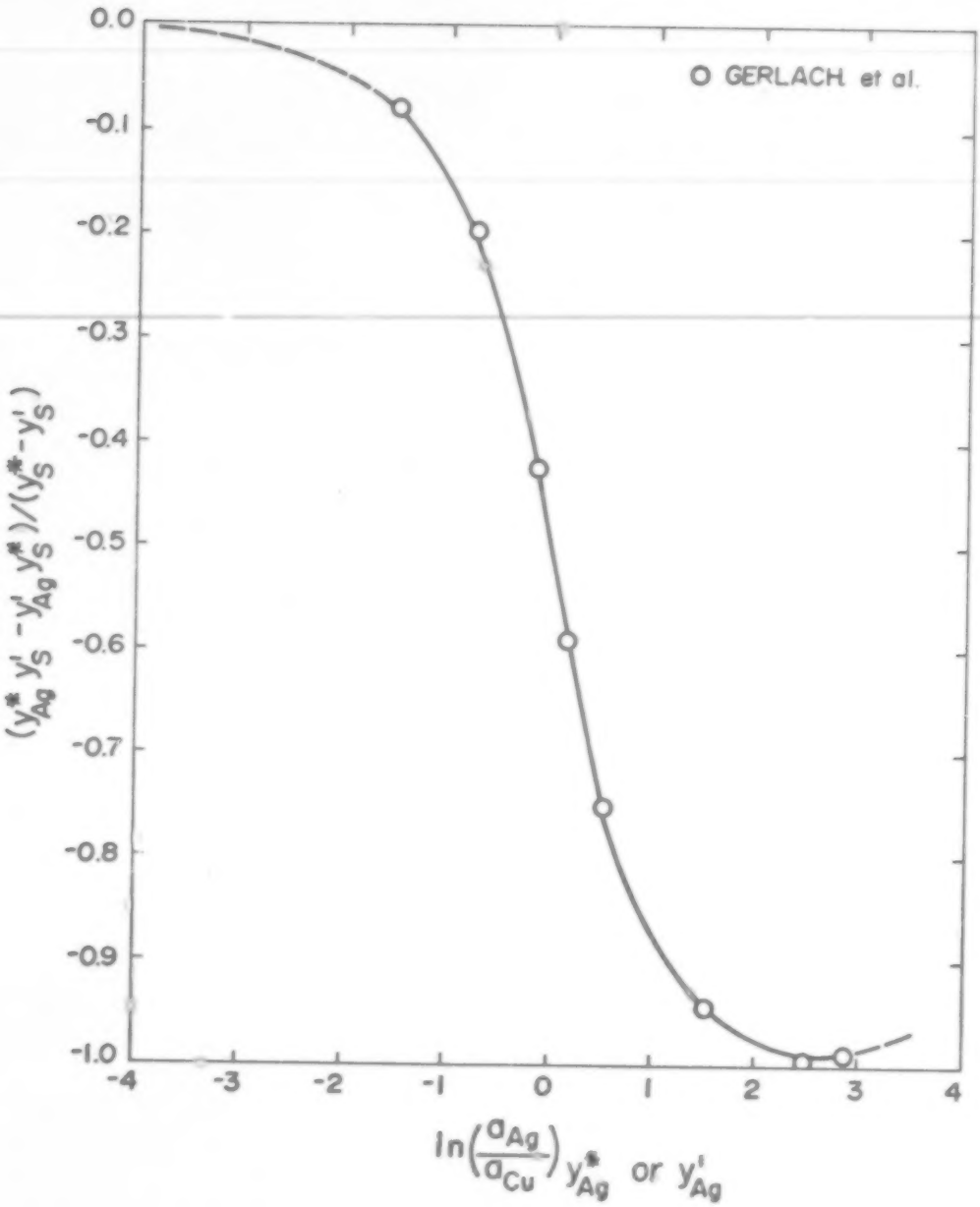

FIGURE 3. Integration plot for deriving the activities of copper and silver at 1473 K in the ternary miscibility gap of the Cu-Ag-S system.

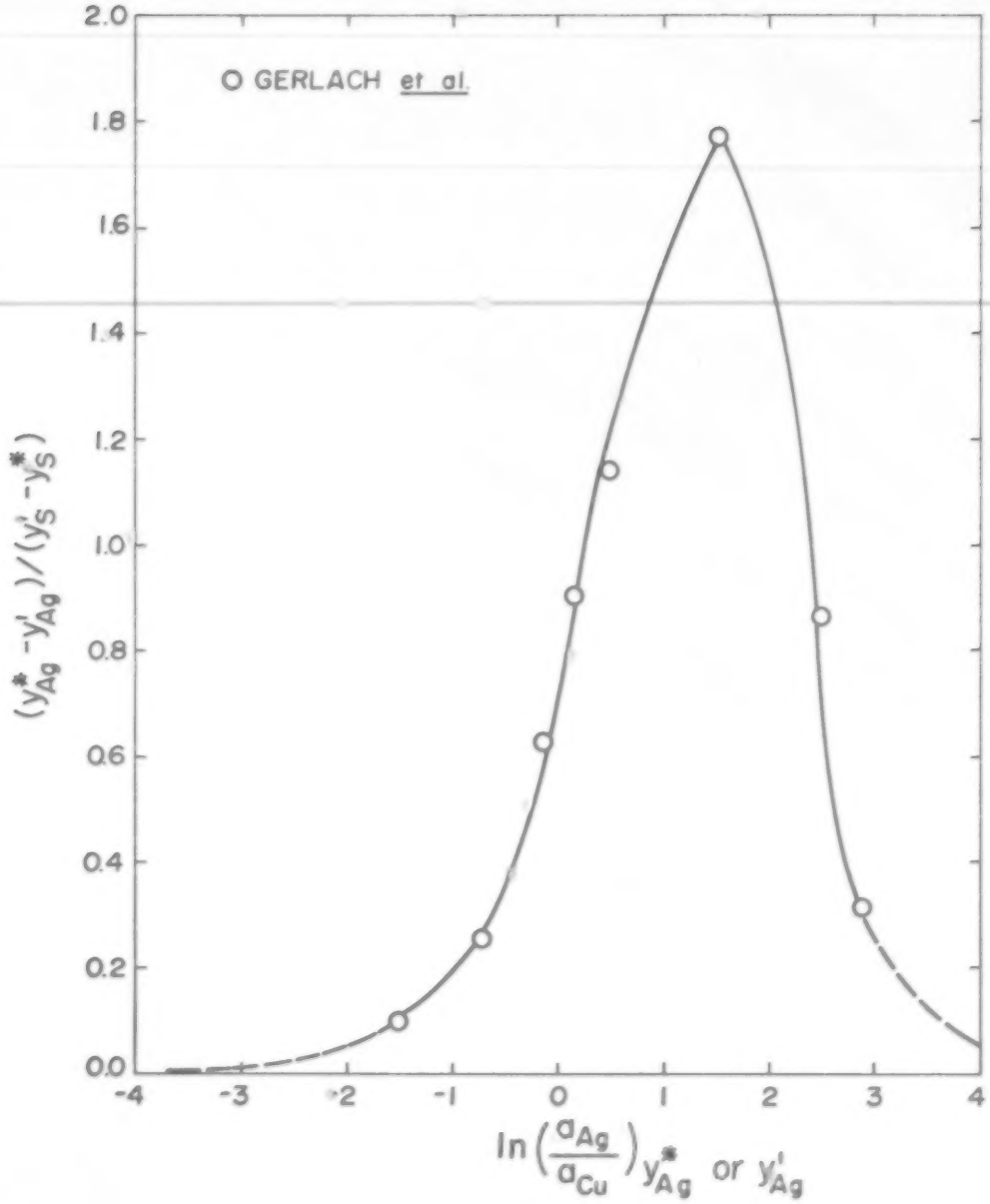

FIGURE 4. Integration plot for deriving the activities of sulfur at 1473 K in the ternary miscibility gap of the Cu-Ag-S system.

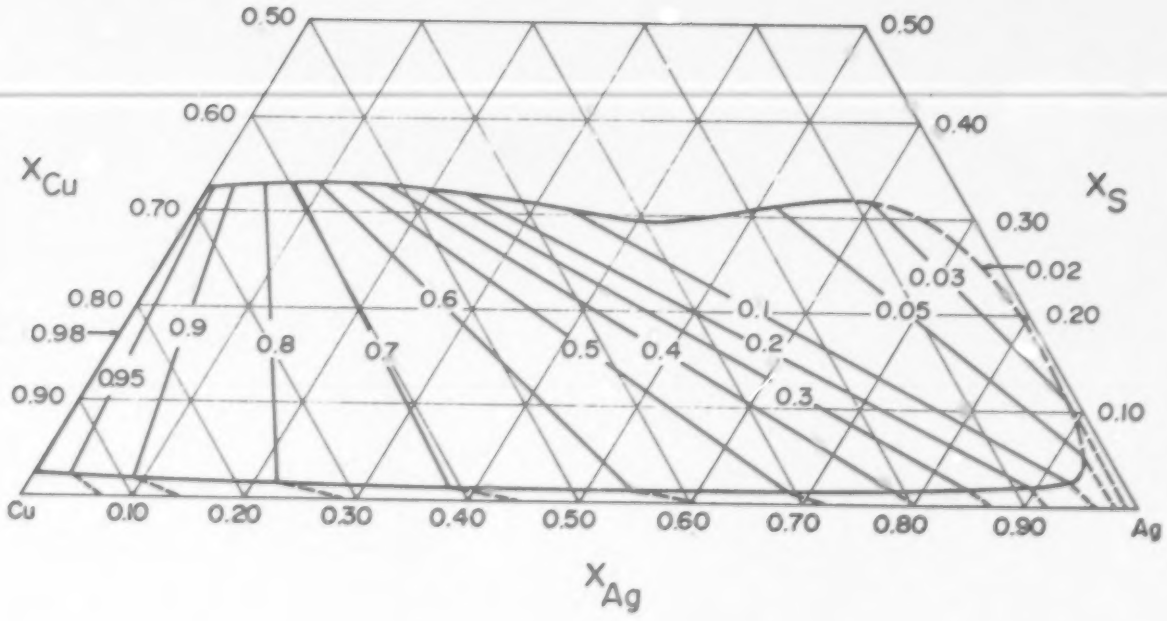

FIGURE 5. Isoactivities of copper in Cu-Ag-S melts at 1473 K (standard state: pure liquid copper).

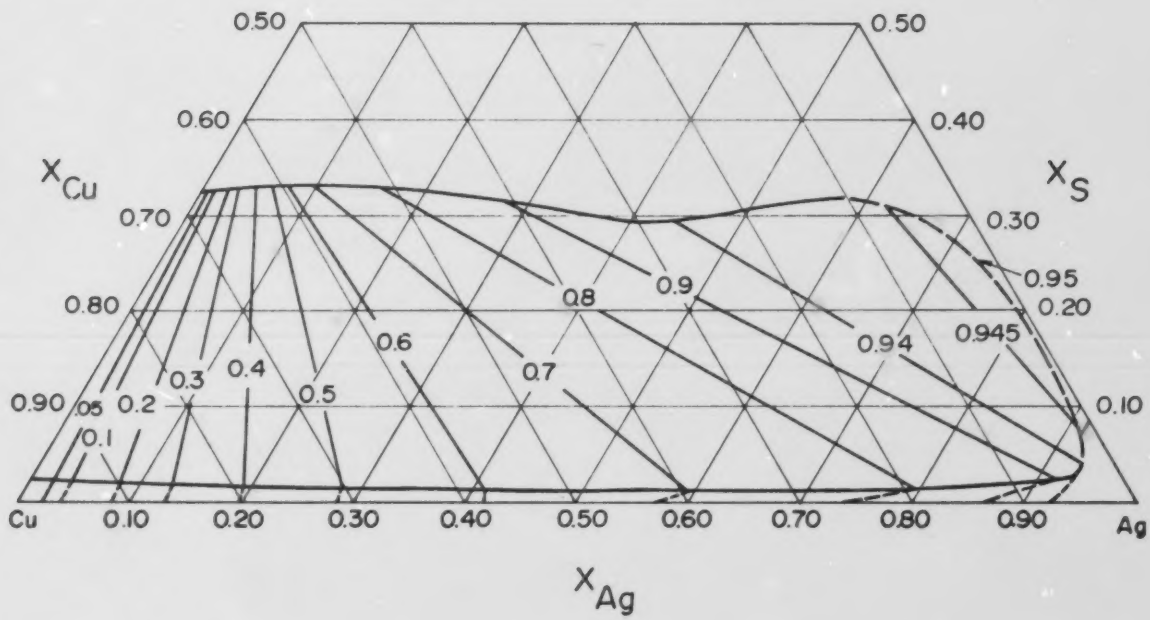

FIGURE 6. Isoactivities of silver in Cu-Ag-S melts at 1473 K (standard state: pure liquid lead).

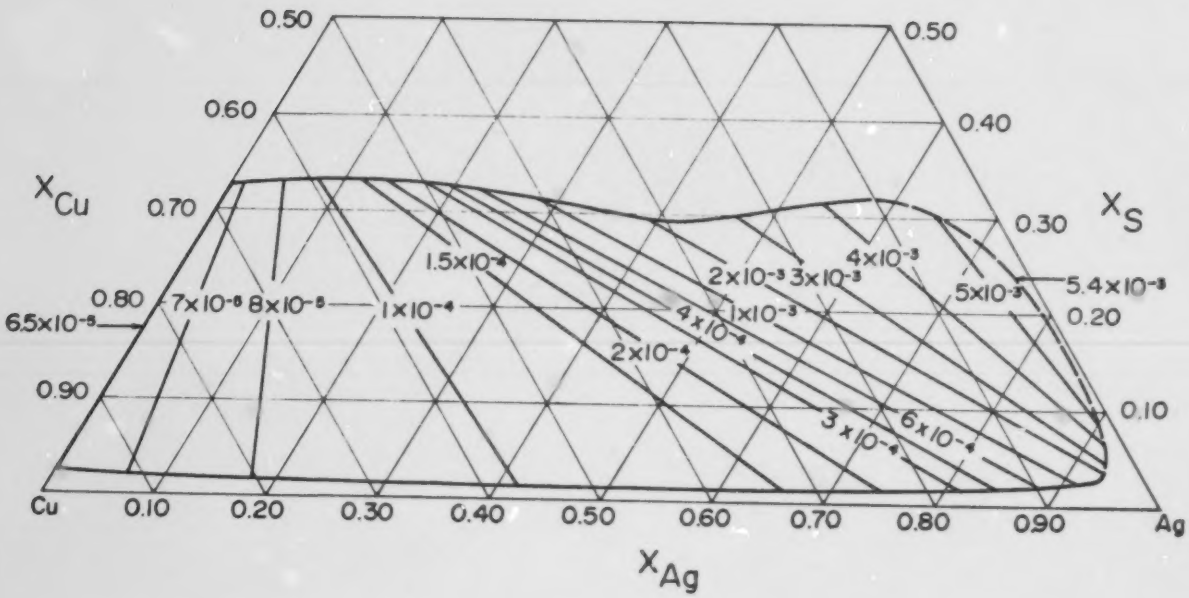

FIGURE 7. Isoactivities of sulfur in Cu-Ag-S melts at 1473 K (standard state: pure liquid sulfur).

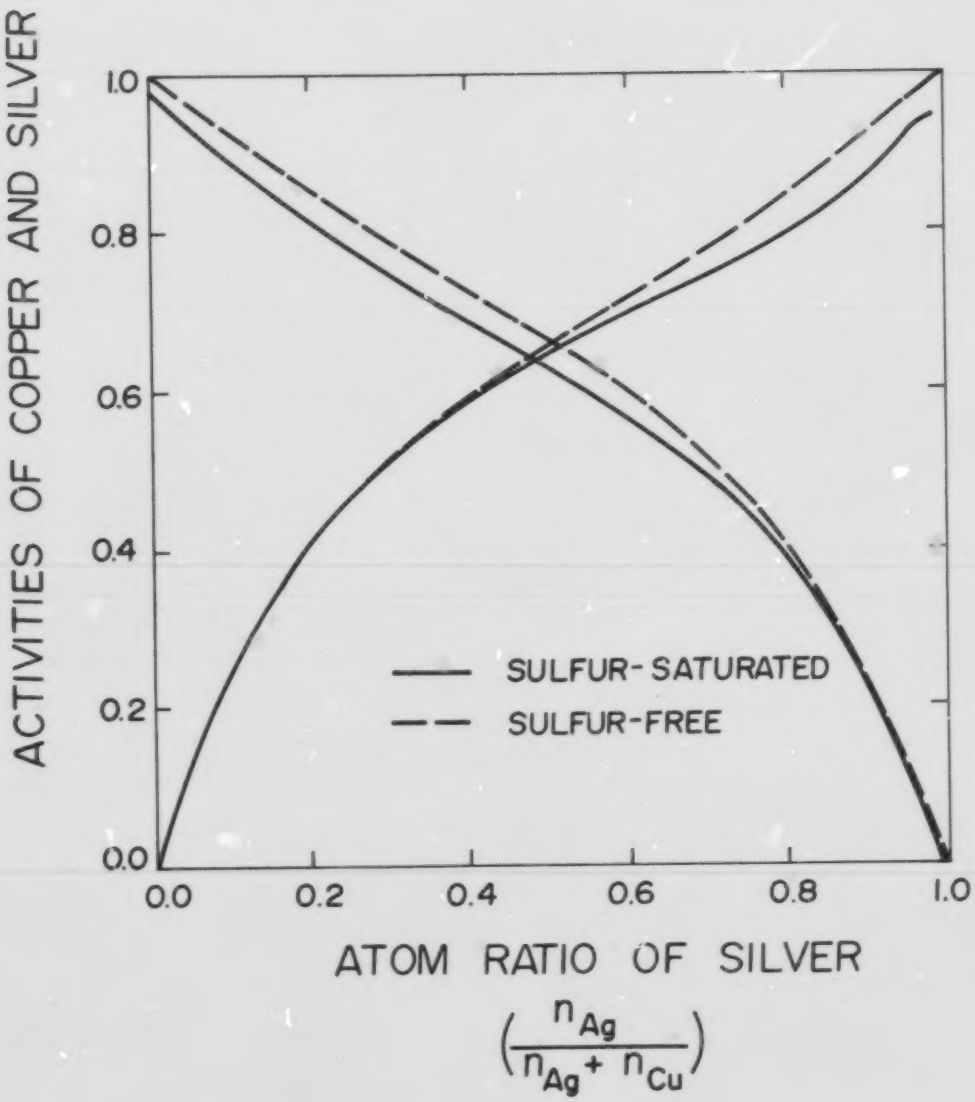

FIGURE 8. Activities of Cu and Ag in sulfur-free and sulfur-saturated copper-silver melts at 1473 K.

868

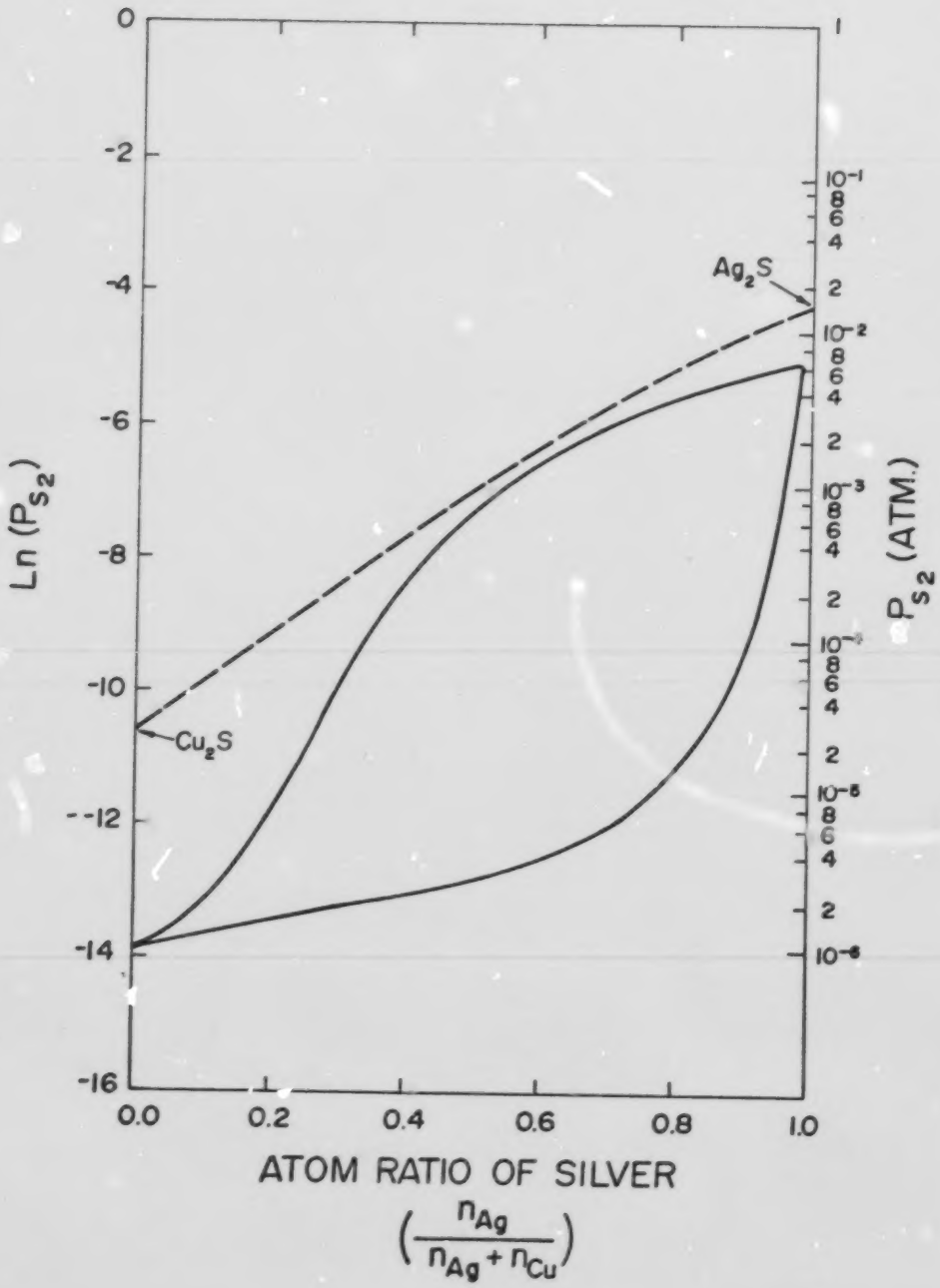

FIGURE 9. Sulfur potential as a function of atom ratio of silver along the ternary miscibility gap and the pseudo-binary section $CuS_{\frac{1}{2}}$-$AgS_{\frac{1}{2}}$ in the Cu-Pb-S system at 1473 K.

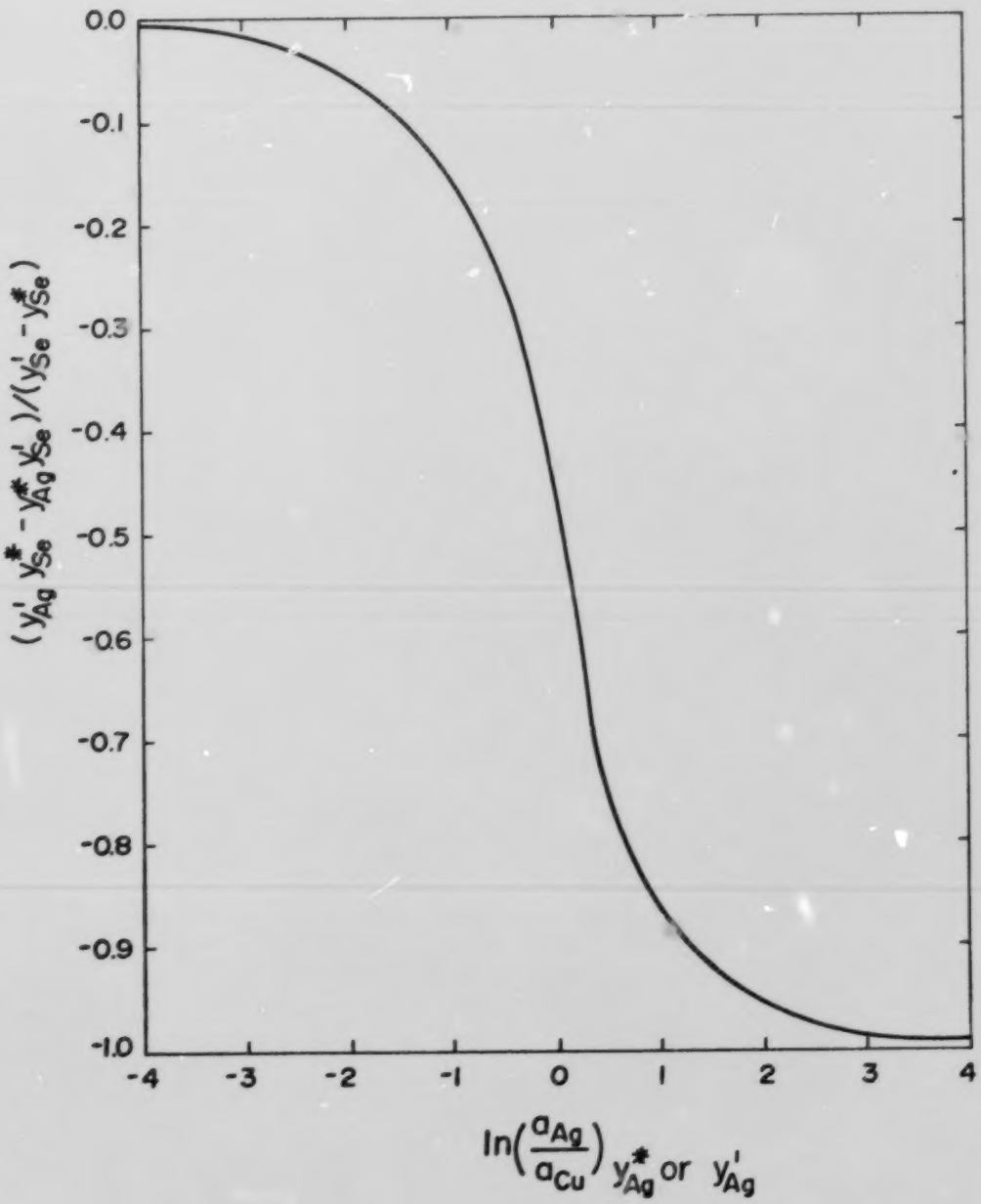

FIGURE 10. Integration plot for deriving the activities of copper and silver at 1473 K in the ternary miscibility gap of the Cu-Ag-Se system.

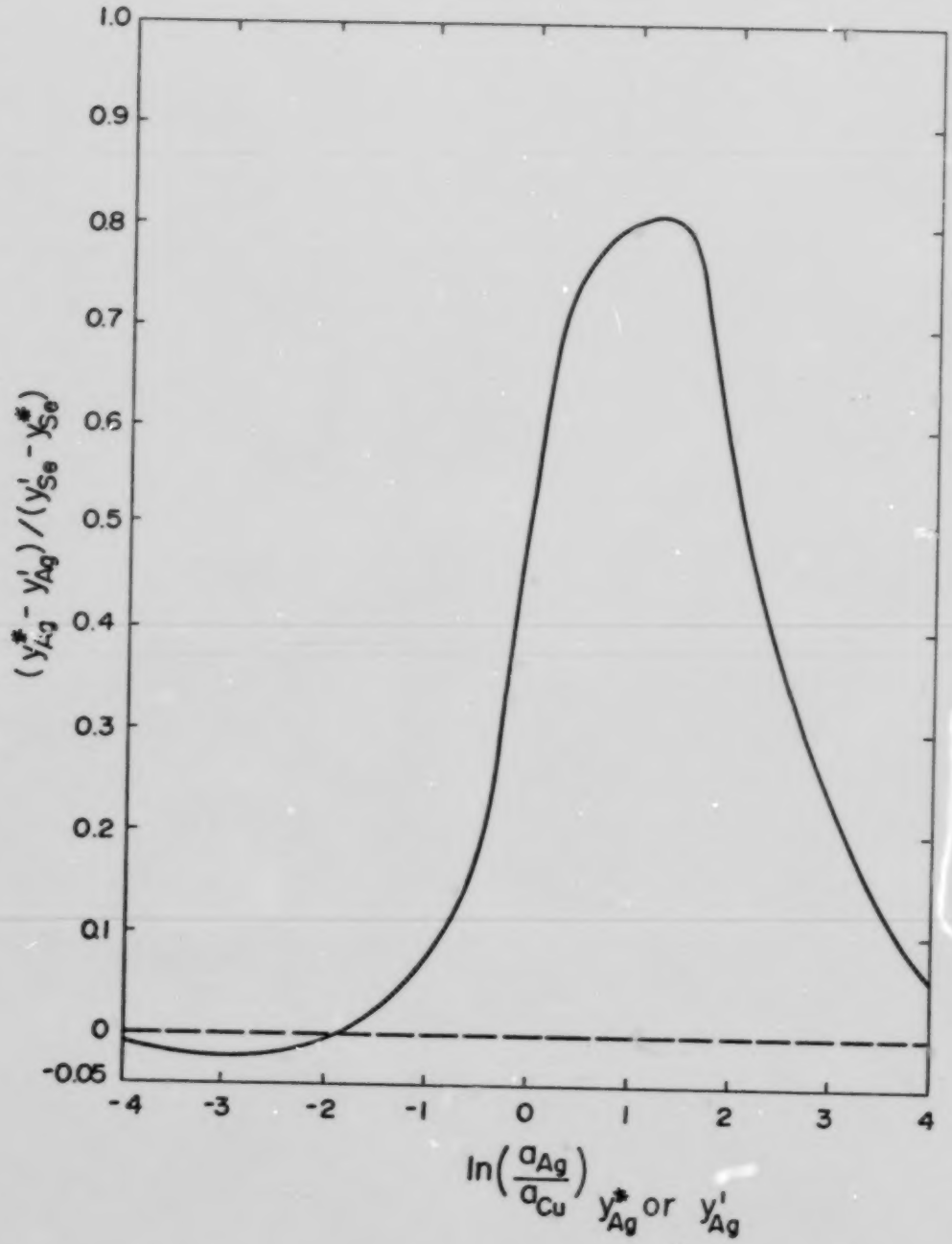

FIGURE 11. Integration plot for deriving the relative activities of selenium at 1473 K in the ternary miscibility gap of the Cu-Ag-Se system.

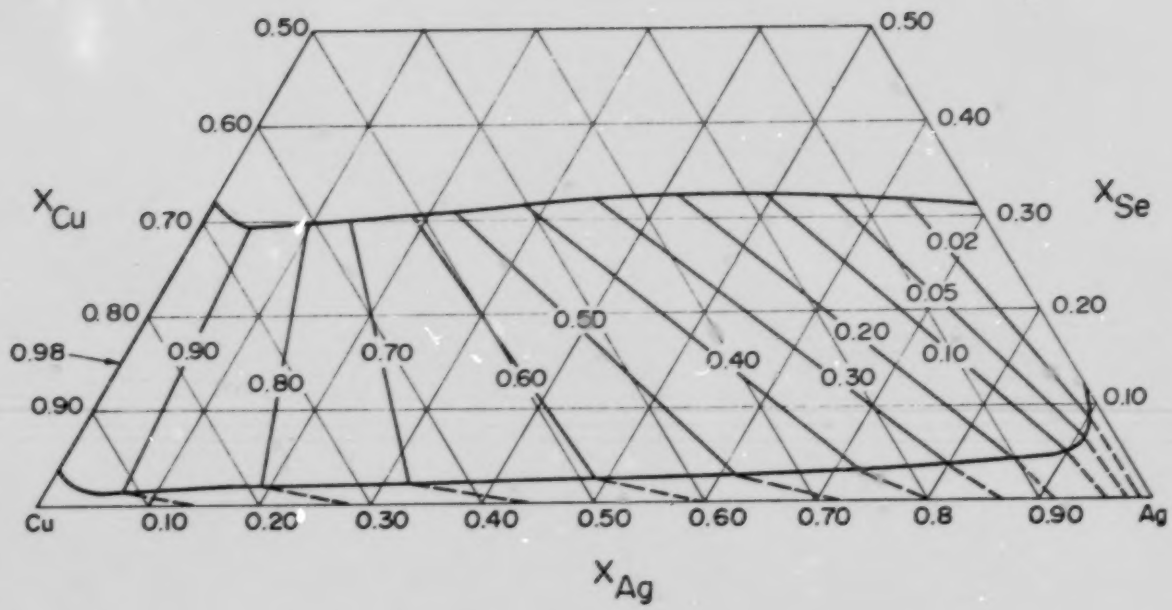

FIGURE 12. Isoactivities of copper in Cu-Ag-Se melts at 1473 K (standard state: pure liquid copper).

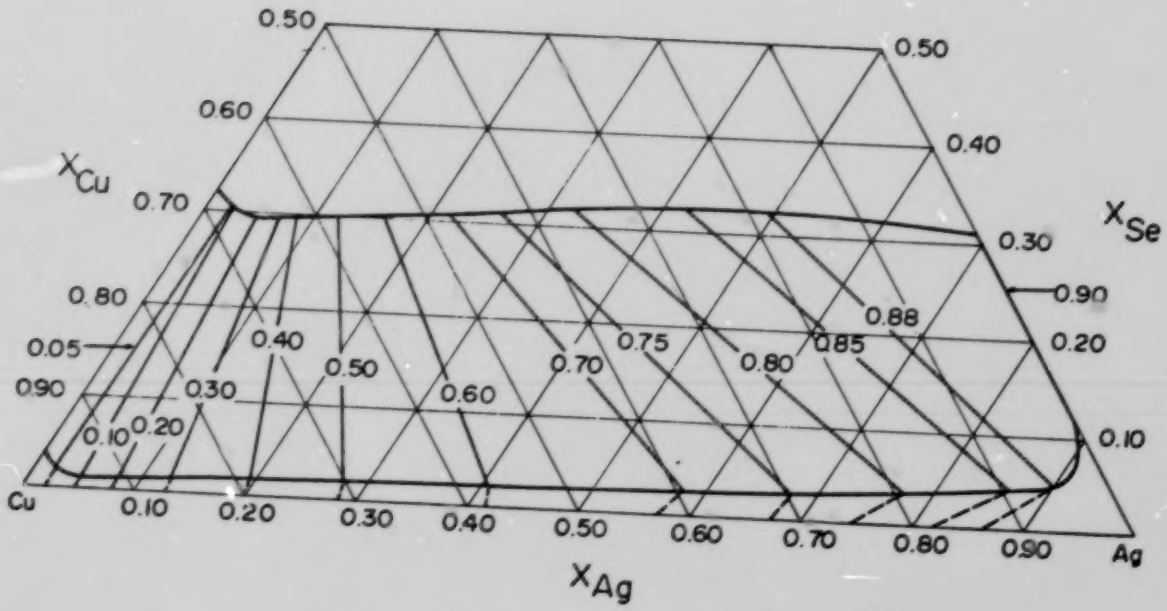

FIGURE 13. Isoactivities of silver in Cu-Ag-Se melts at 1473 K (standard state: pure liquid silver).

871

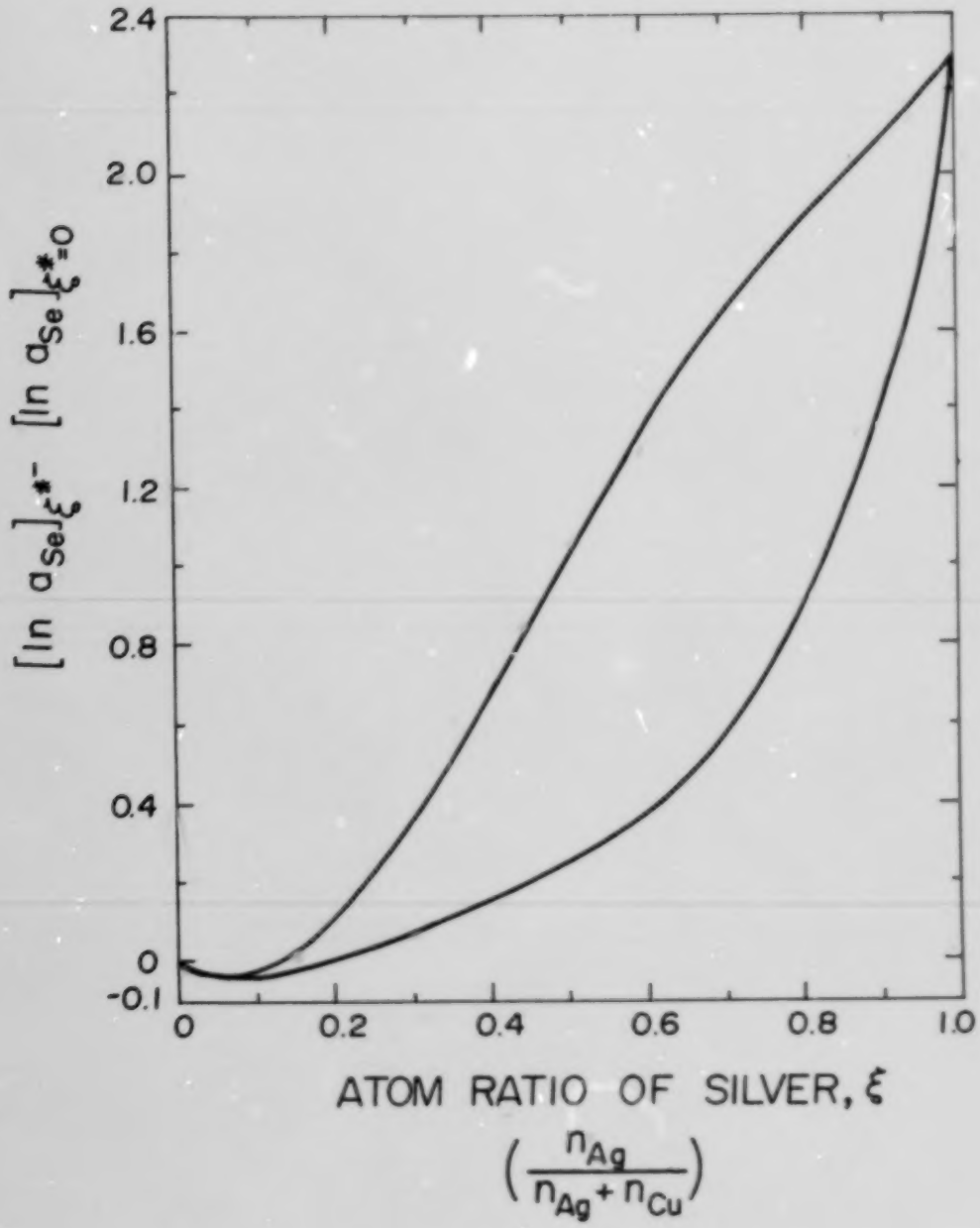

FIGURE 14. Relative activities of selenium in Cu-Ag-Se melts at 1473 K.

National Bureau of Standards SP-496, Applications of Phase Diagrams in Metallurgy and Ceramics
Proceedings of Workshop held at NBS, Gaithersburg, Md., January 10-12, 1977

THE MATHEMATICAL REPRESENTATION OF ACTIVITY DATA IN THREE COMPONENT SYSTEMS

Issac Eliezer and Reed A. Howald

Chemistry Department of Montana State University, Bozeman, Montana 59715

The activity coefficient of each species in a three component system (and other thermodynamic properties as well) can be expressed as a Redlich-Kister expansion in the sum of the other two mole fractions, $T = X_j + X_k$.

$$\log \gamma_i = T^2 \left[A_i + B_i(-3+4T)+C_i(-5+6T)(-1+2T)+D_i(-7+8T)(-1+2T^2+ \ldots \right]$$

The coefficients in this equation are functions of S defined as $X_j/(X_j+X_k)$, the Redlich-Kister coefficients for the three binary subsystems, and an additional set of parameters describing interactions of all three components at once (B_3^a, C_3^a, C_3^b, etc.).

Typical equations for the calculation of the coefficients A_i through H_i are shown. We have derived these equations, and programmed them for computer calculation. The operation of our computer program is described. By transforming the parameter matrix, activity coefficients and activities can be calculated and printed for each of the three components.

The terms which are required beyond those for the binary systems, B_3^a etc., correspond to equations for the excess quantities of mixing of the form:

$$Y^e = N_3^i \; X_1 \; X_2 \; X_3 \; T^{n-2} \; (-1+2S)^{i-1}$$

An alternative form with orthogonal functions is considered briefly.

The equations and programming have been checked by application to the solid and liquid phases in the iron-nickel-carbon system. Parameters are shown for several three component systems, and calculations of phase equilibria in three component systems are outlined and compared to the original experimental data.

As an example of the use a large quantity of data for a ternary system to determine the parameters in the equations, the system benzene - carbon tetrachloride - acetonitrile is analyzed.

INTRODUCTION --- The thermodynamic properties of solutions can be expressed as power series in the mole fractions. A variety of different power series have been proposed for binary systems, and an even wider range of choices is possible for three component systems. The selection among these choices will ultimately be made on the basis of convenience, assuming they all represent the thermodynamic properties to the same degree of accuracy. In this paper we wish to present a system of equations which makes full use of the expressions obtained for the three binary pairs making up the three component system, which is easily extended to include additional parameters for higher powers of mole fractions, and which is well adapted to computer calculation.

The Augmented Redlich-Kister Formalism. --- For reasons outlined in an accompanying paper[1] we have selected the Redlich-Kister equations[2] to express data for two component systems. These equations have the advantage that the same coefficients (the Redlich-Kister coefficients A, B, C, etc.) appear in expressions for each of the partial molal properties and for the excess functions of mixing, Y^e:

$$\bar{Y}_1 = X_2^2 \left[A_{12}+B_{12}(-1+4X_1) + C_{12}(-1+6X_1)(-1+2X_1) + D_{12}(-1+8X_1)(-1+2X_1)^2 \ldots\right] \quad (1)$$

$$\bar{Y}_2 = X_1^2 \left[A_{12}+B_{12}(-3+4X_1) + C_{12}(-5+6X_1)(-1+2X_1) + D_{12}(-1+8X_1)(-1+2X_1)^2 \ldots\right] \quad (2)$$

$$Y^e = X_1X_2\left[A_{12} + B_{12}(-1+2X_1) + C_{12}(-1+2X_1)^2 + D_{12}(-1+2X_1)^3 \ldots\right] \quad (3)$$

The quantity Y^e is defined as:

$$Y^e = X_1\bar{Y}_1 + X_2\bar{Y}_2 \quad (4)$$

These equations satisfy the Gibbs-Duhem relationship. They can be written in a variety of forms. For example: $-1+2X_1$ can be written in a variety of ways:

$$-1+2X_1 = X_1 - X_2 = 1-2X_2 \text{ etc.} \quad (5)$$

which are entirely equivalent in binary systems but are no longer equal when a third material is present. The proper expressions to use for three component solutions are the main concern of this paper, but for a start we can pick any two of the three mole fractions as independent variables, with the third determined from:

$$X_1 + X_2 + X_3 = 1 \quad (6)$$

The lowest power of mole fraction appearing in any of the expressions is 2, and there are three and only three independent quadratic terms in X_1 and X_2:

$$\bar{Y}_1 = AX_1^2 + A'X_1X_2 + A''X_2^2 + \ldots \quad (7)$$

Similarly there are only four independent cubic terms:

$$\bar{Y}_1 = \ldots + BX_1^3 + B'X_1^2X_2 + B''X_1X_2^2 + B'''X_2^3 + \ldots \quad (8)$$

five quartics etc. Thus the Redlich-Kister "A" values for the three binary systems are the only quadratic terms required, and the expression for Y^e to this degree of approximation can be written as:

$$Y^e = A_{12}X_1X_2 + A_{13}X_1X_3 + A_{23}X_2X_3 \tag{9}$$

It is desirable that three of the four cubic coefficients be B_{12}, B_{13}, and B_{23}, however one additional B coefficient is required. Similarly there will be two C's and three D's etc. beyond the values which are determined for the three binary subsystems. Thus we are led to consider an augmented Redlich-Kister formalism for three component systems.

The Redlich-Kister form for the B_{12} contribution to the activity coefficients in the two-component system is:

$$\log \gamma_1 = B_{12}X_2^2 (3-4X_2) + \ldots \tag{10}$$

and our initial expectation was to find an expression for $\log \gamma_1$ in the three-component system which was similarly a product of three terms. There is, however, nothing which factors this far and still satisfies the Gibbs-Duhem relationship. After a long period of trial and error we found a correct expression:

$$\log \gamma_1 = B_{12}X_2(2X_1-X_2-2X_1^2+2X_1X_2) \ldots \tag{11}$$

This equation has a somewhat neater appearance when written as a function of X_2 and X_3:

$$\log \gamma_1 = B_{12}\left[X_2^2(3-4X_2) + X_2X_3(2-6X_2-2X_3)\right]+\ldots \quad (12)$$

The corresponding equation for $\log \gamma_2$ and $\log \gamma_3$ are:

$$\log \gamma_2 = B_{12}\left[X_1^2 (-3+4X_1) + X_1X_3(-2+6X_1+2X_3)\right] \quad (13)$$

$$\log \gamma_3 = B_{12}X_1X_2(-2X_1+2X_2) \quad (14)$$

Equations 12 - 14 can be combined to give the contribution of B_{12} to G^e, the excess free energy of mixing:

$$G^e = X_1 \log \gamma_1 + X_2 \log \gamma_2 + X_3 \log \gamma_3 \quad (15)$$

$$G^e = B_{12} X_1X_2 (X_1-X_2) + \ldots \quad (16)$$

Similar expressions are valid for B_{13} and B_{23}

$$G^e = B_{13}X_1X_3 (X_1-X_3) + \ldots \quad (17)$$

$$G^e = B_{23} X_2X_3 (X_2-X_3) + \ldots \quad (18)$$

These expressions are simple enough to permit extrapolation to higher Redlich-Kister terms:

$$G^e = C_{12}X_1X_2(X_1-X_2)^2 + D_{12}X_1X_2(X_1-X_2)^3 + \ldots \quad (19)$$

Similarly, the extra terms give reasonably simple expressions for Y^e. For example, the extra B term which we can write as B_3^a, corresponds to an excess free energy of mixing which must go to zero when any one of the three mole fractions goes to zero. The simplest function with this behavior is $X_1X_2X_3$, so we may attempt:

$$G^e = B_3^a \; X_1X_2X_3 + \ldots \tag{20}$$

Expression for $\bar{Y}_i$ for the Redlich-Kister terms. --- From the definition for a partial molal quantity:

$$\bar{Y}_3 = \frac{\partial Y}{\partial n_3}\Bigg|_{n_1,\, n_2} \tag{21}$$

and the expression for Y in terms of Y^e:

$$Y = n_1Y_1^o + n_2Y_2^o + n_3Y_3^o + (n_1+n_2+n_3)\, Y^e \tag{22}$$

where Y^o is the molar value of the pure material, we can readily derive the relation between $\bar{Y}_3$ and Y^e:

$$\bar{Y}_3 = Y_3^o + Y^e + (n_1+n_2+n_3)\; \frac{\partial Y^e}{\partial n_3}\Bigg|_{n_1,n_2} \tag{23}$$

The only complication is in taking the partial derivative. This is easiest if we write Y^e as a function of $S \equiv X_1 / (X_1+X_2)$ and (24)

$T \equiv 1-X_3 = X_1 + X_2$. The choice of these independent variables is dictated by the advisability of having one variable closely related to n_3, and one which is unchanged as n_3 varies holding n_1 and n_2 constant. Then one can rewrite the partial derivative: (25)

$$\left.\frac{\partial Y^e}{\partial n_3}\right|_{n_1,n_2} = \left.\frac{\partial Y^e}{\partial T}\right|_{S} \qquad \left.\frac{\partial T}{\partial n_3}\right|_{n_1,n_2} \tag{26}$$

$$= (dY^e/dT)\ \frac{-(n_1+n_2)}{(n_1+n_2+n_3)^2} \tag{27}$$

$$= (dY^e/dT)\ (-T)\ (1/(n_1+n_2+n_3) \tag{28}$$

The expression for $\bar{Y}_3 - Y_3^o$ is then :

$$\bar{Y}_3 - Y_3^o \doteq Y^e - T(dY^e/dT) \tag{29}$$

The general expressions for Y^e from equation 19 are :

$$Y^e = N_{12}\, X_1X_2\, (X_1 - X_2)^n + \ldots \tag{30}$$

$$Y^e = N_{13}\, X_1X_3\, (X_1 - X_3)^n + \ldots \tag{31}$$

$$Y^e = N_{23}\, X_2X_3\, (X_2 - X_3)^n + \ldots \tag{32}$$

which can be rewritten using:

$$X_1 = ST \tag{33}$$

$$X_2 = (1-S)T = T-ST \tag{34}$$

$$X_3 = 1-T \tag{35}$$

as:

$$Y^e = N_{12}\, T^{n+2}\, S(1-S)(-1+2S)^n + \ldots \tag{36}$$

$$Y^e = N_{13}\, T(1-T)(-1+T+ST)^n S + \ldots \tag{37}$$

$$Y^e = N_{23}\, T(1-T)(-1+2T-ST)^n\, (1-S) + \ldots \tag{38}$$

Equation 36 is easy to differentiate, giving:

$$\bar{Y}_3 - Y_3^o = N_{12}\, (S)(1-S)(-1+2S)^n\, (T^{n+2} - T(n+2)T^{n+1}) + \ldots \tag{39}$$

$$\bar{Y}_3 - Y_3^o = N_{12}\, (S)(1-S)(-1+2S)^n\, (n+1)(-1)\, T^{n+2} + \ldots \tag{40}$$

The other two derivations are somewhat more involved, but eventually lead to the equations:

$$\bar{Y}_3 - Y_3^o = N_{13}\, S\, T^2\, (-1+T+ST)^{n-1}\, (-1-n-nS+T+ST+nST) + \ldots \tag{41}$$

$$\bar{Y}_3 - Y_3^o = N_{23}\, (1-S)\, T^2\, (-1+2T-ST)^{n-1}\, (-1+2n+nS+2T+2nT-ST-nST) \tag{42}$$

It is useful to convert these power series in T to the Redlich-Kister form:

$$\bar{Y}_3 - Y_3^o = T^2 \left[A_3' + B_3' (-3+4T) + C_3' (-5+6T)(-1+2T) + \ldots\right] \qquad (43)$$

and each of the Redlich-Kister coefficients from the binary systems will make a contribution to the "pseudobinary" Redlich-Kister coefficient, A_3', B_3', etc. The transformation from power series into Redlich-Kister coefficients can be accomplished by multiplying by the upper triangular matrix $\mathbb{L}^{-1}$ shown in Table 1. The denominators of the fractions in Table 1 are simply $n2^{(n-1)}$ and come directly from the Redlich-Kister equations. The numerators can be calculated by starting with 1 along the diagonal and adding successive binomial coefficients, $n!/i!(n-i)!$.

Thus the T^{n+2} appearing in equation 40 transforms into columns of Table 1 multiplied by appropriate factors. These results are shown in Table 2.

Equations 41 and 42 contain numerous powers of T with complex coefficients and the transformation is more difficult. This transformation has not yet been accomplished for the general n^{th} term, but the first eight terms transform to the simple expressions shown in Tables 3 and 4 and these relations can probably be extrapolated indefinitely.

The extra terms of the augmented Redlich-Kister formalism. -- Just as one has a choice for binary systems between using the Margules, Redlich-Kister, and Bale-Pelton equations, one has a choice between power series in mole fractions, simple powers of T and S, or orthogonal power series in expressing the experimental data on three component system. The extra terms beyond those which can be evaluated for the three binary substems can all be represented by terms for the excess quantity of mixing which can be written as:

$$Y^e = NX_1 X_2 X_3 F(a, b) + \ldots \tag{44}$$

where F is a function of two concentration variables. The first term, for which we have used the coefficient B_3^a, has simply F=1:

$$Y^e = B_3^a X_1 X_2 X_3 + \ldots \tag{45}$$

The simplest symmetrical first power term is $X_1 - X_2 = T(-1+2S)$, giving:

$$Y^e = C_3^b X_1 X_2 X_3 (X_1 - X_2) = C_3^b X_1 X_2 X_3 T(-1+2S) \tag{46}$$

The function $X_1 - X_2$, is part of an E pair of functions in the C_{3v} symmetry of this problem. The other part, orthogonal to this, is $-\frac{1}{3} + X_3$, possibly multiplied by a suitable normalization constant. Our initial treatment of a three component system using C terms[3] gave equations which correspond to:

$$Y^e = C_{321} X_1 X_2 X_3 (-\tfrac{1}{3} + X_3) + \ldots \tag{47}$$

However, when this is converted to showing F as a function of S and T, one gets:

$$Y^e = C_{321} X_1 X_2 X_3 (\tfrac{2}{3} - T) + \ldots \tag{48}$$

and it is considerably more convenient to use a linear combination of equations 45 and 48, which eliminates the constant, $\frac{2}{3}$.

$$Y^e = C_3^a X_1 X_2 X_3 T + \ldots \tag{49}$$

The relations between our older[3] and new terminology can be written as:

$$C_{123} = C_3^b \tag{50}$$

$$B_{123} = B_3^a - (\tfrac{2}{3})C_3^a \tag{51}$$

$$C_{321} = (\tfrac{1}{3})C_3^a \tag{52}$$

The D terms can all be written with T^2:

$$Y^e = D_3^a X_1X_2X_3 T^2 + \ldots \quad (53)$$

$$Y^e = D_3^b X_1X_2X_3 T^2(-1+2S) + \ldots \quad (54)$$

$$Y^e = D_3^c X_1X_2X_3 T^2(-1+2S)^2 + \ldots \quad (55)$$

Here the alphabetical superscript (i in D_3^i) corresponds to the power of -1+2S appearing in the equation. This form and notation can be extended indefinitely:

$$Y^e = E_3^d X_1X_2X_3 T^3(-1+2S)^3 + \ldots \quad (56)$$

$$Y^e = H_3^d X_1X_2X_3 T^6(-1+2S)^3 + \ldots \quad (57)$$

The sacrifice of orthogonality and even correct C_{3v} symmetry in this formulation is more than compensated by the ease of manipulation of the equations in these relatively simple forms. For example; the second orthogonal function of A symmetry is:

$$F(a,b) = X_1^2 + X_2^2 + X_3^2 - \tfrac{1}{2} \quad (58)$$

$$F(a,b) = \tfrac{1}{6}\left[(2-3T)^2 + 3T^2(-1+2S)^2 - 1\right] \quad (59)$$

This not only involves all three powers of T, which is a nuisance in converting to the pseudobinary Redlich-Kister form, but it cannot be

factored into a function of S times a function of T. If this form is used, the various pseudobinary Redlich-Kister terms will be different and complex functions of S. On the other hand, expressions of the form:

$$Y^e = N_3^m X_1 X_2 X_3 \, T^n(-1+2S)^m + \ldots \tag{60}$$

are readily converted into the pseudobinary form. First they are rewritten as a function of S and T only:

$$Y^e = N_3^m S(1-S)(1-T)T^{n+2}(-1+2S)^m + \ldots \tag{61}$$

This equation can be differentiated and equation 29 then gives:

$$\bar{Y}_3 - Y_3^o = N_3^m S(1-S)(-1+2S)^m \left[(n+2)T^{(n+2)} - (n+1)T^{(n+1)} \right] \tag{62}$$

This expression is easily converted into the pseudobinary form using Table 1. The functions of S carry through unchanged, being simply multiplied by the binomial coefficient divided by 2^n. Table 5 shows the values for the first eight extra terms, and the extension to further terms is clear.

Tables 2 through 5 outline a method for calculation log γ_3 for a particular composition of the ternary system. Log γ_1 and log γ_2 can be calculated using the same equations and the same computer program if one firsts renumbers the components as:

$$1 \rightarrow 2$$
$$2 \rightarrow 3 \qquad (63)$$
$$3 \rightarrow 1$$

As a result of this renumbering A_{12} becomes A_{23}, A_{13} becomes $A_{21} = A_{12}$ and A_{23} becomes $A_{31} = A_{13}$. The transformations of the B_{ij}'s are:

$$B_{12} \rightarrow B_{23}$$
$$B_{13} \rightarrow B_{21} = -B_{12} \qquad (64)$$
$$B_{23} \rightarrow B_{31} = -B_{13}$$

The same kinds of transformations occur for all the N_{ij} with sign changes for the even numbered ones, B, D, F, H, etc.

The transformation of the extra, N_i^m, terms is somewhat more complicated. In choosing powers of $(1-X_3)$ and $(X_1 - X_2)$ to express Y^e, we have picked one material as special, and a substantial transformation is required to change to $(1-X_2)$ and $(X_3 - X_1)$ for the independent variables. Even if we chose symmetry adapted expressions for Y^e, we would need a transformation of this type for the terms of E symmetry since they are neither symmetric nor antisymmetric with respect to the rotations of 120°. The transformation matrix **M** to convert the N_3^m coefficients to N_2^m (ready to claculate $\log Y_2$) is the matrix specified by the equation:

$$\left| B_2^a\ C_2^a\ C_2^b\ D_2^a\ D_2^b\ D_2^c\ E_2^a \ldots \right\rangle = \mathbf{M} \left| B_3^a\ C_3^a\ C_3^b\ D_3^a\ D_3^b \ldots \right\rangle \qquad (65)$$

The first 10 x 10 portion of the matrix $\mathbf{M}$ is shown in Table 4. The individual columns are not difficult to evaluate. One must multiply out $(1-\frac{1}{2}T-\frac{1}{2}ZT)^m\ (-1+\frac{3}{2}T-\frac{1}{2}ZT)^h$ and collect powers of Z and T.

It is not likely that more than 10 of these extra coefficients will be required in practice. Our current computer program will handle 28 of these coefficients together with up to 24 Redlich- Kister coefficients for the three binary subsystems (8 each).

The section of this computer program for the calculation of Redlich- Kister coefficients (BETA (IK, I, I2)) for pseudobinary systems is shown in Table 7. The parameters used for the calculation are stored in the matrix form shown in Table 6.

Evaluation of constants. --- There are two ways to approach the problem of finding values for the coefficients in an augmented Redlich-Kister treatment of a ternary system. For systems close to ideal or which otherwise involve only a small number of coefficients, one can best start with data for the binary subsystems, and then evaluate B_3^a, C_3^a, and C_3^b from a few experiments with all three materials present. This approach will break down if there are many extra coefficients to determine. When a lot of experimental data is required, the best way to organize it is probably to consider the data for a particular ratio of two mole fractions at one time, and obtain pseudobinary Redlich-Kister coefficients for a whole series of values of S. We will illustrate these two approaches with appropriate examples.

The solid gamma Fe-Ni system is close enough to ideal that the enthalpy and activity coefficient data can be well represented by two Redlich-Kister coefficients.[3] The Fe-C and Ni-C systems are very far from ideal, but the limited solubility of graphite in these metals[4] means that all the data is over a small concentration range. For this reason the data requires at the most, three Redlich-Kister coefficients for a fit within experimental error. We have recently reexamined[3] the data on these three subsystems to obtain the N_{ij} values shown in Table 9. Then the values of B_3^a and C_3^b were obtained by selecting two compositions for which the activity coefficient of carbon was known. Using

$B_3^a = 0$ and $C_3^b = 0$, we calculated log γ_3 for carbon from the values for Redlich-Kister coefficients for all the binary subsystems. The difference between the experimental[5] and calculated values for log γ_3 then gives an equation for B_3^a and C_3^b.

$$\log \gamma_{exp} - \log \gamma_{calc} = B_3^a(1-X_3)^2(S)(1-S)(-5-.5(-1+4X_3)) + C_3^b(1-X_3)^2 \quad (66)$$

$$(S)(1-S)(-1+2S)(.25+.50(-1+4X_3)+.25(-1+6X_3)(-1+2X_3))$$

B_3^a and C_3^b can be calculated form two equations of this type, giving the values $B_3^a = -3.75$ and $C_3^b = -.40$.

The liquid Fe-Ni-C system was treated similarly, however in this case there is additional data on the activity of iron in solutions saturated with carbon,[6] and it is possible to estimate C_3^a in addition. These values are shown in Table 10.

If one needs only three extra coefficients and there are measurements of all three activities at $X_1 = X_2 = X_3 = 1/3$, then one can evaluate them from the three equations:

$$\log \gamma_3 - \log \gamma'_3 = -(1/27)(B_3^a) \quad (67)$$

$$\log \gamma_2 - \log \gamma'_2 = -(1/27)(B_3^a + C_3^a - C_3^b) \quad (68)$$

$$\log \gamma_1 - \log \gamma'_1 = -(1/27)(B_3^a + C_3^a + C_3^b) \quad (69)$$

We can illustrate the systematic treatment of a large quantity of data on the activity of one material in a three component system by a consideration of the system benzene - carbon tetrachloride - acetonitrile. This system was chosen because there is a substantial amount of good data available[7], and also because there are statements in the literature[7, 8] that the coefficients for the binary subsystems in this case adequately represent the ternary data. For liquids in this system it is easy to measure the total vapor pressure and the composition of the equilibrium vapor. Hence, one can calculate partial pressures for each component, but we will consider here only the information on the activity of acetonitrile since in many systems, one activity can be measured more accurately than the others. It is customary to correct for non-ideality of the vapor using the equation:

$$\log \gamma_3 = \log(Y_3 P/X_3 P_3^o)+(1/2.303\ RT)\quad (B_{33}-V_3^o)(P-P_3^o) + P(S_{13}Y_1(1-Y_3) + S_{23}Y_2(1-Y_3) - S_{12}Y_1Y_2 \qquad (70)$$

developed by Scatchard[8] where Y_i stands for mole fractions in the vapor and X_3 is the mole fraction of acetonitrile in the liquid. Values for B_{33} and S_{ij} are given in reference 7, and the calculation of $\log \gamma_3$ at each experimental composition in Table II of reference 7 is quite straightforward. For each composition one must also calculate $S = X_{\text{benzene}} / (X_{\text{benzene}} + X_{\text{carbon tetrachloride}})$. The data points are grouped around certain S values, however to bring them to exactly constant values of S as in Table 11, one must interpolate. The interpolation was performed

linearly between two experimental points or between an experimental point and a calculated value for log γ_3 at S = 0 or S = 1.0. The corrected data in Table 11 were then fitted to a Redlich-Kister expansion:

$$\log \gamma_3 = (1-X_3)^2(A'_3 + B'_3(1-4X_3) + C'_3(1-6X_3)(1-2X_3) + \ldots) \quad (71)$$

using four terms at each S value. The values of A'_3, B'_3, C'_3, and D'_3 obtained are plotted against S in figures 1 through 4. The extreme scatter for D'_3 in figure 4 suggests that the fourth term is not really necessary to fit the data for most S values. The data at S = .59 is clearly less accurate than that at other values, and these points are omitted from the graphs and from the fitting procedure.

The A'_3 values have contributions from every parameter used as indicated in Tables 2 through 5. Fortunately, the S dependencies are all quite simple except for the N_{13} and N_{23} terms which should be well known from data on these two binary mixtures. We can thus calculate A'_3(corrected)by subtracting contributions from A_{13}, B_{13}, C_{13}, D_{13}, A_{23}, B_{23}, C_{23}, and D_{23}:

$$A'_3(\text{corrected}) = A'_3 - A_{13}(S) + B_{13}(1/2)(S)(1-S) - C_{13}(1/4)(S)(1-S)^2 \quad (72)$$

$$+ D_{13}(1/8)(S)(1-S)^3 - A_{23}(1-S) + B_{23}(1/2)(1-S)(S)$$

$$- C_{23}(1/4)(1-S)(S)^2 + D_{23}(1/8)(1-S)(S)^3$$

The extension of equation 72 to cases where E and F terms are needed for the binary subsystem is quite straightforward.

The values obtained for A_3'(corrected) are then fitted to a Redlich-Kister type expansion in powers of (-1+2S)

$$A_3'(\text{corrected}) = (S)(1-S)\left[A_a + B_a(-1+2S) + C_a(-1+2S)^2 + \ldots\right] \tag{73}$$

and the coefficients in this expansion are simple functions of the remaining parameters:

$$A_a = -A_{12} + (1/2)B_3^a + (1/4)C_3^a + (1/8)D_3^a \tag{74}$$

$$B_a = -(3/2)B_{12} + (1/4)C_3^b + (1/8)D_3^b \tag{75}$$

$$C_a = -(7/4)C_{12} + (1/8)D_3^c \tag{76}$$

etc. The coefficients in these equations come from Tables 2 and 5. In this particular case, A_3'(corrected) is well fitted by $A_a = -.2418$ and $B_a = -.2125$. No C_a term is needed, and so $D_3^c = 0$. This is a further indication (beyond the scatter in figure 4) that D_3^n terms are not required in this ternary system. Since A_{12} and B_{12} are known, only one additional equation is required:

$$A_b = .0158 = (1/2)B_3^a + (1/2)C_3^a \tag{77}$$

to evaluate:

$$B_3^a = -.7904 \tag{78}$$

$$C_3^a = .8220$$

$$C_3^b = -.8464$$

completing the full set of coefficients for the ternary system benzene-carbon tetrachloride - acetonitrile listed in Table 12. The solid lines in Figures 1-4 are values for A_3', B_3', etc., calculated from the constants in Table 12. One is likely to encounter more complex systems where equations 74 through 76 have 9 unknowns, and the full set of additional equations 81-87 may be needed. These equations come from similar corrections of B_3', C_3' etc., for contributions from N_{13} and N_{23}:

$$B_3'(\text{corrected}) = B_3' - (1/2)B_{13}(S)(1+S) + (1/2)C_{13}(S)(1+S)(1-S) - (3/8)D_{13}(S)(1+S)(1-S)^2 - B_{23}(1/2)(1-S)(2-S) + C_{23}(1/2)(1-S)(2-S)(S) - D_{23}(3/8)(1-S)(2-S)(S)^2 \quad (79)$$

$$C_3'(\text{corrected}) = C_3' - C_{13}(1/4)(S)(1+S)^2 + D_{13}(3/8)(S)(1+S)(1-S) - C_{23}(1/4)(1-S)(2-S)^2 + D_{23}(3/8)(1-S)(2-S)^2(S) \quad (80)$$

The coefficients and functions of S in equations 79 and 80, are taken from tables 3 and 4. The corrected values B_3', C_3' etc., are then fitted to power series like:

$$B_3'(\text{corrected}) = S(1-S)\left[A_b + B_b(-1+2S) + C_b(-1+2S)^2 + \ldots\right] \quad (81)$$

and the equations for A_b, B_b, and A_c etc., are obtained from Tables 2 and 5:

$$A_b = (1/2)B_3^a + (1/2)C_3^a + (3/8)D_3^a \tag{82}$$

$$B_b = -(1/2)B_{12} + (1/2)C_3^b + (3/8)D_3^b \tag{83}$$

$$C_b = -(4/4)C_{12} + (3/8)D_3^c \tag{84}$$

$$A_c = (1/4)C_3^a + (3/8)D_3^a \tag{85}$$

$$B_c = (1/4)C_3^b + (3/8)D_3^b \tag{86}$$

$$C_c = -(1/4)C_{12} + (3/8)D_3^c \tag{87}$$

References

1. I. Eliezer and R. A. Howald, "A Program for Binary Phase Equilibria Using the Redlich-Kister Equations", this volume, paper TPSI-6.

2. O. Redlich, A. T. Kister, and C. E. Turnquist, Chem. Eng. Progr., Symposium Series, 48 (2), 49 (1952)

3. I. Eliezer and R. A. Howald, J. Chem. Phys., submitted

4. J. F. Elliott, M. Gleiser, and V. Ramakrishna, Thermochemistry for Steelmaking, Addison-Wesley Pub. Co., Reading, Mass. (1963)

5. T. Wada, H. Wada, J. F. Elliott and J. Chipman, Metal. Trans., 2, 2199 (1971)

6. C. Petot and E. Bonnier, Bull. Soc. Chim. France, 1967, 836 (1967)

7. H. A. Clarke and R. W. Missen, J. Chem. Eng. Data, 19, 343 (1974)

8. G. Scatchard, L. B. Ticknor, J. R. Goates, and E. R. McCartney, J. Am. Chem. Soc., 74, 3721 (1952)

TABLE 1

The transformation matrix, $\mathbb{L}^{-1}$, to obtain Redlich-Kister coefficients from a power series in T.

$$|A, B, C\ldots\rangle = \mathbb{L}^{-1} \; |C_1, C_2, C_3, \ldots\rangle$$

1	3/4	7/12	15/32	31/80	63/192	127/448	255/1024
0	1/4	4/12	11/32	26/80	57/ 192	120/448	247/1024
0	0	1/ 12	5/32	16/80	42/192	99/448	219/1024
0	0	0	1/32	6/80	22/192	64/448	163/1024
0	0	0	0	1/80	7/192	29/448	93/1024
0	0	0	0	0	1/192	8/448	37/1024
0	0	0	0	0	0	1/448	9/1024
0	0	0	0	0	0	0	1/1024
0	0	0	0	0	0	0	0

Table 2

Contributions to terms in the pseudobinary equation for log γ_3

$$\log \gamma_3 = T^2 \left[A'_3 + B'_3 (-3+4T) + C'_3 (-5+6T)(-1+2T)\ldots\right]$$

from Redlich-Kister coefficients for components 1 and 2.

CONTRIBUTION

to	from A_{12}	B_{12}	C_{12}	D_{12}	E_{12}
A'_3	$-S(1-S)$	$-\frac{3}{2}S(1-S)(1-2S)$	$-\frac{7}{4}S(1-S)(1-2S)^2$	$-(\frac{15}{8})S(1-S)(1-2S)^3$	$-(\frac{31}{16})S(1-S)(1-2S)^4$
B'_3	0	$-\frac{1}{2}S(1-S)(1-2S)$	$-(\frac{4}{4})S(1-S)(1-2S)^2$	$-(\frac{11}{8})S(1-S)(1-2S)^3$	$-(\frac{26}{16})S(1-S)(1-2S)^4$
C'_3	0	0	$-(\frac{1}{4})S(1-S)(1-2S)^2$	$-(\frac{5}{8})S(1-S)(1-2S)^3$	$-(\frac{16}{16})S(1-S)(1-2S)^4$
D'_3	0	0	0	$-(\frac{1}{8})S(1-S)(1-2S)^3$	$-(\frac{6}{16})S(1-S)(1-2S)^4$
E'_3	0	0	0	0	$-(\frac{1}{16})S(1-S)(1-2S)^4$

Table 3

Contributions to terms in the pseudobinary equation for $\log \nu_3$

$$\log \nu_3 = T^2 \left[A'_3 + B'_3 (-3+4T) + C'_3 (-5+6T)(-1+2T)\ldots\right]$$

from Redlich-Kister coefficients for components 1 and 3

CONTRIBUTION

to	from A_{13}	B_{13}	C_{13}	D_{13}	E_{13}
A'_3	S	$-(\frac{1}{2})S(1-S)$	$\frac{1}{4}(S)(1-S)^2$	$-\frac{1}{8}(S)(1-S)^3$	$\frac{1}{16}(S)(1-S)^4$
B'_3	0	$(\frac{1}{2})S(1+S)$	$-\frac{1}{4}(S)(1-S)(1+S)$	$\frac{3}{8}(S)(1-S)^2(1+S)$	$-\frac{4}{16}(S)(1-S)^3(1+S)$
C'_3	0	0	$\frac{1}{4}(S)(1+S)^2$	$-\frac{3}{8}(S)(1-S)(1+S)^2$	$\frac{6}{16}(S)(1-S)^2(1+S)^2$
D'_3	0	0	0	$\frac{1}{8}(S)(1+S)^3$	$-\frac{4}{16}(S)(1-S)(1+S)^3$
E'_3	0	0	0	0	$\frac{1}{16}(S)(1+S)^4$

Table 4

Contributions to terms in the pseudobinary equation for log γ_3

$$\log \gamma_3 = T^2 \left[A'_3 + B'_3 (-3+4T) + C'_3 (-5+6T)(-1+2T)\ldots \right]$$

from Redlich-Kister coefficients for components 2 and 3

CONTRIBUTION

to	from A_{23}	B_{23}	C_{23}	D_{23}	E_{23}
A'_3	$(1-S)$	$-\frac{1}{2}S(1-S)$	$(\frac{1}{4})(S)^2(1-S)$	$-(\frac{1}{8})(S)^3(1-S)$	$(\frac{1}{16})(S)^4(1-S)$
B'_3	0	$(\frac{1}{2})(2-S)(1-S)$	$-(\frac{1}{2})(S)(2-S)(1-S)$	$(\frac{3}{8})(S)^2(2-S)(1-S)$	$-(\frac{4}{16})(S)^3(2-S)(1-S)$
C'_3	0	0	$(\frac{1}{4})(2-S)^2(1-S)$	$-(\frac{3}{8})S(2-S)^2(1-S)$	$(\frac{6}{16})(S)^2(2-S)^2(1-S)$
	0	0	0	$(\frac{1}{8})(2-S)^3(1-S)$	$-(\frac{4}{16})(S)(2-S)^3(1-S)$
E'_3	0	0	0	0	$(\frac{1}{16})(2-S)^4(1-S)$

Table 5

Contributions to terms in the pseudobinary equation for $\log \gamma_3$

$$\log \gamma_3 = T^2 \; A'_3 + B'_3(-3+4T) + C'_3(-5+6T)(-1+2T) \ldots$$

from the extra terms in the ternary system.

CONTRIBUTION to	from B_3^a	C_3^b	C_3^a	D_3^c
A'_3	$(1/2)(S)(1-S)$	$(1/4)(S)(1-S)(-1+2S)$	$(1/4)(S)(1-S)$	$(1/8)(S)(1-S)(-1+2S)^2$
B'_3	$(1/2)(S)(1-S)$	$(1/2)(S)(1-S)(-1+2S)$	$(1/2)(S)(1-S)$	$(3/8)(S)(1-S)(-1+2S)^2$
C'_3	0	$(1/4)(S)(1-S)(-1+2S)$	$(1/4)(S)(1-S)$	$(3/8)(S)(1-S)(-1+2S)^2$
D'_3	0	0	0	$(1/8)(S)(1-S)(-1+2S)^2$

Table 5 (continued)

CONTRIBUTION from D_3^b to	D_3^b	D_3^a	E_3^d	E_3^c
A'_3	$(1/8)(S)(1-S)(-1+2S)$	$(1/8)(S)(1-S)$	$(1/16)(S)(1-S)(-1+2S)^3$	$(1/16)(S)(1-S)(-1+2S)^2$
B'_3	$(3/8)(S)(1-S)(-1+2S)$	$(3/8)(S)(1-S)$	$(4/16)(S)(1-S)(-1+2S)^3$	$(4/16)(S)(1-S)(-1+2S)^2$
C'_3	$(3/8)(S)(1-S)(-1+2S)$	$(3/8)(S)(1-S)$	$(6/16)(S)(1-S)(-1+2S)^3$	$(6/16)(S)(1-S)(-1+2S)^2$
D'_3	$(1/8)(S)(1-S)(-1+2S)$	$(1/8)(S)(1-S)$	$(4/16)(S)(1-S)(-1+2S)^3$	$(4/16)(S)(1-S)(-1+2S)^2$
E'_3	0	0	$(1/16)(S)(1-S)(-1+2S)^3$	$(1/16)(S)(1-S)(-1+2S)^2$

Table 6

The transformation matrix from the N_3^i to the N_2^i coefficients.

$$|B_2^a\ C_2^a\ C_2^b\ D_2^a\ D_2^b\ D_2^c\ E_2^a \ldots\rangle = M\ |B_3^a\ C_3^a\ C_3^b\ D_3^a\ D_3^b\ D_3^c\ E_3^a \ldots\rangle$$

M =	1	1	-1	1	-1	1	1	-1	1	-1
	0	-(1/2)	(3/2)	-1	2	-3	-(3/2)	(5/2)	-(7/2)	(9/2)
	0	-(1/2)	-(1/2)	-1	0	1	-(3/2)	(1/2)	(1/2)	-(3/2)
	0	0	0	(1/4)	-(3/4)	(9/4)	(3/4)	-(7/4)	(15/4)	-(27/4)
	0	0	0	(1/2)	-(1/2)	-(3/2)	(3/2)	-(3/2)	-(1/2)	(9/2)
	0	0	0	(1/4)	(1/4)	(1/4)	(3/4)	(1/4)	-(1/4)	-(3/4)
	0	0	0	0	0	0	-(1/8)	(3/8)	-(9/8)	(27/8)
	0	0	0	0	0	0	-(3/8)	(5/8)	-(3/8)	-(27/8)
	0	0	0	0	0	0	-(3/8)	(1/8)	(5/8)	(9/8)
	0	0	0	0	0	0	-(1/8)	-(1/8)	-(1/8)	-(1/8)

Table 7

Listings of sections of a computer program for ternary systems.

1. Calculation of pseudobinary coefficients (A_3', B_3', C_3', etc.). The values are stored in BETA(KI, I, I2). FC(I) stores I!.

```
                                                                                1793
113.    160 CONTINUE                                                            1794
114.        DO 230 I=1,8                                                        1795
115.    230 BETA(KI,I,I2)=0.                                                    1796
116.        S=X1/(X1+X2)                                                        1797
117.        IF (S.EQ.0) S=1.0E-50
118.        Q=1-S
119.        IF (Q.EQ.0) Q=1.0E-50
120.        XK=X1+X2                                                            1798
121.        Z=1+2*S                                                             1799
122.        IF (Z.EQ.0.0) Z=1.0E-50                                             1800
123.        DO 220 I=2,8                                                        1801
124.        DO 220 K=1,I                                                        1802
125.        C2=FC(I-1)/(FC(K-1)*FC(I-K)*2**(I-1))                               1803
126.        ITM=I+2
127.        DO 220 J=4,ITM
128.        BETA(KI,K,I2)=BETA(KI,K,I2)+C2*S*(1-S)*((Z      )**(J-4))*RT(I,J)   1805
129.    220 CONTINUE                                                            1806
130.        DO 232 I=1,8                                                        1807
131.        C1=2./(-2**I)                                                       1808
132.        C4=-C1*(-1)**I                                                      1809
133.        C3=1.                                                               1810
134.        DO 232 J=1,8                                                        1811
135.        BETA(KI,I,I2)=BETA(KI,I,I2)+C4*S*(1-S)*((-Z    )**(J-1))*RT(J,1)   1812
136.        C2=(-C1)*FC(J-1)/(FC(I-1)*FC(J-I)*(-2)**(J-I))                      1813
137.        BETA(KI,I,I2)=BETA(KI,I,I2)+C2*S*(Q**(J-I))*((1+S)**(I-1))
138.       2 *RT(J,2)                                                           1815
139.        BETA(KI,I,I2)=BETA(KI,I,I2)+C2*(S**(J-I))*(1-S)*((2-S)**(I-1))      1816
140.       2 *RT(J,3)                                                           1817
141.        C3=C3*2*FC(J)/(FC(I-1)*FC(J+1-I))                                   1818
142.        C4=-C3*(-.5)**J                                                     1819
143.    232 CONTINUE                                                            1820
144.        I=KI                                                                1821
145.        IF (IOPT(6)-8) 181,181,200
146.    181 WRITE(108,703) TEMP(I),(BETA(I,J,I2),J=1,4)                         1823
147.    182 WRITE(108,703) TEMP(I),(BETA(I,J,I2),J=5,8)                         1824
148.    703 FORMAT('T=',F9.3,4F13.8)                                            1825
149.    200 CONTINUE                                                            1826
150.        TPK=TP                                                              1827
```

Table 7 (continued)

2. Rearrangement of the coefficients stored in RT so that pseudobinary coefficients can be calculated for the other components. CMM stores the elements of the matrix M shown in Table 6.

```
      IF (IOPT(6)-9) 250,251,251
  250 WRITE(108,710) II,X3,GF(JJ,I2),AF(JJ,I2),AF(JJ,I2),GL
  710 FORMAT('X',I1,'=',F10.8,F11.5,E13.7,'ACT=',3F11.5)
  251 IC=IC+1
      KZZ(1)=KZK
      IF (IC-4)  69,61,999
   69 CONTINUE
      DO 301 J=1,8
      X=RT(J,1)
      RT(J,1)=RT(J,2)*(-1)**(J-1)
      RT(J,2)=RT(J,3)*(-1)**(J-1)
  301 RT(J,3)=X
      L=0
      DO 328 I=2,10
      ITM=I+2
      DO 328 J=4,ITM
      L=L+1
  328 RKK(L)=RT(I,J)
      DO 329 I=1,28
      RKL(I)=0.
      DO 329 J=1,28
  329 RKL(I)=RKL(I)+CMM(J,I)*RKK(J)
      L=0
      ITM=I+2
      DO 332 I=2,8
      DO 332 J=4,ITM
      L=L+1
  332 RT(I,J)=RKL(L)
      X=X1
      X1=X3
      X3=X2
      X2=X
      KZZ(1)=1
      KI=1
      GO TO 160
```


905

Table 8

A useful matrix form for augmented Redlich-Kister coefficients for a ternary system.

A_{12}	A_{13}	A_{23}	0	0	0	0	0
B_{12}	B_{13}	B_{23}	B_3^a	0	0	0	0
C_{12}	C_{13}	C_{23}	C_3^a	C_3^b	0	0	0
D_{12}	D_{13}	D_{23}	D_3^a	D_3^b	D_3^c	0	0
E_{12}	E_{13}	E_{23}	E_3^a	E_3^b	E_3^c	E_3^d	0
F_{12}	F_{13}	F_{23}	F_3^a	F_3^b	F_3^c	F_3^d	F_3^e

Table 9

Redlich-Kister Coefficients for the Binary Subsystems of the Fe - Ni - C gamma phase.

Components	Coefficient	log ν at 1000 K	Enthalpy (cal mol^{-1})
Fe - Ni	A_{12}	-.64667	-3904.
	B_{12}	.42750	2533.
Fe - C	A_{13}	5.1823	28971.
	B_{13}	-5.7708	-27380.
	C_{13}	1.9685	8933.
Ni - C	A_{23}	5.5121	13328.
	B_{23}	-3.0	0.

Table 10.

Coefficients found for the Fe - Ni - C liquid system.

Enthalpy (cal mol^{-1})

	subscripts and superscripts				
N	12	13	23	3a	3b
A	-4545	-24280	-17705	0	0
B	2482	4696	0	0	0
C	0	0	0	0	0

$\log \gamma_{1000}$

	subscripts and superscripts				
N	12	13	23	3a	3b
A	-.75554	-.37940	-2.7448	0.0	0.0
B	.41473	-.65530	.0162	3.5	0.0
C	0.0	.62925	0.0	6.0	0.80

Table II

Data for $\log\gamma$ for acetonitrile from Clarke and Missen[7] corrected for non-ideality of the vapor and interpolated to selected values of $S = X_{benzene}/(X_{benzene} + X_{carbon\ tetrachloride})$

S = .13		S = .23		S = .375	
X_3	$\log\gamma_3$	X_3	$\log\gamma_3$	X_3	$\log\gamma_3$
.4036	.2304	.1833	.4418	.3147	.2717
.4960	.1672	.3044	.3063	.4194	.1969
.5897	.1194	.4221	.1899	.5101	.1461
.6602	.08297	.4918	.1534	.5778	.1109
.7310	.05382	.5633	.1122	.6460	.07579
.7824	.03643	.6401	.07578	.7131	.05393
.8170	.03252	.7460	.03941	.7550	.03442
.8560	.01618	.7884	.02461	.7966	.02509
.8780	.00827			.8144	.01916
.9030	.01099				

Table 11 (continued)

S = .59		S = .65		S = .73		S = .92	
X_3	$\log \gamma_3$	X_3	$\log \gamma_3$	X_3	$\log \gamma_3$	X_3	$\log \gamma_3$
.3827	.2001	.1671	.3345	.1516	.3178	.1560	.3331
.5138	.1273	.2990	.2484	.2881	.2461	.2811	.2316
.6032	.05829	.4026	.1791	.3959	.1683	.3952	.1663
.6585	.06402	.4926	.1261	.4794	.1231	.5047	.1135
.7118	.04430	.5748	.09271	.5540	.08942	.5699	.09026
.7680	.03512	.6452	.06666	.6312	.06304	.6397	.06670
.8180	.02023	.7081	.04369	.6670	.05736	.7061	.04900
		.7623	.03428	.7167	.03737	.7575	.03201
		.8121	.02068	.7588	.02583	.7958	.02096
				.7786	.02038	.8294	.01760

Table 12

A set of augmented Redlich-Kister paramaters for the ternary system benzene - carbon tetrachloride - acetonitrile.

A	.0521	.4419	.7792	0	0	0
B	.00058	.0056	.0817	-.7904	0	0
C	0	.04815	.1114	.8220	-.8464	0
D	0	0	.06835	0	0	0

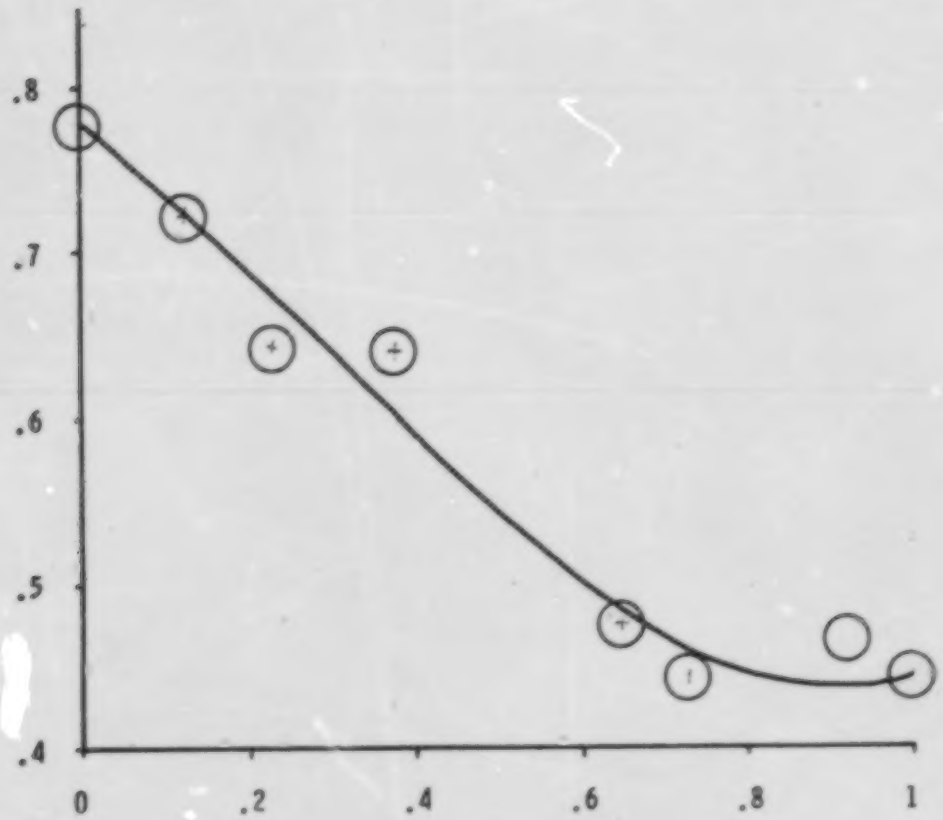

Figure 1

Plot of A_3' vs. $S = X_1/(X_1 + X_2)$ for the system benzene-carbon tetrachloride-acetonitrile. The solid line is calculated from the values in Table 12.

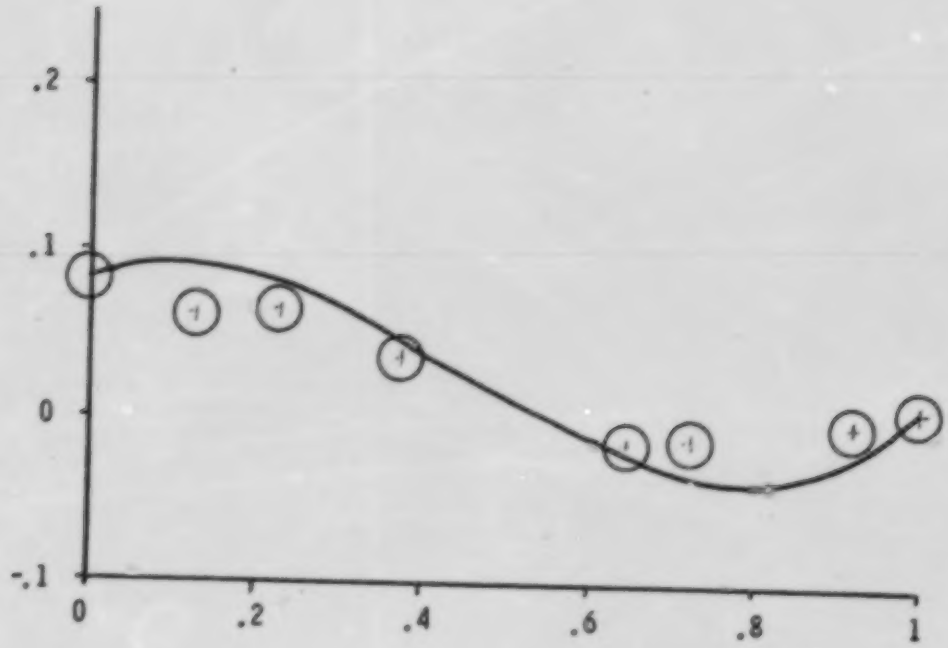

Figure 2

Plot of B_3' vs. $S = X_1/(X_1 + X_2)$ for the system benzene-carbon tetrachloride-acetonitrile. The solid line is calculated from the values in Table 12.

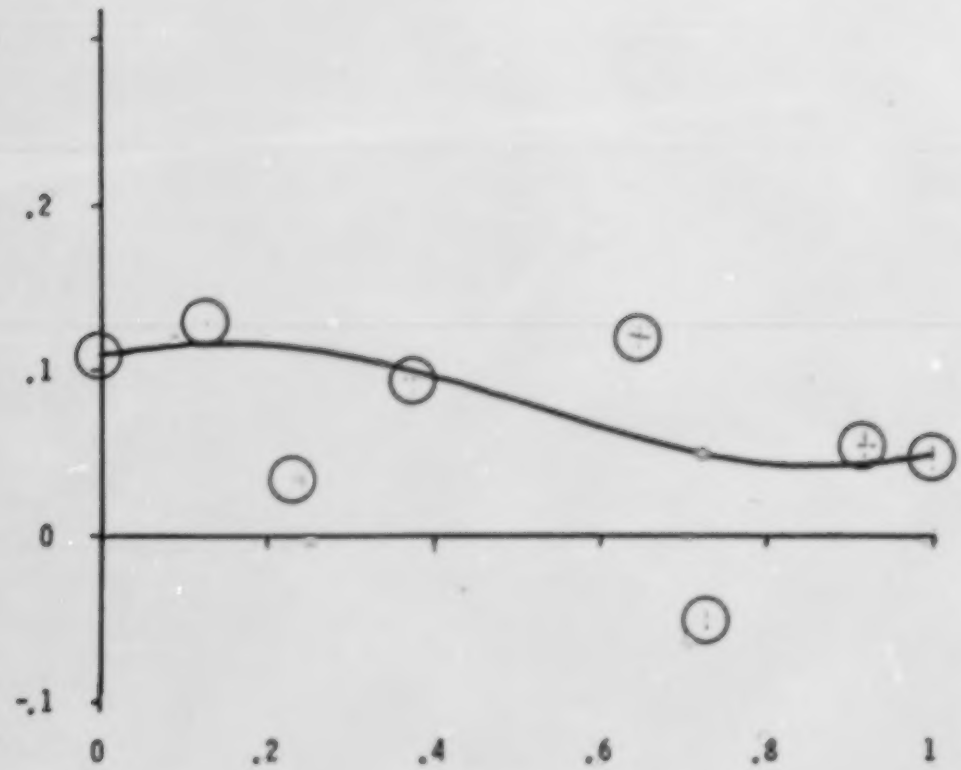

Figure 3

Plot of C_3' vs. $S = X_1/(X_1 + X_2)$ for the system benzene-carbon tetrachloride-acetonitrile. The solid line is calculated from the values in Table 12.

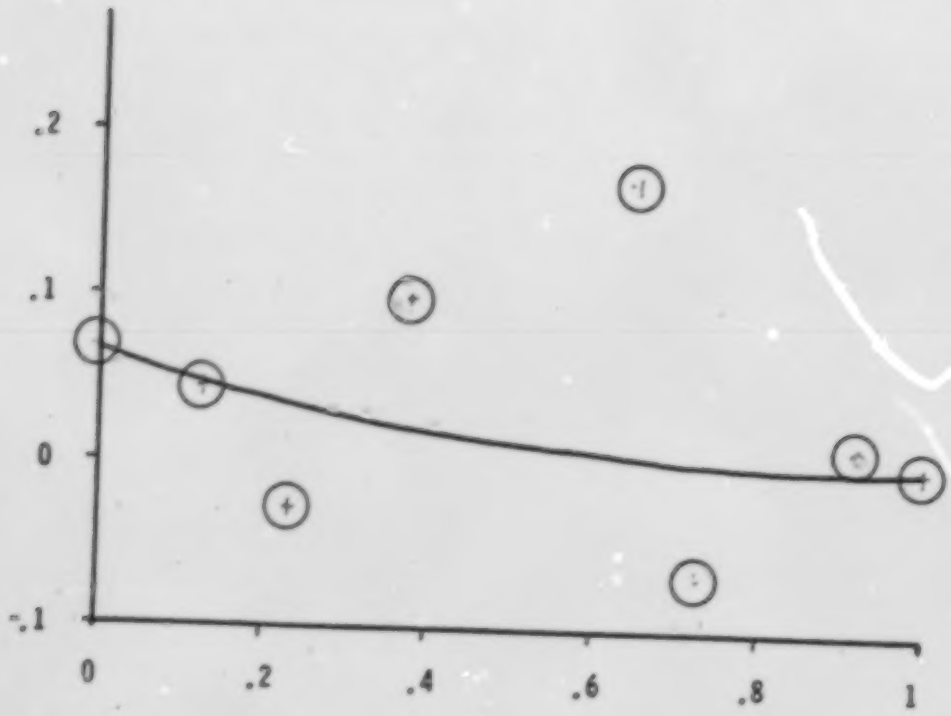

Figure 4

Plot of D_3' vs. $S = X_1/(X_1 + X_2)$ for the system benzene-carbon tetrachloride-acetonitrile. The solid line is calculated from the values in Table 12.

National Bureau of Standards SP-496, Applications of Phase Diagrams in Metallurgy and Ceramics
Proceedings of Workshop held at NBS, Gaithersburg, Md., January 10-12, 1977

A PROGRAM FOR BINARY PHASE EQUILIBRIA USING THE REDLICH-KISTER EQUATIONS

Isaac Eliezer and Reed A. Howald

Chemistry Department of Montana State University,
Bozeman, Montana, 59715

Abstract

Several mathematical forms have been proposed and used to describe the relationship between thermodynamic properties and composition in binary systems. No consensus has been reached on what are the best forms, primarily because there is a basic conflict between the requirement of convenience and the requirement of satisfying the Gibbs-Duhem relationship. The subject is currently of special importance because the availability of large high speed computers permits the application of the equations to a wide range of materials problems encountered in many engineering applications.

Power series in mole fraction are well adapted to the general representation of data and to computer calculation of phase diagrams. At least two series in mole fraction have now been programmed for computers: a simple power series and the modified Legendre polynomials of Bale and Pelton.

We have chosen to program the Redlich-Kister equations

$$\log \gamma_1 = (1-X_1)^2 \left[A+B(-1+4X_1)+C(-1+6X_1)(-1+2X_1)+D(-1+8X_1)(-1+2X_1)^2 + \ldots\right]$$

$$\log \gamma_2 = X_1^2 \left[A+B(-3+4X_1)+C(-5+6X_1)(-1+2X_1)+D(-7+8X_1)(-1+2X_1)^2+ \ldots\right]$$

primarily because the same set of coefficients appears in the equation for both components. These coefficients are the coefficients in a simple power series expansion of the excess free energy of mixing in the variable (-1+2X). Other advantages and disadvantages of the three polynomial forms are discussed, along with the conversion matrices used to convert from one polynomial form to another. It is suggested that both Redlich-Kister and Bale-Pelton coefficients should be reported when experimental data are fitted.

The capabilities of our program are described in terms of the subroutines currently available. Applications to multiphase binary systems of engineering importance are shown, including calculated phase diagrams.

INTRODUCTION --- The earliest generalized power series expansion for thermodynamic properties of binary systems was provided by the Margules equations[1]:

$$\bar{Y}_1 = (1-X_1)^2(A_1 + B_1X_1 + C_1X_1^2 \ldots) \quad (1)$$

$$Y^e = X_1(1-X_1)(A_e + B_eX_1 + C_eX_1^2 \ldots) \quad (2)$$

$$\bar{Y}_2 = X_1^2(A_2 + B_2X_1 + C_2X_1^2 \ldots) \quad (3)$$

The Margules equations are still widely used. However they have two major drawbacks which have led to many efforts to develop alternative formulations. The first difficulty is that different coefficients appear in all three equations, and there are another three sets of coefficients if the expansions are written as power series in X_2 instead of X_1. Conversions from one set of coefficients to another are not too difficult (they involve multiplication by an upper triangular matrix as illustrated in Table 1), But it is still confusing and tedious to have three or more similar but distinct sets of coefficients.

The second drawback concerns the extreme non-orthogonality of power series over the range from 0 to 1. In this region, X_1^5 and X_1^6 are very similar. We can define the degree of non-orthogonality of two functions by a parameter P, defined as:

$$P = \left[\int f\,g\,dx\right]^2 / \int f^2\,dx \int g^2\,dx \quad (4)$$

In this particular case, we have:

$$P = \left[\int X^5X^6\,dX\right]^2 / \int X^{10}\,dX \int X^{12}\,dX = .9931 \quad (5)$$

Orthogonality, P = 0, is useful[2] because then the values of the first coefficients do not depend strongly on the number of coefficients selected to represent the data. At the other extreme, P values greater then 0.99 require that the coefficients be determined and recorded with more significant figures than are present in the original data. Bale and Pelton have shown that even DOUBLE PRECISION computer calculation is inadequate for a 19 term Margules expansion[2].

The Legendre polynomials are exactly orthogonal over the interval from -1 to 1, and an expansion in Bale-Pelton coefficients, q_i,[2,3] works very well:

$$Y^e = X_1X_2(q_0 + q_1(X_1-X_2) + q_2P_2(X_1 - X_2) + q_3P_3(X_1-X_2) \ldots) \quad (6)$$

In this equation the first two Legendre polynomials, $P_0 = 1$, and $P_1(X_1 - X_2) = X_1 - X_2$, have been written explicitly.

Unfortunately, derivatives of the Legendre polynomials can get quite complicated, and the easiest way to apply the Gibbs-Duhem relation to Y^e in this form is to define two new sets of coefficients, a_i and b_i:

$$\bar{Y}_1 = X_2^2 \sum_i a_iP_i(X_1 - X_2) \quad (7)$$

$$\bar{Y}_2 = X_1^2 \sum_i b_iP_i(X_1 - X_2) \quad (8)$$

It is impossible to keep exactly orthogonal polynomials in all three equations without having three different sets of coefficients.

The Redlich-Kister equations[4] provide a reasonable compromise between the conflicting requirements of simplicity, convenience, and

orthogonality. The Redlich-Kister coefficients appear in the expansion of Y^e as X_1X_2 times a power series in $X_1 - X_2$.[5]

$$Y^e = X_1X_2(A+B(X_1 - X_2) + C(X_1 - X_2)^2 + D(X_1 - X_2)^3 \ldots) \tag{9}$$

It might appear that non-orthogonality might be as serious a problem here as with the Margules equations, but since the interval of integration is changed to -1 to +1, one has exact orthogonality between odd and even powers. For seven Redlich-Kister coefficients the largest value one encounters for the non-orthogonality parameter P is:

$$P = \left[\int X^4X^6\, dX\right]^2 \Big/ \int X^8\, dX \int X^{12}\, dX = .9669$$

This is a substantial improvement over P = .9931. This same conclusion can be substantiated by an examination of Tables 2 and 3, the conversion matrices from Bale-Pelton coefficients to Margules and Redlich-Kister coefficients respectively. The largest entry in absolute value in Table 3 is -(693/16) = -43.3125, so that at worst only two additional significant figures are required for eight Redlich-Kister terms beyond the best orthogonal formulation. On the other hand the Margules coefficients would need 4 additional significant figures for the same accuracy, corresponding to an entry of 16632 in the eighth column.

The major advantage of the Redlich-Kister coefficients is the existence of relatively simple expressions for $\overline{Y}_1$ and $\overline{Y}_2$ using the same coefficients:

$$\overline{Y}_1 = X_2^2\left[A+B(-1+4X_1) + C(-1+6X_1)(-1+2X_1) + D(-1+8X_1)(-1+2X_1)^2 + E(-1+10X_1)(-1+2X_1)^3 \ldots\right] \tag{10}$$

$$\overline{Y}_2 = X_1^2 \left[A + B(-3+4X_1) + C(-5+6X_1)(-1+2X_1) + D(-7+8X_1)(-1+2X_1)^2 + E(-9+10X_1)(-1+2X_1)^3 \ldots\right] \quad (11)$$

The earliest publication of these equations was by Scatchard[5]. However the coefficients were used in an earlier paper of Redlich and Kister[6], and they are responsible for popularizing the method[4]. Thus, referring to equations 9-11 as the Redlich-Kister equations is well justified as well as standard practice[7-8].

Conversions between various sets of coefficients. --- The Redlich-Kister polynomials are simple and easy to use, but they are not orthogonal. For comparisons of independent determinations using different numbers of coefficients it will often be best to convert to Bale-Pelton coefficients. We suggest that, in reporting calculations on binary systems, both Redlich-Kister and Bale-Pelton coefficients be tabulated. Conversions to and comparisons with power series in X_1 and X_2 will also continue to be important. There are many significant interconversions (at least 91), and some way of keeping them straight is important. Figure 1 illustrates how any conversion of coefficients can be accomplished going through the Redlich-Kister coefficients with seven conversion matrices (𝕁 through ℙ) and their inverse matrices. A few of the easier conversions along the circumference are also shown.

One can go back and forth between Redlich-Kister and Bale-Pelton coefficients with the matrices 𝕄 and $\mathbb{M}^{-1}$ shown in Table 3. The columns in $\mathbb{M}^{-1}$ are the coefficients of the Legendre polynomials, so these matrices can be extended indefinitely. Table 4 shows 𝕂 and $\mathbb{K}^{-1}$ for conversions between Redlich-Kister coefficients and the

Margules constants of eqn. 2. The columns of $\mathbb{K}$ are the constants in an expansion of $(-1+2X)^n$. These two matrices are especially significant because all the conversion matrices can be written as products of $\mathbb{K}$ and $\mathbb{N}$ with the two simple matrices $\mathbb{D}$ and $\mathbb{P}$ shown in Table 5. This is illustrated in Table 6 for all the matrices shown explicitly in Figure 1. A number of these equations show products of the form $\mathbb{P}\,\mathbb{K}\,\mathbb{P}$; however, these triple products are very easy to evaluate since one needs only to change the sign of certain of the off diagonal matrix elements (along diagonals). For example, $\mathbb{P}\,\mathbb{K}\,\mathbb{P}$ is just like $\mathbb{K}$ except that all the signs are positive, and $\mathbb{F} = \mathbb{P}\,\mathbb{D}\,\mathbb{P}$.

Overview of the BPHD Program --- The BPHD program is designed primarily for the calculation of equilibrium constants and activities as a function of composition in binary systems. Equilibrium constants are calculated by interpolation of stored free energy function data, and activity calculations are based upon the Redlich-Kister equations[4]:

$$\log \gamma_1 = (1-X)^2 \left[A + B(-1+4X) + C(-1+6X)(-1+2X) \ldots\right] \tag{12}$$

$$\log \gamma_2 = X^2 \quad A + \left[B(-3+4X) + C(-5+6X)(-1+2X) \ldots\right] \tag{13}$$

The program includes provisions for calculating the free energy function and the Redlich-Kister coefficients as a function of temperature. However, this requires known expressions for the heat capacities as a function of temperatures, known enthalpies, and a full set of Redlich-Kister coefficients at one standard temperature. Since much of the development was undertaken for high temperature equilibria, the

standard temperature is usually 1000 K, but much of the program will operate with a standard temperature of 298.15 K as well.

Since the program is meant to be very general, applicable to any binary system, the data for particular components and systems are not included in the program. Such data must be provided from the terminal or from a data file before the calculations will proceed. It is expected that most of the use of this program will involve entering new data files, for new systems or for more accurate representation of old systems. The separation of data files from the program is designed to facilitate such updating of old files and the development of new data files.

Data files are normally read under a 12G.4 format. The card

700 FORMAT (12G.4)

appears in almost all subroutines. It allows for the reading of up to twelve numbers on a single line. Successive numbers must be separated by one or more spaces, but this format does not require that numbers occupy any set locations on a line. It allows for the entry of both integers and decimal fractions. Decimal fractions can be entered in either decimal or exponential notation: 0.00435 or .435E-2. The decimal point must be included in all numbers which are not read as integers, or there is likely to be a mistake in reading the numbers. We have found the 12G.4 format convenient since when such errors occur, a factor of 10^4 error is usually evident. For example all temperature data should be entered with a decimal point as in 1400., while the value 1400 will be interpreted as 0.14. For computers which do not accept a widthless format, we suggest the use of 700 FORMAT (6G10.4) cards instead.

Obtaining Coefficients by Least Squares

Redlich-Kister coefficients and power series expressions for heat capacities which appear in the data files are often obtained by least squares procedures. We have not included a least squares fitting procedure in the BPHD program primarily because most users and computer centers have their own least squares and multiple regression programs with which they are already familiar. There are however, certain features of the particular power series we have chosen to use which need to be explained.

We have chosen to express heat capacities as a power series in $T-T_o$, where T_o is a standard temperature usually 1000 K. In this form, the first term is a heat capacity at T_o, which is usually an experimentally accessible temperature. Thus, the value used is quite easy to check in contrast to the value A in the series.

$$C_p = A + BT + CT^2 \ldots \quad (14)$$

The series we have chosen as standard is:

$$C_p = A + B(T-T_o) + C(T-T_o)^2 + D(T-T_o)^3 + E(T-T_o)^4 \quad (15)$$

When using a heat capacity expression in BPHD for the first time, it is advisable to print out the full results of the calculation and compare the heat capacity values calculated at different temperatures with the original heat capacity data you are trying to fit. If these agree reasonably well, then the calculated values for the enthalpy and the free

energy function are presumably correct as well.

Equations of the Redlich-Kister form can also be set up for enthalpy, heat capacity, etc. For instance, for the total enthalpy of a binary system, we can write:

$$H/(n_1+n_2) = H_2^{\circ} + (H_1^{\circ}-H_2^{\circ})X + X(1-X)\left[A + B(-1+2X) + C(-1+2X)^2 \ldots\right] \qquad (16)$$

where n=number of moles, X = mole fraction, H° = enthalpy of standard state. Alternatively the excess enthalpy, ΔH_m can be defined:

$$\Delta H_m = H/(n_1 + n_2) - H_2^{\circ} - (H_1^{\circ} - H_2^{\circ})X \qquad (17)$$

and so, using (5):

$$\Delta H_m = X(1-X)\left[A + B(-1+2X) + C(-1+2X)^2 + D(-1+2X)^3 \ldots\right] \qquad (18)$$

A similar expression can be used for the activity coefficients:

$$X_1 \log \gamma_1 + X_2 \log \gamma_2 = X(1-X)\left[A + B(-1+2X) + C(-1+2X)^2 \ldots\right] \qquad (19)$$

Sometimes this will give better values for the Redlich-Kister coefficients than either of the separate equations for the individual activity coefficients:

$$\log \gamma_1 = (1-X)^2\left[A + B(-1+4X) + C(-1+6X)(-1+2X) + D(-1+8X)(-1+2X)^2 \ldots\right] \qquad (20)$$

and:

$$\log \gamma_2 = X^2\left[A + B(-3+4X) + C(-5+6X)(-1+2X) + D(-7+8X)(-1+2X)^2 \ldots\right] \quad (21)$$

We have chosen to use base 10 logarithms in the equations for the activity coefficients. However, one could use natural logarithms instead, if all the coefficients are multiplied by ln 10 = 2.30259.

Calculation of the Free Energy Function

The standard equilibrium expression:

$$K_T = 10^{-\Delta H_T/2.303RT}\ 10^{\Delta S_T/2.303R} \quad (22)$$

can be rewritten as:

$$K_T = 10^{-\Delta H^\circ_{298.15}/2.303RT}\ 10^{\Delta \bar{\Phi}_T/2.303R} \quad (23)$$

where the temperature dependence of both ΔH and ΔS is put into the free energy function, $\bar{\Phi}$, defined by $\bar{\Phi} = -\dfrac{G^\circ_T - H^\circ_{298.15}}{T}$. It is then possible to calculate equilibrium constants at any temperature from values of $H^\circ_{298.15}$ for each compound and from tables of $\bar{\Phi}$ as a function of temperature like the JANAF tables.[9] For phase equilibria calculations it is often necessary to know K to four significant figures. In most cases, one can obtain this accuracy to interpolating from tables of $\bar{\Phi}$, provided the interval in the table is as small as 20 to 30 K. The program BPHD can be used to create tables of the free energy function at any set of temperatures that one chooses.

The free energy function can be calculated at any temperature if its value is known at some standard temperature and if a heat capacity expression valid over the temperature range of interest including the

standard temperature is known. For the temperature range from 1000 K to 2000 K, we have picked 1000 K as a standard temperature, T_o, and most heat capacity data can be accurately represented over this temperature range by power series of the form:

$$C_p = A + B(T-1000) + C(T-1000)^2 + D(T-1000)^3 + E(T-1000)^4 \qquad (24)$$

This information for a particular species such as graphite can be provided to the computer in three lines of an input file:

```
C       (S, GRAPHITE)
10   4   1      3.020      2324.      2824.
2    5.15465    .00159627    -.13423E-5    .45542E-9
```

The first line is just an identifying label and can say anything. The second line starts with three integers. The first two numbers serve as an identifying label for the computer, specifying the component and the phase. In the example shown above, carbon (graphite) is component 10 of phase 4. The program is currently dimensioned to handle up to 10 components in up to 4 phases.

The free energy function can be calculated from the formula:

$$(\Phi_T) = (\Phi_{T_o}) - H(T_o) - H(298.15)\left(\frac{1}{T} - \frac{1}{T_o}\right) - \frac{1}{T}\int_{T_o}^{T} C_p\,dT + \int_{T_o}^{T} (C_p/T)dT \qquad (25)$$

The two integrals can be evaluated analytically for the heat capacity expressions used here. There is substantial cancellation between the two integrals and this is recognized in the programming of this computation in subroutine PPI.

The third integer is normally given the value 1. This number identifies the position used for the standard temperature. It is followed by the value of the free energy function at 1000 K, $H^{\circ}_{1000} - H^{\circ}_{298.15}$, and finally by the enthalpy at 1000 K defined as $\Delta H^{\circ}_{f,298.15} + (H^{\circ}_{1000} - H^{\circ}_{298.15})$. In the particular case of graphite, since it is the reference state for carbon, $\Delta H^{\circ}_{f,298.15} = 0.0$ and the last two numbers are the same. Note that the enthalpies are given in calories mol^{-1}, and not kcal mol^{-1}.

When the third line starts with the integer 2, the next five numbers in the line are coefficients in the power series expansion of the heat capacity. Thus the expression used here for the heat capacity of graphite is:

$$C_p = 5.15465 + .00159627(T-1000) - .13423 \times 10^{-5}(T-1000)^2 + .45542 \times 10^{-9}(T-1000)^3 + 0(T-1000)^4 \quad (26)$$

When the third line starts with 1, the computer will read three lines of heat capacity data, with several options available as to the form of the heat capacity expression.

The program will read in data for up to 40 materials (10 components of 4 phases) in any order from the input file. However, it is necessary

for the file to identify the last material. The computer will continue until it finds component zero of phase zero. Thus the last two lines in the file should be:

END (or any other arbitrary name)

0 0 1

A sample file is shown in Table 7.

Once the data file is ready, it is assigned a number to identify it and the program is run. The instructions required to assign an identifying number to a file, to compile a Fortran program and to run it will vary from one computer installation to another. Each individual using this program should find out the directions for these three operations at his own computing center. For the Sigma 7 at Montana State University, an example of control commands is:

```
!FORT SPHD OVER BPHD
 BC
!SET F:12 DC/CRIS; IN
! LINK BPHD OVER LMPD
!LMPD.
```

The program starts by typing the key, OPTIONS. At this point if you wish to calculate and tabulate values for the free energy function, you should type in 1792. This series of four integers with no spaces controls a series of IF statements in the main program and in subroutine GNN to call the subroutines TPIN (for entering the temperatures) and PHIC (for calculating the free energy functions). The program then proceeds to type the key, ENTER NUMBER OF TEMPERATURES AND N TEMP VALUES. The example shown in Table 8, uses three tem-

perature values, but any number up to 20 can be used. The first temperature entered must be the standard temperature chosen in building the input files. If some of the later temperatures are left blank, the program will continue the series of equally spaced temperatures suggested by the last two values entered.

Typing a substantial table from a terminal can be quite tedious. In most cases where we want a full table, we operate this part of the program in BATCH so that the output is printed on a high speed line printer. From the terminal we usually suppress part or all of the printing by entering a value for IOPT(6). The value 4 entered in 17920004 or 9 2 0 0 0 4 suppresses printing completely. 9 2 0 0 0 2 is a useful compromise which prints only part of the output. If you want to decide for each species in a file whether to print the results or not, you should use 17920006 or 9 2 0 0 0 6. The options for printing and skipping in this case, are 1 and 4 respectively.

The Calculation of Equilibrium Constants

It is easy to calculate equilibrium constants by hand from a table of H^{o}_{298} and free energy function values, but the calculation is also programmed in subroutine EPHI. This subroutine is called by the value 7 for IOPT(1), the first of the 9 IOPT values called for at the beginning of subroutine GNN. You can type in the free energy function and H^{o}_{298} values that you need for the calculation, but this is not necessary if you have been through subroutine PHIC. All that is usually needed is to enter the number of phases and then enter the coefficients of the balanced chemical equation following the keys:

ENTER THE COEFFICIENTS AND THEN THE H0298 VALUES, PHASE N

Table 9 shows calculations of K's for the melting of tridymite and for the:

$$SiO_2(\text{tridymite}) = SiO_2(\text{cristobalite})$$

equilibrium. Where a lone question mark appears on a line, a line of zeros has been entered by hitting the return key.

A table of equilibrium constant values at the set of temperatures last used in PHIC is automatically typed, and further temperatures can be used by interpolation if desired.

Following the KEQ value, the program prints the values for ΔH and ΔG at each temperature. It is often desirable to correct the entries for one or more of the species to get better values for K or for ΔH. Changing Φ°_{1000} will raise or lower all the K values by a particular factor, and ΔH can be changed by changing values for H°_{1000}. If you want to change ΔG without changing H°_{298}, the values of $H^\circ_{1000} - H^\circ_{298}$ and H°_{1000} should both be adjusted by the same amount.

The Calculation of Activities Given X_1

Like the free energy function, Redlich-Kister coefficients are functions of the temperature and values for a particular temperature can be obtained by interpolation in a table. The program allows for reading a table of values at nine successive temperatures or for calculating such a table (with or without printing it) from the values at 1000 K, Redlich-Kister coefficients for enthalpy at 1000 K and heat capacity power series coefficients.

$$A(T) = A(T_o) - AH(T_o)\left[(1/T) - (1/T_o)\right]/4.5756 \qquad (27)$$

$$B(T) = B(To) - BH(To)\left[(1/T) - (1/To)\right]/4.5756 \qquad (28)$$

etc. There are additional terms required if there is a substantial change in the heat capacity on mixing the components, and these integrals are included in the program. However in most cases, values of zero can be used for the heat capacity coefficients. We will discuss first the procedure for calculating a set of Redlich-Kister coefficients from the values at 1000 K and enthalpy and heat capacity coefficients. This part of the program uses a data file which usually has the form:

A	B	C	D . . .
A(H)	B(H)	C(H)	D(H) . . .
0.			
0.			
0.			
0.			

The particular file for carbon in liquid iron is:

-3.79398	-.655295	.629251
-24280.	4696.	0.
0.		
0.		
0.		
0.		

The four lines after the enthalpy coefficients represent coefficients in a power series in temperature for the excess heat capacity of mixing. However, there are almost no high temperature systems where the heat capacity is known accurately as a function of composition and one ordinarily assumes that the excess heat capacity of mixing is negligibly small at all temperatures, so that there are zeroes in all four of these lines. In this case, the Redlich-Kister coefficients are linear in 1/T as in the equation:

$$A = A_{1000} + (A(H)/4.5756)(1/T - 1/1000) \qquad (29)$$

When there is a zero in the second line as well, i.e. the enthalpy coefficients are also zero, the Redlich-Kister coefficients used do not vary with the temperature. Large enthalpy terms (like -25280. cal mol^{-1} for A(H) in the above example) give Redlich-Kister coefficients with a large temperature dependence, and here it is necessary to calculate the Redlich-Kister coefficients at the exact temperatures to be used or else to interpolate over very short temperature intervals, no larger that 25 degrees.

This calculation is easily performed once a file of the input data has been prepared. The file is assigned an identifying number and the program is run with either 1791 as the initial input or the values 9 and 1 for IOPT(1) and IOPT(2) in subroutine GNN. The same subroutine as above (TPIN) is used for the selection of the temperatures to be used in the calculation, and the first temperature in the file must be that for which the first line of the input file is valid, normally 1000 K.

If the temperatures you want have already been entered, you may keep the same set by simply hitting the return key.

The computer will then type the key: IDENTIFY THE PHASE AND THEN THE INPUT FILE. You should answer this by entering two integers: A number from 1 to 4 to identify the phase you are using and then the value for IDATA needed to read the input file. The computer will then calculate and print eight Redlich-Kister coefficients for each temperature you have specified and store them under the phase number you used.

If you wish to do this same calculation without printing the results, use the commands 17910002 or 9 1 0 0 0 2. The value IOPT(6) = 2 suppresses the printing step.

The calculated Redlich-Kister coefficients are stored in the file BETA. The dimensions of BETA are BETA (12, 20, 4) allowing for 12 Redlich-Kister coefficients (although the program now uses only 8), 20 temperatures, and 4 phases.

Once the beta values are in, the calculation of log γ and activity proceeds using subroutines GOM and GOMM. There are many ways to call these subroutines, but the one which we use most is with the IOPT values 8 5. This way one starts with the key:

IOP(7) = 0 ENTER TEMP. AND MOLE FRACTION

Then if you type in a temperature in the range covered by the values you have entered and a mole fraction, the activities of each of the components will be calculated and printed. An example of a Redlich-

Kister coefficient calculation is given in Table 10.

Finding a Mole Fraction Given an Activity

Quite often you will have a value for the activity of one of the components and want to know what mole fraction gives that activity. Our program for this calculation is called automatically after using GOM with the IOPT values 8 and 5, or it can be entered directly with 8 and 6. This subroutine, CLM, starts with the key, 5 YOU ARE IN CLM, ENTER KZZ VALUES TO CONTROL ACTIONS. You will ordinarily follow this command by entering a single integer, 1, 3, or 4. The value 3 specifies that you are going to enter a value for the activity of component 1. The value 4 similarly specifies component 2. The value 1 will let you choose. It prints the key WHICH COMPONENT? ENTER HC(J), J = 1, 4, NOW: followed by 4 values. HC(J) are the coefficients in the balanced equilibrium equations and the program is set up to look for the value of $a_1^{HC(1)} * a_2^{HC(2)} * a_3^{HC(3)} * a_4^{HC(4)}$ which you have chosen by setting the HC(J) values. Of course the most common entries are 1.0, 0. and 0., 1.0 for activities of components 1 and 2 respectively. However for an equilibrium like $KAlO_2$ (s) = $KO_{.5}$(in β-$AlO_{1.5}$) + $AlO_{1.5}$(β) you will be looking for a composition of the beta phase where $a_{KO.5}^{1.0} * a_{AlO1.5}^{1.0}$ is equal to the equilibrium constant, and you would want to enter the values 1.0 1.0. Table 8 show several examples of the use of CLM. The key ENTER TEMPERATURE, ACTIVITY, AND INTEGERS is preceeded by two integers, the first of which is I1 and the second of which is I2, the number identifying the phase. If you have the wrong phase,

I2 can be changed by returning to GNN and using the value IOPT(1) = 16. This results in an unkeyed input request line which should be two integers, 1 for I1 and then the value for I2.

There are several interesting features in CLM. It ordinarily starts with $X_1 = 1.0 \times 10^{-28}$ and increases X_1 by steps of 0.01 until it passes the correct value, and then searches for the exact root. It will ordinarily note any maxima or minima found along the way. Some times when there are maxima or minima, the root found will not be the one you really want. When this happens, you will want to start the search for roots at a different value of X_1. This is accomplished by entering the temperature, the activity, and then the integer 1 following the key ENTER TEMPERATURE, ACTIVITY, AND INTEGERS. The starting value for X_1 is then entered on the next line.

If no roots are found before $X_1 = 1.0$, the program will not print the ROOT BETWEEN line, but it will ordinarily go back and print the values of mole fractions and activities for your starting value of X_1, so you can perhaps see where the problem lies.

Many of the subroutines, including GOM and CLM , will return to the beginning so that the same calculation can be repeated for a different temperature or for some change in mole fraction or activity. This feature is needed to get enough values to plot activity vs. mole fraction or a solubility line on a phase diagram. The ordinary way to get out of these repeating subroutines is to hit return, entering a line of zeroes.

Equilibrium Between Two Phases of Variable Composition

The last major type of calculation required for two component

phase diagrams is to search for the values of activities and mole fractions at equilibrium between two phases, both of which have variable composition. In this case, you need two equilibrium constants:

$$K_1 = \frac{a_1 \text{ in phase 2}}{a_1 \text{ in phase 1}}$$

and:

$$K_2 = \frac{a_2 \text{ in phase 2}}{a_2 \text{ in phase 1}}$$

The calculation normally proceeds by assuming a value for one of the activities in one phase, calculates the activity for the other component in the other phase, and searches for suitable mole fractions for this other phase. If you make the right choice of components and phases, the calculation will usually converge after 4 to 16 steps of alternating between the phases. Subroutine ALTNT has been written to do the activity calculations and the alternating of phases automatically. It is written to start with an activity of .98 for component 2 in phase 2, so phase 2 is ordinarily selected as the phase which is richest in component 2. Subroutine ALTNT is called from GNN with the IOPT values 0 7. The IOPT values 0 7 1 and 0 7 9 will give more and less printed output respectively. It is necessary to have the Redlich-Kister coefficients available in the storage locations BETA and to have the equilibrium constants K_1 and K_2 ready to enter. However, the values $1/K_1$ and $1/K_2$ are equally acceptable.

The first key in ALTNT is ENTER TEMPERATURE AND A CONTROL INTEGER. For the calculation described here no control integer is necessary and one merely enters a temperature value, with

a decimal point. The computer then asks you to ENTER TWO EQUILIBRIUM CONSTANTS, and you type in the values for K_1 and K_2. If you have values for $1/K_1$ and $1/K_2$ instead, type them in but type 1 after the two values. This calculates K_1 and K_2 and uses them in the computation. Table 12 shows examples of these two entries. The program starts with the value 0.98 for a_2 in phase 2 and prints the successive values for a_1 in phase 1 that it obtains at each iteration. When the computer is satisfied that the calculation has converged, it will print the results for each phase, but more often it will ask : SHALL WE CONTINUE. The integer 1 means yes, but 0 and -1 will both take you back to the beginning to enter a new temperature, to reenter the old temperature, or to leave the subroutine (by pressing the RETURN key). Sometimes convergence is very slow, and you can improve this by guessing at a better starting value for the activity of component 2 in phase 2. If you want to do this, you need a fourth entry, the value 1, in the line following the key ENTER TWO EQUILIBRIUM CONSTANTS. Then on the next line, you type in the value you want to try for a_2 in phase 2.

This is sufficient instruction in the program to repeat a calculation of a phase diagram using a copy of our input files. Tables 13 - 19 show a calculation of the Ni-C phase diagram shown in Figure 2 The thermodynamic data for solid and liquid Ni and C are shown in Table 13. The values for Ni and for graphite are those selected to agree with the JANAF tables. The values for liquid C are selected to fit the equation $K = 1.33 - 5460/T$ for the equilibrium constant for the melting of carbon. This means that $\Delta C_p = 0$ for this reaction, and ΔH

is independent of temperature.

We have used two Redlich-Kister coefficients for carbon in solid Ni, the values A = 5.5121 + (13328/4.5756)(1/T - 1/1000) and B = -3.6. Similarly, two coefficients are used for the liquid phase. Table 13 and 14 are listings of the input files including the thermodynamic data for the calculation of equilibrium constants and of Redlich-Kister coefficients. The calculation of Redlich-Kister coefficients at three temperatures is shown in Table 15. The calculations of equilibrium constants for the melting of Ni and C are shown in Table 16. Table 17 shows the calculation of the solubility of graphite in solid Ni, and the corresponding calculation for the liquid phase is in Table 18. The last 2 lines of the phase diagram, describing the equilibrium between the solid and liquid Ni rich phases, are calculated using ALTNT as in Table 19. The activities of liquid carbon are always very small, and this is a case where the initial estimate a_2 in phase 2 = 0.98 made in ALTNT will not work at all.

It is possible to use ALTNT for cases where a single phase separates into two different compositions, as in cases of two immissible liquids. It is quite possible to represent such phases by a single set of Redlich-Kister coefficients. To use such a set in a phase equilibrium calculation it is necessary to read the values twice, once for phase 1 and once for phase 2.

Figure 3 is a flow chart showing the main sequences in which the subroutines are called.

Every new system to which the program is applied, is likely to bring up new problems. Some of these will be ones which we have already dealt with, and the modifications of BPHD needed may already be present. BPHD has developed by the continuous incorporation of

new features, always attempting to keep the older calculations in working order. This makes the program versatile, but somewhat complex. This kind of complete discussion of the program is available in a manual written for users of the program.[10]

Figure 4 shows a portion of the SiO_2-$KO_{0.5}$ phase diagram calculated with the coefficients listed in Table 20. This system is chosen here as an example of listing and using a large number of parameters. The values shown are of little more than historic interest because at the time they were selected there was insufficient accurate data on this binary system to fix seven parameters.

References

1. M. Margules, Sitzungsber. Wien. Akad., (2), 104, 1243 (1895)
2. C. W. Bale and A. W. Pelton, Metal. Trans., 6A, 1963 (1975)
3. R. A. Howald and I. Eliezer, Metal. Trans., in press
4. O. Redlich, A. T. Kister, and C. E. Turnquist, Chem. Eng. Progr., Symposium Series, 48(2), 49 (1952)
5. G. Scatchard, Chem. Revs., 44, 7 (1949)
6. O. Redlich and A. T. Kister, Ind. Engng. Chem., 40, 345 (1948)
7. E. A. Guggenheim, Thermodynamics, North Holland Pub. Co., Amsterdam, pp. 249-250 (1957)
8. J. M. Smith and H. C. Van Ness, Introduction to Chemical Engineering Thermodynamics, McGraw-Hill Book Co., New York, pp. 332-3 (1975)
9. JANAF Thermochemical Tables, Nat. Stand. Ref. Data Ser. 37 (1971)
10. R. A. Howald and I. Eliezer, BPHD: a Computer Program for the Calculation of Multiphase Equilibria (1976)

Table 1.

Typical conversion matrices for the Margules equations.

From eqn. 1 to eqn. 2:

$$|A_e\ B_e\ C_e\ D_e \ldots\rangle = \mathbf{E}\ |A_1\ B_1\ C_1\ D_1 \ldots\rangle$$

$$\mathbf{E} = \begin{pmatrix} 1 & 0 & 0 & 0 & 0 \\ 0 & (1/2) & 0 & 0 & 0 \\ 0 & 0 & (1/3) & 0 & 0 \\ 0 & 0 & 0 & (1/4) & 0 \\ 0 & 0 & 0 & 0 & (1/5) \end{pmatrix} \qquad \mathbf{E}^{-1} = \begin{pmatrix} 1 & 0 & 0 & 0 & 0 \\ 0 & 2 & 0 & 0 & 0 \\ 0 & 0 & 3 & 0 & 0 \\ 0 & 0 & 0 & 4 & 0 \\ 0 & 0 & 0 & 0 & 5 \end{pmatrix}$$

From eqn. 2 to eqn. 3:

$$|A_2\ B_2\ C_2\ D_2 \ldots\rangle = \mathbf{F}\ |A_e\ B_e\ C_e\ D_e \ldots\rangle$$

$$\mathbf{F} = \begin{pmatrix} 1 & -1 & 0 & 0 & 0 \\ 0 & 2 & -2 & 0 & 0 \\ 0 & 0 & 3 & -3 & 0 \\ 0 & 0 & 0 & 4 & -4 \\ 0 & 0 & 0 & 0 & 5 \end{pmatrix} \qquad \mathbf{F}^{-1} = \begin{pmatrix} 1 & (1/2) & (1/3) & (1/4) & (1/5) \\ 0 & (1/2) & (1/3) & (1/4) & (1/5) \\ 0 & 0 & (1/3) & (1/4) & (1/5) \\ 0 & 0 & 0 & (1/4) & (1/5) \\ 0 & 0 & 0 & 0 & (1/5) \end{pmatrix}$$

872

Table 1 (continued)

From eqn. 1 to eqn. 3:

$$|A_2\ B_2\ C_2\ D_2\ \ldots\rangle = \mathbf{G}\,|A_1\ B_1\ C_1\ D_1\ \ldots\rangle$$

$$\mathbf{G} = \mathbf{KF} = \begin{pmatrix} 1 & -(1/2) & 0 & 0 & 0 \\ 0 & 1 & -(2/3) & 0 & 0 \\ 0 & 0 & 1 & -(3/4) & 0 \\ 0 & 0 & 0 & 1 & -(4/5) \\ 0 & 0 & 0 & 0 & 1 \end{pmatrix} \qquad \mathbf{G}^{-1} = \begin{pmatrix} 1 & (1/2) & (1/3) & (1/4) & (1/5) \\ 0 & 1 & (2/3) & (2/4) & (2/5) \\ 0 & 0 & 1 & (3/4) & (3/5) \\ 0 & 0 & 0 & 1 & (4/5) \\ 0 & 0 & 0 & 0 & 1 \end{pmatrix}$$

Table 2.

Conversion matrices from Bale-Pelton to Margules coefficients.

From eqn. 6 to eqn. 2:

$$|A_e\ B_e\ C_e\ D_e \ldots\rangle = \mathbb{M}\,|q_0\ q_1\ q_2\ q_3 \ldots\rangle$$

$$\mathbb{M} = \begin{matrix} 1 & -1 & 1 & -1 & 1 & -1 & 1 & -1 \\ 0 & 2 & -6 & 12 & -20 & 30 & -42 & 56 \\ 0 & 0 & 6 & -30 & 90 & -210 & 420 & -756 \\ 0 & 0 & 0 & 20 & -140 & 560 & -1680 & 4200 \\ 0 & 0 & 0 & 0 & 70 & -630 & 3150 & -11550 \\ 0 & 0 & 0 & 0 & 0 & 252 & -2772 & 16632 \\ 0 & 0 & 0 & 0 & 0 & 0 & 924 & -12012 \\ 0 & 0 & 0 & 0 & 0 & 0 & 0 & 3432 \end{matrix}$$

$$\mathbb{M}^{-1} = \begin{matrix} 1 & (1/2) & (1/3) & (1/4) & (1/5) & (1/6) & (1/7) & (1/8) \\ 0 & (1/2) & (3/6) & (9/20) & (28/70) & (90/252) & (297/924) & (1001/3432) \\ 0 & 0 & (1/6) & (5/20) & (20/70) & (75/252) & (275/924) & (1001/3432) \\ 0 & 0 & 0 & (1/20) & (7/70) & (35/252) & (154/924) & (637/3432) \\ 0 & 0 & 0 & 0 & (1/70) & (9/252) & (54/924) & (273/3432) \\ 0 & 0 & 0 & 0 & 0 & (1/252) & (11/924) & (77/3432) \\ 0 & 0 & 0 & 0 & 0 & 0 & (1/924) & (13/3432) \\ 0 & 0 & 0 & 0 & 0 & 0 & 0 & (1/3432) \end{matrix}$$

Table 3.

The conversion matrix from Redlich-Kister to Bale-Pelton coefficients.

From equations 9-11 to eqn. 6:

$$|q_0\ q_1\ q_2\ q_3 \ldots\rangle = \mathbb{M}\,|A\ B\ C\ D \ldots\rangle$$

$$\mathbb{M} = \begin{pmatrix}
1 & 0 & (1/3) & 0 & (1/5) & 0 & (1/7) & 0 \\
0 & 1 & 0 & (3/5) & 0 & (27/63) & 0 & (143/429) \\
0 & 0 & (2/3) & 0 & (20/35) & 0 & (110/231) & 0 \\
0 & 0 & 0 & (2/5) & 0 & (28/63) & 0 & (182/429) \\
0 & 0 & 0 & 0 & (8/35) & 0 & (72/231) & 0 \\
0 & 0 & 0 & 0 & 0 & (8/63) & 0 & (88/429) \\
0 & 0 & 0 & 0 & 0 & 0 & (16/231) & 0 \\
0 & 0 & 0 & 0 & 0 & 0 & 0 & (16/429)
\end{pmatrix}$$

$$\mathbb{M}^{-1} = \begin{pmatrix}
1 & 0 & -(1/2) & 0 & (3/8) & 0 & -(5/16) & 0 \\
0 & 1 & 0 & -(3/2) & 0 & (15/8) & 0 & -(35/16) \\
0 & 0 & (3/2) & 0 & -(30/8) & 0 & (105/16) & 0 \\
0 & 0 & 0 & (5/2) & 0 & -(70/8) & 0 & (315/16) \\
0 & 0 & 0 & 0 & (35/8) & 0 & -(315/16) & 0 \\
0 & 0 & 0 & 0 & 0 & (63/8) & 0 & -(693/16) \\
0 & 0 & 0 & 0 & 0 & 0 & (321/16) & 0 \\
0 & 0 & 0 & 0 & 0 & 0 & 0 & (429/16)
\end{pmatrix}$$

Table 4.

One of the conversion matrices from Redlich-Kister to Margules coefficients.

From equations 9-11 to eqn. 2:

$$|A_e\ B_e\ C_e\ D_e \ldots\rangle = \mathbb{K}\ |A\ B\ C\ D \ldots\rangle$$

$$\mathbb{K} = \begin{matrix} 1 & -1 & 1 & -1 & 1 & -1 & 1 & -1 \\ 0 & 2 & -4 & 6 & -8 & 10 & -12 & 14 \\ 0 & 0 & 4 & -12 & 24 & -40 & 60 & -84 \\ 0 & 0 & 0 & 8 & -32 & 80 & -160 & 280 \\ 0 & 0 & 0 & 0 & 16 & -80 & 240 & -560 \\ 0 & 0 & 0 & 0 & 0 & 32 & -192 & 672 \\ 0 & 0 & 0 & 0 & 0 & 0 & 64 & -448 \\ 0 & 0 & 0 & 0 & 0 & 0 & 0 & 128 \end{matrix}$$

$$\mathbb{K}^{-1} = \begin{matrix} 1 & (1/2) & (1/4) & (1/8) & (1/16) & (1/32) & (1/64) & (1/128) \\ 0 & (1/2) & (2/4) & (3/8) & (4/16) & (5/32) & (6/64) & (7/128) \\ 0 & 0 & (1/4) & (3/8) & (6/16) & (10/32) & (15/64) & (21/128) \\ 0 & 0 & 0 & (1/8) & (4/16) & (10/32) & (20/64) & (35/128) \\ 0 & 0 & 0 & 0 & (1/16) & (5/32) & (15/64) & (35/128) \\ 0 & 0 & 0 & 0 & 0 & (1/32) & (6/64) & (21/128) \\ 0 & 0 & 0 & 0 & 0 & 0 & (1/64) & (7/128) \\ 0 & 0 & 0 & 0 & 0 & 0 & 0 & (1/128) \end{matrix}$$

Table 5.

Two simple conversion matrices which combine with $\mathbb{N}$ and $\mathbb{K}$ from Tables 3 and 4.

$$\mathbb{D} = \begin{matrix} 1 & 1 & 0 & 0 & 0 \\ 0 & 2 & 2 & 0 & 0 \\ 0 & 0 & 3 & 3 & 0 \\ 0 & 0 & 0 & 4 & 4 \\ 0 & 0 & 0 & 0 & 5 \end{matrix} \qquad \mathbb{D}^{-1} = \begin{matrix} 1 & -(1/2) & (1/3) & -(1/4) & (1/5) \\ 0 & (1/2) & -(1/3) & (1/4) & -(1/5) \\ 0 & 0 & (1/3) & -(1/4) & (1/5) \\ 0 & 0 & 0 & (1/4) & -(1/5) \\ 0 & 0 & 0 & 0 & (1/5) \end{matrix}$$

$$\mathbb{P} = \mathbb{P}^{-1} = \begin{matrix} 1 & 0 & 0 & 0 & 0 \\ 0 & -1 & 0 & 0 & 0 \\ 0 & 0 & 1 & 0 & 0 \\ 0 & 0 & 0 & -1 & 0 \\ 0 & 0 & 0 & 0 & 1 \end{matrix}$$

Table 6.

Summary of conversion matrices shown in Figure 1.

$\mathbf{E} = \mathbf{K}\,\mathbf{D}^{-1}\,\mathbf{K}^{-1}$ see Table 1

$\mathbf{F} = \mathbf{P}\,\mathbf{D}\,\mathbf{P}$ see Table 1

$\mathbf{G} = \mathbf{K}\,\mathbf{F}\,\mathbf{D}^{-1}\,\mathbf{K}^{-1} = \mathbf{K}\,\mathbf{P}\,\mathbf{D}\,\mathbf{P}\,\mathbf{D}^{-1}\,\mathbf{K}^{-1}$ see Table 1

$\mathbf{H} = \mathbf{K}\,\mathbf{N}^{-1}$ see Table 2

$$\mathbf{J} = \mathbf{K}\,\mathbf{D} = \begin{matrix} 1 & -1 & 1 & -1 & 1 \\ 0 & 4 & -8 & 12 & -16 \\ 0 & 0 & 12 & -36 & 72 \\ 0 & 0 & 0 & 32 & -128 \\ 0 & 0 & 0 & 0 & 80 \end{matrix} \qquad \mathbf{J}^{-1} = \begin{matrix} 1 & (1/4) & (1/12) & (1/32) & (1/80) \\ 0 & (1/4) & (2/12) & (3/32) & (4/80) \\ 0 & 0 & (1/12) & (3/32) & (6/80) \\ 0 & 0 & 0 & (1/32) & (4/80) \\ 0 & 0 & 0 & 0 & (1/80) \end{matrix}$$

$$\mathbf{L} = \mathbf{K}\,\mathbf{F} = \begin{matrix} 1 & -3 & 5 & -7 & 9 \\ 0 & 4 & -16 & 36 & -64 \\ 0 & 0 & 12 & -60 & 168 \\ 0 & 0 & 0 & 32 & -192 \\ 0 & 0 & 0 & 0 & 80 \end{matrix} \qquad \mathbf{L}^{-1} = \begin{matrix} 1 & (3/4) & (7/12) & (15/32) & (31/80) \\ 0 & (1/4) & (4/12) & (11/32) & (26/80) \\ 0 & 0 & (1/12) & (5/32) & (16/80) \\ 0 & 0 & 0 & (1/32) & (6/80) \\ 0 & 0 & 0 & 0 & (1/80) \end{matrix}$$

$$\mathbf{M} = \mathbf{N}\,\mathbf{F} = \begin{matrix} 1 & -1 & 1 & -1 & 1 \\ 0 & 2 & -2 & 2.4 & -2.4 \\ 0 & 0 & 2 & -2 & (18/7) \\ 0 & 0 & 0 & 1.6 & -1.6 \\ 0 & 0 & 0 & 0 & (8/7) \end{matrix} \qquad \mathbf{M}^{-1} = \begin{matrix} 1 & (1/2) & 0 & -(2/16) & 0 \\ 0 & (1/2) & (1/2) & -(2/16) & -(3/8) \\ 0 & 0 & (1/2) & (1/16) & -(3/8) \\ 0 & 0 & 0 & (1/16) & (7/8) \\ 0 & 0 & 0 & 0 & (7/8) \end{matrix}$$

$$\mathbf{O} = \mathbf{N}\,\mathbf{D} = \begin{matrix} 1 & 1 & 1 & 1 & 1 \\ 0 & 2 & 2 & 2.4 & 2.4 \\ 0 & 0 & 2 & 2 & (18/7) \\ 0 & 0 & 0 & 1.6 & 1.6 \\ 0 & 0 & 0 & 0 & (8/7) \end{matrix} \qquad \mathbf{O}^{-1} = \begin{matrix} 1 & -(1/2) & 0 & (2/16) & 0 \\ 0 & (1/2) & -(1/2) & -(2/16) & (3/8) \\ 0 & 0 & (1/2) & -(1/16) & -(3/8) \\ 0 & 0 & 0 & (1/16) & -(7/8) \\ 0 & 0 & 0 & 0 & (7/8) \end{matrix}$$

Table 6 (continued)

$$R = N F N^{-1} = \begin{matrix} 1 & -1 & 1 & -1 & 1 \\ 0 & 2 & -3 & 3 & -3 \\ 0 & 0 & 3 & -5 & 5 \\ 0 & 0 & 0 & 4 & -7 \\ 0 & 0 & 0 & 0 & 5 \end{matrix} \qquad R^{-1} = \begin{matrix} 1 & (1/2) & (1/6) & (1/12) & (1/20) \\ 0 & (1/2) & (3/6) & (3/12) & (3/20) \\ 0 & 0 & (1/3) & (5/12) & (5/20) \\ 0 & 0 & 0 & (1/4) & (7/20) \\ 0 & 0 & 0 & 0 & (1/5) \end{matrix}$$

$$S = N D N^{-1} = \begin{matrix} 1 & 1 & 1 & 1 & 1 \\ 0 & 2 & 3 & 3 & 3 \\ 0 & 0 & 3 & 5 & 5 \\ 0 & 0 & 0 & 4 & 7 \\ 0 & 0 & 0 & 0 & 5 \end{matrix} \qquad S^{-1} = \begin{matrix} 1 & -(1/2) & (1/6) & -(1/12) & (1/20) \\ 0 & (1/2) & -(3/6) & (3/12) & -(3/20) \\ 0 & 0 & (1/3) & -(5/12) & (5/20) \\ 0 & 0 & 0 & (1/4) & -(7/20) \\ 0 & 0 & 0 & 0 & (1/5) \end{matrix}$$

$$T = N F D^{-1} N^{-1} = \begin{matrix} 1 & -1 & 1 & -1 & 1 \\ 0 & 1 & -2 & 3.5 & -2.7 \\ 0 & 0 & 1 & -2.5 & 3.5 \\ 0 & 0 & 0 & 1 & -2.8 \\ 0 & 0 & 0 & 0 & 1 \end{matrix} \qquad T^{-1} = P T P$$

$$U = U^{-1} = L P L^{-1} = K F P F^{-1} K^{-1} = \begin{matrix} 1 & (3/2) & 2 & (5/2) & 3 \\ 0 & -1 & -(8/3) & -5 & -8 \\ 0 & 0 & 1 & (15/4) & 9 \\ 0 & 0 & 0 & -1 & -(24/5) \\ 0 & 0 & 0 & 0 & 1 \end{matrix}$$

Table 7

```
K2O (G)
        7           3           1 71.11     10462.6    -23537.4
        2 14.904
FE (G)
        9           3           1 46.141    4033.      103533.
        2 5.86152  -.41359E-3 .75550E-6 -.1603E-9
FE (C, GAMMA)
        9           2           1 10.026    6789.      6789.
        2 7.73018   .0020027   -.41615E-8
K2CO3 (L)
        4           4           1 57.546    27309.     -242911.
        2 50.0
ALO1.5 (C, BETA, 6-77)
        8           4           1 13.0705   9317.      -188988.
        2 14.908    .0023471   -.12717E-5 .34615E-9
LI(CO3).5 (S)
       10           2           1 18.522    12540.5    -132779.5
        2 23.109    .01551      -.0000200
LI(CO3).5 (L)
       10           1           1 23.0615   13036.     -127779.
        2 22.16
KALO2(S)
       10           3           1 31.3415   16317.     -256645.8
        2  24.005   .0033071 -.12717E-5 .34615E-9
 KALO2 (L)
       10           4           1 32.779    16706.     -249320.5
        2 28.762    .0018
KO.5 (G)
        8           3           1 61.358    6287.      21887.
        2 9.12996  .27908E-3 -.2310E-7
KALSI3O8 (L, CLASS)
        9           1           1 94.72     47988.     -886596.
        2 77.049    .014243     .3525E-4
ALO1.5 (C, GAMMA)
        7           4           1 13.000    9317.      -188283.
        2 14.908    .0023471   -.1272E-5 .3462E-9
K2SO4 (S, BETA)
        1           4           1 61.69     31630.     -311030.
        2 46.90     .0201
K2SO4 (LIQUID)
        2           4           1 69.2907   31630.     -300924.5
        2 47.28
NEXT TO LAST CARD
        0           0           1
```

Table 8

```
!SET F:12 DC/TCBT;IN

!SET F:13 DC/TBCT;IN

!SET F:14 DC/CRIS;IN

!LINK BPHD ØVER LMPD
     LINKING  BPHD
'P1' ASSØCIATED.
     LINKING  SYSTEM LIB

!LMPD.
ØPTIØNS?
?1792
 0 ENTER NUMBER ØF TEMPERATURES, AND N TEMP VALUES
?3 1000. 1073. 1473.
IDENTIFY THE INPUT FILE
?14
KØ.5 IN LIQUID SIØ2
CØMPØNENT   1 ØF PHASE  1 HØ298 IS   -89562.1875
AT1000.000 HØ = -81000.18750 AND PHI IS  25.476303 CP=   11.45000
AT1073.000 HØ = -80159.50000 AND PHI IS  25.085655 CP=   11.58140
AT1473.000 HØ = -75382.93750 AND PHI IS  29.001068 CP=   12.30140
SIØ2 (LIQUID)
CØMPØNENT   2 ØF PHASE  1 HØ298 IS  -215010.0000
AT1000.000 HØ =-205669.00000 AND PHI IS  18.202774 CP=   16.61000
AT1073.000 HØ =-204447.68750 AND PHI IS  18.946747 CP=   16.85214
AT1473.000 HØ =-197407.81250 AND PHI IS  22.656967 CP=   18.41333
KØ.5 (C,IN TRIDYMITE
CØMPØNENT   1 ØF PHASE  2 HØ298 IS   -80000.0000
AT1000.000 HØ = -71655.00000 AND PHI IS  18.000000 CP=    9.09700
AT1073.000 HØ = -70938.31250 AND PHI IS  18.589844 CP=    9.16708
AT1473.000 HØ = -67244.68750 AND PHI IS  21.291153 CP=    9.55108
SIØ2 (C,TRIDYMITE)
CØMPØNENT   2 ØF PHASE  2 HØ298 IS  -217270.0000
AT1000.000 HØ =-206702.52500 AND PHI IS  17.559998 CP=   16.72176
AT1073.000 HØ =-205476.56250 AND PHI IS  18.319580 CP=   16.86310
AT1473.000 HØ =-198613.62500 AND PHI IS  22.076843 CP=   17.39197
SIØ2 (C,CRISTØBALITE
CØMPØNENT   4 ØF PHASE  2 HØ298 IS  -215687.0000
AT1000.000 HØ =-205670.00000 AND PHI IS  18.136993 CP=   16.72176
AT1073.000 HØ =-205443.93750 AND PHI IS  18.859131 CP=   16.86310
AT1473.000 HØ =-198581.00000 AND PHI IS  22.477097 CP=   17.39197
SIØ2 (C,QUARTZ)
CØMPØNENT   5 ØF PHASE  2 HØ298 IS  -217970.0000
AT1000.000 HØ =-207130.00000 AND PHI IS  16.973007 CP=   16.48000
AT1073.000 HØ =-205920.56250 AND PHI IS  17.750580 CP=   16.65518
AT1473.000 HØ =-199066.43750 AND PHI IS  21.568054 CP=   17.61519
ENTER IDATA FØR FILE TØ BE REWØUND, IT IS NØW  -2
?14
IN GNN, ENTER 9 IØPT VALUES   9  2  0  0  0  0  0  0  0
?7
ENTER THE NUMBER ØF PHASES AND IØPT(9)
?2
ENTER ICØMP, IPHASE, AND THEN  2 VALUES FØR PHI
```

Table 9

Calculation of some equilibrium constants for reactions of SiO_2.

```
CP-V C1B AT YOUR SERVICE
ON AT 16:48 SEP 13,'76
LOGON PLEASE: 156,ELIEZER,

C1B IN ... NORMAL CHARGES AGAIN...DOWN AT MIDNIGHT FOR
TYPE NEWS FOR USER INFO, ENTER FOR SUGGESTIONS


!C CRIS TO ME
KO.5 IN LIQUID SIO2
1 1 1  25.4763 8562. -81000.2
2 11.45 .00180
SIO2 (LIQUID)
2 1 1 18.20277 10341. -205669.
2 16.61 .0032268 .12384E-5
KO.5 (C,IN TRIDYMITE)
1 2 1 18.000 8345. -71655.
2 9.097 .00096
SIO2 (C,TRIDYMITE)
2 2 1 17.560 10567.4 -206702.6
2 16.72175 .00205366 -.00000165179 .64630E-9
SIO2 (C,CRISTOBALITE)
4 2 1 18.137 10017. -206670.
2 16.72175 .00205366 -.00000165179 .6463E-9
SIO2 (C,QUARTZ)
5 2 1 16.973 10840. -207130.
2 16.480 .0024
END
0 0 1

!SET F:14 DC/CRIS:IN

!LMPD.
OPTIONS?
?17920006
 0 ENTER NUMBER OF TEMPERATURES, AND N TEMP VALUES
?3 1000. 1073. 1473.
IDENTIFY THE INPUT FILE
?14
KO.5 IN LIQUID SIO2
?4
SIO2 (LIQUID)
?
COMPONENT   2 OF PHASE  1 HO298 IS  -216010.0000
AT1000.000 HO =-205669.00000 AND PHI IS  18.202774 CP=   16.61000
AT1073.000 HO =-204447.68750 AND PHI IS  18.946747 CP=   16.35314
AT1473.000 HO =-197407.81250 AND PHI IS  22.656967 CP=   18.41333
```

Table 9 (continued)

```
KO.5 (C,IN TRIDYMITE
?4
SIO2 (C,TRIDYMITE)
?
COMPONENT   2 OF PHASE  2 HO298 IS  -217270.0000
AT1000.000 HO =-206702.62500 AND PHI IS  17.559999 CP=   16.72176
AT1073.000 HO =-205476.56250 AND PHI IS  18.319590 CP=   16.86310
AT1473.000 HO =-198613.62500 AND PHI IS  22.076843 CP=   17.39197
SIO2 (C,CRISTOBALITE
?
COMPONENT   4 OF PHASE  2 HO298 IS  -216637.0000
AT1000.000 HO =-206670.00000 AND PHI IS  18.136993 CP=   16.72176
AT1073.000 HO =-205443.93750 AND PHI IS  18.859131 CP=   16.86310
AT1473.000 HO =-198581.00000 AND PHI IS  22.477097 CP=   17.39197
SIO2 (C,QUARTZ)
?4
ENTER IDATA FOR FILE TO BE REWOUND, IT IS NOW ###
?14
IN GVV, ENTER 9 IOPT VALUES   9  2  0  0  0  4  0  6  0
?7
ENTER THE NUMBER OF PHASES AND IOPT(9)
?2
ENTER ICOMP, IPHASE, AND THEN   2 VALUES FOR PHI
?
ENTER THE COEFFICIENTS AND THEN THE HO298 VALUES, PHASE  1
?0. 1.
ENTER THE COEFFICIENTS AND THEN THE HO298 VALUES, PHASE  2
?0. -1.
AT 1073.00K, KEQ =  .759327E 00 .102887E 04 .587050E 03
AT 1473.00K, KEQ =  .870642E 00 .120581E 04 .405478E 03
 0 DO YOU WANT TO CALCULATE KEQ AT OTHER TEMPERATURES?
?
IN GVV, ENTER 9 IOPT VALUES   7  0  0  0  0  0  0  0  5
?7
ENTER THE NUMBER OF PHASES AND IOPT(9)
?2
ENTER ICOMP, IPHASE, AND THEN   2 VALUES FOR PHI
?
ENTER THE COEFFICIENTS AND THEN THE HO298 VALUES, PHASE  1
?
ENTER THE COEFFICIENTS AND THEN THE HO298 VALUES, PHASE  2
?0. -1. 0. 1.
AT 1073.00K, KEQ =  .998097E 00 .326250E 02 .406201E 01
AT 1473.00K, KEQ =  .100225E 01 .326250E 02-.657300E 01
 0 DO YOU WANT TO CALCULATE KEQ AT OTHER TEMPERATURES?
?3
ENTER THE COEFFICIENTS AND THEN THE HO298 VALUES, PHASE  1
?0. 1.
ENTER THE COEFFICIENTS AND THEN THE HO298 VALUES, PHASE  2
?0. 0. 0. -1.
AT 1073.00K, KEQ =  .760775E 00 .996250E 03 .582988E 03
AT 1473.00K, KEQ =  .868639E 00 .117319E 04 .412051E 03
 0 DO YOU WANT TO CALCULATE KEQ AT OTHER TEMPERATURES?
?
IN GVV, ENTER 9 IOPT VALUES   7  0  0  0  0  0  0  0  5
?
SORRY, NO OTHER SYSTEMS ARE AVAILABLE YET
DO YOU WANT TO CONTINUE?  USE 1 FOR YES
?
 *STOP* 0
```

Table 10

Calculation of Redlich-Kister coefficients at 1300K in the $KO_{.5}$-$AlO_{1.5}$ system.

```
!C CLUM
-13.155 -4.587
-71352. -25971.
0.
0.
0.
0.
-.546255 7.34730 14.4529 7.56354
3298.85 20269.3 36991.3 20376.3
0.
0.
0.
0.
-97.484095 -129.7985 14.4529 7.56354 0. 170.
3298.85 20269.3 36991.3 20376.3
0.
0.
0.
0.

!SET F:12 DC/CLUM;IN

!LMPD.
ØPTIØNS?
?1791
 0 ENTER NUMBER ØF TEMPERATURES, AND N TEMP VALUES
?2 1000. 1300.
IDENTIFY THE PHASE BY 1,2, ØR 3, AND THEN THE INPUT FILE
?1 12
T=  1000.000 -13.15499973  -4.58699989     .00000000     .00000000
            .00000000     .00000000     .00000000     .00000000
T=  1300.000  -9.55640316  -3.27716827     .00000000     .00000000
            .00000000     .00000000     .00000000     .00000000
ENTER THE NUMBER FØR ANØTHER PHASE IF THERE IS ØNE
?2
T=  1000.000   -.54625499   7.34729958  14.45289993   7.56354046
            .00000000     .00000000     .00000000     .00000000
T=  1300.000   -.71263057   6.32502937  12.58726501   6.53587532
            .00000000     .00000000     .00000000     .00000000
ENTER THE NUMBER FØR ANØTHER PHASE IF THERE IS ØNE
?1
T=  1000.000 -97.48410034-129.79849243  14.45289993   7.56354046
            .00000000 170.00000000     .00000000     .00000000
T=  1300.000 -97.65046692-130.82075500  12.58726501   6.53587532
            .00000000 170.00000000     .00000000     .00000000
ENTER THE NUMBER FØR ANØTHER PHASE IF THERE IS ØNE
?
IN GNN, ENTER 9 IØPT VALUES   9  1  0  0  0  0  0  0  0
?8 5
IØP(7)=  0  ENTER TEMP. AND MØLE FRACTIØN
?1300. .08
     .000000   -8.239993 -578.357178   -5.974330   -3.701484
    .08000?    .00000=ACTIVITY ØF      .00000  .84872E-08 -.18585E 02
    .92000?    .00020=ACTIVITY ØF      .00018  .18294E-03
```

Table 11

Use of subroutine CLM

A. Redlich-Kister coefficients for the Fe-C liquid system.

```
!EDIT BSTEEL
EDIT HERE
*TY 1-6
   1.000 -3.79379 -.655295 .629251
   2.000 -24280. 4696. 0.
   3.000 0.
   4.000 0.
   5.000 0.
   6.000 0.
*END

!SET F:13 DC/BSTEEL;IN

!LMPD.
ØPTIØNS?
?1791
 0 ENTER NUMBER ØF TEMPERATURES, AND N TEMP VALUES
?4 1000. 1573. 1773.
IDENTIFY THE PHASE BY 1,2, ØR 3, AND THEN THE INPUT FILE
?1 13
T=  1000.000  -3.79378986   -.65529501    .62925100    .00000000
          .00000000    .00000000    .00000000    .00000000
T=  1573.000  -1.86082745  -1.02914905    .62925100    .00000000
          .00000000    .00000000    .00000000    .00000000
T=  1773.000  -1.48029613  -1.10274792    .62925100    .00000000
          .00000000    .00000000    .00000000    .00000000
T=  1973.000  -1.17591231  -1.16142464    .62925100    .00000000
          .00000000    .00000000    .00000000    .00000000
ENTER THE NUMBER FØR ANØTHER PHASE IF THERE IS ØNE
?
```

Table 11 B

Use of CLM to find the solubility of carbon in liquid iron

```
IN GNN, ENTER 9 IØPT VALUES   9  1  0  0  0  0  0  0  0
?8 5
IØP(7)=  0  ENTER TEMP. AND MØLE FRACTIØN
?1773. .8
     .000000    -2.471651    -0.776355     -.098866    -1.136867
    .80000?     .79640=ACTIVITY ØF       .63712  .63712E 00 -.45C79E 00
    .20000?     .07297=ACTIVITY ØF       .01459  .14594E-01
?
  5 YØU ARE IN CLM, ENTER KZZ VALUES TØ CØNTRØL ACTIØNS
?4
  1  IENTER TEMPERATURE, ACTIVITY, AND IITEGERS
?1773. .01781\011
 .954902E 00 MINIMUM AT X =     .06324393    .97270314
 .978954E 00 MAXIMUM AT X =     .18828118    .99675554
RØØT BETWEEN
   .78655638    .78665686 AT T =     1773.000
     .000000    -2.505487    -1.743021     -.114038    -1.078530
    .78656?     .75906=ACTIVITY ØF       .60499  .60499E 00 -.50255E 00
    .21334?     .08344=ACTIVITY ØF       .01780  .17801E-01
  1  IENTER TEMPERATURE, ACTIVITY, AND IITEGERS
?1573. .00722598 1
?.7
RØØT BETWEEN
   .81015253    .81015301 AT T =     1573.000
     .000000    -2.659728    -2.162739     -.095862    -1.419507
    .81015?     .80193=ACTIVITY ØF       .64969  .64969E 00 -.43126E 00
    .18985?     .03806=ACTIVITY ØF       .00723  .72260E-02
  1  IENTER TEMPERATURE, ACTIVITY, AND INTEGERS
```

Table 12

Examples using subroutine ALTNT

```
 !C BETA
 -.3966 2.4089 5.5772 -.5137 -1.76 1.76 4.4
 0 0 14458.8 -28002.6 0 0 0
 0.
 0.
 0.
 0.
 -3.25
 -9151.2
 0.
 0.
 0.
 0.
 END
 0 0 1

 !SET F:13 DC/BETA:IN

 !LMPD.
 OPTIONS?
 ?17910002
  0 ENTER NUMBER OF TEMPERATURES, AND N TEMP VALUES
 ?15 1000. 1840. 1860.
 ?
 IDENTIFY THE PHASE BY 1,2, OR 3, AND THEN THE INPUT FILE
 ?1 13
 ENTER THE NUMBER FOR ANOTHER PHASE IF THERE IS ONE
 ?2
 ENTER THE NUMBER FOR ANOTHER PHASE IF THERE IS ONE
 ?
 IN GVN, ENTER 9 IOPT VALUES   9  1  0  0  0  2  0  2  0
 ?0 7
 ENTER TEMPERATURE AND A CONTROL INTEGER
 ?1900.
 ENTER TWO EQUILIBRIUM CONSTANTS
 ?709.655 .977530 1
     .957980
 WILL YOU ACCEPT GAMMA OF  .498214E-02 .812682E-05 .116097E-04
 ?1
     .975949
     .976290
      .000000   -1.303731    4.500839   -1.145228     .017726
      .000000   -2.302638   -2.302638   -2.296866    -.000004
     .062757    .071577 GIVES ACTIVITY IN PHASE  1 OF     .004492  .44919
 4E-02
     .937243   1.041660 GIVES ACTIVITY IN PHASE  1 OF     .976289  .97628
 9E 00
     .001254    .005043 GIVES ACTIVITY IN PHASE  2 OF     .000006  .53297
 5E-05
     .998746    .999992 GIVES ACTIVITY IN PHASE  2 OF     .998738  .99873
 8E 00
```

Table 12 (continued)

```
 ENTER TEMPERATURE AND A CONTROL INTEGER
 ?1920.
 ENTER TWO EQUILIBRIUM CONSTANTS
 ?696.351 .983015 1
     .963355
     .981640
     .981971
      .000000   -1.287062    5.572861   -1.152577     .016062
      .000000   -2.291673   -2.291673   -2.286860    -.000003
     .053685    .070376 GIVES ACTIVITY IN PHASE  1 OF     .003778  .37781

 5E-02
     .946315   1.037675 GIVES ACTIVITY IN PHASE  1 OF     .981967  .98196

 7E 00
     .001050    .005166 GIVES ACTIVITY IN PHASE  2 OF     .000005  .54256

 5E-05
     .998950    .999994 GIVES ACTIVITY IN PHASE  2 OF     .998944  .99894

 4E 00
 ENTER TEMPERATURE AND A CONTROL INTEGER
 ?1920.
 ENTER TWO EQUILIBRIUM CONSTANTS
 ?696.351 .983015 1 1
 ?.9989
     .981934
     .981977
     .053677    .070379 GIVES ACTIVITY IN PHASE  1 OF     .003778  .37777

 6E-02
     .946323   1.037672 GIVES ACTIVITY IN PHASE  1 OF     .981972  .98197

 2E 00
     .001050    .005166 GIVES ACTIVITY IN PHASE  2 OF     .000005  .54250

 8E-05
     .998950    .999994 GIVES ACTIVITY IN PHASE  2 OF     .998944  .99894

 4E 00
 ENTER TEMPERATURE AND A CONTROL INTEGER
 ?1920.
 ENTER TWO EQUILIBRIUM CONSTANTS
 ?.00143606 1.017278
     .963355
     .981640
     .981971
      .000000   -1.287062    5.572861   -1.152577     .016062
      .000000   -2.291673   -2.291673   -2.286860    -.000003
     .053685    .070376 GIVES ACTIVITY IN PHASE  1 OF     .003778  .37781

 5E-02
     .946315   1.037675 GIVES ACTIVITY IN PHASE  1 OF     .981967  .98196

 7E 00
     .001050    .005166 GIVES ACTIVITY IN PHASE  2 OF     .000005  .54256
```

Table 12 (continued)

```
 6E-05
     .998950     .999994 GIVES ACTIVITY IN PHASE  2 OF      .998944  .99994

 4E 00
 ENTER TEMPERATURE AND A CONTROL INTEGER
 ?1960.
 ENTER TWO EQUILIBRIUM CONSTANTS
 ?671.606 .994233 1
     .974349
     .993223
     .993653
      .000000     -.665728    14.465683     -.653675      .001196
      .000000    -2.270414    -2.270414    -2.267893     -.000001
     .99367 8
    .990966 COMP. 2 AT T =    1960.0000.1002725E 01.9936779E 00
      .000000     -.664044    14.482361     -.652101      .001182
     .00903?      .22279=ACTIVITY OF      .00201  .20126E-02 -.620833E 01
     .99097?    1.00272=ACTIVITY OF      .99367  .99367E 00
    .000555 COMP. 1 AT T =    1960.0000.5396448E-02.2996723E-05
      .000000    -2.270414    -2.270414    -2.267893     -.000001
     .00056?      .00540=ACTIVITY OF      .00000  .29967E-05 -.12718E 02
     .99944?    1.00000=ACTIVITY OF      .99944  .99944E 00
     .0053964SHALL WE CONTINUE?
 ?1
     .993679
     .009013     .223068 GIVES ACTIVITY IN PHASE  1 OF      .002011  .20105

 4E-02
     .990987    1.002713 GIVES ACTIVITY IN PHASE  1 OF      .993676  .99367

 6E 00
     .000555     .005396 GIVES ACTIVITY IN PHASE  2 OF      .000003  .29936

 3E-05
     .999445     .999998 GIVES ACTIVITY IN PHASE  2 OF      .999444  .99944

 4E 00
 ENTER TEMPERATURE AND A CONTROL INTEGER
 ?
```

Table 13

Input thermodynamic data for iron, nickel, and carbon.

```
!C FENIC
C(GRAPHITE)
5 1 1 3.03 2824. 2824.
2 5.18396 .00122208 -.529846E-6
NI(S)
2 1 1 10.77 5215. 5215.
2 7.86096 .00314322 -.35278E-5 .890841E-9
FE(GAMMA)
3 1 1 10.025 6789. 6789.
2 7.73018 .0020027 -.416124E-8
FE(ALPHA)
4 1 1 10.123 5820. 5928.
2 13.2341 -.0253213 .486523E-4 -.272654E-7
FE(L)(JANAF)
3 2 1 11.7639 6134. 9272.
2 10.1877 .37823E-3 .139724E-7
C IN FE GAMMA
1 1 1 7.274 2824. 13376.
2 5.18396 .00122208 -.529846E-6
C IN FE(L)
1 2 1 7.03 2824. 8245.
2 5.18396 .00122208 -.529846E-6
NI(L)
2 2 1 12.1700 5215. 8060.5
2 10.30
C,GRAPHITE,JANAF
6 1 1 3.020 2824. 2824.
2 5.15465 .00159627 -.13423E-5 .45542E-9
C(L) IN FE(L) XC=1
5 2 1 -23.0722  2824. 12457.7
2 5.15465 .00159627 -.13423E-5 .45542E-9
C(L) IN FE(L) X=0
4 2 1 7.001 2824. 8224.
2 5.15465 .00159627 -.13423E-5 .45542E-9
END
0 0 1
```

Table 14

Input file for the calculation of Redlich-Kister coefficients for the nickel-carbon system.

```
!QUIT

!BUILD BENIC
   1.000 5.5121 -3.
   2.000 13328. 0.
   3.000 0.
   4.000 0.
   5.000 0.
   6.000 0.
   7.000 -2.7448 .0162
   8.000 -17705. 0.
   9.000 0.
  10.000 0.
  11.000 0.
  12.000 0.
  13.000

!SET F:12 DC/BENIC;IN
```

Table 15

Calculation of Redlich-Kister coefficients for the liquid Ni-C system.

```
!LMPD.
ØPTIØNS?
?1791
 0 ENTER NUMBER ØF TEMPERATURES, AND N TEMP VALUES
?4 1000. 1773. 1573. 1973.
IDENTIFY THE PHASE BY 1,2, ØR 3, AND THEN THE INPUT FILE
?1 12
T=  1000.000    5.51210022  -3.00000000     .00000000     .00000000
          .00000000     .00000000     .00000000     .00000000
T=  1773.000    4.24215603  -3.00000000     .00000000     .00000000
          .00000000     .00000000     .00000000     .00000000
T=  1573.000    4.45104122  -3.00000000     .00000000     .00000000
          .00000000     .00000000     .00000000     .00000000
T=  1973.000    4.07561970  -3.00000000     .00000000     .00000000
          .00000000     .00000000     .00000000     .00000000
ENTER THE NUMBER FØR ANØTHER PHASE IF THERE IS ØNE
?2
T=  1000.000   -2.74479961     .01620000     .00000000     .00000000
          .00000000     .00000000     .00000000     .00000000
T=  1773.000   -1.05779743     .01620000     .00000000     .00000000
          .00000000     .00000000     .00000000     .00000000
T=  1573.000   -1.33528137     .01620000     .00000000     .00000000
          .00000000     .00000000     .00000000     .00000000
T=  1973.000    -.83656979     .01620000     .00000000     .00000000
          .00000000     .00000000     .00000000     .00000000
ENTER THE NUMBER FØR ANØTHER PHASE IF THERE IS ØNE
?
```

Table 16

Calculation of equilibrium constants for the melting of C and Ni

```
!SET F:13 /FENIC;IN

!LMPD.
ØPTIØNS?
?17920004
 0 ENTER NUMBER ØF TEMPERATURES, AND N TEMP VALUES
?11 1000. 1600. 1620.
IDENTIFY THE INPUT FILE
?13
ENTER IDATA FØR FILE TØ BE REWØUND, IT IS NØW ###
?13
IN GNN, ENTER 9 IØPT VALUES   9  2  0  0  0  4  0  4  0
?7
ENTER THE NUMBER ØF PHASES AND IØPT(9)
?2 5
ENTER ICØMP, IPHASE, AND THEN  10 VALUES FØR PHI
?
ENTER THE CØEFFICIENTS AND THEN THE HØ298 VALUES, PHASE  1
?0. 0. 0. 0. 0. -1.
ENTER THE CØEFFICIENTS AND THEN THE HØ298 VALUES, PHASE  2
?0. 0. 0. 0. 1.
AT 1600.00K, KEQ =   .826935E-02 .249830E 05 .152462E 05
AT 1620.00K, KEQ =   .911174E-02 .249830E 05 .151245E 05
AT 1640.00K, KEQ =   .100162E-01 .249830E 05 .150028E 05
AT 1660.00K, KEQ =   .109854E-01 .249830E 05 .148811E 05
AT 1680.00K, KEQ =   .120219E-01 .249830E 05 .147594E 05
AT 1700.00K, KEQ =   .131283E-01 .249830E 05 .146377E 05
AT 1720.00K, KEQ =   .143072E-01 .249830E 05 .145159E 05
AT 1740.00K, KEQ =   .155611E-01 .249830E 05 .143942E 05
AT 1760.00K, KEQ =   .168927E-01 .249830E 05 .142725E 05
AT 1780.00K, KEQ =   .183045E-01 .249830E 05 .141508E 05
 0 DØ YØU WANT TØ CALCULATE KEQ AT ØTHER TEMPERATURES?
?
IN GNN, ENTER 9 IØPT VALUES   7  0  0  0  0  0  0  0  5
?9 2 0 0 0 4
 0 ENTER NUMBER ØF TEMPERATURES, AND N TEMP VALUES
?11 1000. 1600. 1620.
IDENTIFY THE INPUT FILE
?13
ENTER IDATA FØR FILE TØ BE REWØUND, IT IS NØW  13
?13
IN GNN, ENTER 9 IØPT VALUES   9  2  0  0  0  4  0  0  0
?7
ENTER THE NUMBER ØF PHASES AND IØPT(9)
?2 5
ENTER ICØMP, IPHASE, AND THEN  10 VALUES FØR PHI
?
ENTER THE CØEFFICIENTS AND THEN THE HØ298 VALUES, PHASE  1
?0. -1.
ENTER THE CØEFFICIENTS AND THEN THE HØ298 VALUES, PHASE  2
?0. 1.
AT 1600.00K, KEQ =   .910820E 00 .396829E 04 .296995E 03
AT 1620.00K, KEQ =   .925022E 00 .400093E 04 .250899E 03
AT 1640.00K, KEQ =   .939206E 00 .403366E 04 .204405E 03
AT 1650.00K, KEQ =   .953375E 00 .406650E 04 .157505E 03
```

Table 16 (continued)

```
 AT 1680.00K, KEQ =   .967525E 00 .409948E 04 .110216E 03
 AT 1700.00K, KEQ =   .981663E 00 .413262E 04 .625222E 02
 AT 1720.00K, KEQ =   .995782E 00 .416596E 04 .144458E 02
 AT 1740.00K, KEQ =   .100989E 01 .419952E 04-.340234E 02
 AT 1760.00K, KEQ =   .102398E 01 .423332E 04-.828755E 02
 AT 1780.00K, KEQ =   .103806E 01 .426740E 04-.132121E 03
  0 DØ YØU WANT TØ CALCULATE KEQ AT ØTHER TEMPERATURES?
 ?
  IN GVN, ENTER 9 IOPT VALUES   9  2  0  0  0  3  0  5  0
  ?7
  ENTER THE NUMBER OF PHASES AND IOPT(9)
  ?2
  ENTER ICOMP, IPHASE, AND THEN   7 VALUES FOR PHI
  ?
  ENTER THE COEFFICIENTS AND THEN THE H0298 VALUES, PHASE  1
  ?0 -1.
  ENTER THE COEFFICIENTS AND THEN THE H0298 VALUES, PHASE  2
  ?0 1.
  AT 1560.00K, KEQ =   .882366E 00 .390312E 04 .387957E 03
  AT 1600.00K, KEQ =   .910820E 00 .396829E 04 .296995E 03
  AT 1640.00K, KEQ =   .939206E 00 .403366E 04 .204405E 03
  AT 1680.00K, KEQ =   .967525E 00 .409948E 04 .110216E 03
  AT 1720.00K, KEQ =   .995782E 00 .416596E 04 .144458E 02
  AT 1760.00K, KEQ =   .102398E 01 .423332E 04-.828755E 02
  AT 1800.00K, KEQ =   .105212E 01 .430177E 04-.181745E 03
   0 DO YOU WANT TO CALCULATE KEQ AT OTHER TEMPERATURES?
  ?1
  ENTER ONE OR MORE TEMPERATURE
  ?1730. 1740. -100.
  AT 1730.00K, KEQ =   .100234E 01 .418280E 04-.975000E 01
  AT 1740.00K, KEQ =   .100989E 01 .419964E 04-.340352E 02
  ENTER ONE OR MORE TEMPERATURE
  ?1726. 1727. 1728. 1728. -10.
  AT 1726.00K, KEQ =   .100002E 01 .417606E 04-.535937E-01
  AT 1727.00K, KEQ =   .100072E 01 .417775E 04-.247974E 01
  AT 1728.00K, KEQ =   .100143E 01 .417943E 04-.490161E 01
  AT 1728.00K, KEQ =   .100143E 01 .417943E 04-.490161E 01
  ENTER ONE OR MORE TEMPERATURE
  ?1725. -10.
  AT 1725.00K, KEQ =   .999312E 00 .417438E 04 .236011E 01
  ENTER ONE OR MORE TEMPERATURE
  ?1725.8 1725.9 1726. -10.
  AT 1725.80K, KEQ =   .999876E 00 .417573E 04 .424072E 00
  AT 1725.90K, KEQ =   .999946E 00 .417589E 04 .183838E 00
  AT 1726.00K, KEQ =   .100002E 01 .417606E 04-.585937E-01
  ENTER ONE OR MORE TEMPERATURE
  ?1725.97
  AT 1725.97K, KEQ =   .999996E 00 .417601E 04 .124512E-01
  IN GVN, ENTER 9 IOPT VALUES   7  0  0  0  0  0  3  0  5
  ?
  SORRY, NO OTHER SYSTEMS ARE AVAILABLE YET
  DO YOU WANT TO CONTINUE?  USE 1 FOR YES
  ?
   *STOP* 0

  !BYE
  PLEASE HANG UP PHONE- CONNECT TIME WILL BE CHARGED!!

  CPU = .0599 CON = :15 INT = 33 CHG = $.61
```

Table 17

Solubility of graphite in solid nickel.

```
!SET F:12 DC/BENIC;IN

!LMPD.
ØPTIØNS?
?17910002
 0 ENTER NUMBER ØF TEMPERATURES, AND N TEMP VALUES
?8 1000. 1300. 1350.
IDENTIFY THE PHASE BY 1,2, ØR 3, AND THEN THE INPUT FILE
?1 12
ENTER THE NUMBER FØR ANØTHER PHASE IF THERE IS ØNE
?
IN GNN, ENTER 9 IØPT VALUES   9  1  0  0  0  2  0  2  0
?8 6
  2 YØU ARE IN CLM, ENTER KZZ VALUES TØ CØNTRØL ACTIØNS
?1
WHICH CØMPØNENT? ENTER HC(J),J=1,4, NØW:####################    .00
?0. 1.
  1  IENTER TEMPERATURE, ACTIVITY, AND INTEGERS
?1550. 1. 1
?.9
RØØT BETWEEN
   .97832537   .97832584 AT T =     1550.000
     .000000   -4.261386     1.738614     -.002002     1.664063
    .97833?     .99540=ACTIVITY ØF       .97383  .97383E 00 -.26523E-01
    .02167?  46.13832=ACTIVITY ØF      1.00003  .10000E 01
  1  IENTER TEMPERATURE, ACTIVITY, AND INTEGERS
?1500. 1. 1
?.9
RØØT BETWEEN
   .98038864   .98038912 AT T =     1500.000
     .000000   -4.223504     1.776496     -.001624     1.707500
    .98039?     .99627=ACTIVITY ØF       .97573  .97573E 00 -.23546E-01
    .01961?  50.99162=ACTIVITY ØF      1.00001  .10000E 01
  1  IENTER TEMPERATURE, ACTIVITY, AND INTEGERS
?1450. 1. 1
?.9
RØØT BETWEEN
   .98244143   .98244190 AT T =     1450.000
     .000000   -4.181175     1.818824     -.001289     1.755512
    .98244?     .99704=ACTIVITY ØF       .97953  .97953E 00 -.20583E-01
    .01756?  56.95239=ACTIVITY ØF      1.00000  .10000E 01
  1  IENTER TEMPERATURE, ACTIVITY, AND INTEGERS
?
```

Table 18

Solubility of graphite in liquid nickel.

```
!LMPD.
ZPTIØNS?
?17910002
 C ENTER NUMBER ØF TEMPERATURES, AND N TEMP VALUES
?11 1000. 1550. 1580.
IDENTIFY THE PHASE BY 1,2, ØR 3, AND THEN THE INPUT FILE
?1 12
ENTER THE NUMBER FØR ANØTHER PHASE IF THERE IS ØNE
?2
ENTER THE NUMBER FØR ANØTHER PHASE IF THERE IS ØNE
?
IN GNN, ENTER 9 IØPT VALUES   9  1  0  0  0  2  0  2  0
?1\8 6
  2 YØU ARE IN CLM, ENTER KZZ VALUES TØ CØNTRØL ACTIØNS
?4
  1  2ENTER TEMPERATURE, ACTIVITY, AND INTEGERS
?1600. .00826935
RØØT BETWEEN
.906287 .906287  AT T =     1600.000
     .000000    -1.251243    -1.283643     -.010989    -1.054327
    .90629?     .97502=ACTIVITY ØF       .88364  .88364E 00 -.12370E 00
    .09371?     .08824=ACTIVITY ØF       .00827  .82694E-02
  1  2ENTER TEMPERATURE, ACTIVITY, AND INTEGERS
?1620. .00911174
RØØT BETWEEN
.903693 .903694  AT T =     1620.000
     .000000    -1.221555    -1.253954     -.011330    -1.024055
    .90369?     .97425=ACTIVITY ØF       .88042  .88042E 00 -.12735E 00
    .09631?     .09461=ACTIVITY ØF       .00911  .91117E-02
  1  2ENTER TEMPERATURE, ACTIVITY, AND INTEGERS
?1640. .0100162
RØØT BETWEEN
.901073 .901073  AT T =     1640.000
     .000000    -1.192596    -1.224997     -.011672     -.994613
    .90107?     .97348=ACTIVITY ØF       .87718  .87718E 00 -.13104E 00
    .09893?     .10125=ACTIVITY ØF       .01002  .10016E-01
  1  2ENTER TEMPERATURE, ACTIVITY, AND INTEGERS
?1700. .0131283
RØØT BETWEEN
.893048 .893049  AT T =     1700.000
     .000000    -1.109843    -1.142243     -.012695     -.910979
    .89305?     .97119=ACTIVITY ØF       .85732  .85732E 00 -.14235E 00
    .10695?     .12275=ACTIVITY ØF       .01313  .13128E-01
  1  2ENTER TEMPERATURE, ACTIVITY, AND INTEGERS
?1740. .0155611
RØØT BETWEEN
.887560 .887561  AT T =     1740.000
     .000000    -1.057874    -1.090274     -.013374     -.858878
    .88756?     .96967=ACTIVITY ØF       .86064  .86064E 00 -.15007E 00
    .11244?     .13840=ACTIVITY ØF       .01556  .15561E-01
  1  2ENTER TEMPERATURE, ACTIVITY, AND INTEGERS
?1573. .00722598
RØØT BETWEEN
.909737 .909737  AT T =     1573.000
     .000000    -1.292620    -1.325020     -.010532    -1.096613
```

Table 18 (continued)

```
    .90974?     .97604=ACTIVITY ØF      .88794   .88794E 00 -.11885E 00
    .09026?     .08005=ACTIVITY ØF      .00723   .72260E-02
  1  2ENTER TEMPERATURE, ACTIVITY, AND INTEGERS
?
IN GNN, ENTER 9 IØPT VALUES   8  6  0  0  0  2  0  3  0
?9 2 0 0 0 4
 0 ENTER NUMBER ØF TEMPERATURES, AND N TEMP VALUES
?
IDENTIFY THE INPUT FILE
?13

?8 5
IØP(7)=  0  ENTER TEMP. AND MØLE FRACTIØN
?1773. .9
     .000000    -1.015677    -1.048077     -.010157     -.848942
    .90000?     .97688=ACTIVITY ØF       .87920   .87920E 00 -.12875E 00
    .10000?     .14160=ACTIVITY ØF       .01416   .14160E-01
?
  5 YØU ARE IN CLM, ENTER KZZ VALUES TØ CØNTRØL ACTIØNS
?4
  1  1ENTER TEMPERATURE, ACTIVITY, AND INTEGERS
?1773. .0178011 1
?.7
RØØT BETWEEN
.882945 .882947  AT T =     1773.000
     .000000    -1.016782    -1.049182     -.013931     -.817936
    .88295?     .96843=ACTIVITY ØF       .85507   .85507E 00 -.15657E 00
    .11705?     .15208=ACTIVITY ØF       .01780   .17801E-01
  1  1ENTER TEMPERATURE, ACTIVITY, AND INTEGERS
?1573. .00722598 1
?.7
RØØT BETWEEN
.909747 .909748  AT T =     1573.000
     .000000    -1.292529    -1.324929     -.010528    -1.096563
    .90975?     .97605=ACTIVITY ØF       .88796   .88796E 00 -.11883E 00
    .09025?     .08006=ACTIVITY ØF       .00723   .72260E-02
  1  1ENTER TEMPERATURE, ACTIVITY, AND INTEGERS
?1773. .0365270 1
?.7
RØØT BETWEEN
.816176 .816176  AT T =     1773.000
     .000000    -1.021109    -1.053509     -.034505     -.701788
    .81618?     .92362=ACTIVITY ØF       .75384   .75384E 00 -.28257E 00
    .18382?     .19871=ACTIVITY ØF       .03653   .36527E-01
  1  1ENTER TEMPERATURE, ACTIVITY, AND INTEGERS
?
IN GNN, ENTER 9 IØPT VALUES   8  5  0  0  0  2  0  3  0

ENTER THE CØEFFICIENTS AND THEN THE HØ298 VALUES, PHASE  1
?0 0 0 0 0  -1.
ENTER THE CØEFFICIENTS AND THEN THE HØ298 VALUES, PHASE  2
?0 0 0 0 1.
AT 1560.00K, KEQ =   .676038E  2 .249830E 05 .154896E 05
AT 1580.00K, KEQ =   .748   .E-02 .249830E 05 .153679E 05
AT 1600.00K, KEQ =   .826935E-02 .249830E 05 .152462E 05
AT 1620.00K, KEQ =   .911174E-02 .249830E 05 .151245E 05
AT 1640.00K, KEQ =   .100162E-01 .249830E 05 .150028E 05
AT 1660.00K, KEQ =   .109854E-01 .249830E 05 .148811E 05
AT 1680.00K, KEQ =   .120219E-01 .249830E 05 .147594E 05
```

Table 19

Finding equilibrium compositions for solid and liquid phases in equilibrium with each other in the Ni-C system using subroutine ALTNT.

```
!SET F:12 /BNIC:IN

!SET F:13 DC/FENIC:IN

.LMPD.
ØPTIØNS?
?17910002
 0 ENTER NUMBER ØF TEMPERATURES, AND N TEMP VALUES
?1000. 1973. 1580.-
 11 1000. 1973. 1580. 1600.
IDENTIFY THE PHASE BY 1,2, ØR 3, AND THEN THE INPUT FILE
?1 12
ENTER THE NUMBER FØR ANØTHER PHASE IF THERE IS ØNE
?2
ENTER THE NUMBER FØR ANØTHER PHASE IF THERE IS ØNE
?
IN GNN, ENTER 9 IØPT VALUES   9  1  0  0  0  2  0  2  0
?8 5
IØP(7)=  0  ENTER TEMP. AND MØLE FRACTIØN
?1500.  .9
     .000000   -1.251651   -1.284050     -.012517   -1.040080
    .900007    .97159=ACTIVITY ØF       .87443  .87443E 00 -.13418E 00
    .100007    .09118=ACTIVITY ØF       .00912  .91184E-02
?
  5 YØU ARE IN CLM, ENTER KZZ VALUES TØ CØNTRØL ACTIØNS
?4
  1  2ENTER TEMPERATURE, ACTIVITY, AND INTEGERS
?1973. .0365270
RØØT BETWEEN
.853199 .853200  AT T =    1973.000
     .000000    -.797482    -.829882     -.017186    -.504112
    .853207    .96120=ACTIVITY ØF       .82010  .82010E 00 -.19833E 00
    .146807    .24882=ACTIVITY ØF       .03553  .36527E-01
  1  2ENTER TEMPERATURE, ACTIVITY, AND INTEGERS
?
IN GNN, ENTER 9 IØPT VALUES   8  5  0  0  0  2  0  3  0
?0 7 9
ENTER TEMPERATURE AND A CØNTRØL INTEGER
?1600.
ENTER TWØ EQUILIBRIUM CØNSTANTS
?.91082 .00826935 0 1
?..011

FØRTRAN RUN-TIME ERRØR IN '9BCDREAD' CALLED AT LØC X'17445'.
..011
 \
ILLEGAL NUMERIC INPUT CHARACTER.  FIELD TERMINATED.

    .000000
    .718277
    .924686
    .975248
    .9754385SHALL WE CØNTINUE?
```

968

Table 19 (continued)

```
 ?1
      .937241
      .990061
      .990845
      .991025
      .9753107SHALL WE CØNTINUE?
 ?1
      .991100
      .991130
      .976413     .994510 GIVES ACTIVITY IN PHASE  1 ØF      .971053   .97105
 3E 00
      .023587   42.019943 GIVES ACTIVITY IN PHASE  1 ØF      .991126   .99112
 5E 00
      .906845     .975309 GIVES ACTIVITY IN PHASE  2 ØF      .884454   .88445
 4E 00
      .093155     .087984 GIVES ACTIVITY IN PHASE  2 ØF      .008196   .81961
 0E-02
 ENTER TEMPERATURE AND A CØNTRØL INTEGER
 ?1520.
 ENTER TWØ EQUILIBRIUM CØNSTANTS
 ?.925022 .00911174 0 1
 ?.008
      .877988
      .801761
      .783949
      .779757
      .9816904SHALL WE CØNTINUE?
 ?1
      .778661
      .778413
      .778322
      .778289
      .9817030SHALL WE CØNTINUE?
 ?1
      .778277
      .979407     .995756 GIVES ACTIVITY IN PHASE  1 ØF      .975250   .97525
 0E 00
      .020593   37.792480 GIVES ACTIVITY IN PHASE  1 ØF      .778276   .77827
 6E 00
      .918941     .981703 GIVES ACTIVITY IN PHASE  2 ØF      .902127   .90212
 7E 00
      .081059     .087484 GIVES ACTIVITY IN PHASE  2 ØF      .007091   .70914
 1E-02
 ENTER TEMPERATURE AND A CØNTRØL INTEGER
 ?1540.
 ENTER TWØ EQUILIBRIUM CØNSTANTS
 ?.939206 .0100162 0 1
 ?.006
      .599030
      .592666
      .591113
      .590761
      .9873246SHALL WE CØNTINUE?
 ?1
      .590643
      .590603
```

Table 19 (continued)

```
    .590590
    .982564     .996914 GIVES ACTIVITY IN PHASE  1 OF      .979532   .97953
2E 00
    .017436  33.872269 GIVES ACTIVITY IN PHASE  1 OF      .590592   .59059
2E 00
    .931791     .937327 GIVES ACTIVITY IN PHASE  2 OF      .919982   .91998
2E 00
    .068209     .085725 GIVES ACTIVITY IN PHASE  2 OF      .005915   .59154
2E-02
ENTER TEMPERATURE AND A CONTROL INTEGER
?1660.
ENTER TWO EQUILIBRIUM CONSTANTS
?.953375 .0109854 0 1
?.005
    .455149
    .432325
    .426674
    .425355
    .9920924SHALL WE CONTINUE?
?1
    .424953
    .424832
    .424793
    .424782
    .9920975SHALL WE CONTINUE?
?1
    .424778
    .935940     .997964 GIVES ACTIVITY IN PHASE  1 OF      .983933   .98393
3E 00
    .014060  30.212734 GIVES ACTIVITY IN PHASE  1 OF      .424780   .42478
0E 00
    .945529     .992097 GIVES ACTIVITY IN PHASE  2 OF      .938057   .93805
7E 00
    .054471     .085667 GIVES ACTIVITY IN PHASE  2 OF      .004666   .46663
5E-02
ENTER TEMPERATURE AND A CONTROL INTEGER
?1680.
ENTER TWO EQUILIBRIUM CONSTANTS
?.957525 .0120219 0 1
?.0035
    .291135
    .281375
    .278996
    .278322
    .9959022SHALL WE CONTINUE?
?1
    .278131
    .278075
    .278060
    .939612     .998872 GIVES ACTIVITY IN PHASE  1 OF      .988496   .98849
6E 00
    .010388  26.768448 GIVES ACTIVITY IN PHASE  1 OF      .278058   .27805
8E 00
    .960328     .995904 GIVES ACTIVITY IN PHASE  2 OF      .956395   .95639
5E 00
    .039672     .084260 GIVES ACTIVITY IN PHASE  2 OF      .003343   .33427
6E-02
```

Table 19 (continued)

```
ENTER TEMPERATURE AND A CONTROL INTEGER
?1700.
ENTER TWO EQUILIBRIUM CONSTANTS
?.981563 .0131283 0 1
?.002
     .152343
     .149075
     .148203
     .147965
     .9985899SHALL WE CONTINUE?
?1
     .147900
     .147883
     .147878
     .993704      .999579 GIVES ACTIVITY IN PHASE  1 OF      .993286   .99328
6E 00
     .006296   23.487122 GIVES ACTIVITY IN PHASE  1 OF      .147877   .14787
7E 00
     .976448      .993590 GIVES ACTIVITY IN PHASE  2 OF      .975072   .97507
2E 00
     .023552      .082429 GIVES ACTIVITY IN PHASE  2 OF      .001941   .19413
7E-02
ENTER TEMPERATURE AND A CONTROL INTEGER
?1720.
ENTER TWO EQUILIBRIUM CONSTANTS
?.999782 .0143072 0 1
?.001
     .059895
     .042333
     .034918
     .032888
     .9999173SHALL WE CONTINUE?
?1
     .032329
     .032175
     .032133
     .032121
     .9999182SHALL WE CONTINUE?
?1
     .032118
     .998418      .999973 GIVES ACTIVITY IN PHASE  1 OF      .998391   .99839
1E 00
     .001532   20.305603 GIVES ACTIVITY IN PHASE  1 OF      .032118   .32117
9E-01
     .994261      .999918 GIVES ACTIVITY IN PHASE  2 OF      .994180   .99418
0E 00
     .005739      .080072 GIVES ACTIVITY IN PHASE  2 OF      .000460   .45951
9E-03
ENTER TEMPERATURE AND A CONTROL INTEGER
?
SORRY, NO OTHER SYSTEMS ARE AVAILABLE YET
DO YOU WANT TO CONTINUE?  USE 1 FOR YES
?1
OPTIONS?
?17
IN GNN, ENTER 9 I2PT VALUES   1  7  0  0  0  0  0  0  0
?16
?1 2
```

Table 20.

Preliminary estimates of constants for the liquid $KO_{0.5}$ - SiO_2 system.

Redlich-Kister coefficients			Bale-Pelton coefficients		
	log γ_{1000}	enthalpy		log γ_{1000}	enthalpy
A	-.3966	0	q_0	1.7391	1053
B	2.4089	0	q_1	2.8550	-3672
C	5.5772	3160	q_2	4.8077	2107
D	-.5137	-6120	q_3	.5767	-2448
E	-1.76	0	q_4	.9691	0
F	1.76	0	q_5	.2235	0
G	4.4	0	q_6	.3048	0

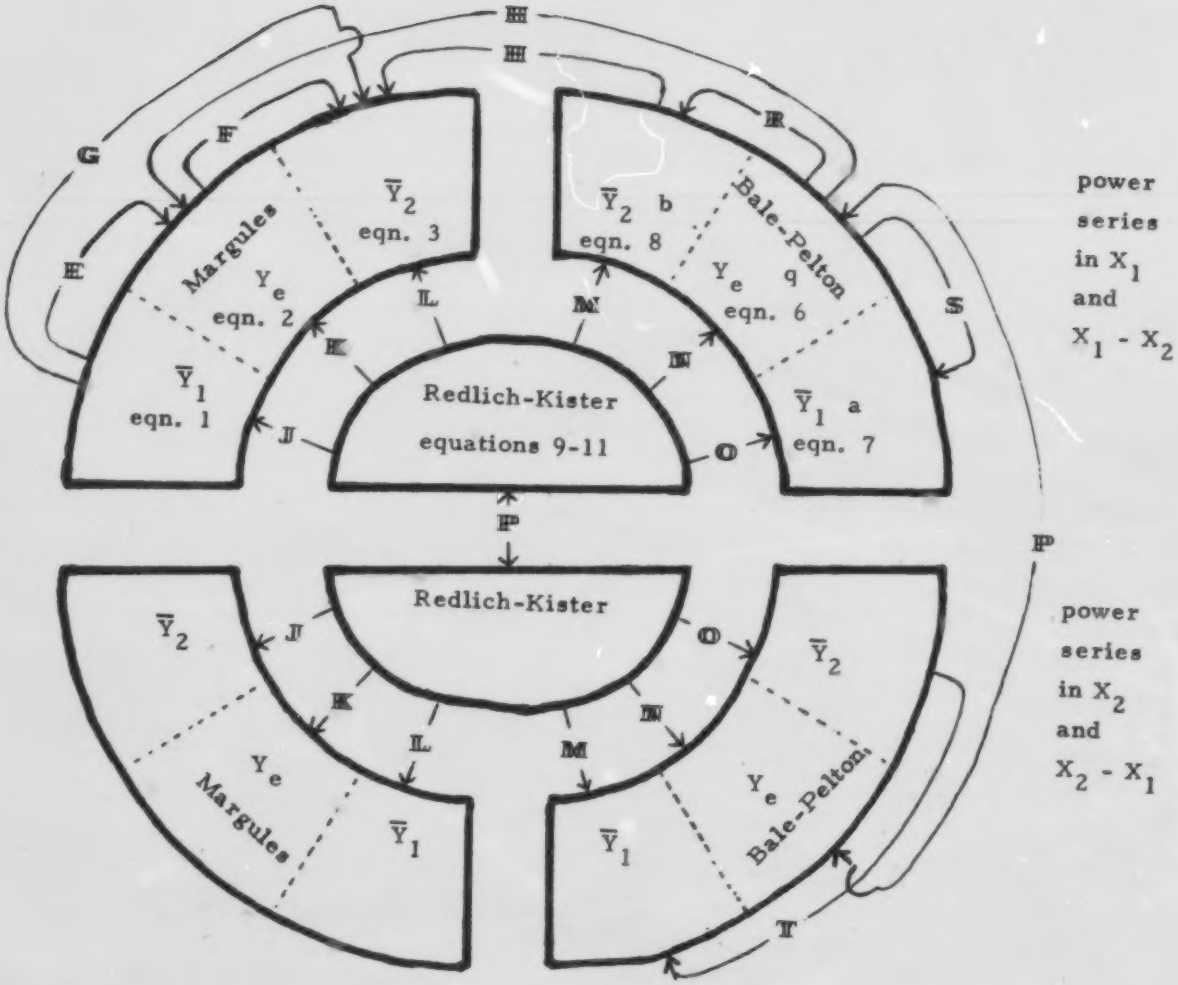

Figure 1

Diagram illustrating the relationships of conversion matrices between various sets of coefficients.

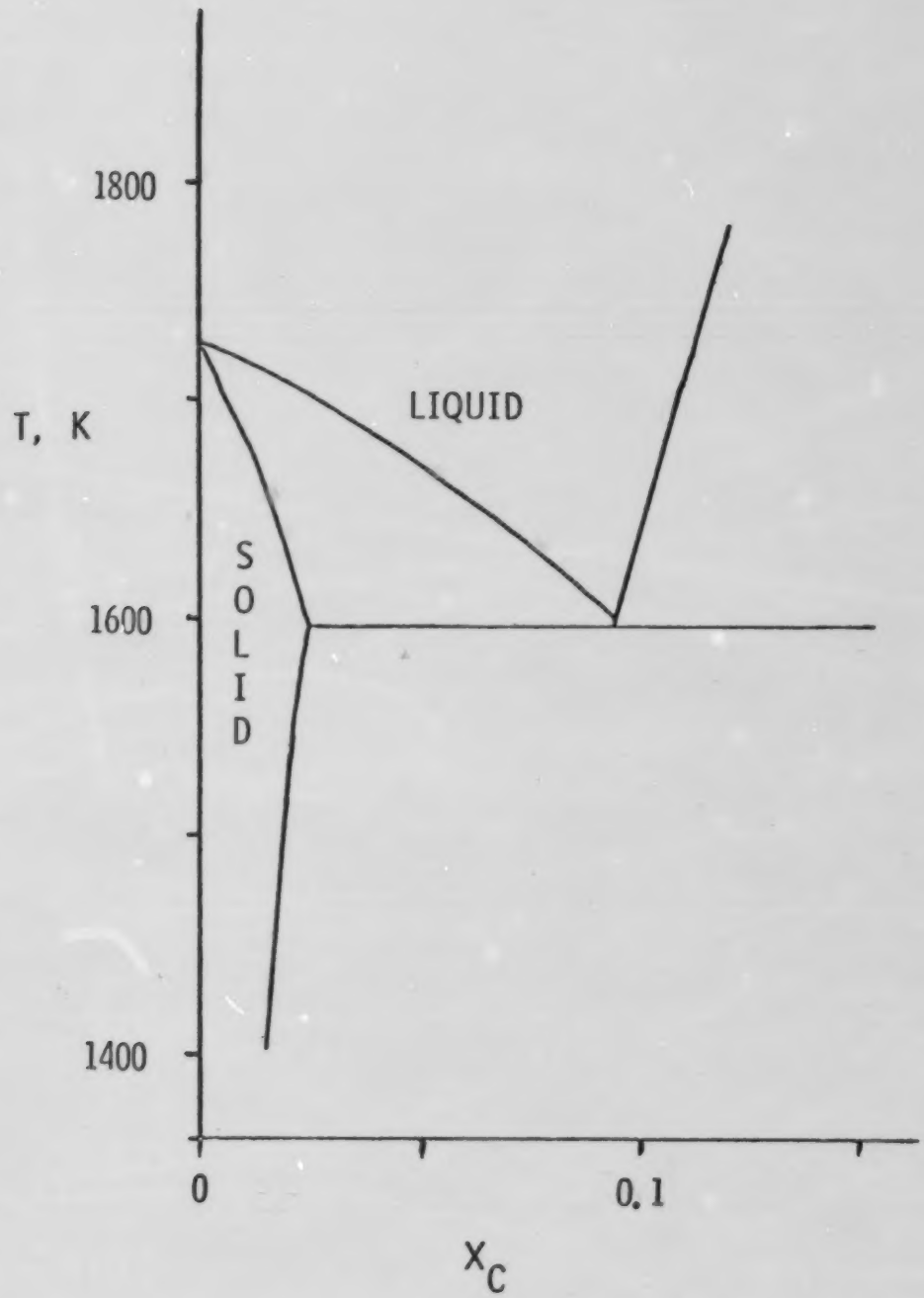

Figure 2

The nickel - carbon phase diagram

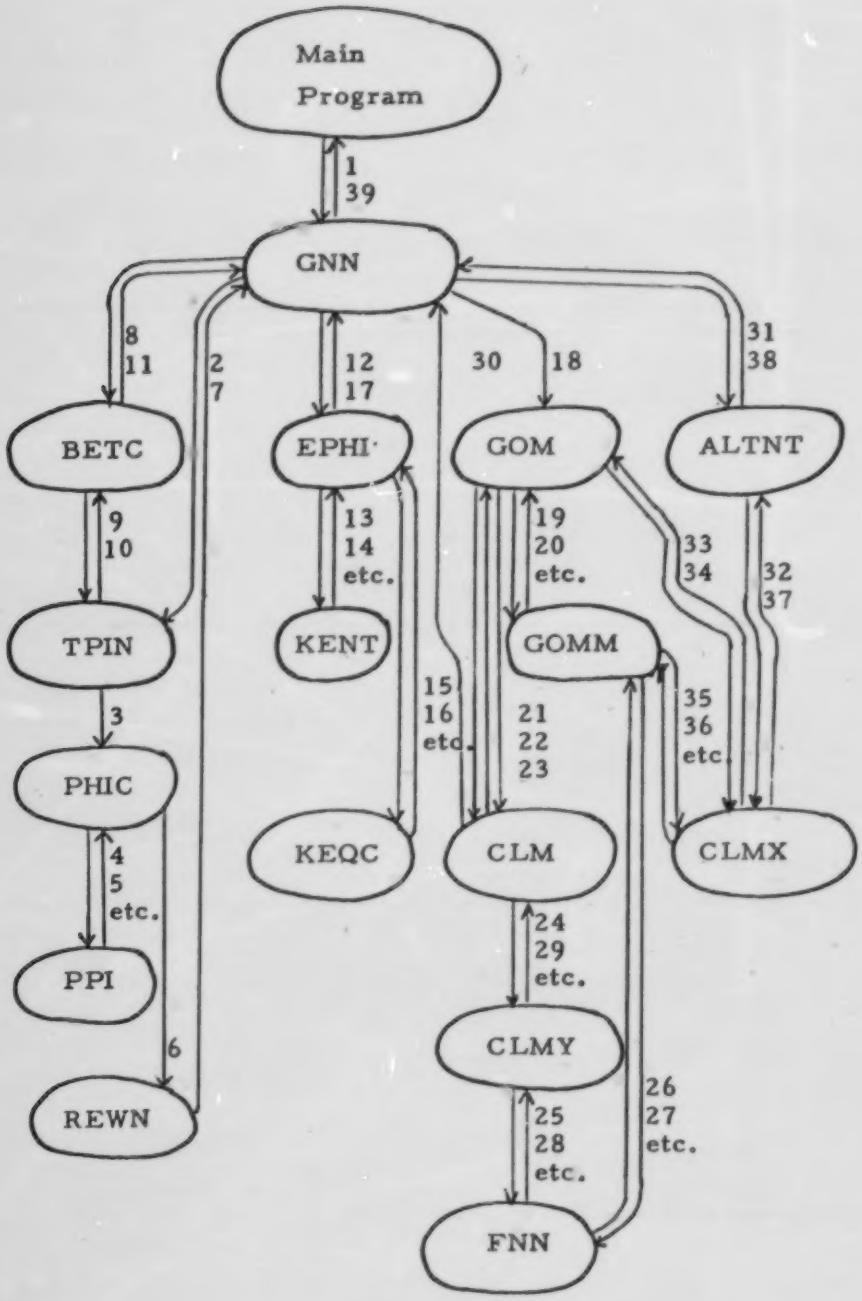

Figure 3

Flow chart of BPHD for some major calculations.

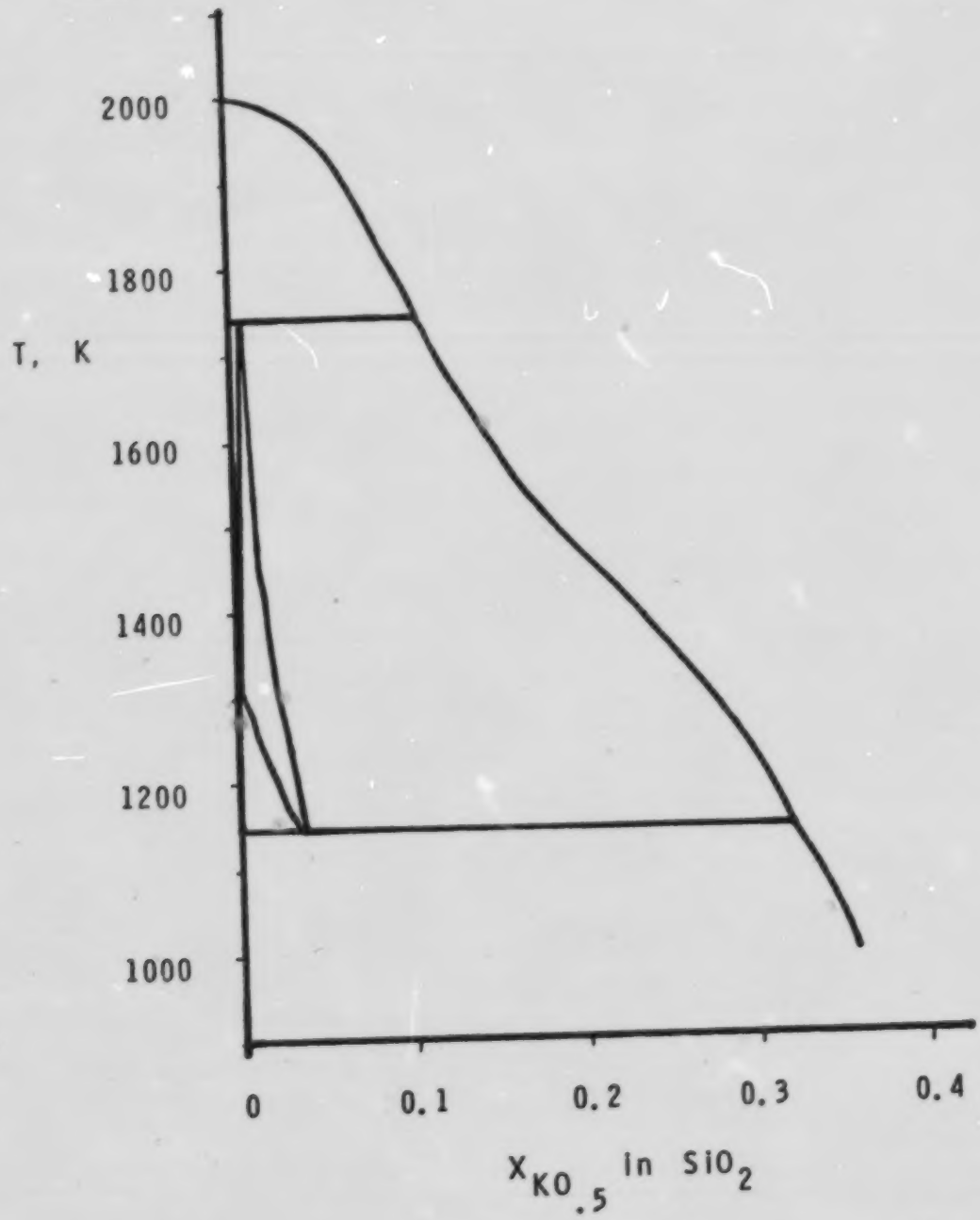

Figure 4. Calculated phase diagram for SiO_2 - $KO_{.5}$.

National Bureau of Standards SP-496, Applications of Phase Diagrams in Metallurgy and Ceramics
Proceedings of Workshop held at NBS, Gaithersburg, Md., January 10-12, 1977

Polynomial Representation of the Excess Free Energy of Multicomponent Systems and their Use in Phase Diagram Calculations

H. Gaye
IRSID - PCM 57
Maizières - les - Metz
France

and

C. H. P. Lupis
Department of Metallurgy and Materials Science
Carnegie - Mellon University
Schenley Park, Pittsburgh, Pa. 15213

Various polynomial formalisms can be proposed for the representation of the excess free energy of multicomponent solutions:

- for the partial molar properties, the "interaction coefficients" approach provides polynomials in terms of solute mole fractions;
- for the integral excess free energy, symmetric expressions in terms of all mole fractions can be used.

An advantage of polynomial formalisms is that the coefficients can be mapped into one-dimensional arrays, so that the number of components and the order of the polynomials can easily remain unrestricted.

Several applications of these formalisms to the integration of the Gibbs-Duhem equation will be presented. To that effect, a new method of integration was derived. It is based upon the expressions:

$$\ln\gamma_1 = \frac{G^E}{RT} - \sum_{j=2}^{m} X_j \frac{\partial(G^E/RT)}{\partial X_j}$$

$$\ln\gamma_i = \ln\gamma_1 + \frac{\partial(G^E/RT)}{\partial X_i} \qquad (\text{for } i = 2,3,\ldots m)$$

The flexibility of polynomials has also been useful in the compilation and exploitation of the phase diagrams of oxide systems. Because many of the solid phases are stoichiometric, a relatively good picture of the diagrams can be derived from the knowledge of the liquidus surfaces. Representing them as polynomials:

$$T_{liq} = P(\text{composition})$$

allows simple interpolations and extrapolations and the calculation of crystallization paths. The example of blast furnace slags (in the system $CaO-SiO_2-Al_2O_3-MgO$) will be presented.

National Bureau of Standards SP-496, Applications of Phase Diagrams in Metallurgy and Ceramics
Proceedings of Workshop held at NBS, Gaithersburg, Md., January 10-12, 1977

Thermodynamic Data for the Fe-O System Evaluated Using a New Computer-Aided Strategy

John L. Haas, Jr. and James R. Fisher
National Center for the Thermodynamic Data of Minerals
U. S. Geological Survey
National Center, Stop 959
Reston, Virginia 22092

This paper will describe the computational techniques employed in evaluating the example given in this abstract

Tables of thermodynamic properties and their confidence limits from 0 to 1800 K at one atm were obtained for the oxides wustite $Fe_{0.947}O$, magnetite Fe_3O_4, and hematite Fe_2O_3. In addition to reflecting the calorimetry accurately, the set is in better agreement with the known phase equilibria than previous sets. We evaluated the published experimental data for the phases and their interactions using the program PHAS20. PHAS20 is a weighted multiple regression routine which combines an empirical equation for the heat capacity with the functional relations among heat capacity, entropy, enthalpy, free energy, equilibrium constants, and electrochemical potentials for a group of chemically related phases. Confidence limits for the tabulated data were obtained from the program RECKON, using the same relations, the refined constants, the variances and covariances, and statistical theory.

The results show that the thermodynamic tables for wustite cannot be significantly improved except by better data for the reported second-order composition- and temperature-dependent structural effects within the solid solution. The thermodynamic tables for hematite can be improved by better data on the solid solution limits for both hematite and magnetite as well as the effect of composition on the activity of the Fe_2O_3 and Fe_3O_4 components in the solid solutions. The thermodynamics of magnetite below 1000 K cannot be significantly improved through existing experimental techniques. There are no indications that magnetite and hematite have a residual entropy at the zero of absolute temperature due to internal disorder.

National Bureau of Standards SP-496, Applications of Phase Diagrams in Metallurgy and Ceramics
Proceedings of Workshop held at NBS, Gaithersburg, Md., January 10-12, 1977

Analysis and Synthesis of Phase Diagrams of the Fe-Cr-Ni, Fe-Cu-Mn and Fe-Cu-Ni Systems.

Mitsuhiro Hasebe and Taiji Nishizawa
Department of Materials Science,
Faculty of Engineering,
Tohoku University, Sendai, Japan

Synopsis

The phase equilibria in the Fe-Cr-Ni, Fe-Cu-Mn and Fe-Cu-Ni systems were examined by microprobe analysis of ternary diffusion couples consisting of their components. The experimental data were analyzed thermodynamically using an extended regular solution model and the thermodynamic data on the binary systems concerned, and the thermodynamic parameters were evaluated by linear programming. The phase diagrams over a wide temperature range were synthesized by computer calculation on the basis of these parameters.

I. Introduction

Most of the previously published phase diagrams for alloy systems have been determined on the basis of the metallographic information alone. The way of constructing phase diagrams, however, requires a great deal of time, labor and materials, particularly in the case of multi-component systems. For this reason, the vacuum deposition of three kinds of metals from three corners[1] and the multi-component diffusion couple technique[2]~[4] have been designed to obtain necessary data over a wide range of composition from one specimen.

Besides, remarkable progress has been made for the analysis and synthesis of the phase diagrams in recent years by means of computer calculation[5]~[7]. It should be noted that this method permits the synthesis of the phase diagrams of real alloys over a wide range of temperature and composition by computation combined with thermodynamic analysis of the experimental data.

Following these lines of both experimental and theoretical approaches, we have made extensive work to establish the phase diagrams of the alloy systems composed of iron and first-row transition elements in the periodic table. In this paper, the phase diagrams of the Fe-Cr-

951

Ni, Fe-Cu-Mn and Fe-Cu-Ni systems are presented.

II. Experimental Procedure

The experiments were carried out mainly for the ternary phase equilibria. The binary Fe-Cu system was also examined to confirm the composition of the γ phase(γFe-Cu solid solution) in equilibrium with the ε phase(Cu-Fe solid solution) or the liquid phase.

II-1. Preparation of specimens

The specimens used in the present work were prepared from pure materials listed in Table 1 by induction-melting and casting in vacuum or under argon atmosphere. After a homogenization-anneal, they were cut into pieces of 5∿10 mm cube and then heated in wet hydrogen flow at about 1100 K for 1∿2 days in order to remove carbon and nitrogen.

The multi-layer diffusion couples were used for determining the equilibrium compositions of the γ phase and the ε phase in the Fe-Cu system. The couples were made by alternatively laminating about ten sheets of pure iron and copper foils of 80∿100 μm thickness, both of which had been thinned by rolling and electroytic polishing.

In the experiments on the ternary systems, a ternary diffusion couple technique was employed for obtaining sufficient data over a wide range of composition from one specimen. As illustrated in Fig. 1, a binary diffusion couple was first prepared from a pair of metals or alloys by joining in a dry hydrogen atmosphere at 1073 K, sealed in a transparent quartz capsule under vacuum or an argon of 1/3 atmospheric pressure, and fully annealed at a high temperature for the moderation of the concentration gradient. Then, a ternary couple was made by joining a third metal piece onto one side of the binary couple. The diffusion couple was sealed again in a quartz capsule and finally equilibrated at fixed temperatures.

In the Fe-Cu-Mn and Fe-Cu-Ni systems, Fe:Fe-50wt%Mn and Fe:Fe-50wt% Ni were chosen as the first couples and pure copper was used as the third metal because it has a lower melting point than the others. In preparing the Fe-Cr-Ni couple, chromium was used as the third metal and the Fe-Ni binary couple was vacuum sealed in a capsule with several pellets of high purity chromium. The ternary couple was spontaneously built up owing to the vaporization and deposition of chromium during

heating at the equilibration temperature.

II-2. Microanalysis of equilibrium composition

The binary and ternary diffusion couples prepared by the method mentioned above were heated at the fixed temperatures between 1123 and 1473 K for 5∿33 days. After quenching in ice brine, they were cut in parallel to the direction of diffusion of the third component, and the concentration profile of each component across the interphase boundary was obtained by microanalysis. The equilibrium compositions were determined by extrapolating the profiles to the position of the interphase boundary. Figure 2 illustrates the microstructure of the cross-section and the concentration profile for a ternary Fe-Cu-Ni couple.

It has been pointed out that the interphase boundary composition in diffusion couples deviates to some extent from the equilibrium value[8][9]. In the present work, however, this may be neglected because the deviations are less than 1% at the most after heating for a long time.

In the investigation of the liquid/solid equilibria, the two-phase alloy specimens were used instead of the diffusion couples. These specimens were quenched from the equilibration temperatures between 1223 and 1523 K for microanalysis of each phase. The determination of composition of the liquid phase was made by counting the average intensity of radiation from an area swept with a width of 40 μm so as to eliminate due to dendritic segregation.

The microanalysis was carried out by Shimazu ARL-EMX microanalyzer using LiF and quartz crystals for K_α radiation and RAP crystal for L_α radiation. The accelerating voltage and the sample current of the electron beam was kept at 20 kV, 3×10^{-8}A or 30 kV, 10^{-8}A. The take-off angle of the spectrometer was 52.5°.

The relative intensities of radiation K_i in the binary system were converted to the weight fractions C_i according to the next equation proposed by Ziebold and Ogilvie[10]:

$$\frac{1-K_i}{K_i} = \alpha_{ij}\frac{1-C_i}{C_i} \quad . \tag{1}$$

The conversion parameters α_{ij} for the i-th component in the binary i-j systems were determined by a calibration experiment as presented in

Table 2.

The conversion of the ternary data was made according to the equation of the form

$$\frac{1-K_i}{K_i} = \bar{\alpha}_i \frac{1-C_i}{C_i} , \qquad (2)$$

where $\bar{\alpha}_i$ is a conversion parameter for the i-th component in the ternary i-j-k system and is approximated by a weighted average of the binary parameters as follows :

$$\bar{\alpha}_i = \frac{\alpha_{ij} C_j + \alpha_{ik} C_k}{C_j + C_k} . \qquad (3)$$

The validity of equations (2) and (3) has been confirmed by a preliminary experiment on several ternary specimens.

III. Thermodynamic Analysis

III-1. Expression of the free energy of solid solution

The free energy of multi-component solid solutions was described by an extended regular solution approximation as follows :

$$G = \sum_{i=1}^{N} x_i ({}^{\circ}G_i + RT \ln x_i) + \sum_{i=1}^{N-1} \sum_{j=i+1}^{N} x_i x_j \Omega_{ij} + \sum_{i=1}^{N-2} \sum_{j=i+1}^{N-1} \sum_{k=j+1}^{N} x_i x_j x_k \Omega_{ijk} , \qquad (4)$$

where x_i is the atomic fraction, ${}^{\circ}G_i$ is the free energy of the i-th component at T K. Ω_{ij} and Ω_{ijk} are the interaction parameters in the binary i-j system and the ternary i-j-k system, respectively. These parameters generally depend upon both temperature and composition, and many studies have been made on the way of describing their dependency[11]. Here, the empirical expressions of the following form were employed :

$$\begin{aligned}
\Omega_{ij} &= \Omega^0_{ij} + \Omega^1_{ij}(x_j - x_i) + \Omega^2_{ij}(x_j - x_i)^2 + \cdots + \Omega^n_{ij}(x_j - x_i)^n , \\
\Omega_{ijk} &= \Omega^i_{ijk} x_i + \Omega^j_{ijk} x_j + \Omega^k_{ijk} x_k , \\
\Omega^n_{ij} &= A^n_{ij} + B^n_{ij} T + C^n_{ij} T \ln T , \\
\Omega^i_{ijk} &= A^i_{ijk} + B^i_{ijk} T + C^i_{ijk} T \ln T .
\end{aligned} \qquad (5)$$

III-2. Analysis by linear programming

The thermodynamic parameters in equations (4) and (5) were evaluated by linear programming on the basis of the experimental results on the ternary systems as well as thermodynamic data on the binary systems.

The phase equilibrium can be described by an equality of chemical potentials, which are related to the free energy of each phase. The activity data can also be described by equations associated with the free energy of each phase. These are rearranged into linear equations concerning the thermodynamic parameters X as follows :

$$a_{i1}X_1 + a_{i2}X_2 + \cdots + a_{in}X_n + e_i = R_i \ . \qquad (6)$$

The coefficient a_{ij} and the right-hand side value R_i are known quantities, and e_i is the corresponding error. Then the parameter X_j is evaluated in such a way as to minimize the objective function :

$$Z = \sum_i |e_i| \ . \qquad (7)$$

Such a linear programming technique has been successfully applied by Rao et al.[12] to the thermodynamic analysis of the binary Pb-Sb system.

Besides an equality like equation (6), the constraint of an inequality was used in this work. For example, the free energy of the liquid phase must be lower than that of the solid phase at the liquidus. This fact is described in the following form and is also of use in linear programming for the evaluation of the parameter X_j :

$$a'_{i1}X_1 + a'_{i2}X_2 + \cdots + a'_{in}X_n < R'_i \ . \qquad (8)$$

III-3. Computation of phase boundaries

The computer calculation of the phase boundary compositions can in principle be divided into two ways. One is to solve the simultaneous equations concerning the chemical potentials of the components in each phase. The other is to search for a set of phases having the best composition to minimize the free energy of the entire alloy system. The former was carried out by Kaufman and Bernstein[13], and the latter by Counsell et al.[14] In this work, the latter was employed because it is simpler in operation and faster to find the equilibrium composition of each phase. The "Simplex" method, the steepest descent method developed by Nelder and Mead[15], was used in performing the calculation.

IV. Results

IV-1. Evaluation of parameters

Experimental results on the equilibrium composition of each phase are given in Tables 3∿8. On the basis of these results, the thermodynamic parameters in equations (4) and (5) were evaluated as listed in Tables 9 and 10. The phase diagrams and thermodynamic data on the binary Fe-Cr[9][16]∿[32], Fe-Mn[18][33]∿[43], Fe-Ni[18][22][34][44]∿[59], Fe-Cu[60]∿[70], Cr-Ni[22][29][32][46][71]∿[77], Cu-Mn[18][78]∿[83] and Cu-Ni[78][84]∿[95] systems and the ternary Fe-Cr-Ni[46][96]∿[99] and Fe-Cu-Ni[14] systems were also employed for the evaluations. The free energy of the component ${}^{\circ}G_i$ used was the literature value[100]∿[103]. The parameters concerning the σ phase were estimated from the data on the Fe-Cr[22] and Cr-Co-Ni[104] systems.

IV-2. Calculation of phase diagram

The phase diagrams are constructed by computation using the above-mentioned parameters. Figures 3∿9 and 10∿20 are the computed diagrams of the binary and ternary systems, respectively. The calculation of the phase equilibria relating to the αFe phase was limited to temperatures above 1073 K, because it has been pointed out by Zener[107], Weiss and Tauer[108], and Hillert et al.[5][21][34] that the thermodynamic functions of αFe solid solution show an anomaly due to the magnetic transition. The phase diagrams over a temperature range below the Curie point will be presented elsewhere.

Comparisons of the accepted diagrams with those obtained in the present work are given in Figs. 13 and 20. There are some discrepancies due to the fact that the accepted diagrams were synthesized by calculation using the binary data alone[14][101] or constructed experimentally in a conventional way[109].

The thermodynamic properties can be calculated by computation as in the case of the phase diagrams. As examples, the activities in the binary Fe-Cr system and the iso-activity lines for chromium in the ternary Fe-Cr-Ni system are shown in Figs. 21 and 22, respectively.

Acknowlegments

The authors wish to express their gratitude to Mr. Y.Kohsaka, now at Technical Research Center, Nippon Kokan K.K., Kawasaki,Japan, for his invaluable assistance throughout the present experiments. Thanks are also due to Prof. H.Takeyama and his staff at the Computer Center, Tohoku University, for their kind help in computer calculation. One of the authors (M.H.) wishes to thank for the financial support of the Sakkokai Foundation.

References

(1) K.Kennedy, T.Stefansky, G.Davy, V.F.Zackay and E.R.Parker : J. Appl. Phys., 36(1965), 3808.

(2) A.Boettcher, G.Haase and R.Thun : Z. Metallk., 46(1955), 386.

(3) G.Kirchner, G.Larbo and B.Uhrenius : Pract. Metallogr., 8(1971), 641.

(4) J.S.Kirkaldy, G.M.Bolze, D.McCutcheon and J.Young : Met. Trans., 4(1973), 1519.

(5) M.Hillert : Phase Transformations, Ed. by M.Cohen, ASM, Cleveland, Ohio, (1969), 181.

(6) International Symposium on Metallurgical Chemistry, England, (1971); International Symposium on Thermodynamics of Alloys, Munster,(1972).

(7) A.D.Pelton and W.T.Thomson : Prog. Solid State Chem., 10(1975),119.

(8) J.R.Eifert, D.A.Chatfield, G.W.Powell and J.W.Spretnak : Trans. Met. Soc. AIME, 242(1968), 66.

(9) T.Nishizawa and A.Chiba : Trans. Japan Inst. Metals, 16(1975), 767.

(10) T.O.Ziebold and R.E.Ogilvie : Anal. Chem., 35(1963), 621; 36(1964), 322.

(11) I.Ansara : Metallurgical Chemistry, Ed. by O.Kubaschewski, HSMO, London, (1972), 403.

(12) M.V.Rao, R.Hiskes and W.A.Tiller : Acta Met., 21(1973), 733.

(13) L.Kaufman and H.Bernstein : Computer Calculation of Phase Diagrams, Academic Press, New York, (1970).

(14) J.F.Counsell, E.B.Lees and J.Spencer : Metallurgical Chemistry, Ed. by O.Kubaschewski, HSMO, London, (1972), 451.

(15) J.A.Nelder and R.Mead : Computer J., 7(1964/5), 308.

(16) F.Adcock : J. Iron Steel Inst., 124(1931), 99.

(17) J.W.Putman, R.D.Potter and N.J.Grant : Trans. ASM, 43(1951), 824.

(18) A.Hellawell and W.Hume-Rothery : Phil. Trans. Roy. Soc. London, Ser.A, 249(1957), 417.

(19) K.Bungardt, E.Kunze and E.Horn : Arch. Eisenhuttenw., 29(1958), 193.

(20) E.Baerlecken, W.A.Fisher and K.Lorentz : Stahl Eisen, 81(1961), 768.

(21) G.Kirchner, T.Nishizawa and B.Uhrenius : Met. Trans., 4(1973), 167.

(22) W.A.Dench : Trans. Faraday Soc., 59(1963), 1279.

(23) C.L.McCabe, R.G.Hudson and H.W.Paxton : Trans. Met. Soc. AIME, 212(1958), 102.

(24) E.Z.Vintaikin : Dokl. Akad. Nauk SSSR, 118(1958), 977.

(25) O.Kubaschewski and G.Heymer : Acta Met., 8(1960), 416.

(26) Y.Jeannin, C.Mannerkantz and F.D.Richardson : Trans. Met. Soc. AIME, 227(1963), 300.

(27) P.B.Reese, R.A.Rapp and G.Pierre : Trans. Met. Soc. AIME, 242(1968), 1719.

(28) D.C.Lidster and H.B.Bell : Trans. Met. Soc. AIME, 245(1969), 2273.

(29) F.N.Mazandarany and R.D.Pehlke : Met. Trans., 4(1973), 2067.
(30) M.Onillon and M.Olette : Compt. Rend. Acad. Sci., C, 264(1967). 46.
(31) R.J.Fruehan : Trans. Met. Soc. AIME, 245(1969), 1215.
(32) S.W.Gilby and G.R.Pierre : Trans. Met. Soc. AIME, 245(1969), 1749.
(33) A.R.Troiano and F.T.McGuire : Trans. ASM, 31(1943), 340.
(34) M.Hillert, T.Wada and H.Wada : J. Iron Steel Inst.,.205(1967), 539.
(35) B.Predel and W.Gust : Arch. Eisenhuttenw., 43(1972), 721.
(36) K.Ishida : Thesis, Tohoku University, Sendai, (1974).
(37) W.B.Kendall and R.Hultgren : Trans. ASM, 53(1961), 199.
(38) K.Sanbongi and M.Ohtani : Sci. Rept. Res. Inst. Tohoku Univ. Ser.A, 7(1955), 204.
(39) J.F.Butler, C.L.McCabe and H.W.Paxton : Trans. Met. Soc. AIME, 221(1961), 479.
(40) R.Smith and R.Shuttleworth : Acta Met., 13(1965), 623.
(41) P.Roy and R.Hultgren : Trans. Met. Soc. AIME, 233(1965), 1811.
(42) R.J.Hawkins : Chemical Metallurgy of Iron and Steel, Iron and Steel Inst., London, (1973), 310.
(43) V.N.Eremenko, G.M.Lukashenko and V.R.Sidorko : Izvest. Akad. Nauk SSSR, 11(1969), 170.
(44) D.Hanson and J.R.Freeman : J. Iron Steel Inst., 107(1923), 301.
(45) T.Kase : Sci. Rept. Tohoku Univ., 16(1927), 491.
(46) C.H.M.Jenkins, E.H.Bucknall, C.R.Austin and G.A.Mellor : J. Iron Steel Inst., 86(1937), 187.
(47) E.A.Owen and Y.H.Liu : J. Iron Steel Inst., 163(1949), 132.
(48) J.I.Goldstein and R.E.Ogilvie : Trans. Met. Soc. AIME, 233(1965), 2083.
(49) W.Steiner and O.Krisement : Arch. Eisenhuttenw., 32(1961), 701.
(50) O.Kubaschewski and L.E.Stuart : J. Chem. Eng. Data, 12(1967), 418.
(51) B.Predel and R.Mohs : Arch. Eisenhuttenw., 41(1970), 143.
(52) K.Ono, Y.Ueda, A.Yamaguchi and J.Moriyama : J. Japan Inst. Metals, 36(1972), 188.
(53) O.Kubaschewski and O.Goldbeck : Trans. Faraday Soc., 45(1948), 948.
(54) R.A.Oriani : Acta Met., 1(1953), 448.
(55) C.Gatellier, D.Henriet and M.Olette : Compt. Rend. Acad. Sci., 271(1970), 453.
(56) R.Speiser, A.J.Jacobs and J.W.Spretnak : Trans. Met. Soc. AIME, 215(1959), 185.
(57) G.R.Zellars, S.L.Payne, J.P.Morris and R.L.Kipp : Trans. Met. Soc. AIME, 215(1959), 181.
(58) G.R.Belton and R.J.Fruehan : J. Phys. Chem., 71(1967), 1403.
(59) K.C.Mills, K.Kinoshita and P.Grieveson : J. Chem. Thermody., 4(1972), 581.

(60) G.Tammann and W.Oelsen : Z. anorg. Chem., 186(1930), 257.

(61) A.G.H.Andersen and A.W.Kingsbury : Trans. AIME, 152(1943), 38.

(62) H.A.Wriedt and L.S.Darken : Trans. Met. Soc. AIME, 218(1960), 30.

(63) A.H.Qureshi : Z. Metallk., 52(1961), 799.

(64) G.R.Speich, J.A.Gula and R.M.Fisher : The Electron Microprobe, Ed. by T.D.Mckinley, K.F.J.Heinrich and D.B.Witty, New York, (1966), 525.

(65) Y.Nakagawa : Acta Met., 6(1958), 704.

(66) W.Oelsen, E.Schurmann and C.Florin : Arch. Eisenhuttenw., 32(1961), 719.

(67) Y.Tozaki, Y.Iguchi, S.Ban-ya and T.Fuwa : Metallurgical Chemistry, Ed. by O.Kubaschewski, HSMO, London, (1972), 130.

(68) J.P.Morris and G.R.Zellars : J. Metals, 8(1956), 1086.

(69) A.D.Kulkarni : Met. Trans., 4(1973), 1713.

(70) B.B.Argent : Chemical Meteallurgy of Iron and Steel, Iron and Steel Inst., London, (1973), 301.

(71) M.Matsunaga : Japan Nickel Review, 1(1933), 347.

(72) C.J.Bechtoldt and H.C.Vacher : Trans. Met. Soc. AIME, 221(1960), 14.

(73) A.Chiba : Thesis, Tohoku University, (1971).

(74) G.Grube and M.Flad : Z. Elektrochem., 48(1942), 377.

(75) O.Kubaschewski and W.A.Dench : Z. Elektrochem., 64(1960), 801.

(76) M.G.Panish, R.F.Newton, W.R.Grimes and F.F.Blankenship : J. Phys. Chem., 62(1958), 980.

(77) L.A.Pugliese and G.R.Fitterer : Met. Trans., 1(1970), 1997.

(78) E.Schurmann and E.Schultz : Z. Metallk., 62(1971), 758.

(79) R.Hultgren, P.D.Desai, D.T.Hawkins, M.Gleiser and K.K.Kelley : Selected Values of the Thermodynamic Properties of Binary Alloys, ASM, Metals Park, Ohio, (1973).

(80) B.F.Peters and D.R.Wiles : Can.J. Chem., 41(1963), 2591.

(81) V.N.Eremenko, G.M.Lukashenko and V.R.Sidorko : Izvest. Akad. Nauk SSSR, 6(1964), 151.

(82) R.W.Krenzer and M.J.Pool : Trans. Met. Soc. AIME, 245(1969), 91.

(83) P.J.Spencer and J.N.Pratt : Trans. Faraday Soc., 64(1968), 1470.

(84) E.A.Feest and R.D.Doherty : J. Inst. Metals, 99(1971), 102.

(85) K.Tanaka and T.Nishizawa : unpublished work

(86) B.D.Bastow and D.H.Kirkwood : J. Inst. Metals, 99(1971), 277.

(87) B.Predel and R.Mohs : Arch. Eisenhuttenw., 42(1971), 575.

(88) O.Kubaschewski, W.A.Dench and V.Genta : Symposium on Physical Chemistry of Metallic Solutions and Intermetallic Compounds, National Physical Laboratory, Teddington, (1958), Vol.I, paper 1G.

(89) R.A.Oriani and W.K.Murphy : Acta Met., 8(1960), 23.

(90) L.Elford, F.Muller and O.Kubaschewski : Ber. Bunsenges. Physik. Chem., 73(1969), 601.

(91) M.G.Benz and J.F.Elliott : Trans. Met. Soc. AIME, 230(1964), 706.

(92) R.N.Dokken and J.F.Elliott : Trans. Met. Soc. AIME, 233(1965), 1351.

(93) R.A.Rapp and F.Maak : Acta Met., 10(1962), 63.

(94) I.Katayama, H.Shimatani and Z.Kozuka : J. Japan Inst. Metals, 37(1973), 509.

(95) A.D.Kulkarni and R.E.Johnson : Met. Trans., 4(1973), 1723.

(96) J.W.Schultz and H.F.Merrick : Met. Trans., 3(1972), 2479.

(97) O.Kubaschewski and L.E.H.Stuart : J. Chem. Eng. Data, 12(1967),418.

(98) W.Slough, J.Spencer and O.Kubaschewski : J. Chem. Thermody., 2(1970), 117.

(99) S.W.Gilby and G.R.Pierre : Trans. Met. Soc. AIME, 245(1969), 1749.

(100) L.Kaufman : Phase Stability in Metals and Alloys, Ed. by P.S.Rudman, J.Stringer and R.I.Jaffee, McGraw-Hill, New York, (1967), 125.

(101) L.Kaufman and H.Nesor : Z. Metallk., 64(1973), 249.

(102) R.J.Orr and J.Chipman : Trans. Met. Soc. AIME, 239(1967), 630.

(103) R.Hultgren, P.D.Desai, D.T.Hawkins, M.Gleiser, K.K.Kelley and D.D.Wagman : Selected Values of the Thermodynamic Properties of Elements, ASM, Metals Park, Ohio, (1973).

(104) M.Hasebe and T.Nishizawa : to be published.

(105) P.Schafmeister and R.Ergang : Arch. Eisenhuttenw., 12(1939), 459.

(106) A.J.Cook and B.R.Brown : J. Iron Steel Inst., 171(1952), 345.

(107) C.Zener : J. Metals, 7(1955), 619.

(108) R.J.Weiss and K.J.Tauer : Phys. Rev., 102(1956), 1490.

(109) A.J.Bradley, W.F.Cox and H.J.Goldschmidt : J. Inst. Metals, 67(1941), 189.

Table 1 Chemical composition of materials.

Materials		Impurities (wt. ppm)
Electrolytic iron	(99.95)	C40, Si40, P30, S40, Cu40, Mn40
Electrolytic chromium	(99.28)	C200, Si80, P10, S260, Al40, Cu5, Pb20, Fe1400
High purity chromium	(99.999)	Fe3, Pb2, Mg<1
Electrolytic manganese	(99.9)	C100, Si100, P100, Fe100, S100, Al Tr.
Mond cobalt	(>99.5)	S60, C100, Fe1200, Ni1200, Si230, Mn60
Electrolytic nickel	(Ni+Co>99.5)	Co<300, Fe<50, Cu<50, Pb<10, Mn<20, S<10, Si<50, C<200
High purity copper	(99.999)	Ag4.0, Au0.1, Fe1.0, Pb0.5, S3.2, Ni,Sn,Zn n.d.

Table 2 Empirical conversion parameters α_{ij} for microanalysis (at 20kV and 30kV).

	i \ j	Fe	Cr	Mn	Ni	Cu
K_α	Fe		1.140	(0.902)	0.760 (0.786)	0.706 (0.725)
	Cr	0.778		-	0.790	-
	Mn	(0.928)	-		-	(0.760)
	Ni	1.100 (1.180)	1.290	-		0.913 (0.858)
	Cu	1.220 (1.180)	-	-	1.010 (1.000)	
L_α	Ni	2.650	2.400	-		-
	Cu	3.620 (5.800)	-	(4.980)	3.650 (5.700)	

values in bracket for 30kV

Table 3 Experimental results of the γ/ε and the γ/liquid equilibrium in the binary Fe-Cu system.

T(K)	x^{γ}_{Cu}	x^{ε}_{Fe}	x^{l}_{Fe}
1173	0.034	0.018	-
1223	0.039	0.022	-
1273	0.064	0.029	-
1323	0.066	0.033	-
1373	0.106	-	0.047
1423	0.103	-	0.031
1473	0.114	-	0.036
1523	0.116	-	0.047
1573	0.129	-	-
1623	0.139	-	-

Table 4 Experimental results of the α/γ equilibria in the ternary Fe-Cr-Ni system.

	α		γ	
	x_{Cr}	x_{Ni}	x_{Cr}	x_{Ni}
1473 K	0.199	0.036	0.177	0.045
	0.233	0.043	0.198	0.069
	0.282	0.070	0.232	0.105
	0.368	0.110	0.285	0.179
	0.390	0.122	0.295	0.200
1373 K	0.420	0.116	0.300	0.200
	0.365	0.085	0.255	0.160
	0.314	0.064	-	-
	0.264	0.055	0.190	0.090
	0.207	0.025	0.158	0.037
	0.560*	0.133*	0.339*	0.309*
1273 K	0.347	0.051	0.230	0.120
	0.365	0.066	-	-
	0.465	0.080	0.285	0.200
	0.523	0.098	0.290	0.275
	0.502	0.105	0.304	0.258
	0.525	0.100	0.313	0.250
	0.497	0.098	0.298	0.260
	0.222	0.017	0.175	0.033
	0.272	0.032	0.210	0.050
	0.320	0.045	0.220	0.100
	0.385	0.062	0.255	0.140
	0.433	0.082	0.271	0.185
	0.668	0.097	0.346	0.361
	0.675	0.092	0.345	0.380
	0.611*	0.099*	0.326*	0.305*
1193 K	0.444	0.060	-	-
	0.465	0.060	0.265	0.215
	0.462	0.069	0.275	0.225
	0.404	0.048	0.250	0.160
	0.350	0.035	0.225	0.110
	0.265	0.025	0.175	0.055
	0.215	0.008	0.150	0.015
	0.380*	0.046*	0.256*	0.122*
	0.678*	0.060*	0.325*	0.292*

* taken from two-phase alloys

Table 5 Experimental results of miscibility gap in the ternary Fe-Cu-Mn system.

	γ		$\gamma'(\varepsilon)$	
	x_{Cu}	x_{Mn}	x_{Cu}	x_{Mn}
1173 K	0.103	0.044	0.923	0.051
	0.129	0.061	0.938	0.059
	0.113	0.077	0.908	0.079
	0.105	0.105	0.916	0.084
	0.109	0.111	0.894	0.105
	0.092	0.109	0.887	0.107
1123 K	0.106	0.025	0.889	0.034
	0.109	0.059	0.913	0.063
	0.108	0.093	0.895	0.094
	0.108	0.122	0.880	0.114
	0.099	0.156	0.850	0.139
	0.095	0.176	0.832	0.149
	0.113*	0.221*	0.767*	0.189*
	0.121*	0.320*	0.722*	0.248*
	0.120*	0.440*	0.609*	0.353*
	0.133*	0.589*	0.413*	0.511*

* taken from two-phase alloys

Table 6 Experimental results of the γ/liquid equilibria in the ternary Fe-Cu-Mn system.

	γ		liquid	
	x_{Cu}	x_{Mn}	x_{Cu}	x_{Mn}
1323 K	0.121	0.062	0.868	0.114
	0.078	0.184	0.762	0.220
	0.075	0.296	0.648	0.295
	0.141	0.503	0.563	0.407
	0.202	0.621	0.456	0.513
1223 K	0.104	0.201	0.782	0.206
	0.090	0.240	0.762	0.226
	0.076	0.266	0.731	0.254
	0.100	0.396	0.674	0.313
	0.127	0.509	0.620	0.368
	0.190	0.546	0.600	0.388
	0.089	0.375	0.669	0.314
1173 K	0.105	0.165	0.770	0.186
	0.147	0.303	0.726	0.248
	0.093	0.354	0.705	0.268
	0.149	0.520	0.624	0.366

Table 7 Experimental results of miscibility gap in the ternary Fe-Cu-Ni system.

	γ		$\gamma'(\varepsilon)$	
	x_{Cu}	x_{Ni}	x_{Cu}	x_{Ni}
1323 K	0.184	0.236	0.868	0.083
	0.214	0.256	0.841	0.103
	0.227	0.242	0.879	0.073
	0.299	0.286	0.778	0.144
	0.283	0.258	0.804	0.114
	0.441	0.265	0.661	0.204
	0.403	0.269	0.693	0.183
	0.151	0.097	0.941	0.035
	0.126	0.089	0.927	0.027
	0.158	0.157	0.909	0.052
	0.186	0.198	0.829	0.067
	0.245	0.250	0.822	0.103
	0.297	0.282	0.761	0.136
1223 K	0.181	0.281	0.881	0.093
	0.188	0.263	0.922	0.062
	0.188	0.299	0.862	0.107
	0.195	0.274	0.882	0.088
	0.243	0.313	0.809	0.130
	0.231	0.305	0.869	0.101
	0.197	0.350	0.776	0.157
	0.304	0.314	0.801	0.147
	0.277	0.352	0.714	0.187
	0.267	0.331	0.751	0.153
	0.342	0.365	0.745	0.198
	0.334	0.343	0.791	0.146
	0.465	0.328	0.713	0.216
	0.138	0.018	0.974	0.018
	0.151	0.108	0.943	0.047
1123 K	0.111	0.079	0.970	0.002
	0.083	0.106	0.946	0.027
	0.103	0.158	0.911	0.040
	0.110	0.189	0.934	0.042
	0.219	0.411	0.799	0.147
	0.205	0.422	0.836	0.131
	0.236	0.434	0.789	0.166
	0.261	0.428	0.819	0.142
	0.241	0.427	0.795	0.162
	0.406	0.383	0.724	0.218
	0.140	0.348	0.873	0.092

Table 8 Experimental results of the γ/liquid equilibria in the ternary Fe-Cu-Ni system.

	γ		liquid	
	x_{Cu}	x_{Ni}	x_{Cu}	x_{Ni}
1523 K	0.180	0.153	0.896	0.054
	0.227	0.220	0.817	0.085
	0.279	0.283	0.792	0.115
	0.374	0.377	0.722	0.190
1423 K	0.209	0.173	0.915	0.039
	0.701	0.170	0.881	0.079
	0.338	0.215	0.908	0.050

Table 9 Evaluated interaction parameters in the binary systems. (J/mol)

system i-j	phase	n	0	1	2
Fe-Cr	l	A^n_{ij}	19310	13360	-
		B^n_{ij}	-11.20	-5.343	-
	α	A^n_{ij}	24710	664	-
		B^n_{ij}	-11.76	1.736	-
	γ	A^n_{ij}	13840	6276	-
		B^n_{ij}	-13.61	-3.310	-
Fe-Mn	l	A^n_{ij}	-26520	-10870	-
		B^n_{ij}	17.10	7.263	-
	α	A^n_{ij}	-10830	-280	-
		B^n_{ij}	8.581	0.533	-
	γ	A^n_{ij}	-19760	-440	-
		B^n_{ij}	13.58	1.127	-
Fe-Ni	l	A^n_{ij}	-16690	-10750	-
		B^n_{ij}	3.592	2.401	-
	α	A^n_{ij}	-10270	-12150	-
		B^n_{ij}	0.306	3.902	-
	γ	A^n_{ij}	-26170	-15140	-
		B^n_{ij}	81.59	33.26	-
		C^n_{ij}	-9.602	-3.807	-

1000

Table 9 (continued)

system i-j	phase	n	0	1	2
Fe-Cu	l	A^n_{ij}	36440	-400	11560
		B^n_{ij}	-2.730	0.738	-4.153
	α	A^n_{ij}	43390	-	-
		B^n_{ij}	-6.197	-	-
	γ	A^n_{ij}	31010	5410	14930
		B^n_{ij}	0	-2.618	-5.627
Cr-Ni	l	A^n_{ij}	-15270	-36170	-
		B^n_{ij}	4.197	15.25	-
	α	A^n_{ij}	23370	-26030	-
		B^n_{ij}	-17.22	4.665	-
	γ	A^n_{ij}	4268	-31080	-
		B^n_{ij}	-15.80	19.23	-
Mn-Cu	l	A^n_{ij}	-2131	-24090	6360
		B^n_{ij}	-0.323	13.89	-6.004
	α	A^n_{ij}	23960	-	-
		B^n_{ij}	-13.64	-	-
	γ	A^n_{ij}	12790	-9837	9749
		B^n_{ij}	-3.893	4.192	-9.816
Ni-Cu	l	A^n_{ij}	10460	-1451	-
		B^n_{ij}	2.087	0.394	-
	γ	A^n_{ij}	8138	-2537	-
		B^n_{ij}	3.009	0.828	-

Table 10 Evaluated interaction parameters in the ternary systems.
(J/mol)

system i-j-k	phase	p	i	j	k
Fe-Cr-Ni	l,α,γ	A^p_{ijk}	0	0	0
Fe-Cu-Mn	l	A^p_{ijk}	0	0	0
	γ	A^p_{ijk}	10460	10460	10460
Fe-Cu-Ni	l	A^p_{ijk}	0	0	0
	γ	A^p_{ijk}	-77400	-111300	-49000
		B^p_{ijk}	72.8	73.2	41.8

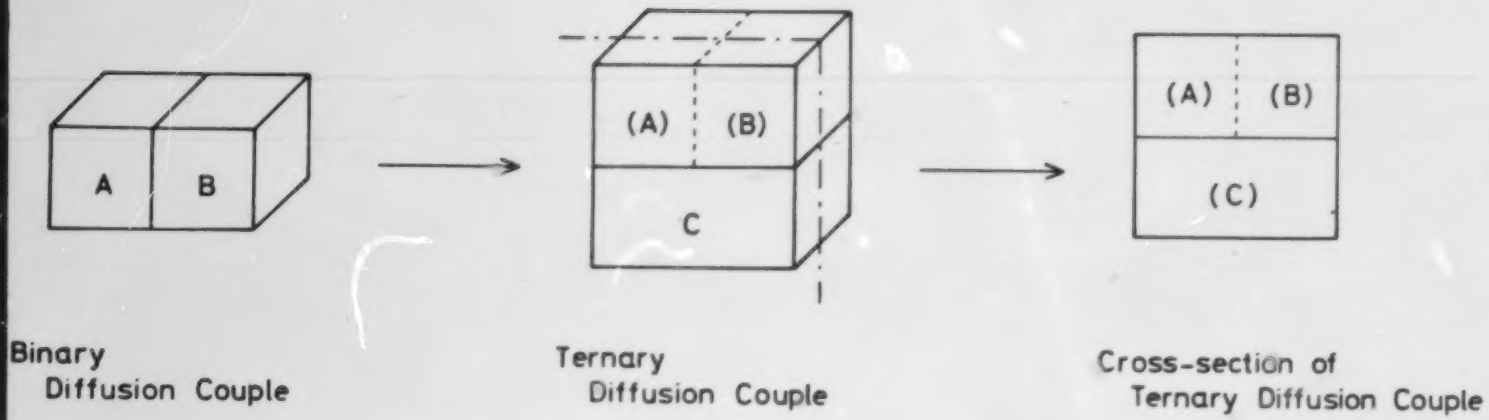

Fig. 1 Construction of a ternary diffusion couple.

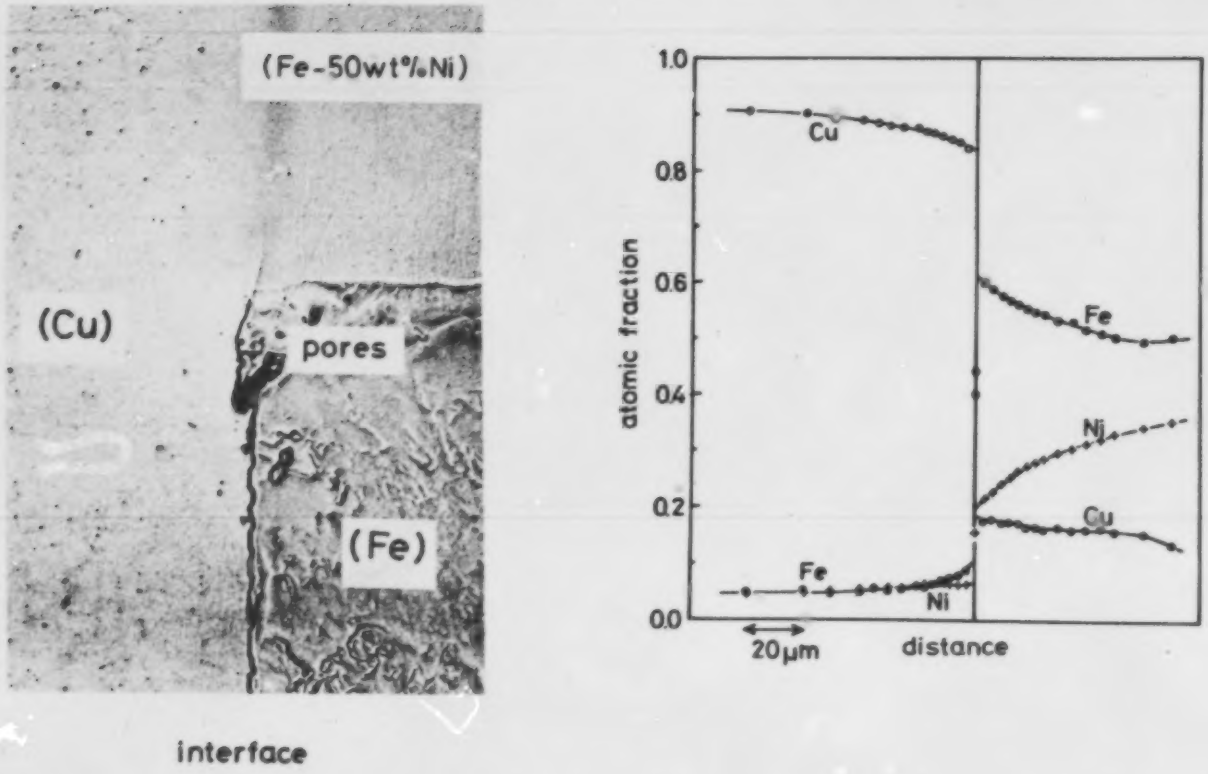

Fig. 2 The cross-section and the concentration profile for a ternary Fe-Cu-Ni diffusion couple heated at 1323 K for 7 days.

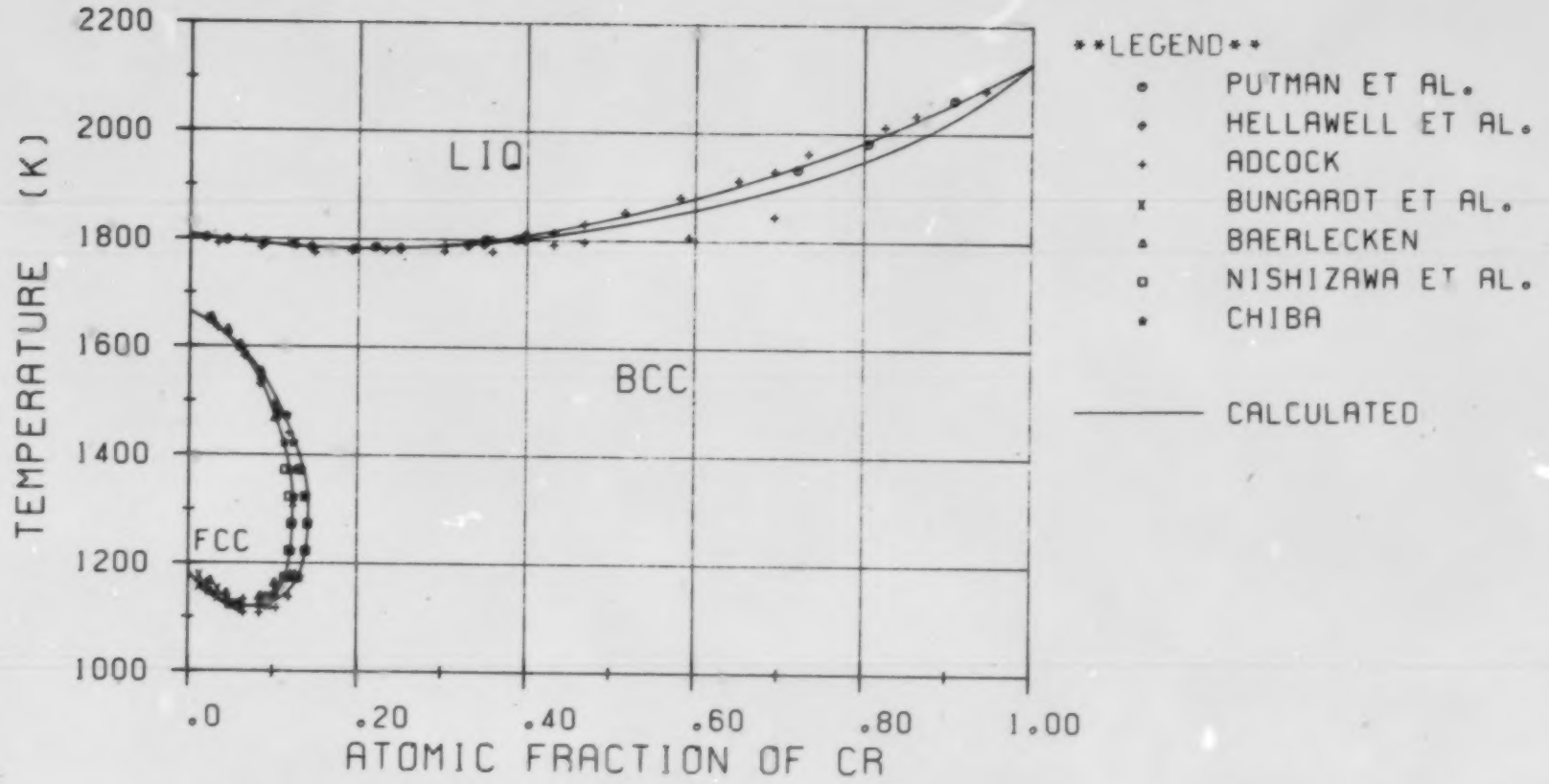

Fig. 3 Computer generated phase diagram in the binary Fe-Cr system.

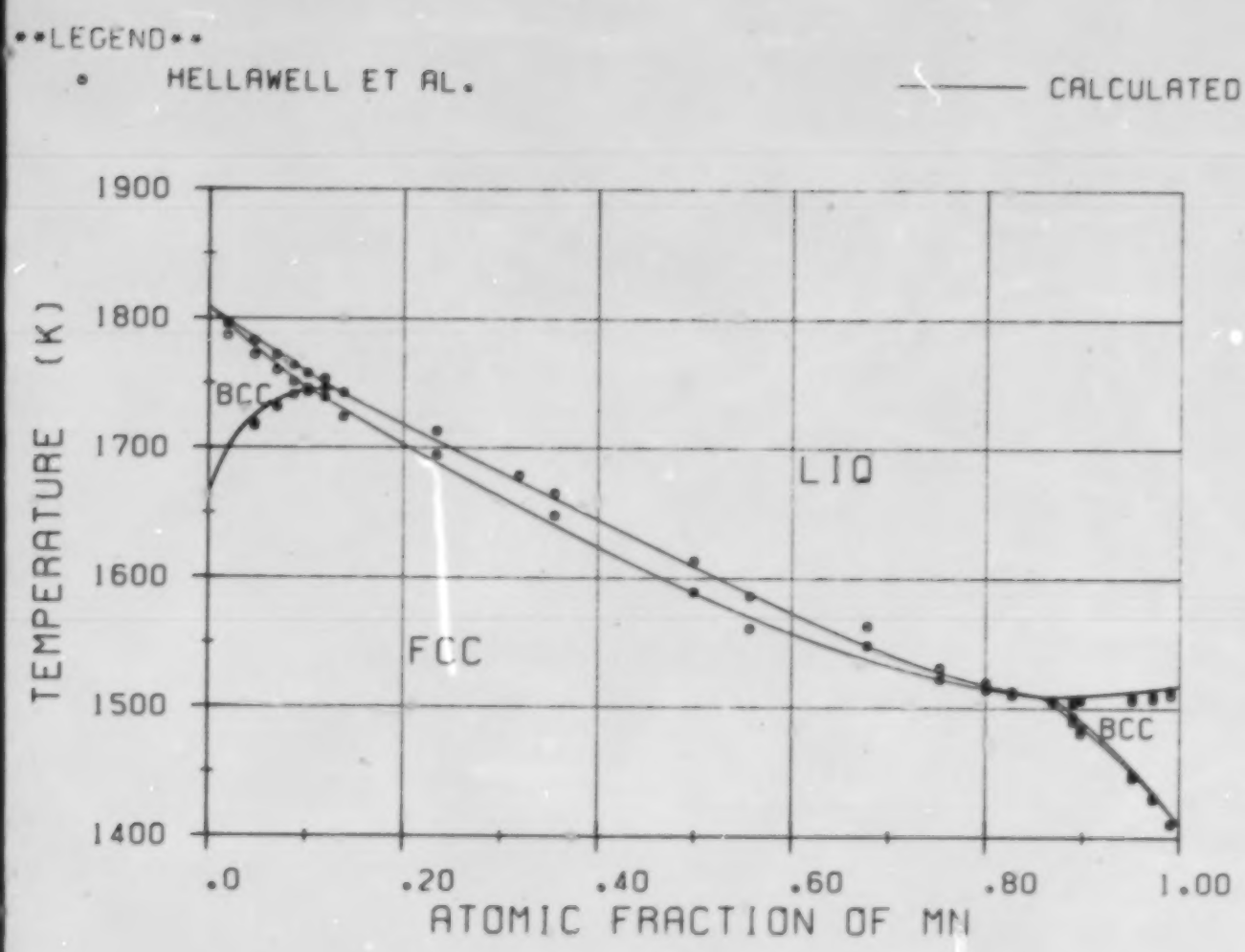

1007

Fig. 4 Computer generated phase diagram in the binary Fe-Mn system.

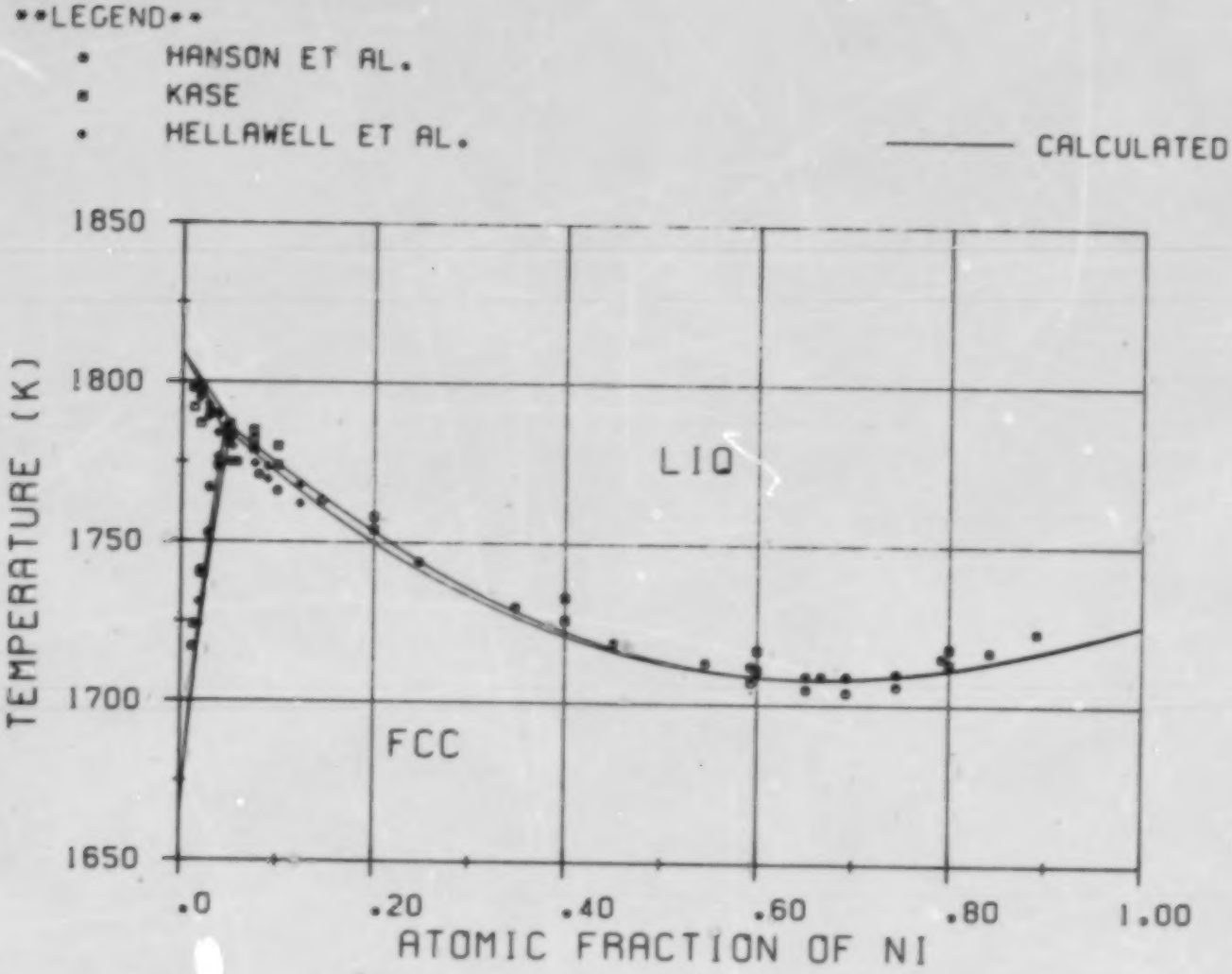

Fig. 5 Computer generated phase diagram in the binary Fe-Ni system.

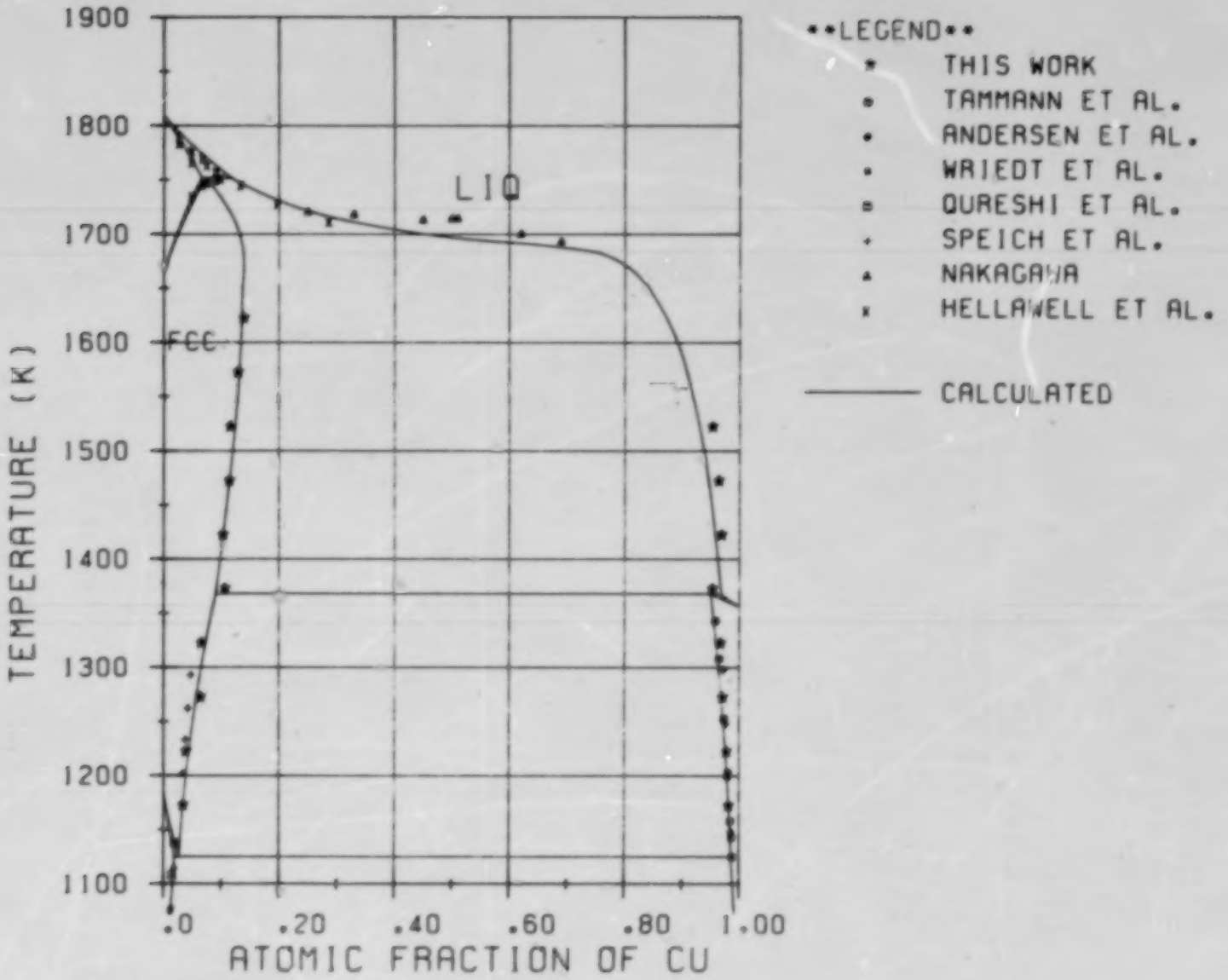

Fig. 6 Computer generated phase diagram in the binary Fe-Cu system.

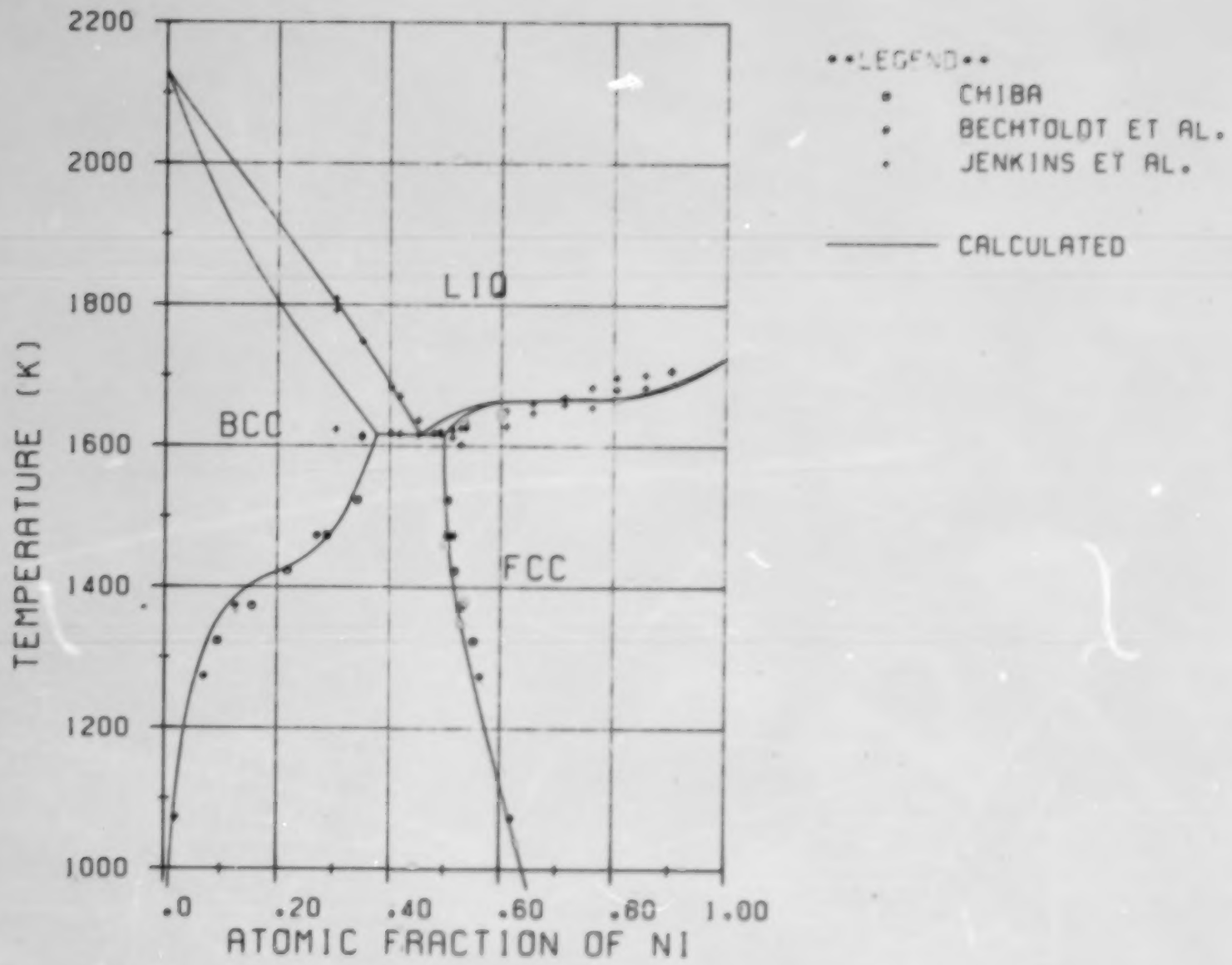

Fig. 7 Computer generated phase diagram in the binary Cr-Ni system.

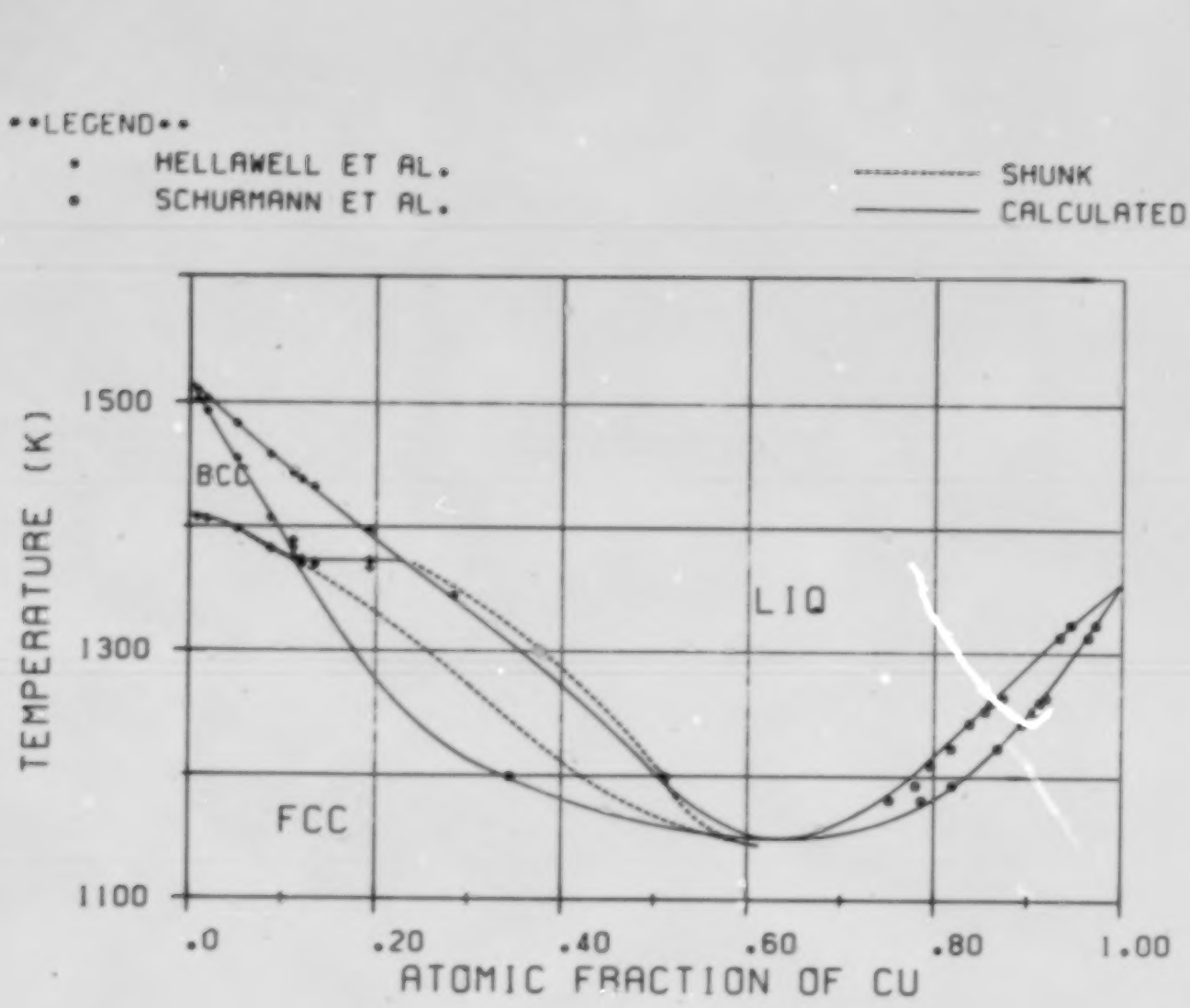

Fig. 8 Computer generated phase diagram in the binary Cu-Mn system.

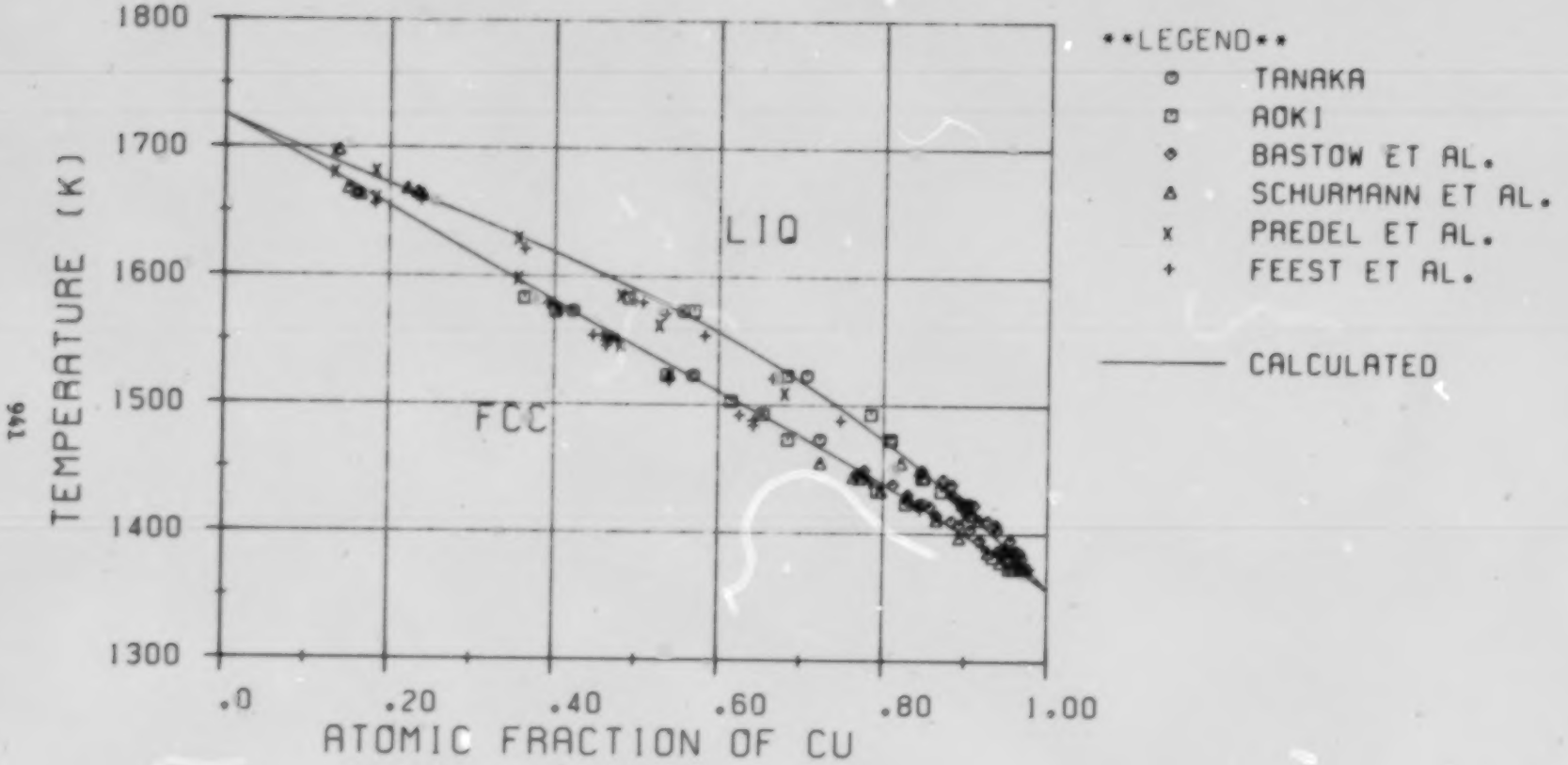

Fig. 9 Computer generated phase diagram in the binary Cu-Ni system.

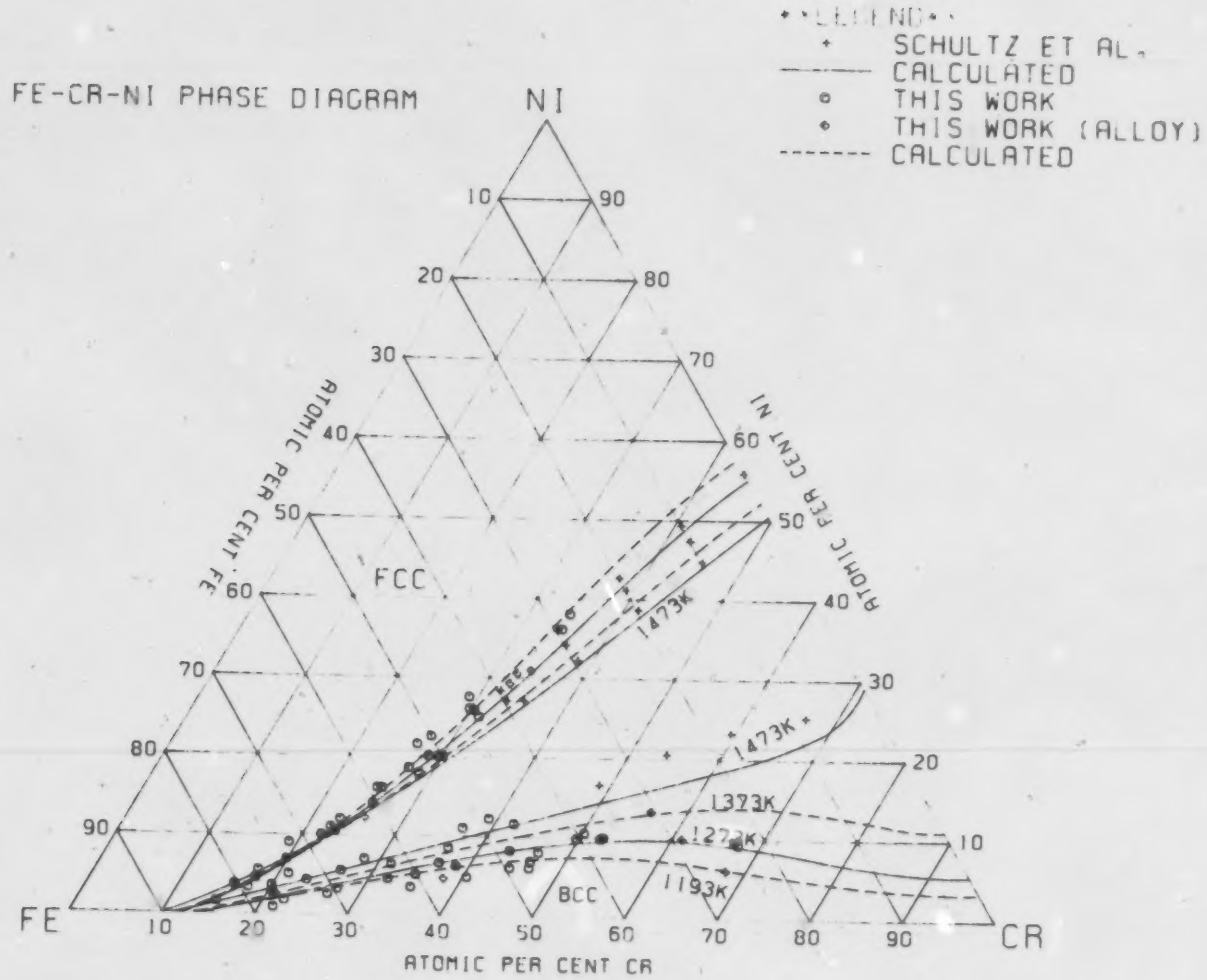

Fig. 10 The α/γ phase equilibria in the ternary Fe-Cr-Ni system between 1193 and 1473 K.

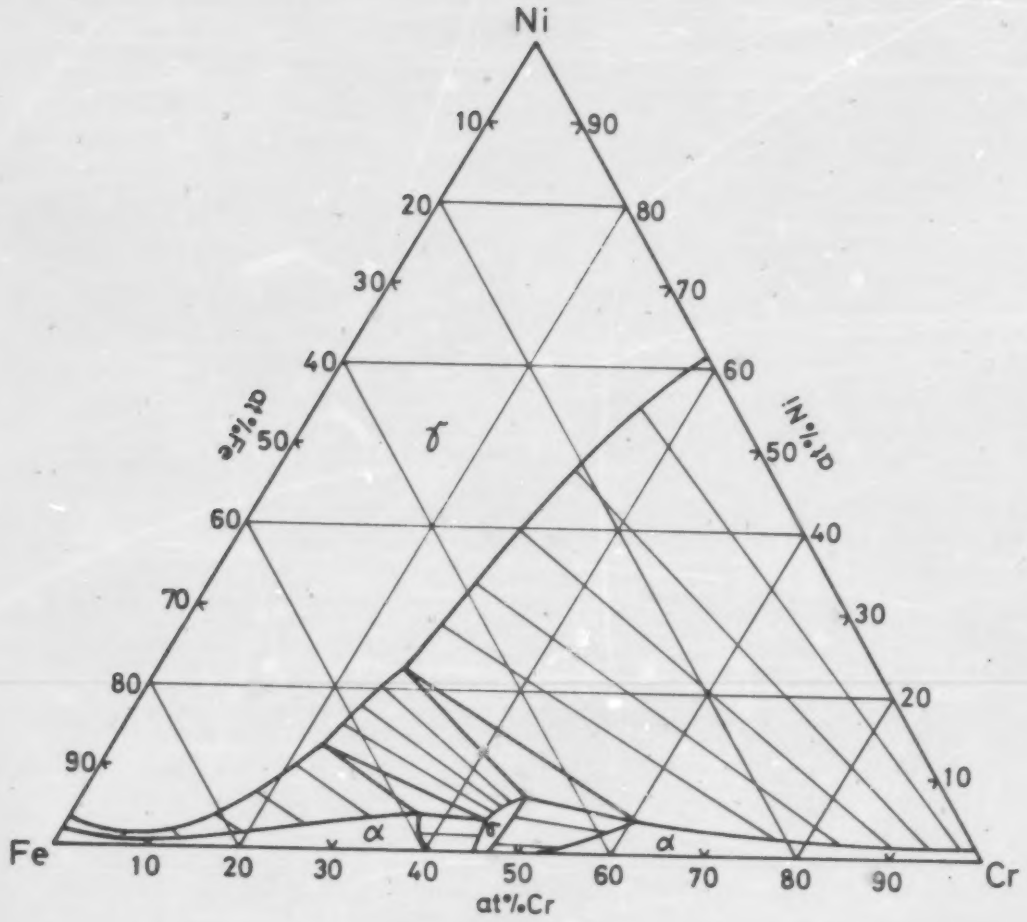

Fig. 12 Isothermal sections of the ternary Fe-Cr-Ni system at 1073 K. (a) Computer calculated.

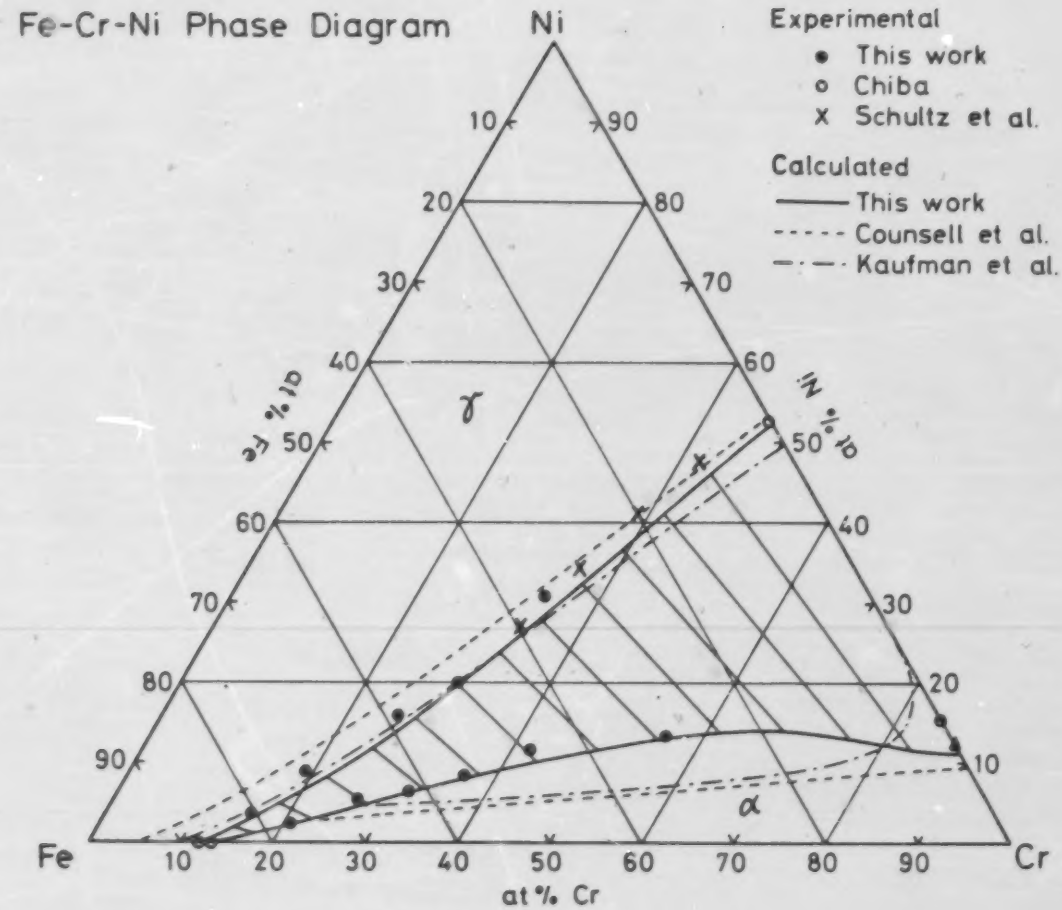

Fig. 13 Comparison between calculated and experimentally determined phase boundaries in the Fe-Cr-Ni system at 1373 K.

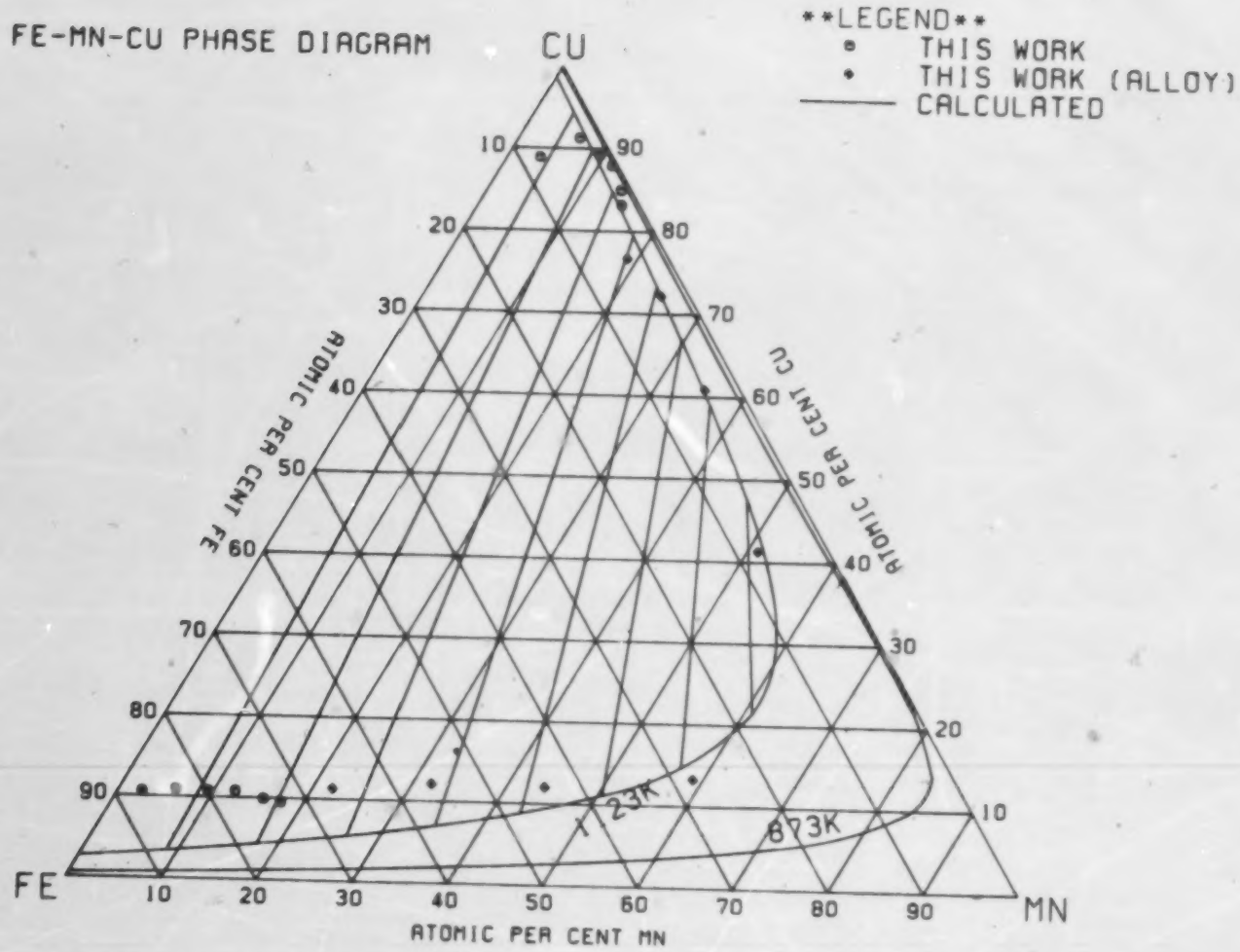

Fig. 14 Miscibility gap in the ternary Fe-Cu-Mn system between 873 and 1123 K.

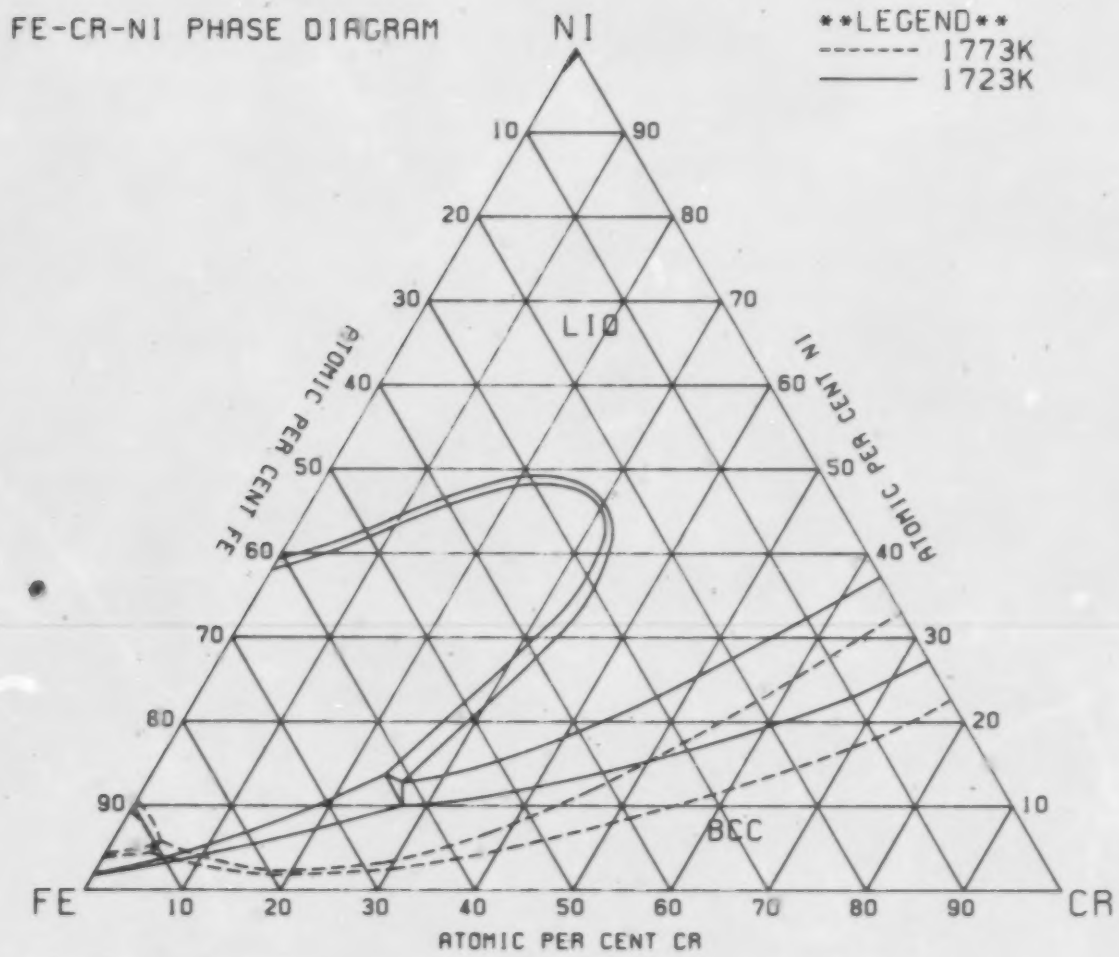

Fig. 11 The solid/liquid phase equilibria in the Fe-Cr-Ni system between 1723 and 1773 K.

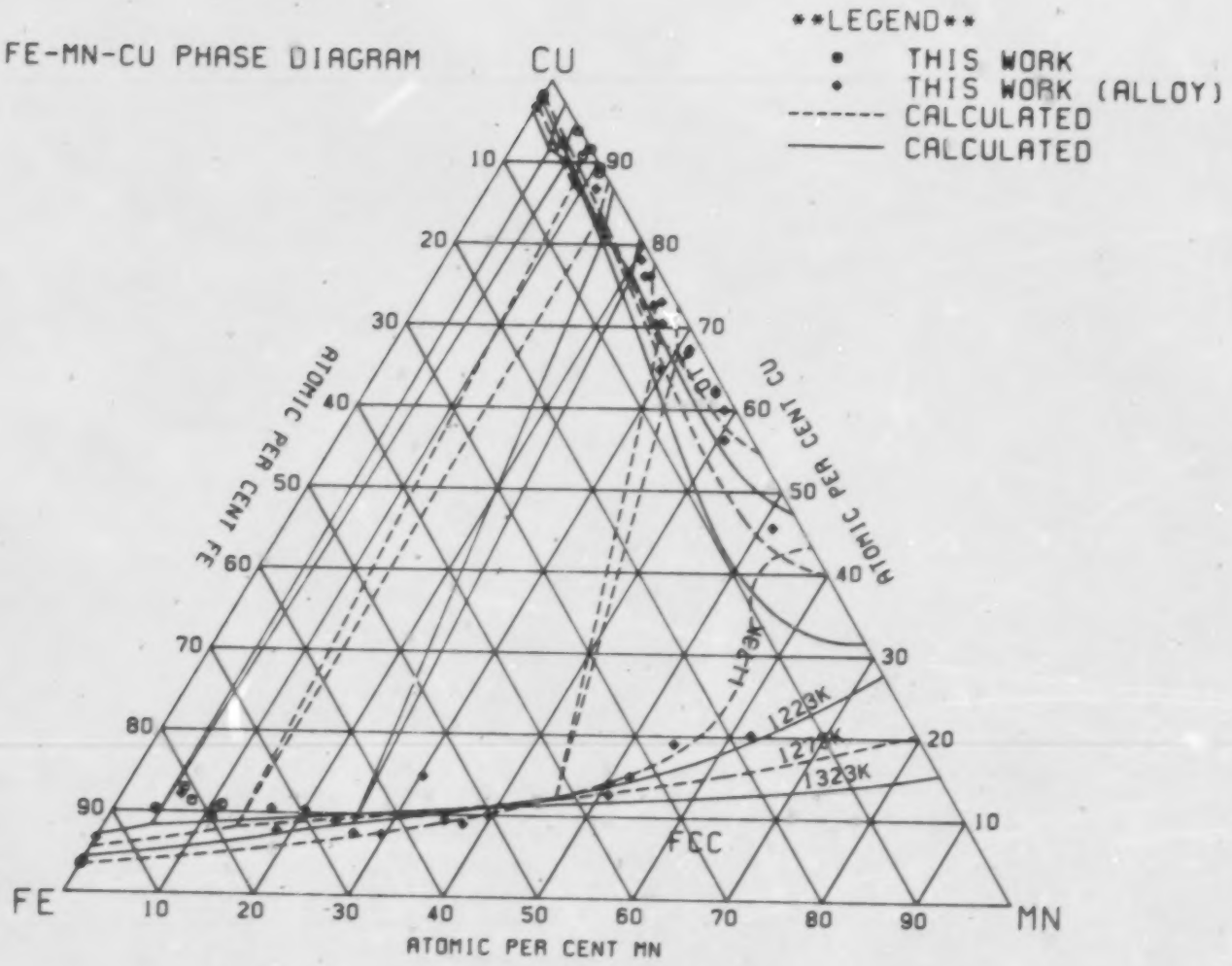

Fig. 15 The γ/liquid phase equilibria in the ternary Fe-Cu-Mn system between 1173 and 1323 K.

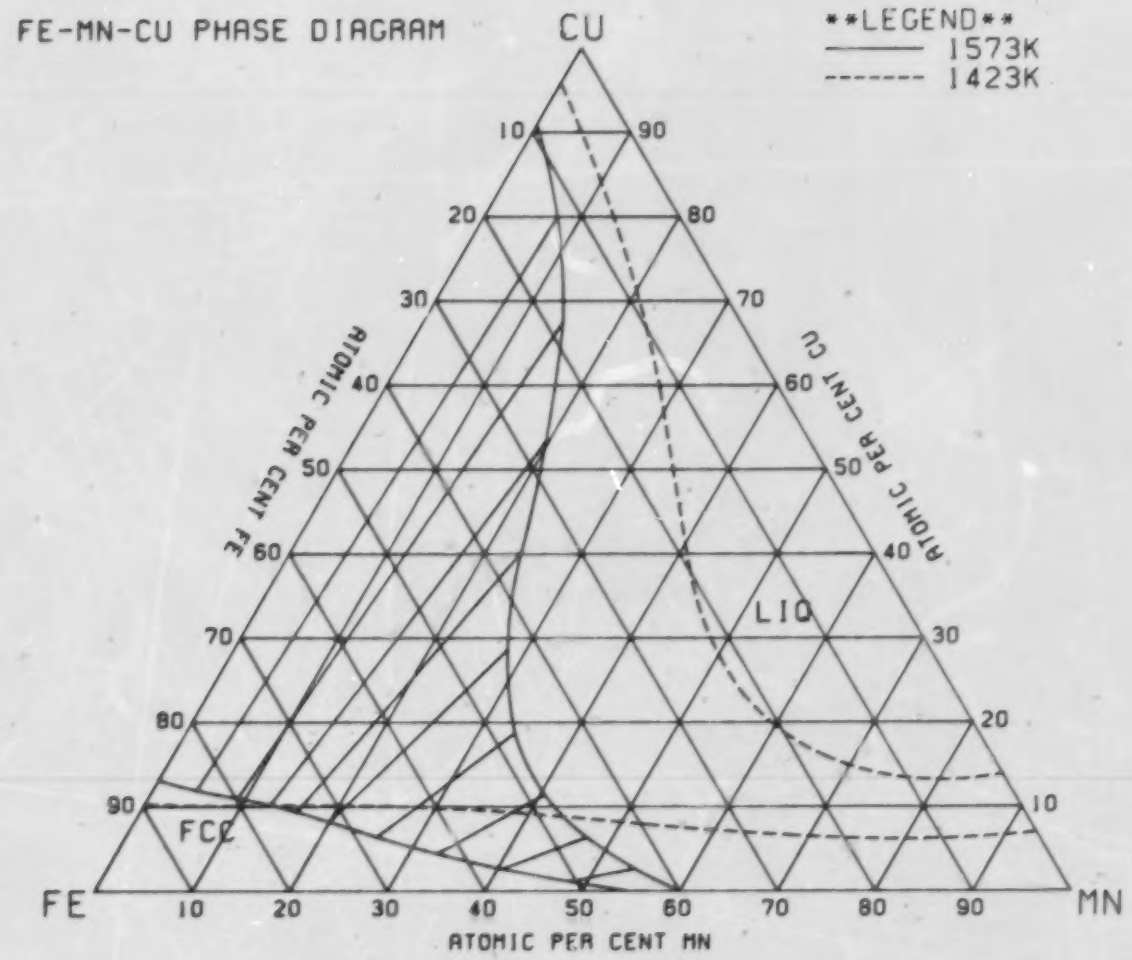

Fig. 16 The γ/liquid phase equilibria in the ternary Fe-Cu-Mn system between 1423 and 1573 K.

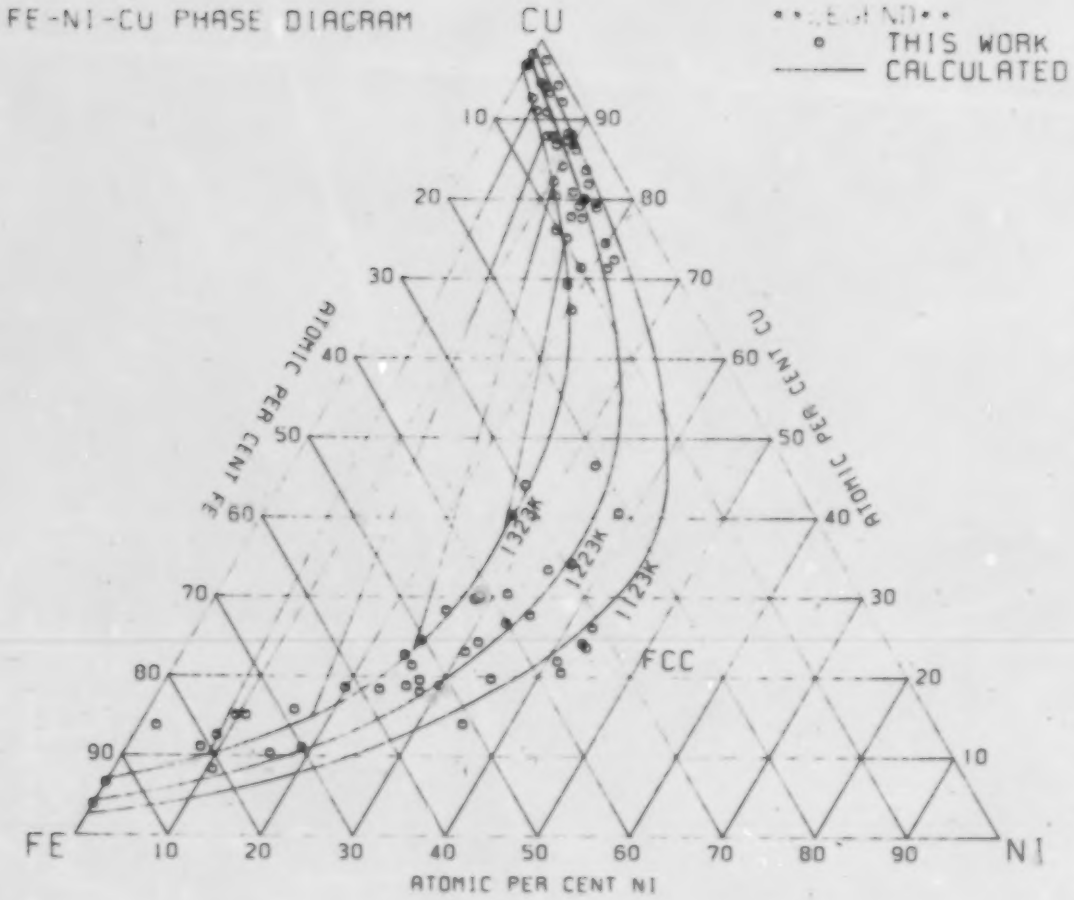

Fig. 17 Miscibility gap in the ternary Fe-Cu-Ni system between 1123 and 1323 K.

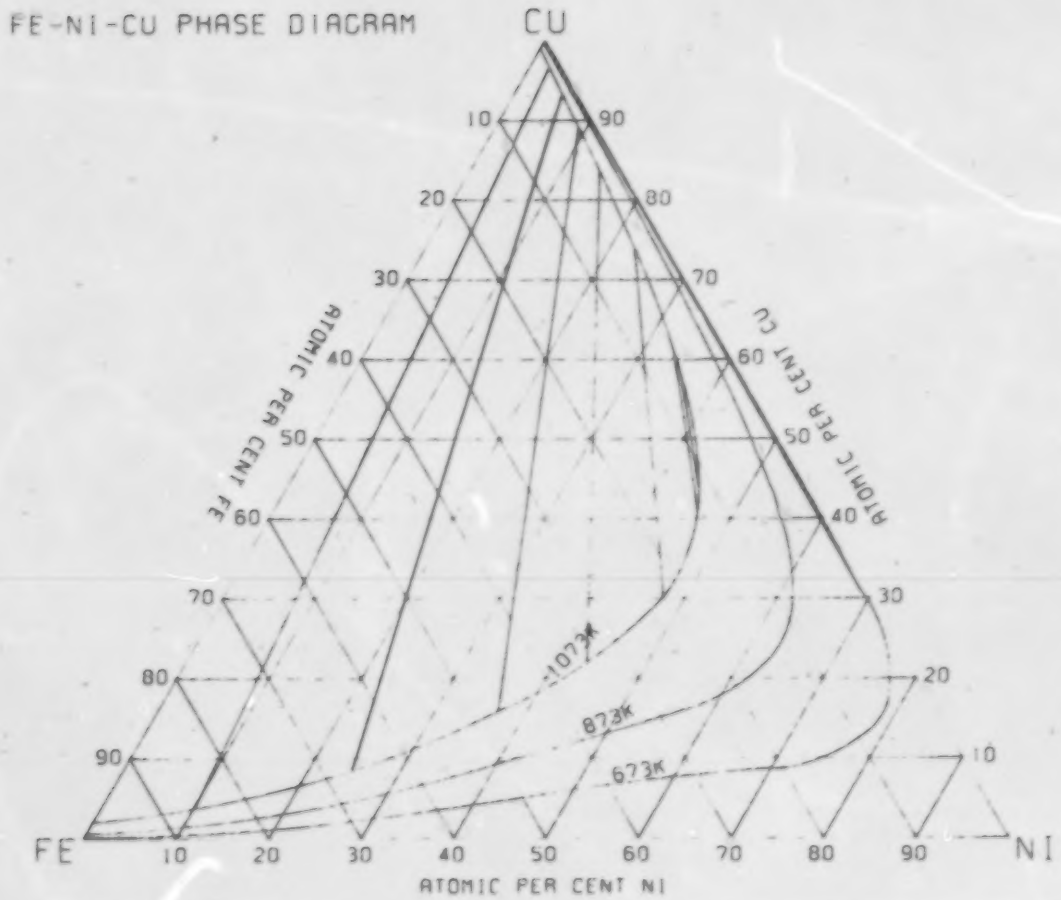

Fig. 18 Miscibility gap in the ternary Fe-Cu-Ni system between 673 and 1073 K.

1022

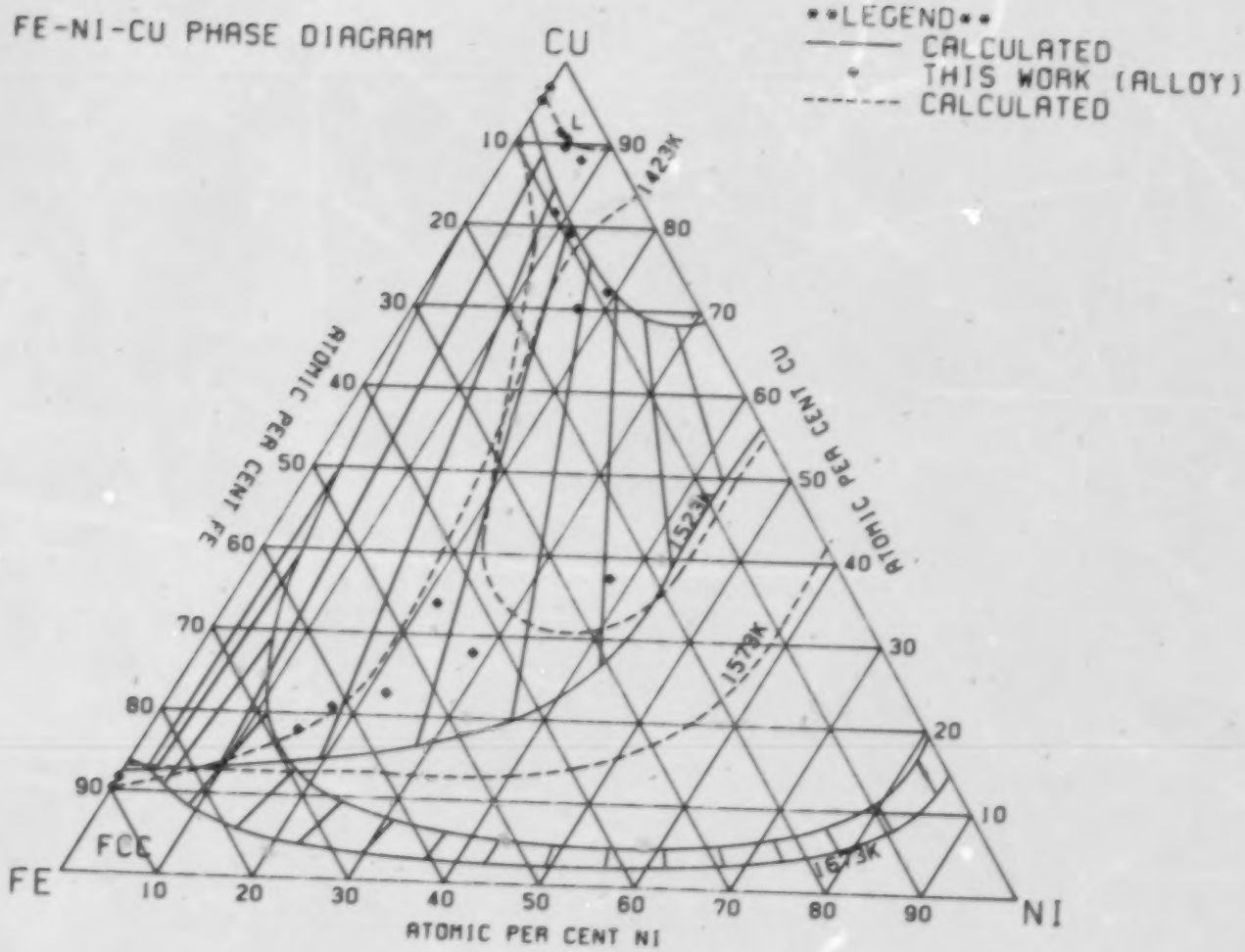

Fig. 19 The γ/liquid phase equilibria in the ternary Fe-Cu-Ni system between 1423 and 1673 K.

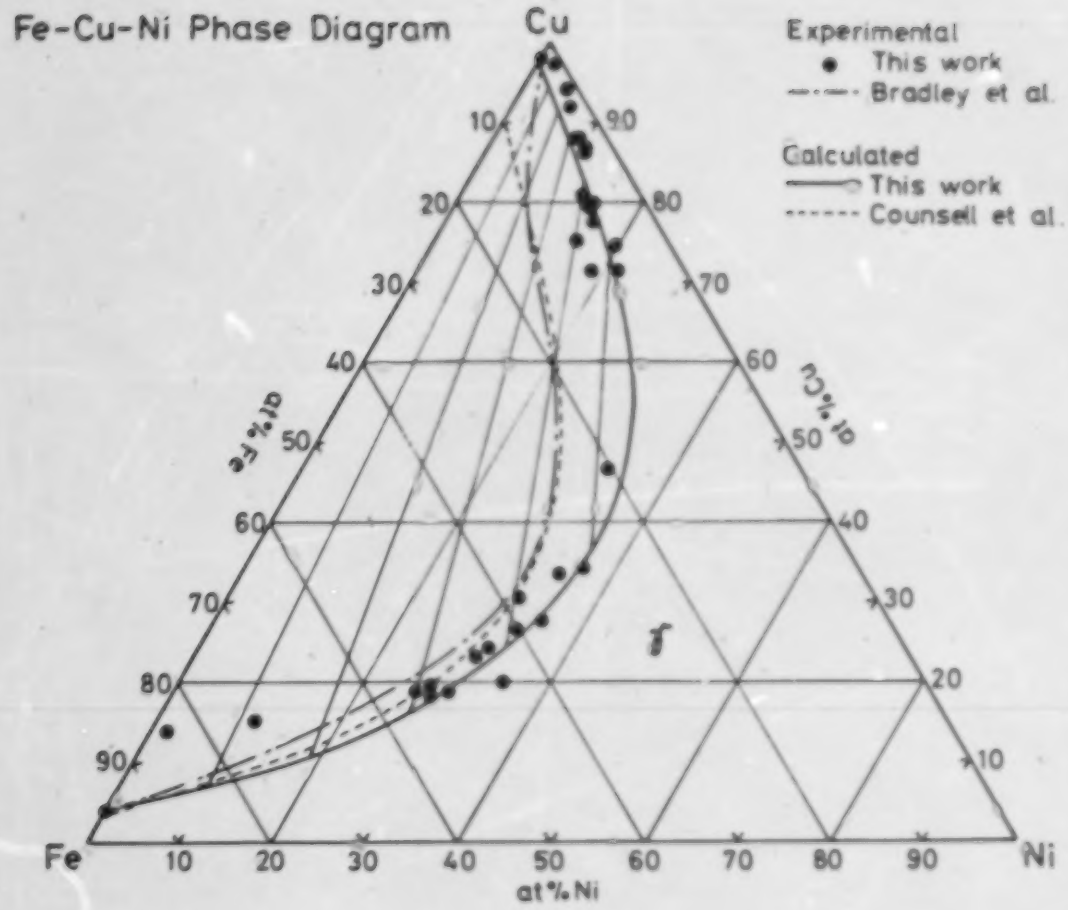

Fig. 20 Comparison between calculated and experimentally determined phase boundaries in the Fe-Cu-Ni system at 1223 K.

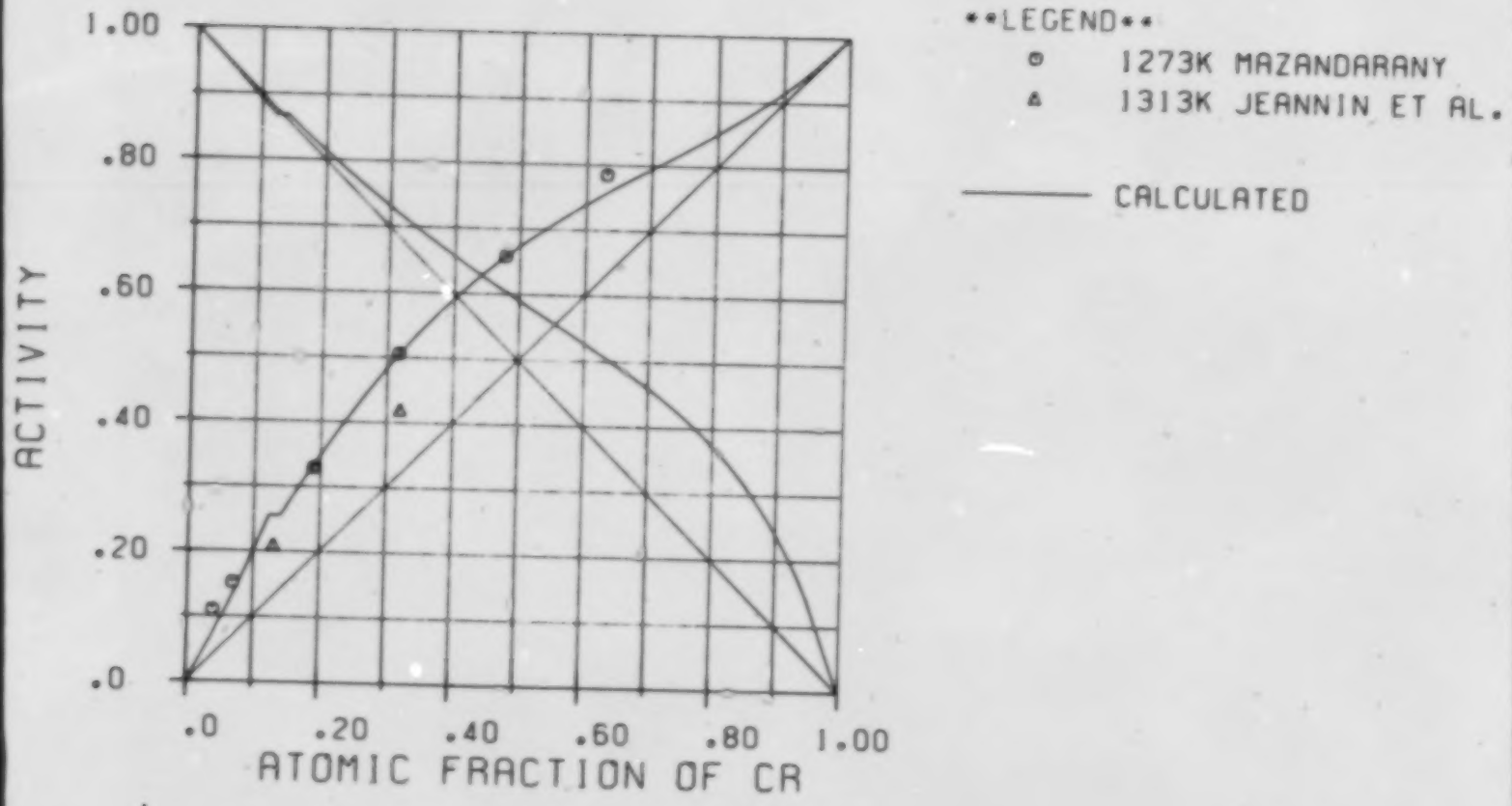

Fig. 21 Activities in the binary Fe-Cr system at 1273 K.

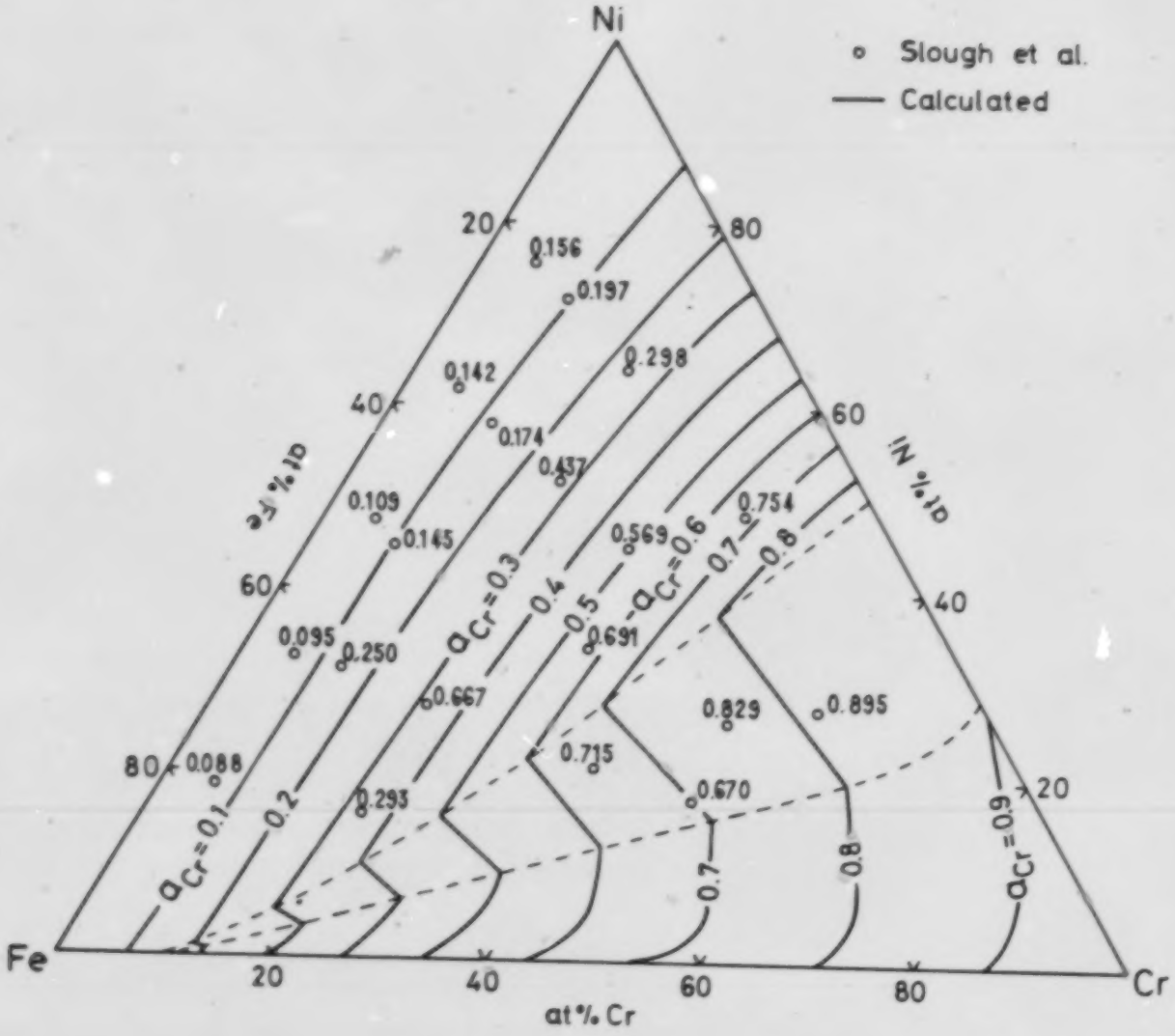

Fig. 22 Iso-activity lines for chromium in the ternary Fe-Cr-Ni system at 1473 K.

National Bureau of Standards SP-496, Applications of Phase Diagrams in Metallurgy and Ceramics
Proceedings of Workshop held at NBS, Gaithersburg, Md., January 10-12, 1977

Optimization of Phase Diagrams by a Least Squares Method Using Simultaneously Different Types of Data.

E.-Th. Henig, H.L. Lukas, B. Zimmermann and G. Petzow
Max-Planck-Institut für Metallforschung, Institut für Werkstoffwissenschaften, Büsnauerstr. 175, 7000 Stuttgart-80, FRG.

Introduction

There are three main problems in constitutional research:

1. Using the existing experimental data the phase diagrams should be as accurate as possible,
2. A powerful tool is necessary to evaluate the enormous number of still unknown multicomponente systems,
3. The information should be storable in a compact form.

The optimal accuracy is obtained if all experimental data are taken into account and if thermodynamic consistency exists between all thermodynamic functions of the different phases and the phase diagram. If these functions are presented analytically they can be extrapolated for systems with one additional component. If the analytical representation uses always the same, standardised pattern, all the information of a system is contained in a set of coefficients and easily stored.

The optimization of a system based on different types of data usually is done by a trial and error method. With increasing number of components and/or increasing number of different types of data, this method becomes more and more cumbersome. Therefore a straight forward method is desirable. As straight forward method the Least Squares method of GAUSS is adapted here [1]. This method is well known for optimization of single functions and also for the determination of the partial free enthalpy (Gibbs energy) from binary phase diagrams [2] or from two phase tie lines of a ternary system [3].

Analytical representation

The goal of the least squares method is the simultaneous calculation of the different thermodynamic functions. Therefore, an analytical formalism is necessary which describes the different functions with coefficients taken from one common set of coefficients. In this way also the thermodynamic consistency is expressed, which is given by the well known and used thermodynamic relations.

We used a combination of the matrix representation of Wiederkehr [4] and the description of binary excess functions by Legendre-polynomials after Bale and Pelton [5].

The formalism is extended by the Kohler [6] extrapolations of the binary excess functions to describe the excess functions of ternary phases. An additional homogeneous polynomial (ternary correction) with the common factor $x_1x_2x_3$, which disappears in the binaries,is also introduced. The coefficients of this polynomial are determined by a few measurements in the ternary. The formulas are shown in appendix 1.

Instead of Kohler's extrapolation we used also the extrapolations of Bonnier and Caboz [7], Toop [8] and Hillert [9]. Those yield different functions and phase diagrams. But after adding the appropriate ternary correction function to each extrapolated function the differencies decrease and become smaller than the accuracy of the measurements.

The matrices of different phases of one system are easily combined into one large matrix of coefficients of the whole system [4]. This is shown in figure 1 where the matrix belongs to the hypothetical system of figure 2.

Not all the coefficients are unknown. Normally the coefficients of the stable phases of the pure elements are known, they are designated with K in figure 1. The coefficients belonging to the ideal solution R in the second column and zero in all

other columns. Coefficients denoted by a dot are not significant, they are taken zero and treated as known coefficients. Only the coefficients quoted U are unknown and subject of the GAUSSian calculation.

Calculation

In the GAUSSian calculation one equation of error belongs to each experimental value. It describes the difference between the calculated and the measured value of one quantity.

Many thermodynamic statements are composed of a set of two or more independent measured values. For example a tie line in a binary system is defined by two independently measured concentration/temperature pairs. These equations are constructed in a form in which one equation is strongly dependent on one and weakly dependent on the other variables. In this way the different accuracy of the measured values affect mainly the related equation of error.

The different types of values (calorimetric, emf or vapor-pressure, phase diagram measurements) have their special equation of error. Also for one type of measurement special equations exist for different number of phases. They are compiled in appendix 2.

By these equations all measurable thermodynamic values can be treated, specially also values, which cannot be treated easily by trial and error methods. For example the change of enthalpy during mixing of two melts of alloys of slightly different composition. Measurements of this kind can be used advantageously for establishing the curvature of the enthalpy concentration curves.

In order to compare the errors of all measurements, they must be weighted and have the same dimension. In our method each error is compared with the accuracy of the corresponding measurement (as given by an author or estimated). If the error is divided by this accuracy, a dimensionless relative error is defined which is expressed in % of the accuracy. In

addition to the measured value itself also the variables temperature and concentration have limited accuracies. To take account of this they are transformed to the dependent variable by multiplying them with the derivative of the dependent variable with respect to the variable in question. Combining all this the weight of the square of the error is:

$$P = 1/(\Delta v)^2 + (\frac{\partial v}{\partial T} \Delta T)^2 + (\frac{\partial v}{\partial x} \Delta x)^2$$

Δv is the accuracy of dependent variable, ΔT of the temperature and Δx of the concentration. If there is more than one concentration involved in a set of measurements there are additional terms of the type $(\frac{\partial v}{\partial x} \Delta x)^2$.

The method described here is applied in the following way:

(i) Optimization of the binary systems.
(ii) Extrapolation of the optimized thermodynamic functions of the binary phases into the ternary.
(iii) Optimization of the correction function using only a few ternary data.
(iv) Extrapolation and optimization for the quaternary system, and so on.

The result of this procedure is a set of coefficients which contains the entire information of the systems in a thermodynamically consistent form. This set of coefficients provides the basis for the calculation of any thermodynamic diagram, in particular the phase diagram.

The method has been used successfully for the calculation of the ternary systems Ag-Bi-Pb [10], Ag-Bi-Tl [11] and Ag-Pb-Tl [12].

The financial support by the Deutsche Forschungsgemeinschaft is greatfully acknowledged.

References

1. B. Zimmermann, Thesis, Uni Stuttgart 1976.

2. R. Hiskes and W.A. Tiller, Mater.Sci.Eng., 2 (1968) 320, 4 (1969) 163 and 4 (1969) 173.

3. G. Kirchner and B. Uhrenius, Acta met., 22 (1974) 523.

4. R.R.V. Wiederkehr, J.Chem.Phys., 37 (1962) 1192.

5. C.W. Bale and A.D. Pelton, Metall.Trans., 5 (1974) 2323.

6. F. Kohler, Monatsh. Chemie, 91 (1960) 738.

7. E. Bonnier and R. Caboz, C.R. Acad.Sci., 250 (1960) 527.

8. G.W. Toop, Trans.Met.Soc.AIME, 233 (1965) 850.

9. M. Hillert, Project Meeting CALPHAD V, 21.-25.6.1976, Düsseldorf.

10. H.L. Lukas, E.-Th. Henig and B. Zimmermann, to be published Z. Metallkde.

11. B. Zimmermann, E.-Th. Henig and H.L. Lukas, Z.Metallkde. 67 (1976) 815.

12. E.-Th. Henig and H.L. Lukas, to be published Z.Metallkde.

1031

Appendix 1

MATRIX REPRESENTATION of Thermodynamic Functions after Wiederkehr [4]

$((T_i)) \cdot ((C_{ij})) \cdot ((X_j)) = \text{value}$

$((T_i))$	= line vector	temperature and type of function (enthalpy, entropy, Gibbs free energy, specific heat)
$((C_{ij}))$	= matrix	coefficients of individual system
$((X_j))$	= column vector	concentration(s) and type of function (integral, partial,.... sum of functions of two phases)

T_i Matrices of Different Functions

H	(1	0	T	$T^2/2$	$-T^{-1}$	$T^3/3$ ...)
S	(0	1	log(T)	T	$-T^{-2}/2$	$T^2/2$ ...)
G	(1	-T	T(1-log(T))	$-T^2/2$	$-T^{-1}/2$	$-T^3/6$ ...)
C_p	(0	0	1	T	T^{-2}	T^2 ...)

X_j Matrices of Different Functions after Bale and Pelton [5]

Binary Phases

(P may be any of the functions H, S, G or C_p)

P	(1-x	x	(1-x)log(1-x) + x log(x)	... $x(1-x)P_1(1-2x)$	...)
P_1	(1	0	log(1-x)	... $x^2 P_1(1-2x)$ $+2x^2(1-x)\,\partial P_1/\partial(1-2x)$	...)
P_2	(0	1	log(x)	... $(1-x)^2 P_1(1-2x)$ $-2x(1-x)^2\,\partial P_1/\partial(1-2x)$	...)
	phase stability terms		ideal solution term	excess terms	

Excess Terms of X_j Matrix of a Ternary Phase

Integral function

$$\ldots x_1 x_2 P_1\left(\frac{x_1 - x_2}{x_1 + x_2}\right) \ldots x_2 x_3 P_1\left(\frac{x_2 - x_3}{x_2 + x_3}\right) \ldots x_3 x_1 P_1\left(\frac{x_3 - x_1}{x_3 + x_1}\right) \ldots$$

$x_1^{n-p-q} x_2^p x_3^q$ ... for $n \geq 3$ ternary correction

$p = 1 \ldots n-2$ (homogeneous polynomial)

$q = 1 \ldots n-1-p$

$$P_1\left(\frac{x_i - x_j}{x_i + x_j}\right)$$ Kohler extrapolation of above formulas

Partial functions are derived from the integral functions by the formula

$$P_i = P + \frac{\partial P}{\partial x_i} - \sum_{j=1}^{3} x_j \frac{\partial P}{\partial x_j}$$

Appendix 2

EQUATIONS of ERROR

Calorimetric Measurements

Nr. of phases	equation
1	$H - (1-x)^{\circ}H_1 - x^{\circ}H_2$ - value = error
2	$H'(T_1) - H''(T_2)$ - value = error
3	$H'(T_1) - \frac{x'''-x'}{x'''-x''} H''(T_2) - \frac{x'-x''}{x'''-x''} H'''(T_2)$ - value = error

4 (ternary systems only)

$$H'(T_1) - \frac{|Det''|}{|Det'|} H''(T_2) - \frac{|Det'''|}{|Det'|} H'''(T_2) - \frac{|Det''''|}{|Det'|} H''''(T_2)$$

- value = error

or

$$\frac{|Det'|}{D} H'(T_1) + \frac{|Det''|}{D} H''(T_1) - \frac{|Det'''|}{D} H'''(T_2) - \frac{|Det''''|}{D} H''''(T_2)$$

- value = error

where $D = |Det'| + |Det''|$

$$|Det'| = \begin{vmatrix} x_3'' & x_2'''' & 1 \\ x_3''' & x_2'''' & 1 \\ x_3'''' & x_2'''' & 1 \end{vmatrix}$$

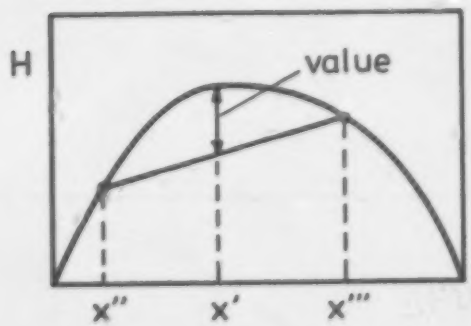

1034

EMF and Vapor Pressure Measurements

Nr. of phases	equation
1	$G_i(x,T) - {}^{o}G_i^r(T) - \text{value} = \text{error}$
2	$G_i'(x,T) - {}^{o}G_i^r(T) - \text{value} = \text{error}$
	$G_i''(x,T) - {}^{o}G_i^r(T) - \text{value} = \text{error}$
	$G' - x'\frac{G''-G'}{x''-x'} - {}^{o}G_1^r(T) - \text{value} = \text{error}$ (i=1)

Symmetrical form of last equation:

i=1 $\quad \frac{G'\,x''}{x''-x'} + \frac{G''\,x'}{x'-x''} - {}^{o}G_1^r - \text{value} = \text{error}$

i=2 $\quad \frac{G'(1-x'')}{x'-x''} + \frac{G''(1-x')}{x''-x'} - {}^{o}G_2^r - \text{value} = \text{error}$

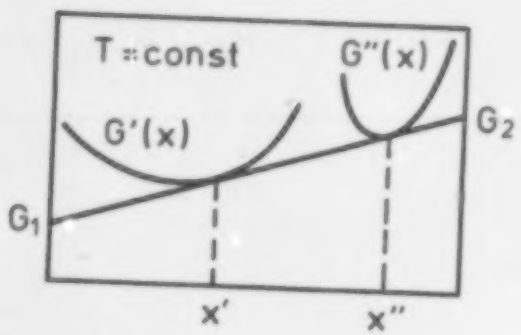

Phase Diagrams

Binary:

2 phases:

$$G'(x') + (x''-x')(\partial G'/\partial x)_{x'} - G''(x'') = \text{error}$$

point on tangent at x" as function of x' — point on curve

$$G''(x'') + (x'-x'')(\partial G''/\partial x)_{x''} - G'(x') = \text{error}$$

See the last picture

3 phases:

2 equations of the type above, weighted by 1/2 (referred to square of error)

$$G'(x'''-x'') + G''(x'-x''') + G'''(x''-x') = \text{error}$$

Ternary:

2 phases:

$$G' + (x_2''-x_2')\left(\frac{\partial G'}{\partial x_2}\right)_{x_2',x_3'} + (x_3''-x_3')\left(\frac{\partial G'}{\partial x_3}\right)_{x_2',x_3'} - G''(x_2'',x_3'') = \text{error}$$

$$G'' + (x_2'-x_2'')\left(\frac{\partial G''}{\partial x_2}\right)_{x_2'',x_3''} + (x_3'-x_3'')\left(\frac{\partial G''}{\partial x_3}\right)_{x_2'',x_3''} - G'(x_2',x_3') = \text{error}$$

$$\left(a\frac{\partial G'}{\partial x_2} + b\frac{\partial G'}{\partial x_3}\right)_{x_2',x_3'} - \left(a\frac{\partial G''}{\partial x_2} + b\frac{\partial G''}{\partial x_3}\right)_{x_2'',x_3''} = \text{error}$$

3 phases:

6 equations of type of equation 1 and 2 above

4 phases:

12 equations of type of equation 1 and 2 above, weighted by 2/3 (referred to square of error) and

$$|Det'|\,G' - |Det''|\,G'' + |Det'''|\,G''' - |Det''''|\,G'''' = \text{error}$$

where $Det' = \begin{vmatrix} x_3'' & x_2'' & 1 \\ x_3''' & x_2''' & 1 \\ x_3'''' & x_2'''' & 1 \end{vmatrix}$

other determinants are formed by cyclic replacement of phase indices in $|Det'|$

Three Phase Equilibrium, where one phase is stoichiometric in one direction

$$G'(x_2', x_3') + (x_i^* - x_i')\,(\partial G'/\partial x_i)_{x_2', x_3'} - G^*(x^*) = \text{error}$$

where $$x_i^* = \frac{x_j''' - x_j'}{x_j''' - x_j''} x_i'' + \frac{x_j'' - x_j'}{x_j'' - x_j'''} x_i'''$$

$$G^*(x^*) = \frac{x_j''' - x_j'}{x_j''' - x_j''} G''(x_2'', x_3'') + \frac{x_j'' - x_j'}{x_j'' - x_j'''} G'''(x_2''', x_3''')$$

x_j is the concentration to which the phase is stoichiometric (either $1 - x_2 - x_3$ or x_2 or x_3)

x_i is the difference of the two other concentrations.

phase 1							2				3	4
K	K	O	U	U	U	U	K	K	O	U	K	U
K	K	-R	U	U	U	U	K	K	-R	U	K	U
K	K	O	U	.	.	.	K	K	O	.	K	U
K	K	O	.	.	.	.	K	K	O	.	K	.

Fig. 1 Matrix of coefficients of a hypothetical binary system containing 4 phases, shown in fig. 2.

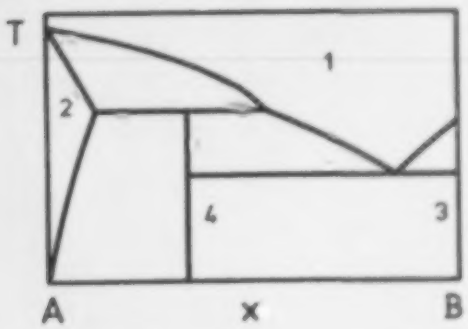

Fig. 2 Hypothetical system of the matrix shown in fig. 1.

National Bureau of Standards SP-496, Applications of Phase Diagrams in Metallurgy and Ceramics
Proceedings of Workshop held at NBS, Gaithersburg, Md., January 10-12, 1977

Theoretical Calculation of Phase Diagrams Using the Cluster Variation Method

Ryoichi Kikuchi*† and Didier de Fontaine†

Abstract

The paper explains how the cluster variation (CV) method and the natural iteration (NI) technique can be used together in calculating phase diagrams. The grand potential Ω (rather than the free energy) is minimized, with temperature and chemical potential μ_i's (rather than composition) kept fixed. The crossing point of Ω vs μ_i curves determines the coexisting phases. The NI technique solves the non-linear simultaneous equations which result from the CV formulation. Unlike the conventional Newton-Raphson iteration method, the NI method always converges and, at each iteration step, the grand potential Ω decreases step by step. The paper discusses the tetrahedron approximation for the fcc lattice, an extrapolation method for making the NI series converge faster, and orthogonality relations in connection with the chemical potential diagram.

*Hughes Research Laboratories, Malibu, CA 90265

†Materials Department, School of Engineering and Applied Science, University of California, Los Angeles, CA 90024

1039

1. Introduction

The companion article ("Fundamental Calculations of Coherent Phase Diagrams")[1] in this volume discusses the background to and the need for using the cluster variation (CV) method in combination with the natural iteration (NI) technique for phase diagram calculations. The application of the CV method in this field has progressed greatly since Golosov et al.[2] and van Baal[3] independently used the tetrahedron approximation of the fcc lattice in calculating diagrams of Cu_3Au and CuAu-type ordered phases.

The NI technique,[4] which was discovered nearly simultaneously with the activities in Refs. 2 and 3, has greatly simplified the calculations required for the CV method. Application of CV-NI methods to ternary systems has been reported recently.[5,6] In this paper, we report detailed computational steps for calculating phase diagrams.

2. Pair Approximation

In this section, we explain the CV method, taking a pair of nearest neighbors as the basic cluster. We discuss the phase-separating case; each lattice point is equivalent and no superlattices are needed.

All the possible configurations of a nearest-neighbor pair are listed in Table I for the example of a binary alloy. As shown in the table, a distribution variable of y_{ij} is assigned to each configuration, with i = 1 used to designate an A atom and i = 2 for a B atom. The

variable y_{12}, for example, is the probability that a certain pair takes the A-B configuration. The y's are normalized to unity:

$$\sum_i \sum_j y_{ij} = 1 \quad . \tag{2.1}$$

Table I. Configurations of a Pair

Configuration	Distribution Variable
A-A	y_{11}
A-B	y_{12}
B-A	y_{21}
B-B	y_{22}

When we formulate the CV method using the notation i and j as in (2.1), it is applicable to the binary case and also to cases with more components. For a ternary system with vacancies, for example, we can choose i = 3 for a C atom and i = 4 for a vacancy.

In addition to the pair variables, the y_{ij}'s, in Table I, we need distribution variables, x_i's, for the configuration of a lattice point. These are listed in Table II. When the number of lattice points in a system is N, and the number of A atoms is N_A, and of B atoms is N_B, then the meaning of x_i is given by the relations:

$$N_A = x_1 N \qquad \text{and} \qquad N_B = x_2 N \quad , \tag{2.2}$$

where the variables x_i and y_{ij} are related by the geometric relation:

$$x_i = \sum_j y_{ij} \quad . \tag{2.3}$$

We will write the free energy (actually the grand potential Ω) in terms of the x's and y's and then minimize Ω with respect to the y's to derive the y values which correspond to the equilibrium state.

Table II. Configurations of a Point

Configuration	Distribution Variable
A	x_1
B	x_2

Energy is the first quantity we examine. For a system with N lattice points and a coordination number 2ω, the total number of nearest-neighbor bonds will be ωN. Since this paper treats only the nearest-neighbor interaction case, the total energy E_N of the system is

$$E_N = \omega N \sum_i \sum_j \epsilon_{ij} y_{ij} \quad , \tag{2.4}$$

where ϵ_{ij} is the nearest-neighbor interaction potential between the i^{th} and j^{th} species. The ϵ_{ij}'s for the binary alloy case are ϵ_{11} for an A-A pair, $\epsilon_{12} = \epsilon_{21}$ for an A-B pair, and ϵ_{22} for a B-B pair.

The entropy for the pair approximation of the CV method for a system of N lattice points is[7,8]

$$S_N = k \ell n \frac{\left[\prod_i (x_i\ N)!\right]^{2\omega-1}}{\left[\prod_i \prod_j (y_{ij}\ N)!\right]^{\omega} N!^{\omega-1}} \quad . \qquad (2.5a)$$

Stirling's approximation allows us to rewrite (2.5a) as

$$S_N = kN\left[(2\omega - 1)\sum_i x_i \ \ell n\ x_i - \omega \sum_i \sum_j y_{ij}\ \ell n\ y_{ij}\right] \quad . \qquad (2.5b)$$

Using S_N in (2.5b) and E_N in (2.4), the Helmholtz free energy F_N, expressed as a function of the y_{ij}'s, is

$$F_N = E_N - TS_N \quad . \qquad (2.6)$$

One method of deriving the equilibrium state is to minimize F_N in (2.6) with respect to the y_{ij}'s, holding the composition $x_1 = 1 - x_2$ fixed. This method yields the equilibrium free energy for the assigned value of x_1.

When the system phase separates, the plot of F_N vs x_1 will be as shown in Fig. 1. In Fig. 1, the coexisting two phases are B and F,

which share the common tangent to the curve. Written mathematically, the coexistence condition is

$$\frac{F_N(F) - F_N(B)}{x_1(F) - x_1(B)} = F'_N(F) = F'_N(B) \quad , \tag{2.7}$$

where F'_N is the derivative of the F_N versus x_1 curve in Fig. 1 and (F) and (B) refer to points in Fig. 1. If we write the common tangent as μN (i.e., $F'_N(F) = F'_N(B) = \mu N$), then (2.7) can be rewritten as

$$F_N(F) - \mu N\, x_1(F) = F_N(B) - \mu N\, x_1(B) \quad . \tag{2.8}$$

This means that if we define a new function

$$\Omega_N = F_N - \mu x_1 N \quad , \tag{2.9}$$

the value of this function will be the same at points B and F. The requirement that μ is the tangent, dF_N/dx_1, leads to the condition

$$\left.\frac{\partial \Omega_N}{\partial x_1}\right)_\mu = \frac{dF_N}{dx_1} - \mu N = 0 \quad , \tag{2.10}$$

which means that the function Ω_N is a minimum with respect to x_1 in equilibrium state for a fixed value of μ.

Taking into account the symmetry of the A and B components, we redefine Ω_N from (2.9) as

$$\Omega_N \equiv F_N - \sum_i \mu_i x_i N \quad , \tag{2.11}$$

which we will call the grand potential. In this expression, μ_1 is the chemical potential for A atoms and μ_2 that for B atoms:

$$\mu_1 = \left(\frac{\partial F_N}{\partial N_A}\right)_{N_B} , \quad \mu_2 = \left(\frac{\partial F_N}{\partial N_B}\right)_{N_A} . \qquad (2.12)$$

Our program is to find the equilibrium state of the system as a minimum of Ω_N with respect to the y_{ij}'s keeping the μ_i's (rather than the x_i's) fixed, and then to plot Ω_N against μ_1 (rather than x_1, as was done in Fig. 1). For the example of a binary alloy for which vacancies are neglected, we can impose a subsidiary condition:

$$\mu_1 + \mu_2 = 0 . \qquad (2.12)$$

When the equilibrium state is found for a fixed value μ_1 (= $-\mu_2$), the grand potential Ω_N is a function of μ_1. For the system of Fig. 1, the Ω_N vs μ_1 curve looks as shown in Fig. 2. In Fig. 2, the points designated by A, B, ···, G, H correspond to those with the same letters in Fig. 1. As expected, the common tangent B-F in Fig. 1 shrinks to a point in Fig. 2. In determining the coexisting phases, it is easier and more accurate to find where two curves cross, as in Fig. 2, than to locate two points of a common tangent, as in Fig. 1. For this reason, we will work with Ω_N in this paper.

In passing, we may comment that a spinodal is represented by an inflexion point, $d^2F_N/dx_1^2 = 0$, in Fig. 1, and by a cusp or spinode in Fig. 2 (points C and G); this indicates the origin of the word spinodal.

3. The Natural Iteration Calculation

In carrying out the computation described in the previous section, it is convenient to use the NI method,[4] a mathematical approach which was designed specifically for solving the equations needed in the CV formulation. Using (2.6), (2.5b), and (2.4), we write the grand potential Ω_N in (2.11) as

$$\Phi \equiv \frac{\beta\Omega_N}{N} = \beta\omega \sum_{i,j} \epsilon_{ij}\, \mu_{ij} - \frac{2\omega - 1}{2}\left[\sum_i \mathscr{L}(x_i) + \sum_j \mathscr{L}(x_j)\right]$$

$$+ \omega \sum_{i,j} \mathscr{L}(y_{ij}) - (\omega - 1) - \frac{\beta}{2} \sum_{i,j} (\mu_i + \mu_j)\, y_{ij}$$

$$+ \beta\lambda\left(1 - \sum_{i,j} y_{ij}\right) \quad , \tag{3.1}$$

where

$$\beta \equiv \frac{1}{kT} \tag{3.2b}$$

and the $\mathscr{L}$-operator is defined as

$$\mathscr{L}(x) \equiv x \ln x - x \quad . \tag{3.2b}$$

This operator originates in the Stirling approximation of the factorial. In the expression Φ, the first term comes from E_N in (2.4). The

two terms $\mathscr{L}(x_i)$ and $\mathscr{L}(x_j)$ are equal and come from the x-term in S_N of (2.5b). In the two $\mathscr{L}(x)$ terms in (3.1), we use the expressions

$$x_i = \sum_j y_{ij} \quad \text{and} \quad x_j = \sum_i y_{ij} \tag{3.3}$$

to make the treatment symmetric. Also for symmetry, the $\mu_i + \mu_j$ sum is written as in (3.1) because

$$\frac{1}{2}\sum_{i,j}(\mu_i + \mu_j)\, y_{ij} = \frac{1}{2}\sum_i \mu_i x_i + \frac{1}{2}\sum_j \mu_j x_j = \sum_i \mu_i x_i \ , \tag{3.4}$$

which is the second term in expression (2.11) for Ω_N. The λ terms in (3.1) take care of normalizing the y's as in (2.1).

When we minimize Φ in (3.1), the y_{ij}'s are regarded as independent and x_i and x_j as dependent through (3.3). Differentiation then leads to

$$\frac{\partial \Phi}{\partial y_{ij}} \equiv \beta\omega\, \epsilon_{ij} - \frac{2\omega - 1}{2} \ln (x_i x_j) + \omega \ln y_{ij}$$

$$- \frac{\beta}{2}(\mu_i + \mu_j) - \beta\lambda = 0 \tag{3.5}$$

or

$$y_{ij} = \exp\left[\frac{\beta\lambda}{\omega} - \beta\epsilon_{ij} + \frac{\beta}{2\omega}(\mu_i + \mu_j)\right] (x_i x_j)^{(2\omega-1)/(2\omega)} \ . \tag{3.6}$$

The NI method works as follows. We fix the values of $\beta = 1/kT$ and μ_1 ($= -\mu_2$) and then begin with the first input value of x_1, which is guessed.

(i) For the input value x_1 (and hence $x_2 = 1 - x_1$), we calculate

$$y_{ij}^{(0)} \equiv \exp\left[-\beta\epsilon_{ij} + \frac{\beta}{2\omega}(\mu_i + \mu_j)\right](x_i x_j)^{(2\omega-1)/(2\omega)} \qquad (3.7)$$

for all values of i and j. Then we determine the normalization factor $\exp(\beta\lambda/\omega)$ using the normalization relation (2.1) as

$$\exp(\beta\lambda/\omega) = \left[\sum_i \sum_j y_{ij}^{(0)}\right]^{-1} \qquad (3.8)$$

Multiplying $y_{ij}^{(0)}$ in (3.7) and $\exp(\beta\lambda/\omega)$ yields the output y_{ij}. In short, step (i) is to calculate the left-hand side of (3.6), y_{ij}, as the output when the inputs x_i and x_j are used on the right-hand side. This output is written as $\hat{y}_{ij}$.

(ii) The next step is to use the output values $\hat{y}_{ij}$ to calculate the next inputs, $\hat{x}_i$ and $\hat{x}_j$, from (3.3). Then we return to step (i) above and repeat the cycle.

This process of going back and forth between steps (i) and (ii) is the NI method. It differs from the well-known Newton method (or the Newton-Raphson method when the number of independent variables is more than one), in that NI has the unique feature that the function being minimized (in the present example, the grand potential Ω_N) always

decreases step by step at each iteration. This property of a monotonic decrease, which can be proved analytically,[4] has the important consequence that the NI procedure converges from whatever initial guess we start with (except for pathological cases).

An example is shown in Fig. 3, which is for bcc ($\omega = 4$) and $\mu_1 = \mu_2 = 0$ for the phase-separating case. Each dot represents output of one iteration cycle. The figure shows two iteration series (one from the right and the other from the left). The point marked $n = \infty$ is the convergence point. In one calculation, the initial guessed value of x_1 was taken as $x_1 = 0.4$, near the top of the right-hand series of dots. If the Newton-Raphson method had been used, the initial guess $x_1 = 0.4$ would have led to the metastable solution at $x_1 = 0.5$, which does not correspond to the phase-separation. The NI method seeks, as illustrated in Fig. 3, the stable solution at $x_1 = 0.02456$. If we start from an initial value x_1 larger than 0.5, NI leads to the other stable solution at $x_1 = 0.97544$. Since the grand potentials for these two points are equal, as are the chemical potentials, they are the two coexisting phases.

As a measure of convergence, we can use

$$\Delta_n \equiv \left| x_1^{(n)} - x_1^{(n-1)} \right| , \qquad (3.9)$$

where n is the number of iterations. The quantity Δ_n decreases exponentially as the iteration proceeds, as shown in Fig. 4. Along with Δ_n, the difference $\left|\Omega^{(n)} - \Omega^{(n-1)}\right|$ also decreases exponentially as

n increases. For the iteration calculation, we can safely regard the iteration as converged when Δ_n becomes less than 10^{-6}. When the iteration has converged, we can prove from (3.1) and (3.5) that

$$\Phi = \Phi - \sum y_{ij} \frac{\partial \Phi}{\partial y_{ij}} = \beta\lambda \quad , \tag{3.10a}$$

which means that the Lagrange multiplier λ, which appears in the normalization factor in (3.8), is the value of the grand potential Ω_N per lattice point:

$$\lambda = \Omega_N / N \quad . \tag{3.10b}$$

4. Tetrahedron Approximation for fcc

The decisive difference between the CV method and the widely used Bragg-Williams method involves the treatment of the ordered phases in the fcc structure. For this structure, the basic cluster of the CV formulation is the tetrahedron made of four nearest-neighbor lattice points.[2,3]

First, we formulate the clustering case. In this case, all lattice points can be treated as equivalent, and superlattices are not needed. As the distribution variables, we use y_{ij} and x_i (defined in Tables I and II) together with the variables z_{ijkl}. A z_{ijkl} is defined as the distribution variable for the configuration i-j-k-l of the tetrahedron. In a ternary system, for example, each i, j, k, and l takes a value 1, 2, or 3 corresponding to an A, B, or C atom.

The energy for a system of N lattice points is written, in place of (2.4), as

$$E_N = 2N \sum_{i,j,k,l} \epsilon_{ijkl}\, z_{ijkl} \quad , \tag{4.1}$$

where 2N is the total number of tetrahedra in the system and the energy per tetrahedron is written as ϵ_{ijkl}. When we write the energy in this form, ϵ_{ijkl} can contain four-body interactions in a tetrahedron. As an example, in the binary system the general expression for the energy paramters are

$$\begin{aligned}
\epsilon_{1111} &= 0 \\
\epsilon_{1112} &= \tfrac{3}{2}\epsilon_{12}(1+\alpha) \\
\epsilon_{1122} &= 2\epsilon_{12} \\
\epsilon_{1222} &= \tfrac{3}{2}\epsilon_{12}(1+\beta) \\
\epsilon_{2222} &= 0 \quad .
\end{aligned} \tag{4.2}$$

In this example, there are three relevant parameters in the binary case: the parameter ϵ_{12} takes care of the nearest-neighbor interaction and α and β are for four-body interactions.[3]

The entropy expression in the tetrahedron approximation for a system of N lattice points is[7,8]

$$S_N = k \ell n \frac{\left[\prod_{i,j} (y_{ij} N)!\right]^6 N!}{\left[\prod_{i,j,k,l} (z_{ijkl} N)!\right]^2 \left[\prod_i (x_i N)!\right]^5} \quad . \qquad (4.3)$$

This may be compared with S_N of the pair approximation in (2.5a).

The grand potential Ω_N is written, corresponding to (3.1), in a symmetric form as

$$\Phi \equiv \frac{\beta\Omega_N}{N} = 2\beta \sum \epsilon_{ijkl} z_{ijkl} + 2 \sum f(z_{ijkl})$$

$$+ \frac{5}{4} \sum \left[f(x_i) + f(x_j) + f(x_k) + f(x_l) \right] + 1$$

$$- \sum \left[f(y_{ij}) + f(y_{ik}) + f(y_{il}) + f(y_{jk}) + f(y_{jl}) + f(y_{kl}) \right]$$

$$- \frac{1}{8} \beta \sum (\mu_i + \mu_j + \mu_k + \mu_l) z_{ijkl}$$

$$+ \beta\lambda \left(1 - \sum z_{ijkl} \right) \quad . \qquad (4.4)$$

Summations are done over the indices in each summand. The last terms multiplied by $\beta\lambda$ takes care of the normalization of z's:

$$1 = \sum_{i,j,k,l} z_{ijkl} \quad . \tag{4.5}$$

For x_i's and y_{ij}'s in the $\mathcal{L}$ terms, we use the geometrical reduction relations:

$$x_i = \sum_{j,k,l} z_{ijkl} \quad , \quad \text{etc.}$$

$$y_{ij} = \sum_{k,l} z_{ijkl} \quad , \quad \text{etc.} \tag{4.6}$$

Comparing Φ in (4.4) with Φ in (3.1) shows the change made as we go from the pair approximation to the tetrahedron approximation.

In deriving the equilibrium state, we minimize Φ in (4.4) with respect to the z_{ijkl}'s while holding $\beta = 1/kT$ and the μ_i's fixed. Differentiation leads to

$$z_{ijkl} = e^{\beta\lambda/2} z^{(0)}_{ijkl} \tag{4.7a}$$

$$z^{(0)}_{ijkl} = \exp\left[-\beta \epsilon_{ijkl} + \frac{\beta}{8}(\mu_i + \mu_j + \mu_k + \mu_l)\right] Y^{1/2} X^{-5/8} \quad , \tag{4.7b}$$

where

$$Y \equiv y_{ij}\, y_{ik}\, y_{il}\, y_{jk}\, y_{jl}\, y_{kl}$$

$$X \equiv x_i\, x_j\, x_k\, x_l \quad . \tag{4.7c}$$

The NI procedure consists of two steps, as in the pair case in Section 3. To start the iteration calculations, we guess initial values of the x_i's and y_{ij}'s. For most calculations, we may specify only the x_i's and then write the y_{ij}'s of the initial guess as

$$y_{ij} = x_i x_j \quad . \tag{4.8}$$

For the iteration calculation, we fix the values of β and of the μ_i's. The two steps in the calculation are given below.

(i) Use the input values x_i and y_{ij} to calculate $z^{(0)}_{ijkl}$ in (4.7b). Then the normalization factor $\exp(\beta\lambda/2)$, as obtained from the normalization relation (4.5), is

$$\exp(\beta\lambda/2) = \left[\sum z^{(0)}_{ijkl}\right]^{-1} \tag{4.9}$$

Multiplying this by $z^{(0)}_{ijkl}$ yields the output $\hat{z}_{ijkl}$ from (4.7a).

In calculating $z^{(0)}_{ijkl}$ of (4.7b), sometimes the product of six y's causes underflow. To avoid this, it is safer to take the logarithm of both sides of (4.7b) and to first calculate $\ell n\, z^{(0)}_{ijkl}$ and then derive $z^{(0)}_{ijkl}$ by exponentiation.

(ii) Using the output values $\hat{z}_{ijkl}$, we derive the output values $\hat{x}_i$ and $\hat{y}_{ij}$ from the geometric reduction relations (4.6). These $\hat{x}_i$ and $\hat{y}_{ij}$ are then used as the input for the next iteration cycle.

Using the same argument as in (3.10a), we can prove that λ in the normalization factor in (4.9) is the grand potential after the iteration has converged:

$$\Phi = \Phi - \sum z_{ijkl} \frac{\partial \Phi}{\partial z_{ijkl}} = \beta\lambda \quad , \tag{4.10a}$$

so that

$$\lambda = \Omega_N / N \quad . \tag{4.10b}$$

In the NI scheme, the iteration proceeds by fixing T and μ_i's. In drawing the isothermal phase diagram of the conventional three-component triangular type, it is convenient to use the diagram in the chemical potential space as a guide. Since the zero point of the μ_i's can, without loss of generality, be chosen arbitrarily, we can impose the relation:

$$\mu_1 + \mu_2 + \mu_3 = 0 \quad . \tag{4.11}$$

Thus, the μ-diagram can be drawn using three μ_i axes 120° apart from each other with the origin as $\mu_i = 0$. An example is shown in Fig. 5(b), which accompanies the composition diagram in Fig. 5(a). A tie line in Fig. 5(a) corresponds to a point in (b). The letters A, B, C, ... in (a) and (b) indicate the same coexisting phases. We will comment more on this figure in Section 7.

5. Ordered Phases in fcc

The treatment in Section 4 applies to the case where all lattice points are equivalent. Therefore, it applies to the analysis of the system where the interaction between different species is repulsive and the system phase-separates, and also to the case where the different species attract but the temperature is high so that the system is in the disordered phase.

For the ordered phases of the fcc structure, we consider the A_3B-type and the AB-type, both of which can be treated based on nearest-neighbor interactions. For these structures, we need sublattices, as shown in Fig. 6, in which the four s.c. sublattices are named α, β, γ, and δ. The amazing feature of the NI formulation is that practically the same formulation in (4.7) can be used for both the ordered and disordered phases.

The only refinement we need on (4.7) in treating the ordered phase is that the sublattice information is used explicitly in the Y and X expressions. When the species i, j, k, and l are located on the α, β, γ, and δ sublattices of Fig. 6, the expressions in (4.7c) are modified as

$$Y = y_{ij}^{(\alpha\beta)}\, y_{ik}^{(\alpha\gamma)}\, y_{il}^{(\alpha\delta)}\, y_{jk}^{(\beta\gamma)}\, y_{jl}^{(\beta\delta)}\, y_{kl}^{(\gamma\delta)} \tag{5.1}$$

$$X = x_i^{(\alpha)}\, x_j^{(\beta)}\, x_k^{(\gamma)}\, x_l^{(\delta)} \quad .$$

Corresponding to these, the four subscripts i, j, k, and l on z and $z^{(0)}$ in (4.7a) are on lattice points α, β, γ, and δ in this order.

Although we used the general designations α, β, γ, and δ in Fig. 6 and in (5.1), actually some of these are grouped together. In the A_3B-type order ($L1_2$), lattice points α, β, and γ are equivalent; in the AB-type order ($L1_0$), α and β are equivalent, and γ and δ are equivalent.

Being able to use practically the same formulation for different phases greatly reduces the potential for human error in computation. This is another advantage of the NI method.

6. Extrapolation Formulation

In Fig. 4, $\left| x_1^{(n)} - x_1^{(n-1)} \right|$ decreases exponentially as NI proceeds. In that expression, n is the number of iterations.

We can prove in general that any variable appearing in the NI formulation approaches its convergence value exponentially for a sufficiently large number of iterations. Each z, y, and x obeys this general property. Using this property, we can extrapolate the iteration calculation from a finite step n to $n \to \infty$. It is done as follows.

To simplify the notation, we will drop subscripts and let x represent any x_i, y_{ij}, z_{ijkl}, $y_{ij}^{(\alpha\beta)}$, etc. Since x behaves exponentially, we can write

$$x(n) = x(\infty) + ae^{-bn} \quad . \tag{6.1}$$

Since the right-hand side contains three unknown constants $x(\infty)$, a, and b, we can solve $x(\infty)$ when we know three values: $x(n)$, $x(n + m)$, and $x(n + 2m)$. Simple arithmetic leads to

$$x(\infty) = x(n) + \frac{x(n + m) - x(n)}{1 - e^{-bm}} \quad , \tag{6.2a}$$

where

$$e^{-bm} = \frac{x(n + 2m) - x(n + m)}{x(n + m) - x(n)} \quad . \tag{6.2b}$$

When we use the extrapolation scheme, the extrapolated value $x(\infty)$ is used as the starting input for the second iteration series. Since $x(\infty)$ is already close to the convergence value, the second iteration series usually converges rapidly. When the convergence is slow, we may need the second extrapolation and the third iteration series.

For this extrapolation to be effective, the exponential convergence of (6.1) must be approximately valid. Since (6.1) is usually not obeyed early in the iteration, we may have to wait until n = 30, 50, or 100 before applying the (6.2) extrapolation. Used with sufficient care, this extrapolation scheme is really helpful. As an extreme example we may quote a certain combination of T and μ, for which n = 100 and m = 50 were used and (6.2) was applied with z_{ijkl} for x. The iteration with the extrapolation converged at 283 total iterations. Starting from the same initial values, the iteration without extrapolation took 5603 iterations before convergence.

7. Orthogonality Relations

When a point in a phase diagram has been determined, to know roughly where the nearby point lies assists in the computation. Such information is provided by the orthogonality theorem.

The binary case is discussed first. The phase diagram is usually drawn in T versus x space, where x is the composition variable. The orthogonality relation, however, holds in T versus μ space. The theorem is derived using a technique similar to the proof of the Clapeyron-Clausius relation. The Helmholtz free energy F satisfies

$$dF = -S\,dT + N\mu\,dx \quad . \tag{7.1}$$

In this expression, μ is the chemical potential corresponding to x and N is the number of lattice points in a system. The grand potential Ω is derived from F as $\Omega = F - N\mu x$ so that from (7.1)

$$d\Omega = -S\,dT - Nx\,d\mu \quad . \tag{7.2}$$

This relation holds for one phase. Along the phase boundary curve on which two phases (I) and (II) coexist in the T vs μ plane, we have two relations:

$$\begin{aligned} d\Omega^{(I)} &= -S^{(I)}\,dT - Nx^{(I)}\,d\mu \\ d\Omega^{(II)} &= -S^{(II)}\,dT - Nx^{(II)}\,d\mu \end{aligned} \tag{7.3}$$

in which dT and dμ are the same. Along the phase boundary curve,

$$d\Omega^{(I)} = d\Omega^{(II)} \quad . \tag{7.4}$$

Substituting (7.3) into (7.4) yields

$$(S^{(I)} - S^{(II)})\, dT + N(x^{(I)} - x^{(II)})\, d\mu \doteq 0 \quad . \tag{7.5}$$

In this expression, $S^{(I)} - S^{(II)}$ and $x^{(I)} - x^{(II)}$ are the differences between the two coexisting phases. The relation (7.5) shows that the vectors $(S^{(I)} - S^{(II)},\ N(x^{(I)} - x^{(II)}))$ and $(dT,\ d\mu)$ are orthogonal. We may also write from (7.5)

$$\frac{d\mu}{dT} = -\frac{S^{(I)} - S^{(II)}}{N(x^{(I)} - x^{(II)})} \quad . \tag{7.6}$$

This relation is used in guessing a nearby point in the T-μ diagram when one point on the phase diagram has been determined.

In Fig. 7 we show the T-μ diagram[9] of the Cu-Au system calculated using the tetrahedron approximation of Section 5. Figure 7 corresponds to the T vs composition diagram, Fig. 5, of the companion paper in this volume.[1] Figure 8 is the entropy vs composition diagram corresponding to Fig. 7. We can see that a tie line in Fig. 8 is orthogonal to the tangent on the T-μ curve of Fig. 7 at the corresponding point after the abscissa scales are adjusted. In the actual computation program, we do not draw the S vs x diagram but let the computer calculate dμ/dT from (7.6).

1060

We next discuss the orthogonality relation in the ternary case. In this case we are usually interested in the isothermal diagram. Thus, corresponding to (7.3), we have

$$d\Omega^{(I)}/N = -\sum_{i=1}^{3} x_i^{(I)}\, d\mu_i$$

$$d\Omega^{(II)}/N = -\sum_{i=1}^{3} x_i^{(II)}\, d\mu_i \quad . \tag{7.7}$$

From the difference between the two relations in (7.7) and the equality $d\Omega^{(I)} = d\Omega^{(II)}$ on the coexisting curve, we derive

$$\sum_{i=1}^{3} \left(x_i^{(I)} - x_i^{(II)} \right) d\mu_i = 0 \quad . \tag{7.8}$$

This suggests that the vectors $x_i^{(I)} - x_i^{(II)}$ and $d\mu_i$ are orthogonal. This can actually be proved[6] by transforming the coordinate axes from those coplanar and 120° apart to the regular cartesian ones. We can verify the validity of the orthogonality that a tie line in Fig. 5(a) is perpendicular to the tangent on the μ-curve at the corresponding point in Fig. 5(b). When a point in the μ-diagram has been calculated, a nearby point on the curve can be roughly estimated using (7.8).

1061

8. Further Comments on the CV-NI Method

When the second-neighbor interaction is to be taken into account in the fcc structure, we need as the basic cluster a double-tetrahedron[10] made of six points. In working with the double-tetrahedron, subsidiary conditions on the distribution variables are needed for symmetry. The method of dealing with such subsidiary conditions within the framework of NI has been worked out.[11]

For the bcc structure, the CV method which is one step better than the pair approximation uses a non-regular tetrahedron. The result was reported previously,[10] and the details will be published shortly.[12]

In addition to the extrapolation formulation of Section 6, other methods have been devised for making the NI approach converge more quickly, and some of these have been tested successfully.[13]

References

1. D. de Fontaine and R. Kikuchi, "Fundamental Calculations of Coherent Phase Diagrams," (this volume).
2. N. S. Golosov, L. Ya. Pudan, G. S. Golosova, and L. E. Popov, Soviet Phys. - Solid State 14, 1280 (1972).
3. C. M. van Baal, Physica (Utr.) 64, 571 (1973).
4. R. Kikuchi, J. Chem. Phys. 60, 1071 (1974).
5. R. Kikuchi, "Ternary Phase Diagram Calculations – I General Theory," Acta Metall. (Dec. 1976).
6. R. Kikuchi, D. de Fontaine, M. Murakami, and T. Nakamura, "Ternary Phase Diagram Calculations – II Examples of Clustering and Ordering Systems," Acta Metall. (1976).
7. R. Kikuchi, Phys. Rev. 81, 988 (1951).
8. D. M. Burley, Phase Transition and Critical Phenomena, Vol. 2, C. Domb and M. S. Green, eds. (Academic Press, New York, 1972) Chapter 9.
9. R. Kikuchi and D. de Fontaine, Scripta Met. 10, 995 (1976).
10. R. Kikuchi and C. M. van Baal, Scripta Met. 8, 425 (1974).
11. R. Kikuchi, "Natural Iteration Method and Boundary Free Energy," J. Chem. Phys. (Dec. 1976).
12. R. Kikuchi, "Structure of Phase Boundaries" (to be published).
13. J.M. Sanchez, Ph.D. Dissertation, School of Engineering and Applied Sciences, UCLA (1977).

1083

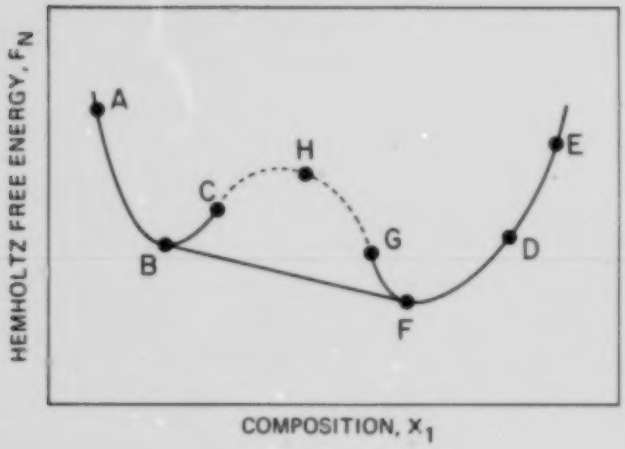

Fig. 1 Schematic diagram of the Helmholtz free energy F_N of a binary alloy plotted against x_1, the density of A atoms.

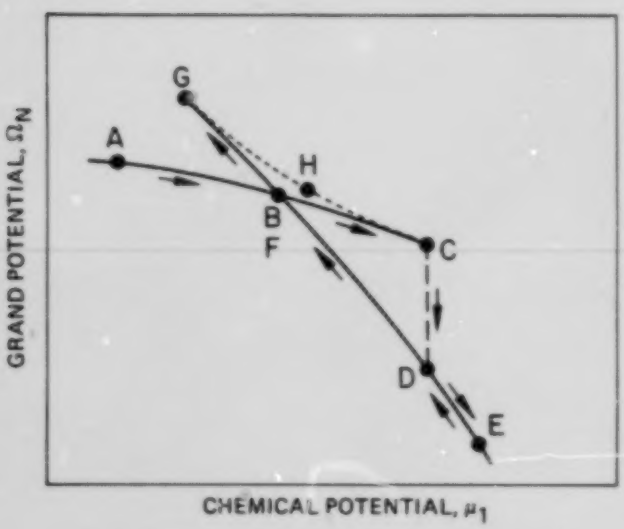

Fig. 2 Schematic diagram of the grand potential Ω_N plotted against μ_1, the chemical potential of the A atom. Letters correspond to those of Fig. 1.

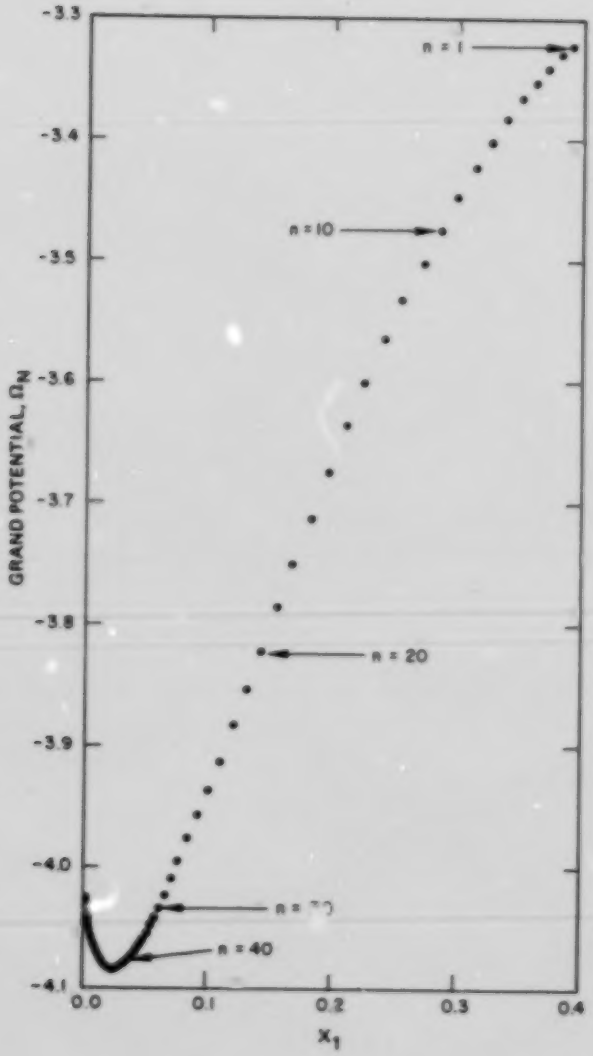

Fig. 3 **Behavior of the grand potential Ω_N as the NI proceeds. The number of iterations is indicated by n.**

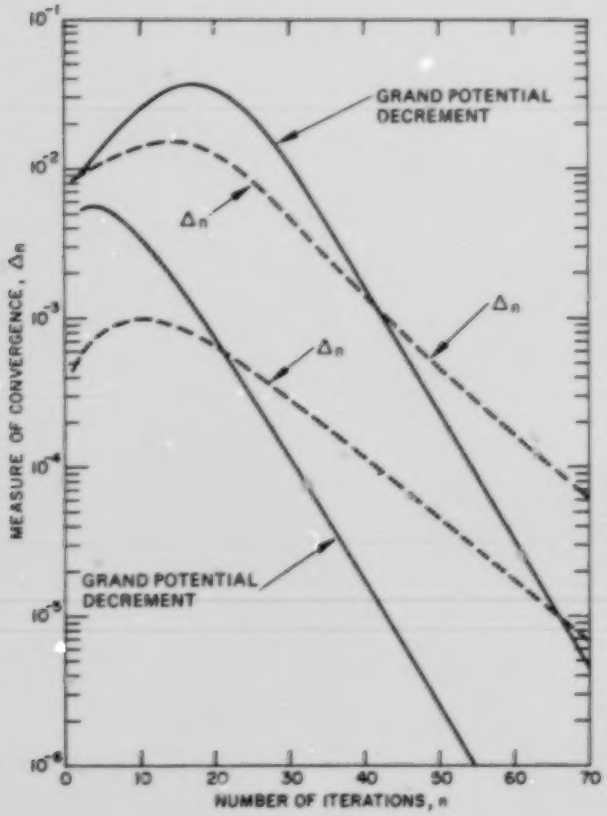

Fig. 4 The number of convergence Δ_n defined in (3.9) plotted against the number of iterations n. The figure also shows $\left|\Omega^{(n)} - \Omega^{(n-1)}\right|$.

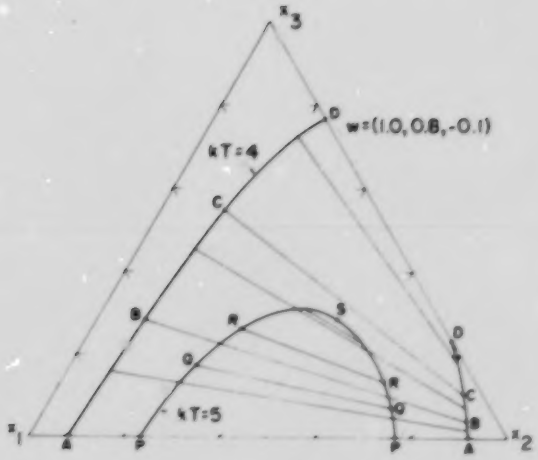

(a)

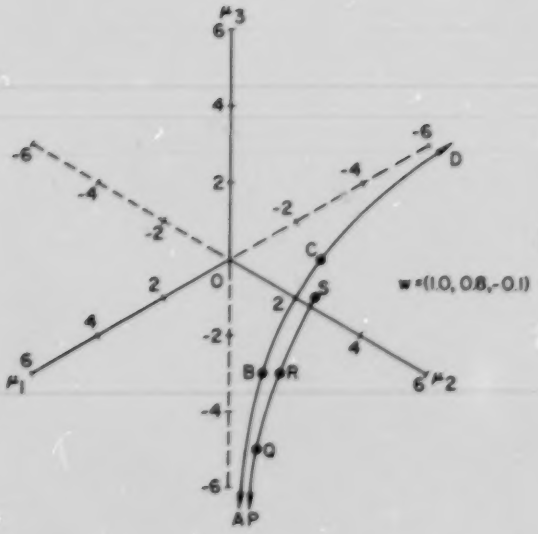

(b)

Fig. 5 **Phase separation diagrams of a ternary system. A tie line in (a) corresponds to a point on the chemical potential diagram in (b).**

1067

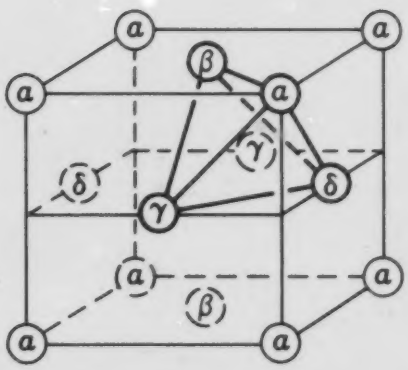

Fig. 6 The basic cluster tetrahedron for an ordered fcc phase.

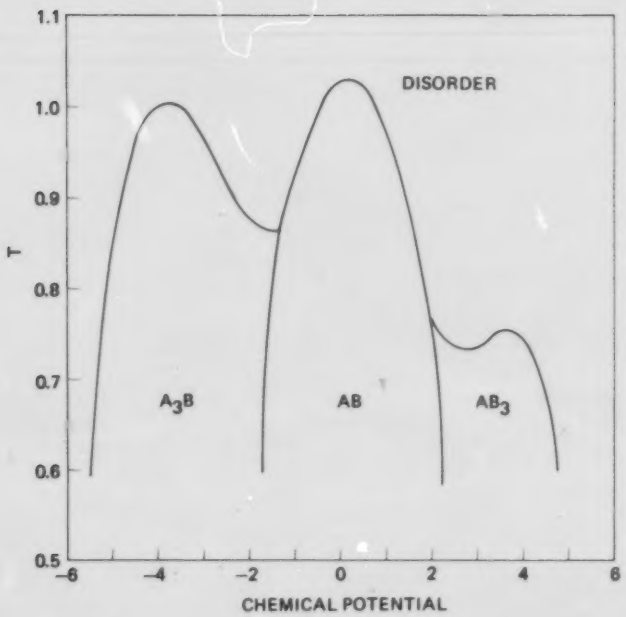

Fig. 7 **The calculated T vs μ diagram of the Cu-Au system.**

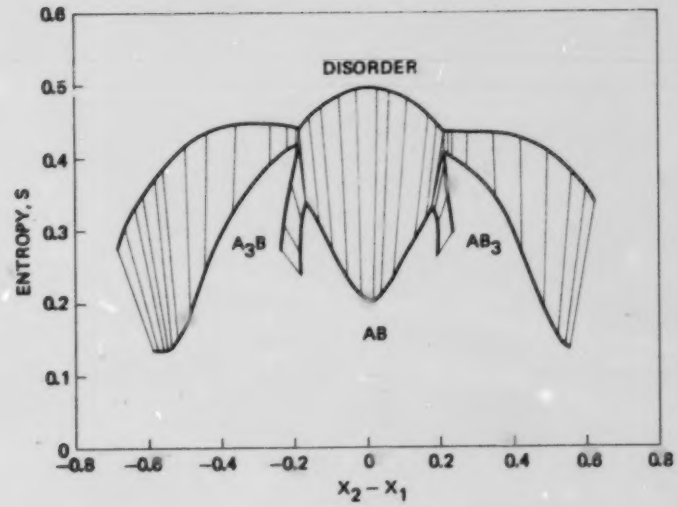

Fig. 8 The calculated diagram of S vs composition x corresponding to Fig. 7.

National Bureau of Standards SP-496, Applications of Phase Diagrams in Metallurgy and Ceramics
Proceedings of Workshop held at NBS, Gaithersburg, Md., January 10-12, 1977

FUNDAMENTAL CALCULATIONS OF COHERENT PHASE DIAGRAMS

Didier de Fontaine and Ryoichi Kikuchi*

Department of Engineering and Applied Science
University of California, Los Angeles

Abstract

By "coherent phase diagram" is meant a temperature-concentration diagram indicating thermodynamic relationships between ordered and disordered solid phases which can all be derived from the same parent lattice. Incoherent phase diagrams cannot, at present, be computed from first principles, but they can be determined experimentally. By contrast, many coherent phase diagrams cannot be readily constructed experimentally, hence a reliable theoretical model yielding useful prototype phase diagrams is highly desirable. Such a model is provided by the Cluster Variation method first developed in 1951. In this method, the configurational entropy is treated in a very accurate manner, in contrast to the regular solution or Bragg-Williams entropy which in many cases can be 100% in error, or lead to phase diagrams which are not even topologically correct. This is illustrated in the case of the Cu-Au system, for which an excellent fit to the experimental phase diagram has recently been obtained, following the ideas of van Baal. The problem of predicting ordered ground states from a knowledge of pair interaction parameters and that of estimating these parameters themselves from band structure calculations is briefly covered.

---

* Permanent Address: Hughes Research Labs, Malibu, California, 90265

1. Introduction

Most computations of temperature-composition phase diagrams to date are semi-empirical, in the sense that separate free energy functions are constructed for the phases which are known to appear in the system[1]. The free energy functions used are usually based on the regular, sub-regular or Bragg-Williams mean-field models, with parameters adjusted to the empirically known portions of the phase diagram or to experimentally determined bulk thermodynamic data. It is of course of considerable interest to inquire whether it is presently possible to perform more fundamental phase diagram calculations which, in some way, can be derived from "first principles". It can be immediately stated that such fundamental calculations of phase diagrams of systems presenting intermediate phases of arbitrary crystal structure, say intermetallic compounds, is presently out of the question. However, for certain classes of binary and ternary systems, namely *coherent* systems, fundamental phase diagram calculations having real predictive power are becoming feasible. The purpose of this communication is to review current progress in this specialized field.

First a definition: by coherent system is meant one in which all phases derive from a unique lattice framework (for instance fcc or bcc) simply by rearranging A, B, C... atoms on the lattice sites in various ordered or clustered configurations. In these systems, when a new ordered phase appears, it must be completely coherent with the parent phase, so that no lattice *discontinuities* are tolerated. Elastic *distortions* may be present, however. Examples of fully coherent systems are Cu-Au (to be examined in detail below), Cu-Pt, Cu-Ag-Au, etc... . Of course, equilibrium phases must generally be separated by incoherent interfaces, but in these simple systems, the incoherent phase

diagram may be regarded as deriving directly from the corresponding, more fundamental, *coherent (metastable) phase diagram*, the only one under consideration here.

It may appear that fully coherent phase diagrams form such a restricted class as to be of little practical interest. This is not the case: most useful materials, alloys in particular, are prepared under conditions which are far removed from thermodynamic equilibrium. Hence, observed microstructures are primarily governed by kinetic effects, and it is known that, for these reasons, coherent products are the first to form in a great many cases. Coherency is often subsequently lost, but the final microstructure then retains essential features which were imparted by the fully coherent early stages of the phase tranformations. Hence, some knowledge of underlying coherent phase equilibria is essential for gaining an understanding of microstructure, and hence of properties, even in "incoherent" systems.

Coherent phase diagrams, being generally of a metastable nature, are not easy to determine experimentally. Therefore, it is particularly fortunate that it is precisely these phase equilibria which are amenable to "fundamental" calculations. Conversely, stable incoherent phase equilibria cannot be calculated at present from "first principles", but incoherent diagrams can in principle be determined experimentally. The theorist's task is then to superimpose the calculated coherent diagram on the experimental incoherent one.

What is needed for a coherent phase diagram calculation? Basically, a reliable configurational free energy function from which one may deduce all coherent ordered phases and their domain of existence in temperature-concentration space. The two contributions to the free energy can be calculated separately, these are: the internal energy (practically equal to the enthalpy in condensed systems) which contains the physics of the problem, and the configurational entropy which is determined from the ways in which

certain sets of symbols can be distributed on lattice sites. The vibrational entropy makes a sizable contribution to the total free energy but its *change* on ordering is regarded as small and shall therefore be neglected. Regular, sub-regular and Bragg-Williams models (referred to collectively in what follows as BW models) are inacceptable for both enthalpy and entropy contributions, as will be shown in the Cu-Au case in Sect. 3. The reason for the failure of mean-field models to predict phase diagrams which, in certain cases, are even topologically correct is twofold: (A) the BW models make the very poor *zeroth or decoupling approximation*

$$\langle \sigma_p \sigma_{p'} \rangle \rightarrow \langle \sigma_p \rangle \langle \sigma_{p'} \rangle \qquad (1)$$

consisting of replacing the average (denoted by brackets) of two-site (and three-site, etc.) occupation by a product of single-site occupation. The symbols σ_p denote occupation parameters with value 1 or 0 depending upon whether lattice site p is or is not occupied by an atom of given type; (B) the BW entropy, of type

$$-k \sum_p \langle \sigma_p \rangle \ln \langle \sigma_p \rangle \, , \qquad (2)$$

where k is Boltzmann's constant, neglects pair (and higher) correlations.

An exact closed-form free energy is not available even under the simplifying assumption that the internal energy consists of a sum of nearest neighbor pair interactions. This would be equivalent to solving the Ising problem in three dimensions, which no one has succeeded in doing to date. One must therefore resort to approximate methods, one of the most successful being the Cluster Variation method (CV) developed in 1951[2]. The basic idea of this method, which constitutes a hierarchy of increasingly accurate approximations, will be presented briefly in Sect. 2, and in more detail in a companion paper[3].

As an illustration, the CV method will be used to calculate the solid-state portion of the Cu-Au phase diagram. This application is presented in Sect. 3, along with a brief historical survey of Cu-Au phase diagram calculations.

The CV method assumes that the phases which appear in the coherent phase diagram are known *a priori*: these are the phases which must be present at absolute zero, the so-called *ordered ground states*. Fortunately, elegant methods[4-7] are now available for predicting ordered ground states in substitutional solutions: the problem is completely solved for ordered structures, based on the fcc and bcc lattices, which are stable for pair interactions limited to second coordination shell. Most commonly occurring ordered structures are thereby predicted. Recent work by Kanamori[8] has extended this to cover the very complicated structures which are stable under the action of up to 4th - neighbor pair interactions.

In both CV and ordered ground state calculations, the pair (or triplet, etc.) interaction parameters are assumed to be given. Of course, for a complete first-principle phase diagram determination, these parameters would have to be obtained from electronic band structure calculations. Reliable numerical values from quantum mechanical calculations appear to be a long way off, however, although significant progress has been made with the advent of pseudopotentials[9,10] and of the Coherent Potential Approximation[11]. Ordered ground states and the problem of calculating pair potentials are very briefly commented upon in Sect. 4.

The topics presented in this article are treated in more detail in a forthcoming review article[12].

2. The Cluster Variation Method

For given crystal lattice, a *basic figure*, or small group of lattice

points is selected. This basic figure may be the nearest-neighbor (n.n) pair, the n.n. tetrahedron (in fcc), the bcc cube, etc... A *cluster* is defined as a particular distribution of A, B, C... atoms on the lattice sites of the basic figure selected. To each distribution is assigned a cluster variable whose value at equilibrium is the frequency of occurrence of that particular cluster in the solid solution. Let us designate all cluster variables collectively by the set $[\alpha]$. Then the free energy of the system in a state characterized by particular values of $[\alpha]$ is defined by the *free energy function*

$$F[\alpha] = E[\alpha] - TS[\alpha] \quad , \tag{3}$$

where T is the absolute temperature and E and S are respectively the internal energy and configurational entropy for which explicit expressions will presently be given. The *equilibrium free energy* F_e is obtained by finding the particular set of cluster variables $[\alpha]$ which minimizes the free energy function (3):

$$F_e = \min_{[\alpha]} F[\alpha] \quad . \tag{4}$$

In general, the larger is the basic figure used in the calculations, the more accurate will be the derived free energy.

The energy $E[\alpha]$ is written as a sum of pair and cluster interactions, while the entropy is calculated from appropriate combinatorial factors, the derivation of which constitutes one of the main features (and difficulties) of the CV method. Consider a specific example, that of an fcc substitutional solution in the n.n. tetrahedron approximation. Let z_{ijkl} be the tetrahedron cluster variables, with i,j,k,l denoting the atomic species occupying the four vertices of the tetrahedron.

The internal energy $E[\alpha]$ is assumed to be given by the sum of the energies of all clusters present in the system. Only the largest clusters need be used explicitly, in the present case the n.n. tetrahedron. Hence,

the energy function is

$$E \equiv E[\alpha] = 2N \sum_{i,j,k,l} \varepsilon_{ijkl}\, z_{ijkl} \qquad (5)$$

where ε_{ijkl} denotes the energy of that particular tetrahedron cluster, and where N is the total number of lattice points. The cluster energies ε can be calculated on the basis of a sum of pair interactions, or distinct clusters may be given distinct energies different from the direct sum of constituent pairs. In this way, many-body interactions can easily be introduced in the internal energy, as will be seen in the next section. The quadruple sum in Eq.(5) runs over the subscript values (1,2) for binary systems, (1,2,3) for ternary systems, etc...

The configurational entropy is obtained from the Boltzmann formula

$$S[\alpha] = k \ln W[\alpha] \qquad (6)$$

where W is the total number of ways of distributing the various clusters over the lattice sites in such a way that the cluster frequencies $[\alpha]$, in the present case the tetrahedron frequencies z_{ijkl}, pair frequencies y_{ij} and point frequencies x_i (concentrations), have specified values. An exact expression for W cannot be found for three-dimensional lattices because of the difficulty of eliminating inconsistencies of site occupation which arise inevitably when different clusters are distributed statistically over the lattice sites. The philosophy of the CV method is to correct systematically and optimally (but approximately) for these overlaps by means of familiar combinatorial factors. In the present case, the weight factor W of the distribution $\{\alpha\}$ for the fcc lattice in the n.n. tetrahedron approximation is[2]

$$W = \frac{(\cdot\!-\!\cdot)^6 N!}{\langle\diamond\rangle^2 (\cdot)^5} \qquad (7)$$

where the standard CV combinatorial notation has been used:

$$\{\cdot\} \equiv \prod_i \{x_i N\}! \tag{8}$$

which, for binary systems containing N_A A atoms and N_B B atoms, reads

$$\{\cdot\} \equiv N_A! N_B! \quad .$$

The pair and tetrahedron symbols in Eq. (7) are given by appropriate generalizations of Eq. (8).

The free energy function $F[\alpha]$ is now obtained by putting (7) into (6), by using Stirling's formula to approximate the logarithms of factorials, and by inserting (6) and (5) into (3). The result in the fcc n.n. tetrahedron approximation is

$$F = N \sum_{ijkl} W_{ijkl} z_{ijkl} + NkT\Big[5 \sum_i x_i \ln x_i - 6 \sum_{i,j} y_{ij} \ln y_{ij} + 2 \sum_{ijkl} z_{ijkl} \ln z_{ijkl}\Big]. \tag{9}$$

This formula is appropriate for the disordered phase. For ordered structures, sublattices must be defined, and Eq. (9) takes on a more complex appearance since now different cluster variables must be defined according to the manner in which clusters straddle the sublattices.

The equilibrium state is found by minimizing equations such as (9) with respect to cluster variables subject to various constraints which are present because of the interdependence of the variables. The practical difficulty here is that the total numbers (ν) of variables and of equal number of (non-linear) equations resulting from the minimization rises rapidly with the number n of components in the system and number m of cluster points, the formula being

$$\nu = n^m. \tag{10}$$

For binary and ternary systems in the tetrahedron approximation, Eq. (10) gives the reasonably tractable numbers 16 and 81, respectively. Recently, the CV method has been applied to the omega displacive transformation[13]

in the eight-point primitive bcc unit cell cluster approximation, with point variables +1, 0, -1; the total number of variables was then $3^8 = 6561$. Such impressively large systems of non-linear simultaneous equations can now be handled successfully through the powerful Natural Iteration algorithm described elsewhere[3,14].

Conditions for phase equilibria are obtained by determining the concentrations for which the equality of chemical potentials hold. The procedure for calculating phase diagrams is thus to minimize the grand potential

$$\Omega = F - N\sum_i \mu_i x_i \qquad (11)$$

rather than F itself as in Eq.(4). The method is explained in more detail in a companion paper[3]. For second-order phase transitions, the critical point is obtained by the standard method of setting equal to zero the determinant of the second derivatives of F with respect to independent configuration variables.

It is important to note that the CV method not only can produce phase diagrams, but also equilibrium values of the cluster variables at any temperature and average concentration. Hence, unlike BW models, the CV method can provide short-range (SRO) as well as long-range order (LRO) information, which may be tested against experimental evidence, such as x-ray or neutron diffraction SRO intensity data.

3. The Cu-Au System

Some of the foregoing considerations will now be applied to the problem of calculating the solid-state portion of the Cu-Au phase diagram. The experimentally determined diagram is shown in Fig. 1[15]. One notes the existence of three ordered regions: two ordered phases have well-

defined transition points where the fcc solid solution (α) transforms by a first-order reaction to the $L1_2$ structure at the Cu_3Au composition and to a long-period modification (II) of the $L1_0$ structure at the CuAu composition. This long-period structure itself transforms at a slightly lower temperature to the true $L1_0$ structure (CuAuI). The structure of Au_3Cu is also $L1_2$ but apparently presents no well-defined common maximum[16] in the ordus and disordus curves[17].

Shockley used a Bragg-Williams n.n. interaction model in 1938[18] to calculate the Cu-Au phase relations, but the resulting phase diagram, shown in Fig. (2), is not even topologically correct. The ordered phase fields are nested, instead of separated, and culminate in a unique second-order transition temperature at the center of the diagram. One must conclude from this disappointing attempt that there is something inherently wrong with the BW approximation which cannot be remedied by more elaborate polynomial expansions of some "excess" free energy.

If one is to discard mean-field theories, then perhaps the Bethe approximation will work better. Unfortunately, this approximation, which is identical to the CV method in the n.n. pair approximation (in the entropy) gives no phase transition at all![19] The next successfull attempt was that of Li[20] in 1949 who used the Guggenheim quasi-chemical theory in the tetrahedron approximation. Li's phase diagram is shown in Fig. 3. Marked improvements over Shockley's diagram are apparent, namely the existence of three distinct phase regions. However, all three ordered phase fields have the same shape, and eutectoid and peritectoid reactions are absent.

The tetrahedron-based configurational entropy formula used by Li is now known to be defective, which led van Baal to try CV method in 1973[21]; the configurational entropy was that of the tetrahedron approximation, Eq. (7), and the internal energy was written as a sum of n.n. pair

interactions. The resulting phase diagram is shown in Fig. 4, as recalculated by one of the present authors[14]. Many essential features of the experimental diagram are present: three separate ordered phase fields, eutectoids, and good qualitative agreement with at least the left (Cu-rich) side of the actual phase diagram. This important calculation by van Baal is very encouraging, particularly when it is recognized that the diagram as drawn in Fig. 4 is based on a *unique free energy function which contains no adjustable parameters*. It follows that Fig. 4 represents a universal phase diagram for all fcc ordering systems with internal energy obtained from n.n. pair interactions alone. Obviously, this is an oversimplification, but the fact that the diagram is by and large topologically correct provides support for the CV method.

The Shockley BW diagram (Fig. 2) also contains no adjustable parameters. Hence a very honest comparison can be made between the BW and CV models: good and bad features of the resulting phase diagrams must reflect the essential qualities of the underlying free energy function, not of any numerical fitting. The conclusion is inescapable: the BW approximation is quite unacceptable, at least for the fcc lattice, while the CV tetrahedron approximation is qualitatively correct, though in need of quantitative improvement.

Van Baal[21] noted that all phase diagrams constructed from an internal energy based on pair interactions with concentration - independent parameters must be completely symmetric about the 50/50 composition. To break the symmetry, either many-body interactions must be introduced or concentration-dependent pair interaction parameters must be used. The former scheme was suggested by van Baal who showed that the energy equation (5) could be written explicitly as

$$E = 12\, N\, \epsilon_{12} \left[(1+\alpha)\, z_{1112} + 2 z_{1122} + (1+\beta)\, z_{1222}\right] \qquad (12)$$

where ε_{12} is the effective pair interaction parameter

$$\varepsilon_{12} = V_{AB} - \frac{V_{AA} + V_{BB}}{2} \qquad (13)$$

in which V_{ij} denotes the interaction energy of a n.n. (i,j = A,B) pair. In Eq. (12), $\varepsilon_{12}(1+\alpha)$ and $\varepsilon_{12}(1+\beta)$ are the energies of n.n. tetrahedra occupied by three A and one B atom, and three B and one A atom, respectively. With $\alpha=\beta=0$, Eq. (12) is the correct energy expression in a purely pairwise scheme. Hence the parameters α and β represent here the fractional deviation of the tetrahedron energy from that which would be calculated from summing its constituent pairs. These parameters therefore represent essential many-body interactions. Equation (12) with $\alpha=0$, $\beta\neq0$ was used by van Baal[21] to show the resulting asymmetry in the transition temperature vs. concentration curves. Corresponding phase diagram calculations were not reported.

The authors recently followed up on van Baal's suggestion and calculated a phase diagram based on the free energy function (9) with internal energy given by Eq. (12). The values $\alpha=0.01$ and $\beta=-0.08$ were chosen, resulting in the phase diagram shown in Fig. 5. Although further refinements are possible, this diagram is remarkably close to the experimental one. The shallow maximum of the Au_3Cu phase field is an unsatisfactory feature, but could be eliminated by fine tuning of the α and β parameters. Of course, the existence of the CuAuII phase cannot be predicted: higher-neighbor interactions would be required

The dashed line in both Fig. 5 and 2 indicate the *ordering spinodal*, i.e. the locus along which the solution becomes inherently unstable to a <100> composition plane wave of infinitesimal amplitude[12,22]. The fact that, in the CV diagram (Fig. 5), the ordering spinodal does not touch the ordus or disordus lines indicates that the ordering reactions are first order, even at the CuAu stoichiometric composition. This is in accordance

with experimental findings, and with the Landau rules[23]. By the same token, note that the BW diagram (Fig. 2) incorrectly predicts a double second-order transition at the 50/50 composition.

Several points may be emphasized in connection with the diagram of Fig. 5:

- a reasonably correct coherent phase diagram has been calculated from a single free energy function in an fcc-based system,
- an ordering spinodal has been constructed,
- the need for many-body (tetrahedron) interactions has been clearly demonstrated, and is seen to play an essential role,
- the calculation yields much more than merely the phase diagram: SRO information is automatically provided in the form of 3 y_{ij} n.n. frequencies and 5 n.n. tetrahedron cluster frequencies at any required concentration and temperature. The pair frequencies can be tested against SRO diffuse intensity data, as mentioned above.

Other fcc and bcc-based phase diagrams may be computed in a similar manner. However, in order to obtain ordered phases other than the $L1_2$ and $L1_0$, it is necessary to include at least next-nearest-neighbor pair interactions. This, in turn, requires the use of a larger basic figure, such as the double tetrahedron for which the CV entropy formula has been derived[24]. A research program aimed at computing prototype coherent phase diagrams for all possible fcc and bcc - based ordered structures is currently underway[25].

4. Ground States and Potentials

In the CV method, ordered phases are simply handled by defining appropriate sublattices. Thus a knowledge of which ordered structures to expect is a separate problem. It may be assumed that candidate ordered

phases of coherent type are those which will be found at absolute zero in the system of interest. By definition, these are the (coherent) *ordered ground states*. Under certain restrictive (but realistic) assumptions, it is now possible to *predict* which ordered structures will be absolutely stable for given ranges of pair interaction parameters and concentrations. The ground state problem is completely solved for fcc and bcc binary substitutional solutions with internal energy given by a sum of first and second neighbor pair interactions, for all ranges of concentrations and pair interaction parameter ratios[4,6,7,26]. Considerable progress is also being made in extending the range of pair interactions to third and fourth neighbors[4,5,8].

The problem is to find that distribution of A, B atom on lattice sites which minimizes the energy E, given the average concentration x of B atoms and the pair interaction parameters ε_s, the latter being given by Eq. (13), extended here to arbitrary coordination shell s=1,2,3,4... . The energy to be minimized can be written

$$E = N \sum_s z_s \varepsilon_s y_s \qquad (14)$$

where y_s is the pair frequency and z_s the coordination number for shell s. The minimization of E in Eq. 14 need not be accomplished by trial and error: indeed Kanamori already devised in 1965[26] a set of inequalities which must hold between linear combinations of pair frequencies y_s and concentrations x, and which allows for the unambiguous determination of ordered ground states. A systematic method for deriving the inequalities was discovered by Kaburagi and Kanamori in 1975[4]; it makes use of clusters of lattice points as does the method of Allen and Cahn[7], developed independently. Linear programming is featured in the latter method and also in that of Kudō and Katsura[5].

It is interesting to note that all the commonly observed binary alloy ordered structures based on the bcc and fcc lattices can be predicted theoretically by the above mentioned methods when only first and second-neighbor interactions are considered. This is not to say that actual interactions do not extend beyond the second coordination shells, nor that many-body forces are unimportant; simply, this means that the stability of ordered structures can, by and large, be rationalized by use of a single parameter: the ratio of first to second neighbor pair interaction, along with the sign of the first-neighbor interaction. In addition, theoretical ground state calculations predict the existence (and stability) of ordered structures which have apparently not yet been observed: examples are the A_2B and A_5B monoclinic structures of space group B2/m[6,7].

Certain known structures owe their stability (at 0°K) to higher-neighbor interactions. An example is the Au_5Mn_2 structure which Kanamori[8] was able to predict on the basis of extremely complex analysis of ordering in the fcc lattice with up to fourth-neighbor interactions. The structure is shown in projection at the top protion of Fig. 6[8]. The Kanamori "S" symbols have arguments

$$S(p_1, p_2, p_3, p_4; x)$$

where the (modified) pair frequencies are

$$p_s = y_s z_s / x,$$

x being the stoichiometric composition. Figure 6 also shows two A_2B structures, illustrating the fact that unit cells may become very large and atomic arrangements very complex when higher-neighbor interactions are taken into account. Figure 7[8] gives an example of two other A_2B structures which are "degenerate", meaning that their pair count up to fourth neightbor is identical. The top structure has space group B2/m, the lower one Immm[27],

which is the Pt_2Mo (or Ni_2V or metastable Ni_2Mo) structure. Fifth neighbor interactions would be required to lift the degeneracy.

To conclude this survey of the possibility of "first-principle" coherent phase diagram calculations, let us briefly mention the problem of theoretically estimating values of the pair interaction parameters ε, which have thus far been regarded as known entities. The problem is an extremely difficult one which formally necessitates the solution of the Schrödinger equation for a solid solution of arbitrary atomic configuration. It appears that accurate solutions are a long way off.

Certain recently developed approximate techniques are quite promising, however. The central problem often consists in finding suitable perturbation expansions which converge sufficiently rapidly so that the expansion may be limited to second order. For pure *simple metals*, it is possible to construct a *pseudopotential*, so that the Schrödinger equation may be solved to second order in this small energy-dependent potential[9,10]. It then follows that the band structure energy may be written conveniently as a sum of pairwise effective interactions. Unfortunately, the list of "simple metals" for which pseudopotentials can be tabulated is not as extensive as one would like. For other metals, particularly the transition elements, i.e. the majority of technologically important materials, the Fermi surfaces have complicated shapes deviating very significantly from the spherical one, and there is considerable overlap of the d-bands in the crystalline state. Hence, the pseudopotential formulation is impractical, and the cohesive energy cannot be written as a sum of pair (or even cluster) interactions[28].

For alloys (solid solutions), the problem is compounded by the fact that ionic potentials differ from site to site so that the crystal potential loses the translation symmetry of the lattice. The customary

way out of that difficulty was to assume an average potential V of the form

$$V = (1-x)V_A + xV_B \qquad (15)$$

where V_A and V_B are the potentials of the constituents. However, this *virtual crystal* method has been shown to give rather poor account of itself in the case of concentrated solutions. Its application to the Hg-Mg system made by Inglesfield[29] in the pseudopotential framework can therefore certainly not be generalized with confidence.

When the difference of the constituent ionic potentials is large with respect to the width of the d-band, a completely different approach must be used. Currently, the most satisfactory method is that of the *Coherent Potential Approximation* (CPA): for the disordered case, one must seek an average single-site potential to be obtained self-consistently, rather than by the simple weighted sum of Eq. (15)[11]. The calculation of cohesive energies then proceeds by standard techniques. It is impractical to obtain (small) ordering energies by taking the difference of two large cohesive energies in the ordered and disordered states. Rather, a way was recently discovered[30] of expanding the concentration fluctuation term, usually neglected in single-site CPA energy calculations, in a convergent generalized perturbation expansion. It is then possible to obtain LRO[31] and SRO[30] configurational energies, though not the total cohesive energy, as sums of effective pairwise interactions, just as in the usual phenomenological theories. This is an important result, as it is clearly desirable to justify, and if possible to calculate, pair interaction parameters which play such a basic role in alloy theory, as shown for example by the considerations set forth in Sect. 2 and 3. It remains to be seen whether truly predictive results can be obtained by this extension of the CPA.

5. Conclusion

Ab initio calculations of *coherent* phase diagrams are becoming feasible thanks to recent theoretical developments. The three basic elements of the calculations are: (a) the estimation of pair (and many-body) interaction parameters, (b) the prediction of ordered ground states of ordering from a knowledge of pair parameter ratios, and (c) the determination of (coherent) phase equilibria and resulting phase diagrams. Corresponding advances in theoretical methods are: (a) recent extensions of the coherent potential approximation to cover LRO and SRO[30,31], (b) the solution of the ground state problem in increasingly general situations[4-8], and (c) the development of rapidly convergent algorithms for the Cluster Variation method[13,14].

We have described the application of the CV method in the tetrahedron approximation to the Cu-Au phase diagram. By the same token, we have demonstrated the inapplicability of the BW model to fcc-based coherent phase diagrams. Despite the very obvious and serious deficiencies of mean-field (BW-like) models, the latter are being consistently used in nearly all current phase diagram calculations. Notable exceptions may be found in recent work carried out in France[32], Germany[33], Holland[34] and the Soviet Union[35]. It is not likely that increasingly elaborate polynomial expansions will remedy the ills of mean-field models; even in those cases for which good fits are obtained numerically (always possible when enough adjustable parameters are used), the fitted parameters may have little physical meaning. In fact, it is not often appreciated that, since the BW models tend to overestimate the configurational entropy by as much as a 100%, the fitted pair interaction parameters and resulting internal energy will be estimated incorrectly in the same proportion.

Investigators have perhaps been put off by the apparent complexity of CV calculations as opposed to BW ones. Actually, as shown elsewhere[36], the CV method in the Natural Iteration scheme turns out to be rather

simpler to handle than the traditional regular solution model in the Newton-Raphson scheme. Furthermore, certain ternary equilibria which are easily missed in the latter method are found without difficulty in the former[36].

It is hoped that the present communication has contributed to bringing new theoretical techniques to the attention of investigators interested in phase diagram calculations; if so, the primary objective of the authors will have been reached.

ACKNOWLEDGEMENTS

The authors thank Professor J. Kanamori of the University of Osaka for having supplied us with copies of Figs. 6 and 7. The calculation of the Cu-Au phase diagram is part of an NSF-funded study of the Ag-Au-Cu ternary system.

DISCUSSION

O. Kleppa - The Au-Ag system has a strong negative enthalpy of mixing in the solid state, so it should form an ordered phase at low temperatures. This has not yet been observed as far as I know.

D. de Fontaine - Yes, we can predict this, but we have to be given the pair interaction parameters. But whether it will be seen or not depends on the kinetics of the system. Maybe it is too low.

M. Hoch - In your Cu-Au system, ordering is parallel to the 100 plane. Now Cu-Pt has complete solid solubility at high temperatures, and a very similar solidus-liquidus. If you cool that, it orders on the 111 plane and you get (Cu, Pt) compounds. My question is, where does your calculation take into effect that in the Cu-Au system we don't get 111 ordering, and in Cu-Pt we don't get 100 ordering?

D. de Fontaine - We haven't done that kind of calculation yet, but it is planned. The difference between these two types of ordering is the following. If you allow both 1st and 2nd neighbor pair interactions in the system, you can differentiate between these and other types of ordering. This has been shown by John Cahn and coworkers and by Kanamori in Japan. You can plot diagrams of ratios of 2nd nn to 1st nn pair interaction parameters, and develop maps this way and stay with absolute

certainty (at T = 0 K), that a certain phase like the (Cu, Pt) or like the (Cu, Au), given the stoichiometry, should be stable in a given range. In order to make our calculation predictive, or useful, for those situations as well, we have to include 2nd nn pair interactions. In the framework of the cluster variation method this can only be done if the cluster size is increased from the single tetrahedron, which contains only first neighbor bonds, to the double tetrahedra or to even large clusters. Recently, at UCLA, one of our students has done a calculation, for a ternary, with an 8-point cluster, which contains up to the fourth neighbor interactions. It is a little bit rough, because the number of simultaneous nonlinear equations you have to solve is 6561. It can be done and it will be done very shortly, I hope.

References

1. L. Kaufman and H. Bernstein, Computer Calculations of Phase Diagrams, Acad. Press, N.Y. (1970)

2. R. Kikuchi, Phys. Rev. 81, 988 (1951).

3. R. Kikuchi and D. de Fontaine (this symposium, preceding paper, TPSI-12a)

4. M. Kaburagi and J. Kanamori, Progress of Theor. Phys. 54, 30 (1975).

5. T. Kudō and S. Katsura, Progress of Theor. Phys. 56, 435 (1976).

6. M. J. Richards and J. W. Cahn, Acta Met. 19, 1263 (1971).

7. S. M. Allen and J. W. Cahn, Acta Met. 20, 423 (1972).

8. J. Kanamori, J. Met. Soc. Japan 15, 35 (1976) [in Japanese].

9. W. A. Harrison, Pseudopotentials in the Theory of Metals, W. A. Benjamin, N.Y. (1966).

10. V. Heine and D. Weaire, Solid State Physics, H. Ehrenreich, F. Seitz, D. Turnbull, Eds., Acad. Press, N.Y. (1970), pg 249-463.

11. H. Ehrenreich and L. M. Schwartz, Solid State Physics, H. Ehrenreich, F. Seitz, D. Turnbull, Eds., Acad. Press, N.Y. (1976), pg. 149-286.

12. D. de Fontaine Solid State Physics, H. Ehrenreich, F. Seitz, D. Turnbull, Eds., Acad. Press, N.Y. (in preparation).

13. J. M. Sanchez, Ph.D. Dissertation, School of Engineering and Applied Sciences, UCLA (1977).

14. R. Kikuchi, J. Chem. Phys. 60, 1071 (1974).

15. M. Hansen, Constitution of Binary Alloys, McGraw-Hill Book Co., N.Y. (1958).

16. D. Gratias, private communication to D.F.

17. Terms coined by P. Bardhan; J. B. Cohen, private communication to D.F.

18. W. Shockley, J. Chem. Phys. 6, 130 (1938).

19. R. Kikuchi and H. Sato, Acta Met., 22, 1099 (1974).

20. Y.Y. Li, J. Chem. Phys. 17, 447 (1949).

21. C.M. van Baal, Physica 64, 571 (1973).

22. D. de Fontaine, Acta Met. 23, 553 (1975).

23. L. D. Landau and E. M. Lifshitz, Statistical Physics, Addison-Wesley, Reading, Mass. (1958).

24. R. Kikuchi and C.M. van Baal, Scripta Met. 8, 425 (1974).

25. Research supported by Army Research Office (Durham), D. de Fontaine principal investigator, UCLA.

26. J. Kanamori, Progress of Theor. Phys. 35, 16 (1966).

27. International Tables for X-Ray Crystallography, edited by N.F.H. Henry and K. Lonsdale, Vol. I, Kynoch Press, Birmingham (1952).

28. J. Friedel, The Physics of Metals, I - Electrons, edited by J.M. Ziman, Cambridge, The University Press (1969), pg 340-408.

29. J. E. Inglesfield, Acta Met. 17, 1395 (1969).

30. F. Ducastelle and F. Gautier, J. Phys. F. Metal Phys. 6, 2039 (1976).

31. F. Gautier, F. Ducastelle and J. Giner, Phil. Mag. 31, 1373 (1975).

32. J. L. Boquet, private communication to R.K.

33. G. Inden, private communication.

34. E. Van Royen and S. Radelaar, private communication.

35. N.S. Golosov, L. E. Popov and L. Ya. Pudan, J. Phys. Chem. Solids, 34, 1149 and 1157 (1973).

36. R. Kikuchi, D. de Fontaine, M. Murakami and T. Nakamura, Acta Met. (in press).

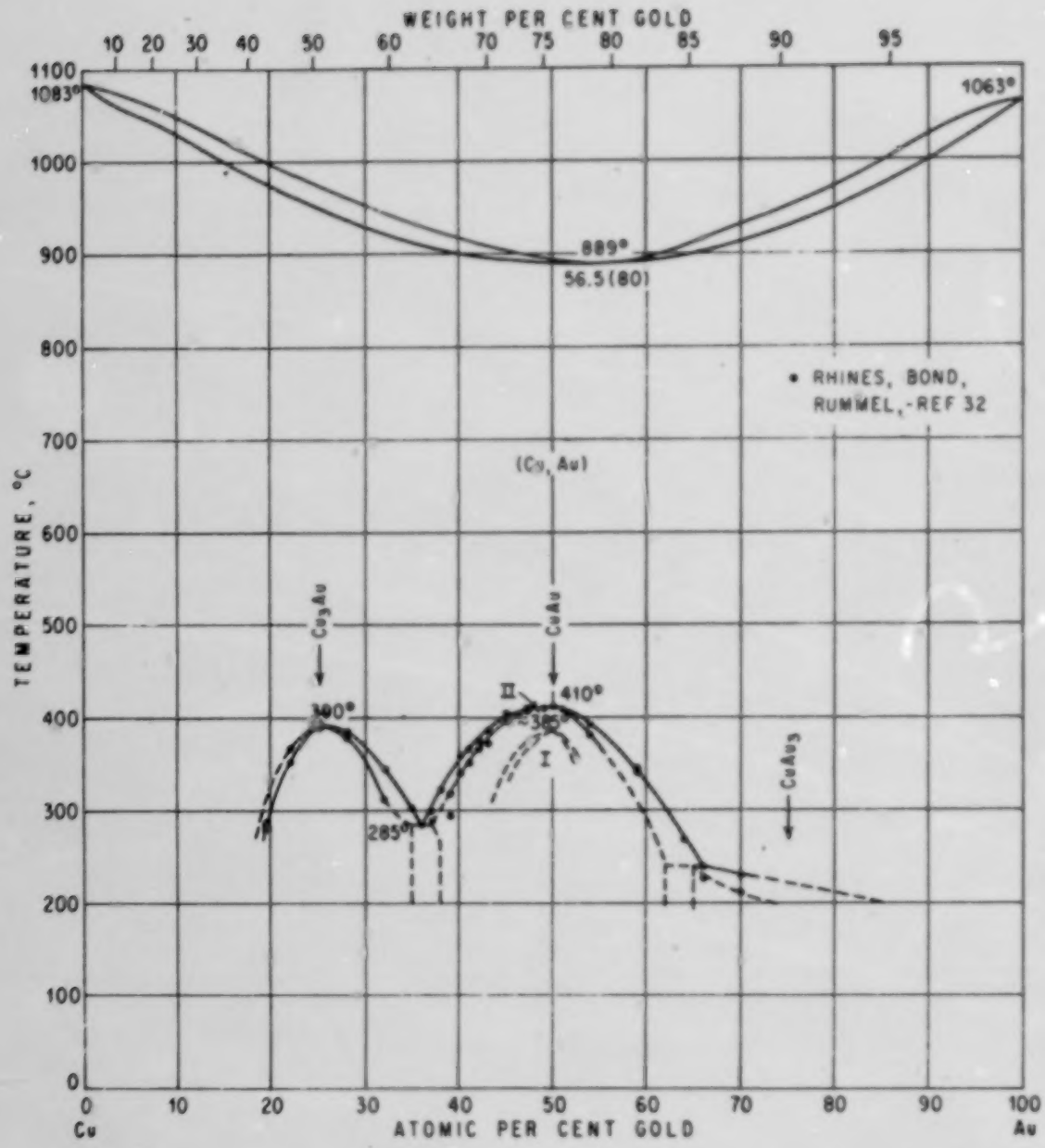

Fig. 1. Experimentally determined Cu-Au phase diagram[15].

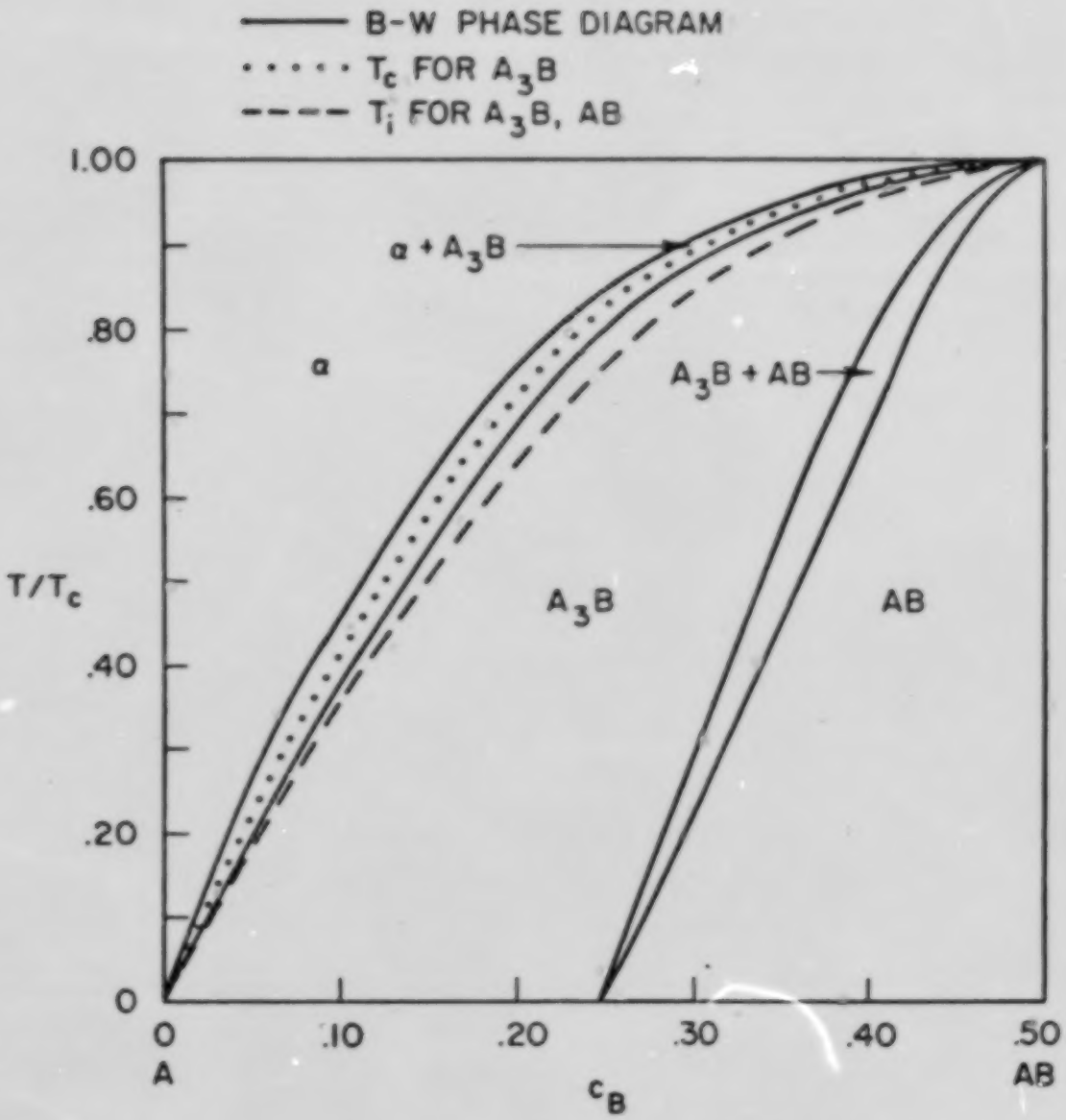

Fig. 2. Cu-Au phase diagram calculated according to the Bragg-Williams model. After Shockely[18].

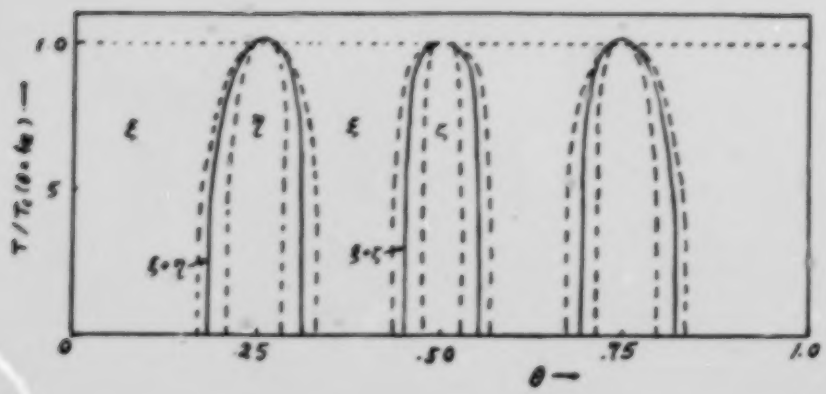

Fig. 3. Cu-Au phase diagram calculated by Li[20] according to the quasi-Chemical theory of Guggenheim (dotted lines). Full lines indicate locus of transition points.

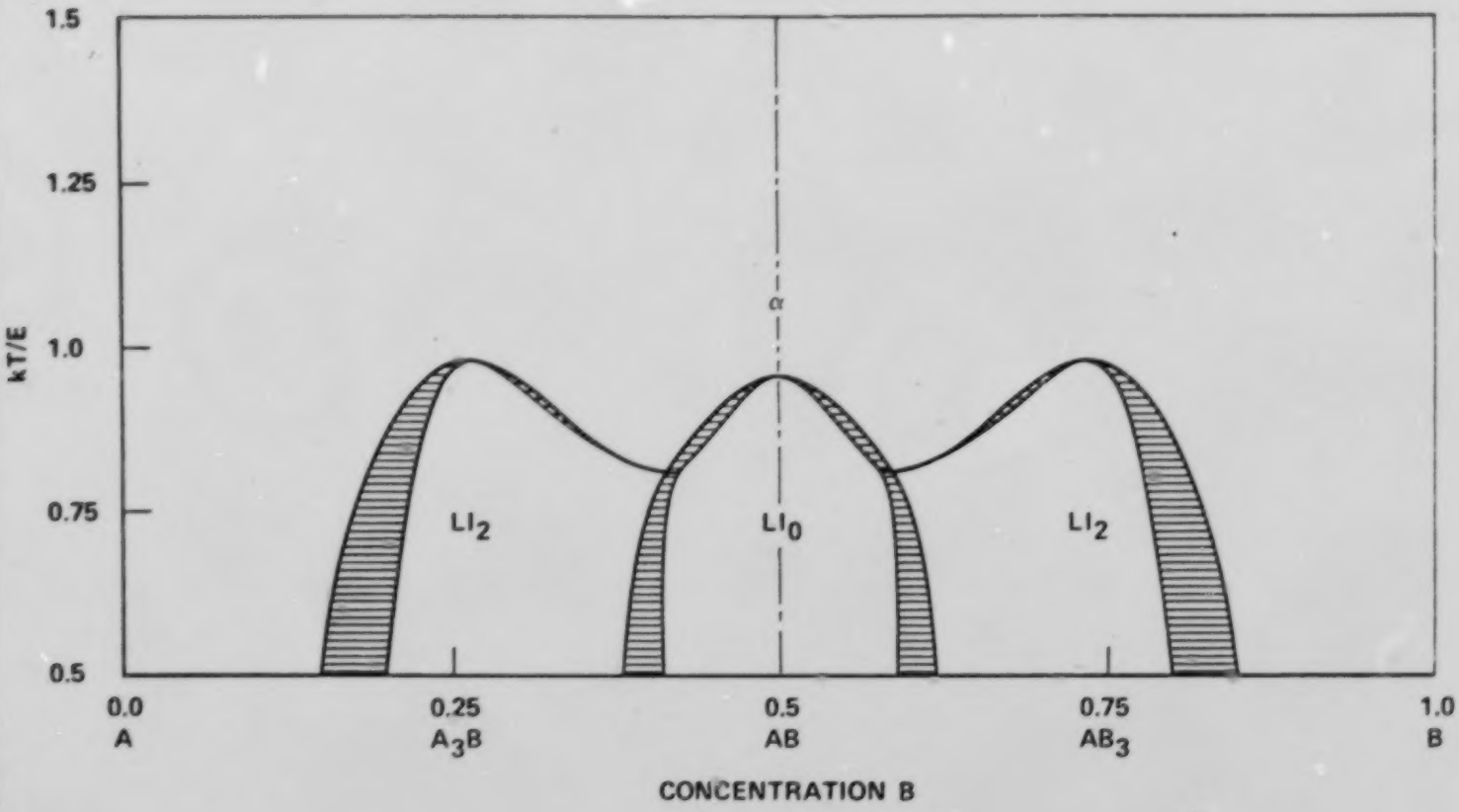

Fig. 4. Cu-Au phase diagram calculated according to the CV model in the tetrahedron approximation with n.n. pair interaction. After van Baal[21] and Kikuchi[14].

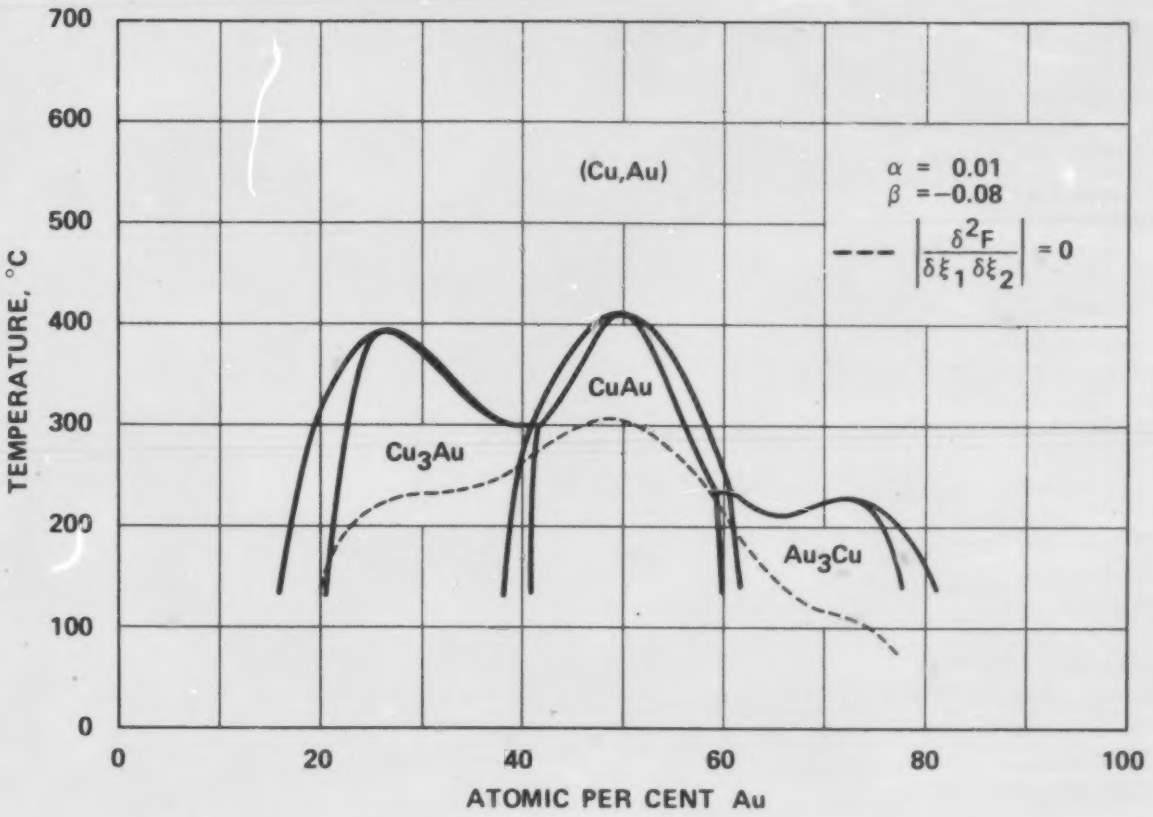

Fig. 5. Cu-Au phase diagram according to the CV model in the tetrahedron approximation with CuCuCuAu and CuAuAuAu many-body interactions.

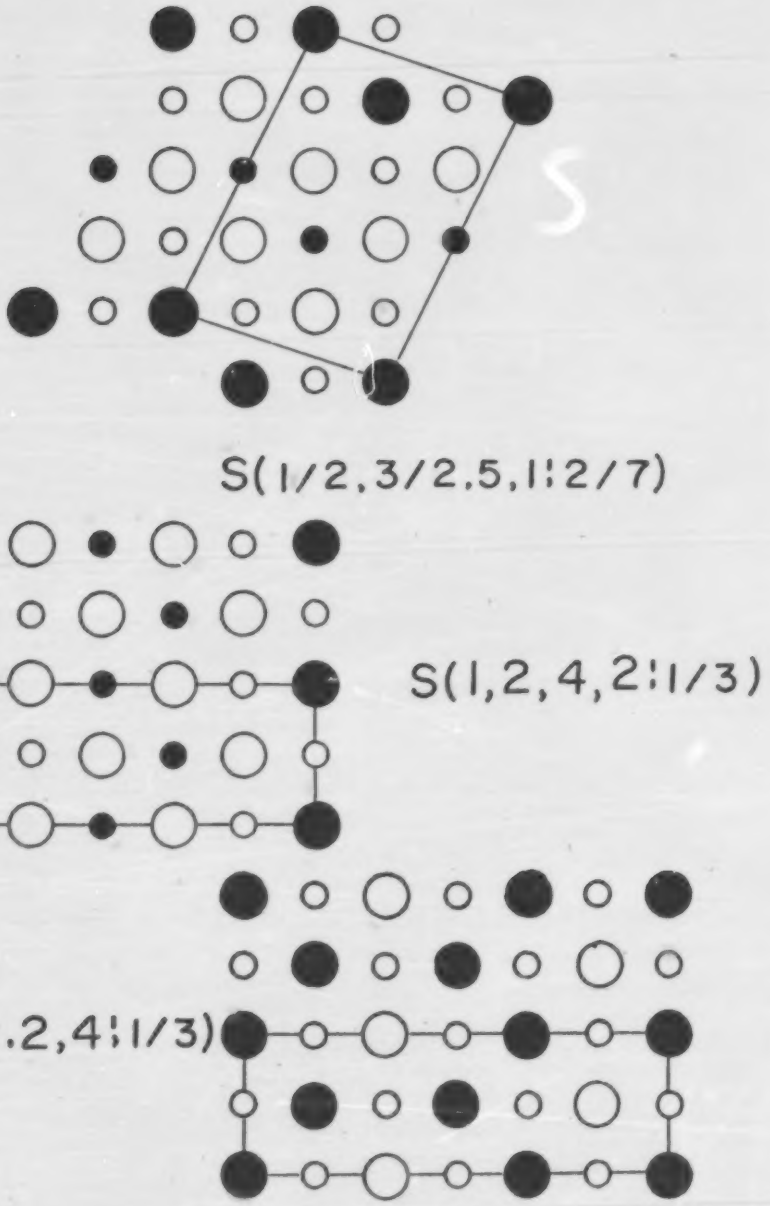

Fig. 6. Projection of the Au_5Mn_2 ordered structure (top) and A_2B structures predicted by Kanamori from a pair interaction model up to fourth coordination shell in the fcc lattice[8]. Open circles: majority component: atoms in planes at integral values of z-coordinate; small circles: atoms at half-integral values of z-coordinate.

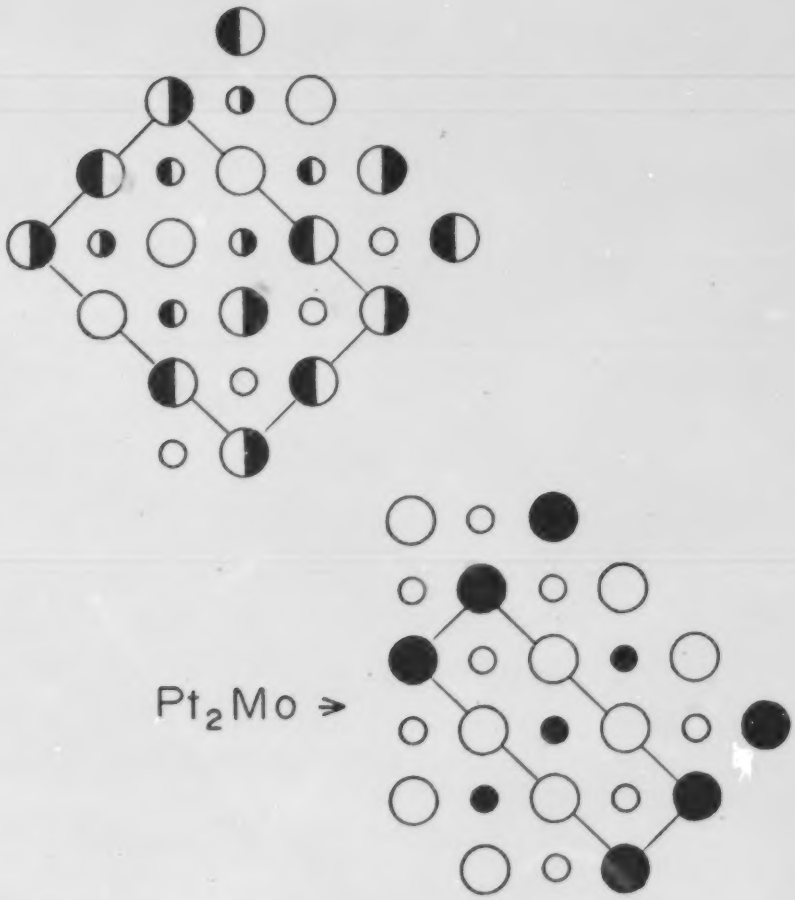

Fig. 7. Projection of two degenerate A_2B ordered structures which have same internal energy in a pairwise model with up to fourth-neighbor interactions[8]. Black-white circles: A-B-A...chains along z axis; white-black circles: B-A-B...chains along z axis.

National Bureau of Standards SP-496, Applications of Phase Diagrams in Metallurgy and Ceramics
Proceedings of Workshop held at NBS, Gaithersburg, Md., January 10-12, 1977

GENERATION OF SELF-CONSISTENT GIBBS ENERGY FUNCTIONS FOR BINARY SYSTEMS: THE Fe-Cu SYSTEM AS AN EXAMPLE*

by J. F. Smith and D. M. Bailey

Ames Laboratory USERDA and Department of Materials Science and Engineering, Iowa State University, Ames, Iowa 50011 U.S.A.

O. Kubaschewski

Lehrstuhl für Metallurgie der Kernbrennstoffe und Theoretische Hüttenkunde der Rheinisch-Westfälischen Technischen Hochschule

5100 Aachen, Germany

Abstract

At present a high level of interest exists concerning the prediction of multicomponent phase equilibria by extrapolation of binary Gibbs energy data. The basic problem is the development of good, self-consistent analytical descriptions of the temperature and composition dependences of the Gibbs energies of formation of the phases in the contributory binary systems. The general process for developing such Gibbs energy functions through combination of experimental thermodynamic data with experimental data concerning binary phase equilibria is illustrated by an analysis of a representative binary system, in this case the Fe-Cu system.

---

*Work was performed in part at the Lehrstuhl für Metallurgie der Kernbrennstoffe und Theoretische Hüttenkunde der Rheinisch-Westfälischen Technischen Hochschule and in part at the Ames Laboratory, for the U.S. Energy Research and Development Administration under Contract No. W-7405-eng-82.

INTRODUCTION

An estimation of the phase equilibria in a multicomponent system can be made if Gibbs energy functions are available for describing the formation of the competitive phases in the system. Such functions can be most simply generated by combination of functions which describe the Gibbs energies of formation of the phases in the contributory binary systems. A number of surveys[1-4] are available which illustrate the various procedures which have been suggested for combination of binary data. The level of interest in the combination of binary data for extrapolation into multicomponent systems is evidenced by the broad-based participation, including scientists in France, Germany, Great Britain, Sweden, and the U.S.A., in the CALPHAD project[5] (CALculation of PHAse Diagrams). However, no combination procedure will produce reliable estimates of multicomponent phase equilibria without good input data. Thus the most basic problem is the development of good analytical descriptions of the temperature and composition dependences of the Gibbs energies of formation of the phases in the contributory binary systems.

The present paper utilizes an analysis of the Fe-Cu system to illustrate what Kaufman[6] has called the ABC procedure. In essence step A is the utilization of the best available thermodynamic data to generate an initial set of Gibbs energy functions. Step B is the input of experimental data pertaining to the phase equilibria to facilitate smoothing and parameter adjustment in the

Gibbs energy functions. Step C is the calculation of an equilibrium temperature-composition diagram from the final set of smoothed and adjusted Gibbs energy functions and the comparison of this calculated diagram with the experimental phase diagram. It may be noted that Gibbs energy functions which are developed in this manner implicitly contain good approximations for the binary interaction parameters. Further, it should be emphasized that the strengths, and thereby the importance, of the interactions decrease with the order of the interactions so that the estimation of multicomponent phase equilibria on the basis of binary interaction parameters includes the dominant interactions. Of course, small additional terms may be added to the Gibbs energy functions of multicomponent phases to include ternary interactions if appropriate thermodynamic and/or phase equilibria data are available. However, the general absence[3] of quarternary and higher order data is not likely to be a serious hindrance to this general approach for the estimation of multicomponent phase equilibria.

In selecting the more reliable from among a number of independent thermodynamic data for any given binary system, two 'thumb' rules may be invoked. First, high-temperature data are normally preferable to low-temperature data because kinetic inhibition of equilibrium is less likely at higher temperatures. Second, enthalpy data tend to be more reliable, albeit not always more precise, than Gibbs energy data. On the basis of this latter observation, the most uncertain terms in experimental data tend to be the excess entropy terms, and these terms therefore have

the most latitude for adjustment when fitting analytical expressions for Gibbs energies to the phase boundaries in experimental temperature-composition diagrams.

Other secondary factors such as the reproducibility of experimental values, comparative repute of different experimental techniques, etc., may also be invoked to select between discordant data. The ultimate criterion is, however, that the Gibbs energy functions which are generated should closely reproduce the phase boundaries of the experimental temperature-composition diagram. When this situation is obtained, the Gibbs energy functions, although they may be less than completely accurate, are at least internally consistent.

REPRESENTATIVE PROCEDURE

Fe-Cu System: The development of Gibbs energy functions for the formation of the competing phases in the Fe-Cu system is here outlined as an example of the generation of self-consistent analytical expressions for a binary system. More specific details are available elsewhere.[7] The present paper is meant to serve only as an illustration of the type of computation and the nature of the successive steps that lead to a satisfactory match between analytical Gibbs energy functions and the experimental phase fields of a temperature-composition diagram. While a portion of the present work was done from a computer terminal interacting with an IBM 360/65 computer, this was done primarily for the convenience arising from the output facility of an associated on-line incremental

plotter. Most of the initial analysis was done with a simple desk calculator in combination with manual graphing, and it is to be emphasized that all of the work, with the possible exception of one item which is later noted, could have been done with almost any of the current generation of programmable desk calculators. This has been verified by repeating representative computations on SR-52 and HP-55 calculators.

In the Fe-Cu system[8] there is an fcc terminal solid solution, the ε-phase, on the Cu-rich side of the system. This phase decomposes peritectically at 1367 K into a Cu-rich liquid plus γ-phase. The γ-phase is the fcc terminal solid solution on the Fe-rich side of the system at intermediate temperatures. On cooling to 1123 K the γ-phase decomposes eutectoidally into ε-phase plus α-phase and on heating to 1751 K the γ-phase decomposes peritectically into δ-phase plus liquid. The α and δ-phases are respectively the low and high temperature terminal bcc solid solutions on the Fe-rich side of the system.

The Liquid Phase: Extensive thermodynamic data are available only for liquid alloys. These data result from independent investigations, five each, of the enthalpies[9-13] and Gibbs energies[14-18] of liquid alloy formation in the temperature range 1700-1900 K. The composite data span the full composition range of the system, and the enthalpy data show reproducibility to ~5% while the reproducibility of the Gibbs energy data is ~15%.

In conformity with the previously noted selection criteria these data were taken to be of good reliability, and a preliminary

Gibbs energy function for the formation of liquid alloys, ΔG_L, was generated from the values selected from these data by Hultgren et al.[19] This was done by first converting the selected values for enthalpies and excess entropies of liquid alloy formation from tabular form to analytical form,

$$J(N_{Fe},N_{Cu}) = N_{Fe}N_{Cu}[a_o+a_1(N_{Fe}-N_{Cu}) + a_2(N_{Fe}-N_{Cu})^2 + a_3(N_{Fe}-N_{Cu})^3]. \quad (1)$$

For the conversion it was found convenient to apply the constraint that for a binary system $N_{Fe} = 1-N_{Cu}$ where N_i represent the mole fraction of the ith component. This constraint allows representation in simple power series

$$J(N_{Fe},N_{Cu}) = J(N_{Fe}) = \Sigma b_n N_{Fe}^n. \quad (2)$$

A least-squares program, such as is commonly available, was then utilized for evaluating the coefficients, b_n, from the tabulated values. The requirements that the enthalpies and excess entropies of alloy formation equal zero at $N_{Fe} = 0$ and $N_{Fe} = 1$ were met by requiring, respectively, $b_o = 0$ and $\Sigma b_n = 0$. After fitting, the functions were inverted to the form of Eq. 1. Liquid Cu and γ-Fe were arbitrarily chosen as the standard states for the Gibbs energy functions for the formation of all phases in the system, and values for the elemental phase transformations[20] were combined with the enthalpy and excess entropy functions in a regular solution approximation to produce the preliminary expression for $\Delta G_L(N_{Fe},N_{Cu},T)$.

The fcc Phases: No experimental thermodynamic measurements for the solid phases in the binary Fe-Cu system were found. However, Counsell et al.[21] had made some calorimetric measurements of the enthalpies of formation of a few solid alloys in the Fe-Cu-Ni ternary system. Through combination of these enthalpy values with thermodynamic data for Fe-Ni and Ni-Cu alloys plus some knowledge of the phase equilibria in certain sections of the ternary system, Counsell et al. developed a set of functions for describing the thermodynamics of formation of the fcc phase in the ternary system. In the present work these functions were extrapolated to the binary limit by setting $N_{Ni} = 0$.

After conversion to the standard states of the present work, graphical representations of the Gibbs energy function vs. composition showed that the fcc phase at intermediate alloy compositions tended to decompose to the ε-phase and γ-phase terminal solutions and at 1367 K the projected equilibrium between liquid and γ-phase showed compositions in reasonable accord with the phase diagram. However, at 1367 K the Gibbs energy of formation of the ε-phase was much too negative to be consistent with peritectic decomposition. This disparity prompted a modification of the excess entropy term, $\Delta S^E_{\gamma,\varepsilon}$, from a value of $2.9805\ N_{Fe}N_{Cu}$ from Counsell et al.[21] to

$$\Delta S^E_{\gamma,\varepsilon} = 2.9805\ \alpha\ N_{Fe}N_{Cu} + 3.308(1-\alpha)\ N^2_{Fe}N_{Cu} \qquad (3)$$

where $2.9805\ N_{Fe}N_{Cu} = 3.308\ N^2_{Fe}N_{Cu}$ at $N_{Fe} = 0.9$ so that $\Delta S^E_{\gamma,\varepsilon}$ is

invariant with respect to α at that composition. Thus $\Delta S^{E}_{\gamma,\varepsilon}$ was made insensitive to the parameter α in the Fe-rich region but highly sensitive in the Cu-rich region so that α could be adjusted to equilibrate the ε-phase with liquid and γ-phase at 1367 K. This is illustrated in Fig. 1.

After adjustment of α, the Gibbs energy function for the formation of fcc alloys indicated equilibrium compositions for the ε and γ-phases over the temperature range 1123-1367 K in acceptable accord with the experimental terminal solubilities.[8,22] Above 1367 K evaluation of the equilibria between liquid and γ-phase predicted a liquidus line in good agreement with the phase diagram for $N_{Fe}<0.15$ but was slightly below the experimental liquidus in the region $0.15<N_{Fe}<0.4$ and beyond $N_{Fe} = 0.4$ drifted significantly above the experimental liquidus. To achieve agreement, the coefficients in the expression for ΔG_L were refined through successive approximations. This refinement was restricted to terms involving higher powers of N_{Fe} so that the refinement did not perturb the agreement already existing in the Cu-rich region. Since the experimental spread among determinations[8] of the liquidus line is about $\pm$ 15 K in the composition range $0.3<N_{Fe}<0.7$, refinement was terminated when the predicted and experimental liquidus lines agreed within this spread. It is worth noting that the refined parameters produce no inconsistency with input thermodynamic data. The refined parameters indicate enthalpies and Gibbs energies of liquid alloy formation agreeing on the average within 3.3% and 5.4%, respectively,

with values tabulated by Hultgren et al.,[19] and this is well below the scatter in the composite of the input experimental data.

The computer program for evaluating the equilibrium compositions at fixed temperature conformed to the following logic sequence. First, at an arbitrarily selected composition, the slope and intercept of the ΔG vs. composition curve were evaluated for the first phase. Second, the slope of the ΔG vs. composition curve for the second phase was evaluated at some selected starting composition. The slopes for the two phases were then compared and, on the basis of the comparison, a new composition was selected for the second phase and the calculation was repeated. Iteration continued with bracketing convergence until the slopes for the two phases matched within a 'good enough' factor. Third, the intercept for the second phase was calculated and compared with the intercept from the first phase. On the basis of the intercept comparison, the composition for the first phase was adjusted and the whole process was repeated until agreement was obtained within 'good enough' limits for both the slopes and intercepts of the two phases being tested for equilibration; such agreement defines a common tangent to the Gibbs energy functions for the two phases. The compositions at the points of tangency were then taken as the calculated phase boundaries.

The bcc Phases: No thermodynamic data were found for the bcc Fe-Cu alloys, but Zener[23] has suggested that for Fe and Fe alloys the greater stability of the bcc structure relative to the fcc structure at low temperatures is due to differences in magnetic

contributions to the Gibbs energies. This suggestion has been pursued by a number of investigators; these include Hillert et al.[24] who have developed a simple formulation for approximating the magnetic contribution to the Gibbs energy of formation of bcc Fe alloys. This approximation requires knowledge of two quantities: first, the change in Curie temperature per mole fraction of alloying component which for Cu alloys was obtained from the phase diagram,[8] and, second, the magnetic contribution to the entropy of bcc Fe which was obtained in analytical form by a least-squares fit to the tabular data developed by Weiss and Tauer.[25]

With this input, the general formulation of Hillert et al.[24] leads to an expression for the Gibbs energy of formation of bcc Fe-Cu alloys from bcc Fe and bcc Cu. The expression contains four adjustable parameters which specify the magnitudes and composition dependences of the non-magnetic contributions to the enthalpies and excess entropies associated with the formation reaction. Conversion of standard state to liquid Cu was accomplished by adding terms for fusion[20] and for the bcc→fcc transformation;[26] conversion of standard state to fcc Fe was accomplished by adding a term for the bcc→fcc transformation which was taken from the critical evaluation of data for pure Fe by Orr and Chipman.[27] This term was evaluated by a least-squares fit to their tabulated data, and satisfactory fitting required powers of temperature ranging from zero through six. The fitting of this term is probably beyond the capability of most desk calculators.

After conversion to the standard states of the present work, the Gibbs energy function for the formation of the bcc phases still contained four adjustable parameters and was in a form suitable for comparison with the Gibbs energy functions for the liquid and fcc phases. The adjustable parameters were then evaluated on the bases of the peritectic reaction at 1751 K which involves the liquid, γ, and δ-phases and the eutectoid reaction at 1123 K which involves the ε, γ, and α-phases. At each of these two temperatures both the magnitude and slope of the bcc Gibbs energy function are constrained at the equilibrium composition of the participating bcc phase, and the constraining limitations are derivable from the Gibbs energy functions already generated for the liquid and fcc phases. Thus there are only four constraints to fix four adjustable parameters plus two additional variables which are the composition of the δ-phase at 1751 K and the composition of the α-phase at 1123 K. This problem was approached by first solving for the magnitudes of the non-magnetic enthalpy and excess entropy of bcc alloy formation without allowing for compositional dependence. The constraints are then sufficient to fix the two magnitudes and the two compositions. The resulting composition for the δ-phase in the peritectic reaction at 1751 K differed by more than an atom per cent from the experimental value of Hellawell and Hume-Rothery,[28] and, in view of the limited terminal solubility, this was considered unacceptable. Parameters defining the compositional dependences were then freed within the limitation that the sums of

the new composition independent and composition dependent terms were not allowed to vary appreciably from the initial composition independent values. Then, in an iterative procedure the calculated composition of the δ-phase at 1751 K was moved into near accord with the Hellawell and Hume-Rothery value and the numerical values of the adjustable parameters were fixed.

RESULTS AND DISCUSSION

The Gibbs energies of formation of the Fe-Cu phases from liquid Cu and fcc Fe which were generated by the foregoing procedure are, in cal/gm-atom, for the liquid,

$$\Delta G_L = 3500\, N_{Fe} + N_{Fe}N_{Cu}[8203+433.3(N_{Fe}-N_{Cu}) + 1808(N_{Fe}-N_{Cu})^2 + 578(N_{Fe}-N_{Cu})^3] - T\{-1.987N_{Fe}\ln N_{Fe}-1.987N_{Cu}\ln N_{Cu} + 1.944N_{Fe} + N_{Fe}N_{Cu}[0.44438+0.39238(N_{Fe}-N_{Cu}) + 0.61813(N_{Fe}-N_{Cu})^2 + 0.56113(N_{Fe}-N_{Cu})^3]\}, \quad (4)$$

for the fcc phases,

$$\Delta G_{\gamma,\varepsilon} = -3120N_{Cu} + 10107\, N_{Fe}N_{Cu}^2 + 12936N_{Fe}^2N_{Cu} - T\{-1.987 N_{Fe}\ln N_{Fe}-1.987N_{Cu}\ln N_{Cu}-2.30N_{Cu}+0.8196N_{Fe}N_{Cu} +2.3983N^2{}_{Fe}N_{Cu}\}, \quad (5)$$

and for the bcc phases,

1110

$$\Delta G_{\alpha,\delta} = N_{Fe}N_{Cu}\{13000+494.7(N_{Fe}-N_{Cu})+1084S_{mag,\alpha}-T[2.500$$

$$+2.542(N_{Fe}-N_{Cu})]\} + T(1.987N_{Fe}\ln N_{Fe}+1.987N_{Cu}\ln N_{Cu})$$

$$+ N_{Cu}(-1620+1.5T) + \Delta G_{Fe,tr}. \qquad (6)$$

In the last expression, $S_{mag,\alpha}$ represents the magnetic entropy of bcc Fe and $\Delta G_{Fe,tr}$ represents the Gibbs energy for the fcc→bcc transformation in pure Fe, and these are:

$$S_{mag,\alpha} = -19.930 + 5.2602\times10^{-2}T - 4.7618\times10^{-5}T^2$$

$$+ 1.9274\times10^{-8}T^3 - 2.9356\times10^{-12}T^4 \qquad (7)$$

and

$$\Delta G_{Fe,tr} = -40027.7 + 158.219T - 0.261351T^2 + 2.30512\times10^{-4}T^3$$

$$-1.14285\times10^{-7}T^4 + 3.01614\times10^{-11}T^5 - 3.30930\times10^{-15}T^6 \qquad (8)$$

Because of the rapid change in the thermodynamic functions of Fe in the vicinity of the Curie temperature, all fitting of data[25,27] was done for values above this temperature so Eqs. 6, 7, and 8 are valid only for temperatures above ~1050 K. Fig. 2 shows the calculated phase diagram (solid lines) together with representative points from the experimental phase diagram with the error bars on the experimental liquidus points in the composition range $0.3<N_{Fe}<0.7$ showing the previously noted $\pm$ 15 K tolerance. Table I shows a comparison of calculated and observed compositions for the two peritectic and one eutectoid reaction.

Obviously the calculation of one binary diagram is by itself a useless endeavor since the experimental diagram is already available. However, the combination of Gibbs energy functions from related phase diagrams to predict multicomponent equilibria is quite worthwhile since the experimental difficulty becomes orders of magnitude more complex, tedious, time-consuming, and expensive when expanding from binary to ternary to quaternary, etc., systems. Thus, even though high precision is not expected in extrapolating binary data to estimate multicomponent equilibria, considerable experimental effort may be saved if one can localize a region of interest. A number of possibilities come readily to mind as examples. If high temperature strength is the desired property, regions of maximal melting might be sought. If oriented eutectics are to be grown, regions of eutectic solidification may be sought. If deleterious phases (e.g. σ-phases) or desirable phases (e.g. age hardening precipitates) are important, their true thermodynamic stability independent of kinetic factors may be tested. If high-temperature superconductors are desired, phase compositions with appropriate electron/atom ratios may be examined for marginal stability or metastability. In short, the possible applications are limited by the ingenuity of the investigator, and the present paper illustrates that the generation of appropriate Gibbs energy functions for reproducing compositions of experimental phase equilibria for a representative binary system to within ~1 at. % is not particularly difficult nor excessively time-consuming. The primary limitation of this ABC approach is that it will not predict the existence of phases which are not functionally represented.

REFERENCES

1. L. Kaufman and H. Bernstein, Computer Calculation of Phase Diagrams, Chaps. 9-13 (Academic Press, New York, 1970).
2. P. J. Spencer, F. H. Hayes, and O. Kubaschewski, Rev. Chim. minerale 9, 13-29 (1972).
3. I. Ansara, in Metallurgical Chemistry Symposium 1971, ed. by O. Kubaschewski, pp. 403-430 (Her Majesty's Stationery Office, London, 1972).
4. O. Kubaschewski and I. Barin, Pure and Appl. Chem. 38, 469-494 (1974).
5. For information contact L. Kaufman, Manlabs, Inc., Cambridge, Mass. 02139, U.S.A.
6. L. Kaufman, in Metallurgical Chemistry Symposium 1971, ed. by O. Kubaschewski, pp. 373-402 (Her Majesty's Stationery Office, London, 1972).
7. O. Kubaschewski, J. F. Smith and D. M. Bailey, Z. Metallk., in process.
8. M. Hansen and K. Anderko, Constitution of Binary Alloys, 2nd ed., pp. 580-582 (McGraw-Hill, New York, 1958).
9. F. Woolley and J. F. Elliott, Trans. Met. Soc. AIME 239, 1872-1873 (1967).
10. W. Oelsen, E. Schürmann, and C. Florin, Arch. Eisenhüttenw. 32, 719-728 (1961).
11. A. Podgornjk, quoted by Oelsen et al., ref. 10.
12. Y. Tozaki, Y. Iguchi, S. Ban-ya, and T. Fuwa, in Chemical Metallurgy of Iron and Steel, Proc. of the Int. Symp. on Met. Chem. - Applications of Ferrous Met. held Univ. of

Sheffield, 19-21 July 1971, pp. 130-132 (Iron and Steel Inst., London, 1973).

13. A. El'-Khasan, K. Abdel-Aziz, A. A. Vertman, and A. M. Samerin, Izvest, Akad. Nauk SSSR, Met. 3, 19-30 (1966).
14. J. P. Morris and G. R. Zellars, J. Metals 8, 1086-1090 (1956).
15. M. Olette and M. Onillon, Comptes Rendus Acad. Sc. Paris 261, 3597-3600 (1965).
16. P. J. Koros and J. Chipman, J. Metals 8, 1102-1104 (1956).
17. F. C. Langenberg, J. Metals 8, 1024-1025 (1956).
18. U. V. Choudary, J. A. Serkin, and G. R. Belton, Met. Trans. 6B, 399-403 (1975).
19. R. Hultgren, P. D. Desai, D. T. Hawkins, M. Gleiser, and K. K. Kelley, Selected Values of the Thermodynamic Properties of Binary Alloys, pp. 737-741 (Am. Soc. for Metals, Metals Park, Ohio 44073, 1973).
20. R. Hultgren, R. L. Orr, P. D. Anderson, and K. K. Kelley, Selected Values of Thermodynamic Properties of Metals and Alloys, pp. 89-95 and 103-112 (John Wiley and Sons, Inc., New York, 1965).
21. J. F. Counsell, E. B. Lees, and P. J. Spencer, in Metallurgical Chemistry Symposium 1971, ed. by O. Kubaschewski, pp. 451-458 (Her Majesty's Stationery Office, London, 1972).
22. G. R. Speich, J. A. Gula, and R. M. Fisher, in The Electron Microprobe, ed. by T. D. McKinely, K. F. J. Heinrich and D. B. Witty, pp. 525-541 (John Wiley and Sons, New York, 1966).
23. C. Zener, Trans. AIME 203, 619-630 (1955).

24. M. Hillert, T. Wada, and H. Wada, J. Iron Steel Inst. 205, 539-546 (1967).

25. R. J. Weiss and K. J. Tauer, Phys. Rev. 102, 1490-1495 (1956).

26. L. Kaufman, Report PB 144220, Office of Technical Services, Cambridge, Mass., 1959.

27. R. L. Orr and J. Chipman, Trans. Met. Soc. AIME 239, 630-633 (1967).

28. A. Hellawell and W. Hume-Rothery, Phil. Trans. Roy. Soc. London A249, 432-433 (1957).

Table I. Comparison of calculated and observed equilibrium compositions (N_{Fe}) for the phases involved in the two peritectic and one eutectoid reaction in the Fe-Cu system.

	Liq.	γ-phase	δ-phase	
Peritectic reaction at 1751 K	0.873	0.920	0.934	(calc.)
	0.897	0.917	0.933	(ref. 28)
	Liq.	ε-phase	γ-phase	
Peritectic reaction at 1367	0.039	0.048	0.942	(calc.)
	0.032	0.045	~0.925	(ref. 8)
	-----	-----	0.940	(ref. 22)
	ε-phase	γ-phase	α-phase	
Eutectoid reaction at 1123 K	0.016	0.982	0.990	(calc.)
	0.012	~0.97	~0.99	(ref. 8)
	-----	0.977	0.981	(ref. 22)

1116

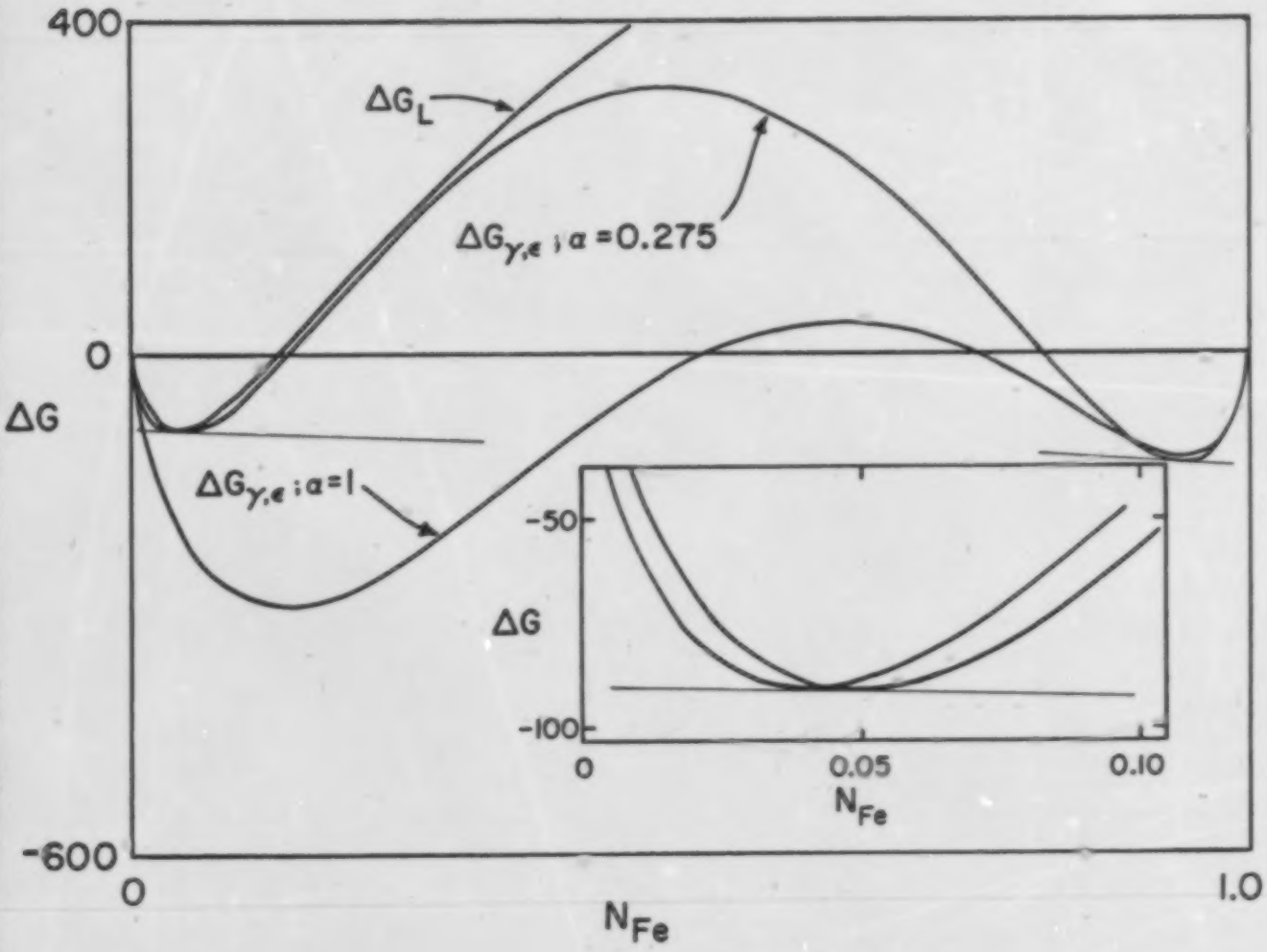

Fig. 1. Adjustment of the parameter α in $G_{\gamma,\varepsilon}$ to effect peritectic equilibrium at 1367 K.

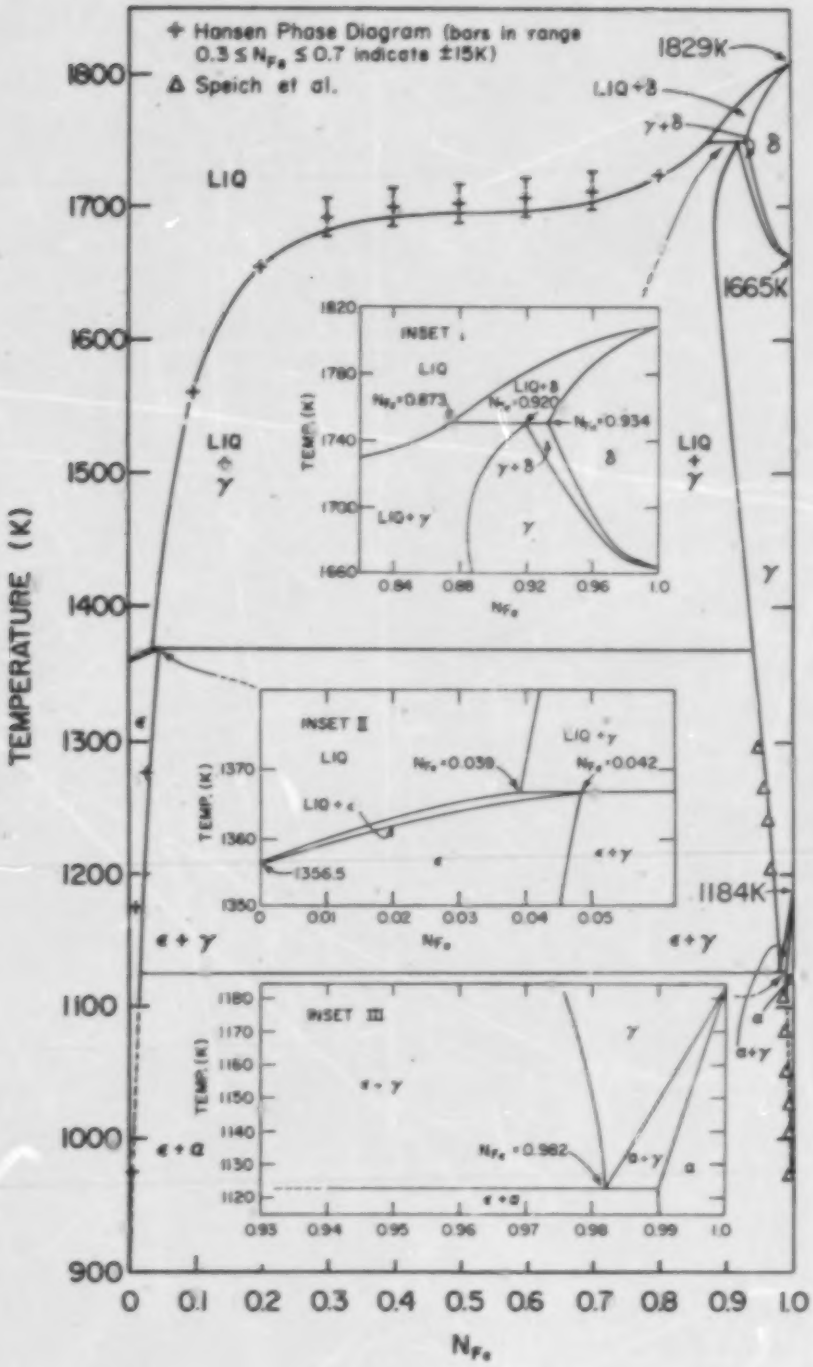

Fig. 2. Comparison of representative points from the experimental Fe-Cu phase diagram with the calculated diagram (solid lines).

National Bureau of Standards SP-496, Applications of Phase Diagrams in Metallurgy and Ceramics
Proceedings of Workshop held at NBS, Gaithersburg, Md., January 10-12, 1977

CHARACTERISTICS AND CALCULATION OF STABILITY DIAGRAMS

Scott McCormick

Metallurgical and Materials Engineering Department
Illinois Institute of Technology
Chicago, Illinois 60616

Yaz Bilimoria

Inland Steel Research Laboratories
East Chicago, Indiana 46312

ABSTRACT

Stability diagrams are equilibrium diagrams that map phase equilibria in systems containing both metallic and non-metallic components as a function of temperature, non-metal chemical potential or activity, and X_M, the ratio of M atoms to metal atoms. They offer an alternative perspective on phase equilibria and reaction paths in these systems. The characteristics and calculation of two forms of stability diagrams for systems containing non-metallic and metallic components will be discussed. In these two types of diagrams phase equilibria are mapped as a function of (1) non-metal activity and X_M at constant temperature, and (2) temperature and X_M at constant or continuously varying non-metal activity.

These diagrams are similar in form to conventional temperature-composition diagrams with horizontal tie lines and eutectic and peritectic-like features. The lever law can be used to calculate the distribution of metal atoms between phases in equilibrium. Non-metal activity-X_M plots are ideal for carrying out ternary Gibbs-Duhem integrations with Schuhmann's method.

These types of diagrams can be calculated from plots of Gibbs free energy versus X_M at constant temperature and non-metal activity. One mole of metal is chosen as the basis for the calculation. The two free energy ordinates are the molar free energies of the two metals. Temperature and non-metal activity are fixed, so that the condensed phases, stable and unstable, have the same non-metal chemical potential. The free energy of the system is therefore minimized when the combined free energies of the two metals are at a minimum. The curves are of the form

$$G^{\eta} = X_A \, {}^{o}G_A^{\eta} + X_B \, {}^{o}G_B^{\eta} + RT \, (X_A \ln a_A^{\eta} + X_B \ln a_B^{\eta})$$

The ${}^{\circ}G_M^{\eta}$ terms are the molar free energies of component M in η-phase standard states at fixed temperature and non-metal activity. The a_M^{η} terms are the metal activities in solution with respect to the ${}^{\circ}G_M^{\eta}$ standard states. To calculate the free energy curves, the thermodynamics of each stable solid or liquid solution must be known.

The Fe-Cr-O-C system is used to illustrate these principles.

1120

CHARACTERISTICS AND CALCULATION OF STABILITY DIAGRAMS

Equilibrium diagrams are maps of the regions of stability of solid, liquid, and gaseous phases as a function of two or more independent thermodynamic variables. The most common choices of independent variables are temperature and composition. Alternative choices of variables allow systems to be examined from different perspectives and can yield different insights into system behavior.

In systems containing both non-metallic and metallic components, it is interesting to map phase equilibria on stability diagrams in which the independent variables are temperature, the chemical potentials or activities of the non-metals, and metal composition as measured by X_i, the ratio of moles of metal i to moles of metal, so that

$$X_i = n_i / (n_i + n_j + \ldots)$$

where n_i, n_j, ... represent moles of metallic components.

Several representative stability diagrams are shown in figures 1-5 for systems containing iron and chromium. The characteristics of these types of diagrams have been discussed by Pelton, Schmalzried, et al.[1-5]. Briefly, figures 1-5 are structurally similar to conventional binary and ternary temperature-composition diagrams. The rules of construction are identical. All n-phase regions must be bounded by regions containing $(n \pm 1)$ phases or $(n + 1)$-phase invariant equilibria. In systems with two metal components, boundaries of one-phase regions must meet with curvatures such that the boundaries extrapolate into the adjacent two-phase regions.

In Figures 1-5 a horizontal line in a two-phase region represents a condition of constant temperature and non-metal activity, a tie line. The metallic compositions can be read at the ends of the tie lines. The distribution of metal between two equilibrium phases can be calculated from the lever law.

It can be seen in Figures 1-3 that on isothermal diagrams of systems containing two metallic components, any variables that fix the non-metal activities can be chosen as independent variables. When the non-metal is oxygen, these could include H_2O/H_2, CO_2/CO, and SO_3/SO_2 pressure ratios or $h_{\underline{o}}$, the Henrian activity of monatomic oxygen in a liquid or solid solution. For carbon one could use $CH_4/(H_2)^2$ or $(CO)^2/CO_2$ pressure ratios or $h_{\underline{c}}$, the Henrian activity of carbon in a liquid or solid solution. When temperature is chosen as an independent variable the non-metal activities can be fixed or allowed to vary continuously with temperature as shown in Figure 4.

Phase equilibria in systems containing three metallic components can be mapped as a function of metal composition at fixed temperature and non-metal potential as shown in Figure 5.

Calculation of Stability Diagrams

Stability diagrams can be calculated from plots of Gibbs free energy versus metal composition at constant temperature, pressure, and non-metal chemical potential. This will be demonstrated for the hypothetical A-B-O system with the aid of Figure 6.

One mole of metal is chosen as the basis for the calculation. The curves in Figure 6b represent the free energies of one mole of metal in each of three phases as a function of X_B at constant T, P, and μ_{O_2}. The condensed phases, stable and unstable, have the same oxygen potential so that the free energy of the system is minimized at any X_B when the combined free energies of A and B are at a minimum. The free energy curves are of the form

$$G^{\eta} = X_A^{\eta}\ {}^{o}G_A^{\eta} + X_B^{\eta}\ {}^{o}G_B^{\eta} + RT\,(X_A^{\eta}\ \ell n\ a_A^{\eta} + X_B\ \ell n\ a_B^{\eta}) \qquad (2a)$$

or, alternatively,

$$G^{\eta} = X_A^{\eta}\ {}^{o}G_A^{\eta} + X_B\ {}^{o}G_B^{\eta} + RT\,(X_A^{\eta}\ \ell n\ X_A^{\eta} + X_B^{\eta}\ \ell n\ X_B^{\eta})$$

$$+ RT\,(X_A^{\eta}\ \ell n\ \gamma_A^{\eta} + X_B^{\eta}\ \ell n\ \gamma_B^{\eta}) \qquad (2b)$$

${}^{o}G_A^{\eta}$ and ${}^{o}G_B^{\eta}$ are the molar free energies of A and B in η-phase standard states at the specified temperature and oxygen potential in the binary A-O and B-O systems, respectively. For example, ${}^{o}G_A^{AO_x}$ represents the molar free energy of A in binary AO_x at the given T and P_{O_2}. The value of ${}^{o}G_A^{AO_x} - {}^{o}G_A^{a}$ can be calculated from the Gibbs-Duhem equation since it is equal to the difference in the molar free energy of A in AO_x at P_{O_2} and in AO_x at $P_{O_2}^{A/AO_x}$, the partial pressure of oxygen in equilibrium with A and AO_x.

$$dG_A^{AO_x} = -x\,dG_O^{AO_x} \qquad (3a)$$

$$\int_{{}^{o}G_A^{a}}^{{}^{o}G_A^{AO_x}} dG_A^{AO_x} = -\frac{RT}{2} \int_{\ell n P_{O_2}^{A/AO_x}}^{\ell n P_{O_2}} x\ d\,\ell n\, P_{O_2} \qquad (3b)$$

$$ {}^{o}G_A^{AO_x} - {}^{o}G_A^{\alpha} = -\frac{XRT}{2}\left(\ell n\, P_{O_2} - \ell n\, P_{O_2}^{A/AO_x}\right) \qquad (3c) $$

Note that the standard states for A and B are defined so that ${}^{o}G_A^{\eta}$ and ${}^{o}G_B^{\eta}$ are functions of both temperature and oxygen potential. If the oxygen/metal atom ratio is a function of oxygen pressure, the ratio must be expressed as a function of P_{O_2} and included within the integral in Equation 3b.

The last term in Equation 2a is the free energy of mixing, the free energy change accompanying the formation of an η-phase solution from A and B in their η-phase standard states. Activities are defined conventionally

$$ \ell n\, a_A^{\eta} = (G_A^{\eta} - {}^{o}G_A^{\eta})/RT \qquad (4) $$

G_A^{η} is the partial molar free energy of A in an η-phase solution. As shown in Figure 6b it is the intercept with the G_A^{η} ordinate of a line tanget to the G^{η} curve at a given composition.

At constant temperature and oxygen pressure the activity of A or B in an $(A, B)O_x$ solution referred to the Raoultian standard state defined above ($a_A^{AO_x}$, for example) is equal to the Raoultian activity of the binary oxide (a_{AO_x}) in the solution. This is shown as follows:

$$ RT\, \ell n\, a_{AO_x} = (G_{AO_x} - {}^{o}G_{AO_x}) \qquad (5a) $$

$$ RT\, \ell n\, a_{AO_x} = (G_A^{(A,B)O_x} - {}^{o}G_A^{AO_x}) + x\,(G_O^{(A,B)O_x} - {}^{o}G_O^{AO_x}) \qquad (5b) $$

But since P_{O_2} is constant, $G_O^{(A,B)O_x} = {}^{o}G_O^{AO_x}$, and

$$ RT\, \ell n\, a_{AO_x} = (G_A^{(A,B)O_x} - {}^{o}G_A^{AO_x}) = {}^{o}G_O^{AO_x} = RT\, \ell n\, a_A^{(A,B)O_x} \qquad (5c) $$

$$a_{AO_x} = a_A^{(A,B)O_x} \tag{5d}$$

Activity coefficients are defined conventionally:

$$\gamma_A^{\eta} = a_A^{\eta} / X_A^{\eta} \tag{6}$$

It follows from Equations 5d and 6 that

$$\gamma_A^{(A,B)O_x} = \gamma_{AO_x} \tag{7}$$

These activities and activity coefficients can be assumed to be independent of oxygen potential unless the oxygen/metal atom ratio varies with oxygen potential. Even for this case the activities will not vary with oxygen potential if the oxygen/metal ratio in solution is a weighted average of the ratios in the binary AO_x and BO_x phases.

For equilibrium between two condensed phases $(A,B)O_x$ and $(A,B)O_y$,

$$G_A^{(A,B)O_x} = G_A^{(A,B)O_y} \tag{8a}$$

$$G_B^{(A,B)O_x} = G_B^{(A,B)O_y} \tag{8b}$$

so that

$$^{o}G_A^{(A,B)O_x} + RT\,(\ell n\, X_A^{(A,B)O_x} + \ell n\, \gamma_{AO_x})$$

$$= {}^{o}G_A^{(A,B)O_y} + RT\,(\ell n\, X_A^{(A,B)O_x} + \ell n\, \gamma_{BO_x}) \tag{9a}$$

and

$$^{o}G_B^{(A,B)O_x} + RT\,(X_B^{(A,B)O_x} + \ell n\, \gamma_{BO_x})$$

$$= {}^{o}G_B^{(A,B)O_y} + RT\,(\ell n\, X_B^{(A,B)O_y} + \ell n\, \gamma_{BO_y}) \tag{9b}$$

From Equations 3 and 9a,

$$-\frac{xRT}{2}\left(\ln P_{O_2} - \ln P_{O_2}^{A/AO_x}\right) + RT\left(\ln X_A^{(A,B)O_x} + \ln \gamma_{AO_x}\right)$$

$$= -\frac{yRT}{2}\left(\ln P_{O_2} - \ln P_{O_2}^{B/BO_x}\right) + RT\left(\ln X_B^{(A,B)O_x} + \ln \gamma_{BO_x}\right) \qquad (10)$$

$$\ln\left(\frac{X_A^{(A,B)O_x}}{X_A^{(A,B)O_y}}\right) = \ln\left(\frac{\gamma_{AO_y}}{\gamma_{AO_x}}\right) + \left(\frac{x-y}{2}\right)\ln P_{O_2}$$

$$+ \frac{y}{2}\ln P_{O_2}^{A/AO_y} - \frac{x}{2}\ln P_{O_2}^{A/AO_x} \qquad (11a)$$

Similarly, for component B,

$$\ln\left(\frac{X_B^{(A,B)O_x}}{X_A^{(A,B)O_y}}\right) = \ln\left(\frac{\gamma_{BO_y}}{\gamma_{BO_x}}\right) + \left(\frac{x-y}{2}\right)\ln P_{O_2}$$

$$+ \frac{y}{2}\ln P_{O_2}^{A/AO_y} - \frac{x}{2}\ln P_{O_2}^{A/AO_x} \qquad (11b)$$

Equations 11 are similar to those derived by Sticker and Schmalzried [5] for equilibrium between metal (A,B) and oxide (A,B)O phases. Similar equations can be derived for systems with three or more metallic components.

To construct stability diagrams, sets of equations similar to 9 or 11 must be solved for pairs of stable phases over the temperature and oxygen potential ranges of interest. A number of computer techniques have been developed to solve equations of this type. The real problem is not computational but thermodynamic. For each phase, ${}^{o}G_{A,B\ldots}^{\eta}$ must be known as a function of temperature and non-metal

potential and $\ell n\ \gamma^{\eta}_{A,B,\ldots}$ or $\Delta G^{\eta,\,xs}$ must be known as a function of composition and temperature.

This is a difficult but not insoluble problem. Data is available for many metallic solutions. Less work has been done on the thermodynamics of oxide, sulfide, nitride, and carbide phases. Although there exists a large body of phase equilibrium measurements at known non-metal chemical potentials. A judicious correlation of this data can yield a large amount of thermodynamic information.

For example, if the non-metal activities and phase boundaries are known on a ternary A-B-O isotherm, metal activities can be calculated from ternary Gibbs-Duhem integrations using Schuhmann's method.[6]

Schuhmann's Equation 6 can be rewritten

$$\left(\frac{\delta G_A}{\delta G_O}\right)_{n_A,\,n_B} = -\left(\frac{\delta n_O}{\delta n_A}\right)_{G_O,\,n_B} \tag{12}$$

The integration is carried out along a path of constant n_A and n_B, vertically in Figure 6, so that in any phase

$$G'_A - G''_A = -\frac{RT}{2}\int_{\ell n P'_{O_2}}^{\ell n P''_{O_2}}\left(\frac{\delta n_O}{\delta n_A}\right)_{G_O,\,n_B} d\,\ell n P_{O_2} \tag{13}$$

For phases with a fixed oxygen/metal atom ratio, the partial derivative within the integral is equal to that ratio. If the ratio varies with oxygen pressure, the integration is more complex.

1127

UTILITY OF STABILITY DIAGRAMS

The limited use of stability diagrams to date in systems containing two or more metallic components is probably due to their limited availability and that few people have thought about what to do with them even if they were available.

These diagrams should be most useful for analyzing phase equilibria and reaction paths in systems open with respect to the non-metallic components. This would involve such systems as the oxidation, sulfidation, or carburization of alloys and the roduction of ores.

Figure 7 shows a reaction path and accompanying microstructure for the oxidation of a hypothetical binary alloy. If continuous protective scale layers are formed and local equilibrium assumed at all interfaces, the oxide-gas interface can be represented by a point somewhere along an oxygen isobar. The value of X_B at this point will depend on the original alloy composition, solid state diffusion rates in the underlying oxide and metal phases, and the reaction kinetics at the oxide-gas interface early in the process. A planar two phase boundary is represented by a path along a two-phase tie line. A two phase scale or internal oxidation is represented by a reaction path that crosses tie lines. If the metallic components are conserved (no volatile metal bearing species formed), any deviation of the reaction path to one side of the vertical X_B line representing the original alloy must be balanced by having part of the path lie on the other side as well. For an oxidation process controlled by solid state diffusion for all $t > 0$, the reaction path will be constant. If surface reaction kinetics were rate-limiting at early stages of the reaction, the path could be time-dependent.

SUMMARY

Stability diagrams are an attractive alternative representation of phase equilibria in systems containing both metallic and non-metallic components. They can be calculated from plots of Gibbs free energy versus metal composition at constant temperature and non-metal chemical potential. Their utility should increase as more diagrams become available.

REFERENCES

1. A. D. Pelton and H. Schmalzried: Met. Trans., 1973, Vol. 4, p. 1395.

2. H. Schmalzried and A. D. Pelton: Ber. Bunsenges Phys. Chem., 1973, Vol 77, p. 90.

3. A. D. Pelton and W. T. Thompson: Progress in Solid State Chemistry, 1975, Vol. 10, p. 119.

4. J. Sticher and H. Schmalzried: Report to the Institut fur Theoretische Huttenkunde und Angewandte Physikolische Chemie der Technischen Universitat Clausthol, May 1975.

5. J. Sticher and H. Schmalzried: Arch. Eisenhuttenw., 1976, Vol. 47, p. 261.

6. R. Schuhmann: Acta Met., 1955, Vol. 3, p. 219.

7. T. Wada, H. Wada, J. F. Elliott, and J. Chipman: Met. Trans., 1972. Vol. 3, p. 2865.

8. R. Benz, J. F. Elliott, and J. Chipman: Met. Trans., 1974, Vol. 5, p. 2235.

9. C. T. Fujii and R. A. Muessner: Trans. Met. Soc. AIME 1968, Vol. 242, p. 1259.

10. K. T. Jacob and C. B. Alcock: Met. Trans. B, 1975, Vol. 68, p. 215.

11. T. Katsura and A. Muan: Trans. Met. Soc. AIME, 1964, Vol. 230, p. 77.

12. P. Riband and A. Muan: Trans. Met. Soc. AIME, 1964, Vol. 230, p. 88.

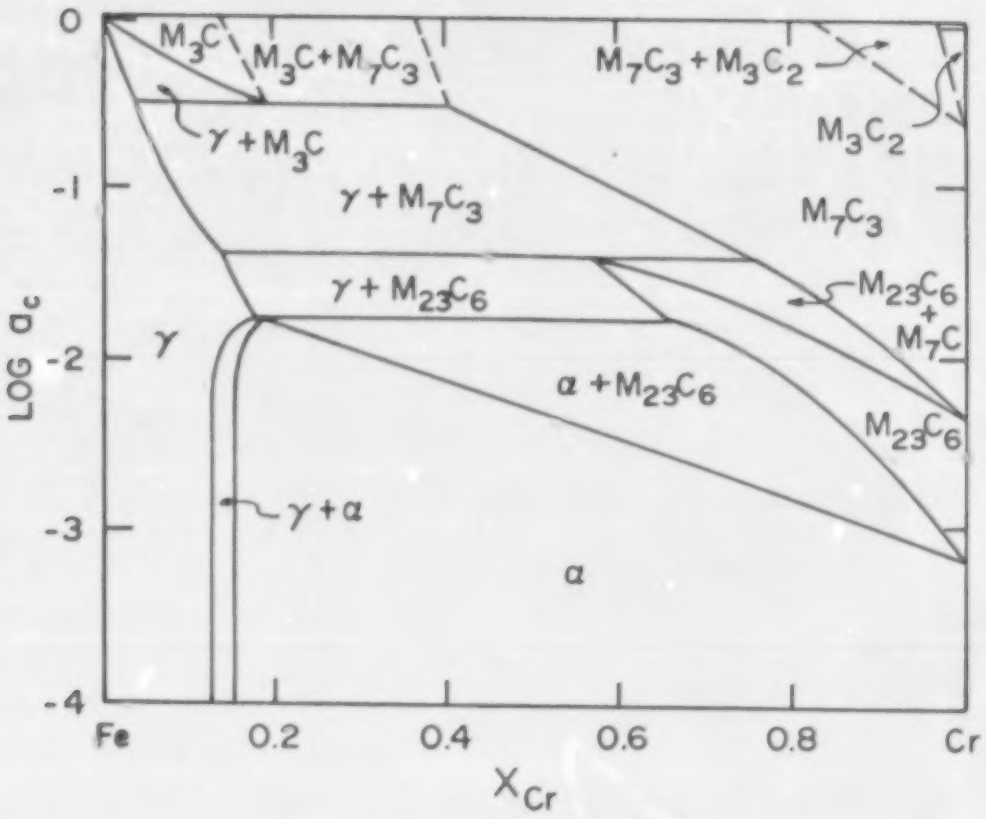

Figure 1. Stability diagram for the Fe-Cr-C system at 1273°K adjusted to match measured phase equilibria [7,8].

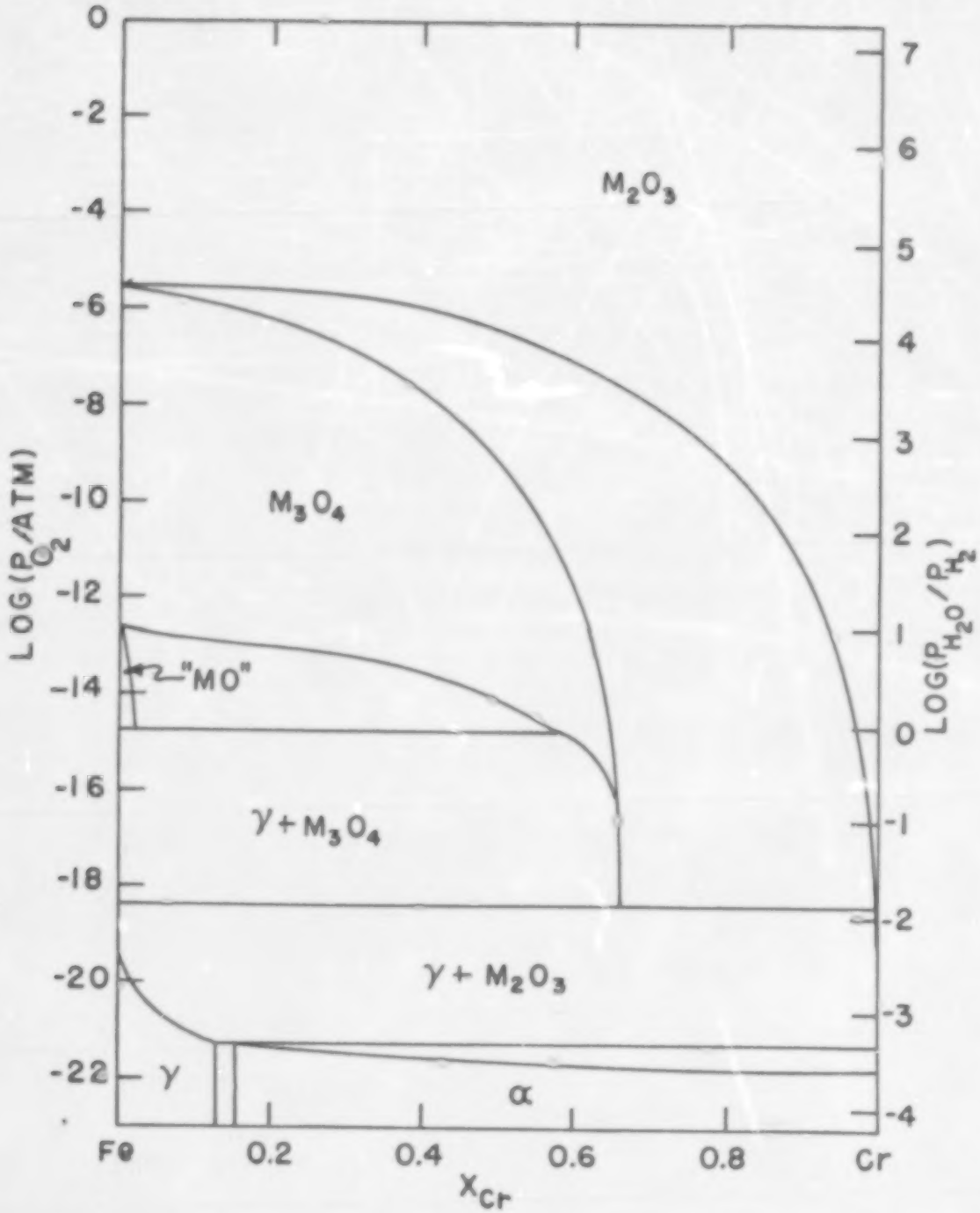

Figure 2. Stability diagram for the Fe-Cr-O system at 1273°K adjusted to match measured phase equilibria [9, 10].

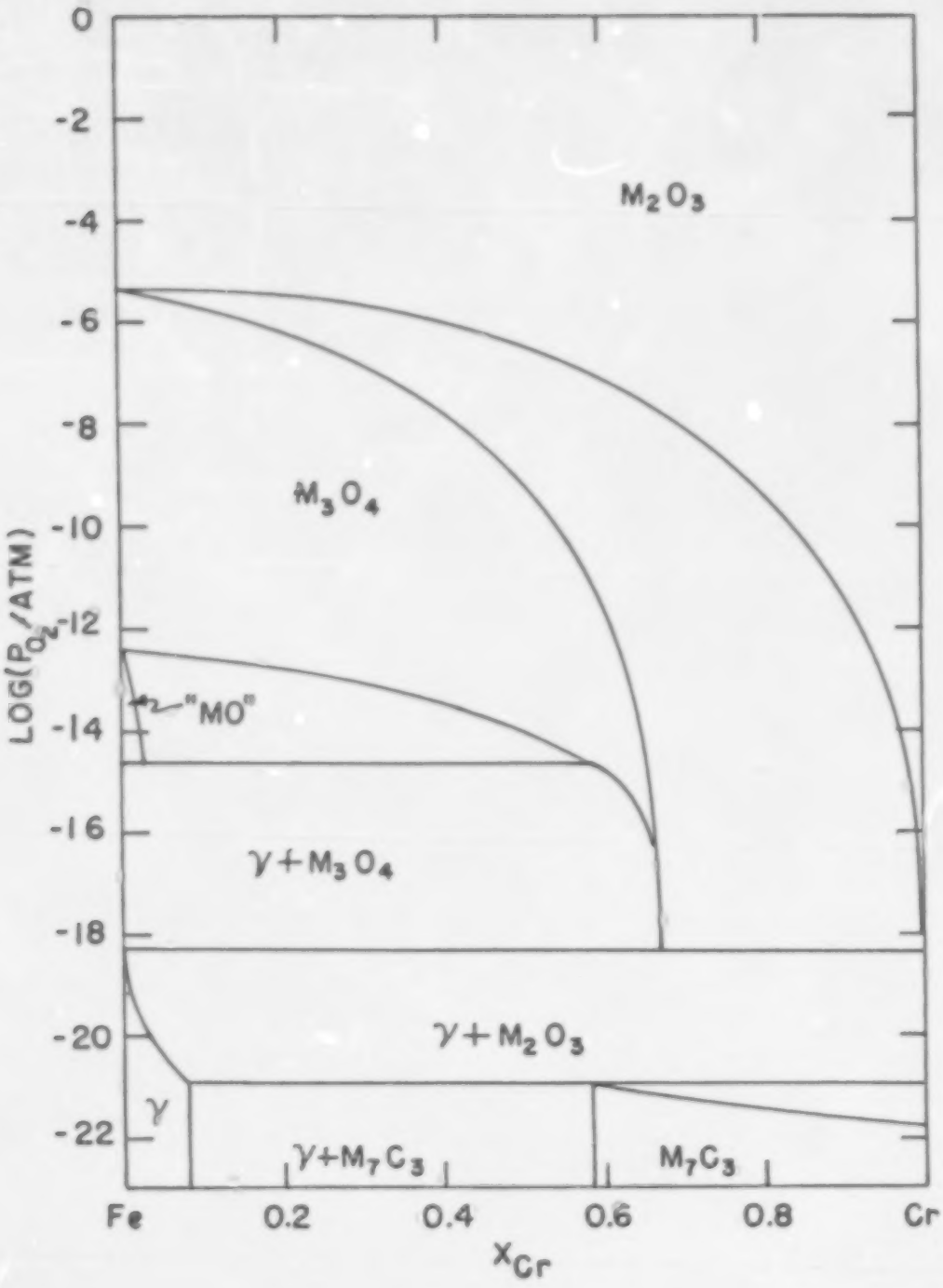

Figure 3. Stability diagram for the Fe-Cr-O-C system at 1273°K at $a_c = 0.1$.

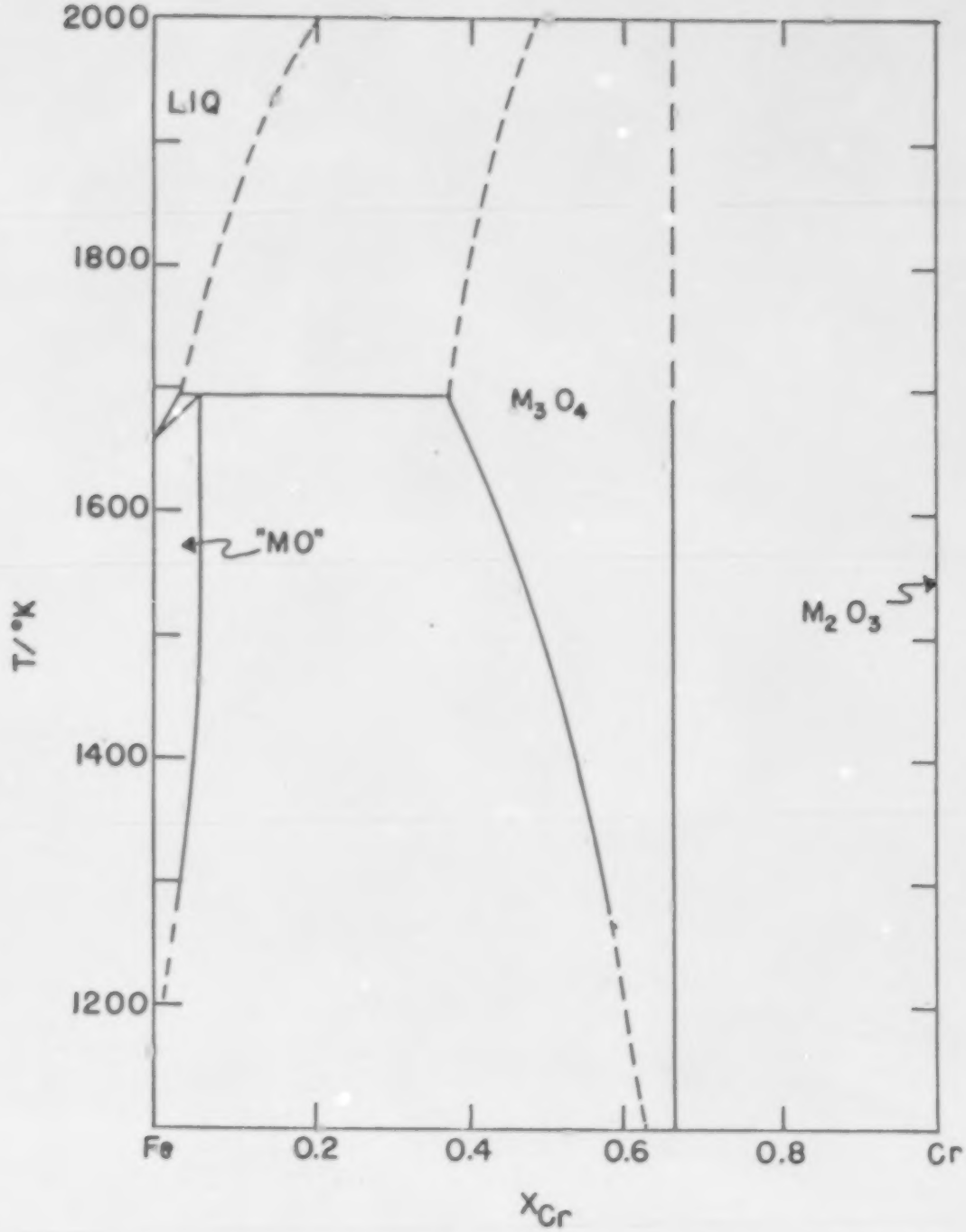

Figure 4. Stability diagram for the Fe-Cr-O system for CO_2/H_2 pressure ratio of 1.0 adjusted to match measured phase equilibria[9,12]

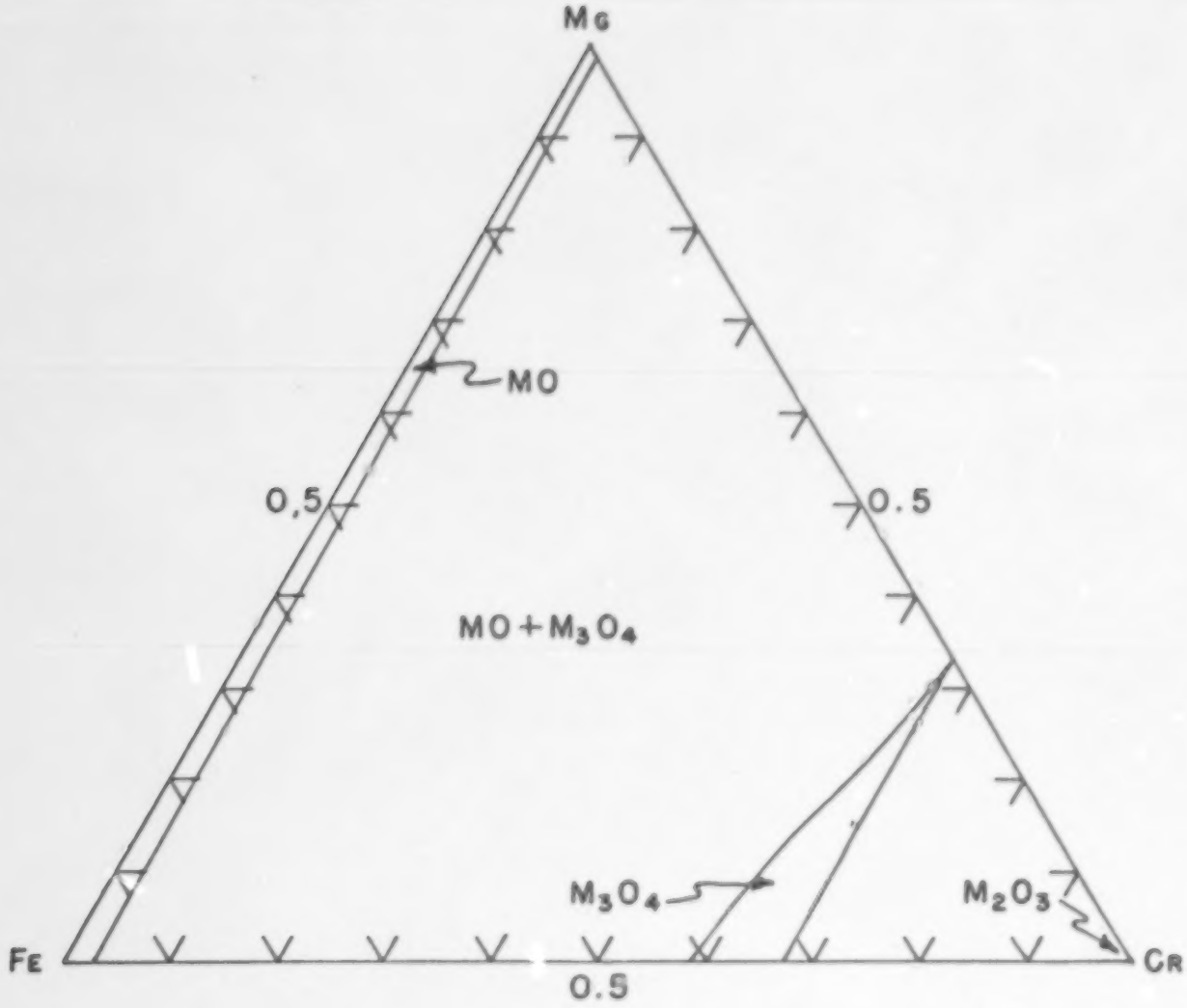

Figure 5. Stability diagram for the Fe-Cr-Mg-O system at 1273°K and $P_{O_2} = CO_2/H_2$ pressure ratio of 1.0.

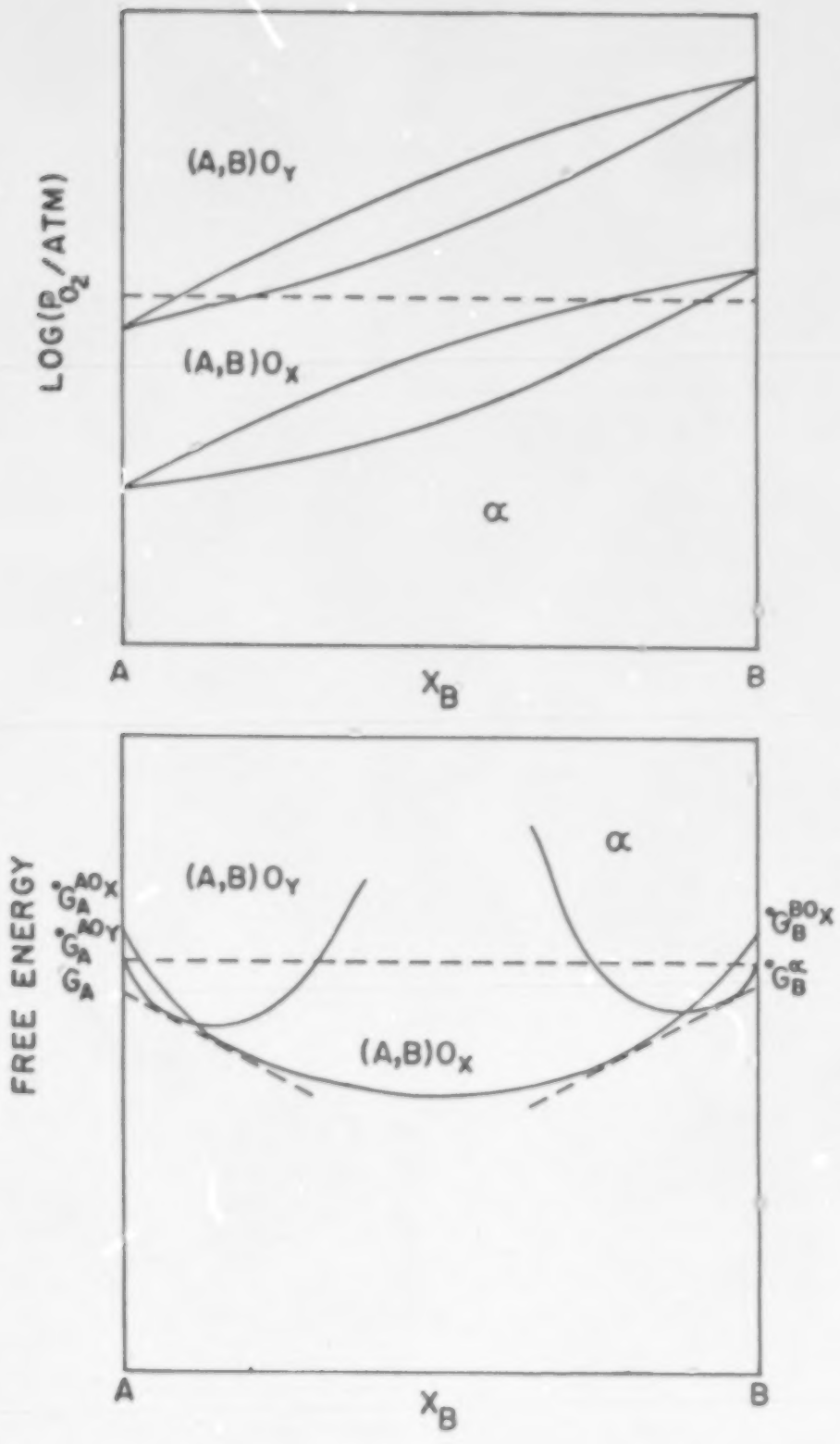

Figure 6. Isothermal stability diagram for a hypothetical A-B-O system.

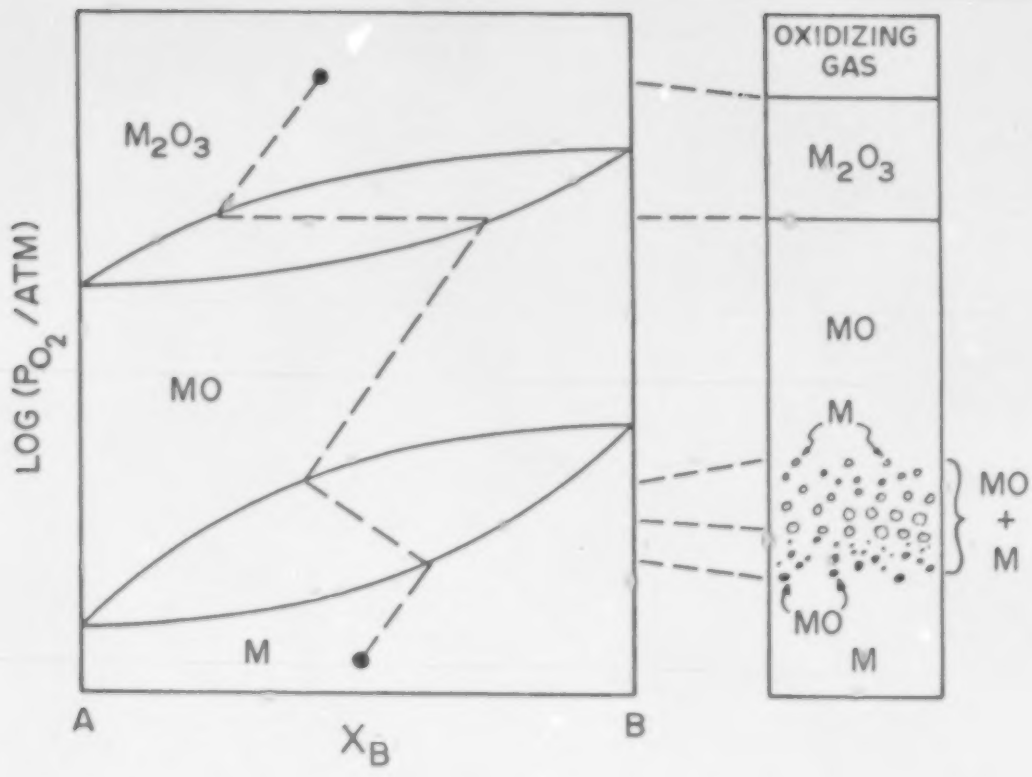

Figure 7. Reaction path and microstructure for oxidation of a hypothetical A-B alloy.

National Bureau of Standards SP-496, Applications of Phase Diagrams in Metallurgy and Ceramics
Proceedings of Workshop held at NBS, Gaithersburg, Md., January 10-12, 1977

UNITED KINGDOM ATOMIC ENERGY AUTHORITY
REACTOR FUEL ELEMENT LABORATORIES SPRINGFIELDS

THE EFFECT OF IRRADIATION ON PHASE STABILITY

L Kaufman,* J S Watkin,† J H Gittus† and A P Miodownik‡

(*MANLABS USA; †UKAEA, RFL Springfields; ‡University of Surrey, UK)

INTRODUCTION

In a recent paper Watkin[1] has noted large variations in the neutron induced void swelling behaviour of a range of annealed austenitic alloys, irradiated to 30 dpa at 600°C in the Dounreay Fast Reactor. These data were analysed in terms of the calculated fraction of sigma phase expected to be present under isothermal conditions from which it was concluded that swelling tended to increase with sigma content. [Fig. 1]

An increasing amount of evidence has now accumulated showing that this assumption may not be tenable. Brown[4] has been unable to detect the presence of sigma-phase in M316** fuel pin cladding irradiated in the Dounreay Fast Reactor at any temperature up to 973 K although this is a temperature range where sigma phase formation is both regularly observed in this alloy, in the absence of irradiation, and predicted by calculated phase diagrams. Instead an ordered fcc phase has been discovered [5] in specimens irradiated at temperatures less than 823 K. At the time of writing some doubt exists as to the precise composition of the phase. Initially it was thought to be $Ni_3(Fe,Mn)$ but more recently it is thought more likely to be based on Ni_3Si. A similar phase is predicted to occur on the calculated ternary diagrams at temperatures below 823 K but not in the 316 composition range. Bilsby[6] has observed an ordered phase in an M316 specimen irradiated by Watkin to 25 atomic displacements per atom at 773 K and has noted the absence of sigma-phase in the same specimen. It is also significant that under normal circumstances 316-type stainless steel is non-magnetic but many reports exist to suggest that after irradiation alloys of this type are slightly magnetic. Cawthorne and Brown[5] suggest that the ordered phase which is magnetic, may be in part responsible for some of the magnetism exhibited by M316 after irradiation, although they have commented that irradiated specimens not containing that phase are also magnetic. Baron, Cadalbert and Delaplace[7] found abnormal magnetism in a 316L (low carbon version of AISI-316 type

**M316 is a UKAEA specification for 316-type stainless steel in which tighter control is kept on the major alloying constituents.

1137

stainless steel) hexagonal tube irradiated in the Rapsodie Fast Reactor, and have tentatively suggested the magnetic behaviour may be due to the formation of a bcc-phase caused by the presence of hydrogen formed from (n,p) transmutations with the major alloying constituents, without however giving direct evidence for their suggestion.

There are therefore three unequivocal facts which must be taken into consideration in the case of irradiated stainless steel:

(a) the non-appearance of sigma-phase at temperatures and durations where this would be observed without irradiation.

(b) the appearance of an ordered phase in a composition range and at temperatures where it would normally not be observed without irradiation.

(c) the appearance of magnetism after irradiation both in the presence and absence of the ordered phase.

An almost parallel situation has been observed in W-Re binary alloys irradiated by Williams, Steigler and Wiffen[8] in EBR II to neutron exposures in the range 6.1 to 37.10^{21} n/cm^2 (> 0.1 MeV). They reported that after irradiation at temperatures equal to or greater than 1373 K, electron diffraction patterns showed the presence of cubic WRe_3 precipitates in an alloy (W-25 at.% Re). Published phase diagrams however predict the alloy to be single phase (bcc) at this temperature. Sigma-phase precipitation could be expected at (> 25 at.%) but WRe_3 would only be expected at Re contents greater than 60 at.%.

Irradiation therefore has a marked effect on the relative stability of certain phases in Fe-Cr-Ni ternary alloys and W-Re alloys. There are three possible reasons for these effects:

(1) That irradiation brings about the true equilibrium structure of these alloys by enhancing diffusion which under normal circumstances would be too slow (at the temperatures in question).

(2) That irradiation changes the relative free energy of various phases by differentially increasing the concentration of defects. This is analogous to the Wigner energy phenomenon in graphite irradiations.

(3) That irradiation inhibits the formation of some phases by bombardment processes which physically knock precipitate atoms back into solution.

In this paper we confine ourselves to determine the changes in the free energy of sigma-phase and Ni_3Fe that are required firstly, to suppress the formation of sigma-phase at the 316 composition for temperatures between 673-873 K and secondly to enhance the stability of Ni_3Fe to encompass the 316 composition for temperatures below 823 K.

THE EFFECT OF VARYING THE FREE ENERGY OF SIGMA-PHASE

The free energy of sigma phase has been formulated by Kaufman and Bernstein[2] and Kaufman and Nesor[3] assuming the phase to be a line compound which runs between $Ni_{0.38}\ Cr_{0.62}$ and $Cr_{0.47}\ Fe_{0.53}$. The general composition of sigma (σ) ($Ni_{x\sigma}$, $Cr_{x\sigma}$, $Fe_{y\sigma}$) is defined by:

$$x_\sigma = 0.62 - 0.283\, y_\sigma \qquad \ldots\ldots (1a)$$

$$y_\sigma = 1 - x_\sigma - z_\sigma \qquad \ldots\ldots (1b)$$

$$z_\sigma = 1 - 0.62 - 0.717\, y_\sigma \qquad \ldots\ldots (1c)$$

The free energy of sigma (G_σ) can be expressed in terms of four components:

$$G_\sigma = \Delta G_1 + \Delta G_2 + \Delta G_3 + \Delta G_4 \qquad \ldots\ldots (2)$$

where $$\Delta G_1 = (z_\sigma\, G_{Ni}^{bcc} + x_\sigma G_{Cr}^{bcc} + y_\sigma\, G_{Fe}^{bcc}) \qquad \ldots\ldots (3)$$

$$\Delta G_2 = [1 - (y_\sigma/x_\sigma)]\, \Delta G_A + [y_\sigma/(1 - x_\sigma)]\, \Delta G_B \qquad \ldots\ldots (4)$$

$$\Delta G_3 = RT\, [y_\sigma \ell n y_\sigma + z_\sigma \ell n z_\sigma - (1 - x_\sigma)\ell n(1 - x_\sigma)] \qquad \ldots\ldots (5)$$

$$\Delta G_4 = C^* y_\sigma\, (0.38 - 0.717\, y_\sigma)/(0.38 + 0.283\, y_\sigma) \qquad \ldots\ldots (6)$$

These four terms can be identified with the characteristics of bcc phase from which sigma derives (ΔG_1); compound parameters specifically associated with the binary sigma phases (ΔG_2); a mixing term (ΔG_3); and finally a ternary excess free energy term (ΔG_4). For the purpose of the current exercise, the free energy of the sigma phase has been varied by altering C*, leaving all other parameters in equation (2 – 6) the same. Table 1 shows the effect of changing C* on the relative stability of sigma-phase at 873 K as measured by its intrusion into the ternary section: the values being obtained from figures 2a to 2d.

Because changes in G_σ caused by varying C* depend upon the precise composition of sigma-phase in equilibrium with the matrix, the free energy increases in Table 1 refer to the composition of sigma-phase at the point of maximum intrusion into the ternary in the reference unirradiated state.

TABLE 1

The effect of changing C* on the relative stability of sigma phase in the Fe-Cr-Ni system at 873 K

Ternary excess parameter C* cal/g.at	Increase in G_σ cal/g.at (J/g.at)	Relative intrusion of sigma phase into theternary	Comments
- 1000	0	1	Reference state corresponding to normal conditions.
+ 1500	233 (975)	½	Arbitary increase in C* until sigma tends to zero.
+ 4000	475 (1987)	1/10	

This exercise was repeated at 673 K, which revealed that sigma-phase was suppressed when C* was set at 1500 cal/g.at i.e. only ~ 200 cal/g.at (~ 1000 J/g at) is required at this lower temperature compared to about 500 cal/g.at (~ 2000 J/g.at) at 873 K.

THE EFFECT OF VARYING THE FREE ENERGY OF $FeNi_3$

The description of the free energy of Ni_3Fe is similar to that employed for sigma phase except in this case the compound is described as running across the nickel corner of the ternary at constant nickel (that is Ni_3Fe to Ni_3Cr). Firstly, because some doubt exists as to the precise composition of the ordered phase found on irradiation, and the distinct possibility that silicon and/or manganese could be present, it was thought prudent to investigate the influence of such an addition on the stability of Ni_3Fe before determining the energy change needed to expand the stability of Ni_3Fe to the 316 composition range. Thus preliminary calculations were carried out at 673, 723 and 773 K to estimate the effect of replacing 1.5 at.% Mn for chromium in $(Ni_{0.75}Mo_{0.25})$. (The level of 1.5 at.% Mn was chosen because such an addition is made to 316 stainless steel.) These calculations revealed an almost constant stabilising effect of Mn at 175 cal/g.at [~ 730 J/g.at] for all temperatures between 673 and 773 K. This value was translated into an equivalent change in C* (12000 cal/g.at) for $Ni_{0.75}(Fe,Cr)_{0.25}$. The effect of this change on the fcc/Ni_3Fe interaction at 673 and 723 K is shown in Figs 3(a) and 3(b). By comparing these figures with 3(c) and 3(d) [the relevant diagrams without a Mn addition], it can be seen that Mn has a potent stabilising effect on Ni_3Fe.

In figure 3(b) further fcc/Ni_3Fe interactions have been calculated with C* set at - 20000, - 22500 and - 25000 which yield a critical C* of - 23700 for the appearance of $Ni_{0.75}(FeMn)$ at the 316 composition. This value translates back to a required energy change of - 350 cal/g.at [- 1460 J/g.at].

As yet we have been unable to determine the effect of silicon (0.5 to 1.2 at.% being usual in 316-type steels), because equivalent thermodynamic data are not available, but the principles used here will be extended to include Si additions when suitable data become available.

CONSIDERATION OF ANALOGOUS CHANGES IN THE W-Re SYSTEM

The free energy curves for the body centred cubic (bcc) and the close packed hexagonal phases (cph) have been calculated for the W-Re system at 1373 K using parameters taken from reference (2), Fig. 4. The free energy of sigma-phase has also been positioned at - 6500 cal/g.at (- 27200 J/g.at) by using the 'tangent rule' in reverse i.e. taking the intersection of the tangent to the G^{bcc} curve at the upper limit of its stability range (26 at.% Re) with the lower compositional extreme of the single sigma-phase field (44 at.% Re). Similarly the free energy of X-phase ($W Re_3$) has been determined from the intersection of the tangent to the G^{cph} curve at 90 at.% Re with the composition $W Re_3$ (W-75 at.% Re) assuming the phase to be a line compound.

For $W Re_3$ to form at the composition W-25 at.% Re, as occurred in Williams experiments,[8] the free energy of sigma-phase must have increased relative to the other phases. The minimum increase is 1500 cal/g.at (6250 J/g.at) and is given by the construction AB in Fig. 4. An alternative view would be that the free energy of $W Re_3$ has been reduced by about 3500 cal/g.at (14650 J/g.at) as shown by the construction CD.

These figures are much higher than the values deduced for the effect of irradiation in the Fe-Cr-Ni system. However further inspection of Fig. 4 shows that the free energy of $W Re_3$ is very sensitive to the slope of the G^{cph} curve where the tangent is drawn (90 at.% Re) and any variation here could have a marked effect on the figures quoted above.

Fuller details of these and other similar calculations will be published in due course.

SUMMARY AND CONCLUSIONS

The aim of this paper has been to determine changes in the free energy of sigma-phase and Ni_3Fe that are required firstly, to suppress the formation of sigma-phase at the AISI 316 composition for temperatures between 673 and 873 K and secondly, to enhance the stability of Ni_3Fe to encompass the 316 composition for temperatures below 823 K; that is, to tailor the Fe-Cr-Ni ternary equilibrium diagram to fit the observations made after irradiation in a fast reactor.

It has been calculated that an increase in free energy of 250-500 cal/g.at (1000-2000 J/g.at) is required to suppress the appearance of sigma-phase in the temperature range 673-873 K. Similarly Ni_3Fe requires a reduction in free energy of 350-500 cal/g.at (1500-2000 J/g.at) to account for its appearance in the range 673-773 K.

In the analogous W-Re binary system, energy changes of somewhat higher values are required 1500-3500 cal/g.at (6500-14500 J/g.at) to account for the observed structural changes on irradiation at 1373 K.

It is envisaged that the establishment of the order of magnitude for such changes will aid the determination of an appropriate mechanism for the required energy change, and the design of alloys with maximum resistance to phase transformations under irradiation.

REFERENCES

1. WATKIN J S. Dependence of void swelling on the electron vacancy concentration. ASTM STP611 1976.

2. KAUFMAN L and BERNSTEIN H. Computer calculation of phase diagrams. Academic Press 1970.

3. KAUFMAN L and NESOR H. Relation of thermochemistry and phase diagrams of condensed systems. Treatise on solid state chemistry. Vol. 5 Changes of State, Plenum Press 1975.

4. BROWN C (private communication).

5. BROWN C and CATHORNE C. Journal of Nuclear Materials (to be published).

6. BILSBY C F (private communication).

7. BARON J L, CADALBERT R and DELAPLACE J. J. Nuclear Materials 1974 51 p266.

8. WILLIAMS R K, STEIGLER J O and WIFFEN F W. Irradiation effects in tungsten-rhenium alloys. ORNL-TM-4500, 1974.

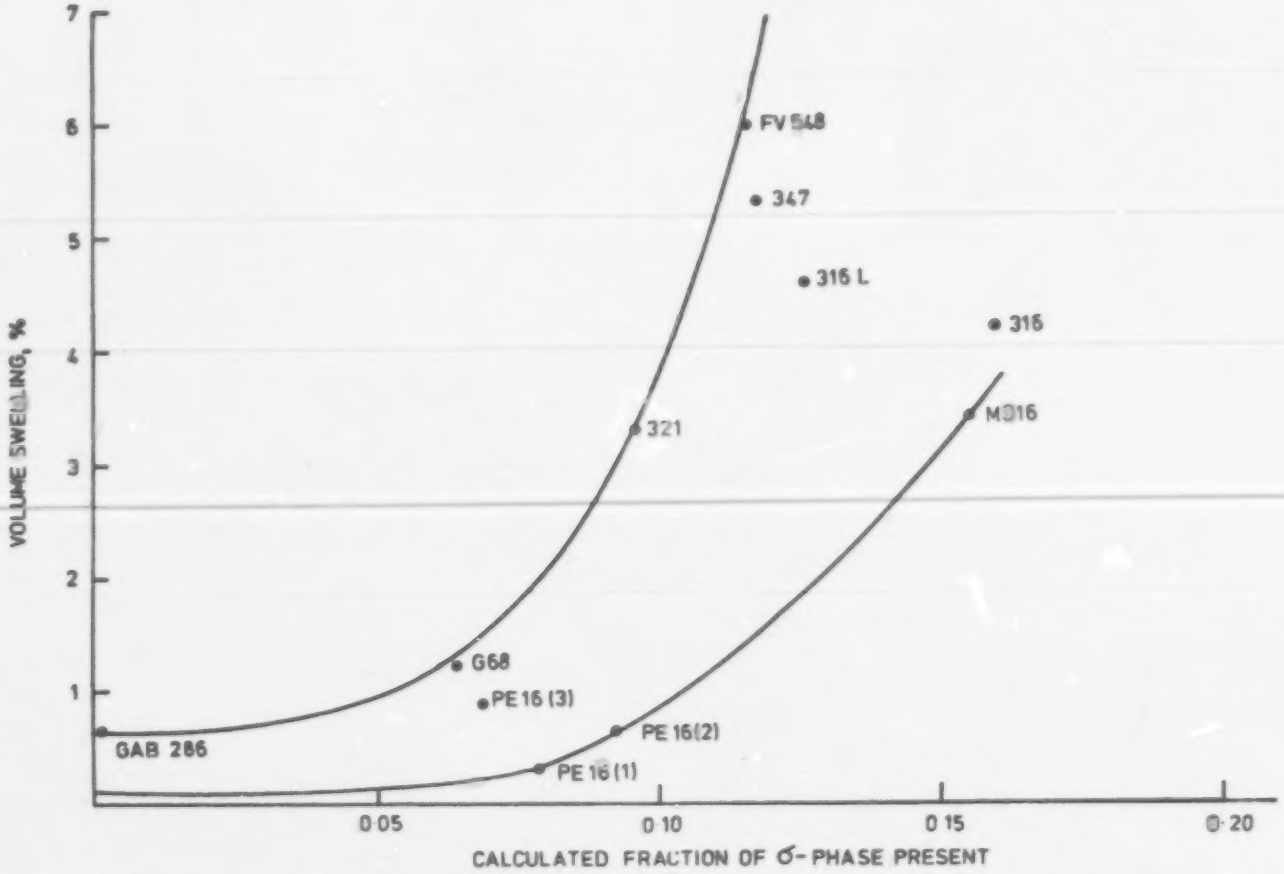

FIG.1. SWELLING AT 30 dpa AND 600°C AS A FUNCTION OF CALCULATED SIGMA CONTENT

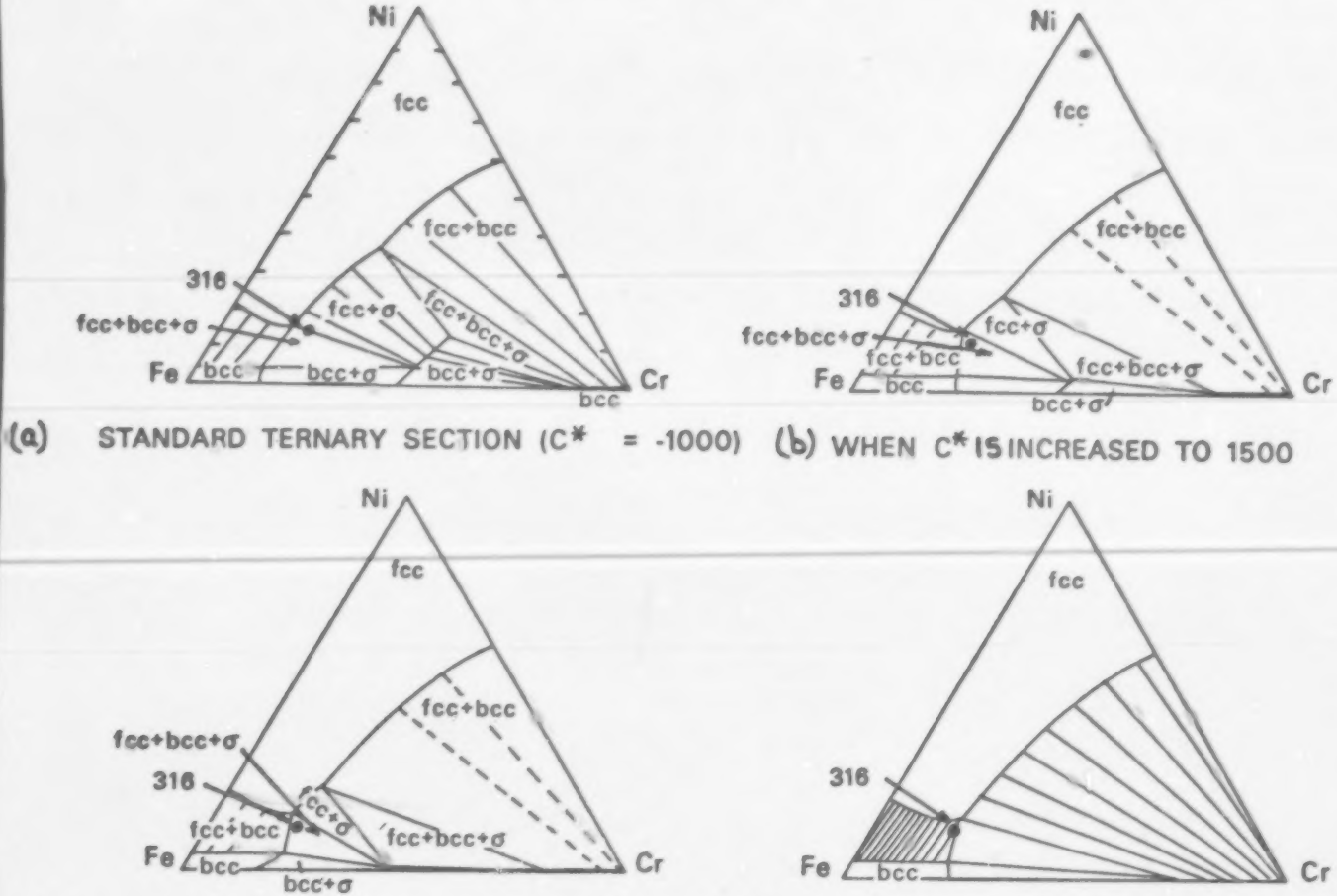

(a) STANDARD TERNARY SECTION (C^* = -1000) (b) WHEN C^* IS INCREASED TO 1500

(c) WHEN C^* IS INCREASED TO 4000 (d) WHEN C^* IS INCREASED TO > 4000

FIG2. THE EFFECT OF DECREASING THE STABILITY OF SIGMA PHASE ON THE Fe-Cr-Ni TERNARY AT 600°C (873 K)

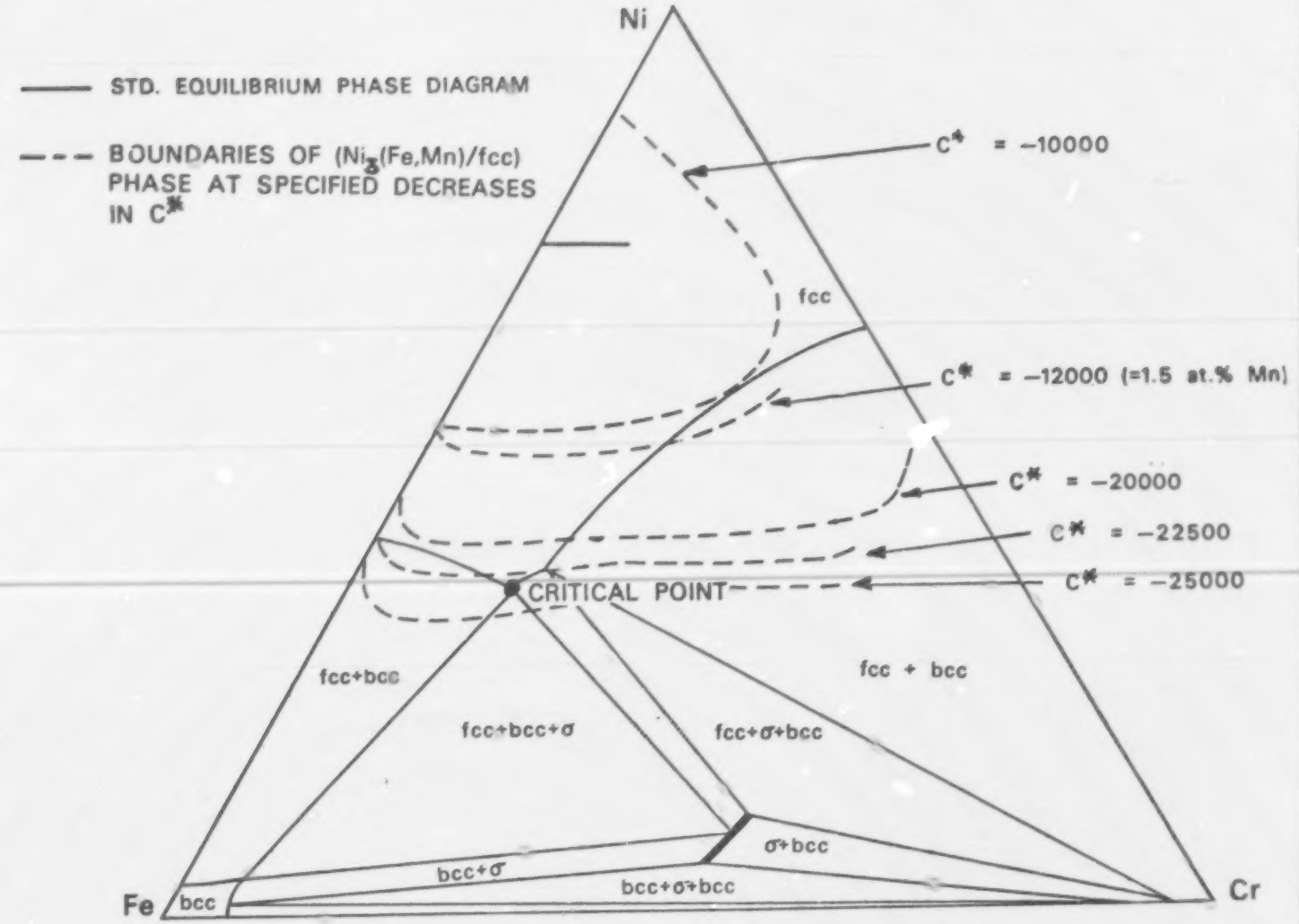

3(a) THE EFFECT OF 1.5 at % Mn ADDITION (C* = −12000) ON THE fcc/Ni_3(Fe,Mn) INTERACTION AT 400°C (673 K)

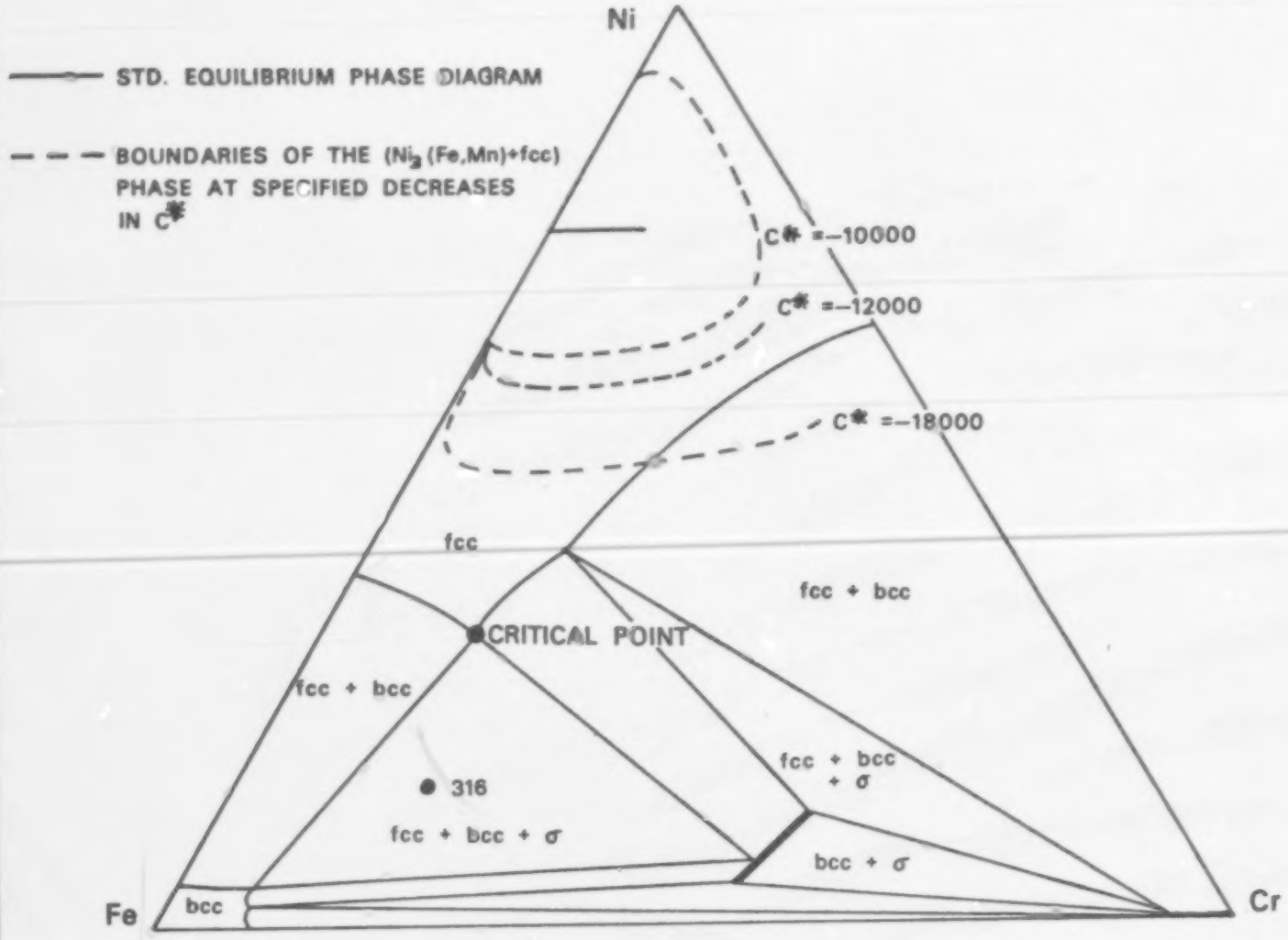

3(b) THE EFFECT OF 1.5 at % Mn ADDITION (C* = –1200) ON THE fcc/Ni_3(Fe, Mn) INTERACTION AT 450°C (723K)

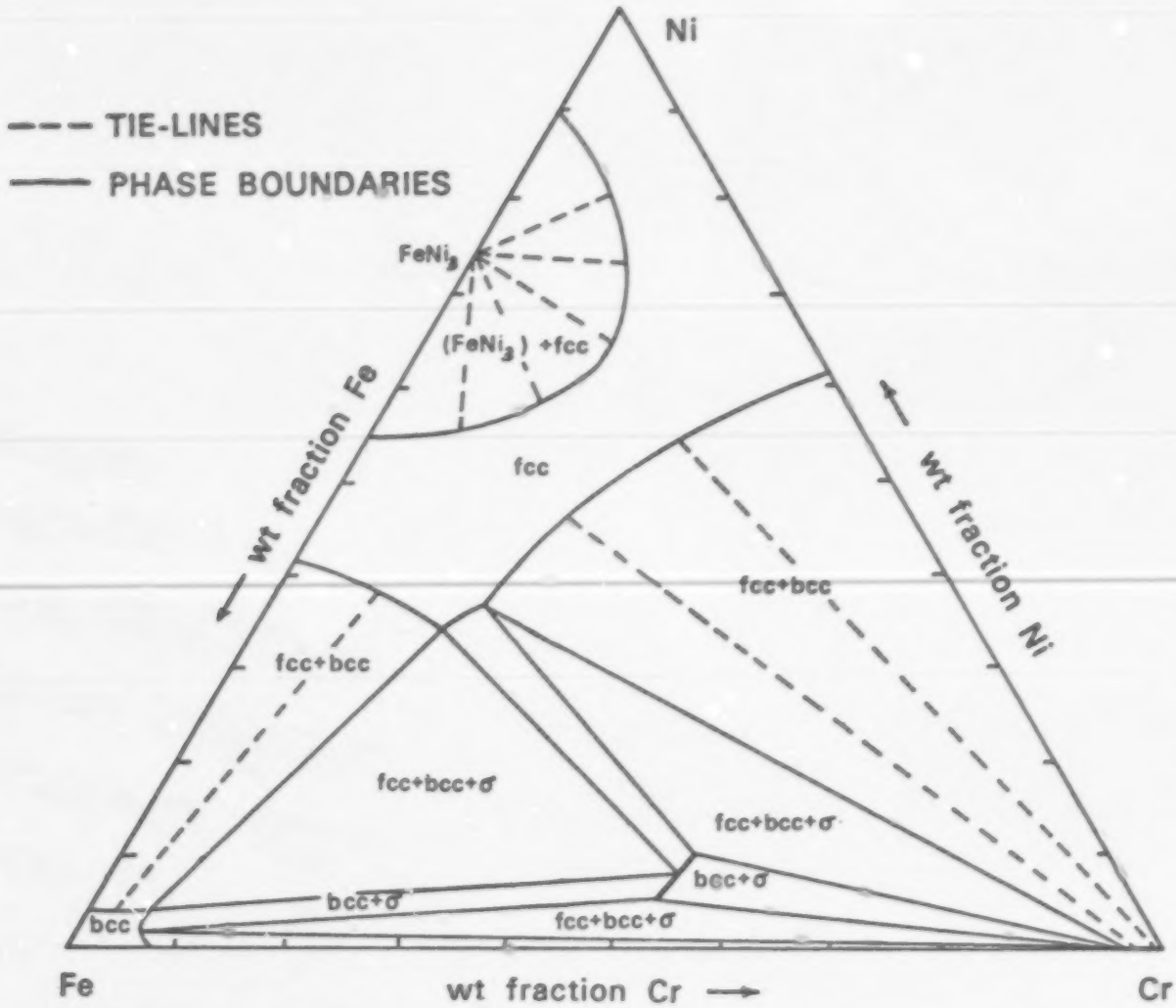

3(c) CALCULATED ISOTHERMAL SECTION OF Fe-Cr-Ni TERNARY DIAGRAM AT 400°C(673K)

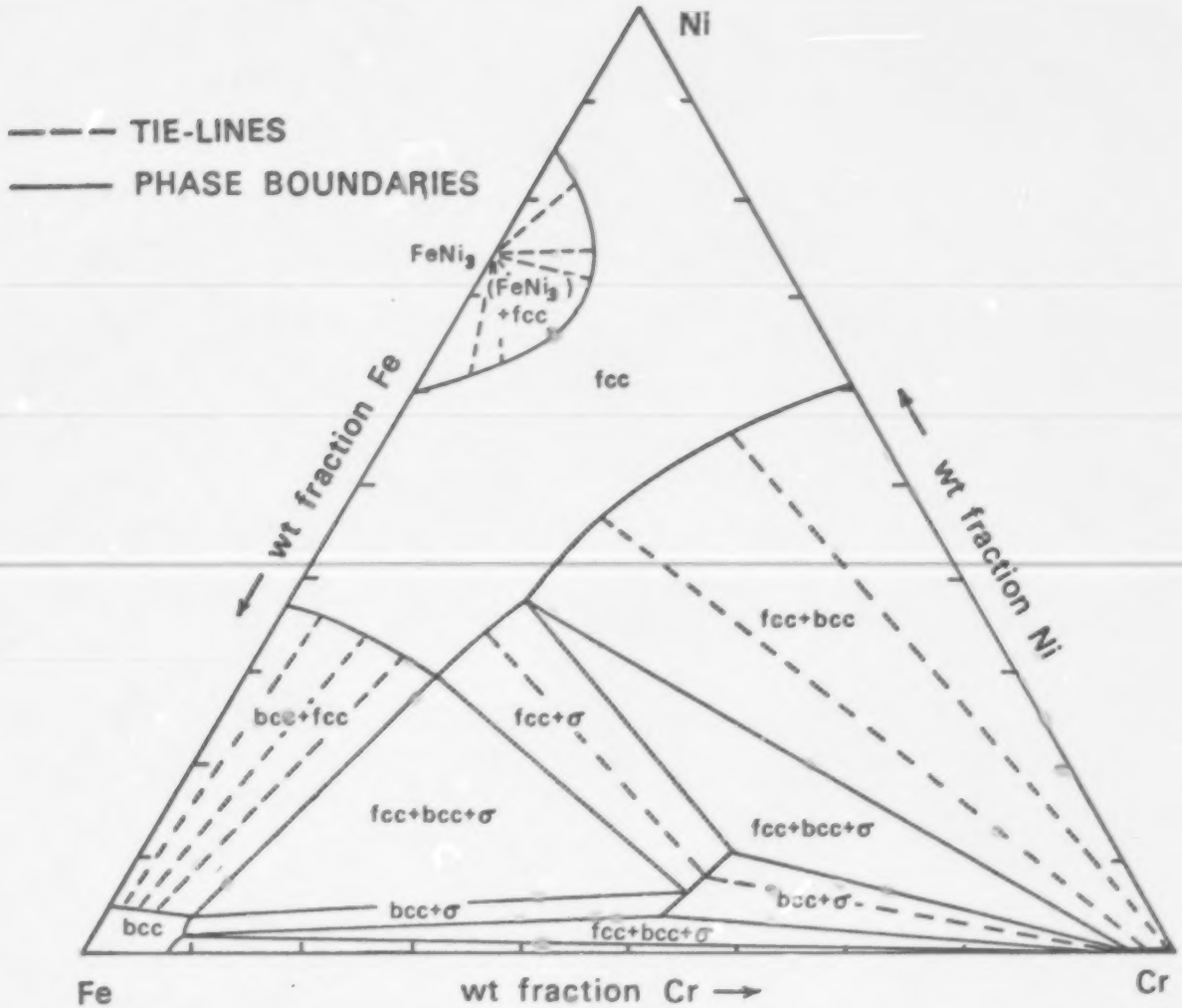

3(d) CALCULATED ISOTHERMAL SECTION OF Fe-Cr-Ni TERNARY DIAGRAM AT 450°C (723 K)

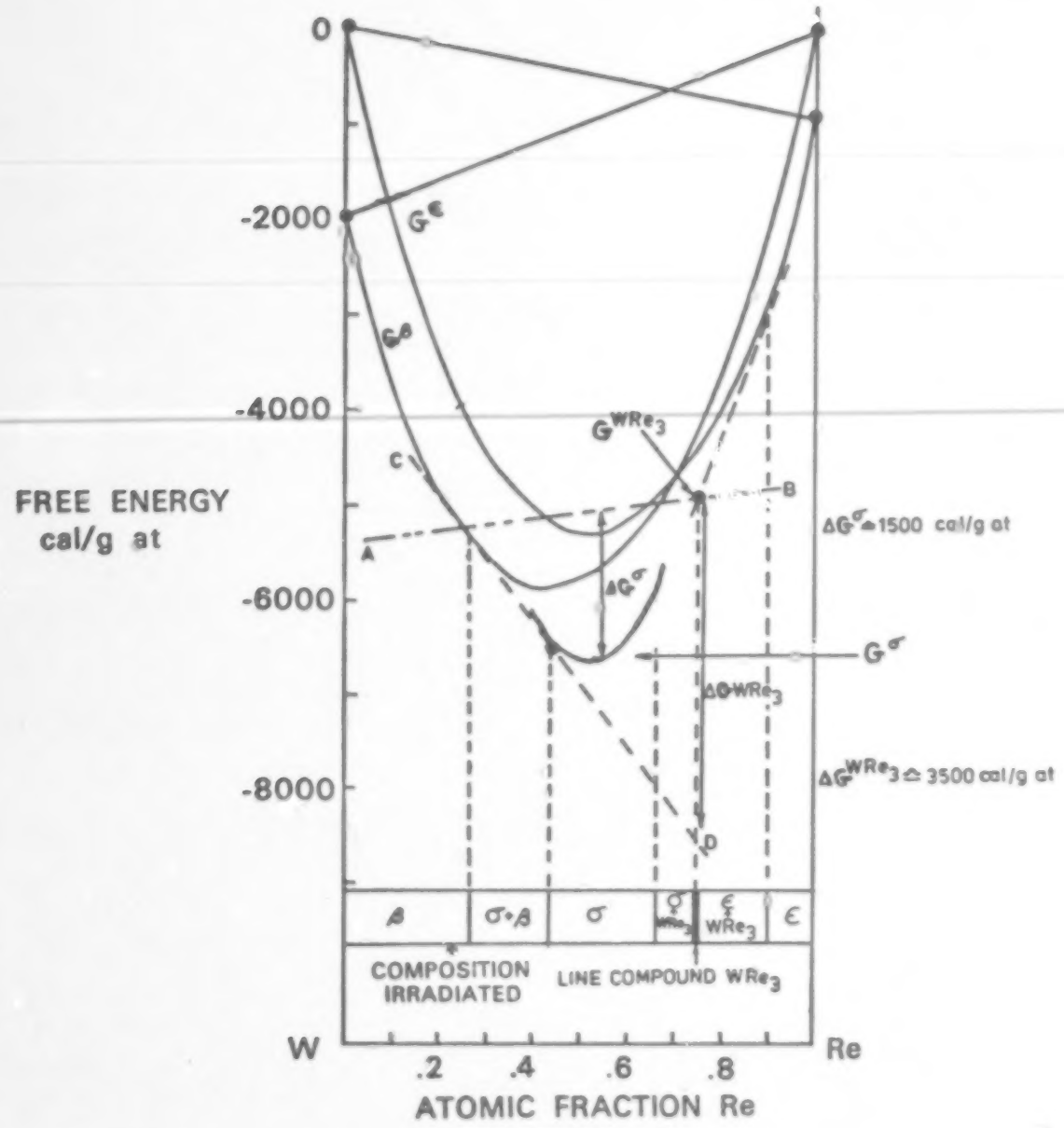

FIG 4 CALCULATED FREE ENERGY - COMPOSITION RELATIONS FOR bcc (β), hcp (ϵ), SIGMA (σ) AND W-Re_3 FOR THE THE W-Re BINARY SYSTEM AT 1100°C (1373 K) 1148

National Bureau of Standards SP-496, Applications of Phase Diagrams in Metallurgy and Ceramics
Proceedings of Workshop held at NBS, Gaithersburg, Md., January 10-12, 1977

F*A*C*T

(FACILITY FOR THE ANALYSIS OF CHEMICAL THERMODYNAMICS)

- A COMPUTERIZED CANADIAN THERMODYNAMIC DATA TREATMENT CENTRE -

A.D. Pelton, C.W. Bale,

Département de génie métallurgique,
Ecole Polytechnique (Université de Montréal),
Montréal, Québec, Canada

W.T. Thompson

Department of Mining and Metallurgical Engineering,
McGill University,
Montréal, Québec, Canada

ABSTRACT

The present state of development of F*A*C*T (Facility for the Analysis of Chemical Thermodynamics), a thermodynamic data treatment centre based in Canada, is described. Users at remote terminals, contacting the system via telephone hook-up, will be able to perform many different thermodynamic calculations using the computer in full conversational mode. The calculations will employ a system data base and/or user-supplied data. A major part of F*A*C*T is devoted to the calculation of phase diagrams with the resulting output printed on the user's terminal. These programs are briefly discussed in this article. These calculate (a) potential-potential phase diagrams for 2-, 3-, 4- and 5-component systems (such as predominance area, Ellingham, stability, combination, and Pourbaix diagrams, etc.); (b) potential-composition diagrams for 2-, 3-, and 4-component systems (such as temperature-composition and chemical potential-composition phase diagrams); and (c) chemical reaction paths (calculations of isothermal, adiabatic, isentropic, etc. chemical reaction paths as well as of the conditions for chemical equilibria). The use of these programs has been illustrated by the calculation of various phase diagrams and reaction paths in the Fe-Ni-S-O system. It is planned to have F*A*C*T on-line with these three programs, with a limited data base, by the end of 1977.

INTRODUCTION

Although the principles of thermodynamic analysis are well-established and its importance is unchallenged, the vast body of thermodynamic data now available is not being put to its best use because the calculations involved are tedious and very time-consuming, usually requiring the knowledge of a specialist.

This article describes the present state of development of F*A*C*T (Facility for the Analysis of Chemical Thermodynamics) - a thermodynamic data treatment centre based in Canada. Users at remote terminals, contacting the system via telephone, will be able to perform many different thermodynamic calculations in conversational mode. All input and output (including graphical output) will be on the remote terminals. The user will not need a CALCOMP or other plotter in order to generate a phase diagram. Calculation will be performed with the use of the system's data base and/or with user-supplied data.

At present, three calculating/plotting programs are in an advanced stage of

1077 1143

development. It is expected that these will be available on-line with a limited data base by the end of 1977. Two of these programs are for the computation and subsequent graphical representation of potential-potential phase diagrams and potential-composition phase diagrams. The third program calculates changes in all of the thermodyanic properties associated with a chemical reaction.

The use of F*A*C*T will now be illustrated for the analysis of heterogeous and homogeneous equilibria in the Fe-Ni-S-O system.

Consider the four independent variables temperature, T; relative chemical potential of oxygen, $RT\ln p_{O_2}$; relative chemical potential of sulfur, $RT\ln p_{S_2}$; and molar metal ratio, $\xi = n_{Ni}/(n_{Ni} + n_{Fe})$ (where n_i = number of moles). If one of these four variables is held constant, a space diagram with the other three as axes can be drawn. (Strictly speaking, the total hydrostatic pressure must also be held constant.) For example, in Fig. 1a is the space diagram T-$RT\ln p_{O_2}$ - ξ at a very low constant p_{S_2}. On the left face of this figure would appear the Ellingham diagram for the Fe-O system (Fig. 4). On the right face would appear the Ellingham diagram for the Ni-O system. These are potential-potential phase diagrams (thermal potential versus chemical potential) in which areas represent one-phase equilibria, lines represent two-phase equilibria, and points represent three-phase equilibria. On the front face, at a constant p_{O_2} sufficiently low that no oxide phases occur, would appear the binary temperature-composition phase diagram for the Fe-Ni system (Fig. 8). This is a potential-composition phase diagram (the potential, in this case, being the thermal potential) in which two-phase equilibria are represented by horizontal tie-lines. In Fig. 1b is the space diagram $RT\ln p_{O_2}$ - $RT\ln p_{S_2}$ - ξ at constant T. On the right and left faces of this diagram would appear the "predominance area phase diagrams" for the Ni-S-O (Fig. 2) and the Fe-S-O systems. These are potential-potential phase diagrams (chemical potential versus chemical potential). On the front face (at very low constant p_{S_2}) would appear the $RT\ln p_{O_2}$ - ξ phase diagram for the Fe-Ni-O system at constant T (Fig. 10). This diagram is a potential-composition phase diagram and obeys the rules of construction of this type of phase diagram.

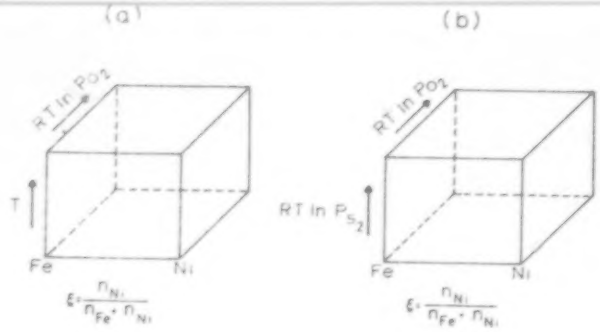

FIG. 1. Space diagrams for the Fe-Ni-S-O system (a) $RT\ln p_{S_2}$ = constant $\ll 0$ (b) T = constant.

An infinite number of other space diagrams for this quaternary system could be drawn. The traces of two-dimensional sections through these space diagrams often yield phase diagrams of the potential-potential or potential-composition type. We may, for example, be interested in a vertical section through Fig. 1a but at a sufficiently high partial pressure of oxygen that oxide phases also appear (Fig. 9). Slices through Fig. 1b at constant p_{SO_2} would also be of interest (Fig. 5). Useful diagrams also result if the independent variables are redefined. We may, for example, be interested in a potential-potential phase diagram of $RT\ln p_{SO_2}$ versus $RT\ln p_{O_2}$ at constant T (Fig. 3).

All these potential-potential or potential-composition sections can easily be calculated with F*A*C*T as will be illustrated in the present article. Furthermore, with the reaction path program, the parameters of the chemical reaction between any two points can be investigated.

The theory of the geometry of various types of phase diagram representations and the detailed procedures involved in calculating these diagrams from thermodynamic data have been discussed previously (1,2).

POTENTIAL-POTENTIAL PHASE DIAGRAMS

In Fig. 2 is the computer-generated "predominance area" phase diagram, $\log_{10}P_{S_2}$-$\log_{10}P_{O_2}$, for the Ni-S-O ternary system at a constant T = 1000 K. A listing of the interactive conversation between the user and computer which generated this particular diagram is given in Table I.

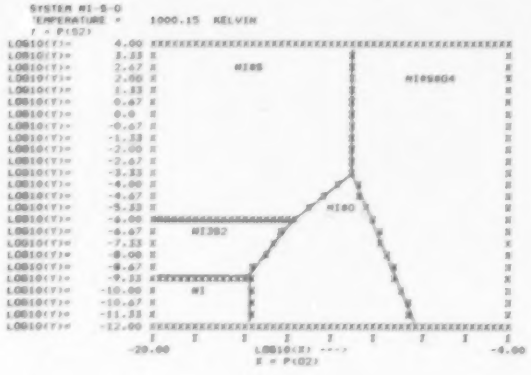

FIG. 2 Predominance area phase diagram for Ni-S-O (Solid lines have been added by hand).

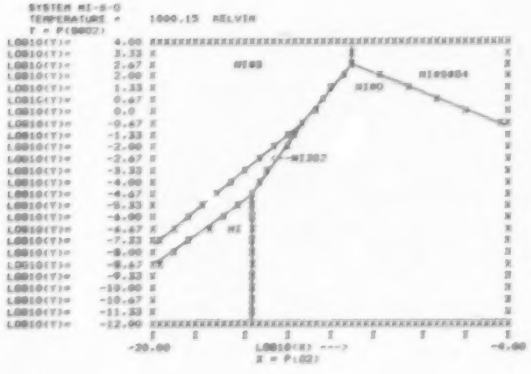

FIG. 3 Predominance area phase diagram for Ni-S-O (Solid lines have been added by hand).

TABLE I

Conversational input used to generate Figs 2 & 3.

1151

It can be seen from Table I that, having called the program, the user has indicated the column width of his terminal, and that he wishes to generate potential-potential diagrams of the three component system, Ni-S-O. The computer has replied that such diagrams for this system can be computed if the user identifies and defines a vertical axis, a horizontal axis, and one independent constant. From the phase rule for a three-component system under a total (theoretical) hydrostatic pressure of 1 atm, the most stable phase can be calculated from a definition of any three independent variables. In Table I, up to and including line 600, the user has identified, and defined the limits of, the vertical axis, $\log_{10} p_{S_2}$, and the horizontal axis, $\log_{10} p_{O_2}$. In line 700, the constant temperature is entered. It is to be noted that the variable T is always specified as either a horizontal axis or a constant.

In F*A*C*T, precautions have been taken to guard against typing or logical errors that might be entered inadvertently by the user. Thus, in line 500, we see that the user has entered P(CL2) as a variable, which clearly cannot be part of the Ni-S-O system. This has been pointed out by the computer. Subsequently, the user has made a correction to the more logical P(02). Also, we note that after line 700 the user is given the option to check and change any numbered line(s) before obtaining the graphical output.

In the graphical output generated at the terminal (Fig. 2), the phases of the predominance area diagram have, where possible, been labelled by the computer. The most stable phase at any position was calculated by comparing the free energies of all condensed phases. The thermodynamic data necessary for this calculation was taken from a data base stored in the computer memory. The actual positions of the two-phase boundary lines were determined by a scanning of the system by a "divided differences technique" within the limits of the axes.

A more useful predominance area phase diagram for the Ni-S-O system is illustrated in Fig. 3. Here, the vertical axis of Fig. 2, $\log_{10} p_{S_2}$, has been replaced by $\log_{10} p_{SO_2}$. This diagram was readily obtained as can be seen from the bottom of Table I where the user has merely indicated that he wishes to continue calculations for the Ni-S-O system and has redefined line 500.

Other types of potential-potential phase diagrams can be computed with this program. In Fig. 4 is the Ellingham diagram for the Fe-O system (relative chemical potential of oxygen, RTln p_{O_2}, versus temperature). In Fig. 5 is the Ellingham diagram for the Fe-S-O system at constant $p_{SO_2} = 10^{-4}$ atm.

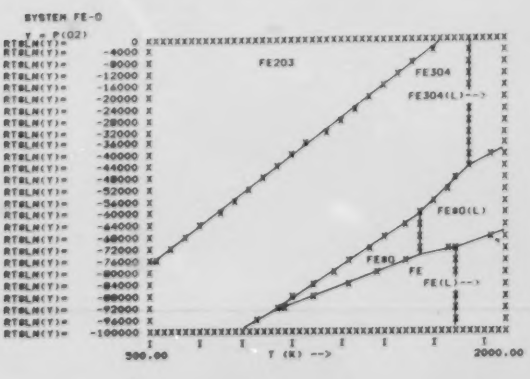

FIG. 4 Ellingham diagram for Fe-O (Solid lines have been added by hand).

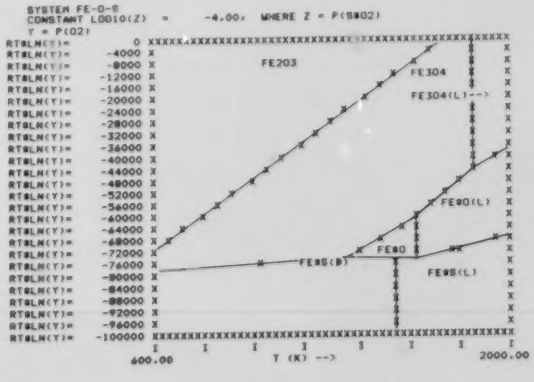

FIG. 5 Ellingham diagram for Fe-O-S at constant p_{SO_2} (Solid lines have been added by hand).

1152

The program can handle systems containing up to five components with complex gas mixtures as variables. We note that, from the phase rule, a potential-potential phase diagram of a five-component system can be calculated from a definition of the horizontal axis, the vertical axis, and three independent constants. For example in Fig. 6 is the predominance area diagram for the Fe-C-O-S-H quinary system at 900 K.

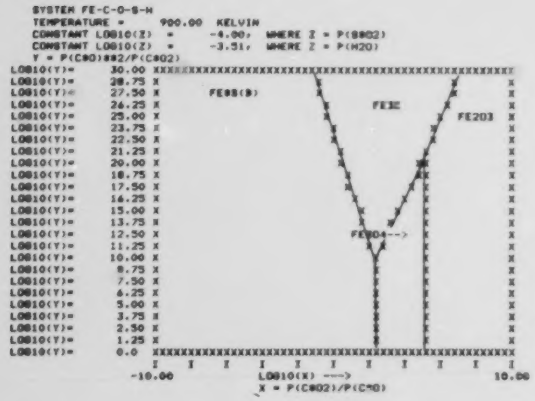

FIG. 6 Combination potential-potential phase diagram for the Fe-C-O-S-H system (Solid lines have been added by hand).

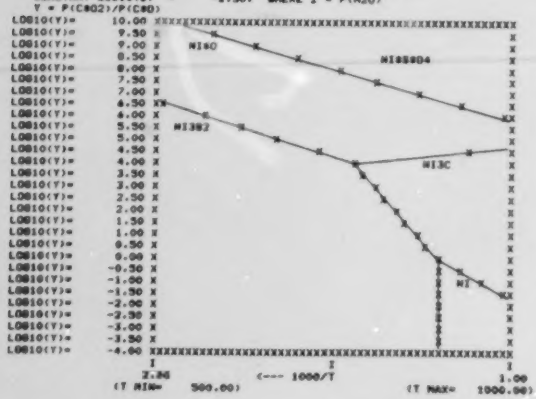

FIG. 7 Combination potential-potential phase diagram for the Ni-C-O-S-H system (Solid lines have been added by hand).

TABLE II

```
###  POTENTIAL - POTENTIAL DIAGRAMS  ###


YOUR TERMINAL (1) CAN, OR (2) CAN NOT PRINT 130 COLUMNS PER LINE
(ENTER 1 OR 2)
2

DEFINE TOTAL NUMBER OF COMPONENTS  (ENTER 2,3,4 OR 5)
5

   SYSTEM  A-B-C-D

   ENTER A  (FOR EXAMPLE CU)
FE

   ENTER B  (FOR EXAMPLE S)
C

   ENTER D  (FOR EXAMPLE O)
O

   ENTER C
S

   ENTER E
H

   AT 1 ATMOS (THEORETICAL) PRESSURE, PREDOMINANCE AREA (OR STABILITY)
   DIAGRAM FOR THE SYSTEM FE-C-O-S-H      CAN BE COMPUTED BY DEFINING
   (I) A VERTICAL AXIS,  (II) A HORIZONTAL AXIS, AND
   (III) 3 CONSTANT(S)


###### IDENTIFY VERTICAL AXIS! (1) LOG10(Y), (2) LN(Y) OR (3) KTB(N(E)) :
1

###200### ENTER VERTICAL VARIABLE Y  (FOR EXAMPLE P(S2)##0.5/P(O2)
P(CO)**2/P(CO2)

###300### DEFINE LOWER AND UPPER LIMITS OF VERTICAL AXIS AND INCREMENTAL STEP
   (IF INCREMENTAL STEP IS UNDEFINED GRAPHICAL OUTPUT WILL BE 25 LINES)
0 30

###### IDENTIFY HORIZONTAL AXIS! (1) LOG10(X), (2) LN(X) OR (3) 1/T  :
1

###400### ENTER HORIZONTAL VARIABLE X  (FOR EXAMPLE P(SO3)/P(SO2) ETC)
P(CO2))/P(CO)
  ERROR ENCOUNTERED IN COLUMN  6
  ')' MUST BE FOLLOWED BY '/' OR '*'
   -PLEASE RE-ENTER
P(CO2)/P(CO
  UNMATCHED PARENTHESES.    -PLEASE RE-ENTER
P(CO2)/P(CO)

###500### DEFINE LOWER AND UPPER LIMITS OF HORIZONTAL AXIS

###700### ENTER CONSTANT TEMPERATURE (KELVINS)
-20
   ERROR, MINIMUM PERMISSIBLE TEMPERATURE IS 298

###700### ENTER CONSTANT TEMPERATURE (KELVINS)
900

######IDENTIFY THE TYPE OF CONSTANT(S) C =  (1) LOG10(Z), (2) LN(Z) OR (3) KTBLN(Z)
1

###900### DEFINITION OF CONSTANT(S)

   ENTER THE VARIABLE Z  (FOR EXAMPLE P(SO2) ETC  )
P(SO2)
   ENTER VALUE OF 'C' (NOTE, 'C' NOT 'Z')
-4

   ENTER THE NEXT VARIABLE Z
P(H2O)
   ENTER VALUE OF 'C' (NOTE, 'C' NOT 'Z')
-3.51

IF YOU WISH TO CHANGE ONE OR MORE OF THE LINES, LIST, IN ORDER, THE LINE
NUMBER(S).  IF NOT PRESS 'RETURN'.


  PRESS 'RETURN' WHEN READY FOR GRAPHICAL OUTPUT
```

Conversational input used to generate Fig. 6.

The vertical axis is $\log_{10}(P_{CO}^2/P_{CO_2})$, the horizontal axis is $\log_{10}(P_{CO_2}/P_{CO})$, and the constants are $P_{SO_2} = 10^{-4}$atm, $P_{H_2O} = 10^{-3.51}$atm, and T = 900 K. In Fig. 7 is the phase diagram for the Ni-C-O-S-H quinary system. The vertical axis is $\log_{10}(P_{CO_2}/P_{CO})$ and the horizontal axis is 1/T corresponding to a temperature range of 500 - 1000 K. The constants are $P_{H_2S}/P_{H_2} = 10^{-3}$, $P_{CH_4}/P_{H_2} = 1.0$, and $P_{H_2O} = 10^{-2.3}$atm. The listing of the interactive conversation which generated Fig. 6 is given in Table II. This particular system has been chosen in order to show how gas mixtures may be employed as either axes or constants, and how typing or logical errors may be readily corrected by the user. (See lines 500 and 700 in Table II).

The usefulness of Figs 6 & 7 for the Fe-Ni-S-O system is apparent when one considers that, experimentally, sulfur potentials are often defined by H_2S/H_2 or SO_2/O_2 mixtures and oxygen potentials by CO_2/CO or H_2/H_2O mixtures. Thus, the possible formation of carbides, carbonates, hydrides, etc. must be considered.

Present developments in F*A*C*T concerned with the calculation of potential-potential phase diagrams include the addition of isobaric (or isoactivity) lines and P_{total} curves on the diagrams, as well as the calculation of Pourbaix (electrical potential, E, versus pH) diagrams. Other developments include the ability to accept user-supplied data and the calculation of metastable phase boundaries.

POTENTIAL-COMPOSITION PHASE DIAGRAMS

A computer-generated T-composition phase diagram for the Fe-Ni binary system is shown in Fig. 8. The calculation is based upon the thermodynamic properties of the phases as given in the critical compilations of the "CALPHAD" group (3).

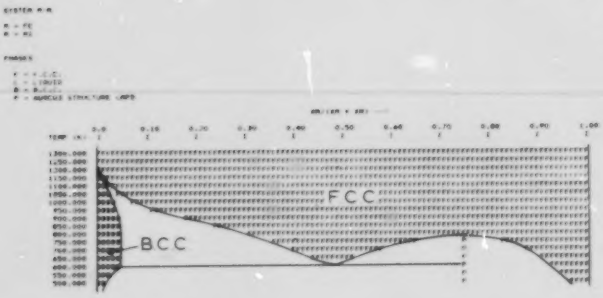

FIG. 8 Temperature-composition phase diagram for the Fe-Ni binary system

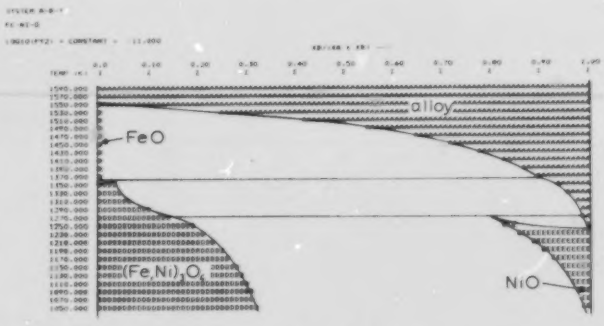

FIG. 9 Temperature-composition phase diagram at constant $P_{O_2} = 10^{-11}$ atm for the Fe-Ni-O system.

For the three-component system Fe-Ni-O, a potential-composition phase diagram can be drawn if another potential is held constant. In Fig. 9 is the computer-generated T-ξ diagram for the Fe-Ni-O system at constant $P_{O_2} = 10^{-11}$ atm. In Fig. 10 is the

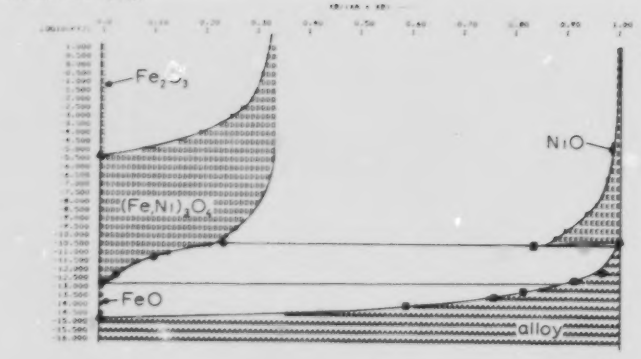

FIG. 10 $\log_{10}P_{O_2}$ - composition phase diagram at constant T for the Fe-Ni-O system ●(ref. 4); ■(ref. 5); ▲(points from standard thermodynamic tables).

computer-generated $\log_{10}P_{O_2}$-ξ diagram at constant T = 1273 K.

In all these computer-generated diagrams, one-phase regions are indicated by a code letter, and two-phase regions by blank areas. The solid lines on Figs 8-16 have been added by hand in order to improve the clarity of the reproduction. Similarly, the labelling of the one-phase fields has also been added. In Table III is a listing of the conversational input which generated the diagram in Fig. 10. After signing on, the user indicates the width of his terminal. (Phase diagrams 50 columns in width can also be generated if the user has only a 72-column wide terminal.) The next few lines in Table III are self-explanatory. At line 1000, the user enters a code number for the system which is taken from a list of systems which have been analyzed and stored in the system's data base. Alternatively, the user may decide to enter all the data himself. In the present example, he chooses the Fe-Ni-O system. The computer then lists the phases for which stored data are available along with the temperature limits for which these data are applicable, and the user indicates which phases he wishes to consider. (One may, for example, choose to ignore certain phases in order to generate metastable phase boundaries.) The user may also choose to add some data sets of his own. The computer then lists the chosen phases along with the code letter to be used in the output for each phase. The user has the

TABLE III

```
IS YOUR TERMINAL (1)CAPABLE, (2)NOT CAPABLE OF (1) 50 OR (2) 72 COLUMN WIDTH?
1
ENTER UNITS OF ENERGY, (1)CAL, (2)JOULES
1
ENTER UNITS OF TEMP, (1)K, (2)C, (3)F
1
DO YOU (1)WANT (2)NOT WANT PROMPTING?
1

@@@@@10000@@@@@ ENTER CODE NUMBER OF SYSTEM,
OR PRESS RETURN IF YOU ARE SUPPLYING ALL DATA YOURSELF.
2

SYSTEM FE-NI-O

PHASE CODE

   1     F.C.C. (GAMMA) ALLOY                    300 - 1800 K
   2     WUSTITE (FEO) (LIME COMPOUND)           800 - 1700 K
   3     FE2O3 SOLID (LIME COMPOUND)             800 - 2400 K
   4     SPINEL                                  800 - 2300 K
   5     NIMO-FERRO SOLID                        800 - 2335 K

REFERENCE PHASES (O + O) ARE NUMBERS  1 FOR A AND  1 FOR B

FREE ENERGIES  TO BE ENTERED AS
 DELTAG = A + BST + C(T*LOG(T)) + D*(T**2) + E*(T**3) + F*TOTALGOUT(T) + G/T
 WHERE T IS KELVINS AND ALOG IS NATURAL LOG

@@@@@11000@@@@@ ENTER CODE NUMBERS OF PHASES TO BE CONSIDERED
1 2 3 4 5
ENTER NUMBER OF ADDITIONAL USER-SUPPLIED PHASES
0

@@@@@11050@@@@@ PHASE A   PHASE CODE NUMBER  1
DO YOU (1) WANT (2) NOT WANT A LISTING OF DATA SET CONTENTS?
1
ENTER PHASE TYPE CODE
   1
ENTER STOICHIOMETRIC FACTORS (I,J)=A OF COMPOUND A(I)B(J)C(K)... AT THE LEFT
 1.00  0.0   0.0
ENTER COEFFTS A+B*C+D*E*F*G OF FREE ENERGY OF  A( 1.00)B( 0.0)C( 0.0) +
   0.0           0.0           0.0           0.0
   0.0           0.0           0.0           0.0
ENTER STOICHIOMETRIC FACTORS (I,J)=A OF COMPOUND A(I)B(J)C(K)... AT THE
 RIGHT
   0.0   1.00   0.0
ENTER COEFFTS A+B*C+D*E*F*G OF FREE ENERGY OF  A( 0.0)B( 1.00)C( 0.0) +
   0.0           0.0           0.0           0.0
   0.0           0.0           0.0           0.0
ENTER COEFFICIENTS (MAX OF  7 TERMS) OF THE SERIES FOR ENTHALPY OF MIXING
DELTAH = X1(X2)(D0 + D1X2 + D2(X2**2) + D3(X2**3) + .....)
  -0.40000E 03  -0.10000E 04   0.0           0.0
   0.0           0.0           0.0
ENTER COEFFTS (MAX OF 7 TERMS) OF SERIES FOR EXCESS ENTROPY OF MIXING
SEXCESS = X1(X2)(D0 + D1X2 + D2(X2**2) + D3(X2**3) + .....)

   0.0           0.0           0.0           0.0
   0.0           0.0           0.0

@@@@@11100@@@@@ PHASE B   PHASE CODE NUMBER  2
DO YOU (1) WANT (2) NOT WANT A LISTING OF DATA SET CONTENTS?
2

@@@@@11150@@@@@ PHASE C   PHASE CODE NUMBER  3
DO YOU (1) WANT (2) NOT WANT A LISTING OF DATA SET CONTENTS?
2

@@@@@11200@@@@@ PHASE D   PHASE CODE NUMBER  4
DO YOU (1) WANT (2) NOT WANT A LISTING OF DATA SET CONTENTS?
2

@@@@@11250@@@@@ PHASE E   PHASE CODE NUMBER  5
DO YOU (1) WANT (2) NOT WANT A LISTING OF DATA SET CONTENTS?
2

@@@@@12000@@@@@  IS WIDTH OF X-AXIS IN MOLE PERCENT, (1) 10     (2)  100
!!!
INPUT CANNOT BE INTERPRETED. REENTER
2

@@@@@13000@@@@@ IS Y-AXIS  (1)T,  (2)LOG10(ACTIVITY(1))+ (3)LOG10(PP2)?
3
ENTER, IN ORDER,  LOWER LIMIT, INCREMENT, AND UPPER  LIMIT OF Y-AXIS
-22 -10  0.25
UPPER LIMIT MUST BE GREATER THAN OR EQUAL TO LOWER LIMIT AND INCREMENT
MUST BE POSITIVE. REENTER
-22 0.25  -10

@@@@@13100@@@@@ ENTER THE CONSTANT TEMPERATURE
1000


IF YOU WISH TO CHANGE A LINE, ENTER ITS NUMBER. IF NOT, PRESS RETURN KEY
 TO START CALCULATION
1310
DO YOU  (1)WANT  (2)NOT WANT  PROMPTING?
2
@@@@@13100@@@@@
1273


IF YOU WISH TO CHANGE A LINE, ENTER ITS NUMBER. IF NOT, PRESS RETURN KEY
 TO START CALCULATION
```

Conversational input used to generate Fig. 10

option of inspecting the stored data for any phase. In Table III he has chosen to do this for phase A, and the computer has listed out the stored thermodynamic data for this phase in the same format, with the same questions asked, as it would if this were a user-supplied data set. In line 1200 the width of the x-axis is specified. In line 1300 the scale of the y-axis (in this case $\log_{10} P_{O_2}$), and the limits and increment of this axis are chosen. Finally, in line 1310 the constant potential (in this case,T) is specified. As was pointed out in the previous section, attempts have been made to make F*A*C*T as error-proof as possible by the incorporation of a large number of error messages which appear if the user makes a logical or typing error. Examples are given at lines 1200 and 1300. The user is now given the chance to go back, if he wishes, to change any section of input by entering its number. In the example in Table III, he has chosen to reenter line 1310 in order to change the temperature from 1000 to 1273 K. At this point, by entering one of the line numbers 1105 to 1125, he would be able to modify the stored data for one of the phases if he so desired. The same opportunity to change some input lines is also offered after the diagram has been printed. The user is thereby permitted to quickly recalculate the diagram for different limits of the axes, for example.

Space does not permit a complete description of the programming techniques to be given here. A detailed discussion will be published shortly. The method used is essentially that of calculating the lowest common tangent to the free energy-composition curves. The thermodynamic data required are the stoichiometry of the phases as well as the free energies of formation (expressed as functions of T) of all compounds as well as expressions for the thermodynamic properties of solution (g^E, Δh, s^E) of all phases. In Table III, Δh and s^E for the Fe-Ni alloy phase (line number 1105) are expressed as simple power series of the mole fractions. However, several other mathematical descriptions can be used (each with its own "phase type code"). Thus, Henrian solutions, spinel solutions, etc. can be treated. This will be the subject of a series of forthcoming articles. In the case of the Fe-Ni-O system, for example, the solution properties of the Fe-Ni alloy phase are expressed as power series in the mole fractions; the FeO and NiO phases are taken to be Henrian solutions; the $(Fe,Ni)_3O_4$ phase is considered to be an ideal mixture of the two inverse spinels Fe_3O_4 and $NiFe_2O_4$; while Fe_2O_3 and $FeNi_3$ are taken to be "line compounds" of fixed composition.

Other computer-generated potential-composition phase diagrams for the Fe-Ni-O system are shown in Figs 11-12. These are T-ξ diagrams at constant ratios of P_{CO}/P_{CO_2} and P_{H_2}/P_{H_2O}. (Such constant ratios fix a constant P_{O_2} at any constant T, but this is not the same P_{O_2} at all temperatures).

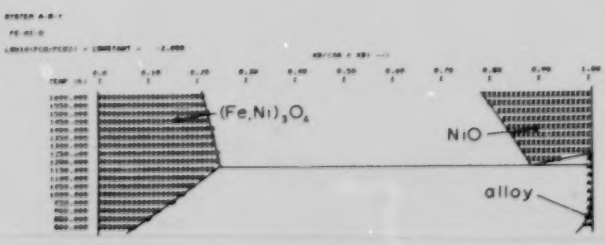

FIG. 11 Temperature-composition phase diagram for Fe-Ni-O at constant $P_{CO}/P_{CO_2} = 10^{-2}$.

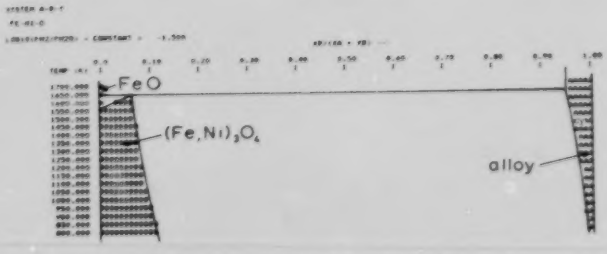

FIG. 12 Temperature-composition phase diagram for Fe-Ni-O at constant $P_{H_2}/P_{H_2O} = 10^{-1.5}$.

For the quaternary Fe-Ni-S-O system, a potential-composition phase diagram can be drawn if two other potentials are held constant. In Fig. 13 is the diagram of $\log_{10} p_{O_2}$-ξ for this quaternary system at constant T = 1173 K and $p_{SO_2} = 10^{-10}$ atm. Since, at constant p_{SO_2}, log p_{O_2} varies inversely as log p_{S_2}, Fig. 13 is also a plot of -log p_{S_2} versus ξ. Thus, Fig. 13 is made up of the log p_{O_2}-ξ diagram for the Fe-Ni-O system (as in Fig. 10) at the top, with the log p_{S_2}-ξ diagram for the Fe-Ni-S system inverted at the bottom. As p_{SO_2} is raised, the two halves of Fig. 13 move together until they intersect as is illustrated in Figs 14-15.

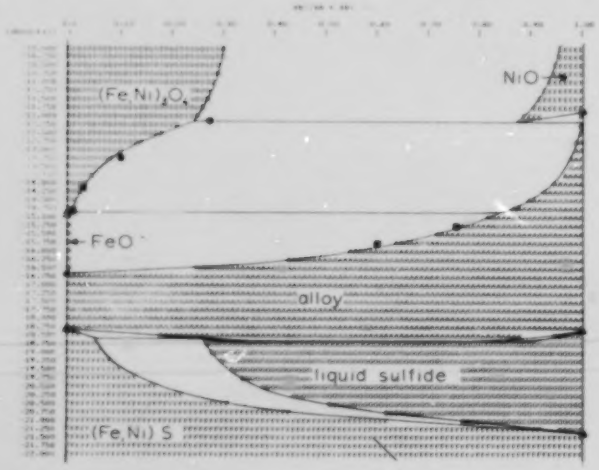

FIG. 13 $\log_{10} p_{O_2}$ versus $\xi = x_{Ni}/(x_{Ni} + x_{Fe})$ for the Fe-Ni-O system at T = 1173 K and $p_{SO_2} = 10^{-10}$ atm. ●(ref. 4); ■(ref. 5); ▲(points from standard thermodynamic tables).

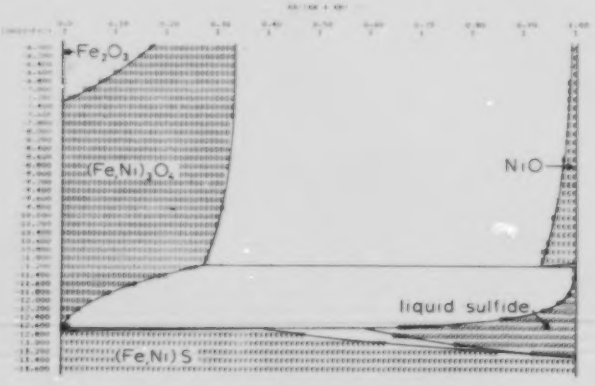

FIG. 14 $\log_{10} p_{O_2}$ versus $\xi = x_{Ni}/(x_{Ni} + x_{Fe})$ for the Fe-Ni-S-O system at T= 1173 K and $p_{SO_2} = 10^{-2.0}$ atm.

In Fig. 16 is an example of a diagram with an expanded x-axis with an attendant resolution of 0.1 mole %. Fig. 16 is a blow-up of a portion of Fig. 13.

Some experimental points (4,5) are shown on Figs 10 & 13 in order to indicate the typical agreement obtained between the calculated diagrams and the experimental diagrams for the limited ranges of T, composition, and partial pressure for which experimental phase diagrams are available.

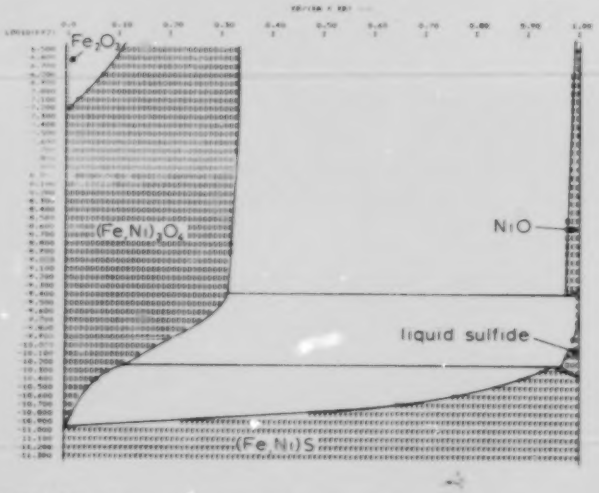

FIG. 15 $\log_{10} p_{O_2}$ versus $\xi = x_{Ni}/(x_{Ni} + x_{Fe})$ for the Fe-Ni-S-O system at T= 1173 K and $p_{SO_2} = 10^{1.0}$ atm.

Present work on this program is concerned mainly with the preparation of a data base for a number of systems of the type A-B-Y where A and B are metals and Y is a non-metal (O,S,C,Cl, etc.). The data base is being obtained from experimental thermodynamic data (curve-fitting), from comparison of calculated and experimental phase diagrams (where available), by interpolation and extrapolation with the aid of statistical models where data are not available, or by a combination of the above.

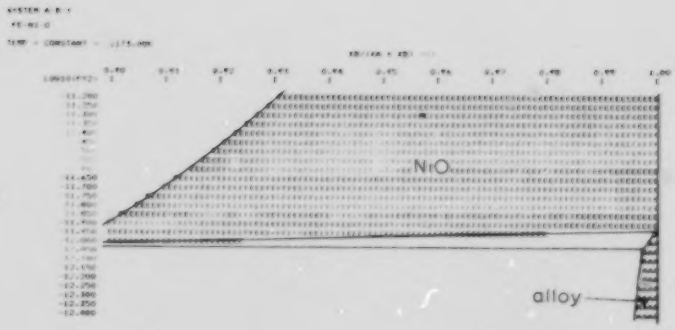

FIG. 16 $\log_{10} P_{O_2}$ versus ξ for the range $0.9 \leq \xi \leq 1.0$ for the Fe-Ni-O system at 1173 K (a blow-up of a portion of Fig. 13)

REACTION PATH CALCULATIONS

This feature of F*A*C*T is intended to complement the phase diagram programs by permitting users to conduct calculations other than those related directly to phase stability. This program computes the changes in the thermodynamic properties H, S, V, U, A, and G between specified or implied initial and final states of a system. Since this routine embraces calculations as elementary as determining the change in G associated with isothermal isobaric chemical reactions to the calculation of ΔH for reactions with many reactants and products at different temperatures and pressures, it is useful not only for important practical problems, but also for educational purposes to give the users a better insight into the significance of the phase diagram programs.

Consider, as an initial example related to the sulfur-oxygen gas equilibrium, the reaction shown in Table IV. The user has entered the balanced chemical equation. Considerable freedom in the style of input is permitted, as long as elements within each compound are separated by a stoichiometric number or by a *(equivalent to a stoichiometric number of 1). In this way, it is possible, for example, to distinguish Co from CO when all alphabetical characters are upper-case. The subscripts are used to identify the states. Algebraic symbols, T and P, for temperature and pressure indicate that the numerical values of these properties are unspecified and will either be entered or calculated later. With the depression of the 'return' key, the information following the equation up to the first row in the tabular output is generated. The changes in the six basic extensive thermodynamic functions are calculated in the indicated units for the system-generated temperature of 298.15 K and pressure of 1.0 atm. In subsequent lines, following each system-generated '?', the user enters in free format two numbers which become the temperature and pressure

TABLE IV

```
ENTER THE CHEMICAL EQUATION
-
 0002     = 1/2  02     +     0003
 (T,P,000)       (T,P,000)       (T,P,000)

CALCULATIONS ARE BASED ON THE NUMBER OF GRAM MOLES OF REACTANTS AND PRODUCTS INDICATED IN THE CHEMICAL EQUATION

 TEMPERATURE   PRESSURE     DELTH      DELTS      DELTV      DELTU      DELTA      DELTG
     (K)         (ATM)      (CAL)    (CAL/K)     (LIT)      (CAL)      (CAL)      (CAL)
    298.1         1.0      -23490.     -22.05     -12.2      -23156.    -16431.    -16727.
    600.0         1.0
    600.0        1.00      -23404.     -22.06     -16.4      -23007.    -16024.    -16457.
    500.0         1.0
    500.0        1.00      -23422.     -22.05     -20.5      -22937.    -15604.    -17160.
    400.0         1.0
    400.0        1.00      -23321.     -22.05     -24.6      -22720.    -9520.     -9915.
    700.0         1.0
    700.0        1.00      -23165.     -22.10     -28.7      -22470.    -6997.     -7692.
    700.0        10.0
    700.0        10.0      -23165.     -19.82     -2.87      -22470.    -8099.     -9296.
    700.0       100.0
    700.0         100.     -23165.     -17.53     -.287      -22470.    -10200.    -10895.
    700.0      1000.0
    700.0    .1000E+04     -23165.     -15.24     -.287E-01  -22470.    -11801.    -12496.
RETURN
```

Conversational input and output using the reaction path program illustrating calculations for isothermal isobaric paths.

1158

defining a new set of property changes which are calculated and printed on the next line after depression of the 'return' key. At no point does the user enter data, since F*A*C*T has its own data base. If data are not in storage, appropriate messages are issued. Table IV shows, for example, that the isothermal standard enthalpy change is virtually constant and that the Gibbs free energy change tends to favour SO_2 at higher temperatures. At 700 K the user has also entered progressively higher values for the pressure. The effect is instructive. ΔH is not altered (gases are presently regarded as ideal) and ΔV diminishes.

It is not necessary that the pressures and temperatures for each compound be assigned values in the tabular output. (n-1) compounds in an n compound reaction may have (possibly different) numerical values set into the subscripts for the temperature and pressure. Furthermore, the same compound may appear on both sides of the reaction. This provides considerable power in solving many problems of practical importance as illustrated in Table V. Hot SO_2 is reacting with an excess of warm air to produce SO_3. The user, by varying the temperature of the products, is examining ΔH. On the fourth entry he has neglected to specify the pressure and so a thermodynamic error message is generated. From the magnitude of the enthalpy changes at 600 and 700 K, it appears that ΔH will be zero near 800 K. The temperature corresponding to $\Delta H = 0$ is the adiabatic reaction product temperature for the isobaric process. This temperature can be directly determined by specifying P = 1.0 atm and $\Delta H = 0$ by entering these values in the appropriate columns. This the user has subsequently done. Asterisks are used in F*A*C*T to indicate those columns left unspecified on entry. The required T has been calculated directly to be 770.8 K. In the next line the user has inadvertently specified three properties. This impossible situation causes F*A*C*T to generate the error message following this line. In the final two lines, the user has entered a zero in the ΔV column and has found that $\Delta V = 0$ when T = 479.8 K. (In a flowing process, reactant and product flow would be the same). This finding is shown to be independent of the pressure.

TABLE V

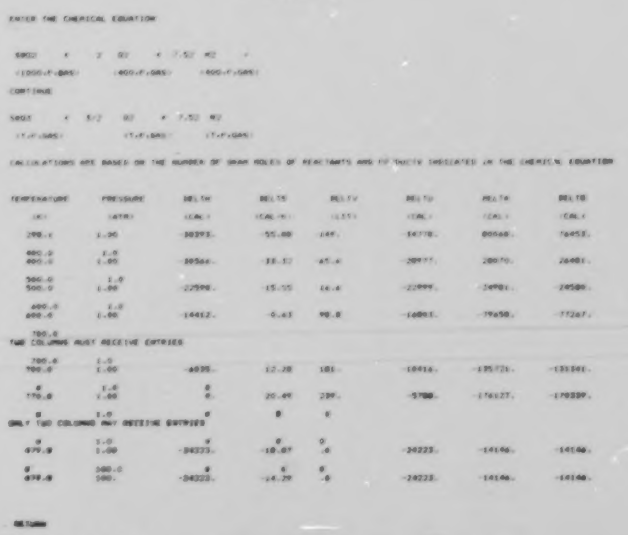

Conversational input and output using the reaction path program illustrating calculations for adiabatic and isovolumetric paths.

In Table VI the user has employed the reaction path program to study the reaction involving Fe, Fe_3O_4 and FeO involved in Fig. 4. In the last line, by setting ΔG to zero (by entering a zero in the ΔG column) the user has determined the precise value of the temperature at the $Fe/Fe_3O_4/FeO$ triple point. The equations entered in Table VII then

TABLE VI

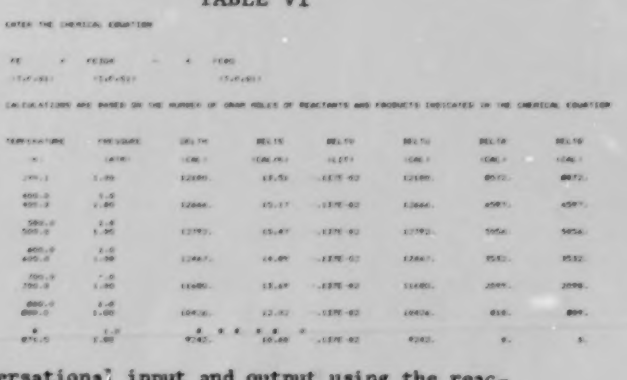

Conversational input and output using the reaction path program illustrating the calculation of the temperature of the $Fe/Fe_3O_4/FeO$ triple point ($\Delta G = 0$).

permit the determination of the partial pressure of oxygen at that triple point since the temperature has been previously established. The number of moles of reactants involved in the equation does not, of course, affect the equilibrium oxygen pressure as illustrated in Table VII by the tabular output for the second equation.

Table VIII illustrates the consequence of not specifying the phase state for one of the compounds. F*A*C*T assumes that the most stable state at the temperature and pressure is desired. In this mode, all of the reactant and product states appear in columns on the extreme right in the order determined by the input equation. It is not possible, when operating in this mode, to set values into columns other than the temperature and pressure columns.

Future developments to this program include the ability to employ user-supplied data, and the ability to indicate that groups of reactants and products exist in solutions. Furthermore, a plotting routine is to be developed to supplement the tabular output.

TABLE VII

Conversational input and output using the reaction path program illustrating the calculation of equilibrium partial pressure of oxygen.

CONCLUSIONS

A brief description has been presented of the present state of development of F*A*C*T (Facility for the Analysis of Chemical Thermodynamics) - a thermodynamic data treatment centre and data bank based in Canada. Users, at standard remote terminals, will be able to 'carry on a conversation' with the computer by means of a telephone connection. F*A*C*T will be able to perform many different thermodynamic calculations in full conversational mode by employing a data base and/or user-supplied data. All resulting outputs, whether they are tables of figures or phase diagrams, will be printed out on the user's terminal. Three main programs have been presented in this article. The use of these programs has been illustrated by the calculation of various phase diagrams and reaction paths in the Fe-Ni-S-O quaternary system and its sub-systems. The diagrams presented include predominance area phase diagrams, Ellingham diagrams, stability diagrams, combination diagrams, and temperature-composition and chemical potential-composition phase diagrams. The chemical reaction paths include adiabatic, isothermal, isovolumetric, and isentropic paths. Work in progress involves the incorporation of an extensive

TABLE VIII

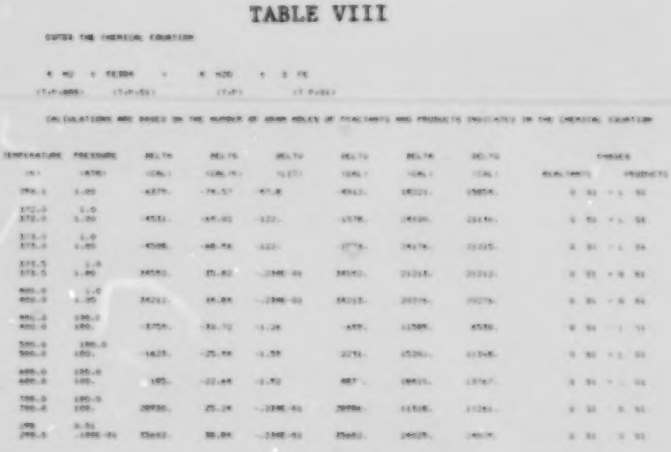

Conversational input and output using the reaction path program illustrating the calculation of the stable phase for a given set of conditions.

data base. Other work in progress is concerned with increasing the scope of the system. Under development are programs involved with the calculation of Pourbaix diagrams, the calculation of ternary composition-composition diagrams with special emphasis on fused salt systems, and the graphical representation of the thermodynamic parameters for various chemical reaction paths, among others.

F*A*C*T is expected to be on-line with the three programs described in this article and a limited data base by the end of 1977. A series of detailed articles describing each of the programs is to be published shortly.

REFERENCES

1. A.D. Pelton and H. Schmalzried, Met. Trans., 4, 1395 (1973).
2. A.D. Pelton and W.T. Thompson, Prog. Sol. State Chem., 10, 119 (1975)
3. "A Sampler of Coupled Thermodynamical and Phase Diagram Data for Metallic Systems", Calphad Project 1975.
4. A. Dalvi and R. Sridhar, to be published.
5. H. Davies and W.W. Smeltzer, J. Electrochem. Soc., 119, 1362 (1972).

ACKNOWLEDGMENTS

The authors are indebted to the National Research Council of Canada for a COOP grant, and to the Canadian department of Energy Mines and Resources for financial support of the project concerned with the calculation of potential-composition diagrams in ternary system. Thanks are due to the computer centres of Ecole Polytechnique and McGill Universities for their help and cooperation.

National Bureau of Standards SP-496, Applications of Phase Diagrams in Metallurgy and Ceramics
Proceedings of Workshop held at NBS, Gaithersburg, Md., January 10-12, 1977

THE CALCULATION OF POURBAIX DIAGRAMS USING A MODIFIED LINEAR PROGRAMMING TECHNIQUE

Barry H. Rosof
Technology Division, Cabot Corporation, Kokomo, Indiana 46901

An algorithm for calculating Pourbaix Diagrams (both partial pressure diagrams and potential pH diagrams) that is particularly suitable for use on a digital computor is presented. The algorithm consists of two principal parts. In the first part, the thermodynamic conditions under which a given phase is stable with respect to all other phases is formulated as a set of linear inequalities. In the second part, the set of linear inequalities is solved by a modified linear programming technique to yield the region in which the subject phase is the stable phase.

Any chemical reaction can be written as

$$0 = \Sigma\, \nu_i A_i, \tag{1}$$

e.g.

$$0 = \frac{3}{2}O_2\ (g) + 2SO_2(g) + Cu_2O - 2CuSO_4(s). \tag{2}$$

By convention Species 3 and 4 are taken as the metal bearing species. The condition that Species 3 is stable wrt Species 4 ($\Delta G_r \leq 0$) can be written after rearranging and after fixing the activities of all species except Species 1 and 2 as

$$a_1\xi_1 + a_2\xi_2 \leq B, \tag{3}$$

where

$$-B = \Delta G_r^\circ + \sum_{i=3}^{n} \nu_i RT\xi_i, \tag{4}$$

$$\xi_i = \ln a_i \text{ or } \ln P_i \tag{5}$$

and

$$a_i = \nu_i RT. \tag{6}$$

In the present case

$$\frac{3}{2}RT \ln P_{O_2} + 2RT \ln P_{SO_2} \leq \Delta G_R^\circ, \tag{7}$$

where the activities of the solid phases have been set equal to unity.

For Species 3 to be stable it must not only be stable wrt Species 4 but also stable wrt all other possible metal bearing species, e.g. Cu_2O must be stable wrt CuS, Cu_2S, Cu, CuO, etc., as well as wrt $CuSO_4$. If there are n metal bearing species there are n-1 stability conditions, each of the form given in Equation 3. The n-1 stability conditions, or constraints, define the region where Species 3 (Cu_2O) is stable as a function of ξ_1 and ξ_2 ($\ln P_{O_2}$ and $\ln P_{SO_2}$). The constraints delimit a polygon in ξ_1-ξ_2 space.

The problem of finding the region (of stability) that satisfies the n-1 constraints can be solved by a modified version of the linear programming technique known as the two phase simplex process.

In Phase 1 the standard tableau is set up, but the cost row is omitted. (The "cost" row for Phase 1 is retained.) The conventional Phase 1 algorithm is executed leading to a basic feasible solution.

1162

A basic feasible solution corresponds to one corner of the polygon delimiting the region of stability. The corner where Cu, Cu_2S and Cu_2O coexist (Fig. 1) is a basic feasible solution for Cu_2O. The object in Phase 2 is to find all basic feasible solutions.

The algorithm for selecting the vector to enter the base in Phase 2 is modified as follows: The two vectors not in the base are labeled A and B. Vector A is chosen to enter the base, Vector B becomes Vector A, and the vector leaving the base becomes Vector B. The vector leaving the base is chosen in the standard fashion so that the new solution is also a basic feasible soluiton. This procedure is repeated until the original basic feasible solution is obtained, yielding all corners of the polygon.

A new species is then chosen as the subject species and the entire procedure repeated to yield the polygon delimiting its region of stability. This procedure is continued until the region of stability is found for all metal bearing species to yield the complete diagram.

Electrochemical as well as high temperature systems can be treated. Additional non-metal bearing chemical species can be included at fixed activities. For example, the $Cu-O_2-SO_2$ diagram changes markedly if chlorine is introduced into the system at a fixed partial pressure of 10^{-10} atm.

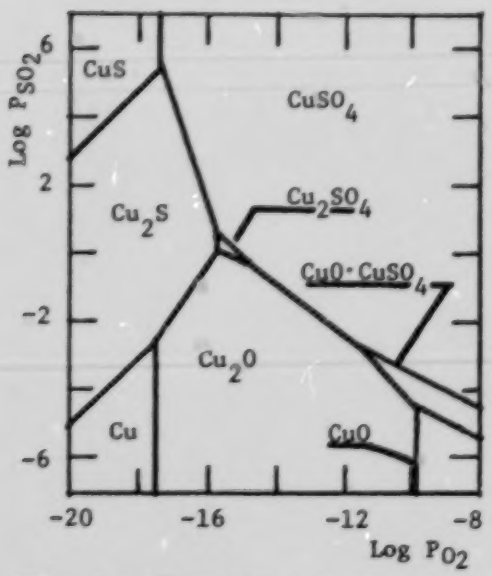

Fig. 1 $Cu-O_2-SO_2$ System
$T = 700°K$.

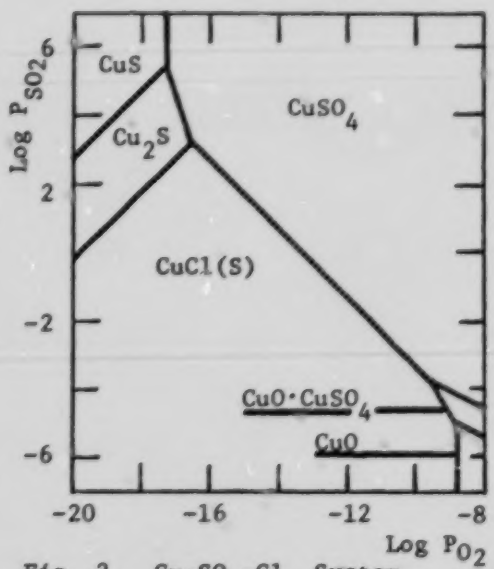

Fig. 2. $Cu-SO_2-Cl_2$ System
$T = 700°K$ $P_{Cl_2} = 10^{-10}$ atm
$P_{CuCl(g)} < 10^{-2}$ atm.
$P_{Cu_3Cl_3(g)} < 10^{-2}$ atm.

Computor software (Fortran IV) has been developed. Calculation of of Pourbaix Diagrams using this software has proved to be very inexpensive and efficient. Copies of the computor software can be obtained by writing to:

Dr. Barry H. Rosof
Technology Division
Cabot Corp.
1020 W. Park Avenue
Kokomo, Indiana 46901

National Bureau of Standards SP-496, Applications of Phase Diagrams in Metallurgy and Ceramics
Proceedings of Workshop held at NBS, Gaithersburg, Md., January 10-12, 1977

THEORETICAL CONCEPTS USEFUL IN THE CALCULATION OR STORAGE OF PHASE DIAGRAMS OF IONIC SYSTEMS*

Marie-Louise Saboungi and Milton Blander
Chemical Engineering Division, Argonne National Laboratory, Argonne, Illinois 60439

Introduction

Solution theories which provide a reasonable representation of the thermodynamic behavior of multicomponent ionic solutions can prove to be important in a variety of applications. One can use theoretical equations:

1. to calculate phase diagrams a priori from the subsidiary binaries,
2. to construct and complete phase diagrams from very few measured points,
3. to check the self consistency of published phase diagrams and consequently to provide a logical basis for the selection of reliable diagrams, and
4. to efficiently store phase diagrams with very few parameters.

We will focus on the conformal ionic solution theory for ternary systems[1-5] since it is the only theory which accounts for coulombic interactions between ions in a rigorous way. The calculations based on a statistical mechanical perturbation method have only been made for simple systems containing ions of the same charge. We will also present empirical extensions for cases where the cations and/or the anions have different charges.

Ternary ionic systems contain four kinds of ions. Those having two kinds of cations and two kinds of anions are ternary reciprocal systems, and those with three kinds of cations (or anions) and one kind of anion (or cation) are additive ternary systems. In the following sections, we will discuss the theory for these two classes of systems.

1. Reciprocal Systems

The calculation for reciprocal systems has been carried out only to second order for the simplest member of the class of reciprocal systems, i.e., the $A^+,B^+/X^-,Y^-$ system. In such a system, there are four constituents, AX, AY, BX and BY, and only three components which can be chosen in

four different ways. If AY, BX and BY are chosen as the three components, then the total molar Gibbs free energy of mixing is given by

$$\Delta G^m = RT[X_A \ln X_A + X_B \ln X_B + X_X \ln X_X + X_Y \ln X_Y] \quad (1)$$

$$+ X_A X_X \Delta G^\circ + \lambda_A X_A X_X X_Y + \lambda_B X_B X_X X_Y + \lambda_X X_X X_A X_B$$

$$+ \lambda_Y X_Y X_A X_B + X_A X_B X_X X_Y \Lambda$$

where ΔG° is the standard Gibbs free energy change for the metathetical reaction $AX + BY \rightleftarrows AY + BY$, the X_i's are ion fractions of the ith ion, the λ's are coefficients deduced from the four subsidiary binaries (e.g., in the binary AX-BX, the excess Gibbs free energy of mixing, $\Delta G_X^E = \lambda_X X_A X_B$) and Λ is calculated to be $\frac{-(\Delta G^\circ)^2}{2ZRT}$ where Z is a parameter taken to be 6.

Reciprocal systems generally have a complex topology which is largely related to the terms containing ΔG°. In the simplest case where no compounds or solid solutions exist, the phase diagram is characterized by two ternary eutectics or one ternary eutectic and one ternary peritectic. If $|\Delta G^\circ|$ is large, the isothermal contours are complex curves which reflect the large deviations from ideality, positive deviations for one pair of constituents (e.g., AX and BY when ΔG° is positive) and negative deviations for the other pair of constituents (e.g., AY and BX).

Equation (1) has been used to calculate liquidus phase diagrams of simple reciprocal systems a priori from data on lower order systems.[6,7] To do this, expressions for activity coefficients of the four constituents are derived from Eq. (1). For the component BY, for example, one can define an activity coefficient by the relation

$$a_{BY} = X_B X_Y \gamma_{BY} \quad (2)$$

1166

where a_{BY} and γ_{BY} are the activity and the activity coefficient of component BY, respectively. The activity coefficients are given by

$$RT \ln \gamma_{BY} = X_A X_X \Delta G^\circ + X_A X_X (X_X - X_Y)\lambda_A + X_X (X_A X_Y + X_B X_X)\lambda_B \qquad (3)$$

$$+ X_A (X_A X_Y + X_B X_X)\lambda_Y + X_A X_X (X_A - X_B)\lambda_X$$

$$- X_A X_X (X_A X_Y + X_B X_X - X_B X_Y)\frac{(\Delta G^\circ)^2}{2ZRT}$$

For those simple systems where neither compounds nor solid solutions are present, liquidus temperatures may be calculated by properly combining Eqs. (2) and (3) with the Schröder-van Laar equation. A comparison between the measured and calculated liquidus phase diagrams for the Li,Na/F,Cl and Li,K/F,Cl systems is illustrated in Figs. 1 and 2, respectively. Even though the phase diagrams for these two systems have rather complex topologies, it can be seen that the relatively simple Eqs. (1)-(3) lead to a reasonably good representation of both systems. However, differences do exist between the measured and calculated phase diagrams. On the one hand, some of these differences arise because of uncertainties in constructing such a complex phase diagram from a limited number of measurements. There were not enough measured points to fully define the shape of most of the liquidus isotherms and it is probable that the shapes calculated from theory are thermodynamically more self-consistent than the reported phase diagrams constructed from a limited amount of data. For example, the 700 and 750°C isotherms in the NaCl phase field of the calculated diagram are probably more reliable than the reported isotherms.

On the other hand, some of the differences between the measured and calculated phase diagrams are related to inadequacies of Eq. (1) which has been derived only to second order. Measurements of enthalpies of mixing

of many binary systems indicate that higher order terms are necessary in order to describe the results accurately. For binary systems having relatively large deviations from ideality, even fourth order terms are needed. Liquidus temperatures are generally fairly insensitive to these higher order terms so that, although necessary, highly precise values of these terms are not needed to improve calculated phase diagrams. Equation (1) can be written to include some of the higher order terms of the binary systems as follows:

$$\Delta G^m = RT[X_A \ln X_A + X_B \ln X_B + X_X \ln X_X + X_Y \ln X_Y] \qquad (4)$$
$$+ X_A X_X \Delta G^\circ + X_A \Delta G^E_A + X_B \Delta G^E_B + X_X \Delta G^E_X + X_Y \Delta G^E_Y$$
$$- X_A X_B X_X X_Y \frac{(\Delta G^\circ)^2}{2ZRT}$$

where ΔG^E_i is the excess Gibbs free energy of mixing of the binary system having the common ion i. For example, ΔG^E_A is the excess free energy of mixing of the mixture AX-AY at an ion fraction X_X (and X_Y) for which the calculation is made. The functions ΔG^E_i can be constructed to describe the binary systems as accurately as desired. As a result, the binary edges of the phase diagram can be made as close to measurements as desired. By thus constraining the edges of the diagrams to be much more precise, the remainder of the diagram, especially the areas near the edges, can be significantly improved. A common form which might be used for ΔG^E_A, for example, is

$$\Delta G^E_A = \underline{a}\, X_X X_Y + \underline{b}\, X_X X_Y (X_X - X_Y) + \underline{c}\, X_X^2 X_Y^2 \qquad (5)$$

Another modification of Eq. (1) involves a different approximation for Λ:

$$\Lambda = -(\Delta G^\circ + \Sigma\, \lambda_i/2)^2/2ZRT \qquad (6)$$

1168

or even a more general form such as

$$A = -\left(\Delta G^\circ + 2\sum_i \Delta G_i^E(\text{50-50 mixture})\right)^2/2ZRT \qquad (7)$$

The form in Eq. (6) has been found to be necessary in order to calculate miscibility gaps in reciprocal systems. In systems where the binary systems exhibit relatively large deviations from ideality, corrections as in Eqs. (6) and (7) compensate, at least in part, for some of the mathematical peculiarities inherent in a series expansion truncated beyond the second order terms.

Thus far we have considered simple systems. To our knowledge, no rigorous theory exists for charge asymmetric systems with cations and/or anions of different charge types. An empirical extension of equations derived from the CIS theory has been tried. The Gibbs free energy of mixing would read as

$$\Delta G^m = RT[X_A \ln X_A + X_B \ln X_B + X_X \ln X_X + X_Y \ln X_Y] \qquad (8)$$

$$+ X'_A X'_X \Delta G^\circ + X'_A \Delta G^E_A + X'_B \Delta G^E_B + X'_X \Delta G^E_X + X'_Y \Delta G^E_Y$$

$$- X'_A X'_B X'_X X'_Y \frac{(\Delta G^\circ)^2}{2ZRT}$$

where ΔG° is now the standard Gibbs free energy change per equivalent in the metathetical reaction and X' represents equivalent fractions. For a number of asymmetric binary systems, as, e.g., the $AX-BX_2$ system, the excess Gibbs free energies of mixing are reasonably well represented by an expression such as

$$\Delta G^E_X = X'_A X'_B \lambda_X \qquad (9)$$

A test of expressions such as Eqs. (8) and (9) has demonstrated that reasonably representative phase diagrams of asymmetric systems may be calculated a priori from minimal information on the binary systems and from data on the free energies of formation of the four constituents.[9] Where equations such as Eq. (9) do not represent the deviations from ideality of the binaries very well, other more accurate forms may be substituted for ΔG_1^E.

The equations described have been used to calculated a number of liquidus phase diagrams of simple and asymmetric reciprocal systems a priori.[5-9] The correspondence between measured and calculated phase diagrams has generally been good. Consequently, the techniques can be used to reliably predict phase diagrams as illustrated in Fig. 3, which shows the calculated liquidus phase diagram for the $Li^+,Na^+/OH^-,CO_3^=$ system. Knowledge of the phase relations in this system is of special interest for fuel cell technology. Again, this computation has been indeed simplified since neither solid solutions nor compounds have been considered. A more accurate calculation should include the two reported binary compounds; this can be done in a relatively simple and standard manner so that the total Gibbs free energy of the system is minimized. (In the particular case of Fig. 3, the binary compounds undoubtedly subtend a very small fraction of the composition field.)

2. Additive Ternary Systems

The conformal ionic solution theory has also been derived for additive ternary systems up to fourth order terms.[4] If we designate an additive ternary system as AX-BX-CX, for example, the theory leads to the expression

$$\Delta G^E = \sum_{i<j}\sum \lambda_{ij}X_iX_j + \sum_{i\neq j}\sum b_{ij}X_i^2X_j + \sum_{i<j}\sum c_{ij}X_i^2X_j^2 \qquad (10)$$

$$+ AX_1X_2X_3 + \sum_{\substack{i\neq j<k \\ 1}} B_iX_i^2X_jX_k$$

where 1, 2 and 3 represent the salts AX, BX and CX, respectively. All of the coefficients in Eq. (10) can be evaluated from data on the three subsidiary binary systems. The coefficients λ_{ij}, b_{ij} and c_{ij} are directly related to the second, third and fourth order terms which describe the three binary systems. The coefficient B_i is given exactly by the relation

$$B_i = 2(c_{ij}c_{ik})^{1/2} \text{ with } i\neq j\neq k \qquad (11)$$

and to a good approximation A is given by

$$A = -(b_{12}^{1/3} + b_{13}^{1/3})(b_{21}^{1/3} + b_{23}^{1/3})(b_{31}^{1/3} + b_{32}^{1/3}) \qquad (12)$$

where $b_{ij} = -b_{ji}(i\neq j)$. Equation (12) is exact when fourth order terms are not included (e.g., $c_{ij} = 0$ and $B_i = 0$). Up to the second order, the equations derived from the CIS theory appear to be adequate for representing phase diagrams of simple systems containing only monovalent ions and having relatively small deviations from ideality.[3] No systems with binary or ternary compounds, solid solutions, or with cations or anions of different charge type have been yet investigated. Similar to what has been done for reciprocal systems, an extension of Eqs. (10)-(12) can be made to represent the thermodynamics of solutions containing ions of different valences.

Another possible empirical form is

$$\Delta G^E = \sum_{\substack{k \\ k\neq i<j}} X'_k\Delta G^E_{ij} + CX'_1X'_2X'_3 + \sum D_iX_i'^2X'_jX'_k \qquad (13)$$

where X' represents equivalent ion fractions, C and D_i are empirical constants and ΔG^E_{ij} is the total excess Gibbs free energy of mixing of the

binary systems i-j at mole fractions such that the ratio (X_i/X_j) in the binary is the same as in the ternary.

Storage of Phase Diagrams

Thus far, theoretical equations and empirical extensions have been only applied to calculate phase diagrams a priori. They can also be used to construct reliable phase diagrams from a relatively small number of experimental points at key compositions. One potential use which has been considered very little is for the computer storage of complex phase diagrams. Such storage, if techniques for accurately representing ternary phase diagrams can be developed, would provide ready and remote access to large collections of phase diagrams stored in central data banks.

For the storage of phase diagrams, one requires equations which can accurately represent known phase diagrams. The accuracy of the equations in representing phase diagrams can be improved if one relaxes the constraints on the coefficients of all the equations considered. The theory defines these parameters within the limitations inherent in the models used. For example, the parameter Z in Eq. (8) is constrained by the theory to be the same for an entire class of conformal solutions. If Z could be considered as a parameter which can have one of several (let us say 10) possible values, the fit of a calculated phase diagram to any given reliable measurements can be improved. Such an adjustment probably would compensate for higher order terms which are not included in the equations.

In order to utilize Eqs. (8) and (9) combined with the Schröder-van Laar equation to calculate phase diagrams, one requires data on enthalpies of fusion and free energies of formation of the four constituents as well as the four binary parameters, λ_{ij}, and Z. If ΔH_m, ΔG° and λ_{ij} can be considered to be independent of temperature, a minimum of 13 parameters is necessary for one system. If the temperature dependence of the parameters needs to be taken into account, more than 13 are required. However, if one considers a large collection of similar phase diagrams, the number of parameters per phase diagram is reduced considerably because some of the parameters are common to several systems. For example, if one considers all the possible phase diagrams one can make from ten different cations and ten different anions, there are 2025 ternary reciprocal systems, 2400 additive ternary systems, 900 binary systems and 100 different constituent compounds.

To store the ternary reciprocal systems separately without considering the commonality of any of the parameters would require at least 26,000 parameters. By considering all the systems together, one can store all the phase diagrams with a minimum of 900 binary parameters, 100 values of the free energies of formation, 100 values of enthalpies of fusion at a standard temperature, and perhaps 10 values of Z. In order to include binary or ternary compounds or solid solutions, at least one more parameter is necessary per compound or solid solution.

Similarly, for additive ternary systems, if only second order equations are required, each phase diagram would require three parameters λ_{ij} plus three enthalpies of fusion giving a minimum of six parameters for one diagram. For a collection of ten cations and ten anions, the 2400 possible additive ternary systems, if considered separately, would require a minimum of over 10^4 parameters. When considered together, there are a minimum of

only 900 binary parameters λ_{ij}, and 100 parameters for the enthalpies of fusion. For all ternary systems, additive and reciprocal, the minimum number required is 900 binary parameters, 100 enthalpies of fusion, 100 values of the free energies of formation at a standard temperature, and ~10 values of Z.

Thus far, we have considered only a minimal set of parameters. More complex expressions for the excess free energies of mixing of the binary systems would require more. Consideration of the temperature coefficients of any of the parameters would also increase the number. For example, the free energies of formation are functions of temperature. However, taking this into account is not as large an improvement as it might seem since the values of ΔG° which are calculated from these are generally relatively independent of temperature, and ΔG° calculated at one standard temperature for all systems may prove to be reasonable at all temperatures. The temperature coefficients of ΔH_m are usually not important unless liquidus temperatures are much lower than the melting points. Further parameters are required if compounds and solid solutions are accounted for. Even when all these (including temperature coefficients) are considered, the number of parameters needed to describe the large number (4425) of ternary systems one can make from ten cations and ten anions is still relatively small (probably less than 9000 parameters). Consequently, if one considers the complexity of ternary phase diagrams, especially of ternary reciprocal systems, theoretical equations hold the promise of being used for the economical storage of phase diagrams in data banks.

Conclusions

Theories of ternary ionic systems permit one to calculate phase diagrams *a priori*. Such calculations also support their utility in the construction of reliable phase diagrams from a small number of well-chosen experimental measurements. One unexplored use is for the computer storage of complex phase diagrams. If calculational techniques and thermodynamically self-consistent extensions of theory can be developed, the economical storage of accurate phase information in large data banks can be effected.

REFERENCES

*Work performed under the auspices of the U. S. Energy Research and Development Administration.

1. H. Reiss, J. L. Katz and O. Kleppa, J. Chem. Phys. 36, 144 (1962).

2. M. Blander and S. J. Yosim, J. Chem. Phys. 39, 2610 (1963).

3. M. L. Saboungi and P. Cerisier, J. Electrochem. Soc. 121, 1258 (1974).

4. M. L. Saboungi and M. Blander, J. Chem. Phys. 63, 212 (1975).

5. M. Blander and M. L. Saboungi, "Fundamental Aspects of Molten Salt Solutions and Their Applications in Technology," in Proceedings of the International Symposium on Molten Salts, ed., Pemsler et al., The Electrochemical Society, Princeton, N. J. (1976) pp. 93-110.

6. M. L. Saboungi and M. Blander, High Temp. Sci. 6, 37 (1974).

7. M. Blander and L. E. Topol, Inorg. Chem. 5, 1641 (1966).

8. M. L. Saboungi, H. Schnyders, M. S. Foster and M. Blander, J. Phys. Chem. 78, 1091 (1974).

9. M. L. Saboungi and M. Blander, J. Am. Ceram. Soc. 58, 1 (1975).

1178

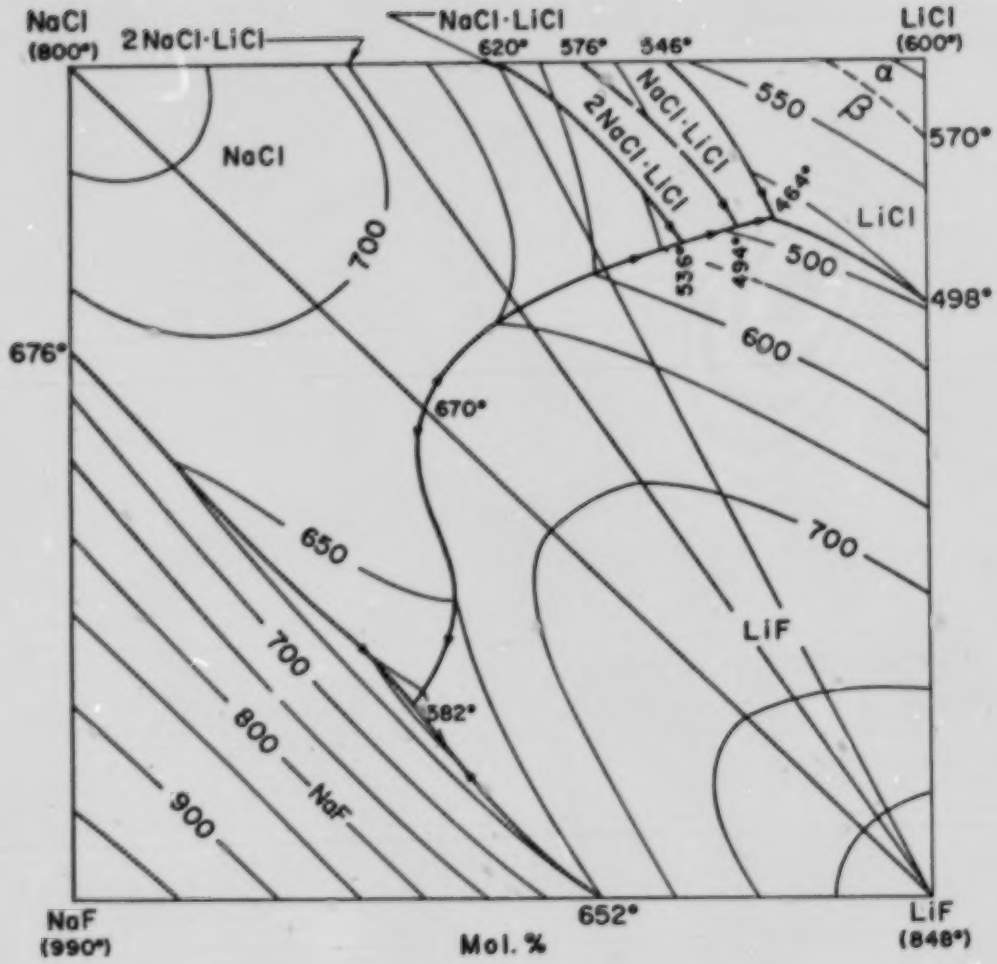

FIGURE 1a. THE MEASURED PHASE DIAGRAM OF $Li^+, Na^+/F^-, Cl^-$

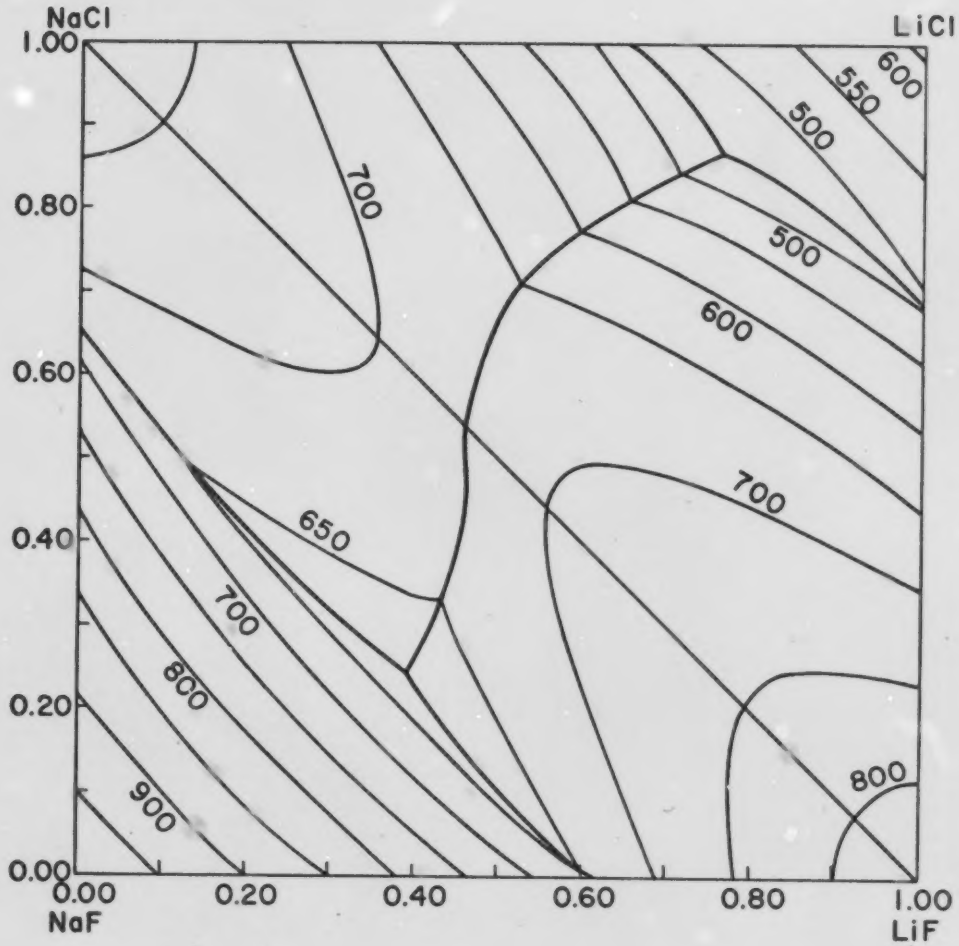

FIGURE 1b. THE CALCULATED PHASE DIAGRAM OF $Li^+,Na^+/F^-,Cl^-$

1178

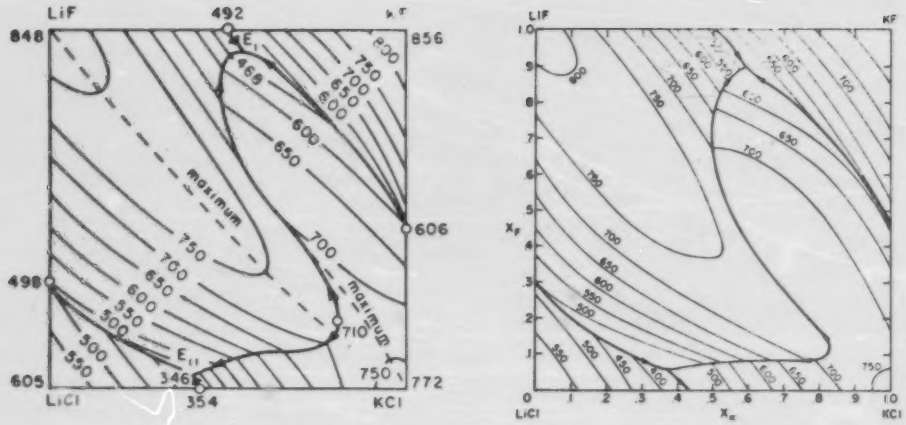

FIGURE 2. THE Li,K/F,Cl PHASE DIAGRAM

a. MEASURED b. CALCULATED

1179

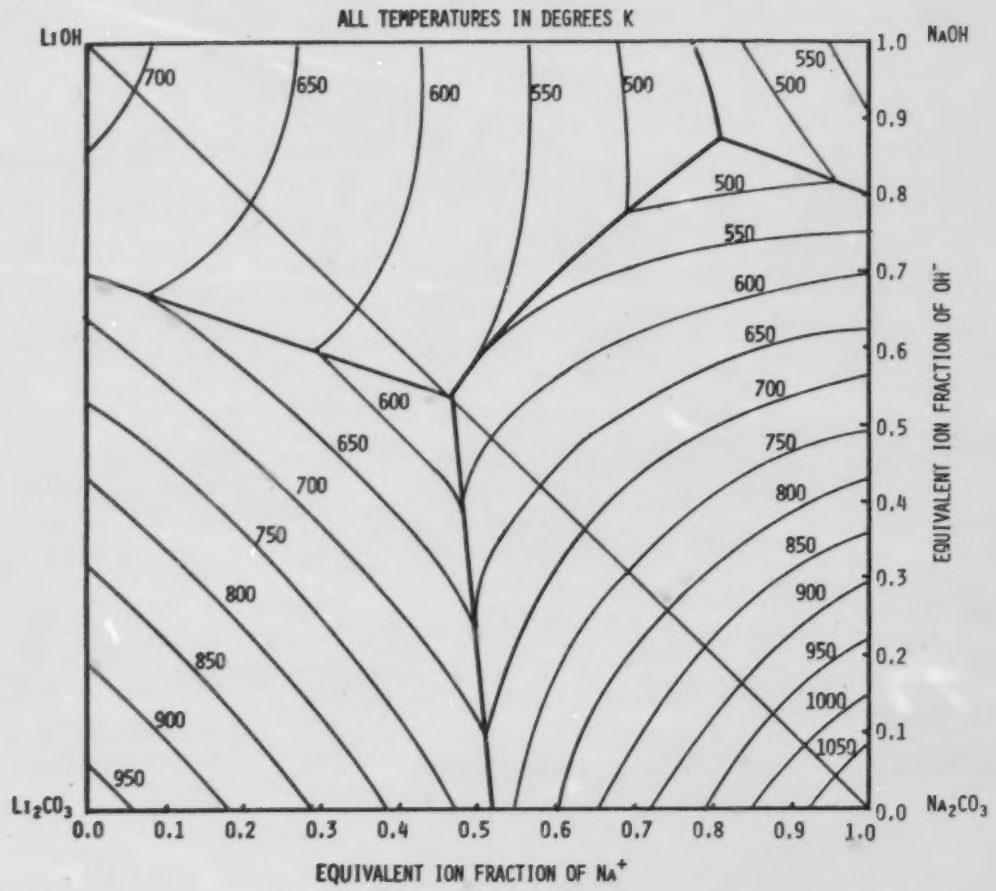

FIGURE 3. COMPUTER GENERATED PHASE DIAGRAM OF THE Li,Na/OH,CO_3 SYSTEM

National Bureau of Standards SP-496, Applications of Phase Diagrams in Metallurgy and Ceramics
Proceedings of Workshop held at NBS, Gaithersburg, Md., January 10-12, 1977

ESTIMATION OF ISOTHERMAL SECTIONS OF TERNARY PHASE DIAGRAMS OF LITHIUM CONTAINING SYSTEMS: THE Al-Li-Mg SYSTEM*

Marie-Louise Saboungi and Chen C. Hsu
Chemical Engineering Division, Argonne National Laboratory, Argonne, Illinois 60439

INTRODUCTION

Currently, in the development of high-temperature batteries at the Argonne National Laboratory, solid Li-Al alloys appear to be the leading candidates for the negative electrode.[1] Despite the overall good performance of the cells, some problems were encountered; after repeated cycling, a loss of capacity accompanied by a change in the morphology of Li-Al alloys was observed.[2] In an effort to overcome these limitations and improve the Li diffusivity in the α-Al, modifications either in the design or in the constituents are being examined. One approach consists of adding an appropriate third element (e.g., Mg) to the Li-Al alloys. Consequently, a knowledge of the phases present in the Al-Li-Mg system and their boundaries at the temperatures of operation of the battery (T ranging from 673 K to 773 K) is vital. In the literature, there are very few and often irreconciliable experimental data related to the phase diagram of the Al-Li-Mg system.[3-6]

These considerations led us to calculate isothermal sections of Al-Li-Mg using a computer-program [7a] developed by Kaufman and Nesor.[7b] In this particular practical case, the numerical method of generating phase diagrams presents several advantages. First, for the subsidiary binary systems, we can check the self-consistency of the measured phase diagrams and the published thermodynamic data and consequently select the most reliable phase diagrams. Second, we can obtain additional information such as the free energy of formation at different temperatures of the reported binary compounds. Third, we can define, to a good approximation, the topological features of the ternary Al-Li-Mg system and therefore minimize the number of measurements necessary to obtain a reliable phase diagram. One needs only few measurements at well-defined compositions to check the accuracy of such calculations.

We report on the calculations of isothermal sections (T = 673 K, 723 K and 773K) of the Al-Li-Mg. An additional temperature (T = 648 K) was investigated to allow for a direct comparison between the calculated phase diagram and earlier data limited to the magnesium-rich corner.

I. Method of Calculations

The numerical method used in this investigation has been extensively described by Kaufman and coworkers. For the sake of brevity, we will only outline the equations used for the solution phase interactions and for the compound-solution interactions in the binary and ternary systems.

1. Solution Phase Interactions

a. Binary Mixtures

In these calculations, an extension of the regular solution model is used to describe the behavior of the mixture. In the i-j system, $G_{ij}(\phi)$, the Gibbs free energy of a solution phase, ϕ, is defined as:

$$G_{i,j}(\phi) = x_i G_i^{\circ}(\phi) + x_j G_j^{\circ}(\phi) + RT[x_i \ln x_i + x_j \ln x_j] + \Delta G_{i,j}^{E}(\phi) \qquad (1)$$

where $G_i^{\circ}(\phi)$ is the Gibbs free energy of the pure ith element in the ϕ phase, x_i is the atomic fraction of the ith element, and $\Delta G_{i,j}^{E}(\phi)$ refers to the excess Gibbs free energy of the solution in the ϕ phase. In what follows, this latter function is assumed to vary with composition according to the equation:

$$\Delta G_{i,j}^{E}(\phi) = x_i x_j [x_i \phi(i,j) + x_j \phi(j,i)] \qquad (2)$$

where $\phi(i,j)$ and $\phi(j,i)$ can be temperature dependent functions. This formulation presents the advantage of taking the asymmetry of the solution into account since $\phi(i,j)$ could differ from $\phi(j,i)$. If $\phi(i,j) = \phi(j,i)$, the

solution is symmetrical. If $\phi(i,j) = \phi(j,i) =$ constant, the solution is regular according to the Hildebrand definition. If $\phi(i,j) = \phi(j,i) = 0$, the solution is ideal. In these calculations, $\phi(i,j)$ and $\phi(j,i)$ are expressed as

$$\phi(i,j) = a + bT \tag{3}$$

and

$$\phi(j,i) = a' + b'T \tag{4}$$

where a, a', b and b' are constants calculated either from reliable thermodynamic data (electromotive force data, calorimetric data, etc.) or from the measured phase diagram using the Schröder-van-Laar equations. Finally, a liquid interaction coefficient can be defined as:

$$L_{i,j}(x_i,x_j) = x_i\, L(i,j) + x_j\, L(j,i) \tag{5}$$

b. Ternary Mixtures

In the ternary system, i-j-k, the Kohler equations[8] are used to describe the solution interactions. The Gibbs free energy of mixing of a solution phase, ϕ, is given by:

$$\Delta G_{i,j,k}(\phi) = G_{i,j,k}(\phi) - \sum_{\alpha} N_\alpha G^\circ_\alpha(\phi) \tag{6}$$

$$= RT \sum_{\alpha} N_\alpha \ln N_\alpha + \frac{1}{2} \sum_{\alpha} \sum_{\beta \neq \alpha} \frac{N_\alpha N_\beta}{(N_\alpha + N_\beta)} [N_\alpha\, \phi(\alpha,\beta) + N_\beta\, \phi(\beta,\alpha)]$$

where α is a running index ($\alpha = i,j,k$) and N_α refers to the atom fraction of the αth constituent ($\sum_{\alpha} N_\alpha = 1$). The quantities, N_α, are easily related to the binary atom fractions, x_α. The coefficients, $\phi(\alpha,\beta)$ and $\phi(\beta,\alpha)$, are those determined in the subsidiary binary, α-β [Eq. (2)]. Consequently, the calculations of the ternary thermodynamic properties can be carried out once the binary coefficients are determined. Using classical relations,

one can derive from Eq. (3), other thermodynamic functions such as $\overline{\Delta G}_\alpha(\phi)$, the partial Gibbs free energy of each element present in the solution, $\Delta S_{i,j,k}(\phi)$, the entropy of mixing and $\Delta H_{i,j,k}(\phi)$, the enthalpy of mixing:

$$\overline{\Delta G}_\alpha(\phi) = \frac{\partial}{\partial n_\alpha} [\Delta G_{i,j,k}(\phi)]_{T,P,n_\beta \neq n_\alpha} \tag{7}$$

$$\Delta S_{i,j,k}(\phi) = - \frac{\partial[\Delta G_{i,j,k}(\phi)]}{\partial T} \tag{8}$$

and

$$\Delta H_{i,j,k}(\phi) = \Delta G_{i,j,k}(\phi) + T\,\Delta S_{i,j,k}(\phi) \tag{9}$$

where n_α is the number of moles of the αth constituent. Finally, the fact that the Kohler equation is symmetrical with respect to each of the components is an advantage over other equations such as the Toop equation.[9]

2. Compound Phase Interactions

a. Binary Mixtures

For the sake of simplicity, all compounds will be considered as having a fixed stoichiometry, i.e., as line compounds. The Gibbs free energy of the compound, P, defined by a fixed stoichiometric composition, x_i^* and x_j^*, is expressed by:

$$G(P) = x_i^* G_i^\circ(\theta) + x_j^* G_j^\circ(\theta) + x_i^* x_j^* [L(x_i^*, x_j^*) - C] \tag{10}$$

where θ is designated as the base phase of the compound, P; $L(x_i^*, x_j^*)$ represents the interactions coefficient in the liquid mixture evaluated at the composition of the compound [Eq. (5)]; and C is defined as the compound parameter.

The choice of the base phase is arbitrary. However, for most of the cases, θ would be identical to the most stable form of either i

or j, at the temperature and pressure of interest. The Gibbs free energy of formation of the compound, P, can be derived from Eq. (10):

$$\Delta G_f(P) = G(P) - x_i^* G_i^\circ(\theta) - x_j^* G_j^\circ(\theta) \qquad (12)$$

$$= x_i^* x_j^* [L(x_i^*, x_j^*) - C]$$

The compound parameter, C, can be computed (i) from data on the thermodynamic functions of formation of the compound, if available; (ii) from the measured phase diagram utilizing mainly the melting point of the compound and some other characteristic liquidus temperatures; (iii) more often, by coupling thermodynamic information with phase diagram data. The compound parameter can be expressed in the following form:

$$C = c_1 + c_2 T \qquad (13)$$

If the compound is unstable, C is usually set equal to zero.

b. Ternary Mixtures

In the ternary system, the present status of the calculations allows for the variation in compound stoichiometry.[10] One can consider a compound, P, defined by a base phase, θ, and having a general composition, N_i, N_j and N_k. The compound is assumed to run between the composition $[(x_i^*)', (x_j^*)']$ in the subsidiary binary, i-j, and the composition (x_j^*, x_k^*) in the adjacent binary, j-k. The general compositions, N_α, can be related to the x_α^* by:

$$N_i = (x_i^*)' - N_j(1+p)$$

$$N_j = 1 - N_i - N_k \qquad (14)$$

$$N_k = (x_j^*)' + N_j p$$

where

$$p = [x_j^* - (x_j^*)']/x_k^* \qquad (15)$$

Then, the Gibbs free energy of the compound can be written as:

$$G(P) = \sum_{\alpha} N_{\alpha} G^{\circ}_{\alpha}(\theta) + RT[N_i \ln N_i + N_j \ln N_j - (1-N_k)\ln(1-N_k)] \qquad (16)$$

$$+ [1 - (N_j/N_k)]\Delta G_f(A) + [N_j/(1-N_k)]\Delta G_f(B)$$

The compound, A, is usually the stable compound positioned on the i-j binary; the Gibbs free energy of formation, $\Delta G_f(A)$, is given by:

$$\Delta G_f(A) = (x_i^*)'(x_j^*)'\left[L[(x_i^*)',(x_j^*)'] - C'\right] \qquad (17)$$

where L and C' are calculated from data on the binary, i-j. The compound, B, positioned on the j-k binary is the "counterphase" of A; the Gibbs free energy of formation of B, $\Delta G_f(B)$, is expressed by:

$$\Delta G_f(B) = x_j^* x_k^* [L(x_j^*, x_k^*) - C] \qquad (18)$$

where L and C are also derived from data on the j-k binary. It should be noted that B can be, and often is, unstable* or even hypothetical; as mentioned earlier, in these cases, C is usually set equal to zero or to an arbitrary value less positive than the value corresponding to A. The compound parameter of B can be considered as an adjustable parameter; for example, if data on the stability of the ternary compound, P, are available, then one can more accurately determine the value of the compound parameter of the counterphase. In this context, the calculations could be improved and set to match the selected data and therefore predict with more reliability the existence of phases and their boundaries in regions inaccessible to measurements.

*By definition, when the Gibbs free energy of formation of a compound is positive, the compound is then metastable or unstable.

The Gibbs free energy of formation of P can be written as:

$$\Delta G_f(P) = G(P) - \sum_{\alpha} N_{\alpha} G^{\circ}_{\alpha}(\theta) \qquad (19)$$

where G(P) is given by Eq. (16). Therefore, the thermodynamic properties of ternary compounds, and consequently the interactions between compounds in the ternary system and the solution phases, are well defined.

II. Results and Discussion

The numerical program used to carry out the present computations has been purchased from L. Kaufman and Nesor (ManLabs, NPL Materials Data Bank). The algorithm has been described elsewhere.[7,10] We will only mention that the interactions in the subsidiary binaries and in the ternary mixture have been calculated on a pair-wise basis.

1. The Al-Li System

As mentioned earlier, the Al-Li alloys appear to be useful as negative electrodes in a high-temperature battery. A rather divergent set of data on the phase diagram of Al-Li exist in the literature.[11-14] The results of the most recent investigation by DTA (differential thermal analyses) techniques complemented by careful metallographic and x-ray analyses are represented in Fig. 1a.[15] Some of the significant differences between the phase diagram of Myles and Settle[15] and that selected by Hansen et al.[16] are:

(i) The shape of the boundary of the solid solutions in the Al-rich side is completely different (one is concave, while the other is convex).

(ii) The melting point of the compound β-LiAl (non-stoichiometric LiAl) is 966 K[15] as opposed to 991 K.[16] In addition, the limits of the solubility of the α-Al (FCC-Al) in the β-LiAl disagree considerably with earlier data.

(iii) The data of Myles and Settle confirm the existence of the compounds Al_2Li_3 and Al_4Li_9 observed first by Tebbe et al.[14] and Hansen and Smith,[13] respectively. The stability of the peritectically melting compound, $AlLi_2$, remains questionable.

In our calculations of the phase diagram of Al-Li, we have tried to couple the thermodynamic information when available[17-20] and the phase diagram of Myles and Settle. The lattice stabilities of the constituents are given in Table I; some [such as $G^{\circ}_{Al}(L) - G^{\circ}_{Al}(FCC)$] are selected from standard thermochemical tables,[21] and others [such as $G^{\circ}_{Al}(L) - G^{\circ}_{Al}(HCP)$] are estimated by Kaufman.[22] The interaction coefficients of the solution phases are calculated from recent emf (electromotive force) measurements[17,18] using Eqs. (2)-(4). The calculated values are given in Table II.

The three compounds, AlLi, Al_2Li_3 and Al_4Li_9, are treated as line compounds. The compound parameter of AlLi was calculated from both emf data[19] obtained between T = 282-389°C and the measured melting point (T = 966 K).

The Gibbs free energy of formation of Al_2Li_3 was calculated at the metastable melting point* from Eqs. (10)-(13). Some values of the liquidus temperatures were also used to calculate the variations of the compound parameter with temperature (Table III).

To our knowledge, there is no thermodynamic information available for Al_4Li_9. Therefore, the liquidus temperatures were used to calculate the compound parameter, C (Table III).

In order to compute the phase diagram, the following interactions were considered: L vs. FCC, L referring to liquid; L vs. LiAl; FCC vs. LiAl; L vs. Al_2Li_3; and L vs. Al_4Li_9. The resultant phase diagram is given in

*The metastable melting point is determined by extrapolating the liquidus up to the stoichiometric composition.

Fig. 1b. The calculated and experimental phase diagrams are in excellent agreement except in the Al-rich side; the shape of the computed solid solution boundary is closer to that selected by Hansen[16] which is consistent with expectations for such solid solutions. The calculations also gave a better defined limit for the solubility of LiAl in Al(FCC). This limit has not been determined experimentally (note the dashed lines in Fig. 1a).

The computations are not only useful in constructing the phase diagrams but also in checking the self-consistency of the published thermodynamic data with the liquidus. For example, the computed Gibbs free energies of formation of the compounds (Table III) are in reasonable agreement with available measurements. For LiAl, our values compare well with those of Yao et al.[19] (Table IV). However, at higher temperatures, the difference between our calculations and the values obtained by extrapolating the least-square fitted equation of Yao et al.[19] increases somewhat: at T = 773 K, ΔG_f(obs.) = -3.24 kcal (g-atom)$^{-1}$ and ΔG_f(calc.) = -2.93 kcal (g-atom)$^{-1}$.

Recently, Selman et al.[20] estimated the Gibbs free energy of formation of Li_3Al_2 from pure liquid Li and pure solid Al(FCC), using emf data in the lithium-rich lithium-aluminum alloys. At 700 K, their value is -14.1 kcal (g-atom)$^{-1}$, while we obtain -15.5 kcal (g-atom^{-1}). If one takes into account the different approximations in either calculation, one realizes that the differences between the two values are not significant.

On the one hand, Selman et al.[20] derived the free energy of formation of Li_3Al_2 from the reactions:

$$Li(L) + Al(FCC) \rightarrow LiAl \qquad (20)$$

and

$$2LiAl + Li(L) \rightarrow Li_3Al_2 \qquad (21)$$

It implies that the solubility of Li in Al(FCC) was neglected and that data from the lithium-poor end member of the range of solid solutions were utilized.[20] In addition, the free energy of reaction (20) was derived from the extrapolation of the data of Yao et al.; the extrapolated values for ΔG_f°(LiAl) differ somewhat from our calculations. On the other hand, we have considered LiAl to be stoichiometric. We have also based our calculations on the experimental phase diagrams.

Finally, for Al_4Li_9, we have derived values of the enthalpies of formation and entropies of formation (Table III). As mentioned earlier, the lack of thermodynamic information does not allow direct comparison between experiments and calculation. However, we believe that the values given in Table III could be considered as a reasonable approximation since the computed and the measured Li-rich portions of the liquidus are in good consonance.

2. The Al-Mg System

The phase diagram selected by Hultgren et al.[23] is given in Fig. 2a. The following compounds have been reported: β-Al_3Mg_2, γ-$Al_{12}Mg_{17}$, ϵ-$Al_{30}Mg_{23}$, and γ' of unknown structure. While thermodynamic properties on liquid alloys (e.g., enthalpy, entropy, etc.) are available in selected tables,[23] there is not thermodynamic information on solid alloys. This lack of data led us to compute a slightly simplified version of the phase diagram. Only two compounds, Al_3Mg_2 and Al_9Mg_{11}, with a fixed stoichiometry have been considered. Therefore, the following interactions are calculated: L vs. FCC, L vs. HCP, L vs. Al_3Mg_2, L vs. Al_9Mg_{11}, FCC vs. Al_3Mg_2, and HCP vs. Al_9Mg_{11}. The values for the lattice stabilities of the components are given in Table I; the interactions in the solution phase (Table II) are approximated by a symmetrical function [ϕ(Al,Mg) = ϕ(Mg,Al) with ϕ = L, FCC and HCP]. The

compound parameters for the two compounds are calculated using the phase field of the compounds and assuming an equal melting point, T = 735 K.

The computed phase diagram is given in Fig. 2b. Except for the fact that the solubility of the compounds in Al(FCC) and in Mg(HCP) is neglected, there is excellent agreement between the two representations. The coordinates of the sets of points separating two different phases are very close (compare on the one hand X_{Mg}(obs.) = 0.19 and X_{Mg}(obs.) = 0.379 to X_{Mg}(calc.) = 0.190 and X_{Mg}(calc.) = 0.350 and on the other hand X_{Mg}(obs.) = 0.699 and X_{Mg}(obs.) = 0.884 to X_{Mg}(calc.) = 0.700 and X_{Mg}(calc.) = 0.880). The calculated enthalpy and entropy of formation for the compounds $Al_{0.45}Mg_{0.55}$ and $Al_{0.6}Mg_{0.4}$ are given in Table III.

3. The Li-Mg System

Hansen and Anderko[16] report two completely different sets of liquidus and solidus curves for the lithium-rich side of the phase diagram of Li-Mg There is no explanation for the inconsistency between the two sets of data since the experimental methods followed in the two investigations are identical. However, in the Mg-rich side, there is substantial agreement between all published results. In this specific case where a choice of liquidus and solidus curves would seem rather arbitrary, the computations of the phase diagram using a thermodynamically self-consistent method would provide a valuable tool for performing this selection.

There is also a rather significant discrepancy in the thermodynamic data for the liquid alloys.[24,25] Recently, one of us has measured the activity of molten lithium-magnesium alloys using an emf technique.[25] The results differ considerably from those of Mashovets and Puchkov[24] derived from the Mg vapor pressure measurements. Mashovets et al. have calculated, using the Gibbs-Duhem equation, the activity of Li from that of Mg. There is no indication of the reproducibility of their data.

In these calculations, we have selected the emf data[25] to compute the liquid interaction coefficients, we have obtained L(Li,Mg) = L(Mg,Li) = -11200 + 10 T (cal mol^{-1}). The solid (FCC, HCP and BCC) interaction coefficients were evaluated using, on the one hand, L(Mg,Li) and L(Li,Mg) and on the other hand, liquidus temperatures on the Mg-rich side for which the published experimental results are in consonance. The values of Φ(Mg,Li) and Φ(Li,Mg) are given in Table II. The compound $LiMg_2$ was not included in our calculations since it has not been corroborated by more recent work. The computations of the phase diagram were performed by calculating the curves representing the following interactions*, L vs. HCP, L vs. BCC and HCP vs. BCC.

The resultant phase diagram, given in Fig. 3a, agrees best with the data of Grube et al.[26] (Fig. 3b), which are the higher set of liquidus and solidus curves from the two alternative sets of phase diagrams given by Hansen. This selection performed on thermodynamic self-consistency basis is different from the rather arbitrary choice of Hultgren et al.[23] It is desirable that such basis for selection would be adopted when several different data are published.

4. The Al-Li-Mg System

Alloys of Al-Li-Mg have been of interest from a practical point of view. They were primary candidates in a search for ductile, malleable structural materials.[6] However, to our knowledge, there is rather incomplete and inconsistent information in the literature on the phase diagram.

Shamrai, in a series of papers, Ref. 3 being the last, reported the phase diagrams of Al-Li-Mg as well as isothermal sections at 20°C and 400°C. The ternary compound $MgLiAl_2$ was identified.

*Lithium is known to have two forms: The α-Li with the HCP structure isotopic with Mg and the β-Li with the BCC structure isotypic with W.[21] In our calculations, Li is considered to be BCC since the transformation from the α-phase to the β-phase occurs at 80 K.

Frost et al.[4] studied the phase relationships at 700°F (≡371°C) for several compositions of the alloys.

Jones et al.[5] reported the 500°F and 700°F isothermal sections of Al-Li-Mg alloys. The ternary compound $MgLi_2Al$ was identified.

Finally, Rowland et al.[5] investigated some isothermal sections of the magnesium-rich corner of the Al-Li-Mg system. Their metallographic and x-ray results did not confirm the existence of the compound $MgLi_2Al$ at equilibrium.

When comparisons are possible, the different investigations show disagreement. The latest data are in contradiction with those of Shamrai; not only the compositions are irreproducible, but also there is a significant difference in the phases. It seems impossible to reconcile the data of Shamrai with the others even by considering the minor differences in temperature (400°C vs. 375°C or 371°C). The four latest investigations show an overall consistency with slight differences in the compositions of the boundaries of different phases. However, the x-ray diffractions data of Rowland et al.[6] do not corroborate the existence of the ternary compound $MgLi_2Al$ observed by Jones et al.[5] and credited to the Dow Chemical Company. To quote them, "From this it must be assumed that an equilibrium compound $MgLi_2Al$ does not exist in the temperature range 100° to 400°C" (Ref. 6, p. 357). We can conclude that if the ternary compound $MgLi_2Al$ does exist, it should be metastable.

Finally, one has to be aware that even in the most recent investigation,[6] the liquidus of the subsidiary binary Li-Al was not well defined. For example, Rowland et al.[6] referred to Li_2Al as a stable compound; as mentioned earlier, it has been proven that Li_2Al is indeed Li_9Al_4. Also, the existence of Li_3Al_2 was not yet known. As a consequence of the

uncertainties and without further experimental evidence, we did not include any ternary compound in our calculations.

The isothermal sections of the Al-Li-Mg system calculated are given in Fig. 4 for T = 673 K, Fig. 5 for T = 728 K, Fig. 6 for T = 773 K and Fig. 7 for T = 648 K. They were computer generated by considering all the possible interactions on a pair-wise basis:

At the Al-rich corner: FCC vs. LiAl, FCC vs. L, FCC vs. Al_3Mg_2, L vs. Al_3Mg_2, L vs. LiAl

At the Li-rich corner: L vs. Li_3Al_2 and L vs. BCC

At the Mg-rich corner: HCP vs. L, HCP vs. BCC, HCP vs. Al_9Mg_{11} and L vs. Al_9Mg_{11}

The interaction coefficients $\Phi(i,j)$ as well as the compound parameters, C, calculated in the subsidiary binaries are used in Eqs. (6)-(19). Only the stable part of the curves representing each couple of interactions are drawn in the final plots given in Figs. 4-7. In the computation of the compound interactions, the counterphase (refer to Section II) always consisted of a hypothetical compound located on the adjacent binary and by definition less stable than the compound studied. In this particular case, we did not use any information from the experimental phase diagram in the calculations (i.e., solubility of LiAl in Mg, etc.). Therefore, we always set the compound parameter of the "counter-phase" equal to zero. It is important to realize the significance of this approximation on the shape of the boundaries between two different regions and even on the stability of some phases. For example, in Fig. 4, a hypothetical compound, H, on the Li-Mg binary was assumed to be the counterphase of Li_3Al_2. If the compound parameter of H was different from zero, it is probable that the phase field of the two-phase region[7] of (Li_3Al_2 + L) would be larger.

This illustrates the importance of the existence of reliable experimental data at "key" compositions of the Al-Li-Mg alloys.

At T = 723 K (Fig. 5), the liquid phase becomes more significant and the phase fields of the Al-Mg compounds less important. At T = 773 K (Fig. 6), only the LiAl and Li_3Al_2 binary phases are stable. As expected, the liquid phase covers a large area. The isothermal section at T = 648 K (375°C) was calculated in order to allow a better comparison with the data of Rowland et al.[6] collected for the Mg-rich corner; indeed, a direct comparison cannot really be done since Rowland et al.[6] were not aware of the existence of Li_3Al_2. However, there is reasonable agreement between our computed isotherm and the experimental data, if one takes into consideration the differences in the binary Li-Al. What is the most striking similarity between Fig. 7 and the x-ray data of Rowland et al.[6] is the non-existence of the liquid phase. Note that a 25 K difference led to the disappearance of the liquid in the Mg-rich side of the system.

Finally, it should be emphasized that these calculations must not be considered as final. It would be desirable to have some experimental information as feedback. Modifications can be easily performed to (i) include ternary compounds (stable or metastable); (ii) change the stability of the compounds generated from the binary compounds; and (iii) include any reliable data on the solubility of a component, C, in a binary solution, A-B. These changes can be easily performed within the framework of the present computer-program. However, there are different limitations inherent in the techniques and models used which one has to be aware.

It is not always possible to represent the thermodynamic properties of the binary solutions by equations such as Eqs. (2)-(4). It has been shown in detail by Darken[27] that simple polynomials could not always be

used for the excess Gibbs free energy of mixing of some binary systems such as Mg-Bi. Particularly in the case of Li-Pb,[28] we have shown that the curve representing the variations of $\overline{\Delta G}^{xs}_{Li}$ versus the atom fraction of Pb, X_{Pb}, exhibits an "S" shape and has an inflection point. In these cases, it would be preferable to use other numerical methods to solve the equations (i.e., one could use a spline function to interpolate the intermediate values).

The thermodynamic representation of ternary solutions can also be improved. The Kohler equations are not as precise as one would desire and particularly when the interactions in the subsidiary binaries are significant. A correctional term to these equations should be considered. In a study of ternary ionic systems, Saboungi and Blander[29] developed equations to represent the thermodynamic properties. Up to the third order expansion, they obtain:

$$\Delta G^{E}_{m} = \sum_{i<j}\sum a_{ij}N_iN_j + \sum_{i\neq j}\sum b_{ij}N_i^2N_j + AN_1N_2N_3 \qquad (22)$$

where A is related to the binary interaction coefficients by:

$$A = -(b_{12}^{1/3} + b_{13}^{1/3})(b_{21}^{1/3} + b_{23}^{1/3})(b_{31}^{1/3} + b_{32}^{1/3}) \qquad (23)$$

A similar term might be introduced in the ternary alloy equations. Different theoretical, rather than empirical, equations should be tried.

CONCLUSION

The method of Kaufman and coworkers is used to provide an estimate of isothermal sections of the Al-Li-Mg system. One starts by calculating the lattice stability of the constituents, the binary interaction coefficients and the binary compound parameters. In the computations, thermodynamic data, when available, were coupled with measured phase diagrams

to provide thermodynamically self-consistent liquidus and solidus curves for the binary systems. Standard enthalpies of formation and entropies of formation were calculated for the reported compounds. The binary system Li-Mg illustrates the use of such calculations in selecting the most reliable representation of the phase diagram.

The calculated binary data were used to compute the phase diagram of Li-Al-Mg, assuming that no ternary compounds exist.

Despite some limitations due mainly to the formalism used (i.e., simple polynomials to fit binary data, the use of the Kohler equations for the thermodynamics of the ternary system), this numerical tool remains useful in providing a reasonable prediction of thermodynamically self-consistent ternary phase diagrams. One of the most attractive features is the fact that the accuracy of the calculations can be improved greatly with a very small amount of experimental information.

ACKNOWLEDGMENTS

We are indebted to both Larry Kaufman and Harvey Nesor for their often-needed help in "debugging" some problems encountered when running the program. Special thanks are due to Milton Blander for his continuous encouragement and advice. We also thank our colleagues Donald Vissers and Michael Roche for keeping us informed of arising technical problems. Finally, we are grateful to Janet Steinquist for typing this manuscript and to the unknown FTS operator who made this long-distance computation possible.

REFERENCES

*This work was performed under the auspices of the U. S. Energy Research and Development Administration.

1. P. A. Nelson et. al., USAEC Report ANL-8058, Argonne National Laboratory, Argonne, Illinois (1974).
2. P. A. Nelson et al., USAEC Report ANL-75-1, Argonne National Laboratory, Argonne, Illinois (1975).
3. F. I. Shamrai, Izvest. Akad. Nauk. S.S.S.R. Otdel. Khim. Nauk., 290-310 (1948).
4. P. D. Frost, J. G. Kura and L. W. Eastwood, Trans. AIME 188, 1277 (1950); Journal of Metals (Oct. 1950).
5. A. Jones, J. H. Lennon, R. R. Nash, W. H. Chang and E. G. Mac Peek, Technical Report 52-169 (1952), U. S. Air Force, Air Research and Development Command, Wright Paterson Air Force Base.
6. J. A. Rowland, Jr., C. E. Armantrout and D. F. Walsh, Trans. AIME, 355 (1955).
7. a) ManLabs - NPL Materials Data Bank
   b) L. Kaufman and H. Nesor, "Treatise on Solid State Chemistry," N. B. Habbay, Ed., Plenum Press, New York 5 179-232, (1975).
8. F. Kohler, Monatsch f. Chemie 19, 738 (1960).
9. G. N. Toop, Trans. Met. Soc. AIME 233, 850 (1965).
10. L. Kaufman and H. Nesor, Z. Metallk. 64, 249 (1973).
11. G. Grube, L. Mohr and L. Breuning, Z. Elektroch. 41, 880 (1935).
12. F. I. Shamrai and P. Ya. Saldau, Izvest. Akad. Nauk. S.S.S.R., Otdel. Khim. Nauk., 631 (1937).
13. D. A. Hansen and J. F. Smith, Acta Cryst. 24, 913 (1968).

14. K. F. Tebbe, H. G. von Schnering, B. Ruter and G. Rabeneck, Z. Naturforsch. 28b, 600 (1973).

15. K. M. Myles, F. C. Mrazek, J. A. Smaga and J. L. Settle, in "Proceedings of the Symposium and Workshop on Advanced Battery Research and Design," March, 1976, U.S. ERDA Report, ANL-76-8, p. B-50.

16. M. Hansen and K. Anderko, Constitution of Binary Alloys, McGraw-Hill Book Co. Inc., New York, 1958.

17. S. P. Yatsenko and E. A. Saltykova, Russ. J. Chem. Phys. 48, 1402 (1974).

18. M. L. Saboungi and M. Blander, J. Electrochem. Soc. (in press).

19. N. P. Yao, L. A. Heredy and R. C. Saunders, J. Electrochem. Soc. 118, 1039 (1971).

20. J. R. Selman, D. K. DeNuccio, C. J. Sy and R. K. Steunenberg (in press).

21. R. Hultgren, P. D. Desai, D. T. Hawkins, M. Gleiser, K. K. Kelley and D. D. Wagman, "Selected Values of the Thermodynamic Properties of the Elements," American Society for Metals, Metals Park, Ohio, 1973.

22. L. Kaufman, personal communication.

23. R. Hultgren, P. D. Desai, D. T. Hawkins, M. Gleiser and K. K. Kelley, "Selected Values of Thermodynamic Properties of Binary Alloys," American Society for Metals, Metals Park, Ohio, 1973.

24. V. P. Mashovets and L. V. Puchkov, Zh. Prikl. Khim. 38(8), 1875 (1965).

25. M. L. Saboungi and M. Blander, J. Electrochem. Soc. 122, 1631 (1975).

26. G. Grube, H. V. Zeppelin and H. Bumm, Z. Elektrochem. 40, 160 1934

27. L. S. Darken, Trans. Metall. Soc. AIME (Am. Inst. Min. Metall. Pet. Eng.) 239, 80 (1967).

28. M. L. Saboungi, J. J. Marr and M. Blander (to be published).

29. M. L. Saboungi and M. Blander, J. Chem. Phys. 63(1), 212 (1975).

Table I

Lattice Stability Values for Aluminum, Lithium and Magnesium

Element	Lattice Stabilities (cal mol^{-1})
Al	$G^\circ(L) - G^\circ(FCC) = 2560 - 2.75\ T$
	$G^\circ(L) - G^\circ(BCC) = 150 - 1.60\ T$
	$G^\circ(L) - G^\circ(HCP) = 1250 - 2.32\ T$
Li	$G^\circ(L) - G^\circ(FCC) = 427 - 1.71\ T$
	$G^\circ(L) - G^\circ(BCC) = 717 - 1.58\ T$
	$G^\circ(L) - G^\circ(HCP) = 727 - 1.71\ T$
Mg	$G^\circ(L) - G\ (FCC) = 1675 - 2.75\ T$
	$G^\circ(L) - G^\circ(BCC) = 1040 - 1.60\ T$
	$G^\circ(L) - G^\circ(HCP) = 2140 - 2.32\ T$

1209

Table II

Calculated Interaction Parameters* for the Solution Phases of the Al-Li, Al-Mg and Li-Mg Systems

$\phi(i,j)$ (cal mol^{-1})	Phase ϕ			
	L	FCC	BCC	HCP
ϕ(Al,Li)	-9600 + 8.0 T	-3000	9999	-3000
ϕ(Li,Al)	-20,000 + 16.0 T	-22,000 + 16.0 T	9999	-22,000 + 16.0 T
ϕ(Al,Mg)	-2400 + 0.8 T	-300	0	0
ϕ(Mg,Al)	-2400 + 0.8 T	-300	0	0
ϕ(Li,Mg)	-11,200 + 10.0 T	-5100 + 3.0 T	-9500 + 7.0 T	-5100 + 3.0 T
ϕ(Mg,Li)	-11,200 + 10.0 T	-9000 + 7.0 T	-13,900 + 10.0 T	-9000 + 7.0 T

*$\Delta G^{E}_{i,j}(\phi) = x_i x_j [x_i \phi(i,j) + x_j \phi(j,i)]$

1201

Table III

Calculated Parameters,* Enthalpies of Formation,** and Entropies of Formation** of the Compounds of the Li-Al and Al-Mg Systems

Compound, P	Compound Parameter, C	$\Delta H_f(P)$	$\Delta S_f(P)$
$Al_{0.308}Li_{0.692}$	13,648 - 10.0 T	-7573	7.047
$Al_{0.40}Li_{0.60}$	15,688 - 11.0 T	-8847	7.838
$Al_{0.5}Li_{0.5}$	7839 + 0.19 T	-7153	5.182
$Al_{0.45}Mg_{0.55}$	3180	-3620	2.948
$Al_{0.60}Mg_{0.40}$	3180 + 0.21 T	-3545	2.892

*The compound parameters, C, are calculated using for the five compounds FCC as the base phase [cal $(g\text{-atom})^{-1}$].

**The enthalpies of formation [in cal $(g\text{-atom})^{-1}$] and entropies of formation [in cal$(g\text{-atom})^{-1}$ K^{-1}] are defined as follows:

$$\Delta H_f(P) = H(P) - x_i^* H_i^\circ(L) - x_j^* H_j^\circ(L)$$

and

$$\Delta S_f(P) = S(P) - x_i^* S_i^\circ(L) - x_j^* S_j^\circ(L)$$

Table IV

Observed[19] and Computed Gibbs Free Energy of Formation of $Li_{0.5}Al_{0.5}$*

T°K	$-\Delta G_f$(obs.) [kcal(g-atom)$^{-1}$]	$-\Delta G_f$(calc.) [kcal(g-atom)$^{-1}$]
573	3.74	3.69
623	3.62	3.50
653	3.54	3.39

$\Delta G_f = G(Li_{0.5}Al) - 0.5\ G^*_{Al}(L) - 0.5\ G^*_{Al}(FCC)$

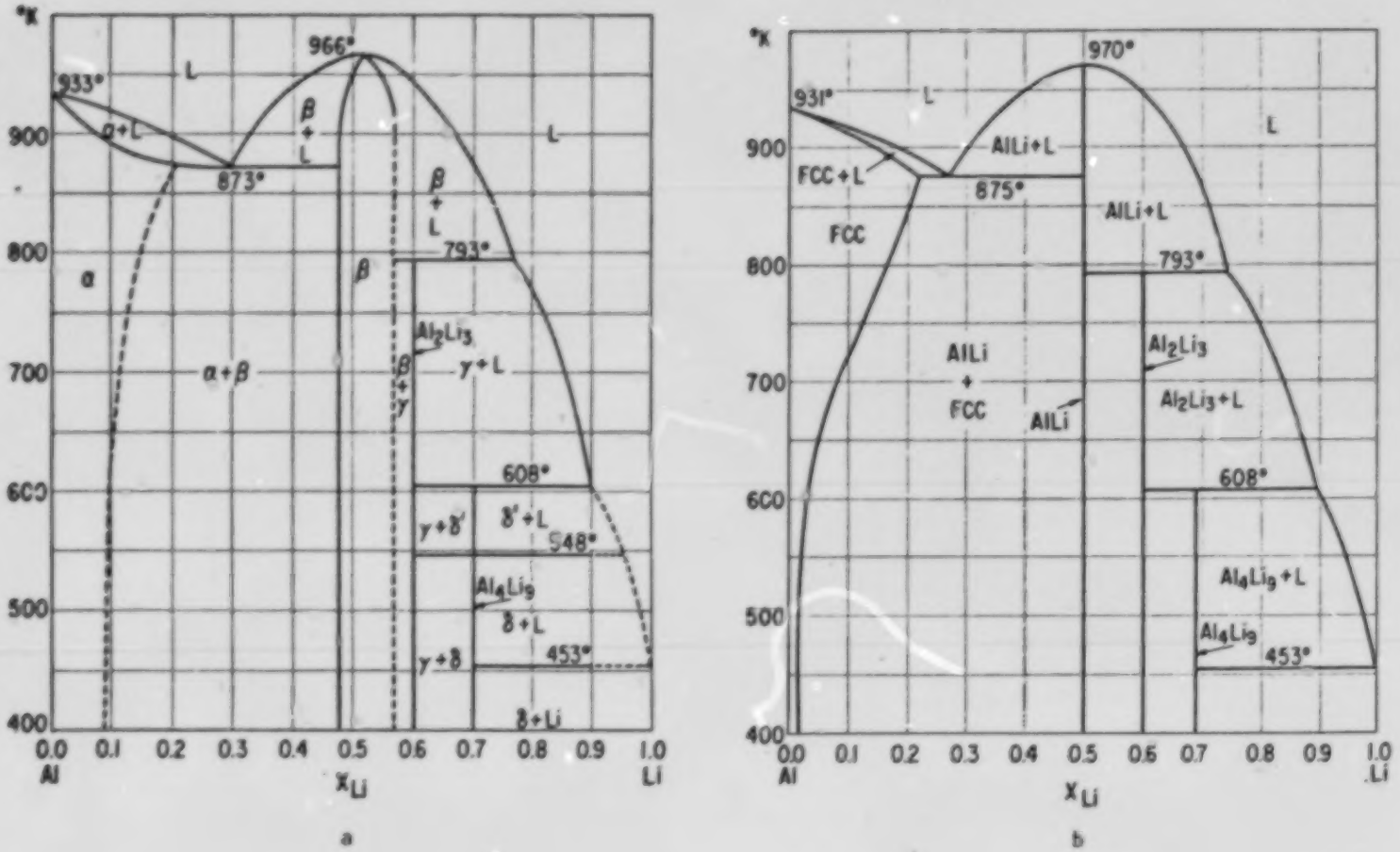

Fig. 1 a. The measured phase diagram of the Al-Li system (Ref. 15).

b. The calculated phase diagram.

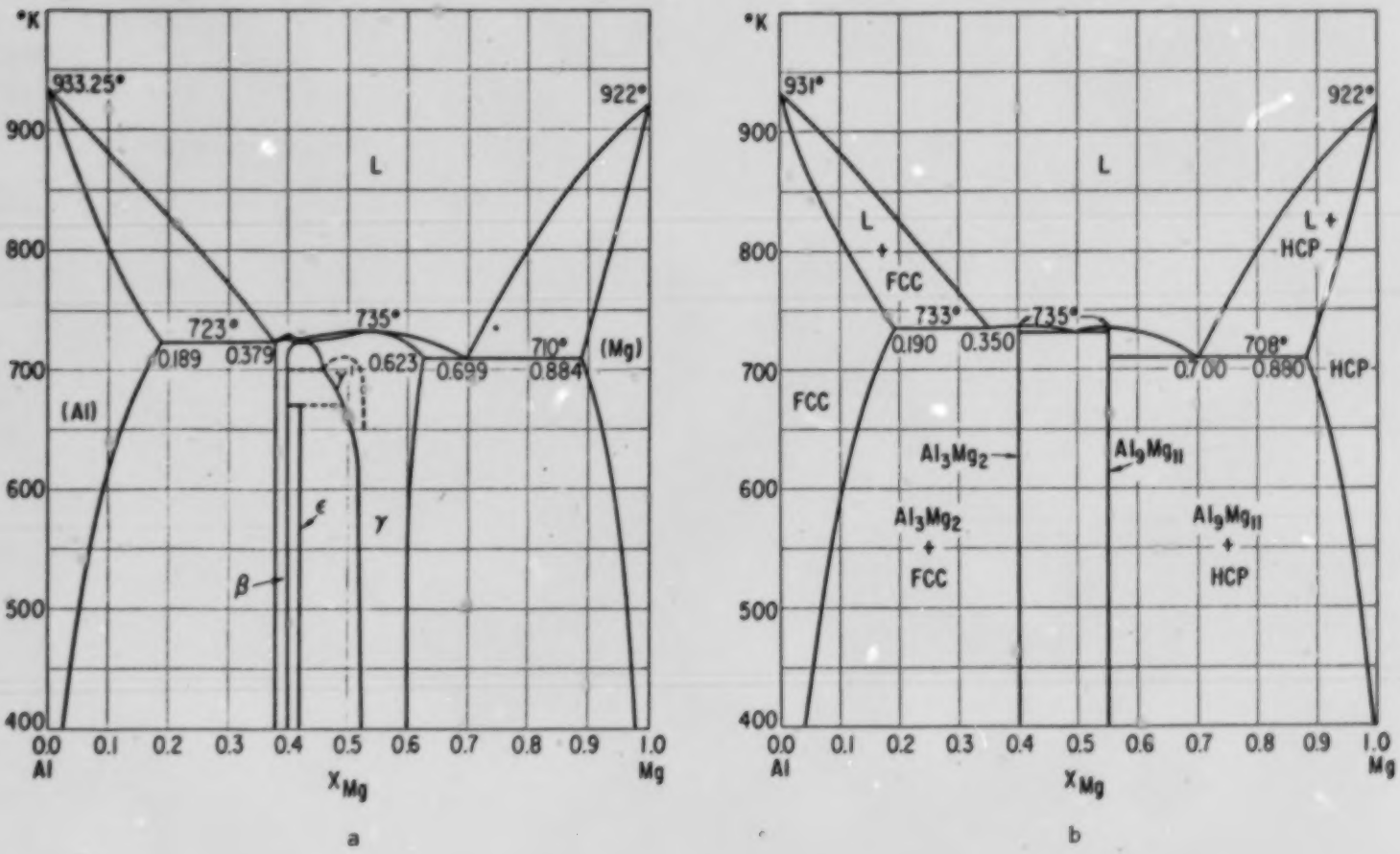

Fig. 2 a. The measured phase diagram of the Al-Mg system (Refs. 16 and 23).

b. The calculated phase diagram.

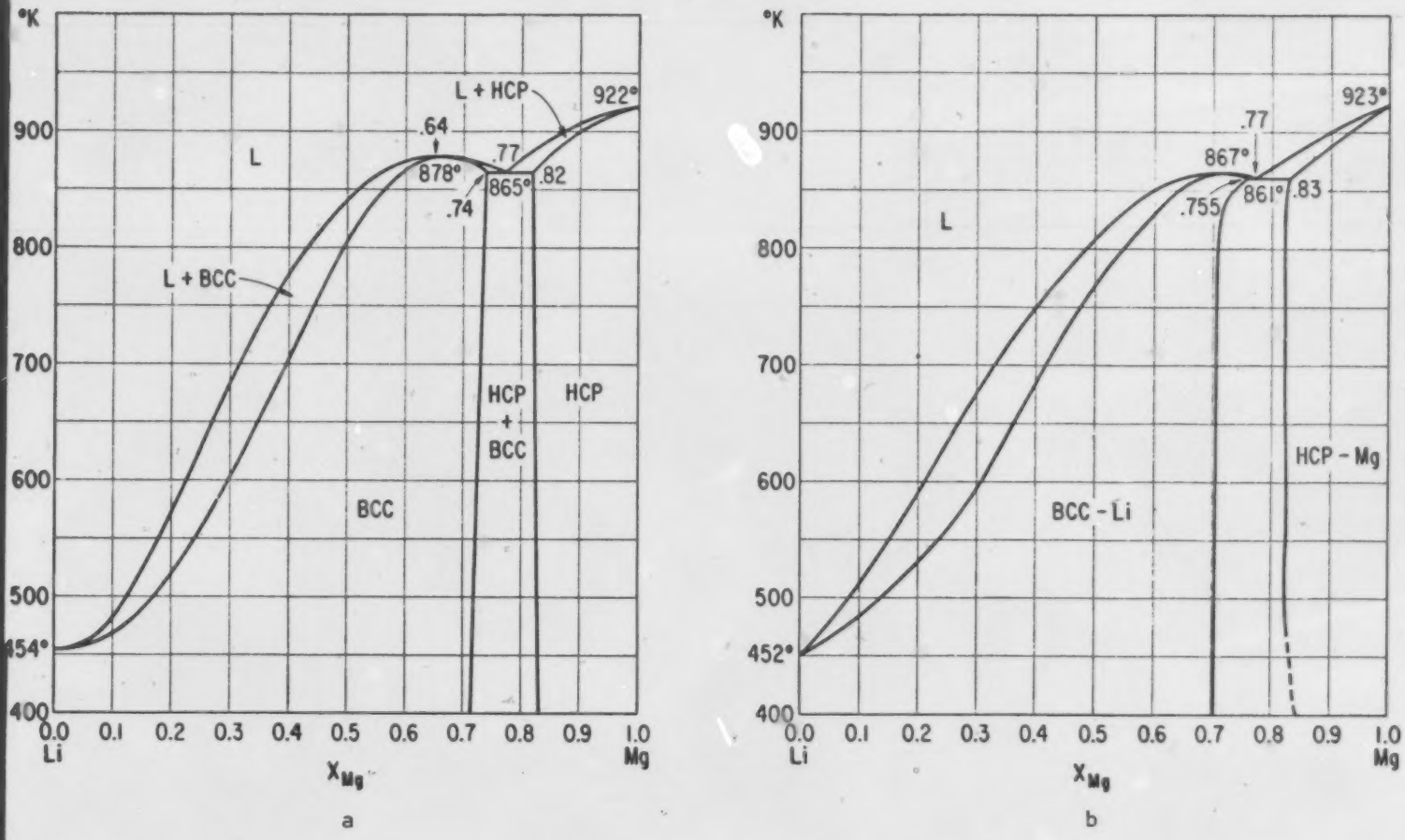

Fig. 3 a. The calculated phase diagram of the Li-Mg system.

b. The measured phase diagram (Refs. 16 and 26).

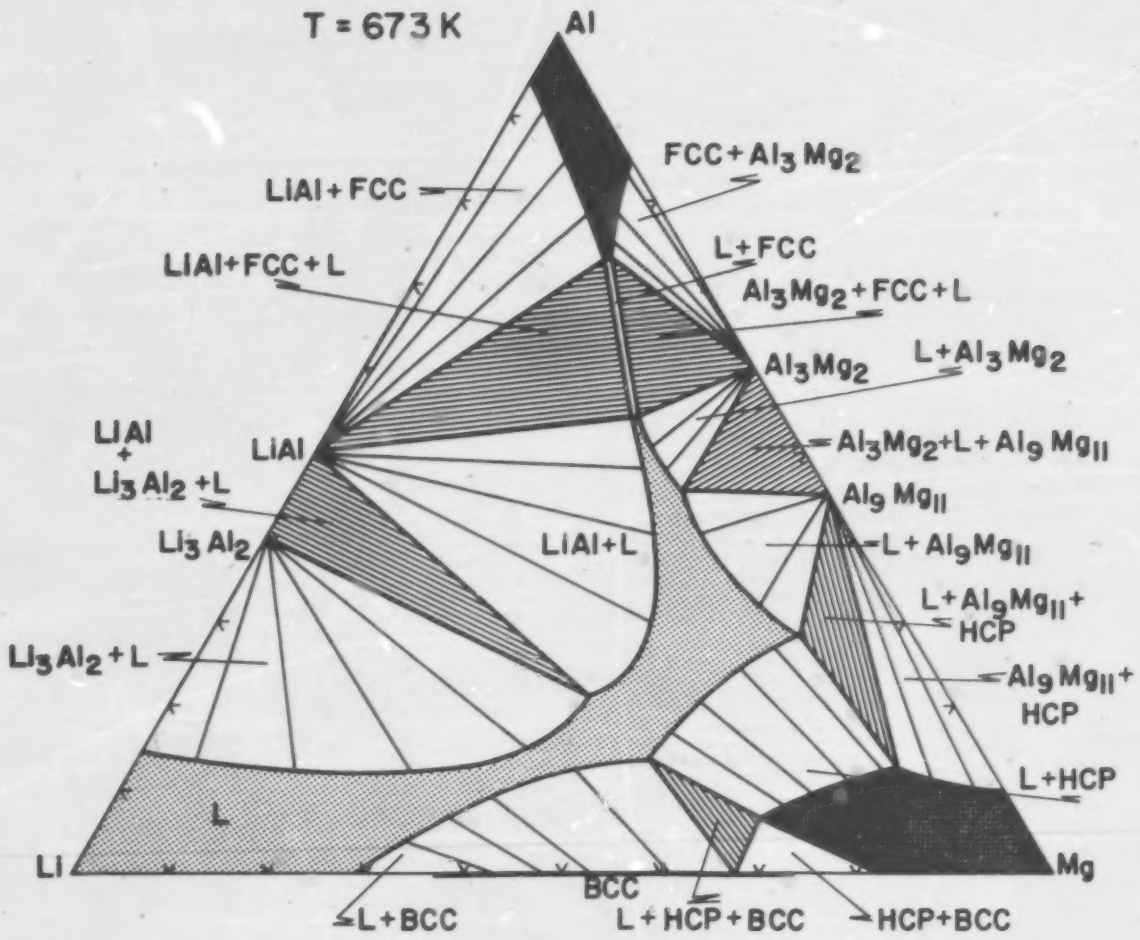

Fig. 4 Computed 673K isotherm of the Al-Li-Mg system.

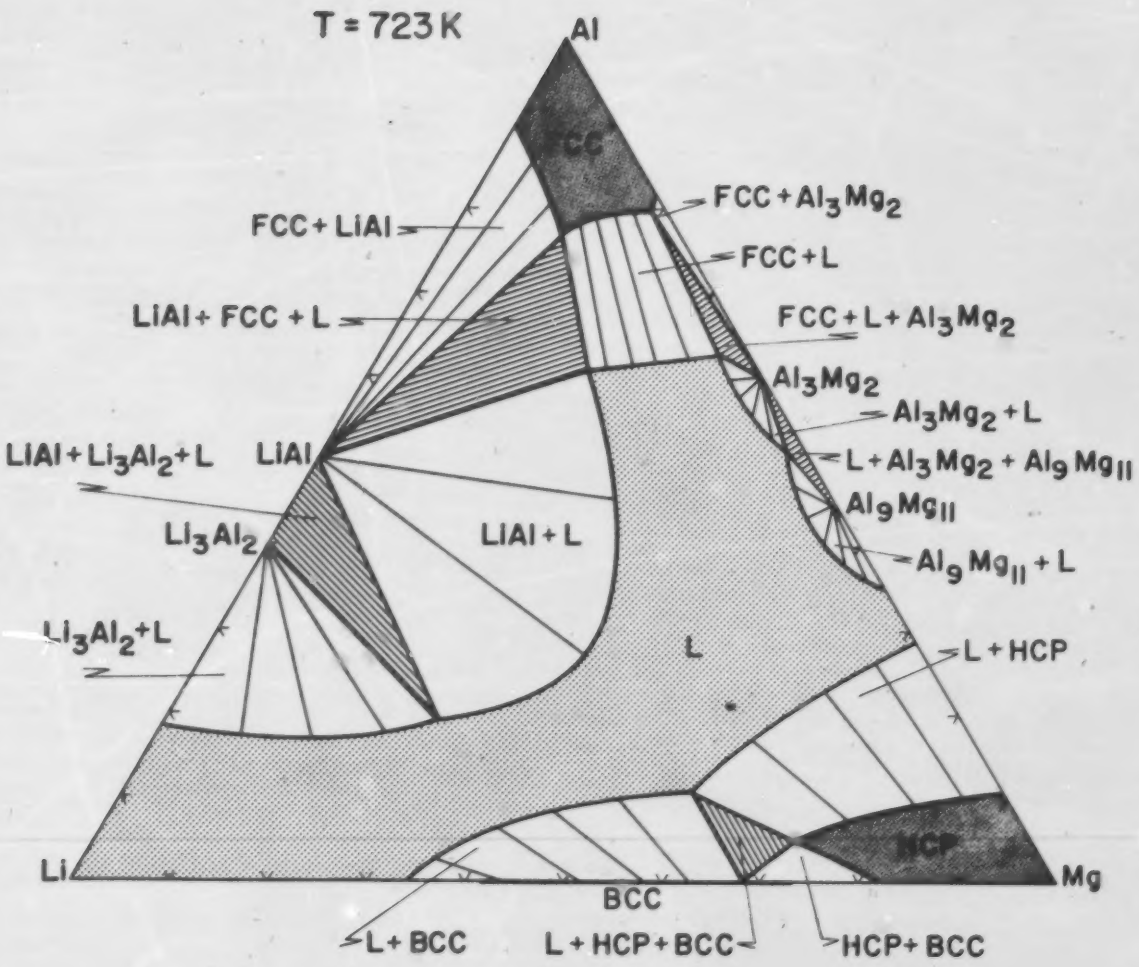

Fig. 5 Computed 723K isotherm of the Al-Li-Mg system.

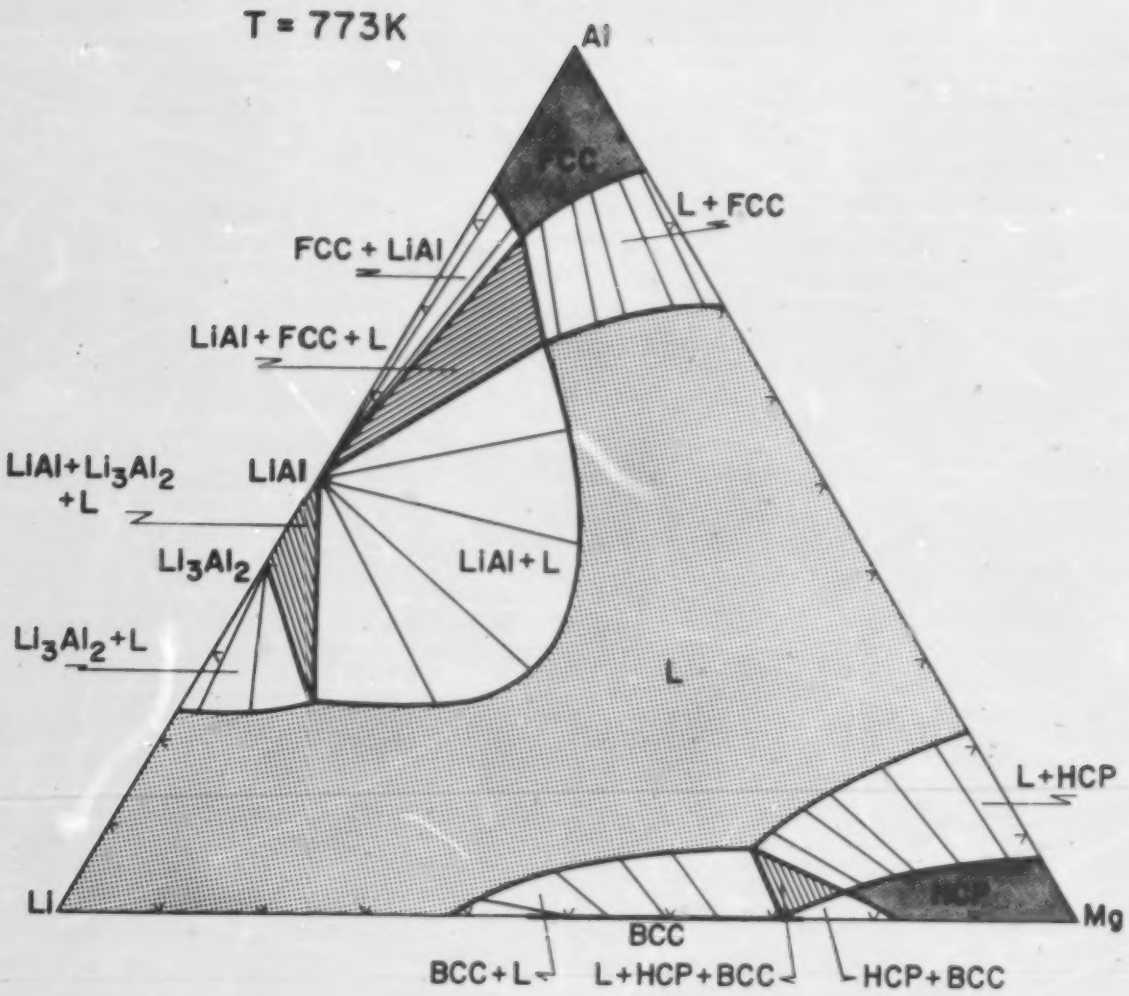

Fig. 6 Computed 773K isotherm of the Al-Li-Mg system.

1209

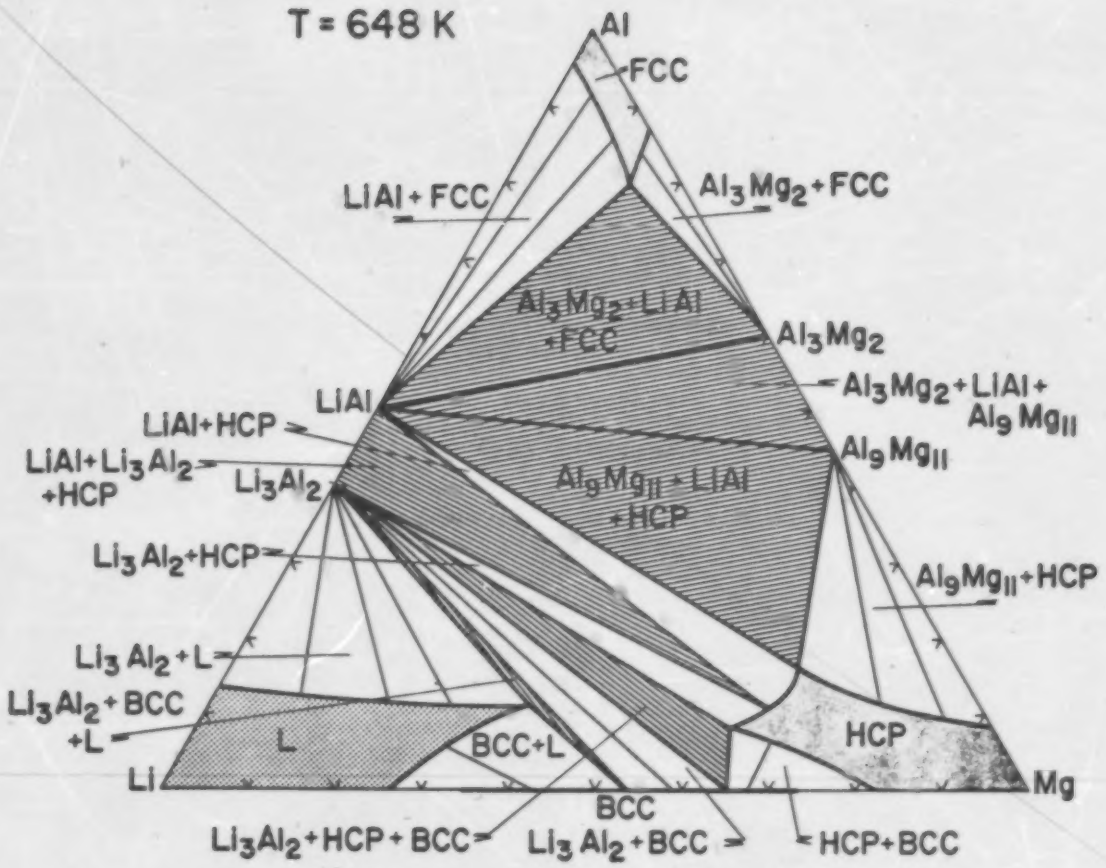

Fig. 7 Computed 648K isotherm of the Al-Li-Mg system.

National Bureau of Standards SP-496, Applications of Phase Diagrams in Metallurgy and Ceramics
Proceedings of Workshop held at NBS, Gaithersburg, Md., January 10-12, 1977

Е.М.Савицкий, В.Б.Грибуля, Н.М.Киселёва

Кибернетическое прогнозирование образования химических соединений в неисследованных системах

Благодаря успехам физики твердого тела, сейчас известно, что все свойства металлов и неметаллов, кроме ядерных, при данном уровне дефектов определяются распределением электронов в поле положительных ионов. Однако расчет существования и устойчивости металлических и других неорганических фаз из "первых принципов" остается пока неразрешенной проблемой. С другой стороны, в химии и металловедении накоплено колоссальное количество экспериментальной информации о зависимости появления и существования фаз от различных факторов (свойств и размеров атомов, состава, температуры, давления, воздействия физико-химических сред, внешних физических полей, кинетики и т.д.). Эти факторы переменны и индивидуальны для конкретных фаз. Традиционные теоретические методы - квантовая механика, термодинамика - в большинстве случаев не дают возможностей для комплексного анализа этих данных с целью поиска новых материалов. Более того, эти методы сами опираются на эмпирические модели взаимодействия частиц, которые, как правило, включают понятия валентности, экранизации заряда ядра, размера атомов, потенциалов взаимодействия.

Принимая во внимание отсутствие эффективных методов использования накопленной информации для прогноза и расчета веществ и материалов, представляющих практический интерес, мы решили использовать новый подход к решению этих проблем. Подход состоит в применении некоторых идей кибернетики из области создания обучающихся автоматических систем к прогнозу физико-химических объектов. Такими объектами, в частности, являются химические элементы, их соединения и смеси, свойства которых определяют структуру фазовых диаграмм. Так как в настоящее время химические элементы изучены наиболее пол-

но по сравнению с более сложными веществами, то мы считаем целесообразным прежде всего использовать широко известные данные о свойствах элементов для прогноза поведения элементов в системах.

Нами была поставлена задача обучить машину различать сочетания химических элементов, обладающих и не обладающих заданным свойством, т.е. классифицировать объекты по свойствам. При этом исходной посылкой служило представление о взаимоотношении элементов в физико-химических системах как о сложной кибернетической системе с взаимообусловленными связями, где данные об элементах неизвестным нам образом обусловливают закономерности наблюдаемых эффектов в системах. После обучения на имеющихся экспериментальных примерах компьютер классифицирует все неисследованные сочетания элементов на заданные классы. Это и составляет задачу кибернетического прогнозирования.

В настоящей работе использованы кибернетические прогнозирующие системы разных типов. В основу первой из них первоначально была положена идеология обучения ЭВМ распознаванию образов / I,9,II/. Вторая система базировалась на методах обучения ЭВМ процессу индуктивного формирования понятий /9,I0/.

Первые исследования в данной области были начаты нами в I966 году /I/. В настоящее время появился целый ряд химических и металловедческих работ, авторы которых обращаются к идее использования распознавания образов /I2-I7/. Область применения этих кибернетических методов широка: от анализа масс-, ИК-, ЯМР-спектров органических веществ /I3,I4,I6/ до поиска новых сплавов с заранее заданными свойствами /I2/. При этом применяются различные методы распознавания образов, включая распознавание с обучением /I2-I4,I7/ и автоматическую классификацию /I4-I6/. Не столь важно, какой алгоритм распознавания образов используется для прогноза, если принимается во внимание спе-

цифика объектов, т.е. объективные и эвристические ограничения, накладываемые на выбор и классификацию объектов обучения для прогноза. Последнее является задачей собственно физико-химии или другой специальной области, но не математики как таковой. Выбор того или иного программного варианта часто определяется возможностями имеющейся вычислительной техники и математического обеспечения. Ввиду отсутствия общей теории распознавания образов, поиск соответствующего метода для решения конкретных задач является проблемой в значительной степени экспериментальной, нежели теоретической. При этом, конечно, нельзя забывать о математических ограничениях того или иного алгоритма.

Стремление получить прогноз из "первых принципов" подсказывает использование в качестве исходных данных фундаментальных характеристик атомов химических элементов - атомного номера, распределения электронов по энергетическим состояниям в атоме и других. Но в зависимости от задачи исследования могут быть использованы различные характеристики химических элементов или известных фаз, представления зонной теории и других физических теорий строения вещества.

Для иллюстрации приводим фрагменты прогноза существования двойных фаз Лавеса /4,5/, б-фаз /6/, фаз типа A-I5 /7/ (рис.I-3). На рисунках вертикальная ось соответствует компонентам A, а горизонтальная - компонентам B в соединениях A_mB_n, где $m \geqslant n$. Знак "+" указывает на прогноз существования фазы данного типа. Знак "$\oplus$" соответствует известным химическим соединениям, которые могли быть использованы для обучения ЭВМ. В приводимых примерах прогноз получен по обучению на экспериментальных примерах существования и отсутствия фаз в системах, в которых химические элементы описаны исключительно данными о распределении электронов в изолированных атомах химических элементов. Оказалось возможным построить логическим путём

аналоги "существенных" признаков для прогнозируемых фаз только из этих данных.

Учитывая перспективность кибернетического прогнозирования, начаты исследования по прогнозу тройных химических соединений и созданию более мощной кибернетической системы, основанной на методе обучения универсальных вычислительных машин формированию понятий /9,10/. Такого рода методы пригодны для выделения сложных закономерностей в больших массивах информации /18/.

Метод формирования понятий был применен для прогнозирования тройных химических соединений состава $A_xB_yC_z$, где A и B - любые элементы периодической системы, а C - кислород или сера. В первую очередь прогнозировались наиболее представительные /по количеству экспериментальных примеров/ классы соединений, имеющие к тому же практический интерес /ABO_4, AB_2O_4, ABO_3/9/, $A_2B_2O_7$, AB_2S_4/, а также наиболее распространённые типы кристаллических структур /перовскиты, шпинели и пирохлоры/. Достоверность прогноза-не ниже 78 %.

В работах по прогнозу тройных соединений мы не ограничивались использованием в качестве системы признаков для описания соединений только совокупностью параметров электронного строения изолированных атомов. Помимо распределения электронов, для описания соединений были использованы ещё две системы признаков. Первая из них включала в себя параметры химических элементов A и B: тип незавершённой электронной оболочки, теплоёмкость элемента, радиус иона элемента в соединении, первые четыре потенциала ионизации, формальную степень окисления элемента в соединении заданного состава. В основу второй системы признаков были положены свойства простых окислов элементов A и B: энтальпия их образования, изобарная теплоёмкость, эффективный радиус катиона в окисле, а также соответствующая ему степень окисления элемента.

Все три системы признаков, используемые для описания соединений, тесно коррелируют. Поэтому прогнозы, полученные в результате обучения ЭВМ с использованием каждого из трёх признаковых описаний, должны, в общем, совпадать. Сравнение прогнозов по разным системам признаков ведёт к значительному повышению достоверности результатов. При этом несовпадающие прогнозы исключаются из рассмотрения.

На рис.4 приведена часть прогнозов возможности образования соединений состава $A^{III}_2B^{IV}_2O_7$ (римскими цифрами помечены степени окисления элементов). Знаком "+" отмечены случаи существования соединений, "-" – отсутствия таковых в системе A–B–O; кружком обведены объекты, использованные для обучения ЭВМ.

На рис.5 дан прогноз соединений со структурой типа пирохлора. В этом случае знак "+" свидетельствует о том, что соответствующее соединение $A^{III}_2B^{IV}_2O_7$ имеет пирохлорную структуру, а "-" удостоверяет противоположное. Следует обратить особое внимание на большое количество прогнозируемых соединений со структурой пирохлора, которые образуют трехвалентные редкоземельные металлы. Вполне возможно, что некоторые из этих соединений будут интересны для исследователей, ведущих поиск новых сегнетоэлектриков.

Следует отметить, что использованные нами кибернетические прогнозирующие системы носят адаптивный характер. Появление совершенно новых экспериментальных данных, неохваченных нашими прогнозами или противоречащих им, способствует дообучиванию системы, уточнению классифицирующих закономерностей и прогнозов. Такая гибкость предложенного подхода является следствием использования быстродействующих ЭВМ, способных для построения классификационной схемы перебрать огромное количество имеющихся вариантов и выбрать из них наилучший с точки зрения разделимости классов.

Полученные прогнозы значительно уменьшают время поиска материалов с заданными свойствами. Они расширят наши возможности теоретического расчёта диаграмм состояния и новых фаз и показывают относительность существующих представлений о диаграммах состояния как инструменте познания физико-химических систем. Они требуют уточнения и формализации понятий химического соединения, условий его образования, стехиометричности, равновесного состояния, кинетических данных и более широкой формулировки термодинамического правила фаз с учётом воздействий различных физических полей, вакуума, дисперсности и т.д.

1216

Литература

1. Е.М.Савицкий, Ю.В.Денингталь, В.Б.Грибуля, ДАН СССР, 1968, 178, №1, с.79-81.

2. E.M.Savitskii and V.B.Gribulya, J.Phys. Chem. Solids, 1972, v.33, 1853-1860.

3. Е.М.Савицкий, В.Б.Грибуля, Изв. АН СССР.Неорганические материалы, 1971, 7, №7, с.1097-1104.

4. Е.М.Савицкий, В.Б.Грибуля, ДАН СССР, 1972, 206, №4, с.848-851.

5. Е.М.Савицкий, В.Б.Грибуля. Предсказание фаз Лавеса при помощи ЭВМ. №4658-72 Деп., М., ВИНИТИ, 1972.

6. Е.М.Савицкий, В.Б.Грибуля, ДАН СССР, 220, №5, 1975, с.1066-1069.

7. Е.М.Савицкий, В.Б.Грибуля, ДАН СССР, 1975, 223, №6, 1383-1386.

8. Е.М.Савицкий, В.Б.Грибуля, в сб. "Структура и свойства жаропрочных металлических материалов", М., "Наука", 1973, с. 3-10.

9. Н.Н.Киселёва, Б.И.Покровский, Н.Д.Ващенко, в сб. "Планирование и автоматизация эксперимента в научных исследованиях", М., "Советское радио", 1974, с.308-315.

10. В.П.Гладун, Кибернетика, 1972, №5, с.109-117; №6, с.28-36.

11. Ю.В.Денингталь, Изв. АН СССР. Техн. кибернетика, 1971, №3, 139-147.

12. Б.Б.Гуляев, Л.Ф.Павленко, Автоматика и телемеханика, 1973, №1, с.131-147.

13. T.R.Brunner, C.L.Wilkins, R.C.Williams, P.J.McCombie, Anal. Chem., 1975, v.47, N.4, pp. 662-665.

14. P.C.Jurs, T.L.Isenhour, "Chemical applications of pattern recognition", N.Y., John Wiley and Sons, 1975.

15. J.M.Koskinen, B.R.Kowalski, J. Chem. Inform. and Comput. Sci.,

1217

1975, v.15, N.2, pp.119-120.

16.B.R.Kowalski, C.F.Bender, J. Amer. Chem. Soc., 1972, v.94, N.126 pp.5632-5639.

17.M.A.Pichler, S.P.Perone, Anal. Chem., 1974, v.46, N.12. pp.1790-1798.

18.E.B.Hunt, J.K.Marin, P.J.Stone, "Experiments in Induction" New York and London, "Academic press", 1966.

1218

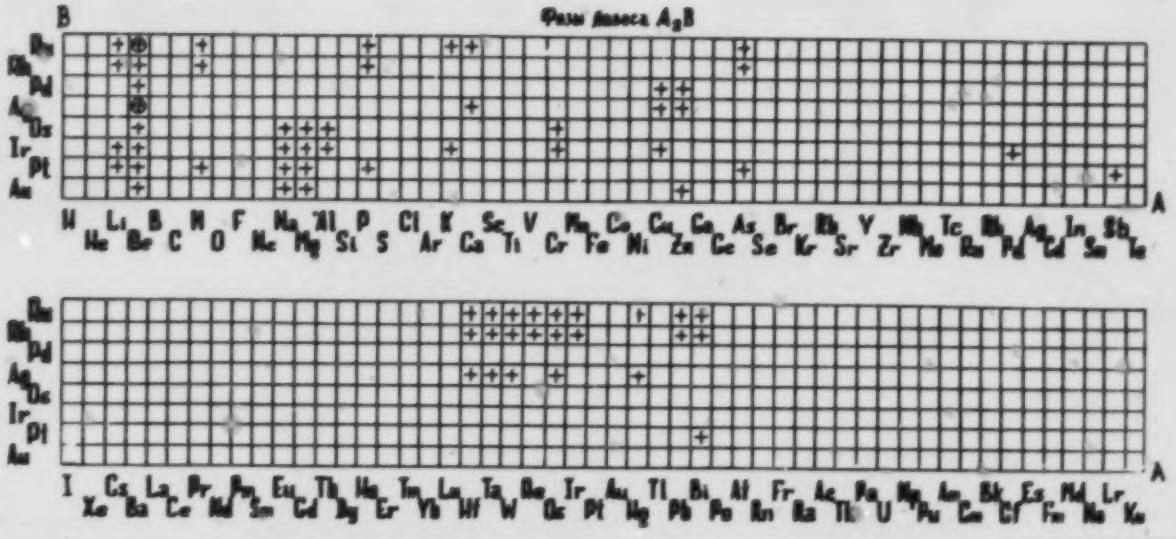

Рис. I Прогноз фаз Лавеса с благородными металлами.

1219

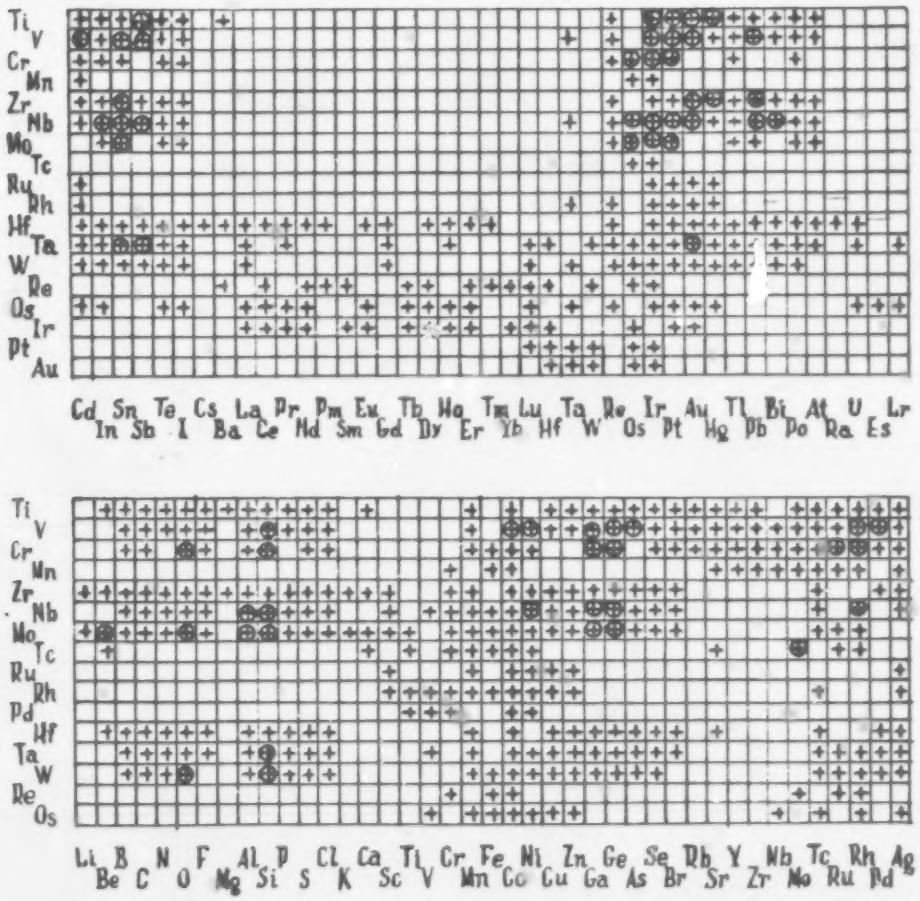

Рис. 2 Прогноз двойных фаз типа A-I5.

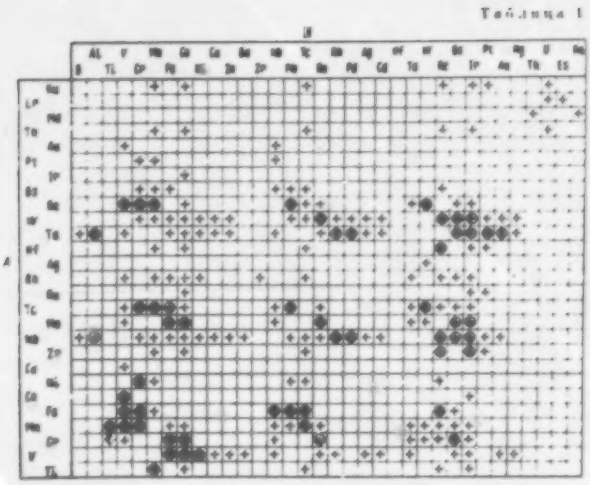

Рис. 3 Прогноз двойных б-фаз.

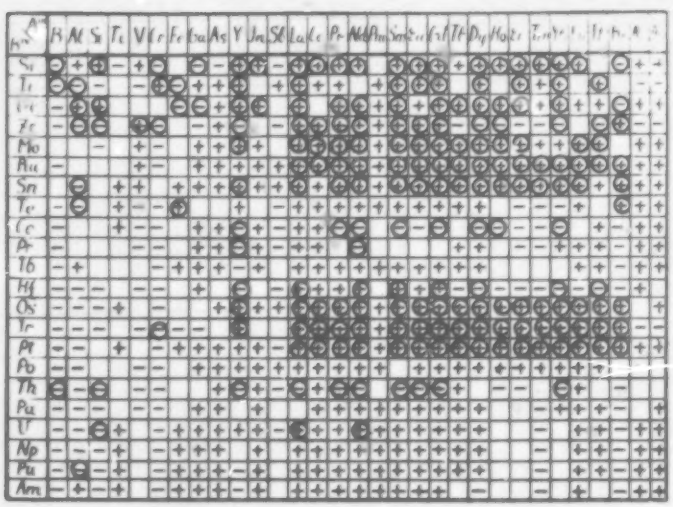

Рис. 4 Прогноз химических соединений состава $A_2^{III}B_2^{IV}O_7$.

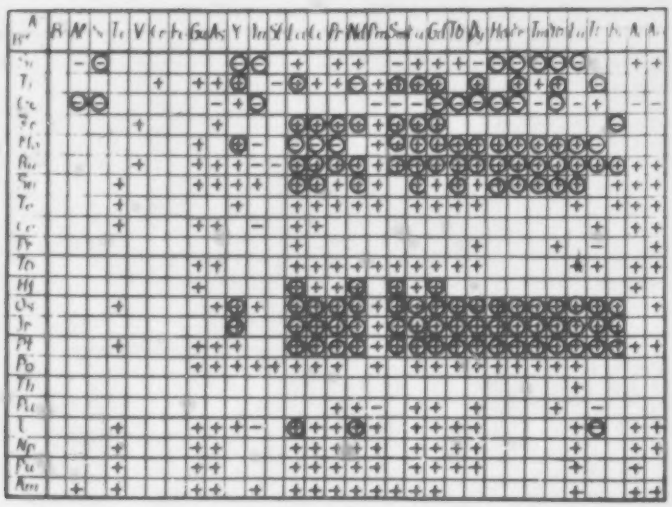

Рис. 5 Прогноз структуры типа пирохлора у соединений состава $A_2^{III}B_2^{IV}O_7$.

National Bureau of Standards SP-496, Applications of Phase Diagrams in Metallurgy and Ceramics
Proceedings of Workshop held at NBS, Gaithersburg, Md., January 10-12, 1977

An English translation prepared by G. Marinenko, Analytical Chem. Div., NBS

Cybernetic Prediction of the Formation of Chemical Compounds in Uninvestigated Systems

E. M. Savitskii, V. P. Gribulya and N. N. Kiselyeva

Baikov Institute of Metallurgy
USSR Academy of Sciences
Institute of Scientific Information
Moscow, USSR

As a result of the advances in solid state physics, it is now known that all properties of metals and nonmetals, with the exception of nuclear properties, under given conditions of defect level, are determined by the distribution of electrons in a field of positive ions. However, the calculation of the existence and the stability of metallic as well as of other inorganic phases on the basis of prima-facie principles still remains an unresolved problem. On the other hand, in chemistry and metal science, an enormous amount of experimental information on the dependence of the occurrence and of the existence of phases on different factors (the properties and atomic size dimensions, composition, temperature, pressure, interaction of physical-chemical media, the external physical fields, kinetics, etc.) has been collected. These factors are variable as well as unique for specific phases. The traditional theoretical methods - quantum mechanics, thermodynamics - in a majority of cases do not provide the possibility for complex analyses of these data in search of new materials. Moreover, these methods in themselves are dependent on the empirical models of the interaction of particles, which, as a rule, include the concepts of valency, nuclear charge shielding, atomic dimensions and interaction potentials.

Taking into account the absence of the effective methods for utilizing the accumulated information for the purposes of prediction and calculations of substances and materials, of practical interest, we have decided to utilize a new approach to the solution of these problems. The approach consists of utilization of certain ideas from cybernetics, from the field known as the generation of learning type of computer systems to the prediction of physical-chemical characteristics of various objects. Such objects in particular, are chemical elements and their compounds and mixtures, the properties of which determine the structure of phase diagrams. Since chemical elements have, at present, been studied in greater detail in comparison with more complex substances, we have decided that it is worthwhile first of all to utilize widely known data on the properties of elements for the prediction of the behavior of elements in various systems.

The problem which we have tackled was to teach the computer to differentiate among the combinations of various chemical elements, those which possess and those which do not possess a prescribed property i.e., objects

according to their properties. In this task the starting point was the concept of interrelationship of elements the physical-chemical systems as being a complex cybernetic system with preconditioned bonds, were the data on elements in a manner unknown to us form the basis for the effects which we observed in these systems. After the study of the available experimental examples, the computer classifies all uninvestigated combinations of elements into prescribed classes. This constitutes the problem of cybernetic prediction.

In this work cybernetic prediction was utilized for various types of systems. The basis for the first problem was to lay down the ideology for teaching the computer to recognize patterns [1,3,11]. The second system was based on the method of teaching the computer of inductive concept formation processes [9,10].

In this area, first investigations began in 1966 [1]. At present a number of chemical and metal science works have appeared, the authors of which turn to the idea of utilizing pattern recognition [12-17]. The area of obligation of their cybernetic methods is very broad; from analyses of mass spectra, IR spectra, NMR spectra of organic substances [13,14,16] to the search for new alloys with specific predesignated properties [12]. In this approach various pattern recognition methods are used, including recognition with learning [12-14,17] and automated classification [14-16]. It is not all that important what type, for the recognition of patterns is utilized for prognosis, if specific objects are taken into account, i.e. the objective and huristic limitations which are placed on the choice and classifications of trained objects for prediction purposes. This letter is a problem of physical chemistry proper, or some other specialized discipline, and not that of mathematics per se. The choice of one or another program variation is frequently determined by the capability of a given computing technology and computation facility. In view of the absence of the general theory of pattern recognition, the search of an appropriate method for solving specific problems is a problem which is to a large extent experimental and not so much a theoretical one. Here one must not forget the mathematical limitations of the different algorithms.

The attempts to obtain prediction from "prima facie principles" suggest the use of fundamental characteristics of the atoms of chemical elements as the starting data-atomic number, distribution of electrons in the atom and others. However, depending on the problem facing the investigation different characteristics of chemical elements or the known phases can be utilized, as well as the concepts of the zone theory and other physical theories of the structure of matter.

For illustration let us cite fragments of the prediction of the existence of the binary Laves phase [4,5], beta-phase [6], A-15 type phase [7] (Figures 1-3). In the figures the vertical axes correspond to components A, while the horizontal axes correspond to component B in $A_n B_n$ type compounds, where n is equal or greater than n. The positive sign indicates the prediction of the existence of a phase of a given type.

The sign "+" corresponds to known chemical compounds, which could have been used for teaching the computer. In cited examples, the prediction was obtained on teaching the machine using experimental examples in which phases in the various systems either existed or were absent, and in which chemical elements were described exclusively by the data on distribution of electrons in the isolated atoms of the corresponding chemcial elements. It was thus found possible to construct in a logical way the analogs of "significant" indices for predicting the phases on the bases of these data alone.

In view of the promise of cybernetic prediction, investigations were started on prediction of ternary chemical compounds and creation of larger capacity cybernetic systems, based on the method of teaching universal computers the concept of formation [9-10]. Such methods are useful for isolation of complex concepts from a larger mass of information [18].

The method of formation concepts was used for predicting ternary chemical compounds of the following composition: $A_xB_yC_z$, where A and B are any elements of the periodic system, while C is either oxygen or sulfur. In the first place predictions were made on the most representative classes of compounds [from the standpoint of experimental examples], which are also of some practical interest [ABO_4, AB_2O_4, ABO_3 [9]], [A_2, B_2, O_7, AB_2S_4], as well as the most wide-spread types of crystal structures [perovskite, spinels and pyrochlores]. The reliability of such prognoses is not lower than 78%.

In the work on ternary compounds we did not limit ourselves to utilization of only combinations of the parameters of electron structures of isolated atoms for the primary indices of the system and a description of the compounds. In addition to electron distribution, for the description of compounds two other indices were utilized. The first index included the parameters of chemical elements A and B; the type of unfilled electronic shell, the heat capacity of the element, the ionic radius of the element in a compound, the first four ionization potentials, and the formal oxidation state of the element in the compound of a given composition. The bases of the second system of indices included properties of simple oxides of the elements A and B; the enthalpy of formation, heat capacity at constant pressure, the effective radius of cation in the oxides, and also the corresponding degree of oxidation of the element.

All three systems of indices which were used for the description of compounds have high degree of correlation. Therefore, the prognosis obtained as a result of teaching the computer to use each of the three descriptive indices must, in general, coincide. The comparison of the predictions from different systems of indices leads to a significant increase in the reliability of the results. In using this approach, the predictions which do not coincide are excluded from consideration.

Figure 4 shows part of the prediction for the possibility of the formation of the compounds of the $A_2^{III}B_2^{IV}O_7$ composition (Roman numerials indicate the oxidation state of the element). The "+" sign denotes those cases when the compounds exists, "-" denotes the absence of such compounds in the A - B - O system; the circles indicate those compounds which were used for teaching the computer.

Figure 5 shows prediction of the existence of the compounds with pyrochlore structure. In this case "+" sign indicates that the existing compound $A_2^{III}B_2^{IV}O_7$ has a pyrochlore structure, while "-" indicates to the contrary. It is worthwhile to turn our attention to the large number of compounds which are being predicted with pyrochlore structure, which are formed by the trivalent rare-earth metals. It is quite possible some of these compounds will be of interest to the researchers who are seeking new piezoelectric materials.

It should be noted that the cybernetic predictary systems which were utilized are flexible in nature. The appearance of completely new experimental data which were not previously included into our predictory systems or which contradict the existing systems, aid in further educating the system, and to refine further the characteristics and prediction classifications. Such flexibility of the proposed approach resulted from the use of high speed electronic digitial computers, capable of examining a tremendous number of possibilities for the construction of the classification scheme and then select from the analyzed variations the best suitable ones from the standpoint of separation of classes.

The predictions which were obtained by us decreased significantly the search time required for materials with the assemblage of desirable properties. They expand our capability of theoretically calculating phase diagrams and prediction of new phases as well as show the pertinence of the existing concepts regarding phase diagrams as an instrument for learning physical chemical systems. They require refinement and formulization of the concepts of chemcial compounds, the conditions under which they are formed, stoichiometry, equilibrium state, kinetic data, as well as broader formulation of the thermodynamic phase rule which would take into account the interaction in various phase fields, vacuum, degree of dispersity, etc.

Bibliography

1. E. M. Savitskii, Yu. V. Devingtal', and V. P. Gribulya, Doklady Akad. Nauk. SSSR (Reports of the Academy of Sciences of the USSR), 1968, Vol. 178, No. 1, pp. 79-81.

2. E. M. Savitskii and V. B. Gribulya, J. Phys. Chem. Solids, 1972, Vol. 33, pp. 1853-1860.

3. E. M. Savitskii and V. P. Gribulya, Izv. Akad. Nauk. SSSR. Neorganicheskiye Matrialy (The news of the Academy of Sciences of the USSR. Inorganic Materials), 1971, 7, No. 7, pp. 1097-1104.

4. E. M. Savitskii and V. P. Gribulya, Doklady Akad. Nauk. SSSR (Reports of the Academy of Sciences of the USSR), 1972, Vol. 206, No. 4, pp. 848-851.

5. E. M. Savitskii and V. P. Gribulya, Predskazaniye Faz Lavesa Pri Pomoshchi Evm. (Prediction of laves phases by means of the electronic digital computer), No. 4658-72, DEP, VINITI, Moscow, 1972.

6. E. M. Savitskii, Yu. V. Devingtal', and V. P. Gribulya, Doklady Akad. Nauk. SSSR (Reports of the Academy of Sciences of the USSR), 1975, Vol. 220, No. 5, pp. 1066-1069.

7. E. M. Savitskii, Yu. V. Devingtal', and V. P. Gribulya, Doklady Akad. Nauk. SSSR (Reports of the Academy of Sciences of the USSR), 1975, Vol. 223, No. 6, pp. 1383-1386.

8. E. M. Savitskii and V. P. Gribulya in the collection "Stiukdurae Svoystva, Zharoprochnykh, Metallicheskikh Materialov" (Structure and properties of refractory metallic materials) NAUKA Publishing House, Moscow, 1973, pp. 3-10.

9. N. N. Kiselyeva, B. I. Pokrovsakiy, N. V. Vashhenko, in a collection "Planiro-Vaniye i avtomatizatatsya eksprimenta v nauchnykh issledovaniyakh" (planning and automation of the experiment in scientific investigations) "SOVETSKOYE RADIO" Publishing House, Moscow, 1974, pp. 308-315.

10. V. P. Gladun, Kibernetika (Cybernetics), 1972, No. 5, pp. 109-117 and 28-36.

11. Yu. V. Devinggal', Izv. Akad. Nauk. SSSR. Tekh. Kibernegika (News of the Academy of Sciences of the USSR Technical Cybernetics), 1971, No. 3, pp. 139-147.

12. B. P. Gulyayev, and L. F. Pavanko, Avtomatika i telemak (automation and telemechanics), 1973, No. 1, pp. 131-147.

1155 1227

13. T. R. Brunner, C. L. Wilkinw, R. C. Williams, P. J. McCombie, Anal. Chem. 1975, v. 47, No. 4, pp. 662-665.

14. P. C. Jurs, T. L. Isenhour, "Chemical applications of pattern recognition", John Wiley and Sons, New York, 1975.

15. J. R. Koskinen, B. R. Kowalski, J. Chem. Inform. and Comput. Sci., 1975, v. 15, No. 2, pp. 119-123.

16. B. R. Kowalski, C. F. Bender, J. Amer. Chem. Soc., 1972, v. 94, No. 126 pp. 5632-5639.

17. M. A. Pichler, S. P. Perone, Anal. Chem., 1974, v. 46, No. 12, pp. 1790-1798.

18. E. B. Hunt, J. K. Marin, P. J. Stone, "Experiments in Induction," Academic Press, New York and London, 1966.

1223

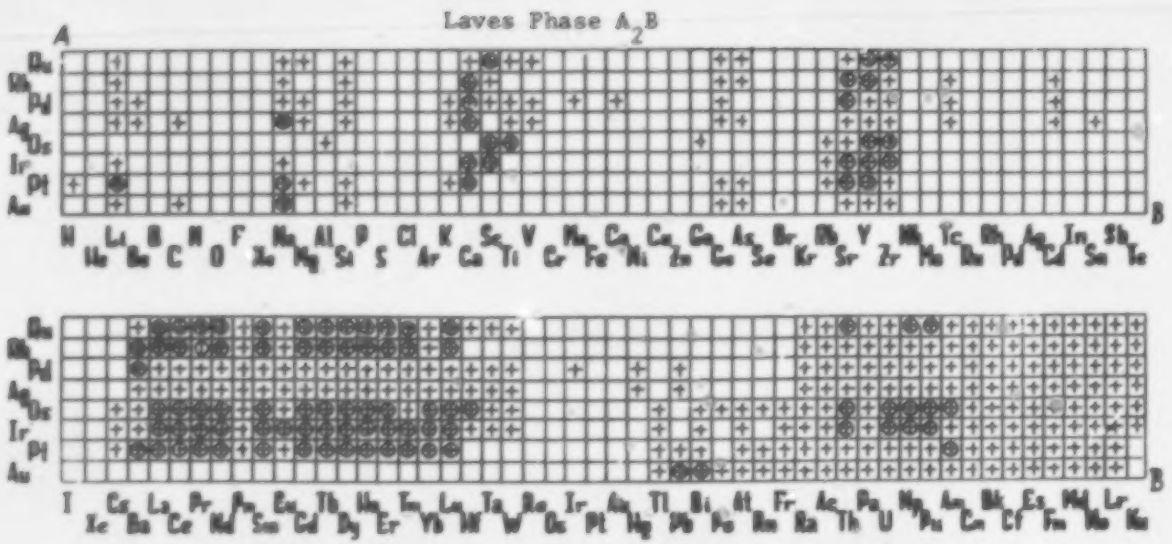

Figure 1. Prediction of laves phases for noble metals.

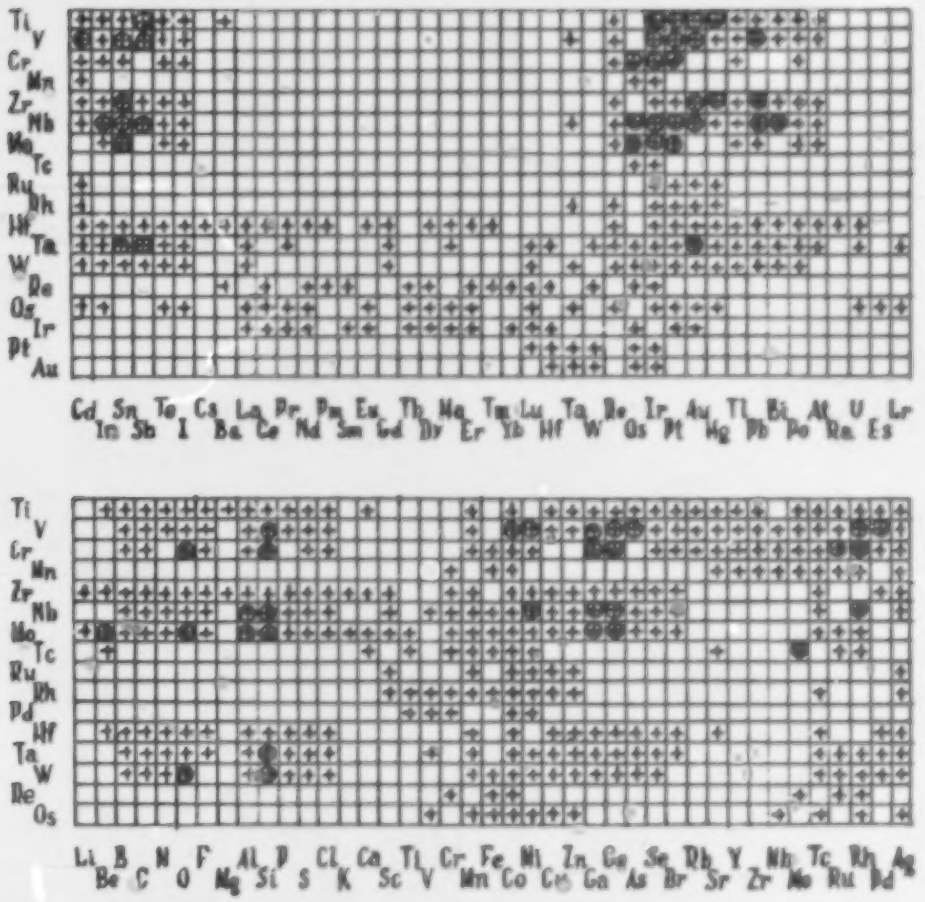
Ti V
Cr Mn
Zr Nb
Mo Tc
Ru Rh
Hf Ta
W Re
Os Ir
Pt Au
Cd Sn Te Cs La Pr Pm Eu Tb Ho Tm Lu Ta Re Ir Au Tl Bi At U Lr
In Sb I Ba Ce Nd Sm Gd Dy Er Yb Hf W Os Pt Hg Pb Po Ra Es
Ti V
Cr Mn
Zr Nb
Mo Tc
Ru Rh
Pd Hf
Ta W
Re Os
Li B N F Al P Cl Ca Ti Cr Fe Ni Zn Ge Se Rb Y Nb Tc Rh Ag
Be C O Mg Si S K Sc V Mn Co Cu Ga As Br Sr Zr Mo Ru Pd

Figure 2. Prediction of binary phases of the A-15 type.

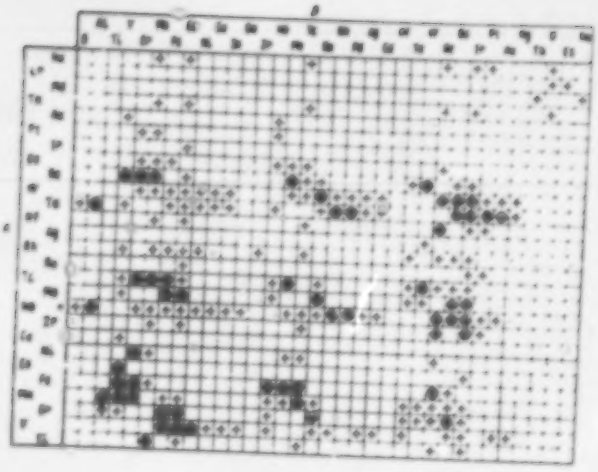

Figure 3. Prediction of the binary σ-phases.

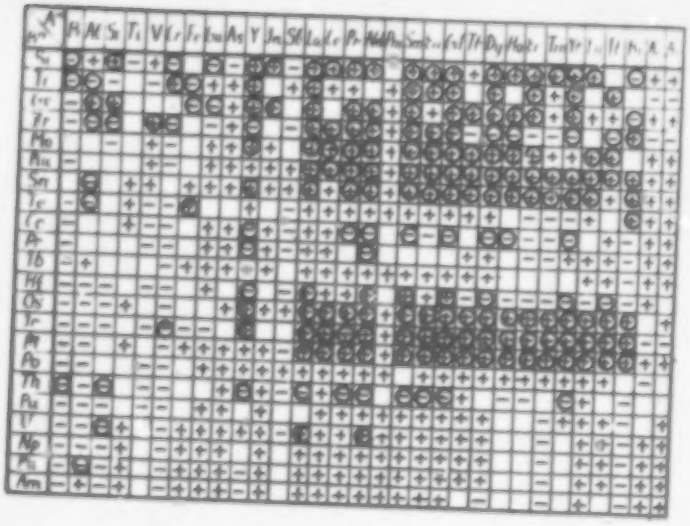

Figure 4. Prediction of chemical compounds of the $A_2^{III}B^{IV}O_7$ composition.

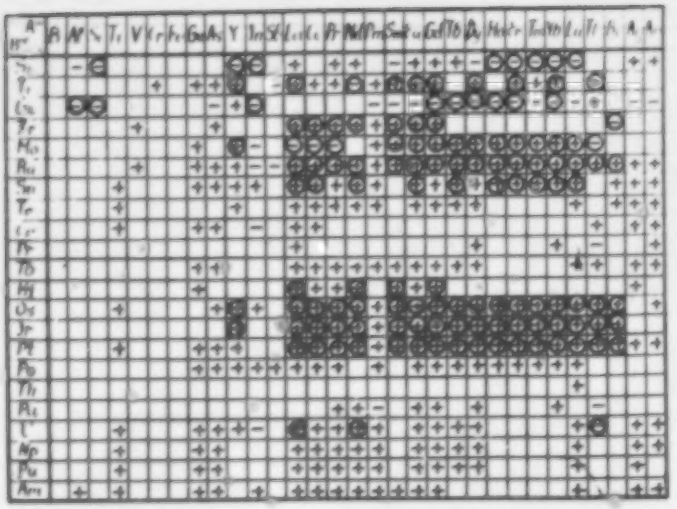

Figure 5. Prediction of the structure of pyrochlore type in compounds of the $A_2^{III}B^{IV}O_7$ composition.

National Bureau of Standards SP-496, Applications of Phase Diagrams in Metallurgy and Ceramics
Proceedings of Workshop held at NBS, Gaithersburg, Md., January 10-12, 1977

THE DETERMINATION AND REPRESENTATION OF METASTABLE PHASE DIAGRAM FEATURES AND OTHER THERMAL CHARACTERISTICS OF METASTABLE ALLOYS, ESPECIALLY AMORPHOUS METALS

Bill C. Giessen

Institute of Chemical Analysis, Applications and Forensic Science
and Department of Chemistry, Northeastern University, Boston, Massachusetts 02115

INTRODUCTION

Recent advances in materials synthetic technology[1-4] have led to the preparation of a considerable number of metastable alloy phases; it was found that metastable phases can be prepared in virtually every alloy system if sufficiently effective nonequilibrium solidification or condensation methods are applied. These results have made it desirable to represent the new phases graphically in modified phase diagrams.

We first list the materials forming the subject of this review. One can differentiate four principal types of non-equilibrium phases[1,2,4] (the term "phase" is used here in the Gibbsian sense to describe a homogeneous constitutional entity[5] and does not necessarily indicate a local free energy minimum, or relate to the ability of the entity to participate in constrained equilibrium reactions, etc.). These materials are:

A. Metastable elemental and near-elemental phases;
B. Metastable extensions of terminal or intermediate solid solutions;
C. Metastable intermediate phases;
D. Amorphous alloys (metallic glasses).

Typical metastable phases representing these four types are listed in Table I, using information compiled primarily in Refs. 2, 4, 6-11. We limit our discussion to phases which require very rapid quenching methods or atomic deposition methods for their preparation and retention to room temperature. This excludes common metastable phases such as martensite and cementite.

Table I: Types of Metastable Alloy Phases

Type	Examples
1. Metastable Elemental Modifications	Ga
2. Extended Terminal or Intermediate Solid Solution	
a) Substitutional	Al(Ni), ε-Pu(Ti)
b) Interstitial or disubstitutional	Pb(Au), Gd(Cu)
c) Based on metastable elemental modification	γ-Sn(Pb), β'-Ga(In)
3. Metastable Intermediate Phases	
a) Disordered phases	
α) Hume-Rothery phases	ζ-(Au-Sb), γ-(Au-Sn)
β) Element-like B and T metal phases	Zn-Ga, In-Bi, ε(Nb-Ni)
b) Ordered phases	NiPb, Cu_2Al_3, Al_3Ge_2
4. Amorphous Metals	
a) Transition metal - metalloid	Fe-B, Pd-Si
b) Transition metal - transition metal	Zr-Cu, Nb-Ni
c) Miscellaneous systems	
α) A metal - B metal	Mg-Zn
β) Actinide - T metal	U-Cr

Following present custom[4] we do not differentiate between amorphous solids prepared from the melt (i.e. glasses in the original sense of the word) and those prepared by atomic deposition methods (e.g. from a vapor) and designate both materials as glasses; see Ref. 8 for a discussion of this point. The types of metastable phases listed above have been the subject of many recent extensive reviews, e.g. Refs. 1, 2, 4. Alloy constitutional aspects have been emphasized in Ref. 1; phase diagram aspects have been presented especially in Ref. 7. In Ref. 12, the constitutional requirements of metastable crystalline phase formation have been discussed in detail and the kinetic aspects have been treated in terms of solidification theory; the formation of amorphous metals is reviewed thoroughly in Ref. 13.

Further, because most of the metastable alloys studied to date either contain two components or components that can be divided into two groups

of closely related elements[4] (such as amorphous metal-metalloid systems T-X where T = Fe, Co, Ni and X = B, C, P), we emphasize binary systems here; we also do not discuss pressure effects; last, because the phases of interest to us are principally prepared from the melt, we focus here on those regions of the phase diagrams which pertain to condensed phases.

Three principal types of data are of importance in the phase diagram representation of metastable phases and will be discussed:

1. Free energy diagrams;
2. Temperature-composition phase diagrams and related diagrams;
3. Diagrams presenting kinetic and other physical/chemical parameters.

We discuss, in order, types of phase diagram representations as listed here, pertinent experimental methods, phase diagram aspects of the formation of metastable phases, and, last, data needed in future research on amorphous metals.

PHASE DIAGRAM AND RELATED DIAGRAM REPRESENTATIONS

1. Free Energy - Composition Diagrams

As free energy diagrams are fundamental to phase diagram representations they are treated first. We begin this discussion by presenting an estimate of the maximum free energy excess ΔG^{exc} of a metastable phase over the equilibrium phases that can be achieved by different preparation methods. The estimate is based on a Carnot cycle thought experiment and has been given by Baker and Cahn.[12] It is readily seen that $\Delta G^{exc}_{max} \leq \frac{\Delta T}{T} \Delta H$ where ΔT is the undercooling and ΔH is the heat added in the first stage of the process. For solidification of a liquid into a crystalline phase, $\Delta H/T = 2$ e.u., $\Delta T/T < 0.3$, and $\Delta G^{exc}_{max} \sim 0.06$ eV (for a metal melting at 1000 K). For condensation of a vapor, $\Delta T/T$ may be unity, $\Delta H/T \sim 20$ e.u. and $\Delta G^{exc}_{max} \sim 2$ eV (for a metal evaporated at 2000 K). While this argument correctly yields the higher capability for metastable phase formation observed for atomic deposition processes, it appears to overestimate this potential considerably. First, this argument is valid only for a reversible process and irreversibility will reduce the ΔG^{exc}_{max}; this will be the case for vapor quenching processes, which are conducted far from equilibrium conditions. Second, it can be expected that any high-energy metastable phase with free energy higher than the corresponding liquid or glass would not form under any conditions, but would relax spontaneously to form a melt or glass, releasing its free energy excess over the latter.

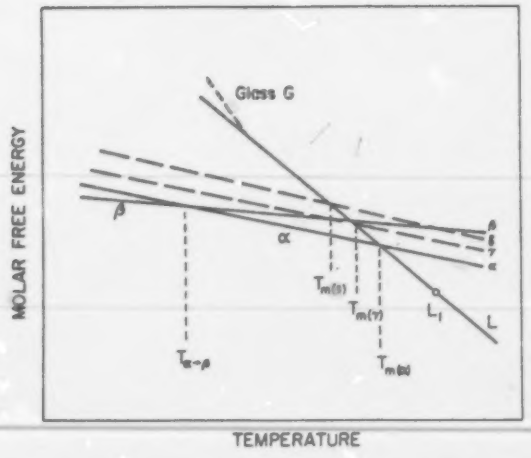

Figure 1. Schematic representation of the free energies of phases present in a hypothetical one-component system as a function of temperature at constant pressure. (From Ref. 1.)

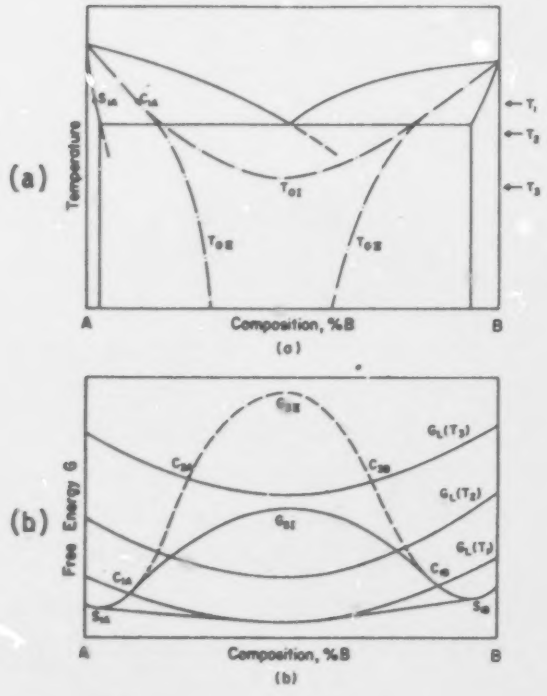

Figure 2. Hypothetical eutectic binary system: (a) phase diagram indicating role of the parameter T_0; (b) free energy diagram for three temperatures $T_{1,2,3}$ and two solid solutions with different positive deviation from Raoult's law. (From Ref. 1.)

---

a. G-T diagrams: Metastable phase and glass formation can be presented particularly readily for one-component systems where free energy(G)-temperature(T) diagrams such as that given in Fig. 1 can be drawn.[4] This figure shows that metastable γ and δ may form in local equilibrium if the system is constrained agains the formation of the lowest-free-energy phase α and, subsequently, the phase β. The formation of the glass at G is also shown; this will occur if the supercooled liquid is no longer able to relax internally as the temperature is reduced and passes through a glass transition.

b. G-x diagrams: A hypothetical, simple eutectic binary phase diagram A-B, where A and B are isostructural, is shown in Fig. 2a. The G-x diagram (x = composition) for this system is as shown schematically in Fig. 2b. These diagrams are discussed extensively in Refs. 1 and 4. The shape of G_S, the free energy curve of the solid, is the principal factor in determining which metastable phases are possible: for a G_S curve such as G_{SI} there exists a

range of temperatures for which G_S lies below G_L, the free energy of the liquid, over the whole composition range, while for G_{SII} no such temperature range exists down to the absolute zero of temperature. This situation is reflected in the T-x diagram by the important T_0 temperatures discussed below (see Fig. 2a). For metastable intermediate phases, G-x diagrams can give comprehensive graphic representations of all phases thermodynamically possible in any given system. An example of such a plot is given in Fig. 3c, which is closely patterned after (though not representative of) the In-Bi system in which many metastable phases have been prepared.[14] This figure, discussed in detail in Ref. 1. shows a large number of competing phases with similar, low excesses of the free energy over those of the equilibrium phases and their combinations.

It may be considered that the G-T diagram of every unary system contains all possible elemental structures at their appropriate free energies if it is extended to sufficiently high values of G; likewise, the free energy diagrams of binary systems contain all binary phases possible at the appropriate composition, both with correct stoichiometries or off-stoichiometrically, and with all values of atomic volume, axial ratio, internal parameters etc., of these phases. However, only a limited number of these phases will have free energies lying below the Carnot process excess free energy discussed previously and can possibly be retained by appropriate experimental techniques.

As an example, the G-x diagram of the Au-Sb system which is discussed below in more detail, is given in Fig. 4d;[1,4] it shows two observed metastable phases ζ[15] and π,[16] for which thermodynamic properties have been determined.[17] We also present a partial G-x diagram for the Zn-rich portion of the Ag-Zn system,[18] Fig. 5a, which includes data for the metastable

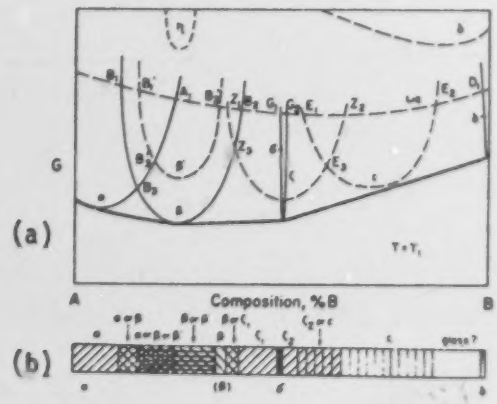

Figure 3. Hypothetical binary system with intermediate phases: (a) free-energy diagram; (b) phases which may be present after nonequilibrium solidification following supercooling of the melt to $T=T_1$. (From Ref. 1.)

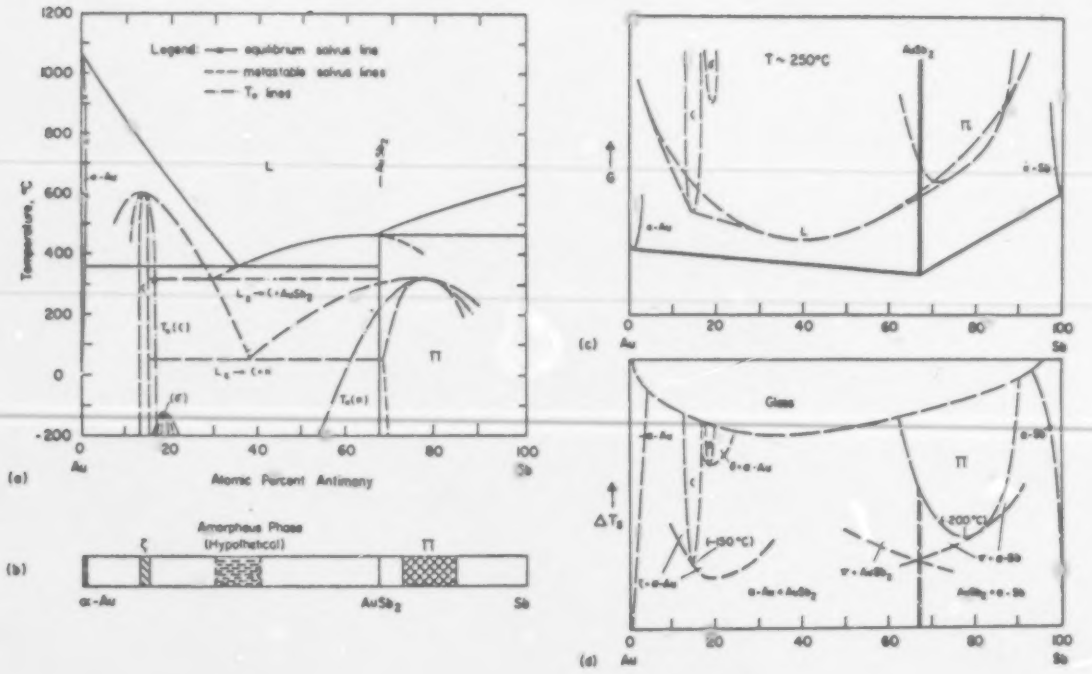

Figure 4. The system Au-Sb: (a) stable and metastable phase diagram; —x—, equilibrium solvus lines; — — —, metastable solvus lines; —·—, T_o lines; (b) quenched-phase plot; (c) hypothetical free energy diagram at $T \sim 250^{\circ}C$; (d) ΔT_s-x diagram showing the role of supercooling in metastable phase formation. (From Refs. 1, 4.)

extensions of two hexagonal phases, terminal η-Zn(Ag) and intermediate ε. The atomic volumes and axial ratios of η and ε approach each other in the metastable range but do not become equal, leading to the preposed G-x diagram.[19]

2. Temperature-Composition Diagrams

The T-x diagrams are the diagrams of greatest general importance concerning metastable phase retention.

a. Phase-vs-composition diagrams: In systems where metastable phases have been prepared by cooling to a certain temperature but where there is no further information on their thermal properties, the most direct representation of metastable phases is in a "quenched phase plot", drawn as shown in Fig. 4b under the phase diagram, Fig. 4a.

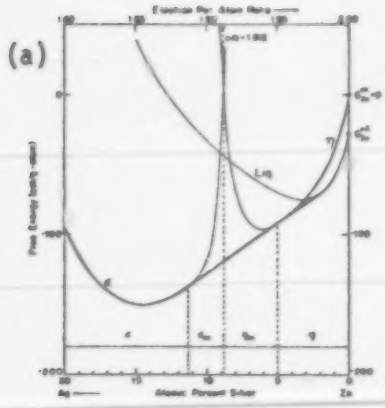

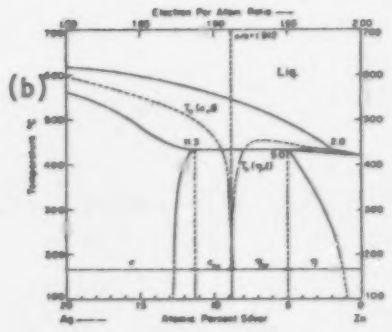

Figure 5.
(a) Free energy configuration for the solid ε and η phases and the liquid phase at the peritectic temperature (430°C) for zinc-silver. The free energy of each phase in its stability range has been calculated from thermodynamic data. The arbitrary energy references are $G^{os}_{Zn} = 0$, $G^{os}_{Ag} = +8000$ cal/g-atom. (From Refs. 18, 19.)

(b) Possible trends of the T_0 temperatures in the zinc-silver system. (From Refs. 18, 19.)

b. T-x diagrams with metastable phases: If thermal data are known from direct measurements, as discussed below for Ga[20] or Bi alloys[21] or by calculation from measured thermodynamic quantities, as shown below for the melting points of Au-Sb alloys,[17] metastable phases and equilibria can be directly represented in a phase diagram as shown for Au-Sb in Fig. 4a. This type of presentation, using dashed lines, has long been standard for equilibria involving metastable phases that can be readily obtained such as those occurring in the metastable Fe-Fe_3C portion of the Fe-C system[22] or the Cd_4Sb_3 phase and the associated equilibria in the Cd-Sb system.[22]

Ideally, such a T-x diagram should be completed as discussed above by including all metastable phases that are thermodynamically able to form from the liquid in constrained equilibrium upon supercooling of the liquid to any temperature, i.e. by including all phases that have lower free energies than the liquid at any temperature ≥ 0 K. At present only the upper temperature region down to 200-300 K below the melting point is

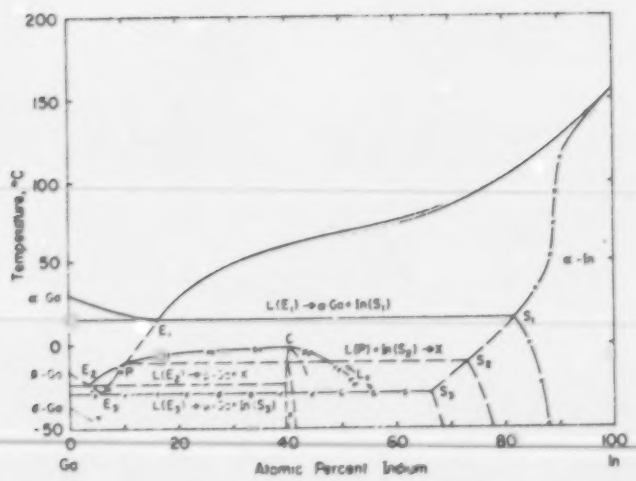

Figure 6. The system Ga-In; stable and metastable phase diagram (after Ref. 20) with additional, hypothetical reactions. ——, equilibrium diagram α-Ga - In (measured); —x—, equilibrium diagram α-Ga - In (assumed); – – –, nonequilibrium diagram β-Ga - In (X forms); —·—·—, nonequilibrium diagram β-Ga-In (X supercooled); ——— , hypothetical congruent melting curve for X. (From Ref. 1.)

experimentally accessible to supercooling experiments because of the intervention of crystallization; moreover, upon supercooling of the liquid to lower temperatures, glass formation will intervene at the glass transition temperature and prevent the crystallization of metastable crystalline phases. However, at least in principle, the total temperature range is accessible by vapor quenching to 0 K. While at present it would be an impossible undertaking to attempt this kind of phase survey for more than a few selected systems, automated methods of examining thin films prepared at very low rates on substrates kept at very low temperatures may make vast portions of the metastable phase diagram accessible.

As examples of direct thermal determinations we present in Fig. 6 measurements on alloys in the metastable Ga-In system[20] which show the formation of metastable β-Ga[23] and its primary liquidus line as well as other equilibria involving a hypothetical metastable intermediate phase. Other examples are the metastable Ga-Al system, discussed in detail in Ref. 1, Fig. 6, and the metastable Sn-Pb system.[24,25]

c. <u>T_0-x diagrams</u>: In T-x diagrams, such as Fig. 2a, T_0 indicates the temperature for which the free energy curves of the liquid and the metastable solid intersect at a given composition x_0 in the corresponding G-x diagram; see Fig. 2b. Compositions with $x > x_0$ cannot be retained as metastable phases by cooling to $T > T_0$, because $G_{solid} > G_{liquid}$ for $x > x_0$ and $T > T_0$.

Alloys with $x = x_0$ can be retained from the melt only upon cooling to $T < T_0$; T_0 thus characterizes the minimum supercooling required for single metastable phase retention at composition x_0.

T_0 curves such as those represented by T_{0I} in Fig. 2a indicate that, at least thermodynamically, a complete range of metastable solid solutions can be retained from the melt if equilibrium phase crystallization is prevented and glass formation does not intervene. By contrast, in the case of T_0 curves such as those represented by T_{0II} this is impossible even upon supercooling to T = 0 K. The Ag-Cu system[26] and probably also the Zn-Cd system[27] are of the former kind, although in the latter case only a small increase of the solid solubility of Cd in Zn has been achieved by splat cooling,[28] apparently due to the failure of reaching sufficiently large undercooling before crystallization occurred.

The T_0-x curves of the Ag-Zn system[18,19] which was introduced above are given together with the T-x phase diagram in Fig. 5b, it is seen that the rapid increases of G in the G-x curves (Fig. 5a) in the intermediate composition range and their intersection lead to a corresponding, deep valley and intersection of the T_0 curves in this region, indicating that supercooling temperatures of $\sim$300 K are required to obtain a single phase alloy at every composition (and coexisting ε and η at the composition of the T_0 intersection).

d. T_c-x diagrams: Such diagrams show the composition dependence of the temperatures of phase transitions T_c involving some property of a metastable phase, such as a magnetic or superconducting transition; these plots are quite analogous to the corresponding ones for equilibrium phases. Examples are plots of the composition dependence of the superconducting transition temperature T_c of the metastable extension of the off-stoichiometric phase $Nb_3(Nb_xGe_{1-x})$ to Nb_3Ge[29] and the plot of the saturation magnetization against composition for ferrimagnetic, amorphous Gd-Fe alloys[30] (see Ref. 4).

e. T_s-x diagrams: The minimum supercooling temperature ΔT_s required to prepare a given metastable phase at a given composition x can be read off from the stable-metastable T-x diagram (e.g., Fig. 4a) and can be plotted directly in a diagram bearing a certain resemblance to an inverted T-x diagram. An example is shown for the Au-Sb system in Fig. 4d;[1] the ΔT_s values for ζ and π are based on Fig. 4a while the other values have not been determined directly. A similar plot of the critical cooling rate T_c required for the retention of a given metastable phase has also been introduced.[31]

3. Kinetic Parameters

Kinetic parameters are especially important in the characterization of amorphous metals,[13] to which the discussion in this section will be limited. There are two principal pertinent quantities.

a. The glass transition temperature, T_g: T_g is the temperature at which properties such as the free energy (Fig. 1a), the atomic volume or some other property depart from a continuous extension of their values for the supercooled liquid due to the inability of the system to stay in internal equilibrium, as shown in Fig. 1a for the free energy. Other property changes taking place at T_g include a decrease of the specific heat by up to 100% and an increase of the viscosity by a factor of 10^5; for amorphous metals, T_g must be approached from below to prevent crystallization and the reverse of these changes is then observed.

T_g depends on the cooling rate of the liquid during supercooling and, if the measurement is made upon heating, the heating rate;[32] thus it is not a quantity of state of the system. In many alloys, the glass transition cannot be observed upon heating because crystallization intervenes; in some systems, on the other hand, crystallization only occurred upon heating to 50 K above T_g.

b. The crystallization temperature, T_c: There may be a sequence of crystallization and recrystallization steps, characterized by T_{c1}, T_{c2}, etc.[33] Like T_g, these temperatures are heating rate dependent, increasing with increasing $\dot{T}$; the activation energy of crystallization can be deduced from the change of T_c with $\dot{T}$.[34] Time-temperature-transformation (TTT) diagrams can be constructed for the equilibration process (see Ref. 8).

Another type of T-T-T diagram is of importance in the formation of amorphous metals; it contains information on the cooling conditions required for the retention of amorphous metals.[35] Representations of the composition dependence of T_g, T_c and the T-T-T diagrams would be useful; these data are presently available only in a few instances.

EXPERIMENTAL METHODS

1. Preparative methods

As the techniques employed to retain metastable phases (in the sense described above) have been discussed frequently in the literature,[1-4] we will limit ourselves here to a brief compilation of the principal methods,

given in Table II. As can be seen, preparative methods are generally classified into liquid (melt) quenching and atomic deposition methods, with the former subdivided into fast quenching (some of which are known as "splat cooling") and slow cooling methods, the latter divided into vapor or solution deposition techniques. There is special emphasis on the droplet supercooling method[21,24] which is suitable for making thermal measurement during cooling, in contrast to the rapid quenching methods; it is primarily based on the prevention of heterogeneous nucleation during cooling and, possibly, a reduction of the equilibrating effect of homogeneous nucleation.

2. Investigative Methods

a. Free energy-composition diagrams: In principle, measurements of the free energy of formation can be made at temperatures sufficiently low to prevent decomposition or transformation of the metastable phases, e.g. by specific heat or EMF measurements. However, the latter measurements which require solid or liquid electrolytes are often difficult to perform at the required low temperatures. An alternate approach is to determine the enthalpy of formation by solution calorimetry and to make suitable assumptions on the entropy term.

b. Temperature-composition data:

i. Thermal analysis: Direct thermal analysis in the metastable range during cooling is readily possible for droplets during supercooling; it has also been attempted during the quenching (splat cooling) of alloy deposits;[36] see also Ref. 2. The thermal analysis of metastable phases by differential thermal analysis (DTA) or differential scanning calorimetry (DSC) during heating is also possible. There are some thermal measurements for metastable crystalline phases[20,21] and a large number of such measurements on metallic glasses.[37,38] For the former, the metastable melting temperatures are of prime interest; for the latter, the glass transition temperature, T_g, and the crystallization and recrystallization temperature(s), T_c, are objects of study. As mentioned, both T_g and T_c depend on the heating rates, as well as on the cooling rate during quenching; the effect of increasing heating rates is an increase (by different amounts) of T_g and T_c.

ii. Indirect methods: An indirect determination of the metastable melting points of crystalline nonequilibrium phases has been carried out for the two metastable Au-Sb phases shown in Fig. 7b;[17] see also Fig. 4a. The

Table II. Methods for the Preparation of Metastable Alloys, Especially Metallic Glasses

Method	Rate of Production	Estimated Cooling Rate, K/sec	Shape of Product
I. Melt Cooling			
A. Rapid Quenching			
1. Gun (splat) method	Very low	10^6 - 10^9	Irreg. foil fragments
2. Hammer-and-anvil method			
a) Arc furnace system	Very low	10^6 - 10^7	Irreg. shaped flat foil
b) Induction system	Very low	10^5 - 10^6	Irreg. shaped flat foil
3. Melt spinning	Very high	10^6	Ribbon
4. Melt extraction	Very high	10^4 - 10^5	Profile wire
5. Dual roller method	low	10^6	Short ribbon
6. Plasma deposition	Medium	10^4 - 10^6	Porous sheet
7. Laser glazing	-	10^5 - 10^6 (est.)	Surface layer
B. Slow Quenching			
Droplet supercooling	Low - medium	10^{-1} - 1	Droplets
II. Atomic Deposition			
A. From Vapor Phase			
1. Vapor deposition	low	Very high*	Thin film
2. Sputtering	Medium	high*	Sheet
B. From Solution			
1. Electrodeposition	Medium	high*	Sheet
2. Electroless deposition	Medium	high*	Sheet

* Effective Cooling Rate

1214

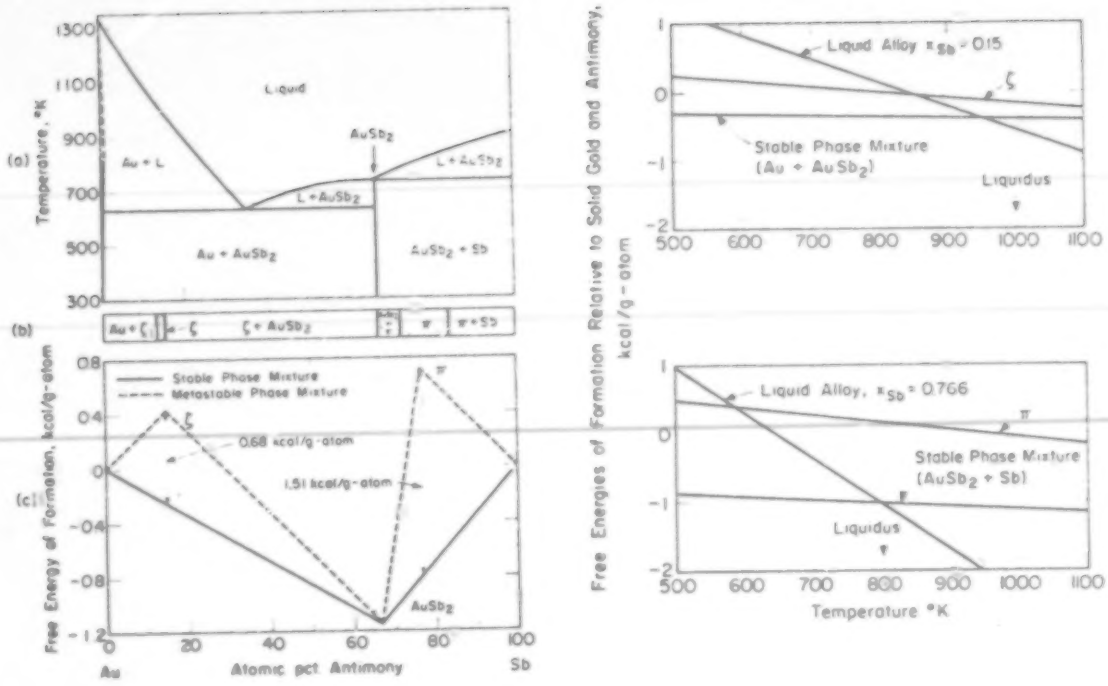

Figure 7. (a) Stable phases in the system gold-antimony. (b) Metastable and stable phases present at 298°K in the splat cooled gold-antimony alloys. (c) Free energies of formation at 298°K of mixtures of stable phases and mixtures of stable and metastable phases in the system gold-antimony. (From Ref. 17.)

Figure 8. Free energies of formation relative to solid gold and antimony of the ζ and π phases, the liquid gold-antimony alloys with x_{Sb}= 0.15 and x_{Sb} = 0.766 and the corresponding mixtures of stable phases. (From Ref. 17.)

heats of formation ΔH_F of ζ-(Au-Sb) and π-(Au-Sb) were measured by tin bath solution calorimetry. The free energies of formation were derived, making a proper assumption on the ΔS_F term, yielding the ΔG_F-x plot, Fig. 7c. This diagram shows that ζ and π are metastable not only with respect to the equilibrium phase mixtures but also with respect to the component mixture.

Further, free energy-temperature (G-T) diagrams can be constructed which yield the metastable melting points of ζ and π (Fig. 8a and b). These temperatures can subsequently be entered into the T-x phase diagram, as shown in Fig. 4a.

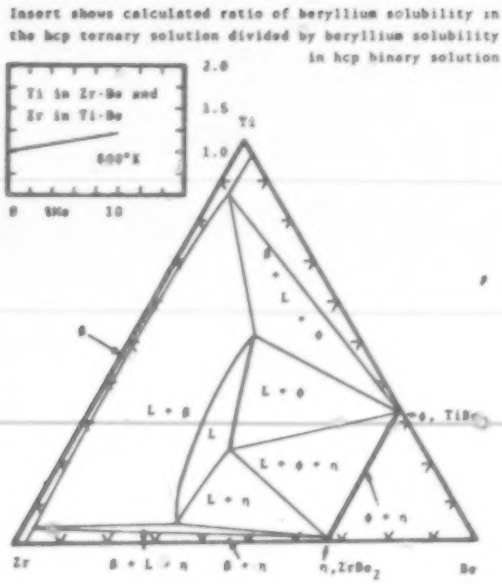

Figure 9. Calculated partial isothermal section in the Ti-Be-Zr system at 1180 K.[41] (From Ref. 42.)

3. Computations

Definitive, first-principle calculations of the thermal data of metastable phases would represent an ideal method for the prediction of metastable phases;[39] unfortunately, at the present state of the art, the accuracy of such calculations is not yet sufficient. However, calculations such as those by Kaufman and others (see review, Ref. 40) can now be used to predict the supercooling required to obtain metastable elemental modifications and element-like intermediate phases in a number of cases. Further, the results of phase diagram calculations made to obtain eutectic compositions may be used to identify possible glass forming compositions in systems with more than two components using the low melting point criterion of ready glass formation discussed in more detail below. As an example, a calculated section of the Be-Ti-Zr system[41] is shown in Fig. 9;[41,42] a high glass forming ability was observed for a number of alloys in this system.[43]

PHASE DIAGRAM ASPECTS OF THE FORMATION OF METASTABLE PHASES

1. Crystalline Phases

The metastable crystalline phases of interest here are of several kinds. For unary systems, there may be metastable modifications of the element or compound involved; for binary and higher order systems there may be metastable

modifications of one or more constituent element(s), with associated solid solution range(s), as well as melting curves and other multi-phase reactions involving these modifications. Further, there may be metastable intermediate phases, both di ordered[44,45] and ordered.[11] The alloy chemistry of these two types o. phases in binary metallic systems has been reviewed extensively in the references given; these aspects are therefore not repeated here.

As shown above for the metastable Au-Sb phases ζ and π, metastable phases are readily represented in T-x diagrams. Besides the interest in metastable equilibria involving such phases, there would be a fundamental interest in "complete" phase diagrams containing all possible metastable phases that could be obtained in a given system by cooling the melt to 0 K, as discussed above. Such information could be used to establish connections between equilibrium diagrams by pointing out structural relationships and fields of isostructural phases or "metastability ranges", as discussed in Refs. 11 and 44. Also, it would provide a basis for the experimental verification of theoretical calculations of structural stability such as those of Heine and Weaire for B-metal phases.[39]

The nucleation and growth rates of various metastable phases from supercooled liquids are generally not known. Ostwald's rule, according to which equilibrium is reached by small steps where possible, with the system passing through a series of metastable states, is sometimes quoted

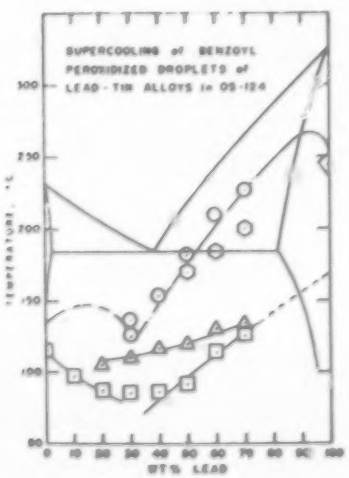

Figure 10. Phase diagram for Sn-Pb indicating undercoolings corresponding to various peroxidation reactions at the droplet surfaces. Squares represent maximum supercooling for benzoyl peroxidized emulsions. The maximum undercooling observed by Hollomon and Turnbull[46] is indicated by the — · — · — curve. (From Ref. 24.)

as a general guide; however, as it is not known beforehand whether discrete intermediate steps (i.e. states of intermediate free energy) exist, this rule has little predictive value.

It would be of interest to relate the occurrence of metastable crystalline phases to features of the equilibrium T-x diagram. Thus, at least in some systems, metastable crystalline phases were found at compositions of relatively low melting point, e.g. in the Au-Si and Al-Ge systems.[7]

Further, we mention plots of other types of composition dependent thermal properties, such as plots of the maximum supercooling obtained, as shown in Fig. 10 for droplet-dispersed and supercooled Pb-Sn alloys.[24]

2. Amorphous Phases

Phase diagram aspects and, particularly, T-x diagrams play an important role in the scientifically and technologically significant effort of categorizing and, hopefully, predicting the occurrence of the amorphous state in alloys prepared under nonequilibrium conditions, especially by rapid quenching from the melt. The latter may be possible because the phase diagram expresses, directly or indirectly, important aspects of the glass forming ability of a given alloy.[4,8,13] Some of these aspects are summarized in Table III (following Ref. 8) and are briefly reviewed in the following; we limit our discussion mostly to systems in which glasses can be formed readily by melt quenching. The eight glass forming phase diagrams presented in Fig. 11 [13] may serve as illustrations of some of the principles involved.

a. Low liquidus temperatures: Probably the most obvious and best-known of the criteria for ready glass formation are connected with the liquidus temperatures. Soon after the accidental discovery that an amorphous Au-Si alloy can be prepared by rapid quenching[47] (splat cooling) the higher glass forming ability of low melting point compositions, frequently at and near eutectics, was recognized. This concept was formalized by Cohen and Turnbull,[48] who related glass forming ability to a low value of the reduced melting temperature

$$\tau_m = kT_m/\Delta H_V \ ,$$

where T_m, the melting (liquidus) temperature, reflects the thermal energy at the melting point and where ΔH_v, the vaporization enthalpy, is a measure of the activation energy required for diffusion processes involved in the nucleation and growth of the equilibrium phases whose formation

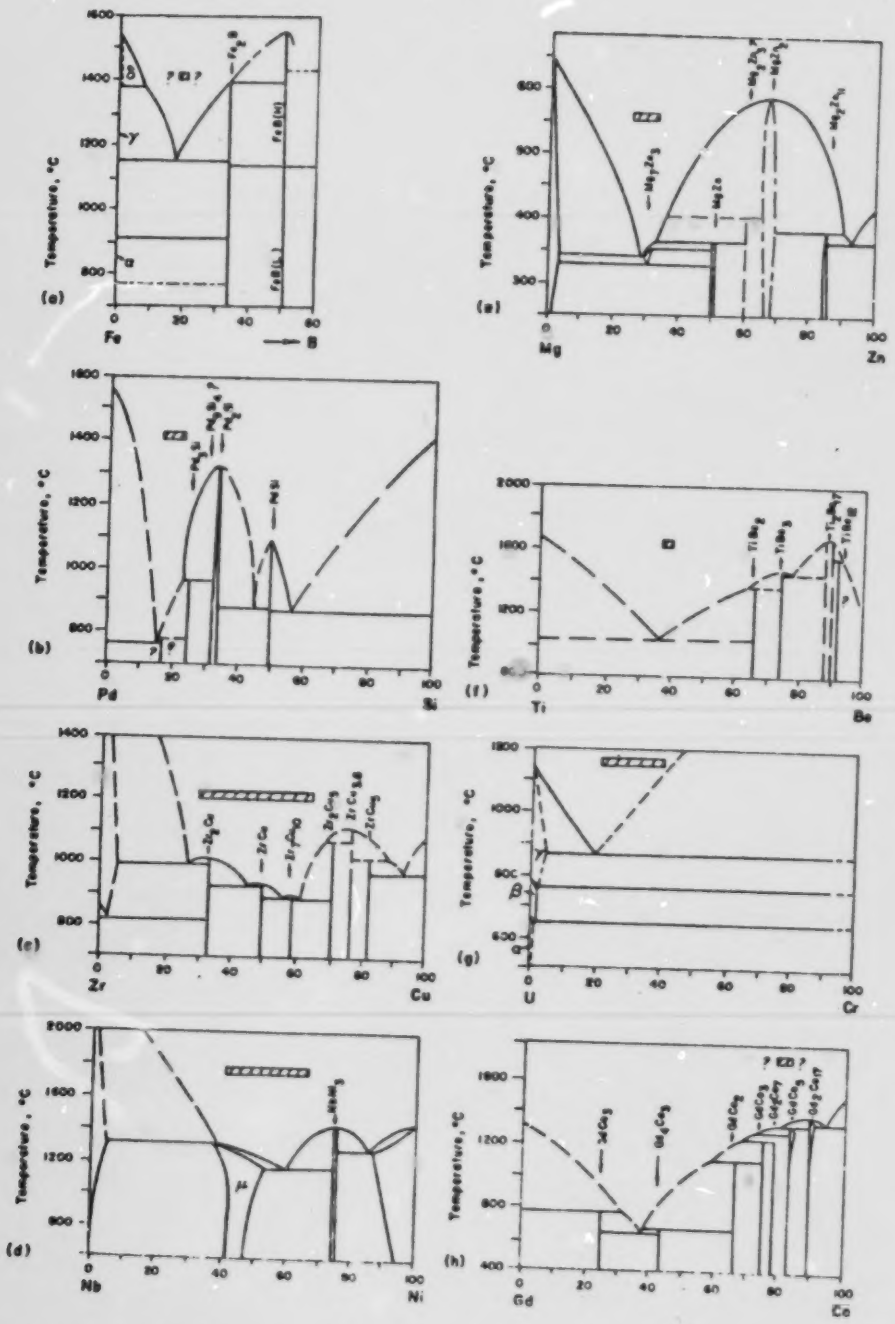

Figure 11. (a)-(g) Constitution diagrams[22,49,50] representative of binary alloy systems which readily form a glass; composition ranges of glasses obtained by rapid liquid quenching are indicated. (h) Constitution diagram[50] of Gd-Co system showing composition range of amorphous alloys formed by sputtering. (From Ref. 8.)

Table III. Criteria for Easy Glass Formation Expressed by the T-x Phase Diagram (After Ref. 8)

Property	Examples
1. Low liquidus temperatures	
a) Narrow region of low T_m (e.g. single deep eutectic)	Pd-Si, Mg-Zn
b) Low T_m over extended composition range	Nb-Ni, Zr-Cu
2. Atomic properties of constituents	
Size difference	Fe-B, Zr-Cu
3. Compositional properties	
a) Crystal chemistry of equilibrium phases	μ(Nb-Ni), Mg_7Zn_3
b) "Confusion principle"	Fe-P-C, Fe-Ni-P-B

Note: Other important criteria not directly expressed by the phase diagram include:

atomic properties of the constituents such as valence difference;

compositional properties such as melt stoichiometry and alloy valence electron concentration.

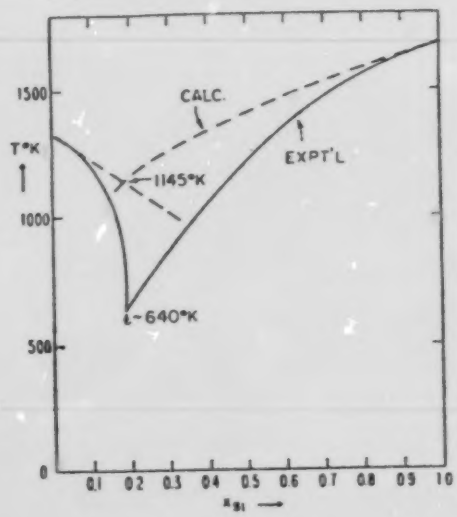

Figure 12. Comparison of experimental phase equilibrium diagram (p = 1 atm) of Au-Si system with diagram calculated assuming that liquid solutions behave ideally. Experimental diagram from Refs. 22 and 49.(From Ref. 40.)

competes with glass formation taking place by continuous cooling of the liquid. τ_m thus is the ratio of the thermal energy available at the melting point to the energy of diffusion in the melt and measures its fluidity.

Composition ranges of relatively low liquidus temperatures thus become prime candidates in a search for readily glass forming alloys. The melting point depression may be expressed as

$$T_{mr} = (\overline{T}_m - T_m)/\overline{T}_m ,$$

the normalized reduction of the melting point T_m from the weighted average $\overline{T}_m$ of the components.[8] An alternate expression is based on the reduction of T_m from the hypothetical melting point as given by ideal solution theory;[51] as an example, observed and calculated values are compared for the Au-Si system in Fig. 12.[40] It is found that the phase diagrams showing large T_{mr} values are primarily of two types:

i. those having narrow regions of low melting points, e.g., a single deep eutectic; examples are transition metal-metalloid systems[22] such as Pd-Si[52] and non - transition metal systems such as Mg-Zn[33] (Fig. 11);

ii. those having low melting points over extended composition ranges, such as Nb-Ni[53] and Zr-Cu;[54] systems of this type generally include one or more intermetallic phase(s) in the glass forming composition range.[8]

Large values of the reduced glass temperature

$$\tau_g = T_g/T_m ,$$

where T_g is the glass temperature, are also associated with high glass forming ability.[13]

b. Atomic properties: Turning to atomic properties of the constituents that are of importance for glass formation and are expressed by features of the phase diagram, one finds the important criterion of atomic size. Generally, a component size ratio of $\gtrsim 1.15$ is required for glass formation; here, the size is not the atomic size of the elements but the "actual" size of the atoms as deduced from equilibrium phases in the system involved. These atomic sizes and their ratios are often reflected in the structure type and thermal stability of the observed equilibrium phases; thus glass forming systems with constituents having a size ratio differing from unity by an amount similar to that given above will often show Laves phases at the compositions appropriate for the formation of such phases (AB_2, AB_3);[45] in general, these compositions are far removed from the glass forming ones.

c. Compositional Properties: Properties of intermediate equilibrium phases may also be used to estimate glass forming ability in another way which is

classified in Table III under the heading of compositional properties. This approach is based on the fact that alloy phases found at or near glass forming compositions generally belong to certain, frequently complex crystal structure types and have similar atomic coordination characteristics. For metal-metalloid glasses, e.g., this observation was made by Polk[55] and was related to a model for the structure of such glasses. Another compositional criterion reflected by the phase diagram is the so-called "confusion principle" which expresses the experience[10] that more complex alloy systems (i.e. systems containing more than two constituents) are often better glass formers than simpler ones; thus, alloys near the ternary eutectic Fe-Fe_3C-Fe_3P form glasses more readily than binary Fe-P or Fe-C alloys. Presumably, all of these factors affect glass forming ability by modifying the quenching T-T-T diagrams discussed above.

5. PHASE DIAGRAM RELATED DATA NEEDED IN FUTURE RESEARCH ON METASTABLE PHASES (ESPECIALLY AMORPHOUS METALS).

The present work on metastable phases, especially the intense current research on amorphous metals would be substantially aided if certain types of phase diagram related information were more readily available. Along with the common thermal data, we include in this discussion alloy chemical data such as the structural information commonly presented in phase diagram compilations and some other related properties. The following data are required:

1. Phase Diagram Information

a. Phase diagrams: There is a need for quantitatively correct phase diagrams, especially diagrams of binary systems with measured solidus and liquidus temperatures in those composition regions in which metastable phase formation is observed. These diagrams should also have well determined phase boundaries, especially for high temperature phases and other phases having limited stability ranges which are often absent in the qualitative phase diagrams on record.[22,49,50] A present need exists particularly for diagrams of transition metals with the metalloids boron, phosphorus and silicon, phase diagrams of the alkaline earths, and a number of diagrams of transition metals and B metals. Liquidus temperatures and high temperature phases are especially important for amorphous metal research.[8]

b. Surveys: There is a need for qualitative phase diagram surveys, especially for ternary systems containing one or two components that are of interest as base metals for metallic glasses. Such data may be useful in several respects. As mentioned above, it is often found that ternary alloys form glasses more readily than binary ones, as recently shown for Ti-Ni-Si alloys;[56] however, this helpful observation is often difficult to utilize without adequate ternary phase diagram data. Such data should include at least an isothermal section and the projection of the melting point troughs in the composition range of interest.

Also, it is often of interest to assess the effect of ternary additions X to glass forming binary alloys (such as Pd-Si-X [57]) [and of quaternary additions X to glass forming ternary alloys (such as Fe-C-P-X [58])] on the thermal stability (as measured by T_g and T_c) and mechanical properties (microhardness) of the base alloy glass. These measurements are generally more difficult to interpret if the effect of the ternary or quaternary addition on the equilibrium phase diagram is not known. Last, quaternary glass forming systems (i.e. systems with four major constituents) almost always have to be studied without guidance from equilibrium phase diagrams because of the absence of data for the systems of interest.

c. Metastable phases: Thermal data and phase equilibria involving metastable phases have been determined only in a few cases. As discussed above, some of these phases are of crystal chemical interest; others are important in connection with their glass forming ability or that of other alloys with the same components. More phase diagram studies of such systems are desirable.

2. Crystallographic Data

Besides the phase diagrams, crystal structure data on intermediate phases are needed. In particular, structure data are missing for many compounds occurring at or near glass forming compositions, where crystal structures would be of particular importance. Possibly, this is the case because compounds at such compositions tend to have complex structures (see previous section) and the structures have therefore not been worked out when the phase diagram was established. This is especially true for complex ternary phases,[59] of which very few are structurally well established.

3. Thermal Characteristics

For fundamental studies on metallic glasses, data on several thermal properties of equilibrium and metastable phases are required. A principal reason

for this is that glass forming systems are generally not among the alloy systems most commonly studied for which data are available in reviews such as Hultgren et al.[60] The following measurements would be useful:

a. Thermodynamic measurements: Data on $\Delta\bar{H}_F$ and $\Delta\bar{G}_F$ are needed for liquids and intermediate stable and metastable phases. This will involve solution calorimetry (generally, using a transition or noble metal bath) and EMF studies (using solid electrolyte cells). Differential scanning calorimetric (DSC) studies of the specific heats of metastable phases continue to be rewarding.

b. Kinetic parameters of metastable phases: Important data include the glass transition temperature $T_g(x, \dot{T})$ as a function of the heating rate (to obtain T_{g_0} and T_{g_∞}),[32] the crystallization temperature(s) $T_c(x, \dot{T})$, and the activation energies of crystallization as obtained by differential thermal analysis using different heating rates.[34]

4. Other, Related Properties

For a theoretical correlation of the thermal parameters of metallic glasses, such as T_g, a quantity characteristic of the vibrational spectrum, such as the Debye temperature θ_D, is required for intermediate alloy phases. The change of θ_D on going from the crystalline to the amorphous state is also of fundamental interest; a substantial reduction of θ_D in alloy glasses had been predicted[61] and observed.[62] More data on other temperature-dependent properties such as the melt viscosity would also be useful.

ACKNOWLEDGEMENT

Research on metastable alloys at Northeastern University is partially sponsored by the Office of Naval Research; this support is gratefully acknowledged. I thank Dr. D.E. Polk for helpful discussions and Ms. T. Utterback for secretarial assistance.

1254

DISCUSSION

T. Massalski - You showed that the bcc phase of Pu can be retained by rapidly quenching, but it would seem to me that by lattice quenching, you eliminate the entropy factor. Therefore, I am surprised that the entropy-stabilized bcc phase of Pu can actually be retained in this process.

W. Giessen - The competing lower temperature solid solutions rise very much in energy by adding a simple transition metal, like Ti, to Pu. You are suppressing the f-electron bonding in the 5f levels. The basic concept is that the f-electron bonding, which stabilizes the 3 low temperature forms of Pu, is suppressed as you add an early transition metal to it. You are, in fact, thermodynamically stabilizing the high temperature modifications to such a degree that you prevent nucleation of the low temperature forms. So your entropy term is certainly working against us, but our enthalpy term is very much in favor of us.

REFERENCES

1. B.C. Giessen and R.H. Willens in Phase Diagrams; Materials Science and Technology, Vol. III., A.M. Alper, Ed., Academic Press, N.Y., p. 103 (1970).
2. H. Jones, Rep. Prog. Phys. 36, 1425 (1973).
3. H. Jones, in Proc. Second Internat. Conf. on Rapidly Quenched Metals, Section I, N.J. Grant and B.C. Giessen, Eds., M.I.T. Press, Cambridge, Mass. p. 1 (1976).
4. A.K. Sinha, B.C. Giessen, and D.E. Polk, in Treatise on Solid State Chemistry, Vol. 3, N.B. Hannay, Ed., Plenum Press, N.Y., p. 1 (1976).
5. L.S. Darken and R.W. Gurry, Physical Chemistry of Metals, McGraw Hill, N.Y., p. 290 (1953).
6. H. Jones and C. Suryanarayana, J. Mater. Sci. 8, 705 (1973).
7. B.C. Giessen, in Developments in the Structural Chemistry of Alloy Phases, B.C. Giessen, Ed., Plenum Press, N.Y., p. 227 (1969).
8. D.E. Polk and B.C. Giessen, in Metallic Glasses, J.J. Gilman and J.H. Leamy, Eds., American Society for Metals, Metals Park, Ohio, p. 1 (1977).
9. S. Takayama, J. Mater. Sci. 11, 164 (1976).
10. P. Duwez, Annual Review of Materials Science, Vol. 6, p. 83 (1976).
11. B.C. Giessen, in Proc. Second Internat. Conf. on Rapidly Quenched Metals, Section I, N.J. Grant and B.C. Giessen, Eds., M.I.T. Press, Cambridge, Mass., p. 119 (1976).
12. J.C. Baker and J.W. Cahn, in Solidification, American Society of Metals, Metals Park, Ohio, p. 23, (1971).
13. F. Spaepen and D. Turnbull, in Proc. Second Internat. Conf. on Rapidly Quenched Metals, Section I, N.J. Grant and B.C. Giessen, Eds., M.I.T. Press, Cambridge, Mass., p. 205 (1976).

14. B.C. Giessen, M. Morris, and N.J. Grant, Trans. Met. Soc. AIME 239, 883 (1967).
15. P. Predecki, B.C. Giessen, and N.J. Grant, Trans. Met. Soc. AIME 233, 1438 (1965).
16. B.C. Giessen, U. Wolff, and N.J. Grant, Trans. Met. Soc. AIME 242, 597 (1968).
17. A.K. Jena, B.C. Giessen, M.B. Bever, and N.J. Grant, Acta Met. 16, 1047 (1968).
18. T.B. Massalski and T. Bienvenu, in Proc. Second Internat. Conf. on Rapidly Quenched Metals, Section I, N.J. Grant and B.C. Giessen, Eds., M.I.T. Press, Cambridge, Mass. p. 95 (1976).
19. T.B. Massalski, L.E. Vassamillet and T. Bienvenu, Acta Met. 21, 649 (1973).
20. E. Delcroix, A. Defrain, and I. Epelboin, J. Phys. Radium 24, 17 (1963).
21. J.H. Perepezko, D.H. Rasmussen, I.E. Anderson, and C.R. Loper, Jr., Proc. Sheffield Internat. Conf. on Solidification and Casting (July 1977), in print.
22. M. Hansen, Constitution of Binary Alloys, McGraw-Hill, N.Y., 1958.
23. L. Bosio, A. Defrain and I. Epelboin, J. Physique 27, 61 (1966).
24. D.H. Rasmussen, J.H. Perepezko and C.R. Loper, Jr., in Proc. Second Internat. Conf. on Rapidly Quenched Metals, Section I, N.J. Grant and B.C. Giessen, Eds., M.I.T. Press, Cambridge, Mass. p. 57 (1976).
25. B.C. Giessen and J. Barrick, to be published.
26. P. Duwez, R.H. Willens, and W. Klement, J. Appl. Phys. 31, 1136 (1960).
27. L. Kaufman, Private Communication.
28. J.C. Baker and J.W. Cahn, Acta Met. 17, 575 (1969).
29. C.C. Tsuei in Proc. Second Internat. Conf. on Rapidly Quenched Metals, Section I, N.J. Grant and B.C. Giessen, Eds. M.I.T. Press, Cambridge, Mass. p. 441 (1976).
30. J. Orehotsky and K. Schröder, J. Appl. Phys. 43, 2413 (1972).
31. T.R. Anantharaman, H.L. Luo, and W. Klement, Jr., Trans. Met. Soc. AIME 233, 2014 (1965).
32. M. Lasocka, in Proc. Second Internat. Conf. on Rapidly Quenched Metals, Section II, N.J. Grant and B.C. Giessen, Eds., Mater. Sci. Eng., 23 173 (1976).
33. A. Calka, M. Madhava, D.E. Polk, B.C. Giessen, H. Matyja and J. Vander Sande, Scripta Met. 11, 65 (1977).
34. H.O.K. Kirchner, in Proc. Second Internat. Conf. on Rapidly Quenched Metals, Section II, N.J. Grant and B.C. Giessen, Eds., Mater. Sci. Eng. 23, 95 (1976).

1256

35. D.Q. Uhlmann, J. Noncryst. Sol. 7, 337 (1972).
36. P. Predecki, A. W. Mullendore and N.J. Grant, Trans. Met. Soc. AIME 233, 1581 (1965).
37. N.J. Grant and B.C. Giessen, Eds., Proc. Second Internat. Conf. on Rapidly Quenched Metals, Section I, M.I.T. Press, Cambridge, Mass. (1976).
38. N.J. Grant and B.C. Giessen, Eds., Proc. Second Internat. Conf. on Rapidly Quenched Metals, Section II, Mater. Sci. Eng. 23/2-3, (1976).
39. V. Heine and D. Weaire, in Solid State Physics, Vol. 24, H. Ehrenreich, F. Seitz, and D. Turnbull, Eds., Academic Press, N.Y., p. 249 (1970).
40. L. Kaufman, Calphad 1, 13 (1977).
41. L. Kaufman and H. Nesor, in Titanium Science and Technology, Vol. 2, R.I. Jaffee and H. Burte, Eds., Plenum Press, N.Y., p. 773 (1973).
42. L. Kaufman and H. Nesor, in Proc. Second Internat. Conf. on Rapidly Quenched Metals, Section II, Mat. Sci. Eng. 23, 119 (1976).
43. L.E. Tanner, R. Ray and C.F. Cline, U.S. Patent No. 3,989,517.
44. B.C. Giessen, in Adv. in X-Ray Analysis, Vol. 12, C.S. Barrett, G.R. Mallett, and J.B. Newkirk, Eds., Plenum Press, N.Y., p. 23 (1969).
45. W.B. Pearson, The Crystal Chemistry and Physics of Metals and Alloys, Wiley-Interscience, N.Y. (1972).
46. J.H. Hollomon and D. Turnbull, Trans. AIME 191, 803 (1951).
47. W. Klement, Jr., R.H. Willens, and P. Duwez, Nature 187, 809 (1960).
48. M.H. Cohen and D. Turnbull, J. Chem. Phys. 31, 1164 (1959).
49. R.P. Elliott, Constitution of Binary Alloys, First Supplement, McGraw-Hill, N.Y. (1965).
50. W.G. Moffatt, Binary Phase Diagrams Handbook, General Electric Co., Schenectady, N.Y. (1976).
51. M. Marcus and D. Turnbull, in Proc. Second Internat. Conf. on Rapidly Quenched Metals, Section II, Mat. Sci. Eng. 23, 211 (1976).
52. P. Duwez, R.H. Willens, and R.C. Crewdson, J. Appl. Phys. 36, 2267 (1965).
53. B.C. Giessen, M. Madhava, D.E. Polk, and J. Vander Sande, in Proc. Second Internat. Conf. on Rapidly Quenched Metals, Section II, N.J. Grant and B.C. Giessen, Eds., Mater. Sci. Eng. 23, 145 (1976).
54. R. Ray, B.C. Giessen, and N.J. Grant, Scripta Met. 2, 357 (1968).
55. D.E. Polk, Acta Met. 20, 485 (1972).
56. D.E. Polk, A. Calka and B.C. Giessen, Acta Met., to be published.
57. H.S. Chen and D. Turnbull, Acta Met. 17, 1021 (1969).
58. M. Naka, S. Tomizawa, T. Masumoto and T. Watanabe, in Proc. Second Internat. Conf. on Rapidly Quenched Metals, Section I, N.J. Grant and B.C. Giessen, Eds., M.I.T. Press, Cambridge, Mass., p. 273 (1976).
59. C.B. Shoemaker and D.P. Shoemaker, in Developments in the Structural Chemistry of Alloy Phases, B.C. Giessen, Ed., Plenum Press, N.Y., p. 107 (1969).
60. R. Hultgren, P.D. Desai, D.T. Hawkins, M. Gleiser, and K.K. Kelley, Selected Values of Thermodynamic Properties, American Society for Metals, Metals Park, Ohio (1973).
61. D. Weaire, M.F. Ashby, J. Logan, and M.J. Weins, Acta Met. 19, 779 (1971).
62. S.R. Nagel, J. Vassiliou, P.M. Horn and B.C. Giessen, Phys. Rev., to be published.

National Bureau of Standards SP-496, Applications of Phase Diagrams in Metallurgy and Ceramics
Proceedings of Workshop held at NBS, Gaithersburg, Md., January 10-12, 1977

THE CALCULATION OF MULTICOMPONENT ALLOY PHASE DIAGRAMS AT THE NATIONAL PHYSICAL LABORATORY

T G Chart

National Physical Laboratory,
Teddington, Middlesex, UK

ABSTRACT

Members of the Division of Chemical Standards, National Physical Laboratory, are currently engaged in the calculation of ternary and quaternary phase diagrams, of relevance to superalloys and other high-temperature materials, from the thermodynamic data for the binary systems concerned. Computer methods involving the minimization of Gibbs energy are utilized. The systems calculable at present involve the transition metals, carbon and aluminium. In order to extend this range a programme of critical assessment of thermodynamic data for binary systems, mainly involving transition metal-silicon and transition metal-boron systems, is being undertaken. Examples of recently calculated phase equilibria in the systems Al-Cr-Zr and Al-Cr-Nb are given.

1258

INTRODUCTION

When accurate thermodynamic data are available for the various phases in a system the phase diagram can be calculated reliably. The modern digital computer allows such calculations to be made rapidly, and for multicomponent systems, very cost-effectively. This approach is an important complementary method to that of experimental determination, and in some cases, eg where equilibration is subject to diffusional delays, can be more reliable. In addition, metastable equilibria can be calculated.

For many years those involved in metallurgical thermodynamics at the National Physical Laboratory have been providing data and developing methods for the calculation of reliable phase diagrams for metallurgical systems of technological importance. This work was initiated by Kubaschewski*, who demonstrated the advantages of calculation procedures when applied to certain binary systems, eg Bi-Zn, Hf-Zr and U-Fe;[1] Ga-Zn, Mg-Cd and Cr-Mo;[2] Fe-Cr;[3] Co-Cu;[4] and Cu-Ni.[5] Later, Counsell and Spencer* made significant advances in the calculation of ternary and quaternary systems using a digital computer:[6] ternary systems calculated by these investigators include Au-Pt-Pd,[7] Fe-Cu-Ni and Fe-Cr-Ni,[8] Fe-Cr-V,[9] and Fe-Co-Cr.[10]

Currently, technologically important ternary and quaternary phase diagrams, mainly of relevance to superalloys and other high-temperature materials, are being calculated. A computerized data base is being established to maximize this effort, and collaboration and interchange

---

* Now at the Rheinisch-Westfälische Technische Hochschule Aachen, Federal Republic of Germany.

of information with other groups in the field is being achieved via the CALPHAD (CALculation of PHAse Diagrams) Project.

OUTLINE OF METHODS EMPLOYED

The principles of the calculation of phase diagrams from thermodynamic data are well established and have been described in a number of monographs, eg by Kaufman and Bernstein,[11] and by Prince.[12] For multicomponent systems the Gibbs energies of formation of the various phases present are represented mathematically as functions of composition and temperature, and phase boundaries computed using minimization of Gibbs energy techniques.[6] Because it would generally be too expensive to measure the thermodynamic properties of multicomponent phases these data are estimated from the thermodynamic properties of the binary systems involved, using empirical equations. The suitability of the equations used, when applied to different types of ternary system, has been scrutinized by various CALPHAD members.[13-15] When multicomponent thermodynamic data or phase equilibria are available they are taken into account to produce the best possible overall representation.

For ternary systems three primary computer programs have been developed to calculate (a) the stable equilibria between various solution phases, eg fig 1(i), (b) the stable equilibria between stoichiometric compounds and various solutions, eg fig 1(ii), and (c) the stable equilibria between two compounds, which are either completely or partly miscible in each other, and various solutions, eg fig 1(iii). When two compounds which exist over a range of compositions are known to be mutually miscible they are represented as a solution, eg fig 1(iv). Any number of phases can be handled simultaneously. The boundaries of three-phase regions are established by the intersection of two two-phase regions, or alternatively, where this is impossible, eg when two compounds are in

equilibrium with a pseudo-binary solution between two other compounds (fig 1(v)), by minimizing the Gibbs energy of formation of a composition within the tie-triangle (point X) for different compositions along the pseudo-binary line (point Y). These programs enable a wide range of types of ternary phase diagram to be calculated. The computer programs which enable the stable equilibria between various solution phases, and between compounds and solutions to be calculated, have been modified to deal with quaternary systems.

EXAMPLES OF CALCULATED TERNARY PHASE DIAGRAMS

Recently calculated phase diagrams include the ternary isothermal sections at 1773, 1673, 1573 and 1523 K for the system Al-Cr-Zr shown in figs 2 to 5. Full details of the calculations and data used will be published shortly. No ternary compounds have been reported to exist in this system[16,17] and the Laves phases $ZrAl_2$ (hexagonal, C14[17]) and Cr_2Zr (cubic, C15, at the temperatures for which calculations were made[18]) have been assumed to be insoluble in each other. The calculated diagrams are in good agreement with the experimental equilibria determined for these temperatures[19] as indicated by fig 6, which shows the calculated and experimentally obtained equilibria[19] for the pseudo-binary section indicated in fig 2, between pure zirconium and the composition represented by point Y. When making such comparisons it should be noted that some of the disagreement may be due to errors in the experimental diagrams, which in the present case indicate the melting point of zirconium to be about 2075 K,[19] which is 50 K lower than the accepted value.[20]

Fig 7 shows a calculated isothermal section at 1773 K for the system Al-Cr-Nb. The thermodynamic data employed for the three binary systems involved were those assessed by Kaufman and Nesor,[21,22] who have also

calculated equilibria in this system.[22] The intermetallic compounds stable at this temperature have been considered stoichiometric and not to form ternary solutions, although there is evidence[23,24] to suggest that the Laves compound Cr_2Nb (cubic, C15) does extend into the ternary phase field, towards $NbAl_3$ (tetragonal, DO_{22}). Nevertheless, the calculation provides a rapid and economic method of determining the composition and temperature ranges in which desired behaviour, such as eutectic solidification, occurs.

CURRENT STATUS AND DIRECTION OF FUTURE WORK

At present over 100 ternary alloy systems, mainly involving transition metal elements, carbon and aluminium, can be reliably calculated from thermodynamic data. A high proportion of the required binary data have been assessed by Kaufman*. The NPL data base is being enlarged so that phase equilibria can be calculated for high-temperature alloy systems involving most combinations of the elements B, C, Al, Si, Ti, Cr, Fe, Co, Ni, Zr, Nb, Mo, Hf, Ta and W. Extant thermodynamic data for binary alloys are being critically assessed to produce sets of values which are consistent with the reliable parts of the binary phase diagrams, (and this programme of work is therefore dependent on the availability of such information). Initially it is planned to deal with transition metal-silicon systems, for which reliable thermodynamic data are available,[25,26] and then to extend the assessments to transition metal-boron systems. It is intended to disseminate these data assessments as widely as possible.

ACKNOWLEDGEMENT

The author gratefully acknowledges the advice received from Dr A J Head.

---

* ManLabs Inc, Massachusetts, USA

REFERENCES

1 Kubaschewski, O, in "Thermodynamics of Nuclear Materials", 1962, IAEA, Vienna, p 219.

2 Kubaschewski, O, Chart, T G, J Inst Met, 1965, 93, 329.

3 Müller, F, Kubaschewski, O, High Temp High Pressures, 1969, 1, 543.

4 Dench, W A, Kubaschewski, O, ibid, 1969, 1, 357.

5 Elford, L, Müller, F, Kubaschewski, O, Ber Bunsenges Phys Chem, 1969, 73, 601.

6 Counsell, J F, Lees, E B, Spencer, P J, Met Sci J, 1971, 5, 210.

7 Kubaschewski, O, Counsell, J F, Monatsh Chem, 1971, 102, 1724.

8 Counsell, J F, Lees, E B, Spencer, P J, in "Metallurgical Chemistry", ed Kubaschewski, O, 1972, HMSO, London, p 451.

9 Spencer, P J, Counsell, J F, Z Metallkd, 1973, 64, 662.

10 Chart, T G, Counsell, J F, Jones, G P, Slough, W, Spencer, P J, Int Metall Rev, 1975, 20, 57.

11 Kaufman, L, Bernstein, H, "Computer Calculation of Phase Diagrams", 1970, Academic Press, New York and London.

12 Prince, A, "Alloy Phase Equilibria", 1966, Elsevier, Amsterdam &c.

13 Ansara, I, in "Metallurgical Chemistry", ed Kubaschewski, O, 1972, HMSO, London, p 403.

14 Spencer, P J, Hayes, F H, Kubaschewski, O, Rev Chim Miner, 1972, 9, 13.

15 Spencer, P J, Hayes, F H, Elford, L, in "Chemical Metallurgy of Iron and Steel", 1973, Iron and Steel Institute, London, p 322.

1263

16 Mondolfo, L F, "Aluminium Alloys: Structure and Properties", 1976, Butterworths, London &c.

17 Pearson, W B, "A Handbook of Lattice Spacings and Structures of Metals and Alloys", Vol 2, 1967, Pergamon, Oxford &c.

18 Eremenko, V N, Prima, S B, Tret'yachenko, L A, Poroshk Metall, 1973, (1), 54.

19 Gruzdeva, N M, Tregubov, I A, in "Diagrammy Sostoyaniya Metallicheskikh Sistem", No 14, ed Ageev, N V, 1970, Viniti, Moscow, p 138.

20 Hultgren, R, Desai, P D, Hawkins, D T, Gleiser, M, Kelley, K K, Wagman, D D, "Selected Values of the Thermodynamic Properties of the Elements", 1973, ASM, Metals Park (Ohio).

21 Kaufman, L, Nesor, H, in "Proceedings of Conference on In-Situ Composites", Vol 3, 1973, National Academy of Sciences - National Academy of Engineering (Publication NMAB-308), Washington DC, p 21.

22 Kaufman, L, Nesor, H, Ann Rev Mater Sci, 1973, 3, 1.

23 Svechnikov, V N, Shurin, A K, Dmitriev, G P, in "Diagrammy Sostoyaniya Metallicheskikh Sistem", No 10, ed Ageev, N V, 1967, Viniti, Moscow, p 125.

24 Hunt, C R, Raman, A, Z Metallkd, 1968, 59, 701.

25 Chart, T G, High Temp High Pressures, 1970, 2, 461.

26 Chart, T G, ibid, 1973, 5, 241.

1284

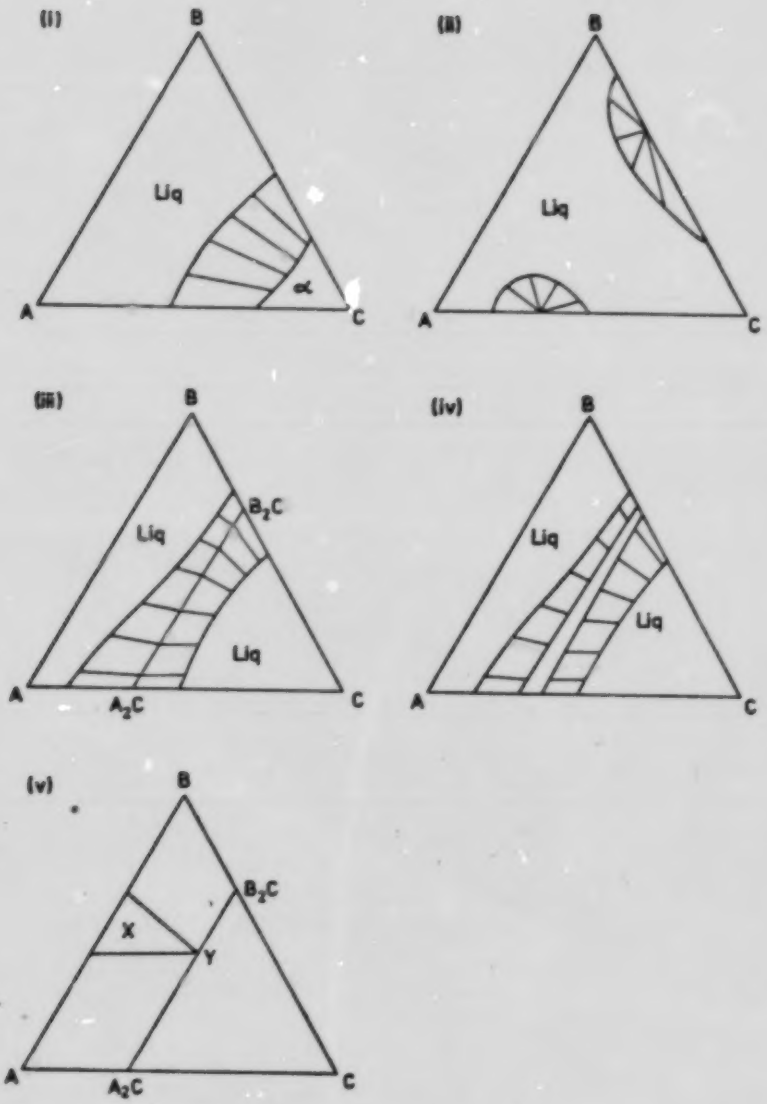

Figure 1 Schematic representation of basic types of ternary phase equilibria calculable from thermodynamic data.

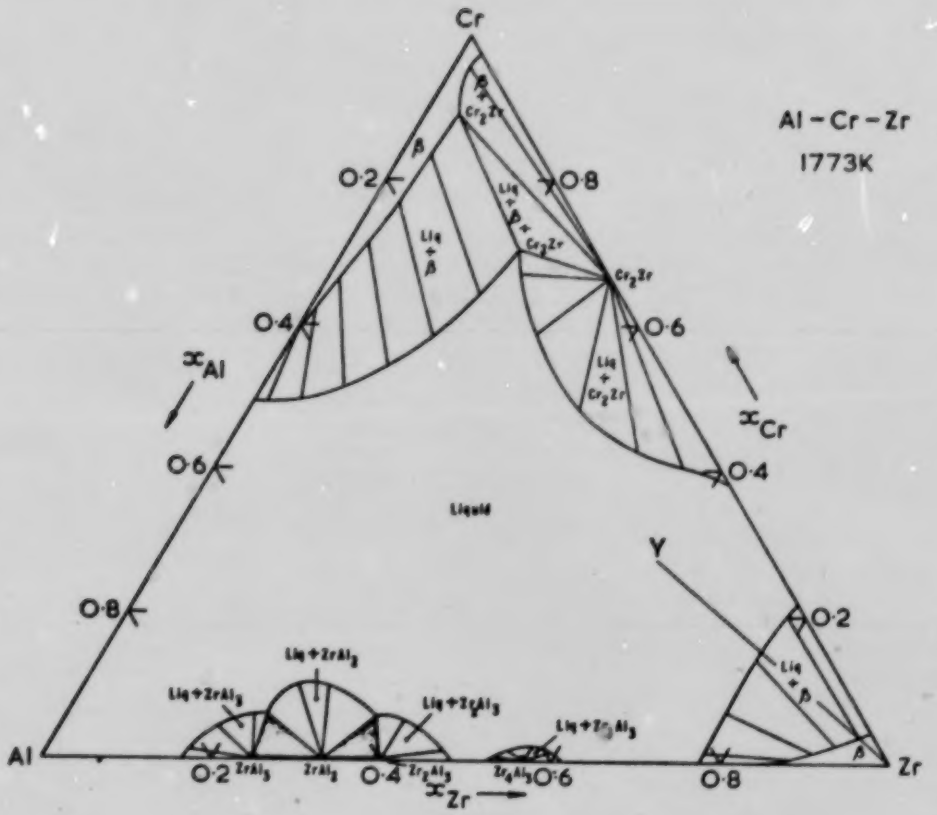

Figure 2 Calculated phase equilibria in the Al-Cr-Zr system at 1773 K.

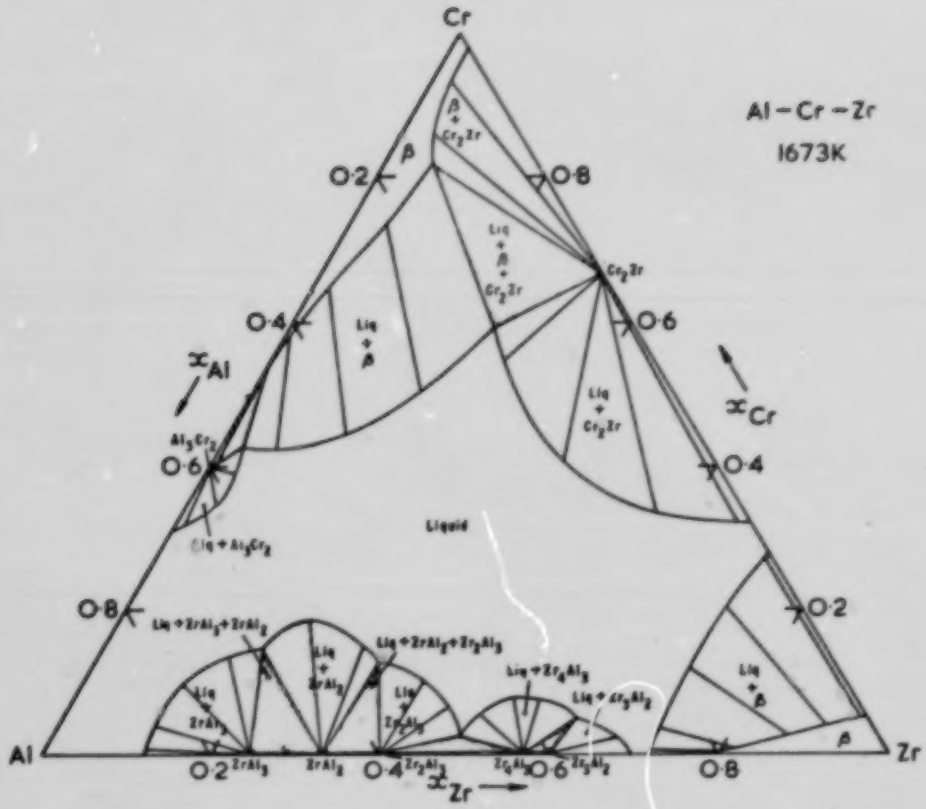

Figure 3 Calculated phase equilibria in the Al-Cr-Zr system at 1673 K.

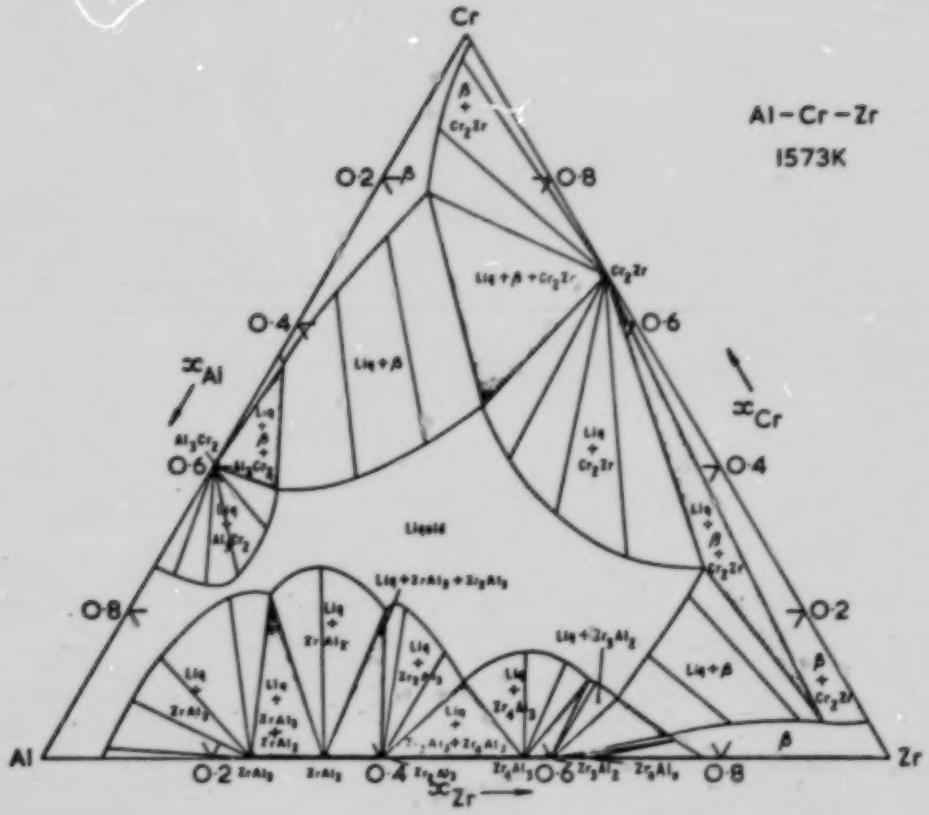

Figure 4 Calculated phase equilibria in the Al-Cr-Zr system at 1573 K.

1263

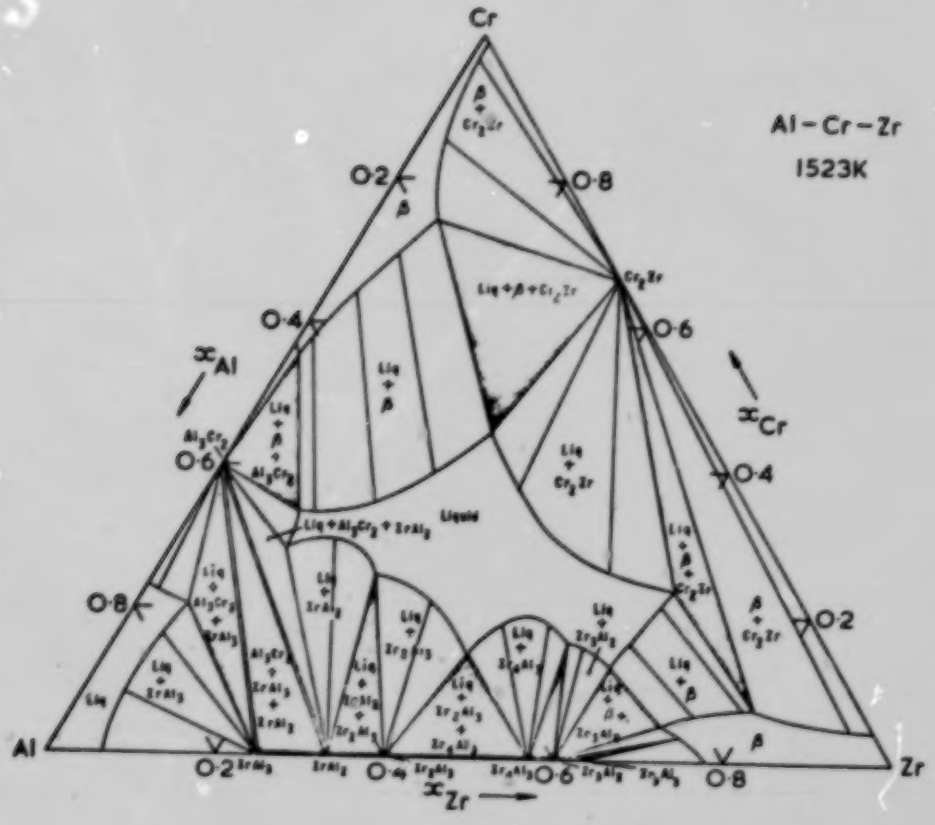

Figure 5 Calculated phase equilibria in the Al-Cr-Zr system at 1523 K.

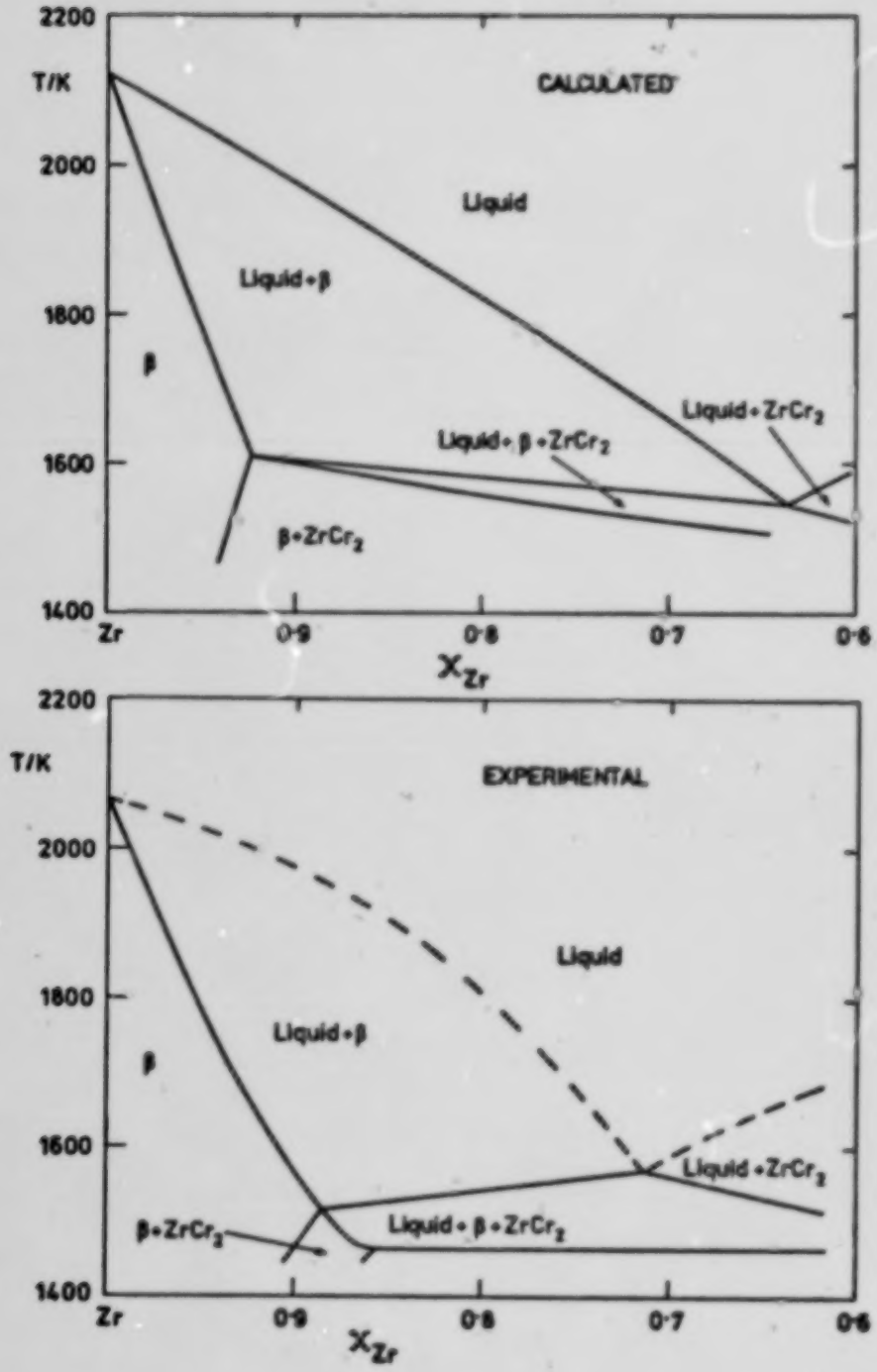

Figure 6 Calculated and experimental phase equilibria in the Al-Cr-Zr system for the pseudo-binary section indicated in figure 2 (see text).

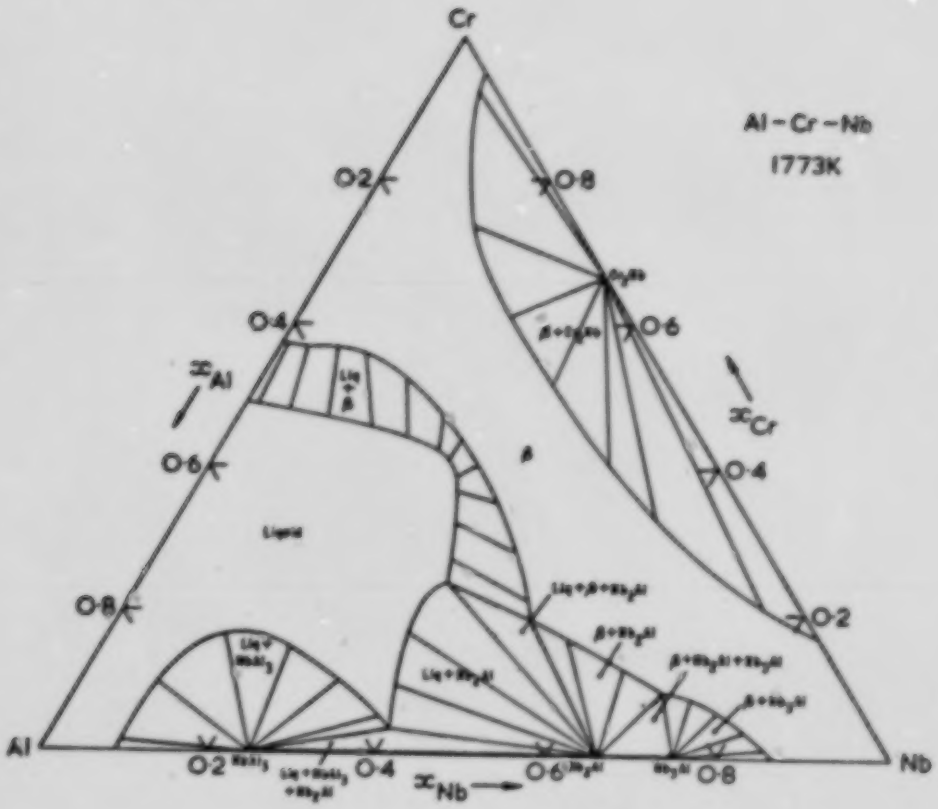

Figure 7 Calculated phase equilibria in the Al-Cr-Nb system at 1773 K.

National Bureau of Standards SP-496, Applications of Phase Diagrams in Metallurgy and Ceramics
Proceedings of Workshop held at NBS, Gaithersburg, Md., January 10-12, 1977

SYNTHESIS OF BINARY METALLIC SYSTEMS

I. ISMORPHOUS SYSTEMS
II. SIMPLE EUTECTIC SYSTEMS

S.S. BALAKRISHNA AND A.K. MALLIK‡
Department of Metallurgical Engineering,
Indian Institute of Technology, Bombay,
INDIA

Introduction:

One of the most important sources of information regarding a materials system is its phase diagram. In fact, before any research or development work is done on a materials problem, it is important to study the phase diagram to know about the nature of the material. Information concerning phase compositions and phase stability are a function of temperature, composition and pressure, and can be obtained from the phase diagrams.

Theoretical synthesis of phase diagrams is a valuable aid in estimating thermodynamic properties in the absence of experimental data and for critical comparison. Using convenient mathematical expressions or statistical thermodynamic models for the free-energy functions involved, one can extend the calculations of the phase diagram to regions where no, or questionable, experimental data are available. This procedure thus forms the basis for extrapolation in phase diagrams.

In order to calculate the phase equilibria in an alloy system, one must express the free energy function of individual phases as a function of composition. Once the free energy functions

‡ Department of Metallurgical Engineering, Indian Institute of Technology, Bombay, INDIA.

1272

of the phases in a system are known, it is in principle possible to calculate the equilibrium state for a certain alloy composition by directly minimising the total free energy. In the present investigation the binary isomorphous and simple eutectic phase diagrams are synthesized using models of statistical thermodynamics (i.e. regular and quasi-chemical) and ideal solution models using and neglecting the C_p data. To solve the system of equations to yield the phase boundaries, the method based on the Newton-Raphson iteration technique[1] offered by Kaufman and Bernstein[2] is utilized.

Thermodynamic Definition of Binary Equilibrium:

Consider an alloy system A-B in which x represents the atom fraction of component B. Suppose that there are two phases liquid (L) and solid solution (α) which exist in the system. The free energy of the liquid phase (L) in the A-B system is defined by

$$F^L = (1-x)\, F_A^L + x\, F_B^L + RT\,[\, x \ln x + (1-x) \ln(1-x)] + F_E^L \quad \text{cals/g.atom} \qquad \ldots (1)$$

where F_A^L and F_B^L are the free energies of pure liquid A and pure liquid B, and F_E^L is the excess free energy of mixing which is zero when x=0 and 1.

The free energy of the solid solution phase (α) in the A-B system is defined in a similar manner to that of liquid phase.

$$F^{\alpha} = (1-x)\, F_A^{\alpha} + x\, F_B^{\alpha} + RT\,[x \ln x + (1-x)\ln(1-x)] + F_E^{\alpha}$$

cals/g.atom .. (2)

where F_A^{α} and F_B^{α} are the free energies of solid forms of pure A and B and F_E^{α} is the excess free energy of mixing in the solid state.

The partial molar free energies of A and B in an alloy containing x atom fraction of B are $\bar{F}_A$ and $\bar{F}_B$ respectively. These quantities are defined as follows:

$$\bar{F}_A = F - x\,\frac{\partial F}{\partial x} \qquad .. (3)$$

$$\bar{F}_B = F + (1-x)\,\frac{\partial F}{\partial x} \qquad .. (4)$$

If, at a temperature T, there exists a two phase ($L+\alpha$) field bounded by compositions XL and $X\alpha$, then equilibrium requirements dictates that for the particular values of T, XL and $X\alpha$

$$\bar{F}_A^{L}\Big|_{XL} = \bar{F}_A^{\alpha}\Big|_{X\alpha} \qquad .. (5)$$

$$\bar{F}_B^{L}\Big|_{XL} = \bar{F}_B^{\alpha}\Big|_{X\alpha} \qquad .. (6)$$

equations (5) and (6) represent the equality of chemical potentials of the components in the two phases. They are the equivalent of the

rule of common tangents. Equations (1-4) yield:

$$\bar{F}_A^L = F_A^L + RT \ln (1-x) + [F_E^L - x\frac{\partial F_E^L}{\partial x}] \quad .. (7)$$

$$\bar{F}_A^\alpha = F_A^\alpha + RT \ln (1-x) + [F_E^\alpha - x\frac{\partial F_E^\alpha}{\partial x}] \quad .. (8)$$

$$\bar{F}_B^L = F_B^L + RT \ln x + [F_E^L + (1-x)\frac{\partial F_E^L}{\partial x}] \quad .. (9)$$

$$\bar{F}_B^\alpha = F_B^\alpha + RT \ln x + [F_E^\alpha + (1-x)\frac{\partial F_E^\alpha}{\partial x}] \quad ..(10)$$

Applying equations (5-6) to equations (7-10) yield:

$$\Delta F_A^{\alpha \rightarrow L} + RT \ln ((1-XL)/(1-X\alpha)) = [F_E^\alpha - x\frac{\partial F_E^\alpha}{\partial x}]_{X\alpha} - [F_E^L - x\frac{\partial F_E^L}{\partial x}]_{XL} \quad .. (11)$$

$$\Delta F_B^{\alpha \rightarrow L} + RT \ln (XL/X\alpha) = [F_E^\alpha + (1-x)\frac{\partial F_E^\alpha}{\partial x}]_{X\alpha} - [F_E^L + (1-x)\frac{\partial F_E^L}{\partial x}]_{XL} \quad .. (12)$$

as the condition for equilibrium. Equations (11) and (12) show directly how the difference in free energies between the two phases of components A and B contribute to final values of XL and $X\alpha$ at a temperature T and thereby lead to the establishment of

the equilibrium diagram.

I. Application to Isomorphous Systems:

a) Ideal Solution.

When $F_E = 0$, the solution is ideal. Equations (11) and (12) reduce to the form

$$\Delta F_A^{\alpha \rightarrow L} + RT \ln \left((1-X_L)/(1-X_\alpha) \right) = 0 \qquad .. (13)$$

$$\Delta F_B^{\alpha \rightarrow L} + RT \ln (X_L/X_\alpha) = 0 \qquad .. (14)$$

Equations (13) and (14) are solved simultaneously for X_L and X_α at different temperatures using and neglecting C_p data. Using the C_p data, $\Delta F_i^{\alpha \rightarrow L}$ (for i = A or B) is expressed as

$$(1/RT)\,\Delta F_i^{\alpha \rightarrow L} = (1/R)\,\Delta H_i^{\alpha \rightarrow L} \left[\frac{1}{T} - \frac{1}{T_i} \right] + \frac{\Delta a_i^{\alpha \rightarrow L}}{R} \left[1 - \frac{T_i}{T} + \ln \frac{T_i}{T} \right] - \frac{\Delta b_i^{\alpha \rightarrow L}}{2RT} [T-T_i]^2 - \frac{\Delta c_i^{\alpha \rightarrow L}}{2R} \left[\frac{1}{T} - \frac{1}{T_j} \right]^2 \qquad ...(15)$$

Neglecting C_p data, $\Delta F_i^{\alpha \rightarrow L}$ is expressed as

$$(1/RT)\,\Delta F_i^{\alpha \rightarrow L} = (1/R)\,\Delta H_i^{\alpha \rightarrow L} \left[\frac{1}{T} - \frac{1}{T_i} \right] \qquad .. (16)$$

b) Regular Solution:

In the regular solution model[3], F_E^L and F_E^α are given by

$$F_E^L = L\ x\ (1-x) \quad \text{cal/g. atom} \qquad .. (17)$$

$$F_E^\alpha = B\ x\ (1-x) \quad \text{cal/g. atom.} \qquad .. (18)$$

where L and B are the interaction parameters of liquid and solid phases respectively.

Introducing these equations (17) and (18) to equations (11) and (12) result

$$\Delta F_A^{\alpha \rightarrow L} + RT \ln \left((1-XL)/(1-x\alpha) \right) = X\alpha^2\ B - XL^2\ L \qquad .. (19)$$

$$\Delta F_B^{\alpha \rightarrow L} + RT \ln (XL/X\alpha) = (1-X\alpha)^2\ B - (1-XL)^2\ L \qquad .. (20)$$

Equations (19) and (20) are solved simultaneously for XL and $X\alpha$ at different temperatures.

c) Quasi-chemical:

In the quasi-chemical model, the excess free energy of mixing is derived by Guggenheim and others[4], [16] as

$$F_E = x(1-x)\Omega[\ 1-x(1-x)\Omega / ZRT] \qquad .. (21)$$

neglecting the higher order terms than the second of (Ω/ZRT), where Ω is the interaction parameter and Z is the coordination number.

The excess free energy terms for liquid and solid phase are written as

$$F_B^L = x\,(1-x)\,L\,[\,1-x(1-x)\,L/ZRT] \qquad ..(22)$$

$$F_B^\alpha = x\,(1-x)\,B[\,1-x(1-x)\,B/ZRT\,] \qquad ..(23)$$

With the introduction of equations (22) and (23) to equations(11) and (12) yield

$$\Delta F_A^{\alpha\rightarrow L} + RT\ln\left(\,(1-XL)/(1-X\alpha)\,\right) = B\,X\alpha^2\left[1-\frac{B}{ZRT}(1-X\alpha)(3X\alpha-1)\right]$$

$$-L\,XL^2\left[1-\frac{L}{ZRT}(1-XL)\,(3XL-1)\right] \qquad ..(24)$$

$$\Delta F_B^{\alpha\rightarrow L} + RT\ln(XL/X\alpha) = B(1-X\alpha)^2\left[1-\frac{B}{ZRT}X\alpha(2-3X\alpha)\right]$$

$$-L(1-XL)^2\left[1-\frac{L}{ZRT}XL(2-3XL)\right] \qquad ..(25)$$

Equations (24) and (25) are solved simultaneously for XL and $X\alpha$ at different temperatures.

II. Application to Simple Eutectic Systems:

a) Ideal Solution:

For the case of simple eutectic system (i.e. no mutual

solid solubilities in each), $X\alpha = 0$ and $XL = XAL$ in equation (13) and $X\alpha = 1$ and $XL = XBL$ in equation (14) and $\alpha = s$, a pure solid. These two requirements reduce the equations (13) and (14) to

$$\Delta F_A^{s \rightarrow L} + RT \ln (1-XAL) = 0 \qquad .. (26)$$

$$\Delta F_B^{s \rightarrow L} + RT \ln XBL = 0 \qquad .. (27)$$

The equations (26) and (27) are solved for XAL and XBL at different temperatures using and neglecting C_p data. The expressions (15) and (16) are valid to apply in equations (26) and (27) using and neglecting C_p data.

b) Regular Solution:

In this case $X\alpha = 0$ and $XL = XAL$ in equation (19) and $X\alpha=1$ and $XL = XBL$ in equation (20). These two requirements reduce the equations (19) and (20) to

$$\Delta F_A^{s \rightarrow L} + RT \ln (1-XAL) = -L(XAL)^2 \qquad .. (28)$$

$$\Delta F_B^{s \rightarrow L} + RT \ln (XBL) = -L(1-XBL)^2 \qquad .. (29)$$

The equations (28) and (29) are solved for XAL and XBL at different temperatures.

c) Quasi-chemical:

In this case $X\alpha = 0$ and XL = XAL in equation(24) and $X\alpha = 1$ and XL=XBL in equation (25). These two requirements reduce the equation (24) and (25) to

$$\Delta F_A^{S \rightarrow L} + RT \ln (1-XAL) = -L\, XAL^2 \left[1 - \frac{L}{ZRT}(1-XAL)(3XAL-1)\right] \quad \ldots.(30)$$

$$\Delta F_B^{S \rightarrow L} + RT \ln XBL = -L(1-XBL)^2 \left[1 - \frac{L}{ZRT} XBL(2-3XBL)\right] \quad \ldots(31)$$

The equations (30) and (31) are solved for XAL and XBL at different temperatures.

Numerical Techniques for Solving the System of Equations:

Rudman's trial and error method[5] has been used to solve the system of equations (19) and (20), (24) and (25), (28) and (29) and (30) and (31) by assigning arbitrary values to the couple of unknown XL and $X\alpha$ or XAL and XBL, so that the whole range of possible compositions is covered, and then selecting the couple of values that best fits the equations. This procedure is time consuming and so the Kaufman and Bernstein method[2] based on Newton-Raphson iteration technique[1] has been used. This method

consists in selecting a couple of approximate equilibrium compositions XL and $X\alpha$ and then calculating a more precise solution XL' and $X\alpha'$ using successive approximations computed by the following formulae:

$$XL_{n+1} = XL_n - \frac{1}{J(XL_n, X\alpha_n)} \begin{vmatrix} F(XL_n, X\alpha_n) & F'_{X\alpha}(XL_n, X\alpha_n) \\ G(XL_n, X\alpha_n) & G'_{X\alpha}(XL_n, X\alpha_n) \end{vmatrix}$$

$$= XL_n - \frac{\Delta_{XL}(n)}{J(XL_n, X\alpha_n)} \qquad .. (32)$$

$$X\alpha_{n+1} = X\alpha_n - \frac{1}{J(XL_n, X\alpha_n)} \begin{vmatrix} F'_{XL}(XL_n, X\alpha_n) & F(XL_n, X\alpha_n) \\ G'_{XL}(XL_n, X\alpha_n) & G(XL_n, X\alpha_n) \end{vmatrix}$$

$$= X\alpha_n - \frac{\Delta_{X\alpha}(n)}{J(XL_n, X\alpha_n)} \qquad .. (33)$$

where $F(XL, X\alpha) = 0$, $G(XL, X\alpha) = 0$,

$$\Delta_{XL}(n) = \begin{vmatrix} F(XL_n, X\alpha_n) & F'_{X\alpha}(XL_n, X\alpha_n) \\ G(XL_n, X\alpha_n) & G'_{X\alpha}(XL_n, X\alpha_n) \end{vmatrix},$$

$$\Delta_{X\alpha}(n) = \begin{vmatrix} F'_{XL}(XL_n, X\alpha_n) & F(XL_n, X\alpha_n) \\ G'_{XL}(XL_n, X\alpha_n) & G(XL_n, X\alpha_n) \end{vmatrix},$$

and the Jacobian

$$J(X_L, X_\alpha) = \begin{vmatrix} F'_{X_L}(X_L, X_\alpha) & F'_{X_\alpha}(X_L, X_\alpha) \\ F'_{X_L}(X_L, X_\alpha) & F'_{X_\alpha}(X_L, X_\alpha) \end{vmatrix} \neq 0$$

This method is effective only when the initial selection of a couple of approximation is sufficiently close to the solution of a system.

Estimation of Interaction Parameters:

The 'electronic component' e_o and the internal pressure term e_p of L described by Kaufman and Bernstein[2] are

$$e_o = 2[\phi_1 \left(\frac{A+B}{2}\right) - \tfrac{1}{2}\phi_1 (A) - \tfrac{1}{2}\phi_1 (B)] \text{cals/g.atom} \quad \ldots (34)$$

$$e_p = 0.3 (V_A + V_B) \left[\left(-\frac{H_A}{V_A}\right)^{\frac{1}{2}} - \left(-\frac{B_B}{V_B}\right)^{\frac{1}{2}} \right] \text{cals/g.atom} \quad \ldots(35)$$

and $L = e_o + e_p$ ...(36)

The strain energy term e_1, the other terms e_2, e_3 and e_4 given by Kaufman and Bernstein[2] are

$$e_1 = -0.5 (H_A + H_B) (V_A - V_B)^2 (V_A + V_B)^{-2} \text{ cals/g.atom.} \quad \ldots(37)$$

$$e_2 = 2[\phi_2 \left(\frac{A+B}{2}\right) - \tfrac{1}{2}\phi_2(A) - \tfrac{1}{2}\phi_2(B)] \quad \ldots(38)$$

$$e_3 = 2[\phi_3 \left(\frac{A+B}{2}\right) - \tfrac{1}{2}\phi_3(A) - \tfrac{1}{2}\phi_3(B)] \quad \ldots(39)$$

$$e_4 = 2[\phi_4 \left(\frac{A+B}{2}\right) - \tfrac{1}{2}\phi_4(A) - \tfrac{1}{2}\phi_4(B)] \quad \ldots(40)$$

$$B = L + e_1 + e_2 \quad \ldots(41)$$

These terms are calculated for the estimation of the interaction parameters of L and B and utilized in the computations of phase equilibria using regular solution and quasi-chemical models.

Results and Discussion:

The regular solution and quasi-chemical solution phase diagrams of the isomorphous and simple eutectic binary systems are computed using the thermodynamic data of heats of fusion, heat capacities, melting temperatures and the interaction parameters using heats of vaporization, molar volumes. The systems considered are Ag-Pd, Cb-Ti, Mo-W, Mo-V, V-W, and Cb-W for isomorphous type and Ag-Si, Sn-Al, Au-Si, Be-Si, and Bi-Cd for simple eutectic type.

The T_o-x computation is the first step in computing the phase diagram, since it discloses the temperature and composition range where the various phases are stable. In the case of isomorphous systems of Cb-Ti, Mo-W, Mo-V, V-W and Cb-W it is found using T_o-x computation that the phases to be considered are only liquid and bcc phases and in case of isomorphous Ag-Pd system, the phases to be considered are liquid and fcc phases. Consequently, the next step in the synthesis is to calculate the two-phase boundaries associated with each T_o-x curve by utilising equations (19) and (20) using regular solution model and equations (24) and (25) using quasi-chemical solution model for isomorphous systems considered. The computations are made using the Newton-Raphson iteration technique described earlier.

In case of simple eutectic systems since liquid phase is in equilibrium with pure components only, the Newton-Raphson iteration technique is relatively simple since it involves the solution of a single variable.

The ideal isomorphous phase diagrams in which the interaction parameters are zero are calculated using equations (13) and (14). With the consideration of C_p data of the pure components, these diagrams are calculated utilizing equations(15) in equations (13) and (14).

The ideal simple eutectic phase diagrams with zero interaction parameters are calculated using equations (26) and (27). With the

consideration of C_p data of the pure components, these diagrams are calculated using equation (15) in equations (26) and (27).

The numerical values of e_o, e_p, e_1, e_2, e_3 and e_4 obtained for the isomorphous systems considered are summarized in table 1, and the resultant interaction parameters are presented in table 2.

Table:1. Interaction Parameters (Cal/g.atom)

System	e_o	e_p	e_1	e_2	e_3	e_4
Ag-Pd	-139,000	2302	438.4	-4110	1990	1415
Cb-Ti	0	3334	28.3	0	0	0
Mo-W	0	1381	7.2	0	0	0
Mo-V	0	585	256	0	0	0
V-W	0	3681	391.3	0	0	0
Cb-W	0	2276	788	0	0	0

Table 2: Resultant Interaction Parameters (Cals/g.atom)

System	L = $e_o + e_p$	B = $L+e_1+e_2$	E = $B+e_3$	A = $E + e_4$
Ag-Pd$^{\varphi}$	-136698	-140370	-138380	-136964
Cb-Ti	3334	3362	3362	3362
Mo-W	1381	1388	1388	1388
Mo-V	585	841	841	841
V-W	3681	4072	4072	4072
Cb-W	2276	3064	3064	3064

φ In case of Ag-Pd system, A is used instead of B, since it forms fcc solid phase.

The interaction parameters computed for the simple eutectic systems are presented in table 3.

Table 3: Interaction Parameters for Simple Eutectic Systems(Cal/g.atom)

System	e_o	e_p	L
Ag-Si	0	+ 190	+ 190
Be-Si	-3589	+ 7254	+ 3565
Bi-Cd	-922.4	+ 80.7	- 842
Au-Si	- 5763	+ 214.2	- 5549
Sn-Al	- 2075.4	+ 3595	+ 1520

The diagrams calculated using ideal, regular and quasi-chemical models are compared in figs. (1) (i.e. a,b,c,d,e,f) and (2) (i.e. g,h,i,j,k) for isomorphous type and simple eutectic type respectively, with the experimental phase diagrams taken from ASM Hand Book[6] and Hansen and Anderko[7].

In the case of phase diagrams of Mo-W, Mo-V, Cb-W and Ti-Cb the experimental solidus lines are in agreement with that computed by the regular solution model and better agreement with that computed by quasi-chemical model. In the V-W diagram, the synthesized solidus lines of regular solution and quasi-chemical models, are away from the idealised solidus lines but lie in between the ideal solidus line and experimental solidus line. In case of Ag-Pd system the agreement is very poor. In all the isomorphous systems,

the synthesized liquidus lines show poor agreement with the experimental liquidus lines.

The ideal model calculations with C_p or without C_p consideration have shown negligible effect on the Ag-Pd, Ti-Cb, and Mo-V systems whereas in other isomorphous systems considered deviation is observed.

In all the simple eutectic systems considered, both the regular solution and quasi-chemical models improved the phase diagrams from ideal to experimental. Though the synthesized models do not agree well with the experimental diagrams, the shape of the synthesized diagrams, agree well with the experimental ones. The ideal model with out without C_p data remain same in all the systems considered.

Summary:

1. The isomorphous binary metallic systems of Ag-Pd, Cb-Ti, Mo-W, Mo-V, V-W and Cb-W have been synthesized. The synthesized solidus lines of Mo-W, Mo-V, Cb-W, and Cb-Ti diagrams are in agreement with the experimental solidus lines. The agreement is poor in Ag-Pd systems. The synthesized solidus line of V-W diagram tends to the experimental solidus line from that of ideal solidus line. In general the synthesized liquidus lines show poor agreement with the experimental liquidus lines.

2. The simple eutectic systems of Ag-Si, Be-Si, Bi-Cd, Au-Si and Sn-Al have been synthesized. The shape of the synthesized diagrams agree well with the experimental ones. The synthesized diagrams tend to approach the experimental diagram from that of ideal diagrams, with the refinement of the statistical thermodynamic models.

References:

1. Kopchenova.N.V and Maron. I.A, 'Computational Mathematics', MIR Publishers, Moscow, 1972.

2. Kaufman.L and Bernstein.H, 'Computer Calculation of Phase diagrams'. Academic Press, New York, 1970.

3. Wagner C, 'Thermodynamics of Alloys', Addison Wesley,Mass, 1952.

4. Rudman, Averbach, Oriani, Acta Met 1954, P 576, Vol.2.

5. Rudman.P.S, 'Advances in Materials Research', Vol.IV, pp.147-293, Interscience Publishers, New York,1969.

6. ASM Metals Hand Book, 'Metallography, Structures and Phase Diagrams', Vol.8., 1973.

7. Hansen.M. and Anderko.K.'Constitution of Binary Alloys', McGraw Hill Book Co., New York,1958.

8. Hultgren.R, Orr.L.R, and Kelley K.K, 'Selected Values of Thermodynamic Properties of Metals and Alloys', John Wiley and Sons,Inc, New York, 1963.

9. Lupis.C.H.P. and Elliott J.F. Acta Met., 1966, Vol.14, PP 529-38: 1967, Vol.15, PP 265-76.

10. Lupis C.H.P. Acta Met, 1968, Vol.16, PP 1365-75

11. Hiskes.R and Tiller W.A. Mater.Sci.Eng. 1967-68, Vol.2, PP 320-30; 1969, Vol.4, PP 163-84.

12. Kaufman L., Acta Met, 1959, Vol.7, PP 575-587.

13. Henri Gaye and Lupis C.H.P., Met. Trans, 1975, Vol.6A, PP 1049-1056.

14. Rao.S.V and Misra S, Trans.IIM, Vol.27, No.5, 1974, PP 311-316.

15. Swalin R.A. 'Thermodynamics of Solids', John Wiley and Sons Inc., New York (1962).

16. Shunk F.A. 'Constitution of Binary Alloys' McGraw-Hill Book Co., New York, (1969).

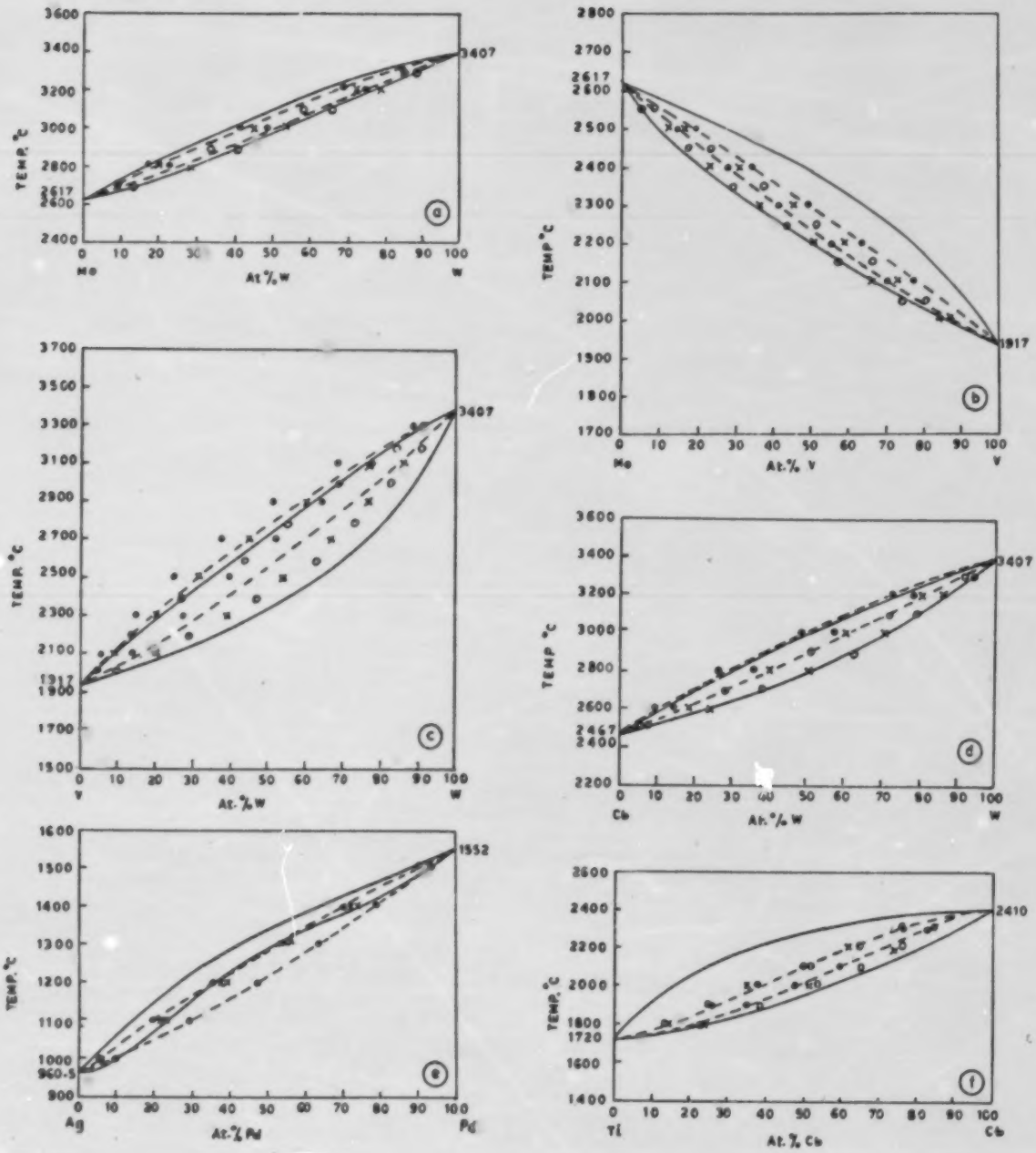

the notations are as follows:

——— Experimental

– – – – – Ideal neglecting C_p

● ● ● ● ● Ideal with C_p

x x x x x x Regular

o o o o o Quasi - chemical

Fig. 1. Isomorphous phase diagrams.

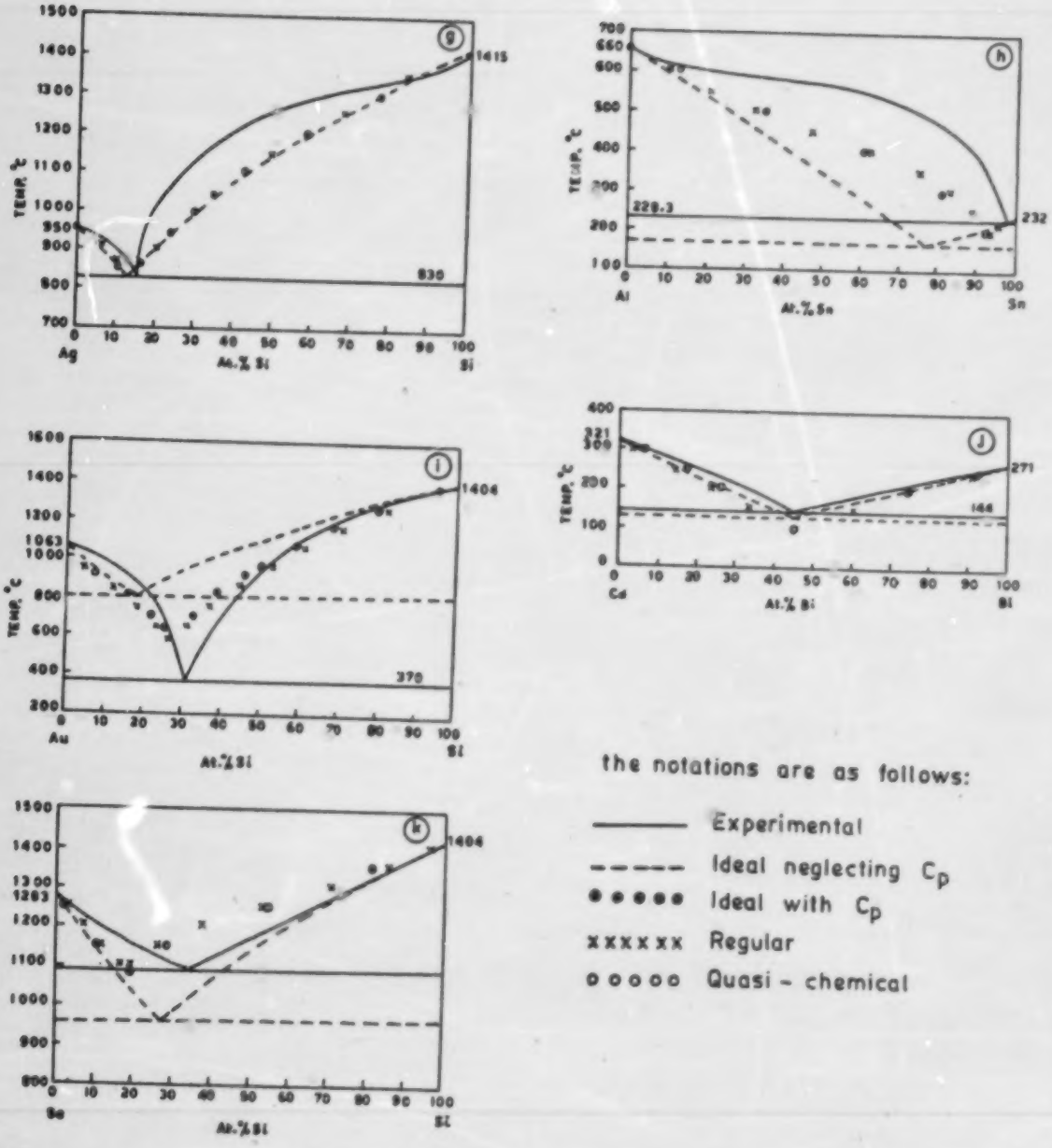

Fig. 2. Simple Eutectic phase diagrams.

National Bureau of Standards SP-496, Applications of Phase Diagrams in Metallurgy and Ceramics
Proceedings of Workshop held at NBS, Gaithersburg, Md., January 10-12, 1977

Quantitative Fits to Phase Lines and High Temperature Thermodynamic Data for Systems Forming Semiconductor Compounds

Robert F. Brebrick
Metallurgy and Materials Science Program
Marquette University, Milwaukee, WI 53233

Introduction

We are primarily interested in binary systems involving compound or elemental semiconductors. Theoretical construction of the phase diagrams involves knowing the appropriate thermodynamic models for the various phases occurring and the values of the parameters in these models that differentiate among specific systems. Although it is commonly believed that the appropriate model is established for a compound semiconductor with not too wide a deviation from stoichiometry, or for an elemental semiconductor containing a small amount of a second component, the same cannot be generally claimed for the liquid phases. Moreover, it has not yet been established that the model parameters, although some progress has been made for crystalline semiconductor phases,[1,2] can be reliably calculated. Therefore the task is to fit available experimental phase diagram lines, as well as any other available high temperature thermodynamic data, in an effort to identify appropriate phase models for chemically similar systems and to establish values for the model parameters. We discuss efforts in this direction below for an A-B system forming a congruently-melting, narrow homogeneity range compound, $A_mB_n(c)$.

Thermodynamic Equation for the Liquidus Line

The appropriate liquidus equation has recently been derived[3] and only the main points are indicated here. An equation is desired that is general in so far as the liquid phase is concerned and which takes account of the

temperature dependence of the enthalpy of formation, ΔH_f, and entropy of formation, ΔS_f, per formula weight of $A_mB_n(c)$ from the pure, liquid elements. As already implied, a basic, plausible, approximation is that at any temperature, T, the integral molar properties are essentially the same at both composition limits of the compound. An important feature of the derivation is that enroute to obtaining the desired liquidus equation, two auxiliary equations are used which link the properties of solid and liquid phases at the congruent melting point, T_{mn}, and the nominal compound composition $x = x^* = n/(m+n)$.

The starting point is in two equilibrium equalities, one between the chemical potentials of A in the coexisting liquid and solid phases, the other between those for component B. Multiplying the former by m, the latter by n, adding, and rearranging gives

$$m(h_A - Ts_A^e) + n(h_B - Ts_B^e) + RT\ln(1-x)^m x^n$$

$$= m\mu_A(c) + n\mu_B(c) - m\mu_A^o(\ell) - n\mu_B^o(\ell) \qquad (1)$$

where if i = A,B then h_i is the relative partial molar enthalpy of I in the liquid, s_i^e is the relative partial molar, excess entropy, and x is the atom fraction of B. The quantity $\mu_i^o(\ell)$ is the chemical potential of pure liquid i. For a narrow homogeneity range compound we assume, with justification from both theory and experiment,[4] that the right hand member of Eq. (1) differs insignificantly from the Gibbs free enthalpy of formation of $A_mB_n(c)$ from the pure liquid elements. This quantity as well as the other integral properties of the compounds are in effect then functions of T along. Writing

$$\Delta G_f = \Delta H_f - T\Delta S_f \qquad (2)$$

and replacing the r.h.m. of Eq. (1) by that of Eq. (2) gives a liquidus equation called[4] the ΔH_f-ΔS_f liquidus equation, since these quantities enter as experimentally determined parameters. Since congruent melting implies a zero change in the Gibbs free enthalpy, two auxiliary relations can be written as

$$\Delta H_f(T_{mn}) = mh_A^* + nh_B^* - H_{mn} \tag{3}$$

$$\Delta S_f(T_{mn}) = ms_A^{*,\ominus} + ns_B^{*,\ominus} - H_{mn}/T_{mn} - R\ln[(1-x^*)^m(x^*)^n] \tag{4}$$

where the asterisk superscript indicates the partial molar quantities for the liquid are evaluated at $x = x^* = n/(m+n)$ and $T = T_{mn}$. In any specific case Eqs. (3) and (4) are two equations between the liquid phase model parameters. Using Eqs. (2), (3) and (4) in (1) and rearranging gives

$$T = \frac{H_{mn}+m(h_A-h_A^*)+n(h_B-h_B^*)-\Delta H_f+\Delta H_f(T_{mn})+T\{\Delta S_f-\Delta S_f(T_{mn})\}}{H_{mn}/T_{mn}+m(s_A^{\ominus}-s_A^{*,\ominus})+n(s_B^{\ominus}-s_B^{*,\ominus})+R\ln\left[\left(\frac{1-x^*}{1-x}\right)^m\left(\frac{x^*}{x}\right)^n\right]} \tag{5}$$

This is the desired "heat-of-fusion" liquidus equation in which the temperature dependence of the enthalpy of compound formation, ΔH_f-$\Delta H_f(T_{mn})$, and that of the corresponding entropy, ΔS_f-$\Delta S_f(T_{mn})$, can be written more explicitly as a function of T in a specific case.[5] In general we do not have an explicit equation for T and must resort to iterative methods for solution. In Eq. (5) the behavior of the relative heat capacity of both the compound and the liquid phase are general. The former is to be fixed by experiment, the latter is fixed upon adoption of a liquid phase model.

In certain cases Eq. (5) can be put into an approximate form, whose validity must be checked in each case, but which has the advantage of being an explicit equation for the liquidus temperature T and so more rapidly solved using a computer.[3] Suppose the Gibbs free enthalpy of compound

formation turns out to depend very nearly linearly upon T. Then one can write

$$\Delta G_f(c) = \Delta\overline{H}_f - T\Delta\overline{S}_f + \delta(T) \tag{6}$$

where the enthalpy and entropy are average, constant quantities and $\delta(T)$ is small in a sense made clear below. One can also write

$$\Delta\overline{H}_f = \Delta H_f(T_{mn}) + \Delta \tag{7}$$

$$\Delta\overline{S}_f = \Delta S_f(T_{mn}) + \Delta/T_{mn} + \delta(T_{mn})/T_{mn} \tag{8}$$

Once the quantity Δ is defined by Eq. (7), then Eq. (8) must follow in order that the correct value of $\Delta G_f(c)$ at T_{mn} be given by Eq. (6). The auxiliary relations, Eqs. (3) and (4) can now be written in terms of the average enthalpy and entropy of formation to give

$$\Delta\overline{H}_f = mh_A^* + nh_B^* - (H_{mn}-\Delta) \tag{3b}$$

$$\Delta\overline{S}_f = ms_A^{*,e} + ns_B^{*,e} - (H_{mn}-\Delta-\delta(T_{mn}))/T_{mn} - R\ln[(1-x^*)^m(x^*)^n] \tag{4b}$$

Eliminating $\Delta\overline{H}_f$ and $\Delta\overline{S}_f$ in Eq. (6) using these equations and then substituting the resulting r.h.m. of Eq. (6) for that of Eq. (1) and rearranging gives

$$T = \frac{H_{mn} - \Delta - \delta(T) + m(h_A-h_A^*) + n(h_B-h_B^*)}{\frac{H_{mn}-\Delta-\delta(T_{mn})}{T_{mn}} + m(s_A^e-s_A^{*,e}) + n(s_B^e-s_B^{*,e}) + R\ln\left[\left(\frac{1-x^*}{1-x}\right)^m\left(\frac{x^*}{x}\right)^n\right]} \tag{9}$$

This liquidus equation is still as exact as that given by Eq. (5). It is always possible to choose $\Delta\overline{H}_f$ and $\Delta\overline{S}_f$ so that the correction term in Eq. (6) is zero at the melting point, i.e. $\delta(T_{mn}) = 0$. However we now neglect the quantity $\delta(T)$ in the numerator of Eq. (9). The assumption is not that $\delta(T) = 0$ everywhere, only that the values of T calculated from Eq. (9) with

$\delta(T) = 0$ and with $\delta(T)$ present differ insignificantly for the purpose at hand. This of course can be checked in a specific case by calculating the denominator of Eq. (9), the error in T incurred by neglecting $\delta(T)$ being the ratio of $\delta(T)$ to this denominator. The approximate equation obtained by setting $\delta(T) = 0$ in the numerator of Eq. (9) is an explicit equation for T whenever the enthalpy and excess entropy of mixing for the liquid phase are independent of T.

One question still remains in the application of these equations when the liquidus line for the compound extends to temperatures below the melting point of either of its elements. The thermodynamic properties of the metastable, supercooled elements are required to obtain ΔH_f and ΔS_f. For definiteness we define the properties of the supercooled melts by taking a zero difference in the constant temperature heat capacity of stable solid element and supercooled melt. This choice can effect the behavior of a particular choice for a liquid phase model, in fact it becomes part of the model, but it does not effect the properties of any stable phase.

An earlier derivation[6] of the liquidus equation of a congruently-melting, narrow homogeneity range compound, A_mB_n, was given by Vieland for the special case, m=n=1. The derivation did not explicitly emphasize the auxiliary relations given here by Eqs. (3) and (4) and relied upon the difference in the constant pressure heat capacity of the compound and that of the supercooled liquid of the same composition. Vieland's liquidus equation has been commonly used in the literature with this ΔC_p set equal to zero. This amounts to a neglect of the temperature dependence of ΔH_f and ΔS_f when the liquid phase model is characterized by a temperature independent enthalpy and excess entropy of mixing (h_i, s_i^e in Eq. (5) independent of T). The liquidus equation is then similar to the approximate

form of Eq. (9), i.e. Eq. (9) with $\delta(T)=0$, differing in absence of the terms Δ and $\delta(T_{mn})$. However the validity of the approximate form of Eq. (9) does not rely upon setting the above ΔC_p equal to zero.

Jordan and Weiner[7] has also derived a liquidus equation for a congruently-melting, narrow homogeneity range compound, AB(s). Their equation (15) can be shown to be equivalent to Eq. (5) with m=n=1, but, in our opinion, is in a relatively awkward form. Again the importance of what we call the auxiliary relations is not emphasized in obtaining the heat-of-fusion liquidus equation. Separate derivations are given for the heat-of-fusion and heat-of-formation liquidus equations whereas a straight forward analysis suffices to obtain both in a single, connected chain of argument.

Liquid Phase Model

Thus far our efforts are most complete for III-V binary systems. It appears that an adequate liquid phase model is one in which the heat and excess entropy of mixing are written in terms of four composition and temperature parameters, W, a, V, and c as

$$\Delta H_M^L = Wx(1-x)\{1+a(x-1/2)\} \tag{10}$$

$$\Delta S_M^{e,L} = Vx(1-x)\{1+c(x-1/2)\} \tag{11}$$

The partial molar quantities necessary to describe the liquidus line can be obtained using thermodynamic definitions. It is seen that the enthalpy and excess entropy of mixing are temperature independent and that the Kopp-Neumann rule for ΔC_p is implicitly assumed for the liquid solution. A number of commonly used models such as the ideal, strictly regular, athermal, and quasi-regular are obtained by setting various parameters in Eq. (10) and (11) equal to zero and so are special cases of this model.

Moreover the model defined by Eqs. (10) and (11) is mathematically equivalent to one used by Kaufmann and Nesor[8] to reproduce the phase diagrams and available thermochemical data in metallic systems. (They also find it necessary to use a more complicated model in certain cases in which ΔH_M^L and $\Delta S_M^{e,L}$ are temperature dependent.) Lupis[9,10] has discussed a model in which ΔH_M^L and $\Delta S_M^{L,e}$ are also independent of T and are given as infinite series in x, the series being truncated where necessary to reproduce the experimental data. The connection between the model used here and other simpler ones, which are derivable from a Braggs-William approximation for nearest neighbor bonding and therefore considered to have a theoretical basis, has already been discussed by Hardy.[11] It should be noted that the choice of factors a(x-1/2) and c(x-1/2) in Eqs. (10) and (11) is one of convenience in that application of the auxiliary relations, Eqs. (3) and (4) then impose restrictions upon W and V alone, a and c not entering. On the other hand, replacement of these factors by any others linear in x yield mathematically equivalent expressions.

Application

The above liquid model has been applied elsewhere[12] in detail to the In-Sb, Ga-Sb, In-As, and Ga-As systems and the experimental data used are tabulated or cited there. Some of these data are shown in Table I. The analysis is described below as a series of steps. For all four compounds a linear temperature dependence with $\delta(T_{mn}) = 0$ and $\delta(T)$ less than 40 cal/mole describes $\Delta G_f(c)$ (see Eq. (6)). Generally the liquidus temperatures calculated using the approximate liquidus equation, Eq. (9) with $\delta(T) = 0$, gives T accurate to 1°C or better, which is sufficient for our purposes. For each system W and V were fixed by Eqs. (3) and (4) and for each given liquidus composition, x_j, a calculated liquidus temperature,

$T_{j,cal}$, was obtained for some fixed values of a and c. These then were varied in an iterative search technique,[13] until a minimum was found for $\sigma(T)$ where

$$\sigma^2(T) = \sum_{j=1}^{N} (T_{j,cal} - T_{j,obs})^2/N \qquad (12)$$

For the liquid model to be considered adequate it is necessary that $\sigma(T)$ be less than a critical value chosen as characterizing the experimental accuracy of the liquidus points. As a corollary, all fits with $\sigma(T)$ less than the critical value are considered equally acceptable at this stage. The corresponding values of a and c lie within a narrow, elongated ellipse in the a-c plane. The major axis of the ellipse is so much longer than the minor axis that one can consider the acceptable values of a and c to be along a "best-fit" line. A similar behavior has been found in the analysis of solidus and liquidus lines in pseudobinary sections between two III-V compounds[14] and in the extraction of second law enthalpies and entropies from Gibbs free enthalpy-temperature measurements.[15] Such behavior can be expected to occur generally in the quantitative fitting of phase diagrams.

Eutectic temperatures are potentially more accurately determined than liquidus temperatures in general and, except for GaAs, were so considered. Moreover an adequate fit to the liquidus points does not necessarily guarantee a eutectic temperature agreeing with the experimental value to within the latter's error. In the second step, only summarized here, the thermodynamic equations between the liquidus of the compound and that of one of the pure elements at their eutectic point were formulated. Specification of a eutectic temperature generates a eutectic composition and another line in the a-c plane, or allowing for the experimental error in

the eutectic temperature, a narrow band in the a-c plane. The intersection of this with the best-fit line, fixed by a fit to the liquidus points, serves to fix the liquid model parameters, a and c to within a negligible uncertainty. In this second step, the eutectic with the Group V element was used, but not that with the Group III element. The latter eutectic is very nearly degenerate with the pure element and variations in the eutectic temperature that are well within experimental error, cause such large shifts in the constraint line between a and c that it is not useful in fixing a and c.

At the end of the second step all the liquid parameters are fixed. The third step consisted of comparing the experimental points on the liquidus of the pure Group V element with that calculated and making a similar quantitative comparison for other high temperature properties. These included the chemical potential of In in In-Sb melt at 627°C, the enthalpy of mixing at x=1/2 for InSb and GaSb melts, and the partial pressures of As_2 over In-saturated InAs(c) and Ga-saturated GaAs(c). In all cases the predicted properties were in quantitative agreement with those measured. A summary is given in Table II.

The final step consisted in allowing for experimental errors in $\Delta H_f(T_{mn})$ and $\Delta S_f(T_{mn})$ which serve to fix the liquid parameters W and V through the auxiliary relations. It was found that the quality of the fits could be maintained over our estimate of the error range for the selected values of $\Delta H_f(T_{mn})$ and $\Delta S_f(T_{mn})$.

In summary it is found that the liquidus lines, Group V eutectic temperatures and compositions, and other high temperature data can all be simultaneously fit in a quantitatively satisfactory way with liquid phase

parameters that are consistent with the measured enthalpy and entropy of compound formation and the temperature dependence of these quantities.

In addition it was also shown that these simultaneous fits cannot be achieved with the special case of the liquid model in which a=c=0 (quasi-regular model). This is illustrated in part for InSb by the plots in the W-V plane shown in Fig. 1. At the best fit point to the InSb liquidus, shown as a square, the value of σ is 7.6°C. However at the point fixed by the auxiliary relations, shown by the cross near W = -3.7 kcal, the value of σ is 18.8°C and too large to be considered satisfactory. The latter point can be made to correspond to a value of 10°C for σ only by assuming it should be shifted to within the 10°C contour for σ due to errors in our selected values for $\Delta H_f(T_{mn}) + H_{mn}$ and for $\Delta S_f(T_{mn}) + H_{mn}/T_{mn}$. These would have to be simultaneous, negative errors of about -2 kcal/mole and -3 e.u./mole which, in view of the overall picture, seem unlikely. Furthermore, as shown in Fig. 1 only an InSb-Sb eutectic temperature of 470°C (lowest dashed line) will allow a value of σ less than 10°C. This is significantly different than the experimental value of 494 $\pm$ 0.5°C.

The agreement between theory and experiment for the four III-V systems considered is so good and so extensive, that we are prompted to suggest that the liquid phase model given by Eqs. (10) and (11) is adequate for all the III-V melts. The agreement also suggests that some of the experimental data for the compounds considered that do not agree with the calculated values be redetermined, e.g. the GaAs-As eutectic temperature. On the other hand, it should be pointed out that the liquid model used here does not give a satisfactory fit to the liquidus lines in more ionic systems such as Pb-Te and Cd-Te when the values of W and V are fixed by the auxiliary relations.[16]

Solidus Lines of a Compound Semiconductor

We now turn to perhaps the most important aspect of the phase diagram for a solid-state chemist, the solidus lines of a semiconductor compound. As an illustration of a somewhat unusual analysis PbTe(c) is considered. The solidus lines have been determined experimentally in terms of electronic carrier concentration for PbTe.[17] The partial pressure of Te_2 has also been measured along the Te-rich leg of the three-phase curve for PbTe and along a short portion of the Pb-rich leg.[18] Thus the solidus lines can be analyzed without reference to the PbTe liquidus lines. The crystalline PbTe is considered to be a non-degenerate semiconductor. It can exist over a range of composition while maintaining the rock-salt structure by the inclusion of the appropriate kind and concentration of atomic point defects. Those associated with an excess of Pb are assumed to be donors that are always z-fold ionized, e.g. Pb interstitials or Te-vacancies. Those associated with an excess of Te are assumed to be acceptors that are also always z-fold ionized. Both kinds of atomic defects are assumed to be randomly distributed upon the appropriate sites of the PbTe lattice and to increase the excess Gibbs free enthalpy of the crystal by an amount per defect that is constant for each type. The resulting equations can be put into a compact form[19] involving the relevant variables as

$$\mu_{Te} = \mu_{Te}(\text{int}) + z\,RT \sinh^{-1}\left(\frac{p-n}{2n_i}\right) + RT \sinh^{-1}\left(\frac{p-n}{2zk_s^{1/2}}\right) \qquad (13)$$

where μ_{Te} is the chemical potential of Te in the pure crystal of fixed composition and hence fixed excess of valence band holes over conduction band electrons, $p-n$; $\mu_{Te}(\text{int})$ is the chemical potential of Te in the pure, intrinsic crystal for which $p-n=0$; n_i is the concentration of electrons in the intrinsic crystals, and k_s is the equilibrium constant equal to the

product of the concentration of z-ionized native donors and that of z-ionized native acceptors. The intrinsic material parameters are therefore $\mu_{Te}(int)$, n_i, and k_s. Assuming an ideal vapor we have

$$\mu_{Te} - \mu_{Te}(int) = 1/2\ RT\ \ln [p_{Te_2}/p_{Te_2}(int)] \qquad (14)$$

so that $p_{Te_2}(int)$ replaces $\mu_{Te}(int)$. If each of the three intrinsic parameters depend exponentially upon T as expected then there are six adjustable parameters. The particular difficulty here lies in the fact that the experimental data considered here require that all six parameters be considered simultaneously. The analysis commonly used in the literature would handle isothermal values of p-n vs p_{Te_2}. Nevertheless it has proved possible to obtain very good fits to the experimental data for PbTe using Eq. (13) with μ_{Te} replaced by p_{Te_2} through Eq. (14). The results are summarized in Table III for two different assumed states of ionization. Recent ion implantation studies[20] give z=2 for Pb-vacancy acceptors and also for Te-vacancy donors. What is not completely indicated in Table III, nor completely developed here, is that the parameters quoted are not unique. Rather there exists a range for each parameter, that for each parameter being correlated, over which almost equally good fits are obtained. It remains to investigate this problem and to apply a similar analysis to SnTe, PbSe, and PbS. Hopefully this can be done and some systematics identified in the values of the intrinsic materials parameters. Then one may be in a position to construct the solidus lines for the solid solutions formed among these compound semiconductors.

This work has been supported by NSF Grant DMR75-09332.

References

1. J. A. VanVechten, J. Electrochem. Soc., 122, 419 (1975).

2. G. B. Stringfellow, J. Phys. Chem. Solids, 33, 665 (1972).

3. R. F. Brebrick, Met. Trans., 7A, 1609 (1976).

4. R. F. Brebrick, Met. Trans., 2, 1657 (1971).

5. In ref. 3 these quantities were given a specific form.

6. L. J. Vieland, Acta Met., 11, 137 (1963).

7. A. S. Jordan and M. E. Weiner, J. Phys. Chem. Solids, 36, 1335 (1975).

8. L. Kaufman and H. Nesor in "Treatise on Solid State Chemistry", Vol. 5, Ed. N. B. Hannay, Plenum Press, N.Y. (1975).

9. C. H. P. Lupis and J. K. Elliott, Acta Met., 14, 529 (1966).

10. H. Gaye and C. H. P. Lupis, Met. Trans., 6A, 1049 (1975).

11. H. K. Hardy, Acta Met., 1, 202 (1953).

12. R. F. Brebrick, Met. Trans. A (in press) Quantitative Fits to the Liquidus Line and High Temperature Thermodynamic Data for InSb, GaSb, InAs, and GaAs.

13. J. A. Nelder and R. Mead, Computer J., 7, 308 (1965).

14. R. F. Brebrick and R. J. Panlener, J. Electrochem. Soc., 121, 932 (1974).

15. R. F. Brebrick, High Temp. Sci., 8, 11 (1976).

16. D. N. Abu-Judom, unpublished, Master's Thesis in Materials Science, Marquette University, Milwaukee, WI (1975).

17. R. F. Brebrick and E. Gubner, J. Chem. Phys., 36, 1283 (1962).

18. R. F. Brebrick and A. J. Strauss, J. Chem. Phys., 40, 3230 (1964).

19. R. F. Brebrick in "Progress in Solid State Chemistry", Vol. 3, p. 244, Ed. H. Reiss, Pergamon Press, Oxford and New York, (1966).
R. F. Brebrick, J. Solid State Chem., 1, 88 (1969).

20. H. Heinrich, A. Lopez-Otero, L. Palmetshofer and L. D. Haas, Inst. Phys. Conf. Ser. No. 23, Ch. 3, p. 264 (1975).

1304

Table I. Thermodynamic Properties of the Compounds AB(c).
Enthalpies in kcal/mole, entropies in e.u./mole, T in °C.

	T_{mn}	H_{mn}	$-\Delta H_f^o(298)$	$-\Delta S_f^o(298)$	$-\Delta H_f(T_{mn})$	$-\Delta S_f(T_{mn})$	$-\Delta \overline{H}_f$	$-\Delta \overline{S}_f$	Eutectic with V T_{eu}	Eutectic with V x_V
InSb	525	11.41	7.40	3.82	13.27	11.53	13.020	11.22	494±.5	0.69
GaSb	709.2	15.80	9.88	2.56	16.30	13.10	16.231	13.03	589±.5	0.88
InAs	942	18.40	14.8	4.25	21.30	11.668	21.458	11.79	731±1	0.87
GaAs	1240	25.18	20.67	2.86	27.753	13.05	27.886	13.14	810?	--

1233

Table II. Summary of Fits to Thermodynamic Data
$\sigma(T,V)$ is the measure of fit to the Group V element liquidus line.
$x_V(eu)$ is the calculated atom fraction of the Group V element at the eutectic temperature, T_{eu}.
$\sigma(p)$ is the root mean square of the fractional difference between calculated and observed values of the partial pressure of As_2.

	W	a	V	c	$\sigma(T)$	$\sigma(T,V)$	T_{eu}	$x_V(eu)$	$\Delta H_M^L(1/2)$	$\sigma(\mu(In))$
	cal		e.u.		°C		°C		cal/gm-atom	cal/gm-atom
InSb	-3720	1.559	0.02377	-395.83	7.2	6.0	494	.689	-930(900°K)	94
GaSb	-1000	12.350	0.4602	-31.35	5.8	1.0	589	.887	-250(1023°K)	--
									$\sigma(p)$	
InAs	-5780	1.98	1.440	-7.80	12.9	15.0	731	.859	0.12	
GaAs	-5186	1.830	1.6735	-4.052	5.7	--	788	.947	0.15	

1234

Table III. Comparison of Experimental and Calculated Values of p-n for PbTe(c) given T and p_{Te_2}. If $\delta = p-n$,

$$\sigma^2 = \sum_{i=1}^{36} [\ln(\delta_{i,cal}/\delta_{i,exp})]^2/36$$

z	W	A	V	B	C	D	σ
2.0	-2939	21.63	-14,790	8.668	-4179	22.32	.164
1.0	-1344	20.116	-11,920	6.148	-5389	23.23	.168

$\log_{10} n_i = W/T + A$: n_i, cm^{-3}

$\log_{10} p_{Te_2}(int) = V/T + B$: p_{Te_2}, atm

$\log_{10} (2zk_s^{1/2}) = C/T + D$; $k_s^{1/2}$, cm^{-3}

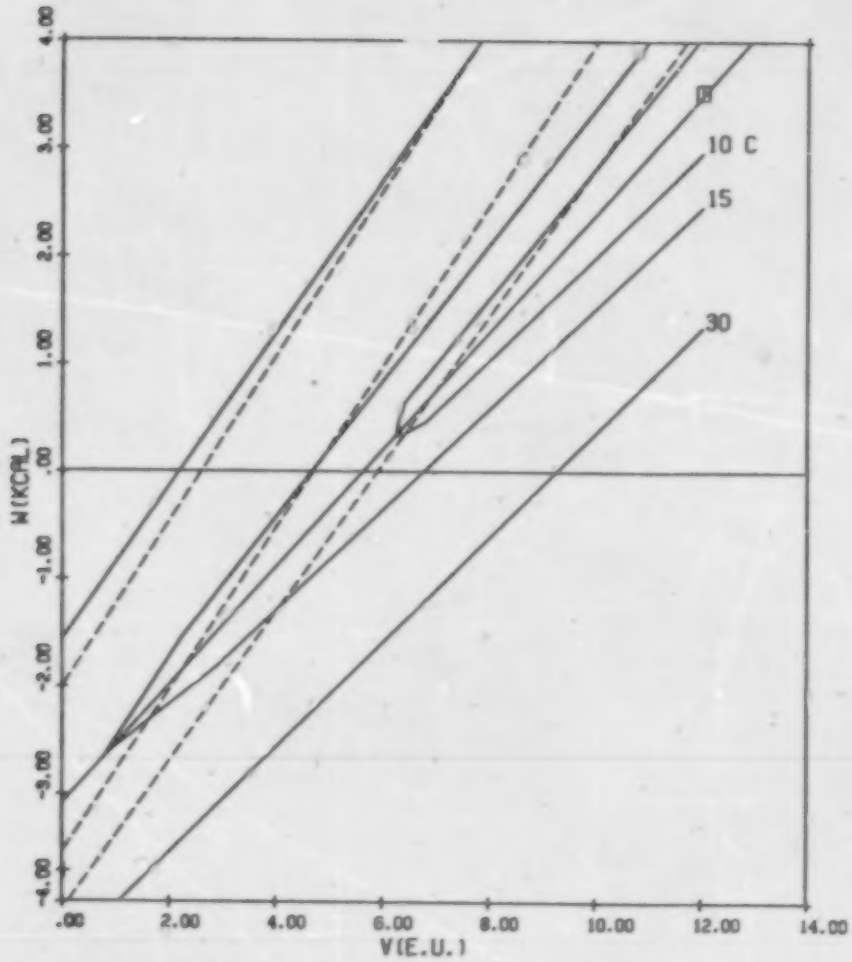

Figure 1 Fit to the InSb liquidus line using the quasiregular model i.e. a=c=0. The best-fit point is the square at the upper right. The lower halves of contours of constant σ are shown as solid curves. The solid straight line bisecting these contours and going through the best-fit point is the so-called best-fit line. The three dashed lines define those values of W and V consistent with an InSb-Sb eutectic temperature of 494°C (upper), 480°C (middle), and 470°C (bottom).

National Bureau of Standards SP-496, Applications of Phase Diagrams in Metallurgy and Ceramics
Proceedings of Workshop held at NBS, Gaithersburg, Md., January 10-12, 1977

NASA TECHNICAL TRANSLATION

NASA TT F-17296

PHASE DIAGRAMS OF METALLIC SYSTEMS (ALPHABETICAL CUMULATIVE ALLOY SYSTEM INDEX AND TABLE OF CONTENTS)

BY N. V. AGEEV, EDITOR

MOSCOW, "VINITI" PRESS, 1959 - 1976

NATIONAL AERONAUTICS AND SPACE ADMINISTRATION
WASHINGTON, D.C. 20546

1237 1311

1. Report No.	2. Government Accession No.	3. Recipient's Catalog No.
NASA TT F-17296		

4. Title and Subtitle	5. Report Date
PHASE DIAGRAMS OF METALLIC SYSTEMS (Alphabetical Cumulative Alloy System Index and Table of Contents)	December 1976
	6. Performing Organization Code
7. Author(s)	8. Performing Organization Report No.
N. V. Ageev, Editor	
	10. Work Unit No.
9. Performing Organization Name and Address	11. Contract or Grant No.
NASA Lewis Research Center Cleveland, Ohio 44135	
	13. Type of Report and Period Covered
12. Sponsoring Agency Name and Address	Translation
National Aeronautics and Space Administration Washington, D.C. 20546	14. Sponsoring Agency Code

15. Supplementary Notes
Translation of "Diagrammy Sostoyaniya Metallicheskikh Sistem." Volumes I - XIX, Moscow, "VINITI" Press, 1959 - 1976, Selected pages.
Translated and compiled by Coulson M. Schumann, Lewis Research Center, Cleveland, Ohio 44135

16. Abstract

The compilation of phase diagram information edited by N.V. Ageev and published in Russian is the most comprehensive publication available on phase diagram information for binary, ternary, and higher order alloy systems. The Tables of Contents in volumes 1 through 17 of the compilation do not list the contents by alphabetic chemical symbols, but in Russian. Volumes 18 and 19 have their Tables of Contents listed by alphabetic chemical symbol. It is a laborious task to use this compilation because no cumulative alloy system index is available. This translation provides individual volume listing of contents by page number with alphabetic chemical symbols and it provides a cumulative alloy system index, listing alloy systems alphabetically by chemical symbol. This publication should facilitate the use of this valuable information source.

17. Key Words (Suggested by Author(s))	18. Distribution Statement
Phase diagrams Binary alloy systems Ternary alloy systems order alloy systems Alloy systems	Unclassified - unlimited Subject category 26

19. Security Classif. (of this report)	20. Security Classif. (of this page)	21. No. of Pages	22. Price*
Unclassified	Unclassified	106	

For sale by the National Technical Information Service, Springfield, Virginia 22161

PREFACE

Phase diagram information is an important factor in the design and development of alloys. Phase diagram information is reasonably accessible for binary systems. Information for higher order systems, however, is not as readily accessible. The most comprehensive source of phase diagram information for binary and higher order systems is the annual compilations edited by N. V. Ageev and produced by the USSR Academy of Sciences.

Several difficulties face the potential user of the Ageev compilations. Typical lag times between cited literature publication dates and supplement publication is about three years. The compilations are somewhat difficult and cumbersome to use by those who cannot read the Russian language because the Tables of Contents through volume 17 are in Russian and because they do not have a cumulative index. Availability of the Ageev compilations is limited within the United States. Volumes 1 through 17 are currently available on microfilm through the Library of Congress. Other partial sets are located at private research laboratories.

This translation addresses the problems of those who cannot read Russian and those who want a cumulative index to aid them in their searches in these Ageev compilations. It is composed of two sections. The first section gives the Tables of Contents for volumes 1 through 19 (1959 - 1976) with the phase diagrams identified by chemical symbol. These volumes are listed in the Bibliography.

The second section of this translation is a cumulative index of phase diagrams included in the Ageev compilations, volumes 1 through 19 (1959 through 1976). The phase diagrams are listed in alphabetical order by chemical symbol. Throughout Section 2, the following convention is used. The volume is given by Roman numerals. Pages are designated by Arabic numerals. For example, the notation 'VII-205' refers to volume 7, page 205. Where data for one system extends to following pages, only the first page is given.

It is hoped that this publication will facilitate use of the Ageev compilations and the enormous amount of phase diagram information which they contain.

Gbulson M. Scheuermann
Lewis Research Center

CUMULATIVE ALLOY SYSTEM INDEX

VOLUMES 1 - 19

CUMULATIVE ALLOY SYSTEM INDEX

System	Location
Ag-Al-Cd	VI-97
Ag-Al-Cu	VII-151, XIX-92
Ag-Al-Cu-Pd	XVIII-244
Ag-Al-Fe	XIX-93
Ag-Al-Mg	V-113, XV-117, XVII-208, XVIII-94
Ag-Al-Mn	III-84, VI-104, VIII-140
Ag-Al-Pd	XV-135
Ag-Al-Sn	IV-110
Ag-Al-Ti	III-86
Ag-Al-Zn	IV-111
Ag-As	V-74
Ag-As-S	XVI-279
Ag-As-Se	XVIII-95
Ag-Au-Co	IV-140
Ag-Au-Cu-Zn	XV-252
Ag-Au-Ge	X-152
Ag-Au-Pt	IV-141
Ag-Au-Si	VIII-183
Ag-Be	XIV-15
Ag-Bi	VIII-26
Ag-Bi-Pb-Te	IX-259
Ag-Bi-Sb-Se-Te	IV-182
Ag-Bi-Te	IX-179
Ag-C	XV-85
Ag-Ca	XVI-65
Ag-Cd	VI-52
Ag-Cd-Cu	I-117, II-73
Ag-Cd-Cu-Sn	VI-172
Ag-Cd-Cu-Zn	I-133, II-99, XIV-266
Ag-Cd-Sb	XIX-93
Ag-Cd-Sn	V-145
Ag-Cd-Zn	VII-205, VIII-191
Ag-Co-Ge	XVIII-97
Ag-Co-Si	XIV-205
Ag-Cr-Pd	VI-162

System	Location
Ag-Cu	XV-60
Ag-Cu-Pd	I-124
Ag-Cu-Se	XVII-345
Ag-Cu-Sn	V-155
Ag-Cu-Ti	XV-207, XVI-259
Ag-Cu-Zn	VIII-205
Ag-D-Pd	XVIII-99
Ag-Dy	XVI-36
Ag-Er	XVI-107
Ag-Eu	XI-62
Ag-Fe	IV-48
Ag-Fe-Ge	XVIII-98
Ag-Fe-Pd	VI-134, VIII-180
Ag-Fe-S	XVI-229
Ag-Fe-Si	II-68
Ag-Ga	V-34
Ag-Ga-In	VIII-171
Ag-Ga-Mg	XVII-265
Ag-Ga-Te	XII-190
Ag-Gd	XVI-28, XVIII-5
Ag-Ge	XII-64
Ag-Ge-Mn	XVIII-98
Ag-Ge-Ni	XVIII-99
Ag-H	XVII-52
Ag-H-Pd	XIX-94
Ag-Hg	IV-86
Ag-Ho	IX-47, XII-67
Ag-In	XVI-53
Ag-In-Mg	XVII-297
Ag-In-Sb	XVII-301
Ag-In-Se	XIII-214
Ag-In-Te	XIII-216
Ag-Ir-Pd	VIII-189
Ag-La	XIII-95
Ag-Lu	XVI-73
Ag-Na	VII-87, XIV-85
Ag-Ni-Si	XIV-214
Ag-O	I-43, XIV-69
Ag-P	V-97

System	Location
Ag-Pb-Sb-Te	IX-269
Ag-Pb-Se	XIII-254
Ag-Pb-Te	XIII-255
Ag-Pd-Rh	VII-234
Ag-Pd-Si	III-114
Ag-Pd-Te	XIV-245
Ag-Pt	III-67
Ag-Pu	XIII-117
Ag-Rh	V-94
Ag-Ru	V-95
Ag-S	IV-88, XIII-130, XVII-162
Ag-S-Sb	V-159, XVI-292
Ag-Sb-Se	XVII-384
Ag-Sb-Sn	IV-168
Ag-Sb-Te	VII-236, IX-252
Ag-Sc	XVI-103
Ag-Se	XVII-161
Ag-Si	XII-97
Ag-Sm	XI-127, XVI-101
Ag-Sr	XVI-104
Ag-Tb	XVI-105
Ag-Te	XVII-165
Ag-Ti	V-96, VI-87, XV-84
Ag-Tm	XVI-106
Ag-Y	XVI-62
Ag-Yb	XVI-58
Ag-Zr	XV-86
Al-As	I-11
Al-As-Ga	XVII-188
Al-As-Ga-Sn	XIX-242
Al-Au	XIII-11
Al-B	VII-5, XIII-6
Al-B-Ce	XVII-183
Al-B-Co	VIII-127, XIX-95
Al-B-Cr	XIX-96
Al-B-Cr-Fe-Si-Ti	IX-271, XIII-271
Al-B-Fe	XII-132
Al-B-La	XVII-182
Al-B-Mn	XIX-97

System	Location
Al-B-Ni	VIII-128, XIX-98
Al-B-Re	XVIII-100
Al-B-Ti	XVIII-101
Al-B-Y	XVII-181
Al-Ba	XVIII-6
Al-Be	XII-5, XVIII-6
Al-Be-Ce	XII-131
Al-Be-Cu	III-80, IV-95
Al-Be-Mg	XII-130
Al-Be-Si	XVIII-102
Al-Be-Ti	XVI-118, XVII-175
Al-Be-Zr	VI-93
Al-Bi	XII-6, XV-7
Al-Bi-Sb	IX-140
Al-C-Co	VI-98
Al-C-Cr-Mo-Nb-Ni-Ti-W	IV-183
Al-C-Fe	V-109, XIV-112, XV-106
Al-C-Fe-Si	XV-239
Al-C-Mo	IX-159
Al-C-Ni-Ti	IV-178
Al-C-W	IX-141
Al-C-Y	XI-146
Al-Ca-Fe	XV-103, XVI-123
Al-Ca-Mg	III-81, V-111
Al-Ca-Mg-Mn	VI-166
Al-Ca-Mn	XV-110
Al-Cd	II-5, XI-7, XIII-13
Al-Cd-Cu	VIII-134, XI-147, XII-140
Al-Cd-Cu-Mn	XI-259, XII-251
Al-Cd-Mn	IX-145, X-115
Al-Cd-Sb	V-110
Al-Cd-Sb-Zn	III-121
Al-Cd-Sn	X-116, XIII-147
Al-Ce	III-12, VII-16, XII-13, XIII-23, XV-15
Al-Ce-Cu	VII-152
Al-Ce-Fe	XV-108
Al-Ce-Ge	XVI-122
Al-Ce-Mg	XIII-150

System	Location
Al-Ce-Mn	IX-153
Al-Ce-Sb	XII-148
Al-Ce-Si	IX-148
Al-Ce-Th	VII-155
Al-Co	XVII-23
Al-Co-Cr	IV-103, VI-99
Al-Co-Cu	XII-142, XVII-205
Al-Co-Cu-Fe-Nb-Ni	XII-265
Al-Co-Cu-Fe-Ni-Si	XII-264
Al-Co-Cu-Fe-Ni-Si-Zr	XII-267
Al-Co-Cu-Fe-Ni-Ta	XII-266
Al-Co-Cu-Fe-Ni-V	XII-263
Al-Co-Fe	IV-100, XII-138, XV-104
Al-Co-Hf	XVII-189
Al-Co-Mn	XVIII-104
Al-Co-Nb	XIV-117
Al-Co-Ni	XII-141
Al-Co-Ta	XIV-118
Al-Co-Ti	XII-143, XIII-148, XV-112
Al-Co-U	X-117, XIV-119
Al-Co-Y	XVII-198
Al-Cr	VI-12, IX-17, XVI-9
Al-Cr-Cu	IV-108, V-115, XIII-152, XVIII-109
Al-Cr-Cu-Zr	XIII-264
Al-Cr-Fe	XV-107, XVI-129
Al-Cr-Fe-Ni	XVIII-245
Al-Cr-Fe-Ni-Ti	III-124
Al-Cr-Fe-Ni-Ti-W	I-135
Al-Cr-Fe-Si-Ti	VI-173, IX-270
Al-Cr-Mg	XIX-99
Al-Cr-Mg-Mn	XIX-243
Al-Cr-Mn	XI-158, XVIII-110
Al-Cr-Mo-Nb-Ni-Ti-W	VII-258, X-219
Al-Cr-Mo-Ni-Ti	XVI-304
Al-Cr-Nb	X-125, XIV-132
Al-Cr-Ni	I-92, IV-109, VII-153
Al-Cr-Ni-Ti	X-213
Al-Cr-Ni-Ti-W	II-101, III-123
Al-Cr-Ni-W	VII-248, VIII-221, X-211
Al-Cr-Si	VII-147, XI-155

System	Location
Al-Cr-Ti	IV-112, IX-162
Al-Cr-Zr	XIII-156, XIV-138, XVI-148, XVIII-113
Al-Cu	I-10, IV-7, VII-9, IX-9, XVIII-7
Al-Cu-Fe	I-81, XVII-196
Al-Cu-Fe-Mn	X-212
Al-Cu-Fe-Ni	III-120
Al-Cu-Fe-Si	VI-165
Al-Cu-In	I-82, II-56
Al-Cu-La	XV-115
Al-Cu-Li	II-58, VI-102, VII-148, IX-151, XI-157
Al-Cu-Li-Mg	XV-241
Al-Cu-Li-Mn	XIV-258
Al-Cu-Mg	I-86, III-83
Al-Cu-Mg-Mn	IX-256
Al-Cu-Mg-Ni	IV-176
Al-Cu-Mg-Si	I-130, VII-249
Al-Cu-Mg-Zn	I-132, V-162, VI-167, VII-250
Al-Cu-Mn	I-88, X-120, XII-144
Al-Cu-Mn-Ni	IV-177
Al-Cu-Mn-Si	I-131
Al-Cu-Nb	XIV-125
Al-Cu-Pd	X-122, XVIII-114
Al-Cu-Si	XIV-120
Al-Cu-Sn	XIV-126
Al-Cu-Ti	IV-106, VI-105, VIII-141, IX-154, XI-160, XVII-209, XIX-99
Al-Cu-V	VII-138, XI-140
Al-Cu-Y	XIV-115, XVII-202, XVIII-115
Al-Cu-Zn	III-85, VI-106, XVIII-116
Al-Cu-Zr	X-123, XIII-153, XVI-137
Al-Dy	XIII-8
Al-Dy-Fe	XIX-100
Al-Dy-U	XIII-144
Al-Er	XI-16, XIII-24
Al-Er-Fe	XVIII-117
Al-Er-Y	XIV-116

System	Location
Al-Fe	IV-4, VI-8, VII-7, XIII-9, XVI-7, XVII-20
Al-Fe-Gd	XIX-105
Al-Fe-Ge	XVIII-118
Al-Fe-Hf	XV-101
Al-Fe-La	XIV-110
Al-Fe-Mg-Si	IV-175
Al-Fe-Mn	VI-95
Al-Fe-Mn-U	XII-252, XIV-255
Al-Fe-Mo	XVI-124
Al-Fe-Mo-Ti-Zr	XVII-413
Al-Fe-Nb	XII-139
Al-Fe-Nd	XVI-126
Al-Fe-Ni	II-55
Al-Fe-Ni-Ti	XIV-256
Al-Fe-Sc	XVI-127
Al-Fe-Si	I-80, VI-94, VII-142, XIII-145, XIV-109
Al-Fe-Si-U	XIX-245
Al-Fe-Ta	XIV-111
Al-Fe-Ti	III-101, IX-142, XV-105, XVI-128, XVII-197, XIX-101
Al-Fe-U	VI-96, VIII-133, IX-143, X-114, XIII-146
Al-Fe-Y	XVII-194
Al-Fe-Zn	XVI-130, XIX-103
Al-Fe-Zr	XIV-113, XV-109
Al-Ga	III-7, IV-3, XIV-7
Al-Ga-In-Sb	I-129, XII-250
Al-Ga-Mg	VII-141, VIII-130, X-113
Al-Ga-Nb	XIX-104
Al-Ga-P	XIX-105
Al-Ga-Sb	I-79, IV-97, V-108
Al-Gd	XI-5, XIII-7
Al-Ge	XVII-19
Al-Ge-La	XVI-121
Al-Ge-Mg	IV-99, XV-102
Al-Ge-Nb	XVII-191
Al-Ge-Nb-Sn	XI-258

System	Location
Al-Ge-P	VIII-132, XI-145
Al-Ge-Sb	VIII-131, XI-144
Al-Ge-Sn	XIX-106
Al-Ge-Y	XVII-190
Al-H	XVII-18
Al-H-Ni	XV-99
Al-Hf	VI-7, VIII-6, XII-7, XVI-6
Al-Hf-Ni	XV-100
Al-Ho	XII-8
Al-In	II-4, XI-6
Al-In-Sb	I-83
Al-La	III-9, XI-8, XIII-15, XV-11
Al-La-V	XV-93
Al-Li	II-6, IV-5, VIII-7, IX-6
Al-Li-Mg	I-84, II-57, XIX-108
Al-Li-Mg-Mn	XVII-393
Al-Li-Mg-Sn	XIX-246
Al-Li-Mg-Zn	XVII-395
Al-Li-Mn	IX-150, XIII-149
Al-Mg	III-10, IX-7
Al-Mg-Mn	III-82, XIX-110
Al-Mg-Mn-Sn	XVI-295
Al-Mg-Nd	XIV-123, XV-116
Al-Mg-Si-Sn	XIV-257
Al-Mg-Sn	IV-104, V-112, XIV-124, XIX-111
Al-Mg-Tl	XIX-111
Al-Mg-Zn	I-87, V-114, VI-103, VII-149, VIII-139
Al-Mg-Zr	XV-118
Al-Mn	IV-6, VI-9, IX-8, XVII-26
Al-Mn-Ni	I-90
Al-Mn-Si	X-118, XI-151
Al-Mn-Ti	I-91, IV-105, IX-152
Al-Mn-U	X-121, XIII-151
Al-Mn-V	XV-94
Al-Mn-Y	XVII-200
Al-Mo	V-8, VI-11, X-7, XVII-28, XVIII-8
Al-Mo-Nb	XIV-128
Al-Mo-Nb-Ni	XV-243
Al-Mo-Nb-Sn	IX-257
Al-Mo-Ni	VI-109, XV-120, XVII-213

System	Location
Al-Mo-Si	VI-100, VII-143
Al-Mo-Ti	VIII-142, IX-155, XV-123, XVI-138, XVIII-119
Al-Mo-Ti-V	X-209
Al-Mo-Ti-Zr	XIV-259
Al-Mo-U	X-124, XV-125, XVII-215
Al-Mo-V	V-907, XII-133
Al-Mo-Zr	XIV-127, XVI-139
Al-Nb	V-9, VII-10, X-8, XII-11, XIV-9
Al-Nb-Ni	VIII-143, XI-161, XII-145, XV-127, XVI-140, XVII-220
Al-Nb-Rh	XVI-142
Al-Nb-Si	VII-144, XIX-112
Al-Nb-Ta	XVI-143
Al-Nb-Ti	V-116, VIII-145, IX-160, XV-130, XVI-144
Al-Nb-V	VII-139, XII-134
Al-Nb-Zr	XIV-133, XVI-146
Al-Nd	XI-9, XIII-16, XV-12
Al-Ni	XVIII-9
Al-Ni-Sc	XIV-129
Al-Ni-Si	VI-101, XVI-136
Al-Ni-Ta	XIV-130
Al-Ni-Ti	VIII-144, XI-162, XIII-154, XIX-113
Al-Ni-U	XIV-131
Al-Ni-V	XI-142, XVII-184
Al-Ni-W	IV-96
Al-Ni-Y	XIV-114
Al-Ni-Zr	XII-147, XV-129
Al-O-Ti	XI-149, XV-111
Al-P	XVII-29
Al-P-Si	VIII-138, XI-154, XVII-207
Al-Pb	XIII-21
Al-Pb-Sn	II-59
Al-Pd	IX-10, X-9
Al-Pr	XII-12, XIII-18, XV-13
Al-Pt	X-10
Al-Pu	VIII-8, X-11, XIII-17
Al-Re	VII-12, IX-11, XVIII-10
Al-Ru	IX-12

System	Location
Al-S-Sb	XI-163
Al-Sb-Si	VIII-136, XI-152
Al-Sb-Y	XVII-204
Al-Sc	XI-11, XIX-3
Al-Si	I-9, III-8, XIII-14, XIV-9, XV-10, XVII-24
Al-Si-Sn	VIII-135
Al-Si-Ta	VII-145
Al-Si-Ti	IX-146, XI-153, XIV-121
Al-Si-U	VII-146, VIII-137, IX-147, X-119
Al-Si-V	VII-137
Al-Si-W	VII-140
Al-Si-Y	XVII-199
Al-Si-Zr	XI-156, XIV-122
Al-Sm	XI-10, XIII-19
Al-Sm-U	XIII-155
Al-Sn	II-7
Al-Sn-Ti	VI-111, VII-154, VIII-146, XV-134
Al-Sn-Ti-Zr	XI-260, XVI-296
Al-Sn-Zn	XIV-134
Al-Sn-Zr	XIV-135
Al-Ta	II-9, V-11, XIX-3
Al-Ta-Ti	IX-161, XII-149
Al-Ta-V	XII-135
Al-Th	V-13, VII-14
Al-Ti	I-12, II-10, III-11, V-12, VII-13, IX-13, XI-12, XII-9, XIII-22
Al-Ti-V	I-78, IX-139, XI-149, XII-136, XIV-107, XV-96, XVI-120, XVII-186
Al-Ti-W	XIX-113
Al-Ti-Zr	X-126, XI-164, XIV-136, XV-136, XVI-147
Al-Tl	IX-15, XV-14
Al-U	VII-15, IX-16, X-12
Al-U-Zr	VII-156, X-129, XIV-137
Al-V	I-7, III-6, V-6, XIX-4
Al-V-Zr	XII-137

System	Location
Al-W	VI-6
Al-Y	V-7, VIII-8, XIII-12, XV-9
Al-Yb	XV-8, XVII-22, XVIII-10
Al-Zn	II-12, VII-17, XVIII-11
Al-Zr	V-14, VIII-9, XI-15, XIV-10, XVI-10, XVIII-13
As-Pu	XII-14
As-Bi	XI-33
As-Bi-Se	VIII-160
As-Bi-Sn	XVIII-120
As-C-Fe	III-105
As-C-Fe-Mn	VI-170
As-Cd	XVI-64, XVIII-13
As-Cd-Ge-In	IX-262
As-Cd-Ge-Sn	XII-258
As-Cd-I-In	XI-263
As-Cd-In	XI-219
As-Cd-Se-Zn	XVII-405
As-Cd-Te	XVIII-122
As-Cd-Zn	X-172
As-Cu	XII-53, XI-205, XVIII-14
As-Cu-Fe	XI-209
As-Cu-Ni	XI-238
As-Cu-Pb	XIII-231
As-Cu-Sn	XII-230
As-Eu	XVII-83
As-Fe	III-31, IV-48
As-Fe-Si	XIII-202
As-Ga	I-25, XV-27
As-Ga-Ge	IX-187, XII-187
As-Ga-Ge-Sn	XIX-247
As-Ga-In	I-101, XII-188, XV-173
As-Ga-P	XVII-267
As-Ga-Sb	I-104, XVII-266
As-Ga-Se-Zn	V-163
As-Ga-Sn	XI-198, XII-189, XIII-187, XVIII-123, XIX-116
As-Ga-Te	XIII-188, XVIII-124
As-Ga-Zn	IV-128, XVIII-125

System	Location
As-Ge-In	IX-193
As-Ge-In-Zn	IX-263
As-Ge-P	XVIII-126
As-Hg	IX-117
As-In-P	IV-144, XVI-237
As-In-Pb	XIII-211
As-In-Pd	XVI-236
As-In-Sb	I-113, II-72
As-In-Se	IV-142, V-141, X-166
As-In-Sn	XIII-210
As-In-Sn-Zn	IX-267
As-In-Te	IV-143, XII-209, XIII-212
As-In-Zn	XIII-213
As-Ni-Sn	XI-246
As-Pb	XIX-5
As-Pb-Sn	XIX-116
As-Pd	IX-95
As-Pd-Te	XVII-364
As-Se	VIII-97
As-Sn-Te	XVI-276, XVII-361
As-Sn-Zn	IX-238
As-Te	XIV-82
As-Te-Zn	XVII-365
As-Th	XIV-84
Au-Be	VIII-10
Au-Bi	VIII-21
Au-Bi-Te	X-140
Au-Bi-Zn	XII-175
Au-C	XV-40
Au-Cd	IV-52, VIII-57
Au-Cd-In	IV-139
Au-Cd-Sb	XIX-120
Au-Co	II-29
Au-Co-Cu	XIII-206
Au-Co-Fe	XVI-212
Au-Co-Pd	II-91
Au-Cr	VI-49
Au-Cs	VII-63

Systems	Location
Au-Cu	I-37, III-36, IV-53, V-44, VIII-58
Au-Cu-Fe	XIII-196
Au-Cu-Pb	I-111
Au-Cu-Pd	I-110
Au-Cu-Zn	XI-218
Au-Dy	XI-58, XIX-6
Au-Er	XI-73
Au-Fe	IX-49
Au-Fe-Ni	VII-192
Au-Ga	XII-52
Au-Ga-Ge	XVII-263
Au-Gd	XI-39
Au-Ge	XII-61
Au-Ge-Sb	X-153, XIV-175, XVII-275
Au-H-Ni	XV-167
Au-Hf	VIII-43
Au-Hg	IV-55, XIII-77
Au-Ho	IX-45, XI-57
Au-In	IV-51, X-50, XVII-91
Au-In-Sb	XIII-205
Au-K	VII-57
Au-Li	VII-58
Au-Lu	XI-68
Au-Mg	XI-69
Au-Mn	X-51
Au-Na	VII-59
Au-Nb	XIX-7
Au-Ni	IV-54, XIV-56, XVII-93
Au-Ni-Pd	VIII-184
Au-Ni-Pt	XIX-121
Au-P	V-48
Au-Pb	I-38, IV-56, V-47, XVII-95
Au-Pb-Sn	XII-208, XIII-207, XIV-194
Au-Pb-Te	XV-194
Au-Pd-Pt	I-112
Au-Pd-Rh	VI-138
Au-Pd-Ru	VIII-185
Au-Pd-W	XV-170

System	Location
Au-Pr	XVII-94
Au-Pt	VI-48
Au-Pt-Rh	X-165
Au-Pu	XIII-75
Au-Rb	VII-60
Au-Rh	V-45, X-52
Au-Ru	V-46
Au-S	VII-62
Au-Sb	XVIII-14
Au-Sb-Si	XVII-294
Au-Sc	XI-70
Au-Se	VII-61, XVII-96
Au-Sm	XIX-8
Au-Sn	XIV-57
Au-Tb	XI-71
Au-Ti	II-30, VIII-59
Au-Tu	XI-72
Au-V	I-14, VI-21, VIII-14
Au-Yb	XI-67, XVI-50
Au-Zn	XVIII-15
Au-Zr	VIII-61
B-Be	VII-18, XIX-9
B-C	IV-10, VII-21
B-C-Cr-Fe	XII-254
B-C-Cr-Fe-Ni	XII-262
B-C-Fe	IX-166, XIII-162
B-C-Hf	VII-159
B-C-Mo	IX-168
B-C-Nb	IX-170, XI-174
B-C-Si	VI-114
B-C-Ta	IX-171, XI-175
B-C-Th	VII-162
B-C-Ti	VII-161
B-C-U	VII-164
B-C-V	IX-163, XI-167
B-C-W	IX-165, XIV-145
B-C-Zr	VII-165

System	Location
B-Ce	XI-26
B-Ce-Cr	XIX-123
B-Ce-Fe	XVIII-127
B-Ce-Ni	XVII-236
B-Ce-Si	XVII-232
B-Ce-Th	XI-176, XIII-168
B-Ce-U	XI-177, XIII-169
B-Co	VI-17, IX-20, XII-22
B-Co-Cr	XII-160, XIV-150
B-Co-Ga	XIX-124
B-Co-Hf	XV-145, XVIII-128
B-Co-In	XVII-228
B-Co-Mn	XII-157
B-Co-Mo	XII-158
B-Co-Nb	XII-161, XIV-149
B-Co-Ni	V-119
B-Co-Re	XIX-124
B-Co-Sb	XI-169
B-Co-Si	V-118, XIX-126
B-Co-Sn	VIII-147
B-Co-Ta	X-132
B-Co-Ti	XIII-163, XVII-230
B-Co-V	XI-166, XIX-127
B-Co-W	XIII-158
B-Co-Zn	IX-167
B-Co-Zr	XI-170, XV-147
B-Cr	IV-11, X-16, XV-17
B-Cr-Fe	XII-156, XVI-155, XIX-127
B-Cr-La	XIX-128
B-Cr-Mn	XV-151
B-Cr-Mo	XV-153
B-Cr-Nb	XV-156
B-Cr-Ni	VI-118, VIII-149, XVIII-128
B-Cr-Re	XV-157, XVI-162
B-Cr-Si	IV-116
B-Cr-Ta	XVIII-129

System	Location
B-Cr-Ti	VI-119
B-Cr-V	XV-140
B-Cr-W	XIV-146
B-Cr-Y	XVI-156
B-Cr-Zr	XIII-170
B-Cu	XI-21, XVI-14, XVII-37
B-Cu-Ni	XI-171
B-Eu	XVII-36
B-Fe	XV-16, XVI-13
B-Fe-Ga	XIX-129
B-Fe-Mn	XII-153
B-Fe-Mo	XII-154
B-Fe-Nb	XIV-148
B-Fe-Ni	XII-155, XV-146, XVIII-130
B-Fe-Si	V-117, XVI-154
B-Fe-Ta	XVII-227
B-Fe-Ti	XIII-161
B-Fe-V	XIX-129
B-Fe-Zr	XI-168
B-Ga-Ni	XV-144, XIX-130
B-Ge	XVI-12
B-Ge-Ni	X-130
B-Hf	XVII-35
B-Hf-N	VII-131
B-Hf-Nb	XVIII-131
B-Hf-Ni	XII-152, XVIII-132
B-Hf-Re	XVI-153
B-Hf-Ta	XVII-226
B-Hf-U	XIII-160
B-Hf-W	XVI-150
B-In-Ni	X-131
B-La	VII-19
B-La-Mo	XVIII-132
B-La-Ni	XIX-131
B-La-Si	XVII-231
B-La-W	XVIII-133
B-Mg-Ni	X-133
B-Mn	XI-20
B-Mn-Mo	XVII-233
B-Mn-Nb	XVIII-134

System	Location
B-Mn-Ni	XV-148
B-Mn-Re	XV-149, XVI-158
B-Mn-Si	V-120, XVI-157
B-Mn-Ti	XV-150
B-Mn-V	XVII-222
B-Mn-W	XVII-223
B-Mo	X-15, XIII-29, XVII-38, XVIII-16
B-Mo-Nb	XVII-234
B-Mo-Ni	VII-160, X-134, XII-162, XV-152
B-Mo-Re	XVI-159
B-Mo-Si	III-88
B-Mo-Ta	XIV-151
B-Mo-Ti	VI-117, XVIII-134
B-Mo-W	XIV-142, XV-141, XVIII-136
B-Mo-Y	XIX-132
B-Mo-Zr	IV-117, XIII-164, XVIII-137, XIX-132
B-N-Ti	I-77, VII-132
B-N-V	XIV-105
B-N-Zr	VII-133
B-Nb	V-20, XVII-40
B-Nb-Ni	X-135
B-Nb-Re	XVI-161
B-Nb-Si	III-89
B-Nb-Ti	I-95, IX-169, XVII-237
B-Nb-W	XII-151
B-Nb-Zr	XVII-240
B-Ni	III-16, VI-18, XI-22, XII-23, XIII-30, XVII-39
B-Ni-P	XIII-165
B-Ni-Re	XVIII-139
B-Ni-Sb	X-136
B-Ni-Si	XVIII-139, XIX-134
B-Ni-Sm	XVI-160
B-Ni-Sn	VIII-148
B-Ni-Ta	X-137, XVII-235
B-Ni-Ti	XI-172, XV-155
B-Ni-V	XIII-157, XIX-135
B-Ni-W	XV-143, XVIII-140
B-Ni-Zn	VIII-150
B-Ni-Zr	XI-173, XIII-166

System	Location
B-Pd	VI-19
B-Pt	XI-24
B-Re	XIV-19
B-Re-Si	XVIII-141
B-Re-Ta	XVII-243
B-Re-Ti	XVII-244
B-Re-V	XV-138, XVI-149
B-Re-W	XIV-144, XVI-151
B-Re-Zr	XIV-152, XVI-163
B-Ru	IX-22
B-Si	V-18, VIII-13, IX-21, XIV-18
B-Si-Ta	III-90
B-Si-V	IV-114
B-Si-W	III-87, IV-115
B-Si-Y	XVII-229
B-Si-Zr	VI-116
B-Ta	V-21, VII-20, XVII-41
B-Ta-Ti	XIV-153
B-Ta-W	XVII-224
B-Ta-Zr	XIII-167
B-Th	XI-25
B-Th-U	VII-163
B-Ti-V	XV-139
B-Ti-W	IX-164, XVI-152, XVII-225
B-U	V-22
B-U-Zr	VIII-151
B-V	V-17
B-W	III-15, XIII-28
B-W-Y	XIX-136
B-W-Zr	XIII-159, XIV-147
B-Zr	III-17, IV-12, XVI-15
Ba-Bi	XII-15
Ba-Cd	XVIII-17
Ba-Cu	V-15, XVII-30
Ba-Ga	XII-16
Ba-Ge	XII-17

System	Location
Ba-In	XII-18
Ba-Li	IV-8
Ba-Mg	III-13
Ba-Mn	X-14, XI-18
Ba-Mn-Si	XI-165
Ba-Na	III-14, VI-13
Ba-Ni	XI-19
Ba-Pd	XVI-11, XVII-31
Ba-Pr	XVII-34
Ba-Pt	XVII-32
Ba-Si	X-13, XI-17
Ba-Sr	II-13
Be-Bi	IV-9, XII-19
Be-C-Si	XII-150
Be-C-U	I-94, XV-137
Be-Ca	XIII-25, XIV-12
Be-Ce	XII-21
Be-Cr	II-14, XIV-16
Be-Cu	VIII-11, XIV-13
Be-Cu-Mn	VI-113
Be-Cu-Ni	IV-113
Be-Cu-Ni-Ti	XV-244
Be-Fe	VI-14, XIV-11
Be-Fe-P	I-93
Be-Fe-Si	VI-112
Be-Fe-Zr	XIV-139
Be-Li	V-16, XIII-26
Be-Na	XIII-27
Be-Nb	IX-18, XIV-14
Be-Nb-Zr	XIV-140
Be-Ni	VI-15
Be-Pu	I-13
Be-Ru	IX-19
Be-Si-U	XVIII-142
Be-Sn-Zr	XIV-141
Be-Th-U	VII-158
Be-Ti	VIII-12
Be-Ti-V	VII-157
Be-W	XII-20
Be-Zr	VI-16, XIV-17

System	Location
Bi-Ca	IX-28, XII-33
Bi-Ca-Pb	III-96
Bi-Cd	XVIII-17
Bi-Cd-Hg	XVI-174
Bi-Cd-In	VII-175
Bi-Cd-Sn	V-124, VII-177
Bi-Cd-Te	XVI-175
Bi-Co	XII-34
Bi-Cs	IV-21
Bi-Cu	VII-28, VIII-22
Bi-Cu-Mg	III-97
Bi-Cu-S	II-61
Bi-Cu-Te	XVII-252
Bi-Cu-U	VIII-159
Bi-Cu-Zn	XII-178
Bi-Dy	XIII-38
Bi-Eu	XVIII-19
Bi-Eu-Th	XVIII-143
Bi-Fe-S	VI-123
Bi-Ga	VI-26
Bi-Gd	XIII-37
Bi-Ge-Te	XI-187
Bi-Hf	XII-31
Bi-Hg	XI-34
Bi-Hg-Pb	XV-163
Bi-Hg-Sn	XV-161, XVI-176
Bi-Hg-Tl	XVI-179
Bi-I-Te	XVII-251
Bi-In	XIX-10
Bi-In-Sb	VII-176
Bi-In-Sb-Te	XIX-248
Bi-In-Sn	XVIII-143
Bi-In-Te	IX-176, XII-176, XIV-168
Bi-Ir	XI-32
Bi-La-Th	XVIII-146
Bi-Lu	XII-36

System	Location
Bi-Mg	XII-37
Bi-Mg-Pb	VI-124, VIII-158
Bi-Mg-Sn	VIII-157
Bi-Mn	II-16, XII-38
Bi-Mn-Sb	IX-177, XIX-136
Bi-Mo	IV-16
Bi-Na	XVI-21
Bi-Na-Sn	XIX-137
Bi-Nb	XII-39
Bi-Nd	XVI-22, XVII-44
Bi-Ni-Rh	XV-160
Bi-O-Te	XIX-138
Bi-Pb	III-21, IV-19, XIII-39
Bi-Pb-Se	VII-178
Bi-Pb-Sn	IV-121
Bi-Pb-Te	V-125, IX-178, XIII-179, XV-164, XVI-180
Bi-Pd	V-25
Bi-Pd-Te	XVII-254
Bi-Pt	VIII-24, XII-40
Bi-Pr	XVII-45
Bi-Rb	III-20, IV-17
Bi-Rh	VIII-25, IX-29
Bi-S	VI-28
Bi-S-Se	V-126, XIII-180
Bi-S-Te	V-127, XVI-181
Bi-Sb	XIV-24
Bi-Sb-Se-Te	IX-260, XI-261
Bi-Sb-Te	XI-188, XIV-169
Bi-Se	I-20, V-26, VI-27
Bi-Se-Sn	XIII-177
Bi-Se-Te	VI-125
Bi-Si	XII-35
Bi-Sn	VIII-23, X-22, XVI-23
Bi-Sn-Te	XIII-178
Bi-Sr	II-17, XII-41
Bi-Te	III-22, IV-20, V-27, XIV-26
Bi-Te-Tl	IX-180
Bi-Th-U	VII-179

System	Location
Bi-Ti	VI-29, XII-42
Bi-Tl	XVI-24
Bi-U	V-28, VII-29, VIII-27
Bi-U-Zr	VII-180
Bi-V	XII-24
Bi-Yb	XII-32
Bi-Zn	I-21
Bi-Zr	IX-30
C-Ce	X-111
C-Ce-Mo	X-190
C-Ce-Th	X-204, XIII-260
C-Ce-U	X-207, XIII-261, XVIII-146
C-Ce-Zr	X-208
C-Co	XIV-72, XVII-113
C-Co-Cr	XV-200, XVII-318, XVIII-147
C-Co-Cr-W	XIV-263, XV-248
C-Co-Fe	XV-185, XVIII-148
C-Co-Mo	XV-199, XIX-139
C-Co-Nb	XI-228, XVIII-148
C-Co-Sn	VI-144
C-Co-Ti	II-80, V-151, VII-208
C-Co-U	IX-218
C-Co-W	VII-185, XVI-187
C-Co-Zn	VII-209
C-Co-Zr	XI-229, XIX-140
C-Cr	III-76, XIII-137
C-Cr-Fe	IV-137, VIII-181, XVI-232, XVIII-149, XIX-141
C-Cr-Fe-Mn-N	XIV-268
C-Cr-Fe-Mo	VIII-224, XIII-266, XVII-401
C-Cr-Fe-N	XII-249, XIII-262, XV-233, XVIII-245
C-Cr-Fe-Ni	VIII-225, XIV-265, XVIII-253
C-Cr-Fe-U	X-218, XIII-268
C-Cr-Fe-V	VIII-222, XIII-265, XIV-260
C-Cr-Fe-W	VIII-223, XVI-299, XVII-396
C-Cr-Hf	XII-195
C-Cr-Mo	XI-243, XVIII-152
C-Cr-Mo-Zr	XVII-412

System	Location
C-Cr-N	XIII-143
C-Cr-Nb	XIV-240, XVIII-153
C-Cr-Ni	I-125
C-Cr-Ni-Ti	XI-265
C-Cr-Re	XII-242
C-Cr-Ta	XIV-252
C-Cr-Ti	I-128, VIII-219, XII-248, XIX-143
C-Cr-U	VII-245, IX-255, X-206
C-Cr-V	XII-173, XIV-167
C-Cr-W	X-150, XIII-186
C-Cr-Zr	XI-257, XIX-144
C-Cu	XV-62
C-Cu-Fe	XI-210, XVIII-153
C-Cu-Ni	VIII-204
C-Cu-U	IX-230
C-Cu-V	VII-171
C-Fe	I-33, V-41, VI-43, VII-55, X-46, XI-66, XII-76, XIV-55, XVI-45, XVII-89, XVIII-19, XIX-10
C-Fe-H	XIX-144
C-Fe-Hf	VIII-173
C-Fe-Mn	X-158, XVII-287, XVIII-155, XIX-145
C-Fe-Mn-Si	III-122, IV-179
C-Fe-Mo	XIV-187, XV-190, XVI-221, XVIII-155
C-Fe-N	VIII-126, XI-138, XIII-140
C-Fe-Nb	XI-212, XVIII-158
C-Fe-Ni	X-161, XV-191, XVI-225, XVIII-159
C-Fe-Ni-Pb	VI-171
C-Fe-Ni-U	XIII-267
C-Fe-Ni-W	X-215
C-Fe-O	VIII-175
C-Fe-P	XVIII-159
C-Fe-Pu	X-162
C-Fe-S	VII-201, XIV-192, XIX-148
C-Fe-Si	V-138, XII-204, XIII-199, XIV-181, XVI-217, XVII-280, XVIII-160
C-Fe-Sn	VII-200
C-Fe-Ti	II-70, III-107, XV-193
C-Fe-U	VII-202, IX-209, X-164

System	Location
C-Fe-V	IX-174, XII-165, XIV-156, XV-158, XVIII-160
C-Fe-W	XIV-170, XVI-182
C-Fe-Zn	VI-137
C-Ge	V-37, XIII-58
C-H-V	XIX-148
C-Hf	VIII-46, XI-52, XVIII-21
C-Hf-Mo	XII-193, XIII-191, XV-175, XVII-272, XVIII-162, XIX-149
C-Hf-Nb	X-151, XI-202, XIII-192, XVII-273
C-Hf-Nb-Zr	IX-261, XII-257
C-Hf-Re	XII-194, XVIII-165
C-Hf-Ta	IX-191, XIII-194
C-Hf-Ti	V-132, XIII-195
C-Hf-U	VII-189, IX-192
C-In-Ni	VI-139
C-Ir	XV-47
C-La	VI-57
C-La-U	XVIII-165
C-Li	III-48
C-Mn	XIX-14
C-Mn-Mo	XVII-334
C-Mn-Si	IV-153
C-Mn-W	XVII-255
C-Mo	XI-106, XII-103, XIII-101, XV-65, XVI-82
C-Mo-N	XVI-117
C-Mo-Nb	VII-213, XIII-234, XVII-356, XIX-150
C-Mo-Nb-Zr	XVII-409
C-Mo-Ni	XV-242, XVII-354, XVIII-166, XIX-150
C-Mo-Ni-Zr	XIX-249
C-Mo-Pu	XIII-236
C-Mo-Re	X-185, XIX-152
C-Mo-Ta	XIV-229, XIX-153
C-Mo-Th	IX-235
C-Mo-Ti	II-89, XI-241, XIII-237, XIV-231, XV-216, XVI-266, XVII-357, XIX-153
C-Mo-Ti-Zr	XVII-410, XIX-251

System	Location
C-Mo-U	IX-236, X-188, XII-232, XIII-240, XIV-234, XVII-358, XIX-154
C-Mo-W	II-62, XVII-258, XIX-157
C-Mo-Zr	IX-237, XI-244, XIII-241, XV-219, XVI-273, XVII-360
C-N-Nb	V-105, VI-92
C-N-O-U	XVII-392
C-N-Ta	V-106
C-N-V	X-112
C-Nb	V-79, VII-102, XIV-91, XVII-140, XVIII-22
C-Nb-Ni	XVIII-167, XIX-158
C-Nb-Re	XIII-246, XIV-239, XVI-285, XVIII-168
C-Nb-Ti	I-126, X-193, XI-247, XVIII-168
C-Nb-U	IV-165, VII-229, X-197, XII-238, XVII-372
C-Nb-W	X-145, XI-193, XIII-184, XVII-260, XVIII-170, XIX-158
C-Nb-W-Zr	XIX-252
C-Nb-Zr	X-198, XI-249, XII-239, XIII-248, XVIII-170
C-Nd-U	XVIII-171
C-Ni	IX-99, X-87, XI-112, XII-109, XIV-89, XVII-137, XIX-14
C-Ni-Pb	VI-159
C-Ni-Ti	II-91, VI-160, VII-225, VIII-213
C-Ni-U	VII-226, IX-239, X-192, XIII-245
C-Ni-W	VII-187
C-Ni-Zn	VII-227
C-Ni-Zr	XIX-159
C-O-Pu	XI-225, XIV-200
C-O-Ta	XIV-201
C-O-Te-U	XVII-406
C-O-Ti	II-76
C-O-U	XII-219, XVI-253
C-O-V	IV-118
C-Pu	VII-114, IX-109
C-Pu-Si	XIII-227
C-Pu-Th	XIII-252
C-Pu-Ti-U	XIII-270

System	Location
C-Pu-U	IX-251, X-199
C-Pu-U-W	XIX-252
C-Pu-W	XVIII-172, XIX-159
C-Re	V-91, IX-112, XI-124, XIX-119
C-Re-Ta	XIII-253, XIV-247, XV-224, XVII-382
C-Re-Ti	XIV-248
C-Re-U	X-200
C-Re-W	IX-186, X-147, XIX-161
C-Re-Zr	XV-225, XIX-160
C-Rh	XV-83, XIX-15
C-Ru	XIX-16
C-Ru-O	XVI-289, XVIII-173
C-Si	V-61
C-Si-U	XIII-229, XIV-216
C-Ta	IX-129, XI-132
C-Ta-Ti	V-160
C-Ta-Ti-W	XIX-253
C-Ta-U	IV-170, VII-238
C-Ta-V	XVI-171
C-Ta-W	VIII-170, XIX-162
C-Ta-Zr	X-202, XII-246
C-Te-U	XVII-381
C-Th	IV-91, XIII-135
C-Th-U	IV-171, VII-240
C-Th-U-Zr	IV-181, VII-257
C-Th-Zr	VII-243, VIII-220, IX-254
C-Ti	II-52, V-102, VII-122
C-Ti-V	X-139, XI-184, XII-169
C-Ti-W	XIX-162
C-Ti-Zr	XIII-258
C-U	VII-129, X-109, XI-134, XII-128, XV-90
C-U-V	XVI-172
C-U-W	X-149, XII-186, XVI-197, XVII-262, XVIII-173, XIX-167
C-U-Y	X-171
C-U-Zr	IV-174, VII-246, XIV-254, XVII-390
C-V	III-19, VIII-19, XI-30, XII-29, XIV-23, XIX-16
C-V-W	VIII-152

System	Location
C-W	IX-33, X-25, XI-37, XII-49, XIX-17
C-W-Zr	XI-194, XVIII-174
C-Y	X-59, XIV-66, XIX-18
C-Zr	XI-135, XII-129
Ca-Cd	XVIII-23
Ca-Ce-Cl	I-118
Ca-Cu	XVII-107
Ca-Eu	XV-35
Ca-Fe-P	II-63
Ca-Fe-Si	VIII-174, XIV-176, XV-179
Ca-Ga	XII-54
Ca-Ge	XI-55, XVII-75
Ca-Hg	XIX-19
Ca-La	IV-61
Ca-Li	III-40
Ca-Mg	I-41, IX-86
Ca-Mg-Mn	V-149
Ca-Mg-Si	XV-195
Ca-Mn	IX-71
Ca-Mn-Si	IX-214, XI-224
Ca-Na	II-34
Ca-Na-Pb	IX-216
Ca-Ni	XI-83
Ca-Pb	V-54
Ca-S-U	XVII-309
Ca-Si	XVIII-24
Ca-Sr	IV-62
Ca-Ti	VI-53
Ca-Zn	IX-73
Cd-Cr-Se	XIX-168
Cd-Cu	VIII-74
Cd-Cu-Hg	I-116, XVI-248
Cd-Cu-Hg-Zn	II-98
Cd-Cu-Sb	XVI-243, XIX-169
Cd-Cu-Sn	V-144
Cd-Cu-Zn	II-75, VIII-190, XIII-219
Cd-Eu	XI-61

System	Location
Cd-Ga	IV-32
Cd-Ga-Pb	VII-188
Cd-Ga-Sb	XI-197
Cd-Ga-Se	XVI-202
Cd-Gd	XVII-63
Cd-Ge-Sb	XV-178, XVI-207
Cd-Hg	XV-49
Cd-Hg-Pb	XVIII-175
Cd-Hg-Sn	XVIII-178
Cd-Hg-Te	XIII-221
Cd-In	V-49, XVII-98
Cd-In-Sb	XVII-296
Cd-In-Sb-Sn	XII-260
Cd-In-Sb-Te	IX-266
Cd-In-Te	IX-211
Cd-La	XIX-20
Cd-Mg	XIII-83, XVII-105, XIX-21
Cd-Mn-S	XIV-199
Cd-Ni	IX-69, XV-48
Cd-Pb	XVIII-27
Cd-Pb-Sb	XVI-245
Cd-Pb-Se	XI-223
Cd-Pb-Sn-Zn	XIII-269
Cd-Pb-Te	X-174
Cd-Pb-Zn	XIII-222
Cd-Pu	XI-79
Cd-S	IX-70
Cd-Sb	VII-71, XIII-84
Cd-Sb-Sn	XII-216, XIX-170
Cd-Sb-Te	XVI-246
Cd-Sb-Zn	V-148, VIII-192, IX-213, X-175
Cd-Se	XII-87
Cd-Sn	V-52, X-61, XIV-67
Cd-Sn-Te	X-173
Cd-Sn-Tl	V-146
Cd-Sn-Zn	IV-146, V-147, XVI-244
Cd-Sr	XI-81
Cd-Te	VIII-75
Cd-Te-Zn	XVI-247

System	Location
Cd-Ti	XVIII-27
Cd-Tl	X-62
Cd-Yb	XVII-100
Cd-Zn	XI-92
Ce-Co	V-51, XII-94, XVII-115
Ce-Co-Fe	V-137
Ce-Co-H	XVIII-182
Ce-Co-La	XIX-170
Ce-Co-Pu	V-150, XII-222
Ce-Co-Si	XVI-255, XVII-314
Ce-Cr	V-104, XV-92, XVI-110
Ce-Cr-O	XVI-254
Ce-Cu	X-77
Ce-Cu-Mn	XIX-171
Ce-Cu-Mn-Zr	XIX-254
Ce-Cu-Pu	XI-239
Ce-Cu-Zr	XVII-350
Ce-Fe	I-36, V-43
Ce-Fe-N	XIX-172
Ce-Fe-Ni-Si	X-217
Ce-Fe-Pu	XIII-204
Ce-Fe-Si	XVI-218, XVII-285
Ce-Ga-V	XVI-164
Ce-Gd	IX-34, X-29
Ce-Ge	XVII-80, XIX-22
Ce-Ge-Se	XVIII-182
Ce-Ge-Si	XII-196
Ce-H	XIX-23
Ce-Hf	XVII-71
Ce-Hg	XII-51
Ce-Ir	XIX-23
Ce-K	XVII-106
Ce-La	IV-66
Ce-La-Mg	XVIII-183
Ce-Mg	VIII-86, XI-102, XVII-123
Ce-Mg-Mn	III-115
Ce-Mg-Zn	XVII-332
Ce-Mn	III-52
Ce-N	XVI-5, XVII-17
Ce-N-V	XIX-173

System	Location
Ce-Na	XIV-86
Ce-Nb	V-80
Ce-Ni	X-88
Ce-Ni-Pu	XIII-243
Ce-Ni-Si	XV-205, XVII-322, XIX-173
Ce-Pd	XIII-112
Ce-Ru	VIII-118
Ce-S-Ti	XVII-388
Ce-Sc	X-106
Ce-Si	XII-98
Ce-Si-Th	XII-226, XIII-228
Ce-Sm	XIV-102
Ce-Te	XIII-132
Ce-Th	III-73, VII-125
Ce-Th-Zr	X-205
Ce-Ti	III-71
Ce-V	VIII-20, XIII-36
Ce-Zn	XI-137
Co-Cr	VI-56, VII-76, XVIII-28
Co-Cr-Fe	V-136, VI-127, IX-197, XIX-174
Co-Cr-Fe-Mo-Ni	XV-258
Co-Cr-Fe-Ni-W	XV-257
Co-Cr-Mo	I-119
Co-Cr-Mo-Ni	XV-253
Co-Cr-Ni	XIX-175
Co-Cr-Ni-W	XV-247
Co-Cr-Si	XI-226
Co-Cr-Ti	IV-148, VI-145, VIII-198
Co-Cr-W	XVIII-185
Co-Cr-Zr	XVIII-186
Co-Cu	II-36, IV-63, XII-91, XVIII-29
Co-Cu-Mn	IV-147
Co-Cu-Pd	II-77
Co-Cu-Si	XIV-202
Co-Dy	XVII-82
Co-Er	XII-95, XVII-116

System	Location
Co-Fe	III-30, XIV-48, XVI-40
Co-Fe-Ge	XIX-176
Co-Fe-Mn	VIII-176
Co-Fe-Mn-U	IX-264
Co-Fe-Mo	XVIII-187
Co-Fe-Ni	XV-183
Co-Fe-O	II-64
Co-Fe-Pd	IV-130, V-135, VII-194
Co-Fe-S	IV-131
Co-Fe-Si	XI-206
Co-Fe-Sn	XIV-183
Co-Fe-U	IX-196, X-157, XI-207
Co-Fe-V	I-96
Co-Fe-Zn	II-67
Co-Gd	VIII-36, XV-23, XVII-65, XIX-24
Co-Ge-Mo	X-154
Co-Ge-Ni	XIX-176
Co-Ge-Si	XVII-276
Co-H	XVII-47
Co-H-La	XVIII-188
Co-Hf	XIV-35, XV-28
Co-Hf-Zr	XVIII-188
Co-Hg	IX-78
Co-Ho	XVII-81
Co-In	XVI-51
Co-La	XIII-90
Co-Mg	XI-86
Co-Mn	VIII-77, XVII-109
Co-Mn-Mo	VI-143
Co-Mn-Pd	X-177
Co-Mn-Si	VIII-197, X-176
Co-Mn-Sn	XIV-207
Co-Mn-Ti	XV-198
Co-Mn-U	IX-217, X-178, XI-227
Co-Mn-Zr	XVIII-189
Co-Mo	IX-77
Co-Mo-Si	XII-220
Co-Mo-Zr	XVII-315

System	Location
Co-Nb	X-67, XII-92, XIII-91, XVI-68, XVIII-30
Co-Nb-Si	XIV-204, XVIII-190
Co-Nb-Sn	XVII-316
Co-Nb-Zr	XIV-208, XVIII-190
Co-Ni-Pd	II-78
Co-Ni-Pd-V	XIV-261
Co-Ni-S	XIX-177
Co-Ni-Sb	III-111, XIX-178
Co-Ni-Si	XIV-203, XIX-178
Co-Ni-Sn	I-120, XIX-179
Co-Ni-U	I-121
Co-Ni-V	III-92
Co-Ni-Zn	II-79
Co-O-W	XI-190
Co-Pb	I-46
Co-Pb-Te	XIV-209
Co-Pd-V	XIV-158
Co-Pu	V-56
Co-S	VII-75, XI-87
Co-Sb	XIX-25
Co-Sb-Si	XIV-206
Co-Se	XVII-111
Co-Si	XIII-89
Co-Si-Ti	XII-221
Co-Si-V	XII-166
Co-Sm	XIV-70, XV-52, XIX-26
Co-Sn	XVII-110
Co-Ta	XIII-92, XVIII-31
Co-Te	V-57, XVIII-32
Co-Th	XII-93
Co-Ti	I-47, VI-54, XIV-71, XVII-112
Co-Ti-Zr	XVII-317
Co-V	I-16
Co-V-Zr	XVIII-191
Co-W	XIII-44
Co-Y	XI-77, XVII-103
Co-Zn	I-48
Co-Zr	XI-88, XVI-69, XVIII-33

System	Location
Cr-Cu	III-54
Cr-Cu-Fe-Mn-Ni	II-102
Cr-Cu-Fe-Ni	II-97
Cr-Cu-Mn-Ni	II-100
Cr-Cu-Nb	XVIII-192
Cr-Cu-Ni	III-117, XIII-233
Cr-Cu-Pd	VI-152
Cr-Cu-Ti	XVI-263
Cr-Cu-Zr	II-87, III-118, XVIII-193
Cr-Fe	VI-45, VIII-55, X-48, XV-39, XVI-48, XVIII-34, XIX-27
Cr-Fe-Mn	IV-135, XIV-186, XIX-179
Cr-Fe-Mn-N-Ni	XIX-265
Cr-Fe-Mn-Nb-Ni-Si-V	VIII-227
Cr-Fe-Mn-Ni	II-96, V-164
Cr-Fe-Mo	III-103, VIII-178, X-160
Cr-Fe-Mo-Ni	XV-251
Cr-Fe-Mo-V	XVIII-254
Cr-Fe-N	IV-94, IX-137, XI-139, XIII-141
Cr-Fe-Nb-Ni	XVIII-248
Cr-Fe-Ni	III-100, VI-133, VII-199, IX-204, XII-207, XVII-290, XVIII-193, XIX-180
Cr-Fe-Ni-Si	XVIII-259
Cr-Fe-Ni-Ti	V-165, XII-259, XVIII-260
Cr-Fe-Ni-W	XV-246
Cr-Fe-O	I-106, XIV-177, XVI-216
Cr-Fe-O-S	XI-262
Cr-Fe-P	XI-216
Cr-Fe-S	IX-206
Cr-Fe-Si	VII-197, VIII-177, XII-206
Cr-Fe-Ti	VI-136, X-163, XI-215
Cr-Fe-V	III-91, XVI-167, XIX-181
Cr-Fe-W	X-142
Cr-Fe-Zr	VIII-182, IX-210, XVI-234, XVIII-195
Cr-Ga	XI-50, XVIII-38
Cr-Gd	X-28
Cr-Ge	XII-66, XIII-59, XIV-44, XVIII-37
Cr-Hf	XI-53, XIV-39, XIX-28
Cr-Hg	IX-122
Cr-Ho	XVIII-38

System	Location
Cr-Ir	XIX-29
Cr-La	VI-58, XIX-30
Cr-Mn	XII-100
Cr-Mn-N	XIV-106
Cr-Mn-Ni	VIII-203
Cr-Mn-Si	XVII-320
Cr-Mn-Zr	XIX-182
Cr-Mo	IX-94, X-83, XII-104, XVII-134
Cr-Mo-Nb	VI-154, VII-217, VIII-208, X-183, XI-240, XV-214
Cr-Mo-Nb-W	XII-256
Cr-Mo-Ni	VIII-207, XIX-182
Cr-Mo-Si	X-182, XII-224
Cr-Mo-Ti	VI-155, VIII-209, XII-231
Cr-Mo-Ti-V	XIV-262
Cr-Mo-U	IV-159, VII-220
Cr-Mo-W	IV-123, V-129, VII-186, VIII-168
Cr-Mo-Zr	XVI-275, XVII-359, XIX-183
Cr-N	III-5, XVII-15, XVIII-38
Cr-N-Pu	XVIII-196
Cr-N-U	XVII-174
Cr-Nb	II-44, IV-80, VII-106, VIII-103, X-94
Cr-Nb-Ni	VI-157, VII-223, VIII-211, XII-234
Cr-Nb-Si	VII-210
Cr-Nb-Ta-Ti	XII-261
Cr-Nb-Ta-Ti-Zr	XV-259, XVII-414
Cr-Nb-Ti	VIII-214, IX-243, X-194, XI-248
Cr-Nb-Ti-Zr	XV-254
Cr-Nb-U	IX-247
Cr-Nb-V	IV-119, V-123
Cr-Nb-Zr	XI-250, XIV-241, XV-222
Cr-Nd	XV-67, XVI-86
Cr-Ni	I-65, III-61, VI-72, VII-93, VIII-99, XVI-89, XVIII-39
Cr-Ni-S	XIX-184
Cr-Ni-Si	VI-147, IX-222
Cr-Ni-Ti	II-92
Cr-Ni-W	III-99

Page	System
3	N-Nb
4	N-Ta
5	Al-B
7	Al-Fe
8	Al-Y
9	Al-Cu
10	Al-Nb
12	Al-Re
13	Al-Ti
14	Al-Th
15	Al-U
16	Al-Ce
17	Al-Zn
18	B-Be
19	B-La
20	B-Ta
21	B-C
22	V-W
23	Hf-V
24	V-Y
25	Sn-V
26	Re-V
27	Th-V
28	Bi-Cu
29	Bi-U
30	Os-W
31	Pd-W
32	Cr-W
33	Fe-Gd
34	Gd-Mg
35	Gd-Zr
36	Ga-K
37	Ga-Na
38	Ga-Hg
40	Ga-Te
41	Fe-Hf
42	Hf-Mo
43	Hf-Ni
44	Fe-Ge
45	Ge-Mn
46	Fe-Y
47	Fe-O
48	Fe-Si
50	Fe-Mo
51	Fe-Ni
52	Fe-Nb
53	Fe-S
54	Fe-Te
55	C-Fe
56	Fe-Zn
57	Au-K
58	Au-Li
59	Au-Na
60	Au-Rb
61	Au-Se
62	Au-S
63	Au-Cs
64	Hg-In
65	Mg-Y
66	Cu-Y
67	Nd-Y
68	Ni-Y
69	Ti-Y
70	Cr-Y
71	Cd-Sb
72	O-Pu
73	O-Zr
75	Co-S
76	Co-Cr
78	Mn-Si
80	Nb-Si
81	Si-Th
82	Mn-Re
83	Cu-Nb
84	Cu-Pu
85	Mo-U
87	Ag-Na
88	Np-Pu
90	Ni-Ru
91	Ni-Se
92	Ni-S
93	Cr-Ni
95	Ni-Zr
96	Nb-Pd
97	Nb-Pt
98	Nb-Re
101	Nb-Ti
102	C-Nb
104	Nb-U
106	Cr-Nb
108	Nb-Zr
109	Hg-Sn
110	S-Sn
111	Sn-Tl
112	Pb-Te
113	Pu-Ru
114	C-Pu
115	Re-Th
116	Cr-Ru
117	Sc-Ti
118	Tl-Zn
119	Ta-Th
120	Cr-Ta
122	C-Ti
123	Ti-U
124	Ti-Zr
125	Ce-Th
126	Th-Zr
129	C-U
130	U-Zr
131	B-Hf-N
132	B-N-Ti
133	B-N-Zr
134	Fe-N-Si
135	Fe-Mn-N
136	Fe-N-Zn
137	Al-Si-V
138	Al-Cu-V
139	Al-Nb-V
140	Al-Si-W
141	Al-Ga-Mg
142	Al-Fe-Si
143	Al-Mo-Si
144	Al-Nb-Si
145	Al-Si-Ta
146	Al-Si-U
147	Al-Cr-Si
148	Al-Cu-Li
149	Al-Mg-Zn
151	Ag-Al-Cu
152	Al-Ce-Cu
153	Al-Cr-Ni

System	Location
Cr-O	III-41
Cr-Os	III-66
Cr-Pd	XIII-111
Cr-Pr	XV-79, XVI-97
Cr-Pt	XIX-31
Cr-Pu	I-71
Cr-Re	V-92
Cr-Rh	XIX-32
Cr-Ru	VII-116, X-105
Cr-Sc	XVIII-40
Cr-Si	III-44, IX-82, X-73, XIV-75
Cr-Si-Ti	XVII-325
Cr-Si-W	VIII-166
Cr-Si-Y	XVII-305
Cr-Sm	XIX-33
Cr-Sn	X-98, XV-74
Cr-Sn-Zr	IV-169, IX-249
Cr-Ta	V-101, VII-120, XIX-33
Cr-Ta-Ti	XII-245, XV-227, XVI-293
Cr-Ta-Zr	XII-247, XIII-257, XV-229
Cr-Tb	XVII-166
Cr-Ti	III-70, IV-90, VIII-121, IX-130, XVII-167
Cr-Ti-V	VIII-155, XI-186, XII-172, XIII-175
Cr-Ti-W	IV-125
Cr-Ti-Zr	XI-256, XIII-259, XV-230
Cr-U	I-75, IX-132
Cr-V	V-24, VI-25
Cr-V-Zr	XVI-173, XVIII-196, XIX-186
Cr-W	VII-32
Cr-W-Zr	XIX-187
Cr-Y	VII-70, XIX-34
Cr-Yb	XIX-35
Cr-Zr	IX-134, XIV-104, XVII-171, XIX-36
Cs-Ga	XIX-36
Cs-Mg	XIII-98
Cs-Na	XVII-135

System	Location
Cu-Zr	XVI-81
Cu-Fe	IV-43, VI-40, XII-69, XIII-69, XVIII-41
Cu-Fe-Mn-Ni	II-95
Cu-Fe-Ni	XVII-289
Cu-Fe-P	XIII-201
Cu-Fe-P-Zn	XIV-264
Cu-Fe-Pd	IX-201
Cu-Fe-Ti	XVI-219
Cu-Ga	XI-44
Cu-Ga-Ge	I-100
Cu-Ga-Ge-Se	XVI-302
Cu-Ga-Te	XIX-187
Cu-Ge	III-29, XII-63
Cu-Ge-Ni	V-134
Cu-Ge-Sb	VII-191
Cu-Ge-Sn	XII-199
Cu-Ge-Te	XIX-188
Cu-H	XVII-48
Cu-Hf	XII-59
Cu-Hg	IX-89, XVII-131
Cu-Ho	IX-46
Cu-In	XVIII-41
Cu-In-Sb	XVII-298
Cu-In-Se	XIII-208
Cu-In-Sn	XVIII-197
Cu-In-Te	XIII-209
Cu-Ir	XV-46
Cu-Li	IV-67
Cu-Mg	III-50
Cu-Mg-Ni	II-82, XVIII-204
Cu-Mg-Sb	V-154
Cu-Mg-Sn	II-83, IX-226
Cu-Mg-Ti	XII-227
Cu-Mg-Zn	I-122, II-84, VI-150
Cu-Mn	VIII-87, XVII-124
Cu-Mn-Ni	IV-154
Cu-Mn-Si	IV-149, VIII-200
Cu-Mn-Sn	XIX-189
Cu-Mn-Zr	XVIII-206

System	Location
Cu-Mo-Nb	XVI-258
Cu-Mo-Ni	XIX-189
Cu-Mo-Zr	XIV-219, XVII-335
Cu-Nb	VII-83, XV-59, XVI-79
Cu-Nb-Ta	XIV-223
Cu-Nb-W	XV-172, XVI-191
Cu-Nb-Zr	XIV-224, XVIII-207
Cu-Ni	IV-71, XVII-126, XVIII-42
Cu-Ni-P	XVII-344
Cu-Ni-Pb	III-116
Cu-Ni-Pd	XI-236, XVII-340
Cu-Ni-S	VI-151
Cu-Ni-Si	III-112, IV-150, XVII-324, XVIII-207, XIX-191
Cu-Ni-Sn	XVII-337
Cu-Ni-Ta	XI-237
Cu-Ni-Ti	XIII-232, XIV-220, XVII-342
Cu-Ni-W	XVI-190
Cu-Ni-Zr	XIV-221
Cu-O	XII-88, XIV-68
Cu-O-Pt	XV-196
Cu-O-Sn	XII-217
Cu-P	XVIII-43
Cu-Pb	I-57, II-40, XVIII-44
Cu-Pb-Te	II-86
Cu-Pu	VII-84, XIII-100
Cu-Rh	XVII-130
Cu-S	VI-64
Cu-Sb	IV-72
Cu-Se-Sn	XIX-192
Cu-Si-Ti	XV-202
Cu-Si-Zn	III-113, V-152, IX-220, X-180
Cu-Si-Zr	XI-233
Cu-Sn	XVI-80, XVII-129
Cu-Sn-Zr	XIV-225
Cu-Sr	XVII-132
Cu-Te	II-41, XIX-37
Cu-Te-Tl	XVII-349
Cu-Th	XVII-133

System	Location
Cu-Ti	IV-73, VI-65, VIII-91, IX-90, XII-101
Cu-Ti-Zn	VIII-206
Cu-Ti-Zr	VII-212
Cu-Tl	I-59, XV-61
Cu-V	VIII-17, X-20, XIII-35
Cu-Y	VII-66
Cu-Yb	XVI-57, XVII-102
Cu-Zn	III-55, VIII-92, XV-63
Cu-Zr	VIII-93, X-78, XVIII-44
D-Lu	XVIII-60
D-Nb	XVIII-60
D-Ni	XVIII-61
D-Pd	XVIII-62
D-Ta	XVIII-63
D-V	XVIII-63, XIX-38
D-Zr	IX-48
Dy-Er	XIX-38
Dy-Hg	XII-51
Dy-Ho	XVI-34, XIX-39
Dy-Ho-Y	XVI-211
Dy-Mg	XI-59
Dy-Mn	XIII-64
Dy-Nd	XVIII-45
Dy-Pb	XIV-45
Dy-Pd	XIX-40
Dy-Sb	XIII-65
Dy-Th	XV-34
Dy-Y	XIII-63
Er-Fe	XVII-90
Er-Gd	X-30
Er-Hf	XVII-73
Er-Hg	XII-51
Er-Ho	XIX-41
Er-Mn	XIII-99
Er-Nd	XVIII-46
Er-Pd	XIX-42
Er-Pt	XVII-154
Er-Rh	XIX-43

1353

System	Location
Er-Sc	X-107
Er-Tb	XIX-44
Er-Th	XV-89
Er-Y	X-60, XIX-45
Eu-In	XI-60
Eu-Mg	XV-36
Eu-Pb	XIII-66
Eu-Te	XVI-37
Fe-Ga	XI-41, XIII-48
Fe-Ga-N	VIII-124
Fe-Gd	VII-33
Fe-Ge	VII-44, X-41, XI-54, XVIII-47
Fe-Ge-Ni	XIX-196
Fe-Ge-S	XV-177
Fe-H	XVII-46
Fe-Hf	VII-41, XII-57, XIV-34, XIX-45
Fe-Hf-Zr	XVIII-209
Fe-Ho	XVI-35
Fe-In	XIII-67, XV-37, XVI-38
Fe-Ir	IX-50, X-42
Fe-Ir-Rh	XIII-197
Fe-La-N	XIX-196
Fe-La-Si	XVIII-209
Fe-Lu	XVIII-48
Fe-Mg	XII-68
Fe-Mg-Ni-O	XVI-303
Fe-Mn	VIII-52, X-44
Fe-Mn-N	VII-135
Fe-Mn-Ni-Zn	VII-254
Fe-Mn-O	XV-181, XVI-213
Fe-Mn-O-S	XVIII-260
Fe-Mn-S	IX-199, XVII-286
Fe-Mn-Si	IV-132
Fe-Mn-Si-V	XII-255
Fe-Mn-Sn	XIV-184
Fe-Mn-Ti	IV-133, XV-189
Fe-Mn-U	IX-200, X-159, XIV-185, XIX-197
Fe-Mn-Zr	XVIII-210

System	Location
Fe-Mo	VII-50, XII-70, XIII-70, XVI-42, XIX-46
Fe-Mo-P	XI-211
Fe-Mo-S	IX-203
Fe-Mo-Si	VII-196, XII-202
Fe-Mo-W	XIX-199
Fe-Mo-Zr	XIV-188
Fe-N	I-5, II-3, XIV-5, XVIII-49, XIX-47
Fe-N-Nb	VIII-125, XIX-200
Fe-N-Si	II-54, III-79, VII-134, XVI-111
Fe-N-U	IX-136
Fe-N-V	XIX-200
Fe-N-Zn	VII-136
Fe-Nb	III-33, VI-41, VII-52, XII-71, XIII-71, XVI-43
Fe-Nb-P	VIII-179, XI-213
Fe-Nb-S	IX-205
Fe-Nb-Si	VI-129, XVIII-211
Fe-Nb-Zr	XIV-190
Fe-Nd	XI-64
Fe-Ni	II-26, III-32, VII-51, XI-65
Fe-Ni-O	I-105, XVI-215, XVII-278
Fe-Ni-P	XVI-226
Fe-Ni-P-S	IX-265
Fe-Ni-Pb	VI-132
Fe-Ni-Pd	VI-131
Fe-Ni-Re	XVI-224
Fe-Ni-S	I-107, III-106, VII-198
Fe-Ni-Sb	XIX-201
Fe-Ni-Si	VI-128, XI-208, XIV-178
Fe-Ni-Sn	XIX-202
Fe-Ni-Ti	XIII-203
Fe-Ni-U	I-108
Fe-Ni-W	III-98, XV-169
Fe-Ni-Zn	IV-136
Fe-Ni-Zr	XIV-189, XIX-202
Fe-O	IV-42, VI-38, VII-47, XIV-46, XVI-39
Fe-O-S	XI-205
Fe-O-Ti	II-65
Fe-O-V	IX-172
Fe-O-Zr	VII-193
Fe-Os	IX-52

System	Location
Fe-P	IV-50, IX-58
Fe-P-S	XIV-193
Fe-P-Si	V-139
Fe-P-Sn	I-109
Fe-P-Ti	V-140, XI-214
Fe-P-V	I-97, XI-180
Fe-P-W	I-99
Fe-P-Zr	IV-138, XI-217
Fe-Pb-Te	XV-192
Fe-Pd	IV-45, V-38, IX-53
Fe-Pt	V-39
Fe-Pu	I-31, III-34
Fe-Rh	IV-46, XIII-73, XVII-85
Fe-Ru	IV-47, VI-42
Fe-S	VII-53, XIV-54, XVII-87, XVIII-50
Fe-S-Sb	VI-135
Fe-S-Si	XIII-198, XIV-180
Fe-S-Ti	IX-208
Fe-S-V	IX-173
Fe-S-W	VII-184
Fe-S-Zr	IX-207
Fe-Sb	XIX-48
Fe-Sb-Si	III-102
Fe-Sc	VIII-53, XV-38
Fe-Se	XIV-53
Fe-Si	II-24, VI-39, VII-48, VIII-50, IX-51, X-43, XI-63, XIII-68, XIV-49, XVI-41
Fe-Si-Sn	VI-130
Fe-Si-Ti	II-69, XII-203
Fe-Si-U	XIX-204
Fe-Si-V	XI-179, XII-164
Fe-Si-W	X-141
Fe-Si-Zn	XIV-182, XV-186
Fe-Sm	XVII-86
Fe-Sn	X-45, XIII-72, XIV-52, XVII-84, XVIII-51
Fe-Sn-Zr	XIV-191

System	Location
Fe-Ta	V-40, XII-73, XIII-74, XVI-44
Fe-Tc	IX-54
Fe-Te	I-32, VII-54
Fe-Th	XII-75
Fe-Ti	II-27, III-35, VIII-54, IX-55, XII-74
Fe-Ti-V	V-121, VI-120, VII-167
Fe-Ti-Zr	XVII-293
Fe-Tm	XVIII-52
Fe-U	IV-49, IX-57, XII-79
Fe-V	XI-28, XVI-16, XIX-49
Fe-V-Zr	XVIII-211
Fe-W	XII-48, XIII-43, XVI-26, XIX-49
Fe-Y	VII-46
Fe-Zn	VII-56, X-49, XVIII-53, XIX-51
Fe-Zr	VI-46, VIII-56, IX-59, XII-80, XVI-49, XIX-52
Fs-Pu-U	XI-251, XII-241
Ga-Ge	I-24, III-25, IV-31, XVII-59
Ga-Ge-Nb	XVIII-212
Ga-Ge-Ni	XIX-204
Ga-Ge-P	IX-188
Ga-Ge-Si-V	XVIII-261
Ga-Ge-Sn	XIX-205
Ga-Ge-Ti	XI-195
Ga-Ge-Zr	XI-196
Ga-Hf	VIII-39
Ga-Hg	VI-35, VII-38
Ga-In	IX-35, XII-53, XV-26, XVIII-54, XIX-53
Ga-In-P	XVI-201, XVII-264, XVIII-213
Ga-In-S	XV-174
Ga-In-Sb	I-102, IV-126, V-130, VIII-172, XVIII-214
Ga-In-Se	XVI-200
Ga-In-Sn	XVI-199
Ga-In-Te	IV-127, V-131

System	Location
Ga-K	VII-36, XIX-54
Ga-La-V	XIV-155
Ga-Li	XIX-54
Ga-Mn	XI-43
Ga-Mo	XIX-55
Ga-Na	II-21, VI-34, VII-37
Ga-Nb	X-31, XI-45, XIV-31, XVIII-54
Ga-Ni	III-26
Ga-O-V	XII-163
Ga-P	X-34
Ga-P-Zn	XII-192
Ga-Pb	IV-34, V-33
Ga-Pd-Zn	XIX-206
Ga-Pt	XIV-33
Ga-Pr-V	XVII-247
Ga-Pu	X-33, XI-47, XIII-49, XVII-61
Ga-Rb	XIX-56
Ga-S	XIII-52
Ga-S-Te	XI-199
Ga-Sb	I-26, IV-35
Ga-Sb-Te	XII-191
Ga-Se	XI-48, XII-55
Ga-Si	IV-33, XVII-60
Ga-Sn	VIII-40, IX-36, X-32, XIV-32
Ga-Sn-Te	XIII-189
Ga-Sr	XII-56
Ga-Ta	XI-49
Ga-Te	VII-40, IX-37
Ga-Ti	III-27, IV-36, VIII-41
Ga-Ti-Zn	XI-200
Ga-Tl	I-28, V-35
Ga-V	X-18, XI-27, XII-26, XIII-32, XIV-20
Ga-V-Y	XVII-245
Ga-Zn	IV-37, IX-38, XI-51
Ga-Zn-Zr	XI-201
Ga-Zr	IV-38, VIII-42, XVI-29
Gd-Hg	XII-51
Gd-La	VIII-37
Gd-Mg	VII-34, XI-40
Gd-Mn	XIII-45

System	Location
Gd-Mo	XII-50
Gd-Pb	XV-24
Gd-Pd	XIX-57
Gd-Pu	XIII-46
Gd-Sb	XIII-47
Gd-Sc	X-26
Gd-Sm	XIV-30
Gd-Tb	X-27
Gd-Th	XV-25
Gd-Ti	VIII-38
Gd-Y	VIII-35
Gd-Zr	VII-35
Ge-In	XVII-74
Ge-In-P	IX-194
Ge-In-Sb	V-133
Ge-In-Te	XI-203, XIX-207
Ge-La	XVII-76, XIX-57
Ge-Li	III-28, XII-62
Ge-Mg	XIV-41
Ge-Mg-Pb	XII-198
Ge-Mg-Sn	XII-197
Ge-Mn	VII-45, XV-32, XVI-30
Ge-Mn-Te	VII-190
Ge-Mo	IX-41
Ge-Mo-W	IX-183
Ge-Nb	XIII-57
Ge-Nb-Ti	XIX-209
Ge-Ni	XVII-77
Ge-O	I-29
Ge-P	VIII-49
Ge-Pb-Se	XII-200
Ge-Pb-Te	X-156, XVIII-215
Ge-Pd-Te	XVII-277
Ge-Pr	XIX-60
Ge-Pt	XII-65
Ge-Rh	II-22
Ge-Ru	VIII-47

System	Location
Ge-S	IX-42
Ge-Sb	XVII-79
Ge-Sb-Si	XVIII-215
Ge-Sb-Sn	XVI-208, XIX-210
Ge-Sb-Te	XI-204, XVI-209
Ge-Se	VIII-48, XIV-42
Ge-Se-Te	XII-201
Ge-Si-Te	X-155
Ge-Si-Th	IX-195
Ge-Si-V	XI-178
Ge-Si-W	VII-183
Ge-Sn-Te	IV-129
Ge-Sr	XVI-33
Ge-Te	VI-36, XI-56, XV-33
Ge-Th	IX-43
Ge-Ti	I-30, IV-41
Ge-Tl	IV-40
Ge-U	VI-37
Ge-V	IV-13
Ge-W	XVII-57
Ge-Y	XVIII-55
Ge-Zr	II-23
H-Hf	VI-30, VIII-28
H-Hf-Zr	XI-189
H-Ir	XIX-61
H-La-Ni	XVIII-216
H-Mo	XVIII-56
H-Mo-Ni	XV-168
H-N-V	XIX-212
H-Nb	IV-22, VI-31, XI-35, XII-43, XV-19, XVIII-57
H-Nb-Ti	VIII-162
H-Nb-Zr	XII-180, XVIII-217
H-Nd	XVII-49
H-Ni	XVII-50, XIX-62
H-Ni-W	XV-166
H-Ni-Zr	IV-122

System	Location
H-O-Ti	VIII-161, XII-179, XIX-212
H-O-V	XIX-213
H-O-Zr	I-98, VII-181, IX-182
H-Pd	XVII-51
H-Rh	XIX-63
H-Ru	XIX-63
H-Sc	XI-36
H-Ta	II-18, VIII-29, XV-20
H-Th	XVII-54
H-Ti	II-19, IV-23, XII-44, XVII-53
H-Ti-Zr	VIII-163
H-U	IV-24, XIII-41, XIV-27
H-U-Zr	V-128, VII-182
H-V	X-17, XII-25, XIX-64
H-Y-Zr	XVIII-219
H-Zr	I-22, II-20, III-23, IV-25, V-29, VI-32, VIII-30, XII-46, XIII-42, XIV-28, XV-21, XVII-55, XVIII-59
Hf-Mn	XIV-36, XV-29
Hf-Mo	VII-42, XIII-53, XVIII-64, XIX-65
Hf-Mo-Nb	XVI-205
Hf-Mo-Re	IX-189, XVI-206
Hf-Mo-Si	XVII-270
Hf-Mo-W	XIII-181
Hf-N-Nb	XIII-139
Hf-N-V	XIX-214
Hf-Nb	X-36, XV-30, XVII-67, XIX-66
Hf-Nb-O	XIII-190, XVI-204, XVII-268
Hf-Nb-Ru	XIX-215
Hf-Nb-Sn	IX-190
Hf-Nb-Ti	XIX-215
Hf-Nb-Ti-Zr	XV-249, XVII-398
Hf-Nb-Zr	XIII-193
Hf-Ni	VII-43, XIII-54, XIV-37, XIX-67
Hf-Ni-O	XVI-203
Hf-O	IX-39, XII-58

System	Location
Hf-Pd	XVIII-65
Hf-Pr	XVII-69
Hf-Pu	XIII-55, XIV-38
Hf-Re	VIII-45, IX-40, XV-31
Hf-Re-W	XII-181
Hf-Ru-Ti	XVIII-219
Hf-Ru-V	XIX-217
Hf-Sc	XIII-56
Hf-Si	XVII-66
Hf-Sn	XVII-68
Hf-Ta	X-39
Hf-Th	IV-39
Hf-Ti	V-36
Hf-Ta-V	XVI-165
Hf-U	XVII-70
Hf-V	VII-23, XIV-21, XIX-67
Hf-W	VI-33, VIII-33, XVIII-66
Hf-Y	VIII-44
Hf-Zr	XII-60, XVII-72
Hg-In	VII-64, VIII-62, IX-61, XVI-52
Hg-La	XII-51
Hg-Mn	IX-87
Hg-Mn-Te	IX-229
Hg-Ni	IX-97
Hg-Pb	XIII-128
Hg-Pb-Se	XIV-249
Hg-Pb-Sn	XVII-375
Hg-Pb-Te	XIV-250
Hg-Pb-Tl	XVI-288, XIX-217
Hg-Pd	XI-120
Hg-Pr	XII-51, XVII-157
Hg-Pt	XIX-68
Hg-Pu	V-88
Hg-Rh	XIII-126
Hg-Sb	VIII-117, IX-118
Hg-Se-Te	VI-163
Hg-Se-Tl	XVII-383
Hg-Sm	XII-51
Hg-Sn	VII-109, IX-103, X-95, XIII-109, XV-72

System	Location
Hg-Tb	XIV-100
Hg-Te	XVI-100
Hg-Th	IX-120
Hg-Ti	IX-119, XIX-69
Hg-Tl	XIX-69
Hg-U	IX-121
Hg-Y	XII-51
Hg-Yb	XIV-61
Ho-Mn	XIII-61
Ho-Pd	XIX-70
Ho-Tb	XIX-71
Ho-Th	XIII-62
Ho-I	XIII-60
I-In	II-31
I-Pb-Se	XII-215
I-Pb-Te	XIII-218, XVI-239
I-Sb-Se	XVIII-221
I-Tl	XVII-104
In-Li	XV-41
In-Mg	XIV-58, XV-42
In-Na	XV-43
In-Ni	XV-44, XIX-72
In-P	III-38, IV-59, XVI-54
In-Pb	IV-57, XV-45
In-Pb-Sb	VIII-187, IX-212
In-Pb-Sb-Sn	XVII-404
In-Pb-Se	XI-220
In-Pb-Sn	I-114
In-Pb-Te	X-168
In-Pb-Tl	IV-145
In-Pd	V-50
In-Pd-Sn	XVIII-221
In-Pr-Se-Te	XI-264
In-Pt	XIX-73
In-Pu	XI-74, XIII-78
In-S	XVIII-66
In-S-Se	XIX-219
In-S-Te	XVII-299

System	Location
In-Sb	IX-65
In-Sb-Se	XII-211, XIII-215, XVI-238
In-Sb-Se-Te	XVIII-262
In-Sb-Sn	I-115, V-142, VIII-186, XII-210, XIV-195
In-Sb-Te	VI-140, X-169, XII-212, XIII-217, XIV-196, XVII-302
In-Sb-Zn	X-170
In-Se	IX-62
In-Se-Sn	XIX-220
In-Se-Te	XI-221
In-Sn	II-32, III-37, X-53
In-Sn-Te	X-167, XVIII-223
In-Sr	XII-81
In-Ta	IX-67
In-Te	X-54
In-Te-Zn	XI-222, XVII-303
In-Th	V-51
In-Ti	IV-58, VIII-65, XVIII-67
In-Tl	IX-66, XII-82
In-V	XVI-17
In-Yb	XVII-97
In-Zr	IV-60
Ir-Mn	I-39
Ir-Mo	XII-83
Ir-Nb	X-55
Ir-Ni-Ta	XIX-221
Ir-O-Zr	VII-204
Ir-Os	X-56
Ir-Pd	III-39, VIII-66
Ir-Pr	XVII-99
Ir-Pt	II-33
Ir-Re	VIII-67
Ir-Re-W	XVI-183
Ir-Ru	X-57, XIX-74
Ir-Th	X-58
Ir-Ti	XI-75, XVI-55
Ir-U	XIV-59
Ir-V	XIII-33
Ir-W	IX-31

System	Location
K-Mg	XIII-85
K-Na	I-40
K-Pb	V-53
K-Yb	XIV-60
La-Mg	XI-95, XVIII-68
La-Nb	V-63
La-Ni	XVIII-68
La-Ni-Re	XVI-256, XVIII-224
La-Pu	XIII-94
La-Re	XIV-76
La-Rh	XV-54
La-Sc	XVI-72
La-Th	XIV-77
La-Ti	III-45
La-V	VI-22, XIII-34
La-Y	VIII-68
Li-Mg-Sn	XV-206, XVII-326, XVIII-224
Li-Mg-Zn	II-81, IV-151, VI-148
Li-Mg-Zr	IX-225
Li-Mn	X-74, XI-96
Li-Mn-Si	XI-230
Li-N	V-5
Li-Na	III-47
Li-Ni	V-64, XI-97
Li-Si	I-50, III-46, V-59, VIII-78, X-68, XI-89
Li-Sr	VIII-83
Li-Ti	IX-83
Li-U	V-65
Li-Zr	V-66
Lu-Mg	XI-98
Lu-Th	XV-55
Mg-Mn	III-49
Mg-Mn-Nd	VIII-202
Mg-Mn-Nd-Ni	XIV-267
Mg-Mn-Ni	XIV-217
Mg-Mn-Th	V-153, VI-149
Mg-Mn-Y	XIV-197, XVI-240
Mg-Mn-Zr	XIII-230

System	Location
Mg-Na	XIII-96
Mg-Nb	IX-85
Mg-Nd	IV-68, VIII-84, IX-84, XI-99
Mg-Nd-Ni	XII-228
Mg-Nd-Pr	XVIII-226
Mg-Nd-Y	XVII-306
Mg-Nd-Y-Zn	XVIII-263, XIX-255
Mg-Nd-Zn	XVII-328
Mg-Pb	XI-101, XVI-74, XVII-122
Mg-Pb-Si	XI-231, XIV-210
Mg-Pd	VIII-85
Mg-Pr	XI-100, XVII-121
Mg-Rb	XIII-97
Mg-Sb-Si	IX-219, XIV-211
Mg-Sb-Sn	IX-228
Mg-Sc	XVIII-69
Mg-Si	XIV-73
Mg-Si-Sn	XII-223
Mg-Sn	XV-56, XIX-74
Mg-Th	IV-69, VI-59
Mg-Th-Zr	IV-152
Mg-Ti	I-52, V-67, XIV-78
Mg-U	II-38
Mg-V	IX-24
Mg-Y	VI-50, VII-65, XI-78, XIV-63
Mg-Y-Zn	XIV-198
Mg-Yb	XI-76
Mg-Zn	III-51
Mg-Zr	X-75
Mn-N	VIII-8, XIII-5
Mn-Nb	VI-60
Mn-Nd	XVI-75
Mn-Ni	XV-57
Mn-Ni-Pd	IV-155
Mn-Ni-Si	VIII-201, X-179
Mn-Ni-Sn	XI-235
Mn-Ni-U	I-123
Mn-Ni-V	XIII-173

System	Location
Mg-Na	XIII-96
Mg-Nb	IX-85
Mg-Nd	IV-68, VIII-84, IX-84, XI-99
Mg-Nd-Ni	XII-228
Mg-Nd-Pr	XVIII-226
Mg-Nd-Y	XVII-306
Mg-Nd-Y-Zn	XVIII-263, XIX-255
Mg-Nd-Zn	XVII-328
Mg-Pb	XI-101, XVI-74, XVII-122
Mg-Pb-Si	XI-231, XIV-210
Mg-Pd	VIII-85
Mg-Pr	XI-100, XVII-121
Mg-Rb	XIII-97
Mg-Sb-Si	IX-219, XIV-211
Mg-Sb-Sn	IX-228
Mg-Sc	XVIII-69
Mg-Si	XIV-73
Mg-Si-Sn	XII-223
Mg-Sn	XV-56, XIX-74
Mg-Th	IV-69, VI-59
Mg-Th-Zr	IV-152
Mg-Ti	I-52, V-67, XIV-78
Mg-U	II-38
Mg-V	IX-24
Mg-Y	VI-50, VII-65, XI-78, XIV-63
Mg-Y-Zn	XIV-198
Mg-Yb	XI-76
Mg-Zn	III-51
Mg-Zr	X-75
Mn-N	VIII-5, XIII-5
Mn-Nb	VI-60
Mn-Nd	XVI-75
Mn-Ni	XV-57
Mn-Ni-Pd	IV-155
Mn-Ni-Si	VIII-201, X-179
Mn-Ni-Sn	XI-235
Mn-Ni-U	I-123
Mn-Ni-V	XIII-173

System	Location
Mo-Nb-U	XV-157, VII-214, IX-231, XIX-222
Mo-Nb-U-Zr	IV-180, VII-255, IX-268, XVII-407
Mo-Nb-V	VI-121
Mo-Nb-W	VIII-167
Mo-Nb-W-Zr	X-216
Mo-Nb-Zr	IX-233, X-184, XIV-227
Mo-Ni	X-79, XIX-76
Mo-Ni-Re	XVIII-227
Mo-Ni-Si	VI-146, XIII-225, XIV-212, XV-203
Mo-Ni-Ta	XV-211
Mo-Ni-Ti	VI-153, XVIII-228
Mo-Ni-W	XIX-222
Mo-Ni-Zr	XIV-226, XV-213, XIX-223
Mo-O	XI-84
Mo-Os	VIII-95
Mo-Os-W	XI-191
Mo-Pd	V-68, X-80
Mo-Pt	IV-75, V-69, XIV-81, XIX-76
Mo-Pt-Re	XVI-264
Mo-Re	III-57, IV-76, V-70, XV-64
Mo-Re-W	VI-126, XIV-172
Mo-Re-Zr	XVI-265
Mo-Rh	V-73, VI-66
Mo-Ru	VI-67
Mo-Si	XIV-74, XVII-117
Mo-Si-Ti	XVIII-229
Mo-Si-V	VIII-153
Mo-Si-W	VIII-164
Mo-Sn-Zr	IV-158, V-156
Mo-Ta-Ti-V	XIX-259
Mo-Ta-V	XI-182
Mo-Ta-W	XVII-257
Mo-Ta-Zr	XIV-230
Mo-Tc	IX-91
Mo-Th	VIII-96
Mo-Th-Zr	X-187
Mo-Ti	IX-92
Mo-Ti-V	II-60, VI-122, VII-172
Mo-Ti-W	XII-182
Mo-Ti-Zr	VIII-210, XIII-238, XIV-232

System	Location
Mo-U	III-58, IV-77, VI-68, VII-85, IX-93, X-82, XVI-83, XVIII-71
Mo-U-V	VIII-154
Mo-U-Zr	IV-160, VI-156, VII-221
Mo-V	IV-14
Mo-V-Zr	XIV-160, XIX-224
Mo-W-Zr	X-144, XI-192, XII-183
Mo-Zr	XIII-103, XVI-84, XVIII-71
N-Nb	VI-5, VII-3, IX-5, X-5
N-Nb-O	VI-91
N-Nb-W	XIII-138
N-Ni-U	IX-138
N-O-Th	XVIII-232
N-O-U	XVI-112
N-Pr-V	XIX-227
N-Pu-U	XIX-228
N-Re	XVII-14, XVIII-72
N-Sc-V	XIX-229
N-Ta	VII-4, XIX-77
N-Ti-V	XIX-229
N-U	XIV-6
N-V	XV-5, XVII-5
N-V-Y	XIX-230
N-V-Zr	XIX-231
N-W	XV-6, XVII-8
N-Y	XIX-78
Na-O	XVII-108
Na-O-V	XVII-249
Na-Pb	I-60
Na-Pb-Te	XVII-366
Na-Sr	III-59
Na-Zn	XIV-87
Nb-Ni	X-84, XII-107, XVIII-73
Nb-Ni-Si	XIV-213, XV-204
Nb-Ni-Sn	XVII-368
Nb-Ni-Ta	II-90
Nb-Ni-Ta-Ti	VII-256
Nb-Ni-Ti	IV-161, XII-233
Nb-Ni-W	XVI-192, XVIII-234
Nb-Ni-Zr	XIV-235, XVI-283

System	Location
Nb-O	VIII-76, IX-74, X-63, XII-89, XIII-86, XVIII-73
Nb-O-Re	VIII-194
Nb-O-Ru	VIII-195
Nb-O-S	XIX-232
Nb-O-Sn-Zr	XIX-261
Nb-O-Ti	VIII-196, XIX-232
Nb-O-W	XIII-182
Nb-O-Zr	XII-218, XVI-250, XVII-310
Nb-Pd	VII-96
Nb-Pt	VII-97
Nb-Re	V-77, VII-98, XV-69
Nb-Re-Ta	XIX-233
Nb-Re-W	XIV-173
Nb-Rh	X-92
Nb-Ru	IX-102, X-93, XI-116
Nb-Ru-Ta	XII-235
Nb-Ru-Ti	XIX-235
Nb-Ru-Zr	XVII-369, XVIII-234, XIX-235
Nb-Sb	XII-110
Nb-Se	XI-117
Nb-Si	I-51, II-37, IV-64, VII-80, XIII-93, XIX-79
Nb-Si-Sn	IX-223
Nb-Si-V	IX-175, X-138
Nb-Si-W	VIII-165, IX-184, X-143
Nb-Sn	V-76, VIII-101, IX-101, X-89, XI-113, XIII-106, XVI-90, XIX-79
Nb-Sn-Ti	IX-240
Nb-Sn-Zr	IV-163, IX-241, XVIII-236
Nb-Ta	IV-78
Nb-Ta-Ti	XV-221
Nb-Ta-Ti-W	XIX-263
Nb-Ta-V	XI-183, XII-168, XIV-163
Nb-Ta-W	XVII-259
Nb-Ta-Zr	IV-164
Nb-Te	VI-75, XI-118, XVIII-74
Nb-Th	I-66, II-43
Nb-Th-Zr	IX-246, X-196

System	Location
Nb-Ti	VII-101, VIII-102, XII-111, XV-70
Nb-Ti-U	IX-242, XIX-237
Nb-Ti-V	III-94, V-122, VII-173
Nb-Ti-V-W	XIX-263
Nb-Ti-W	XII-184, XVI-194
Nb-Ti-W-Zr	XVI-301
Nb-Ti-Zr	VII-228, VIII-217, XII-236, XIII-247, XIV-237, XVI-286, XVII-370
Nb-U	III-63, IV-79, VII-104, XVI-91, XVII-141
Nb-U-Zr	IV-166, VII-230, XVII-373
Nb-V	I-18
Nb-V-Zr	XIII-174, XIV-164, XV-159, XVI-168
Nb-W	IV-28, XVIII-75
Nb-W-Zr	VIII-169, IX-185, XVI-195
Nb-Y	VIII-70
Nb-Zn	XI-119
Nb-Zr	I-67, III-64, VII-108, VIII-104, XV-71, XVII-142, XVIII-75, XIX-80
Nd-Pr	XII-105
Nd-Pt	IX-96, XVII-136
Nd-Pu	XIII-104, XV-66
Nd-Rh	XVI-85
Nd-Sb	XVIII-76
Nd-Te	XI-108, XII-106
Nd-Th	XIII-105, XIV-88
Nd-Ti	VI-69
Nd-Y	VII-67
Ni-O	I-42
Ni-O-Ta	XVI-249
Ni-O-W	XVI-186
Ni-Pb	I-63, VI-70, XV-68
Ni-Pd-V	XIV-161
Ni-Pu	I-62
Ni-Re	XVI-87
Ni-Re-Sc	XVI-284, XVIII-236
Ni-Re-Y	XVI-242, XVIII-237
Ni-Rh	XI-110
Ni-Ru	VII-90, X-86

System	Location
Ni-S	II-42, VII-92
Ni-Sb-Sn	X-191
Ni-Se	VII-91
Ni-Si	VIII-80, XI-91
Ni-Si-Ti	XII-225, XVII-321
Ni-Si-V	XII-167
Ni-Si-W	XIV-171
Ni-Si-Y	XVII-304
Ni-Si-Zn	XIV-215
Ni-Si-Zr	XIII-226
Ni-Sn	I-61, X-85
Ni-Sr	XI-111
Ni-Ta	VIII-98
Ni-Ta-Ti	IV-162
Ni-Te	VI-71, XVI-88
Ni-Th	XVIII-77
Ni-Ti	I-64, III-60, IX-98
Ni-U	IX-100, XVII-139
Ni-V	XVI-19
Ni-V-Zr	XIV-162
Ni-W	XVI-27, XVIII-78
Ni-W-Zr	XVI-193
Ni-Y	VI-51, VII-68
Ni-Yb	XIX-81
Ni-Zr	III-62, VI-74, VII-95, XVIII-79
Np-Pu	VII-88
Np-U	V-75
O-Pt-Zr	VII-206
O-Pu	VII-72
O-Rh-Zr	VII-207
O-Sc	XV-50
O-Si-V	XIV-157
O-Sn-Ti	XVI-251, XVIII-238
O-Ta	I-44, V-55, X-64, XII-90, XVI-66, XVIII-80
O-Te	X-65
O-Te-U	XVII-312
O-Th	XV-51

1372

System	Location
O-Ti	I-45, II-35, IX-75, X-66
O-Ti-V	VII-169
O-Ti-W	XIII-183
O-Ti-Zr	XIII-224, XVII-313
O-U	IX-76, XI-85, XIII-87, XVI-67
O-U-Zr	III-110
O-V	I-15, III-18, XVI-18, XVII-42, XVIII-81
O-W	VIII-34
O-Y	XIX-82
O-Zr	VII-73, XIII-88
Os-Pd	IX-104
Os-Pr	XVII-148
Os-Pu	I-69
Os-Re	VIII-110
Os-Re-Ru	IX-250
Os-Ru	VIII-111, XIX-82
Os-Ti	XVII-149, XVIII-82
Os-U	IX-105
Os-V	XII-28
Os-W	VII-30
P-Pd	XII-116
P-S	IV-87
P-Si	V-62, VIII-82
P-Th	XIII-136
P-Ti	XI-133
Pb-Pd	XIX-83
Pb-Pd-Te	XVII-380
Pb-Pr	XVII-158
Pb-Pu	I-70, XV-77
Pb-Rh	XVIII-83
Pb-S-Sb	VI-164
Pb-S-Te	XII-243
Pb-Sb-Se	VII-235
Pb-Sb-Sn	IX-248
Pb-Sb-Te	XI-253, XIII-256, XVI-291
Pb-Sb-Zn	V-157

System	Location
Pb-Se	II-48, XII-121
Pb-Se-Sn-Te	XIX-264
Pb-Se-Te	II-94, XI-252, XVI-290
Pb-Si	XVII-119
Pb-Sn	IV-82, VIII-106, XVI-93
Pb-Sn-Te	IV-167, XIII-249
Pb-Sn-Zn	XIII-250
Pb-Te	II-49, VII-112, XI-128
Pb-Te-Tl	XV-226
Pb-Te-U	XVIII-239
Pb-Ti	I-72
Pb-Tl	XVI-102
Pb-Y	XIII-80
Pb-Yb	XIII-79
Pb-Zr	IX-126
Pd-Pt-Ru	II-93
Pd-Pu	XIII-110
Pd-Re	VIII-112
Pd-Re-W	X-146
Pd-Rh	V-85
Pd-Ru	II-46, V-86, VI-79, XIX-84
Pd-Sb	XVII-151
Pd-Sb-Te	XVII-381
Pd-Sc	XVII-150
Pd-Si	III-42, XVII-119
Pd-Sm	XIX-84
Pd-Sn	V-81
Pd-Ta	X-99
Pd-Tc	IX-106
Pd-Th	X-100
Pd-Ti	IV-84, VI-80, XI-121, XIV-94, XVIII-84, XIX-85
Pd-U	II-47, X-101, XIV-95
Pd-V	IV-15
Pd-W	VII-31, X-23
Pd-Y	XIX-86
Pd-Zr	V-87, VIII-113, XVII-152

System	Location
Pr-Pt	XVII-153
Pr-Pu	XIII-114, XV-75
Pr-Re	XVII-156
Pr-Se	XII-117
Pr-Te	XVI-95
Pr-Th	XIII-125, XIV-96
Pr-Tl	XVII-159
Pr-Zn	XVI-98
Pt-Pu	XIII-113
Pt-Ru	XVIII-85, XIX-87
Pt-Si	X-71, XV-53
Pt-Ta	XI-122
Pt-Tc	IX-108
Pt-Te	IX-107
Pt-Th	X-102
Pt-U	VI-81
Pt-Zr	XIX-88
Pu-Rh	XIII-115
Pu-Ru	VII-113, XIII-116
Pu-Si	XI-92, XIII-118
Pu-Sn	XV-76
Pu-Th	III-68, XI-123, XIII-121
Pu-Ti	XIII-119, XVII-155
Pu-U	V-89
Pu-U-Zr	XIV-246
Pu-V	I-17
Pu-Y	XIII-81
Pu-Zn	XIII-122
Pu-Zr	VI-82, X-103, XIII-123, XV-78
Re-Rh	VIII-114
Re-Ru	VIII-115
Re-Sc	XII-118
Re-Si-W	XV-171
Re-Sn	XVI-92, XVII-143
Re-Ta	VI-83, XV-80
Re-Ta-W	XIII-185, XIV-174, XIX-237
Re-Tb	XIV-97
Re-Tc	IX-111
Re-Th	VII-115, XIV-98
Re-Ti	V-90, XV-81

System	Location
Re-U	IX-113
Re-V	VI-23, VII-26, XV-18
Re-W	V-31, XV-22
Re-W-Zr	XVI-196
Re-Zr	V-93, XV-82
Rh-Ru	XIX-88
Rh-Sb	IV-85, IX-114
Rh-Se	XIII-127
Rh-Ta	X-104
Rh-Tc	IX-115
Rh-Th	IX-116
Rh-Ti	XI-125, XII-120, XVIII-86, XIX-89
Rh-U	XIV-99
Ru-Sc	XVII-160
Ru-Si	XI-93
Ru-Ta	XI-126
Ru-Th	IX-124
Ru-Ti	IX-123, XVIII-86
Ru-U	XIV-101
Ru-V	IX-25
Ru-V-Zr	XIX-238
Ru-W	X-24
Ru-Y	XVIII-87
Ru-Zr	IX-125
S-Sb	VI-86
S-Sn	IV-83, VII-110, XII-113
S-Sr-U	XVII-387
S-Te-U	XIX-239
S-Ti	XIII-131
S-U	XVII-164
Sb-Se-Sn	XIV-242
Sb-Se-Te	XI-255
Sb-Se-Tl	I-127, XIX-240
Sb-Si	XVII-120
Sb-Sn	VI-76, XII-114, XVII-144
Sb-Sn-Te	XII-240, XIII-251
Sb-Sn-Te-Tl	VIII-226
Sb-Te	V-98, IX-127, XIV-103
Sb-Te-Tl	XII-244, XIV-251
Sb-Te-Zn	XVII-389

1376

System	Location
Sb-Tl	XVI-108
Sb-U	VI-88
Sb-Y	XVI-63
Sb-Zn	IV-89
Sc-Ti	VII-117, VIII-119
Sc-V	XVII-43
Sc-Y	XII-84
Sc-Zr	XII-123
Se-Sn	XII-112, XIV-92
Se-Sn-Te	XIV-243
Se-Ta	II-50, XI-129
Se-Te	VI-85, XII-122
Se-Te-Tl	V-158
Se-U	XVII-163
Si-Sn	V-60
Si-Sr	X-72, XI-94
Si-Ta-V	III-93
Si-Th	VII-81, IX-80
Si-Th-U	IX-224
Si-Ti	VIII-81, IX-79, XVI-71
Si-Ti-V	VII-170, XI-181
Si-Ti-W	XVI-188
Si-Tl	IV-65
Si-U	III-43, IX-81
Si-U-Zr	VII-211
Si-V	II-15, IX-23
Si-V-W	XIII-171
Si-W	III-24, XIX-90
Si-Zn	XVIII-88
Sm-Zn	XIII-129
Sn-Te	X-96
Sn-Te-U	XVIII-240
Sn-Th	X-97
Sn-Ti	I-68, II-45, III-65, VI-77, VIII-108
Sn-Ti-V	III-95
Sn-Ti-Zr	VI-161, VII-232, VIII-218, XIV-244, XVI-287

1377

System	Location
Sn-Tl	V-82, VII-111, VIII-107, XII-115, XIV-93, XVI-94, XVII-146
Sn-Tl-V	XIX-241
Sn-V	VII-25, XIX-91
Sn-Y	IX-68, XIV-64
Sn-Zn	V-84
Ta-Te	V-100, XI-131
Ta-Th	VII-119, XVIII-88
Ta-Ti	IX-128, XV-88
Ta-Ti-V	VII-174, XVI-169
Ta-Ti-W	XVIII-240
Ta-Ti-Zr	X-201
Ta-V	V-23, VI-24, VIII-18, X-21, XI-29
Ta-V-W	XIV-154
Ta-V-Zr	XIV-166
Ta-W	XVIII-89
Ta-W-Zr	X-148
Ta-Y	VIII-71
Ta-Zr	III-69, VIII-120, XII-124, XVIII-90
Tb-Th	XIII-134
Tb-Y	XIII-82
Tc-V	XIV-22
Tc-W	IX-32
Tc-Zn	X-108
Te-Tl	VI-89
Te-Yb	XVI-61
Th-Ti	II-51
Th-Ti-Zr	IX-253, X-203
Th-U	IV-92, XVIII-90
Th-U-W	XVIII-242
Th-U-Zr	IV-172, VII-244, XVIII-243
Th-V	VII-27, IX-27
Th-W	XVIII-91
Th-Zn	III-75
Th-Zr	IV-93, V-103, VII-126, XVIII-92

System	Location
Ti-U	I-74, VII-123
Ti-U-Zr	III-119, V-161, VII-239, XIV-253, XIX-242
Ti-V	IX-26
Ti-V-W	VII-166
Ti-V-Zr	IV-120, VIII-156
Ti-W	IV-30, XIV-29, XVII-58, XVIII-92
Ti-W-Zr	XII-185
Ti-Y	VII-69, VIII-72, XIV-65
Ti-Zn	VIII-123, XII-125
Ti-Zr	VII-124, XII-126, XVII-168
Tl-Zn	I-73, VII-118, XI-130
U-W	I-23
U-Zn	III-77
U-Zr	I-76, II-53, III-78, VII-130, IX-133, XVI-109, XVII-169
V-W	VI-20, VII-22
V-Y	VII-24, VIII-15
V-Zn	XII-30
V-Zr	I-19, XVIII-93
W-Zr	XVIII-93
Y-Zn	XII-85
Y-Zr	VIII-73
Yb-Zn	XII-86, XIV-62
Zn-Zr	VI-90

BIBLIOGRAPHY

The following is a list of the volumes of "Diagrammy Sostoyaniya Metallicheskikh Sistem," edited by N. V. Ageev and published by VINITI in Moscow, USSR, which were used in making this compilation.

Volume	Publ. Date
I	1959
II	1959
III	1960
IV	1961
V	1962
VI	1962
VII	1963
VIII	1964
IX	1966
X	1966
XI	1968
XII	1968
XIII	1970
XIV	1970
XV	1971
XVI	1972
XVII	1973
XVIII	1975
XIX	1976

1380

National Bureau of Standards SP-496, Applications of Phase Diagrams in Metallurgy and Ceramics
Proceedings of Workshop held at NBS, Gaithersburg, Md., January 10-12, 1977

Standards for Publication of Phase Equilibrium Studies

Eric R. Kreidler
General Electric Company, Lighting Research and Technical Services Operation, Nela Park, Cleveland, Ohio

INTRODUCTION

A paper on phase equilibria typically receives a review before publication and may not be critically evaluated again until it is included in a compilation. Since most phase diagrams will eventually be published in handbooks or compilations such as Phase Diagrams for Ceramists, it is important that the initial review process be critical and constructive. Critical evaluations after publication are of limited value because there is usually no opportunity for a response from the original authors. It is suggested that a set of published standards for phase equilibrium papers would assure more uniform treatment of data and would help both journal reviewers and compilers to properly assess the value of individual papers. A brief survey of the literature quickly reveals the wide variation in quality. Papers range from speculations based on a few haphazard experiments to thorough studies based on hundreds of experiments and using complementary experimental techniques. The purpose of standards should not be to preclude publication of incomplete or exploratory work, but to assure that such works are based upon sound data. Standards should be used to prevent publication of erroneous diagrams, and if properly written and disseminated can help improve the general quality of phase equilibrium studies.

The establishment of standards raises some difficult questions. Among them being: how demanding should standards be?; how rigorously should standards be applied?; and what aspects of phase equilibrium work should be subject to standardization? If a set of standards is to gain

wide acceptance, it must represent a concensus of informed opinion and satisfy the main needs of all concerned disciplines. For these reasons, the establishment of standards should be the responsibility of the scientific community. A committee of phase equilibrium experts representing the disciplines metallurgy, ceramics, mineralogy, geochemistry, semiconductor technology, etc. could accomplish the task.

The purpose of this work is not to formulate standards but to point out some of the problem areas and suggest ways to handle them. Most of the comments and opinions result from the author's experiences while handling the review process for thirty phase equilibrium papers over the last three years. The most significant impression gained from that activity is that a majority of phase equilibrium studies are poorly conceived and conducted. Furthermore, there seems to be a widespread lack of understanding of basic phase rule principles among scientists engaged in phase equilibrium studies. It is important to explore ways of upgrading the field; hence the motivation for this discourse.

The majority of problems fit into one or more of the following broad categories, ranked in order of importance.

A. Failure to test for equilibrium.

B. Use of inappropriate experimental methods.

C. Accuracy and precision of experimental results.

D. Failure to provide adequate documentation of experimental data.

E. Diagrams which violate the phase rule.

F. Terminology and phase diagram format.

G. Poor exposition.

Each of these areas are discussed in greater detail in the following sections.

A. Tests of equilibrium

Although the phase rule applies only to systems at equilibrium, tests of equilibrium are a widely ignored aspect of experimental phase diagram determinations. This single factor probably leads to more errors than any other. It is estimated that if sensible tests of equilibrium were a prerequisite to publication, fewer than one in five diagrams would be published. Admittedly, tests of equilibrium are sometimes difficult, but serveral methods are available and should be put to more extensive use.

Theoretically a system is at equilibrium when the components have interacted in such a way as to obtain the minimum free energy possible with those components for a given composition, temperature, and pressure. Furthermore at equilibrium, there cannot be any gradients in chemical potential, temperature, or pressure. Although these are the best criteria for equilibrium, they are seldom used because adequate thermodynamic data are lacking and because it is tedious to prove that individual phases have reached homogeneous equilibrium (i.e. they are free of composition gradients).

The experimental test most often employed is to perform periodic phase analyses on samples held at specified conditions. If the phase assemblage remains constant with time, equilibrium is then assumed. The test is frequently abused because the time intervals studied are too short. This test is usually open to question because it is impossible to determine a priori what the time scale should be.

A better test is to approach equilibrium from two (or more) directions. This technique is much more flexible and generally yields more information than the "constancy with time" criterion. For rapid reversible reactions,

such a test can take the form of DTA scans in both the upward and downward directions at several heating and cooling rates. If sharp heat effects are observed in both directions, one can evaluate, from the thermal hysteresis, how readily the system approaches equilibrium. For sluggish systems, it is often possible to obtain more than one set of phases for a given composition. These can be studied in paired experiments to determine if a common set of assemblages is reached from the two different initial sets. If so, equilibrium can be reasonably assumed. If both initial sets of phases remain unchanged or fail to converge, the investigator immediately knows that equilibrium has not been attained.

At equilibrium, the number of observed phases must be in accord with the predictions of the phase rule. If there is a discrepancy, either the system is not at equilibrium, or the components were incorrectly chosen. This simple criterion is often overlooked, and incorrect diagrams for condensed binary systems have been occasionally presented, showing extensive areas of three and even four phase coexistence. Fortunately, most errors of this sort are eliminated during the review process.

A first rate study should contain convincing tests of equilibrium. The "time invariance" criterion should give way to the "two directions" criterion whenever possible. In all cases the number of observed phases must be in accord with the predictions of the phase rule.

B. Inappropriate Experimental Techniques

In order to select appropriate experimental techniques, something must be known of the system kinetics. The rate at which reactions proceed should dictate the methods used. Generally little is known about the kinetics of phase reactions in new systems, and such knowledge

must be generated by various tests of equilibrium. The two extremes are most easily studied. Rapid reversible reactions are amenable to dynamic methods such as DTA or hot stage microscopy. Very sluggish reactions are best evaluated by static methods such as quenching. Serious experimental problems can lie between the two extremes and may require the use of in situ high temperature methods. Generally these should be static measurements.

In general no one method is suitable for an entire system, and a judicious mixture of static and dynamic methods will yield the greatest amount of information. A classic example is the system SiO_2 where both rapid reversible (α-β quartz transition) and sluggish (critobalite - liquid) reactions are encountered.

Many other errors in experimental technique can be found in the literature. One of the more common is to fail to control or specify the oxygen fugacity in systems containing multivalent oxides. These errors lead to inaccurate results as indicated in the next section.

C. Accuracy and Precision of Experimental Results

A phase diagram is only as good as the accuracy with which temperature, pressure, and composition are measured and controlled. Temperature measurements, although the easiest to make, are frequently of questionable accuracy. One of the more common errors is the use of dynamic methods to measure sluggish transitions. It is not uncommon to find polymorphic transitions which are off by 20°C or more due to superheating and supercooling effects. The precision in temperatures should be realistically stated, taking into account such factors as stability of furnaces, possible temperature gradients, and pyrometer calibration. If a furnace used for equilibration studies is stable to

only $\pm$ 5°C it is not valid to claim precision of $\pm$ 1°C which may be the accuracy of a thermocouple calibration. It appears that the precision of temperature measurements made by optical pyrometry is often grossly overstated.

Pressure measurements have many difficulties which need not be discussed here. As with temperature measurements, estimates of the accuracy and precision of such measurements is mandatory.

Compositional inaccuracy can arise from a number of causes: reactions with containers, reactions with atmospheric components, incongruent vaporization, etc. For this reason, it is essential that investigators state as accurately and completely as possible the nature of containers or other materials in contact with samples as well as the atmospheres used. Where applicable, possible changes in oxidation state should be evaluated and commented upon. Any assumptions regarding the final composition of samples derived by pyrolysis of more complex materials should be checked by chemical analysis. It is not always valid to assume that all CO_2, H_2O, etc. has been removed by heating to high temperatures. Aside from the problem of gross composition, one is faced with a myriad of problems relating to the composition of liquid and solid solutions.

X-ray lattice parameter shifts are commonly used to estimate compositions of solid solutions. Often as not, the method is misused because the calibration curve is obtained from mixtures of phases rather than single phase samples. For the method to be valid, the actual compositions of the solid solutions used in constructing the calibration curve must be accurately known. If a mixture of phases is involved, this is not possible unless the phases can be separated and chemically

analyzed. Liquid compositions are infrequently determined by chemical analysis, but if more effective methods of separating high temperature melts from their conjugate solids could be devised, the problem of accurate liquidus determinations could be greatly simplified.

D. Failure to Provide Adequate Documentation of Experimental Data

Since many journals no longer publish extensive tabular data, it is becoming more and more common for authors not to provide such information. Other, less desirable, methods of documenting phase equilibrium data are being used. One method is to place symbols directly on the phase diagram in an effort to indicate what experiments were done. Although somewhat useful, such symbols do not convey as much information as a well constructed table. The lack of well organized tables often leads to lengthy verbal descriptions of the data. Such discussions tend to read poorly, becoming so bogged down in details that the main points are missed. In some cases the experimental data are simply not documented, and only the phase diagram itself is given.

Tables of well documented phase equilibrium data should be provided along with any diagram submitted for publication! Such tables are placed in data depositories and are available to interested readers. From the viewpoint of the reviewer (or other critical reader), it is inherently unfair to expect that the conclusions of a study (i.e. a phase diagram) be accepted, when the data upon which they are based is unavailable for inspection.

A well constructed table should contain at least the following information:

1. Sample composition

2. Initial phases present
3. Equilibration conditions -- temperature, time at temperature, pressure, atmosphere, etc.
4. Phases present after equilibration
5. Methods of phase analyses -- x-ray diffraction, microscopy, others.

Any conditions or methods common to the entire study should be stated in a footnote and not be endlessly repeated in the table. A sample table incorporating these ideas is shown in Table I. The information density in such a table can be very high, and one might consider replacing the "Experimental" section of a study with such an annotated table. With such a presentation it is an easy matter to document the history of any given sample along with the phase assemblage finally obtained. Table I shows that by indentation of temperatures alone, the sequence of heat treatments given any sample is easily documented. Thus Sample #2 was heated at 900°C for 48 hours in an open platinum crucible, cooled, a portion was packed into a platinum tube which was then sealed, held at 1200°C for 15 hours, and finally quenched into water.

With this kind of detailed information the reviewer is able to fairly judge the plausibility of the author's conclusions. Without it he cannot exercise much independent judgement, and the value of the review declines accordingly.

E. Diagrams Which Violate the Phase Rule

The geometry of phase diagrams must be consistent with the phase rule. There is a tendency among less expert workers to "pepper" a system with experimental points and then map out areas of like phase assemblages without much regard for the requirements of the phase rule. The resulting

diagrams can be very strange and their various parts sometimes cannot be connected together to make a correct, whole diagram. Non-equilibrium phase assemblages are frequently the underlying cause of such implausible diagrams.

Impossible geometries are sometimes found in published diagrams. They can be grouped into "absolutely impossible" and "impossible but approachable in the limit" categories. A few examples of each type which have been found in the recent literature are illustrated in Figures 1 - 4. A greater variety and higher frequency of errors can be found in ternary and quaternary systems. Some of the impossible configurations probably result from poor draftsmanship, but whatever their cause, they should be eliminated before a diagram is published. A brief set of rules for the geometric construction of unary, binary, ternary and quaternary systems and their various sections might be useful. A short compendium of impossible configurations might also help.

F. Formats and Terminology

The formatting of phase diagrams need some attention. Although some conventions do exist, and are in wide use, a formalized statement of these conventions would be of great value both to authors and reviewers. A principal concern is that speculative phase relationships be clearly indicated on the diagrams. This is commonly done by using dashed curves for speculative portions of the diagram. However, this convention is not universally followed. Extraneous material such as the height of DTA peaks should not be superimposed on phase diagrams. Isofracts, lattice parameters or other data useful in constructing the phase diagram may be displayed on separate "property" diagrams but should not be plotted on the phase diagram itself.

A uniform terminology across all disciplines, using phase diagrams, should be possible and is desirable. Our present terminology is incomplete in some respects and confusing in others. Even in simple binary systems, a few rather common features either have no names or are referred to by cumbersome phrases such as "lower temperature limit of stability" (Fig. 5e). A few of these unnamed features are shown in Figures 5a - 5f.

Invention of jargon to supplant more suitable terminology, already in existence, must be strenuously discouraged. The use of generic terms such as "invariant point" should be discouraged whenever the use of a more specific term such as "eutectic point" or "peritectic point" is possible.

An example of faulty terminolgy is illustrated by Figure 6. This diagram was repeatedly referred to as a "planar square iso-electronic phase diagram". Granted the diagram is planar and square, but it certainly is not iso-electronic. (The number of electrons per formula unit are given in parentheses.) The diagram is iso-equivalent which is what the author meant. A lot of trouble could have been saved if the diagram had been referred to by its proper term "reciprocal salt system". Suprisingly, this obviously faulty term almost made it into the literature.

G. Poor Exposition

The exposition of phase equilibrium studies is probably no better or worse than is to be found in other fields of science. A long discourse could be written about what constitutes good and bad scientific writing, but it is not appropriate here. From the reviewer's point of view, there are several particularly annoying faults which should be avoided:

1. Do not expect reviewers to be ghost authors. The English

in some manuscripts is appalling. The responsibility of writing well belongs to the author not his reviewers or editors. The reviewer's main responsibility is to judge the scientific aspects of the work, his responsibility for exposition should be secondary and mostly of a cosmetic nature.

2. Do not engage in extensive discussions which are unsupported by well documented experimental evidence. Speculations should be clearly stated, labled as such, and occupy the minimum possible space. A corollary is -- Do not build an extensive case on data which are really of questionable value.
3. Keep the use of jargon to a minimum. The aim of writing is to communicate, and jargon or excessive use of specialized terminology can only restrict the size of the potential audience.
4. Do not indulge in criticism of prior work unless your own work is clearly more definitive.
5. Do yourself justice. Do not negate a good piece of work with sloppy writing.

CONCLUSION

Much can and should be done to improve the quality of published work on phase equilibria. It is suggested that an interdisciplinary committee of experts could formulate a set of standards or guidelines for the publication of phase equilibrium studies. Although incomplete and certainly debatable in some particulars, it is hoped that the remarks herein might serve as a starting point for such an effort.

A set of well written standards could make the review process more constructive and less subject to the vagaries of individual tastes and expectations. If potential authors could know what standards their work would be evaluated against, they could do a better job of planning and executing their work. The end result should be a general improvement in the quality of phase equilibrium studies.

Table I

Suggested Format for Reporting Phase Equilibrium Data

Composition	T (°C)	Time (hr.)	Phases Present	Comments
ABC	900	48	AB + C	a, x
	1200	15	AB + LIQ.	b, x, m
	1500	5	LIQUID	b, x, m
	1400	20	LIQUID	a, m
	900	48	AB + C	b, x, m
	1000	48	AB + C	b, x, m
	1100	48	AB + C	b, x, m
A_2BC	900	48	A_2B + C	a, x
	1000	1	A_2B + LIQ.	b, x, m

a. Open Pt crucibles, cooled by plunging into air, ~10 gram samples.

b. Sealed Pt capsule, quenched into water, ~10 mg. samples.

x = x-ray diffraction, m = microscopy in polarized light.

The atmosphere in contact with all samples was air.

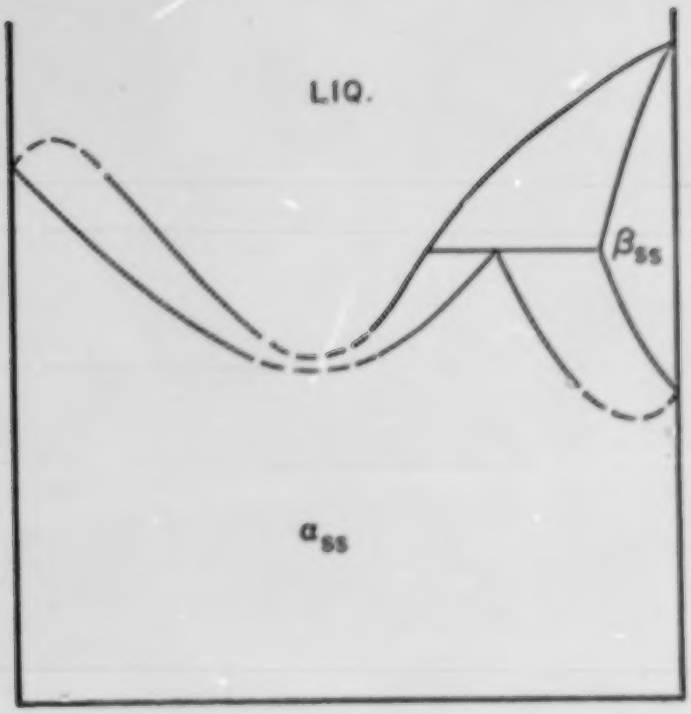

FIGURE 1

Some impossible configurations (dashed curves). Liquidus and solidus curves must be tangent in such a system.

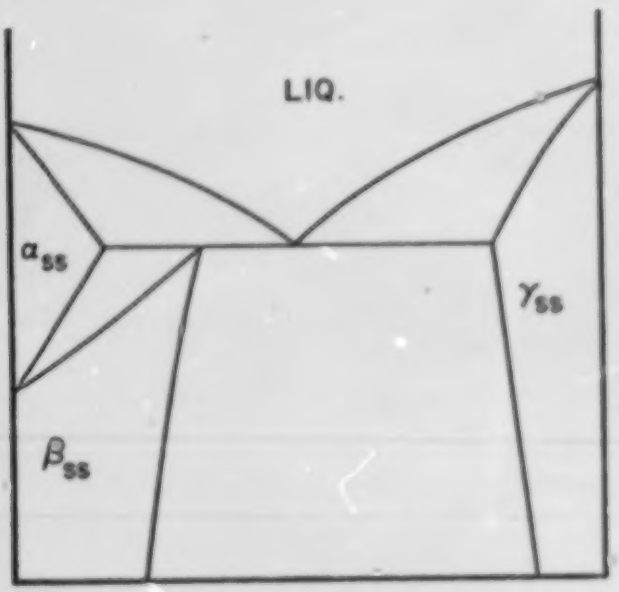

FIGURE 2

However narrow, there must be an $\alpha_{ss} + \gamma_{ss}$ region.

1320 1394

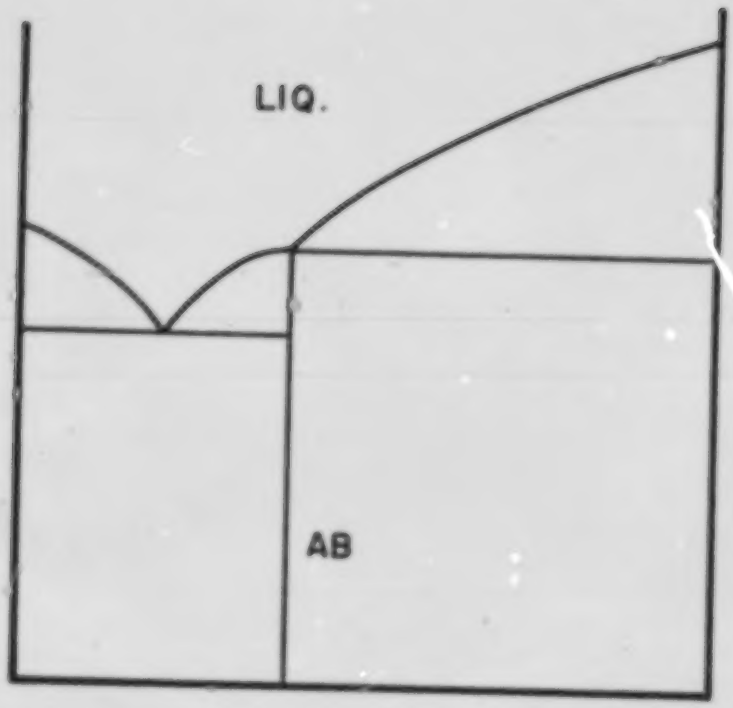

FIGURE 3

Approachable as a limit, but generally the compound AB must melt either congruently or incongruently.

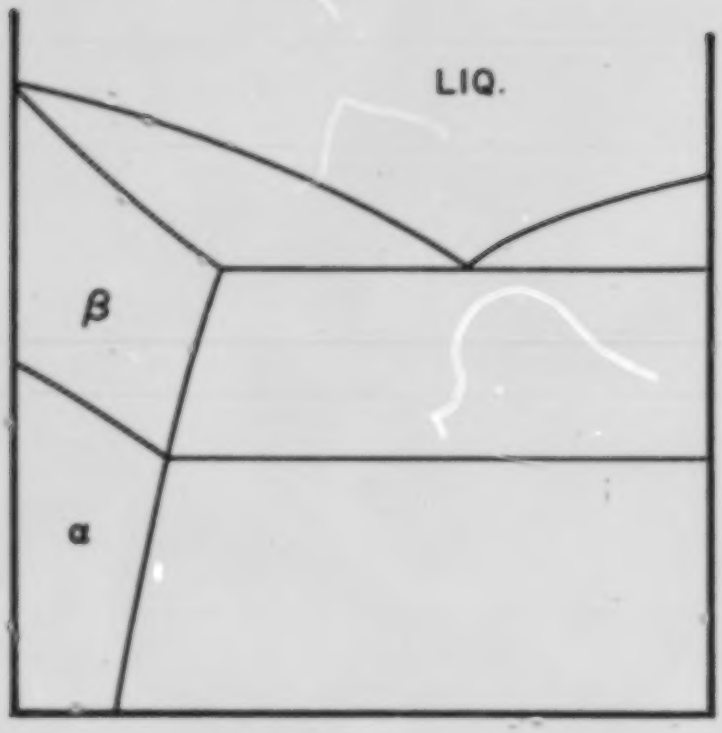

FIGURE 4

If α and β are distinct phases, they must be separated by an α + β region.

1396

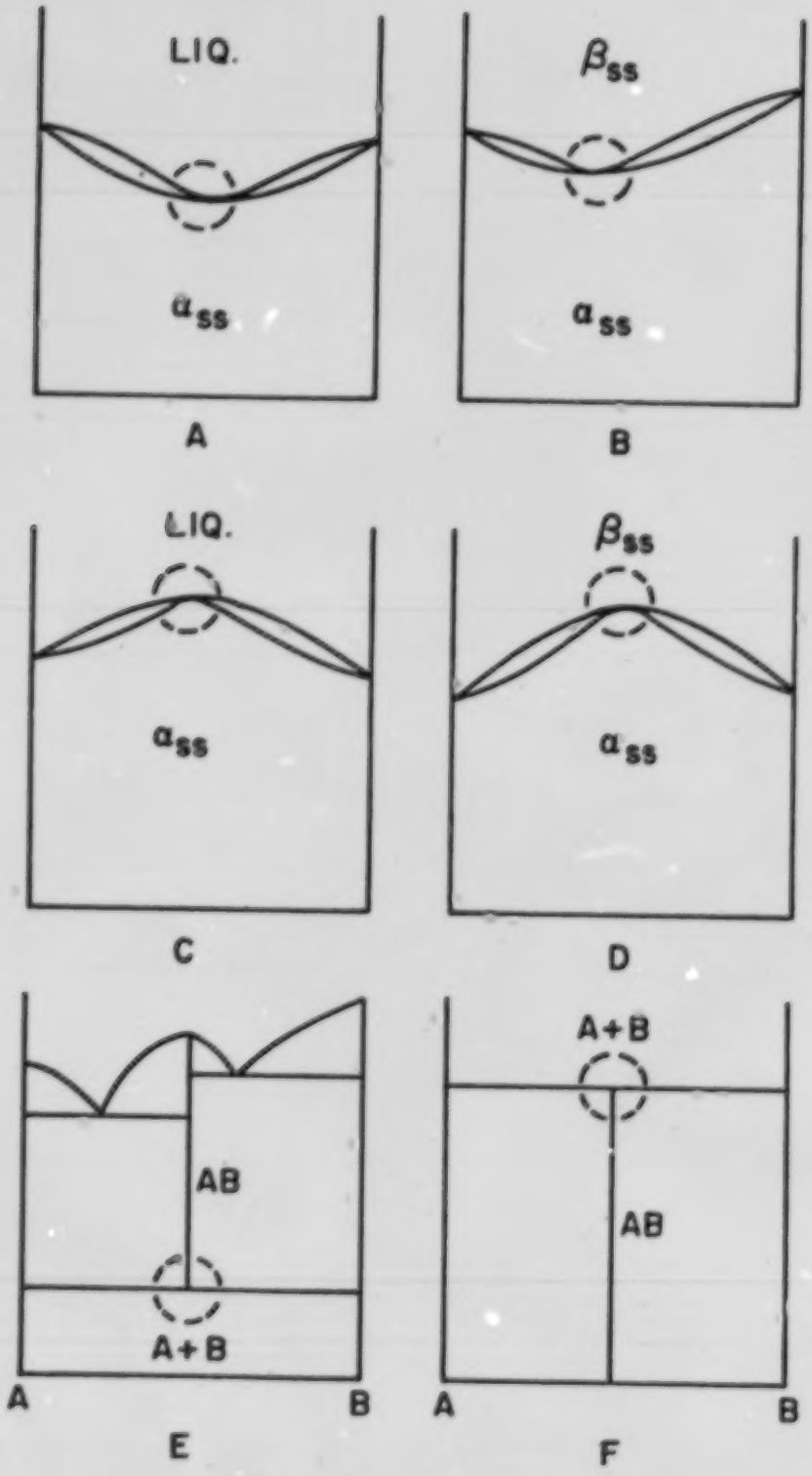

FIGURE 5

Some unnamed features in binary condensed systems (circled).

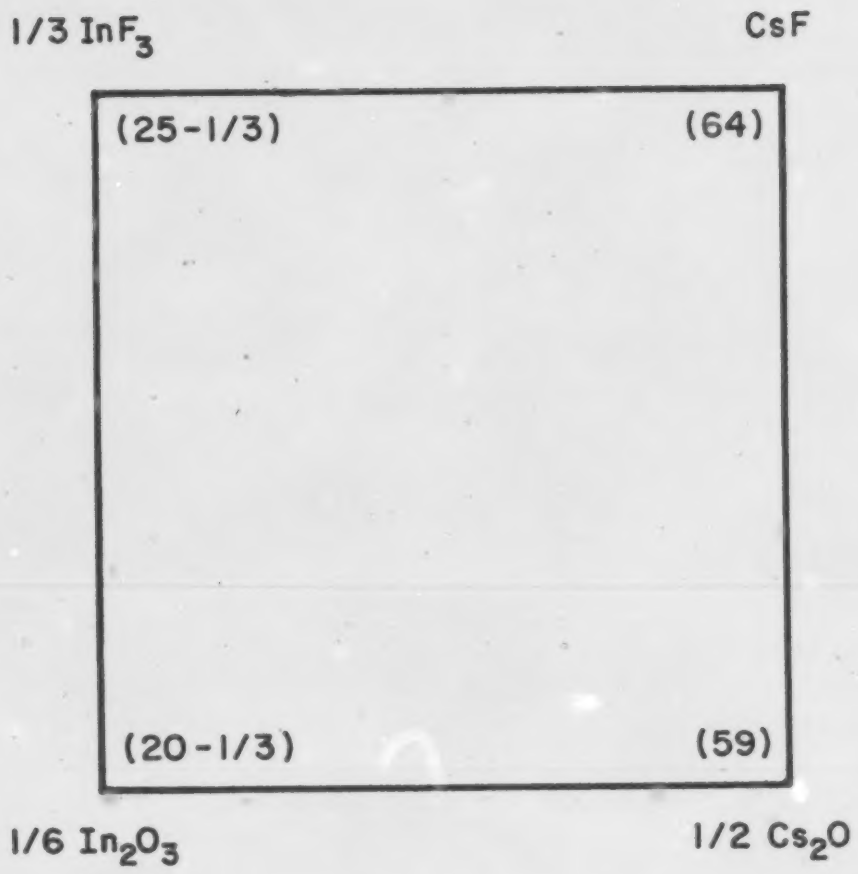

FIGURE 6

An example of poor terminology. "Planar square iso-electronic phase diagram" or "Reciprocal salt diagram"? (Number of electrons per formula unit given in parentheses.)

1398

National Bureau of Standards SP-496, Applications of Phase Diagrams in Metallurgy and Ceramics
Proceedings of Workshop held at NBS, Gaithersburg, Md., January 10-12, 1977

FORMATTING AND DISTRIBUTING EVALUATED REFERENCE DATA: THE OFFICE OF STANDARD REFERENCE DATA AT THE NATIONAL BUREAU OF STANDARDS

S. P. Fivozinsky and G. B. Sherwood
Office of Standard Reference Data
National Bureau of Standards
Washington, D.C. 20234

The Office of Standard Reference Data at the National Bureau of Standards manages a complex of data evaluation centers located in university, industrial, and other Government laboratories as well as within NBS. The centers are engaged in the compilation and critical evaluation of numerical data on physical and chemical properties retrieved from the world scientific literature. This system of centers, the National Standard Reference Data System (NSRDS), is a means of coordinating on a national scale the production and dissemination of critically evaluated reference data in the physical sciences. The primary focus of the NSRDS is on well-defined physical and chemical properties of well-characterized materials or systems.

The Office of Standard Reference Data, as coordinator of the system:

- establishes needed data centers in technical areas which fall within the scope of the program
- maintains close contact with other data compilation activities both in the U.S. and abroad to encourage exchange of data and avoid needless duplication of effort
- identifies, by contacts with users, areas where needs for evaluated reference data are increasing or decreasing, and formatting procedures which will make the outputs of the system as useful as possible
- distributes evaluated reference data through a variety of output channels

The output channels include:

- Journal of Physical and Chemical Reference Data
  a quarterly journal containing data compilations and critical data reviews, published for the National Bureau of Standards by the American Institute of Physics and the American Chemical Society.
- NSRDS-NBS Series
  a publication series distributed by the Superintendent of Documents, U.S. Government Printing Office

- appropriate publications of technical societies and commercial publishers. Handbook publications are an important element of this category

- magnetic tape data files - sold through the National Technical Information Service

The outputs of several NSRDS centers are directly or indirectly related to phase diagram applications in metallurgy and ceramics; examples include alloy data, data on diffusion in metallic systems, properties of substances at high pressures; properties of superconducting materials, and thermodynamic data of minerals. Some recent publications on these subjects are:

1. Butrymowicz, Daniel B., Manning, John R., Read, Michael E., "Diffusion in Copper and Copper Alloys, Part IV. Diffusion in Systems Involving Elements of Group VIII," J. Phys. Chem. Ref. Data, 5(1) 103-200 (1976).

2. Chang, Y. Austin, "Phase Diagrams and Thermodynamic Properties of Ternary Copper-Silver Systems," J. Phys. Chem. Ref. Data (in process).

3. Donnay, J.D.H. and Ondik, Helen M., Crystal Data Determinative Tables, Third Edition, Vol. 1, Organic Compounds, Vol. 2, Inorganic Compounds, Swarthmore, PA, Joint Committee on Powder Diffraction Standards, Vol. 1 (1972), Vol. 2 (1973).

4. Hultgren, R. and Desai, P. D., Selected Thermodynamic Values and Phase Diagrams for Copper and Some of Its Binary Alloys, New York, International Copper Research Association, Inc. (1973).

5. Roberts, B. W., "Survey of Superconductive Materials and Critical Evaluation of Selected Properties," J. Phys. Chem. Ref. Data, 5(3) 281-821 (1976).

6. Stull, D. R. and Prophet, H., JANAF Thermochemical Tables, Second Edition, NSRDS-NBS 37, U.S. GPO (1971).

   Reprint No. 50, "JANAF Thermochemical Tables, 1974 Supplement," J. Phys. Chem. Ref. Data, 3(2) 311-480 (1974).

   Reprint No. 60, "JANAF Thermochemical Tables, 1975 Supplement," J. Phys. Chem. Ref. Data, 4(1) 1-175 (1975).

In general, current NSRDS projects fall into the following categories:

1400

Energy and Environmental Data - This program includes projects dealing with data that have an important application in some aspect of energy R&D or environmental quality improvement. Projects in chemical kinetics, nuclear properties, spectroscopic data, and interaction of radiation with matter are currently incorporated in this program. The output of these projects is particularly important in R&D on new energy sources, environmental monitoring techniques, and prediction of the effects of pollutants introduced into air, water, or land.

Industrial Process Data - Projects dealing with thermodynamic, transport, colloid and surface, and physical properties of industrially important substances are included in this program. Such data have particular application to design of new processes in the chemical and metallurgical industries, optimization of currently used processes, and general productivity enhancement.

Materials Utilization Data - This program covers properties required for material selection and R&D on new materials. The structural, optical, electric, magnetic and mechanical properties of solid materials are included.

Physical Science Data - Projects which involve basic data of very broad applicability, or which are associated with an important frontier field of science, are included in this program. Examples are fundamental physical constants, data on fundamental particles, and data relevant to radioastronomy.

The data centers currently included in the National Standard Reference Data System are given below. Inquiries on data may be directed to all these centers.

Energy and Environmental Data

Atomic Energy Levels Data Center

Dr. W. C. Martin
Optical Physics Division
National Bureau of Standards
Washington, D.C. 20234
Telephone: (301) 921-2011

Data Center for Atomic Transition Probabilities and Atomic Line Shapes and Shifts

Dr. W. L. Wiese
Optical Physics Division
National Bureau of Standards
Washington, D.C. 20234
Telephone: (301) 921-2071

Direct inquiries to: Ms. Georgia Martin, (301) 921-3374

Atomic Collision Cross Section Information Center

Dr. E. C. Beaty
Joint Institute for Laboratory Astrophysics
University of Colorado
Boulder, Colorado 80309
Telephone: (303) 499-3672

Data Center for Atomic and Molecular Ionization Processes

Dr. H. M. Rosenstock
Physical Chemistry Division
National Bureau of Standards
Washington, D.C. 20234
Telephone: (301) 921-2792

Chemical Kinetics Information Center

Dr. R. F. Hampson, Jr.
Physical Chemistry Division
National Bureau of Standards
Washington, D.C. 20234
Telephone: (301) 921-2174

Radiation Chemistry Data Center

Dr. Alberta B. Ross
University of Notre Dame
Radiation Laboratory
Notre Dame, Indiana 46556
Telephone: (219) 283-6527

Molten Salts Data Center

Dr. G. J. Janz
Rensselaer Polytechnic Institute
Department of Chemistry
Troy, New York 12181
Telephone: (518) 270-6356

X-ray and Ionizing Radiation Data Center

Mr. J. H. Hubbell
Center for Radiation Research
National Bureau of Standards
Washington, D.C. 20234
Telephone: (301) 921-2685

1492

Photonuclear Data Center

Dr. E. G. Fuller
Nuclear Sciences Division
National Bureau of Standards
Washington, D.C. 20234
Telephone: (301) 921-2625

Table of Isotopes Center

Dr. M. Lederer
Lawrence Radiation Laboratory
University of California
Berkeley, California 94720
Telephone: (415) 843-2740 x5995

Industrial Process Data

Chemical Thermodynamics Data Center

Mr. D. D. Wagman
Physical Chemistry Division
National Bureau of Standards
Washington, D.C. 20234
Telephone: (301) 921-2773

Aqueous Electrolyte Data Center

Dr. B. R. Staples
Physical Chemistry Division
National Bureau of Standards
Washington, D.C. 20234
Telephone: (301) 921-3632

Thermodynamics Research Center

Dr. B. J. Zwolinski
Texas A & M University
Department of Chemistry
College Station, Texas 77843
Telephone: (713) 846-8765

Cryogenic Data Center

Mr. N. A. Olien
Cyrogenics Division
National Bureau of Standards
Boulder, Colorado 80302
Telephone: (303) 499-1000 x3257

Center for Information & Numerical Analysis and Synthesis

Dr. Y. Touloukian
Purdue University
CINDAS
2595 Yeager Road
W. Lafayette, Indiana 47906
Telephone: (317) 463-1581

Direct inquiries to: Mr. W. H. Shafer

High Pressure Data Center

Dr. H. T. Hall
574 Clark Library
Brigham Young University
Provo, Utah 84601
Telephone: (801) 374-1211 x3477

Direct inquiries to: Dr. Leo Merrill

Alloy Data Center

Dr. L. H. Bennett
Metallurgy Division
National Bureau of Standards
Washington, D.C. 20234
Telephone: (301) 921-2917

Materials Utilization Data

Crystal Data Center

Dr. H. M. Ondik
Inorganic Materials Division
National Bureau of Standards
Washington, D.C. 20234
Telephone: (301) 921-2900

Diffusion in Metals Data Center

Dr. J. R. Manning
Metallurgy Division
National Bureau of Standards
Washington, D.C. 20234
Telephone: (301) 921-3351

1404

Superconductive Materials Data Center

Dr. B. W. Roberts
General Electric Company
Research & Development Center
P.O. Box 8
Schenectady, New York 12301
Telephone: (518) 377-2271

Physical Science Data

Fundamental Particle Data Center

Dr. A. H. Rosenfeld
Lawrence Radiation Laboratory
University of California
Berkeley, California 94720
Telephone: (415) 843-2740 x6301

Microwave Spectral Data Center

Dr. F. J. Lovas
Optical Physics Division
National Bureau of Standards
Washington, D.C. 20234
Telephone: (301) 921-2021

1405

PANEL II

PRIMARY METAL PRODUCTION

(User Needs for Phase Diagram Information)

Moderator: Prof. John F. Elliott, Dept. of Materials Science and Engineering, M.I.T. Cambridge, MA

Panel Members:

Dr. Peter Crimes, Ledgemont Laboratory, Kennecott Copper Corp., Lexington, MA

Dr. Harold R. Larson, American Smelting and Refining Company, Plainfield, NJ

Dr. Robert D. Pehlke, Metallurgy Division, University of Michigan, Ann Arbor, MI

National Bureau of Standards SP-496, Applications of Phase Diagrams in Metallurgy and Ceramics
Proceedings of Workshop held at NBS, Gaithersburg, Md., January 10-12, 1977

PANEL DISCUSSION: PRIMARY METAL PRODUCTION

John F. Elliott
Dept. of Materials Science
and Engineering, M.I.T.
Cambridge, MA

To start the ball rolling, I would like to make a few comments on how phase equilibria and phase diagrams fit in extractive metallurgy. The pyrometallurgy of copper is the area from which the example is drawn. Figure 1[1] is a stability diagram for the copper-iron-silica-oxygen system at 1200°C in which the sides are the copper-iron-oxygen, iron-silica-oxygen and copper-silica-oxygen systems. Log P_{O_2} is the vertical axis. This is a type of phase diagram that is coming into more general use today. The iron-silicate phase on the right is reasonably well understood. There is also the liquid copper-silicate slag at the upper left which is stable at relatively high oxygen pressures. A point of interest technically for newer methods for smelting sulfide copper ores is how the two liquid slag fields may join as the temperature is raised. We think that the joining occurs at approximately 1250°C. The fields of stability of these slags are important to our understanding of what controls the loss of copper to the smelting slags, particularly for newer processes. Dr. Crimes will probably have more to say on the matter in a few minutes.

The copper-oxygen-silica ternary system is a portion of the quaternary system just mentioned. We have devoted considerable attention to this system in the recent past. Reference 2 covers the results of a portion of our work.

It is interesting to note that the liquid field in the Cu-Fe-O-S-SiO_2 system at 1400°C extends continuously from pure liquid copper through the oxysulfied phase (matte) to the silicate phase.

One of the diagrams of importance in nonferrous extractive metallurgy is the iron-copper-sulfur system (Fig. 2). We know quite a bit about this system from the work of Krivsky and Schumann[3]. Technically we are interested in the regions of stability of the liquid sulfide field (matte) near saturation with iron and with copper. There is also great technical interest in this phase with additions of oxygen, of lead, of nickel, etc., but our information on the phase relationships in the pertinent quaternary systems are relatively meager.

The principal point to be made is that these systems are of great techinal importance, but our knowledge of them is rather incomplete, principally because of experimental compilations.

References

1. J. F. Elliott; Met. Trans., 1976, vol. 7B, p. 17.
2. A. Luraschi and J. F. Elliott; Proceedings, International Symposium on Copper Extraction and Refining, J. C. Yannopoulos and J. Agarwal, ed., TMS-AIME, 1976, p. 90.
3. W. A. Krivsky and R. Schuhmann; Trans., TMS-AIME, 1957, vol. 209, p. 981.

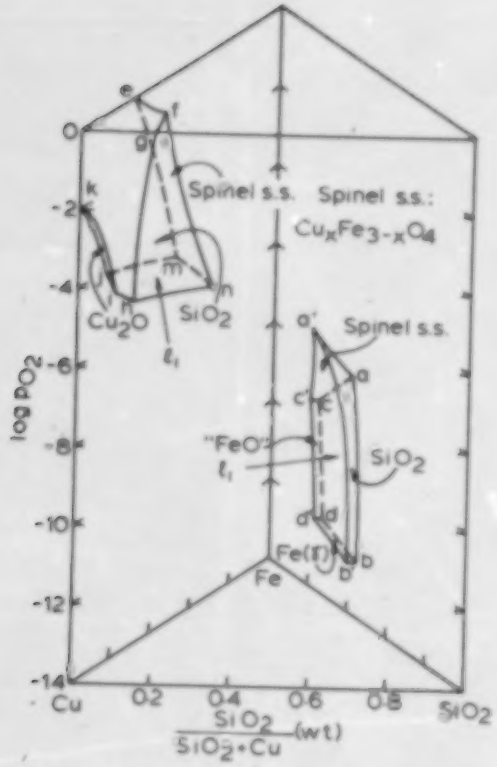

Fig. 1 Stability Diagram of the Cu-Fe-O-SiO_2 System at 1200°C[1].

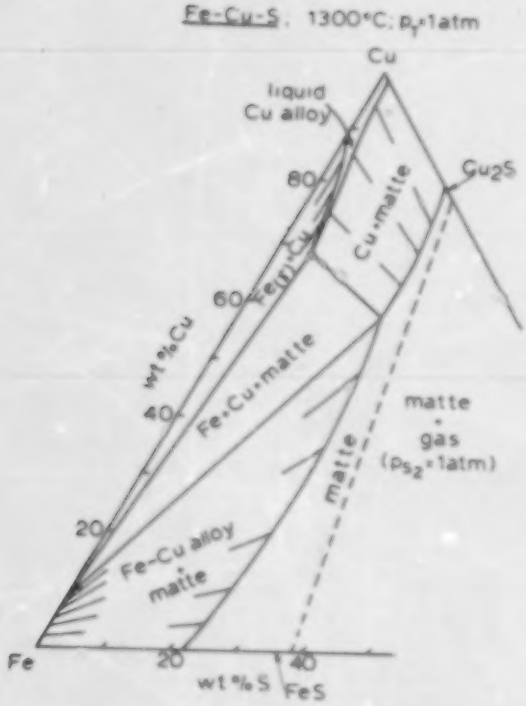

Fig. 2 The Cu-Fe-S System at 1300°C[3].

National Bureau of Standards SP-496, Applications of Phase Diagrams in Metallurgy and Ceramics
Proceedings of Workshop held at NBS, Gaithersburg, Md., January 10-12, 1977

Needs for Phase Diagram Information in Non-Ferrous Industry

P. R. Ammann[1]

Kennecott Copper Corporation
Ledgemont Laboratory
Lexington, Massachusetts

Introduction

Professor Elliott, members of the panel, and ladies and gentlemen. I am pleased to have an opportunity to convey to you some of our thoughts on the future of the non-ferrous industry and the need for and use of fundamental data.

A large fraction of primary copper, nickel, cobalt, zinc, etc. is produced by the conversion of intermediate concentrates into metal through pyrometallurgical processes. In these processes, the sulfides are heated and reacted with air to produce sulfur-dioxide-bearing offgases and molten metal or metal intermediates and molten slag wastes. For many years, copper, nickel, cobalt (as well as lead and zinc) have been produced in smelters. In the modern plants, as well as in their age-old predecessors, the key to the pyrometallurgical process is the highly favorable separation of the desirable metal from the undesirable molten wastes (e.g., iron).

Now the non-ferrous metal industry, particularly in the United States, is in a state of change. Both economic and environmental pressures have reduced the profitability of the copper and nickel businesses, as well as those of other non-ferrous industries. These pressures pose both a threat to the health of these businesses and a challenge to these industries to continue to provide the world needs for these metals. The future health of primary metals production lies in a technological base for improving present operations and for innovation in the areas of metal production such that a new generation of processes will develop. Such an evolution could be akin to the transition from the vacuum tube computers of twenty-years ago to solid-state systems we know today.

In the next few minutes I would like to make some remarks on the use of phase diagram information from the point of view of Industrial Research and Development. The metals industry may respond to economic and environmental pressures in several ways.

---

[1] Paper given by Dr. P. B. Crimes, Ledgemont Laboratory

SLIDE 1

One response is to improve the performance and operability of existing plants. In such systems, the process metallurgy is known. But, improvements in the systems, such as:

(1) closer process control,
(2) higher metal throughput,
(3) minimization of gaseous and other waste products, and
(4) improved quality of the product,

may require a better definition of the process thermodynamics.

SLIDE 2

The second alternative is to replace conventional process plants by new processes which will lower operating costs. Examples of this approach are:

(1) the development of the Outokompu Flash Furnace, the Noranda Direct Converting and Mitsubishi Continuous Smelting Processes to replace the reverberatory furnace-converter system for making copper; and
(2) the development of an alternative process to the Hall Cell for making aluminum.

The substitute processes derive their advantage largely for advances in engineering design. However, more sophisticated processes reach their maximum potential from a complete definition of the thermodynamics in each step.

SLIDE 3

A third direction for R & D is to combine with existing or future processes the capability for the recovery of byproduct metals. Cobalt, and often copper, are byproducts of treating nickel sulfide concentrates. Gold and silver are profitable byproducts of producing copper from copper sulfide concentrates. But there are other metals, such as molybdenum and iron, which could be profitably produced from the non-ferrous smelters as well.

SLIDE 4

Fourth, plants which smelt metal sulfide concentrates generate wastes, such as slags and dusts from offgas streams. These materials contain metal values, which because of present technology limitations, are discarded without being recovered.

SLIDE 5 Finally, metals may derive from new raw materials. For example, many companies now look at deep sea nodules as a source for nickel, copper, cobalt, and perhaps even manganese. Although much published information on processing sea nodules describes hydrometallurgical processes, at least one process has been described by Inco in which the dried material is smelted to separate the small mass of metals from the bulk of the nodule material.

Let us now look at the role of the phase diagram in a couple of copper and nickel smelting processes.

(1) Copper Smelting.

Copper sulfide concentrates consist of chalcopyrite, $CuFeS_2$ and pyrite, FeS_2. These sulfides are oxidized and heated to 1250°C where a molten iron-copper sulfide matte is produced. Sulfur dioxide gas is generated and iron oxide is fluxed with silica to make a molten slag
SLIDE 6 which is a waste product. These reactions are described simply in the next slide. The molten copper-iron sulfide matte is denser than, and completely immiscible with, the iron silicate which thus permits separation of copper from most of the iron. Depending upon composition, mattes are molten above 1000 to 1100°C. Slags, on the other hand, are more complex, containing in addition to FeO and SiO_2, Fe_2O_3, CaO, Al_2O_3, Na_2O and MgO. Fayalite ($2FeO \cdot SiO_2$), the principle slag former has a stated melting point of 1205°C, but higher slag temperatures are used in furnaces.

SLIDE 7 The smelting process is described by the two-phase diagrams in the next slide. A typical copper concentrate contains about 30 per cent copper, 30 per cent sulfur and 40 per cent iron, as shown at the center of the phase diagram on the right. When the sulfide is heated to say 1000°C and oxidized, the sulfide phase becomes enriched in copper, as shown by the red line on the diagram. As the iron is oxidized to FeO, silica is added to produce a low melting, low density slag phase which is immiscible with the sulfide phase. A range of acceptable slag compositions is shown in the $FeO-Fe_2O_3-SiO_2$ diagram to the left of the slide. When the iron is completely oxidized, the sulfide or matte phase will consist essentially of Cu_2S, plus small amounts of valuable metals such as gold, silver and

trace amounts of impurities such as bismuth, and arsenic. In the final step of the process, the Cu_2S is oxidized with air to blister copper and SO_2.

The overall process may be carried out in one step (and one vessel), or it may be carried out in several steps.

An example of improving existing operations is related to the smelting of the copper sulfide concentrates in reverberatory furnaces. These furnaces are long - over 100 feet - and have a relatively wide but shallow bath of about 5 feet, as shown in this side and top view. In routine operation, sections of the bath solidify, reducing the effective volume of the furnace bath and consequently, the performance of the equipment. In a study described by Kim et al, at the 1976 Annual AIME Meeting, a determination was made of the cause of the formation of these solid materials. Samples were taken throughout the furnace to establish composition profiles and they showed extensive buildups in the furnace. The solids were found to be composed of FeO, SiO_2, Al_2O_3, and Cr_2O_3. An $FeO \cdot (Al\ Cr)_2O_3$ (aluminum chromite) phase crystallized in the slag bath as shown here. The study showed that by better control over

SLIDE 8

SLIDE 9

SLIDE 10

(1) the amount of chrome-alumina in the furnace,
(2) the bath temperature, and
(3) the depth of the slag,

the rate of bottom buildup could be reduced and, therefore, the productivity and performance of the furnace enhanced.

For this slag system, only part of the phase equilibria is known but with this limited information, some improvements could still be made in future operations. However, if the complete system equilibrium were known, it might be possible to make even further improvements in productivity.

As an example of new process technology, the reverberatory furnace just described is being replaced by new copper smelting processes, for example, the Noranda Process. Copper sulfide concentrates are oxidized in one step to crude copper, as shown in the diagram. Such a one-step conversion produces a highly oxidized slag which contains 5 to 10 per

SLIDE 11

cent copper - a significant fraction of the feed copper. To recover this copper, the slag is slow-cooled from 1200°C to 550°C under controlled conditions, in which oxidized copper in the slag is transformed to

SLIDE 12

particles of copper sulfide. These phases are shown in the next slide. The copper values are recovered selectively by milling and flotation; and the copper sulfide is resmelted. This process is an improvement over the conventional reverberatory furnace-converter process. It achieves high copper recovery (better than 95 per cent overall) and acceptable capital and operating costs. In addition, plants can be designed to capture most of the sulfur dioxide and dust emissions, thus meeting todays environmental standards.

But what about opportunities for byproduct metal recoveries? In the flowsheet shown, copper, gold and silver are recovered from the cooled slag, but the iron and the nickel or molybdenum, which occur in some slags in appreciable concentrations, are not recovered. Furthermor. significant amounts of dusts are carried with the furnace gases and are cooled and recovered. Although the dusts contain copper, they are enriched in other elements such as zinc, lead, and antimony.

SLIDE 13

The Noranda process can be modified to employ an electric furnace for recovery of copper from slags. The costs are competitive with the slag milling flowsheet shown in the previous slide, but it allows two other options:

(1) recovery of iron, molybdenum, nickel, cobalt (if any), zinc and lead from the slag by reduction in a second furnace,
(2) dusts containing metal impurities can be processed in the electric furnace. If we are clever enough, a process could be developed for the total recovery of not only copper, gold and silver; but also separation and recovery of other metals such as bismuth, lead, and zinc.

We are exploring a number of process flowsheets, for separating and recovering some of the byproduct and metal impurities, but we find that

the required phase diagrams are not available for defining appropriate process conditions to make the necessary metal separations.

(2) Nickel Smelting.

A large amount of the world's nickel is recovered from sulfide minerals. Copper sulfides usually occur in the same ores, so that when metal sulfides, including iron sulfide, are concentrated from the ore, the copper/nickel ratio may vary from 1/2 or 1/3, to as low as 1/12 (Cobalt is another co-product which occurs in these sulfides, but in smaller concentrations.) The smelting processes involve melting the concentrate at about 1250°C, and then oxidizing the iron and sulfur, (making slag and SO_2 gas), and leaving a nickel-copper sulfide matte which contains less than 2 per cent iron. This first step, making a nickel copper sulfide matte, may be carried out by any of several smelting processes. However, the second step, of separating the nickel-copper values, is the most important.

In one early pyrometallurgical process - the now extinct Orford Process - sodium sulfide was added to the liquid nickel-copper sulfide matte. The copper sulfide would selectively dissolve in the sodium sulfide and the lighter copper-sodium and heavier nickel phases would separate upon cooling.

SLIDE 14

This process was replaced by Inco, at Copper Cliff, Canada, in 1948, with a slow-cooling process in which Cu_2S and Ni_3S_2 are selectively formed. Matte from the converter is poured into large pits where it cools slowly over about 3 days. When the temperature reaches about 1700°F, Cu_2S crystallizes first, and when the temperature reaches about 1300°F, a copper/nickel alloy precipitates. Finally at 1070°F, Ni_3S_2 crystals form. The advantage of this process is that the solubility of nickel in the Cu_2S is low (less than 0.5 per cent) and copper in the nickel sulfide is also relatively low. Although Ni_3S_2 contains 6 per cent copper at 1067°F, in slow cooling to 700°F, copper is rejected

SLIDE 15

resulting in a phase containing less than 0.5 per cent copper. This

micrograph shows the resulting phases. At the Inco Copper Cliff plant, the cooled matte is crushed, milled to a fine size and the phases separated by flotation.

This process is probably a classic example of the use of phase equilibria for the primary production of non-ferrous metals. Through the knowledge of the phase behavior of the copper-nickel-sulfur system, Inco can achieve both high recovery and high separation of the copper and nickel values.

I would now like to mention briefly some future needs for Phase Diagram information. The extensive information published on binary and ternary systems is used in developing new processes for primary metal production, and also for processes to recover byproduct metals and for processing wastes, such as flue dusts. To predict specific needs for phase diagram information in the future is to crystal ball the directions industry will take in the future to produce the primary metals. And this, of course, is a chancy business.

SLIDE 16

Let me suggest generally that the quaternary systems need more definition. In particular, we have been looking at a process to extract molybdenum from copper smelting slags. It involves the reduction of molybdenum from slags into a sulfide phase. There is only limited information on the metallic-sulfide phase, Mo-Fe-Cu-S, as shown in the slide. Our researchers have attempted to obtain some data on this system. Of interest also is the slag phase, consisting principally of Mo-Fe-SiO_2-oxygen. (As I noted earlier, such slags usually contain other important components such as MgO, Al_2O_3, CaO, which have an impact on equilibria and melting points.) After the molybdenum and copper have been extracted from the slag into the metal sulfide, it is necessary to separate and recover the molybdenum and copper values. Although this step can be achieved by conventional hydrometallurgical processes, we have been intrigued by Inco's slow-cooling process, just described as a possible alternative route.

The recovery of byproduct nickel and cobalt from certain smelter slags is analogous to the molybdenum system, and should be important in

the future. In addition, the smelting of nickel sulfide concentrates will probably undergo some important changes in the near future in order to meet environmental requirements and to accommodate new ores. Therefore, I see a need for further information on this system.

Another system of interest includes bismuth and lead in copper smelting. The need is two-fold: (1) to control the level of these impurities in the copper product, and (2) to devise processes for separating and recovering these metals. At present, there is a lack of pertinent information on the phase relationships in these complex systems. I might just add another area of importance - the presence of trace elements in copper products. Small amounts of impurities such as As, Bi, Te, S, Sb, Pb, etc., can affect the properties of copper product markedly and additional information on these systems is also needed.

Summary

To summarize; in the future, pyrometallurgical processes for producing copper and nickel will become more efficient and sophisticated. A sound thermodynamic base is essential for smelting processes to meet our future needs in these areas. In these past few minutes I have tried to show how phase diagrams are used and to suggest some future directions for equilibria studies in commercially important systems.

OPPORTUNITIES FOR R & D IN NON-FERROUS METAL PRODUCTION

1. IMPROVE PERFORMANCE AND OPERABILITY OF EXISTING PROCESSES
2. DEVELOP NEW PROCESSES WITH LOWER COSTS
3. INCREASE RECOVERY OF BY-PRODUCT METALS
4. PROCESS WASTE STREAMS FOR SAFE DISCARD OR FOR METAL PRODUCTION
5. TREAT NEW RAW MATERIALS

SLIDES 1 to 5

Description of Opportunities for R&D in Non-Ferrous Metal Industry

PRINCIPLE COPPER SMELTING REACTIONS

$$2CuFeS_2 + 2\tfrac{1}{2}O_2 + SiO_2 = Cu_2S \cdot FeS + FeO \cdot SiO_2 + 2SO_2$$

$$FeS_2 + 2\tfrac{1}{2}O_2 + SiO_2 = FeO \cdot SiO_2 + 2SO_2$$

Slide 6

Principle Oxidation Reactions for Smelting Copper Concentrates

1417

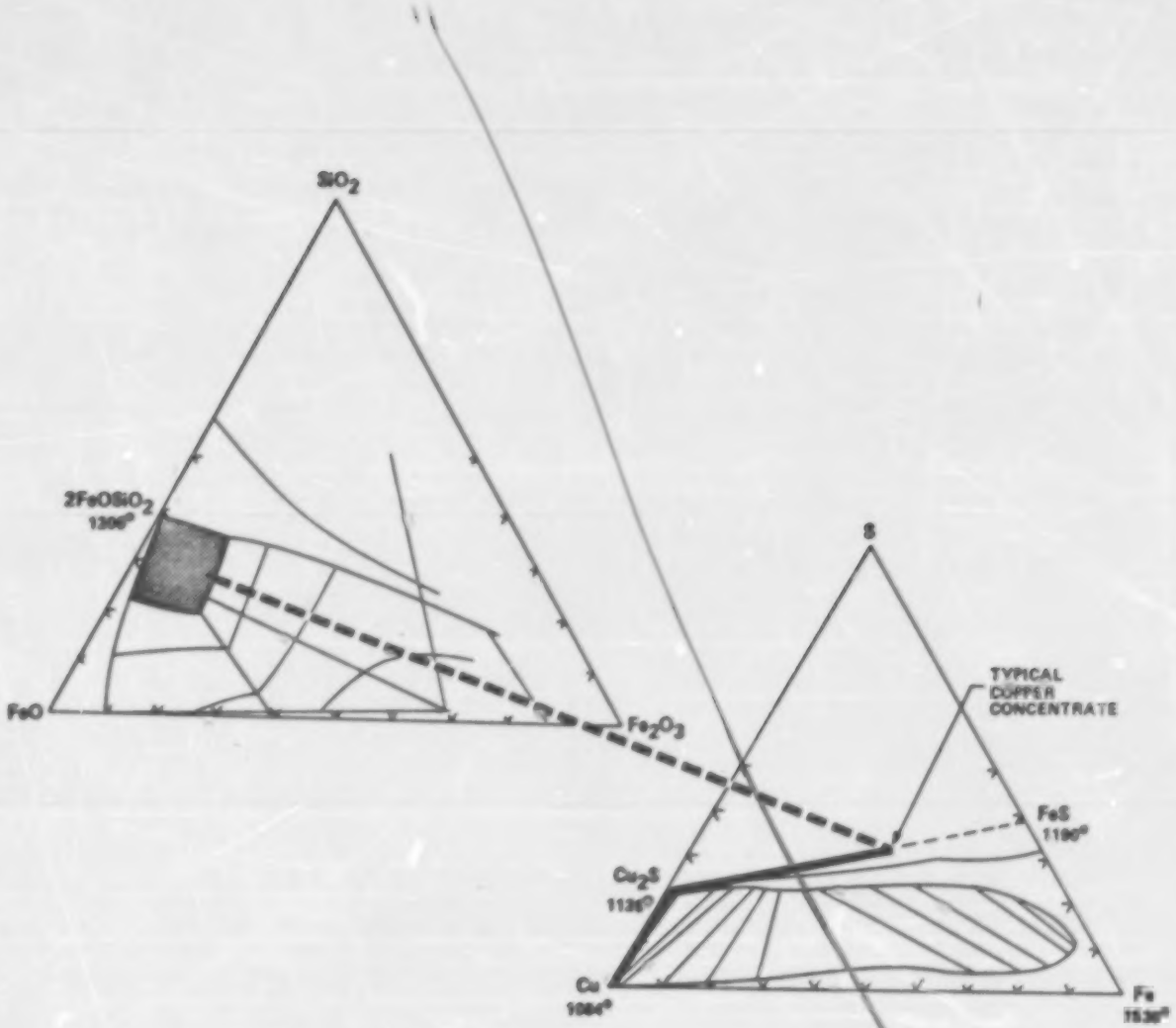

Slide 7

PRA1677

Key Phase Diagrams for Smelting Copper Concentrates Showing Formation of Matte/Copper and Slag Phases

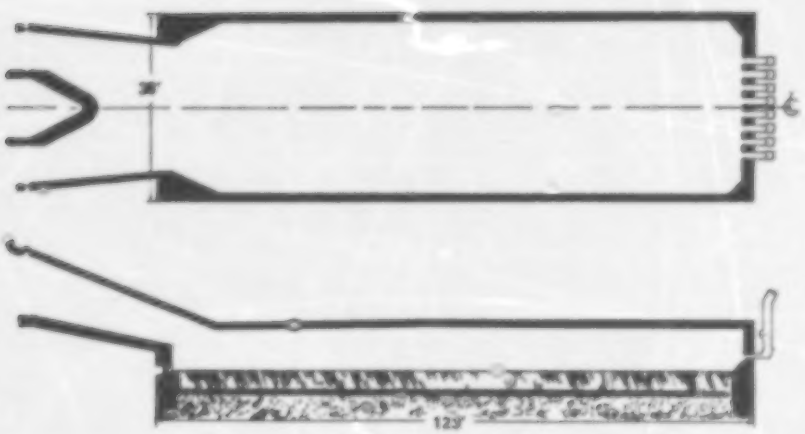

PLAN – REVERBERATORY FURNACE

Slide 8

Plan and Side Views for Typical Reverberatory Furnace Used For Smelting Copper Concentrates

1419

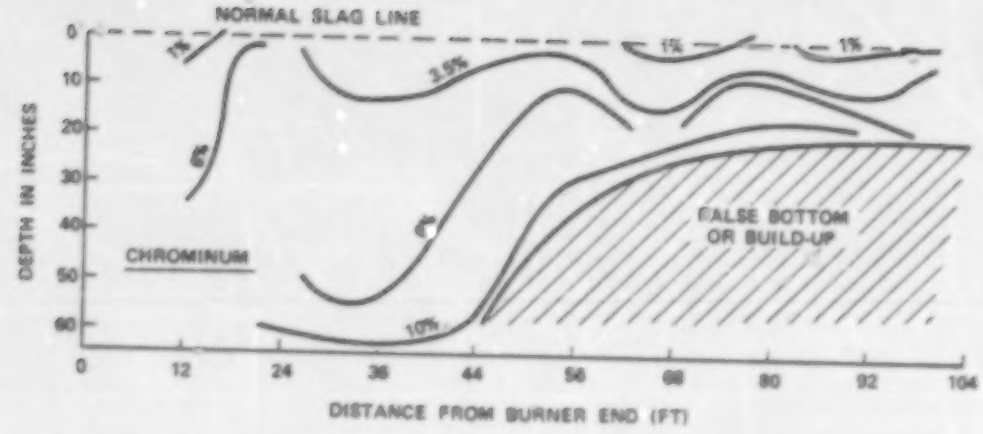

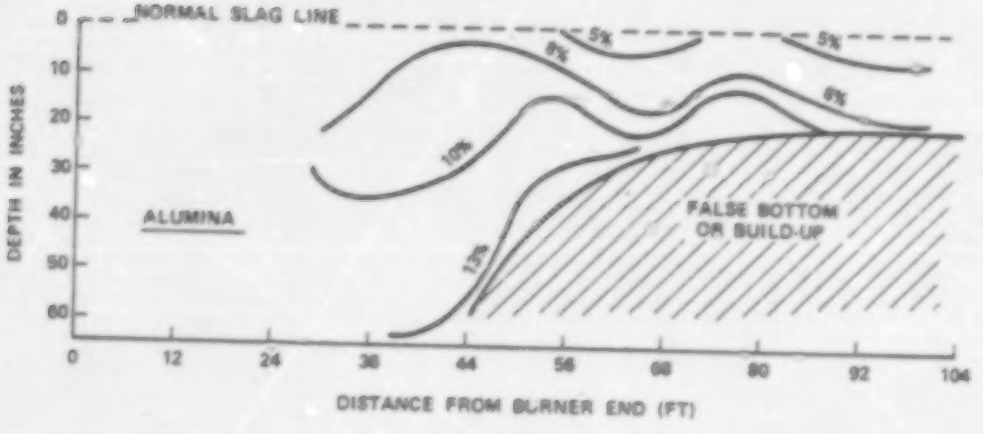

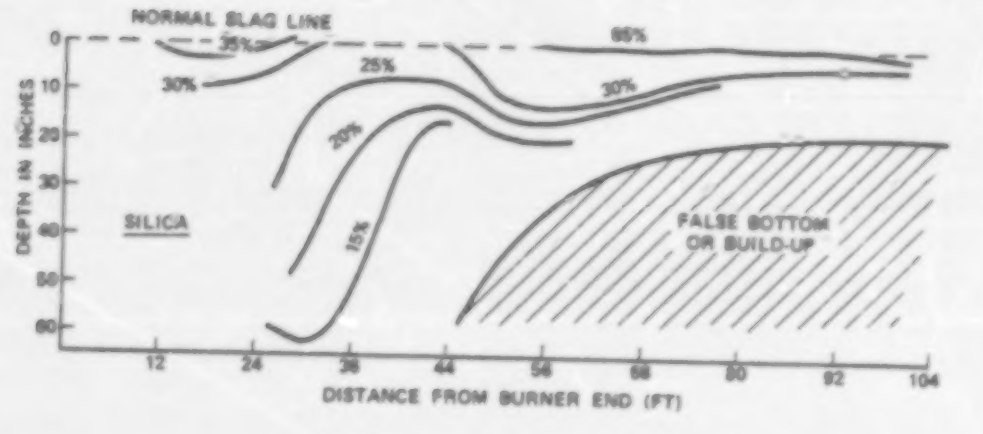

CONCENTRATION PROFILE OF SLAG

Slide 9

Concentration Profiles for Chromium, Alumina and Silica in Reverberatory Furnace

MICROGRAPH OF BOTTOM LAYER OF SLAG

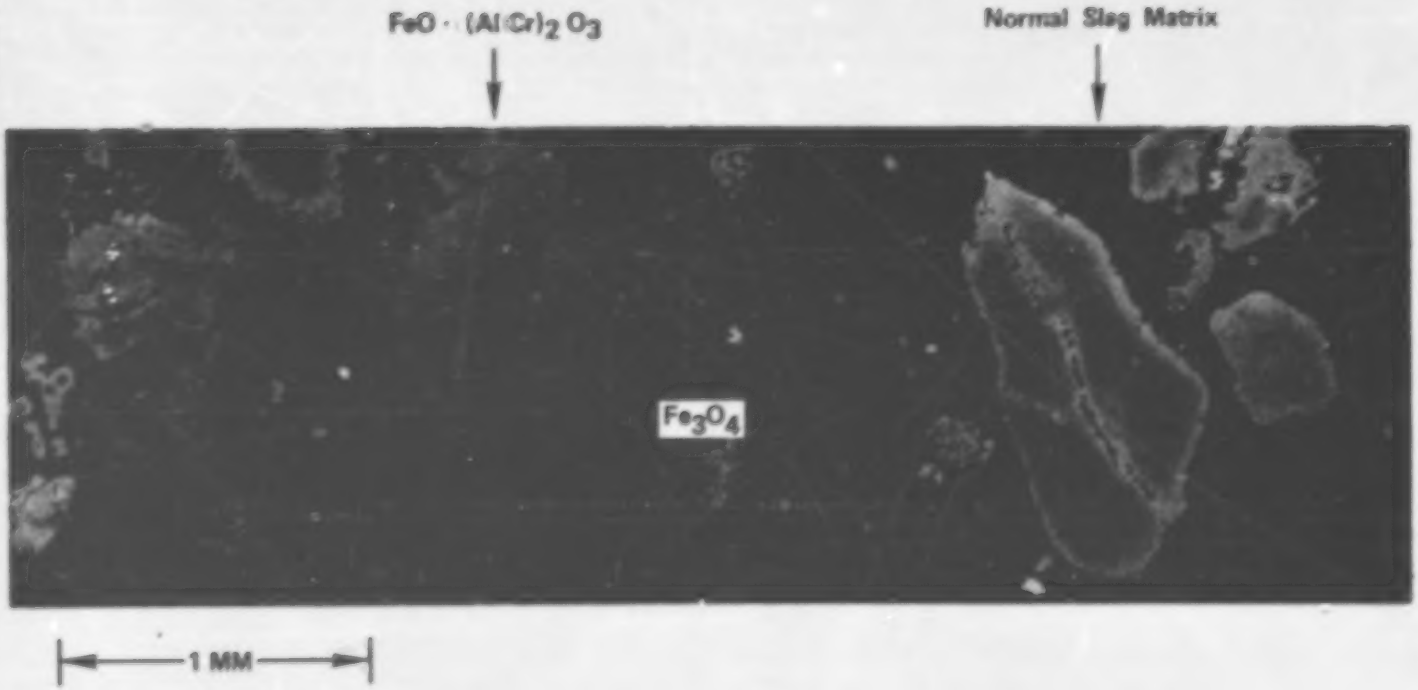

Slide 10

Photomicrograph Showing Major Phases in Reverberatory Furnace Bottom
(Ref. Kim, J.J. et al, Int. Symposium on Copper Extraction & Refining, AIME, Feb. 22-26, 1976, pp 139-153)

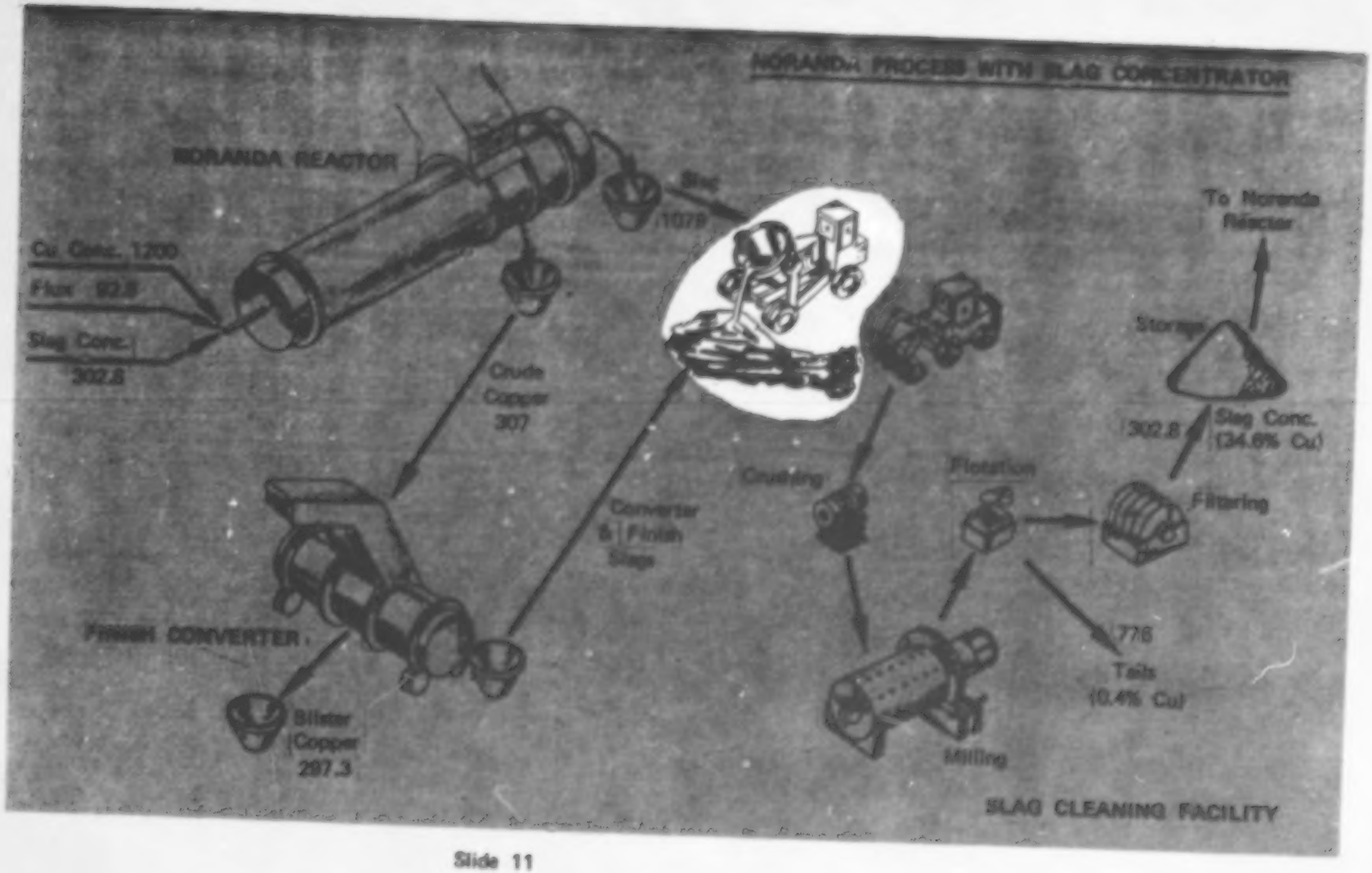

Slide 11

Schematic Diagram of Noranda Process Showing Cooling of Slag as Important Process Step

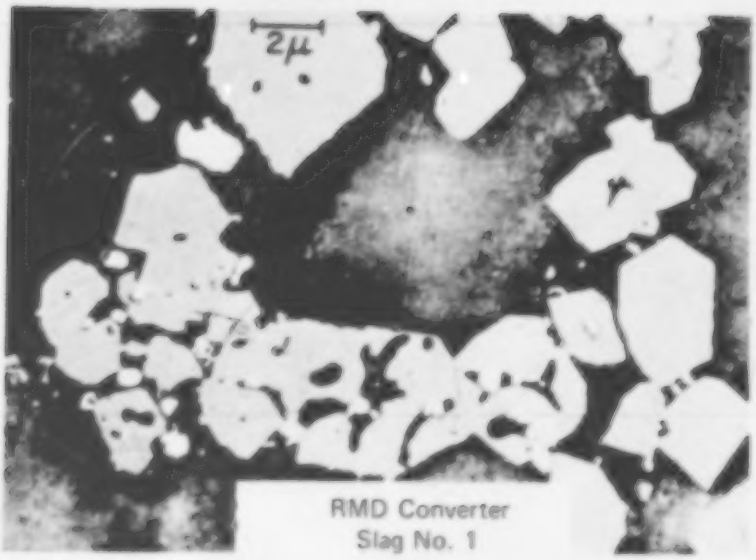

Slide 12

Photomicrograph Showing Copper and Magnetite Phases in Cooled Converter Slag

1424

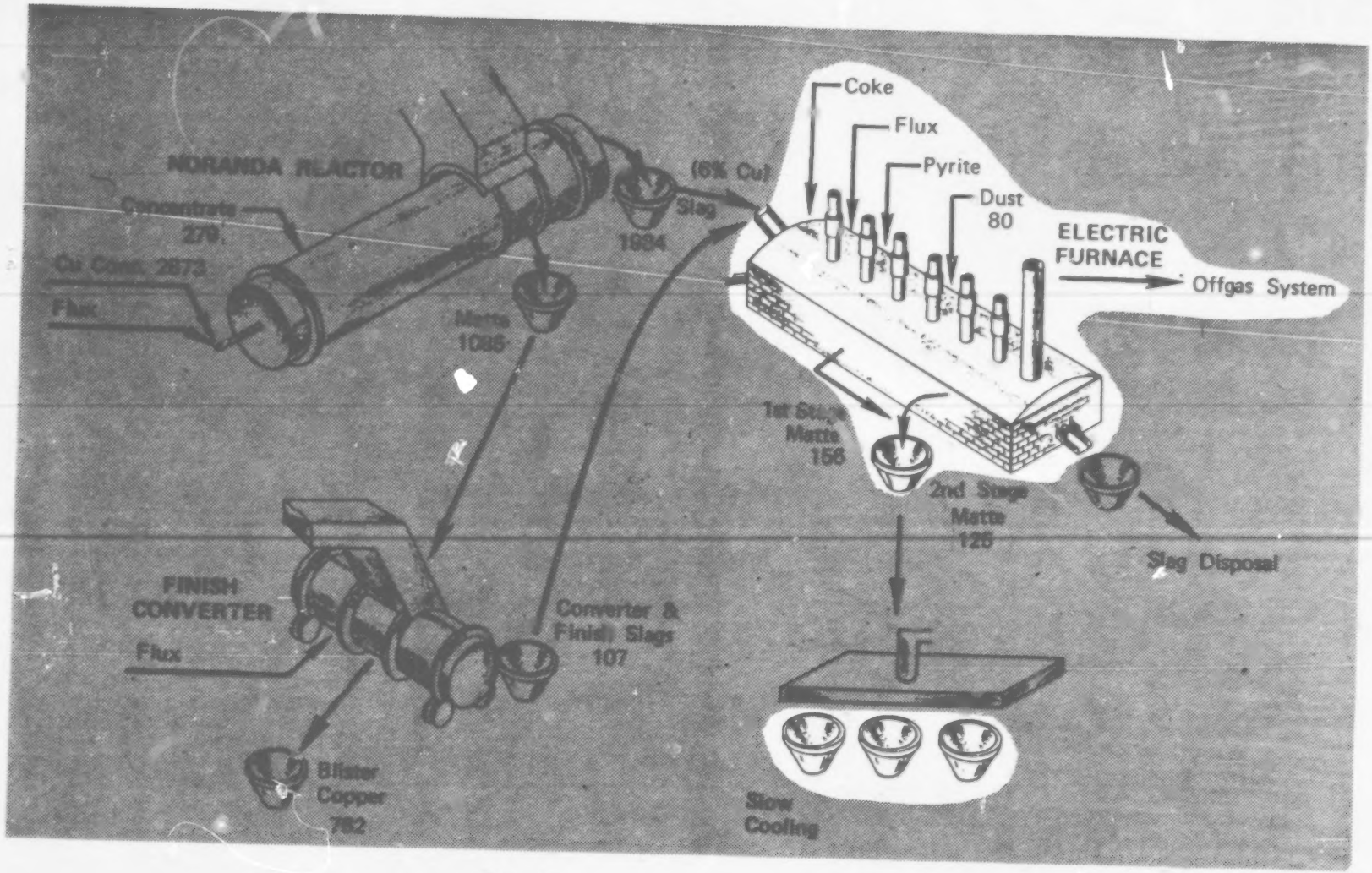

Slide 13

Schematic Diagram Showing Electric Furnace Slag Cleaning for Noranda Process

1349

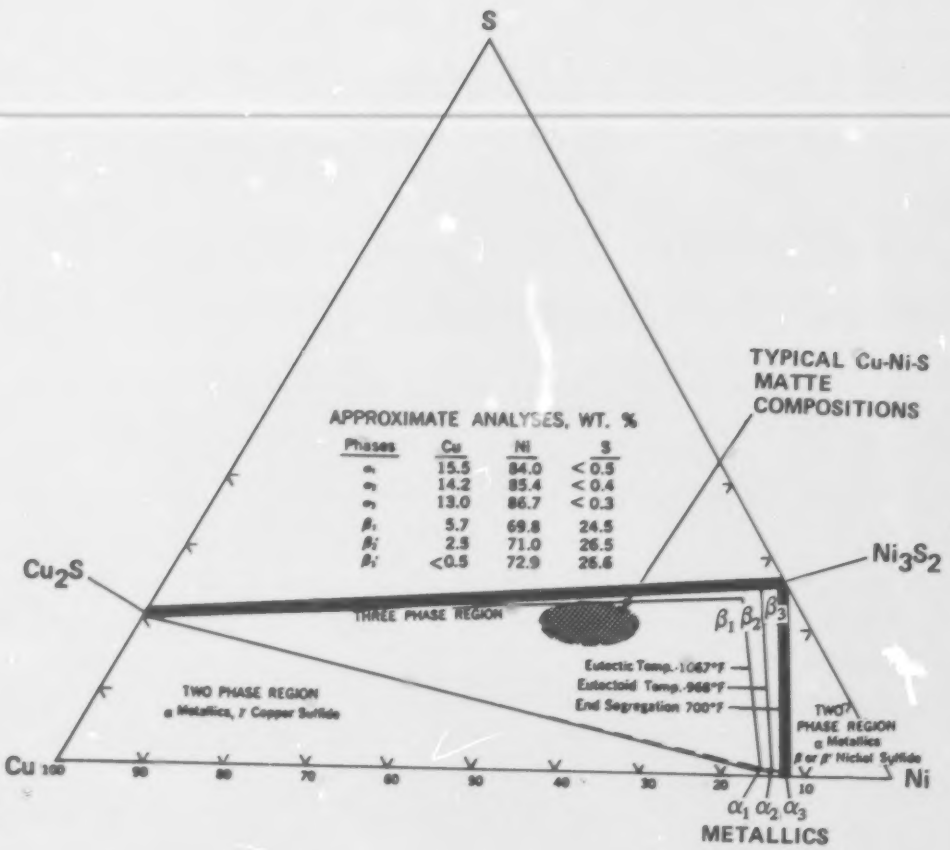

Slide 14

Diagram Showing the Phase Separation for Copper – Nickel Sulfide Matte as a Function of Temperature and Composition (Ref. Boldt, J.R. & Queneau, P., "The Winning of Nickel," D. Van Nostrand Company, Inc., Princeton, N.J., p. 278)

1427

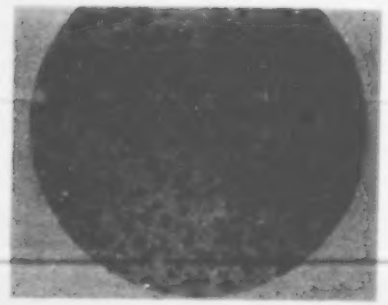

QUENCHED MATTE

SLOW COOLED MATTE

Ref: The Winning of Nickel

Slide 15

Photomicrograph Showing Effect of Cooling Rate on Grain Size for Copper and Nickel Sulfides (Ref. Boldt, J.R. & Queneau, P., "The Winning of Nickel," D. Van Nostrand Company, Inc., Princeton, N.J., p. 276)

SYSTEMS OF POSSIBLE FUTURE INTEREST

- Mo - Fe - Cu - S
  Mo - Fe - SiO_2 - O
- Bi - Pb - Cu - Fe - S - (O)
- Cu - Fe - SiO_2 - O - (S)
- Ni(Co) - Fe - SiO_2 - O - (S)

Slide 16

Metallurgical Systems of Future Interest

DISCUSSION

J. F. Elliott - Thank you, Peter, for your interesting remarks. I might add that phase diagrams often are equivalent to road maps for the process metallurgist. He uses them to find his way through the equivalent of unfamiliar terrain.

Bruce Connor - I wish to thank Dr. Crimes for his excellent review of important aspects of copper and nickel smelting. I would like to add that we have a lot of other phase equilibria that need to be understood in the handling of recycling of secondary copper and nickel alloys. Because precious metals, such as iridium, platinum, pladium, gold and silver are obtained when processing copper and nickel ores, we also have need for more information on the binary, ternary and quaternary phase diagrams of these metals.

J. F. Elliott - It might be noted that nonferrous metals producers usually have to contend with virtually all of the metals and many of the nonmetals in the periodic table. Accordingly, they face great complexity in their systems.

P. Crimes - It may be of interest to the audience to know that we have made considerable progress in understanding kinetic and mass-transfer aspects of our systems, and now we are greatly in need of more and better information on equilibrium relationships.

National Bureau of Standards SP-496, Applications of Phase Diagrams in Metallurgy and Ceramics
Proceedings of Workshop held at NBS, Gaithersburg, Md., January 10-12, 1977

Primary Metals Production

Dr. H. R. Larson
ASARCO Incorporated
Central Research Department

Asarco is a large, diverse, primary non-ferrous company involved among other things in the smelting of Cu, Pb, Zn and precious metals. We are largely a custom smelter treating a wide variety of materials. This fact has an important effect on our outlook and on some of the remarks I will make today. Our metallurgy is extremely complex. We have many materials flowing between plants i.e., from Cu smelter to Pb smelter, etc. In addition to the primary metals we recover a large array of by-product elements which are very important to us. Several of our plants have what must be considered high impurity loads. This adds to the complexity.

What is our interest in Phase Diagrams?

We are of course interested in anything that improves our understanding of the processes used in our plants. I think however that there are a few areas of practical considerations where phase diagrams can be especially important. (Slide 1) First, factors controlling or affecting metal losses to slag are highly important. Our operating revenues are derived from a smelting charge. Obviously, metal losses reduce profitability. Secondly, we are interested in multicomponent multiphase equilibria. The distribution of elements between phases during smelting and pyrometallurgical refining operations is of importance. In particular, the distribution of impurity, by-product elements between phases is of interest. Third, a good deal of our work at the Research Department involves the theoretical evaluation of process alternatives. This can range anywhere from minor changes in an existing process to consideration of a new continuous smelting process. In any of these considerations phase diagrams can be of particular use when they are available. As an example, I could point to the published work of Queneau and Schuhmann on the application of the Q-S process to lead smelting.

Let me start off by making the point that our use of phase diagrams is limited. This is primarily because they are not readily available for the systems of most interest to us. We do use the standard compilations of diagrams, such as: 1. Hansen and 2. Elliott and Shunk's supplements, 3. "Phase Diagrams for Ceramicists" by Muan and Osborn, and I tend to also use 4. W. Guertler et.al. "Compendium of Constitutional Ternary Diagrams of Metallic Systems" as translated from German and published by the U. S. Department of Commerce. In general, the real world systems of interest are more complex than those for which diagrams are available. We use the compilations of diagrams to gain insight into our real systems. Often we are interested in multicomponent systems not adequately described in the literature.

Let me digress for a minute and say something about the phases that are of most interest to us. (Slide 2)

Metal

Here we are in the best shape. Good information is available on all binary systems and many ternary systems. Impurity elements of interest are often in relatively dilute solutions. In the case of lead refining, concentrations may be appreciable and available data serves us well. There is a lack of information on impurity interactions. Activity data would be of great use were it available particularly at varying sulfur and oxygen potentials. The formalization of interaction coefficients available for elements dissolved in iron which has been used for many years should be extended to Cu solutions and Pb solutions. In some cases, such as Pb, the activity of alloying elements would be of interest in the liquid state over a fairly large temperature range.

Alloy development work, i.e., brasses, bronzes and solders is hampered by the lack of phase diagrams or their equivalent for multicomponent systems. Here I am talking of conditions where the substitution of a relatively small amount of a substance can have rather profound effects on alloy properties.

Slag

Of all the phases I have listed slags are perhaps the most interesting, most important, most investigated and least well understood. Metal losses to slag are a major concern. The copper content of reverb slag put to waste at a single smelter can easily exceed $1,000,000/yr. The Cu content of throw away slags is nearly as high as the ore that is mined from the earth.

Our slags are essentially $CaO-FeO-SiO_2$, a system well defined in the literature. However, our slag will contain several percent Al_2O_3 and usually more than 1% MgO. The slag may or may not be saturated with magnetite. ZnO is usually present and, in the case of lead slags, can run to levels of 10-15%. Frequently the slags are equilibrated with a sulfur bearing matte and the slag will contain some sulfur. These complex real slags are not adequately described by phase diagrams. A recent monogram by Prof. Diaz sponsored by INCRA "The Thermodynamic Properties of Copper-Slag Systems" has gathered a great deal of information on copper smelting slags. Similar data is not available for lead smelting slags.

Metal losses in slag occur both as solution and as particulate entrainment. The interrelation of composition and slag viscosity and surface tension are of importance.

The operation of conventional lead blast furnaces requires special properties in sinter. Up until the time of fusion the sinter must maintain enough strength to support a column of burden on top of it. A sharp melting point is important. Once smelted it must form a free flowing low viscosity slag. The presence of a mush or partially molten mass can be disastrous. Selection and control of slag composition is important in this regard. Additional phase diagrams could be of help.

Matte

Matte is a phase consisting of several sulfides in solution. In its simplest form we think of matte as a mixture of Cu_2S and FeS. Again this binary is well defined as is the Cu-Fe-S ternary. Real mattes, especially at a custom smelter, will contain PbS, As_2S_3, Sb_2S_3, NiS and in the case of dross reverb matte Na_2S_x.

Added confusion comes from the ability of matte to dissolve magnetite. Activities of impurities in matte are not well known. Interaction data is almost totally non-existent.

Speiss

Speiss is a very interesting phase that is often overlooked. Speiss can be thought of as a solution of metal arsenides. It consists primarily of Cu, Pb, As and Sb. Antimony can substitute fairly freely with As. Several intermetallic compounds are present. I have never seen a Cu-Pb-As-Sb phase diagram. Little data is available on the ternary systems. It would be especially interesting. Speiss can also contain appreciable quantities of Fe, Ni, Sn, In, Ag, S and Bi. Phase diagrams for complex, multicomponent, arsenide systems are non-existent.

Perhaps the most complex thermochemistry occurring anywhere takes place in the dross reverb furnace of a lead smelter. Three phases, bullion, speiss and matte interact with each other with a considerable temperature gradient existing across the three phase bath. The distribution of at least 7 elements between these phases is of importance. These include Pb, Cu, As, S, Sb, Na and Ag.

DISCUSSION

J. F. Elliott - Thank you very much, Dr. Larson. There certainly are a number of interesting phase relationships in the field in which you work.

Reed Howald - Are there good data on the binary systems in the copper-lead-arsenic-antimony system?

Dr. Larson - The binaries are reasonably well known; the ternaries are not. We know essentially nothing about the quaternary system.

PRACTICAL CONSIDERATIONS

1. METAL LOSSES TO SLAG

2. DISTRIBUTION OF ELEMENTS BETWEEN PHASES

3. THEORETICAL BASIS FOR THE EVALUATION OF ALTERNATE TECHNOLOGIES

PHASES

1. METAL

   Blister Cu, Anode Cu, Lead Bullion

2. SLAG

   Reverb Slag, Converter Slag, Blast Furnace Slag

3. MATTE

   Reverb Matte, Converter Matte, Dross Reverb Matte

4. SPEISS

   Dross Reverb Speiss

National Bureau of Standards SP-496, Applications of Phase Diagrams in Metallurgy and Ceramics
Proceedings of Workshop held at NBS, Gaithersburg, Md., January 10-12, 1977

Use of Phase Diagrams in Iron and Steelmaking

Robert D. Pehlke
Department of Materials and Metallurgical Engineering
The University of Michigan, Ann Arbor, MI 48109

INTRODUCTION

Phase diagrams are particularly important in iron and steelmaking. In fact, the processing and products of the iron and steel industry can be described essentially in terms of the iron-carbon phase diagram. Furthermore, the phase relationships, particularly in oxide systems, reflect the refining steps during smelting and converting of iron in the ironmaking and steelmaking processes, respectively.

The iron and steel industry is presented with several processing problems that can be solved in part on the basis of phase diagrams. Consequently, there is a pressing demand for the study of certain phase relationships in iron and steelmaking systems. The following paragraphs summarize current processing and the requirements for solution of several problems, as well as the development of new processing based on these thermochemical relationships.

IRON AND STEELMAKING VIA PHASE RELATIONSHIPS

The phase diagram central to iron and steel production is that for the iron-carbon system, as illustrated in Figure 1. This phase diagram reflects the structural relationships which define the wide variety of cast irons and steels, as reflected in their heat treatment, in terms of the temperature-composition diagram for the iron-carbon system.

Recognizing that phase equilibrium relationships are of direct importance in iron and steelmaking, several challenges in processing as well as the potential for new processes, should be considered in terms of phase relationships. Some examples are presented i the following paragraphs.

EXAMPLES OF PHASE EQUILIBRIA REQUIRED FOR IMPROVED IRON AND STEELMAKING

The iron and steel industry faces a wide variety of challenges in terms of raw materials, energy and the environment. New and improved processes are necessary to meet these needs. In many cases, phase equilibria are required for the development of new technologies. The following examples are representative of instances where phase equilibria must be defined to accomplish these processing advances.

The iron blast furnace must utilize new charge materials, some of which contain higher concentrations of the alkali oxides, K_2O and Na_2O which have recently become a major concern to the ironmaking industry. High slag basicities and high hearth temperatures can result in concentration of these materials, even at relatively low concentrations in the burden, to cause operating problems such as high blast pressures, burden hangup and coke deterioration, and also to reduce lining life by inducing physical abrasion and chemical attack of refractories.

At the present time several blast furnaces in the industry are being monitored with respect to alkali input. However, an opportunity exists for control of these alkali metals in terms of the particular slag and fluxing

agents employed, as well as by controlling gas phase reactions in terms of oxygen potentials, CN reactions, and other aspects of the gas phase composition and temperature profiles in the furnace. It is widely recognized that recirculation with possible concentration of elements exists for alkali metals and also for silicon, in terms of SiO formation. Further studies of these phase equilibria are required.

The iron and steel industry has periodically undergone reviews of substitutes for fluorspar as a flux, particularly in steelmaking. At the present time the supply of fluorspar and its relative cost, as well as an increase in usage with the adoption of the oxygen steelmaking process, require that substitutes be developed. First of all, the fluxing role of fluorspar, particularly in reducing the liquidus temperatures for phases in equilibrium with dicalcium silicate, has not been fully defined, nor has the chemical role of fluorspar in the steelmaking process. In considering a potential shortage of fluorspar, the steel industry has undertaken a wide variety of full scale plant tests on many substitutes. These include the boron-bearing materials colmonite, razorite and borax. Manganese-bearing materials such as manganese ore, cametco briquettes and urucum ore have been studied. Materials relatively high in calcium oxide and containing some iron oxide including red lime, BOP dust mixed with lime, and alaflux have been tested. Aluminum oxide-bearing materials have been employed in plant trials on aluminum dross, bauxite, and topaz as fluxing agents. In addition, the titanium-bearing materials, ilmenite and sorelflux, have also been considered.

A dozen or more specific processing steps for heat treatment, stress relieving, preheating for welding, carburizing, nitriding, solution treating, preparation for forging, and other hot working operations, as well as the development of desired structures, can be described in terms of this basic phase diagram, as shown in Figure 2. Furthermore, the influence on this phase diagram on various elements which commonly appear in steels has been developed for most alloying additions.

The refining of iron and steel is dependent upon the use of a suitable slag system. Normally, basic processing is used in which a slag with relatively high concentrations of calcium oxide (and magnesium oxide) is used to refine the iron-base liquid. Phase relationships in the $CaO-SiO_2-FeO$ system represent a base system for steelmaking; calcium oxide is added as lime flux, silica is a reaction product in the steelmaking process, and iron oxide is developed by oxidation of the iron bath during the conversion of steel. This phase diagram is presented in Figure 3. Of particular interest are the liquidus phase equilibria for dicalcium silicate ($2CaO \cdot SiO_2$), a high melting reaction product which must be fluxed in the steelmaking process.

In the iron blast furnace process, the $CaO-SiO_2-Al_2O_3$ (or $AlO_{1.5}$), system is particularly important. An activity plot for SiO_2 in this system is presented in Figure 4 to emphasize the importance of the interrelationship between activities of components in systems and their phase equilibria. It should be noted that this diagram was developed by John Chipman utilizing both phase equilibra and thermochemical data to calculate the activity of silica in this system, an important chemical parameter in the blast furnace process.

The fact that plant tests have been conducted indicates the seriousness of the problem, as well as the commitment of the industry to adoption of new fluxing materials. In all cases, phase relationship information is lacking and sorely needed.

Tramp elements represent a serious threat to the economical production of many high quality steel products. Arsenic and antimony which are present in some iron ores, and copper, nickel and tin which result from the use of relatively low quality scrap present challenges to current processes. These elements have a deleterious influence on product properties and service performance, and are not removed in the standard practices for iron or steelmaking. A knowledge of phase equilibria is required to develop control of tramp elements. This question can be presented in a different manner. The result is to be a processing step in which these tramp elements are selectively removed from the iron-base product. The processing systems to be used, which typically are specified, in this case remain to be defined.

Finally, an understanding of phase equilibrium relationships is needed for control of sulfur and phosphorus, the bane of a steelmaker's existence. A number of studies have been made of sulfur distribution between metal and slag under a wide variety of conditions. Unfortunately, in many instances the oxygen potential was undefined and the studies are of questionable value in terms of development of new processing systems to improve sulfur removal. A substantial amount of capital investment and operating costs are now being directed toward sulfur control. These industrial processing steps could be

enhanced by a better understanding of the role of oxygen potential as well as the phase distribution relationships for sulfur between slag, metal, and gas under a wide variety of composition and temperature conditions. Phase equilibria in liquid and solid iron are required for sulfides and oxy-sulfides of various alloying elements and refining additives.

Phosphorus has not presented a major problem for western hemisphere steelmaking in that for the most part we have been blessed by relatively low phosphorus burden materials. However, as new iron-steelmaking processing systems are being adopted worldwide, e.g. the direct reduction-electric furnace melting system, the role of phosphorus has taken on a new aspect. First of all, phosphate phase equilibria in normal iron and steelmaking slags have not been thoroughly defined. Furthermore, pre-reduced iron ores containing phosphates can be greatly improved if the phosphorus remains as phosphate and is not reduced during direct reduction processing. An improvement in quality and development of control measures to optimize direct reduction processing of iron ore for use in subsequent steelmaking operations requires additional information on the phase equilibria which prevail during phosphate reduction.

The few examples presented here are only illustrative of the wide variety of challenges and potential improvement in iron and steelmaking processing which can be accomplished through a knowledge of phase equilibria. The further spinoff of such knowledge in areas of nonferrous processing as well as other high temperature processing such as coal conversion and other energy generating systems should also be recognized. One example is the thermochemistry of iron oxides. This system is central to slag formation

in iron and steelmaking, but also is important in magnetic separation of iron concentrates in mineral processing systems, the undesirable formation of high melting magnetite-rich phases in copper concentrate smelting, and the processing of iron-bearing materials in the production of various electronic components. The control of iron oxide chemistries in a wide variety of high temperature chemical reactions is dependent upon a knowledge of the thermochemistry and phase relationships in the iron-oxygen system.

SUMMARY

Phase relationships play a very significant and prominent role in production of iron and steel. These phase relationships are reflected in the variety of products and structures which can be produced, and are particularly important in the processing steps that are utilized to achieve them. The refining of iron and steel as reflected by slag-metal equilibria and the corresponding phase relationships are most important to development of present and future industrial processes.

A wide variety of specific systems relating to present and future iron and steelmaking processes are in need of further investigation and clarification. The interrelationship between thermochemical data and phase diagrams should be recognized and applied to interpret and evaluate phase equilibria, and should be utilized in their deployment as the foundations of process development.

1413

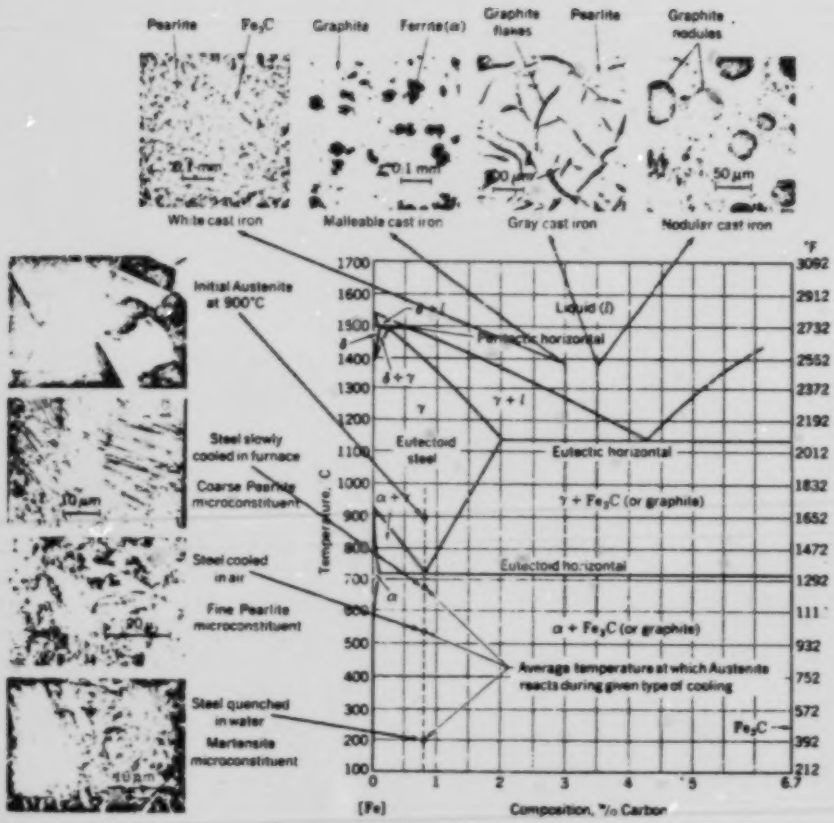

Figure 1. The iron-carbon phase diagram and photomicrographs illustrating the nonequilibrium behavior of a eutectoid steel (0.8 wt% C) and of typical cast irons. (*Photomicrographs from Research Laboratory, U.S. Steel Corporation, Malleable Research and Development Foundation, and International Nickel Company.*) From: Essentials of Materials Science, A.G. Guy, McGraw-Hill, 1976, p. 93.

Basic Guide to Ferrous Metallurgy

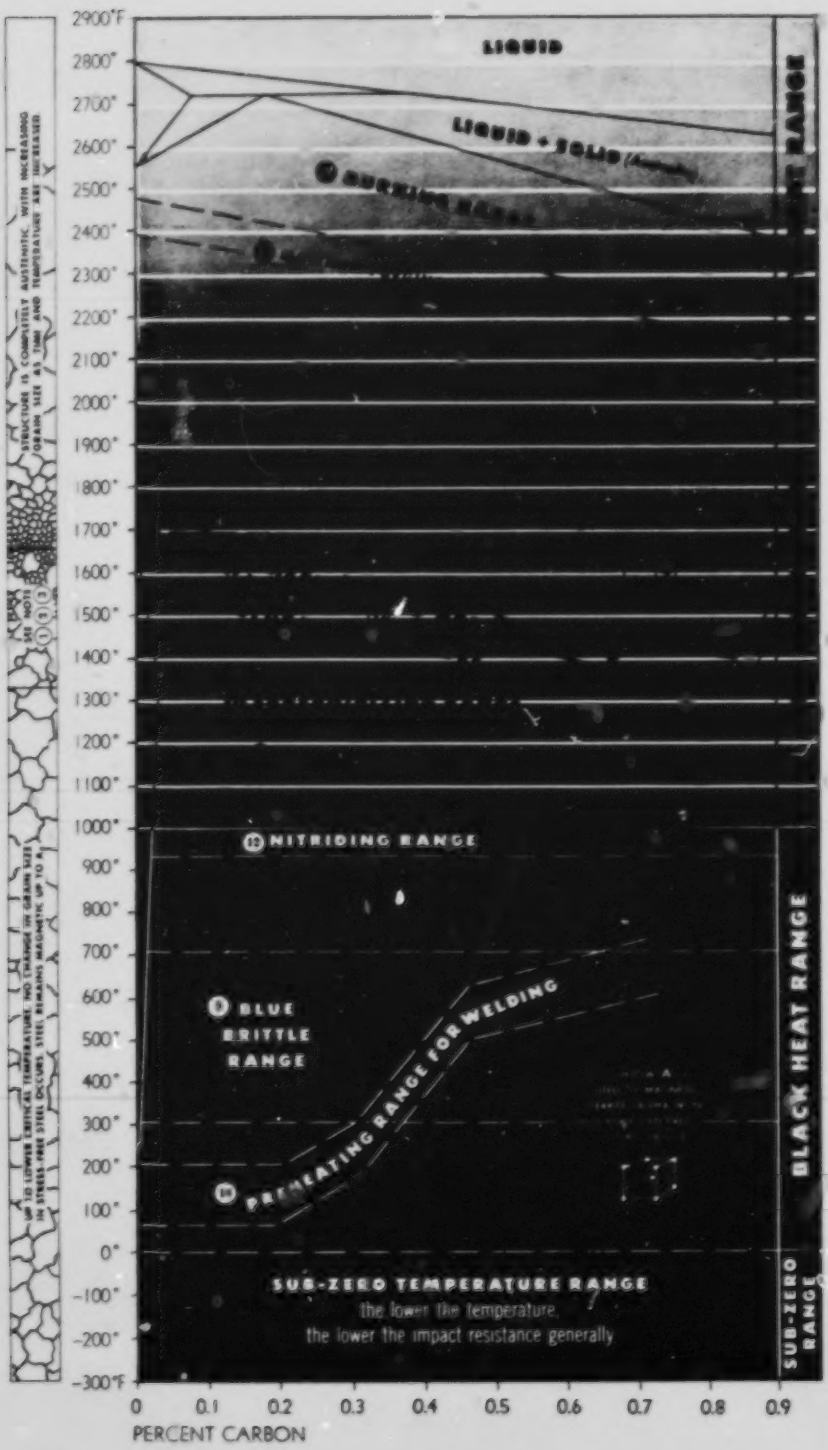

TRANSFORMATION RANGE. In this range steels undergo internal atomic changes which radically affect the properties of the material.

LOWER TRANSFORMATION TEMPERATURE (A$_1$). Termed Ac_1 on heating, Ar_1 on cooling. Below Ac_1 structure ordinarily consists of FERRITE and PEARLITE (see below). On heating through Ac_1 these constituents begin to dissolve in each other to form AUSTENITE (see below) which is non-magnetic. This dissolving action continues on heating through the TRANSFORMATION RANGE until the solid solution is complete at the upper transformation temperature.

UPPER TRANSFORMATION TEMPERATURE (A$_3$). Termed Ac_3 on heating, Ar_3 on cooling. Above this temperature the structure consists wholly of AUSTENITE which coarsens with increasing time and temperature. Upper transformation temperature is lowered as carbon increases to 0.85% (eutectoid point).

FERRITE is practically pure iron (in plain carbon steels) existing below the lower transformation temperature. It is magnetic and has very slight solid solubility for carbon.

PEARLITE is a mechanical mixture of FERRITE and CEMENTITE.

CEMENTITE or IRON CARBIDE is a compound of iron and carbon, Fe_3C.

AUSTENITE is the non-magnetic form of iron and has the power to dissolve carbon and alloying elements.

ANNEALING, frequently referred to as FULL ANNEALING, consists of heating steels to slightly above Ac_3, holding for AUSTENITE to form, then *slowly* cooling in order to produce small grain size, softness, good ductility and other desirable properties. On cooling slowly the AUSTENITE transforms to FERRITE and PEARLITE.

NORMALIZING consists of heating steels to slightly above Ac_3, holding for AUSTENITE to form, then followed by cooling (in still air). On cooling, AUSTENITE transforms giving somewhat higher strength and hardness and slightly less ductility than in annealing.

FORGING RANGE extends to several hundred degrees above the UPPER TRANSFORMATION TEMPERATURE.

BURNING RANGE is above the FORGING RANGE. Burned steel is ruined and *cannot be cured* except by remelting.

STRESS RELIEVING consists of heating to a point below the LOWER TRANSFORMATION TEMPERATURE, A_1, holding for a sufficiently long period to relieve locked-up stresses, then slowly cooling. This process is sometimes called PROCESS ANNEALING.

BLUE BRITTLE RANGE occurs approximately from 300° to 700° F. Peening or working of steels should not be done between these temperatures, since they are more brittle in this range than above or below it.

PREHEATING FOR WELDING is carried out to prevent crack formation. See TEMPIL® PREHEATING CHART for recommended temperature for various steels and non-ferrous metals.

CARBURIZING consists of dissolving carbon into surface of steel by heating to above transformation range in presence of carburizing compounds.

NITRIDING consists of heating certain *special steels* to about 1000°F for long periods in the presence of ammonia gas. Nitrogen is absorbed into the surface to produce extremely hard "skins".

SPHEROIDIZING consists of heating to just below the lower transformation temperature, A_1, for a sufficient length of time to put the CEMENTITE constituent of PEARLITE into globular form. This produces softness and in many cases good machinability.

MARTENSITE is the hardest of the transformation products of AUSTENITE and is formed only on cooling below a certain temperature known as the M_s temperature (about 400° to 600°F for carbon steels). Cooling to this temperature must be sufficiently rapid to prevent AUSTENITE from transforming to softer constituents at higher temperatures.

EUTECTOID STEEL contains approximately 0.85% carbon.

FLAKING occurs in many alloy steels and is a defect characterized by localized micro-cracking and "flake-like" fracturing. It is usually attributed to hydrogen bursts. Cure consists of cycle cooling to at least 600°F before air-cooling.

RIMMING STEEL has not been completely deoxidized and the ingot solidifies with a sound surface ("rim") and a core portion containing blowholes which are welded in subsequent hot rolling.

KILLED STEEL has been deoxidized at least sufficiently to solidify without appreciable gas evolution.

SEMI-KILLED STEEL has been partially deoxidized to reduce solidification shrinkage in the ingot.

A SIMPLE RULE. Brinell Hardness divided by two, times 1000, equals approximate Tensile Strength in pounds per square inch. (200 Brinell = 2 × 1000 = approx. 100,000 Tensile Strength, p.s.i.)

Copyright 1954, TEMPIL® HAMILTON BOULEVARD • SOUTH PLAINFIELD, NEW JERSEY 07080

Figure 2. Iron-Carbon phase diagram showing processing temperatures for steels. (Permission is granted by Tempil Corporation to use its Basic Guide to Ferrous Metallurgy in these proceedings).

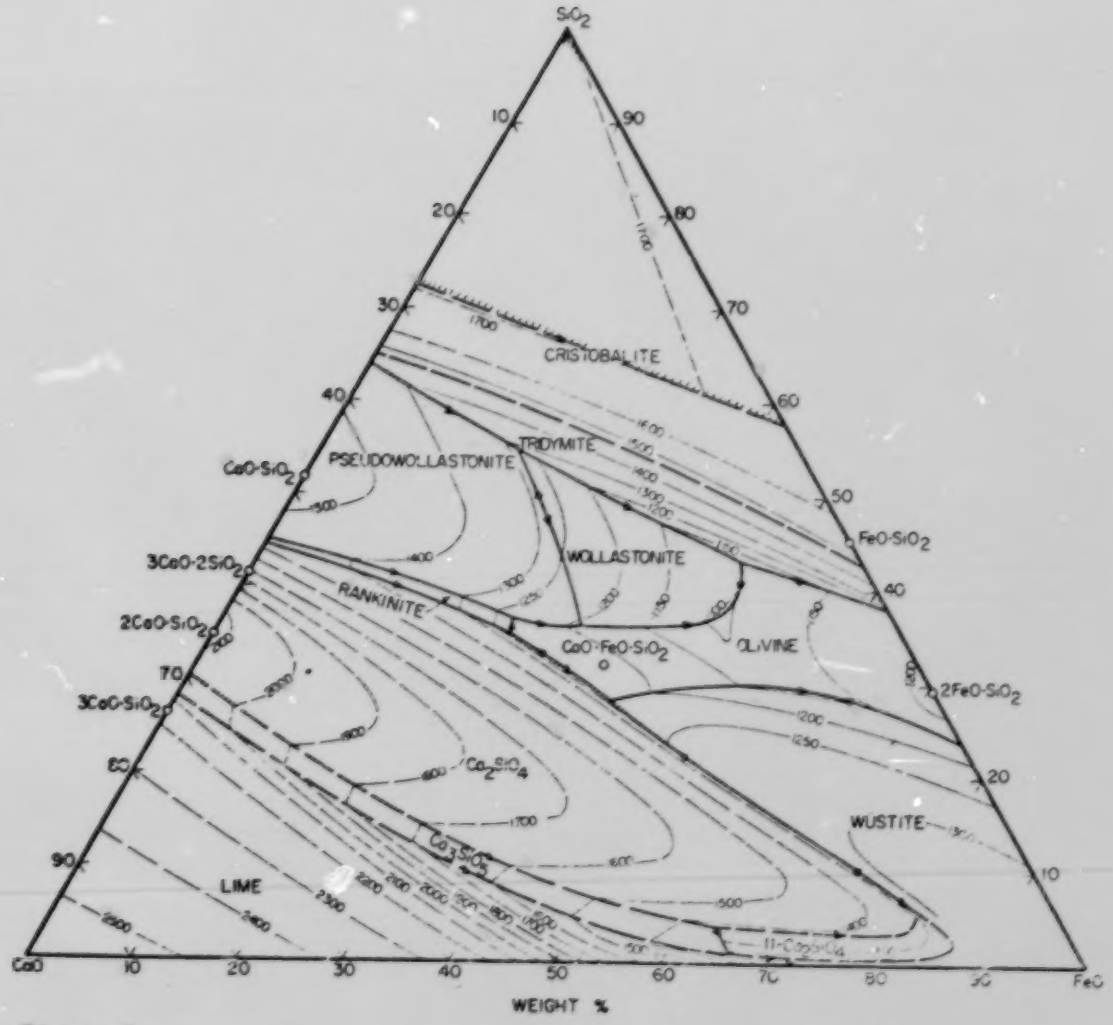

Figure 3. Phase relations in the system CaO-iron oxide-SiO_2 in contact with metallic iron, based mainly on data of Bowen, Schairer, and Posnjak[274] and of Allen and Snow.[275] The system is not ternary. From: Phase Equilibria Among Oxides in Steelmaking, A. Muan and E.F. Osborn, Addison-Wesley, 1965, p. 113.

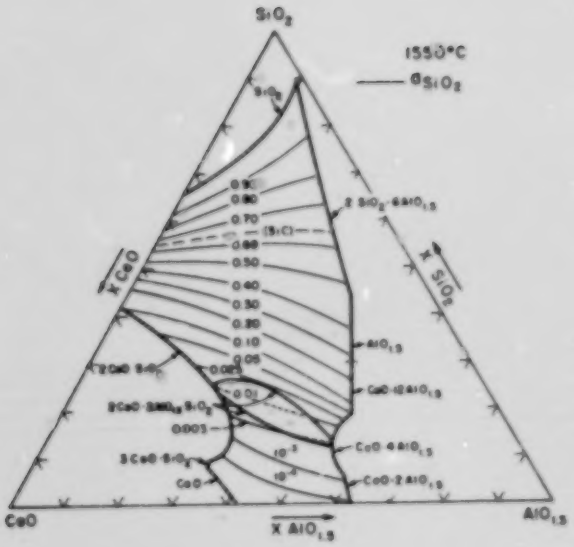

Figure 4. Activity of SiO_2 in SiO_2-CaO-Al_2O_3 slags at 1550°C. From: J. Chipman, Trans. Met. Soc.-AIME, Vol. 233, 1965, p. 419.

1417

DISCUSSION

J. F. Elliott - Thank you, Professor Pehlke, for a very succinct statement concerning some very interesting problems where phase equilibria are important. Would you comment on the possible importance of phase diagrams in problems of solidification of steels?

R. Pehlke - One area where phase relationships are of great importance in determining the properties of steel products is that governing the formation of oxysulfides during solidification. Specifically, the Mn-Fe-O-S system. Another is equilibria between gases and the liquid and solid metal phases during solidification of steels.

Gil Speich - What is the state of our understanding of the phase relationships related to the use of calcium as an agent for deoxidizing and desulfurizing steels?

R. Pehlke - That is a good question because just now I am looking at desulfurization of liquid iron-base alloys. The desulfurization with calcium forms calcium sulfide and other products. The equilibrium constant for the reaction to form calcium sulfide is reasonably well known. Also calcium is very effective as a desulfurizer. An interesting aspect in the use of calcium is that it is a vapor at steelmaking temperatures, but a liquid at temperatures employed in ironmaking and iron foundry operations. This, of course, influences the choice of agents and addition methods when using calcium as a deoxidizer or desulfurizer.

J. F. Elliott - Currently there is a strong interest in the use of rare earths for control of sulfides in steels.

R. Pehlke - Yes, and there is very little information on the phase relationships involved. Work on the use of rare earths for this purpose is in progress at McMaster University in Canada.

D. DeFontaine (excerpted) - I would like to raise a point regarding the size of the task ahead of us if we are to meet the needs of the industrial world. If we take 80 elements as being important, there are 3,000 possible binary systems. In the last 50 years, it appears on the average that we have completed work on one binary a week. There are approximately 50,000 ternaries. Assuming conservatively that at the same tempo of work it takes five times as long to complete a study on a ternary system as it does on a binary, it would be possible to complete 10 a year. This takes us forward 5,000 years. If we go to quaternary systems and assume that by that time our techniques have advanced sufficiently so that we can then do a complete quaternary system in about the same time it now takes us to do a ternary system, it would appear that an additional 100,000 years would be required. This overly simplified statement brings out the enormity of the task before us. It seems to me that we must ask ourselves what are the realistic goals and where do we stop. We must be honest with the industrialists and say that we never really are going to be able to develop all of the information that is needed in the next hundred thousand years.

J. F. Elliott - I feel that the question is highly pertinent. One of the answers is that we must be highly selective as to the systems on which we work because of limitations of funding and of the available manpower. It seems to me that the latter is the more important constraint. We must also be aware that there are limits

to the patience of those who ultimately must pay the bills - the public. We must provide the industrial researcher with background information to assist him to get started in his work even though he may have to develop detailed information on the system that is of immediate interest to him.

Question - Are there common interests in phase relationships across the industrial world where what is known in one area can be used to assist workers in another?

J. F. Elliott - One example that comes readily to mind is the liquid oxide systems CuO-FeO-SiO_2 and CaO-SiO_2-Al_2O_3 which are the bases for many slags that are used in the ferrous and nonferrous systems. Another example is the iron-oxygen system which is very broadly applicable. The answer would be yes.

F. L. Carter - In response to Professor DeFontaine's problem, it appears to me that we should fix our attention on some of the systems of major importance and then use various types of simple and sophisticated chemical and computer models to help us determine the behavior of minor constituents when added to these systems.

P. Crimes - We know quite a bit about a number of basic systems which we have discussed. However, it seems improbable that in the near future we can develop models of sufficient precision to predict in an acceptable way the behavior of all of the components

that might be found in the basic systems that are of interest to process metallurgy. As in the past, we may be forced to continue to rely on empiricism for our predictions.

F. L. Carter - Professor Brewer is not here so I must respond on his behalf. It is absolutely necessary that we develop predictive models because of the scale of our problem, as has been pointed out earlier.

I would like to bring to the panel the questions before the workshop: that is, the questions of the relative importance of depth of coverage versus range of materials covered, and the importance of factors such as high precision, presence of metastable phases, magnetic transitions. Can the panel respond?

R. Pehlke - On the issue of magnetic properties. Magnetic processing is of great importance in the treatment of iron-bearing minerals. With regard to the other questions, it depends on the specific system. One does not really know how much detail one needs on a specific system until one encounters an obstacle. It is only then that one needs detailed information. One has to decide case by case and I find it difficult to generalize on these matters.

H. Larson - I would say that we do not have general information on a number of systems as yet. The calcium-iron-silica system at various potentials of sulfur and oxygen is not well known, even though we know the system quite well at low oxygen pressures.

Other examples are the iron-copper-sulfur system to which arsenic or lead has been added. One can also point out that very little is known about the distribution of elements such as arsenic, antimony and tellurium between the matte and slag phases.

J. F. Elliott - It is unusual to find four liquid phases in a system. In the hearth of a blast furnace there may be bullion, matte speiss and slag - a very complex system which is poorly understood.

P. Crimes - The equilibria involving the distribution of minor elements between phases is indeed of great interest in process metallurgy. Elements such as arsenic, antimony, tellurium, selenium and bismuth, as well as most of the previous metals, are important.

B. Connor - There are four general levels of information that I think are needed in a compilation on phase equilibria. The first is a picture of the phase diagram. The second is an evaluated diagram with annotated references and with the name of the evaluator given to permit one to judge the evaluation itself. The third is a reference which notes from whom and where one can obtain computer-based treatments of the system. The fourth level is fitting in with the diagram quantitative information on the thermodynamic behavior of components of phases and the thermodynamics of reactions involving components in the system.

J. F. Elliott - You place a very tall order with the compiler. However, this has been the goal of several compilations in the field.

B. Rosof - The needs of minor industries in the area of phase diagrams are often not met. The companies in these industries (my company being one) are important to the general economy and often have a high technical base.

J. F. Elliott - I would like to thank our panel members and the audience for a fruitful session. The session is adjourned.

PANEL III

MATERIALS PROCESSING (fabricating, machining, heat treating, etc.)

(User Needs for Phase Diagram Information)

Moderator: W. Rostoker, Dept. of Materials Engineering, University of Illionois, Chicago, IL

Panel Members:

E. R. Kreidler, Lamp Business Div., General Electric Co., Cleveland, OH

R. McNally, Ceramics Research, Corning Glass Works, Corning, NY

L. Mondolfo, Consultant, Clinton, NY

S. Prochazka, Ceramics Branch, Physical Chemistry Laboratory, General Electric Co.

G. R. Speich, Research Laboratories, United States Steel, Monroeville, PA

National Bureau of Standards SP-496, Applications of Phase Diagrams in Metallurgy and Ceramics
Proceedings of Workshop held at NBS, Gaithersburg, Md., January 10-12, 1977

User Needs for Phase Diagrams for Materials Processing: Glasses

R. C. Doman
R. N. McNally

Corning Glass Works
Corning, NY 14830

Introduction:

Phase diagrams are essential for the understanding of materials. These data are employed on a routine basis for developing new products. In many of our developments the phase diagrams were either not available or incomplete resulting in substantial phase equilibria studies to understand the manufacturing and end use. It is imperative that basic phase equilibria data be done in the temperature range 1500°C to 3500°C and in varying atmospheres where materials with unique properties exist. Outlined below are only a few of the important parameters, applications and examples of our requirements for phase equilibria data.

I. Applications for High Temperature Materials (>1000°C)
   - A. Glasses
   - B. Glass-Ceramics
   - C. Ceramics

II. Important Phase Equilibria Systems
   - A. Oxides
   - B. Intermetallics
   - C. Metals
   - D. Composites

1456

III. Processes Related to Phase Equilibria

A. Melting

B. Forming

C. Sintering

IV. Commercial Applications Where Phase Equilibria is Important

A. Refractories for steel and glass industry

B. Technical ceramics - zirconia; nitrogen containing materials

C. Honeycomb ceramics - auto exhaust; engine components

D. Glass systems

E. Glass-ceramics

V. Type Data Needed

A. Melting points, liquidus curves

B. Eutectics, peritetics, compound formation, solid solutions, sub-solidus, kinetics of solution - exsolution

C. Environment - oxidizing, reducing, neutral, vacuum

D. Vapor pressure data

VI. Some Key Data Needed for Determining Phase Equilibria Diagrams at High Temperatures

A. Chemical analysis

B. Microstructural analysis

C. Physical properties

D. Instrumental analysis

VII. Some Problems

A. Greatest need is at higher temperatures - 1500 to 4000°C where experimental problems increase by 4th power

B. Time = money

C. Basic supporting data isn't known

VIII. Examples

Example I: Fusion-Cast MgO-Chromite Product in order to understand this system it was necessary to:

A. Break up nine components system to binarys, ternarys, quarternarys etc. systems.

B. Had to determine melting points of end members.

C. Work out all binary systems - $MgO-Al_2O_3$, $MgO-Cr_2O_3$-MgO-CaO etc. - liquidus, solidus, sub-solidus, solid solutions, etc.

D. Ditto ternarys etc.

E. Ditto in various atmosphere conditions

F. Determine - surface tension at liquidus, vapor pressure, vapor species.

G. Determine phase equilibria data between metallurgical stage and refractory materials

H. Without this work there would not be commercial progress because of the strong relationship of phase equilibria to properties

Example II: up to 3500°C

A. Group IVB, VB, VIB, carbides, borides, silicides, nitrides, oxycarbides, oxynitrides, oxyborides; the need for phase equilibria data even more imperative for the current need for these type materials

Example III: ZrO_2 Solid Solutions - Effect of phase distributions on resulting properties of ZrO_2

A. Example - ZrO_2 electrolytes

B. Example - Relationship to strength

Example IV: Li_2O Stabilization of $MgO-R_2O_3$ Solid Solutions

A. Without original work on $MgO-R_2O_3$ phase equilibria, this work would not have been done

National Bureau of Standards SP-496, Applications of Phase Diagrams in Metallurgy and Ceramics
Proceedings of Workshop held at NBS, Gaithersburg, Md., January 10-12, 1977

EQUILIBRIUM DIAGRAMS IN NON-FERROUS ALLOYS

L. F. Mondolfo

Dept. of Chemical Engineering and Materials Science
Syracuse University
Syracuse, New York 13210

SUMMARY

In non-ferrous alloys, the equilibrium diagram explains why in the continuous casting of brasses, the 60/40 brass cannot be cast with the same technique as used for the 70/30 and 80/20 brasses and suggests the technique changes necessary. The location of the cracking in the welding of AlMgZn alloys is explained by the equilibrium diagram, and the effect of Cu additions. In Mg base alloys the equilibrium diagram indicates that better castability can be obtained by Si additions; in the zone refining of Al the diagrams indicate the movement of impurities and, in a general way, the amount of refining obtainable. Equilibrium diagrams explain the neutralization of Pb in zinc die casting alloys, the choice of heat treatment temperature for durals as function of Si content, Mn additions to improve the corrosion resistance of AlMg alloys, additions of Co or Mn to AlSi alloys to improve the ductility.

The two major difficulties with equilibrium diagrams, namely reliability and availability are discussed, together with the problems arising, especially in Al alloys, because of the complexity of the alloys and the necessity to account for every element present. Also mentioned are some reasons for the decrease of research on equilibrium diagrams and some of the difficulties in equilibrium diagram work.

The equilibrium diagram is for the material engineer what a map is for a surveyor. Not only the map tells the actual relief, but oftentimes when the relief is masked by overgrowth, the knowledge of the location of the ground, even if not visible, permits the surveyor to predict how much to cut to reach bare ground. Similarly for the material engineer non-equilibrium conditions may mask the true equilibrium, but to know where and how far the material has to go to reach equilibrium is often more valuable. Although materials can be handled without equilibrium diagrams, the use of the diagram makes life much easier. In the 100 or so years that equilibrium diagrams have been in use, material science has made more progress than the thousands of years that preceeded it! Every material engineer can tell about the many cases in which the equilibrium diagram has been of great help if not essential, the few examples reported here will show some of the cases in the author's experience.

In the continuous casting of large slabs of brass for subsequent rolling to coils, the casting conditions that produce good slabs are very similar for the 80/20 and the 70/30 brasses: same mold, same settings for the cooling water, same speed of descent. The only difference is that the 80/20 brass requires a pouring temperature some 50^{o}C higher than the 70/30. However when one tries to cast the 60/40 brass with the same conditions as the 70/30, the results are appalling; after a few inches of ingot have been cast, molten metal starts to pour into the pit. The metal shell that forms inside the mold is not solid enough to support the hydrostatic pressure and molten metal breaks through. The obvious answer is to increase the cooling in the mold to build up a stronger shell. This

produces the desired result: no more spill-out. However the problem only changes, casting can proceed to completion, but when one goes to remove the ingot from the pit, one is faced with two half ingots, most times completely split. In Fig. 1 is shown the pertinent part of the diagram C [illegible], as given by Hansen and Anderko[1]. The three vertical lines mark the 80/20, 70/30 and 60/40 alloys. As can be seen, the difference of composition between the first solid and last liquid to freeze is relatively small and approximately the same for the 80/20 (A) and the 70/30 (B) brasses, but the range of freezing temperature is some 50°C higher for the 80/20. The 60/40 on the other hand freezes over approximately the same range of temperature of the 70/30, but the difference in composition between the first solid and the last liquid (C) is much larger. In addition both the 80/20 and the 70/30 in the solid state are composed mostly if not all of alpha phase, whereas the 60/40 is mostly beta phase. Freezing during continous casting is definitely in non-equilibrium conditions; solidification may start with a solid with the composition shown by the equilibrium diagram, but at the point at which in equilibrium conditions it should end, there is still an appreciable amount of liquid, of a composition more or less corresponding to that shown by the diagram. Thus solidification continues and ends at a temperature lower than required by the equilibrium diagram. The lowering of the solidification end is proportional to the difference in composition between solid and liquid. This explains why in the 60/40 brass the shell formed in the mold is not as strong as in the other brasses, the actual range of solidification is larger and more mushy metal is present.

When increased cooling in the mold is used to thicken the shell, internal tensions, due to the quenching of the shell, build up. The shell, mostly of beta phase, is less plastic than if it were composed of the more ductile alpha phase and because of the internal tensions, cracks. Once this information is available, the cure is obvious. The splitting requires a reduction of the internal tensions which means a lesser quenching, the spill-out requires more build up of the shell. Reduction of the cooling in the mold and below reduces the internal tensions and eliminates the splitting, a slower descent speed that allows more time in the mold permits the thickening of the shell necessary to avoid spill-out. Of course all of this could have been done without equilibrium diagram by varying the casting conditions one at the time and then two at the time and so on, until the proper set-up was found. This was actually done at the beginning, but an enormous amount of work was expended and once the proper conditions were found, nobody knew what to do when minor accidental variations of practice crept in and suddenly all the production was scrap!

Fig. 2 shows the equilibrium diagram of the AlMgZn alloys[2], with the crosshatched square marking the range of commercial compositions. As can be seen by comparing the liquidus and the solid state distribution of the phases, the alloys when in equilibrium are well within the range of solid solutions and so far away from the eutectic line, that even the non-equilibrium conditions that may result from commercial welding practice, do not produce sufficient coring to cause the appearance of eutectics. Thus the alloys freeze as solid solutions and toward the end of freezing there is little liquid to feed the shrinkage. Microporosity develops in

the weld, that weakens the weld zone and concentrates in it cracking due to internal tensions. When Cu is added to the alloys, the equilibrium diagram, if available, would show the presence of an eutectic near the alloy composition range. This eutectic toward the end of freezing of the weld acts to feed the shrinkage, thus reducing substantially the microporosity and its weakening effect. No more cracking of the weld zone results. However in the zone surrounding the fused metal eutectic melting takes place, that weakens the material and cracking due to internal tensions concentrates there. Of course the advantage of the equilibrium diagram in this case is limited, it explains what is happening, but not how to remedy it. However, once it is known what the problem is, it is usually reasonably easy to find an answer.

A similar case in which the equilibrium diagram does not give the right answer is that of the Mg base alloys that contain Al and Zn in amounts well below their maximum solubility. They freeze as solid solutions and, also because of the high shrinkage coefficient of Mg, they show extensive microshrinkage in all but the simplest castings. In the MgSi diagram (Fig. 3) at the Mg end there is an eutectic at 1.4% Si[1]. This suggests that if some Si is added to the MgAlZn alloys, the problem of lack of eutectic should be solved. Experiments show that this is the case, as little as 0.4 - 0.5% Si produces all the eutectic that is necessary, and sound castings are produced. What the equilibrium diagram does not tell is that the Si addition so embrittles the castings, that they may shatter if dropped on a hard floor!

In the zone refining of aluminum a look at the binary equilibrium

diagrams will predict that Cu, Mg, Zn, Si whose eutectic composition is quite different from the solid solubility limit, can be moved to the end fairly rapidly and easily, whereas Mn, which has an eutectic point very close to the solid solution limit, will move only extremely slowly, Cr, Ti, V, Zr which undergo peritectic reactions with Al, will move backwards to the starting end. Experimental results shown in Table I confirm the predictions. It is to be noticed that in this case use of the binary diagrams

TABLE I

ANALYSES OF Al (PRODUCED BY DEPOSITION FROM ORGANIC SALTS) BEFORE AND AFTER ZONE REFINING[3]

Element	Before	After	Change	k Factor*
Cu	0.3	0.006	- 150	0.17
Cr	0.004	0.01	+ 2.5	2.0
Mg	1.0	0.01	- 100	0.5
Mn	0.031	0.030	- 0.3	0.94
Si	1.0	0.05	- 20	0.13
Ti	0.05	0.5	+ 10	11.0
V	0.01	0.03	+ 3	4.0
Zn	0.06	<0.001	- 100(?)	0.88
Zr	0.04	0.05	+ 0.25	2.5

for multi-component alloys will predict the right direction, but not even an order of magnitude change. For example Si, with the lowest k factor,

*k = ratio of amount of addition soluble in the solid to amount soluble in the liquid at freezing temperature.

should be the easiest to be removed, followed in the order by Cu and Mg, and far away by Zn and Mn. For the peritectic elements, Ti should be the most concentrated and then in order V, Zr, Cr. Instead the most easily removed is Cu, followd by Zn, Mg and with Si far behind. The only element that follows predictions of the binary diagram is Mn. In the peritectics, Ti concentrates in the right amount but the changes for the other elements are in the proper direction, but not in the proper order or of the right magnitude.

Zinc-base die casting alloys contain some 4 - 5% Al which give to the alloy its excellent castability and strength. Accordingly Zn die castings are extensively used because they are cheap, easily polished and plated to excellent appearance, and stronger than plastics. Most Zn, unless specially refined, contains a few thousands of a percent of Pb. Neither Zn nor Al form compounds with Pb, thus the Pb is present in the alloys as elemental Pb. Solubility of Pb in Zn decreases with decreasing temperature. The age hardening phenomena that result from it have little effect on the mechanical properties, but make the alloys susceptible to intergranular corrosion, to the point that early failure may result even in mildly corrosive conditions. Since removal of the last amount of Pb is expensive, neutralization of the Pb is necessary. As shown by the MgPb diagram, (Fig. 4) a compound Mg_2Pb is formed[1], which is very stable and does not dissolve to any great extent in Zn. This reduces the precipitation of Pb and eliminates the intergranular corrosion susceptibility. The amount of Mg necessary for the neutralization is only a few thousands of a percent and even if for safety sake few

hundreds are added, the cost is infinitesimal, especially if one compares it to the cost of refining Zn to remove the last trace of Pb.

Many commercial Al alloys are subjected to heat treatment, which permits a 3 - 4 fold increase of strength over the annealed properties. Heat treatment relies upon producing a supersaturated solid solution and then controlling its movement toward equilibrium to produce the structure with the desired properties. The best means of supersaturating a solution is to heat the alloy at the highest temperature possible to dissolve the largest amount of solute possible. Since solid solubility increases exponentially, even a few degrees make a substantial difference in the amount dissolved. On the other hand exceeding the lower melting point of the alloy, even by few degrees and for few seconds, deteriorates the alloy beyond repair. In most heat treatments of Al alloys the margin of safety is small: heat treatment temperatures only 5 to 10°C below the melting point of the lowest eutectic are common. Obviously knowledge of the eutectics present in the alloy is necessary.

A typical case are the durals. These are alloys that contain Cu and Mg and sometimes added Si. In addition they contain Mn and the normal impurities of Al: Fe and Si. Neither Mn nor Fe have an appreciable effect on low melting eutectics; the structure of the alloys is basically controlled by the Mg/Si ratio: depending on it several different eutectics can be present in the alloys. Fig. 5 shows the quaternary diagram AlCuMgSi[2]. As can be seen, 3 eutectics are formed in that part of the diagram that covers the durals. In Table II are listed three typical dural compositions, their Mg/Si ratios, the eutectics in them and the

TABLE II

NOMINAL COMPOSITION OF COMMERCIAL DURALS, THEIR Mg/Si RATIO EUTECTICS PRESENT IN THEM WITH THEIR MELTING POINT AND HEAT TREATMENT TEMPERATURE RECOMMENDED

Alloy	Cu	Mg	Si	Ratio Mg/Si	Eutectic	Melting Point	Heat Treatment Temperature °C
2014	4.4	0.5	0.8	<1	$Al + CuAl_2 + Cu_2Mg_8Si_6Al_5 + Si(?)$	507	500 ± 5
2017	4.0	0.5	0.25	≈1.7	$Al + Mg_2Si + CuAl_2$	515	505 ± 5
2024	4.4	1.5	0.25	>>1.7	$Al + CuAl_2 + Mg_2Si + CuMgAl_2$	500	490 ± 5

prescribed heat treatment temperature. It is to be noticed that in the first alloy listed the Si content is insufficient for the Si phase to appear, thus there is no quaternary eutectic in it. The lowest melting point of the alloy is somewhere on the line between the points Q (512°C) and R (507°C). With the equilibrium diagram and the analysis of the alloy, heat treatment temperature can be set with assurance that maximum benefit will be obtained, without danger of deterioration.

AlMg alloys have excellent resistance to corrosion, if properly compounded and treated. The usual Al impurities Fe and Si, form in them the two compounds $FeAl_3$ and Mg_2Si. Mg_2Si has an electrolytic potential anodic to the matrix[4] and in corrosive conditions Mg_2Si is rapidly dissolved to protect the matrix, leaving a pit more or less the size of the Mg_2Si particle. Since Si is kept low and Mg_2Si particles are easily dispersed and thus small, their solution produces only a slight roughening of the surface. $FeAl_3$ on the other hand, is strongly positive to the matrix[4]

thus the matrix around the $FeAl_3$ particle corrodes to protect it, until the particle comes loose. When this happens a pit several times larger than the particle has formed. If one looks at the AlFeMn diagram (Fig. 6) (one should really look at the AlFeMgMnSi diagram or at least to the AlFeMgMn diagram, but neither of the two diagrams is sufficiently known for the purpose) one sees that when Mn is present, the Fe tends to replace Mn in the $MnAl_6$ compound, giving rise to a $(FeMn)Al_6$ compound, that has a structure and properties very close of those of the $MnAl_6$. Of interest in this case: the $MnAl_6$ has an electrolytic potential very close to that of Al[4], and so does the $(FeMn)Al_6$. As a result addition of Mn to AlMg alloys in amounts equal to the Fe content replaces the $FeAl_3$ compound, strongly positive in respect to the matrix, with a $(FeMn)Al_6$ one with practically the same potential as the matrix, and which therefore will not give rise to pronounced pitting corrosion.

Al alloys with more than 12% Si have excellent wear resistance, low thermal expansion coefficients, good castability and, if they contain sufficient high melting point metals, reasonably good strength at elevated temperatures. Thus they are extensively used in the automotive industry for pistons and cylinder blocks. In the Al foundry iron pickup is always a serious problem; sources for iron are innumerable. Even if one does not use cast iron pots for holding the melts, iron can come from stirring tools, mold washes, galvanized iron roofs, steel chips from the saws that cut the ingots and risers, etc., etc. In addition the automotive industry is extremely cost conscious and secondary metal, which usually contains more Fe than primary, is the rule for their castings.

The high Si alloys are particularly sensitive to Fe contamination, if the Fe content is above 0.7 - 0.8% Fe correction is necessary or else the castings may be as brittle as glass. A look at the AlFeSi diagram explains the Fe limit: with Fe above 0.7% the $FeSiAl_5$ phase is primary. This phase is extremely brittle and tends to form large platelets (Figure 7). The problem is to prevent the formation of these primary crystals. The best way would be to reduce the Fe content, but this is economically impossible, sweetening an alloy with 0.9% Fe down to an acceptable 0.6% Fe requires the addition of almost the same amount of low Fe metal!

Several elements combine with Fe to form compounds less embrittling than $FeSiAl_5$: the most common are: Cr, Mn, Ni and Co. The equilibrium diagrams (Fig. 8) can help in the choice of the best corrector. In the AlCrFeSi diagram (Fig. 8a) the compound in equilibrium with Al is most probably $(CrFe)_4Si_4Al_{13}$ which contains large amounts of Si and Cr, but little Fe. A large amount of it forms, which reduces the fluidity of the alloy, with only a limited improvement on ductility. In the AlFeMnSi system (Fig. 8b) the compound formed is $(FeMn)_3Si_2Al_{15}$ which contains less Si and in which Fe can greatly exceed the Mn, thus a small addition of Mn can absorb a large amount of Fe, Ni and Co do not form compounds with Si thus the Fe is absorbed by them through the formation of $FeNiAl_9$ (Fig. 8c) or by displacing up to 50% of the Co in Co_2Al_9 to form a $(CoFe)_2Al_9$ compound (Fig. 8d). The $FeNiAl_9$ compound unfortunately crystallizes as long needles which, although better than $FeSiAl_5$ still embrittle the alloys. Thus neither Cr nor Ni are suitable for the purpose and the choice is

between Mn and Co. Co is better because for any given amount of Fe to be neutralized less compound is formed. For example in the alloy marked x in Figs. 8b and d, using the lever rule, the ratio of Si to $(CoFe)_2Al_9$ can be calculated at approximately 0.12; in the AlFeMnSi diagram, for the same alloy, the ratio is approximately 0.18. Thus in the latter alloy there is some 50% more Fe bearing compound. However the price of Co is much higher than that of Mn, thus economically Mn is more attractive, whereas functionally Co is better. At this point equilibrium diagrams give place to economics: if quality is the major factor, Co wins, if cost, Mn is preferred.

In most examples shown it is obvious that the equilibrium diagram alone is not sufficient and that additional information is needed to solve the problems. However the role of the diagram is basic: it is the framework to which additional information is attached to give a complete, coherent picture.

There are two problems in the use of equilibrium diagrams: availability and complexity. Not only many diagrams are only partially known or even completely unknown, but even those supposedly well established may not be as reliable as one would expect from work widely accepted. Fig. 9 shows several AlZn equilibrium diagrams. As shown by the references[5-13], the names of many well known metallurgists are attached to them. Obviously only one of them can be correct and there is a good probability that the last one is not it. There are good reasons to expect that the actual diagram is the one shown by Hanson and Gayler, published in 1922, and later discarded.

The other serious problem is that the more knowledge of metals increases, the more one becomes aware of the disproportionate role that some small impurity may play on structure and properties. Thus to account, even approximately, for the structure of commercial alloys one has to consider multicomponent systems. In steel and most Cu or Ni alloys many alloying elements are in solution and only small modifications to the binary or ternary systems can account, at least approximately, for these additions. An easily legible diagram can serve for most purposes. In Al alloys the contrary is true. Even commercially pure Al, which contains Fe and Si as normal impurities is a multiphase alloy: in addition to the Al phase, $FeAl_3$, Fe_2SiAl_8, $FeSiAl_5$ and Si may be present (Fig. 10). Thus even before the start of alloying, one is dealing with a ternary diagram. Very few commercial alloys contain only one addition and many of them contain three or four. For example durals are AlCuFeMgMnSi alloys (6 elements), the 7000 group alloys AlCuFeMgSiZn alloys (also 6 elements) but usually with additions of at least one of Cr, Mn, Zr, Ag and often Ti, B.

Ternary diagrams are easily plotted: liquidus and one or two sections can give a reasonably complete and accurate picture. Quaternary diagrams can be plotted by the method of Phragmen[14] in which the pyramid vertex that represents the base element is used as projection point for the diagram (Fig. 11). The picture that one obtains is not as accurate, but one can gather a reasonable idea of invariant reactions, phases present and their approximate distribution. For a quinary system this is impossible: sections have to be used and following a phase or a reaction

through them becomes a major project. Until computers can be trained to read equilibrium diagrams there is little that can be done on this problem.

In the early years of this century every fourth paper published was an investigation of an equilibrium diagram, today one has to wade through an enormous amount of literature to find equilibrium diagram work. Granted that the most important parts of binary diagrams are already established reasonably accurately, but how many useful ternary or quaternary diagrams are known with certainty, if at all?

This dearth of equilibrium diagram work is particularly noticeable in American publications; Russian, Japanese, German magazines stil report a fair amount of equilibrium diagram work. One of the reasons for this is that in American Universities equilibrium diagram work is considered routine and unfit for PhD. theses. It is true that a good part of the work is routine and repetitive, but so is most good reasearch. Granted that one can take a bunch of alloys, prepared by a technician and give them to another technician to determine their X-ray diffraction pattern, and from this work publish an equilibrium diagram, but how much reliance can one put on this kind of research? With the large number of variables in any research one experiment, no matter how brilliantly conceived or executed, is not sufficient to prove anything. One of the most important principles of research is that unless an experimental result can be confirmed by another method, preferably also by another investigator, it should be considered only tentative.

In equilibrium diagram work, where non-equilibrium conditions are

the rule, rather than the exception, one should use as many methods of investigation as possible. On the other hand a judicious selection of methods is necessary. There is no method invented for investigating metals that cannot be used for the determination of equilibrium diagrams. Already the selection of the methods to be used is a series of decisions that require both knowledge and judgement: it is useless to make the most accurate lattice parameter measurements to determine a solid solubility that is below 0.1%! Any one who has investigated equilibrium diagrams knows how much ingenuity and hard work are necessary to assemble all the experimental data and to coordinate them to make them fit a smooth and plausible picture that obeys all the thermodynamic laws.

Among the non-ferrous metals, Al and Mg, which were born in an era when metallurgy was becoming a science, are in a favorite position: many more complex equilibrium diagrams are available for Al and Mg alloys than for the older metals. However even in the Al and Mg industries there is need for more diagram work. The Concorde plane uses large amount of Hyduminiums, which are AlCuFeMgNiSi alloys, yet the AlCuFeNi diagram, that is vital for the understanding of these alloys is very poorly investigated and far from established. Those people that have the money to fly the Concorde should be asked "How does it feel to fly a plane whose equilibrium diagram is not known?".

1474

REFERENCES

1. M. Hansen and K. Anderko, "Constitution of Binary Alloys," McGraw-Hill New York, 1958.

2. L. F. Mondolfo, "Aluminum Alloys, Structure and Properties," Butterworths, 1976.

3. G. Revel, Mem. Artillerie Franc., 1969, 43, 343.

4. E. Franke, Werkstoffe u. Korr., 1953, 4, 4.

5. E. S. Shepard, J. Phys. Chem., 1905, 9, 504.

6. W. Rosenhaim, S. L. Archbutt, Phil. Tr. Roy. Soc., 1912, 212, 315.

7. O. Bauer, O. Vogel, Inter. Z. Metallographie, 1916, 8, 101.

8. D. Hanson, M. L. V. Gayler, J. Inst. Metals, 1922, 27, 267.

9. T. Tanabe, J. Inst. Metals, 1924, 32, 415.

10. T. Tshiwara, J. Inst. Metals, 1925, 33, 73.

11. E. Schmid, G. Wassermann, Z. Metallkunde, 1934, 26, 145.

12. W. L. Fink, L. A. Willey, AIME Tr., 1936, 122, 244.

13. A. A. Presnyakov, Y. A. Gorban, V. V. Chernyakova, Zh. Fiz. Khim, 1961, 35, 1289.

14. G. Phragmen, J. Inst. Metals, 1950, 77, 489.

1475

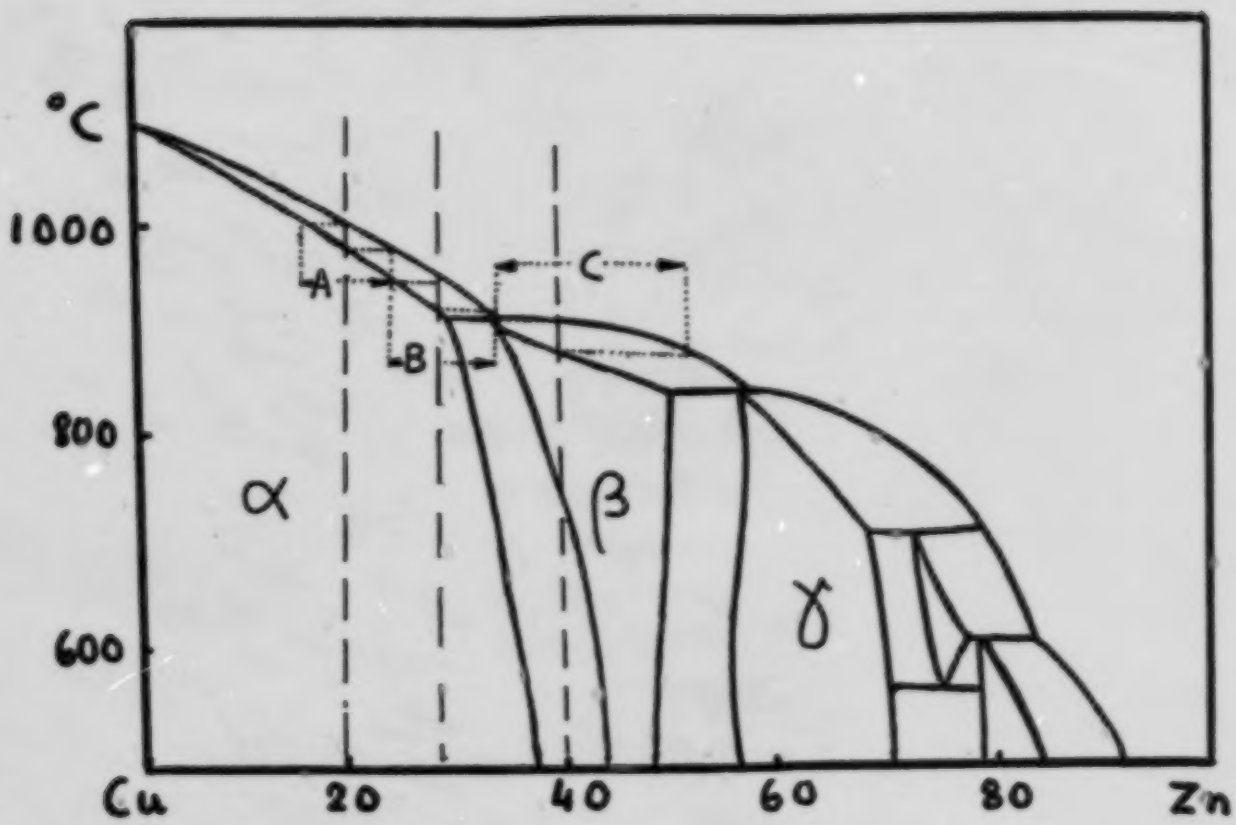

FIG. 1 CuZn DIAGRAM, SHOWING THE 80/20, 70/30, 60/40 BRASSES AND THE SIZE OF THE DIFFERENCE OF COMPOSITION BETWEEN THE FIRST SOLID AND THE LAST LIQUID TO FREEZE IN EQUILIBRIUM CONDITIONS.

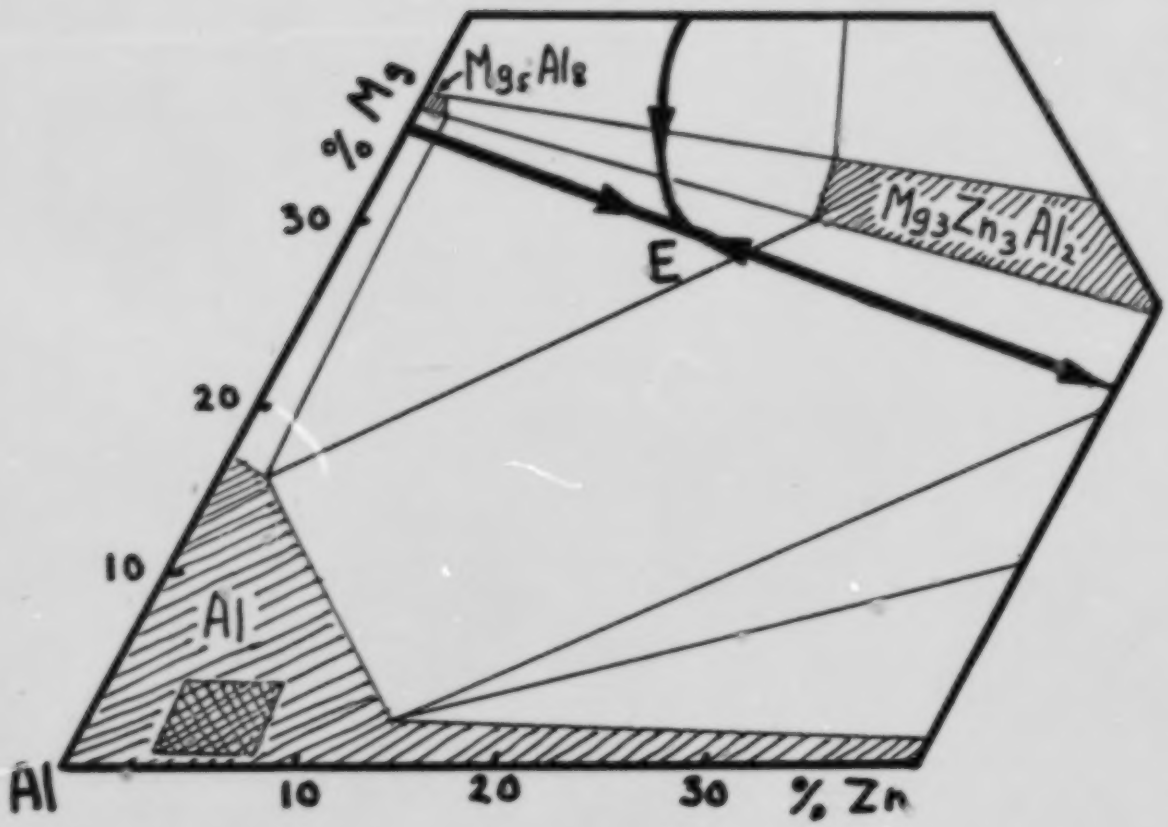

FIG. 2 AlMgZn DIAGRAM, Al CORNER, LIQUIDUS LINES (HEAVY), EUTECTIC E AND PHASE DISTRIBUTION IN THE SOLID STATE (LIGHT LINES). THE CROSSHATCHED AREA REPRESENTS THE RANGE OF COMPOSITION OF COMMERCIAL ALLOYS. NOTICE ITS DISTANCE FROM THE EUTECTIC LINES.

1479

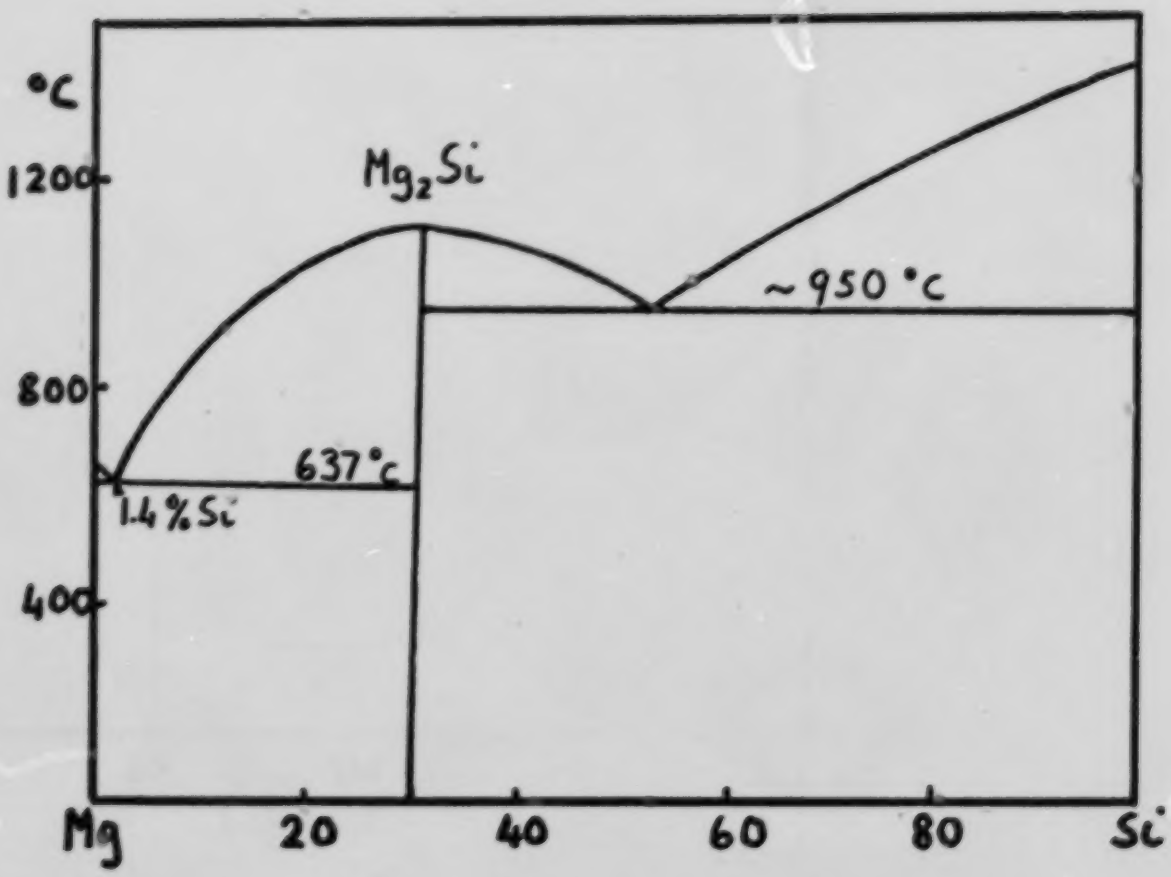

FIG. 3 MgSi EQUILIBRIUM DIAGRAM SHOWING THE PRESENCE OF AN EUTECTIC AT 1.4% Si.

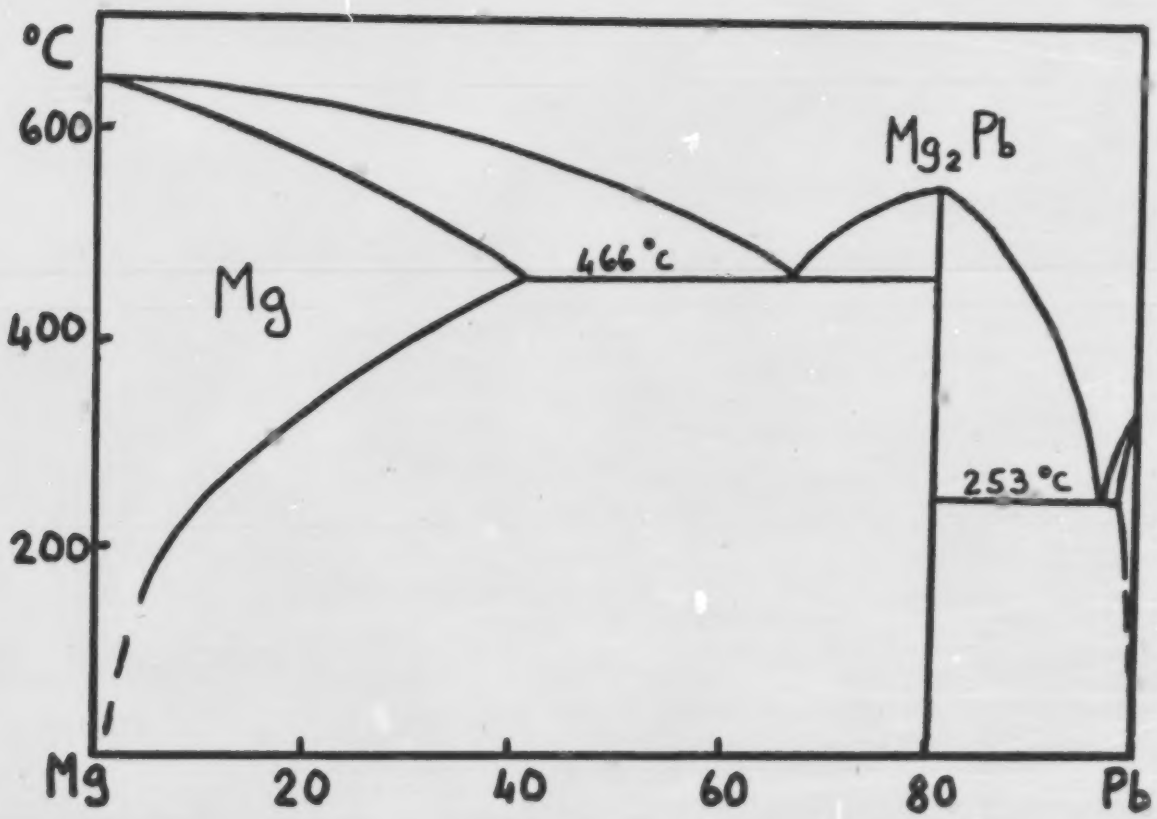

FIG. 4 MgPb DIAGRAM SHOWING THE PRESENCE OF A Mg_2Pb COMPOUND, WITH HIGH Pb CONTENT.

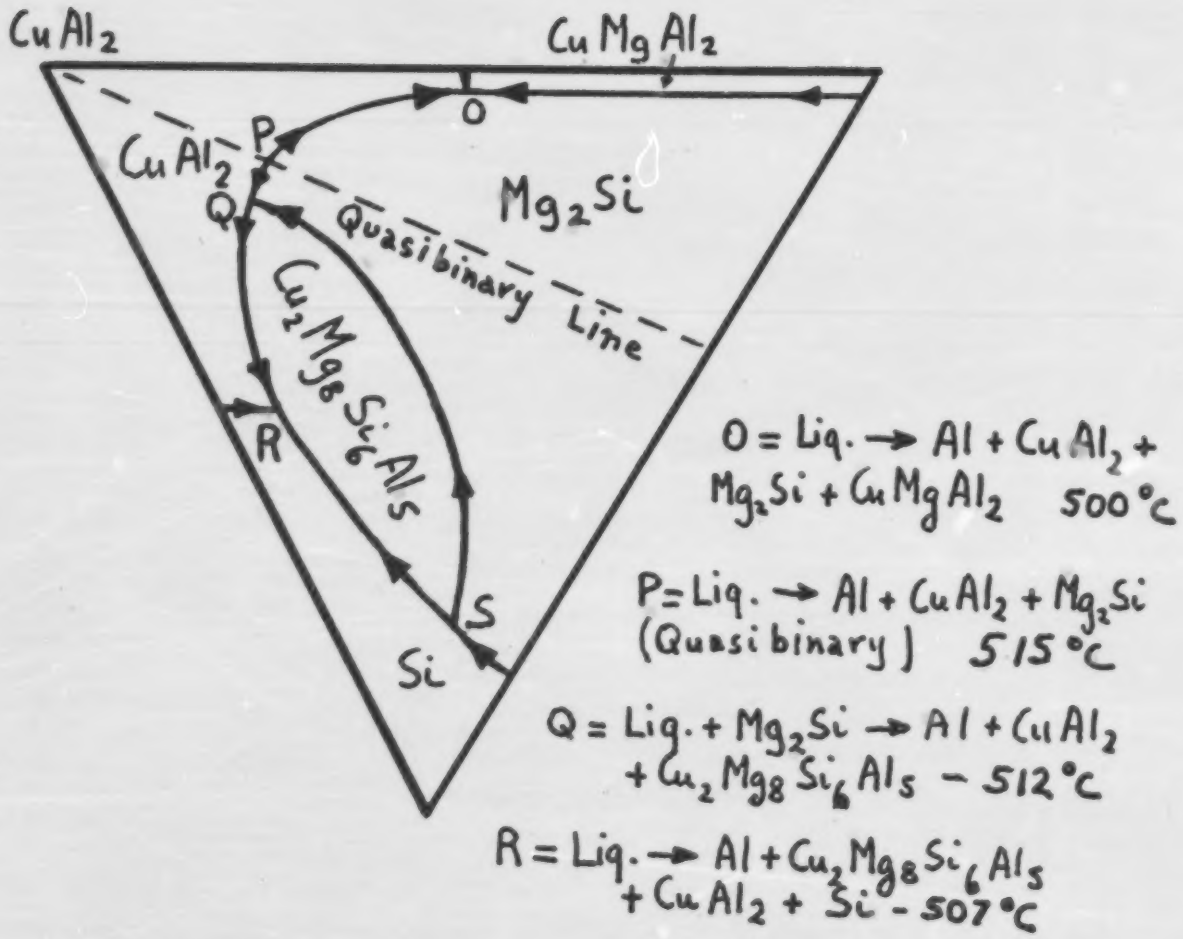

FIG. 5 CORNER OF THE PROJECTION OF THE AlCuMgSi LIQUIDUS, SHOWING THE LOCATION OF THE QUATERNARY EUTECTICS, THE PHASES PRESENT IN THEM AND THEIR MELTING POINT.

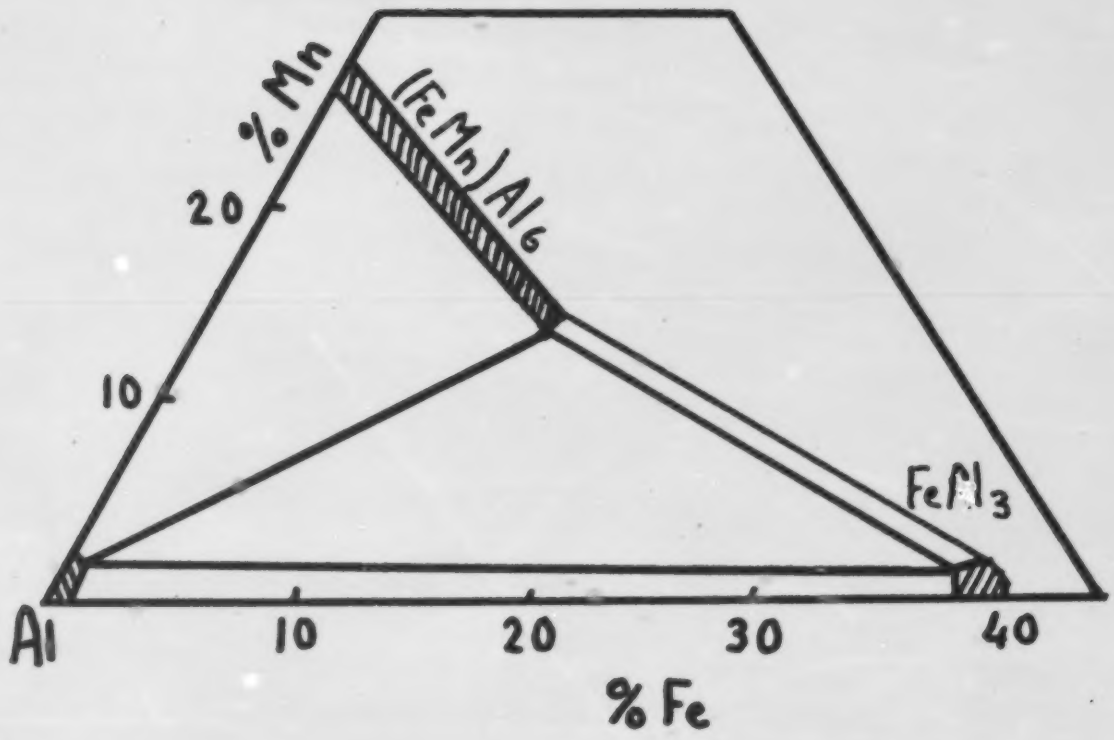

FIG. 6 Al CORNER OF THE AlFeMn DIAGRAM SHOWING THE RANGE OF COMPOSITION OF THE $(FeMn)Al_6$ PHASE.

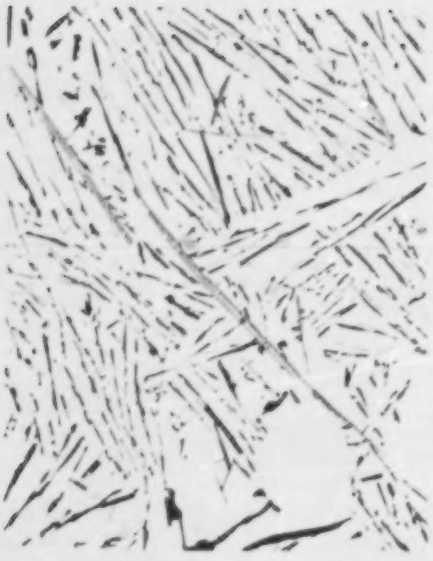

FIG. 7 Al ALLOY WITH 10% Si, 0.9% Fe, SAND CAST. LARGE PRIMARY NEEDLES OF $FeSiAl_5$ (LIGHT) IN A BACKGROUND OF EUTECTIC AlSi. X 250 NOT ETCHED.

1452

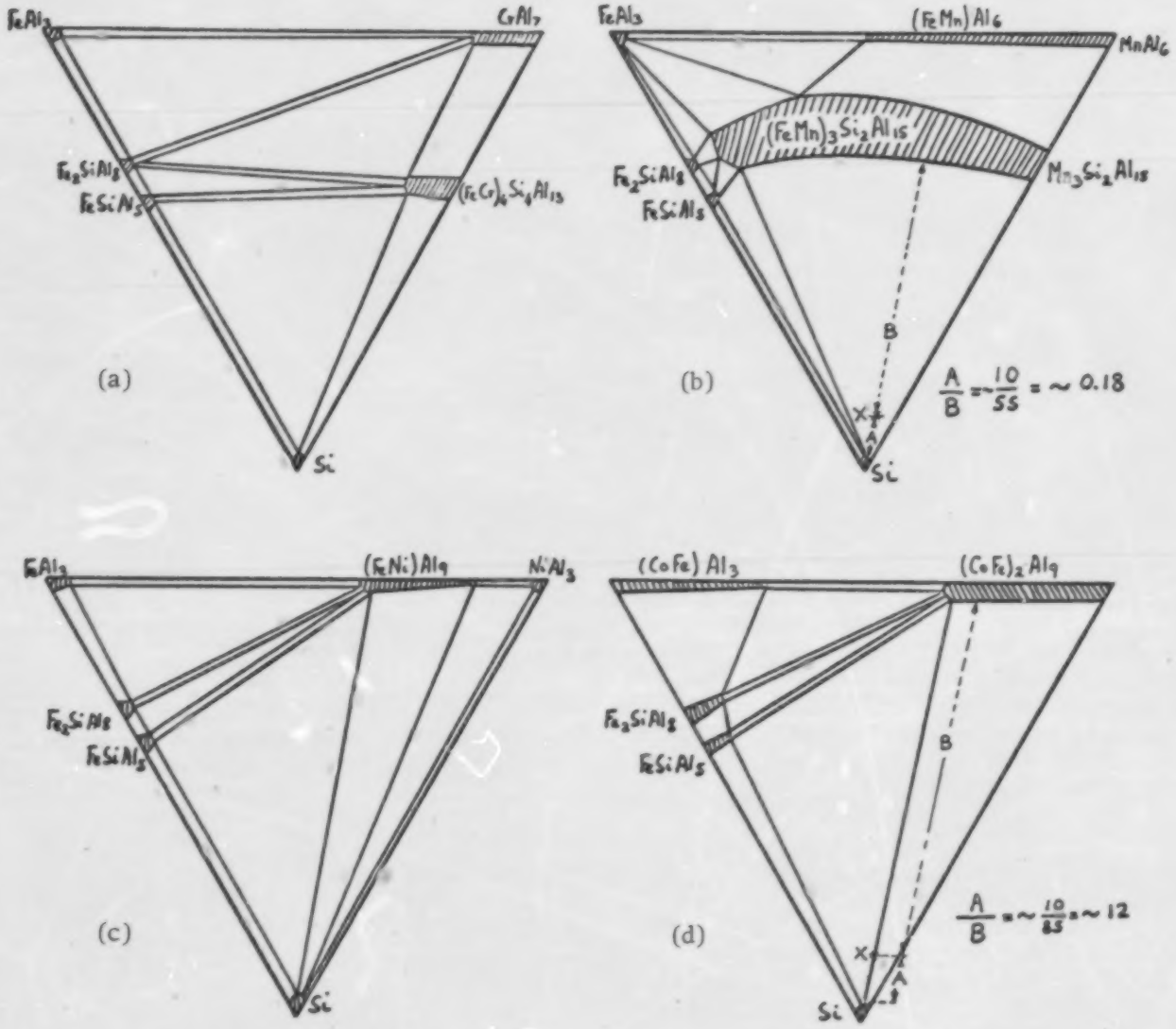

FIG. 8 PROJECTION OF THE PHASE DISTRIBUTION IN THE SOLID IN THE DIAGRAMS a) AlCrFeSi, b) AlFeMnSi, c) AlFeNiSi, d) AlCoFeSi. NOTICE SMALL AMOUNT OF Fe in $(FeCr)_4Si_4Al_{13}$ AND THE LARGE AMOUNT OF Si, AS EVIDENCED BY THE LIMITED PROTRUSION IN THE QUATERNARY FIELD AND PROXIMITY TO THE Si CORNER. ALSO NOTICE HOW IN THE ALLOY X THE RATIO OF COMPOUND TO Si is 0.18 IN THE AlFeMnSi DIAGRAM, BUT ONLY 0.12 IN THE AlCoFeSi SYSTEM.

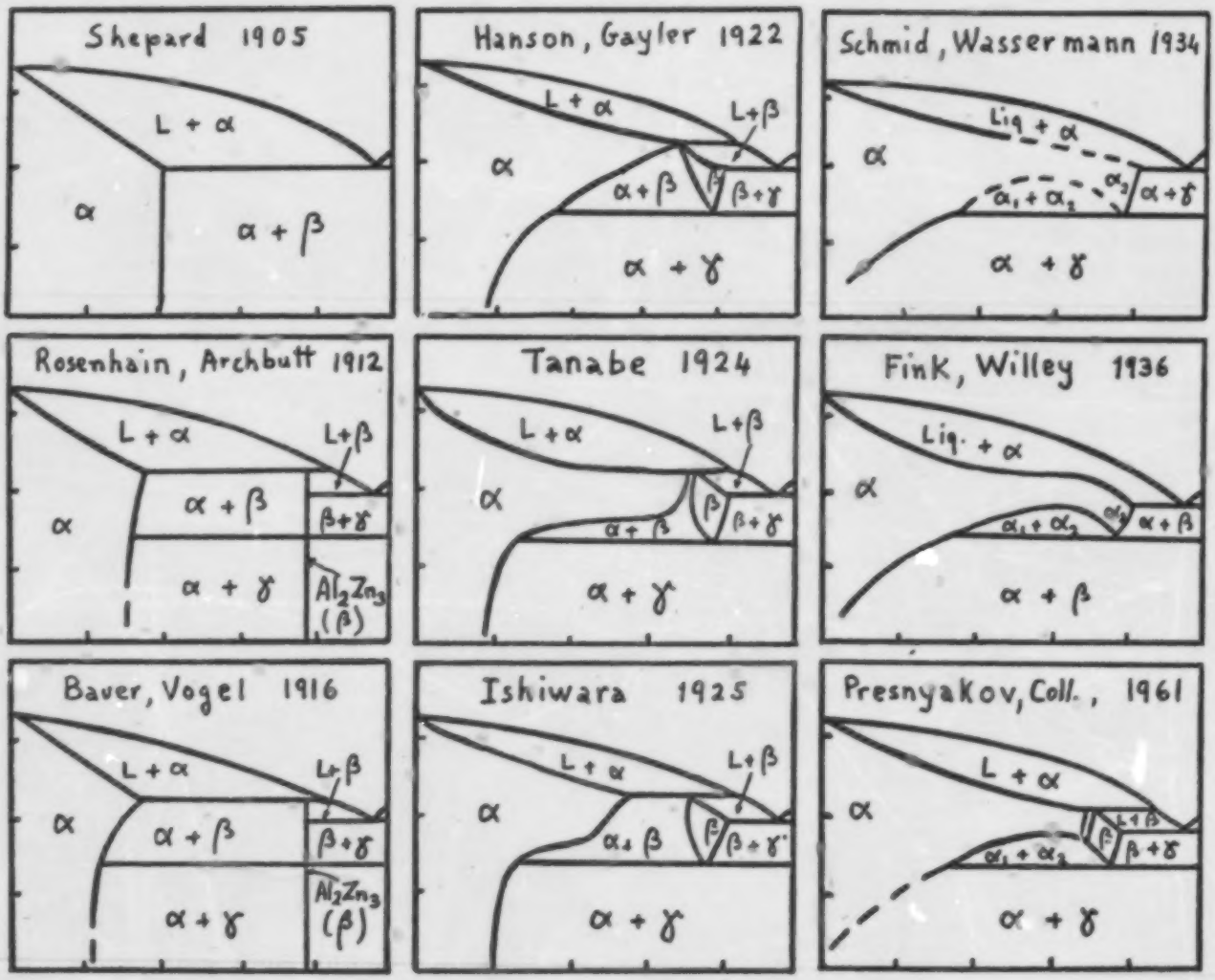

FIG. 9 SOME OF THE AlZn EQUILIBRIUM DIAGRAMS PUBLISHED WITH NAMES OF THE INVESTIGATORS AND DATE (SEE ALSO REFERENCES).

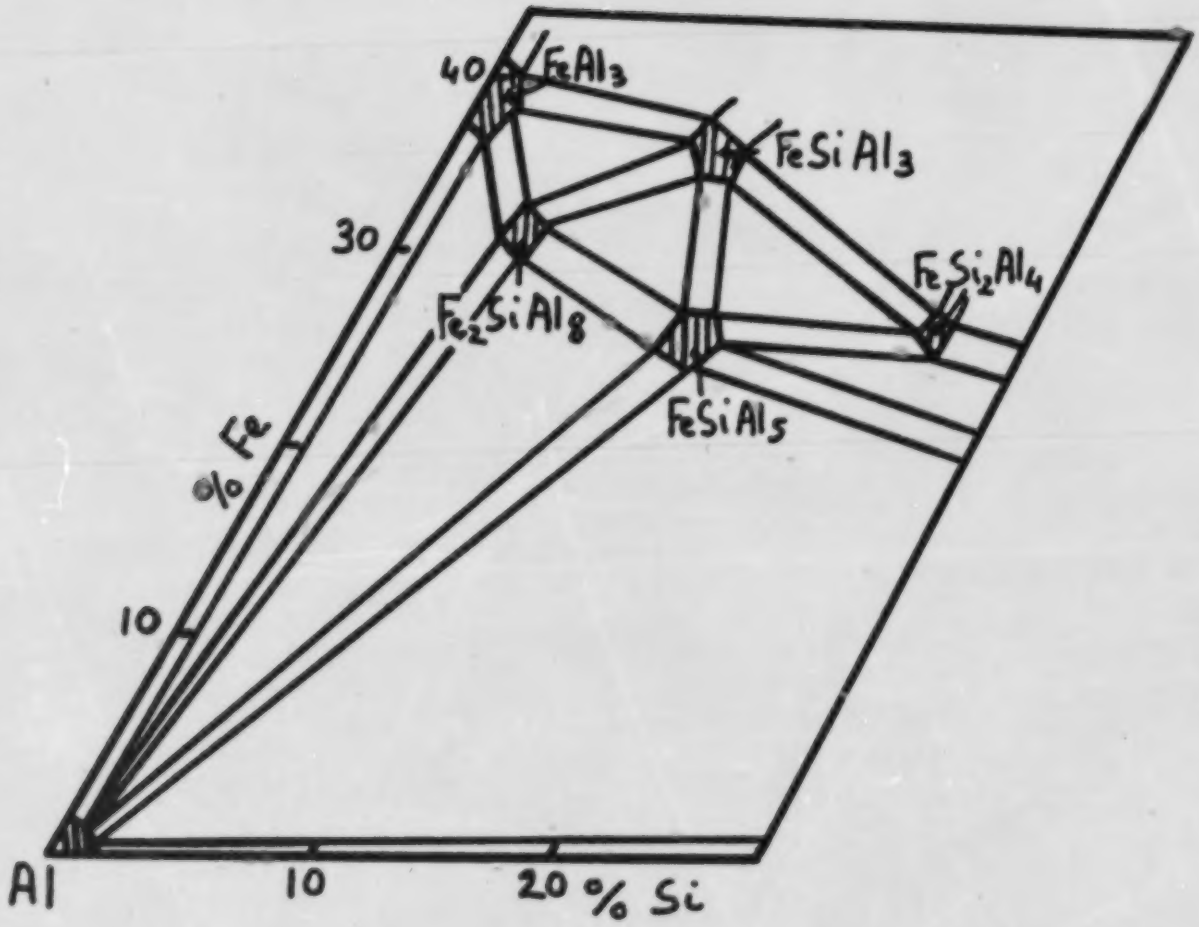

FIG. 10 THE AlFeSi EQUILIBRIUM DIAGRAM, THAT REPRESENTS THE STRUCTURE OF COMMERCIALLY PURE Al.

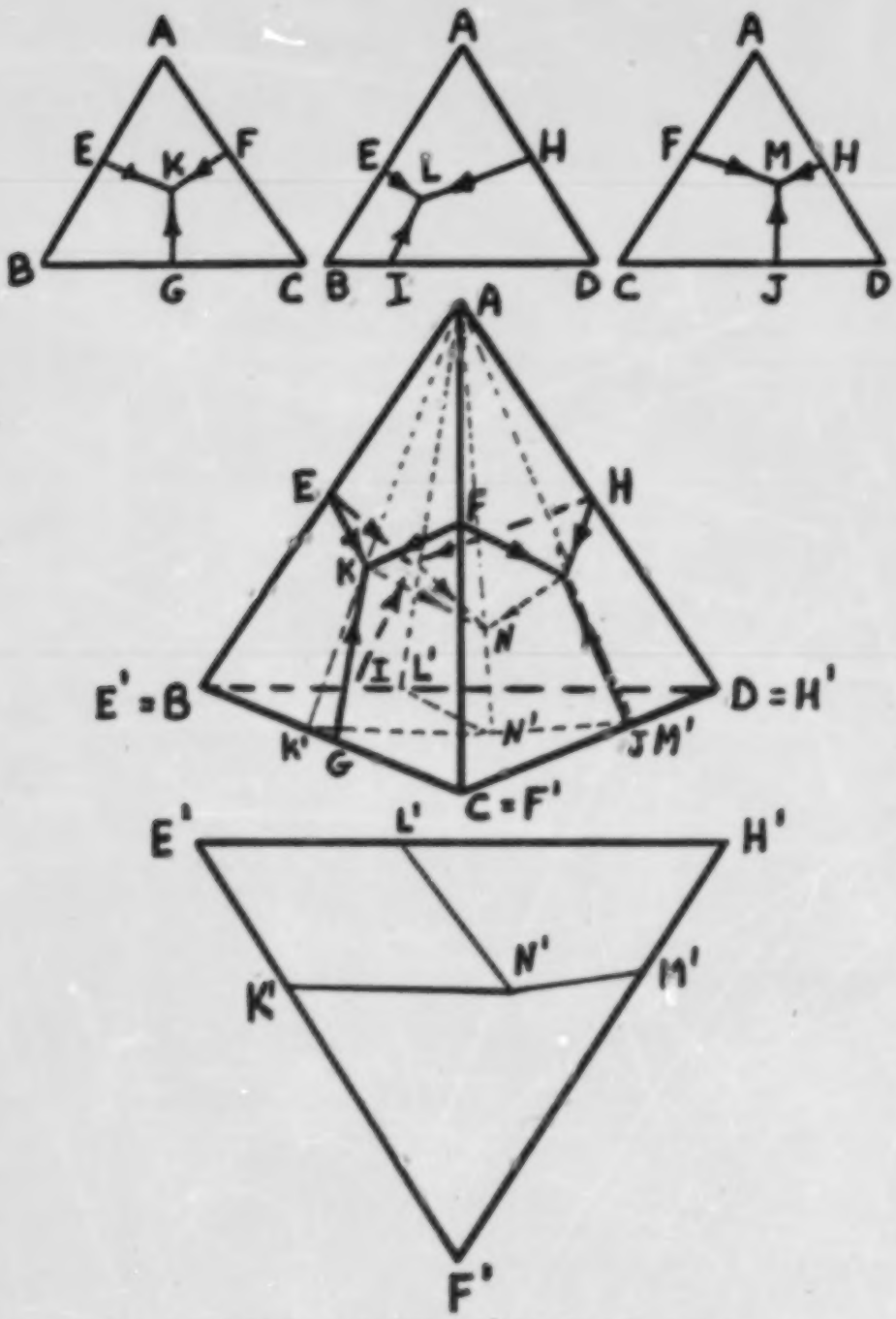

FIG. 11 PHRAGMEN'S METHOD OF PROJECTING QUATERNARY DIAGRAMS ON A PLANE. AT THE TOP THE LIQUIDUS OF THREE HYPOTHETICAL DIAGRAMS ABC, ACD, ABD. IN THE CENTER THE QUATERNARY PYRAMID AND (DASHED) THE EUTECTIC LINES IN THE QUATERNARY DIAGRAM. DOTTED LINES SHOW HOW THE PERTINENT POINTS ARE PROJECTED ON THE BASIS OF THE PYRAMID, AND BELOW IS SHOWN THE PROJECTION THAT RESULTS.

National Bureau of Standards SP-496, Applications of Phase Diagrams in Metallurgy and Ceramics
Proceedings of Workshop held at NBS, Gaithersburg, Md., January 10-12, 1977

Phase Equilibria in the Development of High Temperature Structural Ceramics

Savante Prochazka
General Electric Research and Development
P.O. Box 8
Schenectady, New York 12345

Oxidation resistance, low thermal expansion and low creep rates are first-approach criteria for the development of high-temperature engineering ceramics (temperatures 1300°C and above). Prime candidates are covalently bonded compounds, SiC, Si_3N_4, Si-Al-O-N solid solutions and perhaps AlN, some transition metal borides and materials based on combinations of these compounds. Single phase ceramics are believed to offer the highest temperature capability, but the presence of some other specific phases is usually required for fabrication purposes and for microstructural control and control of related properties. All consolidation processes developed for these materials involve chemical reactions, additions and thermal treatments. Information on phase equilibria is essential for understanding fabrication processes, which are usually established empirically, and the behavior of the materials at high temperature and their interactions with the environments.

The types of chemical processes and equilibria which need to be understood in this field of ceramics may be grouped into the following categories.

A. Pure compound in equilibrium with its decomposition products:

ex. $SiC_{(s)} \rightarrow C_{(s)} + Si_{(g)} + Si_2C_{(g)} + SiC_{2\ (g)} + \ldots$

$Si_3N_4 \rightarrow N_{2(g)} + Si_{(g)} + SiN_{(g)} + Si_2N_{(g)} + \ldots$

B. Stability of polymorphs and the effect of some species on phase transitions between polymorphs:

ex. β - SiC → α - SiC

effect of N_2, O_2, metals (Si) etc.

α - Si_3N_4 → β Si_3N_4

effect of O_2, metals (Si) etc.

C. Limits of nonstoichiometry in pure compounds.

D. Solubility limits in pure compounds of species used to promote sintering.

ex. B, Be, Al, La, in SiC

E. Phase relations, composition ranges and esp. solidus and liquidus temperatures in systems of interest:

ex. Si - Al - N - O

Si - Mg - N - O

Si - C - B

Si - Al - C - N

F. Phase relations in oxidation products:

ex. $Si_3N_4 + MgO \rightarrow SiO_2 + Mg_2SiO_4 \rightarrow 2\ MgSiO_3$

G. Interaction of the parent material and its oxidation products in the environment of combustion products containing

CO, SO_2, Na_2O, V_2O_5 etc.

H. Interaction of nickel and cobalt based refractory alloys with the base material.

Much of the information does not exist; its generation will be slow and will require unconventional techniques.

National Bureau of Standards SP-496, Applications of Phase Diagrams in Metallurgy and Ceramics
Proceedings of Workshop held at NBS, Gaithersburg, Md., January 10-12, 1977

Phase Diagram Information for Processing of Superconductors*

David Dew-Hughes
Metallurgy and Materials Science Division
Department of Applied Science
Brookhaven National Laboratory
Upton, New York 11973

High critical temperature (>20 K) superconductors, and conductors developed therefrom, are essential if superconductivity is to make a serious impact upon electrical engineering practice. The highest critical temperatures are found in compounds with the A15 crystal structure based upon vanadium or niobium. V_3Ga and Nb_3Sn are already established as commercially available conductors, with T_c's of 15 K and 18 K, respectively. The potentially superior compounds Nb_3Al (19 K), Nb_3Ga (20.3 K) and Nb_3Ge (22.5 K) have yet to be developed as conductors.

The superconducting properties of A15 compounds are maximized in well-ordered, stoichiometric samples (see, for example, reference [1] for a review of the properties of A15 superconductors). In the Nb-Al, Nb-Ga and N-Ge systems the equilibrium A15 phase field does not include the stoichiometric composition. The problem is that of phase competition referred to by Professor Massalski in the first session of this meeting. The presence of a stable σ or σ-related compound pushes the range of homogeneity of the A15 compound to the niobium-rich side of the 3:1 composition, as shown in figure 1. The extreme example is Nb_3Ge, which can have a T_c as high as 23 K. When prepared by

*Research carried out under the auspices of the United States Energy Research and Development Administration under Contract No. EY-76-C-02-0016.

bulk melting techniques, the composition of the A15 phase corresponds to Nb_4Ge with T_c of only 6 K. The phase diagram can be beaten by non-equilibrium techniques such as sputtering, chemical vapor deposition, and high vacuum evaporation, all of which can yield thin film material with T_c 22-23 K. It is possible that the addition of a third element will alter the relative stability of the A15 and σ phases, allowing the A15 phase to form at stoichiometry. A precise understanding of phase stability might enable the nature of this third element to be predicted. In the Nb-Al-Ge ternary system, an A15 compound, $Nb_3(Al_{.8}Ge_{.2})$ forms close to stoichiometry. This is believed to be due to a miscibility gap between Nb_2Al and Nb_5Ge_3 just allowing the A15 phase field to advance to the stoichiometric composition, figure 2. A similar situation exists in the Nb-Al-Si system. The existence of the miscibility gap has been related to the presence of a eutectic in the Al-Ge and Al-Si systems[1]. There is also a eutectic in the Al-Ga system, and a miscibility gap between Nb_2Al and Nb_5Ga_3[2]. It is important to know if this is a general rule, and if so, are there other ternary systems based on niobium which allow of the formation of a high T_c stiochiometric A15 phase.

Conductor wire based on Nb_3Sn is fabricated by the 'bronze' process[3]. In this process, filaments of niobium are drawn down in a bronze (Cu-Sn) matrix and subsequently reacted to form a layer of Nb_3Sn. The process is also applicable to V_3Ga, but not to Nb_3Al, Nb_3Ga and Nb_3Ge. Again, the more stable σ and σ-related phases intervene. The system is now a ternary between niobium, copper and a third element. Diffusion between two phases in a ternary system follows the two-phase tie-lines[4]. If there is no tie-line route leading directly from the copper

solid solution to the A15 phase, then it is unlikely that the phase will form. In the case of Nb-Cu-Sn, there are direct tie-lines from the copper-tin solid solution (bronze) to the A15 phase, Nb_3Sn, figure 3, and the process is successful for Nb_3Sn. In the Nb-Cu-Ge ternary the tie-lines from the copper-germanium solid solution lead only to either of the phases Nb_5Ge_3 or Nb_3Ge_2, at low and high germanium concentrations, respectively[5] (see Fig. 4). These phases are more stable than Nb_3Ge, and therefore do not allow the latter to form[6]. A Nb-Al-Cu ternary μ-phase intervenes between the Cu-Al solid solution and Nb_3Al in the Nb-Al-Cu ternary[7]. In the V-Cu-Si system the tielines lead to V_3Si at low, ~1% Si concentrations in the copper but to V_5Si_3 as the silicon content is increased[8].

A knowledge of the various ternary diagrams is necessary in order to predict diffusion routes. It would also be advantageous to know whether the addition of a fourth element is likely to alter phase stability and tie-lines such that the desired A15 phases become accessible by a direct diffusion path.

References

1. D. Dew-Hughes, Cryogenics 15, 435 (1975).
2. M. Drys, J. Less Common Metals 44, 229 (1976).
3. M. Suenaga, W. B. Sampson and C. J. Klamut, IEEE Transactions on Magnetics MAG-11, 231 (1975).
4. J. B. Clark and F. N. Rhines, Trans. A.S.M. 51, 199 (1959).
5. R. H. Hopkins, G. W. Roland and M. R. Daniel, Metallurgical Transactions 8A, 91 (1977).
6. T. S. Luhman, O. Horigami and D. Dew-Hughes, Applied Polymer Symposium No. 29, 61 (1976).
7. C. R. Hunt, Jr. and A. Raman, Zeit. Metallkunde 59, 701 (1968)
8. J. D. Livingston, to be published.

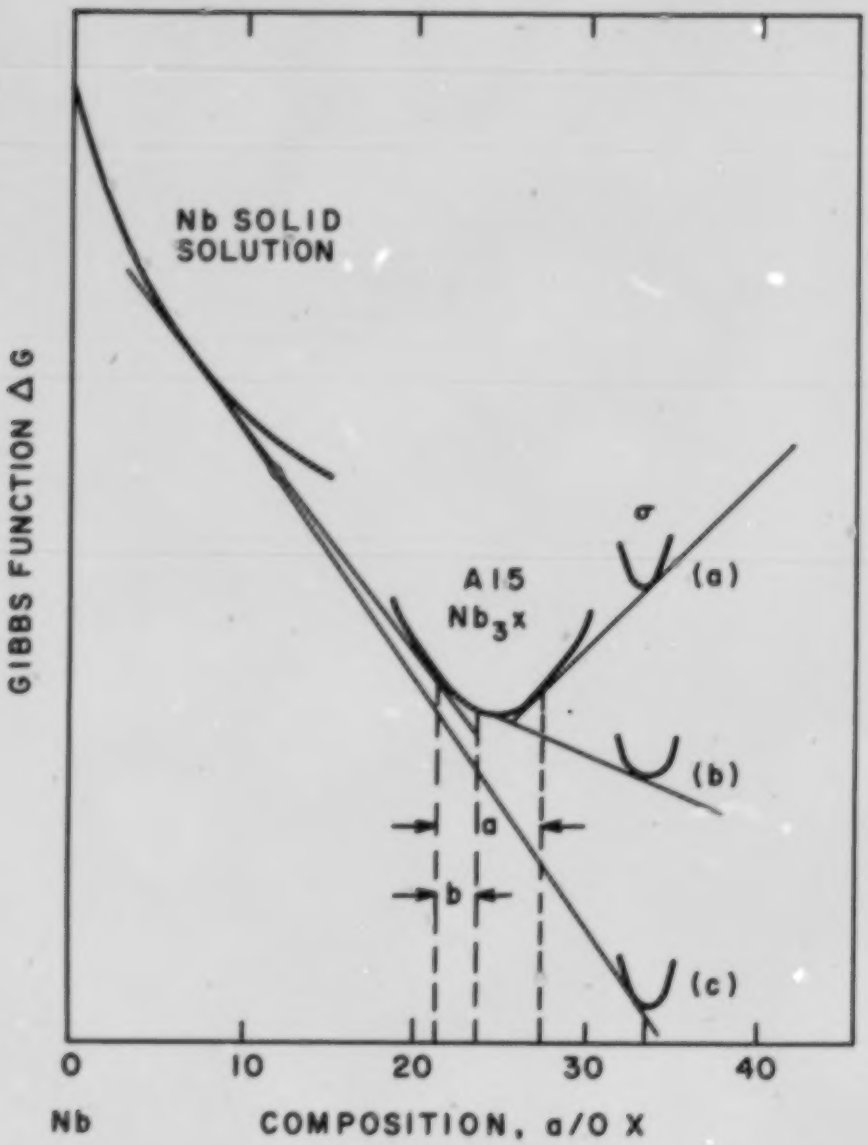

FIGURE 1. Hypothetical Nb-X binary system, showing how the range of homogeneity of the Nb_3X A15 phase is reduced by increasing stability (lower ΔG) of the competing σ phase.

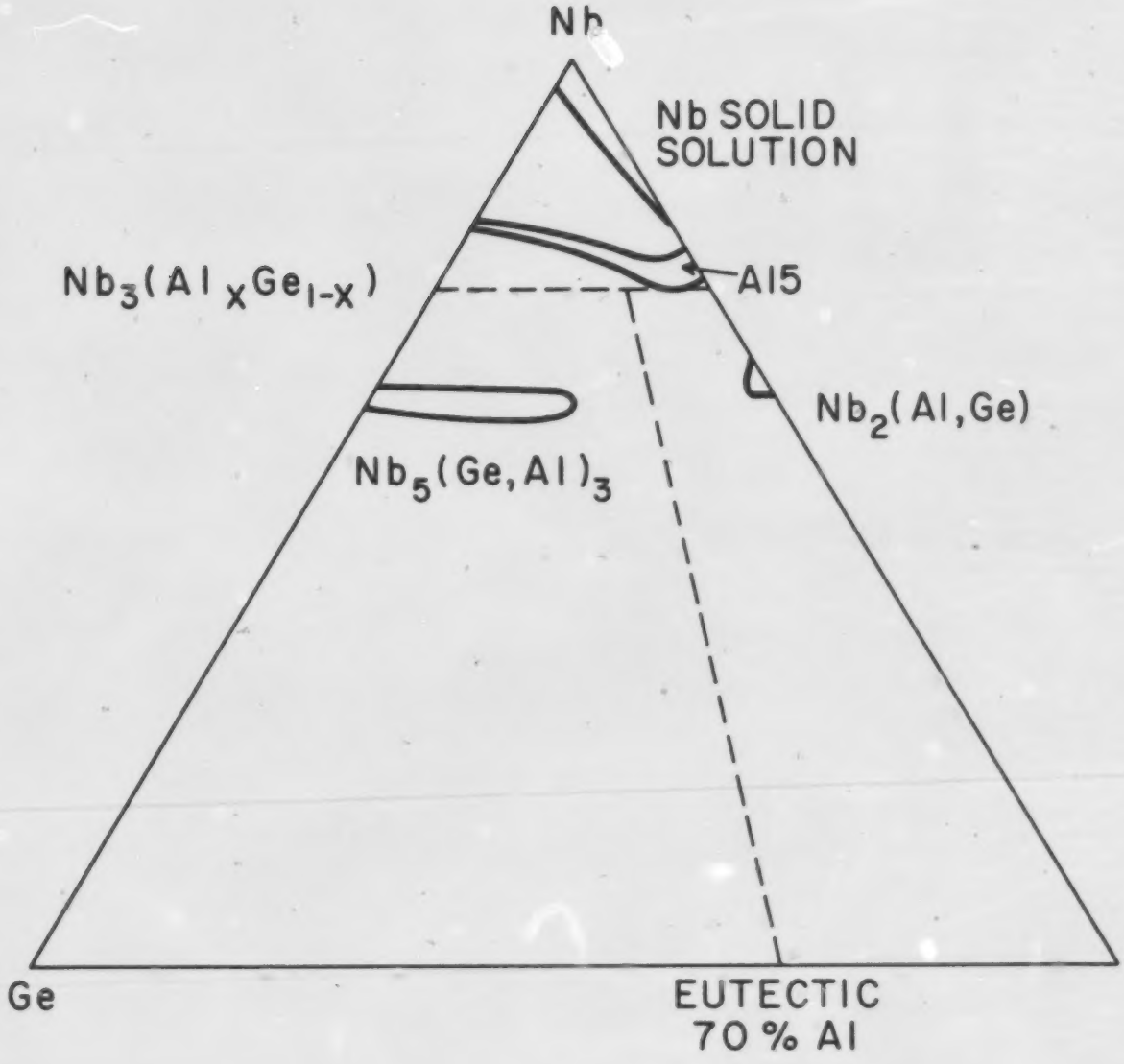

FIGURE 2. A section of the Nb-Al-Ge ternary phase diagram at 1840°C (after reference (1)).

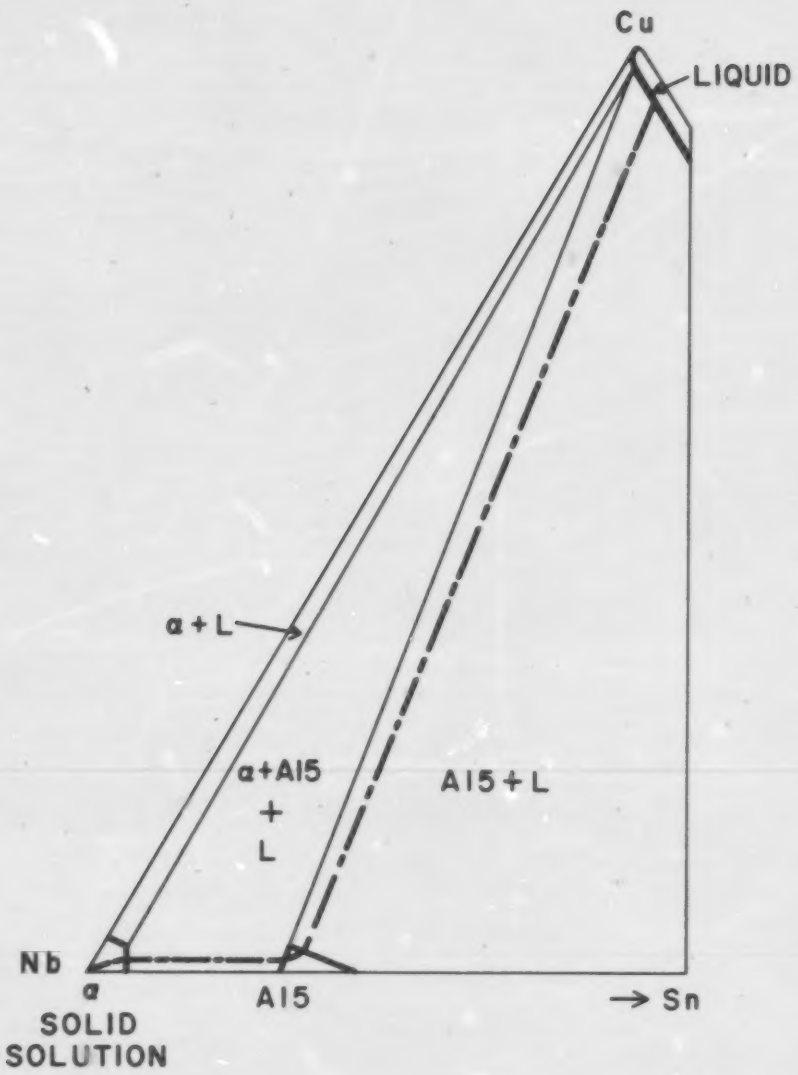

FIGURE 3. A section of the Nb-Sn-Cu ternary phase diagram at 1100°C, showing the diffusion path between Nb and Cu-Sn solid solution, via Nb_3Sn (after reference (5)).

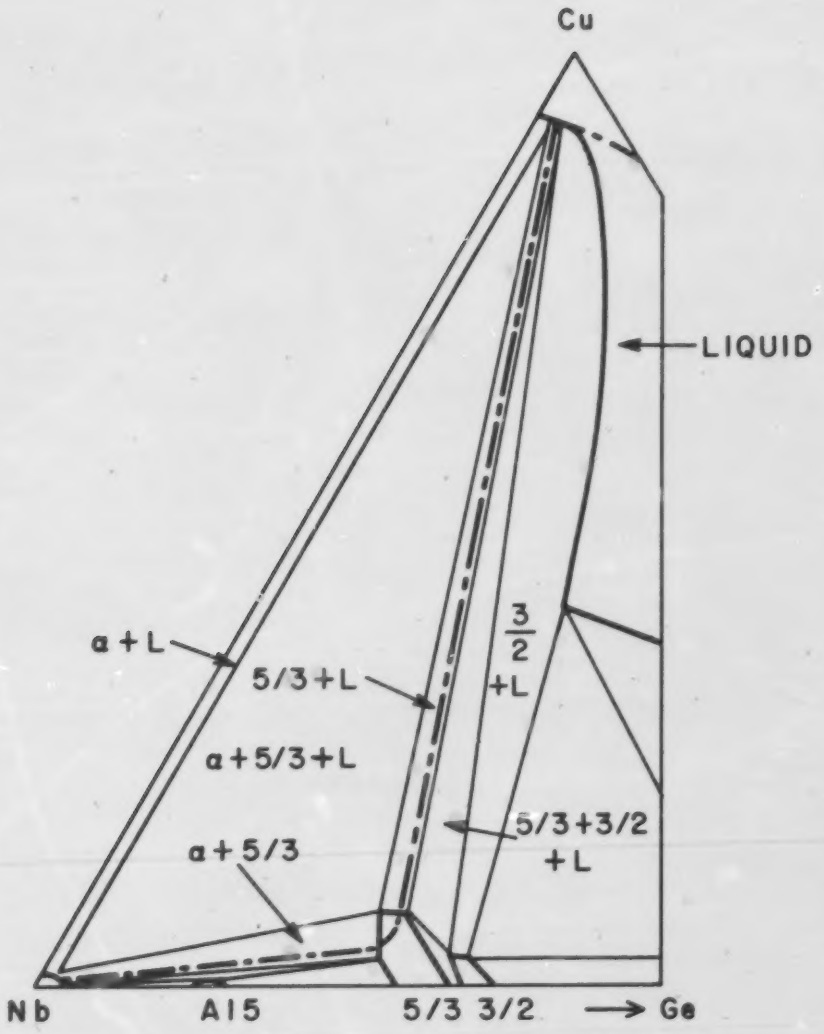

FIGURE 4. A section of the Nb-Ge-Cu ternary phase diagram at 1100°C, showing the diffusion path between Nb and Cu-Ge solid solution. The Nb_3Ge phase is cut off by the intervention of the 5/3 phase (after reference (5)).

PANEL IV

Product Applications

(User Needs for Phase Diagram Information)

Moderator: F. L. VerSnyder, Materials Engineering and Research, Pratt and Whitney Aircraft, U.T.C., E. Hartford, CT

Panel Members:

C. Greskovich, Research and Development Center, General Electric Co., Schenectady, NY

R. I. Jaffee, Fossil Fuel & Advanced Systems Div., Electric Power Research Institute, Palo Alto, CA

B. H. Kear, Materials Engineering and Research Laboratory, Pratt and Whitney Aircraft, U.T.C., Middletown, CT

A. I. Mlavsky, Sr. Vice President of Technology, Tyco Laboratories, Inc., Waltham, MA

P. Slick, Bell Telephone Laboatories, Allentown, PA

National Bureau of Standards SP-496, Applications of Phase Diagrams in Metallurgy and Ceramics
Proceedings of Workshop held at NBS, Gaithersburg, Md., January 10-12, 1977

PANEL DISCUSSION: PRODUCT APPLICATIONS

Opening Remarks by the Moderator

F. L. VerSnyder
Materials and Engineering Research*
Pratt and Whitney Aircraft, U.T.C.
E. Hartford, CT 06108

After introducing the panel members, Chairman VerSnyder gave a brief example of phase diagram applications to a bonding method called Transient Liquid Phase Bonding which is used in the production of gas turbine engines. This method produces high quality bonds with properties that are equivalent to the materials being joined, with the simplicity in production that is characteristic of a simple brazing operation, thus avoiding exceedingly costly processes.

A summary of VerSnyder description of the Transient Liquid Phase Bond (TLP Bond), follows in these paragraphs.

In TLP bonding a thin (.001 - .004") interlayer alloy of specific composition is placed between the mating surfaces of the parts to be joined. The parts are held together under slight compressive pressure (only a few psi is necessary) and heated to the bonding temperature (typically 2000 - 2200°F) in protective atmosphere (vacuum or inert gas). At the bonding temperature, the interlayer initially melts filling the gaps between the mating surfaces with a thin liquid layer. While the parts are held at the bonding temperature, interdiffusion between the interlayer and the parent material raises the melting point of the joint and causes it to solidify isothermally, thus forming a bond. At the completion of isothermal solidification, the joint microstructure generally resembles that of the base metal except for some residual compositional and structural heterogeneity. At this stage the bond has excellent properties although not fully equivalent to the parent metal. To obtain bonds with strengths similar to that of the parent metal, the bond thermal cycle can be continued to further homogenize the joint composition and structure until it is essentially equivalent to the base metal.

Unlike most other practical metallurgical processes, the TLP bonding process occurs under equilibrium conditions. For this reason, the pertinent phase relationships existing during a TLP bond cycle can be viewed with respect to a classic equilibrium phase diagram. The TLP interlayer alloys are designed so they are similar in composition to the alloys being joined, with the principle exceptions that 1) some parent metal elements are either excluded or limited in amount to avoid unwanted phase formation and 2) a melting point depressant is added (currently, boron is utilized as our primary melting point depressant).

---

*presently Manager, Materials Technology, United Technologies Research Center, East Hartford, CT 06108

This view of TLP bonding as an equilibrium process aids further in understanding the influence of many of the bond process variables, the principal variables being base alloy and interlayer composition, bond temperature and bond time. Depending on the base alloy being bonded (or dissimilar metal combination, which is also possible), the interlayer is "tailored" to provide as homogeneous a joint in as short a time as possible. This is done by matching the solute/hardener content of the interlayer as close as possible to the base alloy. For example, titanium is normally excluded since it promotes the formation of undesirable stable precipitates in the joint. Also, the melting point depressant, boron, is added at levels just sufficient to cause enough melting for good bonding. In most cases, less than 100% melting is required (interlayer composition is in the $\alpha + L$ region at the bond temperature). While these interlayers are brittle in bulk form, P&WA has developed and patented a method for making them as ductile foil.

The TLP bonding process is now utilized for the production bonding of low pressure turbine vane clusters for the JT9D engine. By clustering vanes in this manner, significant engine performance improvements are realized primarily as a result of reduced turbine air leakage between vanes. Simple ceramic fixtures are used to hold the vanes in the proper position and also to provide the dead weight loading used during the bond cycle. Both new and previously used vanes (for retrofit into existing engines) have been clustered. Since 1972 over 116,000 clusters have been bonded at a yield well in excess of 99%. These figures demonstrate the production applicability and reliability of this joining process.

VerSnyder concluded:

"I do not think we would ever expect anyone to try to work out all of the details of the foil composition, because, like the superalloy itself, it contains at least five or six components, perhaps not ten, but, at least five or six. General phase information on these superalloy systems is very helpful and with an adequate supply of information we then can carry forward and complete the in-depth process of getting information that finally leads to the application."

National Bureau of Standards SP-496, Applications of Phase Diagrams in Metallurgy and Ceramics
Proceedings of Workshop held at NBS, Gaithersburg, Md., January 10-12, 1977

"IMPORTANCE OF PHASE DIAGRAMS IN THE ELECTRIC POWER INDUSTRY"

R. I. Jaffee
Electric Power Research Institute
Palo Alto, California 94304

To talk on behalf of phase diagrams is like talking on behalf of truth and love, because everybody is in favor of them. In the electrical power industry, equipment must last for lifetimes of 20-40 years at elevated temperatures in many cases. Under these conditions, equilibrium has a very good chance of being attained. In fact, many problems occur because materials are placed in service that are not in equilibrium, and become equilibrated in service, with an accompanying detrimental change in properties.

It is true that many commercial alloys are complex with many alloying components, generally greater than four. Thus, phase diagram information, which is generally limited to ternary equilibrium at best, is not strictly applicable. However, it is my observation that most alloys are dominated by two or three elements, and that a great deal of useful information can be obtained from binary and ternary phase diagrams. In cases where more accurate information is needed, quaternary and even quintanary sections, where the base composition is kept fixed, and alloy elements are varied over limited alloying ranges, can be developed. It is surprising, therefore, that the conference is so negative about the difficulty of the problem of dealing with multi-component equilibrium. Generally, one is concerned with a fairly specific composition, whose deviation from equilibrium is of primary concern. This problem certainly can be handled.

A major problem is metastable equilibrium, which is usually encountered in industry. A typical example is carbide equilibrium in steel. The formation of carbides takes place by kinetic and not equilibrium forces, such that the easiest carbide to form generally forms first. It then may transform to other carbides during elevated temperature service. Ultimately, the carbide itself may be metastable, and one ends up as graphite. No one would develop a practical steel on the basis of the iron-graphite diagram. In real life, one must deal with metastable equilibrium systems.

As an example, take pressure vessel steels for coal conversion. The pressure vessel is generally maintained at 400-500C maximum. In the case of coal liquefaction, it contains 40-50% hydrogen and hydrogen sulfide at pressures up to several hundred atmospheres. A type of phase diagram is used to design such pressure vessels. It is called a Nelson diagram in which the safe operating temperatures and hydrogen pressures are plotted for various pressure vessel steels. A typical Nelson curve is shown in Figure 1. These curves are based on operating experience, in that at some time decarburization or actual failure of pressure vessels made of the particular steel occurred under T-P conditions above the line, and satisfactory operation has been obtained below the line.

The pressure vessels may fail by hydrogen attack at elevated temperatures or hydrogen embrittlement at low temperatures. In the hydrogen attack case, hydrogen diffuses into the steel and reacts with carbides, forming

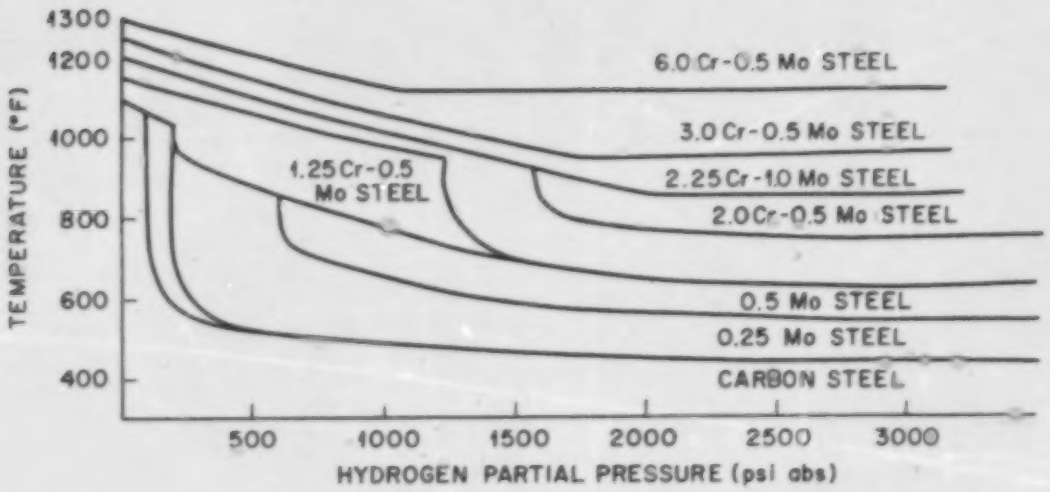

Fig. 1. Operating limits for steels in hydrogen service - the Nelson curves.

internal methane at high pressure, which is trapped at the point of formation, and facilitates crack propagation. In the case of hydrogen embrittlement, the solubility of hydrogen decreases with temperature. A high internal hydrogen pressure may develop if the vessel is cooled too rapidly for the hydrogen to diffuse out of the steel. These are all situations that can be described by phase diagrams involving hydrogen and methane in equilibrium with steel. The carbide in the steel may itself be in a stage of metastable equilibrium. Much higher methane pressures are developed with iron carbide than with alloy carbides. Thus, for safe operation of pressure vessels, it is important to employ heat treatment schedules which develop the equilibrium carbides.

Another example of interest to the electric power industry has to do with the segregation of non-metallic elements such as phosphorus, antimony,

tin and silicon to the grain boundaries of steel during elevated temperature operation. Grain boundary segregation reduces low temperature ductility and is called temper embrittlement. The problem was not properly understood for many years until improved methods to study grain boundaries were developed. The principal technique was Auger electron spectroscopy, which permits the extent of grain boundary segregation to be measured. In this regard, it is clear that phase equilibrium at grain boundaries is considerably different from equilibrium within the grain itself. It might be worthwhile to develop phase diagrams in which equilibrium at grain boundaries and surfaces are described.

Another industrial problem of interest to both steam and gas turbines is the phase stability of the alloys, which are exposed to elevated temperatures over long periods of service. It is desirable to be able to predict the approach to equilibrium. Considerable use has been made of the electron vacancy concept known as "Phacomp".* This is essentially an adaptation of the rigid band model of electron structure of transition metals. If the maximum number of stable d electrons is taken as 10, the electron vacancy is the average group number subtracted from 10 after allowing for the stable compounds such as carbides that precipitate from solid solution before the alloy is placed in service. The electron vacancy number of alloys is then correlated with the occurrence of embrittling phases such as Laves or sigma phases, which are found to occur in specific ranges. The alloy designer tries to keep his alloy composition away from these ranges. Another phase stability method being developed

*Editor's note: The paper by R. L. Dreshfield (Panel I) in these proceedings gives a more detailed description of the Phacomp concept.

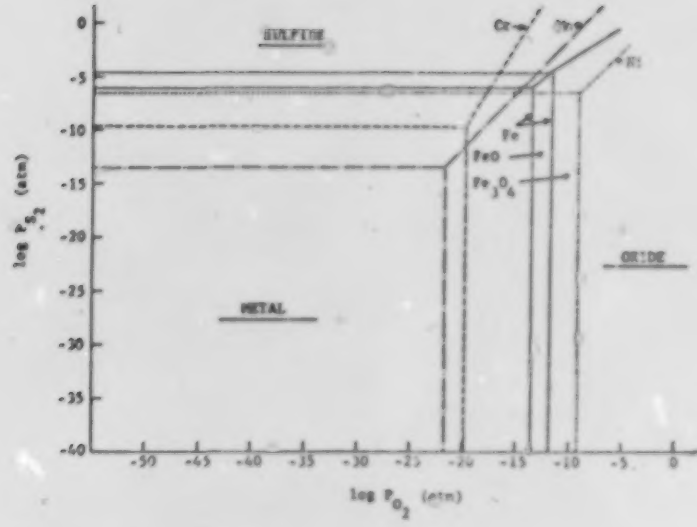

Fig. 2. Comparison of Metal-S-O Diagrams at 1366°K (2000°F) for Cr, Mn, Fe and Ni.

by Machlin at Columbia uses a pair potential method, where the energy in the complex alloy is summed up and minimized. The pair potential method has an advantage over Phacomp in that it does not require the constant electron vacancy value for each group of the Periodic table.

Another type of phase diagram of interest in the power industry has to do with equilibrium between non-metallic phases and alloys. These are important in hot corrosion of turbines and boilers. An area of current interest is the solubility of impurities in steam. In the low pressure steam turbine, highest concentration of impurities precipitate first, and can cause pitting and stress corrosion. For example, high caustic concentration droplets may form on the blades, discs and shafts of the LP turbine, which creates a stress corrosion and corrosion fatigue hazard.

The last example is the use of so-called phase stability diagrams in hot corrosion. These are Pourbaix-Ellingham diagrams which are constructed from the standard free energy formation of the oxides, sulfides or carbides converted to an equivalent dissociation pressure from the relationship, $\Delta G^{O} = RT\ln K$. For the reaction $M + \frac{1}{2}O_2 = MO$, $K = \frac{a_{MO}}{a_M \times P_{O_2}^{\frac{1}{2}}}$

Taking activities of the solids at unity, $\Delta G^{O} = RT\ln P_{O_2}^{-\frac{1}{2}}$

This permits the oxygen partial pressure to be calculated as a function of temperature. Figure 2 shows Metal-S-O diagrams for Cr, Mn, Fe, and Ni. The stable phases that form as a function of P_{O_2}, P_{S_2}, and a_C of a multi-component gas or condensed salts in contact with metallic alloys can be predicted from these diagrams. They are also helpful in guiding conditions of operations to avoid excessive corrosion that might occur if the reaction products are molten.

National Bureau of Standards SP-496, Applications of Phase Diagrams in Metallurgy and Ceramics
Proceedings of Workshop held at NBS, Gaithersburg, Md., January 10-12, 1977

Summary of Presentation on User Needs of Phase Diagrams: The Solar Energy Field

A. I. Mlavsky
Sr. Vice President of Technology
Tyco Laboratories, Inc.
Waltham, MA

Several requirements in the solar energy field were outlined that could be met with better phase diagram information.

Heat Storage

The ability to store heat at various pre-selected temperatures in compact systems would be of great value in a variety of solar energy systems. Salt mixtures with eutectic temperatures of 160°F for space heating and hot water, 220°F for absorption air conditioners, and 500 - 800°F for steam turbine or Rankin cycle engines would be of great value.

Solar Cells

Low cost silicon solar cells for terrestrial use require non-noble metal contacts to silicon surfaces, these contacts meeting certain stringent criteria. They must be ohmic, and of low resistance; they must be applied to the silicon by low cost techniques such as plating (electro or electroless) or screen printing; they must be adaptable to either copper or aluminum wires as power leads. Although there clearly have been developed many excellent ohmic contacts to silicon, the criteria of low cost both in the metals chosen and their means of application are quite specific to the solar cell requirements. Detailed phase information will be necessary to permit the development of such contacts. Although simple binaries between metal and silicon are well defined, there is seldom any detailed information in the 99 - 99.9% silicon-rich range. The interface region at a contact is indeed in this range.

The problem becomes even more acute in making contact to compound semiconductors where at least three component systems must be considered.

Any information which could be generated by practitioners of classical phase equilibria techniques would find a very ready audience among developers of low cost solar cells.

1505

National Bureau of Standards SP-496, Applications of Phase Diagrams in Metallurgy and Ceramics
Proceedings of Workshop held at NBS, Gaithersburg, Md., January 10-12, 1977

Summary of Presentation given for Panel IV by

P. Slick
Bell Telephone Laboratories
Allentown, PA 18103

on

The Use of Phase Equilibria in the Manufacture of Spinel Ferrites

(summary prepared by the editor of these proceedings)

The importance of use of the condensed and phase equilibria for the manufacture of low-loss manganese-zinc-ferrites was discussed by Slick. Multicomponent equilibrium diagrams were said not to be available for the complex processes of deriving manganese-zinc-ferrite spinels, but existing information on condensed phase equilibria for simpler, related systems was said to be used to infer this information for the actual processes. To better understand the mechanisms involved, additional data on phase equilibria were said to be important.

The material manganese-zinc-ferrite, discussed by Slick, is employed in magnetic components of inductors used in filter circuits for telecommunication networks and these materials were said to require close control manufacturing conditions, since the important properties are very dependent on chemistry, microstructure, and defect state (i.e. cation vacancies, nonmagnetic inclusions of second phase and porosity, and compositional inhomogeneity).

Slick noted that one of the most important requirements for low loss ferrite materials is to have a high resistivity phase at grain boundaries. The formation of a high resistivity phase at grain boundaries is needed to reduce eddy current losses, and is exemplified by a condensed phase equilibrium. Minute quantities of calcia and silica, added to the spinel ferrites were said to produce this high resistivity boundary. The exact composition and phase, or phases are not known in the grain boundary, but analysis confirms the segregation of calcia and silica in the grain boundary.

Slick indicated that it is felt that the segregation of calcia and silica, at grain boundaries in manganese-zinc-ferrites may be manifested by a low temperature eutectic of some composition, even though no local phase has been found for the amounts of calcium silicate added in these materials. He noted that it would be of specific interest in this application to develop a phase equilibrium diagram of minute amounts of phases with a specific manganese-zinc-ferrite or any particular ferrite composition, calcia and silica, to better understand the mechanism for producing the segregation of calcium silicate in the grain boundary and especially its influence on high quality manganese-zinc-ferrite properties.

National Bureau of Standards SP-496, Applications of Phase Diagrams in Metallurgy and Ceramics
Proceedings of Workshop held at NBS, Gaithersburg, Md., January 10-12, 1977

THE APPLICATION OF THE PHASE DIAGRAM TO THERMAL ENERGY STORAGE TECHNOLOGY

Jerry E. Beam
Air Force Aero Propulsion Laboratory
Wright-Patterson Air Force Base, OH 45433

and

Joseph E. Davison, Ph.D.
University of Dayton Research Institute
Dayton, OH 45469

1.0 INTRODUCTION

In our program, we are evaluating the potential of phase change thermal energy storage devices to provide heat energy to operate a Vuillieumier cooler for space satellite applications. We have selected the liquid-solid transformation as the energy storage mechanism. Our next step has been to identify liquid-solid transformations which have the largest storage capacity in the temperature range for our application. In this presentation, we have identified those pure components which are of primary interest and the type of data available in the phase diagram which can be utilized to assess the relative merits of different materials.

2.0 SELECTION OF MATERIALS

The tabulated values for the enthalpy of fusion and the melting temperature of the pure components provide a quantitative basis for the selection of phase change thermal energy storage materials. Values for selected elements, inorganic oxides, and inorganic fluorides are presented in Table 1. Extensive compilations of these values for different classes of pure components have been prepared and are available (1-11). The selection of a pure component as the energy storage media limits the application temperature to the melting temperature of the component. This limitation can be circumvented to some extent by selecting intermediate compositions between or among pure components. These intermediate compositions can be readily identified from the appropriate phase diagram. As an example, the melting points of the fluorides of lithium and magnesium are respectively 848°C and 1242°C.

TABLE 1

SELECTED VALUES FOR THE ENTHALPY OF FUSION AND THE MELTING TEMPERATURE

	Enthalpy of Fusion K Joules/gram	Melting Temperature Deg. C	Ref.
a. Elements			
Carbon	(8.71)	(4327)	5
Boron	(2.05)	2027	5
Silicon	1.80	1412	5
Beryllium	1.36	1287	5
Phosphorus (red)	0.61	597	1
Germanium	0.51	937	5
Lithium	0.43	181	5
Vanadium	(0.41)	1902	5
Aluminum	0.40	660	5
b. Oxides			
ThO_2	4.61	2952	3
BeO	2.53	2547	1
Li_2O	(1.96)	1570	1
MgO	(1.92)	2825	1
Al_2O_3	1.16	2042	1
c. Fluorides			
LiF	1.04	848	1
MgF_2	0.93	1242	1
NaF	0.79	996	1
CaF_2	0.61	1127	1
FeF_2	(0.55)	(1100)	1
ScF_3	0.49	1227	3
TiF_3	0.48	1227	3
KF	0.47	858	1

The phase relations in the binary system of these two components has been studied (11,12) and an eutectic transformation has been identified at 724°C and at 33 mode percent MgF_2. Additional invariant points of ternary eutectic compositions at lower temperatures may be obtained by adding NaF or KF. Thus, the temperature of the liquid-solid transformation can be tailored to the particular application. The types of liquid-solid transformations which

we have identified for our applications are the eutectic transformation and the congruent melting of an intermediate compound. The selection of these transformations is based on their reproducibility during cycling between the liquid and solid states. Although the peritectic reaction is reversible in a thermodynamic sense, the time required to attain an equilibrium state on cooling through the peritectic horizational was judged to be unsatisfactory for short duty cycles.

2.1 THE ENTHALPY OF THE LIQUID-SOLID TRANSFORMATION

The amount of heat energy which can be stored or released in the isothermal and reversible transformation between a pure solid and liquid phase at constant pressure is obtained directly from the value for the enthalpy of fusion of the substance. However, when two solid phases of different compositions react to form a single liquid phase, then the value for the enthalpy of mixing must be taken into account to determine the amount of heat energy involved in the liquid-solid transformation.

The effect of the enthalpy of mixing on the energy storage capacity of a liquid-solid transformation can be assessed by consideration of the following thermodynamic cycle. The isothermal and reversible reaction between two solid phases may be considered as the sum of the following processes:

$$\begin{array}{ccccc} n\,A(\ell) & + & m\,B(\ell) & \xrightarrow{\text{step 3}} & (n+m)\;AB(\ell, \text{sol'n}),\quad T_2 \\ \text{step 1}\uparrow & & \text{step 2}\uparrow & & \text{step 4}\downarrow \\ n\,A(s) & + & m\,B(s) & \xrightarrow{\text{step 5}} & (n+m)\;AB(\ell, \text{sol'n}),\quad T_1 \end{array} \qquad (1)$$

Step 1: Heat "n" moles of component A from temperature T_1 to T_2. The enthalpy change of this step is given by,

$$\Delta H_1 = n \int_{T_1}^{T_A} C_{P,A}\,dT + n\,\Delta H_{M,A} + n \int_{T_A}^{T_2} C_{P,A}\,dT, \qquad (2)$$

where T_A represents the melting point of pure A.

Step 2: Heat "m" moles of component B from temperature T_1 to T_2. The enthalpy change for this step is given by,

$$\Delta H_2 = m \int_{T_1}^{T_B} C_{P,B} dT + m \Delta H_{M,B} + m \int_{T_B}^{T_2} C_{P,B} dT, \quad (3)$$

where T_B represents the melting point of pure B.

Step 3: React the two separate liquid components to form the AB liquid solution at a temperature of T_2. The enthalpy change for this step is given by,

$$\Delta H_3 = (n+m) \Delta H (mix), \quad (4)$$

Step 4: Cool the AB liquid solution from temperature T_2 to T_1. The enthalpy change for this step is given by,

$$\Delta H_4 = (n+m) \int_{T_2}^{T_1} C_{P,AB} dT. \quad (5)$$

Step 5: The value for the enthalpy of the liquid-solid transformation between the two solid phases, A and B, and the liquid solution, AB, at the temperature, T_1, can be expressed as the sum of the enthalpies of the first four steps, and is as follows,

$$\Delta H_5 = n \Delta H_{M,A} + m \Delta H_{M,B} + (n+m) \Delta H(mix.) +$$

$$n \int_{T_1}^{T_A} C_{P,A} dT + n \int_{T_A}^{T_2} C_{P,A} dT + m \int_{T_1}^{T_B} C_{P,B} dT +$$

$$m \int_{T_B}^{T_2} C_{P,B} dT + (n+m) \int_{T_2}^{T_1} C_{P,AB} dT. \quad (6)$$

In the absence of data for the heat capacities of the liquid phase, the Neumann-Kopf Rule states that the heat capacity of a substance may be taken as the sum of the heat capacities of the elemental constituents. The application of this rule in the present analysis gives a zero value to the sum of heat capacity terms. As a result, the heat energy which can be stored in the isothermal liquid-solid transformation is given by,

$$\Delta H_5 \approx n\,\Delta H_{M,A} + m\,\Delta H_{M,B} + (n+m)\,\Delta H(\text{mix}). \qquad (7)$$

The first two terms on the right-hand side of this expression are properties of the individual components. The last term on the right is the contribution due to the enthalpy of mixing. The effect of the enthalpy of mixing on the heat of the liquid-solid transformation can be either positive or negative depending on whether the reaction is endothermic or exothermic. If the reaction is endothermic, then the enthalpy of mixing is positive and additional heat energy can be stored in the transformation. If the reaction is exothermic, then the converse is true and less heat energy can be stored in the transformation than would be predicted from the properties of the individual components.

Unfortunately, the data for the enthalpy of mixing are available for relatively few systems. In order to obtain values for the enthalpy of mixing we have combined experimental data which is presented in the phase diagrams with analytical thermodynamic models to obtain the required data.

2.2 THE ENTHALPY OF MIXING

Analytical expressions for the liquidus and solidus phase boundaries can be obtained by combining basic thermodynamic principles with a thermodynamic model of the alloying behavior of the system. When the regular solution model is utilized to represent the alloying characteristics of the system, the following expressions have been obtained for the liquidus and solidus boundaries (13).

$$\Delta H_{fA}(T/T_A - 1) - RT \ln (X_A^{\alpha}/X_A^{L}) = W_1^{\alpha}(X_B^{\alpha})^2 - W_1^{L}(X_B^{L})^2, \qquad (8)$$

and

$$\Delta H_{fB}(T/T_B - 1) - RT \ln (X_B^{\alpha}/X_B^{L}) = W_1^{\alpha}(X_A^{\alpha})^2 - W_1^{L}(X_A^{L})^2. \qquad (9)$$

The values of the parameters, W^{α} and W_1^L, were calculated from Equations (8) and (9) with the known values for the enthalpies of fusion, ΔH_{fA} and ΔH_{fB}, the melting points, T_A and T_B, of the pure constituents, and the composition of the liquidus boundary, X_A^L and X_B^L, and the solidus boundaries, X_A^{α} and X_B^{α}, at the temperature, T. The enthalpy of mixing of the liquid solution is related to the parameter, W_1^L, by the expression,

$$\Delta H \text{ (mix)} = X_A^L X_B^L W_1^L. \qquad (10)$$

An underlying assumption in this approach is that the crystal structures of the two solid phases, A and B, are the same. If the crystal structures are different, then the enthalpy of the solid state transformation between the two structures must be known to obtain an exact solution. In the absence of any data, a zero value was assigned to the enthalpy of the solid state transformation. The data taken from selected phase diagrams and the results of the computations for the parameters W_L and W_S are presented in Table 2. The values of the composition of the solidus boundary were available on only a few of the systems studied. In the absence of any experimental data, a value of 0.999999 was assigned to the solidus composition. The calculated values for the enthalpy of mixing at a mole fraction of 0.5 are compared to experimental values which have been measured on these systems in Table 3. The negative values for the enthalpy of mixing have the effect of decreasing the energy storage capacity of the binary systems in accord with the relation 7. However, the magnitude of the decrease for the system, LiF - KF, represents less than 15 percent of the value for the enthalpy of fusion of the LiF.

3.0 SPECIFIC USER NEEDS

The phase diagrams which are of special interest to a phase change thermal storage technology base for space satellite applications are those which have the largest value for the enthalpy of the liquid-solid transformation

TABLE 2

EXPERIMENTAL DATA FOR THE TEMPERATURE AND COMPOSITION OF THE LIQUIDUS AND SOLIDUS PHASE BOUNDARIES

System A	System B	Temp. Deg. C	Mole Fraction Liquidus	Mole Fraction Solidus	W_L K Joules per Mole	W_S K Joules per Mole
a. Chlorides:						
AgCl	KCl	306	0.695	*	-10.2	---
$AlCl_3$	KCl	250	0.495	*	-40.5	---
$AlCl_3$	NaCl	152	0.490	*	-60.4	---
$CaCl_2$	$FeCl_2$	592	0.445	*	4.0	---
$CaCl_2$	$MgCl_2$	621	0.428	0.877	5.3	20.1
$CaCl_2$	NaCl	500	0.52	*	-11.4	---
$FeCl_2$	NaCl	370	0.43	*	-19.4	-4.8
$FeCl_3$	NaCl	158	0.54	*	-39.5	---
KCl	LiCl	358	0.586	*	-16.8	---
LiCl	RbCl	312	0.5525	*	-19.2	---
b. Fluorides:						
KF	LiF	492	0.5	*	-17.2	---
KF	MgF_2	778	0.85	*	-47.6	---
KF	NaF	710	0.6	0.88	-0.01	22.4
LiF	MgF_2	724	0.68	0.94	-1.3	37.5
LiF	NaF	649	0.61	*	-6.4	---
LiF	RbF	450	0.47	*	-18.0	---
MgF_2	NaF	987	0.64	*	-39.5	---
MgF_2	RbF	883	0.625	*	-65.9	---
NaF	RbF	664	0.33	*	-0.1	---
c. Oxides:						
B_2O_3	Li_2O	715	0.55	*	-27.2	---
Bi_2O_3	Li_2O	730	0.92	*	-272.	---
Li_2O	MoO_3	570	0.75	*	-25.3	---
Li_2O	V_2O_5	621	0.835	*	-10.4	---
Li_2O	WO_3	800	0.63	*	-41.1	---

* In the absence of any experimental information, the mole fraction of the solidus boundary is assumed to be 1.000.

TABLE 3

CALCULATED AND EXPERIMENTAL VALUES
FOR THE ENTHALPY OF MIXING

System		ΔH mix, N = 0.5 K Joules per Mole Calc.	Exp.
AgCl	KCl	-2.5	-0.84[1], -2.31[2]
KCl	LiCl	-4.2	-4.39[2], -3.98[3]
LiCl	RbCl	-4.8	-5.02[2]
LiF	KF	-4.3	-4.47[3]
$Li_2O \cdot 2B_2O_3$*		-6.0*	-3.3[4]*

1. K. Stern, J. Phys. Chem. 60, 679, (1956).
2. L.S. Hersch, O.J. Kleppa, J. Phys. Chem. 42, 3752, (1956).
3. E. Aukrost, B. Bjorge, H. Flood, T. Forlan, Amer. N.Y. Acad. Sci. 79, 830, (1960).
4. JANAF Thermochemical Tables, Dow Chemical Company, Midland, Mich. (1962).

* The calculated and experimental values are for the composition of $Li_2O \cdot 2B_2O_3$.

on a per-unit mass basis. The value for this transformation depends for the most part on the values of the enthalpy of fusion of the pure components and the enthalpy of mixing of the pure components in the liquid phase. The pure components can be selected on the basis of the tabulated values for their enthalpies of fusion. In Table 1 we presented these values for metal oxides and metal fluorides which have the largest values in their respected groups on a per gram basis. Next, we reviewed the number of phase diagrams compiled by the American Ceramic Society (14) which contain one of these pure components. In Table 4 are tabulated the pure component and the total number of phase diagrams presented which contain that component, and many of the systems which have been compiled have been only partially investigated. More comprehensive coverage of systems which contain these components would be of significant value in the selection process.

TABLE 4

THE NUMBER OF PHASE DIAGRAMS COMPILED WHICH CONTAIN A PURE COMPONENT WITH A LARGE VALUE FOR THE ENTHALPY OF FUSION ON A PER-UNIT WEIGHT BASIS

System	Total No. of Systems	No. of Binary Systems	No. of Ternary Systems
LiF	128	42	50
MgF_2	27	12	14
NaF	195	46	91
CoF_2	3	3	0
FeF_2	2	2	0
ScF_3	8	6	2
TiF_3	---	--	--
KF	134	37	52
ThO_2	25	13	11
BeO	36	17	18
Li_2O	94	16	52
MgO	158	35	70
Al_2O_3	207	53	70

The data of primary interest within a particular system are the composition, temperature, and type of liquid-solid transformation.

An assessment of the reliability and the accuracy of thermodynamic models to calculate the enthalpy of mixing from data presented in the phase diagram would likewise be of significant value. If this method can produce reliable thermodynamic data, then a significant increase in our data base for values for the enthalpy of mixing can be made available from the phase diagrams which have been compiled.

4.0 SUMMARY

The applications of the phase diagram to phase change energy storage technology has been presented. Our particular needs are for materials which have large values for the enthalpy of the liquid-solid transformations. Two properties which determine this enthalpy value are the enthalpies of fusion of the pure components and the enthalpy of mixing of the pure components. Values for the enthalpy of mixing can be determined from the data presented in the phase diagram when coupled with a thermodynamic model of the alloying behavior. We hope that our comments will have been of value to assist investigators in assessing the importance of phase diagrams in providing for a technology base for thermal energy storage.

REFERENCES

1. JANAF Thermochemical Tables, 2nd Edition, Dow Chemical Company, Midland, Michigan.

2. Kabaschewski and Evans, Metallurgical Thermochemistry, 3rd Edition, Pergamon Press, New York, 1958.

3. Wicks and Block, Thermodynamic Properties of 65 Elements, Bureau of Mines Bulletin, 605, 1963.

4. Handbook of Materials Science, Volume 1, General Properties, CRC Press, Cleveland, Ohio, 1974.

5. Hultgren et al., Supplement to Selected Values of Thermodynamic Properties of Metals and Alloys, ASM, Metals Park, Ohio, 1974.

6. Thermal and Other Properties of Refractories, LA-5937-MS Informal Report dated March 1975 by Dwayne T. Vier of the Los Alamos Scientific Laboratory, Los Alamos, New Mexico.

7. Janz, George J., Molten Salts Handbook, Academic Press, New York, 1967.

8. Phase Change Materials Handbook, NASA Contractor Report Number NASA CR-61363, dated September 1971 by Hale, Hoover, and O'Neill of Lockheed Missiles and Space Company, Huntsville, Alabama.

9. Determination and Analysis of the Potentialities of Thermal Energy Storage Materials, ASD Technical Report 61-187 dated June 1961 by Wilson, Beahm, and Cooper of the Callery Chemical Company, Callery, Pennsylvania.

10. Survey and Selection of Inorganic Salts for Application to Thermal Energy Storage, ERDA-59 dated June 1975 by Alina Borucka, Borucka Research Company, Livingston, New Jersey.

11. Evaluation of Eutectic Fluoride Thermal Energy Storage Unit Compatibility, AFAPL-TR-79-92-Part 1 by Joseph E. Davison, dated October 1975, University of Dayton, Dayton, Ohio.

12. Voskresenskaya, N.K., Handbook of Solid-Liquid Equilibria in Systems of Anhydrous Inorganic Salts, Volume 1. Available from the U.S. Department of Commerce Clearinghouse for Federal Scientific and Technical Information, Springfield, Virginia.

REFERENCES (concluded)

13. Davison and Rice, Application of Computer Generated Phase Diagrams to Composite Synthesis, NMAB 308-III, dated January 1973. Proceedings of the Conference on In-Situ Composites, September 5-8, 1972, Reported by the National Materials Advisory Board, Washington, D.C.

14. Levin, Robbins, and McMurdie, Phase Diagrams for Ceramists, 1964 (also see the 1969 and 1975 Supplements), The American Ceramic Society, Columbus, Ohio.

National Bureau of Standards SP-496, Applications of Phase Diagrams in Metallurgy and Ceramics
Proceedings of Workshop held at NBS, Gaithersburg, Md., January 10-12, 1977

THE NEEDS FOR PHASE EQUILIBRIA DATA IN THE DEVELOPMENT OF MAGNETOHYDRODYNAMICS*

R. A. Howald and I. Eliezer
Chemistry Department
Montana State University
Bozeman, MT 59715

ABSTRACT

The study of magnetohydrodynamic power production with the use of coal, necessitates a major effort to elucidate to the phase equilibria and thermodynamic properties of a variety of inorganic substances: Liquid or gaseous slag constituents, sulfur compounds and other inorganic materials dissolve protective oxide layers on alloys and have deteriorating effects on ceramic materials used in MHD channels and other components of the MHD power plant. The electrical conductivity in the MHD power generators and the emission of pollutants are also affected by the slag constituents, seed and sulfur compounds, and other inorganic materials. The study of the high temperature equilibria of the materials involved in MHD power generation includes broad ranges of temperature, pressure and oxidation potential, i.e. 1000-2500 K, 1-20 bars, excess oxygen, excess carbon, various moisture contents, etc.

The addition of potassium seed compounds (K_2SO_4, K_2CO_3, etc.) is essential to achieve sufficiently high electrical conductivity in open cycle MHD, and so the interactions between potassium oxide and various refractory oxides are particularly important. Coal slag has actually been used in operating MHD channels as a continually replaced protective coating over the electrodes. Thus the vapor pressures of potassium oxide over typical slag compositions have to be known. For economic reasons

it will be necessary to recover and recycle most of the seed compound, presumably as K_2SO_4. In this connection additional phase equilibria data on solubilities of various oxides in liquid potassium sulfate are needed. Cesium compounds should also be studied since they are used in closed cycle MHD systems.

Large high temperature heat exchangers constitute one of the major capital expenses for MHD. Thus phase relations involved in the preparation and useful lifetime of high temperature ceramics should be investigated in detail.

To summarize, information on the solid, liquid and gas phase relations in a variety of MHD systems is vital both to establish the extent of interaction and to locate temperature and pressure regimes in which deleterious reactions will and will not occur.

Much of the above information is useful for gas turbine engine development as well as for MHD.

Introduction

Of the several alternative energy sources to the conventional power plant, the MHD system seems to have the best efficiency potential which derives mainly from the very high temperature generation of the MHD generator.[1-3] The thermodynamic characteristics of the materials involved at these temperatures are thus of crucial importance to the proper design and operation of an MHD power plant.[4] However, in most cases such information is scant or totally lacking. Therefore a major research program on the thermodynamic properties and phase equilibria of the substances involved is essential if magnetohydrodynamic power production is to become competitive.

Open Cycle MHD Power Generation From Coal

In open cycle MHD power generation the operating substance is a high-temperature plasma made up of hot combustion products and preheated air. In order to obtain the required electrical conductivity, it is necessary to add ionizable substances such as potassium carbonate or sulfate. It is generally accepted that in an economically feasible MHD power generating system the MHD generator is to be coupled to a steam bottoming plant. A schematic representation of an MHD/steam combined cycle plant is given in Figure 1.

Oxidation and Corrosion

Open cycle MHD systems have been operated for periods of up to a hundred hours burning clean fuels. However, MHD can provide a significant contribution to world energy needs only if it can utilize a fuel available in larger, cheaper quantities such as coal. All coals contain substantial quantities of ash and slag constituents causing corrosion of ceramic and metal parts, as is the case for other high temperature systems such as gas turbines.

Metallic and ceramic materials that are exposed to high temperatures are usually protected from oxidation and corrosion by an adhering layer of oxide such as Al_2O_3 or Cr_2O_3. The combustion gases contain vapor species and particulates which condense to liquid sulfates, carbonates, oxides, etc. These liquids are corrosive under both oxidizing and reducing conditions, and may dissolve the protective oxide layers on alloys and ceramics causing serious deterioration of the ceramic or metal parts of the system. Since the physico-chemical interactions in

question will obviously impose severe limitations on the design and operation of the system they must be elucidated. This necessitates thermodynamic information on the vapor pressures of the various species in question, their free energies, their solubilities, the activities of the volatile species when dissolved in typical coal slag liquid oxides, the heat of mixing of the oxides, and the temperature dependence of all these quantities.

The slag may also have beneficial effects on the MHD components, acting as a continually renewable protective coating of the electrode and insulator surfaces and preventing arcing. These effects will again depend on the composition and properties of the slag.

Electrical Conductivity

In the MHD process, the combustion gases are expanded from combustor pressure (1-20 bars) and temperature (1-3 kK) through a duct with a transverse magnetic field (3-7 Tesla) for production of electric power. The gas velocity is of the order of Mach 1. The electrical conductivity of the gas is dependent on the free electron density and the electron mobility. In principle, the conductivity is also dependent on the ions but these are too heavy to contribute appreciably to the conductivity.

The electron density will be reduced by the presence of gaseous species with high electron affinities. The resultant ions can also have adverse effects on the conductivity because they reduce the electron mobility due to their large scattering cross-section. It is therefore important to know the negative ions which are likely to be formed, their electron affinities and their concentrations.

At the temperatures attainable by the combustion of coal with preheated air, it is essential to have a material with a low ionization potential (seed) present to achieve sufficient electrical conductivity. The ionization potential of sodium atoms is slightly too high, but one can use the heavier alkali metals. At the high temperatures involved, substantial alkali metal atom concentrations are obtained from practically any compound. However, it is best to avoid halides because of the electron affinities of halogen atoms. For closed cycle MHD, one can probably recover enough of the seed to consider using expensive material such as cesium metal. With open cycle systems, less seed can be recovered and cost considerations together with the ionization potential and electron affinity considerations mentioned above limit one almost completely to K_2CO_3 and K_2SO_4 as seed compounds. Thus the most important data for the calculation of electron concentrations and conductivities are the equilibria involving potassium atoms and all major potassium containing gaseous species. Much of this information is currently available;[5-8] however, there is still room for improvement in the thermodynamic data for such important species as $K_2SO_4(g)$, $KOH(g)$, $K_2O_2(g)$, and $KO_2(g)$. In addition, data are needed on the interaction of potassium and potassium oxide with various materials which may be present on or in the channel walls.

In MHD coal combustion the main species involved in the formation of negative ions will be carbon, sulfur, nitrogen and metal oxides. Precise thermodynamic data will be necessary for these negative ions as well as the related gases and liquids, since neutral species with high electron momentum transfer collision cross sections, such as SiO, are also important.

Pollution and Seed Recovery

In MHD, as in other power plants, a basic requirement is that pollution levels be kept below EPA requirements. The main species in question are sulfur dioxide and nitrogen oxides.

Another requirement, if MHD is to be economically feasible, is that most of the seed material must be recovered and recycled.

Fortunately, these two requirements interact favorably because the reaction with seed will control sulfur dioxide emission, i.e., the precipitation of potassium sulfate can reduce sulfur in the effluent to very low levels. However, achievement of such a combination of seed recovery and SO_2 emission reduction requires thermodynamic data on the K-S-H-O system at the relevant temperatures and pressures.

Proper separation of the seed from the slag will require phase equilibria data on seed-slag oxide systems including K_2SO_4-K_2O-Al_2O_3-SiO_2-FeO-Fe_2O_3-MgO-CaO. Vaporization data on these seed-slag oxides systems are essential. Gaseous species like K_2SiO_3 and $KAlO_2$ may be stable and data for gaseous aluminum species such as AlO_2 and $HAlO_2$ are poor.

Inorganic oxide systems like the above are very far from ideal. At present, only a few of the binary and ternary subsystems have been analyzed thermodynamically. However, this is sufficient to show that general power series such as the Redlich-Kister[9] and Bale-Pelton[10] equations can represent the data for binary systems, and that it is possible in principle to extend the treatment to multi-component oxide solutions. Working with high temperature oxide systems is very frustrating because while there is a lot of experimental data bearing on the

thermodynamics of these systems, in most cases it has not been collected and evaluated, and there is no standard form for expressing activities and heats of mixing for the few systems which have been analyzed in detail.

At the present time we have available computers and programs which make possible a fully consistent thermodynamic treatment of four or five component oxide systems. In many cases additional activity data from vapor pressures, high temperature e.m.f., solubility, redox equilibria, etc., is required. Many of these systems are slow to reach equilibrium on a macroscopic scale. However, the recent work of Aksay and Pask[11] illustrates how improved solubility data can be obtained with modern techniques such as electron microprobe analysis of diffusion couples. The major additional requirement in most of the systems is good enthalpy data so that activity data can be accurately extended to additional temperatures.

Improved enthalpy data can be obtained either by high temperature calorimetry or by room temperature calorimetry coupled with accurate heat capacity measurements or drop calorimetry for the same compositions. In many cases all that would be required is careful DTA measurement of heats of melting for pure compounds and eutectic compositions. Collection of this data is not particularly glamorous work because there will be few surprises. However, it is essential to supplement the more interesting activity measurements, and those involved in funding research should recognize the importance of obtaining and interpreting enthalpy data on high temperature solutions.

Thus the design of the entire seed regenerator section of the MHD system is subject to the availability of thermodynamic and, in particular, phase equilibria data. For closed cycle MHD systems similar data will be required for cesium compounds.

As to nitrogen oxides, these may be controlled by fuel rich combustion, adding additional oxygen downstream from the MHD channel, but a better way would be their recovery and conversion into fertilizer. This again requires data on the equilibria involved.

Another potential pollution problem in MHD power generation concerns the distribution of toxic trace elements in particulate emissions. In conventional power plants the very small fly ash particles, ($<1\mu$) have been found to be enriched in arsenic, antimony, cadmium, lead, selenium, and thallium.[12,13] This effect and also the concentration of various elements at the surface of fly ash particles[14] is related to partial vaporization of the oxides during combustion. The effects of higher temperature combustion in the MHD process upon these phenomena have not yet been investigated either experimentally or theoretically. However, it is clear that additional data on the high temperature vaporization equilibria of complex oxide systems will be required for a full understanding of the distribution of toxic trace elements in particulate emissions of any coal combustion system.

Refractory Materials

High temperature refractory materials are of major importance in MHD power generation both in the large heat exchangers which constitute a major item of the MHD system and for other purposes, e.g., as conducting

ceramics for electrode materials. Many of them are new materials such as $LaCrO_3$, SiN_4, ZrB_2, etc. Thermodynamic data and phase relations involved in the preparation and useful lifetime of high temperature ceramics and their reactions and products with slag and combustion gases should be known in detail.

Conclusion

Thermodynamic and phase equilibria data needed for the development of MHD include seed and slag interaction with metal alloys and ceramics, slag protection of electrodes, control of polluting effluents, seed recovery and gaseous ions and neutral species influencing electrical conductivity.

The main species involved are gaseous and liquid coal slag components (mostly oxides such as SiO_2, Al_2O_3, FeO, Fe_2O_3, CaO, MgO), seed compounds (such as K_2SO_4, K_2CO_3, Cs_2SO_4. Rb_2CO_3) and related sulfur compounds (such as K_2S, SO_2, $K_2S_2O_3$), slag-seed interaction compounds (such as K_2SiO_3, $K_2Al_{22}O_{34}$, $K_2Al_2Si_2O_6$, $FeSiO_3$), refractory materials (such as Al_2O_3, SiO_2, ZrO_2, $LaCrO_3$, BN) and combustion gases and ions (such as K^+, e^-, OH^-, SO_4^-, AlO_2^-, CO_3^-, NO_2^-).

Thermodynamic and phase equilibria data such as the above are needed not only for MHD power generation but also for gas turbine engine development and for other high-temperature coal conversion processes.

ACKNOWLEDGEMENT

We should like to acknowledge helpful comments by W. Beezhold.

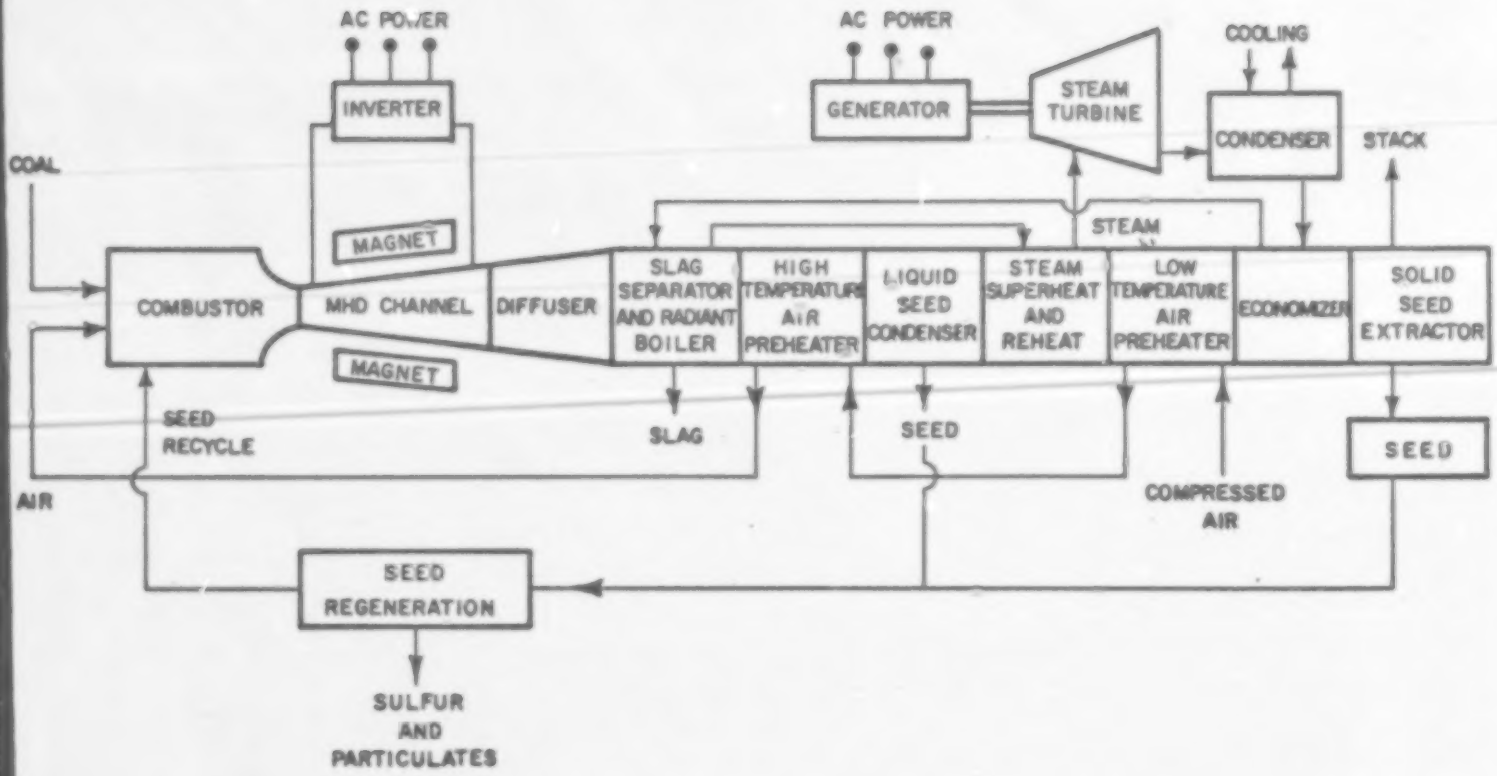

FIGURE 1. A schematic representation of an MHD/steam combined cycle plant.

References

*This work was supported by ERDA under Contract No. E(49-18)-1811.

1. W. D. Jackson, "MHD Electrical Power Generation: Prospects and Issues," AIAA 9th Fluid and Plasma Dyn. Conf., San Diego, California, July 14-16 (1976).
2. ECAS [Energy Conversion Alternatives Study], Westinghouse Electric Corporation Research Laboratories, NASA, CR-134941 (1976).
3. R. J. Rosa, "Magnetohydrodynamic Energy Conversion," McGraw-Hill, New York (1968).
4. J. B. Heywood and G. J. Womack, "Open Cycle MHD Power Generation," Pergamon Press, Oxford (1969).
5. I. Eliezer and R. A. Howald, J. Chem. Phys. 65, 3053 (1976).
6. JANAF Thermochemical Tables, Nat. Stand. Ref. Data Ser., Nat. Bur. Stand. 37 (1971).
7. JANAF Supplements, J. Phys. Chem. Ref. Data 3, 311 (1974); 4, 1 (1975).
8. E. R. Plante, C. D. Olson and T. Negas, 6th International Conference on MHD Electrical Power Generation, Volume II, p. 211, Washington, D.C., June 9-13 (1975).
9. O. Redlich, A. T. Kister and C. E. Turnquist, Chem. Eng. Progr. Symp. Ser. 48 (1952).
10. C. W. Bale and A. D. Pelton, Metal. Trans. 5, 2323 (1974); 6A (1963, 1975).
11. I. A. Aksay and J. A. Pask, J. Amer. Ceram. Soc. 58, 507 (1975).
12. D. F. S. Natusch, J. R. Wallace and C. A. Evans, Jr., Science 183, 202 (1973).
13. J. W. Kaakinen, R. M. Jorden, M. H. Lawasani and R. E. West, Environ. Sci. Technol., 9, 826 (1975).
14. R. W. Linton, D. F. S. Natusch, C. A. Evans, Jr. and P. Williams, Science 191, 852 (1976).

DISCUSSION

L. Kaufman - I would like to make a general comment. I believe that it was pointed out yesterday that you must couple in this environment the thermochemistry and phase diagrams to provide guidence for all these areas. I would like to list several. In the case of Bill Speich's talk, we have much data stored in the [Man Labs - NPL] data-base on solubility products for alloying elements of steels. Those are data that are there now. We have similar data on the range of stability of austentic martensite. Those data are stored there now. We can carry out calculations of tie lines, in copper-niobium or copper-aluminum-X, that's information that's available now. Procedures are being developed to deal with oxides, carbides and borides. That data-base is more fragmetary but the techniques are available now. We don't yet know in general how to do an 8-component system. But 10 years ago we could barely do a binary system and in the last 10 years those of us who operate in this field have advanced from doing binaries routinely, to ternaries routinely and some to quaternaries routinely. So my two points are: a) the correlation and compilation of phase diagrams must be coupled with thermochemistry if we're going to make rational progress, and b) those of you who are interested in phase diagram information, don't stop there. Ask "is there thermochemistry available?" Because often times, information may really be what you want to know.

B. Rosof - I also have a general comment. We have talked about elegant uses of phase diagrams or how important it would be to have a phase diagram solve an elegant problem. All of us here, I'm sure, use phase diagrams in elegant ways. But most [outside] people, wo use phase diagrams, don't. I'll tell you a little short research problem I had that will illustrate this point and is most typical of phase diagram users. I was melting, lets call it, a 10 component alloy in an arc furnace with the usual problems of chrome and carbon equilibrium, of silicon control and aluminam control, etc. And somewhere in this big complex problem I had to add some tantalum. Now you just don't throw tantalum into a furnace. It will sink to the bottom and it's melting point is too high, so it doesn't alloy properly. You want to add this as a Ta-X alloy so it will melt in quickly. You go and grab Hansen off the shelf. You look up... lets see... Ta-Al, Ta-Fe, Ta-Ni, and go through all the components of your system with tantalum. You find one that would make a suitable alloy with a suitably low melting point and in basically less than half an hour you have a solution to your problem. Ah!... the Ta-Fe system looks much better than the Ta-Co system. So you tell the technician, "Take the tantalum, put some iron with it, put it in a vacuum - induction furnace", and now you have your ferro-alloy which is useful, and a solution to the research problem. The point here is that so many of our research problems in the use of phase diagrams are little tiny problems relative to the full complex problems encountered in research. We have to make sure that our phase diagrams are useful in this sense as well as in the elegant senses that everybody else here talked about.

C. Williams - I'd just like to make some sort of an "amen" to what the gentleman just said in terms of specific information that you can get from a phase diagram. In my particular application [at Union Carbide], I deal with ceramics and metals, also in combinations of these two, not necessarily only in the binaries, but usually in the ternary type situation. I think that maybe it would be somewhat helpful if ceramists and metallurgists would get together in sense of compiling some data that would be a little more useful in terms of what's happening at that particular interface and what kind of phases are forming at that particular interfacing. I also would like to ask more or less a question that was not answered, relating to this question of metals-and-ceramics. If anyone of you in the audience or on the panel would have any information or could direct me to some source of information concerning this metals-and-ceramics problem, it would be very much appreciated.

Also, I would like to thank the Bureau for the occasion and thank the committee and the various people that contributed to this session.

National Bureau of Standards SP-496, Applications of Phase Diagrams in Metallurgy and Ceramics
Proceedings of Workshop held at NBS, Gaithersburg, Md., January 10-12, 1977

SUMMARY REMARKS

by

John F. Elliott
Dept. of Materials Science
and Engineering, M.I.T.
Cambridge, MA

Summarization of a workshop of the type held at the National Bureau of Standards this week should include these things. First, one should capture the general feeling that the participants have had towards the formal and informal parts of the workshop. Second, there should be some remarks covering what might be termed the "sense of the meeting" regarding the major issues that have been expressed explicitly and implicitly. Third, some conclusions should be drawn from the results of all facets of the workshop. The summary should not be all inclusive, nor should it necessarily reflect but one final opinion on each of the primary points being considered.

GENERAL REMARKS

From the nature of the formal and informal discussions during the three days of the workshop, it seems clear that the plan to bring people together from diverse areas to discuss a common general interest in phase diagrams was very successful. On the other hand, some came only to sessions of the workshop which were of particular interest to them, and they did not attend all sessions. Fortunately there were many who stayed for the full three

days, and they provided continuity in the discussion which is so essential to a successful workshop.

The informal discussions in the halls, at meals, and at poster sessions indicated that the participants found the sessions stimulating and enjoyable. The times set aside for discussion during the sessions necessarily were limited, particularly during the early part of the workshop, and the informal discussions served to compensate. The organization of the workshop did bring together people from very diverse fields who have a common interest in phase diagrams. All attending the workshop profited from sharing very different points of view with others whom they ordinarily would not meet in their usual professional activities. Such interactions help to develop a better perspective for all involved as to the development and use of thermodynamic data and phase diagrams. It also brings home the international character of the work in progress in the field.

The poster sessions were highly successful in bringing together people with different perceptions of the development and use of phase diagrams. Both the postors and posters provided the participants with stimulating and productive exposures regarding many topics. Of particular interest was the use of computers, computational methods and graphical methods for treating data.

The participation in the workshop has shown again that the interest in phase diagrams is international. This is advantageous

because, as will be noted later, pertinent data are generated in many countries, the results of any work is shared across the world, and the task of assembling, compiling and collating data on phase diagrams is enormous It can be assumed that the task must be shared by groups and laboratories across the world.

DISCUSSION OF AREAS OF COVERAGE

It is helpful in a summary to look at the general issues covered in the workshop from a different point of view than that presented in the formal organization. Thus it may be useful to start with a discussion of where and how data on phase relationships and phase diagrams are utilized, and then move back through the sessions in reverse order.

User Needs

The speakers in the three areas of primary production of metals, materials processing and product application pointed out that the need for information on phase relationships and phase diagrams for each particular application being discussed was extensive and detailed. Often the success of a processing sequence or the property of a material depends on the fine detail of a small area of a phase diagram. The cases cited were numerous and need not be reexamined here. A few examples can be listed to illustrate the range: (a) more complete information is needed on

fields of stability in terms of temperature, pressures of oxygen and sulfur, and composition of the matte and slag phases in copper-iron-sulfur-oxygen-silica systems and how the presence of minor elements such as nickel, lead, etc., influences these fields of stability; (b) a better understanding of the condition of equilibrium between the crystalline phase and the parent liquid phase is required for the conditons existing when semiconductor materials are grown from the melt; and (c) information of a detailed nature is needed for each of the many phase relationships that are pertinent to the processing of metals, alloys and various ceramic materials. It was interesting for people to see the sophisticated ways in which information on phase diagrams is employed by many users. It was also apparent that a user quickly ran out of information when progressing from binary to ternary and then quaternary systems.

Another point of interest was that users seek information on phase relationships in many different forms. The traditional T-X or P-T-X types of diagrams are useful, but other types such as the various types of stability diagrams are desired. It was clear that much more powerful means are needed to handle information about ternary, quaternary and higher order systems because the usual two dimensional charts and plots in most cases are inadequate to meet the user's requirements. This points up the general need for information on phase relationships to be put in forms that are readily adapted to computer use. Perhaps in the longer term it will be possible to prescribe ways of presenting information by investigators to facilitate the use by the computer in various ways and

thus make data of more direct use by many users.

In certain respects, the academic world has some special requirements for information on phase diagrams. There is the need in many research areas for information on phase relationships which is similar in many respects to that which has been expressed for the industrial area. In addition, however, there is the need for this information in forms that facilitate the teaching and learning about phase stability, phase diagrams of all sorts and the uses of these diagrams. Several interesting instructional movies to meet this need were presented during the workshop. However, it would appear that much more must be done, especially with multicomponent systems. It would seem that greater use of computer methods will be helpful in meeting this need.

Methods of Phase Diagram Calculations

The poster and discussion sections on this subject were very helpful in acquainting the participants of the workshop with current activities in a wide range of efforts. As the program schedule shows, the work includes: the treatment of methods for correlating experimental data, use of mathematical methods for expressing thermodynamic functions, development of methods for computing information on activities and other thermodynamic functions from data on phase diagrams, and the reverse in using thermodynamic data for calculating phase relationships. In a number of cases,

the work was directed quite effectively towards meeting some of the user needs as outlined earlier. The methods discussed often involved the use of the computer. These sessions indicated that a diversity of approaches was being employed. It is anticipated that the information displayed and the discussions during the meeting will lead to the development of greater harmony and unity in the use of computer methods. Calphad will undoubtedly help in this.

Review of Phase Diagram Representations

The papers and discussion in this session, the results of Dr. Carter's questionnaire and the various statements from the users' panels present us with the principal dilemma of the compiler of data of any kind. This dilemma arises because, on the one hand, the compiler may not have the time and resources to treat in great detail the information that may be available on a given system. This was noted in the session Present Status of Phase Diagrams. On the other hand, it was clear in the later sessions of the workshop that many users look for a high degree of sophistication and detail in the compiled information, often in a small and obscure portion of a system. In contrast, many who responded to the questionnaire indicated a need for only a moderate degree of sophistication in phase diagrams and phase relationships.

A possible means of resolving this dilemma is to focus the programs of compilation and collation on areas of need. Then one places principal emphasis on the materials, system, and phases of primary interest in an area and either borrows from other compilations or gives less time and effort to that which is of secondary or collateral interest. As an example, in compiling data pertinent to the pyrometallurgical processing of iron and steel[1], emphasis was placed on iron and its alloys and oxide systems typical of slags utilized in the blast furnace and steelmaking furnaces. Systems involving copper, zinc, etc., and liquid alkali-silicate systems were given less detailed coverage. If compilation work were focussed in this manner, it probably would be possible to provide for the needs of people in the current principal areas of application. The areas of lesser emphasis and possible newer areas of scientific and technical interest would be short-changed by this strategy.

The results of the questionnaire also indicate other general needs. As has already been noted, much more must be done with ternary and multicomponent systems. Treatment of metastable phases and of special crystal structures also was considered to be of medium importance. Coverage of these topics adds greatly to the work of the compiler for many systems. Surprisingly, surface phases were not considered to be of great interest. There may be three explanations for this: (a) the interest may in fact be low,

(b) people working in areas with surface phenomena did not respond to the questionnaire, or (c) those people do not perceive how knowledge of phase diagrams are of importance to their work. It seems probable that surface phases may receive much greater emphasis in the future. [Editor's note: Some very fine research on surface phases is being carried out by Prof. G. A. Somorjai et al. at U.C., Berkeley. Unfortunately, this group was unable to attend our workshop, thus causing this topic to seem less important than it is. Applications are, of course, in materials such as used, for example, in catalysis].

SUMMARY

Those of us working in various areas of science and technology see many places and problems where both in the short and long term there are serious and critical needs for continued effort to assimilate, collate and compile information on phase diagrams and phase equilibria. It is apparent that there is much pertinent information now in the literature, particularly with regard to alloy systems, that has not been sought out and compiled for general use. With the present levels of publication of scientific information in the world as compared to the present levels of effort at compilation, we are falling ever farther behind as the years pass in utilizing the information that becomes available. The demands for information on phase equilibria and phase diagrams continues to expand as new devices, materials and processes are developed. Inherent in this situation is the certainty that our technological advancement is slower and more expensive than might be the case. An engineer designing a system must make allowances in the materials chosen and the design of a system for deficiencies

and uncertainties in the behavior of materials and substances in the system. Accordingly, the failure to have up-to-date information on phase stability and equilibria may be costly in the design and operation of a system, and may lead to unexpected failure of that system. For example, those of us who work with energy conversion systems see many places where problems of the type described above ultimately could possibly limit severely the performance and economic viability of many systems being planned today.

The proposals for definitive and exhaustive compilations of phase diagrams and phase equilibria on a grand scale are appealing because it would be desirable to have all such information collected in a usable form in one place. This is a Herculean task, and it seems highly doubtful that it would be possible in the foreseeable future to find funding and talent necessary to carry it out. Thus we collectively are caught up in the dilemma that was mentioned earlier of breadth versus depth of coverage for a compilation. From the discussions of the past three days, it is apparent that a number of steps can be taken to increase the effectiveness of use of resources that are available. One of the most productive steps would be to obtain better coordination of the work of compilation of groups in various countries. Another step, which might be a series of steps, is to break down the work of compilation into smaller and more manageable pieces

rather than undertake a massive overall effort. The preparation of a complete bibliography of phase diagrams that is kept up-to-date could serve as a Baedeker for investigators who were looking for sources, particularly where specific and detailed information is being sought. The next level of sophistication would be to use very simple and compact methods to cover information on simple systems, particularly those that have been covered reasonably well in the literature previously. An example is the section in Landolt-Börnstein[2] where binary systems are collected by type; simple eutectics, peritectics, etc. There a system is covered in a single line on the page in which, for a eutectic, there is a two-numbered entry giving the eutectic composition and entries for the melting point of each component and numbers giving the principal references for the diagram. One could easily add columns giving the limits of solubility of component 1 in component 2, and vice versa, at the eutectic temperature, etc., and reference numbers to guide the reader to an acceptable diagram from a relatively easily available source. This number might in the future also indicate a computer file from which data and diagrams could be extracted. These two relatively simple and compact ways of storing information are inexpensive to prepare and distribute. They also permit the application of resources and expert talent to more complex, difficult and demanding analyses and systems.

The next level of complexity and coverage is to direct the attention of a compiler, or group of compilers, to an area of science and technology where information on phase diagrams and phase equilibria are of importance. An example of this is the volume Selected Thermodynamic Values and Phase Diagrams for Copper and Some of Its Binary Alloys by Hultgren and co-workers of the INCRA Monograph Series on the Metallurgy of Copper[3]. In such a compilation, the systems of principal interest to the field would be covered carefully and in as much detail as is permitted by the available data. Several types of diagrams might be employed to represent the compiled information. Systems that are peripheral to the main interests of the field would be covered in much less detail and might be taken directly from other sources. The compilers for such an effort should be conversant with the field of interest, or should be advised as to the level and coverage of systems by someone who was. It appears that this type of compilation has been reasonably successful in recent years. One of the problems to be faced is that fields tend to broaden, and the task of revising a work may be very large. Another problem is that there may not be sufficient support or interest in a field to develop information at a critical stage in the growth of the field.

The next step in level of coverage is to concentrate the work of compilers on classes of materials. Examples of this are the Phase Diagrams for Ceramists by Levin and co-workers[4], which has

been carried out over the years by the National Bureau of Standards, and the Hansen, Anderko, Elliott and Shunk series on The Constitution of Binary Alloys[5]. The use of advisory groups to aid in coordinating the work and even in selecting areas to be covered as has been followed in the ceramics work is effective and useful. It is perhaps important to raise again the point that one should be wary of undertaking the effort of covering a class of materials in depth with inadequate resources. If the program is started with a high degree of sophistication, and then it is necessary later to draw back in part from such a commitment in quality, the reputation of the whole effort may suffer.

There is interest in seeking out methods and models by which it is possible from first principles to "predict" the phase diagrams of higher-order systems, and the behavior of many different solutes in multi-component solvents. Models by which this may be done still elude us, but people of talent and originality should be encouraged to pursue these efforts.

Computer modelling today is still very limited and tends to be quite empirical in character. It does, however, show promise in being able to provide a user with a limited class of answers on a somewhat limited number of systems. A great deal more needs to be done with this modelling effort to expand its capability and utility.

The Workshop has shown that the business of compilation of data on phase diagrams and phase equilibria is in a state of disarray. There are data in the literature that need attention and pertinent new information continues to appear day by day. Users have many needs that are not being met. The resources and manpower available for compilation of this type of data are neither adequate to keep up with the newly found information, nor to put the information in forms as needed by the users. An aftermath of the Workshop could be the crystallization of a small group of people who will be able to generate a program and attract resources that will begin to dispel this disarray.

REFERENCES

1. J. F. Elliott, M. Gleiser and V. Ramakrishna; Thermochemistry for Steelmaking, Vol. I and II, Addison-Wesley Press, No. Reading, Mass., 1960, 1963.
2. Landolt-Bornstein, Zahlwerte und Funktionen, II Band, 3. Teil. Schmelzgleighgewichte und Grenzflachenerscheinungen; K. Schafer und Zllen Lax, ed., Springer-Verlay, Berlin, 1956.
3. R. Hultgren and P. D. Desai; Selected Thermodynamic Values and Phase Diagrams for Copper and Some of Its Binary Alloys, International Copper Research Association, Inc., New York City, 1971.
4. E. M. Levin, C. R. Robbins and H. F. McMurdie; Phase Diagrams for Ceramists and Supplements, The American Ceramic Society, Columbus, Ohio, 1964, 1969 and 1975.
5. M. Hansen and K. Anderko; Constitution of Binary Alloys, Mc-Graw Hill Book Co., Inc., New York, 1958. Also R. P. Elliott, First Supplement, 1965; and F. A. Shunk, Second Supplement, 1969.

DISCUSSION:

J. F. Elliott - Can we now have some general remarks about the Workshop?

R. Howald - The Workshop was valuable to me because it provided information on many activities where phase equilibria are important of which I was not aware.

J. F. Elliott - Dr. F. L. Carter raised the question earlier as to when and if there should be another workshop or conference of this type. Does anyone wish to comment?

B. Rosof - Until I have been able to digest what has been reported and discussed, I am not able to give an opinion.

(In a brief general discussion on the question, there was consensus that the meeting was successful, and that holding another of similar character at some undefined future time would be desirable. J. Westbrook suggested that CODATA's International Committee on Industrial Needs for basic scientific information might be helpful in planning future meetings of this kind.)

I. Ansara - The topic of the Workshop was of interest to many people in Europe. More would have attended had it been publicized more widely.

G. Armstrong - With the broad demands for use of information on phase equilibria, there appears to be little choice but to follow

Professor Brewer's statement that more systematic means are needed for interpreting the behavior of systems. Such means will help to maximize the use of data, and extend its use in predicting the behavior of related systems.

M.McNeil - It might be useful to use the vehicle of a brief annual review in one or two journals to keep people abreast of activities in the field of phase diagrams. One example of such a review is the annual article titled "What is Going on in Process Metallurgy" that appears in the Journal of Metals.

H. White, Jr. - There is a large variety of needs to be met in a work of compilation. As has been noted, this is what makes the effort both challenging and interesting. The needs are increasing rather than decreasing. This is usually not appreciated by people who are not familiar with the field. One often encounters a remark like "Are there not enough phase diagrams already?".

J. F. Elliott - Although many people ask for a great deal of information in a compilation of phase diagrams, there is a danger to the compiler who strives to meet this need. The amount of work in covering a large number of systems at this level is enormous, and there is

serious danger of not being able to maintain the level for all systems. It may be wiser not to attempt too much because a sin of commission seems to be worse than one of omission.

S. Snyder - It appears to me from my experience with phase diagrams that it is better to summarize data where possible in a compilation. Also the reporting of two reasonable, but conflicting diagrams may be the best way out when the compiler cannot choose between them.

J. Livingston - Many have commented on the large amount of effort that is required to treat ternary and high order systems. It appears that it would be wise for a compiler working on them to limit his coverage to the best developed and most important systems with the aim of completing the work in two to three years.

J. F. Elliott - It appears that we have had a highly successful Workshop. (Adjournment)

National Bureau of Standards SP-496, Applications of Phase Diagrams in Metallurgy and Ceramics
Proceedings of Workshop held at NBS, Gaithersburg, Md., January 10-12, 1977

Evaluation of Conference

by

Reed A. Howald
Chemistry Department
Montana State University
Bozeman, MT

There are a lot of different viewpoints represented at this conference so it is not surprising that it is not easy or even possible to reach a consensus on what kind of evaluated compilation of phase diagram data is required. The range of conference papers makes it clear that there are rapid new phase diagram developments on a variety of fronts. This means that many of our individual prejudices are now seriously outdated, and perhaps the most significant achievement of the workshop is an increased openness of the participants to developments beyond their own areas: in pure theory or in power series representation of empirical data, in experimental techniques or in thermodynamic interpretation of data, in large computer data banks or in hand calculators. Probably we need time to digest these new perspectives before we make any definitive recommendations, but I would like to take the opportunity provided by the workshop proceedings for a few comments of my own on the future direction of phase diagram compilations.

I believe that within ten years we will be seeing the regular publication of updated thermodynamically evaluated computer drawn phase diagrams. Whenever new thermodynamic data for a phase become available from either a theoretical computation or new measurements, a revised phase diagram for the binary and ternary systems containing it could be calculated and made available. This job could be delegated to a large centralized facility, but I do not believe that this will be the direction taken by the United States. I see instead a large group of academic and industrial users with similar programs using compatible files of thermodynamic data and power series coefficients from which phase diagrams are computed.

1519

National Bureau of Standards SP-496, Applications of Phase Diagrams in Metallurgy and Ceramics
Proceedings of Workshop held at NBS, Gaithersburg, Md., January 10-12, 1977

Evaluation of Conference

by

J. E. Selle
Oak Ridge National Laboratory
P.O. Box X
Oak Ridge, Tennessee 37830

Throughout this conference several participants have made appeals, either directly or indirectly, for complete and unequivocable accuracy in phase diagram compilations. Referring to the 2nd Supplement to Hansen by Shunk, it has been inferred that unless a compilation is 100% accurate and complete it is not worth doing at all. I strongly disagree. Strict interpretation and adherence to this philosophy will only serve to intimidate the compilers with the end result that only a few diagrams will be completed each year. I understand the thermodynamicists and theoreticians need for such accuracy and can appreciate their needs, but they are in the distinct minority and if they need the accuracy they claim, they should do their own reviews. The overwhelming percentage of users of phase diagrams, the people in the shops and laboratories do not always need the accuracy or detail demanded. They need information on solid solution, eutectic temperatures (5-10°C in usually accurate enough), potential for compound formation, or potential for second phase formation after heat treatment. Insistence on complete accuracy and its attendant delays in transmitting this information to users will be a catastrophy. The time delay since the publication of Shunk in excessive and it is time to get on with an update and not force a slow down in order to satisfy a very small (through vocal) minority of phase diagram users.

I would hope that somewhere in the NBS budget there will be room for programs to determine phase diagrams for systems that have never been worked on. My own survey of Hansen Elliott and Shunk, the wall chart, "Summary of Binary Phase Diagrams", indicates that for about 15% of the possible binary systems for 55 of the more common metals, no information is available. This in another deficiency that should be addressed.

The NBS should be complimented on their initiative in organizing this conference and attempting to get on with the very crucial task of disseminating phase diagram information to potential users.

National Bureau of Standards SP-496, Applications of Phase Diagrams in Metallurgy and Ceramics
Proceedings of Workshop held at NBS, Gaithersburg, Md., January 10-12, 1977

COMMENTS ON THE PHASE DIAGRAM WORKSHOP JAN. 10-12, 1977

by
Didier deFontaine, Professor of Engineering
School of Engineering and Applied Science
Materials Department
University of California, Los Angeles, CA

This was a timely meeting, indeed, on a very important topic. As a most interested participant, I would like to comment briefly on the meeting itself (1st, 2nd, and 3rd days) and then offer general impressions and even recommendations.

FIRST DAY

The first day's program was the one which I felt to be most relevant to the purpose of the workshop. The presentations on compilation, given in the morning, were most welcomed and the information presented will hopefully be accessible to a large audience; it is of the utmost importance.

The afternoon program was noteworthy as it proved, once again, the effectiveness of poster sessions, particularly in fields such as this one where a great deal of rather intricate graphical information has to be conveyed to the participants.

SECOND DAY

It was a particularly good idea to bring in a solid-state theorist to present the status of current work in the field. This, Dr. Watson did admirably, although, perhaps purposely, he did not attempt to predict when and if reliable computations of such things as alloying potentials would be forthcoming.

Currently, there is no cause for rejoicing: although in principle one knows quite well how to proceed; the business of getting reliable numbers is enormously difficult. Extremely lengthy computations are required to obtain just a single number, say a heat of mixing, and it is not surprising that present computations often result in numbers which are incorrect in both magnitude and sign! The problem of predicting crystal structures of compounds from first principles is many orders of magnitude more difficult yet: in principle, one should perform calculations on all possible structures, then decide on the correct one by minimizing the energy. This means that a small numerical error of perhaps less than one percent will lead to an incorrect structure.

Clearly, the theoretical determination of phase diagrams, even binaries, is presently out of the question. In fact, it appears that such calculations may never reach the truly predictive stage. To some participants of the workshop, this was very discouraging. But are we not asking for too much? After all, despite early optimism, dislocation theory still cannot help us predict work hardening properties of a given polycrystalline alloy, say, and probably never will. Yet dislocation theory is essential for an understanding of plasticity and mechanical behaviour, and has helped to completely reorient our thinking on such matters. Hence, theories (and theorists) should generally be required to give ideas, principles, guidelines. Accurate numbers can only be provided by Nature itself; actual experimental determination of phase diagrams must remain the only reliable way of proceeding.

This brings me to the topic of "computation and prediction of phase diagrams", the object of the morning panel, of which I was a member. First of all, the people working in this field who claim that they are predicting phase diagrams

are kidding themselves. There can be no "prediction", as such with the methods employed (nor, as stated above, with my other method known presently or projected). At best, sub-regular solution methods used currently can be regarded as convenient analytical representations of phase diagram data which can, under favorable circumstances, be extrapolated into unknown domains. The solution models on which these extrapolations are based have little theoretical validity and are, in fact, basically incorrect. This is not to minimize this line of approach; on the contrary, the techniques used by Kaufman, Ansara and others can be most useful from a practical standpoint, and constitute in fact the only currently practical methods available for extrapolation into the unknown for the purpose of making educated guesses. However, these methods should not be considered for attempting to extract basic physical parameters for a given system, as values of parameters obtained by such curve-fitting procedures do not have a clear physical meaning.

The Cluster Variation method proposed by Kikuchi and deFontaine is theoretically meaningful, but is presently limited to a small class of phase diagrams, the so-called "coherent" ones, as explained in our contributed papers. Again, this method can in no way be considered as "predictive", in the strict sense of the word.

What we can do now, but perhaps was not sufficiently discussed, is what I would call a perturbation approach to phase diagram calculations. For example, given an experimentally determined binary diagram, how will small additions of a ternary component modify the equilibria? Or, given a quatenary system containing a small percentage of element X, how will its replacement by Y affect the equilibrium? Answering these questions quantitatively is quite feasible provided that the "perturbation" on the given system to be in some way "small". Also,

this is not an idle academic pursuit, but has real practical applications.

Afternoon talks, were, for me, particularly enjoyable.

THIRD DAY

I found the presentation of industry's needs very disappointing: I could detect no trend, no policy, no clear general statement of requirements. Most panel members told a little anecdote about their favorite phase diagram, and generally made the profound statement that "much more work is needed". The questions of "how much work?" and "who is going to do it?" and "with what funds?" were hardly touched upon.

Of these questions, the one dealing with how much work can be done is the easiest to answer. I suggested that it would take about 8000 years to do all 32,160 possible ternary phase diagrams (based on a total of 80 components), and 100,000 years to do all 15,181,580 quaternaries. These are sobering numbers. Even if we could determine all ternaries, say, in a reasonable amount of time, storing that information (at an average of let us say five book pages per diagram) would require about 160,000 pages or roughly 200 volumes! Hence the first question to be answered is "what do we really want to do, what can we conceivably do?"

It appears that what can be done, and should be done, is a complete determination, evaluation, and compilation of binary phase diagrams. There are but 3,160 of these (again on the basis of 80 elements), so that this is a reachable goal. The problem is finite: once the goal has been reached, a mere six-volume set of binary diagrams, let us say, should satisfy all needs for generations to come.

GENERAL REMARKS

Thermodynamical measurements and phase diagram determinations are no longer regarded as glamourous fields. A few highly experienced and trustworthy old-timers

are still active, but little new blood is being transfused. Consequently, this type of work is often performed nowadays by ill-prepared teams whose primary interest is to obtain specific, immediate answers to specific questions. Phase diagrams result as bi-products, and the published data cannot always be taken very seriously. Frequently, published phase diagrams are even found to violate the phase rule.

Surely, this haphazard uncoordinated and random approach to data collection cannot endure. One group, one organism should take charge and exercise the most rigid scientific control over published data. One cannot insist too much on the need of absolutely top-flight people to preside over such a project: Thermodynamics is a very demanding field, where even long-time practioners are often guilty of ignoring fundamental principles. There is perhaps no basic field in which so many bad mistakes are consistently made. A case in point: a certain number of educational films shown at the workshop were made (presumably at a considerable cost)by a group (I believe) at Penn State. Well, every single Gibbs free energy curve I saw depicted in these movies was drawn incorrectly: if the drawings are taken seriously, then the problem of purifying materials becomes trivial(and the semiconductor industry could save billions if they could only use the Penn State free energy curves) and phase diagrams which violate the phase rule could logically be constructed.

The question is then: "how do we bring very gifted young people into the field?" Unfortunately, I do not know the answer, but a generous injection of funds would help. Probably the type of support needed could be found in Europe where long-term funding policy of basic research is far more sensible than it is in this country right now.

SOME RECOMMENDATIONS

In summary, the workshop accomplished something important; it got people together from various disciplines, initiated dialogues, and made representatives from various fields aware of common needs (Thermodynamics is a great equalizer!) Unfortunately, the participants did not delineate objectives, define realistic goals, or propose methods of implementing these.

Perhaps a second get-together is now required to look into these matters in detail. This should be done quite soon, before too much grass is allowed to grow on the field. I would recommend participation by invitation only, and limited to about 50 persons at most. Participants should be discouraged from elaborating on their own pet projects, concentrating instead on general objectives and modes of implementation.

As mentioned above, the first question to be asked should be: "what can one actually accomplish in the relatively near future?" I would answer " the complete determination, evaluation, compilation, and publication of some 3000 "elemental" binaries (as opposed to "pseudo-binaries" such as NaCl-KCl for example)". In practice, this merely means doubling the size of the present Hansen-Elliott-Shunk series, surely an attainable goal.

Second question: "who shall do this?" It seems to me that since the disappearance of the Hultgren and K.K.Kelley groups, only the National Bureau of Standards can do the job. The NBS's task should not only be that of collecting data and publishing it, but also of evaluating and even generating it. I see no alternative to setting up a well-equipped central facility to crank out phase diagrams in a systematic and consistant manner, with well trained full-time technicians doing practically nothing but that, under the supervision of one top-flight thermodynamist, perhaps assisted by "rotating" post-docs. I repeat, the

task is a finite one; it can be done in reasonable time and gotten over with.

Next in order of complexity are the pseudo-binaries, usually regarded as the province of ceramist. Here, for the time being, I would only envision compilation and evaluation.

Ternaries pose an almost insurmountable problem (8000 years!). The best we can hope for at present is mere compilation and, in parallel, calculations à la Kaufman, with increased attention paid to the "perturbation techniques" alluded to above.

These are challenging tasks. Let us hope that means can be found to reach some limited goals. Needless to say, major technological problems confronting society today cannot be solved without adequate phase diagrams and thermodynamic data.

National Bureau of Standards SP-496, Applications of Phase Diagrams in Metallurgy and Ceramics
Proceedings of Workshop held at NBS, Gaithersburg, Md., January 10-12, 1977

THE RELATION BETWEEN BOND LENGTH AND CRYSTAL STRUCTURES IN METALS

A. P. Miodownik
University of Surrey
Guildford, UK GU2 5XH

Introduction

The changes which occur in the distance of closest approach when an element is placed into a different lattice [1,2] are important in connection with the calculation of lattice strains[3], the estimation of critical size ration[5,6], and the assessment of solid solubility limits[7,8]. Such changes are usually associated with a corresponding change in bond strength and/or the type of bonding arrangement, and therefore also form a useful indicator for the estimation of hardness, melting point, heats of formation, and other properties of alloys and intermetallic compounds[5,6,8,10]

One of the earliest attempts to give general guidance on the magnitude of these changes is the set of predicted percentage changes known as the Goldschmidt conversion factors [11]. These have been extensively used in the tabulation of atomic diameters appropriate to 12-fold co-ordination, particularly for the conversion of the diameters of those elements which occur naturally in the BCC lattice with its 8-fold first co-ordination shell. The figure of 3% given by Goldschmidt for a change in Z from 12→8 was derived empirically from very limited evidence (iron and a copper-palladium alloy); this figure has nonetheless gained wide acceptance, and is in fact a very good approximation for the changes subsequently observed in similar transformations that have now been observed in some 14 other elements [1,12]. Although there is some controversy over the use of Goldschmidt correction factors in relation to solid solubility limits[9], their use is sufficiently wide-spread for several attempts too have been made to produce the same values theoretically. Thus Pauling[13] has applied the relationship:-

Note* Reader in Physical Metallurgy, Department of Metallurgy and Materials Technology, The University of Surrey, Guildford.

$$d_n = d_1 - 0.60 \log_{10} n \quad \ldots\ldots\ldots\

distances it follows that:-

$$d_{BCC} = d_1 - 0.60 \log f\, V/8 \quad \ldots\ldots(4)$$

$$\text{and } (2/\sqrt{3})d_{BCC} = d_1 - 0.60 \log (1 - f)\, V/6 \quad \ldots\ldots(5)$$

$$\text{whence } 0.60 \log 3f/4(1 - f) = 0.1554 d_{BCC} \quad \ldots\ldots(6)$$

From the introduction of the parameter (f), it follows that equation (2) must be replaced by equation (7) where:-

$$\Delta d = (d_{BCC} - d_{FCC}) = 0.60 \log 3f/2 \quad \ldots\ldots(7)$$

The value of f can be determined from equation (6), and it can be seen by inspection that Δd (BCC - FCC) for a given element will now be smaller than the value derived with equation (2), and that the value of Δd is no longer constant, but a function of d (equation 5). (Table I) shows the agreement between theory and experiment obtained by Thewlis for the elements Fe, Ti, Zr and Tl, and the marked improvement obtained by including second nearest neighbour interactions.

This improved fit between theory and experiment must nonetheless be considered partly a consequence of the restricted number of elements analysed by Thewlis. (Figure 1) shows that the value of Δd predicted by equation (7) underestimates the values obtained by experiment for a larger range of elements, particularly those with a large atomic radius. Since the basic Pauling equation does not appear to account for the observed changes in the newly discovered allotropic elements, metallurgical practice to obtain the appropriate atomic radius for a change in co-ordination number has generally reverted to the use of the empirical Goldschmidt factor, or an interpolated value taken directly from the experimental data summarised in Figure 9 (8). The criterion of a zero volume change for the BCC - FCC transformation leads to a predicted 2.6% change in diameter, and can be invoked on the grounds of current electron theory[15], but clearly does not account for the large volume changes that occur in transformations involving lattices with other co-ordination numbers.

In the context of this situation the present paper

1560

attempts to reconsider the basis of Pauling's equation and to apply a modified form of this equation to a more accurate prediction of changes in interatomic spacing resulting from FCC/CPH to BCC transformations.

A general relation between bond strength and interatomic distances

Gilman[16] has shown that the shear modulus for elements of a given crystal structure is a simple function of the distance of closest approach, a family of straight lines of characteristic slope being obtained when these two variables are plotted on logarithmic axes. (Figures 2,3) show that a similar relationship occurs if the bulk modulus is substituted for the shear modulus, which is to be expected with the values of Poisson's ratio characteristic for most metals. All bulk moduli have been taken from the compilation of Köster and Franz[17] with the exception of the data for the allotropes of tin[18] This relationship can be expressed in the form:-

$$\log(K_a/K_b) = k_G \log (d_a/d_b) \quad \ldots\ldots\ldots\ldots\ldots\ldots\ldots\ldots\ldots\ldots(8)$$

where the constant (k_G) has the characteristic values shown in Table II.

At this point it is necessary to enquire whether any systematic error is introduced into the measured slopes through the use of room temperature values of the variables in question, rather than the values appropriate to a series of homologous temperatures. Examination of the expression derived by Mott and Jones[19] for the variation of compressibility with temperature suggests that, to a first approximation, the slopes may well remain largely unaffected providing both variables are referred to the same temperature:-

$$\text{According to Mott } \frac{dX}{dT} = -\frac{\alpha X}{\gamma} V^2 d^2(\log \nu)/dV^2 \quad \ldots\ldots\ldots\ldots\ldots\ldots\ldots(9)$$

where X is the compressibility, V the atomic volume, α the coefficient of expansion, ν the characteristic vibration frequency of the lattice, and γ is Grünheisen's constant[19,20]. Since α and X are inversely proportional to each other, and Grünheisen's constant equals $-d(\log\nu)/d(\log V)$, the rate of change of compressibility with temperature appears to be largely

a function of V^2, or the sixth power of the interatomic distance. This is of the same order as the slopes of the bulk modulus versus interatomic distance plots.

Table II lists the slopes derived from Figure 2 and 3 for various crystal structures and bond types. In the light of the variations accepted in numerous other groupings of physical constants, such as Lindemann's constant and Leibfried numbers[20], it seems valid to use the relationship expressed by equation 8, and the average slopes given in Table II as a valid basis for further discussion of the changes in bond distance occurring during phase transformations. Also included for comparison in Table II are the equivalent slopes calculated for several materials on the basis of various simple bonding models [21 - 24].

The relationship between the Pauling's Equation and the Gilman formulation

Equation (8) clearly indicates that a reduction in interatomic distance will result from an increase in bond strength, where changes in the latter variable are produced by moving from one element to another. The Pauling equation expresses the same conclusion, but relates to changes in bond strength which result from varying the number of bonds between otherwise identical atoms. There is obviously a close connection between the two formulations as can be seen from (Figure 3), where the force constants (f) appropriate to various carbon bonds have been plotted on a logarithmic basis. A slope of approximately -3 is obtained, which forms the basis of Badger's Rule[25]. It is significant that the dimensional relationship between force constants and modulus values is given by $K = f.d^{-1}$, so that Badger's rule corresponds to a slope of ~ -4 for plots of modulus versus interatomic distance. Although many attempts have been made to combine interatomic distances, force constants and bond number[26 - 28] there does not seem to exist a formal description of how the Pauling equation (1) can be related to logarithmic plots of the type used by Gilman.

Alternative form of the Pauling equation

The general form of Pauling's equation is expressed by:-

$$d_a - d_b = k_p \log (n_b/n_a) \quad \ldots\ldots(9)$$

where the constant k_p is left unspecified instead of entering a specific value such as 0.70.

Dividing both sides by d_b

$$(d_a - d_b)/d_b = (k_p/d_b) \log (n_b/n_a) \quad \ldots\ldots(9a)$$

Since $x \gtrsim 2.3 \log (1 + x)$ when x is small, $(d_a - d_b)/d_b$ can be replaced by $2.3 \log \left[1 + (d_a - d_b)/d_b\right]$ and hence:-

$$2.3 \log (d_a/d_b) \simeq (k_p/d_b) \log (n_a/n_a) \quad \ldots\ldots(10)$$

Rearrangement yields:-

$$\log (n_a/n_b) \simeq \left(\frac{-2.3d_b}{k_p}\right) \log (d_a/d_b) \quad \ldots\ldots(11)$$

and comparison with equation (8) shows that the slope A in Gilman plots should be related to the constant k_p of Pauling's equation by the simple relationship:-

$$k_p \simeq -2.3d_b/k_G \quad \ldots\ldots(12)$$

if it is accepted that the bulk modulus is equivalent to the bond number as a criterion of bond strength. The validity of equation (12) can be tested by comparing the calculated values of (k_p) for carbon and a typical metal such as iron, with the empirical values used by Pauling (Equations 1 and 2); Table III shows that values of the correct magnitude are obtained.

The dependence of $\Delta d_{FCC \rightarrow BCC}$ on the distance of closest approach

Equation (12) suggests that the value of k_p in Pauling's equation will be directly proportional to the distance of closest approach for groups of elements whose bonding characteristics are similar (constant value of k_G). This has a number of interesting consequences.

Thus replacing $k_P = 0.60$ by $k_P = 2.3\, d_{BCC}/k_G$ in equation (6):-

$$\log 3f/4(1-f) = \frac{-0.155\, k_G}{2.3} \qquad \ldots\ldots\ldots\ldots\ldots\ldots\ldots\ldots\ldots\ldots(13)$$

Hence the value of f is now a constant independent of the value of d_{BCC} and only a function of the value of (k_G). A similar substitution in equation (7) yields the result that:-

$$\Delta d = d_{BCC} - d_{FCC} = \frac{-2.3\, d_B}{k_G} \log(3f/2) \qquad \ldots\ldots\ldots\ldots\ldots\ldots(14)$$

This leads to the conclusion that the value of Δd should be directly proportional to the distance of closest approach d. Figure 2 indicates that, for BCC/FCC/CPH transformations, A has a value lying between 8 and 9, and the derived values of Δd calculated on this basis are shown in Table IV. It can be seen that there is good agreement with the experimental values available in the literature[8,12] and equations (13 and 14) in effect define the pragmatic dependence of Δd as used by Gschneidner[8], and illustrated in Figure 1. Substituting a value of k_G equal to 8.7 (Table IV) into equation (13) yields $f = 0.84$, and subetituting this value into equation (14) and rearranging gives:-

$$\Delta d_{BCC-FCC}/d = \frac{-2.3}{8.7} \log \frac{3 \times 0.84}{2}$$

$$= -2.6\% \qquad \ldots\ldots\ldots\ldots\ldots\ldots\ldots\ldots\ldots\ldots\ldots\ldots(15)$$

This confirms the initial empirical value of 3% suggested by Goldschmidt. It should however be noted that the small difference between 2.6% and 3% may become significant in high pressure experiments and cases where transformation stresses are important. The inherent geometrical volume change that will occur on changing from FCC to BCC configuration assuming no change in atomic diameter is easily deduced to be:-

$$\frac{V_{BCC} \cdot N_{FCC}}{V_{FCC} \cdot N_{BCC}} = 2\left(\sqrt{\frac{2}{3}}\right)^3 = 1.0872 \qquad \ldots\ldots\ldots\ldots\ldots\ldots(16)$$

Where V_{BCC} and V_{FCC} are the appropriate volumes of the unit cells, and N_{BCC} and N_{FCC} the corresponding numbers of atoms per unit cell.

The net volume change which occurs when a change in atomic diameter is included is given by:-

$$\Delta V_{net} = 1.0872 \ (d_{BCC}/d_{FCC})^3 \quad \ldots\ldots\ldots\

This value is in good agreement with the mean value derived from the carbides listed in Table V (6.9 ± 1.5%) and it may therefore be worth considering that this is a more suitable value to use in metallic systems.

Since the sodium chloride lattice is also favoured by ionic bonding, it is interesting to note that Pauling[13] calculates an expected expansion of 9.1% for a change in ligancy from 6 → 12, with an average Born exponent of 9 which is equivalent to an 8.4% contraction based on 12 fold co-ordination). A change in the proportion of ionic bonding is therefore not going to produce a great deal of difference in the interatomic distances observed in practise, and this situation favours a high degree of resonance consistent with the high melting point and hardness of these carbides. These considerations serve to complement the arguments used by Robins[10] to account for the existence of these carbides, and remove some of the anomalies which result when a conventional Pauling analysis is made of the apparent bond numbers in these compounds[10].

III The A4 → A5 Transformation in Group IV Elements

Jamieson[29] has shown that the allotropic transformation which occurs in pure tin can occur under pressure in other materials possessing a diamond structure (Table VI). It is therefore of interest to see whether the observed changes in interatomic distance can be predicted by means of the present treatment. The A5 (white tin) structure is characterised by two distances of closest approach[1]:-

$$4 \text{ atoms at } (a^2/4 + c^2/16)^{1/2} \quad \ldots\ldots\ldots\ldots\ldots\ldots\ldots\ldots\ldots\ldots (19)$$

$$\text{and } 2 \text{ atoms at } c \quad \ldots\ldots\ldots\ldots\ldots\ldots\ldots\ldots\ldots\ldots\ldots\ldots\ldots\ldots (20)$$

This can be rearranged to yield the difference between the two distances of closest approach Δd_{1-2}:

$$\Delta d_{1-2} = a\left[c/a - 0.518\right] \quad \ldots\ldots\ldots\ldots\ldots\ldots\ldots\ldots\ldots\ldots\ldots\ldots (21)$$

The fraction of the total bond strength (f) associated with the four nearest neighbours may be calculated in an analogous way to the method used for BCC structures (equations 4 to 6), and this value then used to calculate the expected change in interatomic distance for the A4 → A5 transformation. Since there is here some doubt as to whether the bonds should be considered metallic or covalent, both values of the constant B have been used in Table VII. Pauling originally treated the tin transformation as an example where there is a change in the effective valency of the element as well as a change in the number of ligands, attributing a metallic valency of 2.5 for white tin as compared to 4 in the case of the diamond structure of grey tin[13]. However a comparison of the experimental results in Table VI with the predicted values from Table VII indicates that the transformation may equally well be considered in terms of an unaltered valency of 4 together with predominantly covalent bonding in both allotropes. Covalent bonding in white tin structures has also been suggested by Yoshioka and Beck[32] on the basis of the alloying behaviour of group IV elements.

The effect of ionic bonding and the B3 - B1 Transformation

It may be noted from Table VII that an increasing value of Δd (A4 → 5) in the case of III - V compounds correlates with an increase in polarisability of these compounds as determined by Folberth and Welker[30]. It therefore seems likely that there is some proportion of ionic bonding involved in this transformation.

While the A5 structure may be considered as a deformed six-fold co-ordination (since the two sets of interatomic distances are reasonably similar) there is no doubt that it is a less suitable structure for ionic bonding than either the sodium chloride lattice or the diamond lattice. Consequently it may be expected that whereas in a transformation from B3(ZnS) → B1(NaCl) the proportion of ionic bonding is likely to increase, in the transformation A4(or B3) → A5 the proportion of ionic bonding is likely to decrease. With increasing polarisability there then arises a situation where in the A4(B3) structure there

will be an increasingly large contribution to resonance bonding whereas there will be a decreasing contribution to resonance in the corresponding A5 structure. This situation is consistant with the observed variation of Δd with polarisability.

According to Folberth and Welker[30] when the polarisability factor exceeds a critical value the ZnS lattice becomes unstable with respect to the NaCl (or CsCl) lattice, since ionic bonding now predominates over the covalent component. Folberth and Welker placed this critical point between InSb and InP, and it is significant that the results as Drickamer[31] shows that InP and InAs (which have very similar values of polarisability) both transform to a B1 (NaCl) lattice in preference to the white tin modification. Table VIII shows that the changes in the distance of closest approach for this transformation also lie very close together (between +7.4% and +3.6%); Table X shows the corresponding calculated values based on both fully ionic and fully covalent models, it can be seen that, as might be expected, the experimental values fall in between these two extremes.

Changes in the interatomic distance arising from a change in co-ordination from 12 ⟶ 4

(Table X) shows that the changes in atomic diameter for silicon, germanium and tin dissolved in FCC lattices center around 14% relative to the diameter in their normal lattice[1], which is good agreement with the value suggested by Goldschmidt (his correction factor of 12% is based on the FCC lattice as a reference point, and this is nearer 14% relative to CN = 4). With this large change in co-ordination, correspondingly larger differences might be expected for different bonding models, as shown in Table XI." The large differences in apparent atomic volume for these elements when present in various intermetallic compounds[32] can be readily rationalised in terms of varying proportions of covalent and metallic bonding, providing the purely geometric volume changes associated with the various structural changes are first eliminated (see Appendix A). According to the principles already used for the other

types of transformation, the calculated values are given by:-

$$\frac{\Delta d_{FCC \rightarrow DIAMOND}}{d} = \frac{-2.3}{k_G} \log 3 \quad \ldots\ldots\ldots\ldots\ldots\ldots\ldots\ldots\ldots\ldots\ldots\ldots(22)$$

Where in this case it is clearly not to be expected that either $k_G = 8.7$ or $k_G = 4.5$ will lead to a universally applicable answer. It is interesting to note that the range of experimentally determined results does lie generally between the two values obtained by assuming totally covalent or totally metallic bonding in both co-ordinations. The suggested intermediate case in Table XI assumes that there is covalent bonding for the co-ordination change $4 \rightarrow 6$ and metallic bonding for the change $6 \rightarrow 12$. Both these changes have been discussed in other sections of this paper, and together total +16%.

It is interesting that if the experimentally determined values for these two sets of transformations are added, the average value and scatter is almost identical + 14 $\pm$ 4% with the results of Table X. Attributing a definite metallic diameter to the Group IV elements (Si, Ge, Sn) is thus difficult, but it seems clear that the appropriate value will be considerably larger than the estimate made by Rudman[12] on the basis of the effective diameter in the A5 structure.

Conclusion

Table XII compares changes in the distance of closest approach, calculated for various transformations on the basis of the modified Pauling equation used in this paper, with the average experimental values obtainable from literature. It may be concluded that this treatment offers a satisfactory general method of rationalising the observed data, and also relates various other empirical methods currently in use. A summary of the effect of different types of bonds (Figure 4) shows that there is considerable similarity in the dimensional changes expected from the major kinds of bonding, and this no doubt contributes to the general uniformity of the observed overall trend. Although this allows more confidence in estimating dimensional changes where the nature of the bond is not known, it means that the reverse procedure of estimating the nature of the bond from observed changes in interatomic distances must be treated with caution.

Acknowledgements

A debt of gratitude is due to Professor F. C. Thompson, who encouraged the author to persist in tackling this topic, and also to the many students and colleagues whose questions have acted as a spur to finding the solution presented here.

Appendix A

The necessary information to evaluate the changes in volume which occur due to geometric factors only is assembled in (Table A1). The ratio of atomic volumes to be expected can then be expressed in terms of a purely geometric factor and a ratio of the effective atomic diameters in the two structures (Table A2).

If it is assumed that no changes occur in the size of the atoms concerned during transformation, the equivalent values of $\Delta V\%$ are very similar for the A4 $\rightarrow$ A5 and A4 $\rightarrow$ B1 transformation, but markedly different from the value of the A4 $\rightarrow$ A1 transformation (Table A3). It can be seen that if allowances are made for the average change in (d) observed for these transformations an entirely different set of values is obtained. The formulae in the main body of the paper can be used to derive the likely changes in ΔV for different bond strengths.

It is clear that similar calculations should be made for each type of lattice change before any significant comparison can be made between the effective atomic volumes per atom.

TABLE A1

Crystal Lattice	Distance of Closest Approach (d)	Volume/Atom
Diamond A4	$(\sqrt{3}/4)a$	$a^3/8 = (8/3\sqrt{3})d^3_{A4}$
White Tin A5	$\frac{a}{4}\left[4 + (c/a)^2\right]^{\frac{1}{2}}$	$a^2c/4 = \frac{1}{2}(c/a)(d_{A5}/.518)^3$
NaCl B1	$(1/2)a$	$a^3/8 = d^3_{B1}$
FCC A1	$(1/\sqrt{2})a$	$a^3/4 = (\sqrt{2/2})d^3_{A1}$

TABLE A2

Transformation	Ratio of Atomic Volumes
A4 → A5*	$.63 \times (d_{A5}/d_{A4})^3$
A4 → B1	$.65 \times (d_{B1}/d_{A4})^3$
A4 → A1	$.46 \times (d_{A1}/d_{A4})^3$

(*based on c/a ratio of 0.55; only marginal differences in c/a observed for this group of products)

TABLE A3

Transformation	Δd%	Ratio d/d_{A4}	Equivalent ΔV%
A4 → A5	0%	1.00	- 37%
A4 → B1	0%	1.00	- 35%
A4 → A1	0%	1.00	- 54%
A4 → A5	+7%	1.07	- 23%
A4 → B1	+8%	1.08	- 18%
A4 → A1	+14%	1.14	- 32%

(a 1% increase in Δd is approximately equivalent to a change of +2% in ΔV)

REFERENCES

1. Pearson, W. B. A Handbook of Lattice Spacings, Pergamon 1958
2. Massalski T. B. Met. Reviews 1958 3 (9) 45
3. Friedel, T. Advances in Physics 1954 3 504
4. Eshelby, J. D. Solid State Physics 1956 3 79
5. Lewes, F. Theory of Alloy Phases 1956 ASM p. 124
6. Stringer, Ed. J. Rudman, P. and Jaffee, J., Phase Stability i Metals and Alloys, McGraw Hill 1967.
7. Waber, J. T. et al. Trans. Met. Soc. AIME 1963 227 717
8. Gschneidner K. et al. U.S. Dept. Commerce Publication LA 2345 1960
9. Hume Rothery, W. Acta Metallurgica 1966 14 17
10. Robins, D. L. Powder Metallurgy 1958 1/2 172
11. Goldschmidt, V. M. Z. Phys. Chem. 1928 133 397
12. Rudman, P. S. Trans. Met. Soc.(AIME) 1965 233 864
13. Pauling, L., The Nature of the Chemical Bond, C.U.P. 1960
14. Thewlis, J. J. Amer. Chem. Soc. 1953 75 (2) 2279
15. Mott, N. F. Proc. Phys. Soc. 1962 25 218-243
16. Gilman, J. J. Amer. Ceram. Soc. Symp. Nat. Bureau of Standards Publication No. 59 p.79 1963
17. Köster, W. and Franz, H. Metallurgical Reviews 1961 6 (21) 1
18. Musgrave, M. J. P. Proc. Roy. Soc. (A) 1963 272 503
19. Mott, N. F. and Jones, H., The Theory of the Properties of Metals and Alloys, O.U.P. 1936
20. Gschneidner K. A. (Jr.) Solid State Physics 1964 16 275
21. Smith C. S. ASM Symposium on Resonance and Relaxation in Metals 1959
22. Pice, O. K. Phase Transformations in Solids 1951 (John Wiley) (7) 212
23. Raynor, G. V. Inst. of Metals Monograph No. 4 1947 90
24. Gurney, V., Ions in Solution, Dover 1939
25. Badger, R. M. J. Chem. Phys. 1934 2 128 ibid 1935 3 710
26. Walsh, A. D. Trans. Farad. Soc. 1946 42 779 et.seq.
27. Gordy, W. J. Chem. Phys. 1947 15 305
28. Waser, J. and Pauling, L. J. Chem. Phys. 1950 18 (5) 747
29. Jamieson, J. C. Science 1963 March 1 845
30. Folberth, O. G. and Welker, H. J. Phys. Chem. Solids 1959 8 14-20

1572

31. Minomura, S. and Drickamer, H. G. Phys. Chem. Solids 1962 Vol. 23 pp. 451-456

32. Yoshioka, T. and Beck, P. A. Trans. AIME Met. Soc. 1965 233 1788

33. Huggins, M. L. Phase Transformations in Solids 1951 (John Wiley) (8) p. 238

1573

TABLE I

Effect of second neighbour interaction on the prediction of changes in the distance of closest approach in BCC allotropic transformations

Element	d CN12 KX (at T_A)	Δd First neighbour interaction only Pauling (13)	Δd First and second neighbour interaction Thewlis (14)	Observed Δd (at T_A)(1,12)
Fe	2.57	4.1%	2.5%	2.5%
Ti	2.95	3.6%	2.4%	2.8%
Zr	3.13	3.3%	2.4%	2.9%
Tl	3.45	3.1%	2.4%	2.7%

TABLE II

Experimental and calculated values of d(logK)/ d(log d) for groups of elements with different crystal structures

	Structure	d(logK)/d(log d)	Reference
Experimental Values	FCC A1	-(8 → 9)	Data from Pearson (1)
	BCC A2	-(8 → 9)	
	CPH A3	-(8 → 9)	
	Diamond A4	-(4 → 5)	Gilmen (16) and Köster (17)
	NaCl B1	-4	
Calculated Values	Aluminium	-8	Smith (21)
	Sodium	-(7 → 8)	Smith (21)
	Vander Waal	-(6 → 8)	Rice (22)
	"Fermi" Metal	-5	Raynor (23)
	Ionic	-4	Gurney (24)

TABLE III

Comparison of calculated values of the Pauling constant with standard values used in the literature

Element	Interatomic Distance(d)	Gilman constant(k_G)	Pauling constant(k_P)	Calculated Pauling constant (Equation 12)
C	1.54	4.7	0.70	0.75
Fe	2.47	8.7	0.60	0.65

TABLE IVa

Comparison of experimental and calculated values of Δd for transformations from BCC to close packed structures

Element	d (CN12) KX (at T_A)	Δd OBSERVED (Refs 1,8,12)	Δd CALCULATED (k_G = 8.7)
Fe	2.57	.063	.069
Mn	2.73	.069	.074
Ti	2.94	.078	.080
Zr	3.23	.090	.088
Tl	3.45	.097	.094
Th	3.65	.101	.099
Ce	3.66	.100	.100
Na	3.76	.103	.102
Ca	3.97	.110	.109
Sr	4.33	.127	.120

TABLE IV b

Variation in the partition coefficient f_{BCC} with the Gilman constant G_K, and the resultant changes in Δd for BCC - CPH and BCC - FCC transformations

Gilman constant k_G	8.0	8.5	8.7	9.0	OBSERVED
Partition coefficient f_{BCC}	0.82	0.83	0.84	0.85	Δd ↓
Calculated Δd^{BCC}_{CPH} Ti	.075	.077	.080	.083	.078
Calculated Δd^{BCC}_{FCC} Ca	.102	.106	.109	.112	.110

TABLE V

Distances of closest approach in cubic transition metal carbides and their relation to the radius for twelvefold co-ordination

System	Metal Carbon distance (10)	Carbon Radius for Z=6 (13)	Effective Metal Radius	Pure Metal Radius for Z=12 (1)	$\Delta d\%$
Ti-C	2.16	0.84	1.32	1.44	8.3%
Zr-C	2.34	0.84	1.50	1.60	6.3%
Hf-C	2.32	0.84	1.48	1.58	6.3%
V-C	2.08	0.84	1.24	1.34	7.5%
Nb-C	2.23	0.84	1.39	1.43	5.6%

1576

TABLE VI

Experimental values for changes in interatomic distance for A4-A5 transformations

Element	Δd	C/a(A5)	Polarization Factor J(30)	Refs
Si	7.0%	0.554	-	(31,32)
Ge	6.3%	0.551	-	"
Sn	7.5%	0.546	-	"
AlSb	5.2%	0.538	35	(29)
GaSb	5.4%	0.549	55	"
InSb	8.9%	0.536	95	"

TABLE VII

Predictions of the change in interatomic distance for the A4 → A5 transformation in Tin

Valency A4	Valency A5	Partition Coefficient f(A5) Σ	Type of Bond	Gilman Constant k_G	Calculated Δ d	References
4	4	.72	Ionic	4	8.0%	Present Work
		.72	Covalent	4.5	7.1%	
		.76	Metallic	8→9	3→4%	
4	2.5	(.79)*	A4 Covalent A5 Metallic	(10)*	6.6%	Pauling (5,13)

* Equivalent values derived from Pauling and Equation (12) basedon the transformation in Tin.

Σ The partition coefficient will be a function of c/a ratio, but for the range of c/a observed in these transformations (Table VI) this is only a second order effect.

TABLE VIII

Experimental values of the change in the distance of closest approach for the B3 → B1 transformation

Compound	d NaCl	Δd(B3 → B1)	Ref
Ag I	3.04	+ 8.6%	(33)
In As	5.51	+ 7.9%	(31)
In P	5.71	+ 7.4%	(31)

TABLE IX

Predicted values for the change in the distance of closest approach for the B3 → B1 transformation

Type of Bond	Δd(B3 → B1)	Ref
100% Ionic (Born exponent = 9)	+ 5.1%	13
100% Covalent (k_G = 4.5)	+ 9.2%	-

TABLE Xa

Variation in apparent atomic diameter for Tin, Silicon and Germanium in various crystal structures (1)

		d_{Si}	d_{Ge}	d_{Sn}
Elemental Form	A4	2.34	2.44	2.80
White Tin Structure	A5	2.52	2.60	3.02
FCC Solid Solution	A1			
(a) Al base		2.73	2.96	-
(b) Cu base		2.59	2.78	3.26
(c) Ag base		-	2.90	3.18

TABLE Xb

Apparent changes in the distances of closest approach in FCC structures relative to the diamond structure

Element	Δ d A4 → A1		
	in Al	in Cu	in Ag
Si	14%	10%	-
Ge	17%	12%	16%
Sn	-	14%	12%

TABLE XI

Predicted change in interatomic distances for the A4 → A1 transformation

Assumed Bonding	Gilman Constant k_G	Predicted $\Delta d/d_{A4}$
Totally Metallic	8.7	+ 12.6%
Totally Covalent	4.5	+ 24.3%
Covalent (Z = 4 → 6) + Metallic (Z = 6 → 12)	4.5 + 8.7	+ 16.5%
Totally Ionic (13)	-	+ 14.2%
Based on (Z = 6 → 4) + (Z = 6 → 12)		

1579

TABLE XII

Comparison of experimentally observed Δd values with the predictions of the modified Pauling equation

Transformation	Δd predicted	Δd observed
FCC - BCC (A1 - A2)	- 2.6%	- 2.8% (± 0.3%)
FCC - NaCl (A1 - B1)	- 7.4%	- 6.8% (± 1.5%)
Diamond - White Tin (A4 → A5)	+ 7.1%	+ 6.6% (± 1.4%)
Diamond - NaCl (A4 → B1)	+ 9.2%	+ 8.0% (± 0.6%)
Diamond - FCC (A4 → A1)	+ 16.5%	+ 14% (± 4%)

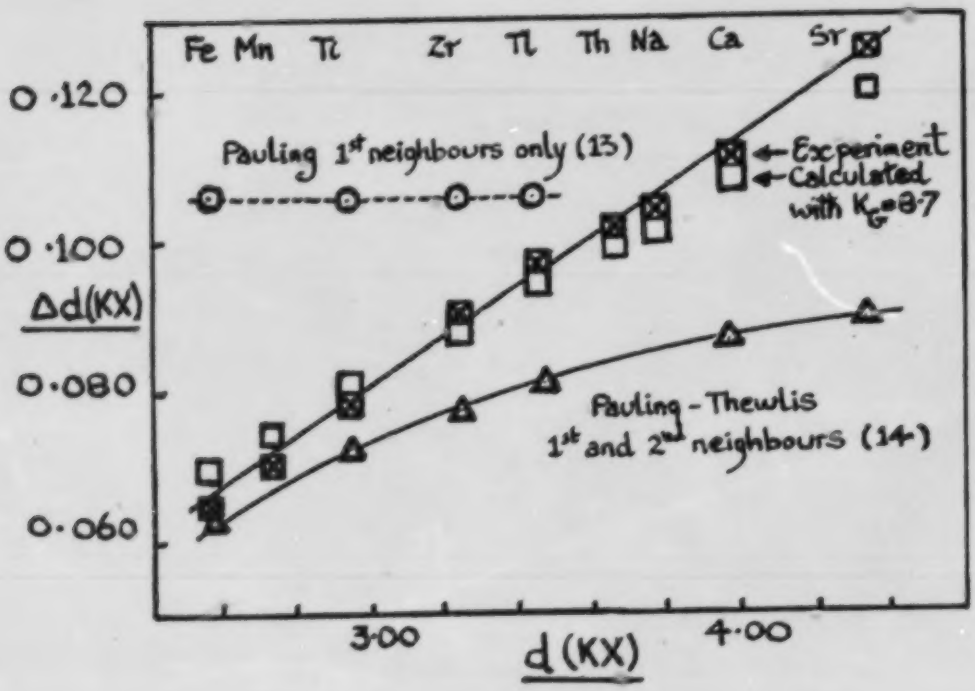

FIG. 1.

The Variation of Δd with d for elements which exhibit BCC-FCC or BCC-CPH Transformations

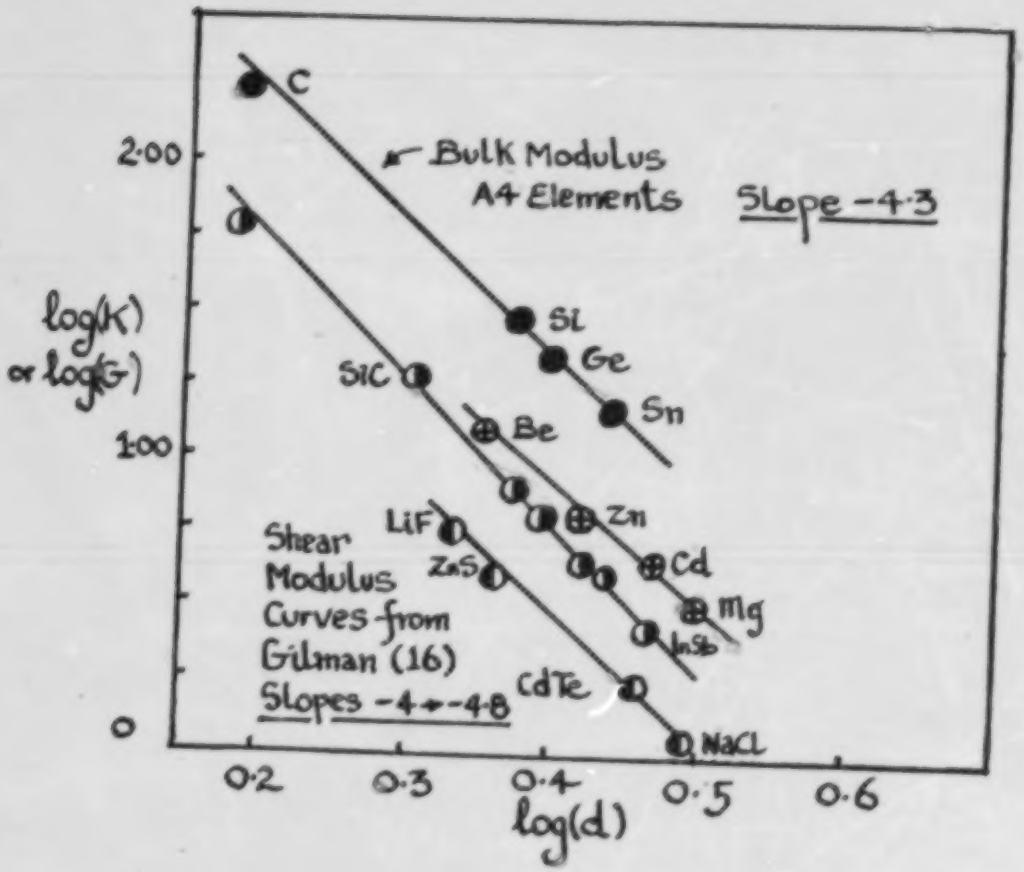

FIG. 2.

The relationship between the elastic modulus and the distance of closest approach for elements and compounds with predominantly covalent and ionic bonding.

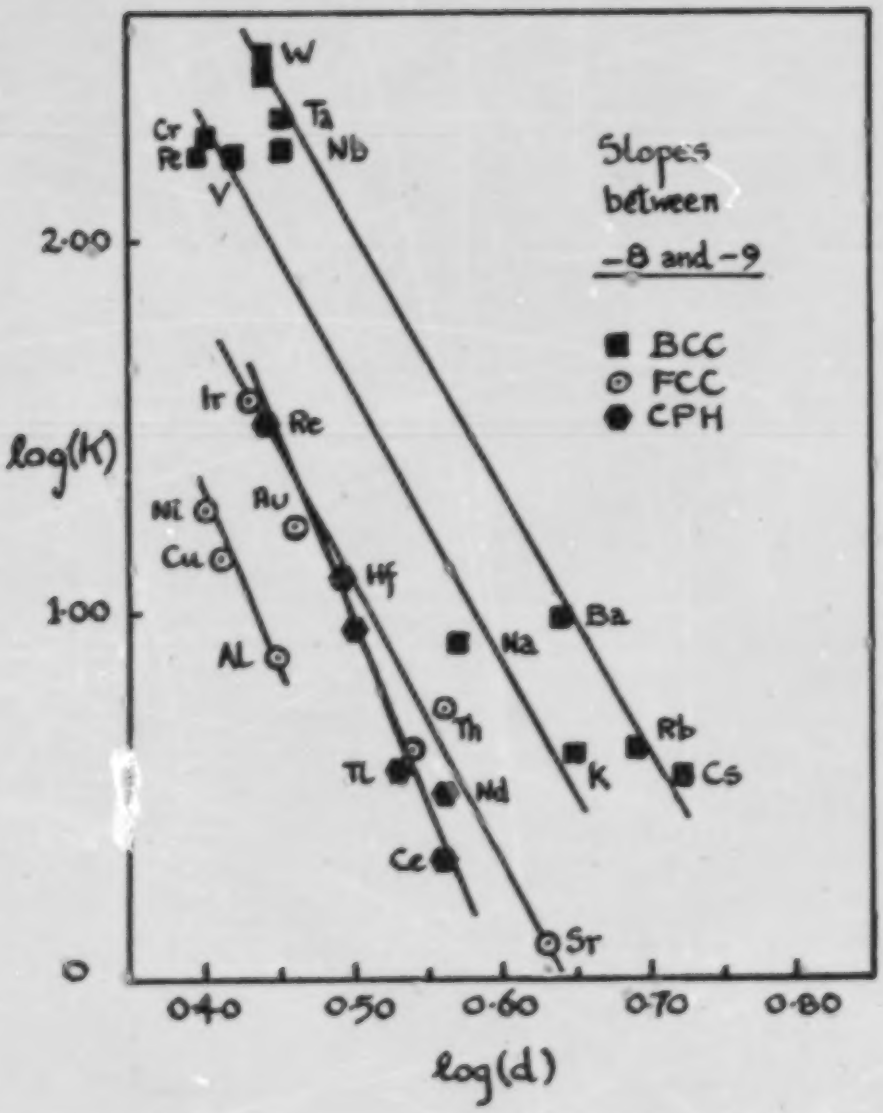

FIG. 3. The Variation of Elastic Modulus with the distance of closest approach in metals with BCC, FCC, and CPH structures.

FIG 4. The variation of Δd with type of bond for different changes in coordination

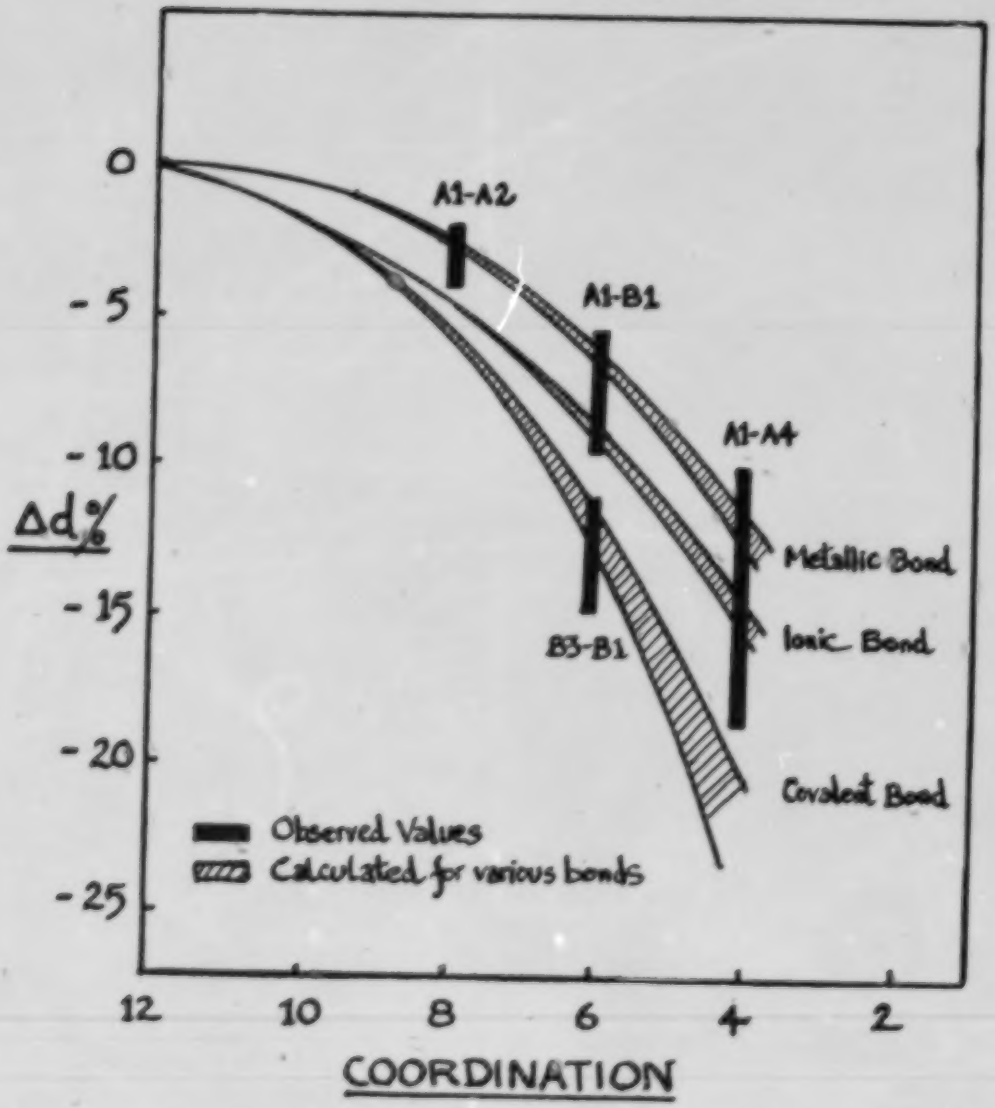

National Bureau of Standards SP-496, Applications of Phase Diagrams in Metallurgy and Ceramics
Proceedings of Workshop held at NBS, Gaithersburg, Md., January 10-12, 1977

On Computerized Construction of Multidimensional Phase Diagrams in a Factographic IRS

I. V. Tulupova and V. S. Stein

"Phase Diagrams" (PD) is a field of knowledge belonging to several sciences--chemistry, physical metallurgy, petrography, etc. Phase diagram data are widely used by scientists and engineers in various professional fields. Naturally, there are quite a number of studies summing up the published data on the PD of two-component systems, including the handbooks by M. Hansen and K. Anderko, R. P. Elliott, F. A. Schunk, and others. A sign of the great importance of PD for various fields of science and technology is the fact that VINITI puts out special collections of abstracts on "Phase Diagrams of Metallic Systems" and "Phase Diagrams of Nonmetallic Systems" on the basis of material covered in its abstract journals "Chemistry" and "Metallurgy."

Constructing a phase diagram from experimental data is a laborious, expensive, and sometimes even practically unfeasible job. This has given rise to several calculative methods of PD construction, some of them computer-based. Methods of computer-based PD construction are being developed by various authors in the USSR and in other countries (D. S. Kamenetskaya, I. L. Aptekar', O. S. Ivanov, A. L. Udovsky, L. Kaufman, C. H. P. Lupis, etc.). A number of studies deal with predictions of the PD pattern and its particular features, for instance, the chemical compounds (V. M. Vozdvizhensky, E. M. Savitsky, and V. B. Gribulya; G. Petzow; and others). Other studies are concerned with experiment planning, which is also very important (F. S. Novik, Yu. P. Adler, etc.). All those studies, however, deal either with particular boundaries or with PD of two-component systems and two-dimensional (isothermal) sections of three-component systems.

Yet PD of multicomponent systems which reflect the interaction of several components are of a particular practical importance. A case in point is PD of materials having special physical properties.

Normally, multicomponent PD are represented by individual sections both in primary publications and in secondary (reference) materials.

Conventional techniques of plotting the PD of a multicomponent system by experimental points (using descriptive geometry) are laborious, lack visuality, and cause difficulties when the PD are put to use in solving calculative problems. So it is clear that reconstruction by computer of PD of multicomponent systems is needed.

The objective of describing a complete PD by means of a computer with a view to its subsequent storage, retrospective searching, and

olution of computational and physical metallurgy problems was first stated by V. S. Stein.

His earlier publications (especially [1,2,3]) described the first attempts at devising machine methods for PD input into a computer (the input information language of PD) and for PD representation in the computer memory (internal information language, PD storage language), and attempts at devising, on this basis, a computer-based information retrieval system.

The concept was to enter PD into the computer in a topological and an analytic notation, describing, respectively, the qualitative and the quantitative aspect of PD structure.

A computer used for information recording, storage, and processing offers, in principle, a mighty capability for highly sophisticated PD calculations and for PD modeling. This is to be done on the basis of experimental data and all information published earlier and accumulated in the system's data base. Since this means bringing together experimental results obtained at different times by different research schools all over the world, one can only conceive such PD modeling within the framework of a computer-based information retrieval system handling a retrospective file of PD data. Such IR systems must be, by their nature, factographic only. Moreover, with the processing of primary information, especially of that extracted from primary texts and graphic material being a very complicated matter, a system of that kind will probably be efficient only if operated as a part of a general integrated IRS. The data items that must be known about each PD are: (1) materials used for PD construction, (2) method used for the study of the sample, (3) constitution of the diagram and the pattern of points and lines, (4) characteristics of system phases, and (5) bibliographic data about the source from which the information has been taken. Data to be extracted from text for items 1, 2, 4, and 5 are not reflected in the geometrical image of PD. Yet, even though the textual information about PD is less important than graphic information, it is very essential for a correct and thorough interpretation of graphic data. This means that the general aspects of automatic text processing should not be overlooked by a designer of an IRS for PD, even though, with the high informativity of geometric description of PD, this is a less urgent issue than in an IRS mainly concerned with verbal information.

This is a difficult problem, but even more difficult is that of the pre-computer description of PD geometry (i.e., creation of the input information language); this must be a description enabling all semantic information about PD stored in a text to be represented by geometrical means. Alongside problems of PD computer system design, this task involves both mathematical problems, e.g., describing the geometrical elements, and pattern recognition problems, particularly during information retrieval and computer input of PD.

A further great difficulty is the absence of automatic printers for efficacious input of PD.

The underlying principles of IRS for PD described in [1,2,3] has been mainly retained and elaborated in [4,5], where a version of topological notation has been developed for PD of condensed simple (nonreciprocal) constant-pressure three- and four-component systems (in principle applicable also to systems of more than four components); it was intended for modeling PD of multicomponent systems from binary PD, two-dimensional sections of PD of multicomponent systems, and projections of the individual surfaces and hypersurfaces of PD.

The information retrieval system under development is to become a part of the integrated IRS for chemistry, itself a component of the ASSISTENT System being designed at VINITI. Along with graphic information, the system will be able to handle natural language text.

In [4], an index of boundary was introduced, which served as an element of the topological notation and denoted the set of names of phase regions adjoining at that boundary. For example, the index of the boundary of the eutectic or peritectic point of PD of two-component systems (figs. 1 and 2) appears as Ж/Жα/Жβ/Жαβ, where "/" separates the sets of symbols denoting the phases of each of the phase regions adjoining at the point.

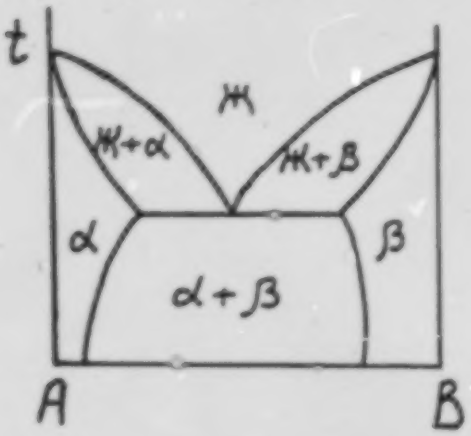

Figure 1

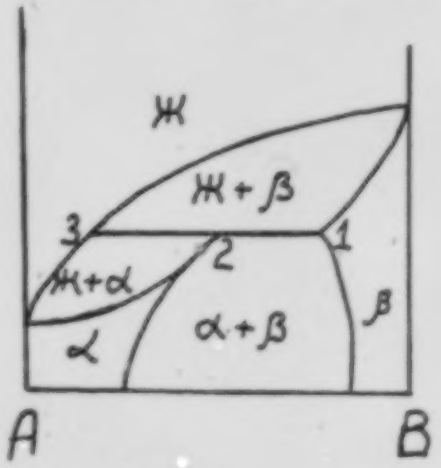

Figure 2

The boundary index gives an expression to one important rule of PD construction. It is the rule of phase grouping, formulated by L.S. Palatnik and A. I. Landau [6], which has several important corollaries. For convenient handling of boundary notations, the so-called index convolution has been introduced. Its left part (to be denoted x) fixes the symbols of the phases of the region which has the least number of phases; the right part (denoted y), does so with those of the region which has most phases. The right and left part of a convolution are separated by "//". The convolution of the above index appears as Ж//Жαβ.

An index should in some fashion indicate all those phase equilibrium regions which, because of a low solubility of components, have merged in the PD with the axis, edge, or face of the coordinates network, degenerated to a point, a vertical straight segment, etc. (i.e., which have undergone a relative degeneration, to use the expression introduced in [6]).

Similarly, the topological notation should record all those phase regions which in the diagram have undergone the so-called absolute degeneration due to the presence of an intensive parameter (temperature). The absolute degeneration is expressed in the fact that a phase equilibrium region having $\underset{\sim}{r} = \underset{\sim}{n}+1$ phases, where $\underset{\sim}{n}$ is the number of components, has one dimension less than the other regions do. In figures 1 and 2, only absolute degeneration has not been eliminated; in figure 3 the relative degeneration has not been eliminated either. Figure 4 shows an example of eutectic-type PD, with both absolute and relative degeneration having been eliminated. Proceeding from the general laws of PD construction, one can obtain a topological notation of a PD even lacking some of its constitutional data.

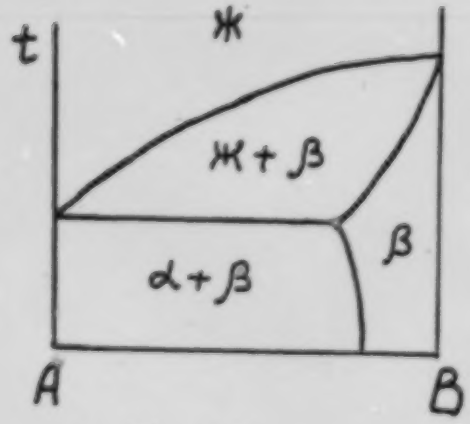

Figure 3

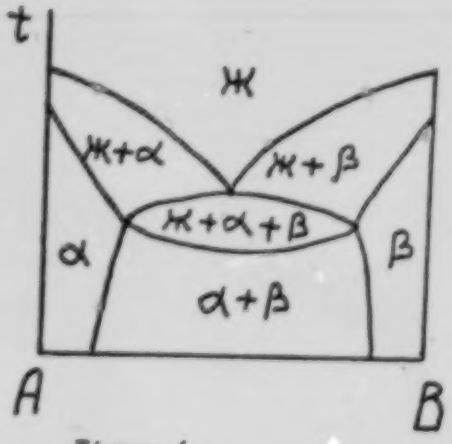

Figure 4

For example, figure 3 shows PD where the phase regions (α) and ($Ж+\alpha$) are absent and it is not known whether subsequent investigation will prove the PD to be eutectic (fig. 1) or peritectic (fig. 2). Nevertheless, it is possible in this case, like in many others, to get a full topological notation of PD. All subsequent refinements of the PD structure will only affect its analytical notation.

An analysis of the convolution of boundary indexes makes it possible to determine the dimensions of (1) the boundary $\underset{\sim}{B}_b$ ($\underset{\sim}{B}_b = \underset{\sim}{n} - \underset{\sim}{y} + \underset{\sim}{x}$), (2) the directrix of boundary $\underset{\sim}{B}_{di}$ ($\underset{\sim}{B}_{di} = \underset{\sim}{n} - \underset{\sim}{y} + 1$), and (3) the generator simplex $\underset{\sim}{B}_{ge}$ ($\underset{\sim}{B}_{ge} = \underset{\sim}{x} - 1$). Since there is a one-one correspondence between boundaries and their index convolutions, it is possible to determine the index for any boundary, and, conversely, given the number of components of a PD, it is possible to determine the nature of each of its boundaries. Index

convolutions are liable to some operations (union, intersection, etc.) which allow the determination of: (1) all phase equilibrium regions adjoining through a boundary obtained by union or intersection of several boundaries, and (2) the dimensions and the type of the new boundary. For example, if boundaries A and B intersect along the boundary C, the index convolution of C is obtained thus: the left term of the C index convolution includes those and only those phases which are comprised at the same time in x_A and x_B, respectively, of the index convolutions of A and B, and the right term of the index convolution of C, (y_C) includes the sum of all phases contained in y_A and y_B of the index convolutions of the respective boundaries. If, for example, we consider the boundaries whose index convolutions are: $\mathcal{H}\alpha//\mathcal{H}'\alpha\beta$ (A), and $\mathcal{H}\alpha V//\mathcal{H}\alpha V\delta\varepsilon$ (B), these boundaries may intersect (i.e., give rise to a new boundary, C) whose index convolution will appear as $\mathcal{H}\alpha//\mathcal{H}\alpha\beta V\delta\varepsilon$. Introducing the sign $\odot$ to denote intersection of boundaries we can represent the derivation of the index convolution of the new boundary as follows:

$$\mathcal{H}\alpha//\mathcal{H}\alpha\beta \odot \mathcal{H}\alpha V//\mathcal{H}\alpha V\delta\varepsilon \rightarrow \mathcal{H}\alpha//\mathcal{H}\alpha\beta V\delta\varepsilon.$$

Since PD contains so-called critical elements (CE) (critical points, critical curves, etc.) and critical figures (CF)* (critical tie-lines, critical tie-triangles, etc.) to which the rule of phase grouping does not apply, a special rule [5] has been formulated enabling the approach described above to be applied for their notation, i.e., index convolutions to be applied for topological notation of CE and CF and the CF boundaries. An example of such a PD is given in figure 5, which shows a possible binary section of a ternary PD with the vanishing line of the binary eutectic.

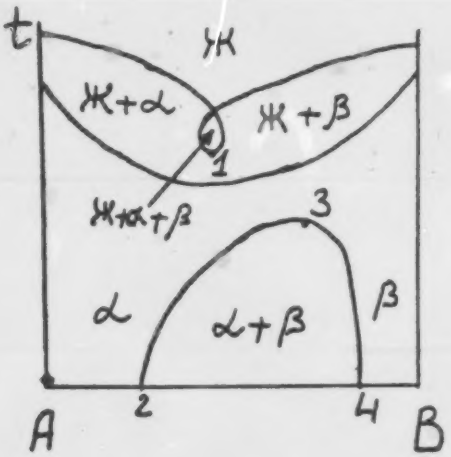

Figure 5

*Critical figure is a geometrical image of whose boundaries at least one is a critical element.

The minimal point (Point 1, fig. 5) on the boundary of the three-phase region ($\mathcal{K}+\alpha+\beta$) with the two-phase ones ($\mathcal{K}+\alpha$) and ($\mathcal{K}+\beta$) belongs to a critical tie-line and has the index convolution $\mathcal{K}(\alpha=\beta)/\!/\mathcal{K}\alpha\beta$, where "$/\!/$" separates the left and right member of the index convolution of the critical element. The sign "=" between symbols of two phases indicates that they are identical. Another possible version of notation for the convolution of the same index is: $\mathcal{K}\alpha=\mathcal{K}\beta/\!/\mathcal{K}\alpha\beta$.

Since for this point the index convolution coincides with the index, another possible notation is $\mathcal{K}(\alpha=\beta)/\mathcal{K}\alpha\beta$. Below the minimal point of three-phase equilibrium, regions ($\mathcal{K}+\alpha$) and ($\mathcal{K}+\beta$) merge into one region, denoted $\mathcal{K}\alpha V\mathcal{K}\beta$ or $\mathcal{K}(\alpha V\beta)$. The sign "V" denotes the logical OR connective. For the binodal curve (line 2-4-3) separating the two-phase region from regions (α) and (β), the position of the critical point may not be known (it does not coincide with the temperature maximum). The index of the binodal curve is $\alpha V\beta/\alpha\beta$. The index of the critical point on that curve is $\alpha=\beta/\alpha\beta$.

Table 1 gives index convolutions of CE, CF, and the CF critical boundaries for two-, three-, and four-component systems, and table 2 gives index convolutions of the noncritical boundaries of CF. The data refer to PD whose two liquid phases are identical. For identical two solid phases, index convolutions are similar. The critical points of a higher order, which are not typical of condensed metal systems, are not considered. The dash indicates absence in the PD of the geometrical element of the respective dimension.

Index convolutions of CD, CF, and CF boundaries and the respective indexes are in one-one correspondence, so that an index convolution can be converted to the index and vice versa. Besides, as has been shown, it is possible for one and the same CF or its boundary to be recorded by a few equivalent alternative indexes.

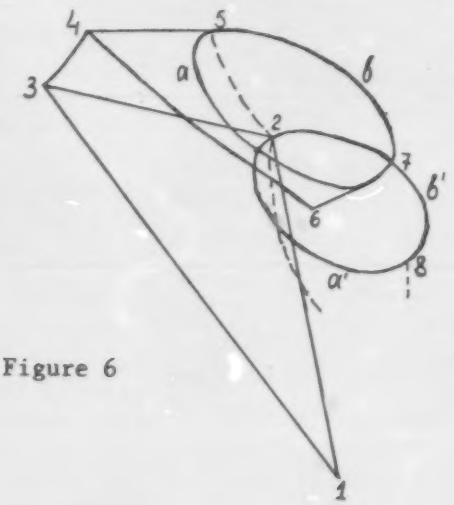

Figure 6

1590

Table 1

		Curvilinear CF	Regular and flat CF and CF boundaries	
Index convolution		$\mathcal{H}_1 = \mathcal{H}_2 \,/\!/\, \mathcal{H}_1 \mathcal{H}_2$		
Dimensions of PD	2	Critical point (extremal)		
	3	Critical curve		
	4	Critical surface		
Index convolution		$\mathcal{H}_1 = \mathcal{H}_2 \,/\!/\, \mathcal{H}_1 \mathcal{H}_2 \alpha$	$(\mathcal{H}_1 = \mathcal{H}_2)\alpha \,/\!/\, \mathcal{H}_1 \mathcal{H}_2 \alpha$	
Dimensions of PD	2	-	-	-
	3	Terminal critical point (vertex of critical tie line)	Critical tie-line (extremal)	
	4	Terminal critical curve	Critical regular surface	
Index convolution		$\mathcal{H}_1 = \mathcal{H}_2 \,/\!/\, \mathcal{H}_1 \mathcal{H}_2 \alpha\beta$	$(\mathcal{H}_1 = \mathcal{H}_2)\alpha\beta \,/\!/\, \mathcal{H}_1 \mathcal{H}_2 \alpha\beta$	$(\mathcal{H}_1 = \mathcal{H}_2)\alpha\beta \,/\!/\, \mathcal{H}_1 \mathcal{H}_2 \alpha\beta$
Dimensions of PD	2	-	-	-
	3	-	-	-
	4	Angular critical point (vertex of critical tie-triangle	Terminal critical tie-line (side of critical tie-triangle)	Critical tie-triangle (extremal)

1591

Table 2

		Curvilinear noncritical CF boundaries	Linear noncritical CF boundaries
Index convolution		$\alpha \parallel M_1, M_2 \alpha$	
Dimensions of PD	2	-	
	3	Noncritical terminal point	
	4	Noncritical curve (boundary of critical regular surface)	
Index convolution		$\alpha \parallel M_1, M_2 \alpha\beta$	$\alpha\beta \parallel M_1, M_2 \alpha\beta$
Dimensions of PD	2	-	-
	3	-	-
	4	Noncritical angular point (vertex of critical tie-triangle)	Terminal noncritical tie-line (side of critical tie-triangle)

Figure 6 shows a fragment of a hypothetical PD of a four-component system with miscibility gap in the quaternary system and in two ternary systems and without miscibility gap in binary systems. In the quaternary system, the miscibility gap region intersects with the surface of the binary eutectic along the closed curve 2-α'-8-b'-2. A fragment of this PD is presented in order to illustrate how the CF and its boundaries are recorded as index convolutions and complete indexes. Note also that 5-α-7, 5-b-7, and 4-6 are monovariant curves defining the equilibrium of two liquid ($ж_1$ and $ж_2$) and one solid (α) phases in one of the three-component systems, 3-4-5-2 is a critical regular surface of the four-component system, and 1-2-3 is a critical tie-triangle. For this PD, it is the temperature maximum of the four-phase region ($ж_1 + ж_2 + \alpha + \beta$). Point 2 is the critical angular point; points 1 and 3 are noncritical angular points.

For the geometrical elements 3-4-5-2, 3-2, 3-2-1, 2, and 3, the index convolutions are:

$$(ж_1 = ж_2)\alpha \barwedge ж_1 ж_2 \alpha,$$

$$(ж_1 = ж_2)\alpha \barwedge ж_1 ж_2 \alpha\beta,$$

$$(ж_1 = ж_2)\alpha\beta \barwedge ж_1 ж_2 \alpha\beta,$$

$$ж_1 = ж_2 \barwedge ж_1 ж_2 \alpha\beta,$$

and

$$\alpha \barwedge ж_1 ж_2 \alpha\beta.$$

The complete indexes are, respectively:

$$(ж_1 = ж_2)\alpha / ж_1 ж_2 \alpha$$

(the index convolution coincides with the index),

$$(ж_1 = ж_2)\alpha / ж_1 ж_2 \alpha / (ж_1 = ж_2)\alpha\beta / ж_1 ж_2 \alpha\beta, \quad (ж_1 = ж_2)\alpha\beta / ж_1 ж_2 \alpha\beta$$

(the index convolution coincides with the index),

$$ж_1 = ж_2 / ж_1 ж_2 / (ж_1 = ж_2)\alpha / (ж_1 = ж_2)\beta / ж_1 ж_2 \alpha / ж_1 ж_2 \beta / (ж_1 = ж_2)\alpha\beta / ж_1 ж_2 \alpha\beta,$$

$$\alpha / (ж_1 = ж_2)\alpha / \alpha\beta / (ж_1 = ж_2)\alpha\beta / ж_1 ж_2 \alpha\beta.$$

The specific feature of the PD fragment is the fact that it has such geometrical elements whose index convolutions would coincide if we do not introduce some additional symbolism (for example, this refers to the critical tie-lines in the three-component PD with a dome). Similar cases also occur in PD without a critical phase--a PD containing both

polymorphism and extremums and the like. On one side of the extremal (by temperature) critical figures (critical tie-triangle, critical regular surface) in figure 6, there lie phase regions separated by usual boundaries; the regions whose phases become identical on the other side of the critical figure merge pairwise, the respective boundaries disappear and in the notations of the phase regions comprised in the index, the sign "V" is introduced.

Let us enumerate the possible alternative positions of phase equilibrium regions relatively to the extremum critical figures.

1. All phase equilibrium regions are treated as ordinary in the following cases:

   1.1 At temperatures above CF, if CF is the minimum of the temperature (isothermal critical tie-figure) or temperatures (regular critical tie-figure with the parallelism plane perpendicular to the axis of temperatures).

   1.2 At temperatures below CF, if CF is the maximum of the temperature or temperatures.

2. Every two phase equilibrium regions each of which comprises the same phases and one differing phase, this differing phase becoming identical on the CE to which the CF directrix belongs, merge pairwise in the following cases:

   2.1 At temperatures below CF, if the latter is the minimum of the temperature or temperatures.

   2.2 At temperatures above CF, if CF is the maximum of the temperature or temperatures.

Index convolutions of CF boundaries can be obtained by the operation of intersection of CE, CF and their boundaries with the ordinary boundaries.

By introducing index convolutions of boundaries, it is possible to write down in the computer memory not only the complete PD, but also PD that have been built just partially.

Apart from points, curves, straight lines, curvilinear and regular surfaces, etc., CE and CF of PD are characterized by the presence of saddle points and extremums, which, in general, are not reflected in index convolutions. Therefore, in reconstructing the complete PD model, it is necessary somehow to include these features in the topological notation. The appearance of extremums and saddle points can be predicted proceeding from the qualitative and quantitative features of PD sections and from the thermodynamic rules. The quantitative description of PD is also affected by the factual insolubility of the components in one or several phases, the presence of polymorphous modifications of phases, etc.

When sections and projections of PD are constructed from the data of two or more experimentors, the experimental points are not normally reported, e.g., in some handbooks and similar publications. When, however, experimental points are not given even in publications by individual authors, i.e., when no thorough preliminary generalization of the results of various authors has been carried out and no estimates of the adequacy of the construction of the particular parts of the PD are given, the process of inputting the sections into the computer building a complete PD is greatly complicated and the reliability of information obtained from processing of input data is weakened.

In plotting PD of a multicomponent system from experimental data, one can resort to methods of descriptive geometry. The drawing of PD and the information about the multidimensional figure it represents express both the qualitative and the quantitative aspect of the PD structure. Applications of descriptive geometry in PD research are discussed by a number of Soviet scientists (V. N. Pervikova, M. G. Podylina, L. N. Lambin, A. G. Kraeva, Yu. A. Maleyev, F. S. Veselova, etc.).

V. N. Pervikova demonstrated (e.g., in [8]) that by attaching a coordinate system to a multidimensional figure to be represented by a drawing, one can dispense with defining the projection mechanisms and replace them with space transformations; a matrix interpretation of drawings makes it possible to pass over from the graphic plottings to the algebraic tools of the present-day geometry.

Some studies use the computer to solve certain special graphic problems in retaining the logic of the graphic method but replacing the geometric plotting with algebraic solutions typical of the analytical method (e.g., finding the common point of four hyperplanes of the four-dimensional space in [9]).

For qualitative description of PD of both binary systems and individual boundaries of the phase regions of the PD of multicomponent systems, the physico-chemical analysts nowadays make use of interpolation and approximation by polynomials of various orders. The polynomial method, however, has a limited application, as it only produces satisfactory results for piece-wise-smooth surfaces.

But, as mentioned, the structure of PD is largely determined by the special points.

In the system under development, the operations performed to reconstruct a complete PD from index convolutions, i.e., operations conducted on the elements of the topological notation, are inseparably linked with those conducted on those elements of the analytical notation which correspond to these index convolutions, e.g., on the equations describing the boundaries whose semantic is expressed by the topological notations.

From Soviet and other publications on the PD of metallic and non-metallic systems, certain rules based on thermodynamics have been selected. Those rules allow prediction of some features of PD structure and verification of the primary experimental data and their interpretations in the very process of PD plotting.

Descriptive-type rules have to be formalized before being entered into the computer. Formalization involves creating a system of concepts and terms and developing the appropriate predicate calculus on which to base a language for description of those rules.

The work on the system of concepts and terms has started by selecting the terms (some 350 altogether) to be in a certain manner correlated with the elements of the graphic image of PD. For the most part, these are names of the phase processes (such as "primary crystallization," "eutectic reaction") and the corresponding geometric elements (e.g., "regular surface"); terms serving to describe the network of coordinates (e.g., "concentration," "weight percentage"); and terms denoting physico-chemical properties ("solubility," "heterogeneity").

Various ways of description of concepts can be used. For example, Hillert's criterion, which determines the type of process (whether eutectic or peritectic), can be represented either mathematically or graphically. The determination of the quasi-binarity of a section can be interpreted as a pattern recognition problem. By feeding into the computer textual information alongside graphic information, it is possible to make corrections and refinements of the description of PD structure. Textual information will be of a particular value where there is no graphic image of PD but just a verbal description of its fragments. Textual information can also be used to add data to a PD which has been built and entered into the IRS earlier.

The IRS under development will make it possible to enter into the computer both graphic and textual information from published sources. Algorithms kept in the computer memory can, not only reconstruct the complete PD from its sections, but also cope with problems involving the plotting of isothermal and polythermal sections, calculation of the quantities of equilibrium phases depending on the mixture composition, etc.

As has been noted, the IRS for PD is to be incorporated in a larger system--the integrated IRS for chemistry, itself a part of the ASSISTENT System under development at VINITI. Along with the data bases of the IRS for PD, files of data will be prepared for other systems as well, including the subsystems for chemical compounds, properties, etc., all incorporated in the ASSISTENT. Data accumulated in these files will eventually allow predictions to be made about properties of chemical structures, the planning of experiments, and so on. It will be also possible to edit all sorts of printed information services on PD and to conduct SDI on permanent interest profiles as well as retrospective searches. All these capabilities will largely expand the scope of applications of ASSISTENT, and particularly of the IRS for PD.

Summary

1. The paper discusses a group of problems involved in the design of an automated information system for PD (in the framework of the integrated IRS for chemistry, a component of VINITI's ASSISTENT System).

2. PD will be constructed on the basis of formal descriptions of the boundaries of two-dimensional sections entered into the computer.

3. The complete record of a PD in the computer will consist of a topological part and an analytical part, expressing the qualitative and the quantitative aspects of PD structure, respectively.

4. The topological notation is based on the so-called boundary index and its convolution. Both index and index convolution serve to record ordinary boundaries as well as CE, CF, and CF boundaries.

5. Algorithms for computer modeling of PD make use of various substantial rules based on laws of thermodynamics. Along with graphic information about PD, some textual information will be used.

6. The IRS under development will allow the carrying out of a variety of operations in PD studies and computations and will provide information services to users in SDI and retrospective-search mode.

References

1. Stein, V. S., Solution of some information problems of the physico-chemical analysis using electronic computers. Thesis for the awardment of the degree of Candidate of Sciences (Technology), Moscow, 1965. (In Russian)

2. Stein, V. S., Design of an information retrieval system for physico-chemical analysis, in "Prikladnaya dokumentalistika," Moscow, Nauka Publishers, 1968. (In Russian).

3. Adler, Yu. P. and Stein, V. S., Composition-property diagrams representation of information for computers, Inform. Stor. and Retr. 4, 1969.

4. Tulupova, I. V. and Stein, V. S., Topology of equilibrium diagrams of multicomponent systems and formal methods of its description, in "Struktura faz, fazovye prevrascheniya i diagrammy sostoyaniya metallicheskikh sistem," Moscow, Nauka Publishers, 1974. (In Russian).

5. Tulupova, I. V. and Stein, V. S., Topology of equilibrium diagrams of multicomponent systems with a critical phase and formal methods of its description, 2454-2474, VINITI, deposited on 9 September 1974. (In Russian).

1597

6. Palatnik, L. S. and Landau, A. I., Phase equilibrium in multicomponent systems, Kharkov, Kharkov University Press, 1961. (In Russian)

7. Cayron, R., Étude théorique des diagrammes d'équilibre dans les systèmes quaternaires, 1, 2, Louvain, 1960.

8. Pervikova, V. N., Theoretical principles of the construction of drawings of multidimensional figures in a synthetic and vectorical presentation as applied to the study of multi-component systems. Thesis for the awardment of degree of Doctor of Sciences (Technology), Moscow, 1972. (In Russian)

9. Frolov, S. A., Automation of the process of graphic solution of problems. Thesis for the awardment of the degree of Doctor of Sciences (Technology), Moscow, 1964. (In Russian)

REGISTRATION LIST

Nazir Ahmad
University of Birmingham
Birmingham, England

Frank Ajersch
Ecole Polytechnique
C.P. 6079 Succ. "A"
Montreal, Quebec H2V-2W8

I. Aldinger
Max-Planck-Institut Für Metallforschung
Busnauerstr. 175
D-7000 Stuttgart, W. Germany

Ernest Ambler
Office of the Director
National Bureau of Standards
Washington, DC 20234

Paul R. Ammann
Kennecott Copper Corp.
Ledgemont Lab
128 Spring Street
Lexington, MA 02173

I. Ansara
Domaine Universitaire
B.P. 44-38401
St. Martin-d'Heres, France

George T. Armstrong
Physical Chemistry Division
National Bureau of Standards
Washington, DC 20234

N. Ault
Norton Co.
Worcester, MA 01606

Donald M. Bailey
Iowa State University
130 Metallurgy Bldg.
Ames, IA 50011

Hugh Baker
American Society for Metals
Metals Park, OH 44073

Chris Bale
Ecole Polytechnique
C.P. 6079
Montreal, Quebec H3C3A7

S. K. Banerji
Foote Mineral Company
Route 100
Exton, PA 19341

Ian R. Bartky
Institute for Materials Research
National Bureau of Standards
Washington, DC 20234

C. J. Bechtoldt
Metallurgy Division
National Bureau of Standards
Washington, DC 20234

Larry H. Bennett
Metallurgy Division
National Bureau of Standards
Washington, DC 20234

Milton Blander
Argonne Nat'l Lab
9700 S. Cass Ave.
Argonne, IL 60439

John H. Blanks
Pennsylvania State University
271 Mat. Res. Lab.
University Park, PA 16802

Edward L. Brady
Office of Information Programs
National Bureau of Standards
Washington, DC 20234

1533

Robert F. Brebrick
Marquette University
1515 W. Wisconsin Ave.
Milwaukee, WI 53233

Leo Brewer
Lawrence Berkeley Laboratory
Univ. of California
Berkeley, CA 94720

Jesse J. Brown, Jr.
VPI & SU
302 Holden Hall
Blacksburg, VA 24061

Daniel Butrymowicz
Metallurgy Division
National Bureau of Standards
Washington, DC 20234

J. W. Cahn
Metallurgy Division
National Bureau of Standards
Washington, DC 20234

Thomas B. Cameron
University of Connecticut
U - 136
Storrs, CT 06268

Cynthia Carter
Metallurgy Division
National Bureau of Standards
Washington, DC 20234

Forrest L. Carter
Naval Research Laboratory
Code 6132
Washington, DC 20034

Y. Austin Chang
College of Engineering
University of Wisconsin-Milwaukee
Milwaukee, WI 53201

James R. Chelikowsky
Bell Labs
600 Mountain Ave.
Murry Hill, NJ 07974

U. V. Choudary
College of Engineering
University of Wisconsin-Milwaukee
Milwaukee, WI 53201

G. W. Cleek
Consultant
5512 N. 24th St.
Arlington, VA 22205

W. Dale Compton
Ford Motor Company
20000 Rotunda Drive
Dearborn, MI 48124

Bruce R. Conard
INCO, Ltd.
Sheridan Park
Mississauga, Ontario, Canada

Lawrence P. Cook
Inorganic Materials Division
National Bureau of Standards
Room B214, Materials Building
Washington, DC 20234

S. R. Coriell
Metallurgy Division
National Bureau of Standards
Washington, DC 20234

Joseph Cox
Watervliet Arsenal
Watervliet, NY 12189

John R. Cuthill
Metallurgy Division
National Bureau of Standards
Washington, DC 20234

Amit DasGupta
Oak Ridge National Lab
Oak Ridge, TN 37830

Didier de Fontaine
University of California
6532 Boelter Hall
Los Angeles, CA 90024

Peter R. Debruyn
Industrial Liaison
National Bureau of Standards
Washington, DC 20234

1600

Joseph E. Davison
Univ. of Dayton
300 College Park
Dayton, OH 45469

R. C. Devries
General Electric
General Electric R & D Center K-1
Schenectady, NY 12345

R. L. Dreshfield
Materials Processing and Joining Section
NASA Lewis Research Center
Cleveland, OH 44135

J. Elliott
Department of Metallurgy & Metals
MIT
Cambridge, MA 02139

S. G. Epstein
Aluminum Association
New York, NY 10017

Maria-Lu'se Fiedler
North Carolina State University
Raleigh, NC 27607

H. Alan Fine
University of Arizona
Dept. of Met. Eng.
Tucson, AZ 85721

Gerhard R. Fischer
Corning Glass Works
SP, FR 1
Corning, NY 14830

Julius Fister
Metals Research Laboratories
Olin Corp.
91 Shelton Ave.
New Haven, CT 06504

Sherman P. Fivozinsky
Office of Standard Reference Data
National Bureau of Standards
Washington, DC 20234

René Flukiger
Dept. Phys. Mat. Cond.
32, Bd. d'Yvoy
Geneva, Switzerland

Paul Fopiano
Watertown Arsenal
Arsenal Street
Watertown, MA 02172

Patrick K. Gallagher
Bell Laboratories
Rm. 6D - 311
Murray Hill, NJ 07974

B. C. Giessen
Department of Chemistry &
Mechanical Engineering
Northwestern University
Boston, MA 02115

F. P. Glasser
University of Aberdeen
Old Aberdeen
Scotland, UK AB9 ZUE

Joseph I. Goldstein
Lehigh University
Bethlehem, PA 18015

J. Ronald Gonterman
Owens/Corning Fiberglas
Technical Center
Granville, OH 43023

Chuck Greskovich
General Electric Co.
K-1, 3C12, P.O. Box 8
Schenectady, NY 12301

K. A. Gschneidner, Jr.
Rare Earth Information Center
Iowa State University
Ames, IA 50010

John L. Haas, Jr.
U.S. Geological Survey
National Center, Stop 959
Reston, VA 22092

David Hansen
Ballistics Research Laboratory
Aberdeen, MD 21005

Ernst-Theo Henig
Max-Planck-Institut für Werkstoffwissensch
Buesnauerstr. 175
D-7000 Stuttgart-80, Germany

Keith A. Hill
Carpenter Technology Corporation
P.O. Box 662
Reading, PA 19603

J. Hilsenrath
National Bureau of Standards
Washington, DC 20234

Michael Hoch
University of Cincinnati
Location 12
Cincinnati, OH 45221

John D. Holder
Oak Ridge National Laboratory
Box X, 4500S S280
Oak Ridge, TN 37830

Emanuel Horowitz
Institute for Materials Research
National Bureau of Standards
Washington, DC 20234

R. A. Howald
Chemistry Dept.
Montana State University
Bozeman, MT 59715

Chen-Chao Hsu
Argonne National Laboratory
9700 S. Cass Ave.
Argonne, IL 60439

David Dew-Hughes
Brookhaven National Laboratory
Building 480
Upton, NY 11973

F. A. Hummel
Pennsylvania State University
Room 214 M.I. Bldg.
University Park, PA 16802

M. R. Jackson
General Electric Co.
CRD, K-1 223 Met
Schenectady, NY 12309

R. I. Jaffee
Electric Power Research Institute
Palo Alto, CA 94303

Ronald B. Johnson
Institute for Materials Research
National Bureau of Standards
Washington, DC 20234

Daniel J. Kahan
Metallurgy Division
National Bureau of Standards
Washington, DC 20234

Larry Kaufman
Manlabs Inc.
21 Erie St.
Cambridge, MA 02146

B. H. Kear
Pratt and Whitney
Materials Engineering &
Research Lab
E. Hartford, CT

S. E. Khalafalla
Dept. of the Interior
P.O. Box 1660
Twin Cities, MN 55111

R. Kikuchi
Hughes Research Laboratories
3011 Malibu Canyon Road
Malibu, CA 90265

R. Kirsch
Applied Mathematics Division
National Bureau of Standards
Washington, DC 20234

O. J. Kleppa
The James Franck Institute
University of Chicago
Chicago, IL 60637

Michael J. Koczak
Drexel University
Dept. of Materials Engineering
Philadelphia, PA 19104

Tamara Kolesnikova
Academy of Sciences of the USSR
Baltijskaya ul., 14
Moscow, USSR

Ram Kossowsky
Westinghouse Research Laboratories
1310 Beulah Road
Pittsburgh, PA 15235

John Krc, Jr.
Parke, Davis & Company
Joseph Campau at the River
Detroit, MI 48232

Eric R. Kreidler
General Electric Co.
Nela Park
Cleveland, OH 44143

A. K. Kuriakose
Norton Research Corp. (Canada) Ltd.
8001 Daly St.
Niagara Falls, Ont., Canada

R. Laudise
Materials Research
Bell Telephone Labs
Murray Hill, NJ 07974

Y. E. Lee
Union Carbide Corp. Metals Div.
4625 Royal Ave.
Niagara Falls, NY 14302

David R. Lide, Jr.
Office of Standard Reference Data
National Bureau of Standards
Washington, DC 20234

James D. Livingston
General Electric Co.
Corp. Res. & Dev.
Schenectady, NY 12308

C. H. P. Lupis
Institute Für Eisenhuttenkunde
Aachen, Germany

Lottie T. McClendon
Institute for Materials Research
National Bureau of Standards
Washington, DC 20234

Scott McCormick
Illinois Institute of Technology
Dept. of Metallurgical and Matls, Eng.
Chicago, IL 60616

H. McKinstry
Materials Research Lab
Pennsylvania State University
University Park, PA 16802

R. McNally
Ceramic Research
Corning Glass Works
Corning, NY 14830

Michael McNeil
National Bureau of Standards
Room A129, Technology Building
Washington, DC 20234

H. F. McMurdie
Inorganic Materials Division
National Bureau of Standards
Washington, DC 20234

Richard Magin
Nat'l Institutes of Health
9000 Rockville Pike
Bethesda, MD 20795

A. I. Malausky
Tyco Laboratories
Waltham, PA

John R. Manning
Metallurgy Division
National Bureau of Standards
Washington, DC 20234

Vincent C. Marcotte
IBM
D/45K B/300 -95
Hopewell Jen, NY 12533

Dennis Marshall
Globe-Union, Inc.
5757 N. Greenbay Ave.
Milwaukee, WI 53201

Robert F. Martin
Institute for Materials Research
National Bureau of Standards
Washington, DC 20234

Thadeus B. Massalski
Carnegie-Mellon University
Schenley Park
Pittsburgh, PA 15213

Leo Merrill
High Pressure Data Center
5093 HBLL, Brigham Young University
Provo, UT 84602

Peter J. Meschter
Univ. of Tennessee
Dept. Chem. & Met. Eng.
Knoxville, TN 37919

Alan D. Mighell
Inorganic Materials Division
National Bureau of Standards
Washington, DC 20234

D. B. Minor
Inorganic Materials Division
National Bureau of Standards
Washington, DC 20234

A. P. Miodownik
University of Surrey
Guildford, UK GU2 5XH

W. G. Moffatt
General Electric Co.
1 River Road P.O. Box 8
Schenectady, NY 12301

B. J. Molino
Office of Standard Reference Data
National Bureau of Standards
Washington, DC 20234

L. F. Mondolfo
Syracuse University
Syracuse, NY 13210

John E. Morral
University of Connecticut
U-136
Storrs, CT 06268

Arnulf Muan
Penn State Univ.
118 M. S. Bldg.
University Park, PA 16802

A. Navrotsky
Chemistry Division
National Science Foundation
Washington, DC 20555

Taki Negas
Inorganic Materials Division
National Bureau of Standards
Washington, DC 20234

T. Nishizawa
Dept. of Metallurgy, Materials
Science & Metal Processing
Tohoku University
Japan

E. F. Osborn
Carnegie Institution of Washington
2801 Upton St., NW
Washington, DC 20008

Robert L. Parker
Metallurgy Division
National Bureau of Standards
Washington, DC 20234

P. Parish
U.S. Army Research Office
Box 12211
Research Triangle Park, NC 27709

Elio Passaglia
Institute for Materials Research
National Bureau of Standards
Washington, DC 20234

David D. Pearson
United Technologies Research Center
Silver Lane
East Hartford, CT 06108

W. B. Pearson
Faculty of Science
University of Waterloo
Waterloo, Canada

Arthur Pelton
Ecole Polytechnique
C.P. 6079
Montreal, Quebec H3C3A7

Guenter Petzow
Met-Planck-Inst. Metallforschung
Buesnauerstr 175
7000 Stuttgart 80, W. Germany

Sri Prakash
Union Carbide Corporation
P.O. Box 5928
Greenville, SC 29606

Svante Prochazka
GE CR & D
P.O. Box 8
Schenectady, NY 11301

Alan Prince
Hirst Research Centre
East Lane, Wembly
Middlesex HA9 7PP, England

Schrade F. Radtke
International Lead-Zinc Research Org.
292 Madison Ave.
New York, NY 10017

Dennis Readey
Division of Physical Research
ERDA
Washington, DC 20545

Curt W. Reimann
Institute for Materials Research
National Bureau of Standards
Washington, DC 20234

R. C. Reno
Dept. of Physics
University of Maryland
Baltimore, MD 21228

Robert J. Reynik
National Science Foundation
1800 G St., NW
Washington, DC 20550

Frederick N. Rhines
University of Florida
Dept. of Mat-Sci. & Eng.
Gainesville, FL 32611

A. D. Romig
Lehigh University
Whitaker Lab. # 5
Bethlehem, PA 18015

Barry H. Rosof
Technology Division, Cabot Corp.
1020 Park Avenue
Kokomo, IN 46901

W. Rostoker
University of Illinois
Chicago Circle, P.O. Box 4348
Chicago, IL 60680

Robert S. Roth
Inorganic Materials Division
Room B214, Materials Building
Washington, DC 20234

William Ruff
Metallurgy Division
National Bureau of Standards
Washington, DC 20234

M. L. Saboungi
Argonne National Lab
Chemical Engineering Div.
Argonne, IL 60439

Saed Safai
Materials Sci. Dept.
SUNY at Stony Brook
Stony Brook, L. I., NY 11794

E. Salkovitz
Office of Naval Research
Arlington, VA 22217

Gary Sandrock
International Nickel Co.
Sterling Forest
Suffern, NY 10901

L. M. Schetky
International Copper Research Assoc.
825 Third Ave.
New York, NY 10022

Coulson M. Scheuermann
NASA Lewis Research Center
21000 Brookpark Road
Cleveland, OH 44135

Fred C. Schwerer
U. S. Steel Research, MS #98
Monroeville, PA 15146

J. E. Selle
Metals and Ceramics Div.
Oak Ridge National Lab
Oak Ridge, TN 37830

M. Semchyshen
Research Laboratory
Climax Molybdenum Corp.
1600 Huron Pkwy.
Ann Arbor, MI 48105

Charles E. Semler
Ohio State Univ.
Refractories Research Center
2041 College Rd.
Columbus, OH 43210

Gertrude B. Sherwood
Office of Standard Reference Data
National Bureau of Standards
Washington, DC 20234

John Shyne
NSF
1800 G St., NW
Washington, DC 20550

W. C. Simmons
AFOSR
Bldg. 410
Bolling AFB, DC 20332

Satish P. Singhal
State University of New York
Materials Science Dept.
Stony Brook, NY 11794

P. Slick
Bell Telephone Laboratories
Murray Hill, NJ 07974

J. F. Smith
Iowa State University
Ames, IA 50010

J. E. Smugeresky
Sandia Labs
Div. 8312
Livermore, CA 94550

Shigeyuki Sōmiya
Tokyo Institute of Technology
Ookayama, Meguro, Tokyo, 152
Tokoyo, Japan

Charles A. Sorrell
Dept. of Ceramic Engineering
Univ. of Missouri
Rolla, MI 65401

Karl E. Spear
Pennsylvania State University
Materials Research Laboratory
University Park, PA 16802

G. R. Speich
U. S. Steel, Research Labs
Monroeville, PA 15146

G. Springer
Falconbridge Nickel Mines Ltd.
8810 Yonge Street, P.O. Box 900
Thornhill, Ontario

Judith K. Stalick
Inorganic Materials Division
National Bureau of Standards
Washington, DC 20234

Kurt H. Stern
Naval Research Laboratory
Code 6130
Washington, DC 20375

C. P. Stroble
Allegheny Ludlum Steel Corp.
Research Center
Brackenridge, PA 15065

Lydon J. Swartzendruber
Metallurgy Division
National Bureau of Standards
Washington, DC 20234

J. Swisher
Energy Research & Development Admin.
Washington, DC 20545

R. E. Thoma
Union Carbide Corporation
P.O. Box X
Oak Ridge, TN 37830

Marshall K. Thomas, Jr.
Naval Air Devel. Center (30231)
Warminster, PA 18974

William Thompson
McGill University
Montreal, Quebec

C. Thurmond
Bell Telephone Labs
Murray Hill, NJ 07974

H. van Olphen
Numerical Data Advisory Board
National Research Council
2101 Constitution Avenue
Washington, DC 20418

E. C. van Reuth
DARPA
1400 Wilson Blvd.
Arlington, VA 22209

Chester J. Van Tyne
Lehigh University
Whitaker Laboratory #5
Bethlehem, PA 18015

Francis L. Ver Snyder
Pratt & Whitney Aircraft Group
400 Main Street
East Hartford, CT 06108

Walter E. Wahnsiedler
Alcoa Laboratories
Alcoa Technical Center
Alcoa Center, PA 15069

J. Waldman
Frankford Arsenal
Bridge & Tacony Streets
Philadelphia, PA 19137

Chang-F. Wan
Pennsylvania State University
271 Materials Res. Lab
University Park, PA 16802

Frederick E. Wang
NSWC
Silver Spring, MD 20910

Richard M. Waterstrat
Polymers Division
National Bureau of Standards
Washington, DC 20234

R. E. Watson
Brookhaven National Laboratory
Upton, NY 11973

Alan Webb
Naval Research Laboratory
Code 6434
Washington, DC 20375

George Wei
ORNL
P. O. Box X
Oak Ridge, TN 37830

J. H. Westbrook
General Electric Co. Bldg. 5-327
1 River Road
Schenectady, NY 12345

Howard J. White, Jr.
National Bureau of Standards
Office of Standard Reference Data
Washington, DC 20234

William B. White
The Pennsylvania State University
Materials Research Laboratory
University Park, PA 16802

Calvin S. Williams
Union Carbide Corporation
P.O. Box 5928
Greenville, SC 29606

Ray Woodriff
Roberts Hall
Montana State University
Bozeman, MT 59715

L. Richard Woodyatt
Bethlehem Steel Corp.
Homer Research Labs
Bethlehem, PA 18015

Han-Il Yoo
Inorganic Materials Division
Room B214, Materials Bldg.
Washington, DC 20234

William Vincent Youdelis
Dept. Engineering Materials
University of Windsor
Windsor, Ontario N9B 3P4

1697

Author Index

Ageev, N. V., 90
Ageeva, D. L., 90
Aldinger, F., 164
Ammann, P., 1334
Ansara, I., 121

Badie, T. M., 550
Bailey, D. M., 1027
Balakrishna, S. S., 1200
Bale, C. W., 1077
Beam, J. E., 1428
Bennett, L. H., 261, 450, 592
Bilimoria, Y., 1047
Blander, M., 1093
Boreni, R., 259
Boyle, M. L., 726
Brebrick, R. F., 1220
Brown, J. J., Jr., 272

Cameron, T. B., 566
Carter, F. L. 763
Carter, G. C., 36, 261, 450
Cassidy, R. T., 272
Chang, L. L. Y., 165
Chang, Y. A., 229, 774
Chart, T. G., 1186
Choudary, U. V., 229, 774
Cleek, G. W., 1, 257
Cook, L. P., 1, 257, 440
Craig, D. F., 272

Davison, J. E., 1428
de Fontaine, D., 967, 999
Dew-Hughes, D., 1411
Doman, R. C., 1378
Dreshfield, R. L., 624

Ehrenreich, H., 592
Eliezer, I., 803 846, 1440
Elliott, J. F., 1332, 1453
Evans, B. L., 226

Fine, H. A., 355
Fisher, J. R., 909
Fivozinsky, S. P., 1325
Flukiger, R., 375
Fopiano, P. J., 567

Gaye, H., 907
Giessen, B. C., 1161
Gittus, J. H., 1065
Glasser, F. P., 407
Goldstein, J. I., 462
Gribulya, V. B., 1139, 1151
Gschneidner, K. A., Jr., 226

Haas, J. L., Jr., 909
Hasebe, M., 911
Henig, E.-Th., 164, 955
Hirano, S., 508
Howald, R. A., 803, 846, 1440, 1470
Hsu, C. C., 1109

Jackson, M. R., 423
Jaffee, R. I., 1420
Johnson, J. R., 483
Jorda, J.-L., 375

Kagan, E. K., 346, 351
Kahan, D. J., 261
Kaufman, L., 1065
Khanna, K. M., 575
Kikuchi, R., 967, 999
Kiseleva, N. N., 1139, 1151
Kolesnikova, T. P., 90
Kreidler, E. R., 1307
Kubaschewski, O., 1027

Larson, H., 1354
Livingston, J. D., 703
Lukas, H. L., 164, 955
Lupis, C. H. P., 907

Mallik, A. K., 1200
McCormick, S., 1047
McNally, R., 1378
Merrill, L., 100
Mighell, A., 259
Minor, D. B., 440
Miodownik, P. A., 1065, 1479
Mlavsky, A. I., 1426
Mondolfo, L., 1382
Morral, J. E., 566
Myers, S. M., 516

1608

Nakamura, K., 508
Negas, T., 1, 257
Neumann, J. P., 229
Nishizawa, T., 911

Ondik, H. 259

Pehlke, R. D., 1360
Pelton, A. D., 1077
Pettrova, L. A., 90
Petzow, G., 164, 955
Prince, A., 660
Prochazka, S., 1409

Rairden, J. R., 423
Reilly, J. J., 483
Reno, R. C., 450
Rhines, F. N., 142
Romig, A. D., Jr., 462
Rosof, B. H., 1090
Roth, R. S., 1, 257

Saboungi, M.-L., 1093, 1109
Saito, S., 508
Sandrock, G. D., 483
Savitskii, E. M., 1139, 1151
Scheuermann, C. M., 1237
Selle, J. E., 1471
Sherwood, G. B., 1325
Sinha, V. K., 578
Slick, P., 1427
Smith, J. F., 1027
Smugeresky, J. E., 516
Sōmiya, S., 508
Spear, K. E., 744
Stalick, J., 259
Stein, V.S., 1506
Swartzendruber, L. J., 450

Tarby, S. K., 726
Thompson, W. T., 1077
Thurmond, C. D., 23
Tulupova, I. V., 1506

Van Tyne, C. J., 726
Verkade, M. E., 226
VerSnyder, F. L., 1418
Vol, A. E., 346, 351

Wachtman, J. W., 1
Wang, F. E., 545
Watkin, J. S., 1065
Watson, R. E., 592
White, H. J., Jr., 709
White, W. B., 251

Zimmermann, B., 955

1609

SUBJECT INDEX

Each paper has been indexed under one or more of these entries for ease of retieval. This index is cursory rather than exhaustive. Those papers giving numerical phase diagram data or phase diagrams on specific systems are listed in the Materials Index.

Acceptor solubilities 26-27
Activity coefficients 726-727, 774, 777-786, 803-845, 1047-1048, 1052-1055
Additive systems (salts) 1093, 1098-1108
Ageev, translated cumulative index 1237-1306
Aircraft industry 262, 1396, 1418-1419
Allen and Cahn 1012, 1017
Alloy physics 84-89, 592-623
  (Also see under spcific terms)
Alloys (see under Metallic systems)
Amorphous materials 261-268, 1161-1185
Analytical representations 672-675
Angular correlation 450-461
Applications (see under Needs and Applications, under main headings of Ceramics systems, Semiconductor systems, High pressure diagrams, or specific terms)
Atomic deposition methods 151, 516-544
  - summary 1172
Autoradiography 566

Bale-Pelton polynomials and coefficients 846-847, 874-875, 902-903, 1445
Band theory 619
Batteries 262, 1109-1138
Bonding, chemical (see also Crystal chemistry) 612-614, 763-773
  -, transient liquid phase (TLP) 1418-1419
Bonnier and Caboz 956
Bragg-Williams 978, 1000, 1008
Brouwer diagrams 27

Calculations of phase diagrams (see under Theories of phase diagrams, specific topics, and see Tuesday's poster session on this subject, pp 726-1236)
Calphad 37, 49, 1188
Calorimetry (including differential scanning calorimetry, DSC) 1171, 1173
Capsule bursting method 508-515
Ceramic systems (see also under specific systems, Materials Index)
  - compilation activities, review 2-5, 12-22, 121-122, 165, 252-256, 257-258, 1327-1331, 1460-1471
  - compilations, review 1-2, 14-22, 256, 407, 1326, 1374
  - needs and applications (see also under Panels II, III, and IV on User Needs, pp 1332-1452) 9-22, 121, 703-708, 1352, 1356-1357, 1361-1366, 1371, 1375-1377, 1378-1381, 1409-1410, 1427, 1442-1450, 1451-1452, 1455-1457, 1471, 1475
  - questionnaire review 5-22

Charge distribution, transfer 607, 615-619, 766
Chatillon-Colinet 141
Chemical analysis 143, 552, 1379
Chemical scan (isothermal) 151
Cluster variation (theory) 967-998, 999-1026, 1474
Coatings of materials 262, 423-439
Coherent phase diagrams 999-1025
Cohesion, cohesion energy 594-603, 616
Compilations (see under Ceramic systems, Semiconductor systems, Metallic systems, High pressure diagrams)
Compilation methods 22, 163, 658, 720-725, 1475-1478
Composites 1378-1381
Compounds (see also the Materials Index) 100-200, 763-773, 1378-1381
Compound prediction 763-773, 1112, 1139-1150, 1151-1160, 1220-1236, 1473
Computerized data banks (see under Crystallography and under Thermodynamics)
Concentration simplex 660-662
Concorde, alloys in use 1396
Coordination numbers, 1479-1491
  - generalized 767
Crystal chemistry 84-89, 101, 545-547, 620-621, 745-746, 763-772, 1139-1150, 1479-1491
Crystallography
  - compilations 82-83, 259-260, 720-725, 1326
  - computerized data bank 259-260
  - theory and prediction of phases 100-109, 659, 763-773, 1139-1150, 1151-1160

Data banks, computerized
  - crystallography 259-260
  - thermodynamics and thermochemistry 37, 40, 41, 43, 45, 49, 121-124, 1077-1089, 1186-1199
Data compilations (see under Cermic systems, Semiconductor systems, Metallic systems, High pressure diagrams, under the subtopic "compilations")
Density of states (esp Ti) 595
Differential thermal analysis, DTA (see under Thermal analysis)
Diffusion couple analysis 142, 149-151, 465, 522-524, 913
Dilatometry 142, 151, 517
Dip sampling 143
Distribution and publication of phase diagrams 262-264, 703-708, 709-719, 720-725, 1325-1326
Donor solubilities 26-27

Electrical conductivity (experimental phase change det.) 143, 517
Electrochemical probe 148
Electron densities 611
Electron diffraction 148
Electron distribution 607, 615-619, 766
Electron energies 594-609

Electron microprobe 148, 156, 462-471
- microscope, reflecting, transmission, scanning (SEM, STEM) 146, 148, 440-449, 462, 471-474
Electronegativity 610-613, 766
Electronic density of states (esp Ti) 595
Electronic materials (see under narrower term, Semiconductor systems, or specific topics)
Ellingham diagrams (see also Metal-gas phase diagrams Solid-vapor diagrams and Pourbaix diagrams) 1077-1088, 1428
Emf measurements in galvanic cells 517
Energy storage/conversion 262, 1109-1138, 1426, 1428-1439, 1440-1450, 1458
Experimental techniques of phase diagram determination (see under specific techniques)

F*A*C*T (Facility for the Analysis of Chemical Thermodynamics) 1077-1089
Field ion microscope 146
Format of phase diagrams
- representation 16-18, 262-264, 265-271, 578-591, 658, 660-702, 1093-1108, 1315-1324, 1458-1460, 1506-1519
- distribution and publication 262-264, 703-708, 709-719, 720-725, 1325-1326
- publication standards 1307-1324

Geometric description of superalloys 628-658
Gibbs energy function, generation of 1027-1046
Glasses (see also specific glasses in the Materials Index)
- ceramic 1378-1381
- metallic 261-268, 1161-1185
- needs 1378-1381
Graphical methods 45, 265-271, 628-658, 1077-1089, 1506-1519

Hardy-type power series 141
High pressure phase diagrams
- compilation activities, review 100-120
- compilations, review 101-108
- needs and applications 261-268, 703-708
- P-T, P-T-X diagrams 121-122, 153, 578-591
Hillert 956
History of data compilations 2, 36, 90, 100
Hot stage microscopy 1310
Hot wire microscopy 355-374
Hume-Rothery 662
Hyperfine techniques (see also under nuclear magnetic resonance, Mossbauer effect, perturbed angular correlation) 450-461

Industrial needs and applications
- ceramics 1378-1381, 1409-1410, 1427, 1440-1450, 1455
- composites 1378-1381
- glasses 1378-1381
- intermetallics 1378-1381
- ionic systems (see salt systems)
- iron and steelmaking 567-574, 1360-1377, 1378-1381, 1421-1423
- non-ferrous 567-574, 1334-1353, 1354-1359, 1378-1381, 1382-1408, 1418-1419, 1423-1425, 1427
- salt systems 1426, 1428-1439
- superconductors 1411-1417
Interaction parameters 1210-1214
Intermetallics (see also under Compounds, or see under specific systems in the Materials Index)
- needs 1378-1381
Internal pressue 1210-1214
International Atomic Energy Agency (IAEA) 38, 45, 60-61, 78-79
Ion backscattering methods 151, 516-544
- implantation methods 151, 516-544
Ionic systems (see also Salt systems, and also specific systems in the Materials Index) 115-120, 165-225, 251-256, 272-345, 1093-1108
Iron and steelmaking (needs) 1360-1377, 1378-1381, 1421-1423
Irradiation effects 1065-1076

Kaburagi and Kanamori 1012, 1017
Kohler 141, 956

Least squares method of optimizing phase diagrams 955-966
Lever rule, enhanced 454

Magnetic effects 594-602
Margules 848, 872, 874, 876, 903
Matte 1356-1357, 1456
Metal-gas phase diagrams (see also Solid-vapor, Pourbaix-, Ellingham diagrams, etc) 1047-1064, 1077-1088, 1090-1092, 1332-1333
Metallic-nonmetallic component diagrams 1047-1064, 1077-1088, 1090-1092
Metallic radii 763
Metallic systems (see also under specific systems, Materials Index)
- compilation activities, review 37-38, 40-48, 49, 92-94, 122, 164, 226-228, 229-250, 751, 1186-1199, 1327-1331, 1460-1471
- compilations, review 36-38, 50-74, 90-94, 122, 227, 234, 346-350, 351-354, 744-762, 1237-1306, 1326, 1374, 1406
- needs and applications (see also under Panels II, III, and IV on user needs, pp 1332-1452) 121, 261-262, 567, 703-708, 725, 1109, 1180-1182, 1352, 1355-1357, 1361-1366, 1371, 1375-1377, 1378-1381, 1382-1408, 1411-1417, 1427, 1447-1448, 1451-1452, 1455-1457, 1471, 1475
- questionnaire review 261-266
Metallographic analysis 142-143, 156, 517

Metastable phases 261-266, 1161-1185, 1421, 1457
Mossbauer effect 152, 450-461, 615
Microanalysis 913, 1379
Microchemical analysis 148, 440
Micro-furnace 357
Micro-indent hardness 148
Micro x-ray diffraction 148
Microscopy (see under specific type, e.g. optical, electron, etc.)

Natural iteration (theory) 967, 974-978
Needs and Applications (see under Ceramics systems, Semiconductor system, Metallic systems, High pressure, etc., and see under Industrial needs).
Newton-Raphson iteration method 967, 976-977, 1017
Non-ferrous phase diagram industrial needs 1334-1353, 1354-1359, 1378-1381, 1382-1406, 1418-1419, 1423-1425, 1427
Non-stoichiometry prediction 770
Nuclear Magnetic Resonance (NMR) 121, 152, 450-461

Olson 730-731
Optical microscopy (color, reflectivity, other) 148, 411-413
Order-disorder 984-998, 999-1026

P-T, P-T-X, diagrams 28, 121-122, 153, 253, 578-591, 1421, 1456
Pair approximation (theory) 968-973, 1009-1010, 1017
Pair potentials 610, 616, 1424
Pauling 620, 763-773, 1479-1491
Perturbed angular coorelation (PAC) 450-461
Phacomp 37, 624-627, 1423
Phase rule 143-144, 162
Physical chemistry and metallurgy, general 84-89
Potential-composition diagrams 1077-1088
Potential-potential diagrams 1077-1088
Potentials (see also under specific potentials) 603-609, 1011-1015
Polar diagrams 662-663, 684
Pourbaix diagrams (see also Metal-gas diagrams, Solid-vapor diagrams, Ellingham diagrams, Stability diagrams, etc.) 1090-1092, 1428
Predictive methods (see under Theories of phase diagrams, Thermodynamics theories, or under specific topics)
Predominance area phase diagrams 1077-1088
Pressure scan 152
Projection methods
- parallel 664-668
- perspective 663-664
Pseudopotentials 603-609, 1014
Publication and distribution 262-264, 703-708, 709-719, 720-725, 1325-1326
Publication standards 1307-1324

Quenching (see also spat-cooling) 1310
- argon jet 383
- rapid quenching methods, summary 1172
Quenched phase plots 1165
Questionnaire, reviews
- ceramic system 5-22
- metallic systems 261-268

Radioactive techniques 148
Raoultian activity coefficient 726-727
Reciprocal systems, representations of 671
- salt systems 1093-1108
Redlich-Kister 803-845, 846-906, 1445
Representations of phase diagrams 16-18, 262-264, 265-271, 578-591, 660-702, 1093-1108, 1315-1324, 1507-1520
Russian literature 44, 46, 50, 51, 92-99, 346-350, 351-354, 1237-1306

Salt systems (see also Ionic systems and see specific systems in the Materials Index) 1093-1108
- needs 1426, 1428-1439
Scratch hardness 148
Second order phase transitions 620
Sectioning methods for phase diagram representations 668-671
Selective chemical solution 148
Semiconductor systems
- compilations, review 23, 346-350, 351-354
- needs and applications (see also under Panels II, III, and IV on User Needs, pp 1332-1452) 27-28, 121, 703-708, 1426, 1471, 1475
Semiconductor compounds, predictive methods 1220-1236
Sigma phase 625-658, 916, 1065
Slags (see also under Materials Index for specific systems) 362-366, 908, 1334-1353, 1356, 1361, 1368-1369, 1374, 1440, 1456
Smelting
- copper 1336-1339, 1342-1349, 1354
- lead 1354
- nickel 1339-1340, 1350-1352
- zinc 1354
Solid state physics (see under Alloy physics or under specific topics)
Solid-vapor diagrams (see also Metal-gas phase diagrams Pourbaix-Ellingham diagrams, etc.) 28, 121-122, 362-374, 1047-1064, 1077-1088, 1090-1092, 1332-1333
Solubilities, donor, acceptor 26-27
Speiss 1357
Splat cooling 383, 1171
Stability diagrams (see also under Pourbaix, Ellingham) 1047-1064, 1077-1088, 1428, 1456
Standards of publication 1307-1324
Stoichiometric description of superalloys 625-627

Strain energy 1210-1214
Strain fields 620
Stress, phase diagrams under external tensile -, or shear stress 575-577
Structural instabilities 769
Sulfur: desulfurization 1372, 1456
Superalloys 37, 262, 423-439, 624-658, 1186
- stoichiometric description 625-627
- geometric description 628-658
- phacomp 37, 624-627, 1423
Superconductivity as technique in phase diagram determination 384-386
Superconductors 262, 375, 387-392, 401, 545-549, 616-618, 770 1148, 1158, 1326, 1411-1417
- needs 1411-1417
Surface phases 262, 268, 1459-1460
Surrounded atom model 141

Temperature scan method 151
Tetrahedron approximation 968, 978-983, 1008
Theories of phase diagrams (see review article pp 592-623, Tuesday's poster session on the topic pp 726-1236, and see under specific topics)
- listing of treatments of the subject 84-89
Thermal analysis, including differential thermal analysis, DTA) 121, 142 377-382, 407, 417-419, 517, 1171, 1310
Thermal gravimetric analysis 517
Thermochemistry (see Thermodynamics)
Thermodata 37, 122
Thermodynamics
- compilations 37, 53, 75-81, 196, 228, 229-250
- computerized data banks 37, 49, 121-124, 1077-1089, 1186-1199, 1451
- theory, including computerized methods (see also Tuesday's poster session on the topic pp 726-1236; and see under specific topics) 37, 121-128, 143-144, 163, 803-845, 846-906, 1077-1089, 1100, 1457-1458, 1472-1475
- listing of treatment of theory 84-89
Toop 141, 730-731, 956
Transient Liquid Phase (TLP) bonding 1418-1419

Variable valency in representation of phase diagrams 671-672
VINITI (see under Russian literature)

Wiederkehr 960

X-ray analysis 143, 156, 407-422, 440-449, 517, 551
- synchrotron light 163

MATERIALS INDEX

This index represents a listing of pages on which quantitative information is given for specific systems: 1) all pages are noted on which phase diagram figures appear; 2) generally, those pages are noted on which data evaluation is discussed; 3) generally, those pages are noted on which related thermodynamic data, or sometimes related crystallographic data appear. A few summarizing data tables occur in these proceedings. No attempt has been made to list these under each individual material. Rather, these are noted under the general material category (e.g. "rare earths", etc.). Alloys have been listed with their components in alphabetical order under the component of lowest alphabetical occurrence. For compounds, the formulas have been alphabetized, but compounds forming components of salt systems are not broken up to further alphabetize, in order to preserve chemical meanings (e.g. CaF_2-AlF_3-Al_2O_3 is listed under AlF_3-Al_2O_3-CaF_2, rather than Al-Ca-F-O).

A-15 compound formation prediction	1148, 1158
$A_2^{III}B^{IV}O_7$ compound formation prediction	1149-1150, 1159-1160
Ac-B	762
Ag laves phase prediction	1147, 1157
Ag-B	770
Ag-Cu	780
Ag-Cu-S	774-797
Ag-Cu-Se	774-802
Ag-Cu-Zn (several temps)	237-246
Ag-Pd	1218
Ag-S	779-780
Ag-Si	219
Al	1407
Al-Au-In	455
Al-B	749, 753-757
Al-Be-Fe	544
Al-Ca-O-Si	1370
Al-Co-Cr-Ni	438
Al-Co-Fe-Si	1392, 1405
Al-Cr-Fe-Ni	438
Al-Cr-Fe-Si	1392, 1405
Al-Cr-Mo-Ni-Ti-W	630-635

Al-Cr-Nb	1189-1190, 1199
Al-Cr-Ni	628-630, 655, 658
Al-Cr-Ni-Pt	439
Al-Cr-Ni-Ti	628-630, 654
Al-Cr-Zr	1189-1190, 1194-1189
Al-Cu	608
Al-Cu-Mg-Si	1389-1390, 1402
Al-Fe-Mn	1391, 1403
Al-Fe-Mn-Si	1392, 1405
Al-Fe-Ni-Si	1392, 1405
Al-Fe-Si	1392, 1394, 1404, 1407
Al-Ge-Nb	1415
Al-Li	1115-1118, 1128-1131
Al-Li-Mg	1109-1138, 1134-1138
Al-Mg	1118-1119, 1128-1129, 1132
Al-Mg-Zn	1385-1386, 1399
Al-Mn	134
Al-Ni-Ti	628-630, 657
Al-Sn	1219
Al-Ti-V (Ti-6Al-4V)	567-574
Al-Zn	1393, 1406
$AlCa_2F_7$, and related cpds.	283-285
$AlCaF_5$-FNa	318
Al_2CaF_9Na	320
AlF-CaF_2	280-285
AlF_3	278
AlF_3-AlF_6Li_3-AlF_6Na	329, 331
AlF_3-AlF_6Na_3-CaF_2	314, 317-324
AlF_3-AlF_6Na_3-Al_2O_3	322-326
AlF_3-AlF_6Na_3-Al_2O_3-CaF_2	333, 335-337

AlF_3-AlF_6Na_3-Al_2O_3-CaF_2-FLi	272-354
AlF_3-AlF_6Na_3-Al_2O_3-CaF_2-FLi	336, 338
AlF_3-AlF_6Na_3-FLi	229, 332
AlF_3-Al_2O_3-CaF_2	328
AlF_3-FLi	300-305
AlF_6Li_3-AlF_6Na_3	306-311
Al_6Li_3-AlF_6Na_3-Al_2O_3	228-330
AlF_6Li_3-Al_2O_3	310, 312
AlF_6Li_3-CaF_2	314, 316
AlF_6Li_3-CaF_2-FLi	329, 333-334
AlF_6Na_3	277
AlF_6Na_3-AlF_3	289-296
AlF_6Na_3-Al_2O_3	296-299
AlF_6Na_3-Al_2O_3-CaF_2	325-328
AlF_6Na_3-CaF_2	285-290
AlF_6Na_3-FLi	305-308
$AlKO_2$-O_2Si	442
Al_2O_3	279
Al_2O_3-AlF_3	300
Al_2O_3-CaF_2	299-300
Al_2O_3-CaO-MgO-Na_2O-O_2Si	362-366, 374
$AlO_{1.5}$-$KO_{0.5}$	884
Al_2O_3-WO_3	221
Alloy 713 and 713LC	642
Am-B	752-756, 762
As-Ga	1233-1234
As-In	1233-1234
Au laves phase prediction	1147, 1157
Au-B	771
Au-Cu	726-743, 984-985, 988, 997-998, 1007-1011, 1020-1024

Au-Cu-Ni	726-743
Au-Mn	1013, 1025
Au-Ni	726-743
Au-Sb (including metastable diagram)	1173
Au-Si	1219
Au-Si (including metastable data)	1178
Au-Te	271

B-Ba	748, 753-757
B-Be	748, 752-757
B-C-Fe	566
B-Ca	748, 753-757
B-Co	749, 752-756, 761
B-Cr	749, 753-756, 759, 768
B-Fe	749, 753-756, 760
B-Fe (including metastable data)	1177, 1178
B-Hf	749, 753-756, 758
B-Ir	749, 753-756, 761
B-La	749, 753-756, 758
B-Mg	748, 753-757
B-Mn	749, 753-756, 760, 768
B-Mo	749, 753-756, 759
B-Nb	749, 753-756, 759, 768
B-Ni	750, 753-756, 761
B-Np	752-756, 762
B-Os	749, 753-756, 760, 770
B-Pa	762
B-Pd	750, 753-756, 761
B-Pt	750, 752-756, 761
B-Pu	752-756, 762
B-Re	749, 753-756, 760

B-Rh 749, 753-756, 761
B-rich systems 752
B-Ru 749, 753-756, 760, 770-771
B-Sc 749, 753-756, 758
B-Sr 748, 753-757
B-Ta 749, 753-756, 759, 768
B-Tc 749, 753-756, 760
B-Th 752-756, 762
B-Ti 749, 753-756, 758
B-transition metal 751
B-U 752-756, 762
B-V 749, 752-756, 759
B-W 749, 753-756, 759, 771
B-Y 749, 753-756, 758
B-Zr 749, 753-756, 758
B-1900 642, 652-653
B_2O_3-WO_3 220
BaO-WO_3 206
Be-Cu 539, 543
Be-Cu-Ne 543
Be-Fe 541
Be-Si 1219
Be-Ti (including metastable data) 1177
Be-Ti-Zr 1174
BeO-WO_3 202
Bi-Nb 1219
Bi_2O_3-WO_3 225
Brasses 1383-1385, 1398

1621

C	857
C-Cr-Fe	1058
C-Cr-Fe-O	1048, 1060
C-Fe	155, 572, 885, 1368
C-Fe (metastable data)	1367
C-Fe-H-O-S	1081
C-Fe-Ni	470, 480, 880
C-Fe-Sb	573
C-H-Ni-O-S	1081
C-Ni (at three pressures)	111
C-Ni	891-901, 904
C-W	770
CO_3-HO-Li-Na	1098, 1108
Ca-Cu-Mg (several temps)	247-250
Ca-Fe-O-Si	1368
CaF_2	279
CaF_2-FLi	310, 313-315
Ca-O-Si	1369
$CaO-WO_3$	204
$CdO-WO_3$	219
Cl-F-K-Li	1095, 1107
Cl-F-Li-Na	1095, 1105-1106
ClK-$(HO)_2$Mg-MgO	511, 514-515
ClLi-$(HO)_2$Mg-MgO	511-512, 515
ClNa-$(HO)_2$Mg-MgO	511, 513, 515
Co-Fe-Ni	479
Co-Gd (including metastable data)	1177
Co-Sm	769
Cr-Fe	916, 935

Cr-Fe-Mg-O	1062
Cr-Fe-Ni	911-954
Cr-Fe-Ni (including irradiation effects)	1066-1069, 1071, 1074-1075
Cr-Fe-O	1059, 1061
Cr-Ni	916, 939
Cr-Ni-Ti	628-630, 656
Cr-O-S	1424
Cr-U (including metastable data)	1177
$Cs_2O \cdot WO_3$-WO_3	201
Cu-Fe	916, 924, 938, 1027-1046
Cu-Fe-Mn	911-954
Cy-Fe-Ni	911-954
Cu-Fe-O-SiO_2	1333
Cu-Fe-O-S-Si	1343
Cu-Fe-S	1333, 1343
Cu-Ge-Nb	1417
Cu-Mn	916, 940
Cu-Nb-Sn	1416
Cu-Ni	726-743, 916, 941
Cu-Ni-S	1350
Cu-O-S	1090-1092
Cu-S	779
Cu smelting	1336-1339, 1342-1349, 1354
Cu ternary alloys	229-250
Cu-Zn	1383-1385, 1398
Cu-Zr (including metastable data)	1177, 1178
Dy_2O_3-O_3Sc_2	553-565
Dy_2O_3-WO_3	211

F-Li	280
Fe-H-O-Ti	503
Fe-H-Ti	456, 498, 500, 506-507
Fe-Mn	916, 936
Fe-Mn-Ti	490-492, 504-505
Fe-Ni	916, 937, 1082, 1084
Fe-Ni (including irridation effects)	1065, 1068-1069
Fe-Ni-Mn (including irridation effects)	1065, 1068, 1072-1073
Fe-Ni-O	1078, 1082-1086
Fe-Ni-O-S	1077-1089
Fe-O	700, 909-910, 1080, 1084
Fe-O-S	1080, 1424
Fe-O-Si	1343
Fe-O-Ti	488-489, 501
Fe-Sb	573
Fe-Ti	486-488, 499
Ga-In-Sb	137, 138, 139
Ga-Nb	387-389, 397, 402-404
Ga-Sb	1233-1234
Ga-Sn-Zn	136
GaO_3-WO_3	222
Ge-Nb	389-392, 405-406
GMR 235	642, 652-653
graphite	857
H-Zr	587, 590-591
HfO_2-WO_3	214
H-Nb-Zr	588-589
H_2O-$(HO)_2Mg$-MgO	511, 515
Ho_2O_3-O_3Sc_2	552-565

In-Sb	1233-1234, 1296
In_2O_3-WO_3	223
IN 100	642, 652-653
IN 731 X	642
Inconel 700	642, 652-653
Inconel 713 C	642, 652-653
Inconel X-750	642, 652-653
Ir laves phase prediction	1147, 1157
$KO_{0.5}$-O_2S	902, 906
$K_2O \cdot WO_3$-WO_3	199
La_2O_3-WO_3	208
Li-Mg	1119-1120, 1128, 1133
$Li_2O \cdot WO_3$-WO_3	197
M 316 stainless (including irradiation effects)	1065
Mar - M 200	642, 652-653
Metal hydrides	610-612
Mg-Pb	1388, 1401
Mg-Si	1386, 1400
Mg-Zn (including metastable data)	1177, 1178
MgO-WO_3	203
Mn-O-S	1424
Mo-P	770
Mo-V	1218
Mo-W	1218

$Na_2O \cdot WO_3 - WO_3$	198
Nb-Ni (including metastable data)	1177
Nb-Ti	1218
Nb-W	1218
$Nb_2O_5 - WO_3$	215
$Nd_2O_3 - WO_3$	210
Ni-based (superalloys)	624-658
Ni-O-S	1078-1080, 1424
Ni smelting	1340-1341, 1350-1352
Ni-Ti	135, 769
Nicrotung	642, 652-653
Nimonic 115	642, 652-653
O-Si	882
Os laves phase prediction	1147, 1157
Oxide systems	165-225, 251-256, 257-258, 272-345, 355-374, 410-422, 440-449, 508-514, 550-562, 909
$PbO-WO_3$	224
Pb-Sn (including metastable data)	1175
Pb-Te	1235
Pd laves phase prediction	1147, 1157
Pd-Si (including metastable data)	1177, 1178
Pt laves phase prediction	1147, 1157
Pt-V	549

Rare earths	110, 226-228, 751-752, 763
- tabulation of structure vs pressure	110, 112-120
$Rb_2O \cdot WO_3 - WO_3$	300
René 41	642, 652-653
Re-W (including irradiation effects)	1066, 1068-1069, 1076
Rh laves phase prediction	1147, 1157
Ru laves phase prediction	1147, 1157
$Sm_2O_3 - WO_3$	209
Sn-V	770
$SrO - WO_3$	205
Steels: 43XX steel	571-572
$Ta_2O_5 - WO_3$	216
$TiO_2 - WO_3$	212
Ti-rich, commercial (Ti-6Al-4V)	567-574
Tool steels	572-573
TRW 1900	642, 652-653
Udimet 500	642, 652-653
Udimet 700	642, 652-653
Unitemp AF	642, 652-653
$UO_3 - WO_3$	217
V-W	1218

Waspaloy	642, 652-653
$Y_2O_3 - WO_3$	207
$ZnO - WO_3$	218
$ZrO_2 - WO_3$	213

NBS-114A (REV. 11-77)

U.S. DEPT. OF COMM. BIBLIOGRAPHIC DATA SHEET	1. PUBLICATION OR REPORT NO. NBS SP-496	2. Gov't Accession No.	3. Recipient's Accession No.

4. TITLE AND SUBTITLE

Applications of Phase Diagrams in Metallurgy and Ceramics—Volume 2
Proceedings of a Workshop Held at the National Bureau of Standards, Gaithersburg, Maryland, January 10-12, 1977

5. Publication Date: March 1978

6. Performing Organization Code

7. AUTHOR(S): G. C. Carter, Editor

8. Performing Organ. Report No.

9. PERFORMING ORGANIZATION NAME AND ADDRESS

NATIONAL BUREAU OF STANDARDS
DEPARTMENT OF COMMERCE
WASHINGTON, D.C. 20234

10. Project/Task/Work Unit No.

11. Contract/Grant No.

12. Sponsoring Organization Name and Complete Address (Street, City, State, ZIP)
National Bureau of Standards; National Science Foundation; Defense Advanced Research Projects Agency; Office of Naval Research; National Aeronautics & Space Administration; Energy Research & Development Administration; U.S. Army Research Office

13. Type of Report & Period Covered

14. Sponsoring Agency Code

15. SUPPLEMENTARY NOTES

Library of Congress Catalog Card Number: 78-2201

16. ABSTRACT (A 200-word or less factual summary of most significant information. If document includes a significant bibliography or literature survey, mention it here.)

The proceedings of a Workshop on Applications of Phase Diagrams in Metallurgy and Ceramics, held at the National Bureau of Standards, Gaithersburg, Maryland, on January 10-12, 1977, is presented in this NBS Special Publication. The Workshop was co-sponsored by the Institute for Materials Research and the Office of Standard Reference Data, NBS, and the National Science Foundation, the Defense Advanced Research Projects Agency, the Office of Naval Research, the National Aeronautics and Space Administration, the Energy Research and Development Administration, and the U.S. Army Research Office.

The purpose of the Workshop was to assess the current national and international status of phase diagram determinations and evaluations for alloys, ceramics and semiconductors, to determine the needs and priorities, especially technological, for phase diagram determinations and evaluations; and to estimate the resources being used and potentially available for phase diagram evaluation. These proceedings reflect the detailed contents of the Workshop for both the tutorial and review sessions as well as four poster sessions and four panel sessions covering the subjects; critical phase diagram availability, user needs of phase diagrams, experimental methods of determination, theoretical methods of calculation and prediction, methods of phase diagram representations of calculation and prediction, methods of phase diagram representations (especially multicomponent) and distribution to the user. Three of the panels addressed the subject of phase diagram needs in industrial applications.

Cont.

17. KEY WORDS (six to twelve entries; alphabetical order; capitalize only the first letter of the first key word unless a proper name; separated by semicolons)

Ceramics; computer predictions; critical evaluations; data compilations; electronic materials; industrial needs; metallurgy; phase diagrams; theory of phase diagrams; thermodynamics.

18. AVAILABILITY

[X] Unlimited

[ ] For Official Distribution. Do Not Release to NTIS

[X] Order From Sup. of Doc., U.S. Government Printing Office Washington, D.C. 20402, SD Stock No. 003-003-01909-3

[ ] Order From National Technical Information Service (NTIS) Springfield, Virginia 22151

19. SECURITY CLASS (THIS REPORT)	21. NO. OF PAGES
UNCLASSIFIED	847
20. SECURITY CLASS (THIS PAGE)	22
UNCLASSIFIED	

USCOMM-DC 60020-P76

16. ABSTRACT *(A 200-word or less factual summary of most significant information. If document includes a significant bibliography or literature survey, mention it here.)*

These proceedings represent documentation of this assessment, and constitute a valuable resource to workers in these areas, especially those planning to initiate phase diagram programs. Most subjects within the overall scope have been dealt with substantially in these proceedings; a few specialized topics such as surface and small particle phases, needed for the study of catalysis, have not been treated in detail. As the Alloy Data Center maintains a continuing phase diagram program, we would like to receive suggestions for similar topics of current and future interest, descriptions of new needs, or addenda and corrigenda to these proceedings. A tear-off sheet has been provided at the end of these proceedings for this purpose to be sent to the NBS Alloy Data Center.

☆ U.S. GOVERNMENT PRINTING OFFICE : 1979 O—278-469

If you wish to send us your suggestions for additional topics of current and future data compilation needs, or if you have any other addenda or corrigenda to these proceedings, please note them on this page and return to the

Alloy Data Center
National Bureau of Standards
Bldg. 223, Room B-150
Washington, DC 20234

Name _____

Affiliation _____

Address _____

City _____ State _____ Zip Code _____

Suggestions:

(cut here)

There's a new look to...

DIMENSIONS/NBS

. . . the monthly magazine of the National Bureau of Standards. Still featured are special articles of general interest on current topics such as consumer product safety and building technology. In addition, new sections are designed to . . . PROVIDE SCIENTISTS with illustrated discussions of recent technical developments and work in progress . . . INFORM INDUSTRIAL MANAGERS of technology transfer activities in Federal and private labs. . . DESCRIBE TO MANUFACTURERS advances in the field of voluntary and mandatory standards. The new DIMENSIONS/NBS also carries complete listings of upcoming conferences to be held at NBS and reports on all the latest NBS publications, with information on how to order. Finally, each issue carries a page of News Briefs, aimed at keeping scientist and consumer alike up to date on major developments at the Nation's physical sciences and measurement laboratory.

(please detach here)

SUBSCRIPTION ORDER FORM

Enter my Subscription To DIMENSIONS/NBS at $12.50. Add $3.15 for foreign mailing. No additional postage is required for mailing within the United States or its possessions. Domestic remittances should be made either by postal money order, express money order, or check. Foreign remittances should be made either by international money order, draft on an American bank, or by UNESCO coupons.

☐ Remittance Enclosed **(Make checks payable to Superintendent of Documents)**

☐ Charge to my Deposit Account No.

Send Subscription to:

NAME-FIRST, LAST

COMPANY NAME OR ADDITIONAL ADDRESS LINE

STREET ADDRESS

CITY | STATE | ZIP CODE

PLEASE PRINT

MAIL ORDER FORM TO:
Superintendent of Documents
Government Printing Office
Washington, D.C. 20402

NBS TECHNICAL PUBLICATIONS

PERIODICALS

JOURNAL OF RESEARCH—The Journal of Research of the National Bureau of Standards reports NBS research and development in those disciplines of the physical and engineering sciences in which the Bureau is active. These include physics, chemistry, engineering, mathematics, and computer sciences. Papers cover a broad range of subjects, with major emphasis on measurement methodology, and the basic technology underlying standardization. Also included from time to time are survey articles on topics closely related to the Bureau's technical and scientific programs. As a special service to subscribers each issue contains complete citations to all recent NBS publications in NBS and non-NBS media. Issued six times a year. Annual subscription: domestic $17.00; foreign $21.25. Single copy, $3.00 domestic; $3.75 foreign.

Note: The Journal was formerly published in two sections: Section A "Physics and Chemistry" and Section B "Mathematical Sciences."

DIMENSIONS/NBS

This monthly magazine is published to inform scientists, engineers, businessmen, industry, teachers, students, and consumers of the latest advances in science and technology, with primary emphasis on the work at NBS. The magazine highlights and reviews such issues as energy research, fire protection, building technology, metric conversion, pollution abatement, health and safety, and consumer product performance. In addition, it reports the results of Bureau programs in measurement standards and techniques, properties of matter and materials, engineering standards and services, instrumentation, and automatic data processing.

Annual subscription: Domestic, $12.50; Foreign $15.65.

NONPERIODICALS

Monographs—Major contributions to the technical literature on various subjects related to the Bureau's scientific and technical activities.

Handbooks—Recommended codes of engineering and industrial practice (including safety codes) developed in cooperation with interested industries, professional organizations, and regulatory bodies.

Special Publications—Include proceedings of conferences sponsored by NBS, NBS annual reports, and other special publications appropriate to this grouping such as wall charts, pocket cards, and bibliographies.

Applied Mathematics Series—Mathematical tables, manuals, and studies of special interest to physicists, engineers, chemists, biologists, mathematicians, computer programmers, and others engaged in scientific and technical work.

National Standard Reference Data Series—Provides quantitative data on the physical and chemical properties of materials, compiled from the world's literature and critically evaluated. Developed under a world-wide program coordinated by NBS. Program under authority of National Standard Data Act (Public Law 90-396).

NOTE: At present the principal publication outlet for these data is the Journal of Physical and Chemical Reference Data (JPCRD) published quarterly for NBS by the American Chemical Society (ACS) and the American Institute of Physics (AIP). Subscriptions, reprints, and supplements available from ACS, 1155 Sixteenth St. N.W., Wash., D.C. 20056.

Building Science Series—Disseminates technical information developed at the Bureau on building materials, components, systems, and whole structures. The series presents research results, test methods, and performance criteria related to the structural and environmental functions and the durability and safety characteristics of building elements and systems.

Technical Notes—Studies or reports which are complete in themselves but restrictive in their treatment of a subject. Analogous to monographs but not so comprehensive in scope or definitive in treatment of the subject area. Often serve as a vehicle for final reports of work performed at NBS under the sponsorship of other government agencies.

Voluntary Product Standards—Developed under procedures published by the Department of Commerce in Part 10, Title 15, of the Code of Federal Regulations. The purpose of the standards is to establish nationally recognized requirements for products, and to provide all concerned interests with a basis for common understanding of the characteristics of the products. NBS administers this program as a supplement to the activities of the private sector standardizing organizations.

Consumer Information Series—Practical information, based on NBS research and experience, covering areas of interest to the consumer. Easily understandable language and illustrations provide useful background knowledge for shopping in today's technological marketplace.

Order **above** *NBS publications from: Superintendent of Documents, Government Printing Office, Washington, D.C. 20402.*

Order **following** *NBS publications—NBSIR's and FIPS from the National Technical Information Services, Springfield, Va. 22161.*

Federal Information Processing Standards Publications (FIPS PUB)—Publications in this series collectively constitute the Federal Information Processing Standards Register. Register serves as the official source of information in the Federal Government regarding standards issued by NBS pursuant to the Federal Property and Administrative Services Act of 1949 as amended, Public Law 89-306 (79 Stat. 1127), and as implemented by Executive Order 11717 (38 FR 12315, dated May 11, 1973) and Part 6 of Title 15 CFR (Code of Federal Regulations).

NBS Interagency Reports (NBSIR)—A special series of interim or final reports on work performed by NBS for outside sponsors (both government and non-government). In general, initial distribution is handled by the sponsor; public distribution is by the National Technical Information Services (Springfield, Va. 22161) in paper copy or microfiche form.

BIBLIOGRAPHIC SUBSCRIPTION SERVICES

The following current-awareness and literature-survey bibliographies are issued periodically by the Bureau:

Cryogenic Data Center Current Awareness Service. A literature survey issued biweekly. Annual subscription: Domestic, $25.00; Foreign, $30.00.

Liquified Natural Gas. A literature survey issued quarterly. Annual subscription: $20.00.

Superconducting Devices and Materials. A literature survey issued quarterly. Annual subscription: $30.00. Send subscription orders and remittances for the preceding bibliographic services to National Bureau of Standards, Cryogenic Data Center (275.02) Boulder, Colorado 80302.